frontiers | Research Topics

Unveiling biomarkers and mechanisms in the tumor-immune nexus

Edited by
Wantao Wu, Pengpeng Zhang, Jiaheng Xie and Uday Kishore

Published in
Frontiers in Immunology
Frontiers in Oncology

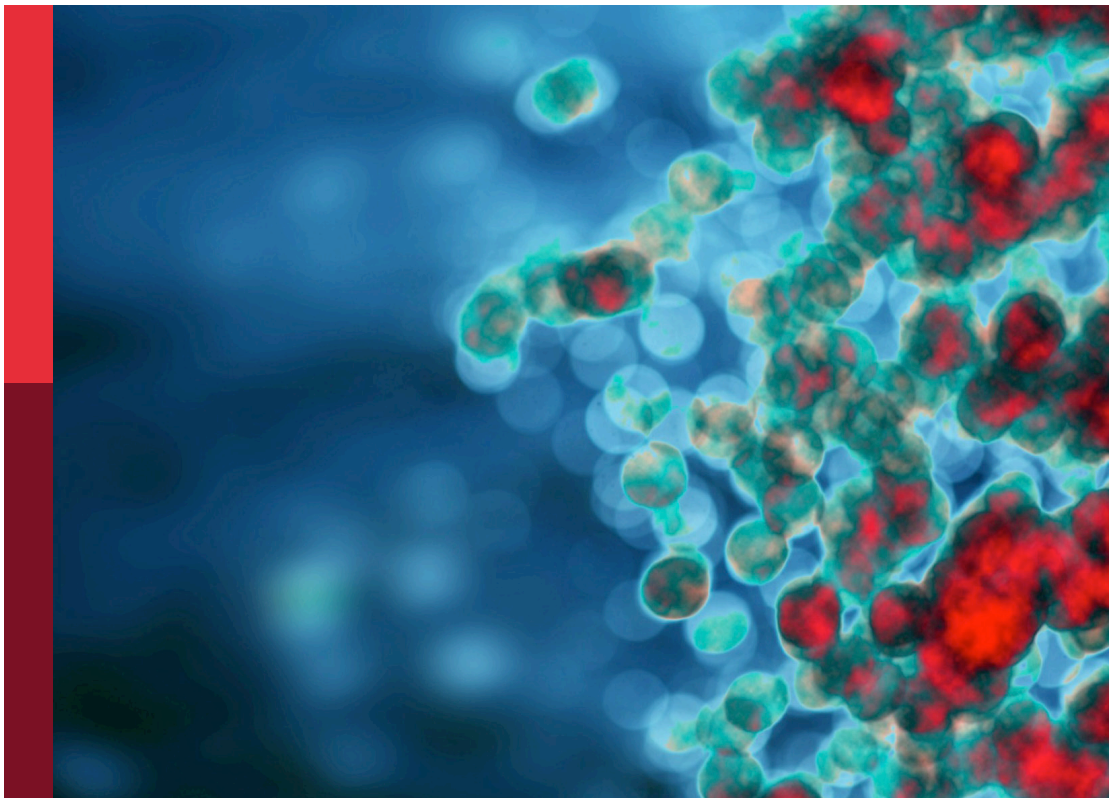

FRONTIERS EBOOK COPYRIGHT STATEMENT

The copyright in the text of individual articles in this ebook is the property of their respective authors or their respective institutions or funders. The copyright in graphics and images within each article may be subject to copyright of other parties. In both cases this is subject to a license granted to Frontiers.

The compilation of articles constituting this ebook is the property of Frontiers.

Each article within this ebook, and the ebook itself, are published under the most recent version of the Creative Commons CC-BY licence. The version current at the date of publication of this ebook is CC-BY 4.0. If the CC-BY licence is updated, the licence granted by Frontiers is automatically updated to the new version.

When exercising any right under the CC-BY licence, Frontiers must be attributed as the original publisher of the article or ebook, as applicable.

Authors have the responsibility of ensuring that any graphics or other materials which are the property of others may be included in the CC-BY licence, but this should be checked before relying on the CC-BY licence to reproduce those materials. Any copyright notices relating to those materials must be complied with.

Copyright and source acknowledgement notices may not be removed and must be displayed in any copy, derivative work or partial copy which includes the elements in question.

All copyright, and all rights therein, are protected by national and international copyright laws. The above represents a summary only. For further information please read Frontiers' Conditions for Website Use and Copyright Statement, and the applicable CC-BY licence.

ISSN 1664-8714
ISBN 978-2-8325-6141-6
DOI 10.3389/978-2-8325-6141-6

About Frontiers

Frontiers is more than just an open access publisher of scholarly articles: it is a pioneering approach to the world of academia, radically improving the way scholarly research is managed. The grand vision of Frontiers is a world where all people have an equal opportunity to seek, share and generate knowledge. Frontiers provides immediate and permanent online open access to all its publications, but this alone is not enough to realize our grand goals.

Frontiers journal series

The Frontiers journal series is a multi-tier and interdisciplinary set of open-access, online journals, promising a paradigm shift from the current review, selection and dissemination processes in academic publishing. All Frontiers journals are driven by researchers for researchers; therefore, they constitute a service to the scholarly community. At the same time, the *Frontiers journal series* operates on a revolutionary invention, the tiered publishing system, initially addressing specific communities of scholars, and gradually climbing up to broader public understanding, thus serving the interests of the lay society, too.

Dedication to quality

Each Frontiers article is a landmark of the highest quality, thanks to genuinely collaborative interactions between authors and review editors, who include some of the world's best academicians. Research must be certified by peers before entering a stream of knowledge that may eventually reach the public - and shape society; therefore, Frontiers only applies the most rigorous and unbiased reviews. Frontiers revolutionizes research publishing by freely delivering the most outstanding research, evaluated with no bias from both the academic and social point of view. By applying the most advanced information technologies, Frontiers is catapulting scholarly publishing into a new generation.

What are Frontiers Research Topics?

Frontiers Research Topics are very popular trademarks of the *Frontiers journals series*: they are collections of at least ten articles, all centered on a particular subject. With their unique mix of varied contributions from Original Research to Review Articles, Frontiers Research Topics unify the most influential researchers, the latest key findings and historical advances in a hot research area.

Find out more on how to host your own Frontiers Research Topic or contribute to one as an author by contacting the Frontiers editorial office: frontiersin.org/about/contact

Unveiling biomarkers and mechanisms in the tumor-immune nexus

Topic editors

Wantao Wu — Chongqing Medical University, China
Pengpeng Zhang — Nanjing Medical University, China
Jiaheng Xie — Central South University, China
Uday Kishore — United Arab Emirates University, United Arab Emirates

Citation

Wu, W., Zhang, P., Xie, J., Kishore, U., eds. (2025). *Unveiling biomarkers and mechanisms in the tumor-immune nexus*. Lausanne: Frontiers Media SA.
doi: 10.3389/978-2-8325-6141-6

Table of contents

06 Editorial: Unveiling biomarkers and mechanisms in the tumor-immune nexus
Chenfeng Ma, Wantao Wu, Pengpeng Zhang and Jiaheng Xie

09 Evaluating the predictive value of angiogenesis-related genes for prognosis and immunotherapy response in prostate adenocarcinoma using machine learning and experimental approaches
YaXuan Wang, JiaXing He, QingYun Zhao, Ji Bo, Yu Zhou, HaoDong Sun, BeiChen Ding and MingHua Ren

24 Sex differences in cancer and immunotherapy outcomes: the role of androgen receptor
Junzhe Zhao, Qian Wang, Alexandra F. Tan, Celestine Jia Ling Loh and Han Chong Toh

39 Causal association between immune cells and lung cancer risk: a two-sample bidirectional Mendelian randomization analysis
Shengshan Xu, Huiying Fang, Tao Shen, Yufu Zhou, Dongxi Zhang, Yongwen Ke, Zhuowen Chen and Zhuming Lu

49 A mitochondria-related genes associated neuroblastoma signature - based on bulk and single-cell transcriptome sequencing data analysis, and experimental validation
Chaoyu Wang, Jiaxiong Tan, Yan Jin, Zongyang Li, Jiaxing Yang, Yubin Jia, Yuren Xia, Baocheng Gong, Qiuping Dong and Qiang Zhao

70 Integrating single-cell and spatial transcriptomic analysis to unveil heterogeneity in high-grade serous ovarian cancer
Haixia Luo, Kunyu Wang and Bin Li

85 A novel artificial intelligence network to assess the prognosis of gastrointestinal cancer to immunotherapy based on genetic mutation features
Bicheng Ye, Zhongyan Li and Qiqi Wang

99 Integrated machine learning identifies a cellular senescence-related prognostic model to improve outcomes in uterine corpus endometrial carcinoma
Changqiang Wei, Shanshan Lin, Yanrong Huang, Yiyun Wei, Jingxin Mao and Jiangtao Fan

117 A novel prognostic signature related to programmed cell death in osteosarcoma
Yu-Chen Jiang, Qi-Tong Xu, Hong-Bin Wang, Si-Yuan Ren and Yao Zhang

139 Comprehensive investigation of tumor immune microenvironment and prognostic biomarkers in osteosarcoma through integrated bulk and single-cell transcriptomic analysis
Shaoyan Shi, Li Zhang and Xiaohua Guo

158 Circadian rhythms and breast cancer: unraveling the biological clock's role in tumor microenvironment and ageing
Yalan Yan, Lanqian Su, Shanshan Huang, Qihui He, Jiaan Lu, Huiyan Luo, Ke Xu, Guanhu Yang, Shangke Huang and Hao Chi

165 Potentially functional variants of *INPP5D* and *EXOSC3* in immunity B cell-related genes are associated with non-small cell lung cancer survival
Guojun Lu, Hongliang Liu, Huilin Wang, Xiaozhun Tang, Sheng Luo, Mulong Du, David C. Christiani and Qingyi Wei

177 Investigating the impact of STING pathway activation on breast cancer treatment outcomes: development and validation of a prognostic model
YangYan Zhong, Hong Cao, Wei Li, Jian Deng, Dan Li and JunJie Deng

192 Elucidating the role of tumor-associated ALOX5+ mast cells with transformative function in cervical cancer progression via single-cell RNA sequencing
Fu Zhao, Junjie Hong, Guangyao Zhou, Tianjiao Huang, Zhiheng Lin, Yining Zhang, Leilei Liang and Huarong Tang

215 Deciphering the role of tryptophan metabolism-associated genes ECHS1 and ALDH2 in gastric cancer: implications for tumor immunity and personalized therapy
Lexin Wang, Xue Zhou, Haisheng Yan, Yaping Miao, Binbin Wang, Yuheng Gu, Weining Fan, Ke Xu, Shangke Huang and Jie Liu

230 Causal effects and metabolites mediators between immune cell and risk of colorectal cancer: a Mendelian randomization study
Qian Yang, Bixia Duan, Jian Yue, Donglin Zhang, Xueping Chen, Mengjia Shi, Jie Kan, Ruochan Li, Hongda Li and Lin Gan

240 Evaluation of the effectiveness and safety of combining PD-1/PD-L1 inhibitors with anti-angiogenic agents in unresectable hepatocellular carcinoma: a systematic review and meta-analysis
Hengzhou Zhu, Wenyue Zhao, Haoyan Chen, Xiaodan Zhu, Jianliang You and Chunhui Jin

254 From single-cell to spatial transcriptomics: decoding the glioma stem cell niche and its clinical implications
Lei Cao, Xu Lu, Xia Wang, Hao Wu and Xiaye Miao

274 Machine learning-based discovery of UPP1 as a key oncogene in tumorigenesis and immune escape in gliomas
Zigui Chen, Chao Liu, Chunyuan Zhang, Ying Xia, Jun Peng, Changfeng Miao and Qisheng Luo

288 Integrated transcriptome analysis of CSE1L regarding poor prognosis and immune infiltration in bladder urothelial carcinoma and experimental verification
Runze Liu, Jiayi Ma, Yong Zhang and Zhongbao Zhou

301 mRNA-seq-based analysis predicts: AEG-1 is a therapeutic target and immunotherapy biomarker for pan-cancer, including OSCC
Lihong Yao, Lixue Liu, Wanqiu Xu, Hualei Xi, Song Lin, Guiyan Piao, Ying Liu, Jinrong Guo and Xiumei Wang

318 Personalized three-year survival prediction and prognosis forecast by interpretable machine learning for pancreatic cancer patients: a population-based study and an external validation
Buwei Teng, Xiaofeng Zhang, Mingshu Ge, Miao Miao, Wei Li and Jun Ma

340 Extracellular vesicles in hepatocellular carcinoma: unraveling immunological mechanisms for enhanced diagnosis and overcoming drug resistance
Lanqian Su, Yuxin Yue, Yalan Yan, Jianming Sun, Lanxin Meng, Jiaan Lu, Lanyue Zhang, Jie Liu, Hao Chi, Sinian Liu, Zhongqiu Yang and Xiaowei Tang

349 Companion diagnostics and predictive biomarkers for PD-1/PD-L1 immune checkpoint inhibitors therapy in malignant melanoma
Zeping Wang, Xiaojing Zou, Haiyan Wang, Zhihui Hao, Gebin Li and Shuaiyu Wang

366 The role of cuproptosis in gastric cancer
Yixian Li, Wenhao Sun, Shaolin Yuan, Xinxin Liu, Ziqi Zhang, Renjun Gu, Pengfei Li and Xin Gu

385 Clinical immunotherapy in glioma: current concepts, challenges, and future perspectives
Jun Liu, Jingjian Peng, Jian Jiang and Yanhui Liu

404 Deciphering the role of NcRNAs in Pancreatic Cancer immune evasion and drug resistance: a new perspective for targeted therapy
Yu Gong, Desheng Gong, Sinian Liu, Xiangjin Gong, Jingwen Xiong, Jinghan Zhang, Lai Jiang, Jie Liu, Lin Zhu, Huiyang Luo, Ke Xu, Xiaoli Yang and Bo Li

412 Impact of bone metastasis on prognosis in non-small cell lung cancer patients treated with immune checkpoint inhibitors: a systematic review and meta-analysis
Yonghua Zhu, Jingyao She, Rong Sun, XinXin Yan, Xinyao Huang, Peijuan Wang, Bo Li, Xiangdong Sun, Changqing Wang and Kai Jiang

428 Prognostic significance of hemoglobin, albumin, lymphocyte and platelet score in solid tumors: a pooled study
Jinze Li, Jing Zheng, Puze Wang and Dong Lv

frontiers | Frontiers in Immunology

TYPE Editorial
PUBLISHED 05 March 2025
DOI 10.3389/fimmu.2025.1581492

Check for updates

OPEN ACCESS

EDITED AND REVIEWED BY
Peter Brossart,
University of Bonn, Germany

*CORRESPONDENCE
Jiaheng Xie
xiejiaheng@csu.edu.cn
Pengpeng Zhang
zpp19940120@163.com
Wantao Wu
wuwantao@hospital.cqmu.edu.cn

RECEIVED 22 February 2025
ACCEPTED 25 February 2025
PUBLISHED 05 March 2025

CITATION
Ma C, Wu W, Zhang P and Xie J (2025) Editorial: Unveiling biomarkers and mechanisms in the tumor-immune nexus. *Front. Immunol.* 16:1581492. doi: 10.3389/fimmu.2025.1581492

COPYRIGHT
© 2025 Ma, Wu, Zhang and Xie. This is an open-access article distributed under the terms of the Creative Commons Attribution License (CC BY). The use, distribution or reproduction in other forums is permitted, provided the original author(s) and the copyright owner(s) are credited and that the original publication in this journal is cited, in accordance with accepted academic practice. No use, distribution or reproduction is permitted which does not comply with these terms.

Editorial: Unveiling biomarkers and mechanisms in the tumor-immune nexus

Chenfeng Ma[1], Wantao Wu[2]*, Pengpeng Zhang[3]* and Jiaheng Xie[4]*

[1]Department of Neurosurgery, The First Affiliated Hospital of Nanjing Medical University, Jiangsu Province Hospital, Nanjing, Jiangsu, China, [2]Department of Thyroid and Breast Surgery, The Second Affiliated Hospital, Chongqing Medical University, Chongqing, China, [3]Department of Lung Cancer Surgery, Tianjin Medical University Cancer Institute and Hospital, Tianjin, China, [4]Department of Plastic Surgery, Xiangya Hospital, Central South University, Changsha, China

KEYWORDS

immunotherapy response biomarkers, tumor-immune interactions, immune evasion mechanisms, tumor microenvironment, next-generation sequencing technologies

Editorial on the Research Topic
Unveiling biomarkers and mechanisms in the tumor-immune nexus

Introduction

Cancer is a multifaceted disease driven by genetic mutations, epigenetic changes, and the evolving interaction with the immune microenvironment (1). Tumor cells often evolve mechanisms to evade immune detection and promote immune suppression (2). Despite the recent breakthroughs in cancer immunotherapy, the identification of novel biomarkers and mechanisms that can predict therapeutic outcomes and provide more targeted treatments remains a significant challenge (3).

The tumor-immune nexus encapsulates the interactions between tumor cells and various immune cells, including T-cells, macrophages, dendritic cells, and natural killer cells (4). These interactions are crucial in determining the immune system's ability to recognize and eliminate tumor cells. This complex ecosystem offers both therapeutic opportunities and challenges.

Biomarkers in the tumor-immune landscape

Biomarkers are essential tools in clinical oncology, offering valuable insights into disease progression, therapeutic efficacy, and patient prognosis (5). Within the tumor-immune microenvironment, biomarkers can indicate the status of immune evasion mechanisms, immune infiltration, and tumor antigen expression (6). For instance, immune checkpoint molecules such as PD-1, PD-L1, and CTLA-4 are well-established biomarkers used in immunotherapy, but they do not fully capture the intricate immune evasion strategies employed by tumors (7).

Recent studies have highlighted additional biomarkers, including tumor-associated antigens (TAAs) and tumor-infiltrating lymphocytes (TILs), that are integral to tumor immunity (7). Moreover, the presence of specific cytokines and chemokines in the tumor microenvironment can serve as indicators of immune activation or suppression (8). These biomarkers, along with emerging technologies such as single-cell and bulk RNA sequencing, hold the potential to reveal new therapeutic targets and to guide personalized treatment regimens. In our Research Topic, Yao et al. conducted mRNA sequencing analysis and found that AEG-1 is highly expressed in various cancer types, and is associated with tumor grading and patient prognosis. Additionally, AEG-1 was found to regulate Th1/Th2 immune homeostasis, promote glycogen accumulation, and facilitate tumor fibrosis. This study highlights the potential of AEG-1 as a key biomarker and therapeutic target, offering new insights into its role in tumor progression, immune regulation, and metabolic reprogramming, which could lead to improved prognostic markers and treatment strategies for cancer.

Mechanisms of immune evasion

Tumor cells employ several strategies to avoid immune detection. One common mechanism involves the downregulation of major histocompatibility complex (MHC) molecules, which are responsible for presenting tumor antigens to immune cells (9). Tumor cells can also secrete immunosuppressive cytokines, such as TGF-β and IL-10, that inhibit the activation of immune effector cells [Wang et al.]. Furthermore, the tumor microenvironment can create physical and metabolic barriers, including hypoxia and acidosis, that hinder immune cell infiltration and function (10).

The concept of immune tolerance is also a central aspect of tumor immunity. Tumor-associated macrophages (TAMs), regulatory T-cells (Tregs), and myeloid-derived suppressor cells (MDSCs) are key players in maintaining immune tolerance within the tumor microenvironment (11). These cells dampen anti-tumor immune responses and support tumor growth. Understanding the molecular mechanisms driving the recruitment and activation of these suppressive cells is crucial for developing strategies to overcome immune resistance.

Emerging therapies and future directions

The increasing understanding of the tumor-immune interplay has paved the way for novel immunotherapies. Cancer immunotherapies, such as immune checkpoint inhibitors, adoptive T-cell therapy, and cancer vaccines, have shown promising results in clinical trials (12). However, the heterogeneous nature of tumors and their immune microenvironment complicates the development of universal treatments.

Future research will focus on the identification of novel biomarkers that can predict patient response to specific therapies. Moreover, combination therapies that target multiple immune evasion mechanisms are likely to enhance the effectiveness of immunotherapy. Recent advances in personalized medicine and precision oncology offer hope for tailored treatments that take into account individual tumor-immune profiles.

In our Research Topic, Zhu et al. conducted a systematic review and meta-analysis to evaluate the effectiveness and safety of combining PD-1/PD-L1 inhibitors with anti-angiogenic agents in patients with unresectable hepatocellular carcinoma (HCC)364. The analysis included five Phase III randomized controlled trials involving 1515 patients and revealed that combination therapy significantly improved overall survival (OS) and progression-free survival (PFS) compared to monotherapy or standard treatments. Additionally, the combination therapy showed a higher objective response rate (ORR), though it was also associated with a higher risk of adverse events (AEs).The significance of this study lies in its contribution to advancing the treatment options for unresectable HCC, a disease with limited effective therapies. The findings underscore the potential of combining immune checkpoint inhibitors and anti-angiogenic agents as a promising therapeutic strategy, providing a new avenue for improving patient outcomes, while also highlighting the need for careful management of adverse events.

Furthermore, the role of the microbiome in modulating the immune response is an emerging area of interest (13). The gut microbiota, in particular, has been shown to influence the efficacy of immunotherapy, opening new avenues for therapeutic intervention.

Conclusion

The tumor-immune nexus remains a critical area of research, with vast potential for advancing cancer therapy. As we continue to uncover the molecular and cellular mechanisms that govern tumor-immune interactions, we are moving closer to a future where personalized and targeted immunotherapies can offer more effective treatment options for cancer patients. However, challenges remain, and continued exploration of novel biomarkers, immune evasion mechanisms, and emerging therapies will be essential in shaping the next generation of cancer immunotherapy.

The research presented in this Research Topic highlights the exciting progress being made in this field and provides a glimpse into the future of cancer treatment, where immune-based therapies play a central role in combating this devastating disease.

Author contributions

CM: Data curation, Investigation, Writing – original draft, Writing – review & editing. WW: Writing – original draft, Writing –

review & editing. PZ: Writing – original draft, Writing – review & editing. JX: Writing – original draft, Writing – review & editing.

Acknowledgments

We deeply thank all the authors and reviewers who have participated in this Research Topic.

Conflict of interest

The authors declare that the research was conducted in the absence of any commercial or financial relationships that could be construed as a potential conflict of interest.

Generative AI statement

The author(s) declare that no Generative AI was used in the creation of this manuscript.

Publisher's note

All claims expressed in this article are solely those of the authors and do not necessarily represent those of their affiliated organizations, or those of the publisher, the editors and the reviewers. Any product that may be evaluated in this article, or claim that may be made by its manufacturer, is not guaranteed or endorsed by the publisher.

References

1. Cao LL, Kagan JC. Targeting innate immune pathways for cancer immunotherapy. *Immunity*. (2023) 56:2206–17. doi: 10.1016/j.immuni.2023.07.018

2. Darvin P, Toor SM, Sasidharan Nair V, Elkord E. Immune checkpoint inhibitors: recent progress and potential biomarkers. *Exp Mol Med*. (2018) 50:1–11. doi: 10.1038/s12276-018-0191-1

3. Mao X, Xu J, Wang W, Liang C, Hua J, Liu J, et al. Crosstalk between cancer-associated fibroblasts and immune cells in the tumor microenvironment: new findings and future perspectives. *Mol Cancer*. (2021) 20(1):131. doi: 10.1186/s12943-021-01428-1

4. Lei X, Lei Y, Li JK, Du WX, Li RG, Yang J, et al. Immune cells within the tumor microenvironment: Biological functions and roles in cancer immunotherapy. *Cancer Lett*. (2020) 470:126–33. doi: 10.1016/j.canlet.2019.11.009

5. Duan Q, Zhang H, Zheng J, Zhang L. Turning Cold into Hot: Firing up the Tumor Microenvironment. *Trends Cancer*. (2020) 6:605–18. doi: 10.1016/j.trecan.2020.02.022

6. McLaughlin M, Patin EC, Pedersen M, Wilkins A, Dillon MT, Melcher AA, et al. Inflammatory microenvironment remodelling by tumour cells after radiotherapy. *Nat Rev Cancer*. (2020) 20(4):203–17. doi: 10.1038/s41568-020-0246-1

7. Kumagai S, Koyama S, Itahashi K, Tanegashima T, Lin YT, Togashi Y, et al. Lactic acid promotes PD-1 expression in regulatory T cells in highly glycolytic tumor microenvironments. *Cancer Cell*. (2022) 40(2):201–18.e9. doi: 10.1016/j.ccell.2022.01.001

8. Ozga AJ, Chow MT, Luster AD. Chemokines and the immune response to cancer. *Immunity*. (2021) 54:859–74. doi: 10.1016/j.immuni.2021.01.012

9. DhatChinamoorthy K, Colbert JD, Rock KL. Cancer immune evasion through loss of MHC class I antigen presentation. *Front Immunol*. (2021) 12:636568. doi: 10.3389/fimmu.2021.636568

10. Hu J, Li X, Yang L, Li H. Hypoxia, a key factor in the immune microenvironment. *BioMed Pharmacother*. (2022) 151:113068. doi: 10.1016/j.biopha.2022.113068

11. Pan Y, Yu Y, Wang X, Zhang T. Tumor-Associated Macrophages in Tumor Immunity. *Front Immunol*. (2020) 11:583084. doi: 10.3389/fimmu.2020.583084. [published correction appears in Front Immunol. 2021 Dec 10;12:775758. doi: 10.3389/fimmu.2021.775758.].

12. Rui R, Zhou L, He S. Cancer immunotherapies: advances and bottlenecks. *Front Immunol*. (2023) 14:1212476. doi: 10.3389/fimmu.2023.1212476

13. Wong-Rolle A, Wei HK, Zhao C, Jin C. Unexpected guests in the tumor microenvironment: microbiome in cancer. *Protein Cell*. (2021) 12:426–35. doi: 10.1007/s13238-020-00813-8

frontiers | Frontiers in Immunology

TYPE Original Research
PUBLISHED 16 May 2024
DOI 10.3389/fimmu.2024.1416914

Check for updates

OPEN ACCESS

EDITED BY
Pengpeng Zhang,
Nanjing Medical University, China

REVIEWED BY
Luo Qiang,
Children's Hospital of Chongqing Medical University, China
Jing Zhang,
University of South Dakota, United States

*CORRESPONDENCE
BeiChen Ding
dingbeichen@hrbmu.edu.cn
MingHua Ren
002051@hrbmu.edu.cn

†These authors have contributed equally to this work

RECEIVED 13 April 2024
ACCEPTED 06 May 2024
PUBLISHED 16 May 2024

CITATION
Wang Y, He J, Zhao Q, Bo J, Zhou Y, Sun H, Ding B and Ren M (2024) Evaluating the predictive value of angiogenesis-related genes for prognosis and immunotherapy response in prostate adenocarcinoma using machine learning and experimental approaches.
Front. Immunol. 15:1416914.
doi: 10.3389/fimmu.2024.1416914

COPYRIGHT
© 2024 Wang, He, Zhao, Bo, Zhou, Sun, Ding and Ren. This is an open-access article distributed under the terms of the Creative Commons Attribution License (CC BY). The use, distribution or reproduction in other forums is permitted, provided the original author(s) and the copyright owner(s) are credited and that the original publication in this journal is cited, in accordance with accepted academic practice. No use, distribution or reproduction is permitted which does not comply with these terms.

Evaluating the predictive value of angiogenesis-related genes for prognosis and immunotherapy response in prostate adenocarcinoma using machine learning and experimental approaches

YaXuan Wang†, JiaXing He†, QingYun Zhao†, Ji Bo, Yu Zhou, HaoDong Sun, BeiChen Ding* and MingHua Ren*

Department of Urology, The First Affiliated Hospital of Harbin Medical University, Harbin, China

Background: Angiogenesis, the process of forming new blood vessels from pre-existing ones, plays a crucial role in the development and advancement of cancer. Although blocking angiogenesis has shown success in treating different types of solid tumors, its relevance in prostate adenocarcinoma (PRAD) has not been thoroughly investigated.

Method: This study utilized the WGCNA method to identify angiogenesis-related genes and assessed their diagnostic and prognostic value in patients with PRAD through cluster analysis. A diagnostic model was constructed using multiple machine learning techniques, while a prognostic model was developed employing the LASSO algorithm, underscoring the relevance of angiogenesis-related genes in PRAD. Further analysis identified MAP7D3 as the most significant prognostic gene among angiogenesis-related genes using multivariate Cox regression analysis and various machine learning algorithms. The study also investigated the correlation between MAP7D3 and immune infiltration as well as drug sensitivity in PRAD. Molecular docking analysis was conducted to assess the binding affinity of MAP7D3 to angiogenic drugs. Immunohistochemistry analysis of 60 PRAD tissue samples confirmed the expression and prognostic value of MAP7D3.

Result: Overall, the study identified 10 key angiogenesis-related genes through WGCNA and demonstrated their potential prognostic and immune-related implications in PRAD patients. MAP7D3 is found to be closely associated with the prognosis of PRAD and its response to immunotherapy. Through molecular docking studies, it was revealed that MAP7D3 exhibits a high binding affinity to angiogenic drugs. Furthermore, experimental data confirmed the upregulation of MAP7D3 in PRAD, correlating with a poorer prognosis.

Conclusion: Our study confirmed the important role of angiogenesis-related genes in PRAD and identified a new angiogenesis-related target MAP7D3.

KEYWORDS

prognosis, angiogenesis, machine learning, PRAD, biomarker

1 Introduction

Prostate adenocarcinoma (PRAD) is the most common solid tumor and the fifth leading cause of cancer death in men, and is now considered a global public health problem (1). Various genetic and environmental factors, including advanced age and family history of PRAD, have been identified as risk factors (2). The majority of patients present with nonspecific symptoms such as decreased urinary flow, urgency, increased nocturia, and incomplete bladder emptying, leading to late-stage diagnosis and high mortality rates (3). While advancements in radiotherapy, targeted therapy, and immunotherapy have improved patient outcomes, the challenge of achieving a complete cure for PRAD patients remains significant. Understanding the etiology and pathogenesis of PRAD and developing new treatment strategies are crucial in addressing this pressing issue.

Angiogenesis is the process of developing new vascular structures from existing capillaries or post-capillary venules. This involves the degradation of the vascular basement membrane, stimulation, proliferation, and migration of vascular endothelial cells, and remodeling to form new blood vessels and networks (4). Hypoxia, particularly within the hypoxic regions of solid tumors, is a key factor influencing tumor cell response by impeding the infiltration of immune cells and reducing their anti-tumor activity (5). The response of tumor endothelial cells to hypoxic signals acts as a switch for angiogenesis (6). Disruption of angiogenesis through anti-angiogenic therapies can result in significant hypoxia and promote resistance to tumor drugs (7). Tumors require new blood vessels to support their growth by supplying oxygen and nutrients and eliminating metabolic waste. Angiogenesis is typically initiated once a tumor reaches a certain size, typically around 1–2 mm in diameter (8). Solid malignant tumors, such as PRAD, rely on a sufficient blood supply to support their growth, development, and spread (9). Recent studies have confirmed the role of exosomal PGAM1 in promoting PRAD angiogenesis, suggesting its potential as a diagnostic marker for PRAD metastasis (10). Interleukin-30 disrupts prostate cancer cross-talk with endothelial cells by enhancing angiogenesis (11). The expression of FOXA1 in prostate cancer is positively associated with cancer vessel lymphatic invasion and metastasis, likely due to its regulation of angiogenesis (12). Additionally, Ephrin-A2 has been found to promote prostate cancer metastasis by stimulating angiogenesis (13). Therapy targeting angiogenesis not only inhibits the growth of tumor blood vessels but also restores their abnormal structure within tumors. This normalization of the vasculature shifts suppressive immune conditions to an immune-stimulated state. The activation of the immune system due to therapy also aids in improving the structure of blood vessels, creating a beneficial cycle of mutual enhancement (14). Therefore, a thorough investigation into the role of angiogenesis in PRAD not only aids in early detection but also holds significant value for immunotherapy in PRAD.

The purpose of this study was to explore the importance of angiogenic genes in the diagnosis, prognosis, and treatment outcome of PRAD. Initially, the ssGSEA algorithm was utilized to assess angiogenesis scores in 498 samples from the TCGA-PRAD dataset (15, 16). Subsequently, 10 prognostic differential genes related to angiogenesis in PRAD were identified using the weighted gene co-expression network analysis (WGCNA) method. Cluster analysis was then conducted based on the expression of these 10 genes to evaluate their correlation with patient prognosis, response to immunotherapy and chemotherapy. An angiogenesis-related diagnostic model was developed using 60 algorithms on the TCGA-PRAD dataset and validated with the GSE62872 dataset. Additionally, a prognostic model focusing on angiogenesis was constructed using the least absolute shrinkage and selection operator (LASSO) algorithm, demonstrating high predictive accuracy for PRAD patient outcomes. Furthermore, the most significant angiogenesis-related prognostic gene, MAP7D3, was identified in PRAD using three machine learning methods. The study has established a close relationship between MAP7D3 and immunotherapy and chemotherapy in patients with PRAD. Additionally, the high correlation between MAP7D3 and angiogenesis-targeting drugs was confirmed using molecular docking methods, suggesting a potential role for MAP7D3 in angiogenesis-targeting therapy.

2 Materials and methods

2.1 Data acquisition

There are 498 PRAD samples and 52 corresponding normal samples from the TCGA database included in the study.

Additionally, our study also includes 264 PRAD samples and 160 normal prostate samples from the GSE62872 dataset. Immunoinfiltration analysis of MAP7D3 in PRAD was conducted using the GSE143791 dataset from the TISCH website. Additionally, 60 cases of PRAD tissue and paired para-cancerous tissue were procured from Shanghai Outdo Biotech Company. The patients included in the tissue chip study underwent surgery between January 2011 and December 2014, with a follow-up period extending from November 2021, spanning 6 to 10 years.

2.2 Consistency cluster analysis

To analyze consistency, we utilized the ConsensusClusterPlus R package (v1.54.0) (17). A total of 100 samples, each comprising 80%, were drawn repeatedly, resulting in the generation of up to 6 clusters. The hierarchical clustering approach involved setting clusterAlg="hc" and innerLinkage='ward.D2'.

2.3 Constructing diagnostic and prognostic models

We utilized multiple machine learning algorithms and developed 108 combinations of different algorithms to build PRAD diagnostic models. The training set consisted of the TCGA-PRAD dataset, while GSE62872 served as the verification set. For each algorithm combination, we computed the AUC value, and the combination with the highest average AUC was deemed the most optimal (18). The prognostic model was characterized by LASSO regression algorithm and 10-fold cross-validation was used for this analysis (19, 20). The R software glmnet package was used for this analysis.

2.4 Immune infiltration and chemotherapeutic drug sensitivity analysis

In order to assess the immune scores of genes related to angiogenesis in PRAD, we utilized the immunedeconv tool (21). For our study, we specifically employed the xCell algorithm due to its ability to evaluate a wide range of immune cell types, making it well-suited for our investigation. Furthermore, we utilized the Genomics Database for Cancer Drug Sensitivity (GDSC) to predict the response to chemotherapy for each sample. This prediction process was conducted using the pRRophetic R package. The tumor immunophenotyping (TIP) method complements the existing ssGSEA and CIBERSORT methods and can systematically track and analyze the proportion of tumor-infiltrating immune cells in the tumor immune cycle (22). Our study utilized the TIP method to investigate the relationship between angiogenesis-related genes and immune cell infiltration in PRAD. Furthermore, we employed the TISCH2 database to assess the correlation between MAP7D3 and immune cell infiltration in PRAD (23).

2.5 Gene Set Enrichment Analysis

In Gene Set Enrichment Analysis (GSEA), we utilized version 3.0 of the GSEA software (24). In the content section of cluster analysis, we grouped the data by cluster 1 and cluster 2. For enrichment analysis on MAP7D3, we utilized the median expression of MAP7D3 as the threshold. Samples with expression levels higher than the median were categorized as the high-expression group, while samples with expression levels lower than the median were categorized as the low-expression group. Then gene sets corresponding to relevant signaling pathways are extracted from the molecular feature database, and the signaling pathways and molecular mechanisms related to gene expression are analyzed (25). The genome sizes were constrained between 5 and 5000, with one thousand resamplings conducted. A statistically significant P value below 0.05 was considered for result interpretation.

2.6 Correlation analysis of MAP7D3 with angiogenesis-targeting drugs

To assess the binding affinity of the key gene MAP7D3 with angiogenic drugs, we employed a molecular docking approach for analysis. The CB-Dock2 website (26) was utilized as a valuable tool in our study, utilizing Vina score to assess the binding affinity of genes and drugs. A Vina score below 5.0 kcal/mol is commonly considered indicative of a more robust binding interaction between the gene and drug.

2.7 Immunohistochemical staining analysis of MAP7D3 expression in PRAD tissues

The PRAD tissue chip underwent a series of preparation steps including heating in an oven at 85°C for 15 minutes, soaking in xylene for 20 minutes, immersion in various concentrations of ethanol, citric acid treatment with antigen retrieval in a pressure cooker, and subsequent rinsing with PBS and hydrogen peroxide solution. The chip was then incubated with MAP7D3 antibody (bs-18668R) overnight at 4°C, followed by rinsing, incubation with secondary antibodies, DAB reagent treatment for color development, and staining with hematoxylin. Immunostaining intensity was scored from 0 to 3 based on reaction strength, and a scale from 1 to 4 was used to assess the proportion of positive staining. The final expression score was calculated by multiplying the intensity and scale scores, with scores ranging from 0 to 5 indicating low expression and scores from 6 to 12 indicating high expression.

2.8 Statistical analysis

All the analysis methods and R package were implemented by R version 4.0.3. The statistical difference of two groups was compared through the Wilcox test. A statistically significant difference is indicated by $p < 0.05$.

3 Results

3.1 Identification of angiogenesis-related genes in PRAD

Within the TCGA-PRAD dataset, 498 samples were analyzed to compute the angiogenesis score for each using the ssGSEA approach. Subsequently, the samples were segregated into two categories depending on the median angiogenesis score. In the analysis conducted, the parameter power for the weight of the adjacency matrix was set to 8 to guarantee a scale-free distribution of the network. WGCNA, a computational method utilized for deriving module information from extensive expression data, characterizes a module as a cluster of genes exhibiting comparable expression profiles (Figure 1A). Pearson correlation analysis was then performed to assess the correlation between module characteristic genes and traits (Figures 1B, C). Notably, the black module exhibited the highest correlation (correlation coefficient of 0.5) with angiogenesis (Figure 1D). Differential analysis of the TCGA-PRAD data set between cancer and normal tissues identified 3125 differential genes (Figure 1E). $P < 0.05$ and Log2 (Fold Change) >1.3 or Log2 (Fold Change) < -1.3 were defined as thresholds for differential expression screening. Subsequently, prognostic gene analysis in the TCGA-PRAD data set revealed 331 prognostic genes. By overlaying these sets using a Venn diagram, we identified 10 prognostic-related angiogenesis differential genes (Figure 1F).

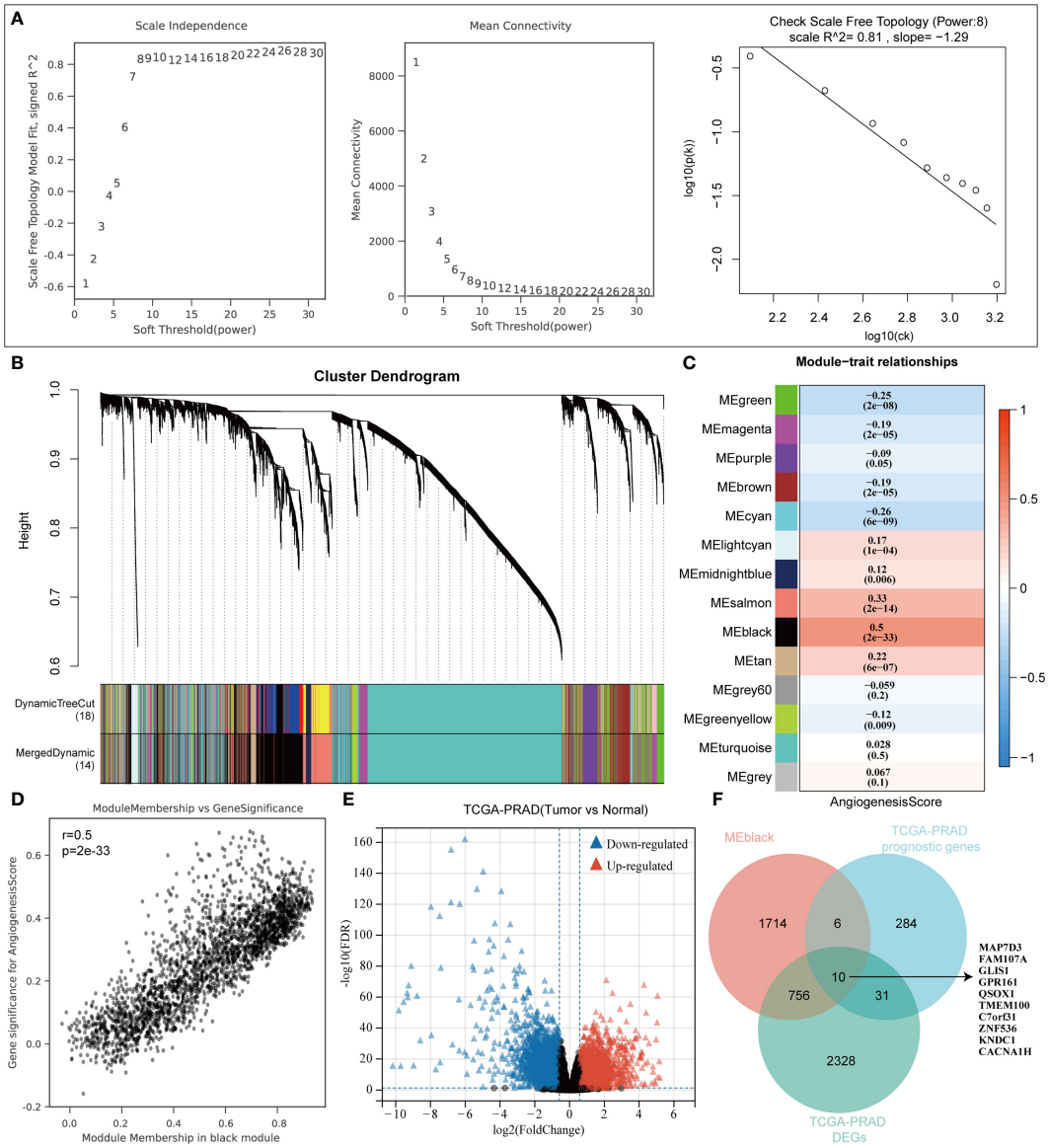

FIGURE 1
WGCNA algorithm screens angiogenesis-related genes. **(A)** WGCNA Network Construction Parameters. **(B)** The upper part of the figure shows the gene clustering tree constructed on the weighted correlation coefficients, and the lower part of the figure is divided into the distribution of genes in each module. **(C)** Heatmap of trait module associations. **(D)** Scatterplot of Angiogenesis and Module Gene Association. **(E)** TCGA-PRAD dataset variance analysis volcano plot. **(F)** Venn diagrams to map angiogenic prognostic differential genes.

10.3389/fimmu.2024.1416914

3.2 Consensus clustering analysis of angiogenesis regulatory factors

The optimal cluster stability for k = 2 was determined by assessing the similarity in expression levels of angiogenic regulatory factors and fuzzy clustering measures (k = 2 to 6). A total of 499 PRAD patients were then classified into two clusters: cluster 1 (n = 245) and cluster 2 (n = 253), based on their expression levels of angiogenic regulatory factors (Figures 2A, B). In addition, according to the average consistency evaluation within the clustering group, here, the number of clusters with the highest average consistency within the group is also K=2 (Figure 2C). Subsequently, we assessed the expression variances of angiogenesis-related prognostic differential genes including MAP7D3, FAM107A, GLIS1, GPR161, QSOX1, TMEM100, C7orf31, ZNF536, KNDC1, and CACNA1H in the two clusters. Our analysis revealed significant differences in all of the mentioned genes (Figure 2D). Patients in cluster 1 exhibited a worse prognosis in terms of both overall survival and disease-specific survival among PRAD patients (Figures 2E, F). Given this conclusion, we are

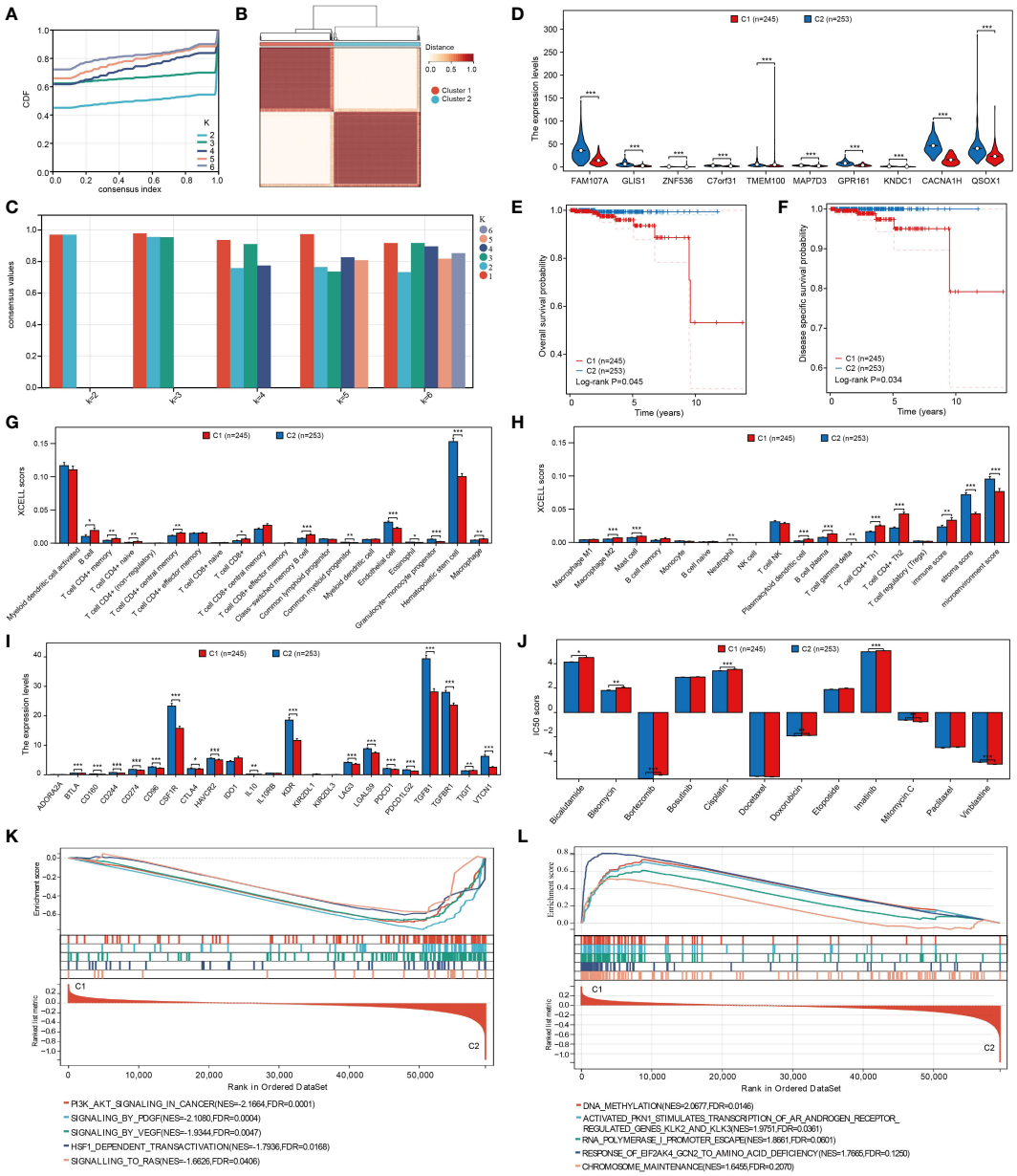

FIGURE 2
Cluster analysis of PRAD patients based on angiogenesis genes. **(A)** Cumulative distribution curve. **(B)** Clustering heatmap. **(C)** Evaluation of average consistency within clustered groups. **(D)** Differential expression of angiogenesis-related genes in clusters. **(E, F)** Differences in overall and disease-specific survival between clusters. **(G, H)** Analysis of different levels of immune cell infiltration between clusters. **(I)** Analysis of expression levels of different immunoinhibitors among clusters. **(J)** Analysis of differences in IC50 scores of different chemotherapeutic agents between clusters. **(K, L)** Analysis of gene enrichment between clusters. *p < 0.05, **p < 0.01 and ***p < 0.001.

interested in understanding the regulatory mechanism. The immune microenvironment plays a crucial role in tumor progression, with angiogenesis closely linked to immune mechanisms in tumors. Therefore, we hypothesize that the difference in prognosis between the two patient clusters may be related to immune mechanisms. This study delved deeper into the relationship between two distinct clusters and immune cell infiltration in patients with prostate adenocarcinoma (PRAD). By utilizing the xCell algorithm, we assessed levels of immune cell infiltration in 38 cells and identified significant differences in 23 cells between the two clusters (Figures 2G, H). This suggests that the varying patient prognoses in these clusters may be associated with differences in immune cell infiltration. As a novel form of tumor immunotherapy drug, immune checkpoint inhibitors are crucial in the field of tumor immunotherapy (27). Our study focused on analyzing the variations in the expression of immunosuppressants across different clusters. Out of the 23 immunoinhibitors studied, 18 displayed significant differences between the clusters (Figure 2I). Furthermore, we analyzed the IC50 scores of commonly used clinical chemotherapy drugs in the two clusters, uncovering significant differences in the IC50 scores of 8 chemotherapy drugs (Figure 2J). In order to deeply analyze the underlying mechanisms of the above results, we also performed gene enrichment analysis on the 2 clusters, and we found that cluster 2 was significantly associated with PI3K/AKT, PDGF, VEGF, and RAS signaling pathways, whereas cluster 1 was associated with factors such as DNA methylation (Figures 2K, L).

3.3 Construction of diagnostic models

Machine learning methods offer a convenient approach for identifying characteristic genes. In our study, we utilized multiple machine learning algorithms to create a diagnostic model related to angiogenesis. By analyzing the TCGA-PRAD and GSE3325 datasets, we used the expressions of FAM107A, C7orf31, TMEM100, GLIS1, QSOX1, KNDC1, MAP7D3, and ZNF536 in the TCGA-PRAD dataset as training data. Our findings revealed that both combinations of machine learning algorithms exhibited strong predictive capabilities for diagnosing PRAD patients in the training set. Subsequently, we validated the expressions of these genes in the GSE3325 dataset to confirm the effectiveness of our diagnostic model. In the verification set of GSE3325, only a few machine learning algorithm combinations showed poor results, while the majority achieved better predictions. Among these combinations, the LASSO+GBM algorithm combination stood out as the best diagnostic model, as it had the highest average AUC value (Figure 3A). Additionally, we presented the number of genes included in each algorithm combination for further clarity (Figure 3B).

3.4 Constructing prognostic models

We examined 10 angiogenesis genes related to PRAD prognosis, including MAP7D3, FAMI07A, GLIS1, GPRI61, QSOX1, TMEM100, C7orf31, ZNF536, KNDC1, and CACNAIH, using the LASSO algorithm to develop a prognostic model. Subsequently, 9 genes, MAP7D3, FAMI07A, GLIS1, GPRI61, QSOX1, TMEM100, C7orf31, ZNF536, and KNDC1, were incorporated into the model (Figures 4A, B). Risk score= (-0.2524) *FAM107A+(1.237) *GLIS1+(-3.0503) *ZNF536 +(-0.8946) *C7orf31+(-0.0732) *TMEM100+(2.6368) *MAP7D3 +(-0.6038) *GPR161+(-0.2713) *KNDC1+(-0.7063) *QSOX1. The expression heatmap of these genes in PRAD samples was presented (Figure 4C). Using the gene expression data, the LASSO algorithm categorizes samples into high-risk and low-risk groups. Patients classified as high-risk typically experience a significantly poorer prognosis compared to those in the low-risk category (Figure 4D). Additionally, we evaluated the model's predictive performance for 1-year, 3-year, and 5-year PRAD prognosis (Figures 4E–G). The ROC curve demonstrated strong predictive capability of the constructed prognostic model, with AUC values of 1, 0.848, and 0.854 for 1 year, 3 years, and 5 years, respectively.

3.5 Correlation analysis of prognostic models with PRAD immune infiltration and chemotherapeutic drug sensitivity

The study compared IC50 scores of various chemotherapy drugs in samples from high-risk and low-risk groups, revealing significant differences in 5 drugs between the groups (Figure 5A). Furthermore, the correlation between the constructed prognostic model and PRAD immune infiltration was examined, showing significant differences in the infiltration levels of 11 immune cells between high and low-risk groups (Figures 5B, C). Additionally, expression differences of immunosuppressants between the groups were analyzed, with 8immunoinhibitor-related genes showing significant differences (Figure 5D). Finally, the relationship between the prognostic model risk score and PRAD immune infiltration was explored using xCell and TIP methods, resulting in a correlation network diagram (Figure 5E).

3.6 MAP7D3 as the best prognostic gene among angiogenesis genes

To delve deeper into identifying prognostic genes associated with angiogenesis, univariate and multivariate COX regression analyses were carried out on these genes along with clinically pertinent pathological factors (T stage, M stage). The findings from the multivariate COX regression analysis revealed that QSOX1, MAP7D3, and M stage could potentially function as prognostic indicators for patients with PRAD (Figures 6A, B). Subsequently, to identify the optimal prognostic biomarkers among these angiogenesis-related genes, we employed three machine learning methods: RF, XGBoost, and GBM. Combining the outcomes of multivariate COX regression analysis, we determined that MAP7D3 emerged as the most promising angiogenesis-related prognostic marker in PRAD (Figures 6C–E). Furthermore, gene enrichment analysis based on the high and low

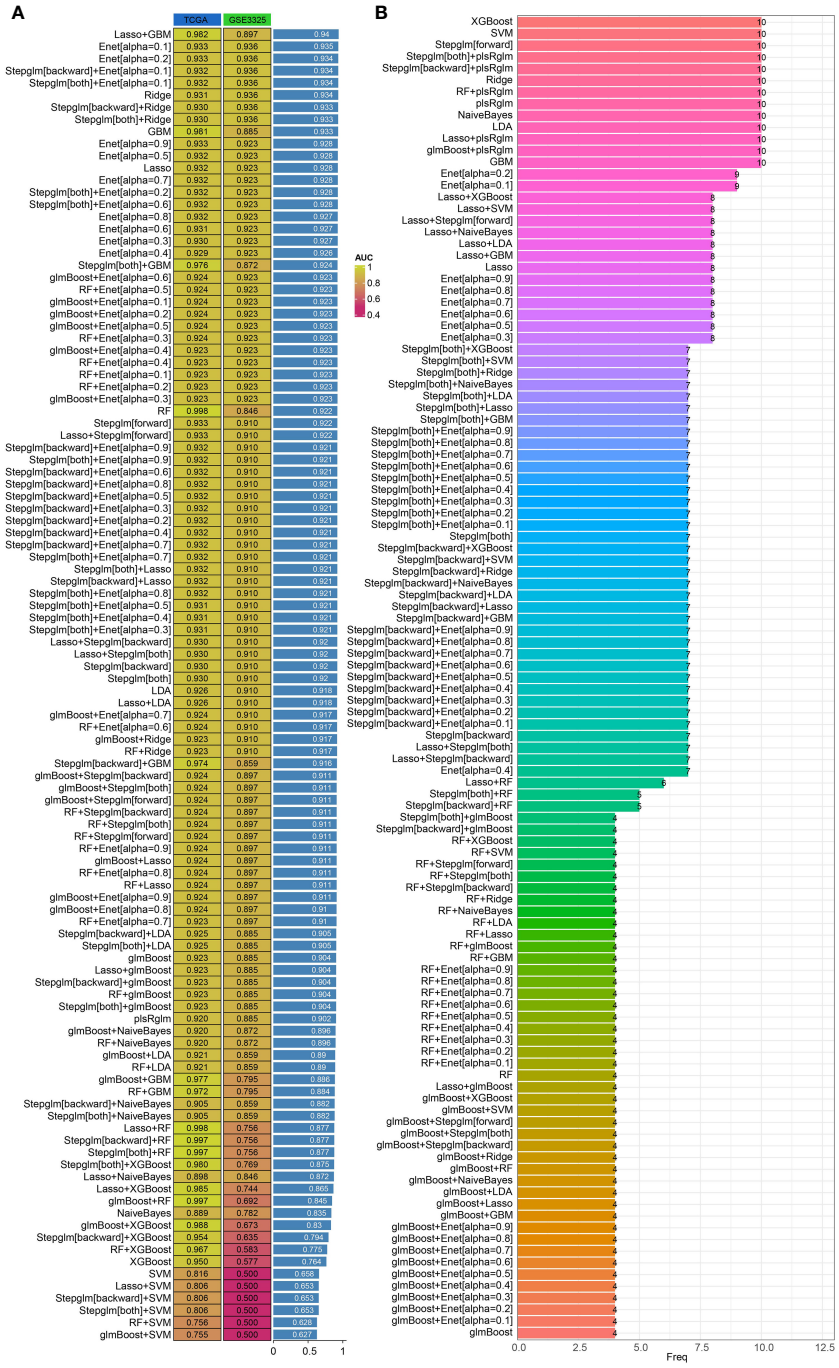

FIGURE 3
Construction of diagnostic models based on integrated machine learning models. **(A)** Predictive effectiveness of different algorithm combinations for PRAD diagnosis. **(B)** Number of genes incorporated by different combinations of algorithms.

expression groups of MAP7D3 validated its association with PRAD angiogenesis. Interestingly, our findings also linked MAP7D3 to the stemness pathway (Figure 6F). The highly vascularized tumor microenvironment provides a conducive setting for the growth of these stem cells, perpetuating a detrimental cycle that contributes to tumor recurrence, metastasis, and drug resistance. Hence, we hypothesize that MAP7D3 may impact the prognosis of PRAD patients by modulating PRAD cell stemness and angiogenesis.

3.7 Analysis of MAP7D3 correlation with PRAD immunotherapy and chemotherapy

The XCELL algorithm was utilized to assess immune cell infiltration levels, unveiling notable variances in the infiltration of 19 immune cell types in PRAD samples categorized by high and low MAP7D3 expression (Figure 7A). Single-cell analysis aids in exploring gene expression patterns within individual cells and

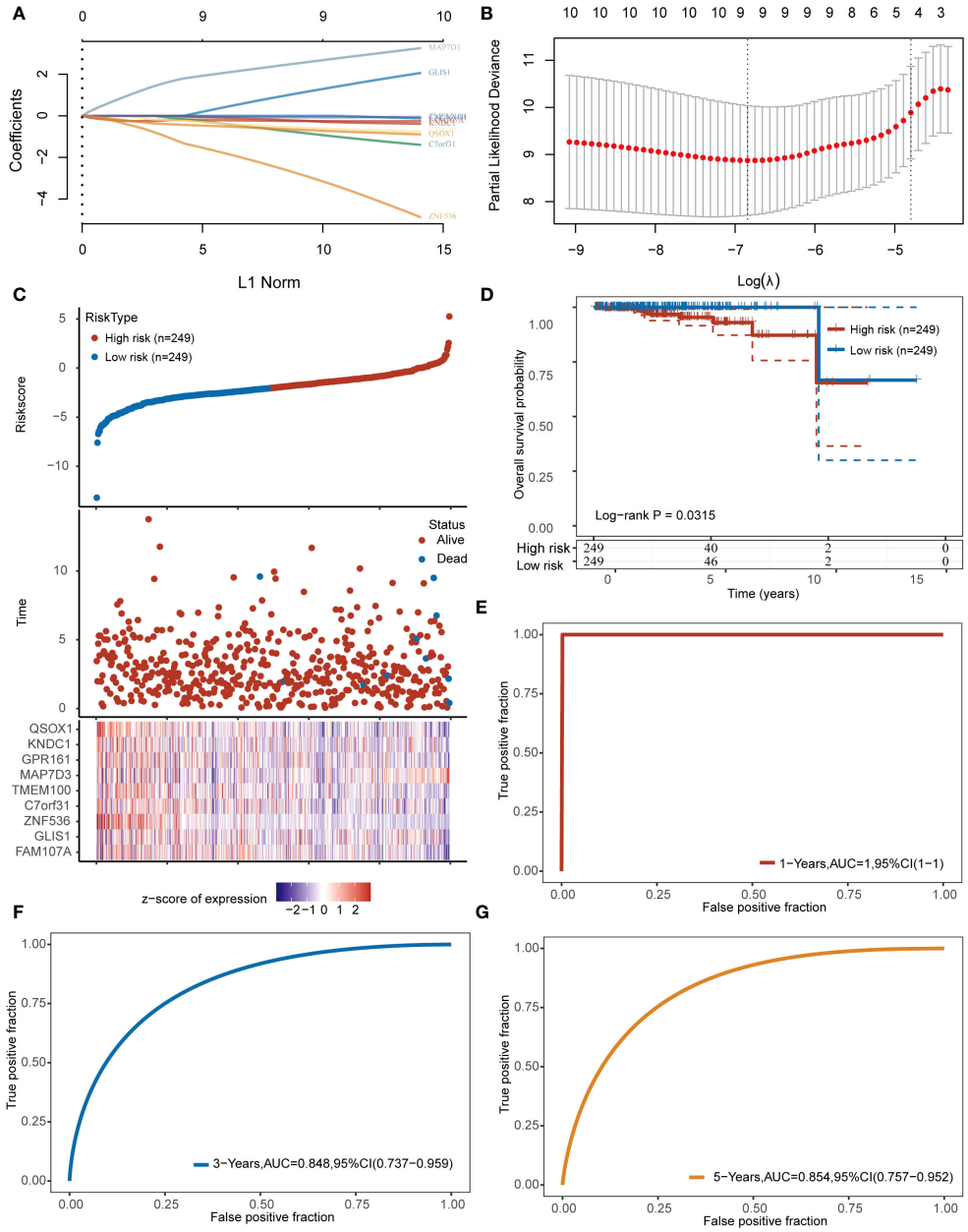

FIGURE 4
Constructing prognostic models based on angiogenesis genes. **(A, B)** 9 angiogenesis-related prognostic genes were included in the prognostic model. **(C)** The top represents the scatter plot of the Riskscore from low to high, the middle represents the scatter plot distribution of survival time and survival status corresponding to the Riskscore of different samples; the bottom represents the expression heat map of the genes included in the model. **(D)** Prognostic differences between high and low risk groups. **(E–G)** Prognostic modeling for predictive analysis of 1,3,5-year prognosis in patients with PRAD.

understanding intercellular signaling networks. Integrating clinical pathology data with scRNA-seq information from tumor samples has the potential to unveil novel diagnostic and prognostic biomarkers (28). Consequently, we investigated the immune infiltration of MAP7D3 through the TISCH2 database, and the findings indicated a significant association with B cells and progenitor cells (Figures 7B, C), aligning with the XCELL algorithm analysis results. Further examination of immunosuppressant-related gene expression in PRAD samples based on MAP7D3 expression levels revealed marked differences in the expression of 22 immunosuppressant-related genes (Figure 7D). Moreover, significant correlations were observed between MAP7D3 and the IC50 scores of 10 commonly used chemotherapy drugs (Figure 7E). Lastly, a correlation network graph depicting the relationship between MAP7D3 and immune cell infiltration levels was constructed using XCELL and TIP algorithms (Figure 7F).

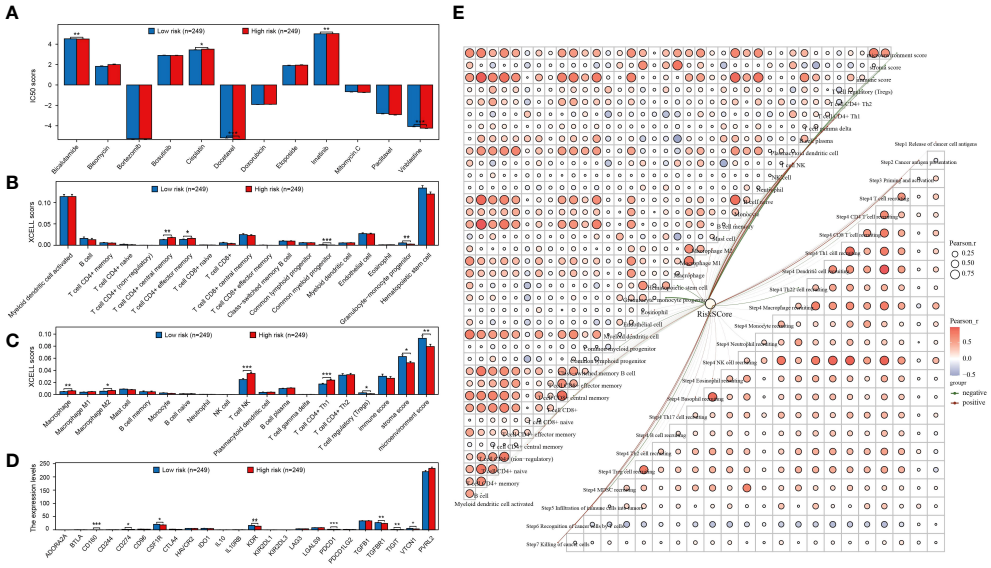

FIGURE 5
Prognostic models are strongly associated with PRAD chemotherapy and immunotherapy. **(A)** Analysis of the difference in IC50 scores of different chemotherapeutic drugs between high and low risk groups. **(B, C)** Analysis of immune cell infiltration levels between different groups. **(D)** Expression level analysis of different immunoinhibitors between high and low risk groups. **(E)** Network diagram of correlation between risk score and PRAD immune infiltration. *p < 0.05, **p < 0.01 and ***p < 0.001.

3.8 Analysis of MAP7D3 correlation with angiogenesis-targeting drugs

In order to further investigate the potential of MAP7D3 as an angiogenesis-targeting drug, a correlation analysis was conducted at the molecular structure level comparing it with established angiogenesis-targeting drugs such as sunitinib, Vandetanib, Thalidomide, Lenalidomide, and Cabozantinib. The molecular structure of MAP7D3 was sourced from the AlphaFold website, while the 3D structures of the angiogenesis-targeting drugs were obtained from the PubChem website. The Vina score was utilized to assess the correlation between MAP7D3 and the other drugs, with a score of less than -5 generally indicating a strong binding activity. The findings revealed that MAP7D3 exhibited good binding activity with the selected angiogenesis-targeting drugs (Figures 8A–E).

3.9 Validation of MAP7D3 expression and prognostic value in PRAD

To ascertain the differential expression and prognostic significance of MAP7D3 in prostate adenocarcinoma (PRAD), we conducted immunohistochemistry experiments on 60 PRAD samples and their corresponding normal prostate tissue samples. Our analysis revealed that MAP7D3 was predominantly expressed in the cytoplasm of PRAD samples (Figures 9A–D). Comparing 60 cases of cancer with 60 adjacent cancer cases, we observed significantly higher MAP7D3 expression in the cancer samples (Figure 9E). Further categorizing the samples based on high and low MAP7D3 expression levels, we discovered a significant correlation between MAP7D3 expression, tumor invasion, and patient survival status (Figure 9F). Detailed examination of tumor invasion and patient survival status in the high and low MAP7D3 expression groups revealed distinct patterns (Figures 9G, H). Kaplan-Meier survival analysis demonstrated a notably worse prognosis for patients with high MAP7D3 expression compared to those with low expression. Additionally, receiver operating characteristic (ROC) curve analysis indicated that MAP7D3 could effectively predict 7-year, 8-year, and 9-year survival rates in PRAD patients (Figures 9I, J). Lastly, ROC curve analysis for the diagnostic potential of MAP7D3 in PRAD patients showed promising results, highlighting its utility in PRAD diagnosis (Figure 9K).

4 Discussion

Immune cells play a crucial role in tumor survival, as cancer cell metabolites and secretions from specific cells in the tumor microenvironment can impact immune cell activation, proliferation, differentiation, and overall function (29–31). The induction of immunosuppression and the ability to evade anti-tumor immune responses have been recognized as significant features in the progression of cancer, particularly through mechanisms such as tumor angiogenesis (32). With strong experimental evidence supporting tumor-dependent angiogenesis, researchers are increasingly focused on developing anti-angiogenic therapies (33). The approval of bevacizumab in 2004, the first FDA-approved anti-angiogenic drug, significantly improved progression-free survival in RCC patients undergoing combination chemotherapy (34). Subsequent studies have furthered anti-angiogenic strategies by proposing the normalization of tumor blood vessels to enhance drug and oxygen delivery. The use of

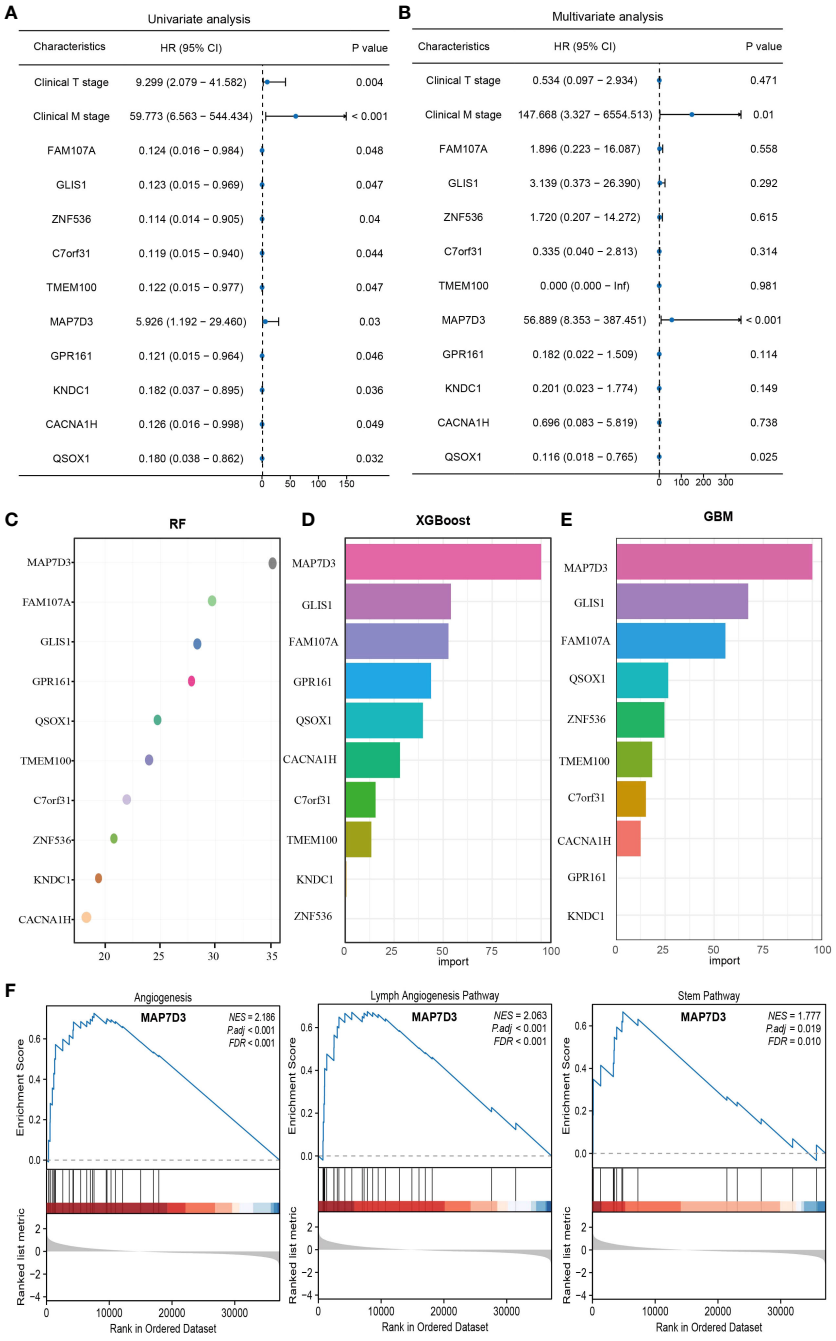

FIGURE 6
Multiple machine learning approaches to identify the best angiogenesis-related prognostic genes in PRAD. **(A)** Univariate COX regression analysis of prognostic differences in relevant indicators. **(B)** Multivariate COX regression to analyze prognostic differences in relevant indicators. **(C–E)** RF, XGBoost and GBM algorithms to screen prognostic genes. **(F)** Gene enrichment analysis based on MAP7D3 expression.

angiogenesis inhibitors in cancer treatment, targeting the formation of new blood vessels in tumors, represents a promising approach for a variety of solid tumors (35). Nevertheless, obstacles like tumor regrowth, resistance to medication, absence of biomarkers, limited duration of effectiveness, and possible negative reactions continue to persist as a result of the intricate aspects of tumor vascularization and insufficient investigation. Even though existing medications that inhibit blood vessel formation may not be optimal for managing PRAD, an enhanced comprehension of the mechanisms driving PRAD vascularization could pave the way for the creation of superior tailored treatments for individuals with PRAD.

WGCNA is a bioinformatics algorithm utilized for extracting module information from high-throughput expression data, known for its efficiency and accuracy in biological data mining (36). In our study, we applied WGCNA to identify genes associated with angiogenesis in PRAD. By integrating differential analysis and prognostic assessment, we successfully pinpointed 10

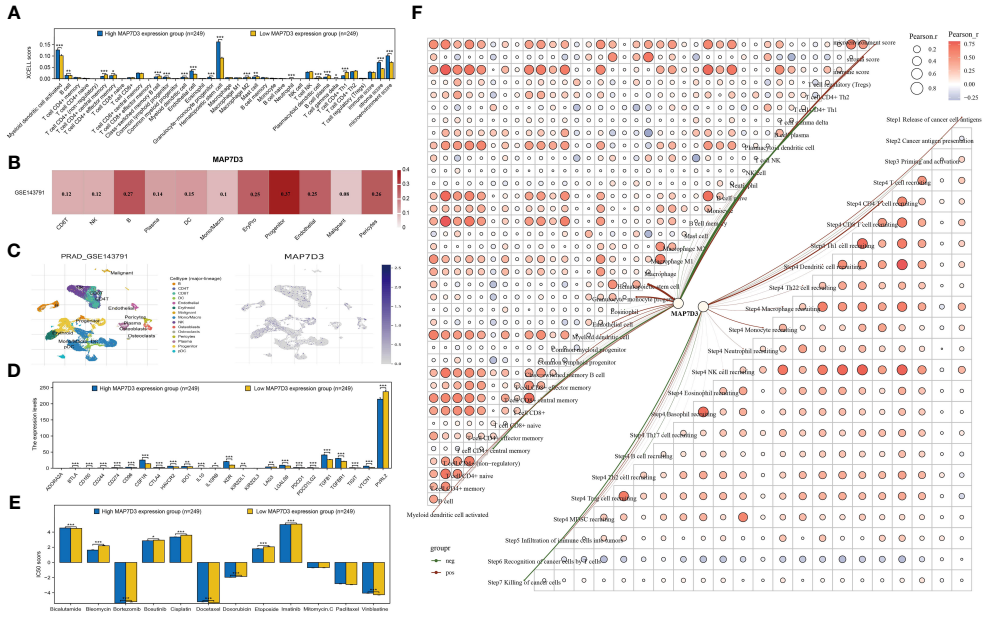

FIGURE 7
MAP7D3 was significantly associated with PRAD immunotherapy and chemotherapy. **(A)** Analysis of MAP7D3 correlation with PRAD immune cell infiltration based on XCELL algorithm. **(B, C)** Analysis of MAP7D3 correlation with PRAD immune cell infiltration based on single-cell dataset. **(D)** Analysis of MAP7D3 correlation with immunoinhibitor-related genes. **(E)** Analysis of the difference in IC50 scores of different chemotherapeutic drugs between high MAP7D3 expression and low MAP7D3 expression groups. **(F)** Network diagram of correlation between MAP7D3 expression and PRAD immune infiltration. *p < 0.05, **p < 0.01 and ***p < 0.001.

angiogenesis-related genes with prognostic significance. Among these 10 angiogenesis-related genes, studies have reported that QSOX1, GLIS1 and FAM107A can be used as prognostic markers for PRAD patients (37–39). In recent years, the concept of precision medicine has emphasized subgroup typing of individual research subjects. Through consensus clustering analysis based on the expression of 10 angiogenesis-related genes, we divided the TCGA-PRAD samples into 2 clusters. Our findings revealed significant differences between these clusters, not only in prognosis but also in sensitivity to immunotherapy and chemotherapy drugs. To further analyze these differences, we conducted gene enrichment analysis and discovered that samples in cluster 2 were primarily associated with VEGF, PDGF, and PI3K/Akt signaling pathways. VEGF-A is a crucial regulator of angiogenesis, exerting a significant influence on tumor proliferation, metastasis and drug resistance. The key signaling pathway involved in both physiological and pathological angiogenesis is VEGF-A/VEGFR-2, which promotes various processes in endothelial cells and solid tumors. Platelet-derived growth factor (PDGF) serves as a primary stimulant for mesenchymal cell types like fibroblasts, smooth muscle cells, and glial cells, contributing to cell growth, wound healing, angiogenesis, and recruitment through paracrine or autocrine mechanisms. PDGF-BB, a well-studied factor in the PDGF family, not only enhances tissue fibrosis but also drives angiogenesis and drug resistance during tumor progression and anti-VEGF therapy (40–42). Additionally, the PI3K/Akt signaling pathway plays a significant role in tumor angiogenesis (43). These findings indirectly support the strong correlation between these 10 genes and angiogenesis. Machine learning is a prominent subject in current research. We utilized various machine learning methods to develop both a diagnostic and prognostic model for PRAD based on the expression of angiogenesis-related genes. Our model results consistently highlight the significant role of angiogenesis in the diagnosis and prognosis of PRAD. We validated the diagnostic model using GSE3325 and obtained satisfactory outcomes. However, due to limited availability of PRAD datasets with prognostic information, our prognostic model lacks validation. This limitation stems from missing gene expression data in the datasets used for model construction.

Multivariate COX regression analysis identified MAP7D3 and QSOX1 as prognostic biomarkers for PRAD among the 10 angiogenesis-related genes. High expression of QSOX1 has been linked to vascular invasion, neural invasion, prostate extension, increased pT stage, and higher pathological tumor stage in prostate cancer. These findings underscore the significant role of QSOX1 in PRAD (37). Subsequently, RF, XGBoost, and GBM machine learning methods were employed to identify the optimal prognostic genes, ultimately confirming MAP7D3 as the top prognostic gene associated with angiogenesis in PRAD. To uncover novel angiogenesis-related prognostic genes, we focused on MAP7D3 for further investigation. Single-cell RNA sequencing is an advanced genomics technology that enables comprehensive analysis of gene expression and genomic features at the single cell level, thereby facilitating in-depth study of cellular properties (44). Therefore, we not only used the XCELL algorithm, but also analyzed the correlation between MAP7D3 and immune cell infiltration in PRAD from the perspective of single cell analysis

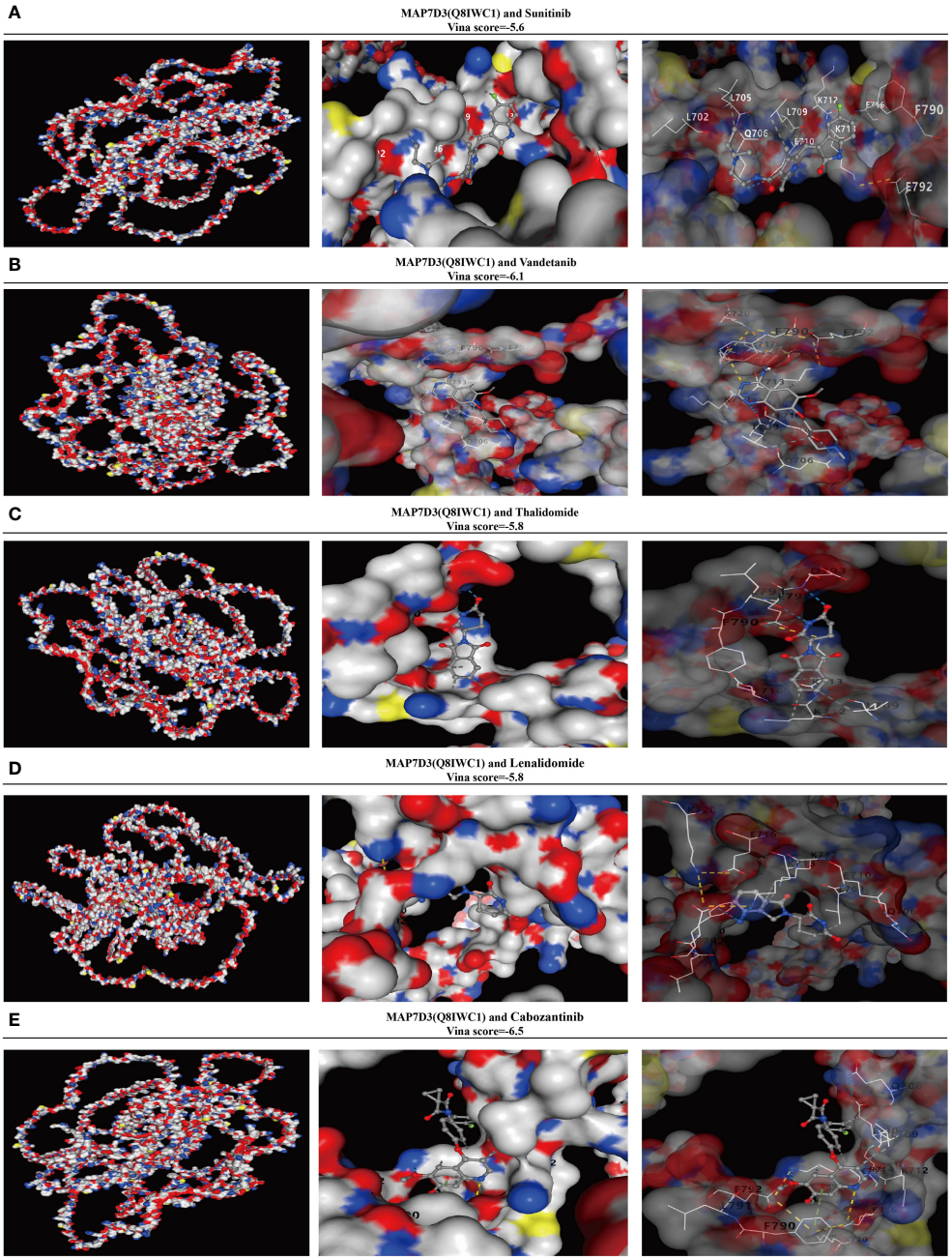

FIGURE 8
MAP7D3 is associated with angiogenesis drugs. **(A–E)** Molecular docking of MAP7D3 with the angiogenesis-targeting drugs sunitinib, Vandetanib, Thalidomide, Lenalidomide, and Cabozantinib.

through the TISCH2 database. Analytical results demonstrated a close correlation between MAP7D3 expression and B cell and progenitor cell infiltration levels in PRAD samples. Furthermore, differences in IC50 scores of immunosuppressant-related genes and common chemotherapy drugs were observed between MAP7D3 high and low expression groups, suggesting a crucial role of MAP7D3 in PRAD immunotherapy and chemotherapy. Gene enrichment analysis indicated that MAP7D3 is not only linked to angiogenesis but also to stem cell pathways. Stem cells are precursor cells that have the ability to self-renew and differentiate into functionally mature, specialized cells in various human tissues Stem cells are precursor cells that have the ability to self-renew and differentiate into functionally mature special cells in various tissues of the human body (45). Importantly, evidence suggests that the interplay between tumor angiogenesis and cancer stem cells promotes tumor growth. Cancer stem cells can contribute to angiogenesis by releasing pro-angiogenic factors and differentiating into vascular endothelial cells, while tumor vasculature supports cancer stem cells (46, 47). This reciprocal interaction between tumor angiogenesis and stemness fuels tumor progression and metastasis. Therefore, the findings suggest that MAP7D3 may drive PRAD progression by regulating both

10.3389/fimmu.2024.1416914

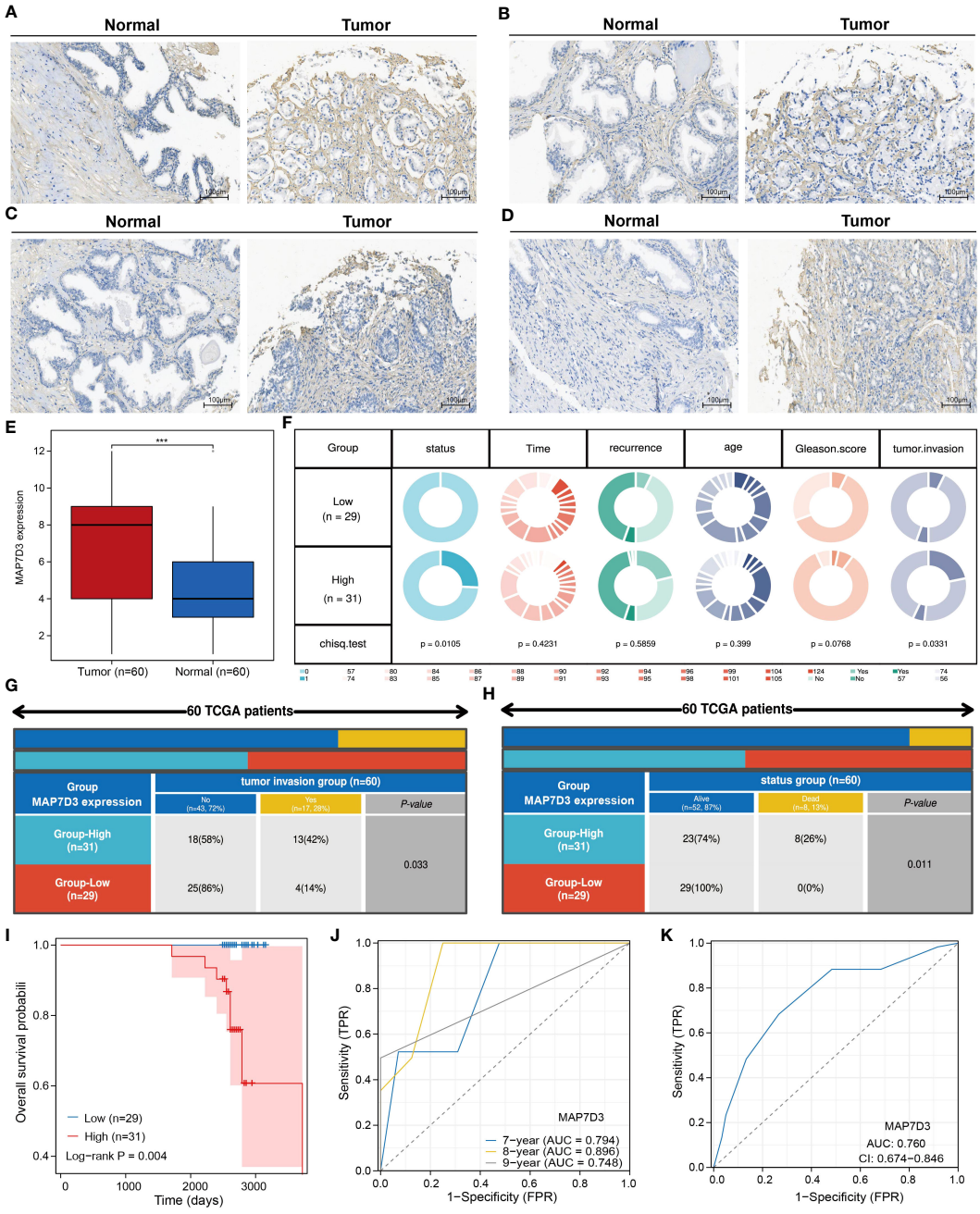

FIGURE 9
MAP7D3 is highly expressed in PRAD and may serve as a prognostic marker. **(A–E)** MAP7D3 expression in PRAD and corresponding normal tissues. **(F–H)** Correlation between MAP7D3 expression and different pathologic parameters in PRAD patients. **(I)** MAP7D3 expression and prognostic KM curves in PRAD patients. **(J)** Predictive ability of MAP7D3 expression for prognosis in PRAD patients. **(K)** Predictive ability of MAP7D3 expression for the diagnosis of PRAD patients. ***p < 0.001.

angiogenesis and stem cells. Sunitinib, vandetanib, thalidomide, lenalidomide, and cabozantinib are currently utilized as angiogenesis-related targeted drugs in clinical settings. To investigate the potential of MAP7D3 as a target for angiogenic drug development, we conducted an analysis of its binding activity with these drugs using molecular docking. Our findings are promising, indicating that MAP7D3 exhibits strong binding activity with the aforementioned drugs, suggesting its potential as an angiogenesis drug target. Our study provides valuable insights into the significant role of angiogenesis in PRAD, drawing from various perspectives. However, it is important to note that the majority of our analyses were conducted using the TCGA-PRAD dataset. To strengthen the robustness of our findings, it is imperative to incorporate a larger sample size and diverse validation sets. Furthermore, conducting additional experiments to validate our conclusions is equally essential.

5 Conclusion

Our study employed a range of machine learning techniques to pinpoint 10 crucial angiogenesis-related genes in prostate cancer. Our findings validate the role of these genes in influencing PRAD immunotherapy, chemotherapy, and patient outcomes. Notably, both machine learning analysis and experimental validation underscore the significant prognostic impact of MAP7D3. Moreover, our research advocates for the potential of MAP7D3 as a promising target for the development of angiogenic drugs.

Data availability statement

The datasets presented in this study can be found in online repositories. The names of the repository/repositories and accession number(s) can be found in the article/supplementary material.

Ethics statement

The studies involving humans were approved by Ethics Committee of Shanghai Outdo Biotech Company. The studies were conducted in accordance with the local legislation and institutional requirements. The participants provided their written informed consent to participate in this study. Written informed consent was obtained from the individual(s) for the publication of any potentially identifiable images or data included in this article.

Author contributions

YW: Conceptualization, Data curation, Formal analysis, Investigation, Writing – original draft. JH: Investigation, Software, Writing – original draft. QZ: Investigation, Methodology, Writing – original draft. JB: Supervision, Writing – original draft. YZ: Validation, Writing – original draft. HS: Methodology, Writing – original draft. BD: Funding acquisition, Writing – review & editing. MR: Funding acquisition, Visualization, Writing – review & editing.

Funding

The author(s) declare financial support was received for the research, authorship, and/or publication of this article. This study was supported by the Natural Science Foundation of Heilongjiang Province (LH2019H030) and National Natural Science Foundation of China (82002680).

Acknowledgments

We would also like to thank the Shengxin Bean Sprout Platform (http://www.sxdyc.com/index) for its help in data statistical analysis.

Conflict of interest

The authors declare that the research was conducted in the absence of any commercial or financial relationships that could be construed as a potential conflict of interest.

Publisher's note

All claims expressed in this article are solely those of the authors and do not necessarily represent those of their affiliated organizations, or those of the publisher, the editors and the reviewers. Any product that may be evaluated in this article, or claim that may be made by its manufacturer, is not guaranteed or endorsed by the publisher.

References

1. Sun L, Tuo Z, Chen X, Wang H, Lyu Z, Li G. Identification of cell differentiation trajectory-related gene signature to reveal the prognostic significance and immune landscape in prostate cancer based on multiomics analysis. *Heliyon*. (2024):e27628. doi: 10.1016/j.heliyon.2024.e27628

2. Feng D, Li D, Xiao Y, Wu R, Wang J, Zhang C. Focal ablation therapy presents promising results for selectively localized prostate cancer patients. *Chin J Cancer Res*. (2023) 35:424–30. doi: 10.21147/j.issn.1000–9604.2023.04.08

3. Satturwar S, Parwani AV. Artificial intelligence-enabled prostate cancer diagnosis and prognosis: Current state and future implications. *Adv Anat Pathol*. (2024) 31:136–44. doi: 10.1097/PAP.0000000000000425

4. Folkman J. Angiogenesis: an organizing principle for drug discovery? *Nat Rev Drug Discovery*. (2007) 6:273–86. doi: 10.1038/nrd2115

5. Ma B, Qin L, Sun Z, Wang J, Tran LJ, Zhang J, et al. The single-cell evolution trajectory presented different hypoxia heterogeneity to reveal the carcinogenesis of genes in clear cell renal cell carcinoma: Based on multiple omics and real experimental verification. *Environ Toxicol*. (2024) 39:869–81. doi: 10.1002/tox.24009

6. El Alaoui-Lasmaili K, Faivre B. Antiangiogenic therapy: Markers of response, "normalization" and resistance. *Crit Rev Oncol Hematol*. (2018) 128:118–29. doi: 10.1016/j.critrevonc.2018.06.001

7. Abou Khouzam R, Brodaczewska K, Filipiak A, Zeinelabdin NA, Buart S, Szczylik C, et al. Tumor hypoxia regulates immune escape/invasion: Influence on angiogenesis and potential impact of hypoxic biomarkers on cancer therapies. *Front Immunol*. (2021) 11:613114. doi: 10.3389/fimmu.2020.613114

8. Rajabi M, Mousa SA. The role of angiogenesis in cancer treatment. *Biomedicines*. (2017) 5:34. doi: 10.3390/biomedicines5020034

9. Melegh Z, Oltean S. Targeting angiogenesis in prostate cancer. *Int J Mol Sci*. (2019) 20:2676. doi: 10.3390/ijms20112676

10. Luo JQ, Yang TW, Wu J, Lai HH, Zou LB, Chen WB, et al. Exosomal PGAM1 promotes prostate cancer angiogenesis and metastasis by interacting with ACTG1. *Cell Death Dis*. (2023) 14:502. doi: 10.1038/s41419–023-06007–4

11. Ciummo SL, Sorrentino C, Fieni C, Di Carlo E. Interleukin-30 subverts prostate cancer-endothelium crosstalk by fostering angiogenesis and activating immunoregulatory and oncogenic signaling pathways. *J Exp Clin Cancer Res*. (2023) 42:336. doi: 10.1186/s13046-023-02902-y

12. Su Y, Zhang Y, Zhao J, Zhou W, Wang W, Han B, et al. FOXA1 promotes prostate cancer angiogenesis by inducing multiple pro-angiogenic factors expression. *J Cancer Res Clin Oncol*. (2021) 147:3225–43. doi: 10.1007/s00432–021-03730–3

13. Zhao Y, Cai C, Zhang M, Shi L, Wang J, Zhang H, et al. Ephrin-A2 promotes prostate cancer metastasis by enhancing angiogenesis and promoting EMT. *J Cancer Res Clin Oncol*. (2021) 147:2013–23. doi: 10.1007/s00432–021-03618–2

14. Gacche RN. Changing landscape of anti-angiogenic therapy: Novel approaches and clinical perspectives. *Biochim Biophys Acta Rev Cancer*. (2023) 1878:189020. doi: 10.1016/j.bbcan.2023.189020

15. Masiero M, Simões FC, Han HD, Snell C, Peterkin T, Bridges E, et al. A core human primary tumor angiogenesis signature identifies the endothelial orphan receptor ELTD1 as a key regulator of angiogenesis. *Cancer Cell*. (2013) 24:229–41. doi: 10.1016/j.ccr.2013.06.004

16. Yang H, Li Z, Zhu S, Wang W, Zhang J, Zhao D, et al. Molecular mechanisms of pancreatic cancer liver metastasis: the role of PAK2. *Front Immunol*. (2024) 15:1347683. doi: 10.3389/fimmu.2024.1347683

17. Jiang S, Yang X, Lin Y, Liu Y, Tran LJ, Zhang J, et al. Unveiling Anoikis-related genes: A breakthrough in the prognosis of bladder cancer. *J Gene Med*. (2024) 26:e3651. doi: 10.1002/jgm.3651

18. Zhang P, Wu X, Wang D, Zhang M, Zhang B, Zhang Z. Unraveling the role of low-density lipoprotein-related genes in lung adenocarcinoma: Insights into tumor microenvironment and clinical prognosis. *Environ Toxicol*. (2024). doi: 10.1002/tox.24230

19. Wang J, Zuo Z, Yu Z, Chen Z, Meng X, Ma Z, et al. Single-cell transcriptome analysis revealing the intratumoral heterogeneity of ccRCC and validation of MT2A in pathogenesis. *Funct Integr Genomics*. (2023) 23:300. doi: 10.1007/s10142–023-01225–7

20. Zhu C, Sun Z, Wang J, Meng X, Ma Z, Guo R, et al. Exploring oncogenes for renal clear cell carcinoma based on G protein-coupled receptor-associated genes. *Discovery Oncol*. (2023) 14:182. doi: 10.1007/s12672-023-00795-z

21. Sun Z, Wang J, Zhang Q, Meng X, Ma Z, Niu J, et al. Coordinating single-cell and bulk RNA-seq in deciphering the intratumoral immune landscape and prognostic stratification of prostate cancer patients. *Environ Toxicol*. (2024) 39:657–68. doi: 10.1002/tox.23928

22. Xu L, Deng C, Pang B, Zhang X, Liu W, Liao G, et al. TIP: A web server for resolving tumor immunophenotype profiling. *Cancer Res*. (2018) 78:6575–80. doi: 10.1158/0008–5472.CAN-18–0689

23. Han Y, Wang Y, Dong X, Sun D, Liu Z, Yue J, et al. TISCH2: expanded datasets and new tools for single-cell transcriptome analyses of the tumor microenvironment. *Nucleic Acids Res*. (2023) 51:D1425–31. doi: 10.1093/nar/gkac959

24. Subramanian A, Tamayo P, Mootha VK, Mukherjee S, Ebert BL, Gillette MA, et al. Gene set enrichment analysis: a knowledge-based approach for interpreting genome-wide expression profiles. *Proc Natl Acad Sci U S A*. (2005) 102:15545–50. doi: 10.1073/pnas.0506580102

25. Liberzon A, Subramanian A, Pinchback R, Thorvaldsdóttir H, Tamayo P, Mesirov JP. Molecular signatures database (MSigDB) 3.0. *Bioinformatics*. (2011) 27:1739–40. doi: 10.1093/bioinformatics/btr260

26. Liu Y, Yang X, Gan J, Chen S, Xiao ZX, Cao Y. CB-Dock2: improved protein-ligand blind docking by integrating cavity detection, docking and homologous template fitting. *Nucleic Acids Res*. (2022) 50:W159–64. doi: 10.1093/nar/gkac394

27. Zhang B, Zhou YL, Chen X, Wang Z, Wang Q, Ju F, et al. Efficacy and safety of CTLA-4 inhibitors combined with PD-1 inhibitors or chemotherapy in patients with advanced melanoma. *Int Immunopharmacol*. (2019) 68:131–6. doi: 10.1016/j.intimp.2018.12.034

28. Zhang P, Zhang H, Tang J, Ren Q, Zhang J, Chi H, et al. The integrated single-cell analysis developed an immunogenic cell death signature to predict lung adenocarcinoma prognosis and immunotherapy. *Aging (Albany NY)*. (2023) 15:10305–29. doi: 10.18632/aging.205077

29. Xiong J, Chi H, Yang G, Zhao S, Zhang J, Tran LJ, et al. Revolutionizing anti-tumor therapy: unleashing the potential of B cell-derived exosomes. *Front Immunol*. (2023) 14:1188760. doi: 10.3389/fimmu.2023.1188760

30. Ren S, Wang W, Shen H, Zhang C, Hao H, Sun M, et al. Development and validation of a clinical prognostic model based on immune-related genes expressed in clear cell renal cell carcinoma. *Front Oncol*. (2020) 10:1496. doi: 10.3389/fonc.2020.01496

31. Zhang P, Dong S, Sun W, Zhong W, Xiong J, Gong X, et al. Deciphering Treg cell roles in esophageal squamous cell carcinoma: a comprehensive prognostic and immunotherapeutic analysis. *Front Mol Biosci*. (2023) 10:1277530. doi: 10.3389/fmolb.2023.1277530

32. Anderson TS, Wooster AL, Piersall SL, Okpalanwaka IF, Lowe DB. Disrupting cancer angiogenesis and immune checkpoint networks for improved tumor immunity. *Semin Cancer Biol*. (2022) 86:981–96. doi: 10.1016/j.semcancer.2022.02.009

33. Shiri P, Ramezanpour S, Amani AM, Dehaen W. A patent review on efficient strategies for the total synthesis of pazopanib, regorafenib and lenvatinib as novel anti-angiogenesis receptor tyrosine kinase inhibitors for cancer therapy. *Mol Divers*. (2022) 26:2981–3002. doi: 10.1007/s11030–022-10406–8

34. Liu J, Zhang Q, Yang D, Xie F, Wang Z. The role of long non-coding RNAs in angiogenesis and anti-angiogenic therapy resistance in cancer. *Mol Ther Nucleic Acids*. (2022) 28:397–407. doi: 10.1016/j.omtn.2022.03.012

35. Ansari MJ, Bokov D, Markov A, Jalil AT, Shalaby MN, Suksatan W, et al. Cancer combination therapies by angiogenesis inhibitors; a comprehensive review. *Cell Commun Signal*. (2022) 20:49. doi: 10.1186/s12964-022-00838-y

36. Zhang S, Jiang C, Jiang L, Chen H, Huang J, Gao X, et al. Construction of a diagnostic model for hepatitis B-related hepatocellular carcinoma using machine learning and artificial neural networks and revealing the correlation by immunoassay. *Tumour Virus Res*. (2023) 16:200271. doi: 10.1016/j.tvr.2023.200271

37. Baek JA, Song PH, Ko Y, Gu MJ. High expression of QSOX1 is associated with tumor invasiveness and high grades groups in prostate cancer. *Pathol Res Pract*. (2018) 214:964–7. doi: 10.1016/j.prp.2018.05.019

38. Peng Q, Xie T, Wang Y, Ho VW, Teoh JY, Chiu PK, et al. GLIS1, correlated with immune infiltrates, is a potential prognostic biomarker in prostate cancer. *Int J Mol Sci*. (2023) 25:489. doi: 10.3390/ijms25010489

39. Ma YF, Li GD, Sun X, Li XX, Gao Y, Gao C, et al. Identification of FAM107A as a potential biomarker and therapeutic target for prostate carcinoma. *Am J Transl Res*. (2021) 13:10163–77.

40. Lin CM, Chiu JH, Wu IH, Wang BW, Pan CM, Chen YH. Ferulic acid augments angiogenesis via VEGF, PDGF and HIF-1 alpha. *J Nutr Biochem*. (2010) 21:627–33. doi: 10.1016/j.jnutbio.2009.04.001

41. Li J, Jiang Z, He J, Yang K, Chen J, Deng Q, et al. Effect of CHRDL1 on angiogenesis and metastasis of colorectal cancer cells via TGF-β/VEGF pathway. *Mol Carcinog*. (2024). doi: 10.1002/mc.23711

42. Sang BT, Wang CD, Liu X, Guo JQ, Lai JY, Wu XM. PDGF-BB/PDGFRβ induces tumour angiogenesis via enhancing PKM2 mediated by the PI3K/AKT pathway in Wilms' tumour. *Med Oncol*. (2023) 40:240. doi: 10.1007/s12032–023-02115–5

43. Yu JR, Liu YY, Gao YY, Qian LH, Qiu JL, Wang PP, et al. Diterpenoid tanshinones inhibit gastric cancer angiogenesis through the PI3K/Akt/mTOR signaling pathway. *J Ethnopharmacol*. (2024) 324:117791. doi: 10.1016/j.jep.2024.117791

44. Zhang P, Pei S, Zhou G, Zhang M, Zhang L, Zhang Z. Purine metabolism in lung adenocarcinoma: A single-cell analysis revealing prognostic and immunotherapeutic insights. *J Cell Mol Med*. (2024) 28:e18284. doi: 10.1111/jcmm.18284

45. Chowdhury MA, Zhang JJ, Rizk R, Chen WCW. Stem cell therapy for heart failure in the clinics: new perspectives in the era of precision medicine and artificial intelligence. *Front Physiol*. (2024) 14:1344885. doi: 10.3389/fphys.2023.1344885

46. Chou PH, Luo CK, Wali N, Lin WY, Ng SK, Wang CH, et al. A chemical probe inhibitor targeting STAT1 restricts cancer stem cell traits and angiogenesis in colorectal cancer. *J BioMed Sci*. (2022) 29:20. doi: 10.1186/s12929–022-00803–4

47. Yang Y, Guo J, Li M, Chu G, Jin H, Ma J, et al. Cancer stem cells and angiogenesis. *Pathol Res Pract*. (2024) 253:155064. doi: 10.1016/j.prp.2023.155064

frontiers | Frontiers in Immunology

TYPE Review
PUBLISHED 28 May 2024
DOI 10.3389/fimmu.2024.1416941

Check for updates

OPEN ACCESS

EDITED BY
Jiaheng Xie,
Central South University, China

REVIEWED BY
Giuseppe Schepisi,
Scientific Institute of Romagna for the Study and Treatment of Tumors (IRCCS), Italy
Prasenjit Dey,
University at Buffalo, United States

*CORRESPONDENCE
Junzhe Zhao
j.zhao@u.duke.nus.edu
Qian Wang
wangqian_16@163.com
Han Chong Toh
toh.han.chong@singhealth.com.sg

†These authors have contributed equally to this work and share first authorship

RECEIVED 13 April 2024
ACCEPTED 16 May 2024
PUBLISHED 28 May 2024

CITATION
Zhao J, Wang Q, Tan AF, Loh CJL and Toh HC (2024) Sex differences in cancer and immunotherapy outcomes: the role of androgen receptor.
Front. Immunol. 15:1416941.
doi: 10.3389/fimmu.2024.1416941

COPYRIGHT
© 2024 Zhao, Wang, Tan, Loh and Toh. This is an open-access article distributed under the terms of the Creative Commons Attribution License (CC BY). The use, distribution or reproduction in other forums is permitted, provided the original author(s) and the copyright owner(s) are credited and that the original publication in this journal is cited, in accordance with accepted academic practice. No use, distribution or reproduction is permitted which does not comply with these terms.

Sex differences in cancer and immunotherapy outcomes: the role of androgen receptor

Junzhe Zhao[1,2*†], Qian Wang[2,3*†], Alexandra F. Tan[4], Celestine Jia Ling Loh[1,5] and Han Chong Toh[2*]

[1]Duke-NUS Medical School, Singapore, Singapore, [2]Division of Medical Oncology, National Cancer Centre Singapore, Singapore, Singapore, [3]Department of Medical Oncology Cancer Hospital of China Medical University/Liaoning Cancer Hospital & Institute, Shenyang, Liaoning, China, [4]Imperial College School of Medicine, London, United Kingdom, [5]Sengkang General Hospital, Singapore, Singapore

Across the wide range of clinical conditions, there exists a sex imbalance where biological females are more prone to autoimmune diseases and males to some cancers. These discrepancies are the combinatory consequence of lifestyle and environmental factors such as smoking, alcohol consumption, obesity, and oncogenic viruses, as well as other intrinsic biological traits including sex chromosomes and sex hormones. While the emergence of immuno-oncology (I/O) has revolutionised cancer care, the efficacy across multiple cancers may be limited because of a complex, dynamic interplay between the tumour and its microenvironment (TME). Indeed, sex and gender can also influence the varying effectiveness of I/O. Androgen receptor (AR) plays an important role in tumorigenesis and in shaping the TME. Here, we lay out the epidemiological context of sex disparity in cancer and then review the current literature on how AR signalling contributes to such observation via altered tumour development and immunology. We offer insights into AR-mediated immunosuppressive mechanisms, with the hope of translating preclinical and clinical evidence in gender oncology into improved outcomes in personalised, I/O-based cancer care.

KEYWORDS

sex, immunotherapy, androgen receptor, tumour microenvironment, gender oncology

1 Introduction

Differences in biological and sociocultural patterns between males and females have led to notable contrast in the characteristics of cancer pathophysiology. Research has revealed sex disparities in cancer incidence and prognosis, which are influenced by sex chromosomes and sex hormones, as well as distinct lifestyles, dietary habits, and environmental exposures (1). Since 2014, the National Institutes of Health have urged scientists to incorporate sex as a biological variable in their study design, aiming to reduce sex-related research biases (2). We now know that sex hormones play a crucial role in the initiation, progression, and treatment

outcomes of cancer. Extensive studies are available on the crucial role of oestrogen and its pathways in the onset and progression of tumours, sometimes notwithstanding the oestrogen receptor (ER) status (3). On the other hand, the role of androgens and their signalling pathways on different cancers is less understood, except in prostate cancer. Emerging evidence on how androgen receptor (AR) affects tumour immunology has once again emphasised the significance of sex difference in response to antitumor therapies (4), prompting further investigation into this intriguing area.

This review collates current knowledge of the connection between biological sex and cancer epidemiology, the interplay between environmental and hormonal factors, AR and cancer sexual dimorphism, as well as the effect of AR on cancer immunology, before suggesting how AR contributes to immunotherapy resistance. Nevertheless, it is necessary to remain cognisant of how human *genders* - sociocultural constructs of the characteristics of men and women - exert significant influence on the lifestyles and exposures experienced by the two *biological sexes*, together shaping the apparent differences in immunotherapy response between males and females.

2 Epidemiology

Recent studies have shown that females tend to have more potent immune functions than males (5), and their overly robust immune system can paradoxically be a double-edged sword that leads to increased occurrence of immune dysregulation (6–8). Therefore, sex has always been an important risk factor for certain infections (6), autoimmune disorders (9), cardiovascular diseases (10) and so on. However, whether certain cancers affect more males than females (or vice versa) remains a contentious topic (11, 12). Based on the GLOBOCAN2020 database (13) regarding the top 10 cancers by incidence and mortality (Figures 1A, B), we can observe that besides the more sex-specific cancers (breast, cervix, prostate), there are 6 male-dominant cancers (bladder, colorectal, liver, lung, oesophagus, stomach) and 1 female-dominant cancer (thyroid) (Figures 1C, D).

Expectably, breast cancer occupies the foremost position in the incidence of cancers in females, accounting for 24.5% of new cancer cases, far more than colorectal cancer (CRC) at 9.4% (Figure 2A). Thyroid cancer (TC) is the only non-reproductive-related cancer that is female-dominant, with a male/female incidence ratio of 0.31 (Figure 1D). Importantly, however, when males do get TC, the male sex seems to be an independent negative indicator of TC prognosis. Data from Canada reveals that men with well-differentiated TC have a higher risk of recurrence than women, with a hazard ratio (HR) of 2.72 (15).

Compared with females, many of the common cancers occur more frequently in men (Figure 2B). Bladder cancer exhibits a notable sex disparity in incidence and mortality (Figure 1D), while females with non-muscle invasive bladder cancer have a higher risk of recurrence than males (16). This could potentially explain why the male/female mortality ratio is lower than the incidence ratio in

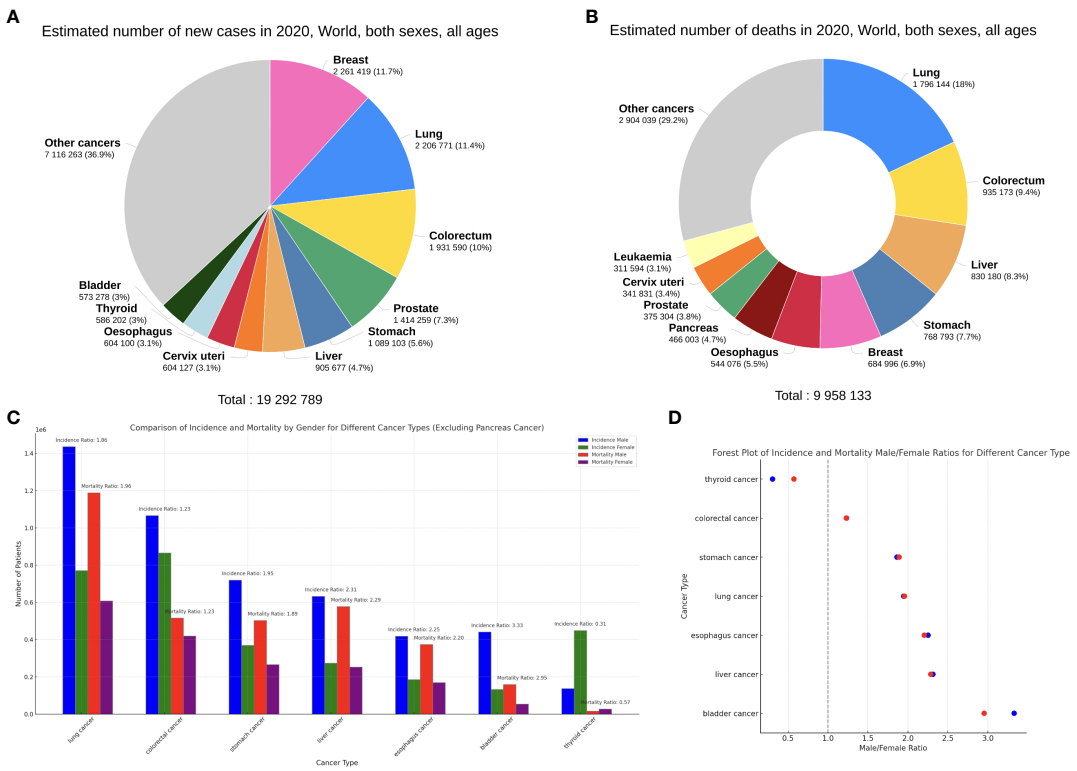

FIGURE 1
(A, B) Top 10 most common cancers worldwide (all ages and sexes) by incidence **(A)** and mortality **(B)**, plotted on the Global Cancer Observatory (GCO) platform (14). **(C)** The incidence and mortality of the 7 sex-neutral cancers in the top 10, females versus males. **(D)** Male/Female ratios of incidence (blue) and mortality (red) of the 7 cancers. Data from GLOBOCAN2020.

bladder cancer. Liver cancer is another male-dominant cancer, ranking third in mortality globally (17). With a male/female incidence and mortality ratio of 2.31 and 2.29 (Figure 1D), the sex disparity is even more pronounced in East Asia (18). Other gastrointestinal tumours, including gastric, oesophageal, and colorectal cancers, also show higher incidence and mortality rates in males, consistent with the trends reported in literature (19–21). Lung cancer is also a male-dominant cancer; yet sex difference in lung cancer incidence is more pronounced within individual subtypes, with a greater male predominance in squamous cell carcinoma (17) and a notable East Asian female predominance in EGFR-mutated adenocarcinoma, the mechanisms of which are still not well understood (22). Notably, recent studies have reported a reversal of the sex disparity in lung cancer, where its incidence has become higher amongst young and middle-aged females (23) with more estimated new cases (17).

Notable sex disparities also exist in cancers with lower incidence rates. For instance, nasopharyngeal carcinoma (NPC) has a strong male predominance amongst Asian cancers, where the male/female incidence ratio ranges from 2:1 to 3:1 (24). Sexual dimorphism also exists in melanoma biology (3), with a male/female incidence ratio in melanoma ranging from 2:1 to 3:1 as well (25). Melanoma in males tends to be more aggressive, while female patients show better prognosis and longer survival (26–28).

3 Non-AR-related factors contributing to sex disparities in cancer incidence

3.1 Modifiable factors

As demonstrated earlier, males generally have higher incidence and mortality rates than females for bladder, colorectal, liver, lung, oesophagus, and stomach cancers (29). These sex disparities cannot solely be explained by the biological sex; lifestyle and environmental exposures are indispensable as well. In the UK, excluding sex-specific cancer types, modifiable risk factors account for 36.4% of male cancer cases and 25.6% of female cases. Tobacco smoking alone contributed to 15% of preventable cancer cases in the UK in 2015 and represents the highest proportion of preventable cancer cases in the US and Australia (30). Male and female smokers are 23 and 13 times more likely to develop lung cancer compared to non-smokers, respectively (31). Chronic alcohol consumption is also strongly linked to various cancers, with dose-response relationships seen in multiple epidemiological studies for liver, colorectal and upper aerodigestive tract cancers (32–34). Subgroup analyses in people with alcohol use disorders have shown that females have a higher risk of developing cancers compared to men (OR=1.767) (35). Additionally, consuming the same amount of alcohol leads to a greater increase in absolute lifetime cancer risk for women (1.4%) compared to men (1%), although these higher cancer rates in women may be attributed to breast cancer (36).

Obesity represents a major public health challenge, with approximately 55% of cancers in females and 24% in males in the USA considered obesity related. Importantly, 42% of new cases of overweight and obesity related cancers are gynaecological and breast cancers. This implies a stronger correlation between high body-mass index (BMI) and female cancers, highlighting the role of aromatase and oestrogen in gynaecological and breast cancer development (37). Non-sex specific cancers have a higher incidence in males, particularly oesophageal (male to female ratio of adenocarcinoma 4.4, squamous cell carcinoma 2.7) and colorectal cancers (38, 39). Obesity also plays a role in the tumorigenesis of these cancers, possibly involving chronic inflammation and systemic insulin and adipokine dysregulation (40, 41) that raise the incidence of metabolic syndrome (including metabolic dysfunction-associated steatotic liver disease, MASLD) particularly in males (42).

Globally, oncogenic viruses contribute to approximately 10% of all malignancies, although this varies between higher and lower income countries (43). The population attributable fractions are higher in females than males, primarily due to the inclusion of sex-specific cancers. Causative agents include human papillomaviruses (HPV), hepatitis B/C viruses (HBV/HCV), Epstein-Barr virus (EBV), and human immunodeficiency virus (HIV) (30). HPV^{+}

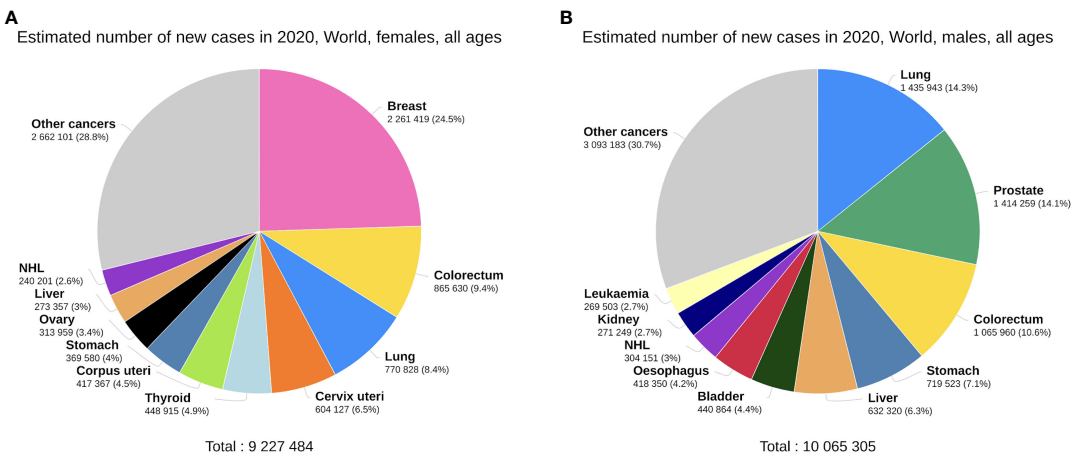

FIGURE 2
Top 10 most common cancers worldwide by incidence, females **(A)** versus males **(B)**, plotted on the GCO platform (14). Data from GLOBOCAN 2020.

head and neck squamous cell carcinoma (HNSCC) (44), EBV-driven NPC (24), as well as HBV/HCV-driven hepatocellular carcinoma (HCC) (45) all show a strong male predominance.

3.2 Sex chromosomes

Sex chromosome differences may also contribute to variations in cancer incidence. Females have XX and males have XY sex chromosome combinations, while intersex individuals such as those with Turner's or Klinefelter's syndrome have chromosomal patterns deviating from the typical configurations. In XX individuals, some pseudoautosomal genes can escape X-chromosome inactivation (XCI) providing a "buffering" effect against allele mutations. Incomplete XCI occurs in 23% of X chromosome genes (46). Thus, a single allele mutation leads to complete alteration of gene function in males, as opposed to a heterozygous alteration in females. This serves as a safeguard, preserving tissue function in the presence of mutations. Many of these genes, including *ATRX*, *KDM5C, KDM6A*, and *MAGEC3*, have tumour suppressor functions. Additionally, mutated alleles on the inactive X chromosome are typically expressed at lower levels or not expressed at all, mitigating their impact on cellular function (47). In females, the selective proliferation of specific mosaic subpopulations exhibiting preferential expression of one X chromosome can lead to skewed XCI (48). This can confer advantageous immunomodulation against cancer – a protective mechanism not available to males who obligatorily express the same mutated maternal X-linked gene.

X-linked genes, including *HUWE1*, *FLNA* and *MED12*, can directly modulate *TP53* expression. This association may render males at a higher risk of p53 dysfunction. Females exhibit a higher incidence of non-expressed mutations among p53-associated X-linked genes. Bioinformatic analyses in 12 non-reproductive cancers have shown that in females, less than half of these exome mutations were transcribed into mRNA, whereas the majority underwent mRNA transcription in males (49). These findings suggest tumour suppressor effects of the X chromosome.

Loss of Y chromosome (LOY) has been implicated in the pathogenesis of lung cancer, renal tumours and up to 40% of bladder cancer (50–52). In muscle invasive bladder cancer, patients exhibiting low Y chromosome gene expression of *KDM5D*, *KDM6C*, *TBL1Y* and *ZFY* demonstrate worse prognosis (52). Mosaic LOY in peripheral leukocytes is also associated with solid tumour incidence. Extreme downregulation of Y is linked to increased cancer risk and resistance against EGFR tyrosine kinase inhibitors (53), which may also impact immunotherapy response downstream. Loss of the entire X chromosome(s) has been documented in early-stage astrocytoma, neuroblastoma and medulloblastoma (54–56).

3.3 Oestrogen and ER

The link between oestrogen or ER and non-reproductive cancers is unclear. At the molecular level, oestrogen and ER affect PD-1 signalling, Wnt/β-catenin pathways and the Ras/MAPK pathway, amongst many other aspects of cancer biology (57–62).

Circulating E1 (oestrone) and E2 (oestradiol) levels were found to have no statistically significant relationship with colon cancer in a cohort of 1000 postmenopausal women (62). However, a 2015 meta-analysis revealed a reduced ratio of ERβ expression in CRC compared to the normal mucosa (OR=0.216), associated with poorer overall and disease-free survival (63). Conversely, exogenous oestrogen reduces the risk of CRC by 37% as demonstrated by the landmark Women's Health Initiative study (64). *In vitro*, ERβ was shown to modify the hypoxic response by downregulating HIF-1α, VEGFA and PDGF (65).

Oestrogen plays a complex role in the liver. It has been implicated in various liver pathologies like fibrosis and fatty liver disease, but its role in HCC remains unclear. In a cohort of 275 men, higher total E2 is associated with increased HCC risk (OR=1.58) (66). A recent cohort study shows a survival advantage for female HCC patients over males in perimenopausal and early-menopausal ages but not in postmenopausal women, possibly due to declining endogenous oestrogen production (67). However, female patients in phase III trials for immune checkpoint inhibitors (ICI) for HCC are found to have worse overall survival (OS) than males (68). Whether this discrepancy can be attributed to oestrogen is unclear. Studies exploring the use of tamoxifen in HCC have yielded mixed results, with some showing prolonged survival but larger studies finding no significant association (69–71).

In lung cancer, oestrogen appears to have a protective effect. A meta-analysis of female lung cancer cases demonstrates that higher levels of sex steroid hormone exposure, both endogenous and exogenous, reduce lung cancer risk by 10% (72), yet the role of ERα or ERβ is unclear. Some studies suggest that ERα is associated with worse prognosis in non-small cell lung cancer (NSCLC) (73), while others find no significant effect. Some meta-analyses indicate an association between ERβ and better prognosis in NSCLC (73, 74), while others consider it an unreliable prognostic marker (75, 76) depending on the methods employed, such as uni- vs multivariate analysis, bioinformatics, or immunohistochemistry (IHC) analysis. Finally, female reproductive factors like breastfeeding are associated with a decreased risk of oesophageal and gastric adenocarcinoma, though parity, menstruation, and the use of hormone replacement therapy have no association (77). Interestingly, the use of tamoxifen, a selective oestrogen receptor modulator (SERM), is associated with an increased risk of gastric adenocarcinoma (78) as well as endometrial cancer. The tissue-specific agonist/antagonist role of SERMs like tamoxifen reflects the complex role of the oestrogen-ER signalling axis in tumorigenesis.

4 Androgens, AR, and tumour pathophysiology

4.1 Androgens and non-reproductive cancers

Androgens include testosterone, dihydrotestosterone (DHT), and dehydroepiandrosterone (DHEA), among others. Testosterone produced by the testes plays a pivotal role in initiating the development of masculine traits, hence exists in higher levels in

males and lower in females. Androgen deficiencies in males can result in the development of feminine traits (79), while increased androgen production in females can lead to a shift from feminine to masculine traits and also be associated with polycystic ovarian syndrome (PCOS) (80). Their biological functions are executed by binding with AR and activating intracellular AR signalling downstream. Besides prostate cancer, the role of androgens in tumorigenesis is less studied compared to oestrogen. Higher concentrations of testosterone are associated with increased risk of liver cancer, particularly in men, while higher levels of DHEA, the adrenal precursor, are associated with a 53% decrease in risk (66, 81). Higher circulating testosterone is associated with a decreased risk of CRC in men, but this is not shown in women (81). The association between testosterone and oesophageal cancer is unclear, with varying degrees of significance across studies (81, 82). Gastric, pancreatic and bladder cancers are also shown to have no significant association with testosterone levels (81). Interestingly, androgen deprivation therapy (ADT) using finasteride has shown improved survival in patients with non-muscle invasive bladder cancer, suggesting a potential strategy to reduce bladder cancer incidence and recurrence (83).

4.2 Overview of AR

AR is a member of the nuclear receptor superfamily acting as a ligand-dependent transcription factor (84). Consisting of eight exons, the AR gene is located on the X chromosome. It comprises a ligand-binding domain (LBD), a DNA-binding domain (DBD), and an N-terminal domain (NTD). In the unbound state, AR forms a complex with co-chaperones, heat shock proteins, and cytoskeletal proteins in the cytoplasm. Ligand binding induces conformational changes, receptor dimerization, and translocation to the cell nucleus. The NTD influences transcriptional activity, while the DBD allows binding to and recognition of androgen response elements (AREs) on target genes where it serves to induce or repress gene expression through binding to chromatin at *cis* AREs (85). AR can also modulate post-translational modifications by phosphorylation, methylation, or ubiquitination (86, 87) (Figure 3). While AR exerts effects mostly in sex hormone-dependent tissues, such as the prostate, testes, ovaries, and endometrium (88, 89), it is also widely expressed in kidneys, liver, urinary bladder, as well as the cardiovascular, immune, musculoskeletal and nervous systems (88, 90–94). It is also noted that membrane androgen receptors (mARs), such as ZIP9 and GPRC6A, are a group of G protein-coupled receptors that directly alter cellular signalling upon androgen stimulation, also known as the non-genomic pathway (95, 96) (Figure 3). While studies have demonstrated the implications of mARs on prostate cancer, they are beyond the scope of this review.

A report of teenagers developing hepatocellular carcinoma due to excess androgen intake have spurred interest in the effect of androgen and AR on cancer (97, 98). In 1980, an article published in *The Lancet* highlighted the association between elevated levels of free testosterone in males and an increased risk of melanoma (99). While multiple observations support the hypothesis that excess androgens may be tumorigenic (100), a definitive mechanistic explanation is still lacking, which necessitates our summary of current knowledge below.

4.3 AR and tumour development/progression

AR signalling is the primary driver of castration resistant prostate cancer (CRPC) (101). Enzalutamide, an AR antagonist, competes with androgens to bind to AR and blocks nuclear ARE binding, thereby inhibiting downstream transcriptional activity (102) and enabling antitumor effect (103). AR and ER exhibit similarities as nuclear receptors, allowing substantial signalling crosstalk (Figure 3) (104). In ER+ breast cancer, AR competes with ER for oestrogen response elements (EREs) and inhibits ER activity, playing a tumour-suppressive role especially in premenopausal patients (105). However, AR may promote cancer progression in certain ER– breast cancers. A study indicated that the luminal AR (LAR) subtype accounts for 15% of triple-negative breast cancer and AR is an attractive therapeutic target (106). Higher AR expression and corresponding aggressive phenotypes are observed predominantly in tissue samples from African American women, with a strong interaction between AR and JAK-STAT signalling (107). Another study shows that *PIK3CA* is highly mutated in the LAR subtype, where PI3K inhibitors can reduce LAR cell proliferation (108). Salivary duct carcinoma (SDC), a male-dominant cancer, is a rare, aggressive malignancy also characterised by high AR expression, ranging from 70% to 97.8% (109–111). Recent studies have found that the occurrence of SDC is closely related to the AR signalling pathway (112), sharing similar molecular profiles with high-grade breast ductal carcinoma and apocrine breast cancer (113). AR-V7, an AR splicing variant, accounts for over 50% of AR in SDC and plays a crucial role in the resistance and progression in CRPC (114). Other studies have reported that *FOXA1* mutations are present in 10% of SDC cases, resulting in drug resistance and tumour progression also via the AR pathway (113).

With its homolog crucial for primary sex determination in *C. elegans* (115), FOXA1 is a key transcription factor necessary for AR and ER activities in prostate and breast cancers (116). AR driven transcription in molecular apocrine breast cancer is mediated by FOXA1 (117). In prostate cancer, *FOXA1* exhibits a high mutation rate, thereby affecting AR transcription (118). Elevated levels of FOXA1 have been associated with poor prognosis in prostate cancer. FOXA1 function in AR signalling and its impact on prostate cancer differs markedly from its role in ER signalling and breast cancer progression (119). A study published in 2012 highlights the significance of FOXA1 and FOXA2 in sexual dimorphism in liver cancer, noting that modulation of these factors can reverse the observed gender differences (120). Other *FOX* family genes are also crucial in regulating the PI3K-AKT-mTOR pathway. FOXO3a, a PI3K/AKT downstream substrate, can induce AR expression as a positive regulator (121). FOXO1, a downstream effector of AR, can also lead to AR hyperactivation in prostate cancer with PTEN loss, independent of androgen binding (122).

The crosstalk between AR and other signalling pathways has also been reported (123, 124). With a strong association between

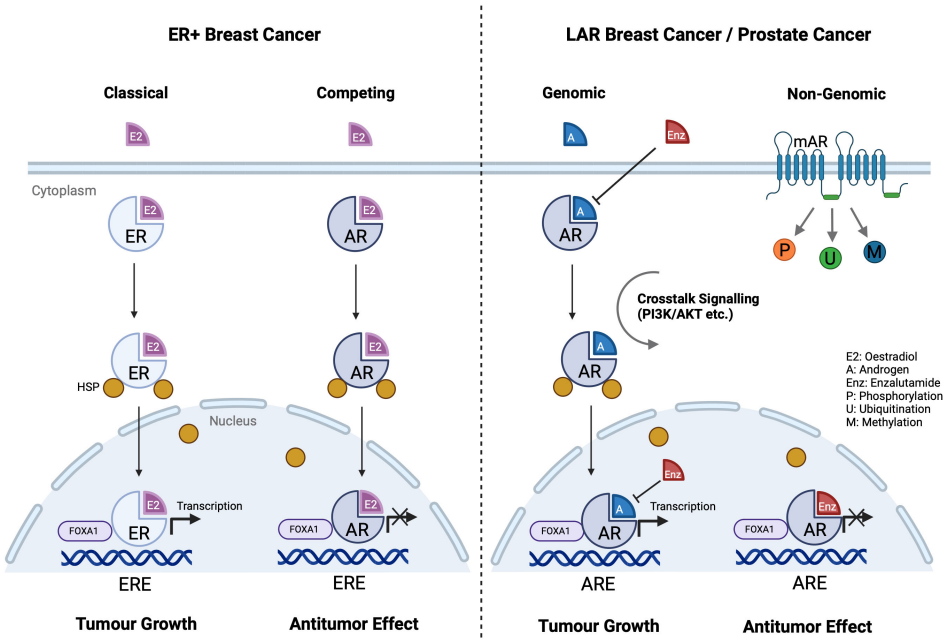

FIGURE 3
AR and ER signalling pathways in different cancer cells. ER and AR share similar structures, and they compete in each other's signalling pathways. In ER+ breast cancer cells, AR substitutes ER on ERE and stops downstream transcription, eliciting an antitumor effect. ER and AR also share the same co-activator FOXA1 on ERE. In LAR breast cancer and prostate cancer, enzalutamide competes with androgen to stop AR activation. (Created with BioRender.com).

nuclear AR expression and Wnt/β-catenin signalling in bladder cancer, ADT has shown great therapeutic potential (124). Moreover, TCF1 and AR have overlapping binding sites on β-catenin (125). β-catenin translocates into the nucleus and interacts with TCF1 and lymphoid enhancer factor, activating the transcription of target genes. TCF1 is required for the self-renewal of stem-like CD8+ T cells in response to viral or tumour antigens, preserving heightened responses to checkpoint blockade immunotherapy (126). This implies not only a causal relationship between AR signalling and tumour progression via β-catenin pathways, but also a connection between AR and antitumor immune responses (more in Section 5.2). In addition, androgens can also influence the effectiveness of BRAF-targeted therapy in melanoma. AR expression is elevated in BRAF-resistant melanoma. Inhibition of both the AR and BRAF/MEK pathways counteracts resistance and hence improves cytotoxicity (127). Intriguingly, blocking AR not only inhibits the proliferation of BRAF-resistant cells, but also enhances the infiltration of CD8+ T cells and promotes cancer cell apoptosis (128). This prompts further investigation on how AR affects immune responses, and targeting AR may offer new combination therapies for cancer treatment.

5 AR and cancer immunotherapy

5.1 Sex difference in clinical trial outcomes

There are several meta-analyses evaluating the comparative efficacy of immuno-oncology (I/O) on various cancers across genders (Table 1). A 2018 meta-analysis summarises 20 clinical trials involving ICIs across various cancer types, with a total of 11,351 participants (129). These trials predominantly focus on melanoma (32%) and NSCLC (31%). The meta-analysis reveals significant sex differences in clinical outcomes, where females experience lower response rates than males. However, the significant heterogeneity calls for analysis specific to individual cancer types and treatments. In 2019, the same team conducted another meta-analysis of chemotherapy and I/O for advanced lung cancer; this time with opposite conclusions compared to a year ago (130). Women with advanced lung cancer seem to derive a larger benefit from the addition of chemotherapy to anti-PD-1/PD-L1 compared with men. Another meta-analysis on NSCLC patients receiving combination chemo-immunotherapy first-line also concludes that females show a more significant improvement in OS and progression-free survival (PFS) (132). These findings highlight the potential impact of gender on the effectiveness of both targeted and combination of chemo-immunotherapies in NSCLC.

In 2020, a meta-analysis on NSCLC includes 13 studies with monotherapy and 5 with combination regimens (KEYNOTE 010/024 with pembrolizumab versus chemotherapy and CHECKMATE 017/026/057 with nivolumab versus chemotherapy), a total of 1028 female and 1435 male patients (131). The result confirms that EGFR wild-type patients could benefit from immunotherapy monotherapy (HR=0.77; $p<0.001$) while those of mutant types experienced no survival benefit (HR=1.11; $p=0.54$). While EGFR mutations are more likely to occur in females (134), there is no apparent efficacy-sex association overall (131). Therefore, to explore

TABLE 1 Summary of meta-analyses evaluating the efficacy of I/O interventions across males and females on different cancers.

Cancer Type	# Patients	Year	Reference	Comparative Arms	Summary of Findings
Advanced solid tumours • 32% melanoma • 31% NSCLC	11,351	2018	Conforti et al (129)	ICI compared with others	Females show lower response rates
Advanced NSCLC/ SCLC Advanced NSCLC	4,923 3,974	2019	Conforti et al (130)	ICI + chemotherapy VS chemotherapy ICI alone OR ICI + chemotherapy	Females benefit more from the ICI + chemotherapy combination
Advanced solid tumours	10,664	2020	Wei et al (131)	13 ICI-alone regimens 5 ICI-based combinations	EGFR mutations are more likely to occur in females No sex difference for ICI monotherapy benefits Females benefit more from ICI-based combinations
Advanced/ recurrent NSCLC	5,830	2022	Takada et al (132)	ICI + non-ICI VS non-ICI	Females show greater benefit in OS and PFS when receiving combined chemoimmunotherapy
Advanced HCC	5,169	2023	Balcar et al (68)	ICI alone OR ICI-based combinations	Females show smaller (pooled) OS benefit from ICI- based therapy Comparable outcomes for Atezo/Bev (on a real-world cohort of 840 patients)
mRCC mUC	4,206 (mRCC) 2,240 (mUC)	2023	Yanagisawa et al (133)	ICI-based combination VS TKI ICI-based combination VS chemotherapy	PFS and OS benefit seen in first-line ICI-based combination; no difference between the sexes OS benefit seen in first-line ICI-based combination; no difference between the sexes

mRCC, metastatic renal cell carcinoma; mUC, metastatic urothelial carcinoma.

the effect of AR in I/O efficacy, confounding factors such as mutations will need to be properly controlled and stratified.

There are no sex differences in the superior OS benefits from first-line ICI-based combination therapies in metastatic renal cell carcinoma (RCC) or metastatic urothelial carcinoma (UC) (133). In locally advanced RCC, however, adjuvant I/O monotherapy reduces recurrence risk in female patients (HR=0.71, 95% CI 0.55–0.93) but not in male patients (133). On the other hand, males with muscle-invasive bladder cancer have better DFS on adjuvant I/O compared to females (133). A meta-analysis on HCC shows single-agent I/O exhibits less OS benefit in females than males. On the other hand, combination atezolizumab-bevacizumab (Atezo/Bev) – a first-line standard of care for advanced HCC – yields comparable efficacy between males and females in a real-world cohort (68). Nevertheless, these studies did not conduct stratified analysis based on AR expression, which may have overlooked the importance of AR in sex disparity.

Other phase III trials in advanced urothelial, hepato-pancreato-biliary and upper or lower gastrointestinal tract cancers have also been individually screened for outcome differences in patients treated with ICI based on sex or AR levels (135–145). However, none of these trials made explicit analysis on how sex or AR affects the outcomes in these cancers. Importantly, though, one study on 23,296 patients enrolled in SWOG trials shows a 49% increased risk of adverse events (AE) in females receiving I/O, especially of haematological AEs (146, 147). It is hoped that more prospective studies on the relationship between sex, AR expression and I/O efficacy and AEs can be carried out to further explore the role of AR signalling in cancer immunology and immunotherapy.

5.2 AR and cancer immunology

While previous sections have attempted to address how genetic, environmental, and hormonal effects lead to distinct tumorigenesis and disease progression patterns between males and females, studies over the past decade have emerged to explain how AR within the tumour microenvironment (TME) conspire to this process and alter patient response to treatments such as ICIs. This section summarises the effect of AR signalling in different TME cell types, laying the foundation for subsequent discussion on another dimension of I/O resistance (Figure 4).

Although AR signalling plays a key role in tumour immunosuppression, it is important to note the caveat when interpreting preclinical studies involving AR and biological sex. Cells harvested from male subjects have long been exposed to androgens and AR signalling. Hence, when manipulating AR-related pathways, male cells may behave very differently compared with female cells. Consequently, when designing and analysing clinical trials for I/O and antiandrogen combination, it is indispensable to include stratification based on biological sex, along with other variables such as circulating androgens, AR mutation/amplification/IHC status, and PD-L1 scoring.

5.2.1 AR signalling in lymphocytes

In murine models of CRC and melanoma, male mice have more aggressive tumours which seemingly depend on $CD8^+$ TILs (4, 148). AR signalling inhibits CD8 T cell stemness by regulating the epigenetic programme of T cell differentiation (4), while reducing IFNγ secretion via USP18 which inhibits NF-κB activation (148). This causes male TILs to be more terminally exhausted

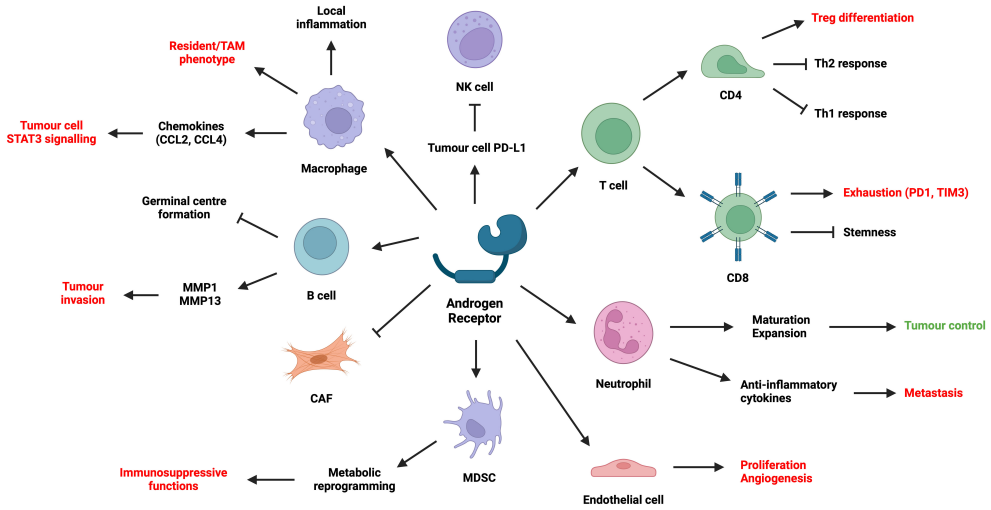

FIGURE 4
Summary of the effect of AR on different cell types in the TME. (Created with BioRender.com).

(PD1$^+$TIM3$^+$) with a loss of stem-cell like state (TCF1$^-$). Surgical castration in combination with ICI improves tumour control. These results correlate well with CRC and melanoma patient data, where AR positively correlates with PD1 and TIM3 expression in CD8$^+$ TILs. In addition, AR signalling transactivates *Tcf7*-centred regulons and directly results in the exhaustion of TCF1$^+$ progenitor CD8$^+$ T cells in murine bladder cancer (149). CD8$^+$-specific *Ar*-KO or systemic use of enzalutamide reduces tumour burden, while combining castration with ICI improves tumour control. These processes do not seem to depend on sex chromosomes, but more on androgen exposure and AR signalling.

Evidence is clear that AR signalling in male CD4$^+$ T cells suppresses Th1 and Th2 responses and favour T_{regs}. AR signalling stabilises *Foxp3*$^+$ T_{regs} during allergen challenge in males (150), possibly via a functional ARE within the *Foxp3* locus (151). Androgens also reduce the differentiation towards Th2 (150) and suppress Th2 functions in males (152), a consequence of AR binding to *Dusp2*. Androgen exposure also reduces Th1 differentiation by inhibiting IL-12 signalling (153). Pan-T cell *Ar*-KO renders severe airway inflammation in male mice during allergen exposure (150, 152).

One recent study has shown that while there are more NK cells in males, they often exhibit reduced cytotoxicity and tumour control (154). Such effect depends on both epigenetic factors (e.g. UTX) on the X chromosome (154) and the effect of sex hormones on tumour cell PD-L1 expression (155, 156). Specifically, high-dose androgen treatment on prostate cancer cells upregulates circFKBP5, which increases their PD-L1 expression and hence NK suppression (155). On the other hand, antiandrogens on bladder cancer cells reduce PD-L1 expression via ADAR2, which in turn increases NK cell cytotoxicity (156). Sorafenib treatment on HCC cell lines also enhances NK cell killing by reducing AR expression, leading to increased IL-12A secretion and NK activation. Further research is needed on the direct effects of AR signalling on NK cells.

There are limited findings on how AR signalling impacts B cell function. Androgens partially facilitate B cell migration away from the follicle centre via CCL21-GPR174 interaction, which prevents germinal centre formation (157). B cell proliferation and IgE synthesis are increased either by reducing circulating androgens (158) or by AR knockout (159), yet these effects do not enhance airway inflammation in allergen challenge (158). In another study, IL-8 increases AR expression on B cells, which promotes bladder cancer cell invasion by upregulating B cell expression of MMP1 and MMP13 (160).

5.2.2 AR signalling in macrophages, DCs, and MDSCs

The direct role of AR signalling on myeloid cell phenotype and function remains a contentious area of research. Androgens upregulate TREM1-associated signalling pathways in THP-1 and induce resident-like phenotypes, promoting prostate cancer cell migration and proliferation (161). Enzalutamide reduces immunosuppressive tumour associated macrophages (TAMs) in prostate cancer patients (161). Nevertheless, while AR signalling in macrophages can increase prostate tumorigenesis via increased CCL4 (162) and consequent STAT3 activation, blocking AR in TAMs or prostate cancer cells may actually promote metastasis via CCL2/STAT3-mediated macrophage recruitment (163). Furthermore, in atherosclerosis (164) and wounds (165), AR signalling promotes local inflammation by enhancing TNFα expression, monocyte differentiation and chemotaxis (166), as well as foam cell formation via altered lipid metabolism. AR signalling in alveolar macrophages also promotes M2 macrophage-mediated eosinophilic inflammation, increasing lung damage in asthma mouse models (167). Hence, the role of AR signalling in macrophages depends not only on its direct effects, but also on the local tissue and disease contexts.

Though analysis has shown that ADT may lead to increased infiltration of myeloid-derived suppressor cells (MDSCs) into the TME (168, 169), there have been few studies looking at the direct effect of AR signalling on MDSCs or dendritic cells (DCs). B16 and 4T1 implantation results in higher tumour burden in female mice that is correlated with a higher plasmacytoid DC infiltration and

less MDSCs compared with male mice (170). Functions of these tumour-associated DCs could depend on FOXO3-regulated AR/ER expression (170). In another seminal study, AR knockout or antagonism on MDSCs facilitate MC-38 tumour progression in mice, resulting from pAMPK-mediated metabolic reprogramming (171). Increased glycolysis and decreased mitochondrial respiration led to immunosuppressive MDSC phenotype (171), which has well been established (172).

5.2.3 AR signalling in neutrophils

Research has shown that androgens promote neutrophil maturation and expansion in the bone marrow, as well as subsequent chemotaxis towards foci of injury or malignancy (173–175). AR-KO mice are often neutropenic and susceptible to acute bacterial infection (176). Male mice castrated prior to melanoma implantation also show impaired neutrophil maturation and function, with elevated metastatic burden that can be ameliorated by rescue testosterone replacement (174). Conversely, women with PCOS and insulin resistance often show increased circulating androgens associated with raised neutrophil count (177). Interestingly, in another study, ADT suppresses neutrophil cytotoxicity via increased TGFβ-RI (178), which is also seen in prostate cancer patients receiving ADT (174). High dose androgens or TGFβ-RI inhibition rescue AR-mediated neutrophil suppression and restore its anti-tumour effects (178).

However, androgen-sensitised neutrophils can also exhibit reduced bactericidal functions or cytotoxicity, hence promoting tumour progression. This phenotype is accompanied by high expression of anti-inflammatory cytokines such as IL-10 (175). For instance, AR signalling promotes hepatic neutrophil accumulation and contribute to MC-38 and B16 liver metastases (LM) (173). Antagonising neutrophil AR signalling axis significantly mitigates LM. Two other studies show tumour infiltrating neutrophils promote AR expression in bladder cancer and RCC cells, which increases their metastatic potential (179, 180). Therefore, systemic administration of antiandrogens often shows equivocal effects on neutrophil-mediated tumour control.

5.2.4 AR signalling in CAFs and endothelial cells

Several studies have demonstrated the important role of AR in preventing fibroblasts from differentiating into CAFs in skin cancers (181, 182) and prostate cancer (183–186). Low AR levels in prostate cancer stroma is associated with poorer patient survival. AR inhibits ANKRD1 (181) and LMO2 (183) expression, both of which are activators of CAF-related gene signatures. AR downregulation or deactivation leads to transition from normal fibroblasts to CAFs, enhancing tumorigenesis, tumour cell stemness and invasion via ECM remodelling and increased MMP expression (186), as well as increased expression of cytokines including IL-6, IL-8, IL-11, CCL2, IFNγ and M-CSF, all of which are also known to induce an immunosuppressive TME (182–185).

Further studies are anticipated on the effects of AR signalling in tumour endothelium and angiogenesis (187). While AR signalling in prostate cancer and RCC cells is known to upregulate angiogenic cytokines including VEGF and CXCL5 (188–190), AR signalling on endothelial cells themselves can also directly increase proliferation (191). AR-deficient or AR-antagonised endothelial cells show reduced angiogenic capacity and failure to activate eNOS (192, 193). How these findings may translate into tangible clinical intervention remains to be elucidated.

5.3 Mechanisms of AR and I/O resistance

Patient scRNA-seq and murine models have suggested that an increased AR signalling may predict I/O resistance, resulting from downregulation of IFNγ and upregulation of $CD8^+$ T cell exhaustion programmes. Indeed, as previous sections have shown, a recurrent *in vivo* finding is that castration or T cell-specific AR knockout can improve I/O response in male mice, while antiandrogens rescue I/O response and tumour control in androgen-exposed females. While it is natural to test I/O-antiandrogen combinations in the clinical setting, I/O nevertheless fails to synergise with AR antagonists in metastatic CRPC after all, as evident in the IMbassador250 trial (194). Why is this?

One explanation, as discussed earlier, is that male $CD8^+$ T cells have experienced long-term androgen exposure, predisposing them towards exhausted phenotypes during tumour progression, irrespective of subsequent AR signalling manipulation. In preclinical studies, castration or cell-specific AR knockout is almost always performed *before* tumour inoculation and I/O treatment. The dynamics of interaction between malignant cells and the TME may well be different from research involving antiandrogens. It reminds us that the sequence of I/O versus AR signalling manipulation is crucial to an optimised patient response.

Another hypothesis is that AR antagonists suppress anti-tumour immunity independently of AR. One study has shown that AR antagonists inhibit initial T cell priming via an off-target effect on GABA-A (195). Even if T cell exhaustion may be reduced with antiandrogen treatment, the initial neoantigen presentation and infiltration into the tumours can also be compromised, cancelling out the beneficial effect of AR antagonist on checkpoint inhibition. Indeed, another study also shows increased monocytic MDSC infiltration, decreased CD8+ TIL number and increased PD-L1 expression in enzalutamide-treated murine Myc-CaP tumours (168). When these tumour cells acquire enzalutamide resistance, they upregulate PD-L1 expression and possess an increased capacity to skew myeloid cells towards MDSCs and M2 macrophages (168, 195), further suppressing T cell function. Strikingly, another study shows a signalling crosstalk between AR and the glucocorticoid receptor (GR) (196). AR inhibition upregulates GR while high-dose steroids confer enzalutamide resistance to a prostate cancer model (196). This finding necessitates a more thorough understanding of the escape mechanisms of tumour cells when treated with combined I/O and antiandrogen (101).

Also importantly, as evident in previous sections, AR signalling exhibits heterogeneous effects on different TME cell types, resulting in equivocal efficacy when combining I/O with systemic antiandrogen administration. While AR on lymphocytes (T, B, NK) negatively regulates their cytotoxic functions in general, AR on macrophages and neutrophils regulate their functions in a sequence-dependent manner. Specifically, AR promotes the proliferation, maturation and

infiltration of macrophages and neutrophils into the tissues. However, it subsequently renders these cells anti-inflammatory in the TME. AR inhibition also enhances the immunosuppressive functions of DCs and MDSCs. Furthermore, increasing evidence has shown that AR prevents fibroblast differentiation towards CAFs and regulates endothelial cell proliferation. Therefore, there is much unknown as to how systemic AR inhibition on a heterogenous TME affect immunotherapy efficacy. Interestingly, a recent analysis of NSCLC exosome and transcriptome datasets show significant enrichment of DCs and T cells as well as a T cell dysfunction phenotype in the TME of female patients, while the male patients generally possess a T cell excluded TME (197). These findings are highly consistent with the effects of AR signalling on TME cell types as described earlier, demonstrating the key role of AR in regulating tumour immunology and I/O response. Future combinatory I/O with AR modulation will require delicate consideration into the individual tumour characteristics.

Specifically in prostate cancer, preclinical studies have shown, as discussed above, how blocking AR signalling can in fact compromise T cell priming or activation (195), upregulate CCL2/STAT3-mediated macrophage recruitment (163), reduce neutrophil maturation or expansion (174), promote CAF accumulation (184), and increasing tumour cell expression of GR (196), all of which may negate the benefits of checkpoint blockade in these patients (198). Future combinatory trials in advanced prostate cancer will need to select patients early in their disease progression, and give careful thoughts on both the checkpoint (PD-1, PD-L1, CTLA4, TIGIT, etc.) to be targeted, as well as the timing of I/O relative to AR inhibition (198, 199).

6 Concluding remarks

The perceived sexual dimorphism in cancer epidemiology is the consequence of a myriad of factors, including socioeconomic and cultural disparities (200), environmental exposures, sex chromosomes, sex hormones, as well as sex hormone receptors such as AR. Indeed, gender oncology is emerging as an important aspect of personalised medicine that recognises and addresses such differences in cancer incidence and therapeutic responses (147). While research has elucidated the role of AR in tumour development and progression, studies have often overlooked the impact of AR signalling on the TME and I/O outcomes. We have shown that AR plays heterogeneous roles in individual TME cell types, sometimes independent of androgens, which potentially explains the equivocal efficacy of antiandrogen and I/O combination so far. It is hoped that future clinical studies on cancers could disaggregate outcomes by sex and stratify androgen/AR level more frequently, hence providing further evidence for antiandrogen and I/O combination or personalised I/O tailored to sex and androgen/AR status. Translational studies on AR modulation of the TME can help design better trials of I/O-based gender oncology with AR as a potential biomarker. By doing so we may optimise treatment strategies and improve individualised patient outcomes.

Author contributions

JZ: Conceptualization, Data curation, Visualization, Writing – original draft, Writing – review & editing. QW: Conceptualization, Data curation, Visualization, Writing – original draft, Writing – review & editing. AT: Conceptualization, Data curation, Writing – original draft, Writing – review & editing. CL: Data curation, Visualization, Writing – original draft, Writing – review & editing. HT: Conceptualization, Resources, Supervision, Writing – review & editing, Writing – original draft.

Funding

The author(s) declare financial support was received for the research, authorship, and/or publication of this article. This work was supported by the National Medical Research Council, Singapore, with grant numbers MOH-STaR21nov-0002 and NMRC/OFLCG/003/2018.

Acknowledgments

JZ would like to thank Caroline Lee and Hanry Yu for their mentorship.

Conflict of interest

The authors declare that the research was conducted in the absence of any commercial or financial relationships that could be construed as a potential conflict of interest.

Publisher's note

All claims expressed in this article are solely those of the authors and do not necessarily represent those of their affiliated organizations, or those of the publisher, the editors and the reviewers. Any product that may be evaluated in this article, or claim that may be made by its manufacturer, is not guaranteed or endorsed by the publisher.

References

1. Haupt S, Caramia F, Klein SL, Rubin JB, Haupt Y. Sex disparities matter in cancer development and therapy. *Nat Rev Cancer*. (2021) 21:393–407. doi: 10.1038/s41568-021-00348-y

2. Clayton JA, Collins FS. Policy: NIH to balance sex in cell and animal studies. *Nature*. (2014) 509:282–3. doi: 10.1038/509282a

3. Kajihara N, Ge Y, Seino K-I. Blocking of oestrogen signals improves anti-tumour effect regardless of oestrogen receptor alpha expression in cancer cells. *Br J Cancer*. (2023) 129:935–46. doi: 10.1038/s41416-023-02381-0

4. Yang C, Jin J, Yang Y, Sun H, Wu L, Shen M, et al. Androgen receptor-mediated CD8+ T cell stemness programs drive sex differences in antitumor immunity. *Immunity*. (2022) 55:1268–83.e9. doi: 10.1016/j.immuni.2022.05.012

5. Bhatia A, Sekhon HK, Kaur G. Sex hormones and immune dimorphism. *ScientificWorldJournal*. (2014) 2014:159150. doi: 10.1155/2014/159150

6. Klein SL, Flanagan KL. Sex differences in immune responses. *Nat Rev Immunol*. (2016) 16:626–38. doi: 10.1038/nri.2016.90

7. Whitacre CC. Sex differences in autoimmune disease. *Nat Immunol*. (2001) 2:777–80. doi: 10.1038/ni0901-777

8. Lockshin MD. Sex differencesxxx inxxx autoimmunexxxx disease. *Lupus*. (2006) 15:753–6. doi: 10.1177/0961203306069353

9. Henze L, Schwinge D, Schramm C. The effects of androgens on T cells: clues to female predominance in autoimmune liver diseases? *Front Immunol*. (2020) 11:1567. doi: 10.3389/fimmu.2020.01567

10. Colafella KMM, Denton KM. Sex-specific differences in hypertension and associated cardiovascular disease. *Nat Rev Nephrol*. (2018) 14:185–201. doi: 10.1038/nrneph.2017.189

11. Shobab L, Burman KD, Wartofsky L. Sex differences in differentiated thyroid cancer. *Thyroid*. (2022) 32:224–35. doi: 10.1089/thy.2021.0361

12. Edgren G, Liang L, Adami H-O, Chang ET. Enigmatic sex disparities in cancer incidence. *Eur J Epidemiol*. (2012) 27:187–96. doi: 10.1007/s10654-011-9647-5

13. Sung H, Ferlay J, Siegel RL, Laversanne M, Soerjomataram I, Jemal A, et al. Global cancer statistics 2020: GLOBOCAN estimates of incidence and mortality worldwide for 36 cancers in 185 countries. *CA Cancer J Clin*. (2021) 71:209–49. doi: 10.3322/caac.21660

14. Ferlay J, Ervik M, Lam F, Laversanne M, Colombet M, Mery L, et al. Global Cancer Observatory: Cancer Today (version 1.0). Lyon, France: International Agency for Research on Cancer. (2020). Available at: https://gco.iarc.who.int/today (Accessed January 10, 2024).

15. Zahedi A, Bondaz L, Rajaraman M, Leslie WD, Jefford C, Young JE, et al. Risk for thyroid cancer recurrence is higher in men than in women independent of disease stage at presentation. *Thyroid*. (2020) 30:871–7. doi: 10.1089/thy.2018.0775

16. Mancini M, Righetto M, Baggio G. Spotlight on gender-specific disparities in bladder cancer. *Urologia*. (2020) 87:103–14. doi: 10.1177/0391560319887327

17. Siegel RL, Miller KD, Wagle NS, Jemal A. Cancer statistics, 2023. *CA Cancer J Clin*. (2023) 73:17–48. doi: 10.3322/caac.21763

18. Li Q, Cao M, Lei L, Yang F, Li H, Yan X, et al. Burden of liver cancer: From epidemiology to prevention. *Chin J Cancer Res*. (2022) 34:554–66. doi: 10.21147/j.issn.1000-9604.2022.06.02

19. Thrift AP, Wenker TN, El-Serag HB. Global burden of gastric cancer: epidemiological trends, risk factors, screening and prevention. *Nat Rev Clin Oncol*. (2023) 20:338–49. doi: 10.1038/s41571-023-00747-0

20. Siegel RL, Miller KD, Fuchs HE, Jemal A. Cancer statistics, 2021. *CA Cancer J Clin*. (2021) 71:7–33. doi: 10.3322/caac.21654

21. Martínez-Rojo E, Berumen LC, García-Alcocer G, Escobar-Cabrera J. The role of androgens and androgen receptor in human bladder cancer. *Biomolecules*. (2021) 11 (4):594. doi: 10.3390/biom11040594

22. Bell DW, Brannigan BW, Matsuo K, Finkelstein DM, Sordella R, Settleman J, et al. Increased prevalence of EGFR-mutant lung cancer in women and in East Asian populations: analysis of estrogen-related polymorphisms. *Clin Cancer Res*. (2008) 14:4079–84. doi: 10.1158/1078-0432.CCR-07-5030

23. Jemal A, Schafer EJ, Sung H, Bandi P, Kratzer T, Islami F, et al. The burden of lung cancer in women compared with men in the US. *JAMA Oncol*. (2023) 9:1727–8. doi: 10.1001/jamaoncol.2023.4415

24. Xie S-H, Yu IT-S, Tse L-A, Mang OW-K, Yue L. Sex difference in the incidence of nasopharyngeal carcinoma in Hong Kong 1983–2008: suggestion of a potential protective role of oestrogen. *Eur J Cancer*. (2013) 49:150–5. doi: 10.1016/j.ejca.2012.07.004

25. Arnold M, Singh D, Laversanne M, Vignat J, Vaccarella S, Meheus F, et al. Global burden of cutaneous melanoma in 2020 and projections to 2040. *JAMA Dermatol*. (2022) 158:495–503. doi: 10.1001/jamadermatol.2022.0160

26. Scoggins CR, Ross MI, Reintgen DS, Noyes RD, Goydos JS, Beitsch PD, et al. Gender-related differences in outcome for melanoma patients. *Ann Surg*. (2006) 243:693–8; discussion 698–700. doi: 10.1097/01.sla.0000216771.81362.6b

27. Manola J, Atkins M, Ibrahim J, Kirkwood J. Prognostic factors in metastatic melanoma: a pooled analysis of Eastern Cooperative Oncology Group trials. *J Clin Oncol*. (2000) 18:3782–93. doi: 10.1200/JCO.2000.18.22.3782

28. Nosrati A, Wei ML. Sex disparities in melanoma outcomes: the role of biology. *Arch Biochem Biophys*. (2014) 563:42–50. doi: 10.1016/j.abb.2014.06.018

29. Dong M, Cioffi G, Wang J, Waite KA, Ostrom QT, Kruchko C, et al. Sex differences in cancer incidence and survival: A pan-cancer analysis. *Cancer Epidemiol Biomarkers Prev*. (2020) 29:1389–97. doi: 10.1158/1055-9965.EPI-20-0036

30. Brown KF, Rumgay H, Dunlop C, Ryan M, Quartly F, Cox A, et al. The fraction of cancer attributable to modifiable risk factors in England, Wales, Scotland, Northern Ireland, and the United Kingdom in 2015. *Br J Cancer*. (2018) 118:1130–41. doi: 10.1038/s41416-018-0029-6

31. Bryant A, Cerfolio RJ. Differences in epidemiology, histology, and survival between cigarette smokers and never-smokers who develop non-small cell lung cancer. *Chest*. (2007) 132:185–92. doi: 10.1378/chest.07-0442

32. Morgan TR, Mandayam S, Jamal MM. Alcohol and hepatocellular carcinoma. *Gastroenterology*. (2004) 127:S87–96. doi: 10.1053/j.gastro.2004.09.020

33. Corrao G, Bagnardi V, Zambon A, La Vecchia C. A meta-analysis of alcohol consumption and the risk of 15 diseases. *Prev Med*. (2004) 38:613–9. doi: 10.1016/j.ypmed.2003.11.027

34. Cho E, Smith-Warner SA, Ritz J, van den Brandt PA, Colditz GA, Folsom AR, et al. Alcohol intake and colorectal cancer: a pooled analysis of 8 cohort studies. *Ann Intern Med*. (2004) 140:603–13. doi: 10.7326/0003-4819-140-8-200404200-00007

35. Verplaetse TL, Peltier MR, Roberts W, Burke C, Moore KE, Pittman B, et al. Sex and alcohol use disorder predict the presence of cancer, respiratory, and other medical conditions: Findings from the National Epidemiologic Survey on Alcohol and Related Conditions-III. *Addict Behav*. (2021) 123:107055. doi: 10.1016/j.addbeh.2021.107055

36. Hydes TJ, Burton R, Inskip H, Bellis MA, Sheron N. A comparison of gender-linked population cancer risks between alcohol and tobacco: how many cigarettes are there in a bottle of wine? *BMC Public Health*. (2019) 19:316. doi: 10.1186/s12889-019-6576-9

37. Steele CB, Thomas CC, Henley SJ, Massetti GM, Galuska DA, Agurs-Collins T, et al. Vital signs: trends in incidence of cancers associated with overweight and obesity - United States, 2005–2014. *MMWR Morb Mortal Wkly Rep*. (2017) 66:1052–8. doi: 10.15585/mmwr.mm6639e1

38. Arnold M, Soerjomataram I, Ferlay J, Forman D. Global incidence of oesophageal cancer by histological subtype in 2012. *Gut*. (2015) 64:381–7. doi: 10.1136/gutjnl-2014-308124

39. Argyrakopoulou G, Dalamaga M, Spyrou N, Kokkinos A. Gender differences in obesity-related cancers. *Curr Obes Rep*. (2021) 10:100–15. doi: 10.1007/s13679-021-00426-0

40. Avgerinos KI, Spyrou N, Mantzoros CS, Dalamaga M. Obesity and cancer risk: Emerging biological mechanisms and perspectives. *Metabolism*. (2019) 92:121–35. doi: 10.1016/j.metabol.2018.11.001

41. Lee CH, Woo YC, Wang Y, Yeung CY, Xu A, Lam KSL. Obesity, adipokines and cancer: an update. *Clin Endocrinol*. (2015) 83:147–56. doi: 10.1111/cen.12667

42. Ballestri S, Nascimbeni F, Baldelli E, Marrazzo A, Romagnoli D, Lonardo A. NAFLD as a sexual dimorphic disease: role of gender and reproductive status in the development and progression of nonalcoholic fatty liver disease and inherent cardiovascular risk. *Adv Ther*. (2017) 34:1291–326. doi: 10.1007/s12325-017-0556-1

43. Elkhalifa AME, Nabi SU, Shah OS, Bashir SM, Muzaffer U, Ali SI, et al. Current Oncology. Available at: https://www.mdpi.com/1718–7729/30/2/150/review_report (Accessed February 27, 2024).

44. Mundi N, Ghasemi F, Zeng PYF, Prokopec SD, Patel K, Kim HAJ, et al. Sex disparities in head & neck cancer driver genes: An analysis of the TCGA dataset. *Oral Oncol*. (2020) 104:104614. doi: 10.1016/j.oraloncology.2020.104614

45. El-Serag HB, Rudolph KL. Hepatocellular carcinoma: epidemiology and molecular carcinogenesis. *Gastroenterology*. (2007) 132:2557–76. doi: 10.1053/j.gastro.2007.04.061

46. Tukiainen T, Villani A-C, Yen A, Rivas MA, Marshall JL, Satija R, et al. Landscape of X chromosome inactivation across human tissues. *Nature*. (2017) 550:244–8. doi: 10.1038/nature24265

47. Dunford A, Weinstock DM, Savova V, Schumacher SE, Cleary JP, Yoda A, et al. Tumor-suppressor genes that escape from X-inactivation contribute to cancer sex bias. *Nat Genet*. (2017) 49:10–6. doi: 10.1038/ng.3726

48. Zito A, Davies MN, Tsai P-C, Roberts S, Andres-Ejarque R, Nardone S, et al. Heritability of skewed X-inactivation in female twins is tissue-specific and associated with age. *Nat Commun*. (2019) 10:5339. doi: 10.1038/s41467-019-13340-w

49. Haupt S, Caramia F, Herschtal A, Soussi T, Lozano G, Chen H, et al. Identification of cancer sex-disparity in the functional integrity of p53 and its X chromosome network. *Nat Commun*. (2019) 10:5385. doi: 10.1038/s41467-019-13266-3

50. Büscheck F, Fraune C, Garmestani S, Simon R, Kluth M, Hube-Magg C, et al. Y-chromosome loss is frequent in male renal tumors. *Ann Transl Med*. (2021) 9:209. doi: 10.21037/atm

51. Willis-Owen SAG, Domingo-Sabugo C, Starren E, Liang L, Freidin MB, Arseneault M, et al. Y disruption, autosomal hypomethylation and poor male lung cancer survival. *Sci Rep*. (2021) 11:12453. doi: 10.1038/s41598-021-91907-8

52. Abdel-Hafiz HA, Schafer JM, Chen X, Xiao T, Gauntner TD, Li Z, et al. Y chromosome loss in cancer drives growth by evasion of adaptive immunity. *Nature*. (2023) 619:624–31. doi: 10.1038/s41586-023-06234-x

53. Cáceres A, Jene A, Esko T, Pérez-Jurado LA, González JR. Extreme downregulation of chromosome Y and cancer risk in men. *J Natl Cancer Inst*. (2020) 112:913–20. doi: 10.1093/jnci/djz232

54. Kool M, Koster J, Bunt J, Hasselt NE, Lakeman A, van Sluis P, et al. Integrated genomics identifies five medulloblastoma subtypes with distinct genetic profiles, pathway signatures and clinicopathological features. *PloS One*. (2008) 3:e3088. doi: 10.1371/journal.pone.0003088

55. Parodi S, Pistorio A, Erminio G, Ognibene M, Morini M, Garaventa A, et al. Loss of whole chromosome X predicts prognosis of neuroblastoma patients with numerical genomic profile. *Pediatr Blood Cancer*. (2019) 66:e27635. doi: 10.1002/pbc.27635

56. Duijf PHG, Schultz N, Benezra R. Cancer cells preferentially lose small chromosomes. *Int J Cancer*. (2013) 132:2316–26. doi: 10.1002/ijc.27924

57. Shuai C, Yang X, Pan H, Han W. Estrogen receptor downregulates expression of PD-1/PD-L1 and infiltration of CD8+ T cells by inhibiting IL-17 signaling transduction in breast cancer. *Front Oncol*. (2020) 10:582863. doi: 10.3389/fonc.2020.582863

58. Kang C, Song C-H, Kim N, Nam RH, Choi SI, Yu JE, et al. The enhanced inhibitory effect of estrogen on PD-L1 expression following Nrf2 deficiency in the AOM/DSS model of colitis-associated cancer. *Front Oncol*. (2021) 11:679324. doi: 10.3389/fonc.2021.679324

59. Liu S, Fan W, Gao X, Huang K, Ding C, Ma G, et al. Estrogen receptor alpha regulates the Wnt/β-catenin signaling pathway in colon cancer by targeting the NOD-like receptors. *Cell Signal*. (2019) 61:86–92. doi: 10.1016/j.cellsig.2019.05.009

60. Clusan L, Ferrière F, Flouriot G, Pakdel F. A basic review on estrogen receptor signaling pathways in breast cancer. *Int J Mol Sci*. (2023) 24(7):6834. doi: 10.3390/ijms24076834

61. McGlynn LM, Tovey S, Bartlett JMS, Doughty J, Cooke TG, Edwards J. Interactions between MAP kinase and oestrogen receptor in human breast cancer. *Eur J Cancer*. (2013) 49:1176–86. doi: 10.1016/j.ejca.2012.11.020

62. Kouzmenko AP, Takeyama K-I, Ito S, Furutani T, Sawatsubashi S, Maki A, et al. Wnt/beta-catenin and estrogen signaling converge in vivo. *J Biol Chem*. (2004) 279:40255–8. doi: 10.1074/jbc.C400331200

63. Niv Y. Estrogen receptor β expression and colorectal cancer: a systematic review and meta-analysis. *Eur J Gastroenterol Hepatol*. (2015) 27:1438–42. doi: 10.1097/MEG.0000000000000471

64. Rossouw JE, Anderson GL, Prentice RL, LaCroix AZ, Kooperberg C, Stefanick ML, et al. Risks and benefits of estrogen plus progestin in healthy postmenopausal women: principal results From the Women's Health Initiative randomized controlled trial. *JAMA*. (2002) 288:321–33. doi: 10.1001/jama.288.3.321

65. Rawłuszko-Wieczorek AA, Lipowicz J, Nowacka M, Ostrowska K, Pietras P, Blatkiewicz M, et al. Estrogen receptor β affects hypoxia response in colorectal cancer cells. *Biochim Biophys Acta Mol Basis Dis*. (2024) 1870:166894. doi: 10.1016/j.bbadis.2023.166894

66. Bravo-Vázquez LA, Méndez-García A, Rodríguez AL, Sahare P, Pathak S, Banerjee A, et al. Applications of nanotechnologies for miRNA-based cancer therapeutics: current advances and future perspectives. *Front Bioeng Biotechnol*. (2023) 11:1208547. doi: 10.3389/fbioe.2023.1208547

67. Pang C, Li J-M, Wang Z, Luo Y-C, Cheng Z-G, Han Z-Y, et al. Age-dependent female survival advantage in hepatocellular carcinoma: A multicenter cohort study. *Clin Gastroenterol Hepatol*. (2024) 22:305–14. doi: 10.1016/j.cgh.2023.07.029

68. Balcar L, Scheiner B, Fulgenzi CAM, D'Alessio A, Pomej K, Roig MB, et al. A meta-analysis and real-world cohort study on the sex-related differences in efficacy and safety of immunotherapy for hepatocellular carcinoma. *JHEP Rep*. (2024) 6:100982. doi: 10.1016/j.jhepr.2023.100982

69. Farinati F, Salvagnini M, de Maria N, Fornasiero A, Chiaramonte M, Rossaro L, et al. Unresectable hepatocellular carcinoma: a prospective controlled trial with tamoxifen. *J Hepatol*. (1990) 11:297–301. doi: 10.1016/0168-8278(90)90211-9

70. Perrone F, Gallo C, Daniele B, Gaeta GB, Izzo F, Capuano G, et al. Tamoxifen in the treatment of hepatocellular carcinoma: 5-year results of the CLIP-1 multicentre randomised controlled trial. *Curr Pharm Des*. (2002) 8:1013–9. doi: 10.2174/1381612024607063

71. Castells A, Bruix J, Brú C, Ayuso C, Roca M, Boix L, et al. Treatment of hepatocellular carcinoma with tamoxifen: a double-blind placebo-controlled trial in 120 patients. *Gastroenterology*. (1995) 109:917–22. doi: 10.1016/0016-5085(95)90402-6

72. Zeng H, Yang Z, Li J, Wen Y, Wu Z, Zheng Y, et al. Associations between female lung cancer risk and sex steroid hormones: a systematic review and meta-analysis of the worldwide epidemiological evidence on endogenous and exogenous sex steroid hormones. *BMC Cancer*. (2021) 21:690. doi: 10.1186/s12885-021-08437-9

73. Castellanos MR, Fanous E, Thaker R, Flory MJ, Seetharamu N, Dhar M, et al. Expression patterns and clinical significance of estrogen receptor in non-small cell lung cancer. *Pathol Res Pract*. (2023) 241:154298. doi: 10.1016/j.prp.2022.154298

74. Kawai H, Ishii A, Washiya K, Konno T, Kon H, Yamaya C, et al. Estrogen receptor alpha and beta are prognostic factors in non-small cell lung cancer. *Clin Cancer Res*. (2005) 11:5084–9. doi: 10.1158/1078-0432.CCR-05-0200

75. Li H, Chen H, Shi J, Fan Q, Zhou Z, Tang X, et al. ERβ overexpression may not be a direct prognostic factor in patients with NSCLC: A meta-analysis. *Int J Biol Markers*. (2022) 37:249–59. doi: 10.1177/03936155221105521

76. Meng W, Liao Y, Chen J, Wang Y, Meng Y, Li K, et al. Upregulation of estrogen receptor beta protein but not mRNA predicts poor prognosis and may be associated with enhanced translation in non-small cell lung cancer: a systematic review and meta-analysis. *J Thorac Dis*. (2021) 13:4281–300. doi: 10.21037/jtd

77. Cronin-Fenton DP, Murray LJ, Whiteman DC, Cardwell C, Webb PM, Jordan SJ, et al. Reproductive and sex hormonal factors and oesophageal and gastric junction adenocarcinoma: a pooled analysis. *Eur J Cancer*. (2010) 46:2067–76. doi: 10.1016/j.ejca.2010.03.032

78. Camargo MC, Goto Y, Zabaleta J, Morgan DR, Correa P, Rabkin CS. Sex hormones, hormonal interventions, and gastric cancer risk: a meta-analysis. *Cancer Epidemiol Biomarkers Prev*. (2012) 21:20–38. doi: 10.1158/1055-9965.EPI-11-0834

79. Raynor MC, Carson CC, Pearson MD, Nix JW. Androgen deficiency in the aging male: a guide to diagnosis and testosterone replacement therapy. *Can J Urol*. (2007) 14 Suppl 1:63–8.

80. Iwasa T, Yamamoto Y, Shinya A, Minato S, Yanagihara R, Kamada S, et al. The effects of androgens on metabolic functions in females. *J Med Invest*. (2021) 68:228–31. doi: 10.2152/jmi.68.228

81. Liu Z, Zhang Y, Lagergren J, Li S, Li J, Zhou Z, et al. Circulating sex hormone levels and risk of gastrointestinal cancer: systematic review and meta-analysis of prospective studies. *Cancer Epidemiol Biomarkers Prev*. (2023) 32:936–46. doi: 10.1158/1055-9965.EPI-23-0039

82. Xie S-H, Ness-Jensen E, Rabbani S, Langseth H, Gislefoss RE, Mattsson F, et al. Circulating sex hormone levels and risk of esophageal adenocarcinoma in a prospective study in men. *Am J Gastroenterol*. (2020) 115:216–23. doi: 10.14309/ajg.0000000000000446

83. Garg H, Wheeler KM, Dursun F, Cooper RE, Pruthi DK, Kaushik D, et al. Impact of finasteride on survival in bladder cancer: A retrospective multi-institutional database analysis. *Clin Genitourin Cancer*. (2023) 21:314.e1–7. doi: 10.1016/j.clgc.2022.10.014

84. Edelsztein NY, Rey RA. Importance of the androgen receptor signaling in gene transactivation and transrepression for pubertal maturation of the testis. *Cells*. (2019) 8(8):861. doi: 10.3390/cells8080861

85. Pietri E, Conteduca V, Andreis D, Massa I, Melegari E, Sarti S, et al. Androgen receptor signaling pathways as a target for breast cancer treatment. *Endocr Relat Cancer*. (2016) 23:R485–98. doi: 10.1530/ERC-16-0190

86. Bennett NC, Gardiner RA, Hooper JD, Johnson DW, Gobe GC. Molecular cell biology of androgen receptor signalling. *Int J Biochem Cell Biol*. (2010) 42:813–27. doi: 10.1016/j.biocel.2009.11.013

87. Kanda T, Jiang X, Yokosuka O. Androgen receptor signaling in hepatocellular carcinoma and pancreatic cancers. *World J Gastroenterol*. (2014) 20:9229–36. doi: 10.3748/wjg.v20.i28.9229

88. Rothman MS, Carlson NE, Xu M, Wang C, Swerdloff R, Lee P, et al. Reexamination of testosterone, dihydrotestosterone, estradiol and estrone levels across the menstrual cycle and in postmenopausal women measured by liquid chromatography-tandem mass spectrometry. *Steroids*. (2011) 76:177–82. doi: 10.1016/j.steroids.2010.10.010

89. Cooke PS, Walker WH. Nonclassical androgen and estrogen signaling is essential for normal spermatogenesis. *Semin Cell Dev Biol*. (2022) 121:71–81. doi: 10.1016/j.semcdb.2021.05.032

90. Gibson DA, Saunders PTK, McEwan IJ. Androgens and androgen receptor: Above and beyond. *Mol Cell Endocrinol*. (2018) 465:1–3. doi: 10.1016/j.mce.2018.02.013

91. Becerra-Diaz M, Song M, Heller N. Androgen and androgen receptors as regulators of monocyte and macrophage biology in the healthy and diseased lung. *Front Immunol*. (2020) 11:1698. doi: 10.3389/fimmu.2020.01698

92. Mantalaris A, Panoskaltsis N, Sakai Y, Bourne P, Chang C, Messing EM, et al. Localization of androgen receptor expression in human bone marrow. *J Pathol*. (2001) 193:361–6. doi: 10.1002/(ISSN)1096-9896

93. Sinnesael M, Boonen S, Claessens F, Gielen E, Vanderschueren D. Testosterone and the male skeleton: a dual mode of action. *J Osteoporos*. (2011) 2011:240328. doi: 10.4061/2011/240328

94. Swerdloff RS, Dudley RE, Page ST, Wang C, Salameh WA. Dihydrotestosterone: biochemistry, physiology, and clinical implications of elevated blood levels. *Endocr Rev*. (2017) 38:220–54. doi: 10.1210/er.2016-1067

95. Lang F, Alevizopoulos K, Stournaras C. Targeting membrane androgen receptors in tumors. *Expert Opin Ther Targets*. (2013) 17:951–63. doi: 10.1517/14728222.2013.806491

96. Papakonstanti EA, Kampa M, Castanas E, Stournaras C. A rapid, nongenomic, signaling pathway regulates the actin reorganization induced by activation of membrane testosterone receptors. *Mol Endocrinol*. (2003) 17:870–81. doi: 10.1210/me.2002-0253

97. Lin AJ, Baranski T, Chaterjee D, Chapman W, Foltz G, Kim H. Androgen-receptor-positive hepatocellular carcinoma in a transgender teenager taking exogenous testosterone. *Lancet*. (2020) 396:198. doi: 10.1016/S0140-6736(20)31538-5

98. Caroppo F, Tadiotto Cicogna G, Messina F, Alaibac M. Association between melanoma and exposure to sex hormones in puberty: A possible window of susceptibility (Review). *Mol Clin Oncol*. (2021) 14:66. doi: 10.3892/mco

99. Rampen FH, Mulder JH. Malignant melanoma: an androgen-dependent tumour? *Lancet*. (1980) 1:562–4. doi: 10.1016/S0140-6736(80)91055-7

100. Pothuri VS, Anzelmo M, Gallaher E, Ogunlana Y, Aliabadi-Wahle S, Tan B, et al. Transgender males on gender-affirming hormone therapy and hepatobiliary neoplasms: A systematic review. *Endocr Pract*. (2023) 29:822–9. doi: 10.1016/j.eprac.2023.05.011

101. Watson PA, Arora VK, Sawyers CL. Emerging mechanisms of resistance to androgen receptor inhibitors in prostate cancer. *Nat Rev Cancer*. (2015) 15:701–11. doi: 10.1038/nrc4016

102. Schweizer MT, Yu EY. AR-signaling in human Malignancies: prostate cancer and beyond. *Cancers*. (2017) 9(1):7. doi: 10.3390/cancers9010007

103. Scher HI, Fizazi K, Saad F, Taplin M-E, Sternberg CN, Miller K, et al. Increased survival with enzalutamide in prostate cancer after chemotherapy. *N Engl J Med*. (2012) 367:1187–97. doi: 10.1056/NEJMoa1207506

104. Wang Q, Li W, Liu XS, Carroll JS, Jänne OA, Keeton EK, et al. A hierarchical network of transcription factors governs androgen receptor-dependent prostate cancer growth. *Mol Cell*. (2007) 27:380–92. doi: 10.1016/j.molcel.2007.05.041

105. Peters AA, Buchanan G, Ricciardelli C, Bianco-Miotto T, Centenera MM, Harris JM, et al. Androgen receptor inhibits estrogen receptor-alpha activity and is prognostic in breast cancer. *Cancer Res*. (2009) 69:6131–40. doi: 10.1158/0008-5472.CAN-09-0452

106. Lehmann BD, Bauer JA, Chen X, Sanders ME, Chakravarthy AB, Shyr Y, et al. Identification of human triple-negative breast cancer subtypes and preclinical models for selection of targeted therapies. *J Clin Invest*. (2011) 121:2750–67. doi: 10.1172/JCI45014

107. Asemota S, Effah W, Young KL, Holt J, Cripe L, Ponnusamy S, et al. Identification of a targetable JAK-STAT enriched androgen receptor and androgen receptor splice variant positive triple-negative breast cancer subtype. *Cell Rep*. (2023) 42:113461. doi: 10.1016/j.celrep.2023.113461

108. Lehmann BD, Bauer JA, Schafer JM, Pendleton CS, Tang L, Johnson KC, et al. PIK3CA mutations in androgen receptor-positive triple negative breast cancer confer sensitivity to the combination of PI3K and androgen receptor inhibitors. *Breast Cancer Res*. (2014) 16:406. doi: 10.1186/s13058-014-0406-x

109. Luk PP, Weston JD, Yu B, Selinger CI, Ekmejian R, Eviston TJ, et al. Salivary duct carcinoma: Clinicopathologic features, morphologic spectrum, and somatic mutations. *Head Neck*. (2016) 38 Suppl 1:E1838–47. doi: 10.1002/hed.24332

110. Williams L, Thompson LDR, Seethala RR, Weinreb I, Assaad AM, Tuluc M, et al. Salivary duct carcinoma: the predominance of apocrine morphology, prevalence of histologic variants, and androgen receptor expression. *Am J Surg Pathol*. (2015) 39:705–13. doi: 10.1097/PAS.0000000000000413

111. Nasser SM, Faquin WC, Dayal Y. Expression of androgen, estrogen, and progesterone receptors in salivary gland tumors. Frequent expression of androgen receptor in a subset of Malignant salivary gland tumors. *Am J Clin Pathol*. (2003) 119:801–6. doi: 10.1309/RVTP1G0Q727WJUQD

112. Mitani Y, Rao PH, Maity SN, Lee Y-C, Ferrarotto R, Post JC, et al. Alterations associated with androgen receptor gene activation in salivary duct carcinoma of both sexes: potential therapeutic ramifications. *Clin Cancer Res*. (2014) 20:6570–81. doi: 10.1158/1078-0432.CCR-14-1746

113. Dalin MG, Desrichard A, Katabi N, Makarov V, Walsh LA, Lee K-W, et al. Comprehensive molecular characterization of salivary duct carcinoma reveals actionable targets and similarity to apocrine breast cancer. *Clin Cancer Res*. (2016) 22:4623–33. doi: 10.1158/1078-0432.CCR-16-0637

114. Morova T, McNeill DR, Lallous N, Gönen M, Dalal K, Wilson DM 3rd, et al. Androgen receptor-binding sites are highly mutated in prostate cancer. *Nat Commun*. (2020) 11:832. doi: 10.1038/s41467-020-14644-y

115. Hodgkin J, Zellan JD, Albertson DG. Identification of a candidate primary sex determination locus, fox-1, on the X chromosome of Caenorhabditis elegans. *Development*. (1994) 120:3681–9. doi: 10.1242/dev.120.12.3681

116. Jozwik KM, Carroll JS. Pioneer factors in hormone-dependent cancers. *Nat Rev Cancer*. (2012) 12:381–5. doi: 10.1038/nrc3263

117. Robinson JLL, Macarthur S, Ross-Innes CS, Tilley WD, Neal DE, Mills IG, et al. Androgen receptor driven transcription in molecular apocrine breast cancer is mediated by FoxA1. *EMBO J*. (2011) 30:3019–27. doi: 10.1038/emboj.2011.216

118. Barbieri CE, Baca SC, Lawrence MS, Demichelis F, Blattner M, Theurillat J-P, et al. Exome sequencing identifies recurrent SPOP, FOXA1 and MED12 mutations in prostate cancer. *Nat Genet*. (2012) 44:685–9. doi: 10.1038/ng.2279

119. Sahu B, Laakso M, Ovaska K, Mirtti T, Lundin J, Rannikko A, et al. Dual role of FoxA1 in androgen receptor binding to chromatin, androgen signalling and prostate cancer. *EMBO J*. (2011) 30:3962–76. doi: 10.1038/emboj.2011.328

120. Li Z, Tuteja G, Schug J, Kaestner KH. Foxa1 and Foxa2 are essential for sexual dimorphism in liver cancer. *Cell*. (2012) 148:72–83. doi: 10.1016/j.cell.2011.11.026

121. Yang L, Xie S, Jamaluddin MS, Altuwaijri S, Ni J, Kim E, et al. Induction of androgen receptor expression by phosphatidylinositol 3-kinase/Akt downstream substrate, FOXO3a, and their roles in apoptosis of LNCaP prostate cancer cells. *J Biol Chem*. (2005) 280:33558–65. doi: 10.1074/jbc.M504461200

122. Liu P, Li S, Gan L, Kao TP, Huang H. A transcription-independent function of FOXO1 in inhibition of androgen-independent activation of the androgen receptor in prostate cancer cells. *Cancer Res*. (2008) 68:10290–9. doi: 10.1158/0008-5472.CAN-08-2038

123. Zheng Y, Izumi K, Yao JL, Miyamoto H. Dihydrotestosterone upregulates the expression of epidermal growth factor receptor and ERBB2 in androgen receptor-positive bladder cancer cells. *Endocr Relat Cancer*. (2011) 18:451–64. doi: 10.1530/ERC-11-0010

124. Li Y, Zheng Y, Izumi K, Ishiguro H, Ye B, Li F, et al. Androgen activates β-catenin signaling in bladder cancer cells. *Endocr Relat Cancer*. (2013) 20:293–304. doi: 10.1530/ERC-12-0328

125. Lee E, Madar A, David G, Garabedian MJ, Dasgupta R, Logan SK. Inhibition of androgen receptor and β-catenin activity in prostate cancer. *Proc Natl Acad Sci U S A*. (2013) 110:15710–5. doi: 10.1073/pnas.1218168110

126. Zhao X, Shan Q, Xue H-H. TCF1 in T cell immunity: a broadened frontier. *Nat Rev Immunol*. (2022) 22:147–57. doi: 10.1038/s41577-021-00563-6

127. Vellano CP, White MG, Andrews MC, Chelvanambi M, Witt RG, Daniele JR, et al. Androgen receptor blockade promotes response to BRAF/MEK-targeted therapy. *Nature*. (2022) 606:797–803. doi: 10.1038/s41586-022-04833-8

128. Samarkina A, Youssef MK, Ostano P, Ghosh S, Ma M, Tassone B, et al. Androgen receptor is a determinant of melanoma targeted drug resistance. *Nat Commun*. (2023) 14:6498. doi: 10.1038/s41467-023-42239-w

129. Conforti F, Pala L, Bagnardi V, De Pas T, Martinetti M, Viale G, et al. Cancer immunotherapy efficacy and patients' sex: a systematic review and meta-analysis. *Lancet Oncol*. (2018) 19:737–46. doi: 10.1016/S1470-2045(18)30261-4

130. Conforti F, Pala L, Bagnardi V, Viale G, De Pas T, Pagan E, et al. Sex-based heterogeneity in response to lung cancer immunotherapy: A systematic review and meta-analysis. *J Natl Cancer Inst*. (2019) 111:772–81. doi: 10.1093/jnci/djz094

131. Wei Y, Li Y, Du Q, Peng X, Jin J, Guo H, et al. Effects of clinicopathological characteristics on the survival of patients treated with PD-1/PD-L1 inhibitor monotherapy or combination therapy for advanced cancer: A systemic review and meta-analysis. *J Immunol Res*. (2020) 2020:5269787. doi: 10.1155/2020/5269787

132. Takada K, Shimokawa M, Mizuki F, Takamori S, Takenaka T, Miura N, et al. Association between sex and outcomes in patients with non-small-cell lung cancer receiving combination chemoimmunotherapy as a first-line therapy: a systematic review and meta-analysis of randomized clinical trials. *Eur J Med Res*. (2022) 27:157. doi: 10.1186/s40001-022-00789-7

133. Yanagisawa T, Kawada T, Quhal F, Bekku K, Laukhtina E, Rajwa P, et al. Impact of sex on the efficacy of immune checkpoint inhibitors in kidney and urothelial cancers: a systematic review and meta-analysis. *World J Urol*. (2023) 41:1763–74. doi: 10.1007/s00345-023-04412-0

134. Shi Y, Au JS-K, Thongprasert S, Srinivasan S, Tsai C-M, Khoa MT, et al. A prospective, molecular epidemiology study of EGFR mutations in Asian patients with advanced non-small-cell lung cancer of adenocarcinoma histology (PIONEER). *J Thorac Oncol*. (2014) 9:154–62. doi: 10.1097/JTO.0000000000000033

135. Finn RS, Qin S, Ikeda M, Galle PR, Ducreux M, Kim T-Y, et al. Atezolizumab plus bevacizumab in unresectable hepatocellular carcinoma. *N Engl J Med*. (2020) 382:1894–905. doi: 10.1056/NEJMoa1915745

136. Zhu AX, Abbas AR, de Galarreta MR, Guan Y, Lu S, Koeppen H, et al. Molecular correlates of clinical response and resistance to atezolizumab in combination with bevacizumab in advanced hepatocellular carcinoma. *Nat Med*. (2022) 28:1599–611. doi: 10.1038/s41591-022-01868-2

137. Abou-Alfa GK, Lau G, Kudo M, Chan SL, Kelley RK, Furuse J, et al. Tremelimumab plus durvalumab in unresectable hepatocellular carcinoma. *NEJM Evid*. (2022) 1:EVIDoa2100070. doi: 10.1056/EVIDoa2100070

138. Doki Y, Ajani JA, Kato K, Xu J, Wyrwicz L, Motoyama S, et al. Nivolumab combination therapy in advanced esophageal squamous-cell carcinoma. *N Engl J Med*. (2022) 386:449–62. doi: 10.1056/NEJMoa2111380

139. André T, Tougeron D, Piessen G, de la Fouchardière C, Louvet C, Adenis A, et al. Neoadjuvant nivolumab plus ipilimumab and adjuvant nivolumab in localized deficient mismatch repair/microsatellite instability-high gastric or esophagogastric junction adenocarcinoma: the GERCOR NEONIPIGA phase II study. *J Clin Oncol*. (2023) 41:255–65. doi: 10.1200/JCO.22.00686

140. Bang Y-J, Van Cutsem E, Feyereislova A, Chung HC, Shen L, Sawaki A, et al. Trastuzumab in combination with chemotherapy versus chemotherapy alone for treatment of HER2-positive advanced gastric or gastro-oesophageal junction cancer (ToGA): a phase 3, open-label, randomised controlled trial. *Lancet*. (2010) 376:687–97. doi: 10.1016/S0140-6736(10)61121-X

141. Bamias A, Davis ID, Galsky MD, Arranz JÁ, Kikuchi E, Grande E, et al. Atezolizumab monotherapy versus chemotherapy in untreated locally advanced or metastatic urothelial carcinoma (IMvigor130): final overall survival analysis from a randomised, controlled, phase 3 study. *Lancet Oncol*. (2024) 25:46–61. doi: 10.1016/S1470-2045(23)00539-9

142. Hoffmann MJ, Gaisa NT, Nawroth R, Ecke TH. *Urothelial Carcinoma: Methods and Protocols*. New York, NY, USA: Springer Nature (2023). doi: 10.1007/978-1-0716-3291-8

143. Balar AV, Kamat AM, Kulkarni GS, Uchio EM, Boormans JL, Roumiguié M, et al. Pembrolizumab monotherapy for the treatment of high-risk non-muscle-invasive bladder cancer unresponsive to BCG (KEYNOTE-057): an open-label, single-arm, multicentre, phase 2 study. *Lancet Oncol*. (2021) 22:919–30. doi: 10.1016/S1470-2045(21)00147-9

144. Cumberbatch MGK, Jubber I, Black PC, Esperto F, Figueroa JD, Kamat AM, et al. Epidemiology of bladder cancer: A systematic review and contemporary update of risk factors in 2018. *Eur Urol*. (2018) 74:784–95. doi: 10.1016/j.eururo.2018.09.001

145. Bellmunt J, de Wit R, Vaughn DJ, Fradet Y, Lee J-L, Fong L, et al. Pembrolizumab as second-line therapy for advanced urothelial carcinoma. *N Engl J Med*. (2017) 376:1015–26. doi: 10.1056/NEJMoa1613683

146. Unger JM, Vaidya R, Albain KS, LeBlanc M, Minasian LM, Gotay CC, et al. Sex differences in risk of severe adverse events in patients receiving immunotherapy, targeted therapy, or chemotherapy in cancer clinical trials. *J Clin Oncol*. (2022) 40:1474–86. doi: 10.1200/JCO.21.02377

147. Berardi R, Rossi F, Papa R, Appetecchia M, Baggio G, Bianchini M, et al. Gender oncology: recommendations and consensus of the Italian Association of

Medical Oncology (AIOM). *ESMO Open*. (2024) 9:102243. doi: 10.1016/j.esmoop.2024.102243

148. Zhang X, Cheng L, Gao C, Chen J, Liao S, Zheng Y, et al. Androgen signaling contributes to sex differences in cancer by inhibiting NF-κB activation in T cells and suppressing antitumor immunity. *Cancer Res*. (2023) 83:906–21. doi: 10.1158/0008-5472.CAN-22-2405

149. Kwon H, Schafer JM, Song N-J, Kaneko S, Li A, Xiao T, et al. Androgen conspires with the CD8+ T cell exhaustion program and contributes to sex bias in cancer. *Sci Immunol*. (2022) 7:eabq2630. doi: 10.1126/sciimmunol.abq2630

150. Gandhi VD, Cephus J-Y, Norlander AE, Chowdhury NU, Zhang J, Ceneviva ZJ, et al. Androgen receptor signaling promotes Treg suppressive function during allergic airway inflammation. *J Clin Invest*. (2022) 132(4):e153397. doi: 10.1172/JCI153397

151. Walecki M, Eisel F, Klug J, Baal N, Paradowska-Dogan A, Wahle E, et al. Androgen receptor modulates Foxp3 expression in CD4+CD25+Foxp3+ regulatory T-cells. *Mol Biol Cell*. (2015) 26:2845–57. doi: 10.1091/mbc.E14-08-1323

152. Ejima A, Abe S, Shimba A, Sato S, Uehata T, Tani-Ichi S, et al. Androgens alleviate allergic airway inflammation by suppressing cytokine production in Th2 cells. *J Immunol*. (2022) 209:1083–94. doi: 10.4049/jimmunol.2200294

153. Kissick HT, Sanda MG, Dunn LK, Pellegrini KL, On ST, Noel JK, et al. Androgens alter T-cell immunity by inhibiting T-helper 1 differentiation. *Proc Natl Acad Sci U S A*. (2014) 111:9887–92. doi: 10.1073/pnas.1402468111

154. Cheng MI, Li JH, Riggan L, Chen B, Tafti RY, Chin S, et al. The X-linked epigenetic regulator UTX controls NK cell-intrinsic sex differences. *Nat Immunol*. (2023) 24:780–91. doi: 10.1038/s41590-023-01463-8

155. Tang M, Sun Y, Huang C-P, Chen L, Liu B, You B, et al. High dose androgen suppresses natural killer cytotoxicity of castration-resistant prostate cancer cells via altering AR/circFKBP5/miRNA-513a-5p/PD-L1 signals. *Cell Death Dis*. (2022) 13:746. doi: 10.1038/s41419-022-04956-w

156. Liu Q, You B, Meng J, Huang C-P, Dong G, Wang R, et al. Targeting the androgen receptor to enhance NK cell killing efficacy in bladder cancer by modulating ADAR2/circ_0001005/PD-L1 signaling. *Cancer Gene Ther*. (2022) 29:1988–2000. doi: 10.1038/s41417-022-00506-w

157. Zhao R, Chen X, Ma W, Zhang J, Guo J, Zhong X, et al. A GPR174-CCL21 module imparts sexual dimorphism to humoral immunity. *Nature*. (2020) 577:416–20. doi: 10.1038/s41586-019-1873-0

158. Aguilar-Pimentel JA, Cho Y-L, Gerlini R, Calzada-Wack J, Wimmer M, Mayer-Kuckuk P, et al. Increased estrogen to androgen ratio enhances immunoglobulin levels and impairs B cell function in male mice. *Sci Rep*. (2020) 10:18334. doi: 10.1038/s41598-020-75059-9

159. Altuwaijri S, Chuang K-H, Lai K-P, Lai J-J, Lin H-Y, Young FM, et al. Susceptibility to autoimmunity and B cell resistance to apoptosis in mice lacking androgen receptor in B cells. *Mol Endocrinol*. (2009) 23:444–53. doi: 10.1210/me.2008-0106

160. Ou Z, Wang Y, Liu L, Li L, Yeh S, Qi L, et al. Tumor microenvironment B cells increase bladder cancer metastasis via modulation of the IL-8/androgen receptor (AR)/MMPs signals. *Oncotarget*. (2015) 6:26065–78. doi: 10.18632/oncotarget.v6i28

161. Cioni B, Zaalberg A, van Beijnum JR, Melis MHM, van Burgsteden J, Muraro MJ, et al. Androgen receptor signalling in macrophages promotes TREM-1-mediated prostate cancer cell line migration and invasion. *Nat Commun*. (2020) 11:4498. doi: 10.1038/s41467-020-18313-y

162. Fang L-Y, Izumi K, Lai K-P, Liang L, Li L, Miyamoto H, et al. Infiltrating macrophages promote prostate tumorigenesis via modulating androgen receptor-mediated CCL4-STAT3 signaling. *Cancer Res*. (2013) 73:5633–46. doi: 10.1158/0008-5472.CAN-12-3228

163. Izumi K, Fang L-Y, Mizokami A, Namiki M, Li L, Lin W-J, et al. Targeting the androgen receptor with siRNA promotes prostate cancer metastasis through enhanced macrophage recruitment via CCL2/CCR2-induced STAT3 activation. *EMBO Mol Med*. (2013) 5:1383–401. doi: 10.1002/emmm.201202367

164. Huang C-K, Pang H, Wang L, Niu Y, Luo J, Chang E, et al. New therapy via targeting androgen receptor in monocytes/macrophages to battle atherosclerosis. *Hypertension*. (2014) 63:1345–53. doi: 10.1161/HYPERTENSIONAHA.113.02804

165. Lai J-J, Lai K-P, Chuang K-H, Chang P, Yu I-C, Lin W-J, et al. Monocyte/macrophage androgen receptor suppresses cutaneous wound healing in mice by enhancing local TNF-alpha expression. *J Clin Invest*. (2009) 119:3739–51. doi: 10.1172/JCI39335

166. Consiglio CR, Gollnick SO. Androgen receptor signaling positively regulates monocytic development. *Front Immunol*. (2020) 11:519383. doi: 10.3389/fimmu.2020.519383

167. Becerra-Díaz M, Strickland AB, Keselman A, Heller NM. Androgen and androgen receptor as enhancers of M2 macrophage polarization in allergic lung inflammation. *J Immunol*. (2018) 201:2923–33. doi: 10.4049/jimmunol.1800352

168. Xu P, Yang JC, Chen B, Nip C, Van Dyke JE, Zhang X, et al. Androgen receptor blockade resistance with enzalutamide in prostate cancer results in immunosuppressive alterations in the tumor immune microenvironment. *J Immunother Cancer*. (2023) 11:e006581. doi: 10.1136/jitc-2022–006581

169. Kohada Y, Kaiho Y, Takeda K, Kuromoto A, Ito J, Teishima J, et al. Analysis of the circulating myeloid-derived suppressor cells during androgen deprivation therapy for prostate cancer. *IJU Case Rep*. (2021) 4:367–70. doi: 10.1002/iju5.12351

170. Thompson MG, Peiffer DS, Larson M, Navarro F, Watkins SK. FOXO3, estrogen receptor alpha, and androgen receptor impact tumor growth rate and infiltration of dendritic cell subsets differentially between male and female mice. *Cancer Immunol Immunother*. (2017) 66:615–25. doi: 10.1007/s00262-017-1972-4

171. Consiglio CR, Udartseva O, Ramsey KD, Bush C, Gollnick SO. Enzalutamide, an androgen receptor antagonist, enhances myeloid cell-mediated immune suppression and tumor progression. *Cancer Immunol Res*. (2020) 8:1215–27. doi: 10.1158/2326-6066.CIR-19-0371

172. Hu C, Pang B, Lin G, Zhen Y, Yi H. Energy metabolism manipulates the fate and function of tumour myeloid-derived suppressor cells. *Br J Cancer*. (2020) 122:23–9. doi: 10.1038/s41416-019-0644-x

173. Tang J-J, Pan Y-F, Chen C, Cui X-L, Yan Z-J, Zhou D-X, et al. Androgens drive sexual dimorphism in liver metastasis by promoting hepatic accumulation of neutrophils. *Cell Rep*. (2022) 39:110987. doi: 10.1016/j.celrep.2022.110987

174. Markman JL, Porritt RA, Wakita D, Lane ME, Martinon D, Noval Rivas M, et al. Loss of testosterone impairs anti-tumor neutrophil function. *Nat Commun*. (2020) 11:1613. doi: 10.1038/s41467-020-15397-4

175. Scalerandi MV, Peinetti N, Leimgruber C, Cuello Rubio MM, Nicola JP, Menezes GB, et al. Inefficient N2-like neutrophils are promoted by androgens during infection. *Front Immunol*. (2018) 9:1980. doi: 10.3389/fimmu.2018.01980

176. Chuang K-H, Altuwaijri S, Li G, Lai J-J, Chu C-Y, Lai K-P, et al. Neutropenia with impaired host defense against microbial infection in mice lacking androgen receptor. *J Exp Med*. (2009) 206:1181–99. doi: 10.1084/jem.20082521

177. Ibáñez L, Jaramillo AM, Ferrer A, de Zegher F. High neutrophil count in girls and women with hyperinsulinaemic hyperandrogenism: normalization with metformin and flutamide overcomes the aggravation by oral contraception. *Hum Reprod*. (2005) 20:2457–62. doi: 10.1093/humrep/dei072

178. Alsamraae M, Costanzo-Garvey D, Teply BA, Boyle S, Sommerville G, Herbert ZT, et al. Androgen receptor inhibition suppresses anti-tumor neutrophil response against bone metastatic prostate cancer via regulation of TβRI expression. *Cancer Lett*. (2023) 579:216468. doi: 10.1016/j.canlet.2023.216468

179. Song W, Li L, He D, Xie H, Chen J, Yeh C-R, et al. Infiltrating neutrophils promote renal cell carcinoma (RCC) proliferation via modulating androgen receptor (AR) → c-Myc signals. *Cancer Lett*. (2015) 368:71–8. doi: 10.1016/j.canlet.2015.07.027

180. Lin C, Lin W, Yeh S, Li L, Chang C. Infiltrating neutrophils increase bladder cancer cell invasion via modulation of androgen receptor (AR)/MMP13 signals. *Oncotarget*. (2015) 6:43081–9. doi: 10.18632/oncotarget.v6i40

181. Mazzeo L, Ghosh S, Di Cicco E, Isma J, Tavernari D, Samarkina A, et al. ANKRD1 is a mesenchymal-specific driver of cancer-associated fibroblast activation bridging androgen receptor loss to AP-1 activation. *Nat Commun*. (2024) 15:1038. doi: 10.1038/s41467-024-45308-w

182. Clocchiatti A, Ghosh S, Procopio M-G, Mazzeo L, Bordignon P, Ostano P, et al. Androgen receptor functions as transcriptional repressor of cancer-associated fibroblast activation. *J Clin Invest*. (2018) 128:5531–48. doi: 10.1172/JCI99159

183. Chen L, Wang Y-Y, Li D, Wang C, Wang S-Y, Shao S-H, et al. LMO2 upregulation due to AR deactivation in cancer-associated fibroblasts induces non-cell-autonomous growth of prostate cancer after androgen deprivation. *Cancer Lett*. (2021) 503:138–50. doi: 10.1016/j.canlet.2021.01.017

184. Cioni B, Nevedomskaya E, Melis MHM, van Burgsteden J, Stelloo S, Hodel E, et al. Loss of androgen receptor signaling in prostate cancer-associated fibroblasts (CAFs) promotes CCL2- and CXCL8-mediated cancer cell migration. *Mol Oncol*. (2018) 12:1308–23. doi: 10.1002/1878-0261.12327

185. Liao C-P, Chen L-Y, Luethy A, Kim Y, Kani K, MacLeod AR, et al. Androgen receptor in cancer-associated fibroblasts influences stemness in cancer cells. *Endocr Relat Cancer*. (2017) 24:157–70. doi: 10.1530/ERC-16-0138

186. Leach DA, Need EF, Toivanen R, Trotta AP, Palethorpe HM, Tamblyn DJ, et al. Stromal androgen receptor regulates the composition of the microenvironment to influence prostate cancer outcome. *Oncotarget*. (2015) 6:16135–50. doi: 10.18632/oncotarget.v6i18

187. Torres-Estay V, Carreño DV, San Francisco IF, Sotomayor P, Godoy AS, Smith GJ. Androgen receptor in human endothelial cells. *J Endocrinol*. (2015) 224:R131–7. doi: 10.1530/JOE-14-0611

188. Guan Z, Li C, Fan J, He D, Li L. Androgen receptor (AR) signaling promotes RCC progression via increased endothelial cell proliferation and recruitment by modulating AKT → NF-κB → CXCL5 signaling. *Sci Rep*. (2016) 6:37085. doi: 10.1038/srep37085

189. Eisermann K, Broderick CJ, Bazarov A, Moazam MM, Fraizer GC. Androgen up-regulates vascular endothelial growth factor expression in prostate cancer cells via an Sp1 binding site. *Mol Cancer*. (2013) 12:7. doi: 10.1186/1476-4598-12-7

190. Boddy JL, Fox SB, Han C, Campo L, Turley H, Kanga S, et al. The androgen receptor is significantly associated with vascular endothelial growth factor and hypoxia sensing via hypoxia-inducible factors HIF-1a, HIF-2a, and the prolyl hydroxylases in human prostate cancer. *Clin Cancer Res*. (2005) 11:7658–63. doi: 10.1158/1078-0432.CCR-05-0460

191. Godoy A, Watts A, Sotomayor P, Montecinos VP, Huss WJ, Onate SA, et al. Androgen receptor is causally involved in the homeostasis of the human prostate endothelial cell. *Endocrinology*. (2008) 149:2959–69. doi: 10.1210/en.2007-1078

192. Yoshida S, Aihara K-I, Ikeda Y, Sumitomo-Ueda Y, Uemoto R, Ishikawa K, et al. Androgen receptor promotes sex-independent angiogenesis in response to ischemia and is required for activation of vascular endothelial growth factor receptor signaling. *Circulation*. (2013) 128:60–71. doi: 10.1161/CIRCULATIONAHA.113.001533

193. Yu J, Akishita M, Eto M, Ogawa S, Son B-K, Kato S, et al. Androgen receptor-dependent activation of endothelial nitric oxide synthase in vascular endothelial cells: role of phosphatidylinositol 3-kinase/akt pathway. *Endocrinology*. (2010) 151:1822–8. doi: 10.1210/en.2009-1048

194. Powles T, Yuen KC, Gillessen S, Kadel EE 3rd, Rathkopf D, Matsubara N, et al. Atezolizumab with enzalutamide versus enzalutamide alone in metastatic castration-resistant prostate cancer: a randomized phase 3 trial. *Nat Med*. (2022) 28:144–53. doi: 10.1038/s41591-021-01600-6

195. Pu Y, Xu M, Liang Y, Yang K, Guo Y, Yang X, et al. Androgen receptor antagonists compromise T cell response against prostate cancer leading to early tumor relapse. *Sci Transl Med*. (2016) 8(333):333ra47. doi: 10.1126/scitranslmed.aad5659

196. Arora VK, Schenkein E, Murali R, Subudhi SK, Wongvipat J, Balbas MD, et al. Glucocorticoid receptor confers resistance to antiandrogens by bypassing androgen receptor blockade. *Cell*. (2013) 155:1309–22. doi: 10.1016/j.cell.2013.11.012

197. Conforti F, Pala L, Pagan E, Bagnardi V, De Pas T, Queirolo P, et al. Sex-based dimorphism of anticancer immune response and molecular mechanisms of immune evasion. *Clin Cancer Res*. (2021) 27:4311–24. doi: 10.1158/1078-0432.CCR-21-0136

198. Cha H-R, Lee JH, Ponnazhagan S. Revisiting immunotherapy: A focus on prostate cancer. *Cancer Res*. (2020) 80:1615–23. doi: 10.1158/0008-5472.CAN-19-2948

199. Rebuzzi SE, Rescigno P, Catalano F, Mollica V, Vogl UM, Marandino L, et al. Immune checkpoint inhibitors in advanced prostate cancer: current data and future perspectives. *Cancers*. (2022) 14(5):1245. doi: 10.3390/cancers14051245

200. Kim S-E, Paik HY, Yoon H, Lee JE, Kim N, Sung M-K. Sex- and gender-specific disparities in colorectal cancer risk. *World J Gastroenterol*. (2015) 21:5167–75. doi: 10.3748/wjg.v21.i17.5167

frontiers | Frontiers in Immunology

TYPE Original Research
PUBLISHED 19 June 2024
DOI 10.3389/fimmu.2024.1433299

Check for updates

OPEN ACCESS

EDITED BY
Zhijia Xia,
Ludwig Maximilian University of Munich, Germany

REVIEWED BY
Chen Li,
Free University of Berlin, Germany
Zhengrui Li,
Shanghai Jiao Tong University, China

*CORRESPONDENCE
Shengshan Xu
xushengshan97@163.com
Zhuming Lu
lzm219@jnu.edu.cn

†These authors have contributed equally to this work and share first authorship

RECEIVED 15 May 2024
ACCEPTED 03 June 2024
PUBLISHED 19 June 2024

CITATION
Xu S, Fang H, Shen T, Zhou Y, Zhang D, Ke Y, Chen Z and Lu Z (2024) Causal association between immune cells and lung cancer risk: a two-sample bidirectional Mendelian randomization analysis. *Front. Immunol.* 15:1433299. doi: 10.3389/fimmu.2024.1433299

COPYRIGHT
© 2024 Xu, Fang, Shen, Zhou, Zhang, Ke, Chen and Lu. This is an open-access article distributed under the terms of the Creative Commons Attribution License (CC BY). The use, distribution or reproduction in other forums is permitted, provided the original author(s) and the copyright owner(s) are credited and that the original publication in this journal is cited, in accordance with accepted academic practice. No use, distribution or reproduction is permitted which does not comply with these terms.

Causal association between immune cells and lung cancer risk: a two-sample bidirectional Mendelian randomization analysis

Shengshan Xu[1*†], Huiying Fang[2,3†], Tao Shen[1], Yufu Zhou[1], Dongxi Zhang[1], Yongwen Ke[1], Zhuowen Chen[1] and Zhuming Lu[1*†]

[1]Department of Thoracic Surgery, Jiangmen Central Hospital, Jiangmen, Guangdong, China, [2]Department of Breast Cancer Center, Chongqing University Cancer Hospital, Chongqing, China, [3]Chongqing Key Laboratory for Intelligent Oncology in Breast Cancer (iCQBC), Chongqing University Cancer Hospital, Chongqing, China

Background: Previous studies have highlighted the crucial role of immune cells in lung cancer development; however, the direct link between immunophenotypes and lung cancer remains underexplored.

Methods: We applied two-sample Mendelian randomization (MR) analysis, using genetic variants as instruments to determine the causal influence of exposures on outcomes. This method, unlike traditional randomized controlled trials (RCTs), leverages genetic variants inherited randomly at conception, thus reducing confounding and preventing reverse causation. Our analysis involved three genome-wide association studies to assess the causal impact of 731 immune cell signatures on lung cancer using genetic instrumental variables (IVs). We initially used the standard inverse variance weighted (IVW) method and further validated our findings with three supplementary MR techniques (MR–Egger, weighted median, and MR-PRESSO) to ensure robustness. We also conducted MR–Egger intercept and Cochran's Q tests to assess heterogeneity and pleiotropy. Additionally, reverse MR analysis was performed to explore potential causality between lung cancer subtypes and identified immunophenotypes, using R software for all statistical calculations.

Results: Our MR analysis identified 106 immune signatures significantly associated with lung cancer. Notably, we found five suggestive associations across all sensitivity tests (P<0.05): CD25 on IgD- CD24- cells in small cell lung carcinoma (OR_{IVW} =0.885; 95% CI: 0.798–0.983; P_{IVW} =0.022); CD27 on IgD+ CD24+ cells in lung squamous cell carcinoma (OR_{IVW} =1.054; 95% CI: 1.010–1.100; P_{IVW} =0.015); CCR2 on monocyte cells in lung squamous cell carcinoma (OR_{IVW} =0.941; 95% CI: 0.898–0.987; P_{IVW} =0.012); CD123 on CD62L+ plasmacytoid dendritic cells (OR_{IVW} =0.958; 95% CI: 0.924–0.992; P_{IVW} =0.017) as well as on plasmacytoid dendritic cells (OR_{IVW} =0.958; 95% CI: 0.924–0.992; P_{IVW} =0.017) in lung squamous cell carcinoma.

Conclusion: This study establishes a significant genomic link between immune cells and lung cancer, providing a robust basis for future clinical research aimed at lung cancer management.

KEYWORDS

Mendelian randomization, lung cancer, immune cells, causal relationship, genome-wide association studies

1 Introduction

Lung cancer remains one of the most prevalent malignancies globally, ranking second in incidence and leading in cancer-related deaths (1–3). Due to its significant incidence and mortality, lung cancer represents a critical public health challenge, emphasizing the need for effective preventive strategies (4, 5). Identifying potential causal relationships between risk factors and lung cancer is essential for developing these strategies.

Recent advancements in tumor immunology have underscored the importance of understanding the role of immune cells within the lung cancer microenvironment. This understanding is crucial for advancing immunotherapy drug development. The immune system plays a complex role in tumorigenesis; it can suppress tumor growth by eliminating cancer cells, yet it can also promote tumor progression by providing growth and survival factors. For instance, the presence of CD3+ tumor-infiltrating lymphocytes is associated with improved overall survival (OS) in non-small cell lung cancer (NSCLC) (6) and hepatocellular carcinoma (7). Elevated levels of FoxP3+ Tregs are linked to poorer outcomes in several cancers, including melanoma and breast cancer. Conversely, an improvement in OS has been reported in colorectal and head and neck cancers, with variable results in lung cancer regarding disease-free survival (DFS) (8). B-cell infiltration has shown mixed outcomes across different cancers, enhancing survival in breast cancer (9) but presenting inconsistent results in melanoma, hepatocellular carcinoma, ovarian and head and neck cancers (10). Despite significant progress in immune cell research, the links between immunophenotypes and lung cancer remain inconsistent, often limited by small sample sizes, study design flaws, and unaddressed confounders (11–13). The introduction of genome-wide association studies (GWAS) has been transformative, providing new pathways to investigate cancer etiology (14, 15).

In this context, Mendelian randomization (MR), which uses genetic variants as instrumental variables (IVs) to establish causal relationships between exposures and outcomes, offers a powerful epidemiological tool (16). MR is advantageous because it uses genotypes that are fixed at conception, thus reducing bias from confounding factors and reverse causation (17, 18). This study employs a two-sample MR approach, using single nucleotide polymorphisms (SNPs) to evaluate the causal impact of immune cells on lung adenocarcinoma (LUAD), lung squamous cell carcinoma (LUSC), and small cell lung carcinoma (SCLC).

2 Materials and methods

2.1 Study design

Our two-sample MR study design is depicted in Figure 1. The validity of our MR analysis was ensured by meeting three essential criteria: the first criterion confirmed a significant link between the IVs and immunophenotypes. Second, the IVs were free from any relationships with confounding elements. Finally, outside of exposure elements, there was no impact of the IVs on outcomes through other pathways (19).

2.2 Genome-wide association study data sources for lung cancer

We obtained GWAS summary data for lung adenocarcinoma (LUAD), lung squamous cell carcinoma (LUSC), and small cell lung carcinoma (SCLC) from J. D. McKay et al. (20) via the IEU-OpenGWAS platform. The study involved 21,363 lung cancer patients, namely, 11,273 LUAD, 7,426 LUSC and 2,664 SCLC patients and 55,483, 55,627, and 21,444 controls (Supplementary Table 1). In the quality assurance stage, SNPs exhibiting suboptimal imputation (R2 < 0.3 or Info < 0.4) or a minor allele frequency greater than 0.01 were excluded. Approximately 8 million SNPs were retained for the GWAS.

2.3 Sources of immunity-wide GWAS data

We sourced comprehensive GWAS data for 731 immunophenotypes from the largest study to date, involving 3,757 Europeans (21). Approximately 22 million SNPs, adjusted for sex and age (including age squared), were genotyped with high-density arrays and imputed employing a reference panel based on Sardinian sequences (22).

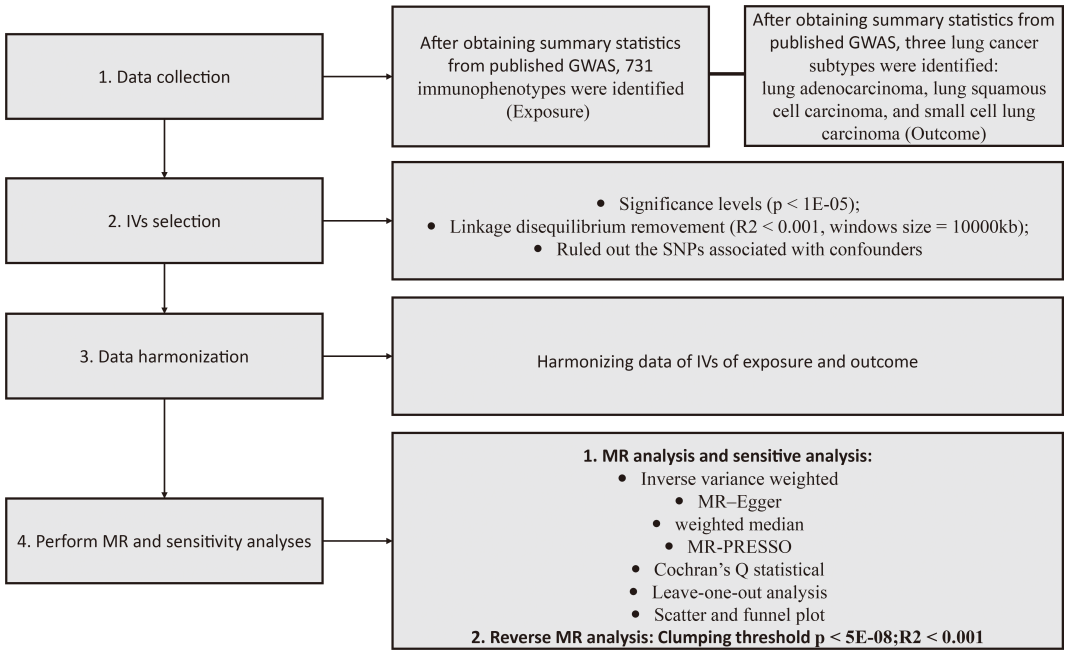

FIGURE 1
Illustrative schematic of the study methodology. GWAS, genome-wide association study; MR, Mendelian randomization; MR-PRESSO, MR pleiotropy residual sum and outlier test; IV, instrumental variables.

2.4 Selection criteria for IVs for 731 immunophenotypes

To identify sufficient SNPs (number >3) for both exposure and outcome analyses, we selected SNPs with genome-wide suggestive significance ($P<1\times10^{-5}$). This method is frequently utilized in MR research as it encompasses a wider array of variations, particularly when there are limited genome-wide significant SNPs available for analysis (23). Independent SNPs were identified using a clumping process with stringent criteria (r2 < 0.001, window size 10,000 kb) using the European 1000 Genomes reference panel (17). Following steps evaluated the robustness of these IVs in predicting causal effects using the F-test (24). The formula used in the design is outlined in Supplementary Table 2. An F-statistic greater than 10 typically signifies strong IVs, and any immunophenotypes with an F-statistic below 10 were discarded (25). The PhenoScannerV2 database (http://www.phenoscanner.medschl.cam.ac.uk/) was employed to identify and remove SNPs directly linked to cancer and other recognized confounders in cancer progression, such as smoking (26, 27) and alcohol consumption (28). In the reverse MR analysis, the threshold for statistical significance was established at $P < 5 \times 10^{-8}$, using a clumping parameter analogous to that used in the forward-direction analysis.

2.5 MR statistical analysis

In this MR study, we investigated the causal associations between immune cell profiles and different subtypes of lung cancer (LUAD, LUSC, SCLC) using the standard inverse variance weighted (IVW) approach. We also applied MR-Egger and weighted median methods as supplementary analyses to IVW, especially in scenarios where a significant fraction of variants (up to 50% or less) might originate from potentially invalid IVs (29, 30). Results were presented as odds ratios (ORs) with 95% confidence intervals (CIs). To identify any potential horizontal pleiotropy or outliers among the SNPs, we implemented the MR-Egger intercept test (29) and the Mendelian Randomization Pleiotropy Residual Sum and Outlier (MR-PRESSO) test (31). The reliability of our MR results was verified using the Cochran Q statistic to evaluate SNP heterogeneity (32). A sensitivity analysis called "leave-one-out" was conducted, where SNPs were sequentially removed. This analysis was complemented by applying the IVW-random method to the remaining set of SNPs to determine the influence of outlying variants on the findings (33). For thorough analysis of heterogeneity, we generated forest and scatter plots. A meta-analysis was then undertaken to elucidate the causal connections between the identified immunophenotypes and lung cancer subtypes by synthesizing MR data from two distinct cohorts (34). In instances of significant heterogeneity or pleiotropy, adjustments were made to the ORs and CIs for the meta-analysis. Based on the degree of heterogeneity observed, the choice was between a fixed-effects model (I2 ≤ 50%) and a random-effects model (I2 > 50%). The conclusions from the meta-analysis were considered the definitive causal relationships (35). To address concerns of multiple testing, a Bonferroni-corrected significance threshold of 6.84×10^{-5} (0.05/731 for the 731 immunophenotypes evaluated) was employed. P values between 6.84 × 10–5 and 0.05 were deemed indicative of suggestive causal links between the exposures and

outcomes. All analyses were conducted using the "TwoSampleMR" and "MRPRESSO" packages in R (version 4.2.0).

3 Results

3.1 Selection of IVs

Our two-sample MR analysis identified 106 immunophenotypes with IVs ranging from 4 to 103 SNPs, indicating suggestive associations at P<0.05. The IVs for each phenotype showed high potency, with F-statistics ranging from 19.546 upwards, confirming their reliability for MR studies.

3.2 Causal effects of immunophenotypes on 3 lung cancer subtypes

Using the IVW method, significant associations were found between 36 immunophenotypes and lung adenocarcinoma (LUAD), 33 with lung squamous cell carcinoma (LUSC), and 37 with small cell lung carcinoma (SCLC), as detailed in Figure 2 and Supplementary Table 3. Notably, certain immunophenotypes such as CD4 Treg %T cells in LUAD (OR_{IVW} =1.071; 95% CI: 1.015–1.131; P_{IVW} =0.013), Unsw mem AC in LUSC (OR_{IVW} =1.134; 95% CI: 1.047–1.228; P_{IVW} =0.002), and CD25 on CD4+ T cells in SCLC (OR_{IVW} =1.174; 95% CI: 1.053–1.310; P_{IVW} =0.004) were associated with increased risk, while CD27 on IgD- CD38br cells (OR_{IVW} =0.909; 95% CI: 0.841–0.984; P_{IVW} =0.018), SSC-A on HLA DR+ CD8br cells (OR_{IVW} =0.897; 95% CI: 0.824–0.977; P_{IVW} =0.012) and CD25 on resting Treg cells (OR_{IVW} =0.840; 95% CI: 0.733–0.963; P_{IVW} =0.013) showed protective effects across different subtypes (Table 1; Supplementary Figures 1-4). Additionally, the presence of CD27 on CD24+ CD27+ cells was associated with an increased risk across all three lung cancer subtypes (for LUAD, OR_{IVW} =1.039; 95% CI: 1.006–1.072; P_{IVW} =0.019; for LUSC, OR_{IVW} =1.041; 95% CI: 1.003–1.080; P_{IVW} =0.032; for SCLC, OR_{IVW} =1.072; 95% CI: 1.010–1.137; P_{IVW} =0.022). Similarly, CD27 on memory B cells also showed increased risks for lung cancer subtypes (for LUAD, OR_{IVW} =1.047; 95% CI: 1.009–1.086; P_{IVW} =0.014; for LUSC, OR_{IVW} =1.053; 95% CI: 1.008–1.099; P_{IVW} =0.020; for SCLC, OR_{IVW} =1.093; 95% CI: 1.002–1.192; P_{IVW} =0.045). The results imply a shared biological pathway among these subtypes of lung cancer, influenced by CD27 expression on CD24+ CD27+ cells and memory B cells, as outlined in Table 2 and Supplementary Figures 5-8. The genetic variants that clarify the links between these immunophenotypes and lung cancer are detailed in Supplementary Tables 4-15.

3.3 Sensitivity and pleiotropy analysis

Due to potential biases from weak instruments in the IVW approach, we expanded our study to incorporate additional sensitivity and pleiotropy assessments, with detailed findings listed in Supplementary Table 3. Noteworthy, pleiotropic effects were observed for SSC-A on HLA DR+ CD8br cells in LUSC ($P_{MR\text{-}PRESSO}$ Global =0.039). The combined outcomes from IVW, MR-Egger, and weighted median methods across immunophenotypes with suggestive links are displayed in Figure 3. Furthermore, we discerned five immunophenotypes with suggestive links that passed all sensitivity analyses (P<0.05) (Table 3; Supplementary Figures 9-12): CD25 on IgD- CD24- cells in SCLC (OR_{IVW} =0.885; 95% CI: 0.798–0.983; P_{IVW} =0.022), CD27 on IgD+ CD24+ cells in LUSC (OR_{IVW} =1.054; 95% CI: 1.010–1.100; P_{IVW} =0.015), CCR2 on monocyte cells in LUSC (OR_{IVW} =0.941; 95% CI: 0.898–0.987; P_{IVW} =0.012), CD123 on CD62L+ plasmacytoid dendritic cells (DCs) of LUSC (OR_{IVW} =0.958; 95% CI: 0.924–0.992; P_{IVW} =0.017), and CD123 on plasmacytoid DCs of LUSC (OR_{IVW} =0.958; 95% CI: 0.924–0.992; P_{IVW} =0.017). Additional validation through MR analysis utilized GWAS data for SCLC (ieu-a-988: 2,791 patients and 20,580 controls) and LUSC (ieu-a-989: 7,704 patients and 54,763 controls), with results detailed in Supplementary Tables 16, 17. Genetic variants clarifying the associations between these five immunophenotypes and lung cancer are summarized in Supplementary Tables 18-22. In reverse MR analyses, a suggestive link was observed for LUSC risk and CCR2 on monocyte cells (OR_{IVW} =0.888; 95% CI: 0.790–0.999; P_{IVW} =0.048). Lung cancer subtypes with at least two robust MR findings were included in the meta-analysis, whose results are compiled in Supplementary Table 23. Four immunophenotypes demonstrated a suggestive correlation with LUSC risk: CD27 on IgD+ CD24+ cells (OR = 1.0567; 95% CI: 1.0263 to 1.0880; P = 0.0002), CCR2 on monocyte cells (OR = 0.9483; 95% CI: 0.9238 to 0.9735; P < 0.0001), CD123 on CD62L+ plasmacytoid DCs (OR = 0.9629; 95% CI: 0.9414 to 0.9850; P = 0.0011), and CD123 on plasmacytoid DCs (OR = 0.9630; 95% CI: 0.9414 to 0.9850; P = 0.0011). Additionally, CD25 on IgD- CD24- cells was linked to a decreased risk of SCLC (OR = 0.8701; 95% CI: 0.8175 to 0.9260; P < 0.0001). The findings indicate the reliability of the causal relationship between the identified immune phenotype and subtypes of lung cancer.

4 Discussion

This MR study marks a significant advance in understanding the causal effects of immune cell signatures on lung cancer, focusing on three specific subtypes. Leveraging a robust two-sample MR framework that incorporates IVW, MR-Egger, and weighted median approaches, our study advances beyond earlier observational research that predominantly concentrated on correlations (36, 37). By utilizing the most comprehensive GWAS datasets currently available for the immunophenotyping of peripheral blood, our research significantly enhances the investigation into the connections between immune cells and disease, expanding the scope further than prior studies (38, 39). Moreover, we utilized meta-analysis to consolidate data from multiple studies, thereby enhancing the robustness of our conclusions. The discovery of 106 immune signatures, particularly five key associations such as CD25 on IgD- CD24- cells in SCLC and CCR2 on monocyte cells in LUSC, enriches our understanding of these cells' causal involvement in lung cancer.

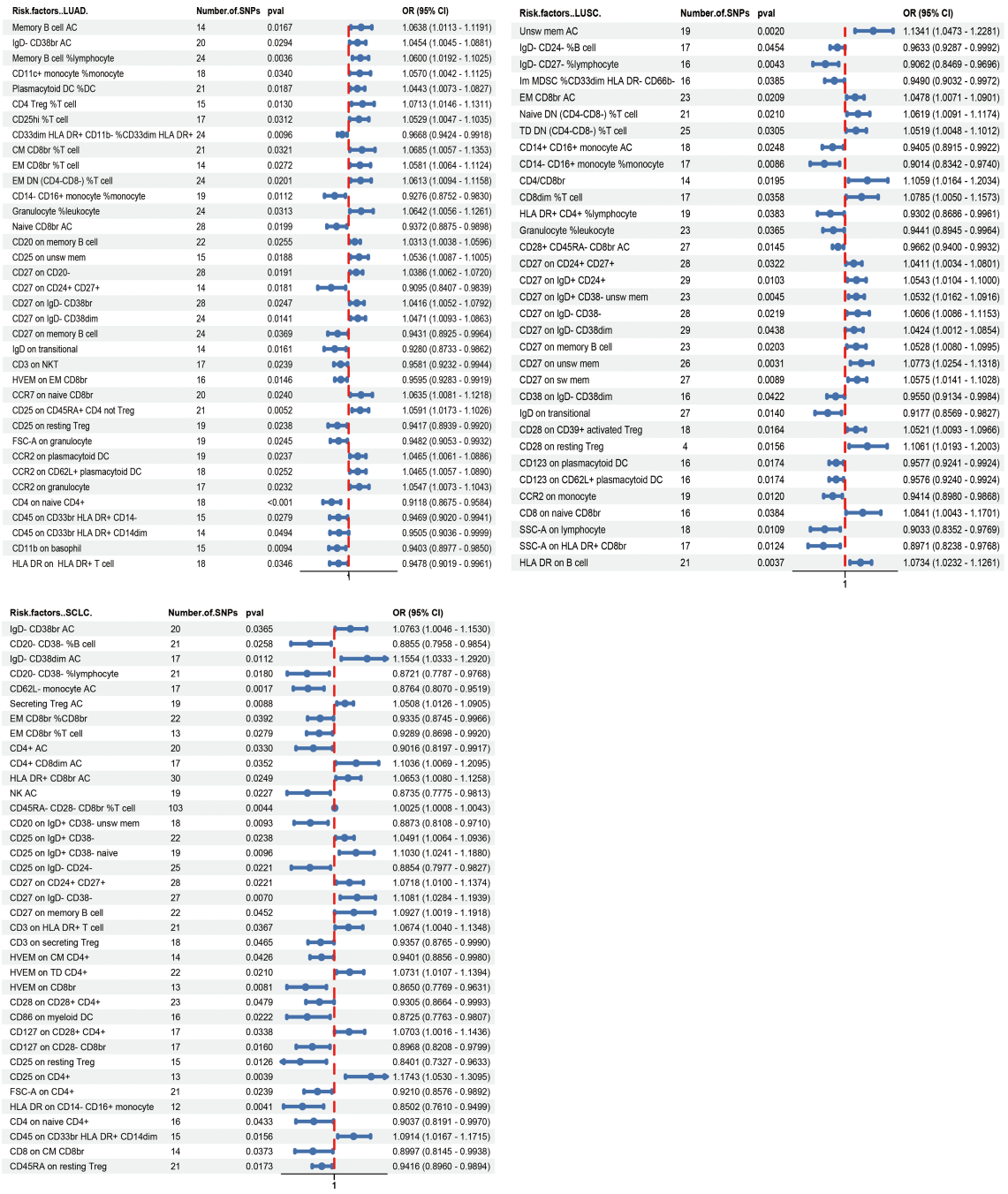

FIGURE 2
Forest plot depicting the Mendelian randomization analyses for associations between various immunophenotypes and lung cancer subtypes.

This research offers insightful hypotheses regarding the mechanistic roles of these immune signatures in lung cancer. The diverse interactions of immune cell subsets within the tumor microenvironment hint at their potential influence on tumor growth, apoptosis, and microenvironment dynamics. The distinct responses observed across lung cancer subtypes emphasize the specificity of immune reactions and suggest potential avenues for therapeutic intervention. Of the 106 immune signatures studied, five showed significant links to lung cancer subtypes, including CD25 on IgD- CD24- cells in SCLC, CD27 on IgD+ CD24+ cells in LUSC, CCR2 on monocyte cells in LUSC, CD123 on CD62L+ plasmacytoid DCs in LUSC, and CD123 on plasmacytoid DCs in LUSC, pointing to their roles in cancer development.

Significantly, our results emphasize the association of CCR2 with monocyte cells in LUSC. CCR2-positive monocytes are attracted to the LUSC tumor microenvironment in response to signals from cancer-associated fibroblasts via CCL2, contributing to an immunosuppressive environment (40, 41). Additionally, these monocytes, once present in inflamed lung areas, tend to reduce local CCL2 levels (42). Concurrent studies, like that by Lei Li and

TABLE 1 The most detrimental and protective factors for lung cancer subtypes.

Trait	Exposure	IVW		MR-Egger		Weighted median	
		OR (95% CI)	P-value	OR (95% CI)	P-value	OR (95% CI)	P-value
Lung adenocarcinoma	CD4 Treg %T cells	1.071 (1.015-1.131)	0.013	1.044 (0.965-1.129)	0.303	1.028(0.960-1.101)	0.427
Lung squamous cell carcinoma	Unsw mem AC	1.134 (1.047-1.228)	0.002	1.050 (0.862-1.280)	0.634	1.075(0.961-1.203)	0.205
Small cell lung carcinoma	CD25 on CD4+ T cells	1.174 (1.053-1.310)	0.004	0.985 (0.829-1.170)	0.866	1.195(1.037-1.378)	0.014
Lung adenocarcinoma	CD27 on IgD- CD38br cells	0.909 (0.841-0.984)	0.018	0.869 (0.608-1.243)	0.457	0.915(0.823-1.019)	0.105
Lung squamous cell carcinoma	SSC-A on HLA DR+ CD8br cells	0.897 (0.824-0.977)	0.012	0.973 (0.848-1.117)	0.703	0.954(0.860-1.059)	0.379
Small cell lung carcinoma	CD25 on resting Treg cells	0.840 (0.733-0.963)	0.013	0.794 (0.516-1.223)	0.315	0.772(0.639-0.934)	0.008

colleagues, have shown high CCL2 levels in the tumor microenvironment as predictors of survival in lung cancer patients (43). There is also evidence that CD24 facilitates interactions among B cells, with CD24-deficient mice displaying B-cell anomalies (44). High CD24 levels have been identified as adverse prognostic factors for progression-free and cancer-specific survival in NSCLC patients (45, 46). Moreover, this research highlights the essential role of DCs in LUSC, where tumor-infiltrating mature DCs correlate with better NSCLC prognosis (47, 48).

Despite its strengths, this study has limitations. Firstly, the cohort comprised mainly European individuals, which might limit the generalizability of the findings to more diverse populations. Second, the selection criteria for IVs were relatively permissive, establishing a significance level at $P < 1 \times 10^{-5}$, potentially leading to the incorporation of false-positive variants, potentially introducing bias into the results. Nevertheless, the F-statistics for all IVs exceeded 10, mitigating the concern for weak instrument bias. Third, despite our thorough examination for possible secondary phenotypes of IVs and the ability to conduct multiple sensitivity analyses, the potential for pleiotropy cannot be entirely dismissed. Fourthly, no immunophenotypes showed a statistically significant association with lung cancer risk after Bonferroni correction.

With further validation in larger populations and additional SNP analysis, identifying these immune signatures as biomarkers could enhance risk prediction, early detection, and prevention strategies in clinical settings. These advances may pave the way for more personalized cancer treatments. Additionally, the identified immune cells serve as promising targets for experimental investigation to determine their impact on lung cancer and the development of innovative immunotherapies. Specifically, focusing on the pathways that regulate these immune cells might facilitate the development of new immunotherapies for lung cancer. As immunotherapy

TABLE 2 Causal effects between CD27 on CD24+ CD27+ cells and CD27 on memory B cells with lung cancer subtypes.

Trait	Exposure	IVW		MR-Egger		Weighted median	
		OR (95% CI)	P-value	OR (95% CI)	P-value	OR (95% CI)	P-value
Lung adenocarcinoma	CD27 on CD24+ CD27 + cells	1.039 (1.006-1.072)	0.019	1.045 (0.992-1.101)	0.113	1.035(0.985-1.088)	0.175
Lung squamous cell carcinoma	CD27 on CD24+ CD27 + cells	1.041 (1.003-1.080)	0.032	1.021 (0.961-1.085)	0.507	1.042(0.987-1.099)	0.135
Small cell lung carcinoma	CD27 on CD24+ CD27 + cells	1.072 (1.010-1.137)	0.022	1.021 (0.923-1.130)	0.689	1.026(0.941-1.118)	0.563
Lung adenocarcinoma	CD27 on memory B cells	1.047 (1.009-1.086)	0.014	1.037 (0.978-1.100)	0.235	1.043(0.993-1.097)	0.093
Lung squamous cell carcinoma	CD27 on memory B cells	1.053 (1.008-1.099)	0.02	1.057 (0.986-1.133)	0.134	1.074(1.012-1.140)	0.018
Small cell lung carcinoma	CD27 on memory B cells	1.093 (1.002-1.192)	0.045	1.089 (0.946-1.254)	0.248	1.077(0.980-1.183)	0.123

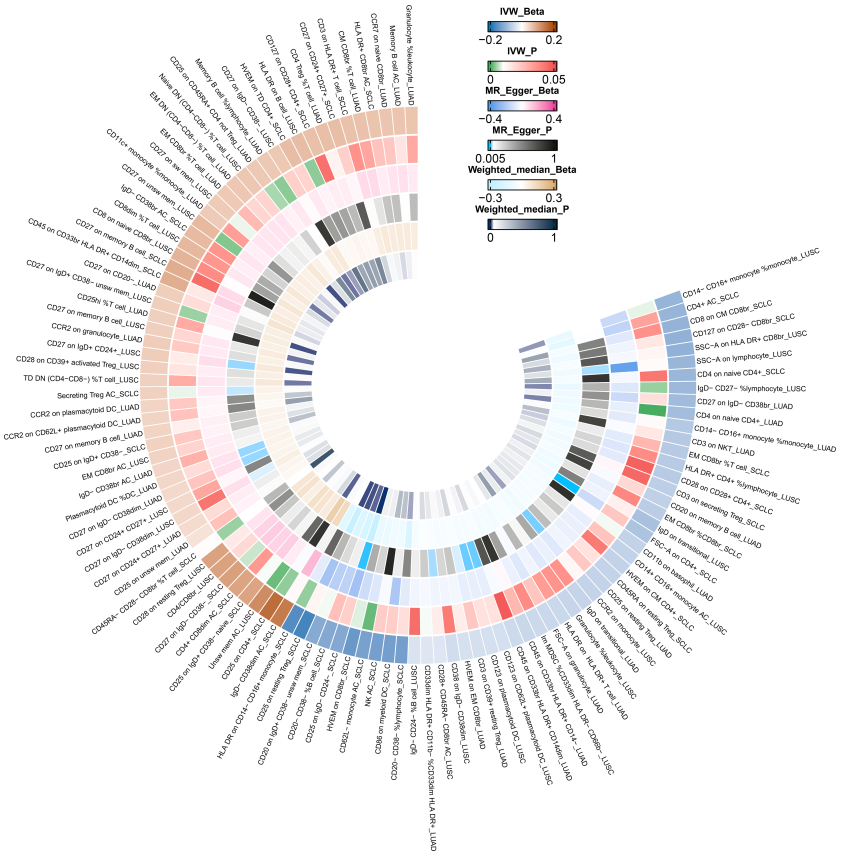

FIGURE 3
IVW Mendelian randomization estimates, MR−Egger estimates, and weighted-median estimates for the associations between immunophenotypes and lung cancer subtypes. IVW, inverse variance weighted; MR, Mendelian randomization.

increasingly becomes a cornerstone of cancer therapy, our results could provide significant contributions to the domain.

In summary, our research offers critical insights into the links between immune signatures and lung cancer, potentially leading to new therapeutic strategies. Continued investigation is essential to fully decipher these interactions and their implications for treating and preventing lung cancer.

5 Conclusion

In conclusion, this investigation marks the first comprehensive MR study to explore the causal links between immunophenotypes and specific lung cancer subtypes using genome-wide data, providing initial insights into how immune cell signatures might affect lung cancer risk. Utilizing the IVW method and various

TABLE 3 Statistically significant association between five potential immune cell signatures and lung cancer.

Trait	Exposure	IVW		MR-Egger		Weighted median	
		OR (95% CI)	P-value	OR (95% CI)	P-value	OR (95% CI)	P-value
Small cell lung carcinoma	CD25 on IgD- CD24- cells	0.885 (0.798-0.983)	0.022	0.790 (0.676-0.923)	0.007	0.772(0.672-0.887)	0
Lung squamous cell carcinoma	CD27 on IgD+ CD24+ cells	1.054 (1.010-1.100)	0.015	1.081 (1.015-1.152)	0.023	1.079(1.018-1.144)	0.011
Lung squamous cell carcinoma	CCR2 on monocyte cells	0.941 (0.898-0.987)	0.012	0.919 (0.864-0.978)	0.017	0.928(0.868-0.992)	0.029
Lung squamous cell carcinoma	CD123 on CD62L+ plasmacytoid dendritic cells	0.958 (0.924-0.992)	0.017	0.938 (0.896-0.981)	0.014	0.950(0.904-0.999)	0.047
Lung squamous cell carcinoma	CD123 on plasmacytoid dendritic cells	0.958 (0.924-0.992)	0.017	0.938 (0.896-0.981)	0.014	0.950(0.903-1.000)	0.049

sensitivity analyses, we identified strong associations between specific immune signatures such as CD25 on IgD- CD24- cells, CD27 on IgD+ CD24+ cells, CCR2 on monocyte cells, and CD123 on both CD62L+ and plasmacytoid dendritic cells with the development of lung cancer. Our results indicate that these immune cell signatures hold potential as valuable biomarkers for the early detection and prevention of lung cancer in clinical settings. These insights open avenues for further studies aimed at understanding the mechanisms through which these immune cells influence lung cancer and developing targeted therapies. While our study has successfully linked numerous immune cell signatures with the incidence of lung cancer, additional research is required to fully understand their roles in the pathogenesis of lung tumors.

Data availability statement

The original contributions presented in the study are included in the article/Supplementary Material. Further inquiries can be directed to the corresponding authors.

Ethics statement

SX, HF, TS, YZ, DZ, YK, ZC, and ZL assure that, for the manuscript "Causal association between immune cells and lung cancer risk: a two-sample bidirectional Mendelian randomization analysis", the following is fulfilled: 1) This material is the authors' original work, which has not been previously published elsewhere. 2) The paper is not currently being considered for publication elsewhere. 3) The paper reflects the authors' research and analysis truthfully and completely. 4) The paper properly credits the meaningful contributions of co-authors. 5) All the authors have been personally and actively involved in substantial work leading.

Author contributions

SX: Conceptualization, Data curation, Funding acquisition, Investigation, Methodology, Software, Writing – original draft, Writing – review & editing. HF: Conceptualization, Funding acquisition, Methodology, Writing – original draft, Writing – review & editing. TS: Formal analysis, Investigation, Writing – review & editing. YZ: Validation, Writing – review & editing. DZ: Writing – review & editing. YK: Writing – review & editing. ZC: Writing – review & editing. ZL: Conceptualization, Funding acquisition, Investigation, Methodology, Supervision, Validation, Writing – original draft, Writing – review & editing.

Funding

The author(s) declare financial support was received for the research, authorship, and/or publication of this article. This work was supported by the Technology Project of Jiangmen (Nos. 2220002000183, 2320002000933), the Medical Science Foundation of Jiangmen Central Hospital (J202401) and the Natural Science Foundation of Chongqing (No. cstc2020jcyj-msxmX0367).

Conflict of interest

The authors declare that the research was conducted in the absence of any commercial or financial relationships that could be construed as a potential conflict of interest.

Publisher's note

All claims expressed in this article are solely those of the authors and do not necessarily represent those of their affiliated organizations, or those of the publisher, the editors and the reviewers. Any product that may be evaluated in this article, or claim that may be made by its manufacturer, is not guaranteed or endorsed by the publisher.

Supplementary material

The Supplementary Material for this article can be found online at: https://www.frontiersin.org/articles/10.3389/fimmu.2024.1433299/full#supplementary-material

SUPPLEMENTARY FIGURE 1
Scatter plots illustrating genetic associations of six distinct immunophenotypes with lung cancer risk across different subtypes: **(A)** CD4 Treg %T cells in LUAD, **(B)** Unsw mem AC in LUSC, **(C)** CD25 on CD4+ T cells in SCLC, **(D)** CD27 on IgD- CD38br cells in LUAD, **(E)** SSC-A on HLA DR+ CD8br cells in LUSC, **(F)** CD25 on resting Treg cells in SCLC.

SUPPLEMENTARY FIGURE 2
Forest plots for six immunophenotypes in lung cancer. **(A)** CD4 Treg %T cells in LUAD, **(B)** Unsw mem AC in LUSC, **(C)** CD25 on CD4+ T cells in SCLC, **(D)** CD27 on IgD- CD38br cells in LUAD, **(E)** SSC-A on HLA DR+ CD8br cells in LUSC, **(F)** CD25 on resting Treg cells in SCLC.

SUPPLEMENTARY FIGURE 3
Leave-one-out plots for six immunophenotypes in lung cancer. **(A)** CD4 Treg %T cells in LUAD, **(B)** Unsw mem AC in LUSC, **(C)** CD25 on CD4+ T cells in SCLC, **(D)** CD27 on IgD- CD38br cells in LUAD, **(E)** SSC-A on HLA DR+ CD8br cells in LUSC, **(F)** CD25 on resting Treg cells in SCLC.

SUPPLEMENTARY FIGURE 4
Funnel plots for six immunophenotypes in lung cancer. **(A)** CD4 Treg %T cells in LUAD, **(B)** Unsw mem AC in LUSC, **(C)** CD25 on CD4+ T cells in SCLC, **(D)** CD27 on IgD- CD38br cells in LUAD, **(E)** SSC-A on HLA DR+ CD8br cells in LUSC, **(F)** CD25 on resting Treg cells in SCLC.

SUPPLEMENTARY FIGURE 5
Scatter plots depicting the genetic correlations between two immune markers and the risk of lung cancer among different subtypes. **(A)** CD27 on CD24+ CD27+ cells in LUAD, **(B)** CD27 on CD24+ CD27+ cells in LUSC, **(C)** CD27 on CD24+ CD27+ cells in SCLC, **(D)** CD27 on memory B cells in LUAD, **(E)** CD27 on memory B cells in LUSC, and **(F)** CD27 on memory B cells in SCLC.

SUPPLEMENTARY FIGURE 6
Forest plots for assessing the association of two immune phenotypes with lung cancer risk. **(A)** CD27 on CD24+ CD27+ cells in LUAD, **(B)** CD27 on CD24+ CD27+ cells in LUSC, **(C)** CD27 on CD24+ CD27+ cells in SCLC, **(D)** CD27 on memory B cells in LUAD, **(E)** CD27 on memory B cells in LUSC, and **(F)** CD27 on memory B cells in SCLC.

SUPPLEMENTARY FIGURE 7
Leave-one-out sensitivity plots for two immunophenotypes across lung cancer subtypes. **(A)** CD27 on CD24+ CD27+ cells in LUAD, **(B)** CD27 on CD24+ CD27+ cells in LUSC, **(C)** CD27 on CD24+ CD27+ cells in SCLC, **(D)** CD27 on memory B cells in LUAD, **(E)** CD27 on memory B cells in LUSC, and **(F)** CD27 on memory B cells in SCLC.

SUPPLEMENTARY FIGURE 8
Funnel plots for two immunophenotypes of lung cancer. **(A)** CD27 on CD24+ CD27+ cells in LUAD, **(B)** CD27 on CD24+ CD27+ cells in LUSC, **(C)** CD27 on CD24+ CD27+ cells in SCLC, **(D)** CD27 on memory B cells in LUAD, **(E)** CD27 on memory B cells in LUSC, and **(F)** CD27 on memory B cells in SCLC.

SUPPLEMENTARY FIGURE 9
Scatter plots depicting the genetic correlations between four immune markers and the risk of lung cancer among different subtypes. **(A)** CD25 on IgD- CD24- cells in SCLC, **(B)** CD27 on IgD+ CD24+ cells in LUSC, **(C)** CCR2 on monocyte cells in LUSC, and **(D)** CD123 on CD62L+ plasmacytoid dendritic cells in LUSC.

SUPPLEMENTARY FIGURE 10
Forest plots for assessing the association of five immune phenotypes with lung cancer risk. **(A)** CD25 on IgD- CD24- cells in SCLC, **(B)** CD27 on IgD+ CD24+ cells in LUSC, **(C)** CCR2 on monocyte cells in LUSC, **(D)** CD123 on CD62L+ plasmacytoid dendritic cells in LUSC, and **(E)** CD123 on plasmacytoid dendritic cells in LUSC.

SUPPLEMENTARY FIGURE 11
Leave-one-out sensitivity plots for five immunophenotypes across lung cancer subtypes. **(A)** CD25 on IgD- CD24- cells in SCLC, **(B)** CD27 on IgD+ CD24+ cells in LUSC, **(C)** CCR2 on monocyte cells in LUSC, **(D)** CD123 on CD62L+ plasmacytoid dendritic cells in LUSC, and **(E)** CD123 on plasmacytoid dendritic cells in LUSC.

SUPPLEMENTARY FIGURE 12
Funnel plots for five immunophenotypes of lung cancer. **(A)** CD25 on IgD- CD24- cells in SCLC, **(B)** CD27 on IgD+ CD24+ cells in LUSC, **(C)** CCR2 on monocyte cells in LUSC, **(D)** CD123 on CD62L+ plasmacytoid dendritic cells in LUSC, and **(E)** CD123 on plasmacytoid dendritic cells in LUSC.

References

1. Siegel RL, Miller KD, Jemal A. Cancer statistics, 2020. *CA: Cancer J Clin*. (2020) 70:7–30. doi: 10.3322/caac.21590

2. Bray F, Ferlay J, Soerjomataram I, Siegel RL, Torre LA, Jemal A. Global cancer statistics 2018: globocan estimates of incidence and mortality worldwide for 36 cancers in 185 countries. *CA: Cancer J Clin*. (2018) 68:394–424. doi: 10.3322/caac.21492

3. Cao P, Zhang Q, Wu S, Sullivan MA, Huang Y, Gong W, et al. Baseline differences in metabolic profiles of patients with lung squamous cell carcinoma responding or not responding to treatment with nanoparticle albumin-bound paclitaxel (Nab-paclitaxel). *Acta Materia Med*. (2023) 2:347–56. doi: 10.15212/amm-2023–0027

4. Yang H, Li C, Xie Q. Advances in the use of nanomaterials in tumor therapy: challenges and prospects. *Cancer Insight*. (2023) 2:20. doi: 10.58567/ci02020004

5. Wang J, Yuan Y, Tang L, Zhai H, Zhang D, Duan L, et al. Long non-coding rna-tmpo-as1 as cerna binding to let-7c-5p upregulates strip2 expression and predicts poor prognosis in lung adenocarcinoma. *Front Oncol*. (2022) 12:921200. doi: 10.3389/fonc.2022.921200

6. Zeng DQ, Yu YF, Ou QY, Li XY, Zhong RZ, Xie CM, et al. Prognostic and predictive value of tumor-infiltrating lymphocytes for clinical therapeutic research in patients with non-small cell lung cancer. *Oncotarget*. (2016) 7:13765–81. doi: 10.18632/oncotarget.7282

7. Yao W, He JC, Yang Y, Wang JM, Qian YW, Yang T, et al. The prognostic value of tumor-infiltrating lymphocytes in hepatocellular carcinoma: A systematic review and meta-analysis. *Sci Rep*. (2017) 7:7525. doi: 10.1038/s41598–017-08128–1

8. Shang B, Liu Y, Jiang SJ, Liu Y. Prognostic value of tumor-infiltrating foxp3+ Regulatory T cells in cancers: A systematic review and meta-analysis. *Sci Rep*. (2015) 5:15179. doi: 10.1038/srep15179

9. Schmidt M, Böhm D, von Törne C, Steiner E, Puhl A, Pilch H, et al. The humoral immune system has a key prognostic impact in node-negative breast cancer. *Cancer Res*. (2008) 68:5405–13. doi: 10.1158/0008–5472.can-07–5206

10. Siliņa K, Rulle U, Kalniņa Z, Linē A. Manipulation of tumor-infiltrating B cells and tertiary lymphoid structures: A novel anti-cancer treatment avenue? *Cancer Immunol Immunother: CII*. (2014) 63:643–62. doi: 10.1007/s00262–014-1544–9

11. Ganesan AP, Johansson M, Ruffell B, Yagui-Beltrán A, Lau J, Jablons DM, et al. Tumor-infiltrating regulatory T cells inhibit endogenous cytotoxic T cell responses to lung adenocarcinoma. *J Immunol (Baltimore Md: 1950)*. (2013) 191:2009–17. doi: 10.4049/jimmunol.1301317

12. Lizotte PH, Ivanova EV, Awad MM, Jones RE, Keogh L, Liu H, et al. Multiparametric profiling of non-small-cell lung cancers reveals distinct immunophenotypes. *JCI Insight*. (2016) 1:e89014. doi: 10.1172/jci.insight.89014

13. Kargl J, Busch SE, Yang GH, Kim KH, Hanke ML, Metz HE, et al. Neutrophils dominate the immune cell composition in non-small cell lung cancer. *Nat Commun*. (2017) 8:14381. doi: 10.1038/ncomms14381

14. Kunkle BW, Grenier-Boley B, Sims R, Bis JC, Damotte V, Naj AC, et al. Genetic meta-analysis of diagnosed Alzheimer's disease identifies new risk loci and implicates Aβ, tau, immunity and lipid processing. *Nat Genet*. (2019) 51:414–30. doi: 10.1038/s41588–019-0358–2

15. Wray NR, Ripke S, Mattheisen M, Trzaskowski M, Byrne EM, Abdellaoui A, et al. Genome-wide association analyses identify 44 risk variants and refine the genetic architecture of major depression. *Nat Genet*. (2018) 50:668–81. doi: 10.1038/s41588–018-0090–3

16. Li Z, Wang Q, Huang X, Wu Y, Fu R, Wen X, et al. A Mendelian randomization analysis reveals no relationship between periodontitis and coronary atherosclerosis. *Int Dental J*. (2024). doi: 10.1016/j.identj.2024.01.027

17. Hemani G, Zheng J, Elsworth B, Wade KH, Haberland V, Baird D, et al. The mr-base platform supports systematic causal inference across the human phenome. *eLife*. (2018) 7:e34408. doi: 10.7554/eLife.34408

18. Zheng T, Liu C, Wang Y, Zhou H, Zhou R, Zhu X, et al. Inflammatory cytokines mediating the effect of oral lichen planus on oral cavity cancer risk: A univariable and multivariable Mendelian randomization study. *BMC Oral Health*. (2024) 24:375. doi: 10.1186/s12903–024-04104–0

19. Davies NM, Holmes MV, Davey Smith G. Reading Mendelian randomization studies: A guide, glossary, and checklist for clinicians. *BMJ (Clinical Res ed)*. (2018) 362:k601. doi: 10.1136/bmj.k601

20. McKay JD, Hung RJ, Han Y, Zong X, Carreras-Torres R, Christiani DC, et al. Large-scale association analysis identifies new lung cancer susceptibility loci and heterogeneity in genetic susceptibility across histological subtypes. *Nat Genet*. (2017) 49:1126–32. doi: 10.1038/ng.3892

21. Orrù V, Steri M, Sidore C, Marongiu M, Serra V, Olla S, et al. Complex genetic signatures in immune cells underlie autoimmunity and inform therapy. *Nat Genet*. (2020) 52:1036–45. doi: 10.1038/s41588–020-0684–4

22. Sidore C, Busonero F, Maschio A, Porcu E, Naitza S, Zoledziewska M, et al. Genome sequencing elucidates sardinian genetic architecture and augments association analyses for lipid and blood inflammatory markers. *Nat Genet*. (2015) 47:1272–81. doi: 10.1038/ng.3368

23. Choi KW, Chen CY, Stein MB, Klimentidis YC, Wang MJ, Koenen KC, et al. Assessment of bidirectional relationships between physical activity and depression among adults: A 2-sample Mendelian randomization study. *JAMA Psychiatry*. (2019) 76:399–408. doi: 10.1001/jamapsychiatry.2018.4175

24. Shim H, Chasman DI, Smith JD, Mora S, Ridker PM, Nickerson DA, et al. A multivariate genome-wide association analysis of 10 ldl subfractions, and their response to statin treatment, in 1868 caucasians. *PloS One*. (2015) 10:e0120758. doi: 10.1371/journal.pone.0120758

25. Holsinger KE, Weir BS. Genetics in geographically structured populations: defining, estimating and interpreting F(St). *Nat Rev Genet*. (2009) 10:639–50. doi: 10.1038/nrg2611

26. Hecht SS, Hatsukami DK. Smokeless tobacco and cigarette smoking: chemical mechanisms and cancer prevention. *Nat Rev Cancer*. (2022) 22:143–55. doi: 10.1038/s41568–021-00423–4

27. Liang R, Li X, Li W, Zhu X, Li C. DNA methylation in lung cancer patients: opening a "Window of life" under precision medicine. *Biomed Pharmacother = Biomedecine Pharmacotherapie*. (2021) 144:112202. doi: 10.1016/j.biopha.2021.112202

28. GBD 2016 Alcohol Collaborators. Alcohol use and burden for 195 countries and territories, 1990–2016: A systematic analysis for the global burden of disease study 2016. *Lancet (London England)*. (2018) 392:1015–35. doi: 10.1016/s0140–6736(18)31310–2

29. Bowden J, Davey Smith G, Burgess S. Mendelian randomization with invalid instruments: effect estimation and bias detection through egger regression. *Int J Epidemiol*. (2015) 44:512–25. doi: 10.1093/ije/dyv080

30. Bowden J, Davey Smith G, Haycock PC, Burgess S. Consistent estimation in Mendelian randomization with some invalid instruments using a weighted median estimator. *Genet Epidemiol*. (2016) 40:304–14. doi: 10.1002/gepi.21965

31. Verbanck M, Chen CY, Neale B, Do R. Detection of widespread horizontal pleiotropy in causal relationships inferred from Mendelian randomization between complex traits and diseases. *Nat Genet*. (2018) 50:693–8. doi: 10.1038/s41588–018-0099–7

32. Cohen JF, Chalumeau M, Cohen R, Korevaar DA, Khoshnood B, Bossuyt PM. Cochran's Q test was useful to assess heterogeneity in likelihood ratios in studies of diagnostic accuracy. *J Clin Epidemiol*. (2015) 68:299–306. doi: 10.1016/j.jclinepi.2014.09.005

33. Burgess S, Thompson SG. Interpreting findings from Mendelian randomization using the Mr-Egger method. *Eur J Epidemiol*. (2017) 32:377–89. doi: 10.1007/s10654–017-0255-x

34. Niu W, Gu M. Adding Mendelian randomization to a meta-analysis-a burgeoning opportunity. *Tumor Biol: J Int Soc Oncodevelopmental Biol Med*. (2016) 37:1527–9. doi: 10.1007/s13277–015-4680–8

35. Jackson D, White IR, Riley RD. Quantifying the impact of between-study heterogeneity in multivariate meta-analyses. *Stat Med*. (2012) 31:3805–20. doi: 10.1002/sim.5453

36. Stankovic B, Bjørhovde HAK, Skarshaug R, Aamodt H, Frafjord A, Müller E, et al. Immune cell composition in human non-small cell lung cancer. *Front Immunol*. (2018) 9:3101. doi: 10.3389/fimmu.2018.03101

37. Riemann D, Cwikowski M, Turzer S, Giese T, Grallert M, Schütte W, et al. Blood immune cell biomarkers in lung cancer. *Clin Exp Immunol*. (2018) 195:179–89. doi: 10.1111/cei.13219

38. Feng Y, Liu X, Tan H. Causal association of peripheral immune cell counts and atrial fibrillation: A Mendelian randomization study. *Front Cardiovasc Med*. (2022) 9:1042938. doi: 10.3389/fcvm.2022.1042938

39. Gong Z, Liu Y, Ding F, Ba L, Zhang M. Natural killer cells-related immune traits and amyotrophic lateral sclerosis: A Mendelian randomization study. *Front Neurosci*. (2022) 16:981371. doi: 10.3389/fnins.2022.981371

40. Xiang H, Ramil CP, Hai J, Zhang C, Wang H, Watkins AA, et al. Cancer-associated fibroblasts promote immunosuppression by inducing ros-generating monocytic mdscs in lung squamous cell carcinoma. *Cancer Immunol Res*. (2020) 8:436–50. doi: 10.1158/2326–6066.cir-19–0507

41. Lesokhin AM, Hohl TM, Kitano S, Cortez C, Hirschhorn-Cymerman D, Avogadri F, et al. Monocytic ccr2(+) myeloid-derived suppressor cells promote immune escape by limiting activated cd8 T-cell infiltration into the tumor microenvironment. *Cancer Res*. (2012) 72:876–86. doi: 10.1158/0008–5472.can-11–1792

42. Maus UA, Wellmann S, Hampl C, Kuziel WA, Srivastava M, Mack M, et al. Ccr2-positive monocytes recruited to inflamed lungs downregulate local ccl2 chemokine levels. *Am J Physiol Lung Cell Mol Physiol*. (2005) 288:L350–8. doi: 10.1152/ajplung.00061.2004

43. Li L, Liu YD, Zhan YT, Zhu YH, Li Y, Xie D, et al. High levels of ccl2 or ccl4 in the tumor microenvironment predict unfavorable survival in lung adenocarcinoma. *Thorac Cancer*. (2018) 9:775–84. doi: 10.1111/1759–7714.12643

44. Nielsen PJ, Lorenz B, Müller AM, Wenger RH, Brombacher F, Simon M, et al. Altered erythrocytes and a leaky block in B-cell development in cd24/hsa-deficient mice. *Blood*. (1997) 89:1058–67.

45. Kristiansen G, Schlüns K, Yongwei Y, Denkert C, Dietel M, Petersen I. Cd24 is an independent prognostic marker of survival in nonsmall cell lung cancer patients. *Br J Cancer*. (2003) 88:231–6. doi: 10.1038/sj.bjc.6600702

46. Lee HJ, Choe G, Jheon S, Sung SW, Lee CT, Chung JH. Cd24, a novel cancer biomarker, predicting disease-free survival of non-small cell lung carcinomas: A retrospective study of prognostic factor analysis from the viewpoint of forthcoming (Seventh) new tnm classification. *J Thorac Oncol: Off Publ Int Assoc Study Lung Cancer*. (2010) 5:649–57. doi: 10.1097/JTO.0b013e3181d5e554

47. Inoshima N, Nakanishi Y, Minami T, Izumi M, Takayama K, Yoshino I, et al. The influence of dendritic cell infiltration and vascular endothelial growth factor expression on the prognosis of non-small cell lung cancer. *Clin Cancer Res*. (2002) 8:3480–6.

48. Goc J, Germain C, Vo-Bourgais TK, Lupo A, Klein C, Knockaert S, et al. Dendritic cells in tumor-associated tertiary lymphoid structures signal a th1 cytotoxic immune contexture and license the positive prognostic value of infiltrating cd8+ T cells. *Cancer Res*. (2014) 74:705–15. doi: 10.1158/0008–5472.can-13–1342

frontiers | Frontiers in Immunology

TYPE Original Research
PUBLISHED 19 June 2024
DOI 10.3389/fimmu.2024.1415736

Check for updates

OPEN ACCESS

EDITED BY
Jiaheng Xie,
Central South University, China

REVIEWED BY
Wenyi Jin,
City University of Hong Kong, Hong Kong SAR, China
Ziwei Liao,
Guangzhou Medical University, China

*CORRESPONDENCE
Qiang Zhao
zhaoqiang@tjmuch.com
Qiuping Dong
qdong@tmu.edu.cn
Baocheng Gong
bcgong@cmu.edu.cn

†These authors have contributed equally to this work and share first authorship

RECEIVED 11 April 2024
ACCEPTED 03 June 2024
PUBLISHED 19 June 2024

CITATION
Wang C, Tan J, Jin Y, Li Z, Yang J, Jia Y, Xia Y, Gong B, Dong Q and Zhao Q (2024) A mitochondria-related genes associated neuroblastoma signature - based on bulk and single-cell transcriptome sequencing data analysis, and experimental validation. *Front. Immunol.* 15:1415736. doi: 10.3389/fimmu.2024.1415736

COPYRIGHT
© 2024 Wang, Tan, Jin, Li, Yang, Jia, Xia, Gong, Dong and Zhao. This is an open-access article distributed under the terms of the Creative Commons Attribution License (CC BY). The use, distribution or reproduction in other forums is permitted, provided the original author(s) and the copyright owner(s) are credited and that the original publication in this journal is cited, in accordance with accepted academic practice. No use, distribution or reproduction is permitted which does not comply with these terms.

A mitochondria-related genes associated neuroblastoma signature - based on bulk and single-cell transcriptome sequencing data analysis, and experimental validation

Chaoyu Wang[1†], Jiaxiong Tan[1†], Yan Jin[1†], Zongyang Li[1], Jiaxing Yang[1], Yubin Jia[1], Yuren Xia[1], Baocheng Gong[1*], Qiuping Dong[2*] and Qiang Zhao[1*]

[1]Department of Pediatric Oncology, Tianjin Medical University Cancer Institute & Hospital, National Clinical Research Center for Cancer, Tianjin's Clinical Research Center for Cancer, Key Laboratory of Cancer Prevention and Therapy, Tianjin, China, [2]Department of Tumor Cell Biology, Tianjin Medical University Cancer Institute and Hospital, National Clinical Research Center for Cancer, Tianjin's Clinical Research Center for Cancer, Key Laboratory of Cancer Prevention and Therapy, Tianjin, China

Background: Neuroblastoma (NB), characterized by its marked heterogeneity, is the most common extracranial solid tumor in children. The status and functionality of mitochondria are crucial in regulating NB cell behavior. While the significance of mitochondria-related genes (MRGs) in NB is still missing in key knowledge.

Materials and methods: This study leverages consensus clustering and machine learning algorithms to construct and validate an MRGs-related signature in NB. Single-cell data analysis and experimental validation were employed to characterize the pivotal role of FEN1 within NB cells.

Results: MRGs facilitated the classification of NB patients into 2 distinct clusters with considerable differences. The constructed MRGs-related signature and its quantitative indicators, mtScore and mtRisk, effectively characterize the MRGs-related patient clusters. Notably, the MRGs-related signature outperformed MYCN in predicting NB patient prognosis and was adept at representing the tumor microenvironment (TME), tumor cell stemness, and sensitivity to the chemotherapeutic agents Cisplatin, Topotecan, and Irinotecan. FEN1, identified as the most contributory gene within the MRGs-related signature, was found to play a crucial role in the communication between NB cells and the TME, and in the developmental trajectory of NB cells. Experimental validations confirmed FEN1's significant influence on NB cell proliferation, apoptosis, cell cycle, and invasiveness.

Conclusion: The MRGs-related signature developed in this study offers a novel predictive tool for assessing NB patient prognosis, immune infiltration, stemness, and chemotherapeutic sensitivity. Our findings unveil the critical function of FEN1 in NB, suggesting its potential as a therapeutic target.

KEYWORDS

neuroblastoma, mitochondria, signature, prognosis, tumor immune microenvironment, FEN1

1 Introduction

Neuroblastoma (NB), the most common extracranial solid tumor in children, originates from embryonic neural crest cells and accounting for 15% of all childhood cancer deaths (1, 2). Characterized by its marked heterogeneity, NB presents a varied clinical spectrum. Patients with low to intermediate-risk NB exhibit a survival rate exceeding 95%, with some cases even showing spontaneous regression without the need for therapeutic intervention; while the long-term survival rate for individuals with high-risk NB remains dismal, falling below 50% (3). There is also significant intratumor heterogeneity between cells within the same individual NB patient, and a hallmark feature of high-risk NB is the presence of multiple cell subsets (4). Therefore, individualized precision treatment is particularly important in NB.

NB is traditionally classified as an immunosuppressive "cold" tumor, characterized by low immunogenicity and a poor response to immunotherapeutic interventions (5, 6). While recent advancements in immunotherapy have significantly improved survival rates for several highly immunogenic adult solid tumors, the treatment efficacy for NB remains substantially challenged by its immunosuppressive microenvironment, with the majority of pediatric patients deriving minimal benefit from current immunotherapeutic approaches (7, 8). Consequently, identifying strategies to transform the immunosuppressive "cold" tumor into an immunostimulatory "hot" tumor, conducive to tumor immune microenvironment (TIME) activation, represents a critical and urgent task for enhancing the efficacy of immunotherapy in the clinical management of NB.

Mitochondria are increasingly recognized for their critical roles in the etiology and advancement of malignant tumors, acting through a plethora of mechanisms (9, 10). Their status and functionality are crucial in regulating tumor cell apoptosis, cell cycle progression, metabolic pathways, and so on (11, 12). The interaction between tumor cells and the tumor microenvironment (TME) is also modulated by mitochondrial dynamics, which extends to affecting the efficacy of immune cells within the TME, facilitating immune evasion, and contributing to the development of resistance to treatments (13, 14). The significance of mitochondria-related genes (MRGs) in malignancies, including but not limited to NB, is evident through their substantial impact on patient prognosis (15–17). Research into MRGs-related prognostic signatures in cancers such as lung adenocarcinoma, stomach adenocarcinoma, and breast cancer has shown promising results (18–20). However, the exploration of such prognostic models in NB is still absent, underscoring a critical gap in current knowledge and presenting a clear opportunity for groundbreaking contributions to personalized cancer therapy.

This study embarks on constructing a prognostic model for NB using MRGs through a series of bioinformatics methods and machine learning algorithms, aiming to categorize patients for more targeted clinical management and therapeutic strategies. This study delves into the application of the MRGs-related signature to delineate the TIME of NB patients, assessing tumor cell stemness, and evaluating chemotherapy drug sensitivity. This comprehensive approach seeks to enhance precision in patient classification, thereby facilitating clinical benefits. Moreover, through single-cell transcriptomic analysis and experimental validation, this research explores the significant role of FEN1, the most critical molecule within the MRGs-related signature, in NB, suggesting FEN1 as a potential therapeutic target and offering new avenues for treatment strategies.

2 Materials and methods

2.1 Data sources

The data of bulk RNA sequencing in GSE49710 (21) and single cell RNA sequencing in GSE137804 (22) were acquired from Gene Expression Omnibus (GEO, https://www.ncbi.nlm.nih.gov/geo/). The microarray data E-MTAB-8248 was obtained from ArrayExpress database (https://www.ebi.ac.uk/biostudies/arrayexpress) (23). The genomic data of NBL (neuroblastoma) project in TARGET (Therapeutically Applicable Research to Generate Effective Treatments) database was downloaded from the Genomic Data Commons (GDC, https://portal.gdc.cancer.gov) (24). The Supplementary Table 1 presents the clinical baseline characteristics of the 4 datasets included in this study. The list of 2,030 MRGs was derived from the study by J. Chang, et al. (19).

2.2 Screening of differentially expressed genes

The "limma" package was used to screen differentially expressed genes (DEGs) in this study (25). Linear models were fitted using the lmFit function of the "limma" package and subsequently empirical Bayesian methods were applied using the eBayes function to stabilize the variance estimates. The P value < 0.05 and $|\log2 \text{Fold change (FC)}| > 1$ were defined as the threshold for DEGs in this study.

2.3 Unsupervised clustering

The consensus clustering method and "ConsensusClusterPlus" package was performed to discover stable and consistent cluster structures in this study (26). One to nine clustering iterations were implemented in the datasets. In each iteration, the data are randomly split into subsets and then the K-means clustering algorithm is applied. Using the consistency matrix, the optimal number of clusters was determined by evaluating the consistency and stability of clusters under different cluster numbers (27).

2.4 Survival analysis

This study employed the "survival" package to conduct Kaplan-Meier (K-M) survival analysis (28, 29), a non-parametric method used to estimate the survival function from time-to-event data. And

the "survminer" package was used to visualize survival estimates and generate the survival curves in this study (30).

2.5 Construction of prognostic signature

Prior to constructing a prognostic signature, this study initially employed K-M survival analysis and univariate Cox proportional hazards regression, both with OS as the endpoint, to screen for genes significantly associated with prognosis. In univariate COX regression models, the criteria were: P value < 0.05, and the 95% confidence interval (CI) of hazard ratio (HR) was consistently distributed ipsilateral to 1. Following the preliminary survival analysis, the machine learning algorithm Least Absolute Shrinkage and Selection Operator (LASSO) regression was utilized in GSE49710 dataset to determine the optimal number of genes and their respective coefficients for the prognostic model. The LASSO method was conducted using the "glmnet" package in R (31, 32). A score was obtained by linearly combining the mRNA expression levels of selected genes, each weighted by their respective coefficients derived from the LASSO regression analysis, which is termed the mitochondria-related risk score (mtScore).

2.6 Validation of prognostic signature

In order to evaluate the signature's predictive capability across diverse patient populations, the same statistical method was applied to the GSE49710 dataset for internal validation and to two independent datasets E-MTAB-8248 and TARGET-NBL for external validation. K-M survival analysis, receiver operating characteristic (ROC) curve analysis and correlation analysis of key clinical features based on mtScore were all validated in the above different datasets. The area under the curve (AUC) value of ROC curves exceeded 0.70 was considered to be efficient prediction (33).

2.7 Analysis of immune infiltration

For the comprehensive evaluation of the immune cell infiltration within the TME, 4 prominent computational methods were employed: ESTIMATE (Estimation of STromal and Immune cells in MAlignant Tumour tissues using Expression data) (34), EPIC (Estimating the Proportions of Immune and Cancer cells) (35), MCPcounter (Microenvironment Cell Populations-counter) (36), and CIBERSORT (Cell-type Identification By Estimating Relative Subsets Of RNA Transcripts) (37). In addition, we also evaluated the infiltration of 28 kinds of immune cells provided by the study from Q. Jia, et al. (38). The infiltration abundance in TME of 28 different types of immune cells was calculated using the single-sample Gene Set Enrichment Analysis (ssGSEA) algorithm as described by D. A. Barbie, et al. (39).

2.8 Calculation of mRNA expression-based stemness index

To quantify the degree of NB cellular dedifferentiation, which is indicative of stemness characteristics within tumor samples, we employed the mRNA expression-based stemness index (mRNAsi). This index was calculated following the methodology developed by T. M. Malta, et al., leveraging a machine learning model predicated on the one-class logistic regression (OCLR) algorithm (40). The gene expression profile of GSE49710 used in this study was mapped against the stemness signature to calculate the mRNAsi score for each sample. The mRNAsi scores range from 0 to 1, with higher values indicating a closer resemblance to the pluripotent state, thereby suggesting higher tumor cell stemness.

2.9 Assessment of chemotherapeutic response

To evaluate the predictive value of mtRisk for drug sensitivity, the Genomics of Drug Sensitivity in Cancer (GDSC, https://www.cancerrxgene.org/) database was utilized to analyze the drug response of patients with varying mtRisk levels to 3 commonly used clinical drugs for NB patients (Cisplatin, Topotecan, and Irinotecan) (41). The half-maximal inhibitory concentration (IC50) serving as a gauge for drug potency computed by the he "DrugResponse" package (42).

2.10 Single-cell data pre-processing and single-cell communication analysis

In this study, single-cell RNA sequencing data from 16 samples, comprising 160,847 cells, were utilized for single-cell analysis. Initial data processing included quality control measures, notably the exclusion of cells characterized by an exceptionally low number of detected genes or elevated mitochondrial gene expression, followed by normalization and mitigation of batch effects. Subsequent data analysis involved dimensionality reduction using the Uniform Manifold Approximation and Projection (UMAP) algorithm, as implemented in the "Seurat" package in R (43). Cell types were annotated based on the cell markers recommended within the GSE137804 dataset.

To investigate the expression patterns of the FEN1 gene within tumor cells, all tumor cells were categorized into two groups based on the median expression level of FEN1: FEN1 high expression group (FEN1-High) and FEN1 low expression group (FEN1-Low). Inter-cellular communication was analyzed separately for FEN1-High and FEN1-Low tumor cells in relation to other cells within the TME. This analysis was facilitated using CellPhoneDB software (version 2.0; Wellcome Sanger Institute, Hinxton, Cambridge, UK) (44).

2.11 Single-cell pseudotime trajectory analysis

This study further explored the dynamic expression of FEN1 within the developmental trajectory of NB tumor cells. This study employed pseudotime trajectory analysis to simulate the continuum of cell differentiation states and to chart the progression of tumor cells from their origin to mature states. For this analysis, the "Monocle" package in R was utilized (45). Cells were ordered in a pseudotime sequence, an inferred temporal continuum that represents the maturation or progression of cells through a developmental pathway, based on their gene expression profiles. FEN1 expression levels were then quantitatively assessed across the pseudotime to elucidate the gene's dynamic expression patterns during the development and differentiation of tumor cells. This differential expression analysis across pseudotime states aimed to identify significant changes in FEN1 expression, employing methods incorporated within the Monocle framework.

2.12 Overexpression and knockdown of FEN1 in NB cell

Human NB cell SH-SY5Y purchased from Meisen Chinese Tissue Culture Collections were cultured in Minimum Essential Medium/Ham's F12 (MEM/F12) medium supplemented with 10% fetal bovine serum (FBS) and 1% penicillin-streptomycin (PS), under a humidified atmosphere containing 5% CO_2 at 37°C to ensure healthy cell growth.

The overexpression (OE) and knockdown (KD) of FEN1 were achieved through infection procedure. Five distinct groups were structured in this study: Vector, FEN1, Scramble, sh-FEN1#1, and sh-FEN1#2. The pCDH-puro-FEN1 plasmid encoding human FEN1 was defined as OE of FEN1 and named "FEN1". The empty pCDH-CMV-MCS-EF1-puro plasmid was defined as a negative control (NC) for OE (named "Vector"). Two short hairpin RNAs (shRNAs) targeting FEN1 was synthesized and inserted into the plasmid to generate the FEN1 KD vectors defines plsi-puro-FEN1–1 and plsi-puro-FEN1–2 (named "sh-FEN1#1" and "sh-FEN1#2"). The shRNAs sequences are shown in Supplementary Table 2. The NC for KD was constructed from a scrambled shRNA inserted into plsi-ctrl-puro plasmid named "Scramble". The cloned plasmids and packaging plasmids (psPAX2 and pMD2-VSVG) were transfected into 293 T cells to synthesize the lentiviral particles. The NB cells were infected with the collected lentiviral particles. The total RNA and total protein of the infected NB cells were collected, and the efficiency of FEN1 OE and KD was verified by quantitative real-time PCR (qRT-PCR) and Western blot analysis.

2.13 Cell counting kit-8 assay

The NB cells were seeded in 96-well plates and cultured at 5% CO_2, 37°C atmospheres. The incubation was continued for 3 hours after adding 10 μL of cell counting kit-8 (CCK-8) solution (CA1210, Solarbio, China) to each well. The absorbance at 450 nm was measured at four distinct time points: 0-, 24-, 48-, and 72-hours post-adherence, using a microplate reader. The relative cell proliferation activity was calculated according to the following formula:

$$\text{Relative proliferation} = (OD_{450mm}^{OE\ or\ KD} - OD_{450mm}^{blank})/(OD_{450mm}^{NC} - OD_{450mm}^{blank})$$

2.14 Plate cloning assay

The single-cell suspensions were prepared using 0.25% trypsin-EDTA solution. The NB cells were seeded in 6-well plates at a density of 1,000 cells per well. After one week of culture, colonies were fixed with 4% paraformaldehyde for 15 minutes at room temperature and subsequently stained with 0.1% crystal violet for 15 minutes. Excess stain was removed by washing the plates with distilled water, and the plates were allowed to air dry. Colonies consisting of more than 50 cells were counted manually under a light microscope.

2.15 Mitochondrial membrane potential ΔΨm assay with JC-1

The mitochondrial membrane potential (MMP) is a critical parameter in the regulation of cell apoptosis, serving as a key indicator of cell health (46). The decline of MMP is a hallmark event in the early stage of apoptosis. The JC-1, an ideal fluorescent probe widely used to detect the MMP ΔΨm (47), was applied as an indicator of apoptosis in this study (C2003, Beyotime, China). In detail, each of the 5 groups of NB cells were trypsinized, collected, and washed twice with cold phosphate-buffered saline (PBS). Cells were resuspended in 500 μL of PBS and subsequently mixed with 500 μL of JC-1 staining solution. The mixture was then incubated for 20 minutes at 37°C in the dark to allow for staining. After incubation, cells were washed twice with dye buffer and immediately analyzed by flow cytometry. For the detection of JC-1 monomers, the analysis conducted through the FITC channel. Conversely, the assessment of JC-1 aggregates, was performed with the PE channel for detection. A minimum of 20,000 events were recorded for each sample.

2.16 Cell cycle analysis

The NB cells in 5 groups were harvested and washed twice with cold PBS. Cells were then fixed in 70% ethanol at 4°C overnight. After fixation, cells were washed with PBS and then resuspended in 100 μL of RNase A solution (CA1510, Solarbio, China) and incubated at 37°C for 30 minutes. The cells were stained with propidium iodide (PI) (CA1510, Solarbio, China) for 30 minutes at 4°C in the dark. For the analysis of DNA content, the emitted fluorescence of PI-stained cells was detected in the PE channel using

a flow cytometer. Data acquisition was performed for at least 20,000 cells per sample to ensure statistical relevance. The Dean-Jett-Fox model, a built-in algorithm within FlowJo, was employed to fit the DNA content histogram and quantitatively assess the proportions of cells in G0/G1, S, and G2/M phases of the cell cycle (48).

2.17 Transwell invasion assay

The invasive potential of the NB cells was assessed using Transwell permeable supports with 8.0 μm pore polystyrene membrane inserts. The upper surface of the insert was coated with 50 μL of Matrigel at a concentration of 2 mg/mL and allowed to solidify at 37°C incubator for 1 hour to form a thin layer of matrix barrier mimicking the extracellular matrix. Then, $1x10^5$ cells in 200 μL of serum-free medium were placed into the upper chamber, and 600 μL of medium containing 10% FBS was added to the lower chamber as a chemoattractant. After 48 hours of incubation at 37°C, non-invading cells on the upper surface of the membrane were gently removed with a cotton swab. Cells that had invaded through the Matrigel and reached the lower surface of the membrane were fixed with 4% paraformaldehyde, stained with 0.1% crystal violet, and counted under a light microscope in five randomly selected fields per well.

2.18 Statistical analysis

Continuous variables were expressed as mean ± standard deviation (SD). For comparisons between two groups, the Student's t-test was employed. Categorical variables were presented as numbers (percentages) and analyzed using the Chi-square test. Correlations between continuous variables were evaluated using Pearson's correlation coefficient. The P value < 0.05 was considered statistically significant for all tests. All experiment were performed in triplicate.

The bioinformatics analysis was carried out using R software (version 4.3.3; R Foundation for Statistical Computing, Vienna, Austria). Post-acquisition flow cytometry data processing was conducted using FlowJo (version 10.8.1; BD Biosciences, San Jose, California USA). Part of the statistical analysis and the generation of corresponding figures were performed with GraphPad Prism (version 9.0; GraphPad Software, San Diego, California USA). Image processing and assembly tasks were accomplished using Adobe Photoshop 2023 and Adobe Illustrator 2023 (Adobe Systems Incorporated, San Jose, California USA).

3 Results

3.1 MRGs-based clustering of NB patients into 2 distinct clusters with unique differences

In this study, we identified 1,694 DEGs between NB patients with and without MYCN amplification in GSE49710 dataset, employing a threshold of P value < 0.05 and |log2FC| > 1, with 730 up-regulated genes and 964 down-regulated genes (Figure 1A). Intersection of these 1,694 MYCN status DEGs with 2,030 MRGs yielded 105 MRGs specifically relevant to NB (Figure 1B). Unsupervised consensus clustering based on the expression profiles of 105 MRGs in the GSE49710 dataset stratified 498 NB patients. The consensus cumulative distribution function (CDF) plot suggested that the optimal k value was 2 (Figure 1C). Consequently, 498 NB patients were categorized into 2 clusters: Cluster A with 361 patients and Cluster B with 137 patients (Figure 1D).

Significant disparities were observed between patients in Clusters A and B in terms of survival, clinical characteristics, and immune cell infiltration. Principal component analysis (PCA) distinctly separated the 2 clusters, validating the classification robustness (Figure 2A). The expression heatmap of the 105 MRGs in Clusters A and B was showed in Supplementary Figure 1. The K-M survival analysis indicated that NB patients in Cluster B had significantly worse overall survival (OS) compared to those in Cluster A (P < 0.001) (Figure 2B). Further analysis of clinical features showed substantial statistical differences between the 2 clusters in key clinical indicators (Figure 2C). Patients for progression and INSS stage 4 (an independent risk factor for NB) (49) were predominantly found in Cluster B (P < 0.0001 for both). Similarly, patients with clinical risk factors, MYCN amplification, and age below 18 months (a factor associated with poorer prognosis) were significantly concentrated in Cluster B (P < 0.0001 for all comparisons). Detailed relations between each clinical characteristic and distribution across Clusters A and B are depicted using Sankey diagrams in Supplementary Figure 2. Additionally, a marked difference in the TME between Clusters A and B was uncovered through 4 distinct immune infiltration analysis algorithms. The ESTIMATE algorithm suggested that patients in Cluster A had higher scores overall in terms of ESTIMATE, immune, and stromal scores compared to Cluster B (Figure 2D). Results from the EPIC algorithm revealed significant statistical differences in cell proportions of all 7 cell types between the two clusters (Figure 2E). In parallel, the analysis using MCPcounter indicated that the cell abundance of T cells, Cytotoxic lymphocytes, B lineage, NK cells, Monocytic lineage, and Myeloid dendritic cells in Cluster A was statistically higher compared to Cluster B (Figure 2F). Finally, the CIBERSORT analysis also reflected that Cluster A patients exhibited higher cell proportions for various immune cells compared to Cluster B (Figure 2G).

To further validate the broad applicability of the clustering based on MRGs, the same cluster analysis was conducted on the E-MTAB-8248 dataset. The consensus CDF plot suggested an optimal number of clusters k = 2 (Figure 3A), subdividing the 223 NB children in the dataset into 138 in Cluster A and 85 in Cluster B (Figure 3B). The heatmap of the expression of 105 MRGs for Clusters A and B within the E-MTAB-8248 dataset is presented in Supplementary Figure 3. The PCA confirmed robust separation between the clusters (Figure 3C). Echoing the results from the GSE49710 dataset, K-M survival analysis within E-MTAB-8248 also demonstrated poorer OS for patients in Cluster B (P<0.001) (Figure 3D). Substantial differences were also observed between clusters A and B in important clinical characteristics within E-

10.3389/fimmu.2024.1415736

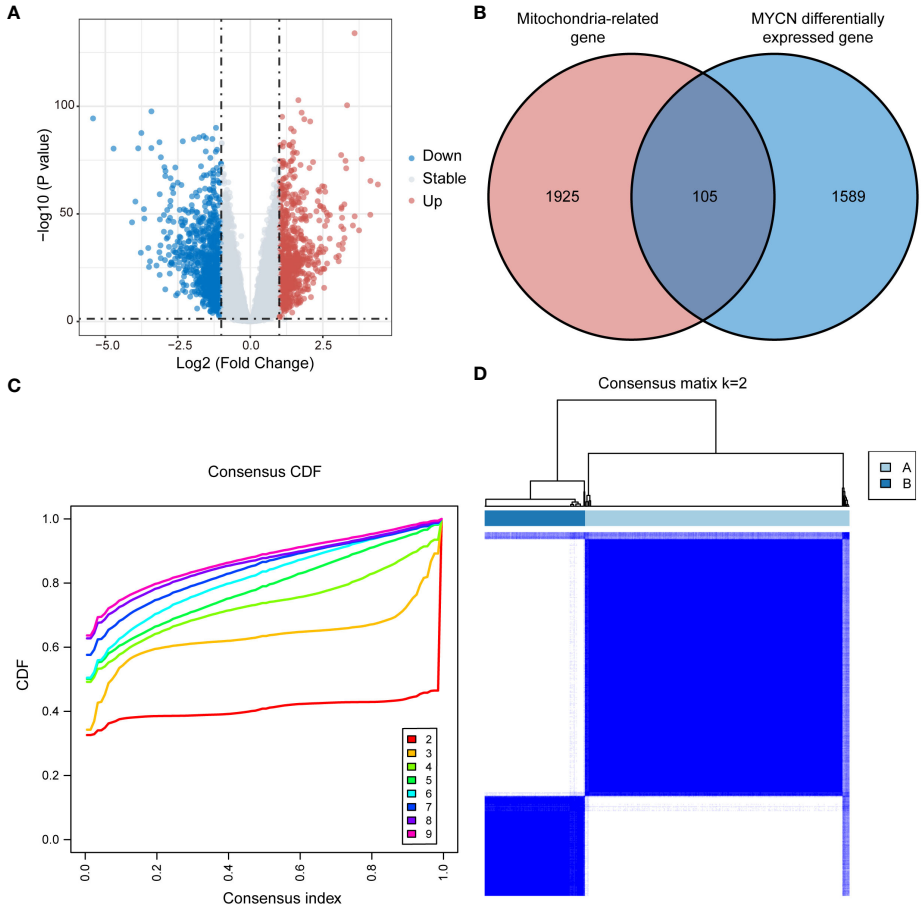

FIGURE 1
Consensus clustering in GSE49710 based on MRGs associated with NB. **(A)** Volcano plot displaying DEGs between MYCN-amplified and non-amplified NB patients in GSE49710 (Genes with P value < 0.05 and |log2FC| > 1 are highlighted). **(B)** Venn diagram illustrating the intersection of MYCN status DEGs with MRGs, identifying 105 MRGs specifically associated with neuroblastoma. **(C, D)** Consensus clustering of NB patients into clusters A and B based on the expression of 105 MRGs, with k=2 as the optimal cluster number. MRGs, mitochondria-related genes; NB, neuroblastoma; DEGs, differentially expressed genes; FC, fold change; CDF, cumulative distribution function.

MTAB-8248 (Figure 3E). Chromosome 1p aberrations, recognized as markers of poor prognosis in NB patients (49), were more frequently observed in patients of Cluster B (P<0.0001). Similarly, patients associated with poor prognostic factors such as INSS stage 4, MYCN amplification, and age under 18 months were predominantly found in Cluster B (all comparisons P<0.0001). Supplementary Figure 4 employs Sankey diagrams to detail the distribution of these significant clinical features between clusters A and B in the E-MTAB-8248 dataset.

3.2 Construction and internal validation of the MRGs-related signature

In an effort to delineate the 2 clusters formed by MRG expression, this study constructed an MRGs-related signature to quantify the distinction through a scoring mechanism. Initially, 1,497 DEGs (618 up-regulated genes and 879 down-regulated genes) between Clusters A and B in the GSE49710 dataset (Figure 4A), and 830 DEGs (369 up-regulated genes and 461 down-regulated genes) between Clusters A and B in the E-MTAB-8248 dataset (Figure 4B) were identified (using a threshold of P < 0.05 and |log2FC| > 1). A Venn diagram depicts the 33 intersecting genes found between the 1,497 DEGs in GSE49710, the 830 DEGs in E-MTAB-8248, and the 105 MRGs specific to NB (Figure 4C). Further, the prognostic implications of the 33 intersecting genes were validated in both the GSE49710 and E-MTAB-8248 datasets, using K-M analysis with OS as the endpoint, categorized by the gene median expression. In GSE49710, K-M analysis revealed statistical survival differences between patients with high and low expression of each of the 33 genes (Supplementary Figure 5). Similarly, in the E-MTAB-8248 dataset, 31 of the 33 genes showed statistically significant survival correlations in K-M analysis (Supplementary Figure 6). Subsequent analysis involved univariate Cox regression to further screen for genes significantly associated with prognosis. Each of the 31 genes underwent univariate Cox regression analysis with OS as the endpoint in both GSE49710 and E-MTAB-8248 (Figure 4D), with only one gene (marked in red in Figure 4D) not showing statistical significance in E-MTAB-8248. Consequently, the remaining 30 genes

10.3389/fimmu.2024.1415736

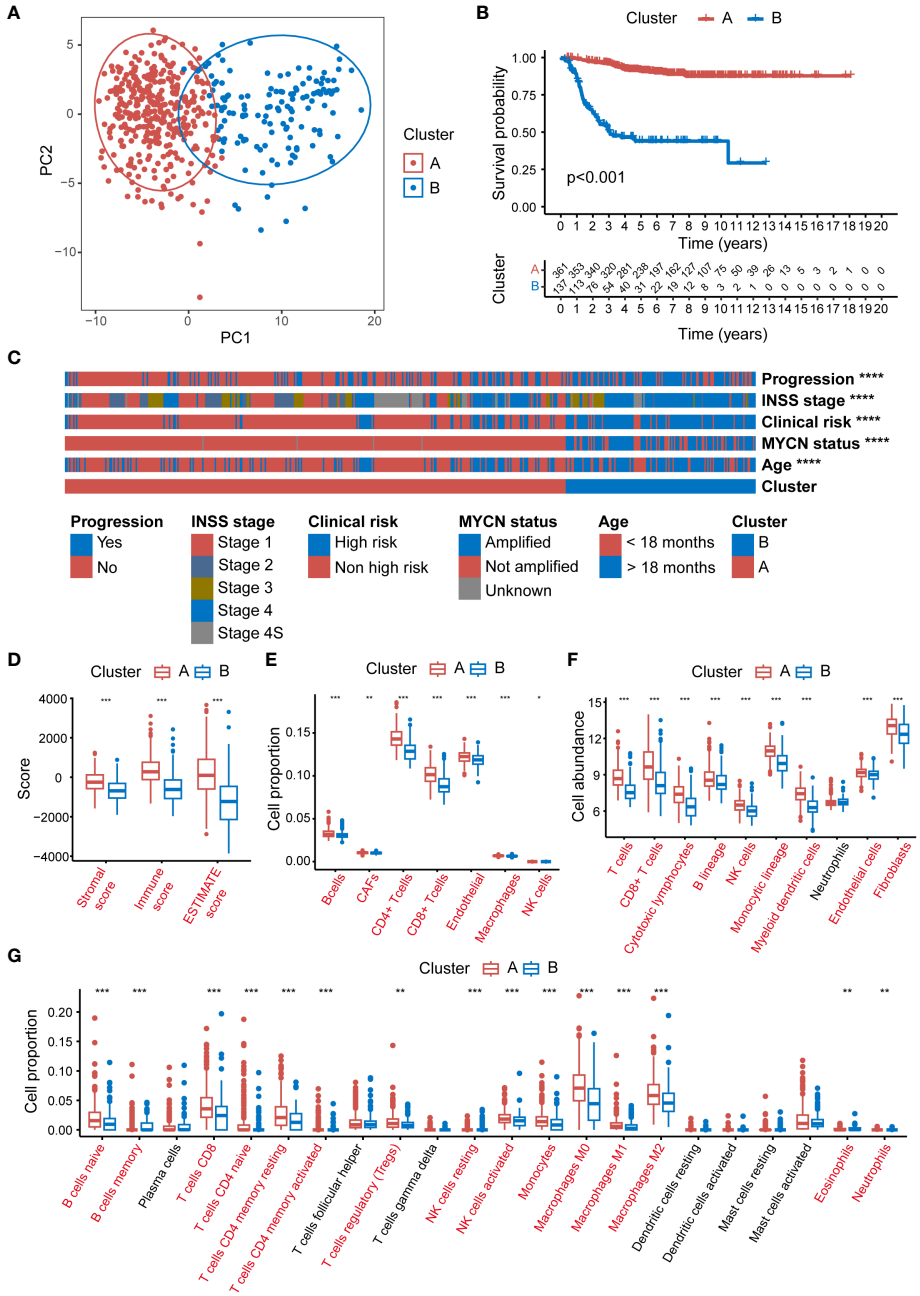

FIGURE 2
Significant disparities between Cluster A and B in GSE49710. **(A)** The PCA scatter plot demonstrating the segregation of NB patients into 2 clusters, Cluster A (blue) and B (red), based on MRG expression profiles. **(B)** The Kaplan-Meier survival curves depicting the OS probability for patients in clusters A and B. **(C)** The heatmap displaying the distribution of progression status, INSS stage, clinical risk, MYCN amplification status, and age in patients within Clusters A and B. **(D)** Box plots representing the ESTIMATE scores in Clusters A and B. **(E)** Box plots illustrating the proportion of various immune cells as analyzed by the EPIC algorithm in Clusters A and B. **(F)** Box plots depicting the cell abundance of different immune cell types as analyzed by the MCPcounter algorithm. **(G)** Box plots detailing the cell proportion of various immune cells as analyzed by the CIBERSORT algorithm in Cluster A and B. PCA, principal component analysis; NB, neuroblastoma; MRG, mitochondria-related genes; OS, overall survival; ESTIMATE, Estimation of STromal and Immune cells in MAlignant Tumour tissues using Expression data; EPIC, Estimating the Proportions of Immune and Cancer cells; MCPcounter, Microenvironment Cell Populations-counter; CIBERSORT, Cell-type Identification By Estimating Relative Subsets Of RNA Transcripts. (*P<0.05, **P<0.01, ***P<0.001, ****P<0.0001).

proceeded to the next phase of analysis. The LASSO regression analysis was applied in GSE49710 to refine the selection to 10 genes, assigning coefficients to each (Figures 4E, F). The mtScore was defined as the linear combination of the mRNA expression levels of the 10 genes, weighted by their respective coefficients provided by LASSO analysis within GSE49710. The formula is as follows: mtScore = (-0.243142218 × the expression of DNM3) + (-0.173523906 × the expression of AGBL4) + (-0.156591746 × the expression of CROT) + (-0.155479922 × the expression of SLC22A4) + (-0.074329063 × the expression of TP63) +

10.3389/fimmu.2024.1415736

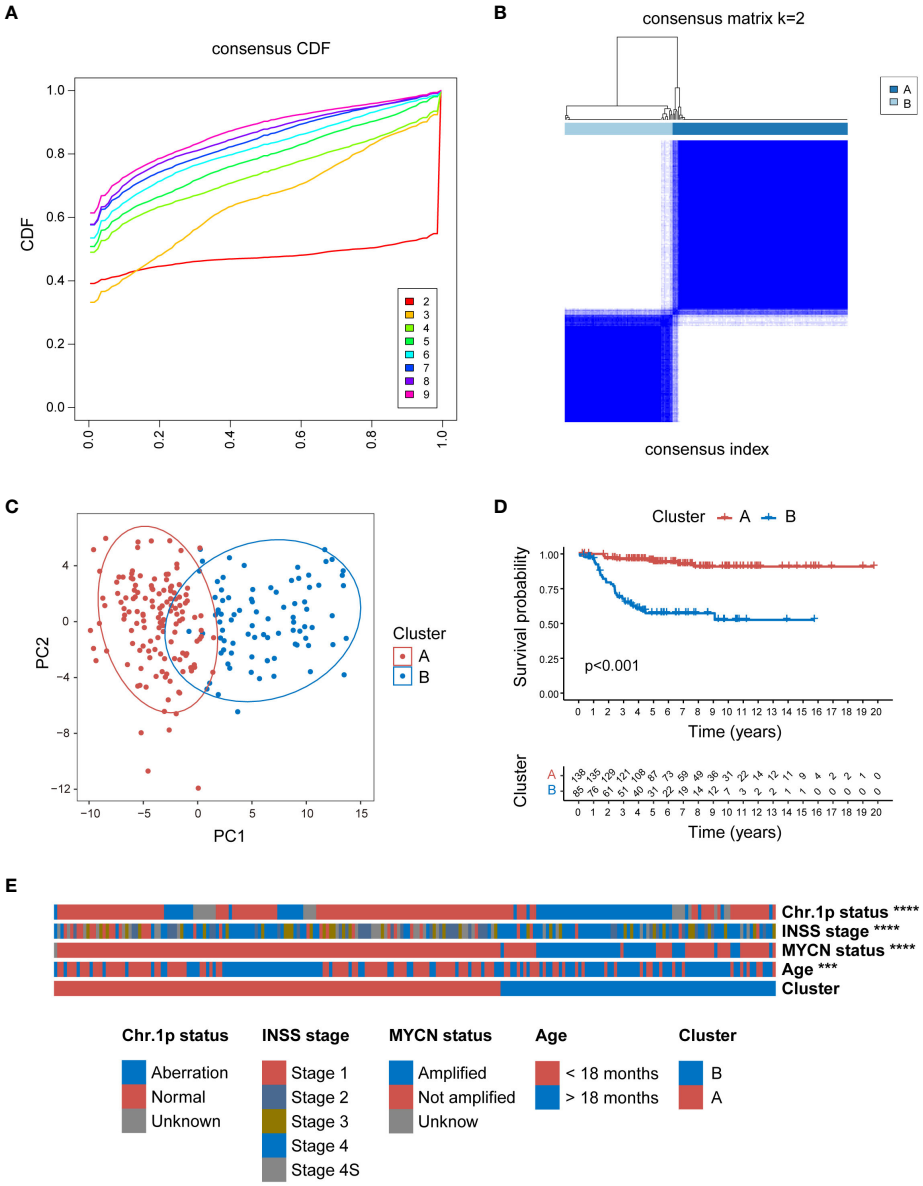

FIGURE 3
Consensus clustering of E-MTAB-8248 dataset into 2 distinct clusters. **(A)** The consensus CDF plot identifying the optimal cluster number (k=2). **(B)** Consensus matrix heatmap at k=2, displaying the robust bifurcation of the dataset into Clusters A and B. **(C)** The PCA demonstrating a clear separation between the two clusters, validating the clustering approach. **(D)** Kaplan-Meier survival analysis revealing a significant survival disadvantage for Cluster B compared to Cluster A (p<0.001). **(E)** The clinical characteristic heatmap exhibiting distinct profiles between Cluster A and B, with chromosome 1p status, INSS stage, MYCN amplification status, and age at diagnosis, underscoring the clinical relevance of the clustering. Chr: chromosome; CDF, cumulative distribution function; PCA, principal component analysis. (***P<0.001, ****P<0.0001).

(-0.001579582 × the expression of PID1) + (0.029877545 × the expression of HK2) + (0.072465418 × the expression of DLGAP5) + (0.196643607 × the expression of TERT) + (0.570707127 × the expression of FEN1).

The mtScore for all 498 patient samples in the GSE49710 dataset was calculated in this study. Following the computation of mtScores, patients were dichotomized into two risk categories, low and high mtRisk, based on the median mtScore value. Internal validation of the predictive value of mtScore and mtRisk was conducted in the GSE49710 dataset. Initially, Figures 5A and B demonstrated that mtScore and mtRisk could effectively discriminate between Clusters A and B, with Cluster B patients exhibiting higher mtScores. The PCA indicated a clear distinction between high and low mtRisk groups (Figure 5C). A bipartite plot of mtScore distribution revealed a concentration of dead patients within the high mtScore group (Figure 5D). The K-M analysis with endpoints of OS (Figure 5E) and Event-Free Survival (EFS) (Figure 5F) showed that high mtRisk NB patients faring worse in both OS and EFS compared to their low mtRisk counterparts. The heatmap in Figure 5G displayed the expression patterns of the 10 genes used in mtScore calculation, with TERT, HK2, DLGAP5, and FEN1 being overexpressed in high mtRisk patients, while PID1,

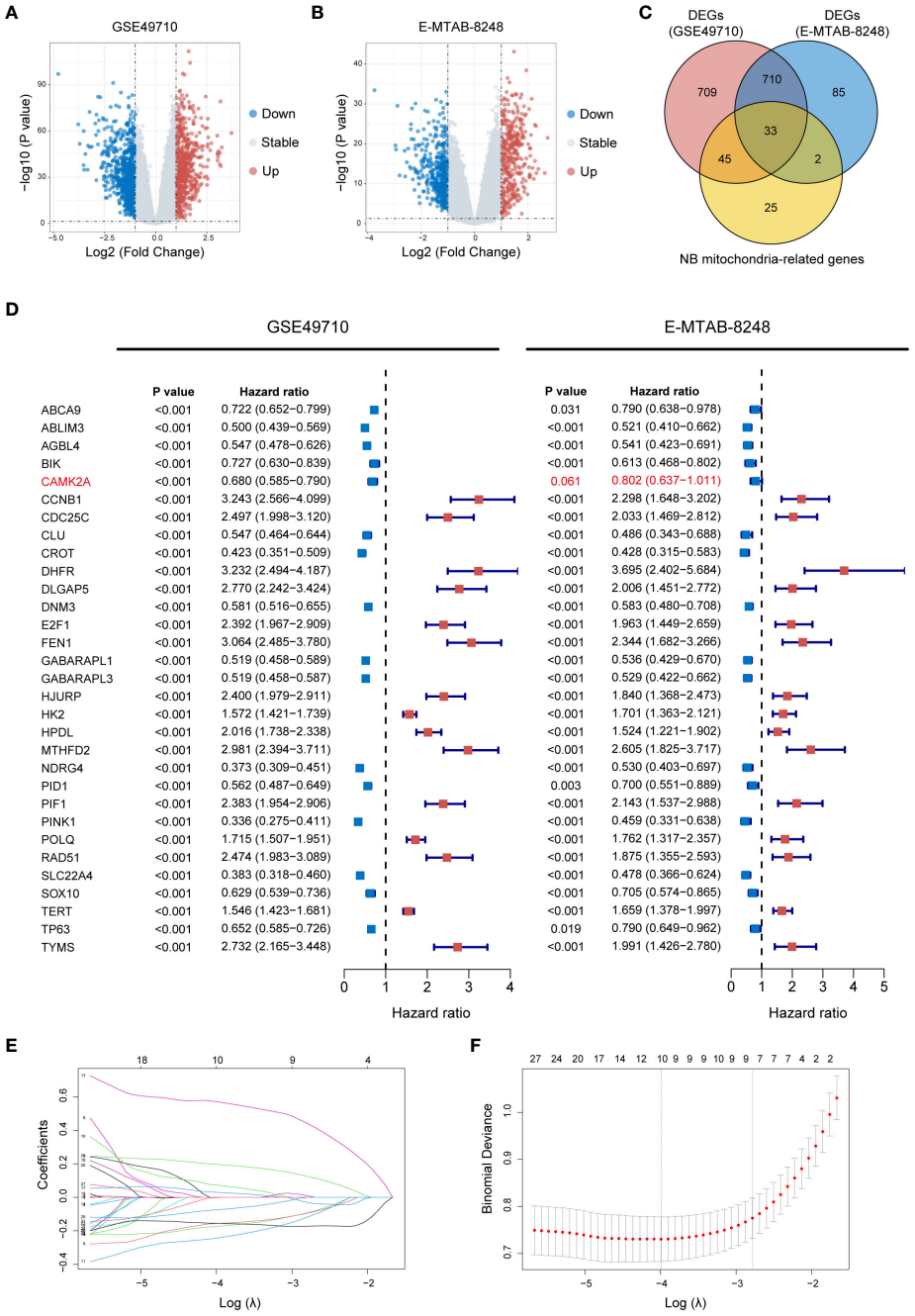

FIGURE 4
Construction of the MRGs-related signature. **(A)** Volcano plot displaying DEGs between Cluster A and B in GSE49710 (Genes with P value < 0.05 and |log2FC| > 1 are highlighted). **(B)** Volcano plot illustrating DEGs between Cluster A and B in E-MTAB-8248 (Genes with P value < 0.05 and |log2FC| > 1 are highlighted). **(C)** Venn diagram demonstrating the 33 intersecting genes found between the 1,497 DEGs in GSE49710, the 830 DEGs in E-MTAB-8248, and the 105 MRGs specific to NB. **(D)** Forest plots of HR for the 33 intersecting genes from GSE49710 and E-MTAB-8248 datasets, indicating their association with OS. P value < 0.05, and the 95% CI of HR was consistently distributed ipsilateral to 1 was considered statistically significant. **(E)** LASSO coefficient profiles of the 30 candidate genes. **(F)** Cross-validation for tuning parameter selection in the LASSO model used in **(E)**. MRGs, mitochondria-related genes; DEGs, differentially expressed genes; FC, fold change; NB, neuroblastoma; HR, hazard ratio; OS, overall survival; CI, confidence interval; LASSO, Least Absolute Shrinkage and Selection Operator.

TP63, DNM3, AGBL4, CROT, and SLC22A4 showed lower expression in the high mtRisk group. The ROC curve illustrated the prognostic prediction capability and accuracy of mtScore. The AUCs of the ROC curve for OS at 3, 5, and 10 years were 0.910, 0.911, and 0.907, respectively (Figure 5H), while for EFS, they were 0.824, 0.819, and 0.843 (Figure 5I). In contrast, the AUCs of the MYCN, a well-established biological indicator of poor prognosis in NB, prediction for OS at 3, 5, and 10 years were only 0.769, 0.692, and 0.672 (Figure 5J). Furthermore, the high and low mtRisk patient groups correlated well with key clinical features (Figure 5K), with significantly more patients with progression, INSS stage 4, clinical risk, MYCN amplification, and age under 18

10.3389/fimmu.2024.1415736

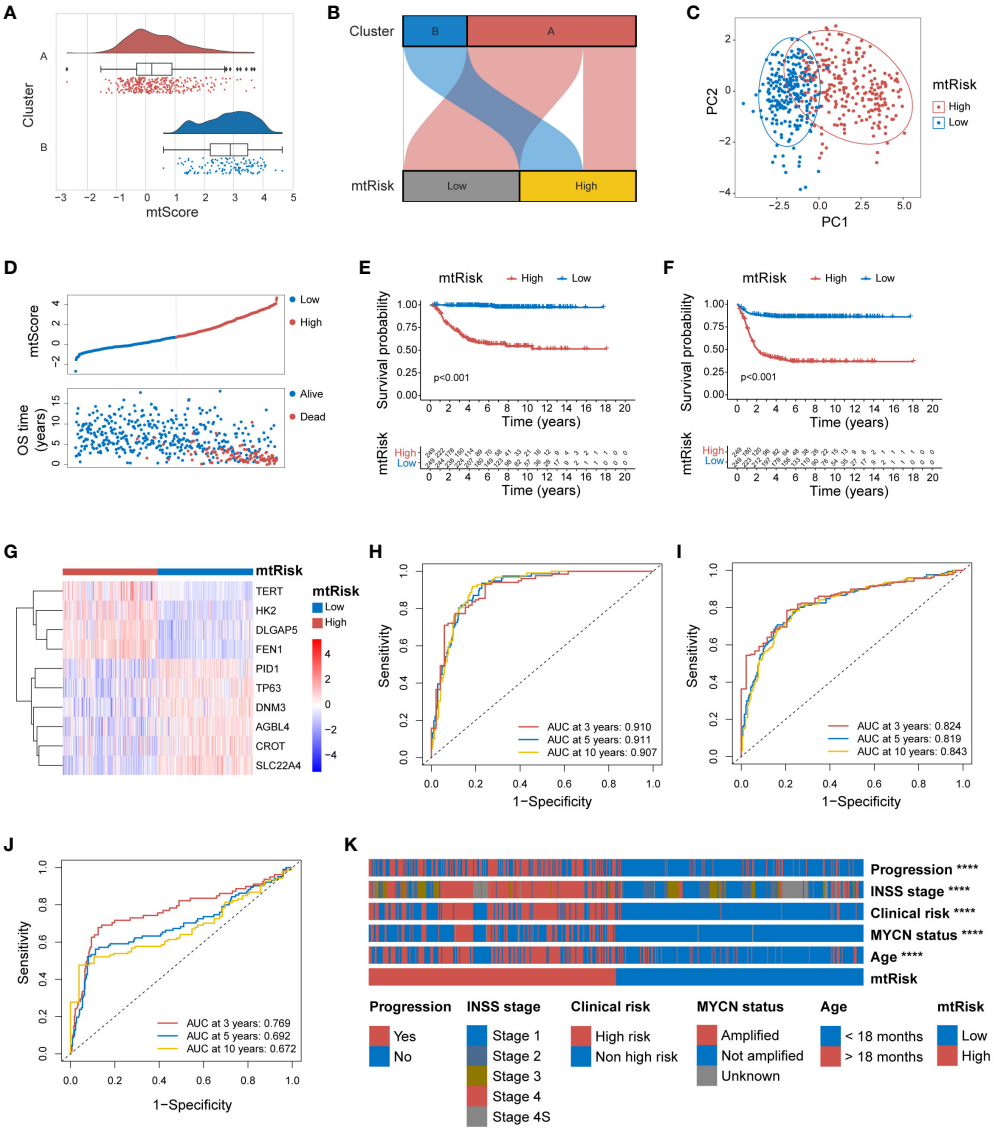

FIGURE 5
Internal validation of the MRGs-related signature in GSE49710. **(A)** Combined violin and box plot with overlaid scatter plot illustrating the distribution of mtScores across clusters A and B. **(B)** Sankey diagram demonstrating the effective discrimination of Clusters A and B using mtRisk. **(C)** PCA plot showing the clear separation between the patients of high and low mtRisk groups. **(D)** Bipartite plot of mtScore against OS time, highlighting the survival status (Alive or Dead) of patients. **(E)** Kaplan-Meier survival curve for OS, between the high and low mtRisk groups. **(F)** Kaplan-Meier survival curve for EFS, between the high and low mtRisk groups. **(G)** Heatmap showing the gene expression profiles of the 10 genes constituting the mtScore across the mtRisk stratified patient groups. **(H)** ROC curve of mtScore for OS. **(I)** ROC curve of mtScore for EFS. **(J)** ROC curve of MYCN for OS. **(K)** Heatmap displaying the association of clinical features with the mtRisk groups. MRGs, mitochondria-related genes; PCA, principal component analysis; OS, overall survival; EFS, event-free survival; ROC, receiver operating characteristic; AUC, area under the curve. (****P<0.0001).

months in the high mtRisk group (P < 0.0001 for all 5 comparisons). The detailed distribution of mtScores across different clinical features is presented as violin plots in Supplementary Figure 7.

3.3 External validation of the MRGs-related signature

To ascertain the general applicability of the MRGs-related signature and its quantitative indices, mtScore and mtRisk, further external validation was undertaken in the E-MTAB-8248 and TARGET-NBL datasets. Within the E-MTAB-8248 dataset, mtScore corresponded well with the identified Cluster A and B. Both the Figures 6A and B effectively demonstrated that mtScore and mtRisk could distinguish between Clusters A and B, with Cluster B associated with higher mtScores and mtRisk. the PCA underscored that patients in the E-MTAB-8248 dataset could be well-separated into high and low mtRisk groups (Figure 6C). The bipartite distribution plot revealed that dead patients predominantly occupied the high mtScore sector (Figure 6D). K-M analysis for OS (Figure 6E) and EFS (Figure 6F) were performed in E-MTAB-8248, demonstrating that high mtRisk patients had poorer prognoses compared to their low mtRisk counterparts (P < 0.01 for both). The heatmap in Figure 6G illustrates the expression

of the 10 genes comprising the mtScore in high and low mtRisk patients within the E-MTAB-8248 dataset. The ROC curves displayed the predictive capacity of mtScore, with AUC values for OS at 3 years (0.837), 5 years (0.857), and 10 years (0.864) (Figure 6H), and for EFS at 3 years (0.765), 5 years (0.775), and 10 years (0.783) (Figure 6I). In comparison, the AUCs of the MYCN prediction for OS were only 0.705, 0.674, and 0.566 at the same time points (Figure 6J). The mtRisk also showed significant statistical correlation with key clinical features in the E-MTAB-8248 dataset (Figure 6K), where more malign clinical features such as chromosome 1p aberration, INSS stage 4, MYCN amplification, and age <18 months were significantly more prevalent in the high mtRisk group (P<0.0001 for all comparisons). The distribution of mtScores across different clinical feature groups is presented as violin plots in Supplementary Figure 8.

External validation of mtScore and mtRisk in the TARGET-NBL dataset reiterated the robust predictive power of the MRGs-related signature. PCA delineated a clear distinction between high and low mtRisk groups in the TARGET-NBL dataset (Figure 6L). K-M survival analysis confirmed the consistent predictive power of mtRisk for prognosis, with high mtRisk patients exhibiting worse outcomes in both OS (Figure 6M) and EFS (Figure 6N) endpoints (P<0.001 and P<0.01, respectively). Beyond prognosis, mtRisk was also correlated with important clinical features in the TARGET-NBL dataset (Supplementary Figure 9A). High-risk COG risk group, unfavorable histology, high MKI, MYCN amplification, INSS stage 4, and age <18 months were statistically more frequent in high mtRisk patients. Supplementary Figures 9B–G display the mtScore distributions for different clinical feature groups as violin plots.

3.4 Predictive efficacy of MRGs-related signature for TIME, stemness, and chemosensitivity

The MRGs-related signature and its quantitative markers, mtScore and mtRisk, developed in this study, not only predict the prognosis of NB patients but also show significant relevance to immune infiltration in the TME. Various algorithms were applied to assess the indication of mtScore and mtRisk towards immune infiltration within the GSE49710 dataset. The ESTIMATE algorithm indicated that patients with low mtRisk had higher scores, with higher total ESTIMATE score, immune score, and stromal score compared to patients with high mtRisk (Figure 7A). According to the EPIC algorithm, the proportion of immune cells such as $CD4^+$ T cells, $CD8^+$ T cells, and macrophages was statistically higher in the TIME of patients with low mtRisk compared to those with high mtRisk (Figure 7B). The MCPcounter algorithm suggested that the cell abundance of T cells, $CD8^+$ T cells, cytotoxic lymphocytes, NK cells, monocytic lineage, myeloid dendritic cells, endothelial cells, and fibroblasts was higher in the low mtRisk patient group than in the high mtRisk group (Figure 7C). CIBERSORT analysis revealed statistically significant differences in the cell proportions of naive B cells, memory B cells, plasma cells, resting memory $CD4^+$ T cells, follicular helper T cells, resting NK cells, activated NK cells, monocytes, M0 macrophages, M2 macrophages, resting mast cells, and activated mast cells between the high and low mtRisk groups (Figure 7D). Additionally, a heatmap displayed the correlation between mtScore, the 10 genes constituting mtScore, and 28 types of immune cells (Figure 7E).

Furthermore, results demonstrated that mtScore is significantly positively correlated with tumor cell stemness. A scatter plot in Figure 7F exhibited the relationship between mtScore and mRNAsi values in the GSE49710 dataset. The scatter plot revealed a strong positive correlation, with an R value of 0.77 ($P < 0.0001$). A trend line drawn through the data points further emphasized this positive linear relationship.

Moreover, mtRisk may also predict the sensitivity to 3 commonly used drugs in NB patients. Results showed that patients in the low mtRisk group had statistically significantly higher IC50 values for Cisplatin (Figure 7G), Topotecan (Figure 7H), and Irinotecan (Figure 7I) compared to the high mtRisk group, suggesting increased sensitivity to these 3 drugs in the high mtRisk patients ($P < 0.001$ for 3 comparison).

3.5 Analysis of FEN1's essential role through single-cell transcriptome sequencing data

This study further validated the significant function and role of FEN1 in NB, the gene with the highest contribution in the MRGs-related signature. Quality control, normalization, and batch effect removal were initially applied to single-cell transcriptomic sequencing data from 160,847 cells of 16 NB patients sourced from GSE137804. Subsequent dimensionality reduction via UMAP clustered the cells into 30 clusters (Figure 8A), and cell type annotation using known markers identified 8 cell types similar to the original GSE137804 study (22), including tumor cells, T cells, B cells, endothelium, plasmacytoid dendritic cell (pDC), Schwann cells, fibroblasts, and myeloid cells (Figure 8B). The markers used for cell annotation are presented in Supplementary Figure 10A.

Tumor cells were segregated into FEN1-high and FEN1-low groups based on the median expression of FEN1. Cell-cell communication analysis further investigated differences between FEN1-high and FEN1-low tumor cells in their interactions with the TME. Compared to FEN1-high tumor cells, FEN1-low tumor cells exhibited increased and stronger communication with surrounding cells. Figures 8C, D respectively show the communication counts of tumor cells (FEN1-high) and tumor cells (FEN1-low) with adjacent cells. Supplementary Figures 10B, C display the communication weights of tumor cells (FEN1-high) and tumor cells (FEN1-low), respectively. Additionally, the exploration of interacting pairs in cell communication revealed that tumor cells primarily interact with other cells via the MIF-(CD74+CXCR4) axis; conversely, other cells predominantly communicate with tumor cells through the PTN-NCL axis (Figures 8E, F).

Pseudotime trajectory analysis illustrated the temporal expression changes of FEN1 in the development of NB tumor

10.3389/fimmu.2024.1415736

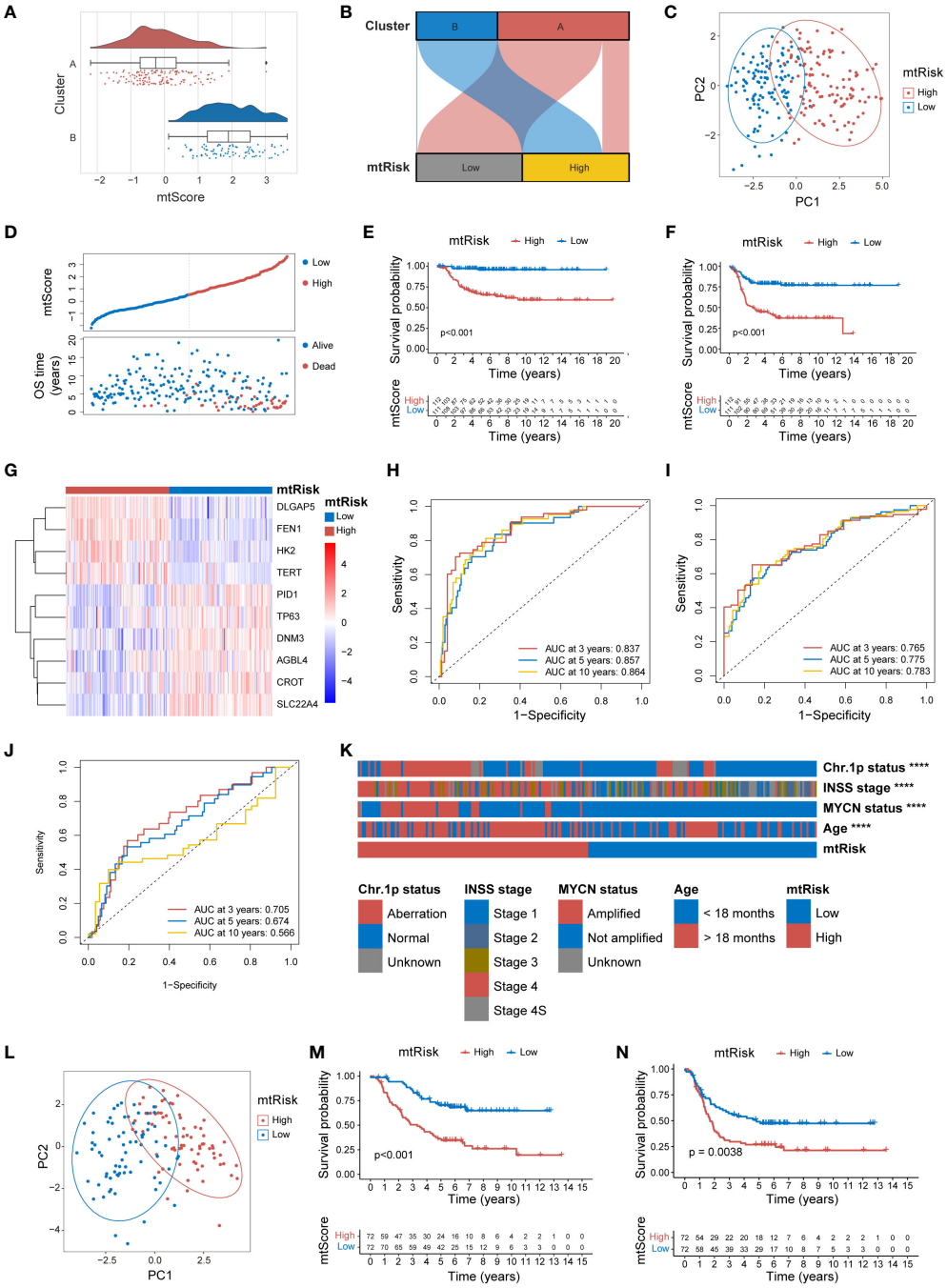

FIGURE 6
External validation of MRGs-related signature in the E-MTAB-8248 and TARGET-NBL datasets. **(A)** Combined violin, box, and scatter plot demonstrating mtScore distribution across Clusters A and B in the E-MTAB-8248 dataset. **(B)** Sankey diagram demonstrating the correlation between mtRisk stratification and Cluster A and B designation in E-MTAB-8248. **(C)** PCA plot distinctly separating high and low mtRisk patient groups in the E-MTAB-8248 dataset. **(D)** Scatter plot of mtScore against OS time in E-MTAB-8248, distinguishing patients by survival status. **(E)** Kaplan-Meier survival curve for OS in E-MTAB-8248 stratified by mtRisk. **(F)** Kaplan-Meier survival curve for EFS in E-MTAB-8248stratified by mtRisk. **(G)** Heatmap of the expression of 10 genes constituting the mtScore in E-MTAB-8248, differentiated by mtRisk groups. **(H)** ROC curve of mtScore predictive capacity for OS in E-MTAB-8248. **(I)** ROC curve of mtScore predictive capacity for EFS in E-MTAB-8248. **(J)** ROC curve of MYCN predictive capacity for OS in E-MTAB-8248. **(K)** Heatmap correlating mtRisk with key clinical features in E-MTAB-8248. **(L)** PCA plot distinctly separating high and low mtRisk patient groups in the TARGET-NBL dataset. **(M)** Kaplan-Meier survival curve for OS in TARGET-NBL categorized by mtRisk. **(N)** Kaplan-Meier survival curve for EFS in TARGET-NBL categorized by mtRisk. MRGs, mitochondria-related genes; PCA, principal component analysis; OS, overall survival; EFS, event-free survival; ROC, receiver operating characteristic; AUC, area under the curve; Chr, chromosome. (****P<0.0001).

10.3389/fimmu.2024.1415736

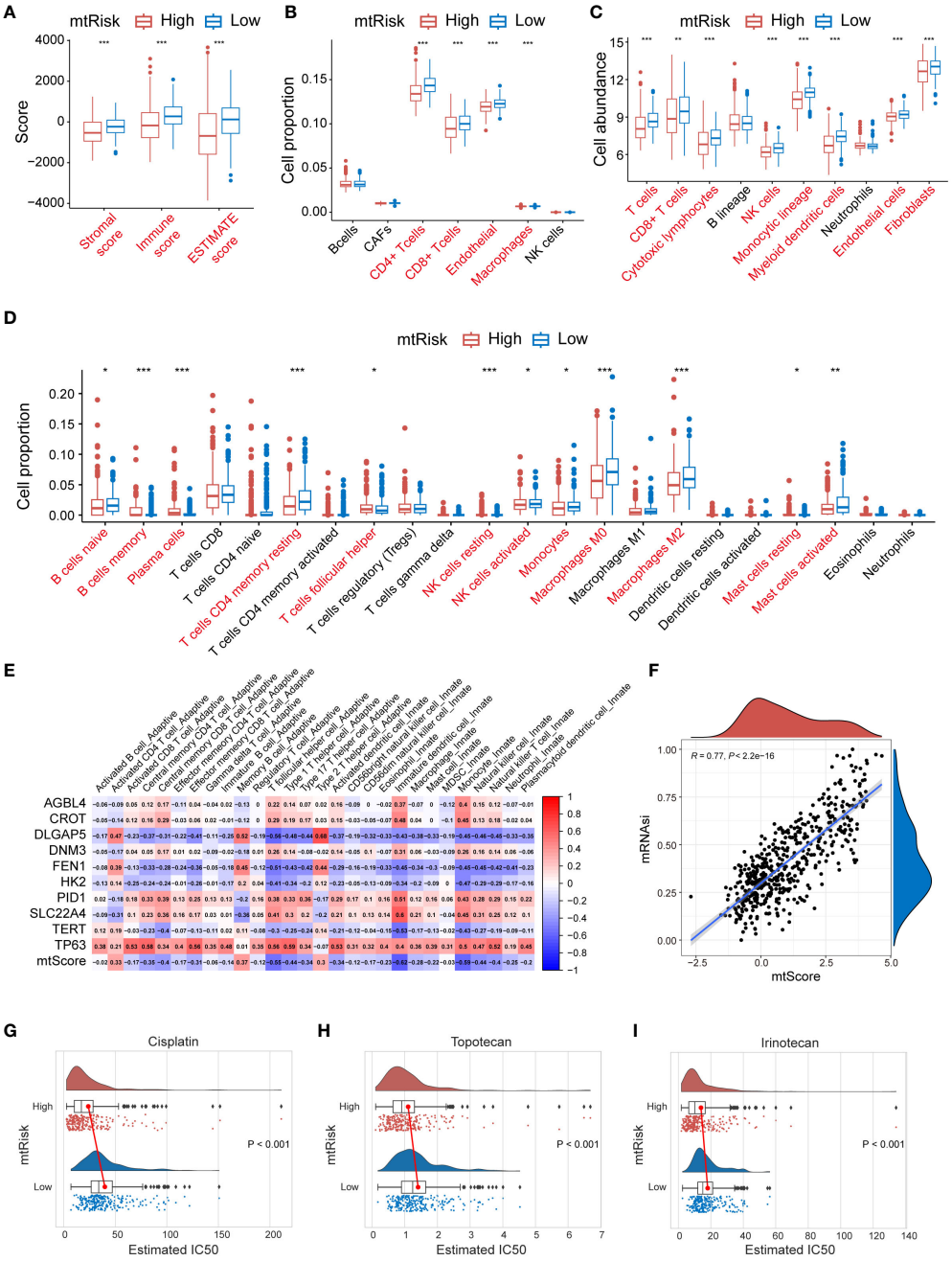

FIGURE 7
Immune profile, stemness, and drug Sensitivity analysis related to MRGs-related signature in GSE49710. **(A)** Box plots representing the ESTIMATE scores stratified by mtRisk groups. **(B)** Box plots illustrating the proportion of various immune cells as analyzed by the EPIC algorithm, stratified by mtRisk groups. **(C)** Box plots depicting the cell abundance of different immune cell types as analyzed by the MCPcounter algorithm. **(D)** Box plots detailing the cell proportion of various immune cells as analyzed by the CIBERSORT algorithm stratified by mtRisk groups. **(E)** Heatmap displaying the correlation between the mtScore, the ten genes comprising mtScore, and 28 immune cell types. **(F)** Scatter plot demonstrating a positive association between mtScore and mRNAsi. **(G–I)** Violin plots illustrating the estimated IC50 values for Cisplatin **(G)**, Topotecan **(H)**, and Irinotecan **(I)**, comparing high and low mtRisk groups. MRGs, mitochondria-related genes; ESTIMATE, Estimation of STromal and Immune cells in MAlignant Tumour tissues using Expression data; EPIC, Estimating the Proportions of Immune and Cancer cells; MCPcounter, Microenvironment Cell Populations-counter; CIBERSORT, Cell-type Identification By Estimating Relative Subsets Of RNA Transcripts; IC50, half-maximal inhibitory concentration. (*P<0.05, **P<0.01, ***P<0.001).

10.3389/fimmu.2024.1415736

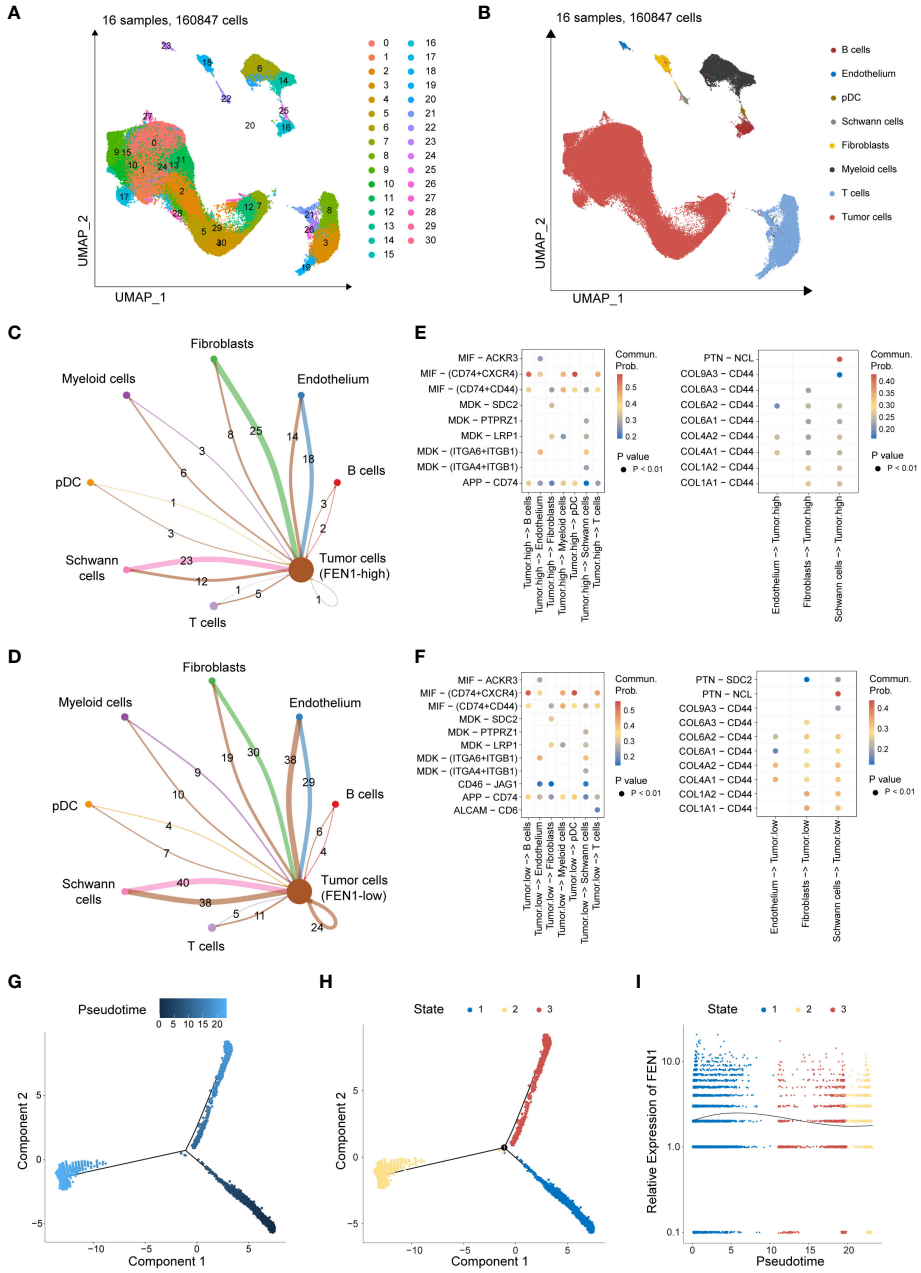

FIGURE 8
Single-cell transcriptomic data analysis revealing the role of FEN1 in NB tumor cells. **(A)** UMAP dimensionality reduction and clustering of 160,847 cells from 16 neuroblastoma patient samples. **(B)** Annotated UMAP Clustering of Cell Types. **(C)** Cell-cell communication counts network of FEN1-high tumor cells with the surrounding microenvironment. **(D)** Cell-cell communication counts network of FEN1-low tumor cells with the surrounding microenvironment. **(E)** Heatmap illustrating significant ligand-receptor pairs between FEN1-high tumor cells and other cell types. **(F)** Heatmap illustrating significant ligand-receptor pairs between FEN1-low tumor cells and other cell types. **(G)** Pseudotime trajectory analysis of NB tumor cells, with color gradient indicating progression through pseudotime. **(H)** Cells are categorized into 3 developmental states along the pseudotime trajectory. **(I)** Trend of FEN1 gene expression across pseudotime, demonstrating its dynamic changes during tumor cell development. NB, neuroblastoma; UMAP, uniform manifold approximation and projection; pDC, plasmacytoid dendritic cell; Commun Prob, communication probability.

cells. Figure 8G depicts the pseudotime trajectory of NB tumor cells, with the cell developmental trajectory divided into 3 states in Figure 8H. The gene expression trend of FEN1 over pseudotime is shown in Figure 8I, indicating that FEN1 expression is higher in the early stages of NB tumor cell development than in later stages.

3.6 Functional validation of FEN1 in NB cell lines

The current study further investigated the important role of FEN1 in NB cell by modulating its expression through lentiviral-

mediated OE or KD in human NB cells. Successful modulation of FEN1 at both RNA and protein levels was confirmed by qRT-PCR (Figure 9A) and Western blot (Figure 9B), achieving the desired OE and KD effects.

The impact of FEN1 on NB cell proliferation was assessed using the CCK-8 assay (Figure 9C). Cells with FEN1 OE showed significantly higher proliferation rates compared to the vector group ($P<0.0001$). Cells with FEN1 KD (sh-FEN1#1 and sh-FEN1#2), demonstrated significantly reduced proliferation compared to the scramble group ($P<0.0001$ for both comparisons). Plate clonogenic assays corroborated these findings (Figure 9D), where FEN1 OE increased colony formation in NB cells compared to NC ($P<0.01$), and KD led to a significant decrease in colony numbers ($P<0.01$ for both sh#1 and sh#2).

To explore changes in apoptosis following FEN1 modulation, we quantified $\Delta\Psi m$ using the JC-1 dye. An increase in red/green fluorescence ratio, indicating higher J-aggregates formation, reflects higher MMP and thus, a lower level of apoptosis. Figure 9E shows that cells with FEN1 OE had a significantly higher Aggregates/Monomer ratio compared to NC ($P<0.001$), whereas FEN1 KD cells displayed a significant reduction, indicating increased apoptosis ($P<0.01$ for both sh#1 and sh#2).

Cell cycle analysis also yielded positive findings (Figure 10A), with FEN1 KD cells showing an increased proportion in the G2/M phase, suggesting G2/M arrest compared to the NC ($P<0.0001$ for sh#1, $P<0.001$ for sh#2). Cells OE FEN1 exhibited a significant increase in the S phase proportion compared to NC ($P<0.0001$), indicative of heightened DNA synthesis and replication activity.

Furthermore, FEN1 may influenced the invasive capacity of NB cells. Transwell assays revealed changes in NB cell invasion following FEN1 OE and KD (Figure 10B). Compared to NC, FEN1 OE enhanced the invasiveness of NB cells, with increased cell numbers traversing the membrane ($P<0.01$). Conversely, FEN1 KD reduced NB cell invasion, with fewer cells penetrating the membrane ($P<0.01$ for both sh#1 and sh#2).

4 Discussion

Our study has successfully constructed a prognostic signature based on MRGs and developed quantitative indices, namely mtScore and mtRisk. Through extensive internal and external validation, the MRGs-related signature exhibited superior prognostic predictive effect and value over the traditional molecular marker MYCN in NB patients. Furthermore, it demonstrated predictive capability for immune infiltration in the TME, tumor cell stemness, and sensitivity to specific chemotherapeutic agents. Furthermore, through single-cell transcriptomic analysis, we underscored the pivotal role played by FEN1, the most contributive molecule in the MRGs-related signature, in the molecular crosstalk and developmental trajectory of NB cells. The experimental validation results underscored that FEN1 expression significantly affects processes such as cell proliferation, apoptosis, cell cycle progression, and invasiveness in NB cells.

In this study, MRGs effectively stratified NB patients into 2 distinct groups with significant differences in prognosis and immune infiltration characteristics. An MRGs-related signature and its quantitative metrics, mtScore and mtRisk, were developed to characterize these 2 patient groups, revealing that lower mtScore and mtRisk are associated with significantly better prognoses. Similar works have been reported in colorectal cancer, hepatocellular carcinoma, and other cancers (50, 51), but this is the first time an MRGs-related signature has been identified and explored in NB, to our knowledge. It's noteworthy that the predictive efficiency of this MRGs-related signature for NB patients surpasses that of MYCN, traditionally recognized as the best genetic marker for forecasting outcomes in NB (52, 53). This highlights the potential of MRGs-related signature to provide a more comprehensive understanding of NB prognosis beyond conventional markers.

In line with the above results, MRGs-related signature not only predicts prognosis, but also identifies key clinical features to a certain extent. MYCN amplification, which is closely related to the poor prognosis of high-risk NB patients (54), was found to be significantly correlated with high mtRisk in this study. INSS4 stage, as an independent risk factor for NB (49), was found to be significantly associated with high mtRisk in this study. Similarly, high mtRisk was profoundly associated with a spectrum of adverse clinical features, including clinical risk, progression, chromosomal 1p aberration, high MKI, unfavorable histology, and high COG risk. The congruence of the MRGs-related signature's predictive capacity for both prognosis and key clinical features in NB patients underscores its utility beyond mere prognostic estimation.

The Further analysis of immune infiltration implies that patients with lower mtScore and mtRisk tend to have a more active immune environment within their tumors. This heightened immune activity is hypothesized to be a key factor contributing to their better prognosis, suggesting a link between mitochondrial function, immune engagement, and cancer outcome. Exploring the TIME and transitioning from "cold" to "hot" tumors could significantly enhance therapeutic efficacy in NB, a tumor traditionally marked by immune suppression and modest responses to immunotherapy (5). The establishment of the MRGs-related signature provides a promising avenue for identifying and modulating the TME. By targeting specific MRGs to activate the immune landscape within NB, it may be possible to convert these traditionally "cold" tumors into "hot" tumors, potentially making them more amenable to immunotherapeutic interventions. This approach, aligning with findings in other cancers, underscores the critical interplay between mitochondrial dynamics and immune responsiveness in determining cancer prognosis and treatment outcomes (14, 55). The results of this study may provide a new target for immunotherapy of NB and other tumors (56–59).

In addition, the significant linear correlation between mtScore and mRNAsi underscores the potential of our developed MRGs-related signature to effectively indicate the stemness of tumor cells in patients. Our team's previous work has developed an mRNAsi-based risk score for NB, which demonstrated excellent performance

10.3389/fimmu.2024.1415736

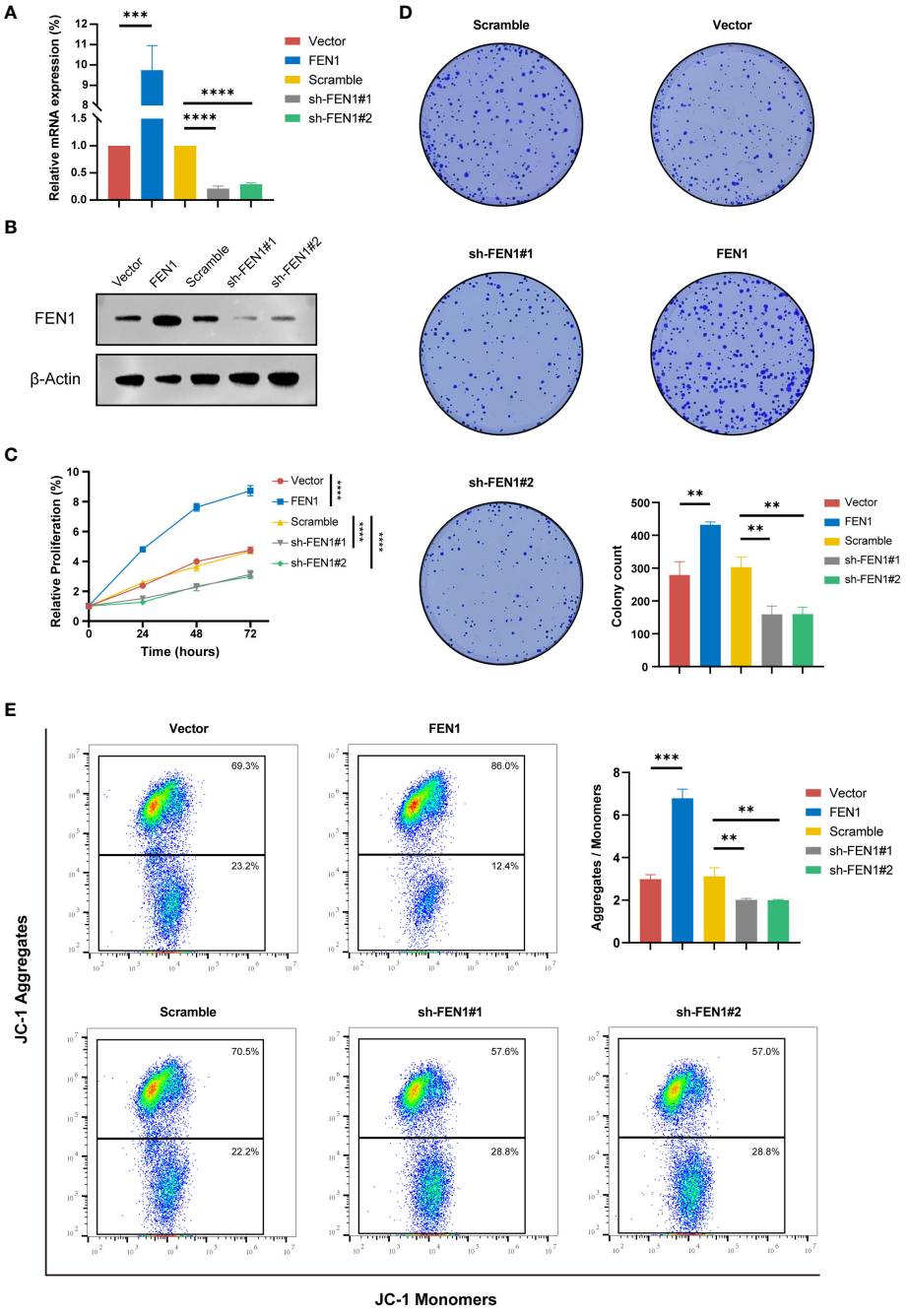

FIGURE 9
Functional validation of FEN1 OE and KD in NB cell lines. **(A)** qRT-PCR Validation of FEN1 OE and KD Efficiency at RNA Level in NB Cells. **(B)** Western Blot Confirmation of FEN1 OE and KD at Protein Level in NB Cells. **(C)** Line graph depicting the relative proliferation of NB cells, measured by CCK-8 assay. **(D)** Representative images and quantification of colony formation assay results. **(E)** Flow cytometry analysis of JC-1 staining to assess MMP (ΔΨm), with the Aggregates/Monomers ratio indicating changes of apoptosis. OE, overexpression; KD, knockdown; NB, neuroblastoma; MMP, mitochondrial membrane potential. (**P<0.01, ***P<0.001, ****P<0.0001).

in predicting patient prognosis, immune infiltration, and treatment response (60). This study extends the prognostic utility of mtScore as a marker of stemness, potentially impacting the clinical management of NB significantly. Patients with elevated mtScores might be identified as harboring a higher burden of tumor stem cells, likely to undergo aggressive disease progression and exhibit poor responses to standard therapies. This observation aligns with the outcomes of poor prognosis and reduced sensitivity to certain chemotherapies among patients with high mtScores. Such insights potentially could facilitate the stratification of patients into more personalized treatment regimens.

In the realm of clinical pharmacotherapy, our findings highlight a significant role of mtRisk in shaping therapeutic responses. At first glance, patients categorized under high mtRisk appear to present a formidable challenge in treatment management due to their poor prognosis, immune-suppressive TME, and pronounced tumor cell

10.3389/fimmu.2024.1415736

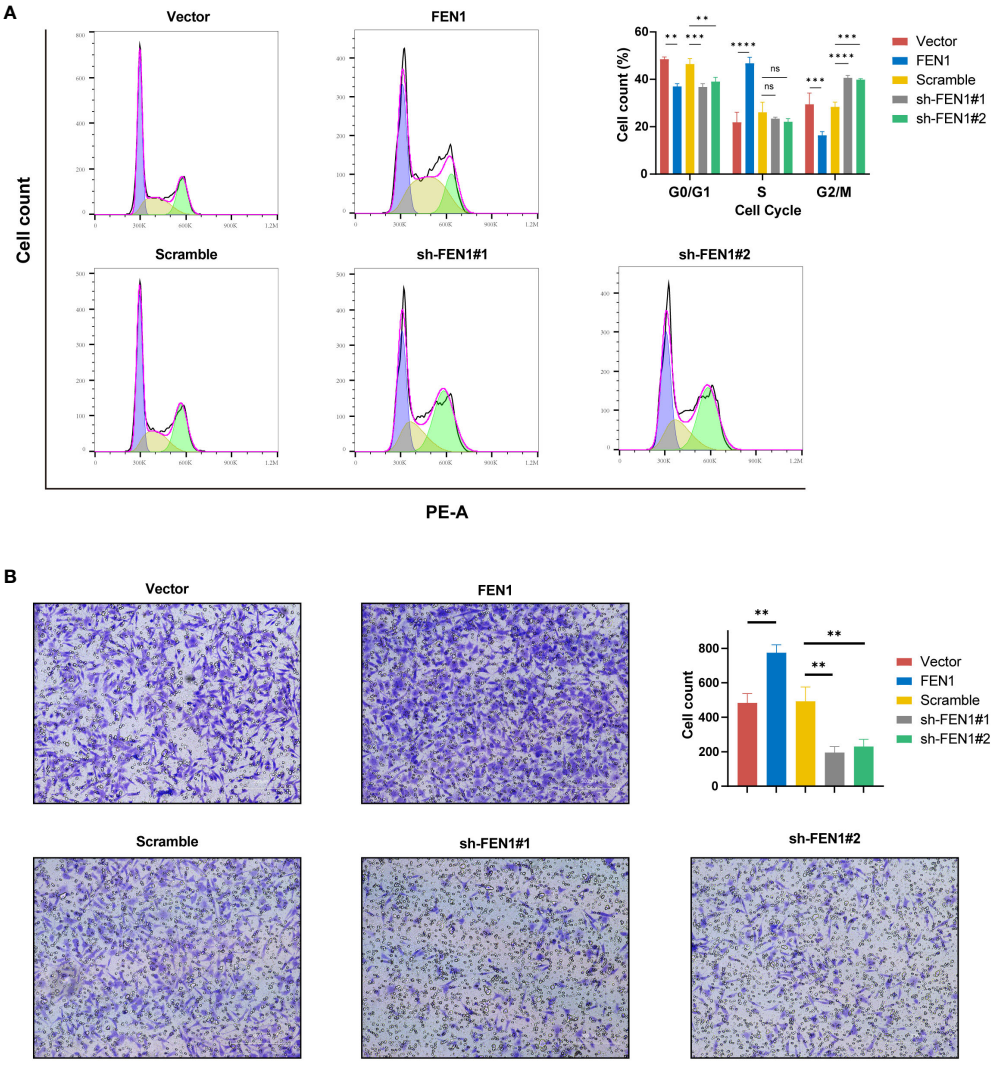

FIGURE 10
Impact of FEN1 modulation on NB cell cycle progression and invasiveness. **(A)** Flow cytometry cell cycle analysis presenting the situation of NB cells in 5 group. **(B)** Transwell invasion assays with representative images and quantitative analysis displaying the invasive capacity of NB cells in 5 groups. NB, neuroblastoma; ns, not significant. (**P<0.01, ***P<0.001, ****P<0.0001).

stemness. However, a pivotal discovery of our study is the heightened sensitivity of high mtRisk patients to 3 clinically prevalent drugs for NB: Cisplatin, Topotecan, and Irinotecan. All 3 drugs are internationally recognized for the treatment of NB patients (61–63). This enhanced drug responsiveness, surpassing that of low mtRisk patients, uncovers a nuanced aspect of mtRisk's clinical implications. This holds some promise for the therapeutic management of patients with high mtRisk, and also re-emphasizes the importance of precise individualized treatment in highly heterogeneous NB patients.

The MRGs-related signature in NB is composed of ten genes: FEN1, TERT, DLGAP5, HK2, PID1, TP63, SLC22A4, CROT, AGBL4, DNM3. FEN1 (Flap endonuclease 1) is crucial in DNA replication and repair, and its overexpression is linked to poor prognosis in various cancers, indicating its potential as a target for cancer therapy (64). TERT (Telomerase reverse transcriptase), the catalytic subunit of telomerase, affects telomere length by affecting telomerase activity, and considered to be a useful marker in diagnosis and prognosis of various cancers and a new therapy approach (65). DLGAP5 (Discs large homolog associated protein 5) is involved in mitotic spindle assembly, and its overexpression is associated with tumor progression and adverse outcomes in cancer patients, highlighting its role in cell division and potential as a therapeutic target (66, 67). HK2 (Hexokinase 2) catalyzes the first step of glycolysis and its upregulation in tumors is linked to enhanced glycolytic metabolism typical of cancer cells, suggesting its involvement in the Warburg effect and as a target for metabolic therapy (68). The role of PID1 (Phosphotyrosine interaction domain-containing protein 1) in cancer involves modulating lipid metabolism and mitochondrial function, indicating its potential impact on tumor metabolic reprogramming and its association with cancer progression (69, 70). A member of the p53 family, TP63 is implicated in the development and progression of several cancers, where it can influence cell cycle regulation, apoptosis, and the

immune response in the TME (71, 72). SLC22A4, a solute carrier protein, has been associated with drug disposition and response in cancer therapy, reflecting its role in modulating chemotherapeutic efficacy and resistance mechanisms in tumors (73). CROT is involved in fatty acid metabolism, and alterations in its expression are linked to changes in cancer cell metabolism and potential effects on tumor growth and patient prognosis (74). AGBL4 (ATP/GTP binding protein-like 4), as a neuronal differentiation marker, participates in neuronal differentiation by promoting mitochondrial axonal growth and axonal transport (75). DNM3 (Dynamin 3), involved in exosomes, endocytosis, and tumor metastasis, is considered as a tumor suppressor gene in a variety of cancers such as non-small-cell lung cancer (NSCLC), hepatocellular carcinoma, papillary thyroid carcinoma, and colon cancer (76–79). Therefore, the MRGs-related signature developed in this study encompasses a range of factors related to patient prognosis, the TIME, apoptosis, cell cycle progression, mitochondrial function, neuronal differentiation, and resistance mechanisms in NB. This comprehensive signature holds potential for guiding therapeutic strategies and prognosis assessment in NB patients.

The single-cell transcriptomics data analysis further explored the role of the most important gene in the MRGs-related signature, FEN1, providing profound insights into this gene's multifaceted functions in NB. The enhanced communication between FEN1-low tumor cells and the surrounding cells, as revealed through our analysis, suggests a more dynamic interplay within the TME. Taken together with the results of bulk sequencing data analysis (FEN1 is an oncogene associated with poor prognosis in NB patients and positively contributes to mtScore), we may be able to make an important hypothesis. High FEN1 expression could lead to a reduced need for external support from the TME, suggesting that these cells might have developed autonomous signaling pathways that promote proliferation, resist apoptosis, and enhance invasion capabilities without the extensive need for stromal or immune cell interactions. This autonomy could be a factor in their increased progression and aggressiveness. The differential communication patterns, particularly through the MIF-(CD74+CXCR4) and PTN-NCL axes, may underscore specific pathways amenable to therapeutic intervention. Furthermore, pseudotime trajectory analysis elucidating the temporal changes in FEN1 expression across the developmental trajectory of NB tumor cells underscores its significance. The observation that FEN1 expression is higher in the early stages of tumor cell development suggests a role in the initial phases of tumorigenesis or in maintaining a stem-like state of the tumor cells. This finding is supported by research from Z. Peng, et al., which confirmed FEN1's capability to promote stemness in tumor cells (80).

FEN1 is an enzyme characterized by its multifunctional enzymatic activities, playing a pivotal role in the processes of DNA replication and repair (81). The exonuclease activity of FEN1 is critical for the maturation of lagging strand Okazaki fragments during DNA replication. This activity facilitates the removal of RNA primers at the termini of these fragments, as well as the trimming of damaged ends during DNA repair mechanisms (82, 83). As an endonuclease, FEN1 recognizes and cleaves flap structures, which are intermediates formed during DNA replication. The precise excision of these flap structures by FEN1 ensures the continuity and fidelity of DNA synthesis. This endonuclease activity is particularly crucial for genomic stability, as it aids in the accurate resolution of structural anomalies encountered during DNA replication and repair processes (84). FEN1 has been implicated in the malignancy progression of various cancers, including gastric cancer, NSCLC, and cholangiocarcinoma (85–87). This study extends the understanding of FEN1's oncogenic role by exploring its functional significance in NB cell lines through OE and KD experiments. Our findings illustrate the multifaceted role of FEN1 in modulating NB cell behaviors, emphasizing its critical involvement in cell proliferation, apoptosis, cell cycle progression, and invasiveness. The pivotal role of FEN1 in supporting NB cell proliferation and colony formation underscores its important contribution to the proliferation and growth of NB. This aligns with FEN1's established roles in DNA replication and repair mechanisms (88). Furthermore, the regulation of FEN1 significantly impacts NB cell apoptosis and cell cycle dynamics. Increased apoptosis in FEN1 KD cells highlights a potential vulnerability that could be therapeutically exploited to induce cell death in NB cells. This observation aligns with existing research indicating FEN1's capacity to inhibit tumor cell apoptosis (89). Cell cycle analysis revealed G2/M phase arrest in FEN1 KD cells and an increase in the proportion of cells in the S phase following FEN1 OE, further evidencing FEN1's regulatory role in cell cycle progression. Such findings suggest that FEN1 is not only indispensable for the replication process but also crucial for the proper progression of the cell cycle, likely by ensuring the fidelity of DNA replication and repair prior to mitotic entry. Alterations in the invasive capacity of NB cells post-FEN1 modulation underscore the gene's role in tumor metastasis. Enhanced invasiveness in FEN1 OE cells could reflect an increased ability to facilitate tumor spread. Coupled with resistance to apoptosis and increased proliferation, these capabilities position FEN1 as a key driver of NB aggressiveness and metastatic potential. In summary, our findings advocate for FEN1's important role in NB cell proliferation, survival, and invasiveness, and emphasize that FEN1 may serve as a potential therapeutic target for NB.

This study presents a pioneering effort in constructing an MRGs-related signature for NB, revealing potential avenues for further research and clinical application. However, there are limitations to consider. Of the ten genes comprising the constructed MRGs-related signature, only one was confirmed in subsequent single-cell data analysis and experimental validation. It is imperative to highlight that the validated gene, FEN1, is not only a part of the signature but its most crucial and significantly contributory element, underscoring its pivotal role within the MRGs-related signature for NB. The roles of the remaining nine genes in NB require further exploration through more extensive data analysis and experimental investigation. Additionally, the validation of the signature and its associated genes would benefit from a broader array of NB cell lines, animal models, and clinical patient samples to confirm their function and impact more definitively. This approach underscores the importance of comprehensive validation to strengthen the findings and potential clinical applications of genomic signatures in cancer research.

In conclusion, this study shows for the first time that MRGs can divide NB patients into two clusters that differ significantly in terms of survival prognosis, clinical features, and TIME. On this basis, this study developed MRGs-related signature and its quantitative indicators mtScore and mtRisk to characterize the above two clusters. The MRGs-related signature constructed in this study can successfully distinguish heterogeneous NB patients in different clusters, which is of great significance for the targeted and precise treatment of NB patients with different characteristics. Notably, the MRGs-related signature can predict the prognosis of NB patients, and the predictive performance is better than that of MYCN. The MRGs-related signature is significantly associated with malignant clinical features including MYCN amplification status. Besides, the MRGs-related signature may indicate the immune infiltration in TIME of NB patients to a certain extent, which may be of great significance for distinguishing "hot" tumors from "cold" tumors and predicting the response of immunotherapy. The MRGs-related signature was also adept at representing tumor cell stemness, and sensitivity to the chemotherapeutic agents Cisplatin, Topotecan, and Irinotecan. Furthermore, the important role of FEN1, the most important gene in MRGs-related signature, in NB was demonstrated by single-cell data analysis and experimental validation in this study. The development of mtScore and mtRisk provides a new perspective and evidence for the precise treatment, prognosis prediction, the conversion of "cold" and "hot" tumors, and the activation of TIME of NB patients. The important role of FEN1 demonstrated in this study also provides a potential new target for the treatment of NB.

Data availability statement

The original contributions presented in the study are included in the article/Supplementary Material. Further inquiries can be directed to the corresponding authors.

Ethics statement

Ethical approval was not required for the studies on humans in accordance with the local legislation and institutional requirements because only commercially available established cell lines were used.

Author contributions

CW: Writing – review & editing, Writing – original draft, Visualization, Validation, Software, Methodology, Investigation, Formal analysis, Data curation. JT: Writing – review & editing, Writing – original draft, Visualization, Validation, Software, Methodology, Investigation, Formal analysis, Data curation. YJ: Writing – review & editing, Writing – original draft, Visualization, Validation, Software, Methodology, Investigation, Formal analysis, Data curation. ZL: Writing – review & editing, Investigation, Data curation. JY: Writing – review & editing, Visualization, Methodology. YBJ: Writing – review & editing, Visualization, Methodology. YX: Writing – review & editing, Investigation, Data curation. BG: Writing – review & editing, Supervision, Resources, Funding acquisition. QD: Writing – review & editing, Supervision, Resources, Funding acquisition. QZ: Writing – review & editing, Supervision, Resources, Funding acquisition.

Funding

The author(s) declare financial support was received for the research, authorship, and/or publication of this article. This study was funded by National Key Research and Development Program of China (2018YFC1313000) and Tianjin Key Medical Discipline (Specialty) Construction Project (TJYXZDXK-009A).

Conflict of interest

The authors declare that the research was conducted in the absence of any commercial or financial relationships that could be construed as a potential conflict of interest.

Publisher's note

All claims expressed in this article are solely those of the authors and do not necessarily represent those of their affiliated organizations, or those of the publisher, the editors and the reviewers. Any product that may be evaluated in this article, or claim that may be made by its manufacturer, is not guaranteed or endorsed by the publisher.

Supplementary material

The Supplementary Material for this article can be found online at: https://www.frontiersin.org/articles/10.3389/fimmu.2024.1415736/full#supplementary-material

References

1. Cheung NK, Dyer MA. Neuroblastoma: developmental biology, cancer genomics and immunotherapy. *Nat Rev Cancer*. (2013) 13:397–411. doi: 10.1038/nrc3526

2. Ngan ES. Heterogeneity of neuroblastoma. *Oncoscience*. (2015) 2:837–8. doi: 10.18632/oncoscience.216

3. Lundberg KI, Treis D, Johnsen JI. Neuroblastoma heterogeneity, plasticity, and emerging therapies. *Curr Oncol Rep*. (2022) 24:1053–62. doi: 10.1007/s11912–022-01270–8

4. Gomez RL, Ibragimova S, Ramachandran R, Philpott A, Ali FR. Tumoral heterogeneity in neuroblastoma. *Biochim Biophys Acta Rev Cancer*. (2022) 1877:188805. doi: 10.1016/j.bbcan.2022.188805

5. Kennedy PT, Zannoupa D, Son MH, Dahal LN, Woolley JF. Neuroblastoma: an ongoing cold front for cancer immunotherapy. *J Immunother Cancer*. (2023) 11. doi: 10.1136/jitc-2023–007798

6. Wienke J, Dierselhuis MP, Tytgat GAM, Künkele A, Nierkens S, Molenaar JJ. The immune landscape of neuroblastoma: Challenges and opportunities for novel therapeutic strategies in pediatric oncology. *Eur J Cancer*. (2021) 144:123–50. doi: 10.1016/j.ejca.2020.11.014

7. Galluzzi L, Chan TA, Kroemer G, Wolchok JD, López-Soto A. The hallmarks of successful anticancer immunotherapy. *Sci Transl Med*. (2018) 10. doi: 10.1126/scitranslmed.aat7807

8. Anderson J, Majzner RG, Sondel PM. Immunotherapy of neuroblastoma: facts and hopes. *Clin Cancer Res*. (2022) 28:3196–206. doi: 10.1158/1078–0432.Ccr-21–1356

9. Wallace DC. Mitochondria and cancer. *Nat Rev Cancer*. (2012) 12:685–98. doi: 10.1038/nrc3365

10. Zong WX, Rabinowitz JD, White E. Mitochondria and cancer. *Mol Cell*. (2016) 61:667–76. doi: 10.1016/j.molcel.2016.02.011

11. Badrinath N, Yoo SY. Mitochondria in cancer: in the aspects of tumorigenesis and targeted therapy. *Carcinogenesis*. (2018) 39:1419–30. doi: 10.1093/carcin/bgy148

12. Pangou E, Sumara I. The multifaceted regulation of mitochondrial dynamics during mitosis. *Front Cell Dev Biol*. (2021) 9:767221. doi: 10.3389/fcell.2021.767221

13. Bai R, Cui J. Mitochondrial immune regulation and anti-tumor immunotherapy strategies targeting mitochondria. *Cancer Lett*. (2023) 564:216223. doi: 10.1016/j.canlet.2023.216223

14. Klein K, He K, Younes AI, Barsoumian HB, Chen D, Ozgen T, et al. Role of mitochondria in cancer immune evasion and potential therapeutic approaches. *Front Immunol*. (2020) 11:573326. doi: 10.3389/fimmu.2020.573326

15. Chai C, Chen Y, Luo Y, Zhang H, Ye Z, He X, et al. Mitochondria-associated gene expression perturbation predicts clinical outcomes and shows potential for targeted therapy in neuroblastoma. *Front Pediatr*. (2023) 11:1094926. doi: 10.3389/fped.2023.1094926

16. Wang Y, Song F, Zhang X, Yang C. Mitochondrial-related transcriptome feature correlates with prognosis, vascular invasion, tumor microenvironment, and treatment response in hepatocellular carcinoma. *Oxid Med Cell Longev*. (2022) 2022:1592905. doi: 10.1155/2022/1592905

17. Liu W, Du Q, Mei T, Wang J, Huang D, Qin T. Comprehensive analysis the prognostic and immune characteristics of mitochondrial transport-related gene SFXN1 in lung adenocarcinoma. *BMC Cancer*. (2024) 24:94. doi: 10.1186/s12885-023-11646-z

18. Li YP, Liu GX, Wu ZL, Tu PH, Wei G, Yuan M, et al. A novel mitochondrial-related gene signature for the tumor immune microenvironment evaluation and prognosis prediction in lung adenocarcinoma. *J Immunol Res*. (2022) 2022:5366185. doi: 10.1155/2022/5366185

19. Chang J, Wu H, Wu J, Liu M, Zhang W, Hu Y, et al. Constructing a novel mitochondrial-related gene signature for evaluating the tumor immune microenvironment and predicting survival in stomach adenocarcinoma. *J Transl Med*. (2023) 21:191. doi: 10.1186/s12967–023-04033–6

20. Wang Y, Wang DY, Bu KN, Gao JD, Zhang BL. Prognosis prediction and risk stratification of breast cancer patients based on a mitochondria-related gene signature. *Sci Rep*. (2024) 14:2859. doi: 10.1038/s41598-024-52981-w

21. Su Z, Fang H, Hong H, Shi L, Zhang W, Zhang W, et al. An investigation of biomarkers derived from legacy microarray data for their utility in the RNA-seq era. *Genome Biol*. (2014) 15:523. doi: 10.1186/s13059-014-0523-y

22. Dong R, Yang R, Zhan Y, Lai HD, Ye CJ, Yao XY, et al. Single-cell characterization of Malignant phenotypes and developmental trajectories of adrenal neuroblastoma. *Cancer Cell*. (2020) 38:716–33.e6. doi: 10.1016/j.ccell.2020.08.014

23. Roderwieser A, Sand F, Walter E, Fischer J, Gecht J, Bartenhagen C, et al. Telomerase is a prognostic marker of poor outcome and a therapeutic target in neuroblastoma. *JCO Precis Oncol*. (2019) 3:1–20. doi: 10.1200/po.19.00072

24. Pugh TJ, Morozova O, Attiyeh EF, Asgharzadeh S, Wei JS, Auclair D, et al. The genetic landscape of high-risk neuroblastoma. *Nat Genet*. (2013) 45:279–84. doi: 10.1038/ng.2529

25. Ritchie ME, Phipson B, Wu D, Hu Y, Law CW, Shi W, et al. limma powers differential expression analyses for RNA-sequencing and microarray studies. *Nucleic Acids Res*. (2015) 43:e47. doi: 10.1093/nar/gkv007

26. Wilkerson MD, Hayes DN. ConsensusClusterPlus: a class discovery tool with confidence assessments and item tracking. *Bioinformatics*. (2010) 26:1572–3. doi: 10.1093/bioinformatics/btq170

27. Monti S, Tamayo P, Mesirov J, Golub T. Consensus clustering: a resampling-based method for class discovery and visualization of gene expression microarray data. *Mach learning*. (2003) 52:91–118. doi: 10.1023/A:1023949509487

28. Therneau TM. *A package For Survival Analysis in R*. (2024).

29. Therneau TM, Grambsch PM. *Modeling Survival Data: Extending the Cox Model*. New York: Springer (2000).

30. Kassambara A, Kosinski M, Biecek P. *Survminer: Drawing Survival Curves using 'ggplot2'*. (2021).

31. Friedman J, Hastie T, Tibshirani R. Regularization paths for generalized linear models via coordinate descent. *J Stat Software*. (2010) 33:1–22. doi: 10.18637/jss.v033.i01

32. Tibshirani R. Regression shrinkage and selection via the lasso. *J R Stat Soc Ser B: Stat Methodology*. (1996) 58:267–88. doi: 10.1111/j.2517-6161.1996.tb02080.x

33. Heagerty PJ, Lumley T, Pepe MS. Time-dependent ROC curves for censored survival data and a diagnostic marker. *Biometrics*. (2000) 56:337–44. doi: 10.1111/j.0006-341X.2000.00337.x

34. Yoshihara K, Shahmoradgoli M, Martínez E, Vegesna R, Kim H, Torres-Garcia W, et al. Inferring tumour purity and stromal and immune cell admixture from expression data. *Nat Commun*. (2013) 4:2612. doi: 10.1038/ncomms3612

35. Racle J, Gfeller D. EPIC: A tool to estimate the proportions of different cell types from bulk gene expression data. *Methods Mol Biol*. (2020) 2120:233–48. doi: 10.1007/978–1-0716–0327-7_17

36. Becht E, Giraldo NA, Lacroix L, Buttard B, Elarouci N, Petitprez F, et al. Estimating the population abundance of tissue-infiltrating immune and stromal cell populations using gene expression. *Genome Biol*. (2016) 17:218. doi: 10.1186/s13059–016-1070–5

37. Newman AM, Liu CL, Green MR, Gentles AJ, Feng W, Xu Y, et al. Robust enumeration of cell subsets from tissue expression profiles. *Nat Methods*. (2015) 12:453–7. doi: 10.1038/nmeth.3337

38. Jia Q, Wu W, Wang Y, Alexander PB, Sun C, Gong Z, et al. Local mutational diversity drives intratumoral immune heterogeneity in non-small cell lung cancer. *Nat Commun*. (2018) 9:5361. doi: 10.1038/s41467-018-07767-w

39. Barbie DA, Tamayo P, Boehm JS, Kim SY, Moody SE, Dunn IF, et al. Systematic RNA interference reveals that oncogenic KRAS-driven cancers require TBK1. *Nature*. (2009) 462:108–12. doi: 10.1038/nature08460

40. Malta TM, Sokolov A, Gentles AJ, Burzykowski T, Poisson L, Weinstein JN, et al. Machine learning identifies stemness features associated with oncogenic dedifferentiation. *Cell*. (2018) 173:338–54.e15. doi: 10.1016/j.cell.2018.03.034

41. Yang W, Soares J, Greninger P, Edelman EJ, Lightfoot H, Forbes S, et al. Genomics of Drug Sensitivity in Cancer (GDSC): a resource for therapeutic biomarker discovery in cancer cells. *Nucleic Acids Res*. (2013) 41:D955–61. doi: 10.1093/nar/gks1111

42. Geeleher P, Cox NJ, Huang RS. Clinical drug response can be predicted using baseline gene expression levels and *in vitro* drug sensitivity in cell lines. *Genome Biol*. (2014) 15:R47. doi: 10.1186/gb-2014–15-3-r47

43. Stuart T, Butler A, Hoffman P, Hafemeister C, Papalexi E, Mauck WM 3rd, et al. Comprehensive integration of single-cell data. *Cell*. (2019) 177:1888–902.e21. doi: 10.1016/j.cell.2019.05.031

44. Efremova M, Vento-Tormo M, Teichmann SA, Vento-Tormo R. CellPhoneDB: inferring cell-cell communication from combined expression of multi-subunit ligand-receptor complexes. *Nat Protoc*. (2020) 15:1484–506. doi: 10.1038/s41596-020-0292-x

45. Qiu X, Mao Q, Tang Y, Wang L, Chawla R, Pliner HA, et al. Reversed graph embedding resolves complex single-cell trajectories. *Nat Methods*. (2017) 14:979–82. doi: 10.1038/nmeth.4402

46. Zamzami N, Kroemer G. The mitochondrion in apoptosis: how Pandora's box opens. *Nat Rev Mol Cell Biol*. (2001) 2:67–71. doi: 10.1038/35048073

47. Salvioli S, Ardizzoni A, Franceschi C, Cossarizza A. JC-1, but not DiOC6(3) or rhodamine 123, is a reliable fluorescent probe to assess delta psi changes in intact cells: implications for studies on mitochondrial functionality during apoptosis. *FEBS Lett*. (1997) 411:77–82. doi: 10.1016/s0014–5793(97)00669–8

48. Dean PN, Jett JH. Mathematical analysis of DNA distributions derived from flow microfluorometry. *J Cell Biol*. (1974) 60:523–7. doi: 10.1083/jcb.60.2.523

49. Irwin MS, Naranjo A, Zhang FF, Cohn SL, London WB, Gastier-Foster JM, et al. Revised neuroblastoma risk classification system: A report from the children's oncology group. *J Clin Oncol*. (2021) 39:3229–41. doi: 10.1200/jco.21.00278

50. Xie YH, Jiang HZ. The exploration of mitochondrial-related features helps to reveal the prognosis and immunotherapy methods of colorectal cancer. *Cancer Rep (Hoboken)*. (2024) 7:e1914. doi: 10.1002/cnr2.1914

51. Shi Y, Huang G, Jiang F, Zhu J, Xu Q, Fang H, et al. Deciphering a mitochondria-related signature to supervise prognosis and immunotherapy in hepatocellular carcinoma. *Front Immunol*. (2022) 13:1070593. doi: 10.3389/fimmu.2022.1070593

52. Brodeur GM, Seeger RC, Schwab M, Varmus HE, Bishop JM. Amplification of N-myc in untreated human neuroblastomas correlates with advanced disease stage. *Science*. (1984) 224:1121–4. doi: 10.1126/science.6719137

53. Huang M, Weiss WA. Neuroblastoma and MYCN. *Cold Spring Harb Perspect Med*. (2013) 3:a014415. doi: 10.1101/cshperspect.a014415

54. Otte J, Dyberg C, Pepich A, Johnsen JI. MYCN function in neuroblastoma development. *Front Oncol*. (2020) 10:624079. doi: 10.3389/fonc.2020.624079

55. Wang SF, Tseng LM, Lee HC. Role of mitochondrial alterations in human cancer progression and cancer immunity. *J BioMed Sci*. (2023) 30:61. doi: 10.1186/s12929-023-00956-w

56. Zhao Y, Liao P, Huang S, Deng T, Tan J, Huang Y, et al. Increased TOX expression associates with exhausted T cells in patients with multiple myeloma. *Exp Hematol Oncol*. (2022) 11:12. doi: 10.1186/s40164–022-00267–0

57. Huang S, Liang C, Zhao Y, Deng T, Tan J, Zha X, et al. Increased TOX expression concurrent with PD-1, Tim-3, and CD244 expression in T cells from patients with acute myeloid leukemia. *Cytometry B Clin Cytom*. (2022) 102:143–52. doi: 10.1002/cyto.b.22049

58. Huang S, Liang C, Zhao Y, Deng T, Tan J, Lu Y, et al. Increased TOX expression concurrent with PD-1, Tim-3, and CD244 in T cells from patients with non-Hodgkin lymphoma. *Asia Pac J Clin Oncol*. (2022) 18:143–9. doi: 10.1111/ajco.13545

59. Chan GC, Chan CM. Anti-GD2 directed immunotherapy for high-risk and metastatic neuroblastoma. *Biomolecules*. (2022) 12. doi: 10.3390/biom12030358

60. Xia Y, Wang C, Li X, Gao M, Hogg HDJ, Tunthanathip T, et al. Development and validation of a novel stemness-related prognostic model for neuroblastoma using integrated machine learning and bioinformatics analyses. *Transl Pediatr*. (2024) 13:91–109. doi: 10.21037/tp-23–582

61. Krystal J, Foster JH. Treatment of high-risk neuroblastoma. *Children (Basel)*. (2023) 10. doi: 10.3390/children10081302

62. Zhang D, Kaweme NM, Duan P, Dong Y, Yuan X. Upfront treatment of pediatric high-risk neuroblastoma with chemotherapy, surgery, and radiotherapy combination: the CCCG-NB-2014 protocol. *Front Oncol*. (2021) 11:745794. doi: 10.3389/fonc.2021.745794

63. Park JR, Scott JR, Stewart CF, London WB, Naranjo A, Santana VM, et al. Pilot induction regimen incorporating pharmacokinetically guided topotecan for treatment of newly diagnosed high-risk neuroblastoma: a Children's Oncology Group study. *J Clin Oncol*. (2011) 29:4351–7. doi: 10.1200/jco.2010.34.3293

64. Zheng L, Jia J, Finger LD, Guo Z, Zer C, Shen B. Functional regulation of FEN1 nuclease and its link to cancer. *Nucleic Acids Res*. (2011) 39:781–94. doi: 10.1093/nar/gkq884

65. Dratwa M, Wysoczańska B, Łacina P, Kubik T, Bogunia-Kubik K. TERT-regulation and roles in cancer formation. *Front Immunol*. (2020) 11:589929. doi: 10.3389/fimmu.2020.589929

66. Shi M, Guo H, Bai Y, Niu J, Niu X, Sun K, et al. Upregulated mitosis-associated genes CENPE, CENPF, and DLGAP5 predict poor prognosis and chemotherapy resistance of Acute Myeloid Leukemia. *Cancer biomark*. (2022) 35:11–25. doi: 10.3233/cbm-203170

67. Tang N, Dou X, You X, Shi Q, Ke M, Liu G. Pan-cancer analysis of the oncogenic role of discs large homolog associated protein 5 (DLGAP5) in human tumors. *Cancer Cell Int*. (2021) 21:457. doi: 10.1186/s12935–021-02155–9

68. Garcia SN, Guedes RC, Marques MM. Unlocking the potential of HK2 in cancer metabolism and therapeutics. *Curr Med Chem*. (2019) 26:7285–322. doi: 10.2174/0929867326666181213092652

69. Erdreich-Epstein A, Robison N, Ren X, Zhou H, Xu J, Davidson TB, et al. PID1 (NYGGF4), a new growth-inhibitory gene in embryonal brain tumors and gliomas. *Clin Cancer Res*. (2014) 20:827–36. doi: 10.1158/1078–0432.Ccr-13–2053

70. Yang J, Li S, He J, Xu Q, Xie M, Yang C, et al. Dual role of PID1 in regulating apoptosis induced by distinct anticancer-agents through AKT/Raf-1-dependent pathway in hepatocellular carcinoma. *Cell Death Discovery*. (2023) 9:139. doi: 10.1038/s41420–023-01405–1

71. Muller PA, Vousden KH. p53 mutations in cancer. *Nat Cell Biol*. (2013) 15:2–8. doi: 10.1038/ncb2641

72. Gonfloni S, Caputo V, Iannizzotto V. P63 in health and cancer. *Int J Dev Biol*. (2015) 59:87–93. doi: 10.1387/ijdb.150045sg

73. Jong NN, McKeage MJ. Emerging roles of metal solute carriers in cancer mechanisms and treatment. *Biopharm Drug Dispos*. (2014) 35:450–62. doi: 10.1002/bdd.1903

74. Fernández-Hernando C, Suárez Y, Rayner KJ, Moore KJ. MicroRNAs in lipid metabolism. *Curr Opin Lipidol*. (2011) 22:86–92. doi: 10.1097/MOL.0b013e3283428d9d

75. Fontanella RA, Ghosh P, Pesapane A, Taktaz F, Puocci A, Franzese M, et al. Tirzepatide prevents neurodegeneration through multiple molecular pathways. *J Transl Med*. (2024) 22:114. doi: 10.1186/s12967-024-04927-z

76. Lu Q, Ni Y, Wang W, Wang L, Jiang T, Shang L. Dynamin 3 inhibits the proliferation of non-small-cell lung cancer cells by suppressing c-MET-GBR2-STAT3 complex formation. *Front Cell Dev Biol*. (2021) 9:641403. doi: 10.3389/fcell.2021.641403

77. Inokawa Y, Nomoto S, Hishida M, Hayashi M, Kanda M, Nishikawa Y, et al. Dynamin 3: a new candidate tumor suppressor gene in hepatocellular carcinoma detected by triple combination array analysis. *Onco Targets Ther*. (2013) 6:1417–24. doi: 10.2147/ott.S51913

78. Lin S, Tan L, Luo D, Peng X, Zhu Y, Li H. Linc01278 inhibits the development of papillary thyroid carcinoma by regulating miR-376c-3p/DNM3 axis. *Cancer Manag Res*. (2019) 11:8557–69. doi: 10.2147/cmar.S217886

79. Ma Y, Guan L, Han Y, Zhou Y, Li X, Liu Y, et al. siPRDX2-elevated DNM3 inhibits the proliferation and metastasis of colon cancer cells via AKT signaling pathway. *Cancer Manag Res*. (2019) 11:5799–811. doi: 10.2147/cmar.S193805

80. Peng Z, Wang S, Wen D, Mei Z, Zhang H, Liao S, et al. FEN1 upregulation mediated by SUMO2 via antagonizing proteasomal degradation promotes hepatocellular carcinoma stemness. *Transl Oncol*. (2024) 44:101916. doi: 10.1016/j.tranon.2024.101916

81. Hosfield DJ, Mol CD, Shen B, Tainer JA. Structure of the DNA repair and replication endonuclease and exonuclease FEN-1: coupling DNA and PCNA binding to FEN-1 activity. *Cell*. (1998) 95:135–46. doi: 10.1016/s0092–8674(00)81789–4

82. Ishimi Y, Claude A, Bullock P, Hurwitz J. Complete enzymatic synthesis of DNA containing the SV40 origin of replication. *J Biol Chem*. (1988) 263:19723–33. doi: 10.1016/S0021-9258(19)77695-9

83. Goulian M, Richards SH, Heard CJ, Bigsby BM. Discontinuous DNA synthesis by purified mammalian proteins. *J Biol Chem*. (1990) 265:18461–71. doi: 10.1016/S0021-9258(17)44775-2

84. Storici F, Henneke G, Ferrari E, Gordenin DA, Hübscher U, Resnick MA. The flexible loop of human FEN1 endonuclease is required for flap cleavage during DNA replication and repair. *EMBO J*. (2002) 21:5930–42. doi: 10.1093/emboj/cdf587

85. Wang K, Xie C, Chen D. Flap endonuclease 1 is a promising candidate biomarker in gastric cancer and is involved in cell proliferation and apoptosis. *Int J Mol Med*. (2014) 33:1268–74. doi: 10.3892/ijmm.2014.1682

86. Zhang K, Keymeulen S, Nelson R, Tong TR, Yuan YC, Yun X, et al. Overexpression of flap endonuclease 1 correlates with enhanced proliferation and poor prognosis of non-small-cell lung cancer. *Am J Pathol*. (2018) 188:242–51. doi: 10.1016/j.ajpath.2017.09.011

87. Yuwei X, Bingzi D, Zhaowei S, Yujie F, Wei Z, Kun L, et al. FEN1 promotes cancer progression of cholangiocarcinoma by regulating the Wnt/β-catenin signaling pathway. *Dig Liver Dis*. (2024) 56:695–704. doi: 10.1016/j.dld.2023.08.050

88. Xiao Y, Yin M, Wang Y, Shi R, Mao S, Hua Y, et al. Post-translational modifications by acyl groups regulate FEN1's activities and play essential roles in cell proliferation and DNA repair. *Protein Pept Lett*. (2023) 30:597–607. doi: 10.2174/0929866530666230529152209

89. Wu H, Yan Y, Yuan J, Luo M, Wang Y. miR-4324 inhibits ovarian cancer progression by targeting FEN1. *J Ovarian Res*. (2022) 15:32. doi: 10.1186/s13048–022-00959–5

frontiers | Frontiers in Immunology

TYPE Original Research
PUBLISHED 21 June 2024
DOI 10.3389/fimmu.2024.1420847

Check for updates

OPEN ACCESS

EDITED BY
Wantao Wu,
Central South University, China

REVIEWED BY
Furong Huang,
Duke University, United States
Weijie Sun,
Anhui Medical University, China

*CORRESPONDENCE
Bin Li
libin@cicams.ac.cn

†These authors have contributed equally to this work and share first authorship

RECEIVED 21 April 2024
ACCEPTED 06 June 2024
PUBLISHED 21 June 2024

CITATION
Luo H, Wang K and Li B (2024) Integrating single-cell and spatial transcriptomic analysis to unveil heterogeneity in high-grade serous ovarian cancer. *Front. Immunol.* 15:1420847. doi: 10.3389/fimmu.2024.1420847

COPYRIGHT
© 2024 Luo, Wang and Li. This is an open-access article distributed under the terms of the Creative Commons Attribution License (CC BY). The use, distribution or reproduction in other forums is permitted, provided the original author(s) and the copyright owner(s) are credited and that the original publication in this journal is cited, in accordance with accepted academic practice. No use, distribution or reproduction is permitted which does not comply with these terms.

Integrating single-cell and spatial transcriptomic analysis to unveil heterogeneity in high-grade serous ovarian cancer

Haixia Luo†, Kunyu Wang† and Bin Li*

Department of Gynecological Oncology, National Cancer Center/National Clinical Research Center for Cancer/Cancer Hospital, Chinese Academy of Medical Sciences and Peking Union Medical College, Beijing, China

High-grade serous ovarian cancer (HGSOC) presents significant challenges due to its heterogeneity and late-stage diagnoses. Using single-cell and spatial transcriptomics to elucidate the complex landscape of HGSOC to understand its underlying mechanism. Our analysis reveals significant inter- and intra-tumoral diversity, manifested through distinct cellular subpopulations and varied microenvironmental niches. Notably, our findings highlight a widespread immunosuppressive environment, marked by complex networks of cell-cell interactions, particularly evident in areas of elevated tumor cell density within metastatic samples. We identify the exclusive presence of COL14A1+ neoplastic cells in metastatic specimens, alongside a strong correlation between CD8A+ NKT cells and poor prognosis, and elevated CHODL expression in HGSOC metastasis tissues. Furthermore, knockdown experiments targeting CHODL demonstrate its role in reducing migration and invasion abilities in HGSOC cells. A pivotal discovery of our study is the delineation of specific cellular signatures correlated with adverse outcomes, notably a subset of CHODL+ neoplastic cells characterized by a distinct metabolic phenotype with a predilection for lipid metabolism. The therapeutic targeting of this metabolic pathway with existing inhibitors appears promising in curbing tumor proliferation. These findings enhance our understanding of HGSOC heterogeneity and reveal potential therapeutic targets, promising more effective management strategies for this aggressive cancer subtype.

KEYWORDS

HGSOC, spatial transcriptomic, multi-omics, heterogeneity, CHODL

1 Introduction

Ovarian cancer ranks as the eighth most common cause of cancer-related deaths among women globally (1). High-grade serous ovarian carcinoma (HGSOC), the deadliest and most prevalent histologic subtype, is responsible for 70–80% of deaths from ovarian cancer (2, 3). It is characterized by an advanced stage at diagnosis and a propensity for rapid metastasis. The genetic architecture of HGSOC is defined by extensive chromosomal instability and signature mutations in key genes such as TP53 and BRCA1/2, alongside numerous disruptions in the pathways responsible for homologous recombination repair (4, 5). These genetic aberrations contribute to the cancer's diverse clinical manifestations and notable resistance to chemotherapy, underlining the complexity of tumor dynamics and therapeutic outcomes in affected individuals.

The tumor microenvironment (TME), primarily composed of fibroblasts, endothelial cells, lymphocytic infiltrates, and extracellular matrix proteins, can directly influence cancer cell growth, migration, and differentiation, presenting a unique opportunity for diagnosis and treatment (6). The immune system significantly shapes the TME; ongoing inflammation leads to the production of various immunologic gene products that create a favorable microenvironment for tumor growth and progression (7). The presence of specific immune cell types, such as intratumor CD8 + T cells, is associated with improved survival in patients with various cancers, including ovarian cancer (8). These findings indicate that TME heterogeneity especially immune cell, plays a crucial role in determining the malignant phenotypes of cancer cells. However, the heterogeneity of the TME in HGSOC and its association with clinical outcomes, as well as the molecular mechanisms by which various TME components promote or inhibit cancer, remain incompletely understood. Additionally, the interplay between different cellular and non-cellular populations and their spatial organization within the TME in HGSOC requires further elucidation.

Recent advances in single-cell technologies have elucidated the complex cellular landscapes within HGSOC, underscoring the dynamic interactions among cancer cells, immune cells, and stromal elements in the TME. Single cell sequencing enables detailed analysis of transcriptomic characteristics across different cell subsets, revealing cell heterogeneity and microenvironmental features that traditional methods cannot capture (9, 10). However, the aforementioned techniques and analyses cannot provide spatial information. Growing evidence across multiple cancer types indicates that the spatial arrangement of various cellular components within the TME, and their positioning relative to tumor cells, immune cells, and blood vessels, can significantly influence both antitumor and protumor responses (11–13). Spatial transcriptomics technology, capturing genome-wide readouts across biological tissue, enables researchers to determine gene expression spatially within the complex TME (14).

In light of these findings, our study employs scRNA-seq and spatial transcriptomics to dissect the cellular and molecular landscapes of primary HGSOC tumors and their distant metastases. By integrating these state-of-the-art technologies, we aim to uncover the heterogeneity within HGSOC tumors, identify key drivers of metastasis, and elucidate the interactions between tumor cells and the TME that facilitate distant spread. We validated these findings through *in vitro* experiments and immunohistochemistry assays, and corroborated the results using both internal and external data from numerous clinical samples. Our research not only contributes to the understanding of HGSOC biology but also holds promise for identifying novel biomarkers and therapeutic targets to combat HGSOC.

2 Materials and methods

2.1 Acquisition and processing of bulk transcriptomic data

For this study on ovarian cancer, transcriptomic data, encompassing RNA expression profiles along with relevant clinical details, were sourced from the TCGA database via the "TCGAbiolinks" package (15). To enhance the survival analysis's reliability, we omitted samples lacking survival data or with a survival duration under 30 days. Subsequently, the data were converted to Transcripts Per Million (TPM) and subjected to log2 transformation in preparation for further analysis (16).

2.2 Acquisition and processing of single-cell and spatial transcriptomic data

Single-cell transcriptomic data were meticulously acquired from the GEO database (17), specifically targeting primary tumor samples from GSE211956 and metastatic samples from GSE147082, resulting in a comprehensive collection of 11 samples. The Read10 × function was utilized to process the Seurat object containing the gene expression data of each sample. After quality control of the cells, encompassing data normalization to correct for technical variances, identification of 2,000 highly variable genes to focus on biologically significant fluctuations, and the application of specific functions to mitigate cell cycle effects. Batch effects were corrected using the harmonization technique, ensuring comparability across samples. Dimensionality reduction was achieved through UMAP (Uniform Manifold Approximation and Projection) and t-SNE (t-Distributed Stochastic Neighbor Embedding), revealing inherent data structures, while the Louvain algorithm facilitated insightful clustering, uncovering previously unrecognized cell populations. Differential expression analysis was conducted with stringent criteria, employing a p-value < 0.05, log2 fold change > 0.25, and expression proportion > 0.1, to ascertain significant gene variations across clusters.

In parallel, spatial transcriptomic analysis of 8 primary tumor samples from GSE211956 was executed with precision using "SpaceRanger" for initial quality checks. This was followed by meticulous normalization and variable gene selection via the "SCTtransform" method, optimizing data for subsequent analysis. The spatial data, characterized by an average of 2515 spots per sample, underwent a thorough examination and visualization

process through Seurat, enabling a spatially resolved understanding of tumor heterogeneity. The CARD algorithm, informed by single-cell annotations, was applied for cutting-edge spatial data deconvolution, adeptly predicting cell type distributions for each spot, thus bridging the gap between single-cell and spatial transcriptomics. Visualization of spatial cell type distributions and signature score calculations were adeptly achieved using CARD and the "GSVA" package, further complemented by Seurat's AddModelScore function, providing a multifaceted view of the tumor microenvironment and its dynamic interplay with cancer progression.

2.3 Cell annotation

We employed a rigorous and detailed approach to categorize cells within the single-cell transcriptomic datasets. Marker genes were meticulously selected based on established literature and database references to ensure high specificity and sensitivity for each cell type. For epithelial cells, markers included "EPCAM" (epithelial cell adhesion molecule), "KRT18" and "KRT19" (keratins 18 and 19), and "CDH1" (E-cadherin) (18), reflecting their pivotal role in maintaining epithelial integrity and function. Fibroblast identification hinged on the expression of "DCN" (decorin), "THY1" (CD90), "COL1A1", and "COL1A2", which are indicative of extracellular matrix production and fibroblast activation (19). Endothelial cells were distinguished by "PECAM1" (CD31), "CLDN5" (claudin-5), "FLT1" (VEGFR-1), and "RAMP2", markers that denote vascular structures and blood vessel lining (20). T-cells were identified through T-cell receptor components "CD3D", "CD3E", "CD3G", and "TRAC", underscoring their role in adaptive immunity. NK cell markers "NKG7", "GNLY" (granulysin), "NCAM1" (CD56), and "KLRD1" (CD94) were chosen for their relevance in innate immune responses. B-cells were annotated using "CD79A", "IGHM", "IGHG3", and "IGHA2", reflecting their antibody production capabilities. Lastly, mast cells were identified by "KIT" (CD117), "MS4A2" (FcεRI), and "GATA2", known for their role in allergic responses and tissue homeostasis. Following cell annotation, we conducted clustering analyses on epithelial cells, immune cells (including T-cells, NK cells, B-cells, and mast cells), and fibroblasts to dissect the tumor heterogeneity further.

2.4 Cell culture and lentivirus packaging

The cell lines 293T, ES-2, OVCAR3, SKOV3, OVCA-429, and TOV-21G were procured from the American Type Culture Collection (ATCC; Manassas, VA, USA). A2780 cells were obtained from the National Experimental Cell Resource Sharing Platform (Beijing, China), and 3AO cells were purchased from the Cell Bank of the Chinese Academy of Sciences (Shanghai, China). 293T cells were cultured in DMEM supplemented with 10% fetal bovine serum (FBS), SKOV3 cells in McCoy's 5A with 10% FBS, and the rest in RPMI 1640 10% FBS.

To generate pLKO.1-puro lentiviruses, HEK293T cells were co-transfected with packaging plasmids psPAX2, pMD2G, and lentiviral vectors. As described previously (21), lentivirus infection was performed in accordance with the manufacturer's guidelines, and puromycin (2 μg/mL) (540222, Sigma) was applied to establish the stable cellular populations. The CHODL shRNA sequences were as follows (5′-3′): sh1, GCAAGTATGAACCAGAGATTA and sh2, GCATATTCATTGATGAGGGTT.

2.5 Tissue microarray

Tissue chips from 125 patients with HGSOC were supplied by the Department of Gynecology Oncology, National Cancer Center/National Clinical Research Center for Cancer/Cancer Hospital. These patients underwent surgical resection from January 2010 to October 2019. Following the exclusion of 3 unsuitable samples, the remaining 119 samples were subjected to further analysis.

2.6 Western blotting

Western blotting procedure was performed as described previously (21). Post-blocking with 5% skim milk, the membranes underwent overnight incubation at 4°C with anti-CHODL (diluted at 1:1000; ab236742, Abcam) and anti-GAPDH (diluted at 1:4000; Abclonal) antibodies. Subsequent visualization of the immunoblots was achieved using the ImageQuant LAS-4000 System (GE).

2.7 Immunohistochemistry

Tissue microarrays were stained with anti-CHODL antibody (1:100; ab236742, Abcam). The images were captured by Aperio ScanScope (Leica, Nussloch, Germany).

2.8 Transwell assays

The migration and invasion capabilities of A2780 cells were evaluated using the transwell assay as described previously (21). Briefly, cells (2×10^4/well) were seeded in 200 μL of serum-free medium. The lower chamber contained 600 μL of medium with 10% FBS. Matrigel (BD Bioscience, USA) was applied to the upper compartment for the invasion assay or omitted for the migration assay. After 24 hours, cells that had invaded or migrated to the lower chamber were stained with 0.1% crystal violet and quantified. Each experiment was conducted independently in triplicate.

2.9 Subclustering analysis of cell populations

We adopted a refined approach to discern intricate subpopulations among immune cells, epithelial cells, and fibroblasts, leveraging the robust capabilities of the Seurat

package. Initially, we performed a high-resolution clustering analysis, adjusting the resolution parameter in Seurat to detect subtle variations within the broad cell types identified. Differential expression analysis between the identified clusters was then performed to select specific markers for each cell type. The UMAP technique was then employed to visualize the subclusters in a two-dimensional space, allowing for the intuitive interpretation of the complex cellular landscape. To enhance the rigor of our subclustering analysis, statistical tests were incorporated to validate the significance of the identified subclusters.

2.10 Copy number variation analysis

We employed the InferCNV software to conduct a comprehensive Copy Number Variation (CNV) analysis on subpopulations of tumor cells, with a specific focus on distinguishing malignant cells within the tumor microenvironment. Immune cells were meticulously chosen as the reference for comparison, based on their stable genomic profile and minimal CNV alterations.

2.11 Pseudotime analysis

For the pseudotime analysis within epithelial cell subpopulations, we utilized the Monocle2 software, specifically employing its DDRTree algorithm for effective dimensionality reduction, while adhering to the default settings for other parameters. This analysis was strategically aimed at delineating the cell differentiation trajectory.

2.12 Transcription factor analysis

We applied the SCENIC software, maintaining default settings for the RcisTarget and GRNBoost databases. The RcisTarget package was deployed to pinpoint transcription factors notably expressed within our gene list, whereas the AUCell package quantified the activity levels of regulatory networks across identified cell types.

2.13 Cell-cell communication

For cell-cell communication assessment, the CellChat package was our tool of choice. Starting with the normalized gene expression matrix, we constructed a CellChat object, followed by the execution of preprocessing functions such as identifyOverExpressedGenes and identifyOverExpressedInteraction, all under default parameters. Subsequent steps involved the computeCommunProb and filterCommunication functions to unveil potential ligand-receptor interactions. The analysis culminated with the aggregateNet function, synthesizing a comprehensive cell communication network.

2.14 Statistical analysis

All data processing, statistical analysis, and plotting were performed using R 4.1.3 software. The Pearson correlation coefficient was used to evaluate the correlation between two continuous variables. The chi-square test was employed for comparison of categorical variables, while the Wilcoxon rank-sum test or t-test was used for comparing continuous variables. Cox regression and Kaplan-Meier analysis were conducted using the survival package.

3 Results

3.1 Single-cell transcriptome atlas of HGSOC

Utilizing single-cell transcriptomics, our investigation revealed a complex cellular landscape within the tumor microenvironment of HGSOC, characterized by the identification of 22 distinct cell clusters. This diversity was elucidated through the detection of specific markers, such as EPCAM and KRT for epithelial cells, DCN and COL1A1 for fibroblasts, PECAM1 and CLDN5 for endothelial cells, and various others for immune cell types including T-cells, NK-cells, B-cells, and mast cells (Figure 1A). Sophisticated visualization methods, like heatmaps (Figure 1B) and t-SNE plots (Figure 1C), effectively demonstrated the unique expression patterns of these markers, highlighting the considerable heterogeneity among the cells present. The deployment of scType software further refined the classification of immune cells, providing deeper insights into the intricacies of the tumor's cellular composition. Notably, these cell types were present in nearly all patients, albeit in differing proportions (Figure 1D). Tumor cells predominated, exhibiting elevated levels of transcripts and copy number variations, indicative of their malignant nature. Among immune cells, T-cells were most prevalent, with a notable reduction in B cells, myeloid cells, and mast cells in primary tumors compared to metastatic samples. Conversely, stromal cells were significantly diminished in the tumor microenvironment of metastatic samples, likely due to the expansion of tumor cells.

3.2 Heterogeneity through spatial transcriptomic expression profiling

We applied the inferCNV software to evaluate copy number variations (CNVs) across eight designated spots within each sample. To dissect the cellular composition of the spatial transcriptomic data, we implemented the CARD algorithm. Spots explicitly identified as tumor cells were categorized accordingly, with remaining cells labeled as non-tumor. For a representative sample (SP1), we showcased a range of visualizations, including hematoxylin and eosin (H&E) staining, CNV score distribution, cellular composition, and clustering results for both tumor and

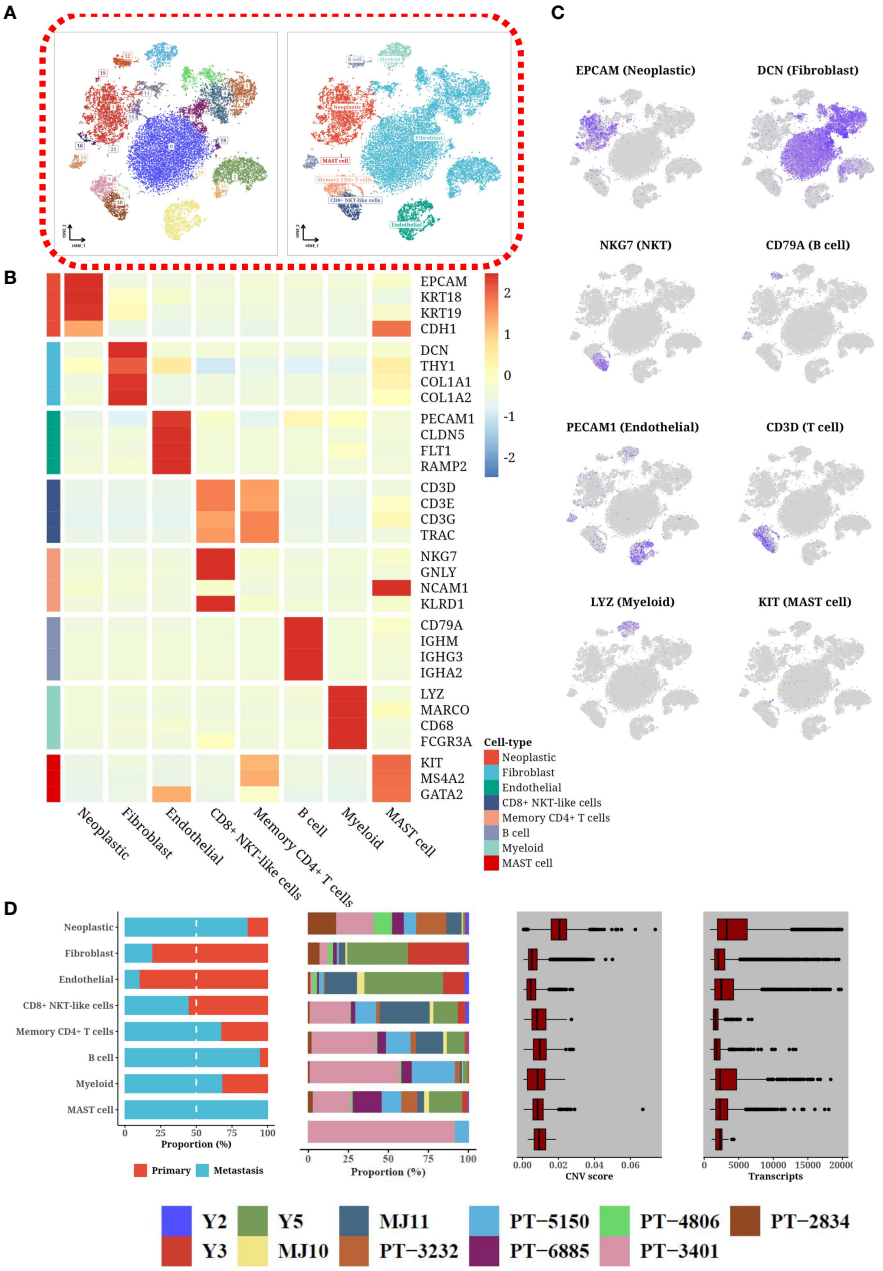

FIGURE 1
Heterogeneity through single-cell expression profiling. **(A)** tSNE plot categorizing single-cell data by clusters and cell types. **(B)** Heatmap displaying the expression levels of marker genes in different cell types. **(C)** tSNE plot illustrating the expression patterns of various marker genes across different cell types. **(D)** Composite plot showing the composition of cell sources, patient composition, number of cells, number of transcripts detected, and copy number variation (CNV) status for different cell types.

non-tumor cells (Figure 2A). SP1, SP4, SP7, and SP8, linked to suboptimal or partial chemotherapy responses, exhibited a predominant tumor cell presence (data not displayed). Further analysis involved segregating spots into tumor and non-tumor groups, followed by dimensional reduction and clustering. The tumor cells were classified into six subgroups, with each subgroup's composition, CNV status, and marker genes elucidated on a tSNE plot (Figure 2B). Non-tumor cells were divided into four subgroups (Figure 2C). A comparative heatmap analysis between samples showing poor responses and those with better or partial responses highlighted a greater prevalence of tumor cells in the former and an increased presence of non-tumor cells, such as fibroblasts, in the latter (Figures 2D, E).

3.3 High heterogeneity of neoplastic cells

Neoplastic (NEO) cells were segregated and subjected to dimensionality reduction and clustering, unveiling five unique subgroups (Figure 3A). A bar graph delineated the cell

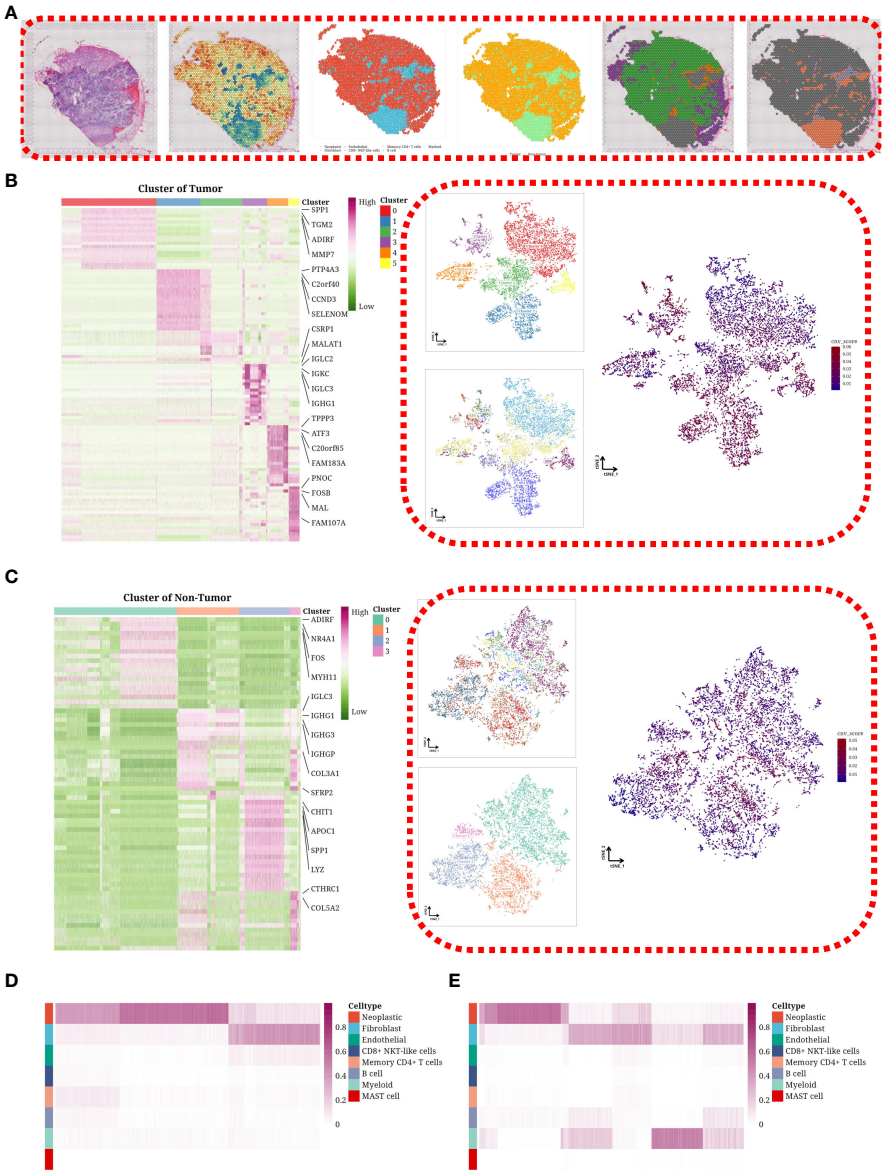

FIGURE 2
Heterogeneity through spatial transcriptomic expression profiling. **(A)** H&E staining image, distribution of CNV scores, cellular composition of the tumor sample, tumor or non-tumor classification, clustering results of tumor cells, and clustering results of non-tumor cells in representative SP2 sample. **(B)** Heatmap showing marker expression of tumor cell subgroups on the left, and tSNE plot illustrating the composition, CNV score, and patient distribution of tumor cell subgroups on the right. **(C)** Heatmap showing marker expression of non-tumor cell subgroups on the left, and tSNE plot illustrating the composition, CNV score, and patient distribution of non-tumor cell subgroups on the right. **(D)** Heatmap depicting the cellular composition differences in poor_response samples. **(E)** Heatmap illustrating the cellular composition differences in good_response/partial_response samples.

composition from varied origins, highlighting KRT14$^+$ NEO cells in primary samples and COL14A1+ NEO cells in metastatic counterparts (Figure 3B). Transcription factor (TF) profiles for each subgroup were analyzed, with a heatmap illustrating the enrichment of specific TFs, such as the heightened activity of FOSL1 in KRT14+ NEO cells indicative of an immunomodulatory phenotype. FOSB and JUNB were notably active in COL14A1$^+$ NEO cells, implicating their roles in differentiation, proliferation, and apoptosis (Figure 3C). Cellular trajectory analysis, using primary cells as a reference, depicted multiple developmental pathways within metastatic samples, indicating subtype diversity (Figure 3D). These pathways culminated in branches rich in CHODL$^+$ NEO cells. Pseudotemporal analysis positioned KRT14$^+$ NEO cells at the onset, whereas COL14A1$^+$ NEO cells were intermediate, with the bulk of cells at the trajectory's end (Figures 3E, F). A scatter plot illustrated the pseudotemporal evolution of six genes (MITF, KIT, VIM, CCL2, C1R, STAT3), with a heatmap showcasing gene expressions linked to pseudotemporal progression (Figures 3G, H). This analysis revealed a loss of the immune-related molecule

10.3389/fimmu.2024.1420847

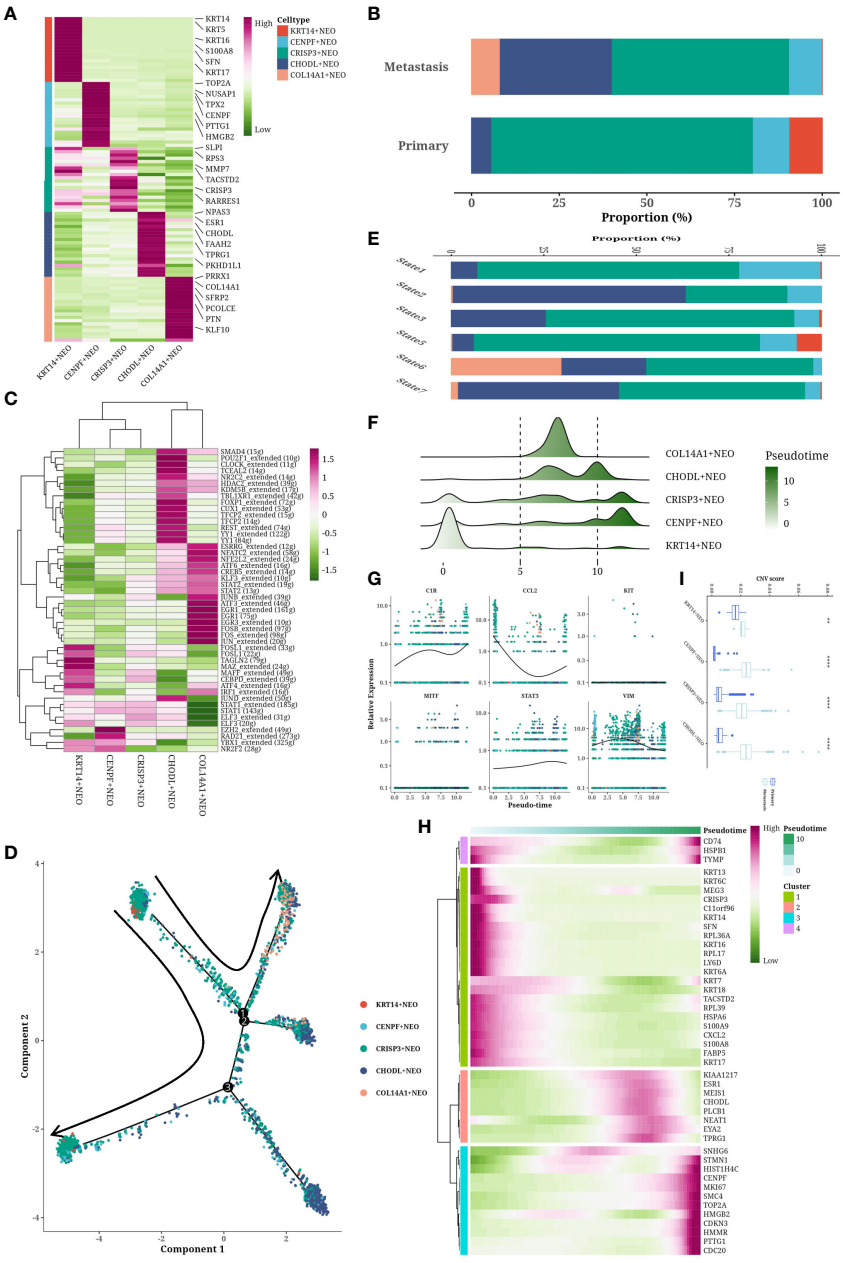

FIGURE 3
Subtyping analysis of tumor cells. **(A)** Cell communication network map of two cell groups. **(B, C)** Cell communication scatterplot depicting intercellular interactions between two cell groups. **(D)** Chord diagram illustrating the signaling pathways of MK. **(E)** Chord diagram depicting the signaling pathways of GALECTIN. **(F)** Spatial expression maps showing the distribution of LGALS9_CD44 in representative samples. **(G)** Spatial expression maps showing the distribution of LGALS9_HAVCR2 in representative samples.

CCL2 over time, contributing to a "cold" tumor microenvironment, and an increase in metastasis-associated molecules like MITF, KIT, and VIM, suggesting a potential transition to a mesenchymal phenotype. CNVs were distinct across cell types and origins (Figure 3I). Metastatic NEO cells, especially those expressing COL14A1, not analyzed in primary samples due to their exclusivity to metastatic sites, displayed a more malignant profile than their primary counterparts, with CHODL$^+$ NEO cells at the developmental culmination exhibiting the highest CNV levels.

3.4 Functional analysis of endpoint cells (CHODL$^+$ NEO cells)

In our comparative analysis of primary and metastatic tumor samples, we noted a markedly higher prevalence of CHODL$^+$ NEO cells in metastatic specimens (Supplementary Figure S1A). A heatmap delineating gene expression differences between CHODL$^+$ NEO cells and their counterparts underscored the upregulation of genes associated with lipid metabolism in the

former group (Supplementary Figure S1B). We further explored lipid metabolism pathways, computing signature scores for both cell populations and illustrating the disparities through heatmap visualization, which highlighted distinct variations in the FATTY_ACID_BETA_OXIDATION pathway (Supplementary Figure S1C). Additionally, SMAD4 was identified as a significantly enriched transcription factor in CHODL+ NEO cells, with its expression profile analyzed within a control dataset. We examined the distribution of FATTY_ACID_BETA_OXIDATION pathway scores in patients SP1 and SP6, categorizing cells based on SMAD4 expression with the mean as a threshold (Supplementary Figure S1D). Violin plots underscored significant disparities in pathway scores between the two groups (Supplementary Figures S1E, F), underscoring the unique metabolic phenotype of CHODL$^+$ NEO cells.

3.5 The anti-tumor immune function of metastatic samples was impaired

T and B cells were isolated from the sample and subjected to dimensionality reduction clustering analysis, which identified nine distinct cell clusters (Figure 4A). Differential gene expression analysis was then performed for each cluster, visually represented as a volcano plot (Figure 4B). To validate cell subtypes, t-SNE plots were utilized to illustrate the expression patterns of subtype-specific marker genes (Figure 4C). The distribution of cells within each cluster was graphically depicted using a bar chart (Figure 4D). Notably, metastatic samples exhibited a significant decrease in C0 (CD8A$^+$ NKT) cells and a significant increase in most B-cells and CD4+ T cells compared to primary samples. Hallmark gene set scores were computed for each cluster and visualized in another heatmap (Figure 4E), indicating stronger activation levels in C6 and C7. Furthermore, immune-related gene expression profiles across different clusters were elucidated through an additional heatmap (Figure 4F). In metastatic samples, there was a notable increase in cells with immunosuppressive effects and a significant loss of cells with cytotoxic functions. To further assess CD8$^+$ cells, cytotoxicity and exhaustion values were determined, revealing notable differences among different CD8$^+$ cell subgroups (Figure 4G). Additionally, the expression distributions of four immune-related genes (GZMB, GZMH, PRF1, GNLY) within CD8$^+$ cells (C0 and C5) were visualized (Figure 4H). Comparing the proportions of C0 in primary and metastatic samples, a significantly higher content was observed in the primary samples (Figure 4I). Importantly, our analysis unveiled a correlation between the diminished abundance of C0 (CD8A$^+$ NKT) cells and poorer survival outcomes in the TCGA-OV cohort (Figure 4J).

3.6 Decreased CCL3-secreting M1 macrophages accelerate metastasis

Through isolation and dimensionality reduction clustering, we delineated seven myeloid cell subtypes, illustrated in Figure 5A. A volcano plot highlighted differentially expressed genes across these subgroups (Figure 5B). t-SNE visualizations confirmed our classifications, showcasing gene expression through subtype-specific markers (Figure 5C). A pie chart detailed the composition of primary versus metastatic subgroups (Figure 5D), revealing notable shifts: a decrease in C4 (CCL3$^+$) cells, and an increase in C2 (CCL22$^+$), C3 (TOP2A$^+$), and C5 (ART3$^+$) within metastatic samples. Hallmark pathway activation levels were analyzed, with C4 and C5 showing heightened activity (Figure 5E). Macrophage trajectory analysis from primary cells (C0+C4+C6) unveiled a unique differentiation pathway (Figure 5F), and a heatmap of immune gene expression within macrophage clusters underscored an active immune function in C4 (Figure 5G). Violin plots further elucidated significant differences between subgroups (Figures 5H, I), suggesting C4 as pro-inflammatory M1 macrophages, C0 as M2 macrophages, and C6 as undifferentiated M0 macrophages.

3.7 Subtyping analysis of stroma cells

We isolated stromal cells and subjected them to dimensionality reduction clustering analysis, which enabled us to identify 14 different cell subtypes and determine their corresponding cellular origins (Figures 6A, B). To ensure the accuracy of our findings, we employed marker genes specific to each subtype and visualized their expression patterns using t-SNE plots (Figure 6C). Notably, we observed that myoCAF, iCAF, and endothelial cells were clustered separately. Subsequently, we performed differential gene expression analysis within each subgroup and presented the results in a differential heatmap (Figure 6D). To gain further insight into the characteristics of each subgroup, we evaluated the Hallmark gene set scores and generated a corresponding heatmap (Figure 6E). Interestingly there was a positive correlation between endothelial and fibroblast expression (Figure 6F). Moreover, we investigated the abundance of fibroblasts and endothelial cells across the spatial transcriptomic samples and found that the content of fibroblasts was higher than that of endothelial cells (Figure 6G).

3.8 Cell communication analysis

We conducted an in-depth analysis of cellular communication in both primary and metastatic cells. This analysis allowed for a comprehensive comparison of the results, enabling us to generate informative network graphs (Figure 7A) and scatter plots (Figures 7B, C) that visually depict the intricate patterns of cellular communication. To further investigate this phenomenon, we carefully examined the chord diagrams representing the MK and GALECTIN signal pathways. As a result, we constructed compelling statistical bar charts (Figures 7D, E) that effectively illustrate the ligand-dependent receptor signaling dynamics. Additionally, we quantified the expression of LGALS9_CD44 and LGALS9_HAVCR2 (Figures 7F, G) in spatial transcriptomic samples. Notably, our findings clearly demonstrated a significantly higher expression level of LGALS9_CD44 compared to LGALS9_HAVCR2.

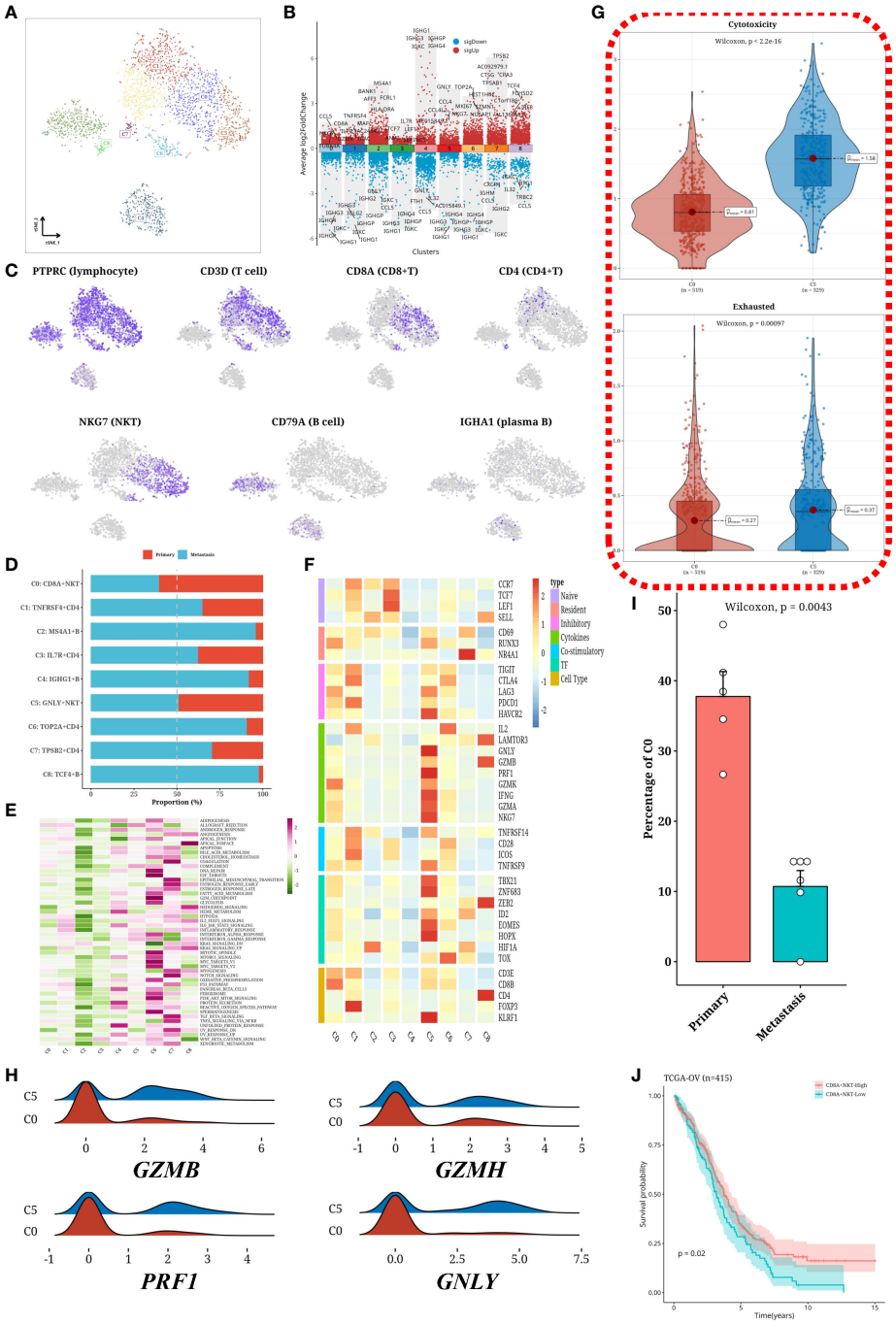

FIGURE 4
Subtyping analysis of T/B cells. **(A)** tSNE plot showing subgroups of T cells and B cells. **(B)** Volcano plot depicting differentially expressed genes in each subgroup. **(C)** tSNE plot illustrating the expression of immune cell markers. **(D)** Bar graph displaying the distribution of T cell and B cell subgroups across different samples. **(E)** Heatmap showing the scores of Hallmark gene sets in each subgroup. **(F)** Heatmap demonstrating the expression of immune-related genes in each subgroup. **(G)** Violin plot comparing the Cytotoxicity and Exhausted values of different subgroups of CD8+ T cells. **(H)** Ridge plot showing the expression levels of four immune-related genes (GZMB, GZMH, PRF1, GNLY) in CD8+ T cell subgroups. **(I)** Bar graph representing the proportion of C0 subgroup in primary and metastatic samples. **(J)** Survival analysis results of C0 (CD8A+NKT) cell content in the TCGA-OV cohort.

3.9 Experimental validation of CHODL

Given the higher risk coefficient of CHODL, we examined the tumor tissues from HGSOC patients, and found that the expression of CHODL was higher in the metastasis tissues compared to that of primary tissues (Figure 8A). Furthermore, high expression of CHODL was associated with worse prognosis (Figure 8B). We selected CHODL for the experimental validation. As shown in Figure 8C, CHODL protein expression was relatively high in the A2780 cell line. Therefore, we knocked down the gene in A2780 cell line (Figure 8D) to further determine its biological significance. Transwell assays demonstrated that knockdown of CHODL

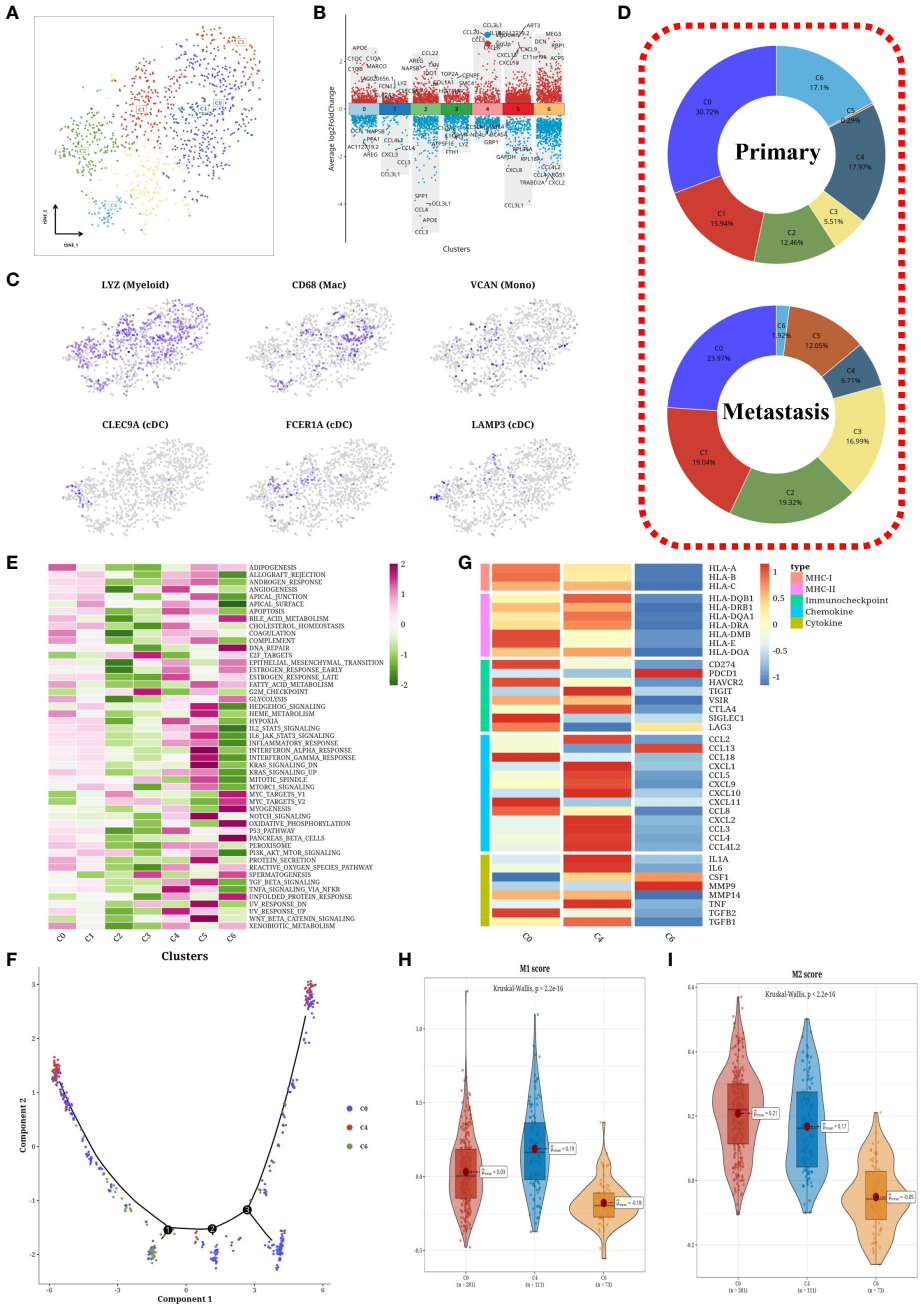

FIGURE 5
Subtyping analysis of myeloid cells. **(A)** tSNE plot of subpopulations of myeloid cells. **(B)** Volcano plots showing differentially expressed genes among each subpopulation. **(C)** tSNE plot of marker expression levels in myeloid cells. **(D)** Pie charts depicting the composition of subpopulations in primary and metastatic samples. **(E)** Heatmaps displaying scores of hallmark gene sets in each subpopulation. **(F)** Cell trajectory analysis plot of macrophages. **(G)** Heatmaps displaying expression levels of immune-related genes in macrophage subpopulations. **(H)** Violin plots showing differential M1 score among subpopulations of macrophages. **(I)** Violin plots showing differential M2 score among subpopulations of macrophages.

strongly inhibited cell migration and invasion in A2780 cells (Figure 8E).

4 Discussion

80% of HGSOC patients present abdominal metastasis initially, which is a foothold for subsequent tumor recurrence and unfavorable prognosis. In this comprehensive investigation, we meticulously analyze the intricate landscape of HGSOC using single-cell and spatial transcriptomic analyses. We aim to discern the transcriptome landscape of the tumor/immune interactions in primary or metastatic HGSOC tissues across spatial and temporal dimensions. Our findings reveal pronounced inter- and intra-tumor heterogeneity in HGSOC, accompanied by a highly suppressive TME and intricate cell-cell communications, particularly in metastatic HGSOC. Notably, CHODL+NEO and CD8A+ NKT cells correlate closely with metastasis and poorer prognosis

10.3389/fimmu.2024.1420847

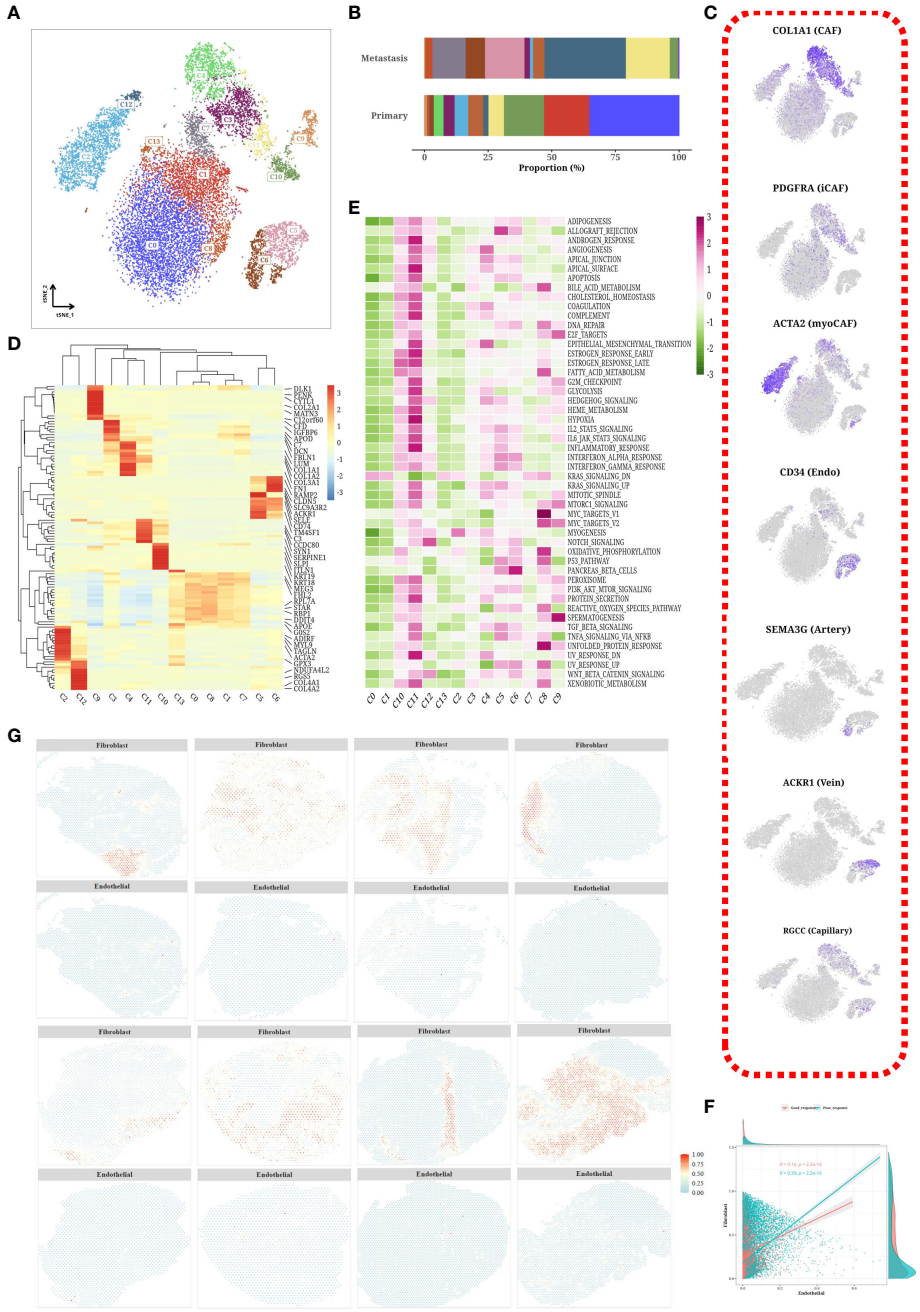

FIGURE 6
Subtyping analysis of stroma cells. **(A)** tSNE plot of subpopulations of stromal cells. **(B)** Bar chart showing the proportion of each subpopulation in different samples. **(C)** tSNE plot of marker expression levels in stromal cell subpopulations. **(D)** Heatmap displaying differentially expressed genes among each subpopulation. **(E)** Heatmap displaying scores of hallmark gene sets in each subpopulation. **(F)** Scatterplot showing correlation between content of endothelial cells and fibroblasts. **(G)** Spatial distribution of content of fibroblasts and endothelial cells in different tumor samples.

among HGSOC patients. Further clinical analysis and experiments support CHODL's potential role as a pivotal regulatory factor in HGSOC metastasis, making it a promising therapeutic target.

We highlighted the considerable intratumoral and intertumoral variability in HGSOC, presenting formidable challenges in the realms of treatment efficacy and prognostication. Through the identification of distinct cellular populations at both primary and metastatic sites, our study elucidates the evolutionary trajectory of tumor cells, shedding light on the metastatic cascade. This diversity spans not only the tumor cells but also the stromal and immune constituents within the TME, all contributing to the tumor's adaptive resilience. Notably, the identification of specific subpopulations, such as CHODL^{+} NEO cells, associated with adverse outcomes and a propensity for metastasis, provides critical insights into the cellular mechanisms underpinning HGSOC dissemination. This concept of cell subclusters driving metastasis resonates with findings in melanoma, where specific cell states are linked to tumor advancement (22, 23). Chondrolectin (CHODL) has emerged as a

10.3389/fimmu.2024.1420847

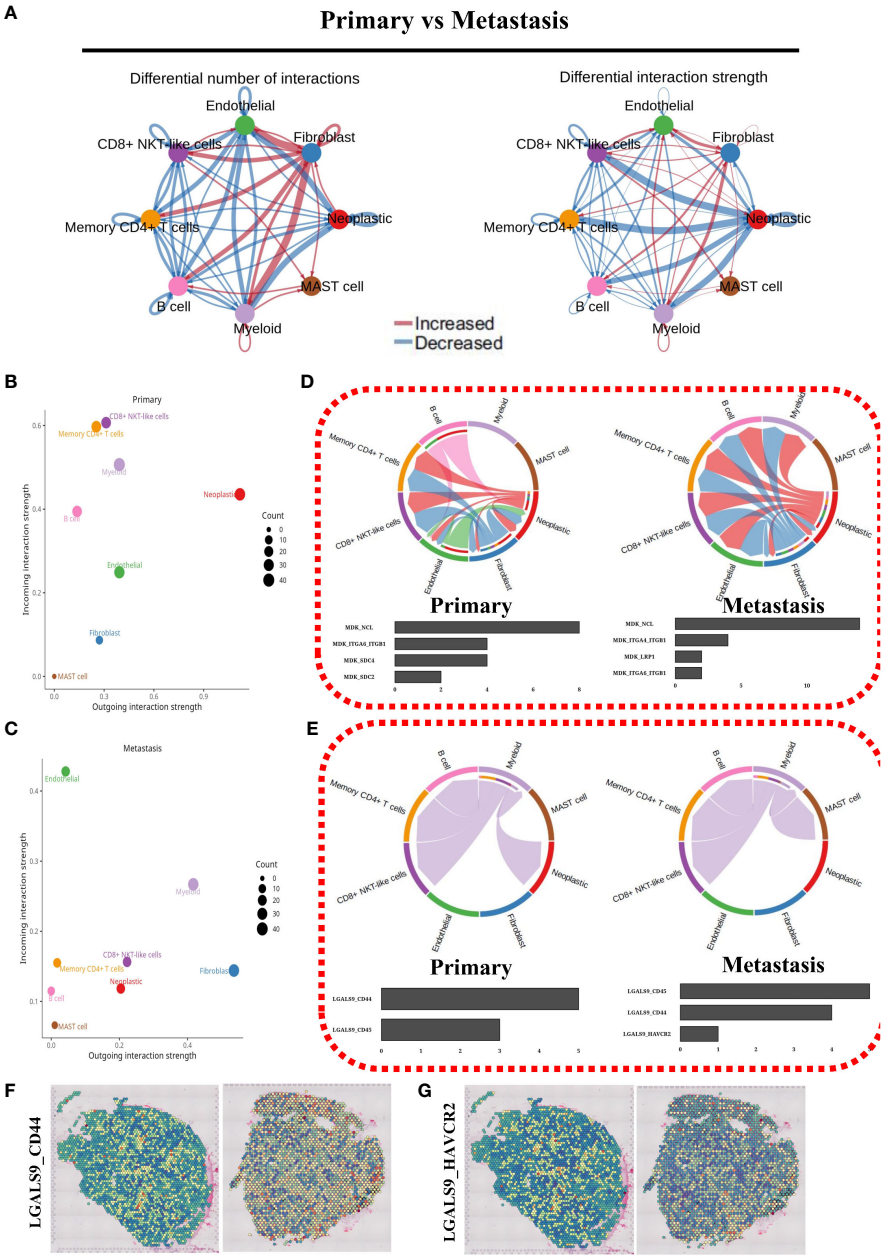

FIGURE 7
Cell communication analysis. **(A)** Cell communication network map of two cell groups. **(B)** Cell communication scatterplot depicting intercellular interactions between two cell groups. **(C)** Chord diagram illustrating the signaling pathways of MK. **(D)** Chord diagram depicting the signaling pathways of GALECTIN. **(E)** Spatial expression maps showing the distribution of LGALS9_CD44 in representative samples. **(F)** Spatial expression maps showing the distribution of LGALS9_HAVCR2 in representative samples.

significant molecular player in the realm of cancer research, particularly in colorectal cancer (CRC) (24) and non-small cell lung cancer (NSCLC) (25). The aberrant hypermethylation of CpG islands is a hallmark of CRC, and CHODL has been identified as a novel gene preferentially methylated in human CRC. Notably, the downregulation of CHODL in CRC, driven by promoter hypermethylation, has been associated with poor survival rates, especially in patients with early-stage CRC (24). Moreover, the expression of CHODL, screened through a comprehensive analysis of gene transactivation in lung cancers, has been correlated with the clinicopathologic significance in patient tissues. The strong positivity of CHODL protein is linked with shorter survival rates in NSCLC patients, underscoring its potential as an independent prognostic factor (25). Given the relatively high-risk coefficient of CHODL in the model, we further validated this gene in cellular models of HGSOC. Our findings suggest that CHODL is a metastasis-related gene that promotes HGSOC cell migration and invasion, and its high expression in the tumor tissues is associated with poor prognosis. However, the mechanism and the participated signaling pathway of CHODL in HGSOC remains to be further investigated, and the possibility of CHODL as a therapeutic target will be further explored in our subsequent study.

10.3389/fimmu.2024.1420847

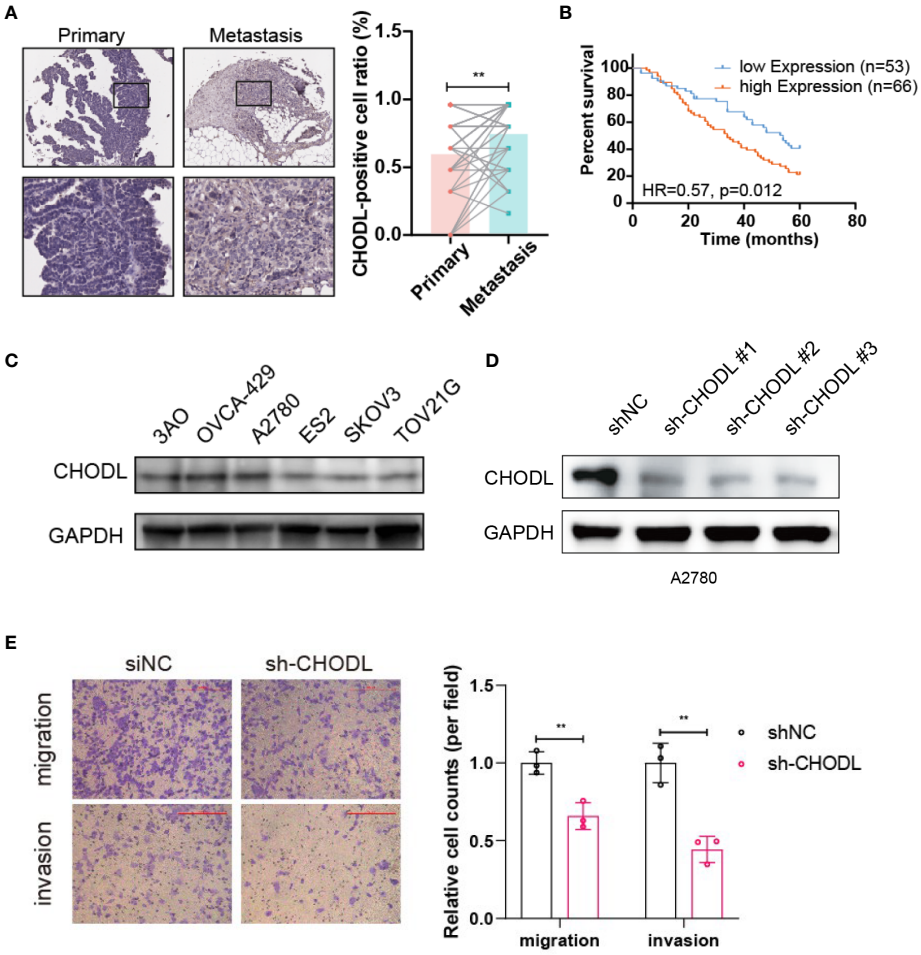

FIGURE 8
CHODL regulates migration and invasion in HGSOC cells. **(A)** Immunohistochemical analysis of CHODL expression in 52 paired samples from primary and metastatic HGSOC tissues. **(B)** The survival data analysis of 119 HGSOC patients. **(C)** Immunoblot depicting the expression of CHODL protein in 6 common HGSOC cell lines. **(D)** Immunoblot demonstrating CHODL expression levels in A2780 cells following CHODL gene knockdown. **(E)** Transwell assays evaluating the effects of CHODL on the invasion capabilities of A2780 cells. Scale bar represents 200 μm. Statistical analysis of transwell assays is presented in the right. The data are presented as the mean ± s.d. values; t-test, $^{**}p < 0.01$; n = 3.

We further elucidate the tumor's metastatic potential through the lens of cellular pathways exploitation, notably those regulated by SMAD4. The augmented activation of lipid metabolism pathways, potentially mediated by SMAD4 in CHODL$^+$ NEO cells, underscores the complexity of cancer progression mechanisms. SMAD4's role as a central mediator in the TGF-β signaling pathway, regulating key cellular processes such as proliferation, differentiation, and apoptosis, is well-documented, with its involvement in cancer highlighting its potential as a therapeutic target. SMAD4, a central mediator in the TGF-β signaling pathway (26), plays a pivotal role in the regulation of cellular processes such as proliferation, differentiation, and apoptosis (27). SMAD4's presence was found to impart vulnerability to ferroptosis, a form of regulated cell death, in highly invasive tumor cells induced by TGF-β1 (28). Ferroptosis is distinct from other forms of cell death, such as apoptosis, and is characterized by the accumulation of iron-dependent lipid peroxides (29). The implication of SMAD4 in ferroptosis suggests a nuanced role in cancer cell survival and death, offering potential therapeutic avenues to exploit this vulnerability in SMAD4-positive cancers.

The highly immunosuppressive TME observed in HGSOC, particularly in tumors with distant metastases, underscores the challenges in harnessing the immune system for therapeutic benefit. The increase in exhausted cells, alongside a decrease in CD8A$^+$ NKT cells in tumors with metastatic involvement, paints a picture of a TME adept at evading immune surveillance. The decrease in CD8A$^+$ NKT cells, known for their potent anti-tumor activity (30), in metastatic tumors highlights a potential mechanism by which HGSOC evades immune-mediated destruction. This finding is particularly intriguing given the emerging role of NKT cells in cancer immunotherapy (31). Research has shown that CD8A$^+$ NKT-like cells not only possess cytotoxic granules, indicative of their potential to directly engage and destroy tumor cells, but also secrete high levels of interferon-gamma (IFN-γ) when stimulated by TCR-matched antigens (32). The secretion of IFN-γ is particularly noteworthy as it plays a crucial role in antitumor immunity by activating other immune cells and increasing the

immunogenicity of cancer cells. Further insights into the distinct populations and functional specializations of NKT cells, including $CD8A^+$ NKT-like cells, highlight the complexity of the immune system's interaction with cancer (33). These cells' unconventional lifestyles and roles in tumor immunity underscore the potential for novel therapeutic strategies that harness their unique capabilities.

The complex cell-cell communications unveiled in our study, especially pronounced in tumors with distant metastases, reveal a sophisticated network of interactions that facilitate tumor progression. The dialogues between stromal, tumor, and immune cells underscore the collaborative nature of the TME in promoting tumor growth and evasion from immune surveillance. This complexity is further exemplified by the role of metabolic reprogramming, particularly the shift towards lipid metabolism in facilitating metastasis. One of the key findings in this area is the discovery of various mechanisms through which lipid metabolism promotes tumor growth and survival, many of which operate independently of traditional cellular bioenergetics. For example, the reprogramming of lipid metabolism in cancer cells can lead to the accumulation of specific lipid species that contribute to the malignant phenotype, influencing processes such as ferroptotic-mediated cell death, tumor metastasis, and interactions with immune cells within the tumor microenvironment (34). Lipid droplets, in particular, have been identified as crucial players in cancer, acting as reservoirs for energy storage and sources of signaling molecules that can protect cancer cells under stressful conditions, such as hypoxia or nutrient deprivation (35). The therapeutic potential of targeting the lipid metabolism pathway, as demonstrated by the efficacy of etomoxir in suppressing metastasis, opens new avenues for intervention (36). This approach aligns with the growing interest in targeting metabolic pathways as a means to thwart cancer progression.

Utilizing single-cell sequencing technology, we have been able to thoroughly analyze the transcriptomic characteristics of different cell subsets in tumor tissues. single-cell sequencing has enabled us to deeply explore cellular heterogeneity and microenvironment characteristics, identify rare cell subpopulations, examine cell-cell interactions, and uncover potential therapeutic targets that traditional methods could not achieve. New sequencing techniques with spatial resolution deepen our understanding of the relationship between a cell's genotype or gene expression and its morphology and interactions with the local environment, thus advancing knowledge in HGSOC development and progression.

While our study provides significant insights into the cellular and molecular underpinnings of HGSOC metastasis, several limitations warrant consideration. The heterogeneity among patients and the limited sample size pose challenges in generalizing our findings. The dynamic nature of cancer biology means that our findings are only a snapshot of time, which may not fully cover the complexity of tumor heterogeneity and the dynamics of TME. Addressing the limitations noted, future studies should aim to include larger and more diverse cohorts. This expansion would allow for a broader generalization of our findings and enable a more detailed validation of the observed phenomena. Additionally, investigating the common mechanisms of metastasis in HGSOC could significantly enhance our understanding of the disease process and potentially unveil novel therapeutic targets. Moreover, advancing beyond the two-dimensional spatial analyses employed in our current study, future research should incorporate three-dimensional imaging techniques. Such approaches will provide a more comprehensive view of the tumor architecture, improving our understanding of how the three-dimensional environment influences cellular interactions and tumor progression. This could lead to breakthroughs in how we approach the prevention and intervention of metastasis in HGSOC.

In conclusion, our study sheds light on the intricate tapestry of cellular heterogeneity, immune evasion, and metabolic reprogramming in HGSOC, particularly in the context of distant metastasis. By unraveling the complex interplay between tumor cells and their microenvironment, we pave the way for novel therapeutic strategies aimed at disrupting these interactions.

Data availability statement

The original contributions presented in the study are included in the article/Supplementary Material. Further inquiries can be directed to the corresponding author.

Ethics statement

Ethical approval was not required for the studies on humans in accordance with the local legislation and institutional requirements because only commercially available established cell lines were used.

Author contributions

HL: Investigation, Validation, Writing – original draft. KW: Investigation, Methodology, Software, Writing – original draft. BL: Funding acquisition, Supervision, Writing – review & editing.

Funding

The author(s) declare financial support was received for the research, authorship, and/or publication of this article. National Natural Science Foundation of China (82272726).

Conflict of interest

The authors declare that the research was conducted in the absence of any commercial or financial relationships that could be construed as a potential conflict of interest.

Publisher's note

All claims expressed in this article are solely those of the authors and do not necessarily represent those of their affiliated organizations, or those of the publisher, the editors and the reviewers. Any product

that may be evaluated in this article, or claim that may be made by its manufacturer, is not guaranteed or endorsed by the publisher.

Supplementary material

The Supplementary Material for this article can be found online at: https://www.frontiersin.org/articles/10.3389/fimmu.2024.1420847/full#supplementary-material

SUPPLEMENTARY FIGURE 1
Functional Analysis of CHODL+NEO. **(A)** Bar graph depicting the proportion of CHODL+NEO cells in different sample sources. **(B)** Heatmap showing the differential gene expression between CHODL+NEO cells and non-CHODL +NEO cells. **(C)** Heatmap displaying the signature scores of lipid metabolism-related pathways in CHODL+NEO cells and non-CHODL+NEO cells. **(D)** Representative spatial expression maps illustrating the scores of SMAD4 and FATTY ACID BETA OXIDATION. **(E)** Violin plots demonstrating the differences in FATTY ACID BETA OXIDATION scores in SP1. **(F)** Violin plots demonstrating the differences in FATTY ACID BETA OXIDATION scores in SP6.

References

1. GBD 2019 Demographics Collaborators. Global age-sex-specific fertility, mortality, healthy life expectancy (Hale), and population estimates in 204 countries and territories, 1950–2019: A comprehensive demographic analysis for the global burden of disease study 2019. *Lancet*. (2020) 396:1160–203. doi: 10.1016/s0140–6736 (20)30977–6

2. Cancer Genome Atlas Research Network. Integrated genomic analyses of ovarian carcinoma. *Nature*. (2011) 474:609–15. doi: 10.1038/nature10166

3. Bowtell DD, Böhm S, Ahmed AA, Aspuria PJ, Bast RC Jr., Beral V, et al. Rethinking ovarian cancer ii: reducing mortality from high-grade serous ovarian cancer. *Nat Rev Cancer*. (2015) 15:668–79. doi: 10.1038/nrc4019

4. Patch AM, Christie EL, Etemadmoghadam D, Garsed DW, George J, Fereday S, et al. Whole-genome characterization of chemoresistant ovarian cancer. *Nature*. (2015) 521:489–94. doi: 10.1038/nature14410

5. Cancer Genome Atlas Research N. Integrated genomic analyses of ovarian carcinoma. *Nature*. (2011) 474:609–15. doi: 10.1038/nature10166

6. Zhang B, Chen F, Xu Q, Han L, Xu J, Gao L, et al. Revisiting ovarian cancer microenvironment: A friend or a foe? *Protein Cell*. (2018) 9:674–92. doi: 10.1007/s13238–017-0466–7

7. Kroeger DR, Milne K, Nelson BH. Tumor-infiltrating plasma cells are associated with tertiary lymphoid structures, cytolytic T-cell responses, and superior prognosis in ovarian cancer. *Clin Cancer Res*. (2016) 22:3005–15. doi: 10.1158/1078–0432.Ccr-15–2762

8. Laumont CM, Wouters MCA, Smazynski J, Gierc NS, Chavez EA, Chong LC, et al. Single-cell profiles and prognostic impact of tumor-infiltrating lymphocytes coexpressing cd39, cd103, and pd-1 in ovarian cancer. *Clin Cancer Res*. (2021) 27:4089–100. doi: 10.1158/1078–0432.Ccr-20–4394

9. Veneziani AC, Gonzalez-Ochoa E, Alqaisi H, Madariaga A, Bhat G, Rouzbahman M, et al. Heterogeneity and treatment landscape of ovarian carcinoma. *Nat Rev Clin Oncol*. (2023) 20:820–42. doi: 10.1038/s41571–023-00819–1

10. Xu J, Fang Y, Chen K, Li S, Tang S, Ren Y, et al. Single-cell rna sequencing reveals the tissue architecture in human high-grade serous ovarian cancer. *Clin Cancer Res*. (2022) 28:3590–602. doi: 10.1158/1078–0432.Ccr-22–0296

11. Ferri-Borgogno S, Zhu Y, Sheng J, Burks JK, Gomez JA, Wong KK, et al. Spatial transcriptomics depict ligand-receptor cross-talk heterogeneity at the tumor-stroma interface in long-term ovarian cancer survivors. *Cancer Res*. (2023) 83:1503–16. doi: 10.1158/0008–5472.Can-22–1821

12. Carstens JL, Correa de Sampaio P, Yang D, Barua S, Wang H, Rao A, et al. Spatial computation of intratumoral T cells correlates with survival of patients with pancreatic cancer. *Nat Commun*. (2017) 8:15095. doi: 10.1038/ncomms15095

13. Gartrell-Corrado RD, Chen AX, Rizk EM, Marks DK, Bogardus MH, Hart TD, et al. Linking transcriptomic and imaging data defines features of a favorable tumor immune microenvironment and identifies a combination biomarker for primary melanoma. *Cancer Res*. (2020) 80:1078–87. doi: 10.1158/0008–5472.Can-19–2039

14. Marx V. Method of the year: spatially resolved transcriptomics. *Nat Methods*. (2021) 18:9–14. doi: 10.1038/s41592-020-01033-y

15. Wang Z, Jensen MA, Zenklusen JC. A practical guide to the cancer genome atlas (Tcga). *Methods Mol Biol*. (2016) 1418:111–41. doi: 10.1007/978–1-4939–3578-9_6

16. Feng S, Xu Y, Dai Z, Yin H, Zhang K, Shen Y. Integrative analysis from multicenter studies identifies a wgcna-derived cancer-associated fibroblast signature for ovarian cancer. *Front Immunol*. (2022) 13:951582. doi: 10.3389/fimmu.2022.951582

17. Barrett T, Wilhite SE, Ledoux P, Evangelista C, Kim IF, Tomashevsky M, et al. Ncbi geo: archive for functional genomics data sets–update. *Nucleic Acids Res*. (2013) 41:D991–5. doi: 10.1093/nar/gks1193

18. Yu M, Bardia A, Wittner BS, Stott SL, Smas ME, Ting DT, et al. Circulating breast tumor cells exhibit dynamic changes in epithelial and mesenchymal composition. *Science*. (2013) 339:580–4. doi: 10.1126/science.1228522

19. Korsunsky I, Wei K, Pohin M, Kim EY, Barone F, Major T, et al. Cross-tissue, single-cell stromal atlas identifies shared pathological fibroblast phenotypes in four chronic inflammatory diseases. *Med*. (2022) 3:481–518.e14. doi: 10.1016/j.medj.2022.05.002

20. Mosquera JV, Auguste G, Wong D, Turner AW, Hodonsky CJ, Alvarez-Yela AC, et al. Integrative single-cell meta-analysis reveals disease-relevant vascular cell states and markers in human atherosclerosis. *Cell Rep*. (2023) 42:113380. doi: 10.1016/j.celrep.2023.113380

21. Wang K, Zhang Y, Ao M, Luo H, Mao W, Li B. Multi-omics analysis defines a cuproptosis-related prognostic model for ovarian cancer: implication of wasf2 in cuproptosis resistance. *Life Sci*. (2023) 332:122081. doi: 10.1016/j.lfs.2023.122081

22. Wei C, Sun W, Shen K, Zhong J, Liu W, Gao Z, et al. Delineating the early dissemination mechanisms of acral melanoma by integrating single-cell and spatial transcriptomic analyses. *Nat Commun*. (2023) 14:8119. doi: 10.1038/s41467-023-43980-y

23. Tirosh I, Izar B, Prakadan SM, Wadsworth MH 2nd, Treacy D, Trombetta JJ, et al. Dissecting the multicellular ecosystem of metastatic melanoma by single-cell rna-seq. *Science*. (2016) 352:189–96. doi: 10.1126/science.aad0501

24. Zhang X, Wu K, Huang Y, Xu L, Li X, Zhang N. Promoter hypermethylation of chodl contributes to carcinogenesis and indicates poor survival in patients with early-stage colorectal cancer. *J Cancer*. (2020) 11:2874–86. doi: 10.7150/jca.38815

25. Masuda K, Takano A, Oshita H, Akiyama H, Tsuchiya E, Kohno N, et al. Chondrolectin is a novel diagnostic biomarker and a therapeutic target for lung cancer. *Clin Cancer Res*. (2011) 17:7712–22. doi: 10.1158/1078–0432.CCR-11–0619

26. Colak S, Ten Dijke P. Targeting tgf-beta signaling in cancer. *Trends Cancer*. (2017) 3:56–71. doi: 10.1016/j.trecan.2016.11.008

27. Tan X, Tong L, Li L, Xu J, Xie S, Ji L, et al. Loss of smad4 promotes aggressive lung cancer metastasis by de-repression of pak3 via mirna regulation. *Nat Commun*. (2021) 12:4853. doi: 10.1038/s41467–021-24898–9

28. Chen HD, Ye Z, Hu HF, Fan GX, Hu YH, Li Z, et al. Smad4 endows tgf-beta1-induced highly invasive tumor cells with ferroptosis vulnerability in pancreatic cancer. *Acta Pharmacol Sin*. (2023) 45(4):844–56. doi: 10.1038/s41401–023-01199-z

29. Zeng F, Nijiati S, Tang L, Ye J, Zhou Z, Chen X. Ferroptosis detection: from approaches to applications. *Angew Chem Int Ed Engl*. (2023) 62:e202300379. doi: 10.1002/anie.202300379

30. Godfrey DI, Uldrich AP, McCluskey J, Rossjohn J, Moody DB. The burgeoning family of unconventional T cells. *Nat Immunol*. (2015) 16:1114–23. doi: 10.1038/ni.3298

31. Mensurado S, Blanco-Dominguez R, Silva-Santos B. The emerging roles of gammadelta T cells in cancer immunotherapy. *Nat Rev Clin Oncol*. (2023) 20:178–91. doi: 10.1038/s41571–022-00722–1

32. Wang C, Liu X, Li Z, Chai Y, Jiang Y, Wang Q, et al. Cd8(+)Nkt-like cells regulate the immune response by killing antigen-bearing dcs. *Sci Rep*. (2015) 5:14124. doi: 10.1038/srep14124

33. Liu X, Li L, Si F, Huang L, Zhao Y, Zhang C, et al. Nk and nkt cells have distinct properties and functions in cancer. *Oncogene*. (2021) 40:4521–37. doi: 10.1038/s41388–021-01880–9

34. Vogel FCE, Chaves-Filho AB, Schulze A. Lipids as mediators of cancer progression and metastasis. *Nat Cancer*. (2024) 5(1):16–29. doi: 10.1038/s43018-023-00702-z

35. Broadfield LA, Pane AA, Talebi A, Swinnen JV, Fendt SM. Lipid metabolism in cancer: new perspectives and emerging mechanisms. *Dev Cell*. (2021) 56:1363–93. doi: 10.1016/j.devcel.2021.04.013

36. Tan Z, Xiao L, Tang M, Bai F, Li J, Li L, et al. Targeting cpt1a-mediated fatty acid oxidation sensitizes nasopharyngeal carcinoma to radiation therapy. *Theranostics*. (2018) 8:2329–47. doi: 10.7150/thno.21451

frontiers | Frontiers in Immunology

TYPE Original Research
PUBLISHED 27 June 2024
DOI 10.3389/fimmu.2024.1428529

Check for updates

OPEN ACCESS

EDITED BY
Jiaheng Xie,
Central South University, China

REVIEWED BY
Jiaxiong Tan,
Tianjin Medical University Cancer Institute and Hospital, China
Weibiao Zeng,
The First Affiliated Hospital of Soochow University, China
Qianhe Ren,
Jiangsu University, China

*CORRESPONDENCE
Qiqi Wang
wzwangqiqi@163.com

†These authors have contributed equally to this work

RECEIVED 06 May 2024
ACCEPTED 14 June 2024
PUBLISHED 27 June 2024

CITATION
Ye B, Li Z and Wang Q (2024) A novel artificial intelligence network to assess the prognosis of gastrointestinal cancer to immunotherapy based on genetic mutation features.
Front. Immunol. 15:1428529.
doi: 10.3389/fimmu.2024.1428529

COPYRIGHT
© 2024 Ye, Li and Wang. This is an open-access article distributed under the terms of the Creative Commons Attribution License (CC BY). The use, distribution or reproduction in other forums is permitted, provided the original author(s) and the copyright owner(s) are credited and that the original publication in this journal is cited, in accordance with accepted academic practice. No use, distribution or reproduction is permitted which does not comply with these terms.

A novel artificial intelligence network to assess the prognosis of gastrointestinal cancer to immunotherapy based on genetic mutation features

Bicheng Ye[1†], Zhongyan Li[2†] and Qiqi Wang[3,4,5*]

[1]School of Clinical Medicine, Yangzhou Polytechnic College, Yangzhou, China, [2]Department of Geriatric Medicine, Huai'an Hospital Affiliated to Yangzhou University (The Fifth People's Hospital of Huai'an), Huai'an, China, [3]Department of Gastroenterology, Wenzhou Central Hospital, Wenzhou, China, [4]Department of Gastroenterology, The Dingli Clinical College of Wenzhou Medical University, Wenzhou, China, [5]Department of Gastroenterology, The Second Afliated Hospital of Shanghai University, Wenzhou, China

Background: Immune checkpoint inhibitors (ICIs) have revolutionized gastrointestinal cancer treatment, yet the absence of reliable biomarkers hampers precise patient response prediction.

Methods: We developed and validated a genomic mutation signature (GMS) employing a novel artificial intelligence network to forecast the prognosis of gastrointestinal cancer patients undergoing ICIs therapy. Subsequently, we explored the underlying immune landscapes across different subtypes using multiomics data. Finally, UMI-77 was pinpointed through the analysis of drug sensitization data from the Genomics of Drug Sensitivity in Cancer (GDSC) database. The sensitivity of UMI-77 to the AGS and MKN45 cell lines was evaluated using the cell counting kit-8 (CCK8) assay and the plate clone formation assay.

Results: Using the artificial intelligence network, we developed the GMS that independently predicts the prognosis of gastrointestinal cancer patients. The GMS demonstrated consistent performance across three public cohorts and exhibited high sensitivity and specificity for 6, 12, and 24-month overall survival (OS) in receiver operating characteristic (ROC) curve analysis. It outperformed conventional clinical and molecular features. Low-risk samples showed a higher presence of cytolytic immune cells and enhanced immunogenic potential compared to high-risk samples. Additionally, we identified the small molecule compound UMI-77. The half-maximal inhibitory concentration (IC50) of UMI-77 was inversely related to the GMS. Notably, the AGS cell line, classified as high-risk, displayed greater sensitivity to UMI-77, whereas the MKN45 cell line, classified as low-risk, showed less sensitivity.

Conclusion: The GMS developed here can reliably predict survival benefit for gastrointestinal cancer patients on ICIs therapy.

KEYWORDS

artificial intelligence, gastrointestinal cancer, genomic mutation, immunotherapy, immune landscape

Introduction

Gastrointestinal cancers constitute a significant health challenge worldwide, accounting for 26% of all cancer diagnoses and 35% of cancer-related fatalities (1). Immune checkpoint inhibitors (ICIs) have emerged as a potentially effective therapeutic strategy for a variety of cancer types, including those of the gastrointestinal cancer (2, 3). However, the response rate to ICIs is limited, varying from 10–20% across different tumor types (3, 4). Consequently, the development of biomarkers capable of accurately identifying patients who are likely to benefit from ICIs therapy is of paramount importance.

Microsatellite instability (MSI), a genetic indicator of tumor responsiveness to ICIs, stands as the sole validated biomarker in clinical trials for gastrointestinal cancers (5, 6). However, MSI-high tumors are relatively uncommon, representing only 0–5% of all metastatic gastrointestinal cancer cases (7). Programmed death ligand-1 (PD-L1) expression is another commonly assessed biomarker for the application of ICIs, but its predictive value is inconsistent across different trials due to heterogeneity and variability of expression and detection (8, 9). Another promising biomarker under investigation is the tumor mutation burden (TMB), which has demonstrated a correlation with response to ICIs in recent research (10). However, TMB is not a reliable biomarker for gastrointestinal cancer (11). Not all mutations have the same immunogenic impact, and some mutations, such as CDKN2A, ARID1A, ARID1B, ARID2, ERBB4, and ZFHX3, may modulate the outcomes of ICIs treatment in positive or negative ways (12–15). Besides, In the context of gastrointestinal tumors, certain genetic mutations are closely linked to the effectiveness of immunotherapy. Mutations in the AKT1 and CDH1 genes have been associated with primary resistance to ICIs (16). These insights highlight the importance of gene mutations in predicting responses to immunotherapy and tailoring personalized treatment approaches for patients with gastrointestinal cancers. TMB scoring systems do not account for the differential effects of these mutations, limiting their predictive value for ICIs (17). To overcome this limitation, some studies have suggested refining the TMB algorithm (18) or constructing gene mutation-based signatures to improve the survival prediction of ICIs in gastrointestinal cancer (17, 19, 20).

Machine learning and deep learning are powerful tools for solving complex problems in medicine using large clinical data sets (20). These methods have demonstrated their achievements and efficiency in prediction and clustering tasks (21). By applying these novel technologies, we can explore the mechanisms of therapy resistance at different levels, such as transcriptional, epigenetic, and translational levels, and find more clues to improve the efficacy of ICIs (22–24). Thus, we developed a novel artificial intelligence network that integrated traditional regression algorithms, machine learning, and deep learning, comprising a total of 22 algorithms and 297 algorithm combinations, greatly surpassing the previous 101 algorithm combinations (25). This comprehensive approach allows us to more accurately analyze and predict the outcomes of immunotherapy for gastrointestinal tumors.

In this work, we used genomic mutation information to develop and validate an artificial intelligence network-based genomic mutation signature (GMS). This study may provide guidance for immunotherapy treatment decisions and improve the clinical outcomes of gastrointestinal cancer.

Methods

Designing research studies and collecting data

We present the overall study design in Figure 1. We collected 233 gastrointestinal cancer cases treated with ICIs from Memorial Sloan Kettering Cancer Center (MSK) as a training cohort to screen for mutations with prognostic potential and to construct a prognostic signature (11). We also obtained two independent validation cohorts of gastrointestinal cancers with ICIs treatment from public databases. The combined Janjigian and Pender cohort comprised 39 cases of metastatic chemotherapy-refractory esophagogastric cancer (26) and 9 cases of metastatic or advanced gastrointestinal cancer (27). The PUCH cohort consisted of 91 patients with gastrointestinal cancer (17). The patient enrollment criteria are as follows: (1) primary gastrointestinal cancers; (2) availability of gene mutation profiles and clinical annotations, including follow-up data; (3) receipt of at least one cycle of a CTLA-4 inhibitor, PD-1/PD-L1 inhibitor or combined treatment. Furthermore, we obtained somatic mutation data, mRNA expression profiles, and copy number variations (CNV) for a non-immunotherapy gastrointestinal cancer cohort consisting of 184 cases of esophageal cancer, 439 cases of gastric cancer, and 380 cases of colorectal cancer from The Cancer Genome Atlas (TCGA) database. The genomic and clinical data for the MSK cohort, the Janjigian and Pender cohorts, and the PUCH cohort, are openly available and were downloaded from the following sources: MSK cohort (http://www.cbioportal.org/study?id=tmb_mskcc_2018), Janjigian cohort (https://www.cbioportal.org/study/summary?id=egc_msk_2017), Pender cohort (http://clincancerres.aacrjournals.org/content/27/1/202.article-info), and PUCH cohort (https://www.bcgsc.ca/downloads/immunoPOG/). The data from the TCGA dataset are available for download at https://portal.gdc.cancer.gov/.

Analysis of mutation data and evaluation of clinical outcomes

Tumor tissues from the MSK and Janjigian cohorts were subjected to sequencing using the MSK-IMPACT sequencing technique, which involved either a 341-gene panel, a 410-gene panel, or a 468-gene panel. For the Pender cohort, whole-genome sequencing (WGS) was utilized for tumor tissue analysis, and whole-exome sequencing (WES) was employed for the PUCH cohort. The mutated gene status was assigned a value of 1, and the wild-type gene status was assigned a value of 0. The primary survival endpoint considered was overall survival (OS). The clinical response was assessed per the Response Evaluation Criteria in

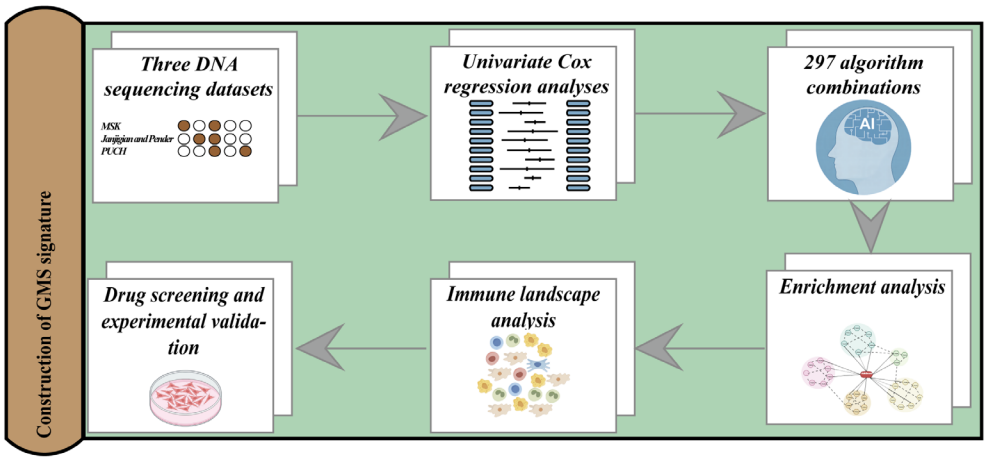

FIGURE 1
An illustration of the general workflow adopted in this study.

Solid Tumors version 1.1. Durable clinical benefit (DCB) met the criteria for complete response (CR), partial response (PR), or stable disease (SD) persisting for ≥6 months. Conversely, no durable benefit (NDB) was defined as progressive disease (PD) criteria or SD <6 months (28).

Artificial intelligence network-based signature generation

We constructed a novel artificial intelligence network based on 297 algorithm combinations, integrating 22 algorithms from traditional regression, machine learning, and deep learning. These algorithms included random survival forest (RSF), supervised principal components (SuperPC), oblique random survival forests (obliqueRSF), gradient boosting with component-wise linear models (GLMBoost), gradient boosting with regression trees (BlackBoost), stepwise Cox, recursive partitioning and regression trees (Rpart), parametric survival model (Survreg), Ranger, conditional inference trees (Ctree), least absolute shrinkage and selection operator (LASSO), partial least squares regression for Cox (plsRcox), survival support vector machine (survival-SVM), Ridge, elastic network (Enet), deephit survival neural network (DeepHit), deepsurv survival neural network (DeepSurv), cox-time survival neural network (CoxTime), extreme gradient boosting (XGBoost), Coxboost, CForest, and variable selection oriented LASSO bagging algorithm (VSOLassoBag). We developed the signature as follows: (1) Prognostic genes were identified via univariate Cox regression in the MSK cohort. (2) Initial signature discovery utilized an artificial intelligence network in the MSK cohort. (3) Further testing of the network occurred in two validation cohorts (Janjigian/Pender and PUCH). (4) Harrell's concordance index (C-index) evaluated each model's performance across all cohorts. The model with the maximal average C-index across the test cohorts was deemed optimal based on its superior predictive ability. The source code and specific parameters of this artificial intelligence network can be found at the following GitHub repository: https://github.com/miaolab1998/AI_network/tree/main.

Functional annotation of the GMS

We collected immune modulators from a previous study (29). We used four algorithms to quantify immune infiltrating cells: the quanTIseq algorithm (30) of 11 immune cells, the estimating the proportions of immune and cancer cells (EPIC) algorithm (31) of eight immune cells, the Microenvironment Cell Populations-counter (MCPcounter) algorithm (32)of ten immune cells, and the Estimation of STromal and Immune cells in Malignant Tumours using Expression data (ESTIMATE) algorithm (33). We also acquired 29 classical immune signatures from the work of He et al. (34). The cytolytic activity scores (CYTs) were estimated using the geometric mean of GZMA and PRF1 (35). Employing the GSVA R package, which is grounded in the single-sample gene set enrichment analysis (ssGSEA) technique, we quantified the enrichment levels of the 29 immune signatures across each sample (36). Utilizing the GSVA method (36) and clusterprofiler (37) R packages, we executed gene set variation analysis (GSVA) and gene set enrichment analysis (GSEA) on the MSigDB database. We also used Metascape for enrichment analysis (38).

Calculation of immunogenomic indicators

We obtained immunogenomic indicators from the pan-cancer immune landscape study (29). In summary, they established the intertumoral heterogeneity (ITH) score to quantify the subclonal genomic fraction, reflecting tumor genome segments unaccounted for by the dominant clone. This was determined via ABSOLUTE, a tool modeling tumor alterations including subclonal and clonal components with varying ploidies. CNV burden metrics were n_segs, indicating segment count per sample, and frac_altered, denoting proportion of bases diverging from baseline ploidy. The aneuploidy score aggregated altered chromosomal arms. Additionally, T-cell

receptor (TCR) and B-cell receptor (BCR) diversity indices like Shannon entropy and richness were calculated from cancer RNA-seq data.

Oncogenic pathway enrichment scores

From the study by Sanchez-Vega et al (39), we obtained ten canonical oncogenic pathways that include 187 oncogenes. We applied the GSVA method, facilitated by the GSVA R package (36), to calculate the enrichment scores for these pathways in each sample.

Uncovering genomic mutational signatures

Employing the maftools R package, we conducted nonnegative matrix factorization (NMF) on a dataset of 96 trinucleotide context mutations from gastrointestinal cancer specimens, which were obtained from the TCGA. We then compared the resulting mutational landscape to the Catalogue of Somatic Mutations in Cancer (COSMIC), employing cosine similarity for the assessment.

Drug prediction

We retrieved data on tumor cell line sensitivity to potential drugs and mutations from the Genomics of Drug Sensitivity in Cancer (GDSC) database. The cell line sensitivity was assessed using the lower half maximal inhibitory concentration (IC50) values of the respective drugs.

Cell line culture

The human gastric cancer cell lines AGS and MKN45 were acquired from the Shanghai Institutes for Biological Sciences, part of the Chinese Academy of Sciences. MKN45 cells were grown in RPMI 1640 medium supplemented with 10% FBS and 1% penicillin-streptomycin. AGS cells were cultivated in Ham's F-12 medium with the same supplements. The cells were incubated at 37°C with 5% CO2.

CCK-8 detection

Cells were seeded into a 96-well plate at an optimal density of 5,000 cells per well. We treated the cells with different concentrations of UMI-77 and incubated them for 48 h and 72 h. We measured and recorded the absorbance value on the cell growth curve and calculated the IC50.

Colony formation assay

1000 untreated cells were cultured in each well of a six-well plate, either with UMI-77, DMSO, or without any treatment, for a period of 2 weeks. Following this, colony formation was analyzed.

Statistical analysis

Categorical data were examined with the chi-square test, and numerical data with the Wilcoxon test. Pearson test was employed for association analysis. Survival curves were generated with the Survival and survminer packages in R. Univariate and multivariate Cox regression analyses were performed to assess the GMS's clinical factor independence. Receiver operator characteristic curve (ROC) and area under the ROC curve (AUC) were used to determine the predictive sensitivity and specificity for survival or response. Statistical significance was defined as a P value below 0.05, unless stated otherwise. All analyses were conducted using R version 4.2.3.

Results

Construction and valiation of the GMS

The characteristics of patients in these three immunotherapeutic cohorts are detailed in Supplementary Table 1. The training cohort consisted of 233 gastrointestinal cancer patients (esophagogastric cancer, N = 123; colorectal cancer, N = 110) from MSK who received ICIs. We identified 74 prognostic genes through univariate Cox analysis and selected seed genes with a mutation frequency greater than 3%. These genes were then subjected to our artificial intelligence network to construct a GMS. The optimal model, comprising a combination of VSOLassoBag and RSF, was determined based on its highest average C-index (C-index = 0.71) among the 297 algorithm combinations evaluated through 10-fold cross-validation (Figure 2A). The VSOLassoBag algorithm selected 23 genes based on curve elbow point detection (CEP) method and used them to construct the most reliable GMS by RSF (Figures 2B, C). The GMS score was determined for each participant and stratified them into high and low-risk groups per the training set (median GMS score = 16.65). The high-risk group had markedly inferior OS versus low-risk (all $p < 0.05$) across all cohorts (Figures 2D–F). In the MSK cohort, 6-month AUC = 0.785, 12-month AUC = 0.799, and 18-month AUC = 0.837 (Figure 2D). In the Janjigian&Pender cohort, 6-month AUC = 0.771, 12-month AUC = 0.823, and 18-month AUC = 0.829 (Figure 2E). In the PUCH cohort, 6-month AUC = 0.782, 12-month AUC = 0.699, and 18-month AUC = 0.697 (Figure 2F). The time-dependent ROC curves demonstrated the strong and consistent performance of the GMS across all cohorts. In the two test cohorts, a notable number of patients with DCB had low GMS scores (all $p < 0.05$). The ROC analyses in these cohorts suggested that the GMS could be a valuable predictive biomarker for immunotherapy clinical benefit, with AUCs of 0.786 and 0.643, respectively (Figures 2G, H). These findings suggest the GMS may act as a robust predictor of responses and outcomes for gastrointestinal cancer patients undergoing immunotherapy.

The strong predictive performance of GMS

Univariate and multivariate Cox regression analyses were conducted across all cohorts to evaluate GMS as an independent

10.3389/fimmu.2024.1428529

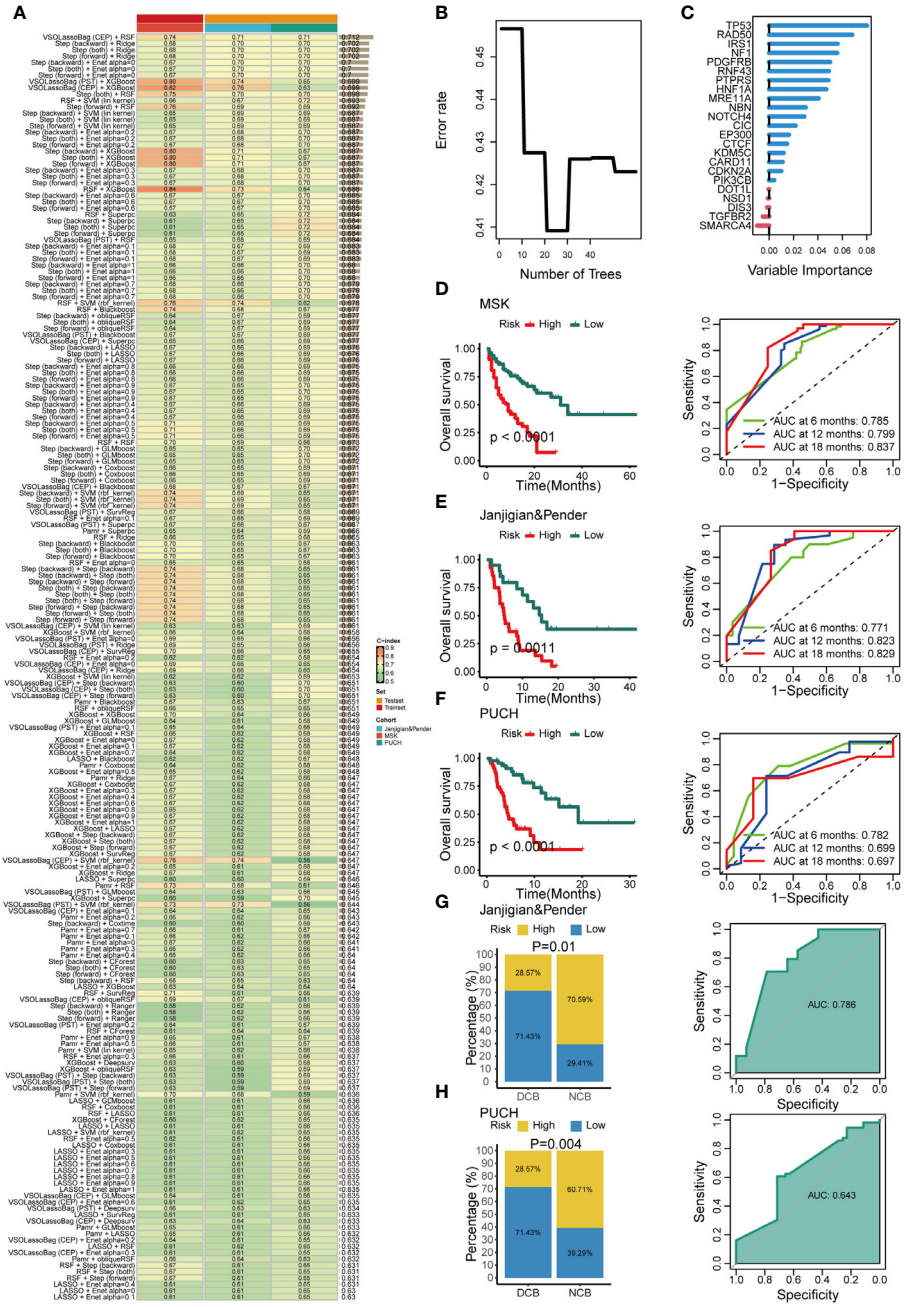

FIGURE 2
Development and validation of an artificial intelligence network using 297 algorithm combinations. **(A)** Evaluation and C-index computation for 297 prediction models across all validation datasets. **(B)** Determination of the number of trees by minimizing error. **(C)** Variable importance of the top 23 genes determined using the random survival forest (RSF) algorithm. **(D-F)** Kaplan-Meier survival analysis (left) and receiver operating characteristic (ROC) (right) curves for overall survival (OS) in the MSK **(D)**, Janjigian and Pender **(E)**, and PUCH **(F)** cohorts. **(G, H)** The correlation between genomic mutation signature (GMS) and response (left), as well as the ROC of GMS predicting clinical response (right) in the Janjigian and Pender cohort **(G)**, and PUCH cohort **(H)**.

predictor of OS in immunotherapy patients. In the univariate and multivariate analyses, GMS emerged as a robust predictor, not affected by adjustments for age, gender, drug category, MSI, PDL-1, and TMB (Figures 3A–C), solidifying its predictive utility in prognosis. To compare the predictive superiority of GMS, we assessed it against common clinical traits and molecular features. GMS exhibited significantly higher accuracy compared to other variables, such as age, gender, drug type, the genomic mutation signature of immunotherapy for gastrointestinal tumors identified in previous studies (GIPS) (17), TMB, MSI, and PD-L1, across all three cohorts (Figures 3D–F). These results indicate that our GMS holds promise as a reliable surrogate for predicting the prognosis of gastrointestinal cancer patients receiving immunotherapy in clinical practice.

10.3389/fimmu.2024.1428529

Potential biological peculiarities of the GMS

We examined the biological mechanisms of GMS in the TCGA dataset. We noted that the GMS displayed a negative correlation with numerous immune pathways, including graft-versus-host disease, natural killer cell-mediated cytotoxicity, cytokine-cytokine receptor interaction, antigen processing, asthma, allograft rejection, and autoimmune thyroid disease pathways (Figure 4A). Conversely, the GMS showed a positive correlation with several tumorigenic pathways, such as DNA replication, mismatch repair, manchette assembly, cytosine DNA methylation, meiotic telomere clustering, and cell cycle pathways (Figure 4A). Further analysis revealed significant differences in immunological and tumorigenic pathways between the high- and low-risk groups (Figure 4B). The genes with high expression in the low-risk group were enriched in immune activation and infiltration pathways (Figure 4C). GSEA using Kyoto Encyclopedia of Genes and Genomes (KEGG) terms showed the low-risk group had enrichment in NK cell cytotoxicity, Th17 cell differentiation, and influenza A, as anticipated (Figure 4D). In contrast, the high-risk group displayed enrichment in DNA replication and cell cycle pathways. These

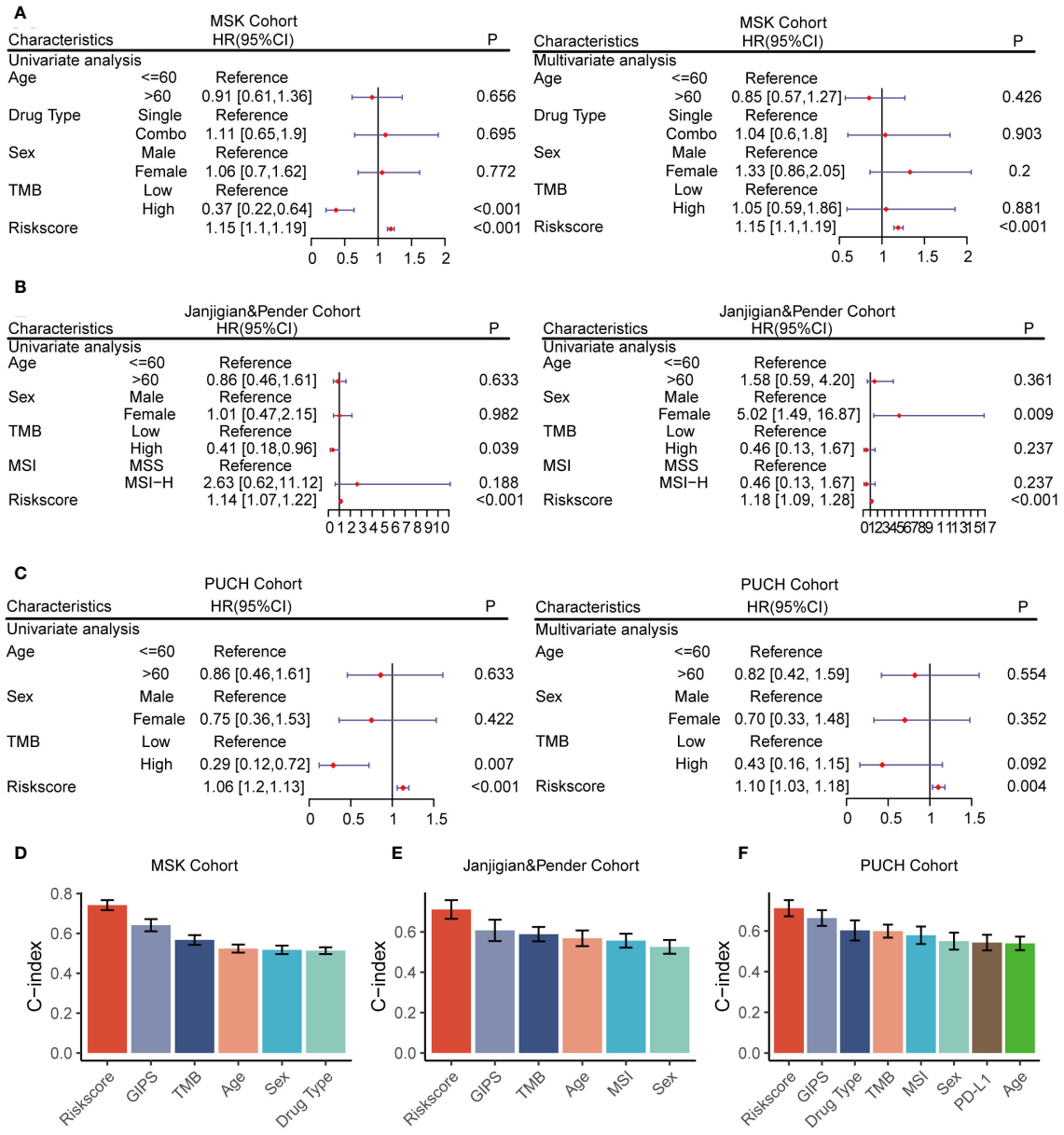

FIGURE 3
Univariate and multivariate Cox regression analyses of the GMS and other characteristics. **(A)** GMS subjected to univariate and multivariate Cox regression analyses in the MSK cohort. **(B)** GMS subjected to univariate and multivariate Cox regression analyses in the Janjigian and Pender cohort. **(C)** GMS subjected to univariate and multivariate Cox regression analyses in the PUCH cohort. **(D)** Comparison of GMS performance with other clinical and molecular variables for prognosis prediction in the MSK cohort. **(E)** Comparison of GMS performance with other clinical and molecular variables for prognosis prediction in the Janjigian and Pender cohort. **(F)** Comparison of GMS performance with other clinical and molecular variables for prognosis prediction in the PUCH cohort.

10.3389/fimmu.2024.1428529

results indicate that a lower GMS score tends to be associated with an inflammatory environment.

Extrinsic immune landscapes of the GMS

We assessed the GMS as an indicator of immune status by analyzing its association with infiltration of immune cells and expression of immune checkpoints. Figures 5A, B show that the low-risk group had increased infiltration of immune cells and immune modulatory activity in the TCGA dataset. Comparison of the 29 immune signatures between groups revealed that the low-risk group had higher prevalence of immune cells including CD8+ T cells ($p < 0.05$) (Figure 5C). To determine if the risk groups corresponded to low and high infiltration cohorts, unsupervised clustering of the 29 immune signatures for TCGA

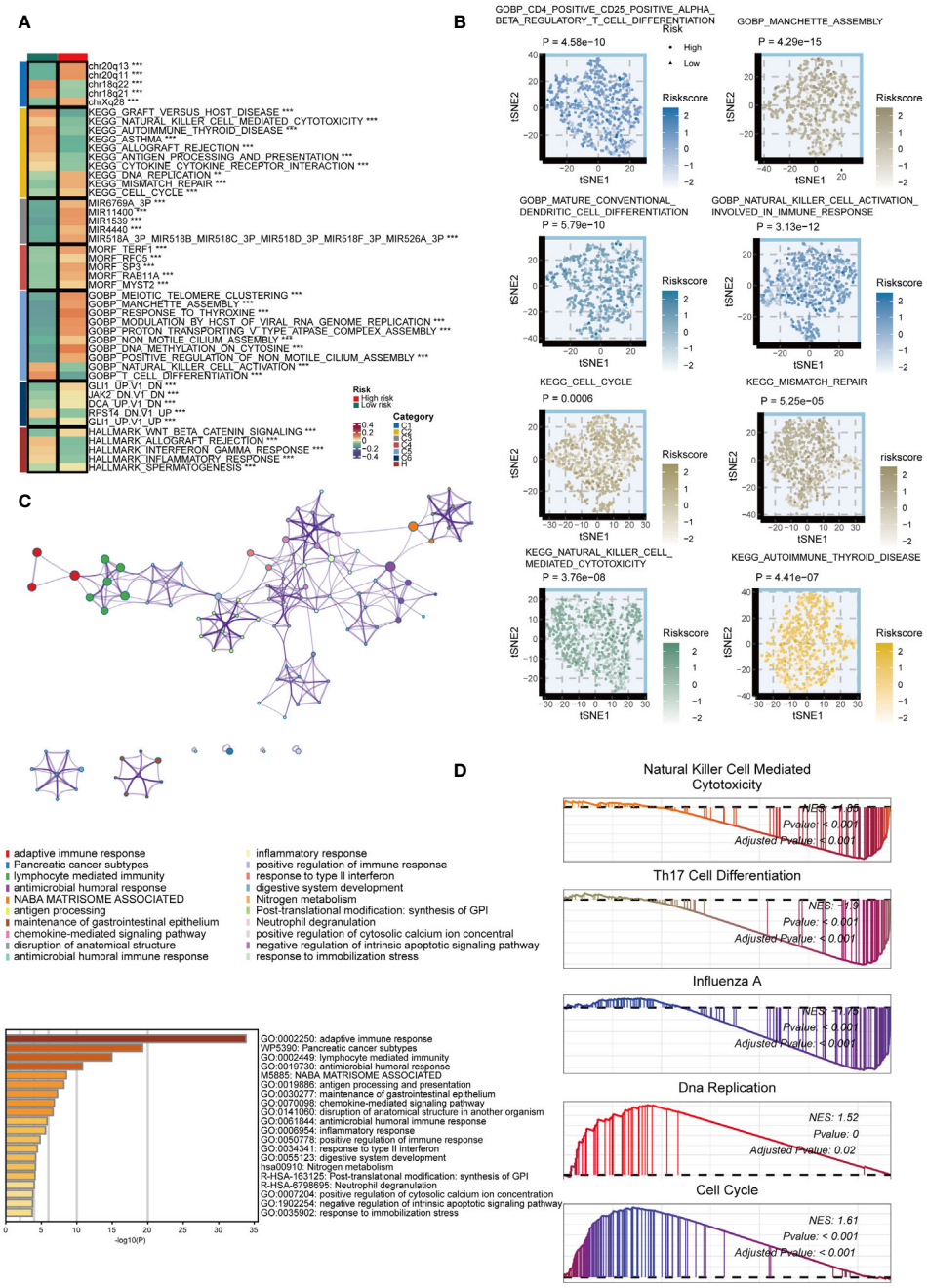

FIGURE 4
Biological peculiarities of the GMS in the TCGA dataset. **(A)** Outlining the biological characteristics of two groups based on GMS using MsigDB-based Gene Set Variation Analysis (GSVA) in the TCGA dataset. **(B)** T-distributed Stochastic Neighbor Embedding (t-SNE) plot to illustrate differences in pathway activity between two GMS groups based on Gene Ontology (GO) and Kyoto Encyclopedia of Genes and Genomes (KEGG) terms. **(C)** Metascape-based enrichment analysis of high expression genes in the low-risk group. **(D)** Gene Set Enrichment Analysis (GSEA) for GO and KEGG terms to investigate biological pathways associated with GMS in the TCGA dataset. **p < 0.01; ***p < 0.001.

patients was performed. This identified two distinct immune patterns: high and low immune infiltration (Figure 5D). Notably, the low-risk group was more common in the high infiltration cluster ($p < 0.05$) (Figure 5E). Furthermore, low-risk tumors were linked to significantly higher CYT scores ($p < 0.05$) (Figure 5F). These results implied a relatively inflamed and immunostimulatory microenvironment, which may be amenable to immunotherapy (40).

Intrinsic immune landscapes of the GMS

To clarify the factors affecting tumor immunogenicity between the two risk groups, we initially examined the neoantigen load, TCR diversity, mutation rate, BCR diversity, CNV burden, aneuploidy, and intertumoral heterogeneity. Compared to the high-risk group (all $p < 0.05$), the low-risk group harbored a higher mutation rate and neoantigen burden alongside significantly greater BCR and TCR diversity (all $p < 0.05$) (Figure 6A). However, the high-risk group exhibited significantly higher aneuploidy and CNV burdens (all $p < 0.05$) (Figure 6A). This aligns with existing research associating tumor aneuploidy with dampened immunotherapy responses (41). Compared to the low-risk group, individuals in the high-risk group exhibited significantly greater intertumoral heterogeneity ($p < 0.05$) (Figure 6A). This finding aligns with the hypothesis that tumors, facing a diminished immune response, may evolve clonally, leading to increased heterogeneity. This suggests that the heightened immunogenicity in the low-risk group might trigger an extrinsic immune response. To further explore the underlying mutational processes, we profiled mutational signatures based on somatic mutation data in both groups. This analysis revealed two distinct mutagenic patterns within the TCGA cohort (Figure 6B). The low-risk group exhibited a higher prevalence of SBS6, a mutational signature associated with defective DNA mismatch repair (Figure 6C). We further analyzed oncogene enrichment in ten key pathways, revealing distinct patterns. Whereas the cell cycle and Wnt pathways were enriched in the high-risk group (potentially linked to immune exclusion) (42), the Notch, PI3K, RAS, TGF beta, and TP53 pathways showed higher activity in the low-risk group (Figure 6D).

Copy number features of the GMS

The high-risk and low-risk groups harbored vastly different chromosomal abnormalities (Figure 7A). Notably, the low-risk group, unlike the high-risk group (Figures 7B, C), exhibited focal amplifications of immune genes, including PD-L1 (9p24.1) and PD-L2 (9p24.1). While 625 amplified genes were shared between the groups, the high-risk and low-risk groups harbored 373 and 1597 unique amplified genes, respectively. We further analyzed these amplified genes using Gene Ontology (GO) biological processes (Figure 7D). The GO enrichment analysis revealed a different pattern in the low-risk group (Figure 7D), including five immune-related processes focused on cell proliferation (mononuclear, lymphocyte, and leukocyte) and adaptive immunity through immunoglobulin superfamily domain recombination. Notably, no such immune pathways enrichment was observed in the high-risk group (Figure 7D). Intriguingly, PD-L1 and PD-L2, key players in immune modulation, reside within the 9p24.1 amplification peak unique to the low-risk group, suggesting their potential contribution to the observed enhanced immune response. Consistent with this, mRNA expression of PD-L1 and PD-L2 mirrored the CNV pattern, with their levels being significantly higher in the low-risk group (Figure 7D), highlighting the influence of tumor copy number variations on immune infiltration patterns.

Identification of small molecule drugs negatively associated with GMS

Based on the GDSC database, we identified that UMI-77, luminespib, lapatinib, and sapitinib exhibited the lowest p-values in the correlation test between GMS score and IC50, with UMI-77 having the smallest p-value ($p < 0.05$) (Figure 8A). We inferred that UMI-77 could be more effective for high-risk patients. To test this hypothesis, we measured the GMS of two cell lines in our laboratory (GMS score of AGS: 17.91; GMS score of MKN45: 4.43) and compared their sensitivity to UMI-77. The IC50 of UMI-77 for AGS and MKN45 was 8μM and 125μM, respectively (Figure 8B). A plate clone formation assay confirmed that AGS was more sensitive to UMI-77 (Figure 8C).

Discussion

A genomic classifier named GMS, consisting of 23 genes, was developed and validated. It was derived from an artificial intelligence network aimed at enhancing the prediction of ICIs therapy efficacy in gastrointestinal cancer patients. The selection of the most efficient model involved utilizing a combination of VSOLassoBag and RSF methods, which displayed the highest average C-index in the test cohorts. The GMS had a prognostic value independent of other factors and showed consistent performance in the validation cohorts. ROC analysis also demonstrated that the GMS had high sensitivity and specificity in predicting 6/12/24 months OS and clinical response. The GMS exhibited a significantly superior level of predictive accuracy in comparison to both clinical attributes (e.g., sex) and molecular characteristics (e.g., MSI, TMB, and PD-L1 expression). This indicates the considerable potential for enhanced clinical translation and utilization of the GMS.

Leveraging the comprehensive data of the TCGA cohort, we delved into the diverse responses of cancers to immunotherapy treatment. The low-risk group stood out for its dense immune cell infiltration, rigorously supported by multiple algorithms. This internal immunological terrain was additionally fortified by potent immunogenic features: elevated mutation rates and a substantial neoantigen burden. In contrast to the high-risk group, the low-risk group also exhibited increased expression of immune checkpoint proteins such as PD-L1, PD-1, and CTLA-4, which

10.3389/fimmu.2024.1428529

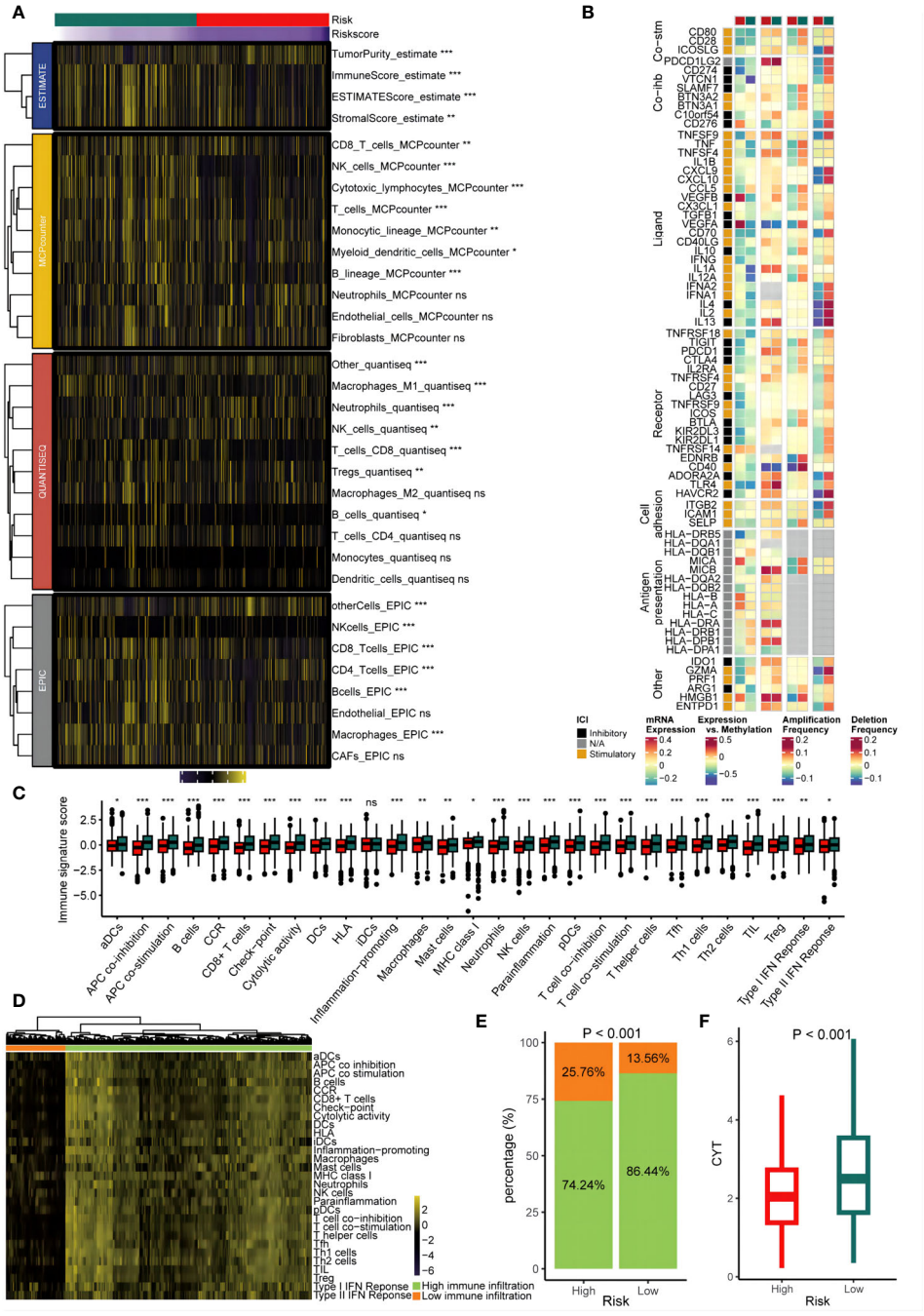

FIGURE 5
Immune infiltrating characteristics of the GMS in the cohort from TCGA. **(A)** The relationship between the GMS and infiltrating immune cell populations. **(B)** The association between the GMS and immune modulatory factors. **(C)** The relationship between the GMS and 29 immune signatures score. **(D)** Unsupervised clustering based on 29 immune signatures. **(E)** The proportions of high and low immune infiltration were estimated in both the high-risk and low-risk groups. **(F)** A comparison of the cytolytic activity scores (CYTs) score was conducted betweenthe high-risk and low-risk groups. NS, no significant; *p < 0.05; **p < 0.01; ***p < 0.001.

could contribute to a more favorable response to ICIs therapy. The activated antitumor immunity, elevated PD-L1, PD-L2 and CTLA-4 expression, and heightened tumor immunogenicity likely explain why the low-risk group benefits from ICI therapy compared to their high-risk counterparts.

Our research offers the following novel contributions and practical implications. Firstly, we have developed an artificial intelligence network that comprises 297 algorithm combinations. This integration encompasses 22 algorithms, drawn from traditional regression, machine learning, and deep learning methodologies. This network featured a diverse and comprehensive set of algorithms, and exhibited superior predictive performance than previous studies (17, 25). Moreover, the optimal combination was VSOLassoBag and RSF, which was

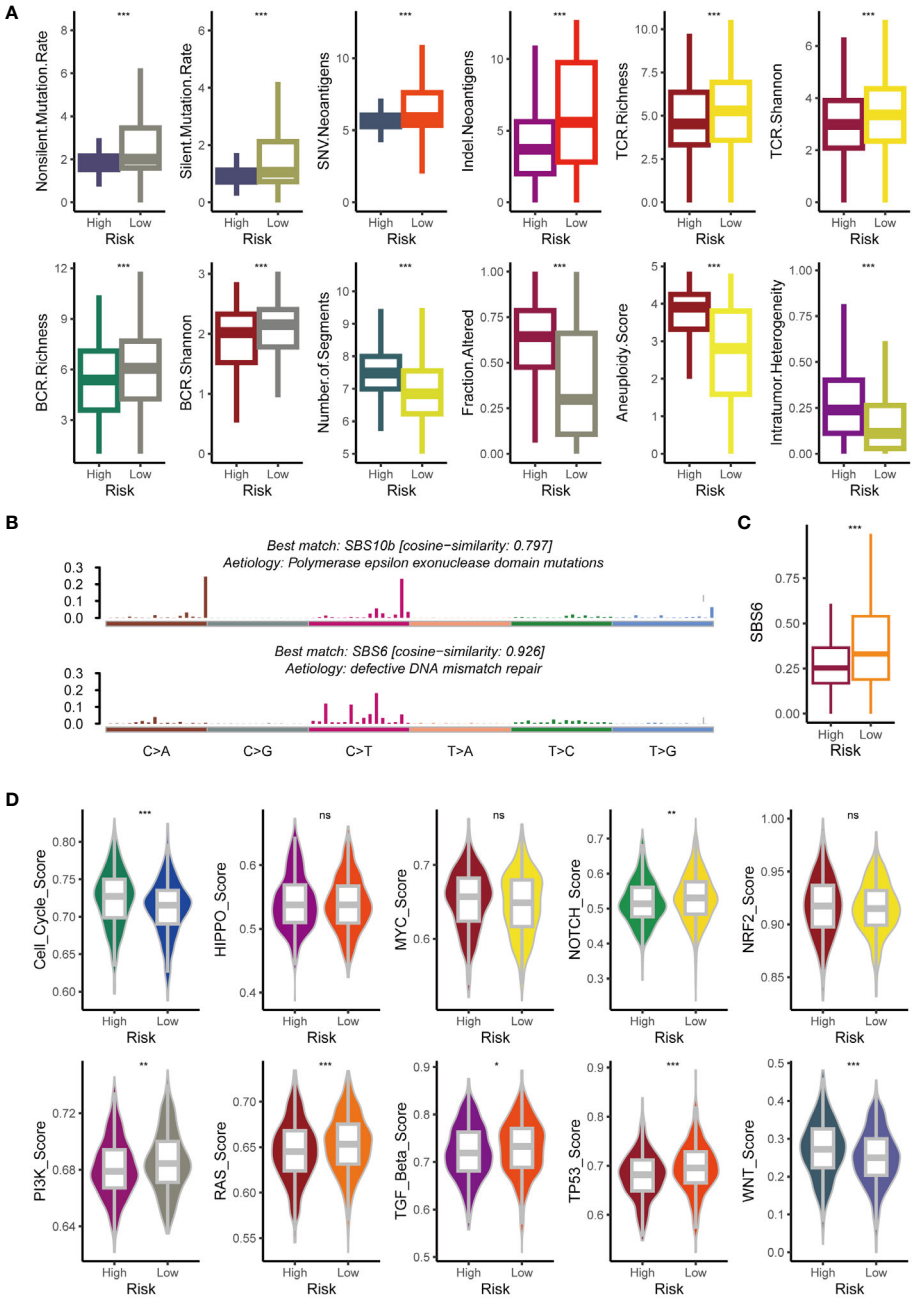

FIGURE 6
Exploration of potential intrinsic immune response and escape landscapes in the high-risk and low-risk groups. **(A)** Comparison of immunogenomic markers between the high-risk and low-risk groups. **(B)** Analysis of mutational activities of two extracted mutational signatures. **(C)** Comparison of the SBS6 signature activity between high-risk and low-risk groups. **(D)** Comparison of enrichment scores for 10 oncogenic pathways between high-risk and low-risk groups. NS, no significant; *p < 0.05; **p < 0.01; ***p < 0.001.

not considered in the prior study (25). The dimensionality of the variables was further reduced by the additional algorithm combinations, making the GMS more simplified and feasible. Secondly, the creation of multibiomarker predictive models demands a thorough comprehension of the elements impacting the dependability and precision of high-throughput assays in clinical scenarios. The variability in biomarker measurements, particularly those that is technical (platform-dependent), is a critical concern. A number of mRNA-based signatures have been developed to forecast clinical efficacy for patients receiving ICI therapy, including the T cell-inflamed gene-expression profile (GEP), which comprises an 18-gene panel (43). The evaluation of mRNA expression is carried out through relative quantification by normalizing it to reference genes (44). The risk scoring and threshold values of mRNA signatures may not be directly applicable for validation with diverse measurement data types. In this study, we have identified specific gene mutations to forecast the clinical effectiveness of ICIs. Consequently, the GMS is resilient to

10.3389/fimmu.2024.1428529

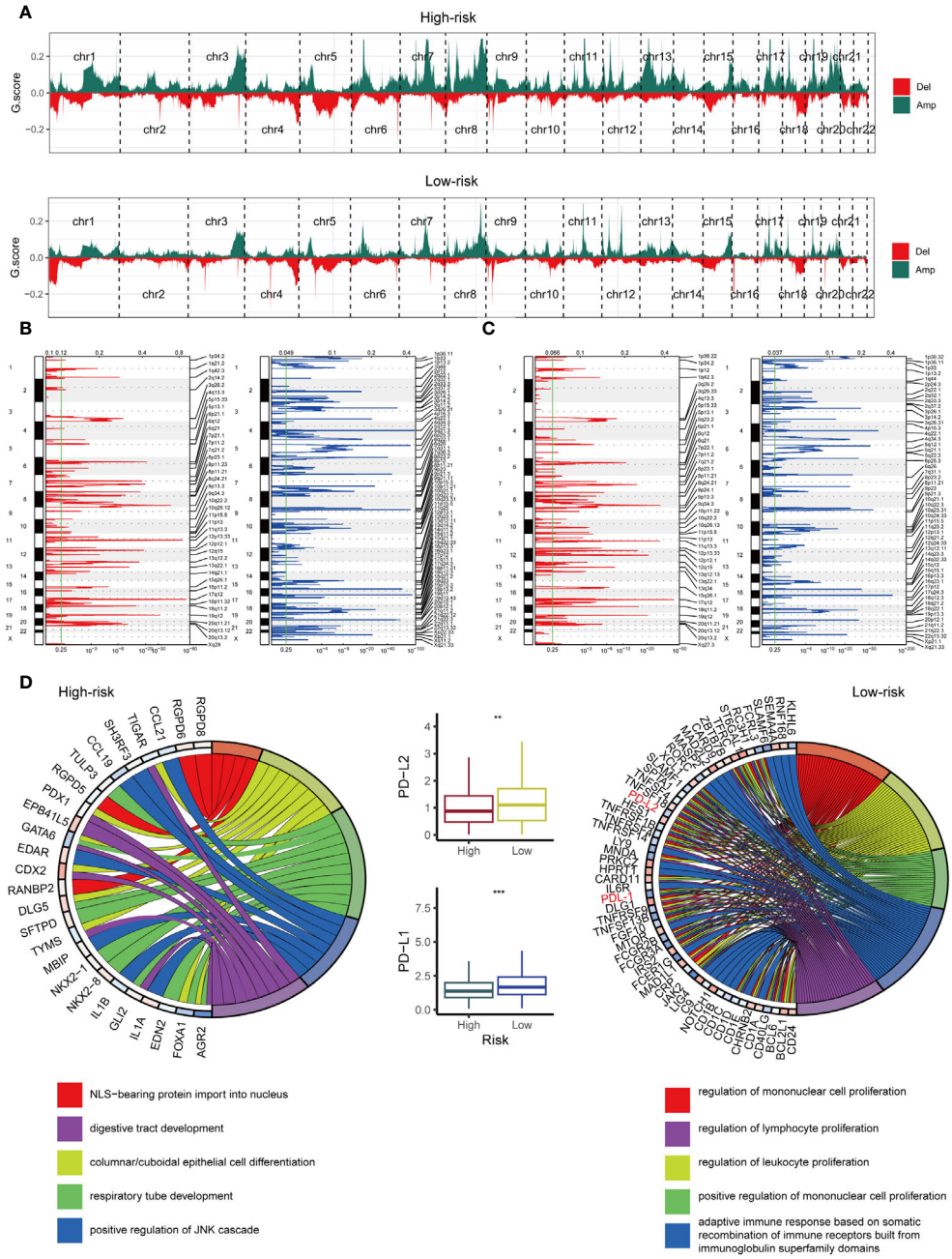

FIGURE 7
Examination of Copy Number Alterations in High-Risk and Low-Risk Groups. **(A)** Displaying copy number profiles for the high-risk group (upper) and low-risk group (lower). **(B)** Elaborating on cytobands with focal amplifications (left) and deletions (right) peaks identified within the high-risk group. **(C)** Exploring cytobands with focal amplifications (left) and deletions (right) peaks detected in the low-risk group. **(D)** Circular plot showcasing the top 5 biological processes along with their corresponding enriched genes in the high-risk (left) and low-risk (right) groups. Additionally, comparing the mRNA expression of PD-L1 and PD-L2 between the high-risk and low-risk cohorts from TCGA (middle). $^{**}p < 0.01$; $^{***}p < 0.001$.

technical variations, even when different platforms are employed across various centers. Thirdly, in clinical practice, the GMS aids in avoiding potential immune-related adverse effects for patients who are unlikely to respond, and it enables the early identification of patients who may benefit from more effective therapies. Additionally, given that the average cost of a treatment regimen often exceeds $120,000 (45), implementing biomarker strategies that improve diagnostic precision can help prevent significant costs for treatments with limited expected benefits. In summary, since obtaining tumor specimens through targeted next-generation sequencing (NGS) of these genes is simpler and less costly compared to assessing TMB, which are complex and expensive in routine practice, the GMS with these refinement merits evaluation. Such an assessment could enhance diagnostic accuracy and cost-effectiveness in clinic.

Utilizing the GDSC, we identified UMI-77, a small molecule drug that demonstrated the most significant p-value and a strong negative correlation with GMS. UMI-77 is an FDA-approved

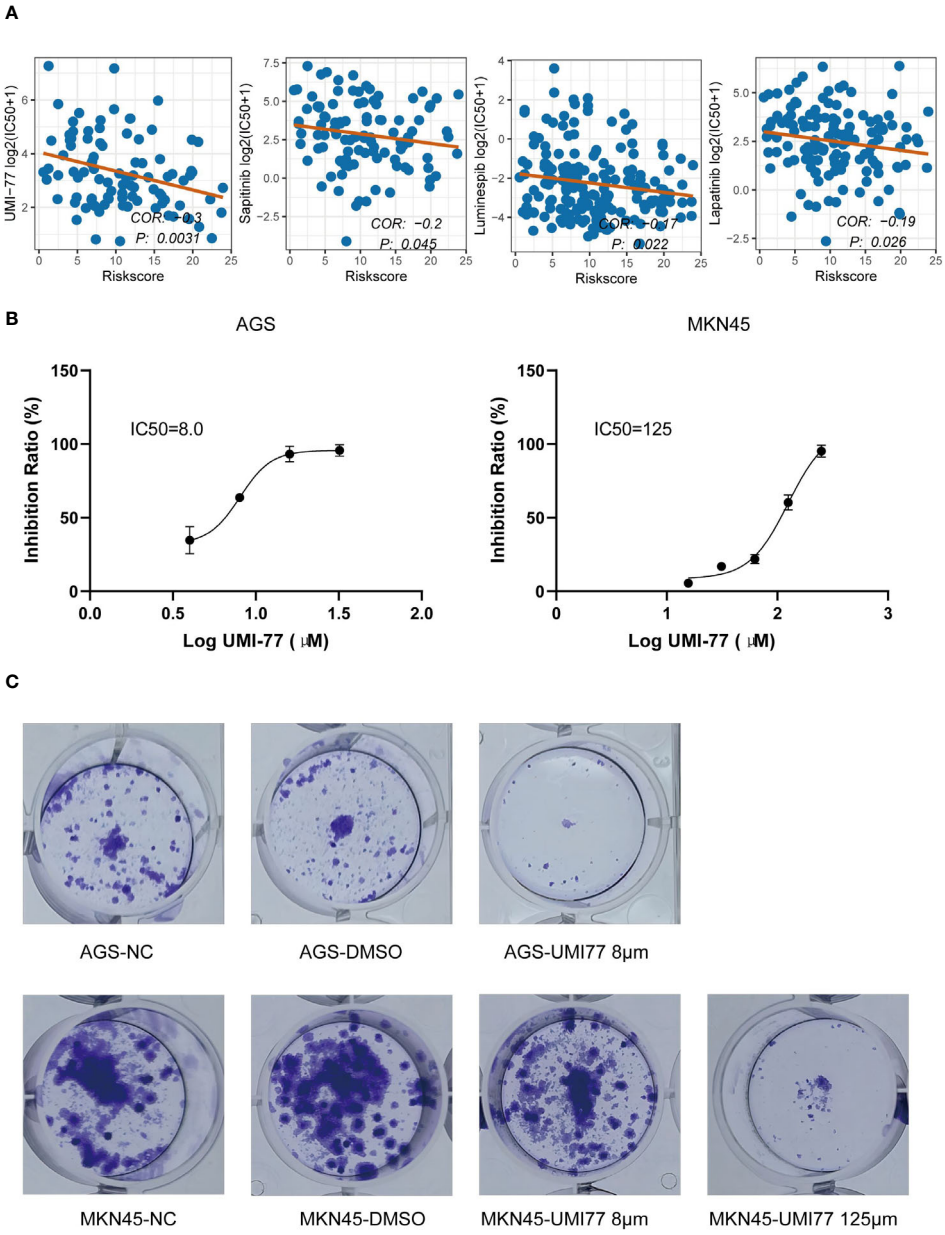

FIGURE 8
Identification of small molecule drugs negatively associated with GMS. **(A)** Correlation of half maximal inhibitory concentration (IC50) with GMS for UMI-77, Luminespib, Lapatinib, and Sapitinib. **(B)** IC50 of UMI-77 of AGS (right) and MKN45 (left). **(C)** Clonogenicity of AGS (above) and MKN45 (below) by using a colony-forming assay.

candidate drug for pancreatic cancer, known to inhibit cell proliferation and induce apoptosis in pancreatic cancer cells (46). Moreover, UMI-77 triggers mitophagy, a process that selectively eliminates damaged mitochondria, making it a potential therapeutic option for Alzheimer's disease (47, 48) and glioma (49). Our observations revealed that the AGS cell line, categorized in the high-risk group, displayed greater sensitivity to UMI-77 than the MKN45 cell line, which belongs to the low-risk group. Based on these findings, we hypothesize that combining UMI-77 with ICIs may enhance the efficacy of ICIs in the high-risk group. However, this hypothesis necessitates further validation through *in vivo* experiments.

Limitations

Our research is not without limitations, which are important to acknowledge. Firstly, we did not have access to comprehensive clinical records for all patients, potentially introducing bias in the data analysis. Secondly, the inclusion of diverse gastrointestinal cancer types and the retrospective nature of the study may have introduced confounding factors. Thirdly, the abundance of immune cells and the expression of immune checkpoints should be substantiated through immunohistochemistry techniques. To address these limitations, further analysis and validation are needed through prospective studies involving a large cohort of

gastrointestinal cancer patients with diverse ethnic backgrounds receiving ICIs therapy. Such studies would help strengthen the findings and implications of our research.

Conclusions

In summary, our GMS emerges as a promising biomarker for both prognosis and prediction of ICI treatment response in gastrointestinal cancer patients. This signature also presents an economical approach to pinpoint patients who may benefit from immunotherapy, a concept that should be further explored through prospective research. The GMS could significantly contribute to the refinement of personalized treatment plans and the enhancement of patient outcomes in gastrointestinal cancer immunotherapy.

Data availability statement

The genomic and clinical data for the MSK cohort, Janjigian and Pender cohort, and PUCH cohort are openly available and were downloaded from the following sources: MSK cohort: http://www.cbioportal.org/study?id=tmb_mskcc_2018; Janjigian cohort: https://www.cbioportal.org/study/summary?id=egc_msk_2017; Pender cohort: http://clincancerres.aacrjournals.org/content/27/1/202.article-info; PUCH cohort: https://www.bcgsc.ca/downloads/immunoPOG/; The DNA-seq and RNA-seq data from the TCGA dataset is available for download at https://portal.gdc.cancer.gov/.

Ethics statement

Ethical approval was not required for the studies on humans in accordance with the local legislation and institutional requirements because only commercially available established cell lines were used.

Author contributions

BY: Methodology, Software, Visualization, Writing – original draft, Writing – review & editing. ZL: Methodology, Software, Visualization, Writing – original draft, Writing – review & editing. QW: Conceptualization, Data curation, Methodology, Software, Writing – original draft, Writing – review & editing.

Funding

The author(s) declare that no financial support was received for the research, authorship, and/or publication of this article.

Conflict of interest

The authors declare that the research was conducted in the absence of any commercial or financial relationships that could be construed as a potential conflict of interest.

Publisher's note

All claims expressed in this article are solely those of the authors and do not necessarily represent those of their affiliated organizations, or those of the publisher, the editors and the reviewers. Any product that may be evaluated in this article, or claim that may be made by its manufacturer, is not guaranteed or endorsed by the publisher.

Supplementary material

The Supplementary Material for this article can be found online at: https://www.frontiersin.org/articles/10.3389/fimmu.2024.1428529/full#supplementary-material

References

1. Arnold M, Abnet CC, Neale RE, Vignat J, Giovannucci EL, McGlynn KA, et al. Global burden of 5 major types of gastrointestinal cancer. *Gastroenterology*. (2020) 159:335–349.e315. doi: 10.1053/j.gastro.2020.02.068

2. Carlino MS, Larkin J, Long GV. Immune checkpoint inhibitors in melanoma. *Lancet (London England)*. (2021) 398:1002–14. doi: 10.1016/S0140-6736(21)01206-X

3. Lu Z, Peng Z, Liu C, Wang Z, Wang Y, Jiao X, et al. Current status and future perspective of immunotherapy in gastrointestinal cancers. *Innovation (Cambridge (Mass))*. (2020) 1:100041. doi: 10.1016/j.xinn.2020.100041

4. Rao D, Parakrama R, Augustine T, Liu Q, Goel S, Maitra R. Immunotherapeutic advances in gastrointestinal Malignancies. *NPJ Precis Oncol*. (2019) 3:4. doi: 10.1038/s41698-018-0076-8

5. Dudley JC, Lin MT, Le DT, Eshleman JR. Microsatellite instability as a biomarker for PD-1 blockade. *Clin Cancer Res*. (2016) 22:813–20. doi: 10.1158/1078-0432.CCR-15-1678

6. Asaoka Y, Ijichi H, Koike K. PD-1 blockade in tumors with mismatch-repair deficiency. *New Engl J Med*. (2015) 373:1979. doi: 10.1056/NEJMc1510353

7. Fuchs CS, Doi T, Jang RW, Muro K, Satoh T, MaChado M, et al. Safety and efficacy of pembrolizumab monotherapy in patients with previously treated advanced gastric and gastroesophageal junction cancer: phase 2 clinical KEYNOTE-059 trial. *JAMA Oncol*. (2018) 4:e180013. doi: 10.1001/jamaoncol.2018.0013

8. Wang F, Wei XL, Wang FH, Xu N, Shen L, Dai GH, et al. Safety, efficacy and tumor mutational burden as a biomarker of overall survival benefit in chemo-refractory gastric cancer treated with toripalimab, a PD-1 antibody in phase Ib/II clinical trial NCT02915432. *Ann Oncol*. (2019) 30:1479–86. doi: 10.1093/annonc/mdz197

9. Huang J, Xu J, Chen Y, Zhuang W, Zhang Y, Chen Z, et al. Camrelizumab versus investigator's choice of chemotherapy as second-line therapy for advanced or metastatic oesophageal squamous cell carcinoma (ESCORT): a multicentre, randomised, open-label, phase 3 study. *Lancet Oncol*. (2020) 21:832–42. doi: 10.1016/S1470-2045(20)30110-8

10. Marabelle A, Le DT, Ascierto PA, Di Giacomo AM, De Jesus-Acosta A, Delord JP, et al. Efficacy of pembrolizumab in patients with noncolorectal high microsatellite instability/Mismatch repair-Deficient cancer: results from the phase II KEYNOTE-158 study. *J Clin Oncol*. (2020) 38:1–10. doi: 10.1200/JCO.19.02105

11. Samstein RM, Lee CH, Shoushtari AN, Hellmann MD, Shen R, Janjigian YY, et al. Tumor mutational load predicts survival after immunotherapy across multiple cancer types. *Nat Genet*. (2019) 51:202–6. doi: 10.1038/s41588-018-0312-8

12. Xue L, Tang W, Zhou J, Xue J, Li Q, Ge X, et al. Next-generation sequencing identifies CDKN2A alterations as prognostic biomarkers in recurrent or metastatic head and neck squamous cell carcinoma predominantly receiving immune checkpoint inhibitors. *Front Oncol*. (2023) 13:1276009. doi: 10.3389/fonc.2023.1276009

13. Zhu G, Shi R, Li Y, Zhang Z, Xu S, Chen C, et al. ARID1A, ARID1B, and ARID2 mutations serve as potential biomarkers for immune checkpoint blockade in patients with non-small cell lung cancer. *Front Immunol*. (2021) 12:670040. doi: 10.3389/fimmu.2021.670040

14. Hu X, Xu H, Xue Q, Wen R, Jiao W, Tian K. The role of ERBB4 mutations in the prognosis of advanced non-small cell lung cancer treated with immune checkpoint inhibitors. *Mol Med (Cambridge Mass)*. (2021) 27:126. doi: 10.1186/s10020-021-00387-z

15. Zhang J, Zhou N, Lin A, Luo P, Chen X, Deng H, et al. ZFHX3 mutation as a protective biomarker for immune checkpoint blockade in non-small cell lung cancer. *Cancer immunology immunotherapy: CII*. (2021) 70:137–51. doi: 10.1007/s00262-020-02668-8

16. Wang Z, Zhang Q, Qi C, Bai Y, Zhao F, Chen H, et al. Combination of AKT1 and CDH1 mutations predicts primary resistance to immunotherapy in dMMR/MSI-H gastrointestinal cancer. *J immunotherapy Cancer*. (2022) 10:e004703. doi: 10.1136/jitc-2022-004703

17. Jiao X, Wei X, Li S, Liu C, Chen H, Gong J, et al. A genomic mutation signature predicts the clinical outcomes of immunotherapy and characterizes immunophenotypes in gastrointestinal cancer. *NPJ Precis Oncol*. (2021) 5:36. doi: 10.1038/s41698-021-00172-5

18. Shim JH, Kim HS, Cha H, Kim S, Kim TM, Anagnostou V, et al. HLA-corrected tumor mutation burden and homologous recombination deficiency for the prediction of response to PD-(L)1 blockade in advanced non-small-cell lung cancer patients. *Ann Oncol*. (2020) 31:902–11. doi: 10.1016/j.annonc.2020.04.004

19. Wang Z, Ge Y, Li H, Fei G, Wang S, Wei P. Identification and validation of a genomic mutation signature as a predictor for immunotherapy in NSCLC. *Bioscience Rep*. (2022) 42. doi: 10.1042/BSR20220892

20. Bai X, Wu DH, Ma SC, Wang J, Tang XR, Kang S, et al. Development and validation of a genomic mutation signature to predict response to PD-1 inhibitors in non-squamous NSCLC: a multicohort study. *J immunotherapy Cancer*. (2020) 8:e000381. doi: 10.1136/jitc-2019-000381

21. Qiu T, Shi X, Wang J, Li Y, Qu S, Cheng Q, et al. Deep learning: A rapid and efficient route to automatic metasurface design. *Advanced Sci (Weinheim Baden-Wurttemberg Germany)*. (2019) 6:1900128. doi: 10.1002/advs.201900128

22. Holder LB, Haque MM, Skinner MK. Machine learning for epigenetics and future medical applications. *Epigenetics*. (2017) 12:505–14. doi: 10.1080/15592294.2017.1329068

23. Zhao S, Wang L, Ding W, Ye B, Cheng C, Shao J, et al. Crosstalk of disulfidptosis-related subtypes, establishment of a prognostic signature and immune infiltration characteristics in bladder cancer based on a machine learning survival framework. *Front Endocrinol*. (2023) 14:1180404. doi: 10.3389/fendo.2023.1180404

24. Ye B, Wang Q, Zhu X, Zeng L, Luo H, Xiong Y, et al. Single-cell RNA sequencing identifies a novel proliferation cell type affecting clinical outcome of pancreatic ductal adenocarcinoma. *Front Oncol*. (2023) 13:1236435. doi: 10.3389/fonc.2023.1236435

25. Liu Z, Liu L, Weng S, Guo C, Dang Q, Xu H, et al. Machine learning-based integration develops an immune-derived lncRNA signature for improving outcomes in colorectal cancer. *Nat Commun*. (2022) 13:816. doi: 10.1038/s41467-022-28421-6

26. Janjigian YY, Sanchez-Vega F, Jonsson P, Chatila WK, Hechtman JF, Ku GY, et al. Genetic predictors of response to systemic therapy in esophagogastric cancer. *Cancer Discovery*. (2018) 8:49–58. doi: 10.1158/2159-8290.CD-17-0787

27. Pender A, Titmuss E, Pleasance ED, Fan KY, Pearson H, Brown SD, et al. Genome and transcriptome biomarkers of response to immune checkpoint inhibitors in advanced solid tumors. *Clin Cancer Res*. (2021) 27:202–12. doi: 10.1158/1078-0432.CCR-20-1163

28. Rizvi NA, Hellmann MD, Snyder A, Kvistborg P, Makarov V, Havel JJ, et al. Cancer immunology. Mutational landscape determines sensitivity to PD-1 blockade in non-small cell lung cancer. *Sci (New York NY)*. (2015) 348:124–8. doi: 10.1126/science.aaa1348

29. Thorsson V, Gibbs DL, Brown SD, Wolf D, Bortone DS, Ou Yang TH, et al. The immune landscape of cancer. *Immunity*. (2018) 48:812–30.e814. doi: 10.1016/j.immuni.2018.03.023

30. Finotello F, Mayer C, Plattner C, Laschober G, Rieder D, Hackl H, et al. Molecular and pharmacological modulators of the tumor immune contexture revealed by deconvolution of RNA-seq data. *Genome Med*. (2019) 11:34. doi: 10.1186/s13073-019-0638-6

31. Racle J, Gfeller D. EPIC: A tool to estimate the proportions of different cell types from bulk gene expression data. *Methods Mol Biol (Clifton NJ)*. (2020) 2120:233–48. doi: 10.1007/978-1-0716-0327-7_17

32. Becht E, Giraldo NA, Lacroix L, Buttard B, Elarouci N, Petitprez F, et al. Erratum to: Estimating the population abundance of tissue-infiltrating immune and stromal cell populations using gene expression. *Genome Biol*. (2016) 17:249. doi: 10.1186/s13059-016-1113-y

33. Yoshihara K, Shahmoradgoli M, Martínez E, Vegesna R, Kim H, Torres-Garcia W, et al. Inferring tumour purity and stromal and immune cell admixture from expression data. *Nat Commun*. (2013) 4:2612. doi: 10.1038/ncomms3612

34. He Y, Jiang Z, Chen C, Wang X. Classification of triple-negative breast cancers based on Immunogenomic profiling. *J Exp Clin Cancer research: CR*. (2018) 37:327. doi: 10.1186/s13046-018-1002-1

35. Rooney MS, Shukla SA, Wu CJ, Getz G, Hacohen N. Molecular and genetic properties of tumors associated with local immune cytolytic activity. *Cell*. (2015) 160:48–61. doi: 10.1016/j.cell.2014.12.033

36. Hänzelmann S, Castelo R, Guinney J. GSVA: gene set variation analysis for microarray and RNA-seq data. *BMC Bioinf*. (2013) 14:7. doi: 10.1186/1471-2105-14-7

37. Yu G, Wang LG, Han Y, He QY. clusterProfiler: an R package for comparing biological themes among gene clusters. *Omics: J Integr Biol*. (2012) 16:284–7. doi: 10.1089/omi.2011.0118

38. Zhou Y, Zhou B, Pache L, Chang M, Khodabakhshi AH, Tanaseichuk O, et al. Metascape provides a biologist-oriented resource for the analysis of systems-level datasets. *Nat Commun*. (2019) 10:1523. doi: 10.1038/s41467-019-09234-6

39. Sanchez-Vega F, Mina M, Armenia J, Chatila WK, Luna A, La KC, et al. Oncogenic signaling pathways in the cancer genome atlas. *Cell*. (2018) 173:321–37.e310. doi: 10.1016/j.cell.2018.03.035

40. Wu W, Liu Y, Zeng S, Han Y, Shen H. Intratumor heterogeneity: the hidden barrier to immunotherapy against MSI tumors from the perspective of IFN-γ signaling and tumor-infiltrating lymphocytes. *J Hematol Oncol*. (2021) 14:160. doi: 10.1186/s13045-021-01166-3

41. Davoli T, Uno H, Wooten EC, Elledge SJ. Tumor aneuploidy correlates with markers of immune evasion and with reduced response to immunotherapy. *Sci (New York NY)*. (2017) 355:eaaf8399. doi: 10.1126/science.aaf8399

42. Luke JJ, Bao R, Sweis RF, Spranger S, Gajewski TF. WNT/β-catenin pathway activation correlates with immune exclusion across human cancers. *Clin Cancer Res*. (2019) 25:3074–83. doi: 10.1158/1078-0432.CCR-18-1942

43. Ott PA, Bang YJ, Piha-Paul SA, Razak ARA, Bennouna J, Soria JC, et al. T-cell-inflamed gene-expression profile, programmed death ligand 1 expression, and tumor mutational burden predict efficacy in patients treated with pembrolizumab across 20 cancers: KEYNOTE-028. *J Clin Oncol*. (2019) 37:318–27. doi: 10.1200/JCO.2018.78.2276

44. Long J, Wang D, Wang A, Chen P, Lin Y, Bian J, et al. A mutation-based gene set predicts survival benefit after immunotherapy across multiple cancers and reveals the immune response landscape. *Genome Med*. (2022) 14:20. doi: 10.1186/s13073-022-01024-y

45. Lu S, Stein JE, Rimm DL, Wang DW, Bell JM, Johnson DB, et al. Comparison of biomarker modalities for predicting response to PD-1/PD-L1 checkpoint blockade: A systematic review and meta-analysis. *JAMA Oncol*. (2019) 5:1195–204. doi: 10.1001/jamaoncol.2019.1549

46. Abulwerdi F, Liao C, Liu M, Azmi AS, Aboukameel A, Mady AS, et al. A novel small-molecule inhibitor of mcl-1 blocks pancreatic cancer growth *in vitro* and *in vivo*. *Mol Cancer Ther*. (2014) 13:565–75. doi: 10.1158/1535-7163.MCT-12-0767

47. Cen X, Chen Y, Xu X, Wu R, He F, Zhao Q, et al. Pharmacological targeting of MCL-1 promotes mitophagy and improves disease pathologies in an Alzheimer's disease mouse model. *Nat Commun*. (2020) 11:5731. doi: 10.1038/s41467-020-19547-6

48. Cen X, Xu X, Xia H. Targeting MCL1 to induce mitophagy is a potential therapeutic strategy for Alzheimer disease. *Autophagy*. (2021) 17:818–9. doi: 10.1080/15548627.2020.1860542

49. Chen C, Zhu S, Zhang X, Zhou T, Gu J, Xu Y, et al. Targeting the synthetic vulnerability of PTEN-Deficient glioblastoma cells with MCL1 inhibitors. *Mol Cancer Ther*. (2020) 19:2001–11. doi: 10.1158/1535-7163.MCT-20-0099

frontiers | Frontiers in Immunology

TYPE Original Research
PUBLISHED 27 June 2024
DOI 10.3389/fimmu.2024.1418508

Check for updates

OPEN ACCESS

EDITED BY
Pengpeng Zhang,
Nanjing Medical University, China

REVIEWED BY
Chunyan Niu,
Southeast University, China
Yuquan Chen,
Monash University, Australia

*CORRESPONDENCE
Jiangtao Fan
jt_fan2018@163.com
Jingxin Mao
2230040@cqmpc.edu.cn

†These authors have contributed equally to this work and share first authorship

RECEIVED 16 April 2024
ACCEPTED 12 June 2024
PUBLISHED 27 June 2024

CITATION
Wei C, Lin S, Huang Y, Wei Y, Mao J and Fan J (2024) Integrated machine learning identifies a cellular senescence-related prognostic model to improve outcomes in uterine corpus endometrial carcinoma. *Front. Immunol.* 15:1418508. doi: 10.3389/fimmu.2024.1418508

COPYRIGHT
© 2024 Wei, Lin, Huang, Wei, Mao and Fan. This is an open-access article distributed under the terms of the Creative Commons Attribution License (CC BY). The use, distribution or reproduction in other forums is permitted, provided the original author(s) and the copyright owner(s) are credited and that the original publication in this journal is cited, in accordance with accepted academic practice. No use, distribution or reproduction is permitted which does not comply with these terms.

Integrated machine learning identifies a cellular senescence-related prognostic model to improve outcomes in uterine corpus endometrial carcinoma

Changqiang Wei[1†], Shanshan Lin[1†], Yanrong Huang[1†], Yiyun Wei[1], Jingxin Mao[2*] and Jiangtao Fan[1*]

[1]Department of Obstetrics and Gynecology, The First Affiliated Hospital of Guangxi Medical University, Guangxi, China, [2]Department of Science and Technology Industry, Chongqing Medical and Pharmaceutical College, Chongqing, China

Background: Uterine Corpus Endometrial Carcinoma (UCEC) stands as one of the prevalent malignancies impacting women globally. Given its heterogeneous nature, personalized therapeutic approaches are increasingly significant for optimizing patient outcomes. This study investigated the prognostic potential of cellular senescence genes(CSGs) in UCEC, utilizing machine learning techniques integrated with large-scale genomic data.

Methods: A comprehensive analysis was conducted using transcriptomic and clinical data from 579 endometrial cancer patients sourced from the Cancer Genome Atlas (TCGA). A subset of 503 CSGs was assessed through weighted gene co-expression network analysis (WGCNA) alongside machine learning algorithms, including Gaussian Mixture Model (GMM), support vector machine - recursive feature elimination (SVM-RFE), Random Forest, and eXtreme Gradient Boosting (XGBoost), to identify key differentially expressed cellular senescence genes. These genes underwent further analysis to construct a prognostic model.

Results: Our analysis revealed two distinct molecular clusters of UCEC with significant differences in tumor microenvironment and survival outcomes. Utilizing cellular senescence genes, a prognostic model effectively stratified patients into high-risk and low-risk categories. Patients in the high-risk group exhibited compromised overall survival and presented distinct molecular and immune profiles indicative of tumor progression. Crucially, the prognostic model demonstrated robust predictive performance and underwent validation in an independent patient cohort.

Conclusion: The study emphasized the significance of cellular senescence genes in UCEC progression and underscored the efficacy of machine learning in developing reliable prognostic models. Our findings suggested that targeting cellular senescence holds promise as a strategy in personalized UCEC treatment, thus warranting further clinical investigation.

KEYWORDS

UCEC, cellular senescence, machine learning, MYBL2, CPEB1

1 Introduction

Uterine Corpus Endometrial Carcinoma (UCEC) stands as one of the most prevalent malignancies in gynecology. In China, its incidence ranks second only to cervical cancer (1). In 2023, an estimated 66,200 new cases and 13,030 deaths are projected in the United States (2).

The pathogenesis and classification of UCEC have garnered considerable attention in medical research. It is primarily categorized into two types based on biological characteristics and clinical behavior: Type I (estrogen-dependent) and Type II (non-estrogen dependent) endometrial carcinoma. Recent studies have further delineated it into four molecular subtypes: POLE ultramutated, microsatellite instability, copy-number stability, and p53 abnormal types (3). This molecular classification enriches our comprehension of UCEC heterogeneity and forms the basis for devising personalized treatment strategies (4).

Early-stage endometrial cancer commonly involves total hysterectomy and bilateral salpingo-oophorectomy (5), whereas in cases of advanced or recurrent endometrial cancer, surgery remains crucial but must be supplemented with systemic treatments such as chemotherapy, immunotherapy, targeted therapy, and endocrine therapy (6). Recent studies have concentrated on molecular markers like mutations in the PTEN, PIK3CA, ARID1A, and KRAS genes, prevalent in Type I endometrial cancers, which foster tumor growth and survival (7). Type II cancers often manifest mutations in the p53 gene and amplification of the HER2 gene (8). These findings aid in delineating distinct biological features and therapeutic targets for various tumor types.

Targeted therapies, including PI3K and mTOR inhibitors, have become essential in UCEC treatment, significantly improving outcomes for certain patients (9). For individuals exhibiting microsatellite instability or mismatch repair deficiencies, immune checkpoint inhibitors like PD-1/PD-L1 present novel therapeutic possibilities (10). The efficacy of these strategies highlights the significance of personalized medicine in UCEC treatment. However, challenges persist in precisely identifying eligible patients and devising novel medications.

Cellular senescence constitutes a multifaceted biological process involving alterations in gene expression, DNA damage accumulation, protein function loss, and cell cycle arrest (11). Serving as a critical tumor-suppressing mechanism, it inhibits cancer by constraining the proliferation of damaged or mutated cells (12). Nonetheless, the accumulation of senescent cells can foster tumor progression via the secretion of pro-inflammatory and pro-tumorigenic factors (13). Studies have demonstrated the pivotal roles of senescence-associated genes, such as p53, RB, and PTEN, in cancer development (11). Targeting SASP factors presents a novel perspective for certain cancer treatments (14, 15).

Studies utilizing public databases such as TCGA and Gene Expression Omnibus have pinpointed specific genes linked to the prognosis and treatment responses of UCEC (16–18). These genes can potentially serve as novel biomarkers for refining prognostic models. Currently, research on cellular senescence related to UCEC remains limited. Employing advanced bioinformatics to investigate the relationship between cellular senescence genes and UCEC is imperative for patient stratification and the identification of new therapeutic targets and immune treatment strategies.

2 Materials and methods

2.1 Data and patient collection

Figure 1 illustrates the methodology employed in this research. Transcriptomic and clinical data for 579 endometrial cancer patients, comprising 544 UCEC cases and 35 control subjects, were obtained from the TCGA database (https://portal.gdc.cancer.gov/). A total of 503 cellular senescence genes were sourced from the CSGene database (https://csgene.bioinfominzhao.org/index.html, Supplementary Table 1).

Furthermore, 20 endometrial cancer tissues and 20 non-cancerous endometrial tissues were collected from the First Affiliated Hospital of Guangxi Medical University. All UCEC diagnoses were confirmed by experienced pathologists, with pertinent clinical details provided in Supplementary Table 2. Following surgery, tissues were promptly transferred to a petri dish using forceps and rinsed thoroughly with physiological saline to eliminate surrounding blood clots. Subsequently, approximately 5g samples were dissected using a surgical blade for subsequent RT-

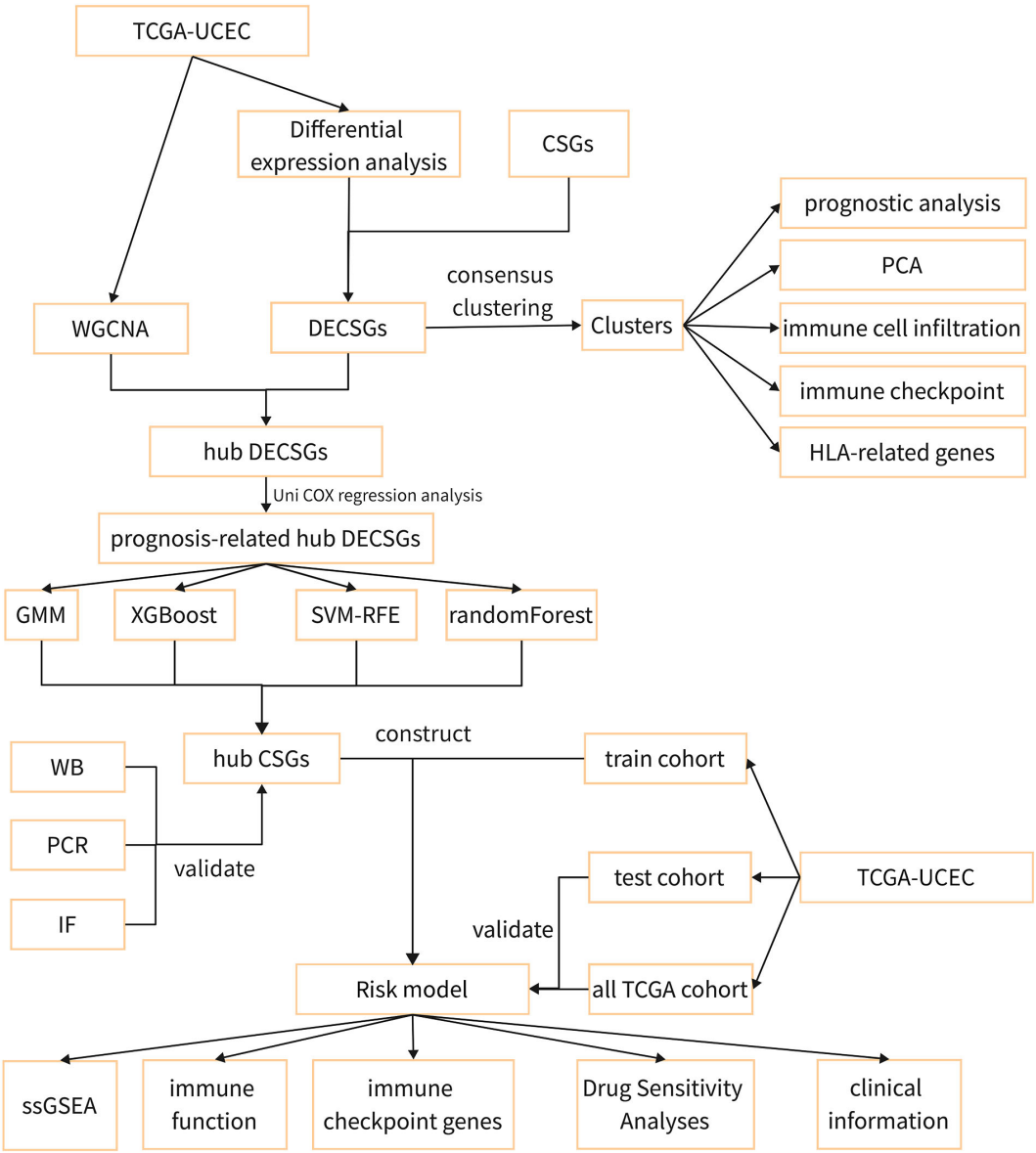

FIGURE 1
The flow diagram of the study.

qPCR and Western blot experiments. Additionally, roughly 10g of tissue was placed in 4% paraformaldehyde fixative, fixed for 24 hours, and then subjected to dehydration and paraffin embedding for sectioning. The study received ethical approval (No. 2023-S033–01), and all participants provided informed consent before undergoing surgery.

2.2 Differential expression analysis

In this study, we utilized the "limma" package (19) in R software to perform differential expression analysis on the UCEC dataset. The filtering criteria were set as: $|\log_2 \text{FoldChange}| \geq 1.5$, and $P<0.05$. Subsequently, the differentially expressed genes and cellular senescence genes were intersected to yield a series of Differentially Expressed Cellular Senescence Genes (DECSGs).

2.3 Consensus clustering and subtype analysis

To identify UCEC subtypes associated with DECSGs, we utilized the "ConsensusClusterPlus" R package for consensus clustering analysis (20). This approach evaluated consistency across multiple clustering runs to determine a more stable final clustering structure, commonly employed in data analysis and bioinformatics. The clustering criteria were as follows: enhanced correlation within subtypes post-clustering, and weakened

correlation between subtypes. We ensured the reliability of our results through 1,000 iterations and utilized the Probably Approximately Correct (PAC) method to determine the optimal number of clusters. Specifically, the PAC method initially generated a set of random datasets and conducted cluster analysis on these datasets to obtain a range of random cluster numbers. The PAC value quantified the dissimilarity between observed clustering results and random clustering results. A higher PAC value indicated greater dissimilarity between the observed clustering structure and random results, indicating a more robust and reliable clustering structure.

Subsequently, we employed principal component analysis (PCA) to discern variations in gene expression patterns among the clusters. Additionally, we conducted differential expression analysis across the clusters and utilized the "ClusterProfiler" (21) and "org.Hs.eg.db" packages to explore potential biological mechanisms through Gene Ontology (GO), Kyoto Encyclopedia of Genomes (KEGG), and Gene Set Enrichment Analysis (GSEA). Furthermore, the "survival" and "survminer" packages (22) were utilized to analyze the overall survival (OS) and progression-free survival (PFS) rates across the different clusters. The tumor microenvironment (TME) of endometrial cancer was assessed using the "estimate" package to understand its characteristics deeply. Based on the "CIBERSORT" package (23), we analyzed the infiltration levels of 22 immune cell types to identify differences in immune cell infiltration across clusters. Lastly, we investigated the expression differences in key immune checkpoint genes and human leukocyte antigen (HLA)-related genes between clusters. This exploration aimed to elucidate mechanisms by which tumors evade immune surveillance, providing valuable insights for the development of novel immunotherapeutic strategies.

2.4 Co-expression network construction

WGCNA was conducted using the "WGCNA" package (24) to construct a scale-free network associated with clinical phenotypes. The process commenced with hierarchical clustering to filter the cases, followed by the selection of an appropriate soft threshold to construct a weighted adjacency matrix. This matrix was then transformed into a topological overlap matrix (TOM), represented with colors and module eigengenes. Additionally, the Pearson correlation coefficient between the module eigengenes and clinical features was calculated to unveil potential links between gene expression patterns and clinical manifestations.

2.5 Cox regression analysis and machine learning algorithms

In this study, we intersected genes from key modules identified by WGCNA with DECSGs to pinpoint key DECSGs. Patients from the TCGA database with complete clinical information and survival times exceeding 30 days were selected for univariate Cox regression analysis to identify prognostically relevant DECSGs.

To accurately identify hub genes associated with UCEC, we employed four machine learning algorithms: GMM, SVM-RFE, Random Forest, and XGBoost. Firstly, GMM analysis was conducted utilizing the "SimDesign" package (25). This method examined the probability distribution of gene expression data and fit it to multiple Gaussian distributions, revealing complex underlying biological information. Subsequently, the SVM-RFE method (26) was implemented using the "e1071," "kernlab," and "caret" packages. This technique constructed a model based on SVM and optimized the feature set by recursively removing the least impactful features. Next, we employed the Random Forest algorithm via the "randomForest" package and the XGBoost algorithm using the "xgboost" package (27, 28). Random Forest is a robust ensemble learning algorithm that builds multiple decision trees and combines their predictions to enhance model accuracy and robustness, widely utilized in classification and regression tasks. XGBoost is an efficient ensemble learning algorithm that incrementally constructs decision trees and corrects errors to optimize model performance, identifying core features. The common genes identified by these algorithms were determined to be the core DECSGs. Finally, the relationship between these core DECSGs and the prognosis of endometrial cancer was analyzed using the external survival prognosis database Kaplan-Meier Plotter (https://kmplot.com/analysis/index.php?p=background).

2.6 Construction and validation of the cellular senescence-relate risk score model

UCEC samples were randomly divided into a training set and a testing set at a ratio of 7:3. Based on the expression of key DECSGs, a prognostic model was constructed within the training set using the LASSO Cox regression method.

This methodology entails an initial fitting of gene expression data and survival time via LASSO regression, followed by cross-validation utilizing the "cv.glmnet" function. Subsequently, the "coef" function is utilized to extract and compute the weights of the selected genes within the model. The model predicts patient survival prognosis through the calculation of a risk score, formulated as: Risk score = Σ (Xi*Yi), where X represents the coefficient of each gene in the model, and Y denotes the expression level of the corresponding gene. Within the training set, UCEC samples were stratified into high-risk and low-risk clusters based on the risk score. Kaplan-Meier survival analysis was employed to compare the OS between these groups, thereby validating the performance of the risk score model. ROC curve analysis, facilitated by the "timeROC" package (29), was conducted to assess the model's accuracy in predicting patient survival rates. Finally, the model's accuracy was further validated utilizing the independent testing set from TCGA, as well as the entire TCGA dataset.

2.7 Differences in immune characteristics and molecular biology between the high-risk and low-risk groups

Using the "GSEABase" and "GSVA" packages, we analyzed the infiltration fractions and immune-related functions of tumor-infiltrating immune cells in UCEC cases. Differences in immune cell infiltration between low-risk and high-risk groups were compared employing the Wilcoxon test. Moreover, the correlation between the risk score and the expression levels of immune checkpoint genes was investigated using Pearson correlation coefficients. Furthermore, comparisons of risk scores across different stages, grades, and subgroups were conducted to assess the prognostic value of the risk score.

2.8 Drug sensitivity analyses

To investigate the association between chemotherapeutic responsiveness and the risk score model, we employed the "oncoPredict" package (30), leveraging data from the Genomics of Drug Sensitivity in Cancer (GDSC) database (www.cancerRxgene.org). This enabled an analysis of drug sensitivity. Subsequently, we conducted comparative analyses of IC50 values across two distinct groups to assess differential therapeutic outcomes, with the aim of identifying potentially efficacious drugs for the treatment of UCEC.

2.9 Reverse transcription quantitative polymerase chain reaction

Total RNA was extracted using TRIzol reagent (Takara, Japan) and reverse-transcribed into cDNA. PCR was performed using the SYBR Green Master Mix kit (Qiagen, Germany), with the expression level of glyceraldehyde 3-phosphate dehydrogenase (GAPDH) serving as the internal reference. The primer sequences were provided in Table 1. The experiment was conducted with at least three technical replicates. We employed the $2^{-\Delta\Delta CT}$ method to calculate the relative mRNA expression levels of hub genes. A CT value difference within 0.5 between replicate wells of the same sample was considered acceptable for analysis.

TABLE 1 The primers of hub DEERGs and GAPDH.

Gene name	Primer orientation	Sequences
MYBL2	Forward	CTTGAGCGAGTCCAAAGACTG
	Reverse	AGTTGGTCAGAAGACTTCCCT
CPEB1	Forward	GTCCTCCCAAAGGTAATATGCC
	Reverse	TGCAGAGCACCGACAAACA
GAPDH	Forward	CAGGAGGCATTGCTGATGAT
	Reverse	GAAGGCTGGGGCTCATTT

2.10 Western blotting

Cells and clinical samples were lysed with RIPA lysis buffer (Solarbio, China), and the protein concentrations were quantified with a BCA protein quantification kit (NCM Biotech, China). The protein samples were then loaded onto a 10% SDS-PAGE gel for electrophoretic separation, followed by transfer to PVDF membranes (Millipore, USA). After blocking with 5% BSA (Solarbio, China) for 1 hour, the membranes were washed three times with Tris-buffered saline containing 0.1% Tween-20 (TBST), with each wash lasting 5 minutes. Next, the PVDF membrane was incubated overnight at 4°C with specific primary antibodies (anti-β-actin, Sigma, USA, 1/10000; MYBL2, Abcam, UK,1/1000; CPEB1, abways, China, 1/1000). The following day, the membrane was incubated for 1 hour at room temperature with HRP-conjugated goat anti-rabbit IgG. Finally, the target protein band was visualized by laser scanning (Thermo Fisher, USA).

2.11 Immunofluorescence assay

Clinical samples were prepared into slides and deparaffinized in xylene, followed by rehydrated in 100% ethanol and sequentially dehydrated in 95%, 85%, and 75% ethanol concentrations. Antigen retrieval was carried out using sodium citrate in a microwave. To block endogenous peroxidases, the samples were treated with 3% hydrogen peroxide (H2O2), followed by incubation in a 3% Bovine Serum Albumin (BSA) solution (Solarbio, China) for blocking purposes. Subsequently, the tissues were incubated with primary antibodies (MYBL2, Abcam, UK, 1/200; CPEB1, abways, China, 1/200)) overnight at 4°C. After the primary antibody incubation, the tissues underwent incubation with secondary antibodies (Goat Anti-Rabbit IgG H&L/AF555 and Goat Anti-Mouse IgG H&L/AF488) for 1 hour at room temperature. DAPI (Solarbio, China) was added, and the samples were briefly incubated before being washed with phosphate-buffered saline. Finally, images were acquired at 400-fold magnification using a confocal microscope (Nikon AIR, Japan).

2.12 Statistical analysis

Data processing, analysis, and visualization were conducted using R (version 4.3.0) and GraphPad Prism (Version 9.4). Differential analysis in R was primarily conducted utilizing the "limma" package. Visualization of data was predominantly achieved through the "ggplot2", "ggpubr", and "enrichplot" packages. Time-dependent ROC curves were calculated and plotted using the "timeROC" package, facilitating comparisons between different models. Statistical comparisons of experimental results between different groups were executed using the Wilcoxon test, with statistical significance set as a p-value of less than 0.05.

3 Results

3.1 Identification of different expression cellular senescence genes

Differential expression analysis was performed on the TCGA-UCEC dataset. The findings revealed 1,132 upregulated genes and 3,839 downregulated genes in the endometrial carcinoma tissues compared to the control group (Figures 2A, B). Intersection analysis of differentially expressed genes with those associated with cellular senescence identified a total of 104 DECSGs (Figure 2C).

3.2 Construction and analysis of cellular senescence gene-related molecular clusters for UCEC

Consensus clustering was conducted based on the expression of DECSGs. As shown in the Figures 3A–C and Supplementary Figure 1, the PAC algorithm determined the optimal number of clusters to be k=2, yielding clusters denoted as C1 (n=229) and C2 (n=315). PCA affirmed the robust intergroup segregation between cluster C2 and cluster C1 (Figure 3D). Subsequent differential analysis of these subtypes identified 1,375 genes exhibiting differential expression. GO enrichment analysis underscored the significant involvement of these DEGs in pathways vital for nuclear division, precise chromosome segregation, and cytoskeleton functions (Figure 3E; Supplementary Table 3). Moreover, KEGG pathway analysis delineated their predominant roles in cell cycle regulation, motor proteins, cellular senescence, and protein digestion and absorption processes (Figure 3F). GSEA further elucidated that cluster C2 is significantly associated with pivotal biological processes encompassing the cell cycle, focal adhesion, pathways pertinent to cancer, spliceosome activity, and ubiquitin-mediated proteolysis (Figure 3G).

Survival analysis between the clusters revealed that patients in cluster C2 exhibit a shorter OS and PFS compared to those in cluster C1 (Figures 3H, I). Analysis of the tumor microenvironment indicated that cluster C2 demonstrates lower immune scores, stromal scores, and ESTIMATE scores, alongside higher tumor purity (Figures 3J–M). Further exploration of the immune landscapes among UCEC patients in the two clusters involved calculating the relative proportions of immune cells using the CIBERSORT algorithm. In comparison to cluster C1, cluster C2 exhibited significantly elevated levels of infiltration by follicular helper T cells, M1 macrophages, M2 macrophages, and activated dendritic cells, while levels of CD8 T cells and regulatory T cells (Tregs) were diminished (Figure 4A).

The majority of immune checkpoint genes (CD274, SIGLEC15, HAVCR2, TIGIT, LAG3, and PDCD1LG2) were highly expressed in cluster C2, while CTLA4 and PDCD1 showed no significant statistical difference between the two risk groups (Figure 4B). Furthermore, the expression levels of most HLA-related genes were significantly elevated in cluster C2, with the exception of HLA-L, which demonstrated decreased expression (Figure 4C).

3.3 Screening of hub prognostic DEGs

In the WGCNA, a β value of 7 (R^2 = 0.75) was chosen to construct a scale-free network (Figures 5A–C), resulting in the identification of 15 modules (Figure 5D). Among these, the darkgreen, royal blue, and salmon modules exhibited the highest correlation with endometrial carcinoma and were selected as hub modules (Figure 5E). By intersecting the WGCNA results with DECSGs, 40 critical genes were identified. Through univariate Cox regression model analysis, 20 DECSGs that displayed prognostic significance were singled out (Figure 6A). Further refinement was conducted using machine learning algorithms to identify hub prognostic DECSGs from these 20 genes, ensuring a more focused selection of genes with significant prognostic value. The XGBoost algorithm ultimately identified 7 central genes with a Gain > 0.01 (Figure 6B). In the GMM regression analysis, after 2^{20} iterations for 20 genes, the model with the highest accuracy (AUC=0.99) was determined, comprising 8 key genes (Figure 6C). In the SVM-RFE process, the classifier error was minimized when the number of signatures was reduced to 6; thus, these 6 genes were identified as central signatures (Figures 6E, F). The Random Forest algorithm, by integrating multiple decision trees, ultimately identified 12 genes with importance scores >1.0 as central features

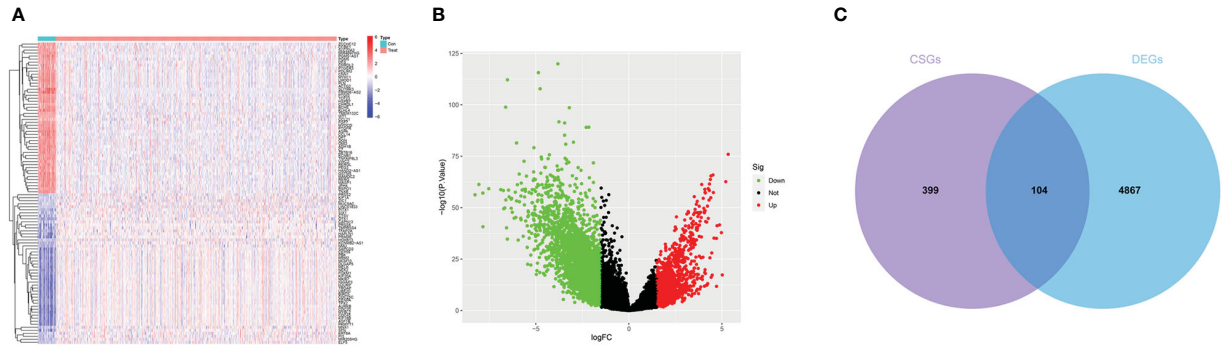

FIGURE 2
(A, B) The heatmap and volcano plot of differential analysis. **(C)** Intersection map of cell senescence genes and differentially expressed genes.

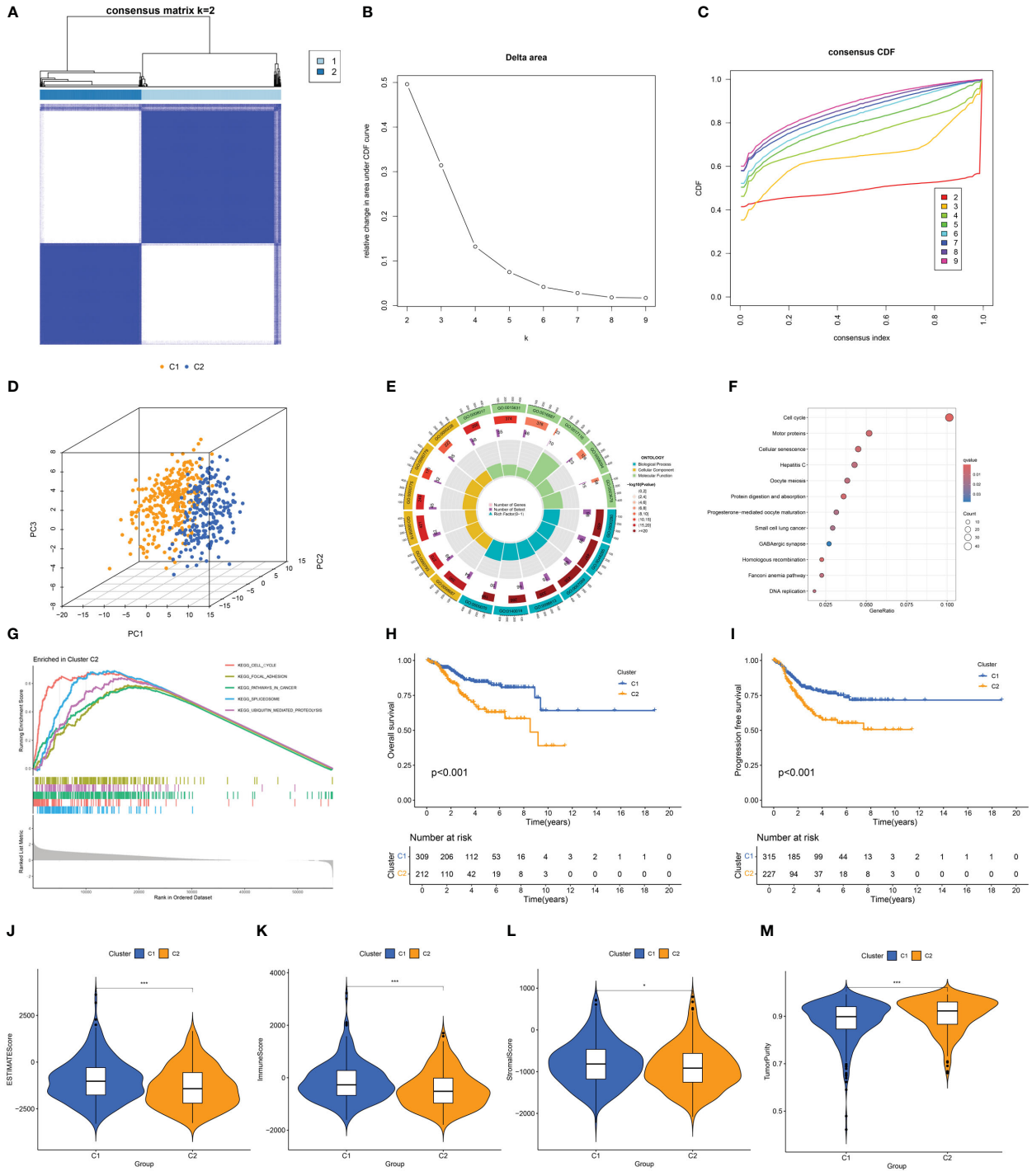

FIGURE 3
(A) Consensus clustering matrix when k = 2. **(B)** Relative alterations in CDF delta area curves. **(C)** Consensus CDF curves when k=2 to 9. **(D)** Three-dimensional Principal Component Analysis delineating the segregation between Cluster C1 and Cluster C2. **(E–G)** GO term enrichment, KEGG pathway analysis, and GSEA results in two clusters. **(H, I)** The difference in OS and PFS between the two clusters. **(J–M)** Differences in ESTIMATEScore, immune scores, stromal scores, and tumor purity between the two clusters (*p<0.05; ***p<0.001).

(Figures 6G, H). The intersection of these selected feature genes identified CPEB1 and MYBL2 as hub prognostic DECSGs (Figure 6D). Survival analyses from the Kaplan-Meier Plotter database revealed a significant decrease in OS of patients with endometrial carcinoma as the expression levels of CPEB1 and MYBL2 increased (Figures 6I, J). Compared to the control group, the expression of MYBL2 was upregulated in endometrial carcinoma, whereas CPEB1 expression was downregulated (Figures 6K, L). ROC curve analysis showed the areas under the curve (AUC) values for CPEB1 and MYBL2 are 0.979 and 0.974, respectively, indicating excellent diagnostic value for UCEC (Supplementary Figure 2).

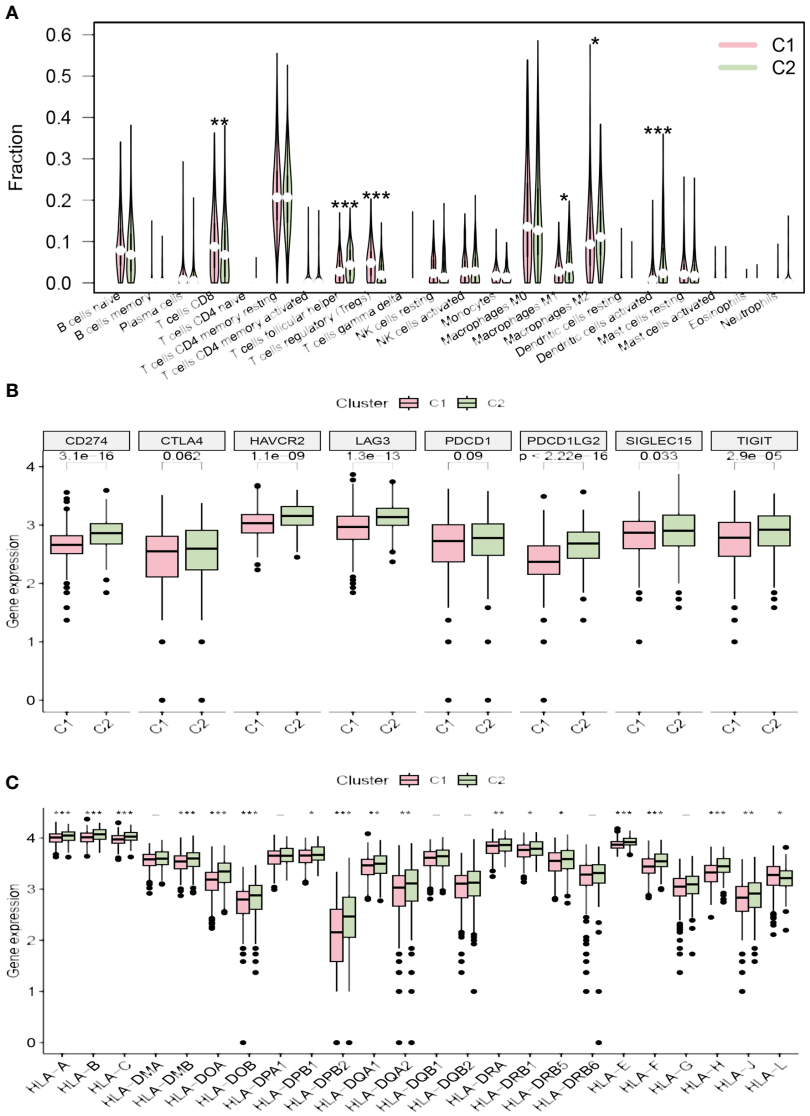

FIGURE 4
(A) The diagram of the difference in immune cell infiltration levels between the two clusters. **(B, C)** The different expression levels of immune checkpoint genes and HLA-related genes in two clusters, respectively (*p < 0.05; **p < 0.01; ***p < 0.001).

3.4 Development and validation of a novel cellular senescence-related prognostic model

After random division, the TCGA training set included 355 patients, while the testing set comprised 156 patients. Utilizing CPEB1 and MYBL2, a risk model incorporating two hub gene risk features was developed through LASSO Cox regression analysis in the TCGA training set (Figures 7A, B). The risk score was calculated as follows: Risk score = (0.1279 × expression of MYBL2) + (0.0879 × expression of CPEB1). UCEC patients were then categorized into high-risk and low-risk groups based on the median risk score. Figures 7C, F, I showed the distribution of risk scores and survival times across the training cohort, testing cohort, and the entire TCGA cohort. Survival analysis results demonstrated a positive correlation between higher risk scores and increased mortality in the training cohort, test cohort, and the entire TCGA cohort. According to Kaplan-Meier analysis, the overall survival of the high-risk group was significantly shorter than that of the low-risk group, indicating a worse prognosis for the high-risk group (Figures 7D, G, J). ROC curves demonstrated that the AUC for the 3-year time-dependent ROC for the three cohorts were 0.624, 0.768, and 0.661, respectively, indicating that the prognostic model exhibits good predictive performance (Figures 7E, H, K).

3.5 Evaluation of TME and drug sensitivity between the two risk score groups

The results obtained from the ssGSEA algorithm revealed distinctive immune infiltration patterns between the high-risk and low-risk groups. Specifically, compared to the low-risk group, the

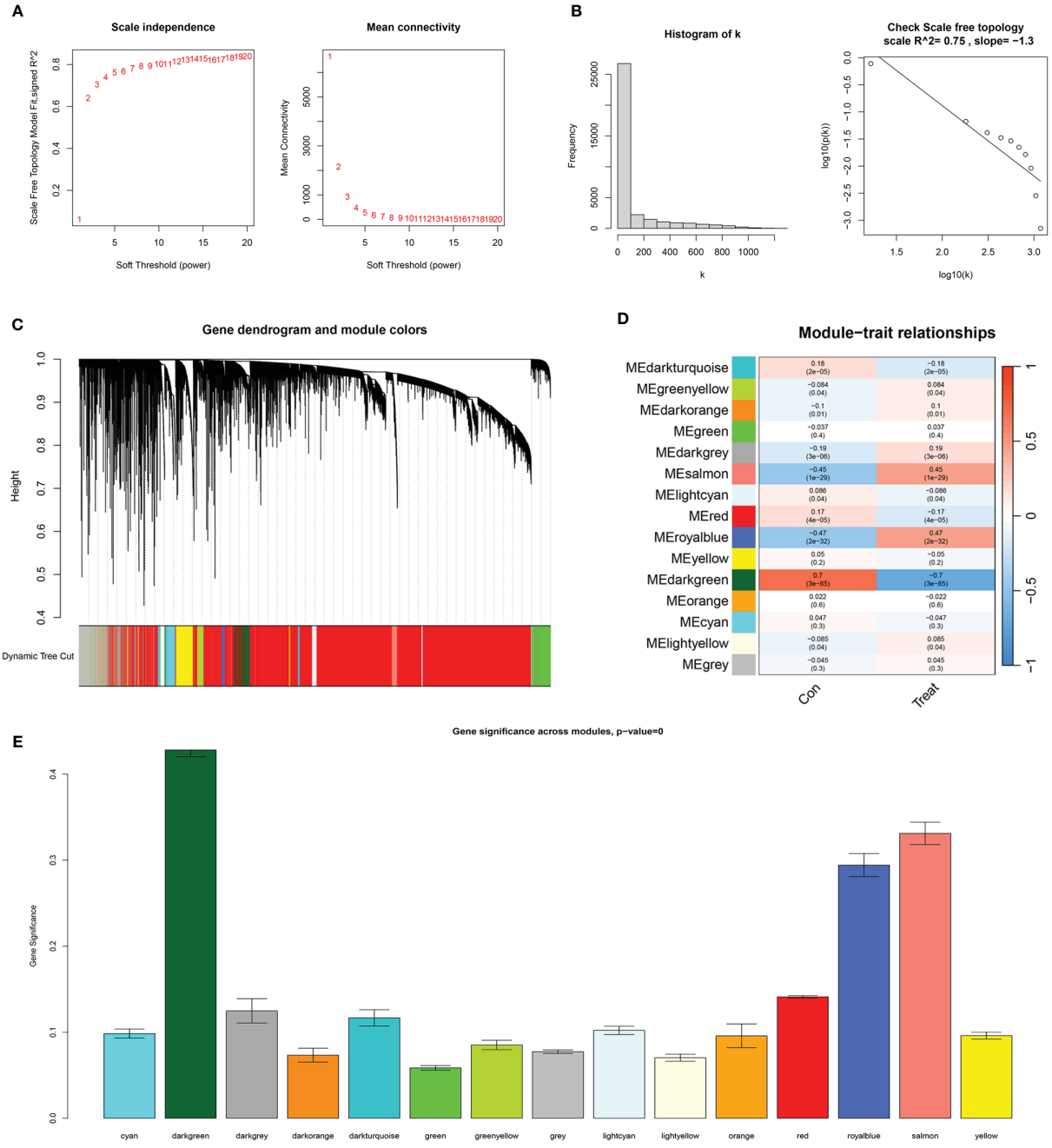

FIGURE 5
WGCNA results. **(A)** The scale-free fit index for various soft-thresholding powers (β) and the mean connectivity for various soft-thresholding powers. **(B)** Histogram of connectivity distribution and the scale-free topology when β=7. **(C)** Dendrogram of genes clustered via the dissimilarity measure. **(D)** Heatmap of the correlation between module and clinical traits. **(E)** Bar plot of gene significance across WGCNA modules.

high-risk group exhibited a unique immune infiltration pattern characterized by significantly lower abundance of most tumor-infiltrating immune cells, except for natural killer cells (Figure 8A). Regarding immune function activity, apart from macrophages and parainflammation, most immune functions were significantly higher in the low-risk group compared to the high-risk group (Figure 8B).

Additionally, our differential analysis of IC50 values between the groups revealed notable differences. Specifically, the IC50 values for Trametinib, PD0325901, Dactolisib, Docetaxel, and Camptothecin were substantially higher in the high-risk group compared to the low-risk group (Figures 8C–G). This suggests that patients with lower risk scores may derive enhanced benefits from these drugs. Conversely, IC50 values for Vincristine, BI-2536, BMS-754807, Bortezomib, and Daporinad were found to be lower in the high-risk group (Figures 8H–L), indicating that these drugs might be particularly effective for patients classified as high risk. These insights highlight the importance of risk stratification in tailoring chemotherapeutic strategies to individual patient profiles, potentially optimizing treatment outcomes.

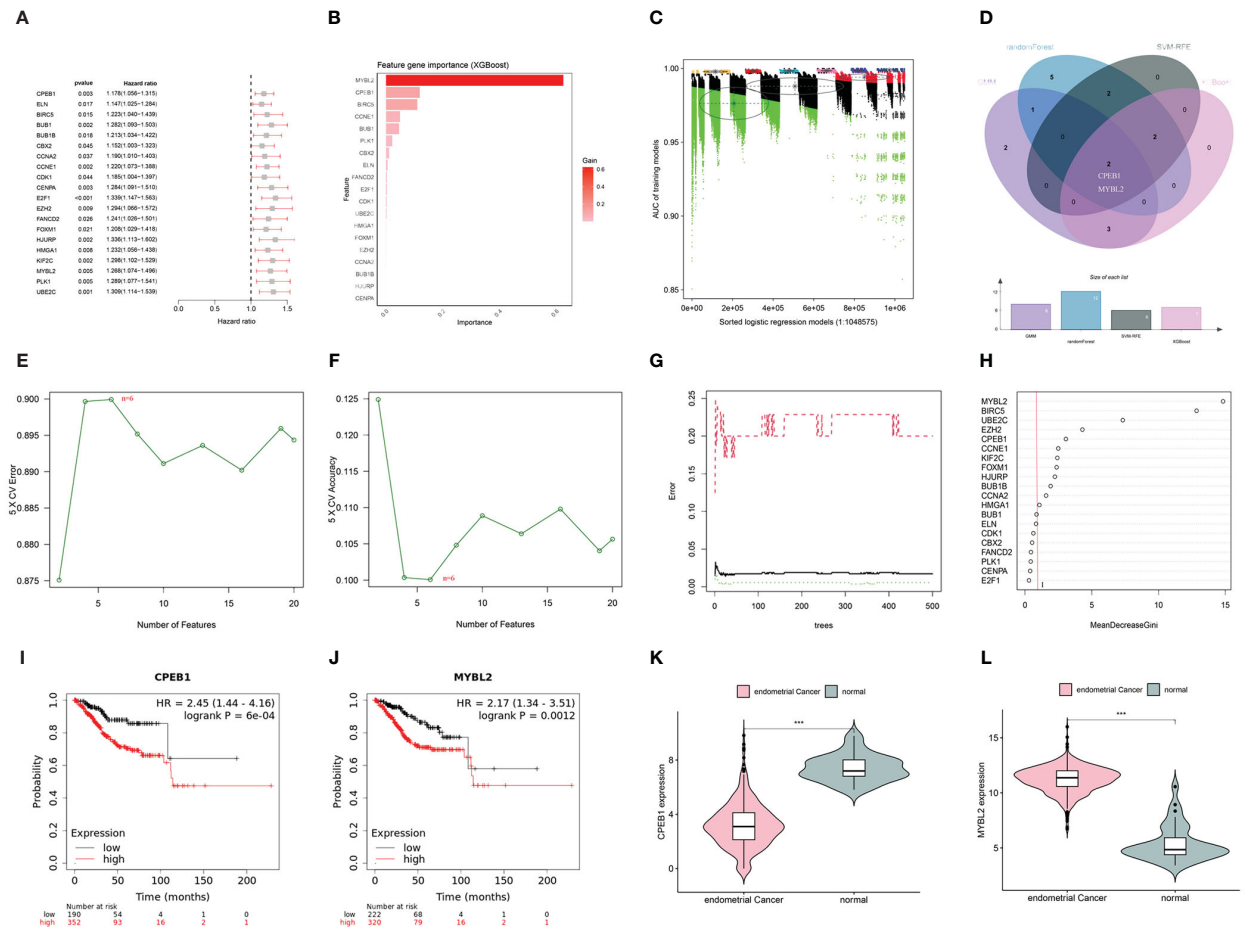

FIGURE 6
(A) Univariate COX analysis shows 20 genes associated with overall survival. **(B)** Screening of diagnostic biomarkers based on XGBoost algorithm (n=7). **(C)** Variable selection in GMM model (n=8); **(D)** Venn diagram of four machine learning results. **(E, F)** Through SVF- RFE algorithm selects the best biomarkers (n=6). **(G, H)** Important features selected by random forest algorithm (n=12). **(I, J)** K-M curves of CPEB1 and MYBL2 in UCEC. **(K, L)** Violin plot show the expression levels of CPEB1 and MYBL2 in TCGA-UCEC cohort(***p < 0.001).

3.6 Correlation of risk scores with clinical information, cellular senescence-related subtypes and immune checkpoints

We conducted a comparison of risk score levels across clinical stages and grades in patients. In the TCGA-UCEC dataset, we observed that higher grades were associated with higher risk scores (Figure 9A). Regarding clinical stages, risk scores for patients in stages II, III, and IV were significantly higher than those in stage I. However, there were no statistical differences in risk scores between stages II, III, and IV (Figure 9B). Subsequently, we explored the correlation between the expression levels of immune checkpoint genes and prognostic risk scores. Notably, there was a significant difference in risk scores between the two subtypes established through cellular senescence genes (Figure 9C). As illustrated in Figure 9D, the expression of most immune checkpoint genes, except for CTLA4, was positively correlated with risk scores. An alluvial diagram illustrated the variations in cellular senescence-related clusters, risk scores, and life states (Figure 9E).

3.7 Verification of the expression of CPEB1 and MYBL2

We conducted further analysis to assess the relative mRNA and protein expression levels of the hub genes CPEB1 and MYBL2 in clinical samples. PCR results indicated that at the transcriptomic level, the relative mRNA expression of MYBL2 was significantly higher in UCEC compared to normal tissue (Figure 10A), while the relative expression of CPEB1 was significantly down-regulated in UCEC (Figure 10B). Results from WB analyses (Figures 10C, D) and immunofluorescence staining (Figures 10E, F) corroborated these findings, demonstrating that the protein expression levels of the two hub genes were consistent with the RT-qPCR results (Figures 9A–D).

4 Discussion

Uterine corpus endometrial carcinoma has been demonstrated to exhibit high levels of heterogeneity (31). The tumor

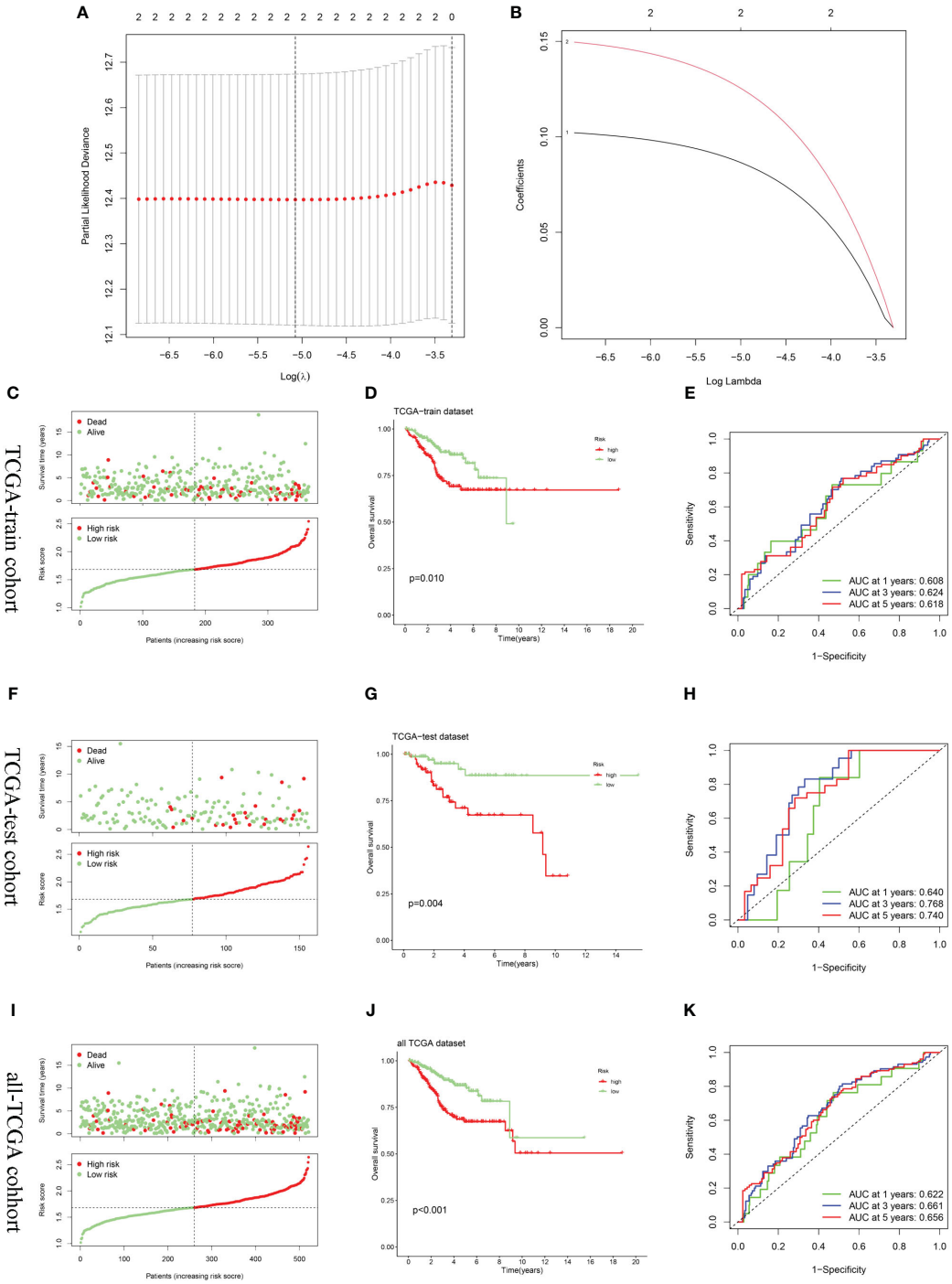

FIGURE 7
Construction and validation of the risk score model. **(A, B)** Constructed a prognostic model in the TCGA-train cohort through LASSO COX regression analysis. **(C, F, I)** Risk scores distribution and survival status of each patient in the TCGA-train cohort, TCGA-train cohort, and all-TCGA cohort, respectively. **(D, G, J)** Kaplan–Meier curves for the OS of the two subtypes in the TCGA-train cohort, TCGA-train cohort, and all-TCGA cohort, respectively. **(E, H, K)** ROC curves illustrated the predictive efficacy of the risk score for 1-, 3-, and 5-year survival in the TCGA-train cohort, TCGA-train cohort, and all-TCGA cohort, respectively.

microenvironment, comprising malignant, immune, endothelial, and stromal components (32), plays a pivotal role in the progression of the cancer and its sensitivity to therapeutic agents (33). The molecular attributes of endometrial cancer cells, along with the composition and dynamics of the tumor microenvironment, significantly influence these processes.

The widespread utilization of genomic sequencing has generated a plethora of biological data, offering enhanced diagnostic and prognostic capabilities across various malignancies. In recent years, researchers have developed diverse prognostic models utilizing gene expression profiles sourced from databases, employing a range of bioinformatics analysis

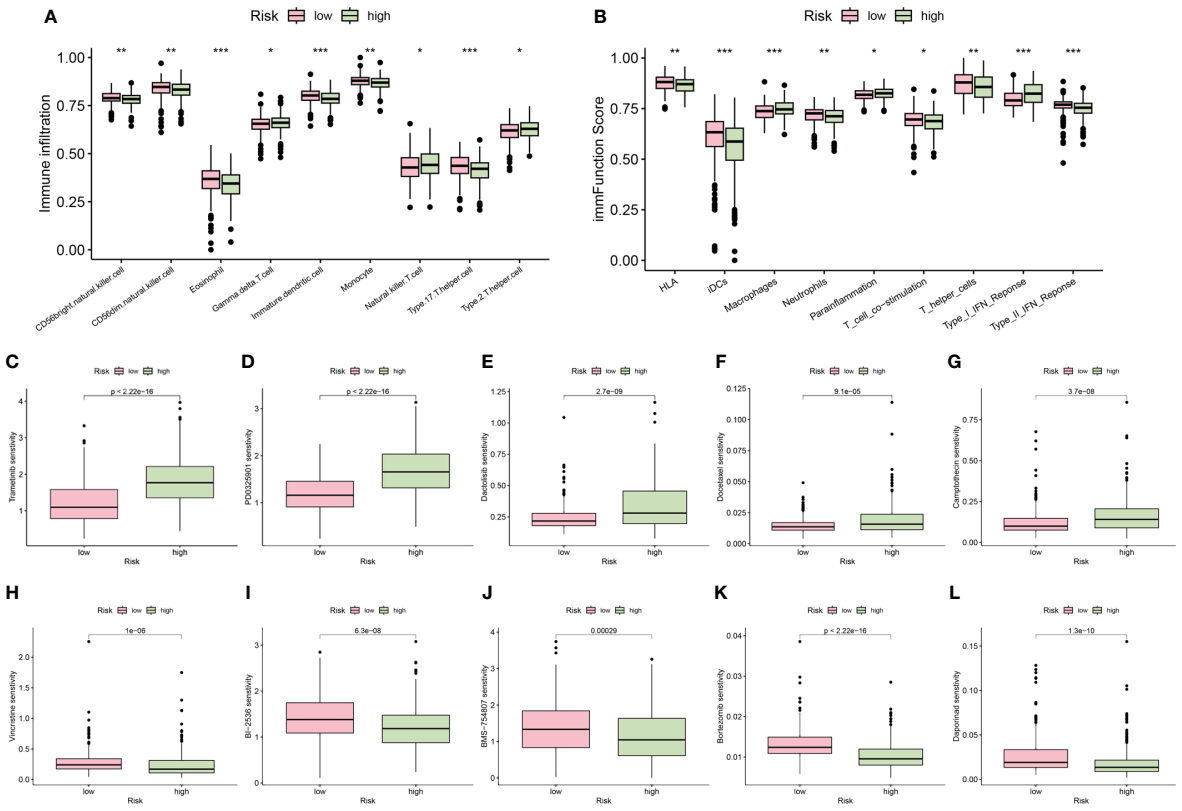

FIGURE 8
The differences of immune infiltrating cells **(A)** and immune function **(B)** between high- and low- risk groups. **(C–L)** Chemotherapy and immunotherapy sensitivity prediction between the low-risk and the high-risk groups (*p < 0.05; **p < 0.01; ***p < 0.001).

methodologies. These models have provided valuable insights into guiding personalized treatment strategies for UCEC (34, 35).

Cellular senescence plays a crucial role in maintaining tissue stability, internal equilibrium, and serves as a natural mechanism to prevent cancer. However, under certain conditions, it can also promote tumor development (36). It has been closely associated with the onset and progression of various diseases and serves as an effective means of stratifying cancer patients (37).

Previous studies have investigated the association between cellular senescence and endometrial cancer. Gao et al. (38) conducted a bioinformatics study focusing on the role of cell senescence-related genes in UCEC and made significant progress. However, their study has certain limitations. Primarily, although they utilized various datasets from TCGA-UCEC and GEO to expand the sample size for analysis, it's worth noting that GSE119041 dataset includes cases of undifferentiated uterine sarcoma. UCEC encompasses pure endometrioid cancer as well as carcinomas with high-risk endometrial histology, including sarcoma. Sarcomas represent uncommon subtypes with a generally poorer prognosis, and the TCGA-UCEC dataset comprises only a limited number of sarcoma cases. Incorporating data from GSE119041 into the analysis may lead to unreliable conclusions.

In our study, all samples were sourced from TCGA-UCEC, avoiding heterogeneity between diseases and samples, as well as batch effects stemming from different datasets. Unlike previous approaches that solely relied on LASSO regression to select feature genes, we employed a stepwise selection process for UCEC feature genes using methods such as WGCNA, Cox regression, and machine learning. Our findings hold promise as diagnostic and prognostic markers for UCEC. WGCNA facilitated the identification of co-expression gene modules in cancer samples, offering a refined and systematic perspective on understanding the molecular mechanisms of cancer by establishing network relationships between genes. Furthermore, the utilization of machine learning, especially in managing and analyzing large biomedical datasets, significantly enhanced the accuracy of analysis and the performance of predictive models. Leveraging these advanced algorithms allowed for the more precise identification of genes closely associated with UCEC. Lastly, we conducted multidimensional experimental validations including PCR, WB, and IF, thereby further confirming the abnormal expression of hub genes. Our study results yielded divergent findings from Gao et al., expanding the realm of research on cell senescence genes and their implications in endometrial cancer.

In this study, we conducted an in-depth exploration of the relationship between UCEC and cellular senescence genes. Utilizing 104 differentially expressed cellular senescence genes, we performed a consensus clustering analysis, ultimately categorizing UCEC into two clusters. We observed significant differences between clusters C1 and C2 in terms of biological functions, prognostic outcomes, tumor microenvironment, immune cell infiltration, immune

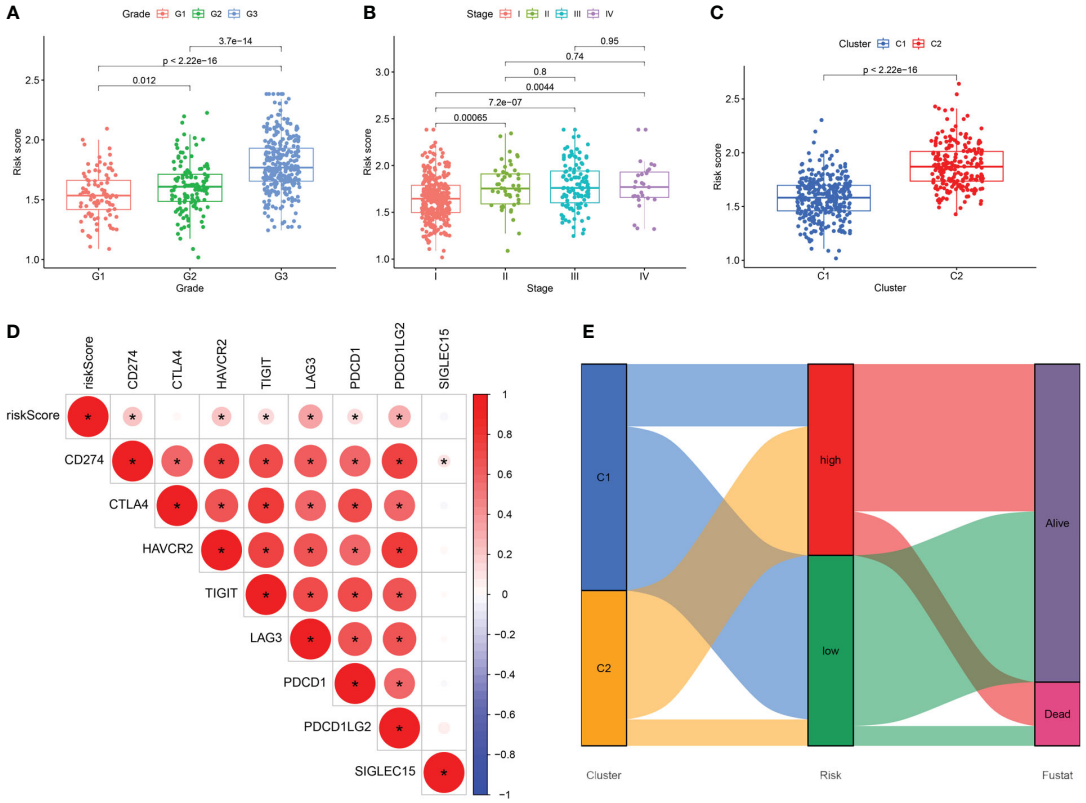

FIGURE 9
(A–C) The difference in risk scores between pathologic grades, clinical stages, and the two subtypes. **(D)** Correlation between the expression levels of immune checkpoint genes and risk score. **(E)** Alluvial diagram of subtype distributions and prognosis of UCEC patients. *, means p-values less than 0.05.

checkpoints, and HLA gene expression. This underscores the presence of substantial tumor heterogeneity within UCEC. The KEGG results indicated that the differentially expressed genes in clusters C1 and C2 were primarily implicated in the cellular senescence pathway, highlighting the pivotal role of cellular senescence genes in UCEC. Furthermore, both KEGG and GSEA analyses indicated the activation of the cell cycle pathway.

In cluster C2, we speculated that aberrant expression of cellular senescence genes may enable damaged or potentially malignant cells to evade senescence defenses and enter a state of uncontrolled proliferation. This not only disrupted crucial cell cycle checkpoints but may also impact the expression and activity of cyclin-dependent kinases (CDKs) and cyclins, as well as their inhibitors, thereby enhancing tumor cells' ability to override growth inhibitory signals. This propensity for unbridled proliferation facilitated the rapid expansion of cluster C2 tumor cells, exacerbating genomic instability and promoting the survival and division of DNA-damaged cells. Consequently, this promoted the malignant transformation of the C2 cluster, ultimately resulting in poor prognosis.

In the tumor microenvironment of cluster C2, we noted a higher tumor purity alongside a lower immune score. Furthermore, most of the HLA class I and class II molecules in cluster C2 were found to be upregulated. HLA class I molecules typically present endogenous antigens to CD8+ T cells, while HLA class II molecules present exogenous antigens to CD4+ T cells (39). Generally, increased expression of HLA molecules should facilitate more effective T-cell-mediated immune responses, thereby enhancing the recognition and elimination of tumor cells, ultimately improving patients' prognosis (40). However, the results from CIBERSORT analysis revealed a decrease in the infiltration levels of CD8 T cells and regulatory T cells in cluster C2, with no significant difference observed in CD4 T cells. Conversely, the proportion of follicular helper T cells, M1 macrophages, and activated dendritic cells was found to increase.

Follicular helper T cells, primarily found in secondary lymphoid tissues, play a pivotal role in facilitating B cells interactions, thereby promoting antibody production and the formation of memory B cells (41). M1 macrophages represent an activated state of macrophages that bolster immune responses by eliminating tumor cells and pathogens (42). Activated dendritic cells capture and present antigens, thereby initiating immune responses in T cells and B cells (43). In cluster C2, combined with the upregulation of most immune checkpoint genes, these immune checkpoint molecules, typically expressed on the surface of immune cells, possessed the capacity to inhibit the activation and proliferation of T cells, fostering a tumor-promoting environment conducive to immune evasion (44). We speculated that despite adequate antigen presentation in cluster C2, the predominant influence of immune checkpoint molecules in UCEC progression renders related T cell

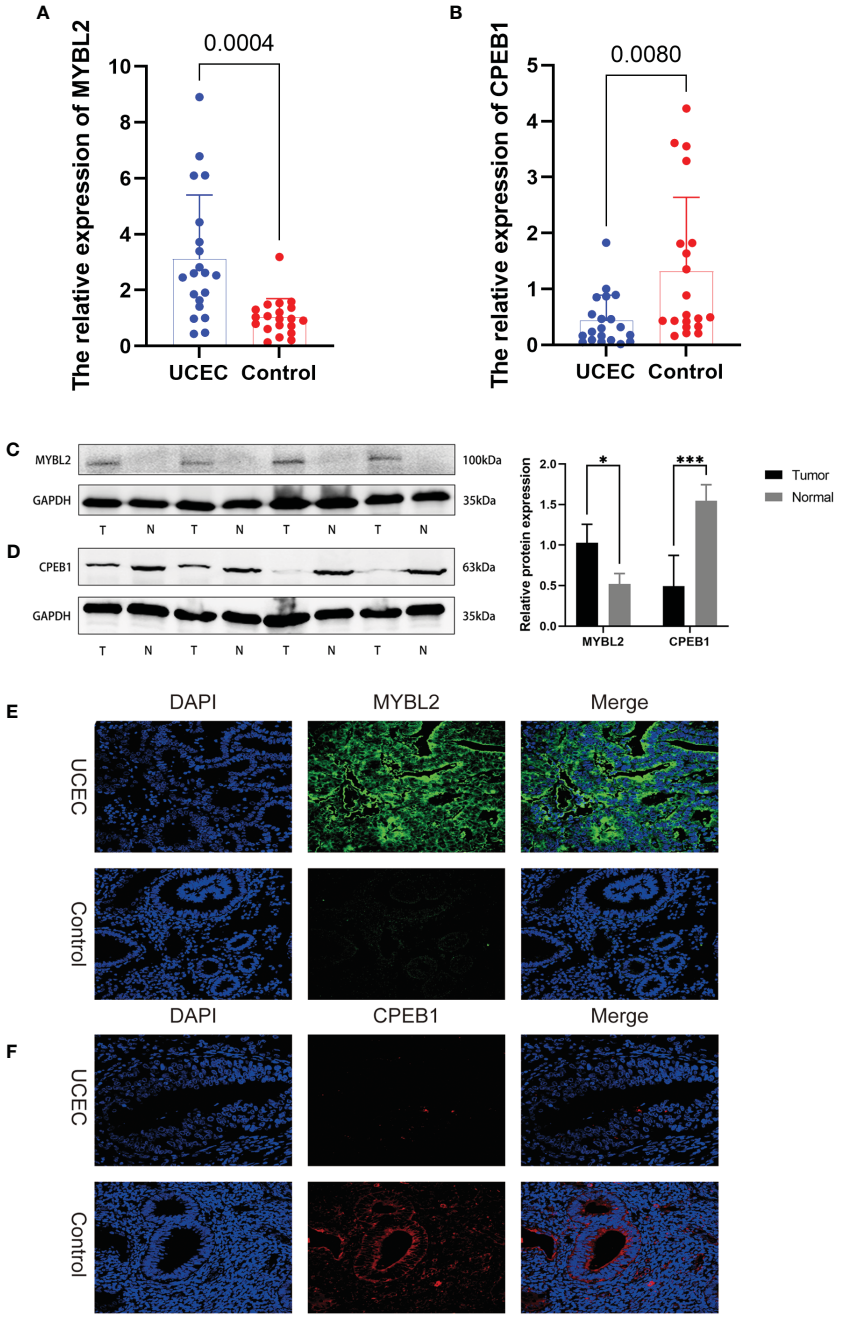

FIGURE 10
The expression levels of 2 hub genes in UCEC tissues and normal tissues were validated by RT-qPCR, WB, and immunofluorescence. **(A, B)** RT-qPCR. **(C, D)** WB assay. **(E, F)** immunofluorescence. *, and ***, means p-values less than 0.05, and 0.001, respectively.

activation ineffective. Moreover, under the influence of abnormally high expression of immune checkpoint molecules, although follicular helper T cells and M1 macrophages showed an increased proportion, their functionality may be compromised by the immunosuppressive environment, thus limiting their anti-tumor activity. Consequently, the anti-tumor immune response in cluster C2 appeared weakened, thereby facilitating tumor growth and dissemination. This underscored the potential utility of immune checkpoint inhibitors in patients within Cluster C2, as these therapeutic agents may help restore the anti-tumor immune response and impede tumor progression.

In summary, the observed upregulation of HLA genes in cluster C2, combined with the decrease in CD8+ T cells and Treg levels, alongside the heightened expression of immune checkpoint genes, revealed a complex immune regulatory network. While theoretically, this network should enhance anti-tumor immune responses, it may inadvertently lead to immune suppression due to tumor cells' strategies for immune evasion. This phenomenon

underscored the importance of emphasizing the value of immune checkpoint inhibitors in exploring immune-based therapeutic strategies for UCEC, aiming to circumvent these inhibitory mechanisms within the tumor microenvironment.

Through the application of WGCNA and Cox regression analysis, in conjunction with a series of advanced machine learning algorithms, we successfully identified CPEB1 and MYBL2 and developed a prognostic risk model. Internal validation results indicated that patients with high-risk scores exhibited significantly worse OS across the training cohort, testing cohort, and the entire TCGA cohort. Furthermore, we observed significant variations in risk scores across two clusters, clinical stages, and grades. These findings suggested that the prognostic risk model holds substantial clinical value in identifying high-risk patients.

MYBL2, a member of the MYB transcription factor family, plays a crucial role in regulating the cell cycle, particularly during DNA replication and mitosis. As a central regulator in tumorigenesis, MYBL2 is involved in the proliferation, apoptosis, and differentiation of cancer cells. Elevated expression of MYBL2 in various tumors is often associated with poor prognosis (45, 46), rendering it a potential therapeutic target in cancer treatment. As a prognostic indicator of unfavorable outcomes in osteosarcoma and a universal marker for immune infiltration across various cancers, MYBL2 exerts regulatory control over proliferation, tumor advancement, and immune cell infiltration within osteosarcoma and broader cancer contexts (47). In clear cell renal carcinoma, MYBL2 promotes malignant characteristics and impedes apoptosis through activation of the hedgehog signaling pathway (48). Within gastric cancer, MYBL2 modulates DNA damage via UBEC2 activation, thereby promoting tumor progression and resistance to cisplatin therapy (49). In ovarian cancer, the MYBL2-CCL2 axis promotes tumor progression and confers resistance to PD-1 therapy by inducing immunosuppressive macrophages (50). In colorectal cancer, MYBL2 expedites cancer progression through an interactive feed-forward activation with E2F2 (51). In our investigation, we observed upregulated expression of MYBL2 in UCEC tissues, thus suggesting its potential utility as a prognostic marker for this malignancy.

CPEB1, also known as Cytoplasmic Polyadenylation Element Binding Protein 1, exerts influence over the stability and translation of its target mRNA molecules, significantly impacting fundamental cellular processes such as growth, differentiation, and apoptosis (52). The expression and function of CPEB1 have garnered considerable attention due to its diverse expression patterns and roles across various types of cancer (53). Research into colorectal cancer metastasis has revealed a novel tumor-suppressive role for CPEB1. High methylation of the CPEB1 promoter, restricting chromatin accessibility and transcription factor binding, diminishes its expression, thereby influencing colorectal cancer progression (54). Additionally, studies have demonstrated that CPEB1 can directly target SIRT1, suppressing its translation and mediating cancer stemness *in vitro* and *in vivo*, suggesting its potential as a therapeutic target in hepatocellular carcinoma (HCC) (55). Overall, recent research has increasingly recognized the multifaceted role of CPEB1 in cellular processes and its impact on various cancers. Currently, there is a lack of research on CPEB1 in the context of endometrial cancer in the existing literature. Our analysis revealed downregulation of CPEB1 expression in endometrial cancer, a finding supported by PCR, WB, and IF assays. While we are the first to report its association with endometrial cancer, further experimental investigations are warranted to fully elucidate the underlying mechanisms.

Carboplatin, in combination with paclitaxel, has emerged as the frontline chemotherapy regimen for endometrial cancer (56). Nonetheless, substantial variability exists among patients in their responses to chemotherapy. Through drug sensitivity analysis, we have identified several drugs that hold promise for UCEC treatment. Significant differences in IC50 values of these drugs observed between distinct risk groups indicate the substantial predictive capacity of our model in predicting drug responses among patients with endometrial cancer.

Immunotherapy, particularly checkpoint inhibitors, has demonstrated high efficacy and generally favorable safety and tolerability profiles. In several clinical trials, checkpoint inhibitors have shown substantial therapeutic effects in patients with recurrent endometrial cancer, especially in those unresponsive to chemotherapy (57). Moreover, studies indicate that the use of checkpoint inhibitors can significantly enhance long-term survival rates in endometrial cancer patients characterized by specific molecular markers (58). Currently, immunotherapy drugs are increasingly being incorporated into the clinical management of endometrial cancer. PD-1 inhibitors, such as pembrolizumab and dostarlimab, have shown efficacy in treating unresectable or metastatic solid tumors with MSI-H or dMMR status. Concurrently, PD-L1 inhibitors, including atezolizumab and avelumab, are under evaluation in clinical trials for their potential in endometrial cancer therapy. Combination therapy, such as pembrolizumab combined with multikinase inhibitors like lenvatinib, is being utilized for endometrial cancer patients experiencing disease progression after prior systemic therapy. Moreover, CTLA-4 inhibitors like ipilimumab are being investigated in combination with PD-1 inhibitors to assess their efficacy in endometrial cancer treatment (59). The advent of immune checkpoint inhibitors (ICIs) has significantly transformed the therapeutic landscape for endometrial cancer, highlighting the substantial immune heterogeneity within UCEC (60). Additionally, a recent review revealed that the addition ICIs to chemotherapy can improve PFS in the overall population compared to chemotherapy alone (61). New treatment guidelines are also being formulated to explore the use of immune checkpoint inhibitors across the four molecular categories of endometrial cancer and their potential prognostic effects (62). However, not all endometrial cancer patients respond favorably to checkpoint inhibitors, particularly those with microsatellite stable (MSS) tumors or low tumor mutational burden (63). Additionally, the high costs and potential toxicities associated with these therapies limit their accessibility to all UCEC patients. Our analysis unveiled that cluster C2 exhibits elevated levels of immune checkpoint genes and a positive correlation between risk scores and immune

checkpoint expression, suggesting that patients in the high-risk group may derive greater benefits from treatment with immune checkpoint inhibitors.

Our advanced bioinformatics analyses, based on a prognostic model centered on cellular senescence genes, provide novel perspectives on UCEC and present opportunities for personalized immune therapies to advance treatment strategies. Nevertheless, our study is not without limitations. Firstly, its retrospective nature and reliance on bioinformatics methodologies underscore the need for further investigations with larger patient cohorts to enhance the generalizability of the results. Additionally, while we validated the dysregulated expression of hub genes at the transcriptomic and proteomic levels, understanding their biological functions and interactions within the tumor microenvironment, particularly with regard to immune checkpoints, necessitates additional experimental exploration.

In summary, our diverse bioinformatics analyses based on senescence-associated genes have unveiled two distinct molecular subtypes of UCEC exhibiting significantly different tumor microenvironments and prognoses. Moreover, the prognostic risk model we established has demonstrated remarkable efficacy in predicting the prognosis and responsiveness to chemotherapy among UCEC patients, indicating its potential clinical applicability.

Data availability statement

Publicly available datasets were analyzed in this study. This data can be found here: https://portal.gdc.cancer.gov/projects/TCGA-UCEC.

Ethics statement

The studies involving humans were approved by the Medical Ethics Committee of the First Affiliated Hospital of Guangxi Medical University. The studies were conducted in accordance with the local legislation and institutional requirements. The participants provided their written informed consent to participate in this study. Written informed consent was obtained from the individual(s) for the collection of clinical specimens during the ethical approval process.

Author contributions

CW: Conceptualization, Data curation, Methodology, Software, Visualization, Writing – original draft. SL: Validation, Conceptualization, Data curation, Formal analysis, Visualization, Writing – original draft. YH: Conceptualization, Data curation, Validation, Visualization, Writing – original draft. YW: Data curation, Validation, Writing – original draft, Investigation, Methodology, Software. JM: Software, Supervision, Visualization, Conceptualization, Writing – review & editing, Formal analysis, Methodology. JF: Funding acquisition, Supervision, Validation, Resources, Project administration, Writing – review & editing.

Funding

The author(s) declare financial support was received for the research, authorship, and/or publication of this article. This work was supported by grants from the National Natural Science Foundation of China (Nos. 81960464) and the construction of clinical intervention protocols Guangxi Key R & D program (Guike AB22080045).

Acknowledgments

Thanks to the R software development team and the TCGA databases for providing many biological information data, and express our gratitude to the support from the National Natural Science Foundation of China.

Conflict of interest

The authors declare that the research was conducted in the absence of any commercial or financial relationships that could be construed as a potential conflict of interest.

Publisher's note

All claims expressed in this article are solely those of the authors and do not necessarily represent those of their affiliated organizations, or those of the publisher, the editors and the reviewers. Any product that may be evaluated in this article, or claim that may be made by its manufacturer, is not guaranteed or endorsed by the publisher.

Supplementary material

The Supplementary Material for this article can be found online at: https://www.frontiersin.org/articles/10.3389/fimmu.2024.1418508/full#supplementary-material

References

1. Zheng RS, Zhang SW, Sun KX, Chen R, Wang SM, Li L, et al. [Cancer statistics in China, 2016]. *Zhonghua Zhong Liu Za Zhi*. (2023) 45:212–20. doi: 10.3760/cma.j.cn112152–20220922–00647

2. Sung H, Ferlay J, Siegel RL, Laversanne M, Soerjomataram I, Jemal A, et al. Global cancer statistics 2020: globocan estimates of incidence and mortality worldwide for 36 cancers in 185 countries. *CA Cancer J Clin*. (2021) 71:209–49. doi: 10.3322/caac.21660

3. Mills AM, Liou S, Ford JM, Berek JS, Pai RK, Longacre TA. Lynch syndrome screening should be considered for all patients with newly diagnosed endometrial cancer. *Am J Surg Pathol*. (2014) 38(11):1501–9. doi: 10.1097/pas.0000000000000321

4. Betella I, Fumagalli C, Raviele PR, Schivardi G, Vitis LAD, Achilarre MT, et al. *A Novel Algorithm to Implement the Molecular Classification According to the New Esgo/Estro/Esp 2020 Guidelines for Endometrial Cancer*, Vol. 32. (2022). pp. 993–1000. Hudson Place, New Jersey, USA: International Journal of Gynecologic Cancer. doi: 10.1136/ijgc-2022–003480.

5. Morice P, Leary A, Creutzberg C, Abu-Rustum N, Darai E. Endometrial cancer. *Lancet*. (2016) 387:1094–108. doi: 10.1016/s0140–6736(15)00130–0

6. Siegel RL, Miller KD, Fuchs HE, Jemal A. Cancer statistics, 2021. *CA Cancer J Clin*. (2021) 71:7–33. doi: 10.3322/caac.21654

7. Xue Y, Dong Y, Lou Y, Lv Q, Shan W, Wang C, et al. Pten mutation predicts unfavorable fertility preserving treatment outcome in the young patients with endometrioid endometrial cancer and atypical hyperplasia. *J Gynecol Oncol*. (2023) 34:e53. doi: 10.3802/jgo.2023.34.e53

8. Vermij L, Léon-Castillo A, Singh N, Powell ME, Edmondson RJ, Genestie C, et al. P53 immunohistochemistry in endometrial cancer: clinical and molecular correlates in the portec-3 trial. *Mod Pathol*. (2022) 35:1475–83. doi: 10.1038/s41379-022-01102-x

9. Janku F, Wheler JJ, Westin SN, Moulder SL, Naing A, Tsimberidou AM, et al. Pi3k/akt/mtor inhibitors in patients with breast and gynecologic Malignancies harboring pik3ca mutations. *J Clin Oncol*. (2012) 30:777–82. doi: 10.1200/jco.2011.36.1196

10. Peters I, Marchetti C, Scambia G, Fagotti A. New windows of surgical opportunity for gynecological cancers in the era of targeted therapies. *Int J Gynecol Cancer*. (2024) 34:352–62. doi: 10.1136/ijgc-2023–004580

11. Kumari R, Jat P. Mechanisms of cellular senescence: cell cycle arrest and senescence associated secretory phenotype. *Front Cell Dev Biol*. (2021) 9:645593. doi: 10.3389/fcell.2021.645593

12. Chambers CR, Ritchie S, Pereira BA, Timpson P. Overcoming the senescence-associated secretory phenotype (Sasp): A complex mechanism of resistance in the treatment of cancer. *Mol Oncol*. (2021) 15:3242–55. doi: 10.1002/1878–0261.13042

13. Schmitt CA, Wang B, Demaria M. Senescence and cancer - role and therapeutic opportunities. *Nat Rev Clin Oncol*. (2022) 19:619–36. doi: 10.1038/s41571–022-00668–4

14. Colucci M, Zumerle S, Bressan S, Gianfanti F, Troiani M, Valdata A, et al. Retinoic acid receptor activation reprograms senescence response and enhances anti-tumor activity of natural killer cells. *Cancer Cell*. (2024) 42:646–61.e9. doi: 10.1016/j.ccell.2024.02.004

15. Guo Y, Wang S, Dong Y, Liu Y. Attenuation of pro-tumorigenic senescent secretory phenotype by stn, a novel derivative of stevioside, potentiates its inhibitory activity on hepatocellular carcinoma. *Food Chem Toxicol*. (2024) 184:114371. doi: 10.1016/j.fct.2023.114371

16. Talhouk A, McConechy MK, Leung S, Li-Chang HH, Kwon JS, Melnyk N, et al. A clinically applicable molecular-based classification for endometrial cancers. *Br J Cancer*. (2015) 113:299–310. doi: 10.1038/bjc.2015.190

17. Liu W, Ma J, Zhang J, Cao J, Hu X, Huang Y, et al. Identification and validation of serum metabolite biomarkers for endometrial cancer diagnosis. *EMBO Mol Med*. (2024) 16(4):988–1003. doi: 10.1038/s44321–024-00033–1

18. Hong S, Fu N, Sang S, Ma X, Sun F, Zhang X. Identification and validation of irf6 related to ovarian cancer and biological function and prognostic value. *J Ovarian Res*. (2024) 17:64. doi: 10.1186/s13048–024-01386–4

19. Ritchie ME, Phipson B, Wu D, Hu Y, Law CW, Shi W, et al. Limma powers differential expression analyses for rna-sequencing and microarray studies. *Nucleic Acids Res*. (2015) 43:e47. doi: 10.1093/nar/gkv007

20. Wilkerson MD, Hayes DN. Consensusclusterplus: A class discovery tool with confidence assessments and item tracking. *Bioinformatics*. (2010) 26:1572–3. doi: 10.1093/bioinformatics/btq170

21. Wu T, Hu E, Xu S, Chen M, Guo P, Dai Z, et al. Clusterprofiler 4.0: A universal enrichment tool for interpreting omics data. *Innovation (Camb)*. (2021) 2:100141. doi: 10.1016/j.xinn.2021.100141

22. Therneau TM, Grambsch PM. *Modeling Survival Data: Extending the Cox Model*, Vol. 65. (2013). pp. 843–4. Tiergartenstrasse 17, Heidelberg, Germany: Springer Science & Business Media. doi: 10.2307/25053321.

23. Newman AM, Liu CL, Green MR, Gentles AJ, Feng W, Xu Y, et al. Robust enumeration of cell subsets from tissue expression profiles. *Nat Methods*. (2015) 12:453–7. doi: 10.1038/nmeth.3337

24. Langfelder P, Horvath S. Wgcna: an R package for weighted correlation network analysis. *BMC Bioinf*. (2008) 9:559. doi: 10.1186/1471–2105-9–559

25. Chalmers R, Adkins M. *Writing Effective and Reliable Monte Carlo Simulations with the Simdesign Package*. (2020). Dr. Penfield Avenue, Montreal, Canada: Tutorials in Quantitative Methods for Psychology. doi: 10.20982/tqmp.16.4.p248.

26. Das P, Roychowdhury A, Das S, Roychoudhury S, Tripathy S. Sigfeature: novel significant feature selection method for classification of gene expression data using support vector machine and T statistic. *Front Genet*. (2020) 11:247. doi: 10.3389/fgene.2020.00247

27. Breiman L, Breiman L. Cutler RAJJoCM. *Random Forests Mach Learning*. (2001) 2:199–228.

28. Chen T, Guestrin C. *Xgboost: A Scalable Tree Boosting System*. San Francisco, California, USA: ACM (2016). doi: 10.1145/2939672.2939785

29. Blanche P, Dartigues JF, Jacqmin-Gadda H. Estimating and comparing time-dependent areas under receiver operating characteristic curves for censored event times with competing risks. *Stat Med*. (2013) 32:5381–97. doi: 10.1002/sim.5958

30. Maeser D, Gruener RF, Huang RS. Oncopredict: an R package for predicting in vivo or cancer patient drug response and biomarkers from cell line screening data. *Brief Bioinform*. (2021) 22. doi: 10.1093/bib/bbab260

31. Tang X, Hu Y. The role of tcga molecular classification in clear cell endometrial carcinoma. *Front Oncol*. (2023) 13:1147394. doi: 10.3389/fonc.2023.1147394

32. Pradhan R, Kundu A, Kundu CN. The cytokines in tumor microenvironment: from cancer initiation-elongation-progression to metastatic outgrowth. *Crit Rev Oncol Hematol*. (2024) 196:104311. doi: 10.1016/j.critrevonc.2024.104311

33. Huang Y, Chen Z, Shen G, Fang S, Zheng J, Chi Z, et al. Immune regulation and the tumor microenvironment in anti-pd-1/pdl-1 and anti-ctla-4 therapies for cancer immune evasion: A bibliometric analysis. *Hum Vaccin Immunother*. (2024) 20:2318815. doi: 10.1080/21645515.2024.2318815

34. Liu J, Wu Z, Sun R, Nie S, Meng H, Zhong Y, et al. Using mrnasi to identify prognostic-related genes in endometrial carcinoma based on wgcna. *Life Sci*. (2020) 258:118231. doi: 10.1016/j.lfs.2020.118231

35. Wu E, Fan X, Tang T, Li J, Wang J, Liu X, et al. Biomarkers discovery for endometrial cancer: A graph convolutional sample network method. *Comput Biol Med*. (2022) 150:106200. doi: 10.1016/j.compbiomed.2022.106200

36. Regulski MJ. Cellular senescence: what, why, and how. *Wounds*. (2017) 29:168–74.

37. Zeng Q, Gong Y, Zhu N, Shi Y, Zhang C, Qin L. Lipids and lipid metabolism in cellular senescence: emerging targets for age-related diseases. *Ageing Res Rev*. (2024) 97:102294. doi: 10.1016/j.arr.2024.102294

38. Gao L, Wang X, Wang X, Wang F, Tang J, Ji J. A prognostic model and immune regulation analysis of uterine corpus endometrial carcinoma based on cellular senescence. *Front Oncol*. (2022) 12:1054564. doi: 10.3389/fonc.2022.1054564

39. Juanes-Velasco P, Landeira-Viñuela A, Acebes-Fernandez V, Hernández ÁP, Garcia-Vaquero ML, Arias-Hidalgo C, et al. Deciphering human leukocyte antigen susceptibility maps from immunopeptidomics characterization in oncology and infections. *Front Cell Infect Microbiol*. (2021) 11:642583. doi: 10.3389/fcimb.2021.642583

40. Aptsiauri N, Garrido F. The challenges of hla class I loss in cancer immunotherapy: facts and hopes. *Clin Cancer Res*. (2022) 28:5021–9. doi: 10.1158/1078–0432.Ccr-21–3501

41. Qin L, Waseem TC, Sahoo A, Bieerkehazhi S, Zhou H, Galkina EV, et al. Insights into the molecular mechanisms of T follicular helper-mediated immunity and pathology. *Front Immunol*. (2018) 9:1884. doi: 10.3389/fimmu.2018.01884

42. Liu J, Geng X, Hou J, Wu G. New insights into M1/M2 macrophages: key modulators in cancer progression. *Cancer Cell Int*. (2021) 21:389. doi: 10.1186/s12935–021-02089–2

43. Mellman I. Dendritic cells: master regulators of the immune response. *Cancer Immunol Res*. (2013) 1:145–9. doi: 10.1158/2326–6066.Cir-13–0102

44. Guo Z, Zhang R, Yang AG, Zheng G. Diversity of immune checkpoints in cancer immunotherapy. *Front Immunol*. (2023) 14:1121285. doi: 10.3389/fimmu.2023.1121285

45. Liu W, Shen D, Ju L, Zhang R, Du W, Jin W, et al. Mybl2 promotes proliferation and metastasis of bladder cancer through transactivation of cdca3. *Oncogene*. (2022) 41:4606–17. doi: 10.1038/s41388-022-02456-x

46. Li Q, Wang M, Hu Y, Zhao E, Li J, Ren L, et al. Mybl2 disrupts the hippo-yap pathway and confers castration resistance and metastatic potential in prostate cancer. *Theranostics*. (2021) 11:5794–812. doi: 10.7150/thno.56604

47. Qiu X, He H, Zeng H, Tong X, Zhang C, Liu Y, et al. Integrative transcriptome analysis identifies mybl2 as a poor prognosis marker for osteosarcoma and a pan-cancer marker of immune infiltration. *Genes Dis*. (2024) 11:101004. doi: 10.1016/j.gendis.2023.04.035

48. Yang W, Chen H, Ma L, Wei M, Xue X, Li Y, et al. The oncogene mybl2 promotes the Malignant phenotype and suppresses apoptosis through hedgehog signaling pathway in clear cell renal cell carcinoma. *Heliyon*. (2024) 10:e27772. doi: 10.1016/j.heliyon.2024.e27772

49. Long J, Zhu B, Tian T, Ren L, Tao Y, Zhu H, et al. Activation of ubec2 by transcription factor mybl2 affects DNA damage and promotes gastric cancer progression and cisplatin resistance. *Open Med (Wars)*. (2023) 18:20230757. doi: 10.1515/med-2023–0757

50. Pan B, Wan T, Zhou Y, Huang S, Yuan L, Jiang Y, et al. The mybl2-ccl2 axis promotes tumor progression and resistance to anti-pd-1 therapy in ovarian cancer by inducing immunosuppressive macrophages. *Cancer Cell Int*. (2023) 23:248. doi: 10.1186/s12935–023-03079–2

51. Fan X, Wang Y, Jiang T, Liu T, Jin Y, Du K, et al. B-myb accelerates colorectal cancer progression through reciprocal feed-forward transactivation of E2f2. *Oncogene*. (2021) 40:5613–25. doi: 10.1038/s41388–021-01961–9

52. Drisaldi B, Colnaghi L, Levine A, Huang Y, Snyder AM, Metzger DJ, et al. Cytoplasmic polyadenylation element binding proteins cpeb1 and cpeb3 regulate the translation of fosb and are required for maintaining addiction-like behaviors induced by cocaine. *Front Cell Neurosci*. (2020) 14:207. doi: 10.3389/fncel.2020.00207

53. Kochanek DM, Wells DG. Cpeb1 regulates the expression of mtdh/aeg-1 and glioblastoma cell migration. *Mol Cancer Res*. (2013) 11:149–60. doi: 10.1158/1541–7786.Mcr-12–0498

54. Shao K, Pu W, Zhang J, Guo S, Qian F, Glurich I, et al. DNA hypermethylation contributes to colorectal cancer metastasis by regulating the binding of cebpb and tfcp2 to the cpeb1 promoter. *Clin Epigenet*. (2021) 13:89. doi: 10.1186/s13148-021-01071-z

55. Xu M, Fang S, Song J, Chen M, Zhang Q, Weng Q, et al. Cpeb1 mediates hepatocellular carcinoma cancer stemness and chemoresistance. *Cell Death Dis*. (2018) 9:957. doi: 10.1038/s41419–018-0974–2

56. Abu-Rustum N, Yashar C, Arend R, Barber E, Bradley K, Brooks R, et al. Uterine neoplasms, version 1.2023, nccn clinical practice guidelines in oncology. *J Natl Compr Canc Netw*. (2023) 21:181–209. doi: 10.6004/jnccn.2023.0006

57. Mutlu L, Harold J, Tymon-Rosario J, Santin AD. Immune checkpoint inhibitors for recurrent endometrial cancer. *Expert Rev Anticancer Ther*. (2022) 22:249–58. doi: 10.1080/14737140.2022.2044311

58. Mahdi H, Chelariu-Raicu A, Slomovitz BM. Immunotherapy in endometrial cancer. *Int J Gynecol Cancer*. (2023) 33:351–7. doi: 10.1136/ijgc-2022–003675

59. Peng H, He X, Wang Q. Immune checkpoint blockades in gynecological cancers: A review of clinical trials. *Acta Obstet Gynecol Scand*. (2022) 101:941–51. doi: 10.1111/aogs.14412

60. Bhangoo MS, Boasberg P, Mehta P, Elvin JA, Ali SM, Wu W, et al. Tumor mutational burden guides therapy in a treatment refractory pole-mutant uterine carcinosarcoma. *Oncologist*. (2018) 23:518–23. doi: 10.1634/theoncologist.2017–0342

61. Bartoletti M, Montico M, Lorusso D, Mazzeo R, Oaknin A, Musacchio L, et al. Incorporation of anti-pd1 or anti pd-L1 agents to platinum-based chemotherapy for the primary treatment of advanced or recurrent endometrial cancer. *A Meta-Analysis Cancer Treat Rev*. (2024) 125:102701. doi: 10.1016/j.ctrv.2024.102701

62. Bruchim I, Capasso I, Polonsky A, Meisel S, Salutari V, Werner H, et al. New therapeutic targets for endometrial cancer: A glimpse into the preclinical sphere. *Expert Opin Ther Targets*. (2024) 28:29–43. doi: 10.1080/14728222.2024.2316739

63. van der Woude H, Hally KE, Currie MJ, Gasser O, Henry CE. Importance of the endometrial immune environment in endometrial cancer and associated therapies. *Front Oncol*. (2022) 12:975201. doi: 10.3389/fonc.2022.975201

frontiers | Frontiers in Immunology

TYPE Original Research
PUBLISHED 01 July 2024
DOI 10.3389/fimmu.2024.1427661

Check for updates

OPEN ACCESS

EDITED BY
Wantao Wu,
Central South University, China

REVIEWED BY
Jingwei Zhao,
Shanghai Jiao Tong University, China
Yucheng Hou,
The First Affiliated Hospital of Soochow University, China

*CORRESPONDENCE
Yao Zhang
zhangyour@126.com

†These authors have contributed equally to this work

RECEIVED 04 May 2024
ACCEPTED 17 June 2024
PUBLISHED 01 July 2024

CITATION
Jiang Y-C, Xu Q-T, Wang H-B, Ren S-Y and Zhang Y (2024) A novel prognostic signature related to programmed cell death in osteosarcoma.
Front. Immunol. 15:1427661.
doi: 10.3389/fimmu.2024.1427661

COPYRIGHT
© 2024 Jiang, Xu, Wang, Ren and Zhang. This is an open-access article distributed under the terms of the Creative Commons Attribution License (CC BY). The use, distribution or reproduction in other forums is permitted, provided the original author(s) and the copyright owner(s) are credited and that the original publication in this journal is cited, in accordance with accepted academic practice. No use, distribution or reproduction is permitted which does not comply with these terms.

A novel prognostic signature related to programmed cell death in osteosarcoma

Yu-Chen Jiang[1†], Qi-Tong Xu[2†], Hong-Bin Wang[1], Si-Yuan Ren[1] and Yao Zhang[1*]

[1]Affiliated Zhongshan Hospital Of Dalian University, Dalian, China, [2]Department of Gastrointestinal Surgery, Shanghai East Hospital, School of Medicine, Tongji University, Shanghai, China

Background: Osteosarcoma primarily affects children and adolescents, with current clinical treatments often resulting in poor prognosis. There has been growing evidence linking programmed cell death (PCD) to the occurrence and progression of tumors. This study aims to enhance the accuracy of OS prognosis assessment by identifying PCD-related prognostic risk genes, constructing a PCD-based OS prognostic risk model, and characterizing the function of genes within this model.

Method: We retrieved osteosarcoma patient samples from TARGET and GEO databases, and manually curated literature to summarize 15 forms of programmed cell death. We collated 1621 PCD genes from literature sources as well as databases such as KEGG and GSEA. To construct our model, we integrated ten machine learning methods including Enet, Ridge, RSF, CoxBoost, plsRcox, survivalSVM, Lasso, SuperPC, StepCox, and GBM. The optimal model was chosen based on the average C-index, and named Osteosarcoma Programmed Cell Death Score (OS-PCDS). To validate the predictive performance of our model across different datasets, we employed three independent GEO validation sets. Moreover, we assessed mRNA and protein expression levels of the genes included in our model, and investigated their impact on proliferation, migration, and apoptosis of osteosarcoma cells by gene knockdown experiments.

Result: In our extensive analysis, we identified 30 prognostic risk genes associated with programmed cell death (PCD) in osteosarcoma (OS). To assess the predictive power of these genes, we computed the C-index for various combinations. The model that employed the random survival forest (RSF) algorithm demonstrated superior predictive performance, significantly outperforming traditional approaches. This optimal model included five key genes: MTM1, MLH1, CLTCL1, EDIL3, and SQLE. To validate the relevance of these genes, we analyzed their mRNA and protein expression levels, revealing significant disparities between osteosarcoma cells and normal tissue cells. Specifically, the expression levels of these genes were markedly altered in OS cells, suggesting their critical role in tumor progression. Further functional validation was performed through gene knockdown experiments in U2OS cells. Knockdown of three of these genes—CLTCL1, EDIL3, and SQLE—resulted in substantial changes in proliferation rate, migration capacity, and apoptosis rate of osteosarcoma cells. These findings underscore the pivotal roles of these genes in the pathophysiology of osteosarcoma and highlight their potential as therapeutic targets.

Conclusion: The five genes constituting the OS-PCDS model—CLTCL1, MTM1, MLH1, EDIL3, and SQLE—were found to significantly impact the proliferation, migration, and apoptosis of osteosarcoma cells, highlighting their potential as key prognostic markers and therapeutic targets. OS-PCDS enables accurate evaluation of the prognosis in patients with osteosarcoma.

KEYWORDS

osteosarcoma, tumor immunology, programmed cell death, machine learning algorithm, prognostic marker

1 Introduction

Osteosarcoma is an exceptionally aggressive cancer that develops in bone tissue, predominantly affecting children and teenagers. This malignancy constitutes nearly half of all bone cancers in this age group. It commonly arises in the metaphyseal regions of long bones, such as the distal femur, proximal tibia, and proximal humerus (1). Characteristically, osteosarcoma is marked by uncontrolled proliferation of bone and cartilage tissue, leading to significant morbidity (2). Recent statistical data indicate that the average 5-year survival rate for osteosarcoma patients is around 70%. However, this rate significantly declines to below 30% for those with distant metastases. The pathogenesis of osteosarcoma involves complex genetic alterations that drive the initiation and progression of the tumor (3).

Osteosarcoma is characterized by aberrant gene expression, which exerts significant influence on the initiation and progression of tumor cells (4, 5). Key molecular pathways implicated in osteosarcoma include the STING/IRF3/IFN-β, PI3K/AKT, and mTOR signaling pathways (6–8). Considering the complexity of osteosarcoma pathogenesis and the heterogeneity of its molecular landscape, identifying critical genes affecting prognosis and constructing a simple yet effective prognostic model is paramount.

With the advancement of cancer biology research, the interaction between programmed cell death (PCD) and malignant tumors has received widespread attention, being considered a crucial component in the occurrence of malignant tumors (9, 10). As research progresses, an increasing number of researchers are focusing on the correlation between PCD and osteosarcoma occurrence (11). Apoptosis, the predominant form of cell death, is essential for the proper functioning of organisms. Abnormal activation of apoptosis pathways may lead to sustained proliferation and abnormal survival of tumor cells, which could promote tumor occurrence and growth (12). Ferroptosis, another form of cell death induced by oxidative stress, has attracted significant interest in the realm of cancer research. Due to the weakened antioxidant capacity of tumor cells, they are more susceptible to iron-dependent cell death (13). Cuproptosis has also attracted researchers' interest, as this form of death may be related to the death and survival of tumor cells (14). Autophagy is an intracellular degradation process crucial for maintaining cellular homeostasis, as it breaks down damaged proteins and organelles (15). PARP-1 is an important factor associated with DNA damage repair and the effectiveness of cancer drugs (16). Pyroptosis is an inflammatory type of cell death that generally happens after the involved cells release cytokines like interleukins and other signaling molecules (17). By aiding the decline of inflammatory cells to control tumor progression and, to a certain extent, modifying the response to treatment (18). Netotic cell death, a distinct form of cellular demise, is triggered by the formation and accumulation of net-like fibrous structures (19). The possibility of this kind of regulation lies in an apoptotic function of the tumor microenvironment. They are interconnected with the consequences of oxidative harm (20). Anoikis is a type of cellular demise initiated by the separation of cells from the extracellular matrix, Dysregulation of extracellular matrix interaction may impact tumor cell survival and metastasis (21). Immunogenic cell death is a type of cellular demise that can provoke an immune response, consequently impacting the survival of tumor cells (22). Disulfidptosis is a type of cell death linked to the formation and disruption of intracellular disulfide bonds. This process may also contribute to tumor initiation and progression (23). In summary, a deeper comprehension of the different forms of programmed cell death and their roles in the development of malignant tumors will yield new insights and targets for cancer prevention and therapy. Further research is essential to explore how these apoptotic pathways function in cancer treatment, aiming to enhance the survival rates and quality of life for cancer patients.

The creation of prognostic models for osteosarcoma has been greatly enhanced by the advancement of machine learning methods. When it comes to understanding the complexity of biological information, the application of different algorithms provides special advantages within the field of machine learning. A selection of 10 algorithms renowned for their intrinsic variable selection properties has been made, encompassing Enet, Ridge, CoxBoost, survivalSVM, Lasso, SuperPC, plsRcox, StepCox, RSF, and GBM. Lasso is a regression analysis method used for feature selection and model sparsity, aiding in identifying key predictor variables (24). Ridge regression constrains the size of model coefficients by adding an L2 regularization term, reducing overfitting, particularly useful for

handling collinear data (25). Elastic Net combines the strengths of Lasso and Ridge, balancing model sparsity and complexity, suitable for high-dimensional and collinear data (26). CoxBoost is a Cox proportional hazards model based on gradient boosting trees, used for modeling and predicting survival data (27). Utilizing support vector machines to capture intricate relationships between variables and survival time, Survival Support Vector Machine is a technique for managing survival data (28). With the advancement of machine learning integration, the establishment of prognosis models for different diseases has significantly improved. The application of various algorithms in the field of machine learning provides distinct advantages. Ten algorithms known for their inherent variable selection capabilities include Enet, Ridge, CoxBoost, survivalSVM, Lasso, SuperPC, plsRcox, StepCox, RSF, and GBM. By integrating these methods, the intricate relationship between programmed cell death (PCD) and osteosarcoma (OS) prognosis can be more thoroughly understood. The complementary nature of these algorithms greatly enhances the model's generalizability and predictive accuracy.

This research employed the integration of several machine learning algorithms to create a prognostic model for osteosarcoma associated with programmed cell death (PCD). The underlying assumption was that combining various algorithms would better capture the complex gene interactions and enhance prediction accuracy. The goal was to improve the accuracy of prognostic predictions for osteosarcoma patients and to identify potential targets for personalized treatment strategies.

2 Methods

2.1 Data download and standardization

We obtained a comprehensive dataset from the Therapeutically Applicable Research to Generate Effective Treatments (TARGET) database. This dataset contained detailed information on 202 osteosarcoma patients, encompassing expression data, clinical details, and chromosomal and gene mutation information (https://ocg.cancer.gov/programs/target). To ensure the robustness of our study, we applied stringent criteria to screen for samples with complete data, resulting in a selection of 88 osteosarcoma patient samples. Furthermore, we enriched our analysis by incorporating three additional datasets from the Gene Expression Omnibus (GEO) database (https://www.ncbi.nlm.nih.gov/geo/): GSE16102, GSE21257, and GSE39058. These datasets collectively contributed an additional 128 osteosarcoma patient samples. Each dataset was carefully chosen based on its relevance and the completeness of the accompanying clinical annotations.

At the outset of osteosarcoma data analysis, we utilized the IOBR package's data transformation function to convert the raw count matrix from the TARGET dataset into Transcripts Per Million (TPM) format. This conversion was crucial for normalizing the expression levels across samples. Next, we utilized the NormalizeBetweenArrays function from the limma package to standardize the data, which helped to reduce batch effects and ensure comparability across various datasets. For the GEO datasets, we reversed the log2-transformed count values to restore the original count values before converting them to TPM format. Batch effects were addressed using the movebatcheffect function from the sva package. These stringent normalization steps were essential to maintain the integrity and reproducibility of our results.

Through a thorough literature review, we identified 15 distinct types of programmed cell death, including disulfidptosis, entotic cell death, netotic cell death, pyroptosis, ferroptosis, anoikis, autophagy, necroptosis, PARP-1-dependent cell death, alkaliptosis, oxeiptosis, immunogenic cell death, and lysosome-dependent cell death. The genes associated with these forms of cell death were sourced from the Gene Set Enrichment Analysis (GSEA) database (http://www.gsea-msigdb.org/gsea/index.jsp) and the Kyoto Encyclopedia of Genes and Genomes (KEGG) database (https://www.genome.jp/kegg/). These genes were then combined using the intersection function, resulting in a comprehensive set of 1621 programmed cell death genes.

2.2 Selection of differentially expressed genes and identification of prognosis-associated genes

Utilizing the limma software for differential expression analysis, we pinpointed genes significantly linked to programmed cell death (PCD) in 88 osteosarcoma samples and their corresponding adjacent normal tissues from the training set. The differential analysis criteria were established at FDR < 0.05 and |log2Foldchange| > 1. Osteosarcoma samples and their adjacent normal tissues were differentiated using TARGET sample IDs. To visualize the differentially expressed genes, we generated a heatmap by randomly selecting a subset of these genes with the pheatmap package. Additionally, we created a volcano plot using the ggplot2 tool to display the fold changes, p-values, and expression levels of these genes.

In our thorough UniCox regression analysis, conducted with the survival package in R, we identified 30 genes significantly correlated with patient survival, applying a stringent p-value threshold of < 0.05. Out of these, 24 genes were found to have protective effects, while 6 were associated with a higher risk prognosis. These findings were illustrated through detailed forest plots, providing clear depictions of hazard ratios and confidence intervals. To further elucidate the intricate relationships between genes associated with prognosis, we constructed chord plots using the igraph, psych, and reshape2 packages. These plots illustrated complex interactions and co-expression patterns among the identified genes. Additionally, lollipop plots and the Circos package were employed to identify and present prognostic genes with copy number variations (CNVs) greater than 4% in the training set of osteosarcoma samples, offering deeper insights into the genomic alterations and their potential impact on prognosis.

2.3 Establishment of osteosarcoma subtypes and mechanism analysis

We utilized the ConsensusClusterPlus package in R to perform unsupervised clustering on the test set of osteosarcoma samples.

The maxK parameter was set to 9, generating subtypes ranging from 2 to 9. Through an in-depth examination of the clustering heatmap and the consensus variation curve, we determined the optimal value of K to be 2. Consequently, the training set samples were categorized into two distinct subtypes, labeled as A and B. The consensus clustering results were subsequently validated using t-distributed stochastic neighbor embedding (tSNE) and Uniform Manifold Approximation and Projection (UMAP) techniques. Kaplan-Meier (KM) survival curves for osteosarcoma patients were created using the survival package in R to depict the prognostic differences between these two subtypes.

To explore the underlying mechanisms behind the survival rate disparities between the subtypes, we conducted a differential expression analysis of prognostically relevant genes using the limma package. We utilized single-sample gene set enrichment analysis (ssGSEA) to determine variations in immune cell abundance between the subtypes. To explore differential pathway enrichment between the subtypes, gene set variation analysis (GSVA) was performed, and the top twenty most differentially enriched pathways were visualized using the pheatmap package. Reference gene sets from the KEGG and GSEA databases were employed, and the Gene Set Enrichment Analysis (GSEA) method was applied to identify pathways significantly enriched in each subtype. Furthermore, we illustrated the expression levels of the 30 prognosis-associated genes in subtypes A and B, along with clinical information for each sample.

2.4 Development of integrated machine learning models

After a preliminary screening, we identified ten machine learning algorithms known for their excellent variable selection properties. We integrated these into a robust ensemble. The chosen algorithms included Enet, Ridge, CoxBoost, survivalSVM, Lasso, SuperPC, plsRcox, StepCox, RSF, and GBM. Leveraging the corresponding R packages, we established fundamental computational protocols for each model. The selection of these algorithms was based on their strengths in handling high-dimensional data, regularization, and boosting, which are critical for robust prognostic modeling.

During model training, we optimized key parameters for each algorithm. For instance, the Lasso and Ridge regressions included tuning the regularization parameter lambda, which controls the strength of the penalty imposed on the coefficients. The Elastic Net model balanced the l1_ratio parameter to combine the penalties of Lasso and Ridge. For the survivalSVM, we adjusted the cost parameter to manage the trade-off between margin maximization and classification error. In the case of the CoxBoost algorithm, the step size and the number of boosting steps were finely tuned to prevent overfitting while ensuring adequate model complexity.

Subsequently, we implemented a strategy where one algorithm was responsible for variable selection, while another algorithm was tasked with model construction. Pairing these ten algorithms in all possible combinations resulted in 101 combinations. Each combination was rigorously cross-validated, with hyperparameters fine-tuned based on performance metrics like the concordance index (C-index) and mean squared error.

The concordance index (C-index) was computed for each model, considering both survival time and status. To ensure robust performance metrics, k-fold cross-validation was employed for model evaluation. Ultimately, the Osteosarcoma Programmed Cell Death Score (OS-PCDS) model was developed using the Random Survival Forest (RSF) algorithm, which exhibited the lowest relative variability and the highest average C-index across validation sets. The exceptional performance of this model is attributed to RSF's ability to handle complex variable interactions and its robustness against overfitting through ensemble learning.

By combining the glmnet R utility with the CalRiskScore function, the parameter type was configured to linear predictor. Subsequently, risk scores were computed for each sample in both the training and validation sets. The median OS-PCDS value from the training set was used as the threshold to classify all osteosarcoma (OS) samples in the dataset into high-risk and low-risk groups.

During the variable selection process, the RSF algorithm identified five genes associated with prognosis, which became the foundation of the prognostic model. Box plots were used to illustrate the expression levels of these five genes in osteosarcoma samples from the training set and adjacent normal tissues. Independent survival analyses were subsequently conducted for the high-expression and low-expression groups of these model genes.

2.5 Verification of model prediction accuracy and exploration of mechanism

We manually curated 61 transcriptome-based prognostic models for osteosarcoma from publicly available sources, the list of models is provided in Supplementary Table S1. In this study, variables were excluded from published models if the proportion of missing model genes in the training set expression matrix exceeded 20%. Consequently, a total of 38 models were selected for comparison. Comparative analyses with previously published osteosarcoma prognostic models involved generating forest plots to represent the C-index for both training and validation sets. Kaplan-Meier (KM) curves, illustrating overall survival across all training and validation sets, were constructed using the survival and survminer R packages. The comparison of survival curves between low-risk and high-risk groups in the training and validation sets was performed using the survdiff function, yielding statistically significant p-values (<0.05). To improve the reliability of prognostic predictions for osteosarcoma patients, ROC (Receiver Operating Characteristic) curves were generated at 1, 2, 3, 4, and 5 years for both the training and validation sets using the timeROC package. Subsequently, the area under the curve (AUC) values were calculated for each ROC curve. Additionally, to validate the prognostic significance of OS-PCDS and explore its potential as a supplementary tool to current clinical data, ROC values were calculated for all clinically relevant information to forecast outcomes at 1-5 years. Following this, the predictive effectiveness of PCDS was evaluated using multiCox regression, which incorporated potential confounding factors from additional clinical data, displayed in forest plot form. By utilizing Sankey

and violin diagrams to illustrate the correlations between various risk groups and subtypes A and B, the objectivity and predictive precision of the model were confirmed. A heatmap was employed to illustrate the relationships between the expression of model genes, survival time, and risk scores.

We employed the CIBERSORT package to assess the relative abundance of 22 distinct immune cell types in each sample from the training set. Violin plots were then used to compare immune cell abundance levels between the high and low PCDS groups. Additionally, the R package estimate was utilized to evaluate potential differences in stromal scores, immune scores, and estimated scores within the tumor microenvironment between these two groups.

2.6 Evaluation of mRNA expression levels in model genes

Total RNA was isolated from the tissues or cells according to the manufacturer's instructions using Trizol reagent (R401, Vazyme).The RNA's quantity and integrity were then verified using a spectrophotometer. Subsequently, cDNA was synthesized from the RNA template employing reverse transcriptase and random primers. This cDNA served as the template for quantitative polymerase chain reaction (qPCR), conducted on a StepOnePlus Real-Time PCR System (ABI, USA), to measure the expression levels of the MLH1, SQLE, EDIL3, MTM1, and CLTCL1 genes. The qPCR procedure followed the manufacturer's instructions, utilizing SYBR Green (Q712, Vazyme) and gene-specific primers. An internal control was utilized instead of beta-actin. Relative gene expression levels were determined using the 2^-ΔΔCT method. Details of the primers can be found in Supplementary Table S2.

2.7 Determination of protein expression levels of model genes

Protein extraction from tissue or cell lysates was performed using radioimmunoprecipitation assay (RIPA) buffer (abs9231, absin). The isolated proteins were subsequently subjected to sodium dodecyl sulfate-polyacrylamide gel electrophoresis (SDS-PAGE) and then transferred onto polyvinylidene fluoride (PVDF) membranes. After transfer, the membranes were incubated with primary antibodies against EDIL3 (ab190692, Abcam), GAPDH (ab9485, Abcam), CLTCL1 (ab21679, Abcam), and SQLE (ab67479, Abcam). Following this, a horseradish peroxidase (HRP)-conjugated secondary antibody (ab6721, Abcam) was applied. Protein bands were detected using an enhanced chemiluminescence (ECL) substrate (E411 Vazyme), which reacts with HRP to produce light, thereby visualizing the proteins on the membrane. GAPDH expression served as the internal control.

2.8 Culturing and transfection of cells

The osteosarcoma cell lines (U2OS, MG-63, and HOS) as well as mesenchymal stem cells (MSCs) were obtained from the American Type Culture Collection (ATCC). Each cell line was cultured and maintained following the specific protocols provided by their respective suppliers. For the osteosarcoma cell lines, Dulbecco's Modified Eagle Medium (DMEM) (Gibco, USA) was used, while a specialized Human Mesenchymal Stem Cell Growth Medium (Gibco, USA) was utilized for the MSCs. The cells were then placed in a humidified incubator set at 37°C with 5% CO2 to ensure optimal growth conditions. Plasmid transfection was performed following the manufacturer's guidelines using Lipofectamine 2000 reagent (cat#11668019, Invitrogen). Plasmids were synthesized by GenePharma.

2.9 Detection of proliferative capacity of osteosarcoma cells after knockdown of model gene expression

Cells were plated at a density of 5,000 cells per well in a 96-well plate and were given 24 hours to attach and acclimate. After this initial period, the cells were cultured for a standardized duration to ensure synchronization across the population. Subsequently, the CCK-8 assay reagent (C0038, Beyotime) was added to each well following the manufacturer's instructions. The plate was incubated for an additional 120 minutes to allow the colorimetric reaction to develop. Cell viability was subsequently evaluated by measuring the absorbance at 450 nm with a microplate reader. The optical density readings were used as indicators of cell proliferation and overall viability.

For the colony formation assay, cells were detached with trypsin and evenly seeded into 6-well plates at a concentration of 1,000 cells per well. The cells were cultured for another 7 days to allow colony formation. Subsequently, the cell monolayers were fixed using a 4% solution of paraformaldehyde and then incubated with a 0.1% crystal violet staining solution (abs817172, absin) to visualize the colonies. Photographs of the stained colonies were captured, and the colony counts were documented and analyzed among the various experimental groups.

2.10 Detection of migration ability of osteosarcoma cells after knockdown model gene expression

When the cell monolayer reached around 90% confluence, a wound was created by gently scraping a specific area of the cell layer with a 200 µl plastic pipette tip, producing a controlled scratch. Images of the scratch wound were taken immediately after its creation and again after a 24-hour incubation period using a phase-contrast or inverted microscope equipped with a digital camera.

2.11 Detection of apoptosis rate of osteosarcoma cells after knockdown of model gene expression

The cells underwent a staining procedure that included a one-hour incubation with Annexin V-FITC (A211, Vazyme) and 7-

AAD in the absence of light and at room temperature. After the designated incubation period, the cells underwent three comprehensive washes using cold phosphate-buffered saline (PBS) in order to eliminate any unbound stains. Following that, the cells were reconstituted in PBS, and a flow cytometer (BD, USA) was utilized to analyze the stained cells.

2.12 Single-cell analysis

Six samples of osteosarcoma (OS) and six samples of normal control make up the GSE162454 dataset. The R program Seurat was used to perform quality control processes for the single-cell sequencing data. The tSNE and UMAP algorithms were then used for dimension reduction and clustering, respectively. The generated two-dimensional graphs were labeled with numbers to identify cell types. Further annotation of cell types was performed using the singleR package in R to identify established cell types that are linked to each cellular subgroup.

2.13 Drug sensitivity analysis

Using the oncoPredict R package, sensitivity scores for 198 anticancer drugs were calculated for samples in the training set. Through iterative analysis, we identified significant sensitivity differences between the OS-PCDS high and OS-PCDS low groups, with a p-value threshold of <0.001. This analysis revealed significant sensitivity differences in 34 drugs: 9 drugs demonstrated increased sensitivity in the PCDS low group, while 25 drugs showed heightened sensitivity in the PCDS high group. The results of the drug sensitivity screening were visually represented using violin plots, highlighting the differences across the various risk categories.

2.14 Osteosarcoma specimen information

To assess the mRNA and protein expression levels of the model genes, we collected tumor specimens and adjacent normal tissue samples from six osteosarcoma patients. These samples were obtained during surgeries performed at the Affiliated Zhongshan Hospital of Dalian University between September 2021 and September 2023. Prior to specimen collection, informed assent was obtained from all patients. In addition, the research protocol, including the collection and use of human tissue samples, has been reviewed and approved by batch number KY2023-115-1 of the hospital's ethical review committee.

2.15 Statistical analysis

Statistical analyses were performed using R software version 4.1.3. Continuous variables were presented as means with standard deviations or as medians with interquartile ranges, while categorical variables were summarized using frequencies and percentages. T-tests were utilized to compare continuous variables between two groups, and one-way ANOVA was applied for comparisons involving more than two groups. For categorical variables, chi-square tests or Fisher exact tests were used as appropriate to identify significant differences.

Survival distributions between different groups were compared using the Kaplan-Meier method along with the log-rank test. The Cox proportional hazards regression model was employed to evaluate the prognostic value of the osteosarcoma programmed cell death score (OS-PCDS), adjusting for potential confounding variables. Model performance was assessed using the concordance index (C-index), and receiver operating characteristic (ROC) curve analyses were conducted to calculate the area under the curve (AUC), thereby evaluating model effectiveness.

To optimize the model, machine learning algorithms such as Lasso, Ridge regression, and Random Survival Forests were employed. These algorithms were selected for their capability to handle high-dimensional data and perform feature selection effectively. Cross-validation was used for parameter tuning to avoid overfitting and ensure the model's robustness.

A two-sided P-value of less than 0.05 was considered statistically significant. Detailed statistical analyses for specific experiments, including qPCR, CCK8 assays, flow cytometry, and other investigations, were performed using Prism software. For qPCR, gene expression levels were normalized to internal controls, and relative quantification was carried out using the 2^-ΔΔCT method. CCK8 assay results were analyzed by comparing optical density values across different time points and treatment groups using repeated measures ANOVA. Flow cytometry data were analyzed by calculating the percentage of cells in different cell cycle stages or the percentage of apoptotic cells, followed by statistical comparisons using T-tests.

3 Results

3.1 Identification of differentially expressed and prognosis-associated genes

Within the training set, 246 genes were found to be differentially expressed between osteosarcoma samples and their corresponding adjacent normal tissues. Among these, 145 genes showed significant downregulation, while 101 genes demonstrated significant upregulation. A heatmap depicted the expression patterns of forty randomly selected genes (Figure 1A). The volcano plot illustrated both upregulated and downregulated genes, with notable upregulated genes including UBE2C, MMP13, TREM2, SPP1, and MMP9, and representative downregulated genes including MAPT, GABARAP, ILK, EEF1A2, and ATP6V0C (Figure 1B).

A total of 30 prognosis-related genes were identified and visualized using a forest plot. This group included 24 protective genes (such as CLTCL1, CALCOCO2, MLH1, MTM1, and ZDHC3) and 6 risk genes (including BAG1, CD36, and CRIP1) (Figure 1C). Additionally, a circos plot was utilized to illustrate the interconnections among these prognosis-associated genes. Genes related to prognosis were highlighted in red, while genes carrying protective or risk factors were depicted with yellow and green

10.3389/fimmu.2024.1427661

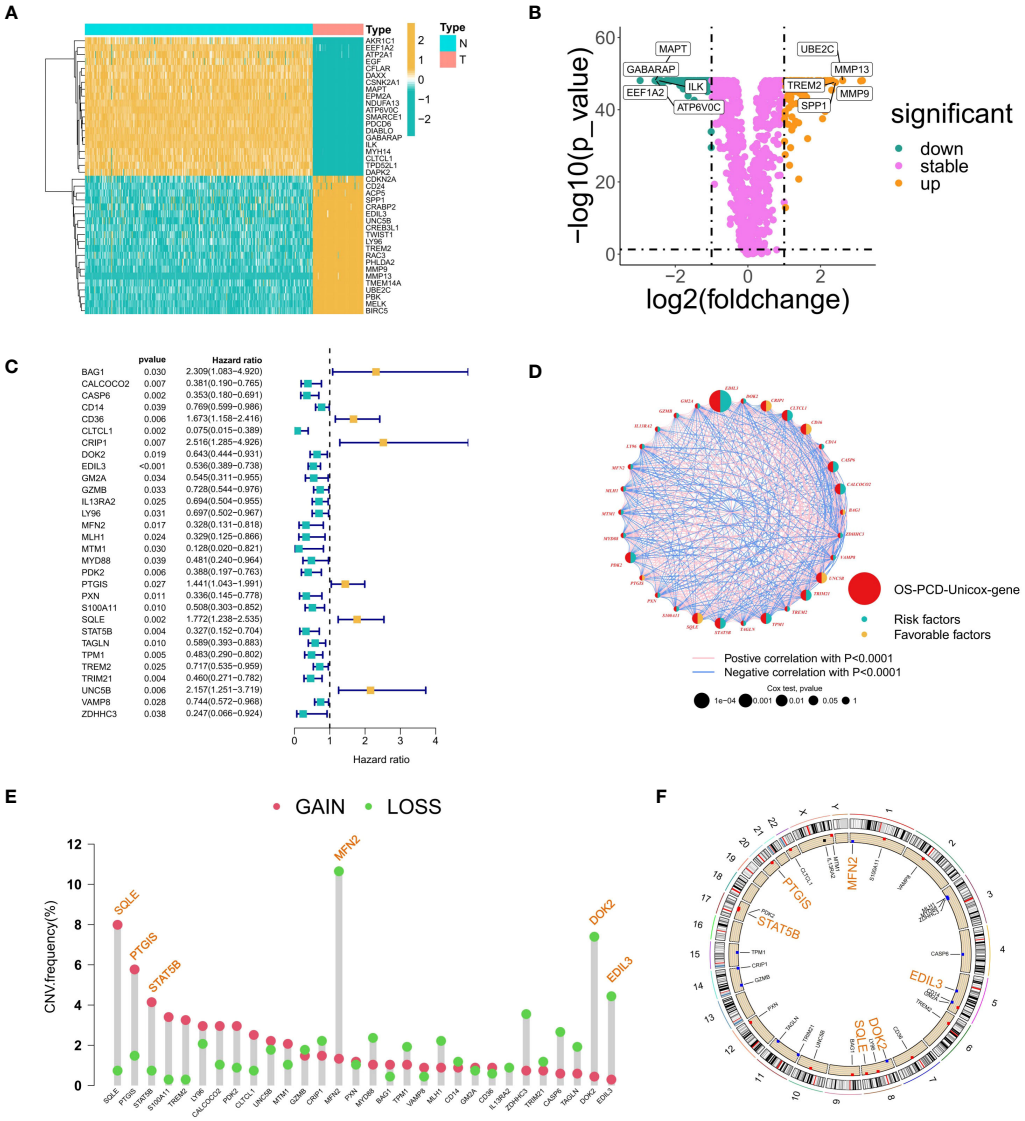

FIGURE 1
Gene Selection Relating to Prognosis and Differentiation. **(A)** Heatmap showing the expression patterns of 40 randomly selected differentially expressed genes between osteosarcoma samples and adjacent normal tissues. The color scale indicates the level of gene expression, with red representing high expression and blue representing low expression. **(B)** A volcano diagram illustrating the correlation between fold changes, P-values, and gene expression levels; yellow dots denote upregulated genes, green dots represent downregulated genes, and purple dots signify insignificant differences in gene expression. **(C)** A forest plot illustrating thirty genes that have been linked to survival prognosis. **(D)** A circos plot depicting the correlations among genes associated with prognosis. **(E)** A lollipop diagram illustrating the frequency of copy number variations (CNVs) in genes associated with prognosis, with particular attention given to CNVs surpassing a 4% threshold. **(F)** Genes with a mutation frequency greater than 4% are highlighted at the position of chromosome mutations. The genomic circumference diagram illustrates the chromosomal locations of genes that display high-frequency CNVs.

semicircles, respectively. The sizes of circles representing p-values from Cox regression analysis served as indicators of the relative importance and relevance of gene interactions within the network. Particularly noteworthy genes included EDIL3, CRIP1, CLTCL1, SQLE, PDK2, and TPM1, which exhibited extensive interaction patterns. Expression correlations between genes were represented by lines connecting them, with positive correlations depicted in pink and negative correlations in blue (Figure 1D).

A bar plot was created to display the frequency of Copy Number Variations (CNVs) impacting prognosis-associated genes, focusing on those with frequencies above 4%. Noteworthy genes with copy number gains included SQLE, PTGIS, and STAT5B, while those with losses comprised MFN2, DOK2, and EDIL3 (Figure 1E). Furthermore, a circular plot depicted the chromosomal locations of these high-frequency CNV-affected genes: MFN2 on chromosome 1, EDIL3 on chromosome 5, SQLE and DOK2 on chromosome 8, STAT5B on chromosome 17, and PTGIS on chromosome 20. Chromosomes 3, 5, 8, and 17, in particular, exhibited high frequencies of CNV events in osteosarcoma (Figure 1F).

3.2 Revealing the establishment and mechanism analysis of osteosarcoma subtypes

The ConsensusClusterPlus R package was employed to determine the optimal number of clusters for unsupervised clustering, categorizing TARGET-OS samples into subtypes A and B (Figure 2A). The optimal clustering number was identified by analyzing the inflection point on the variation rate curve of the Cumulative Distribution Function (CDF) (Figures 2B, C). A heatmap was generated to display the subtype and clinical information for each sample (Figure 2F). Additionally, dimensionality reduction of the osteosarcoma expression matrix to two dimensions was performed using the t-distributed Stochastic Neighbor Embedding (tSNE) and Uniform Manifold Approximation and Projection (UMAP) algorithms, with each sample assigned a point value (Figure 2D). Both algorithms effectively distinguished subtypes A and B, confirming the objectivity of PCD-related osteosarcoma subtyping. Kaplan-Meier (KM) curves further validated prognostic differences between the subtypes (P = 0.002), with subtype B showing better survival outcomes than subtype A (Figure 2E).

An in-depth analysis was subsequently conducted to uncover the molecular mechanisms underlying the prognostic differences among the subtypes. The limma package facilitated differential expression analysis of prognosis-associated genes between subtypes, with results presented via box plots (Figure 3A). A total of 19 genes displayed significant differential expression between subtypes A and B, with 18 genes upregulated in subtype B and only one gene upregulated in subtype A. The ssGSEA algorithm computed the abundance of 33 distinct immune cell types in each training set sample. Box plots visualized the differences in immune cell expression levels between the subtypes (Figure 3B). Significant variations were observed in the abundance of 24 immune cell types, with all being more abundant in subtype B, except for nine cell types, including immature dendritic cells, eosinophils, Th17 cells, and Th2 cells.

The GSVA algorithm was utilized to examine differential enrichment pathways between the subtypes. A heatmap highlighted the top 20 pathways with significant enrichment differences, all upregulated in subtype B (Figure 3C). GSEA curves depicted the top five pathways most enriched in each subtype (Figures 3D, E). Subtype A showed significant upregulation in the Focal Adhesion and Neuroactive Ligand-Receptor Interaction pathways, while subtype B

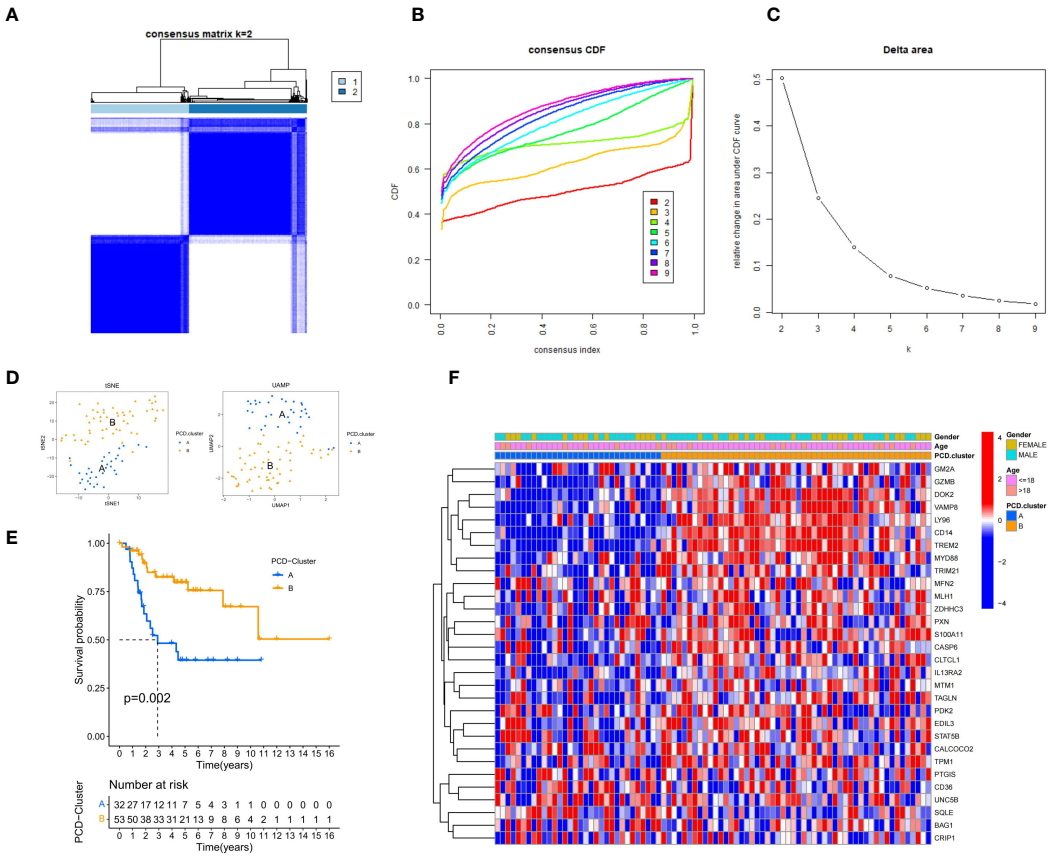

FIGURE 2
Clinical Information and Subtype Differentiation Are Illustrated in Figure 2. **(A)** By employing the R package ConsensusClusterPlus and non-parametric clustering, TARGET-OS samples were categorized into subtypes A and B. **(B)** The determination of the optimal number of clusters is based on the x-coordinate of the inflection point on the variability curve of the CDF. **(C)** Cluster number CDF curves spanning the range of 2 to 9. **(D)** The osteosarcoma expression matrix is reduced to two dimensions by the UMAP and tSNE algorithms, which distinguish the expression patterns of the two subtypes. **(E)** K-M survival analysis curve. The Kaplan-Meier diagram (P = 0.002) provides validation for the prognostic distinctions among the four subtypes. **(F)** A pheatmap presents the subtype and clinical information of each sample.

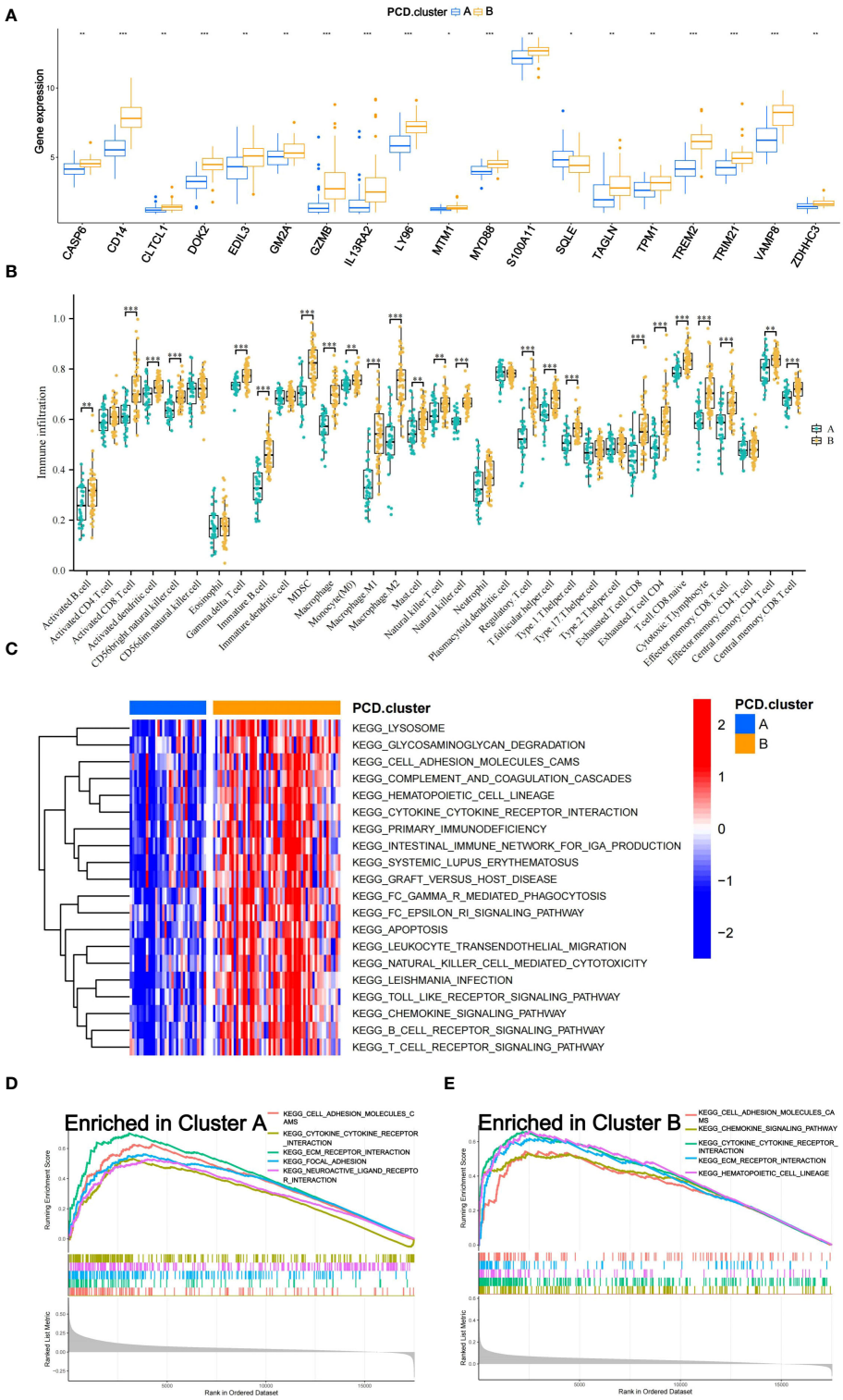

FIGURE 3
Mechanisms of Subtypes of Osteosarcoma Associated with PCD. **(A)** Box diagram depicting the variation in prognostic gene expression among distinct subtypes. **(B)** The differences in 33 immune cell abundances between the two subtypes are depicted in the box diagram. **(C)** The Gene Set Variation Analysis (GSVA) method was applied to identify pathways that varied in expression between two subtypes. **(D, E)** Gene Set Enrichment Analysis (GSEA) shows which five pathways within each subtype have the highest level of enrichment. The following p-value ranges: * < 0.05, ** < 0.01, and *** < 0.001.

demonstrated substantial upregulation in the Hematopoietic Cell Lineage and Chemokine Signaling Pathway pathways. Additionally, three pathways—Cell Adhesion Molecules (CAMs), Cytokine-Cytokine Receptor Interaction, and Extracellular Matrix (ECM) Receptor Interaction—were notably upregulated in both subtypes.

3.3 Construction of machine learning integration models

The integration of the machine learning algorithm generated a total of 101 possible combinations. The optimal model was identified to be the one constructed by the RSF algorithm, which exhibited the highest average consistency index and relatively low variability in the consistency index. This model's scoring system was termed OS-PCDS. The model generated by the RSF algorithm ranked highest across all three GEO validation sets, with an average C-index of 0.943 (Figure 4A). During the variable selection process, the RSF algorithm identified all five prognostic-related genes, namely MTM1, MLH1, CLTCL1, EDIL3, and SQLE. The mRNA expression levels of these five genes showed significant differences between osteosarcoma samples and adjacent normal tissues, as depicted in the boxplots (Figure 4B). Specifically, EDIL3 and SQLE exhibited significant upregulation in osteosarcoma samples, suggesting their roles in promoting angiogenesis and cholesterol biosynthesis, respectively. EDIL3, known for its involvement in endothelial cell adhesion, may facilitate tumor angiogenesis, while SQLE, an enzyme in the cholesterol biosynthesis pathway, could support membrane biogenesis in rapidly proliferating tumor cells. While MTM1, MLH1, and CLTCL1 showed significant upregulation in adjacent normal tissues. By integrating clinical information from all datasets with the OS-PCDS, a nomogram model was developed to predict the prognosis of OS patients (Figure 4C).

3.4 Validation of machine learning integration models

A comparative analysis was conducted on osteosarcoma prognostic models published in the last five years. The C-index for both training and validation sets was illustrated using forest plots, with significant differences indicated by asterisks. Across all three GEO validation sets, the TARGET-OS training set, and the combined meta-cohort from the three validation sets, OS-PCDS consistently ranked highest in C-index values (Figure 5A). Samples were classified as high-risk or low-risk based on the median OS-PCDS value from the training set. Kaplan-Meier plots for each dataset showed significant survival differences ($p < 0.05$) between high-risk and low-risk groups in both the training set and the three validation sets. The prognosis of the low-risk group consistently surpassed that of the high-risk group in all datasets (Figures 5B–E).

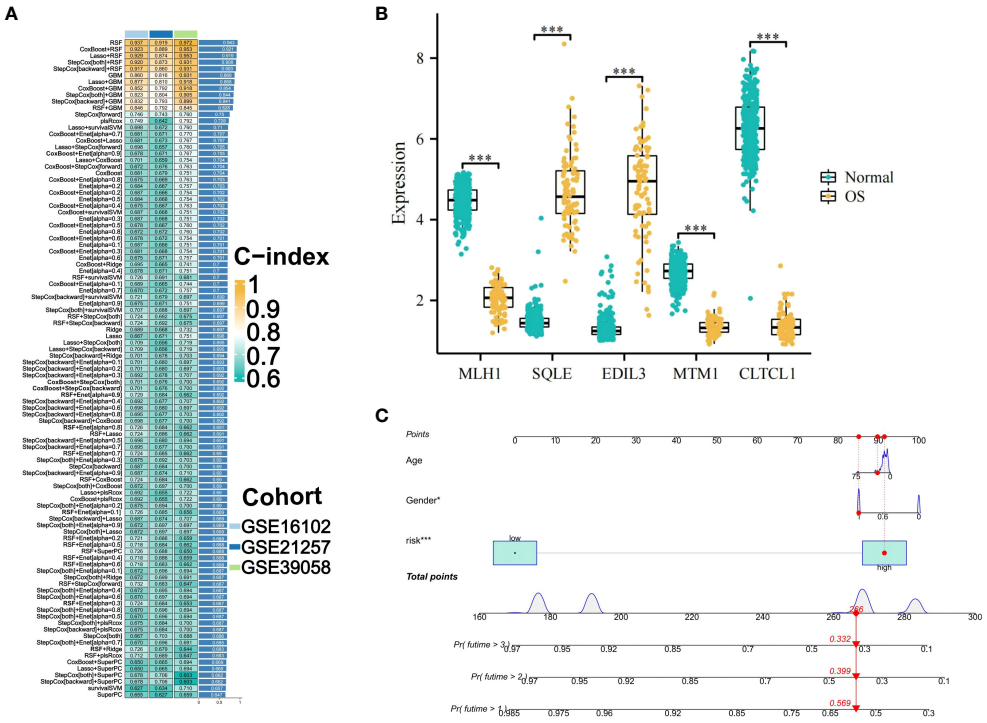

FIGURE 4
Construction and Selection of an Machine Learning Integration Model. **(A)** A cumulative sum of 101 iterations generated by ten distinct machine learning algorithms was employed in the development of prognostic models, with the Concordance index (C-index) being computed. The optimal model was determined to be the RSF algorithm, and its score was designated OS-PCDS (Osteosarcoma Programmed Cell Death Score). **(B)** The OS-PCDS gene expression levels in adjacent normal tissues and osteosarcoma are depicted in the box plot. **(C)** A nomogram model was developed by incorporating PCDS, gender and age variables. P values for *** is less than 0.001.

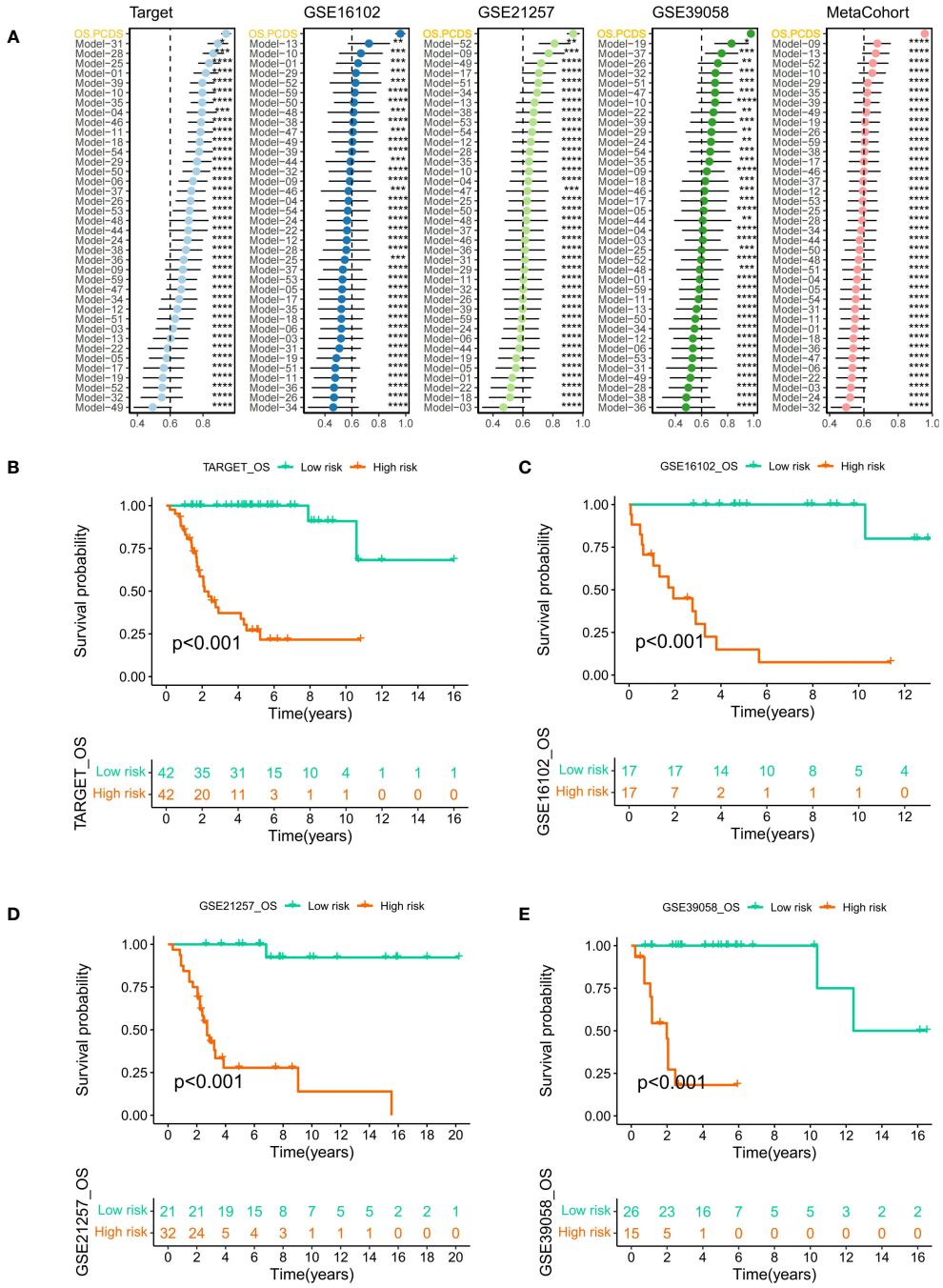

FIGURE 5
(A) A forest plot illustrating the OS-PCDS's Superiority in published osteosarcoma models according to the C-index. Calculations were done for the TARGET-OS training set, several GEO validation sets, and a meta-cohort consisting of the GEO validation sets. **(B–E)** The median PCDS of the TARGET−OS training set was used as the cut-off value to separate all data into PCDS−high and PCDS−low categories. After that, Kaplan-Meier plot was generated for each dataset. Various degrees of importance are indicated by the following symbols: P values for *, **, ***, and **** are less than 0.05, 0.01, 0.001, and 0.0001, respectively.

In both training and validation sets, the Area Under the Curve (AUC) values for PCDS at 1, 2, 3, 4, and 5 years were calculated using Receiver Operating Characteristic (ROC) curves. The 5-year AUC values for the TARGET, GSE16102, GSE21257, and GSE39058 cohorts were 0.994, 0.906, 0.959, and 0.769 respectively (Figures 6A–D), indicating the model's exceptional stability. Violin plots displayed significant differences in OS-PCDS risk scores between subtypes A and B. Subtype B had lower risk scores associated with better prognostic outcomes, whereas subtype A had higher risk scores linked to poorer survival (Figure 6E). Additionally, the Sankey plot (Figure 6F) showed a significant correlation between the distribution of high-risk and low-risk categories and the A and B subtypes.

Using ESTIMATE analysis, violin plots were created to depict significant differences in stromal and immune scores between the high

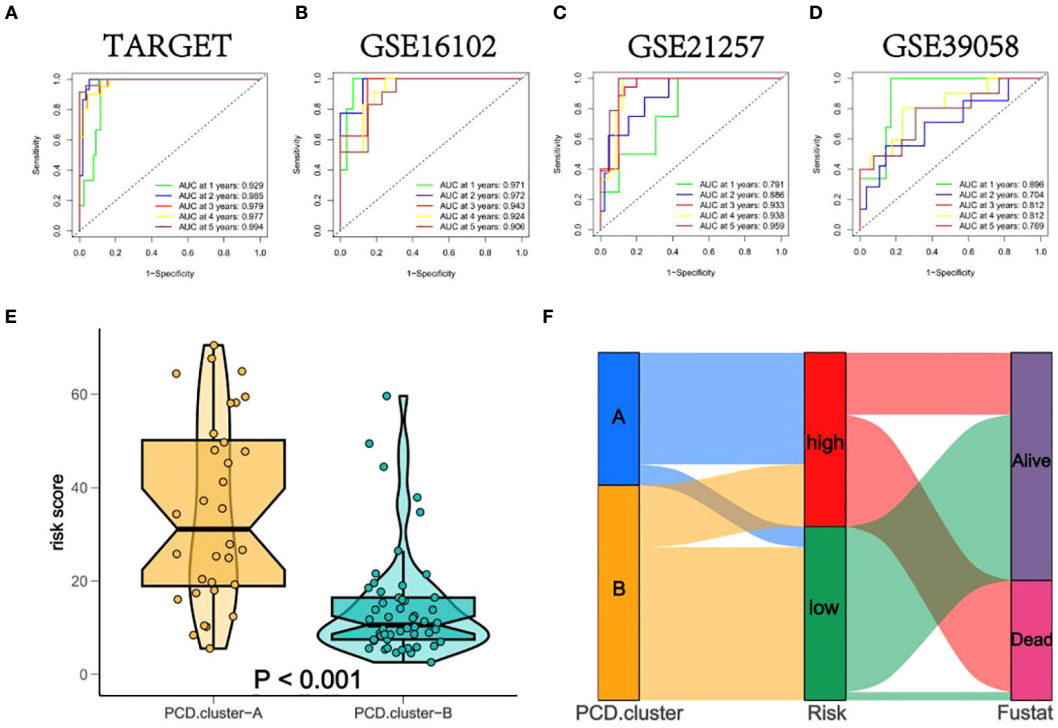

FIGURE 6
(A–D) The Area Under the Curve (AUC) values of PCDS at 1, 2, 3, 4, and 5 years for all training and validation sets. **(E)** Box diagrams indicate that the risk scores for subtypes A and B differ significantly. **(F)** A Sankey plot depicting noteworthy correlations between the sample distributions of the PCD-Cluster and OS-PCDS.

and low OS-PCDS groups (Figure 7B). The CIBERSORT algorithm was then applied to determine the abundance of 22 different immune cell types in each sample (Figure 7A). Violin plots revealed an increase in memory B cells and macrophage M2 cells in the low OS-PCDS group, while the high OS-PCDS group had elevated levels of naive B cells and resting dendritic cells. Correlation scatter plots further validated the relationship between these immune cells and OS-PCDS (Figures 7C–F). Additionally, a heatmap was generated to show the correlation between the abundance of immune cells and the expression levels of the five model genes, with significance levels indicated as * $p < 0.05$, ** $p < 0.01$, *** $p < 0.001$ (Figure 7G).

3.5 The mRNA expression levels of the model genes were evaluated

In comparison to osteosarcoma samples, the mRNA expression levels of the CLTCL1, MTM1, and MLH1 genes were significantly elevated in adjacent normal tissues (P=0.015, P=0.009, and P<0.001, respectively). On the other hand, the expression levels of SQLE and EDIL3 genes were considerably higher in osteosarcoma samples compared to the adjacent normal tissues (P=0.033 and P=0.026, respectively) (Figure 8A).

Quantitative polymerase chain reaction (qPCR) analysis of model genes in Mesenchymal Stem Cells (MSCs) and three different osteosarcoma cell lines (HOS, MG63, and U2OS) showed no significant differences in the expression levels of MLH1 and MTM1 genes between MSCs and the osteosarcoma cell lines. However, mRNA expression levels of EDIL3 and SQLE genes were markedly higher in osteosarcoma cell lines compared to MSCs. Furthermore, the CLTCL1 gene expression was significantly greater in MSCs than in the osteosarcoma cell lines (Figure 8B).

3.6 Expression levels of model genes encoding proteins

In adjacent normal tissues, the protein expression levels of CLTCL1 were significantly higher than those observed in osteosarcoma samples. Conversely, the protein expression levels of SQLE and EDIL3 were markedly elevated in osteosarcoma samples compared to the adjacent normal tissues (Figure 9A). Additionally, when compared to MSC cell lines, human osteosarcoma cell lines showed significantly higher protein expression levels of SQLE and EDIL3, whereas CLTCL1 demonstrated significantly higher protein expression levels in MSC cell lines than in human osteosarcoma cell lines (Figure 9B).

3.7 Impact of gene knockdown on osteosarcoma cell proliferative capacity

To evaluate the differential expression of CLTCL1, SQLE, and EDIL3 genes in OS cells (U2OS), individual gene silencing was

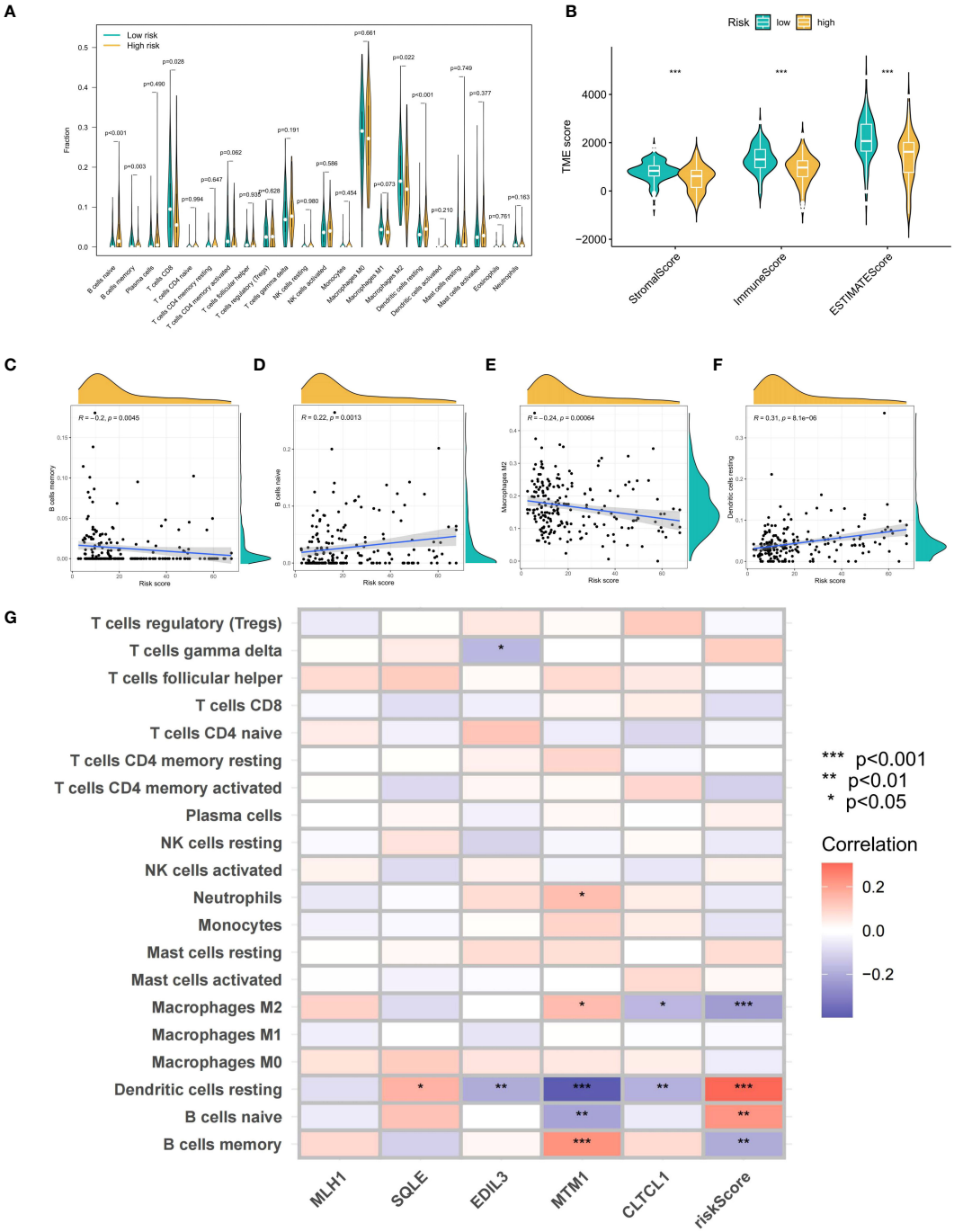

FIGURE 7
(A) shows violin plots generated by the CIBERSORT algorithm to compare the quantity of 22 immune cell types across groups with high and low scores. **(B)** Violin graphs showing statistically significant differences in stromal and estimate scores between PCDS-high and PCDS-low groups are produced using estimate analysis. **(C–F)** Correlation scatter graphs show how PCDS is related to four different kinds of immune cells. **(G)** A heatmap showing the correlation between immune cell abundance and five model gene expression levels. The following is a notation for the importance levels: The following p-value ranges: * < 0.05, ** < 0.01, and *** < 0.001. P-values are considered statistically significant when they are less than 0.05.

conducted, and the differences in proliferation capacity between the silenced and control groups were assessed. In the CCK8 assay, the optical density (OD) values for the si-CLTCL1 group significantly increased from day one, showing a notable contrast to the control group. Conversely, the OD values for the si-SQLE group significantly decreased from day two, demonstrating a marked difference from the control. Similarly, the si-EDIL3 group exhibited a significant reduction in OD values compared to the control group from day one onward (Figure 10A).

Results from the colony formation assay showed a significant increase in the number of OS cell clones in the CLTCL1 knockdown group compared to the control. In contrast, there was a substantial decrease in the number of OS cell clones in the SQLE knockdown group. Additionally, the EDIL3

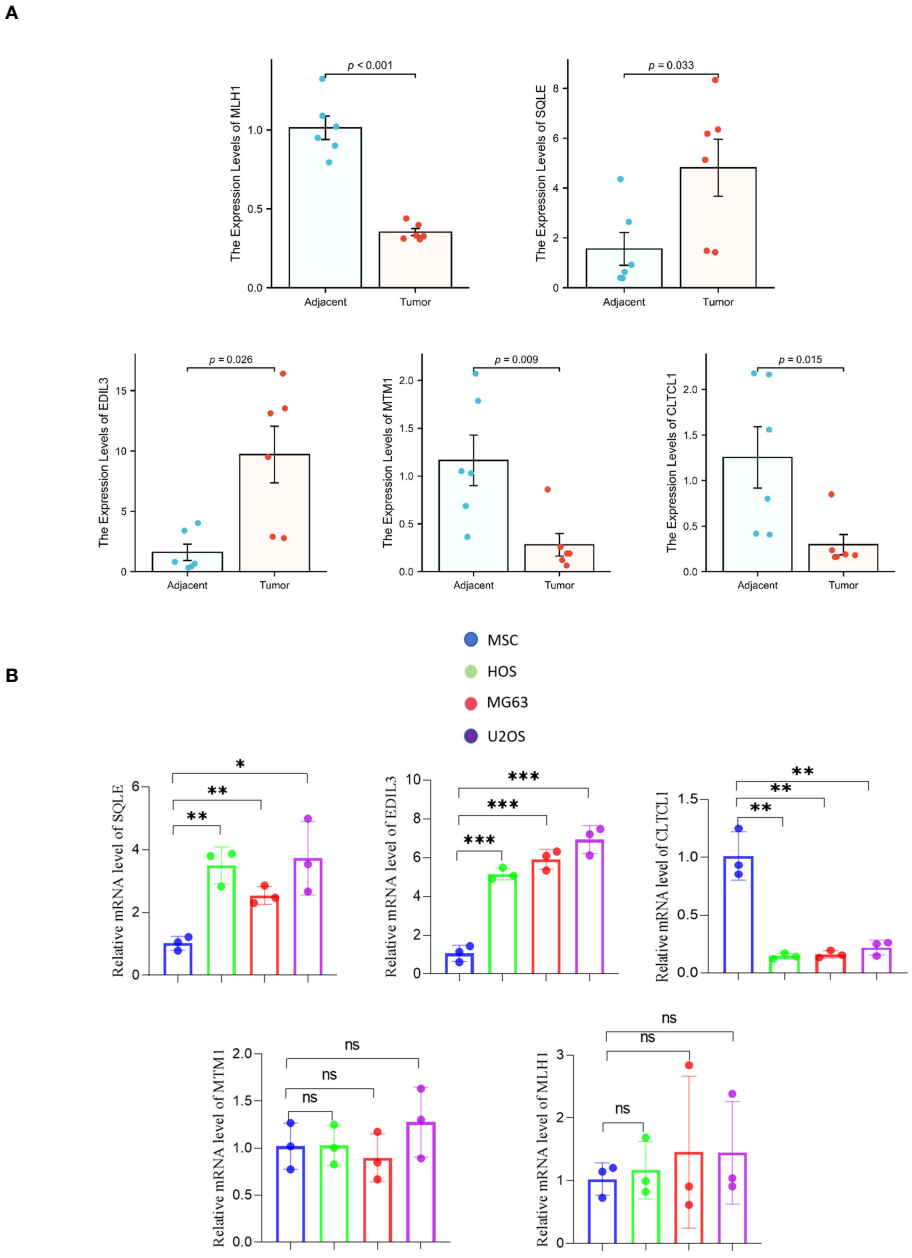

FIGURE 8
(A) The differential mRNA expression of the model gene between osteosarcoma samples and adjacent normal tissues. **(B)** A comparison is made between human osteosarcoma cell lines (HOS, MG63, U2OS) and mesenchymal stem cell (MSC) cell lines with respect to the mRNA expression of the model gene. The levels of significance are denoted as follows: *pvalue < 0.05, **pvalue < 0.01; ***pvalue < 0.001. P-values that are below 0.05 are deemed to be statistically significant.

knockdown group also displayed a reduction in OS cell clone numbers (Figure 10B).

3.8 Repercussions of gene knockdown on the migratory capacity of osteosarcoma cells

The results of the cell scratch assay revealed that, compared to the 0-hour time point, all four cell groups exhibited healing after 24 hours. Additionally, OS cells treated with CLTCL1 gene knockdown showed significantly enhanced migratory capacity compared to the control group, while those treated with SQLE and EDIL3 gene knockdown demonstrated weakened migratory abilities (Figure 11).

3.9 Repercussions of knockdown model genes on the apoptotic rate of osteosarcoma cells

The bar chart below depicts the comparison of apoptosis rates among different groups (Figure 12). Compared to the control group,

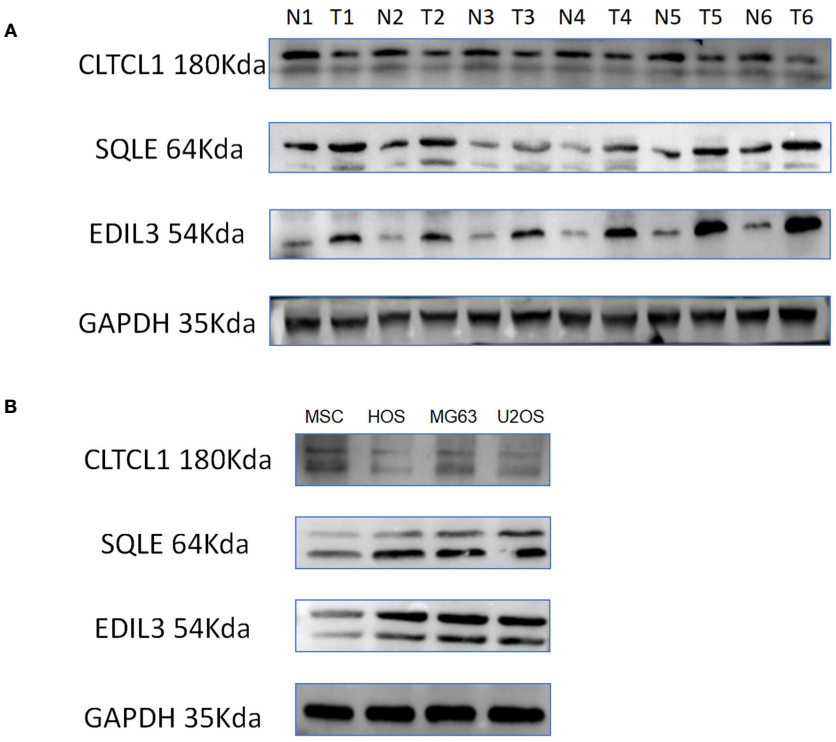

FIGURE 9
(A) The differences in the expression levels of CLTCL1, EDIL3, and SQLE proteins in 6 pairs of osteosarcomas and their adjacent normal tissues were demonstrated, with N representing normal tissues, T representing osteosarcoma tissues, and GAPDH protein being the internal reference protein. **(B)** The discrepancy between human osteosarcoma cell lines (HOS, MG63, U2OS) and MSC (mesenchymal stem cell) cell lines in terms of protein expression of the model gene is illustrated.

a significant decrease in the apoptosis rate of osteosarcoma cells was observed following CLTCL1 gene knockdown ($P<0.001$), while a substantial increase was noted after SQLE gene knockdown ($P<0.001$) and EDIL3 gene knockdown ($P<0.01$).

3.10 Single-cell analysis

The GSE162454 dataset, which includes six osteosarcoma samples, underwent various analyses, and the results were compared to ensure validity. Cell subclusters identified through Seurat dimensionality reduction clustering and annotated known cell types from singleR were visually represented using UMAP plots (Figures 13A, B). Bubble plots depicted the correspondence between cell subclusters (Figure 13D). Furthermore, UMAP and violin plots were utilized to illustrate the expression levels of model hub genes within individual cell subclusters (Figure 13C). A notable finding was the significant upregulation of EDIL3 expression, particularly in chondrocytes and tissue stem cells.

3.11 Identification of OS-PCDS-related anticancer medications

The violin plot clearly illustrates substantial differences in drug sensitivity between the high and low PCDS groups, highlighting a set of 34 drugs with divergent responses. Specifically, eight drugs, including Acetalax, BI-2536, Daporinad, and Lapatinib, showed increased sensitivity in the low PCDS group (Figure 14A). In contrast, 26 drugs, such as Axitinib, Dabrafenib, Entospletinib, and Mitoxantrone, exhibited enhanced sensitivity in the high PCDS group (Figure 14B).

4 Discussion

Osteosarcoma is a common and highly aggressive bone cancer that predominantly affects individuals during their teenage years (29).Despite progress in surgical techniques and chemotherapy, the 5-year survival rate for osteosarcoma patients has seen little improvement over the last twenty years (30, 31).The pathogenesis of osteosarcoma is exceedingly intricate, with single genes, protein markers, or conventional clinical data falling short in fully elucidating its complexity (32). These approaches are relatively rudimentary and overlook the heterogeneity inherent in osteosarcoma. Studies indicate that markers like B7-H3, GD2, and HER2, while closely linked to osteosarcoma pathogenesis, offer limited prognostic value when examined in isolation (33). As recent literature underscores, integrating molecular data is pivotal for enhancing prognosis (34). Traditional multigene models have been found lacking in exploring the interplay of genetic information in osteosarcoma. They overlook gene

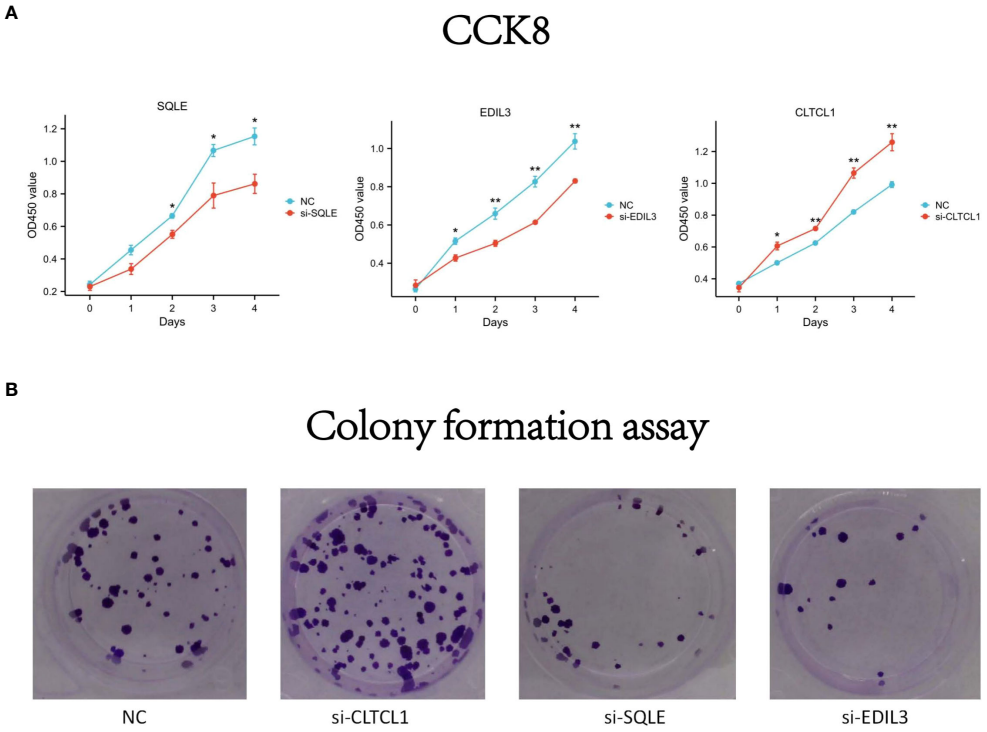

FIGURE 10
(A) The differences in optical density (OD) values over time compared to the negative control (NC) following knockdown of CLTCL1, SQLE, and EDIL3 gene expression levels in the CCK8 experiment. **(B)** The results of a colony formation assay. Four groups are depicted: negative control (NC), and cells treated with small interfering RNA (siRNA) against CLTCL1 (si-CLTCL1), SQLE (si-SQLE), and EDIL3 (si-EDIL3), respectively. The plates have been stained to visualize the colonies. Significance levels are indicated as *p value < 0.05, **p value < 0.01 ***p value < 0.001. P-values less than 0.05 are considered statistically significant.

interactions and pathway crosstalk, thus constraining their predictive capability (35). Recent research endeavors have aimed to employ multi-gene panels in osteosarcoma, emphasizing the imperative for more intricate and comprehensive investigations into the disease (36, 37). The fifteen forms of programmed cell death play a crucial role in cancer (38). Therefore, this study screened genes highly correlated with programmed cell death and osteosarcoma, unveiling numerous potential therapeutic targets,

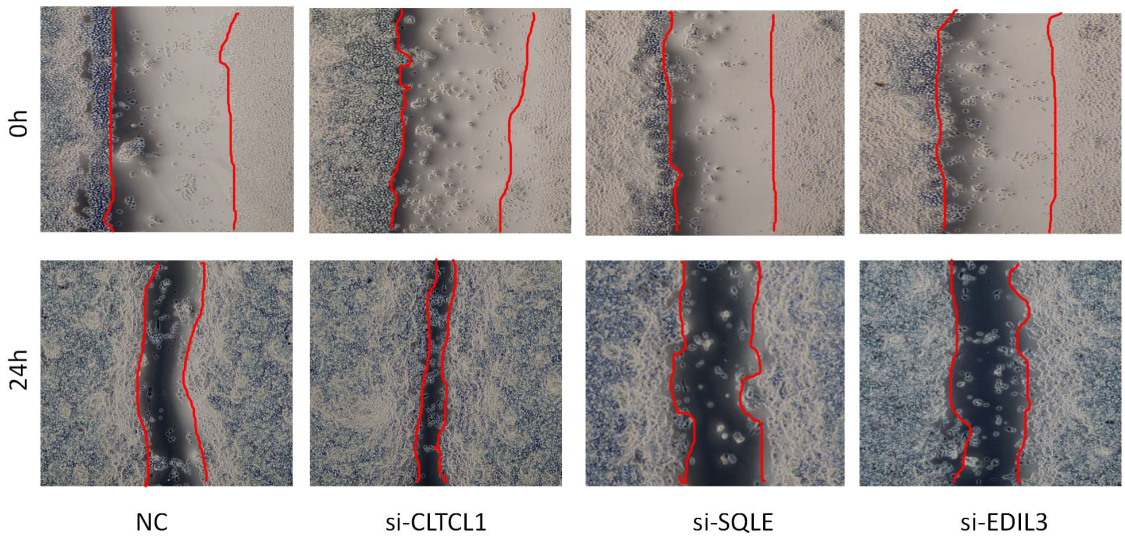

FIGURE 11
The image depicts a wound healing assay conducted to evaluate cell migration over a 24-hour period.

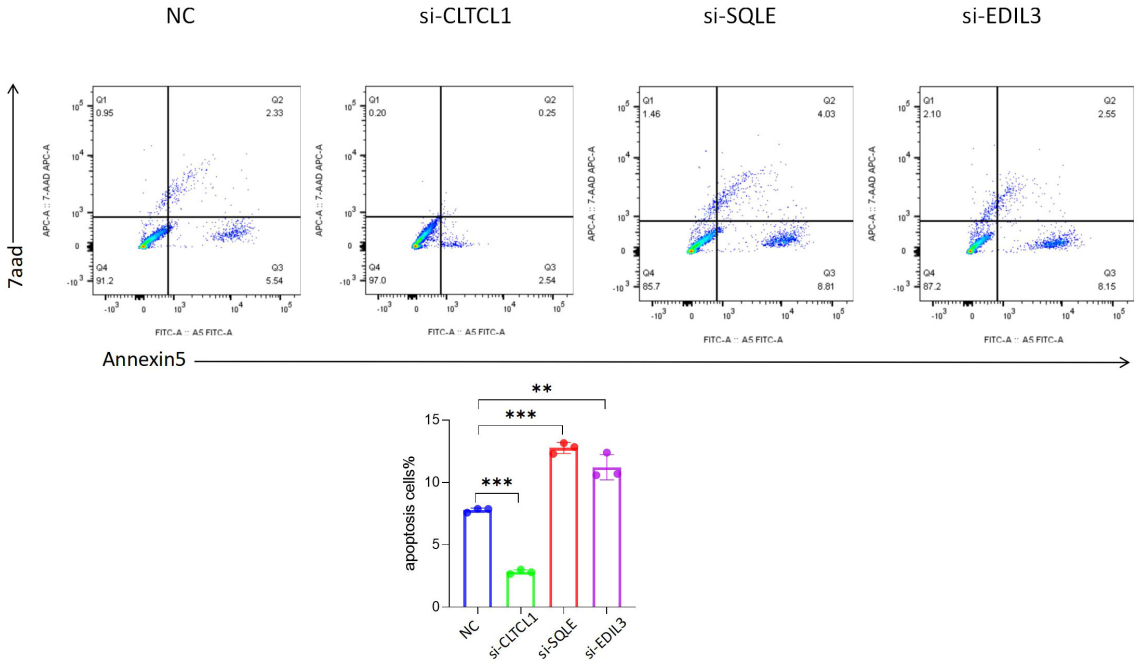

FIGURE 12
The results showed that compared with the negative control (NC), the apoptosis rate of osteosarcoma cells was changed after the expression levels of CLTCL1, SQLE and EDIL3 were reduced. Significance levels are indicated as *p value < 0.05, **p value < 0.01 ***p value < 0.001. P-values less than 0.05 are considered statistically significant.

pathways, and immune cells. By leveraging highly sophisticated machine learning integration, a prognostic model for osteosarcoma was constructed to furnish a more precise prognosis assessment for osteosarcoma patients.

Using unsupervised clustering, the osteosarcoma (OS) patient database was classified into A and B subtypes, revealing a poorer survival prognosis in subtype A. There were 19 genes with significant differential expression between the two subtypes, among which only one gene, SQLE, was highly expressed in subtype A. Previous research has demonstrated that the p53 transcription regulator can inhibit tumor cell growth through suppression of SQLE expression (39). Meanwhile, research has confirmed the role of CASP6, a gene highly expressed in subtype B, in reducing the risk of osteosarcoma patient prognosis (40). There was significant variation in immune cell infiltration abundance between the two subtypes. While 9 out of 33 immune cell types showed no significant distribution difference between subtypes, the remaining 24 immune cell types were significantly more abundant in subtype B. This suggests that the low abundance of immune cell infiltration is one of the factors contributing to the poorer survival prognosis in subtype A patients. Pathway enrichment analysis revealed differences between the two subtypes. Subtype A exhibited significant enrichment in the focal adhesion pathway, a finding consistent with previous studies that have associated this pathway with increased cancer cell growth and migration (41). In summary, by studying differences in survival prognosis between different subtypes, immune cell abundance, differential gene expression, and enriched pathways, we explore key factors leading to different survival prognoses in OS patients, providing a foundation for subsequent research on molecular targeted therapy for osteosarcoma.

In recent years, various prognostic models for osteosarcoma have been developed, mostly constructed using single machine learning algorithms and single forms of cell death to build prognostic risk models for osteosarcoma (42–44). However, the molecular characteristics of osteosarcoma are extremely complex, and using single screening criteria cannot accurately predict the prognosis of osteosarcoma patients. A study utilized multiple machine learning integration to construct a prognostic model for ovarian cancer and established a prognostic model for breast cancer patients using various forms of cell death (45, 46). However, these methods have not been applied to osteosarcoma disease. Samples of osteosarcoma patients and 15 sets of genes associated with PCD were extracted from the database. Prior to filtering out genes associated with prognosis, genes differentially expressed between osteosarcoma samples and adjacent normal tissues were screened. These genes were then intersected with PCD genes. The model utilized in this investigation was constructed using this gene set as its foundation.

As demonstrated in the text, our study's machine learning integration model exhibits significant improvements compared to traditional methods. The use of multiple integrated machine learning algorithms resulted in improved accuracy of prognostic predictions for osteosarcoma, as evidenced by higher concordance index scores compared to traditional methods. The experimental results are consistent with findings from other studies, which have used similar methodologies and analytical frameworks (47–50). OS samples from all datasets are classified by the OS-PCDS into high-

10.3389/fimmu.2024.1427661

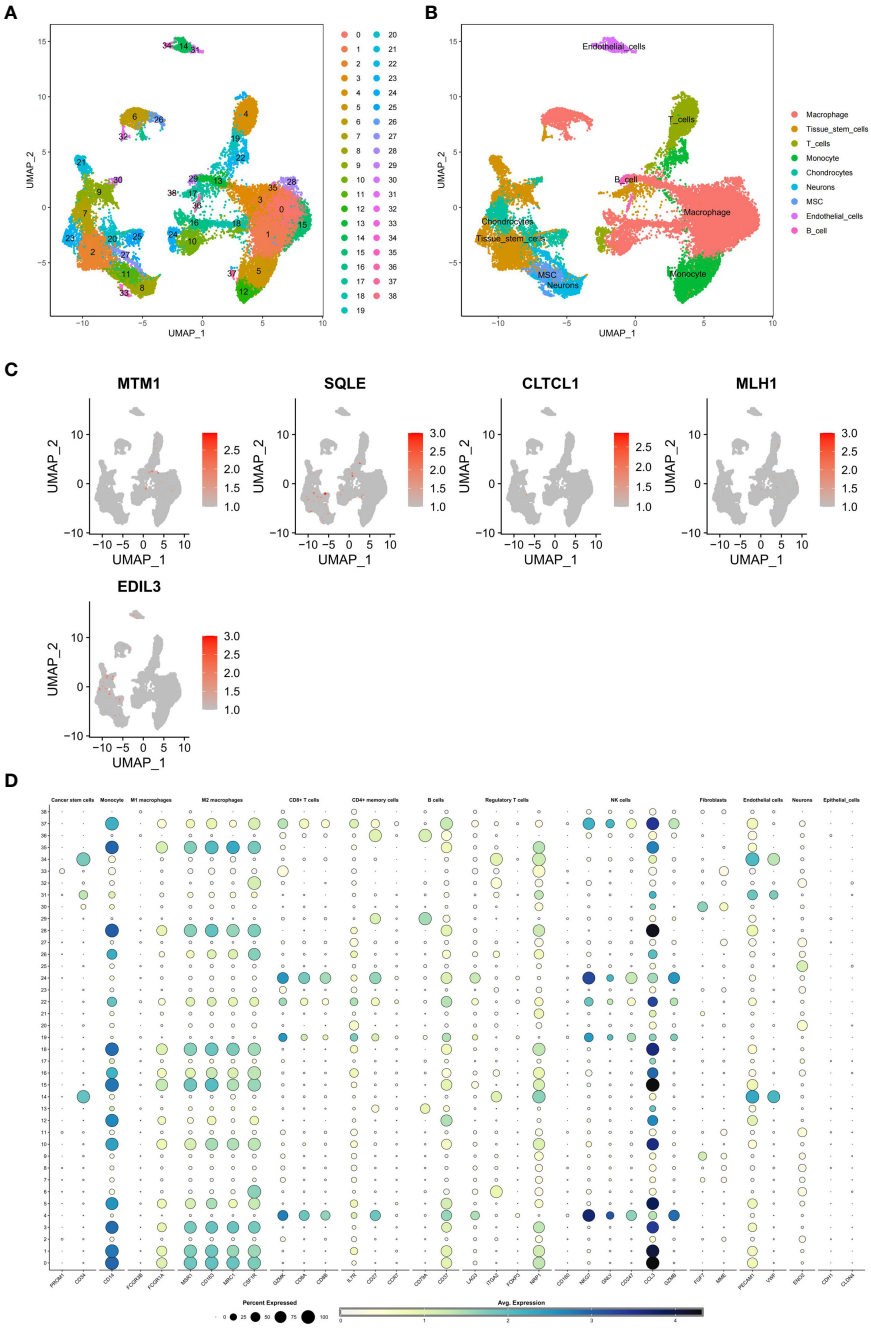

FIGURE 13
(A, B) A single-cell analysis was conducted on the GSE162454 dataset in order to examine the processes of dimensionality reduction and clustering of single-cell data. **(C)** To visually represent the expression levels of critical genes in various cell subgroups within the model, UMAP plots were employed. The dot plot illustrated the relationship between subgroups of cells. **(D)** The bubble map illustrates the expression levels of key genes in different cell subpopulations.

risk and low-risk groups, with survival analysis indicating that a lower prognosis is associated with the low-risk group and a higher prognosis is associated with the high-risk group. ROC curve analysis further validates the robustness of OS-PCDS. After undergoing internal validation, the predictive performance of OS-PCDS was compared to that of 38 other prognostic models for osteosarcoma based on transcriptomes that were published within the last five years. In order to mitigate discrepancies that may have emerged from sources other than the TARGET and GEO databases, all models underwent training and validation using homogeneous datasets. The results demonstrate that our model exhibits stronger stability and accuracy compared to existing prognostic tools, thus confirming its significant advantage and potential utility in clinical practice.

The machine learning integration selected five model genes: MLH1, MTM1, CLTCL1, EDIL3, and SQLE. In recent years, the

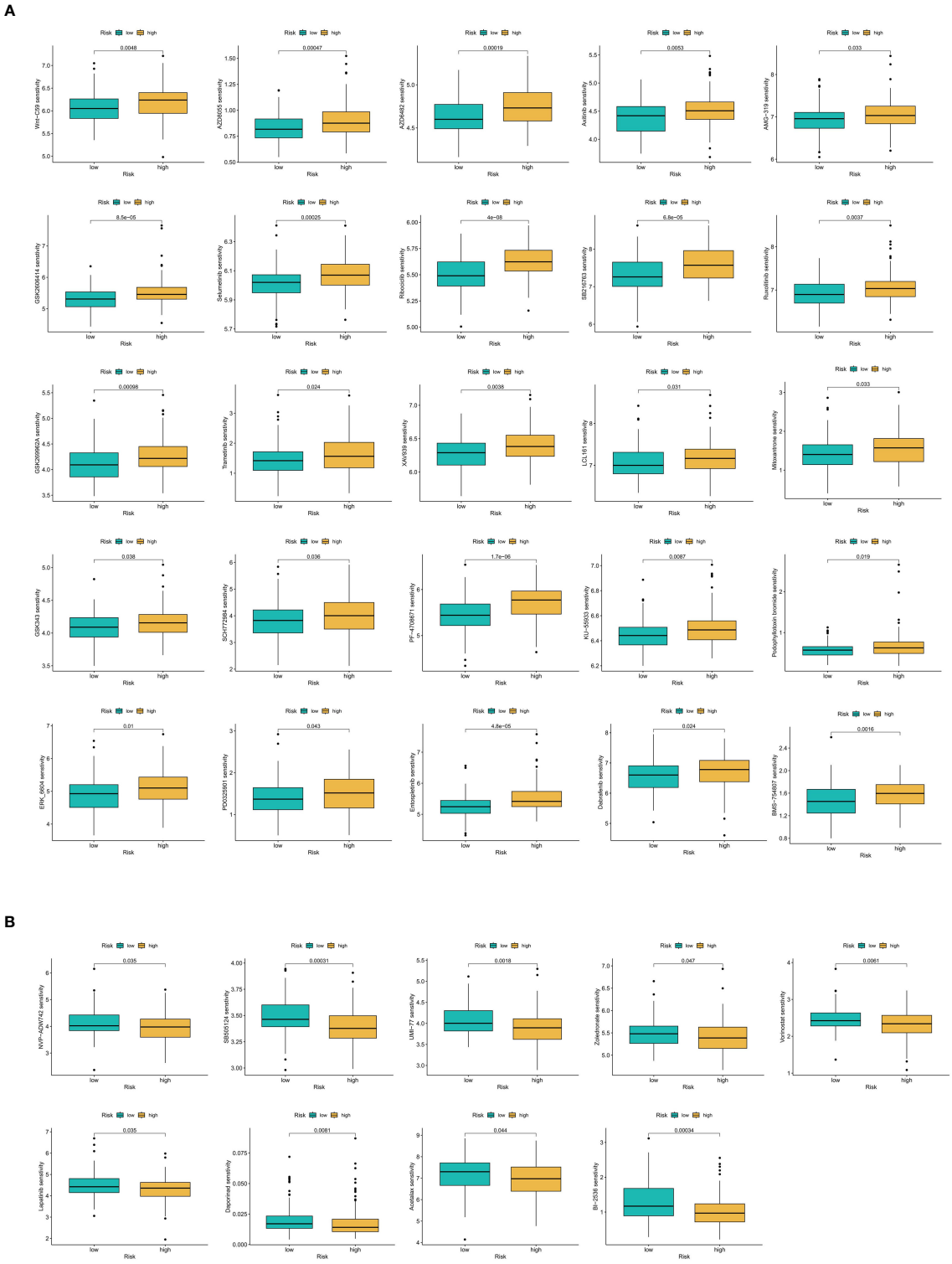

FIGURE 14
(A) Anticancer drug screening in relation to model scores. Twenty-five compounds demonstrate increased sensitivity in the OS-PCDS-high group. **(B)** Nine drugs show greater sensitivity in the OS-PCDS-low group. P-values less than 0.001 are considered statistically significant.

roles of MLH1 and SQLE genes in osteosarcoma have garnered attention. Recent studies have indicated an association between the expression level of MLH1 and the prognosis of osteosarcoma patients. Specifically, the expression level of MLH1 shows a negative correlation with patients' risk scores, suggesting that higher MLH1 expression is associated with lower risk scores and better prognosis (51). Kun reported that SQLE can promote the proliferation and migration of osteosarcoma cells (52). These studies suggest that MLH1 may act as a protective factor, with higher expression potentially reducing the risk and improving the

prognosis of osteosarcoma patients, while SQLE may serve as a risk factor, with its higher expression possibly increasing the prognosis risk for osteosarcoma patients. Visualization of the expression levels of model genes in osteosarcoma samples and adjacent normal tissues from databases revealed that MLH1 was downregulated in osteosarcoma samples but significantly upregulated in adjacent normal tissues, whereas SQLE was significantly upregulated in osteosarcoma samples but downregulated in adjacent normal tissues. The expression patterns of MLH1 and SQLE suggest differential roles in osteosarcoma pathology. MLH1 was downregulated in osteosarcoma samples, potentially indicating a tumor suppressive function, whereas SQLE was upregulated, suggesting a role in tumor progression. The experimental results align with the conclusions of previous studies, suggesting that MLH1 and SQLE genes could serve as biomarkers for osteosarcoma prognosis and therapeutic targets. However, the precise mechanisms by which these genes influence osteosarcoma development remain to be fully elucidated. Various cellular experiments were conducted to elucidate the functional roles of the identified genes and their impacts on osteosarcoma cells. Specifically, the mRNA and protein expression levels of CLTCL1 were significantly reduced in osteosarcoma cells, indicating its potential role as a tumor suppressor gene. Bioinformatics analysis suggested that CLTCL1 might exert protective effects in osteosarcoma. Inhibition of CLTCL1 expression led to increased proliferation and migration of osteosarcoma cells, along with a significant reduction in apoptosis, validating its role as a protective molecular marker.

Further investigation into the regulatory mechanisms of risk genes, such as EDIL3 and SQLE, revealed that these genes are potential candidates for therapeutic targeting, as indicated by their significant role in the progression and prognosis of osteosarcoma. Downregulation of EDIL3 and SQLE in the U2OS osteosarcoma cell line was essential for exploring potential treatment strategies and understanding osteosarcoma pathology. Bioinformatics analysis indicated a positive correlation between the high expression of SQLE and EDIL3 and osteosarcoma cell development. Knockdown experiments showed that reduced expression of these genes led to a significant decrease in proliferation and migration abilities, along with an increase in apoptosis rates, suggesting their roles as risk factors that promote tumor development.

Additionally, the differential expression analysis using the limma package and subsequent gene set enrichment analyses (GSEA and GSVA) provided insights into the functional pathways and regulatory networks involving these differentially expressed genes. For instance, the upregulation of genes in the focal adhesion pathway in subtype A may promote cancer cell growth and migration, while the enriched immune-related pathways in subtype B indicate potential immunogenic responses. The mechanistic insights from these analyses highlight the complex interplay between gene expression patterns and osteosarcoma progression, emphasizing the need for further research to uncover the underlying biological mechanisms and therapeutic implications.

By integrating these findings, we can better understand the biological significance of the differentially expressed genes and their roles in osteosarcoma development and progression. This comprehensive approach lays the groundwork for future investigations into targeted therapies and prognostic biomarkers in osteosarcoma, enhancing the potential for personalized treatment strategies.

Risk genes are often utilized in the development of therapeutic targets. In our research, EDIL3 and SQLE may also serve as potential therapeutic targets. Therefore, we validated their functions by downregulating their expression levels in the human osteosarcoma cell line U2OS. This approach is essential for investigating potential treatment strategies and advancing our understanding of osteosarcoma pathology. In osteosarcoma cells, both the mRNA and protein expression levels of SQLE and EDIL3 genes show significant elevation. Combining the bioinformatics analysis results from this study, SQLE and EDIL3 are likely to be genes associated with risk, indicating a positive correlation between their high expression and the development of osteosarcoma cells. Knockdown of SQLE and EDIL3 gene expression in osteosarcoma cells resulted in a significant decrease in proliferation and migration abilities, accompanied by a notable increase in apoptosis rate. These findings suggest that SQLE and EDIL3 genes serve as risk factors in osteosarcoma, promoting tumor development.

In osteosarcoma cells, the mRNA expression levels of MTM1 and MLH1 genes were significantly decreased, suggesting their functions may be inhibited in these cells. Although further experimental validation of these two genes was not conducted in this study, combining the predictive results suggests that MTM1 and MLH1 genes are likely negatively correlated with tumor development. This conclusion awaits further experimental investigation.

While the prognostic model for osteosarcoma developed in this study demonstrates remarkably high predictive accuracy, it is imperative to acknowledge the inherent limitations of this research methodology. One significant constraint lies in the retrospective nature of the osteosarcoma patient data utilized, which were primarily sourced from the TARGET and GEO databases. This reliance on retrospective data may limit the generalizability of the findings to broader clinical contexts. Additionally, the variability in patient demographics and treatment protocols across different datasets could introduce biases that affect the model's performance.

To conclusively ascertain the efficacy and robustness of the prognostic model, further validation through prospective clinical trials is essential. These trials would provide more controlled and comprehensive data, allowing for a more accurate assessment of the model's predictive capabilities. Moreover, prospective studies could help in understanding how the model performs across diverse patient populations and in different clinical settings, thereby enhancing its applicability and reliability.

Recognizing these limitations aids in a fair assessment of the study's scope and practicality, thereby furnishing crucial insights for subsequent inquiries. Further exploration of the molecular mechanisms governed by the genes identified in the model may unveil previously undiscovered therapeutic targets, potentially advancing more effective approaches to treating osteosarcoma. For instance, investigating the regulatory pathways and interactions of

these genes could provide deeper insights into their roles in tumor progression and response to treatment. This understanding could lead to the development of targeted therapies that are more precise and effective in managing osteosarcoma.

In summary, while the current study provides a robust framework for prognostic modeling in osteosarcoma, addressing its limitations through future research and validation efforts is crucial for translating these findings into clinical practice. Continuous refinement and validation of the model will ensure its long-term utility and effectiveness in improving patient outcomes.

5 Conclusion

This study integrated multiple machine learning algorithms and selected five model genes, including CLTCL1, SQLE, EDIL3, MTM1, and MLH1. Utilizing these five genes, a programmed cell death-related osteosarcoma prognostic risk model was constructed, enabling a more precise and comprehensive analysis of prognostic factors in osteosarcoma patients. According to all experimental results, CLTCL1, MTM1, and MLH1 are likely tumor suppressor genes exerting inhibitory effects on osteosarcoma development, while SQLE and EDIL3 may function as targets promoting tumor proliferation, thus presenting new therapeutic potential. Further research, including *in vivo* studies and clinical trials, is crucial for validating the roles of these genes in osteosarcoma progression and assessing their potential as therapeutic targets.

Data availability statement

The datasets presented in this study can be found in online repositories. The names of the repository/repositories and accession number(s) can be found in the article/Supplementary Material.

Ethics statement

The studies involving humans were approved by Ethics Review Committee of Affiliated Zhongshan Hospital Of Dalian University. The studies were conducted in accordance with the local legislation and institutional requirements. The participants provided their written informed consent to participate in this study.

Author contributions

Y-CJ: Writing – original draft, Writing – review & editing. Q-TX: Writing – review & editing, Conceptualization, Software, Visualization, Writing – original draft. H-BW: Data curation, Visualization, Writing – review & editing. S-YR: Data curation, Validation, Writing – original draft. YZ: Writing – review & editing, Formal analysis, Supervision.

Funding

The author(s) declare that no financial support was received for the research, authorship, and/or publication of this article.

Conflict of interest

The authors declare that the research was conducted in the absence of any commercial or financial relationships that could be construed as a potential conflict of interest.

Publisher's note

All claims expressed in this article are solely those of the authors and do not necessarily represent those of their affiliated organizations, or those of the publisher, the editors and the reviewers. Any product that may be evaluated in this article, or claim that may be made by its manufacturer, is not guaranteed or endorsed by the publisher.

Supplementary material

The Supplementary Material for this article can be found online at: https://www.frontiersin.org/articles/10.3389/fimmu.2024.1427661/full#supplementary-material

SUPPLEMENTARY TABLE 1
A curated compilation of 61 published transcriptomic osteosarcoma prognostic models.

SUPPLEMENTARY TABLE 2
Sequence information of qPCR primers for the five model genes.

References

1. Shoaib Z, Fan TM, Irudayaraj JMK. Osteosarcoma mechanobiology and therapeutic targets. *Br J Pharmacol.* (2022) 179:201–17. doi: 10.1111/bph.15713

2. Chen C, Xie L, Ren T, Huang Y, Xu J, Guo W. Immunotherapy for osteosarcoma: Fundamental mechanism. *rationale Recent breakthroughs Cancer Lett.* (2021) 500:1–10. doi: 10.1016/j.canlet.2020.12.024

3. Smrke A, Anderson PM, Gulia A, Gennatas S, Huang PH, Jones RL. Future directions in the treatment of osteosarcoma, cells, 10. *Future Directions in the Treatment of Osteosarcoma.* (2021) 10(1):172. doi: 10.3390/cells10010172

4. Atiye J, Wolf M, Kaur S, Monni O, Böhling T, Kivioja A, et al. Gene amplifications in osteosarcoma-CGH microarray analysis. *Genes Chromosomes Cancer.* (2005) 42:158–63. doi: 10.1002/gcc.20120

5. Sadikovic B, Yoshimoto M, Chilton-MacNeill S, Thorner P, Squire JA, Zielenska M. Identification of interactive networks of gene expression associated with osteosarcoma oncogenesis by integrated molecular profiling. *Hum Mol Genet.* (2009) 18:1962–75. doi: 10.1093/hmg/ddp117

6. Li H, Shen X, Ma M, Liu W, Yang W, Wang P, et al. ZIP10 drives osteosarcoma proliferation and chemoresistance through ITGA10-mediated activation of the PI3K/AKT pathway. *J Exp Clin Cancer Res.* (2021) 40:340. doi: 10.1186/s13046-021-02146-8

7. Wu W, Zhang Z, Jing D, Huang X, Ren D, Shao Z, et al. SGLT2 inhibitor activates the STING/IRF3/IFN-β pathway and induces immune infiltration in osteosarcoma. *Cell Death Dis.* (2022) 13:523. doi: 10.1038/s41419-022-04980-w

8. Yuan B, Shi K, Zha J, Cai Y, Gu Y, Huang K, et al. Nuclear receptor modulators inhibit osteosarcoma cell proliferation and tumour growth by regulating the mTOR signaling pathway. *Cell Death Dis*. (2023) 14:51. doi: 10.1038/s41419-022-05545-7

9. Zhang Q, Fan X, Zhang X, Ju S. Ferroptosis in tumors and its relationship to other programmed cell death: role of non-coding RNAs. *J Transl Med*. (2023) 21:514. doi: 10.1186/s12967-023-04370-6

10. Wang M, Yu F, Zhang Y, Li P. Programmed cell death in tumor immunity: mechanistic insights and clinical implications. *Front Immunol*. (2023) 14:1309635. doi: 10.3389/fimmu.2023.1309635

11. Wang Y, Ji Y, Hu Z, Jiang H, Zhu F, Yuan H, et al. Riccardin D induces cell death by activation of apoptosis and autophagy in osteosarcoma cells. *Toxicol In Vitro*. (2013) 27:1928–36. doi: 10.1016/j.tiv.2013.06.001

12. Hadian K, Stockwell BR. The therapeutic potential of targeting regulated non-apoptotic cell death. *Nat Rev Drug Discovery*. (2023) 22:723–42. doi: 10.1038/s41573-023-00749-8

13. Gao W, Wang X, Zhou Y, Wang X, Yu Y. Autophagy, ferroptosis, pyroptosis, and necroptosis in tumor immunotherapy. *Signal Transduct Target Ther*. (2022) 7:196. doi: 10.1038/s41392-022-01046-3

14. Xie J, Yang Y, Gao Y, He J. Cuproptosis: mechanisms and links with cancers. *Mol Cancer*. (2023) 22:46. doi: 10.1186/s12943-023-01732-y

15. Onorati AV, Dyczynski M, Ojha R, Amaravadi RK. Targeting autophagy in cancer. *Cancer*. (2018) 124:3307–18. doi: 10.1002/cncr.31335

16. Zhou Y, Liu L, Tao S, Yao Y, Wang Y, Wei Q, et al. Parthanatos and its associated components: Promising therapeutic targets for cancer. *Pharmacol Res*. (2021) 163:105299. doi: 10.1016/j.phrs.2020.105299

17. Rao Z, Zhu Y, Yang P, Chen Z, Xia Y, Qiao C, et al. Pyroptosis in inflammatory diseases and cancer. *Theranostics*. (2022) 12:4310–29. doi: 10.7150/thno.71086

18. Zeng C, Zeng B, Dong C, Liu J, Xing F. Rho-ROCK signaling mediates entotic cell death in tumor. *Cell Death Discovery*. (2020) 6:4. doi: 10.1038/s41420-020-0238-7

19. Skendros P, Mitroulis I, Ritis K. Autophagy in neutrophils: from granulopoiesis to neutrophil extracellular traps. *Front Cell Dev Biol*. (2018) 6:109. doi: 10.3389/fcell.2018.00109

20. Tang D, Kang R, Berghe TV, Vandenabeele P, Kroemer G. The molecular machinery of regulated cell death. *Cell Res*. (2019) 29:347–64. doi: 10.1038/s41422-019-0164-5

21. Taddei ML, Giannoni E, Fiaschi T, Chiarugi P. Anoikis: an emerging hallmark in health and diseases. *J Pathol*. (2012) 226:380–93. doi: 10.1002/path.3000

22. Kroemer G, Galassi C, Zitvogel L, Galluzzi L. Immunogenic cell stress and death. *Nat Immunol*. (2022) 23:487–500. doi: 10.1038/s41590-022-01132-2

23. Zheng P, Zhou C, Ding Y, Duan S. Disulfidptosis: a new target for metabolic cancer therapy. *J Exp Clin Cancer Res*. (2023) 42:103. doi: 10.1186/s13046-023-02675-4

24. Yuan Q, Ren J, Wang Z, Ji L, Deng D, Shang D. Identification of the real hub gene and construction of a novel prognostic signature for pancreatic adenocarcinoma based on the weighted gene co-expression network analysis and least absolute shrinkage and selection operator algorithms. *Front Genet*. (2021) 12:692953. doi: 10.3389/fgene.2021.692953

25. Arashi M, Roozbeh M, Hamzah NA, Gasparini M. Ridge regression and its applications in genetic studies. *PloS One*. (2021) 16:e0245376. doi: 10.1371/journal.pone.0245376

26. Basu A, Mitra R, Liu H, Schreiber SL, Clemons PA. RWEN: response-weighted elastic net for prediction of chemosensitivity of cancer cell lines. *Bioinformatics*. (2018) 34:3332–9. doi: 10.1093/bioinformatics/bty199

27. Scholl S, Roufai DB, Chérif LL, Kamal M. RAIDS atlas of significant genetic and protein biomarkers in cervical cancer. *J Gynecol Oncol*. (2023) 34:e74. doi: 10.3802/jgo.2023.34.e74

28. Lynch CM, Abdollahi B, Fuqua JD, de Carlo AR, Bartholomai JA, Balgemann RN, et al. Prediction of lung cancer patient survival via supervised machine learning classification techniques. *Int J Med Inform*. (2017) 108:1–8. doi: 10.1016/j.ijmedinf.2017.09.013

29. Kager L, Tamamyan G, Bielack S. Novel insights and therapeutic interventions for pediatric osteosarcoma. *Future Oncol*. (2017) 13:357–68. doi: 10.2217/fon-2016-0261

30. Wang Z, He Z, Wan J, Chen A, Cheng P, Zhu W. EphA2-specific microvesicles derived from tumor cells facilitate the targeted delivery of chemotherapeutic drugs for osteosarcoma therapy. *J Nanobiotechnology*. (2024) 22:89. doi: 10.1186/s12951-024-02372-0

31. Simpson E, Brown HL. Understanding osteosarcomas. *Jaapa*. (2018) 31:15–9. doi: 10.1097/01.JAA.0000541477.24116.8d

32. Ma C, Nie XG, Wang YL, Liu XH, Liang X, Zhou QL, et al. CBX3 predicts an unfavorable prognosis and promotes tumorigenesis in osteosarcoma. *Mol Med Rep*. (2019) 19:4205–12. doi: 10.3892/mmr

33. Gill J, Gorlick R. Advancing therapy for osteosarcoma. *Nat Rev Clin Oncol*. (2021) 18:609–24. doi: 10.1038/s41571-021-00519-8

34. Fountzilas E, Tsimberidou AM, Vo HH, Kurzrock R. Clinical trial design in the era of precision medicine. *Genome Med*. (2022) 14:101. doi: 10.1186/s13073-022-01102-1

35. Thayanithy V, Sarver AL, Kartha RV, Li L, Angstadt AY, Breen M, et al. Perturbation of 14q32 miRNAs-cMYC gene network in osteosarcoma. *Bone*. (2012) 50:171–81. doi: 10.1016/j.bone.2011.10.012

36. Lei T, Qian H, Lei P, Hu Y. Ferroptosis-related gene signature associates with immunity and predicts prognosis accurately in patients with osteosarcoma. *Cancer Sci*. (2021) 112:4785–98. doi: 10.1111/cas.15131

37. Zhao X, Zhang J, Liu J, Chen Q, Cai C, Miao X, et al. Identification of mitochondrial-related signature and molecular subtype for the prognosis of osteosarcoma. *Aging (Albany NY)*. (2023) 15:12794–816. doi: 10.18632/aging.v15i22

38. Liu J, Hong M, Li Y, Chen D, Wu Y, Hu Y. Programmed cell death tunes tumor immunity. *Front Immunol*. (2022) 13:847345. doi: 10.3389/fimmu.2022.847345

39. Sun H, Li L, Li W, Yang F, Zhang Z, Liu Z, et al. p53 transcriptionally regulates SQLE to repress cholesterol synthesis and tumor growth. *EMBO Rep*. (2021) 22:e52537. doi: 10.15252/embr.202152537

40. Yang M, Zheng H, Su Y, Xu K, Yuan Q, Cai Y, et al. Novel pyroptosis-related lncRNAs and ceRNAs predict osteosarcoma prognosis and indicate immune microenvironment signatures. *Heliyon*. (2023) 9:e21503. doi: 10.1016/j.heliyon.2023.e21503

41. Lin X, Zhuang S, Chen X, Du J, Zhong L, Ding J, et al. lncRNA ITGB8-AS1 functions as a ceRNA to promote colorectal cancer growth and migration through integrin-mediated focal adhesion signaling. *Mol Ther*. (2022) 30:688–702. doi: 10.1016/j.ymthe.2021.08.011

42. Wang H, Li J, Li X. Construction and validation of an oxidative-stress-related risk model for predicting the prognosis of osteosarcoma. *Aging (Albany NY)*. (2023) 15:4820–43. doi: 10.18632/aging.204764

43. Hua L, Lei P, Hu Y. Construction and validation model of necroptosis-related gene signature associates with immunity for osteosarcoma patients. *Sci Rep*. (2022) 12:15893. doi: 10.1038/s41598-022-20217-4

44. Yang J, Zhang J, Na S, Wang Z, Li H, Su Y, et al. Integration of single-cell RNA sequencing and bulk RNA sequencing to reveal an immunogenic cell death-related 5-gene panel as a prognostic model for osteosarcoma. *Front Immunol*. (2022) 13:994034. doi: 10.3389/fimmu.2022.994034

45. Boehm KM, Aherne EA, Ellenson L, Nikolovski I, Alghamdi M, Vázquez-García I, et al. Multimodal data integration using machine learning improves risk stratification of high-grade serous ovarian cancer. *Nat Cancer*. (2022) 3:723–33. doi: 10.1038/s43018-022-00388-9

46. Zou Y, Xie J, Zheng S, Liu W, Tang Y, Tian W, et al. Leveraging diverse cell-death patterns to predict the prognosis and drug sensitivity of triple-negative breast cancer patients after surgery. *Int J Surg*. (2022) 107:106936. doi: 10.1016/j.ijsu.2022.106936

47. Kawaguchi K, Miyama K, Endo M, Bise R, Kohashi K, Hirose T, et al. Viable tumor cell density after neoadjuvant chemotherapy assessed using deep learning model reflects the prognosis of osteosarcoma. *NPJ precis oncol*. (2024) 8:16. doi: 10.1038/s41698-024-00515-y

48. Huang X, Chen Z, Xiang X, Liu Y, Long X, Li K, et al. Comprehensive multi-omics analysis of the m7G in pan-cancer from the perspective of predictive, preventive, and personalized medicine. *Epma J*. (2022) 13:671–97. doi: 10.1007/s13167-022-00305-1

49. Li GQ, Wang YK, Zhou H, Jin LG, Wang CY, Albahde M, et al. Application of immune infiltration signature and machine learning model in the differential diagnosis and prognosis of bone-related Malignancies. *Front Cell Dev Biol*. (2021) 9:630355. doi: 10.3389/fcell.2021.630355

50. Xu QT, Qiang JK, Huang ZY, Jiang WJ, Cui XM, Hu RH, et al. Integration of machine learning for developing a prognostic signature related to programmed cell death in colorectal cancer, Environ Toxicol. (2024) 39(5):2908–26. doi: 10.1002/tox.24157

51. Liu Z, Zhong Y, Meng S, Liao Q, Chen W. Identification of a seven-gene prognostic signature using the gene expression profile of osteosarcoma. *Ann Transl Med*. (2022) 10:53. doi: 10.21037/atm

52. Zheng K, Hou Y, Zhang Y, Wang F, Sun A, Yang D. Molecular features and predictive models identify the most lethal subtype and a therapeutic target for osteosarcoma. *Front Oncol*. (2023) 13:1111570. doi: 10.3389/fonc.2023.1111570

frontiers | Frontiers in Immunology

TYPE Original Research
PUBLISHED 23 July 2024
DOI 10.3389/fimmu.2024.1424950

Check for updates

OPEN ACCESS

EDITED BY
Wantao Wu,
Central South University, China

REVIEWED BY
Bo Li,
Sun Yat-sen University, China
Zhigang Ji,
Peking Union Medical College Hospital, China
Yi He,
Huazhong University of Science and Technology, China

*CORRESPONDENCE
Xiaohua Guo
guoxh_1981@126.com

RECEIVED 29 April 2024
ACCEPTED 08 July 2024
PUBLISHED 23 July 2024

CITATION
Shi S, Zhang L and Guo X (2024) Comprehensive investigation of tumor immune microenvironment and prognostic biomarkers in osteosarcoma through integrated bulk and single-cell transcriptomic analysis.
Front. Immunol. 15:1424950.
doi: 10.3389/fimmu.2024.1424950

COPYRIGHT
© 2024 Shi, Zhang and Guo. This is an open-access article distributed under the terms of the Creative Commons Attribution License (CC BY). The use, distribution or reproduction in other forums is permitted, provided the original author(s) and the copyright owner(s) are credited and that the original publication in this journal is cited, in accordance with accepted academic practice. No use, distribution or reproduction is permitted which does not comply with these terms.

Comprehensive investigation of tumor immune microenvironment and prognostic biomarkers in osteosarcoma through integrated bulk and single-cell transcriptomic analysis

Shaoyan Shi, Li Zhang and Xiaohua Guo*

Honghui Hospital, Xi'an Jiaotong University, Xi'an Honghui Hospital North District, Xi'an, Shanxi, China

Osteosarcoma (OS) is an aggressive and highly lethal bone tumor, highlighting the urgent need for further exploration of its underlying mechanisms. In this study, we conducted analyses utilizing bulk transcriptome sequencing data of OS and healthy control samples, as well as single cell sequencing data, obtained from public databases. Initially, we evaluated the differential expression of four tumor microenvironment (TME)-related gene sets between tumor and control groups. Subsequently, unsupervised clustering analysis of tumor tissues identified two significantly distinct clusters. We calculated the differential scores of the four TME-related gene sets for Clusters 1 (C1) and 2 (C2), using Gene Set Variation Analysis (GSVA, followed by single-variable Cox analysis. For the two clusters, we performed survival analysis, examined disparities in clinical-pathological distribution, analyzed immune cell infiltration and immune evasion prediction, assessed differences in immune infiltration abundance, and evaluated drug sensitivity. Differentially expressed genes (DEGs) between the two clusters were subjected to Gene Ontology (GO) and Gene Set Enrichment Analysis (GSEA). We conducted Weighted Gene Co-expression Network Analysis (WGCNA) on the TARGET-OS dataset to identify key genes, followed by GO enrichment analysis. Using LASSO and multiple regression analysis we conducted a prognostic model comprising eleven genes (ALOX5AP, CD37, BIN2, C3AR1, HCLS1, ACSL5, CD209, FCGR2A, CORO1A, CD74, CD163) demonstrating favorable diagnostic efficacy and prognostic potential in both training and validation cohorts. Using the model, we conducted further immune, drug sensitivity and enrichment analysis. We performed dimensionality reduction and annotation of cell subpopulations in single cell sequencing analysis, with expression

profiles of relevant genes in each subpopulation analyzed. We further substantiated the role of ACSL5 in OS through a variety of wet lab experiments. Our study provides new insights and theoretical foundations for the prognosis, treatment, and drug development for OS patients.

KEYWORDS

osteosarcoma, tumor microenvironment, transcriptome sequencing, prognostic model, single-cell sequencing

1 Introduction

OS is the predominant primary malignant bone tumor, representing 20%-40% of all bone cancers (1). Globally, the annual incidence is approximately 1–3 cases per million individuals (2), with around 800 new cases diagnosed annually in the United States (3). Among children and adolescents, OS has the highest incidence, with a median age of 18 years, positioning it as the third most prevalent malignant tumor within this demographic (4, 5). The disease demonstrates a bimodal distribution, with the initial peak typically manifesting during adolescence (with an average age of 10–14 years for females and 15–19 years for males), followed by a second peak occurring after the age of 65 (6). Among OS patients, the 5-year relative survival rates are approximately 60% for individuals under 30 years old, 50% for those aged 30–49, and diminish to 30% for patients aged 50 or older (7). OS commonly affects the long bones of the limbs, whereas tumors in the chest and pelvic bones present a higher risk of metastasis OS (8). Chemical agents such as methylcholanthrene, beryllium oxide, and zinc beryllium silicate are potential inducers of OS, along with radiation exposure, electrical burns, and genetic factors (9). Gender and race significantly influence the incidence of OS. Males are more frequently affected than females across all age groups. Additionally, the highest incidence rates are observed among black individuals (10). Survival rates are highly correlated with tumor location and staging (11). Tumors detected at an earlier stage and located in more accessible regions generally have a better prognosis compared to those found at advanced stages or in less accessible areas such as the pelvis or chest. These factors underscore the importance of early detection and tailored treatment strategies for improving patient outcomes.

For suspected OS patients, initial cost-effective screening involves X-ray examinations, followed by CT or MRI scans to further evaluate tumor involvement (12). The standard treatments for OS encompass neoadjuvant multidrug chemotherapy, typically involving cisplatin, doxorubicin, methotrexate (commonly known as MAP therapy), and ifosfamide. This is typically followed by surgical intervention and subsequent postoperative chemotherapy (13). Despite its rarity, OS carries a poor prognosis, with surgical intervention being the primary curative treatment; however, patients undergoing surgery alone have a survival rate of only about 15% (14). For patients who are not candidates for surgical resection or those with residual tumors at the resection margins, as well as for OS patients with poor response to chemotherapy, radiation therapy serves as an effective method for local control and symptom relief (15). Additionally, many OS patients have small lung metastases at diagnosis. The 5-year survival rate is over 78% for localized disease but falls to 25% for metastatic or recurrent OS (16). Metastatic OS is highly invasive with a poor prognosis, emphasizing the urgent need for early diagnosis and targeted therapy. Continued investigation into the mechanisms underlying the onset and progression of OS, especially those contributing to elevated recurrence and metastasis rates, is paramount. The identification of pivotal biomarkers and exploration of essential target genes are crucial for enhancing the diagnostic, therapeutic, and prognostic approaches for OS.

Currently, numerous studies have investigated the role and mechanisms of specific gene families in OS (17, 18), such as the presence of pro-inflammatory FABP4^{+} macrophage infiltration observed in pulmonary metastatic OS lesions. In comparison with primary osteoblastic OS lesions, sub-osteoclast infiltration has been observed in chondroblastic, recurrent, and pulmonary metastatic OS lesions OS (19). It has been suggested that TME promotes tumor cell proliferation and immune evasion (20), yet its value as an immunotherapeutic target in OS remains unknown (21). We analyzed bulk transcriptome sequencing data of OS and healthy control samples, as well as single cell sequencing data, obtained from public databases. Initially, we assessed the expression differences of four TME-related gene sets between tumor and control groups. Next, we performed unsupervised clustering analysis on tumor tissues, identifying two distinct clusters. We calculated the GSVA score differences of the four TME-related gene sets between Clusters 1 (C1) and 2 (C2) and conducted single-variable Cox analysis. For the two clusters, we analyzed survival rates, clinical-pathological distribution differences, immune cell infiltration, immune evasion, immune cell abundance, and drug sensitivity. DEGs of the two clusters were subjected to GO and GSEA. We performed WGCNA on the TARGET-OS dataset to identify key genes, followed by GO enrichment analysis. Using LASSO and multiple-factor regression analysis, we constructed a prognostic model comprising eleven genes (ALOX5AP, CD37, BIN2, C3AR1, HCLS1, ACSL5, CD209, FCGR2A, CORO1A,

CD74, CD163). The model demonstrated good diagnostic performance and prognostic evaluation potential in both training and validation cohorts. Next, using the model, we conducted immune analysis, drug sensitivity analysis, and enrichment analysis. In single-cell sequencing, we performed dimensionality reduction and annotated cell subtypes, followed by analyzing the expression of relevant genes in each subtype. We further validated the potential impact of ACSL5 inhibition on the invasive behavior of OS cells through various wet lab experiments. Our study offers novel insights and a theoretical framework for the prognosis, treatment, and drug development targeting OS patients.

2 Material and methods

2.1 Data acquisition and preprocessing

In this study, we used the "TCGAbiolinks" R package to retrieve bulk transcriptomic data of OS from the public database The Cancer Genome Atlas (TCGA, https://portal.gdc.cancer.gov/), specifically the TARGET-OS dataset comprising 86 patients. We obtained healthy control bulk transcriptomic data from the public database Genotype-Tissue Expression (GTEx, www.org/home/index.html). Additionally, we downloaded bulk transcriptomic datasets of OS, including GSE21257 (53 patients) and GSE16091 (34 patients), as well as single cell sequencing datasets GSE162454 and GSE198896, from the public database GEO (https://www.ncbi.nlm.nih.gov/geo/). We excluded samples with missing information from the analysis. Using the "ComBat" function from the "sva" package, we standardized the TARGET-OS and GTEx datasets into bulk matrices in Transcripts per million (TPM) formats. All open-access public databases utilized in this study allow unrestricted access and utilization without the need for additional ethical approval. Our data retrieval and analysis processes adhered to relevant regulations.

2.2 Investigation of expression levels of tumor microenvironment-related gene sets

Utilizing the "signature_collection" function of the "IOBR" package, we identified four TME-related gene sets (TMEscoreA_CIR, TMEscoreB_CIR, TMEscoreA_plus, and TMEscoreB_plus) within the merged dataset of TARGET-OS/GTEx. Subsequently, we employed heatmaps to illustrate the expression disparities of these four relevant gene sets between the tumor and normal groups.

2.3 Hierarchical clustering and TME landscape analysis

We used the "ConsensusClusterPlus" package to perform unsupervised clustering analysis on tumor tissues. The optimal number of clusters (k) was determined by scoring and evaluating matrix plots, Cumulative Distribution Function (CDF) curves, and Proportion of Ambiguous Clustering (PAC) curves. High intra-cluster cohesion, low inter-cluster coupling, a smooth CDF curve, and the lowest PAC curve value are included as our selection criteria. Following multiple standard screenings, we identified two significantly different clusters. Using the "GSVA" package, we calculated scores for four TME-related gene sets in the TARGET-OS dataset (GSVA: gene set variation analysis for microarray and RNA-seq data). We used heatmaps and box plots to show the differences in GSVA scores of the four TME-related gene sets between Clusters 1 (C1) and 2 (C2). We then performed univariate Cox analysis on these gene sets and displayed the differences in hazard ratios with forest plots. Additionally, we conducted survival analysis on the two clusters and displayed the prognostic differences using Kaplan-Meier curves. We used a stacked bar graph to show the compositional differences in clinical pathological information such as Age and Stage between the two clusters.

We utilized five immune cell infiltration prediction algorithms (CIBERSORT, TIMER, MCPcounter, EPIC, quanTIseq) to assess the immune cell infiltration status of the two clusters and visualized the results using box plots. From the TISIDB database (http://cis.hku.hk/TISIDB/), we downloaded 150 immunomodulators and chemokines, including 41 chemokines, 24 immunoinhibitors, 46 immunostimulators, 21 MHC molecules, and 18 receptors. Furthermore we generated a heatmap to illustrate the expression differences of immune modulators between the two clusters. We employed the TIDE (Tumor Immune Dysfunction and Exclusion) database (http://tide.dfci.harvard.edu/) to predict tumor immune escape via immune checkpoint analysis for the two clusters. We visualized the different responses of the two clusters to immune checkpoints using stacked bar graphs. Additionally, we assessed the efficacy of immune checkpoint blockade (ICB) through TIDE scoring. Three immune-suppressive cell types (MDSCs, TAM.M2, and CAFs) were selected, and violin plots were employed to demonstrate the differences in immune-suppressive cell infiltration abundance between the two clusters. Additionally, using the "OncoPredict" package, we predicted the sensitivity of the two clusters to four drugs (Bortezomib, XAV939, Selumetinib, Trametinib).

2.4 Enrichment analysis and weighted gene co-expression network analysis

We employed the "limma" package to identify DEGs between the two clusters and visualized the upregulated and downregulated genes using volcano plots. Subsequently, we conducted GO enrichment analysis on the DEGs and presented bar graphs showing the top ten pathways in each of the BP, CC, and MF subclasses. Following this, we performed GSEA on the DEGs and demonstrated the downregulated pathways within the C2 category. For the TARGET-OS dataset, we conducted WGCNA, selecting appropriate soft thresholds based on Scale Independence and Mean Connectivity. Utilizing the optimal soft threshold, we constructed a co-expression network, partitioned genes into modules, and depicted a Cluster Dendrogram for visualization. We computed the correlation between modules and clinical traits (futime, fustat, age, stage, cluster), illustrating the correlation heatmap. We identified the module most correlated with the cluster as the key

module and selected key genes within this module based on criteria of MM (module membership) > 0.6 and GS (gene significance) > 0.3. We then performed GO enrichment analysis on these key genes.

2.5 Construction and validation of machine learning prognostic models

We chose the TARGET-OS dataset as the training set, while two GEO datasets served as validation sets. Utilizing the Least Absolute Shrinkage and Selection Operator (LASSO) and multiple regression analysis, we constructed the prognostic model (22). In the TARGET-OS dataset, we identified prognostic hub genes by obtaining the optimal parameter λ. Through multiple Cox regression analysis, we determined the coefficients of each gene in the model and visualized them using bar graphs. We determined the risk score of the model by summing the product of the expression level of each gene and its respective coefficient.

$$\text{Risk score} = \sum_{i=1}^{n} [Exp_{gene_i} * \beta_i]$$

In this context, Exp_{gene_i} denotes the expression level of the model gene, and β_i represents the coefficient corresponding to the model gene. We divided the training and validation sets into high-risk and low-risk groups based on the median score of each dataset. We then observed survival differences over time between these groups in all three datasets. Additionally, we conducted ROC curve analysis to evaluate the model's performance at 1-year, 3-year, and 5-year intervals.

2.6 Model-based immune analysis, drug sensitivity analysis, and enrichment analysis

Immune cell infiltration analysis was conducted using the CIBERSORT algorithm to identify relevant immune cell subtypes. Box plot analysis was conducted to evaluate the distribution disparities among various subtypes across two risk groups. Additionally, we utilized box plots to illustrate the expression differences of M2 markers and depleted T cell markers between the two risk groups. We obtained the data from the Progenitor Cell Biology Consortium (PCBC, https://www.synapse.org), and violin plots were generated to display the mRNAsi index of two risk groups, allowing for an analysis of cellular stemness differences between the two risk groups. We analyzed the sensitivities of nine drugs in the two risk groups. Following this, we conducted differential gene expression analysis between the groups and used GSEA to identify dysregulated pathways.

2.7 Single-cell sequencing analysis

Analysis of single cell sequencing data was conducted utilizing both the "Seurat" package and the "SCP pipeline." Data underwent quality control and data cleaning to ensure the accuracy and reliability of subsequent analyses, with quality control criteria set as follows: nFeature_RNA< 9000, percent.mt< 25. We used the harmony method for batch correction of data across multiple samples. Utilizing the Uniform Manifold Approximation and Projection (UMAP) method, we performed dimensionality reduction on the integrated single-cell sequencing data. We annotated ten major cell subtypes using specific markers for each and visualized them. To show the correlation between these subtypes and individual genes, we created violin plots. We used SingleR for automatic annotation and CopyKAT to identify malignant cells. We computed the upregulated and downregulated genes in each cell subtype and displayed the top five of each in volcano plots. GO_BP analysis was conducted, with dot plots illustrating the enriched upregulated pathways in each cell subtype. Using Seurat, we evaluated the activity level of prognostic models in the single-cell dataset.

2.8 Cell culture and siRNA transfection

We acquired OS cell lines MG63 and Saos-2 from Procell Life Science & Technology, China, and cultured in Dulbecco's Modified Eagle's Medium (DMEM) containing 10% fetal bovine serum (FBS) at 37°C in a humidified atmosphere with 5% carbon dioxide. Small interference RNA (siRNA) targeting ACSL5 was transfected using sequences sourced from HANBIO, China, and LipoFiter 3.0 (HANBIO, China) was employed for the transfection process. The specific sequences for siRNA were as follows:

si-NC Sense: UUCUCCGAACGUGUCACGUTT;
Antisense: ACGUGACACGUUCGGAGAATT;
Si-ACSL5–1 Sense: CAAATACTTTCGGACCCAAA;
Antisense: CTCTTCTTGACCTGAACAAT;
Si-ACSL5–2 Sense: CATGATAGTTTCTGGGACAA;
Antisense: CCAAGTTGTAAGGGAAGCCAT

2.9 Real-time PCR

Total RNA extraction utilized Trizol reagent (Solarbio Science & Technology, China), with subsequent reverse transcription into cDNA employing a two-step RNA reverse transcription kit (TaKaRa Bio Inc., Japan). The RT-qPCR reaction comprised cDNA, RT-qPCR SYBR Green (TaKaRa Bio Inc., Japan), and primers, following cyclic parameters: initial denaturation at 95°C for 30 seconds, succeeded by 40 cycles of denaturation at 95°C and annealing at 60°C for 34 seconds. The primers used for cDNA amplification were as follows: ACSL5-F: 5′-GGCATTGGTGCTGATAGG-3′ and ACSL5-R: 5′-TCTTCTCCCCTCTTTGCTT-3′; β-actin-F: 5′-CAAGAGATGGCCACGGCTGCT-3′ and β-actin-R: 5′-TCCTTCTGCATCCTGTCGGCA-3′ (23, 24).

2.10 Cell proliferation assay

We assessed cell viability employing the CCK-8 kit (Seven, China). we seeded a 96-well plate with a single-cell suspension at a density of 5×10^3 cells per well. Subsequently, we added 10 μL of

CCK-8 solution to each well every 24 hours, and the plate was then incubated for 2 hours. (25) We measured the optical density (OD) at 450 nm using a multifunctional enzyme-linked immunosorbent assay reader (Synergy H1, BioTek, USA).

2.11 Cell migration and invasion assays

We evaluated cell migration and invasion utilizing transwell chambers featuring an 8.0-μm pore size (Corning, USA). We loaded the lower chamber with 500 μL of medium supplemented with 10% FBS, while 2×10^4 cells in serum-free medium were seeded onto the upper chamber. For invasion assessments, we coated the transwell membrane with 1 mg/ml Matrigel. After a 24-hour incubation at 37°C, we gently removed the non-migrated cells using cotton swabs. Cells that migrated to or invaded the underside of the membrane were stained with crystal violet and quantified. Three randomly chosen microscopic fields were tallied for each well.

2.12 EdU assay

We assessed the proliferation capacity of cells post-knockdown using the EdU Cell Proliferation Assay Kit (Beyotime, China). We subjected MG63 and Saos-2 cells to knockdown and cultured them on six-well plate. We prepared a 2x EdU working solution in serum-free medium using a 10 mM EdU solution, preheated it, and mixed it with the culture medium to obtain a 1x EdU solution. The cells were incubated with this solution for 12 hours. After incubation, we fixed the cells with 2.5 mL of PBS containing polyformaldehyde for 15 minutes at room temperature. We then washed the cells three times with 2.5 mL of PBS for 5 minutes each. Next, we treated the cells with 2.5 mL of permeabilization buffer for 20 minutes at room temperature. After removing the permeabilization buffer, we washed the cells twice with 2.5 mL of PBS and then removed the washing solution. We prepared Click-iT reaction mixture and added to each slide (100 μl), followed by incubation in the dark at room temperature for 30 minutes. Subsequently, we removed the reaction mixture, and each well was washed once with 2.5 mL of PBS, followed by removal of the washing solution. We also performed DAPI nuclear staining and captured images under a microscope for further analysis.

2.13 Colony-formation assays

Cells in logarithmic growth phase were trypsinized, resuspended in complete culture medium supplemented with 10% fetal bovine serum, and counted. We seeded MG63 and Saos-2 cells in six-well plates at a density of 700 cells per well and cultured for 14 days, with media changes every 3 days and continuous monitoring of cell status. We captured images of the cells under a microscope, followed by a single wash with PBS. Cells were then fixed with 1 mL of 4% polyformaldehyde per well for 30 minutes, washed once with PBS, and stained with crystal violet solution (Beyotime, China) for 10 minutes. After several washes with PBS, the cells were air-dried and photographed.

2.14 Statistical analysis

We performed statistical analyses using R software (version 4.1.3). For single cell sequencing analysis, we used the "Seurat" package and "SCP pipeline." We used the "IOBR" package for gene set acquisition and immune infiltration analysis, and "oncoPredict" for drug sensitivity analysis. We employed "SingleR" for cell annotation and "copykat R" for tumor cell identification. We used the "ConsensusClusterPlus" package for unsupervised clustering analysis, and "clusterProfiler" for enrichment analysis. Differential expression analysis was implemented using the "limma" package. A threshold of $p < 0.05$ was considered statistically significant (* $p < 0.05$; ** $p < 0.01$; *** $p < 0.001$; **** $p < 0.0001$).

3 Results

3.1 Exploration of expression levels of tumor microenvironment-related gene sets

We analyzed the expression differences of four TME-related gene sets (TMEscoreA_CIR, TMEscoreB_CIR, TMEscoreA_plus, and TMEscoreB_plus) between tumor and normal groups using integrated bulk expression matrices from the TARGET-OS and GTEx datasets. Heatmaps illustrate that most genes within the four gene sets exhibit significantly higher expression in the tumor group (Figures 1A–D).

3.2 Hierarchical clustering and TME landscape analysis

Utilizing the "ConsensusClusterPlus" package, we conducted unsupervised clustering analysis on tumor tissues based on scoring. We computed GSVA scores for four TME-related gene sets in the TARGET-OS dataset and presented heatmap illustrations depicting score disparities of these genes between clusters C1 and C2. Notably, TMEscoreA_CIR and TMEscoreA_plus exhibited significantly higher scores in C2 compared to C1, whereas differences in scores for TMEscoreB_CIR and TMEscoreB_plus between the two groups were minimal (Figure 2A).Univariate Cox analysis was performed on the four TME-related gene sets, revealing significantly higher hazard ratios for TMEscoreA_CIR and TMEscoreA_plus compared to TMEscoreB_CIR and TMEscoreB_plus, indicating an unfavorable prognosis associated with the scores of TMEscoreA_CIR and TMEscoreA_plus (HR>1, Figure 2B). The matrix plot indicates high intra-cluster cohesion and low inter-cluster coupling (Figure 2C). Results for cluster numbers ranging from k=2 to k=9 were demonstrated, with k=2 showing a

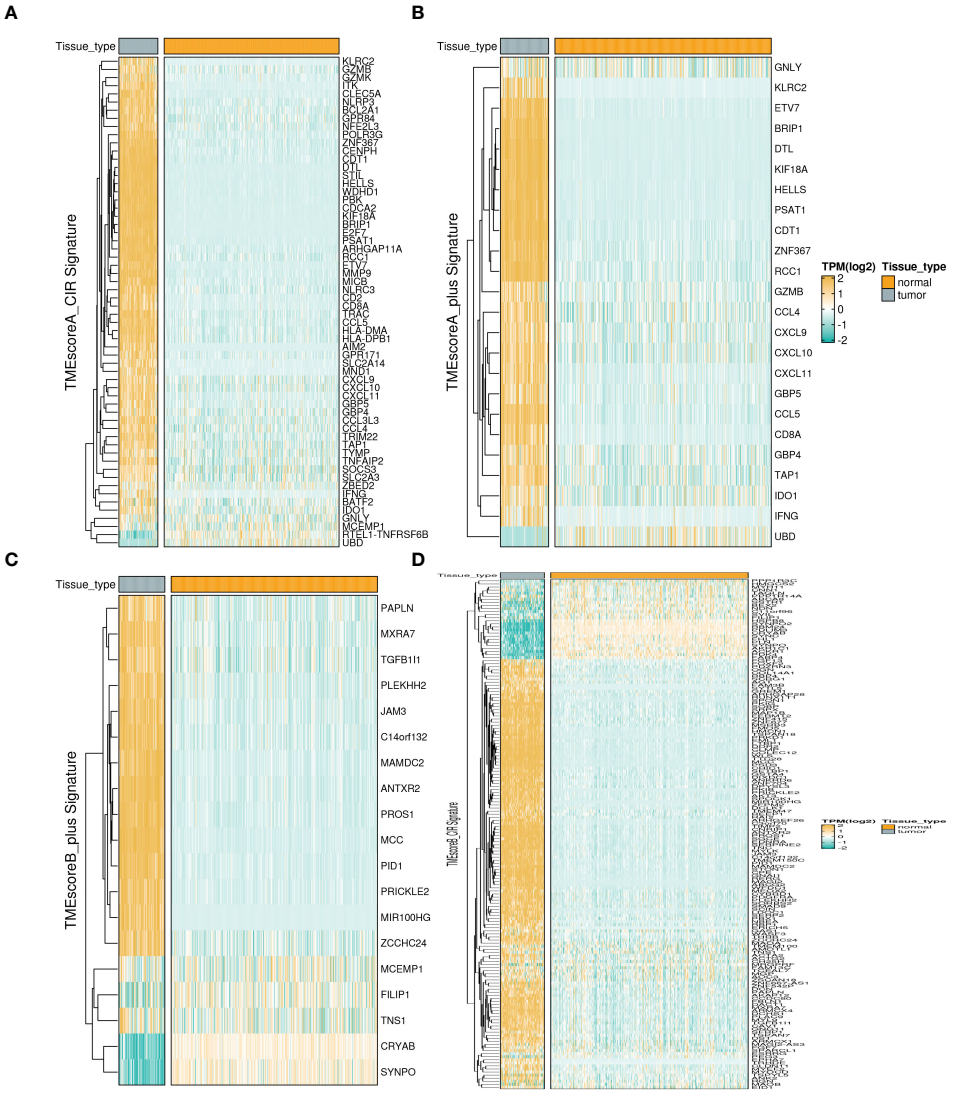

FIGURE 1
Expression profiles of TME-related Signatures in OS. The expression patterns of four TME-related signatures including TMEscoreA_CIR **(A)**, TMEscoreA_plus **(B)**, TMEscoreB_CIR **(C)**, and TMEscoreB_plus **(D)**.

smooth CDF curve (Figure 2D) and the lowest PAC score (Figure 2E), thus suggesting k=2 as the optimal cluster number. Boxplots based on GSVA scores demonstrated that, except for TMEscoreB_CIR, scores for each TME-related gene set were higher in cluster C2 than in C1, with TMEscoreA_CIR and TMEscoreA_plus showing particularly significant differences (Figure 2F). Survival analysis was conducted on clusters C1 and C2, with KM curves illustrating a superior prognosis for C2 compared to C1 (Figure 2G). Additionally, stacked bar plots depicted distribution disparities of C1 and C2 across different clinical-pathological parameters. While patients aged over 15 years were slightly more predominant in C1 compared to C2 in terms of age distribution (Figure 2H), C2 exhibited a higher proportion of late-stage cases than C1 based on tumor stage distribution (Figure 2I). For immune cell infiltration analysis, we employed five algorithms, namely CIBERSORT, TIMER, MCPcounter, EPIC, and quanTIseq. Boxplots revealed that in CIBERSORT analysis, most immune cell infiltration levels were lower in cluster C1 compared to C2, whereas the infiltration level of Macrophages_M0 was lower in C2 than in C1. Results from MCPcounter indicated that the infiltration levels of various cell types were significantly higher in C2 than in C1. In quanTIseq analysis, the difference in infiltration levels between the two groups was minimal overall, but in the "Other" category, infiltration levels were slightly higher in C1 than in C2. EPIC analysis showed that CD4_Tcells and Endothelial cell infiltration levels were higher in C2 than in C1, while in the "OtherCells" category, infiltration levels were higher in C1 than in C2. TIMER analysis showed similar infiltration levels between the two groups, with C2 being higher than C1 in most cases (Figure 3A). Heatmaps of immunomodulators and chemokines along with the two clusters demonstrated higher expression of these 150 immunomodulators and chemokines in C2 (Figure 3B). We

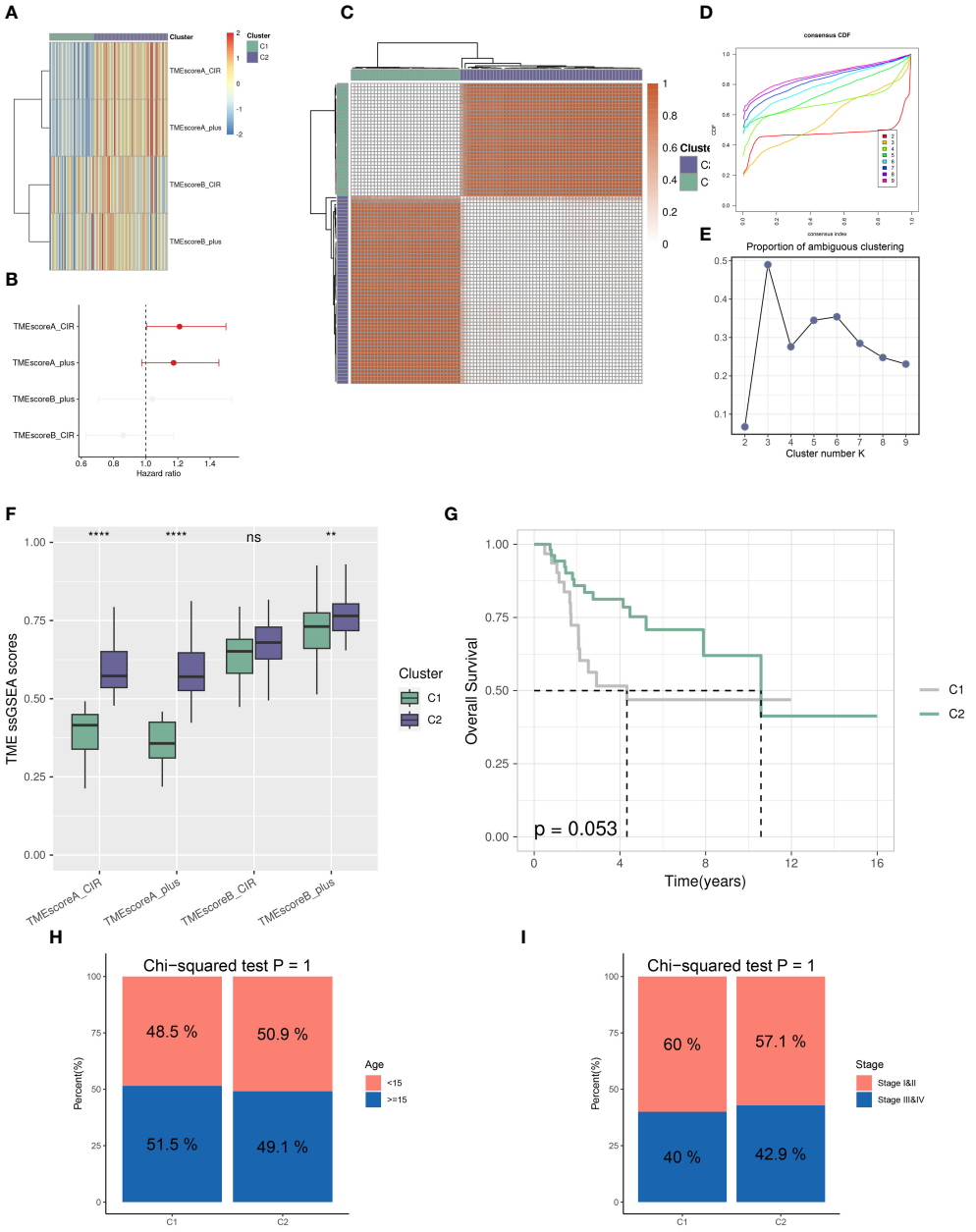

FIGURE 2
Distinct TME landscapes in OS. **(A)** The GSVA scores of each TME-related signature between two TME subclusters. **(B)** Forest plot illustrating the hazard ratio of each TME-related signature determined by Univariate Cox regression analysis. **(C)** The consensus score matrix of glioma samples in TARGET-OS when the clustering number k = 2. The consensus score represents the intensity of interaction between two samples. **(D, E)** The CDF curves **(D)** and PAC scores **(E)** of the consensus matrix for each (k) **(F)** Boxplots showing the distribution of GSVA scores of each TME-related signature between two TME subclusters. **(G)** The survival differences between two TME subclusters, analyzed by Kaplan-Meier curves with the log-rank test. **(H, I)** Stacked Bar plots illustrating the distributions of age populations **(H)** and stages **(I)** between two TME subclusters. P values were calculated by the Chi-squared tests. ** p<0.01; **** p<0.0001.

predicted tumor immune escape by examining immune checkpoints in clusters C1 and C2, with a stacked bar graph showing a higher response to immune checkpoints in C2 compared to C1 (Figure 4A). Violin plots displaying TIDE scores for the two clusters showed no statistically significant differences (Figure 4B).We selected three immune-suppressive cell types, CAFs, MDSCs, and TAM.M2, and presented violin plots illustrating the abundance of immune-suppressive cells between the two groups. In MDSCs and TAM.M2, infiltration was higher in C1 than in C2, with TAM.M2 showing particularly significant differences, while there was no significant difference between C1 and C2 in CAFs (Figure 4C).Furthermore, we conducted drug sensitivity analysis on four relevant drugs, Bortezomib, XAV939, Selumetinib, and Trametinib, for clusters C1 and C2. The IC50 values for all four drugs were lower in C2 than in C1, indicating higher sensitivity and better drug efficacy in C2 (Figure 5).

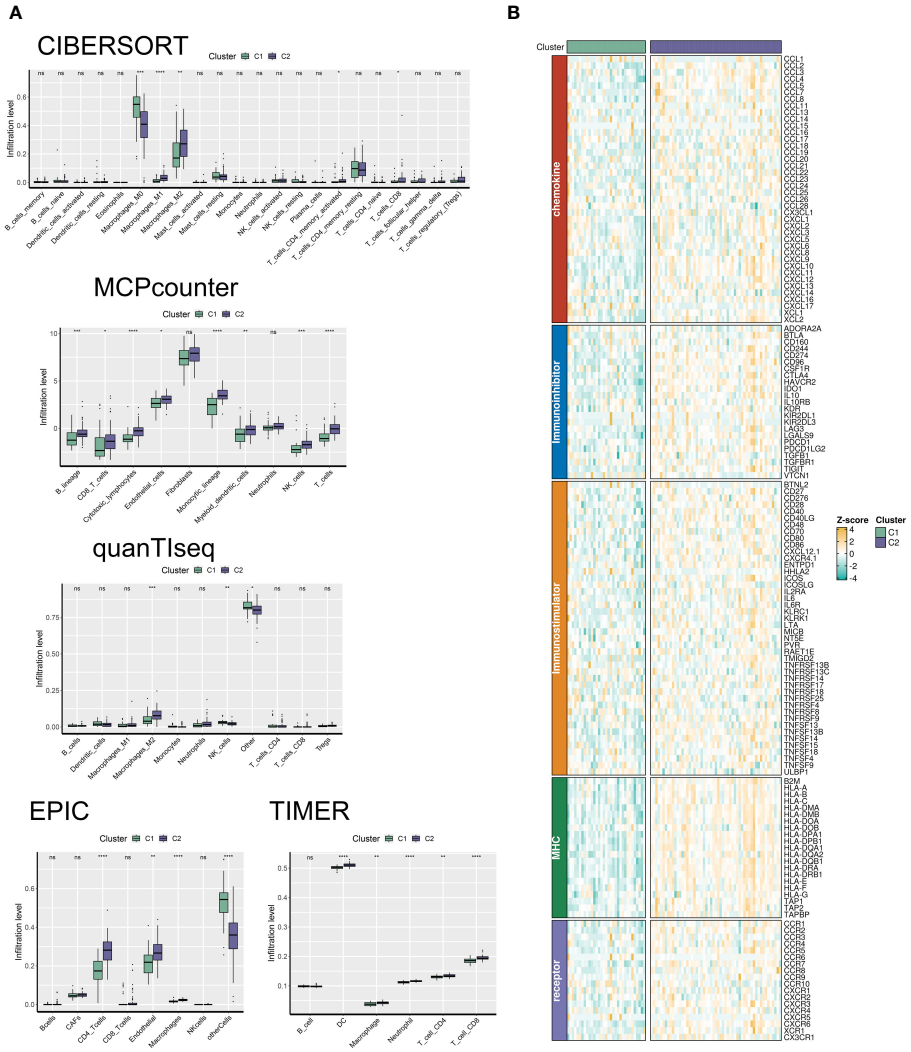

FIGURE 3
The C2 TME subcluster shapes a hot-TME in OS. **(A)** The infiltration abundances of immune cell subsets evaluated by CIBERSORT, MCP-counter, quanTIseq, EPIC, and TIMER for two TME subclusters. **(B)** The expression patterns of immunoregulators for two TME subclusters. * p<0.05; ** p<0.01; *** p<0.001; **** p<0.0001.

3.3 Enrichment analysis and weighted gene co-expression network analysis

We evaluated the differences between groups C1 and C2 in two directions: differential fold change and differential significance level. We identified DEGs between the two groups and displayed upregulated and downregulated genes using volcano plots (Figure 6A). Next, we performed GO enrichment analysis on the DEGs and illustrated the top ten pathways in the BP, CC, and MF categories using lollipop plots. In the MF category, the DEGs were enriched in pathways like gated channel activity, monoatomic cation channel activity, and monoatomic ion gated channel activity. The CC category showed consistent enrichment levels. In the BP category, the genes were enriched in pathways related to feeding behavior, response to hydrogen peroxide, and regulation of dendrite development. (Figure 6B). Furthermore, we performed GSEA on the DEGs, displaying the downregulated pathways in C2 (Figure 6C). Subsequently, we applied WGCNA to the TARGET-OS dataset, determining an appropriate soft threshold based on Scale Independence and Mean Connectivity (Figure 7A). Using the optimal soft threshold, we constructed a co-expression network, partitioned genes into modules, and visualized a dendrogram for clustering (Figure 7B). We computed the correlation between modules and clinical traits, depicting the results in a heatmap. The correlation between modules and the futime trait was generally low with minimal variation, while more modules exhibited negative correlations with the fustat trait. Modules were mainly positively correlated with age and stage. The MEbrown module had a strong positive correlation with the cluster trait, while the MEgrey module had a strong negative correlation. (Figure 7C). We identified the MEbrown module, which had the highest correlation with the cluster trait, as the key module. Subsequently, we filtered out key genes of the module based on Module Membership (MM) and Gene Significance (GS) criteria (MM > 0.6 & GS > 0.3) (Figure 7D). We conducted GO enrichment analysis on the key genes, revealing enrichment in pathways such as immune receptor activity in MF,

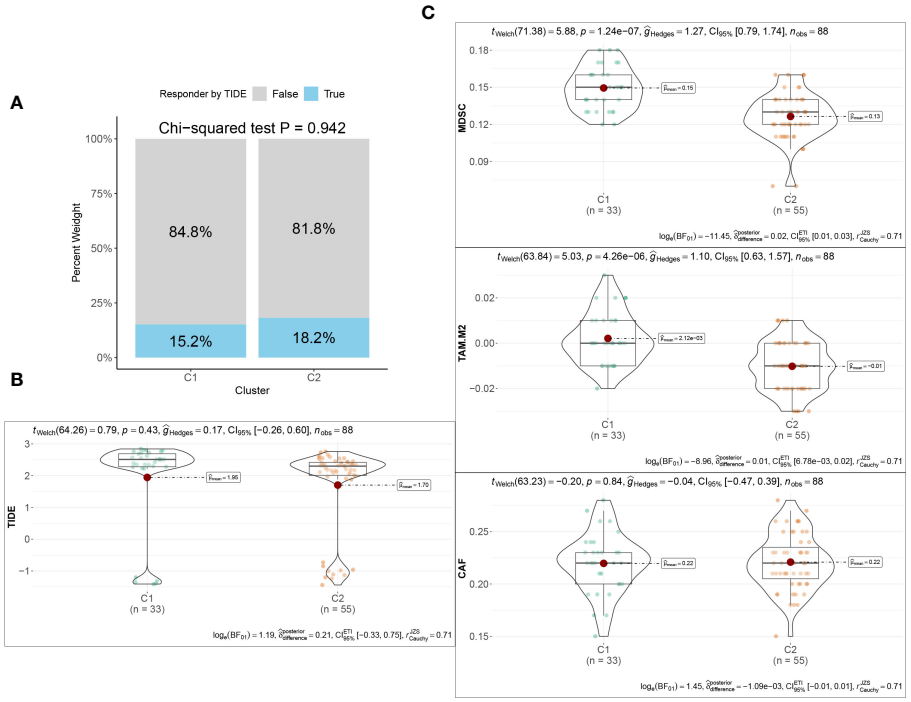

FIGURE 4
Immunotherapeutic response between the two TME subclusters. **(A)** Stacked Bar plots illustrating the distributions of predicted ICB responders between the two TME subclusters. **(B)** The TIDE scores between the two TME subclusters. **(C)** Violin plots showing the infiltration abundances of MDSC, M2-TAM, and CAF between the two TME subclusters.

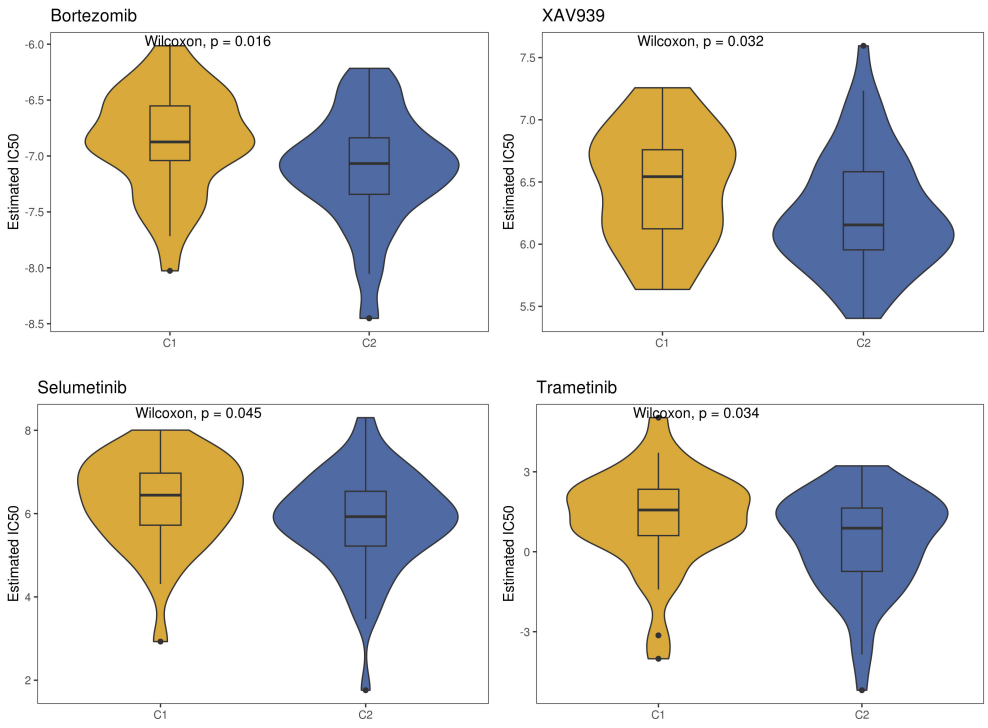

FIGURE 5
Drug sensitivity between the two TME subclusters.

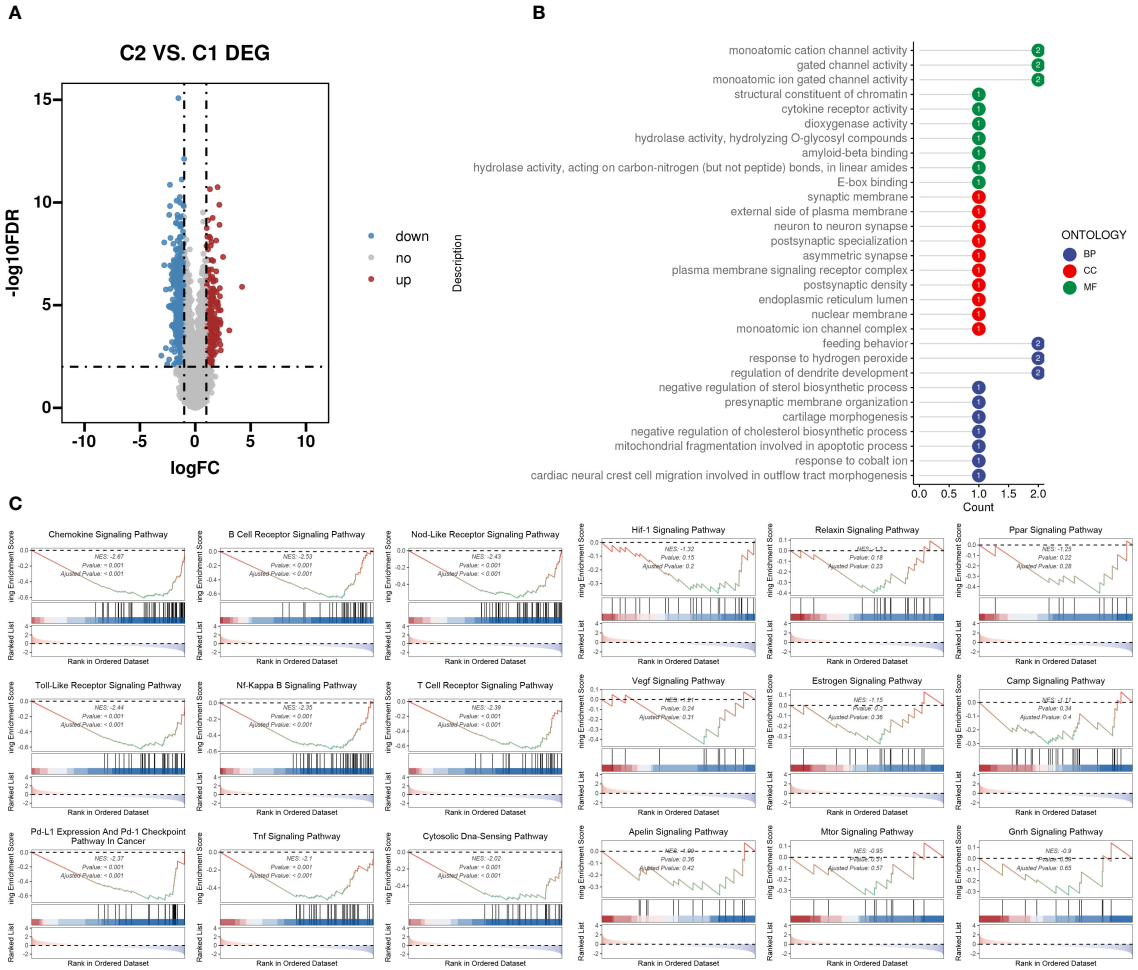

FIGURE 6
DEGs between the two TME subclusters. **(A)** Volcano plot showing the upregulated (colored in red) and downregulated (colored in blue) genes between the two TME subclusters. **(B)** Top ten enriched GO terms of hub genes. **(C)** GSEA of dysregulated pathways in the C2 TME subcluster.

secretory granule membrane in CC, and positive regulation of cytokine production in BP. Overall, the number of genes enriched in BP pathways was significantly higher than those in MF and CC pathways (Figure 7E).

3.4 Construction and validation of machine learning prognostic model

We selected TARGET-OS as the training set and two GEO datasets as the validation sets. LASSO and multivariable Cox regression analyses were performed, retaining coefficients for 11 genes. The optimal parameter λ=0.040 was determined through coefficient distribution analysis (Figure 8A). A lollipop plot displayed the coefficients of the 11 genes obtained (Figure 8B). Using the median of each dataset, we divided the training and validation sets into high-risk and low-risk groups. Throughout both the training set TARGET-OS and the validation sets GSE21257 and GSE16091, the low-risk cohort consistently demonstrated markedly superior survival prognosis compared to the high-risk cohort, with the disparity in survival rates escalating over time. ROC curve analysis revealed that the area under the curve (AUC) for all three datasets at 1, 3, and 5 years was greater than 0.8, indicating good diagnostic performance of the model at these time points (Figure 8C).

3.5 Further analysis of the model and drug prediction

Using CIBERSORT, we conducted immune cell infiltration analysis to screen for relevant immune cell subgroups. Interestingly, we did not observe any significant differences between the two groups in terms of various immune cell populations (Figure 9A). We generated box plots to show the expression differences of M2 markers and exhausted T cell markers between the high and low-risk groups. In the high-risk group, most markers had higher expression levels compared to the low-risk group, except for CXCL13, which was lower in the high-risk group. (Figures 9B, C). Violin plots visually depicted the disparity in cellular stemness analysis between the high and low-risk groups based on the mRNAsi index, revealing a higher mRNAsi index in the high-risk

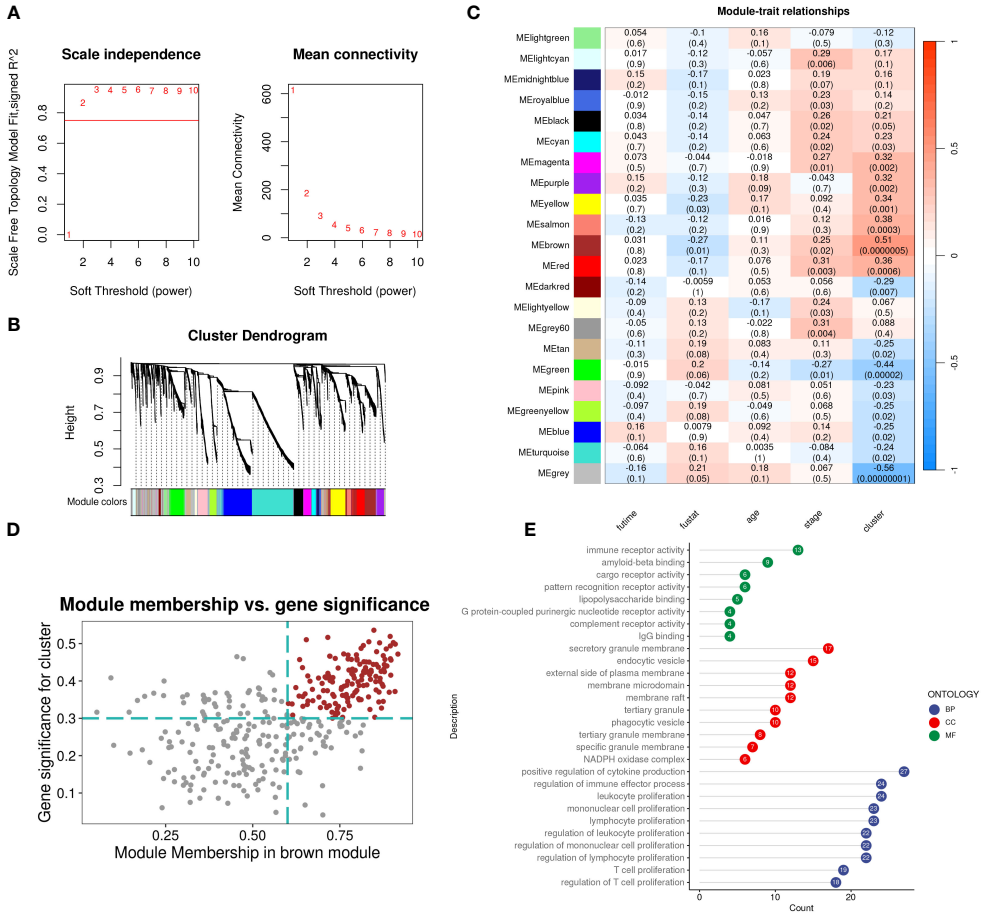

FIGURE 7
WGCNA identifies subcluster-related modules and hub genes inside. **(A)** Analysis of network topology for different soft-threshold power. The left panel shows the impact of soft-threshold power (power = 3) on the scale-free topology fit index; the right panel displays the impact of soft-threshold power on the mean connectivity. **(B)** Cluster dendrogram of the coexpression modules. Each color indicates a co-expression module. **(C)** Module-trait heatmap displaying the correlation between module eigengenes and clinical traits. **(D)** Correlation between module membership and gene significance in the brown modules. Dots in color were regarded as the hub genes of the corresponding module (MM > 0.6 & GS > 0.3). **(E)** Top ten enriched GO terms of hub genes.

group (p=0.01, Figure 9D). We also conducted drug sensitivity analyses for nine selected drugs, comparing the high and low-risk groups. Violin plots demonstrated higher IC50 values in the high-risk group, indicating reduced drug sensitivity (Figure 10). Differential gene expression analysis between the two risk groups was followed by Gene Set Enrichment Analysis (GSEA) to identify commonly dysregulated pathways. The high-risk group exhibited upregulation in most frequently altered tumor pathways (Figure 11).

3.6 Single-cell sequencing analysis

We conducted an analysis of the acquired single cell sequencing data. We used UMAP dimensionality reduction clustering on the integrated single-cell data (Figure 12A), and ten cell subgroups annotated and visualized ten cell subgroups based on cell-specific markers (Figure 12B). We examined the expression of various genes across the ten cell subgroups, revealing higher expression of COL3A1 in MSCs, Malignant cells, and Osteocytes, with significant upregulation of IGF1R in Malignant cells (Figure 12C).Utilizing SingleR for automated annotation combined with copycat for malignant cell identification, we computed the upregulated and downregulated genes in each cell subgroup and presented volcano plots showing the top five upregulated and downregulated genes (Figure 12D). GO_BP analysis indicated significant upregulation of multiple pathways in Macrophages, monocytes, T cells, NK cells, and B cells (Figure 12E). Furthermore, we evaluated the distribution of prognostic model scores within the single-cell dataset, revealing a significant regional pattern (Figure 12F).

3.7 Knockdown of ACSL5 inhibited the proliferation, invasion, and migration of OS cells

To assess the potential impact of ACSL5 inhibition on the aggressive behavior of OS cells, we used siRNA to downregulate ACSL5 expression in MG63 and Saos-2 cells. We selected two siRNA sequences and confirmed by RT-qPCR. As depicted in Figure 13A, both sets of sequences effectively reduced ACSL5

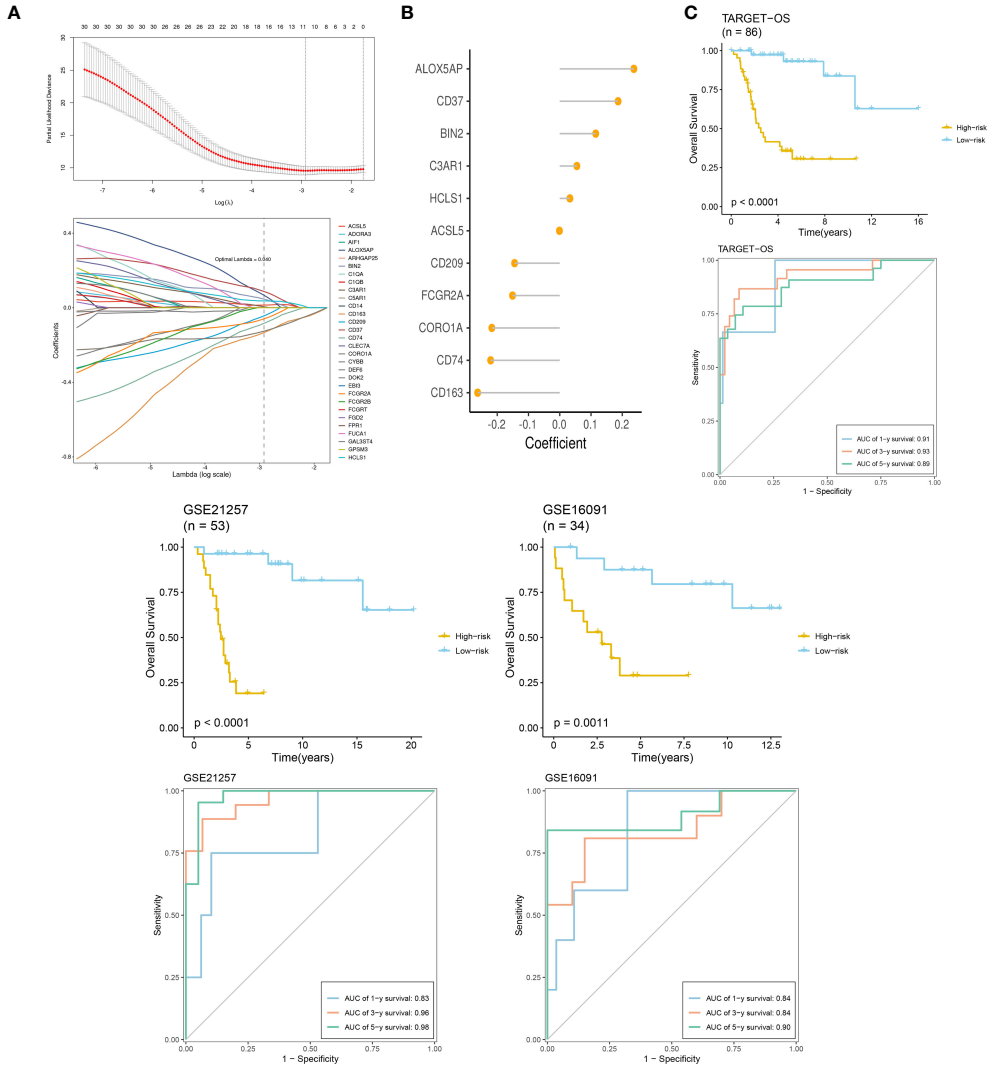

FIGURE 8
TME-related prognostic signature construction and validation. **(A)** The selection of prognostic hub genes based on the optimal parameter λ that was obtained in the LASSO regression analysis. **(B)** Lollipop chart of the coefficients of signature genes determined by the multiCox regression analysis. **(C)** Survival differences between two groups in the three datasets. Time-dependent ROC analysis of the model in the three datasets.

expression in MG-63 and Saos-2 cells, with si-ACSL5–2 demonstrating notably superior knockdown efficacy compared to si-ACSL5–1. As illustrated in Figure 13B, ACSL5 knockdown significantly curtailed cell proliferation within 72 hours. Figures 13C, D further demonstrated that ACSL5 knockdown markedly impeded the invasion and migration of both MG-63 and Saos-2 cells. We further used more experiments to explore the effect of ACSL5 on proliferation. EdU staining results indicated that the proliferation capacity of both MG63 and Saos-2 knockdown groups was significantly lower compared to the NC group, indicating inhibited cell proliferation post-knockdown (Figures 14, 15A). Colony formation assay results revealed that the proliferation capacity of the NC group was significantly superior to that of the knockdown groups (Figures 15B, C). Hence, our findings suggest that silencing ACSL5, a pro-oncogene, could attenuate the oncogenic behaviors of proliferation, migration, and invasion in OS cells.

4 Discussion

OS stands as the prevailing primary malignant bone tumor, presenting with the highest occurrence in children and adolescents, thereby securing the third position among malignant tumors within this age group. Though rare, OS has a poor prognosis. Surgery is the main curative treatment, but patients undergoing only surgery have a survival rate of about 15%. The 5-year survival rate is over 78% for localized OS but drops to 25% for metastatic or recurrent cases. For those unable to have surgery, radiotherapy is effective for local control and symptom relief. However, advanced-stage OS is highly invasive and has a poor prognosis. Therefore, investigating the mechanisms underlying OS-related genes, particularly those implicated in its elevated metastatic potential and recurrence rates, deciphering pivotal biological markers, and exploring essential target genes emerge as critical endeavors for enhancing the diagnosis, treatment, and prognosis of OS.

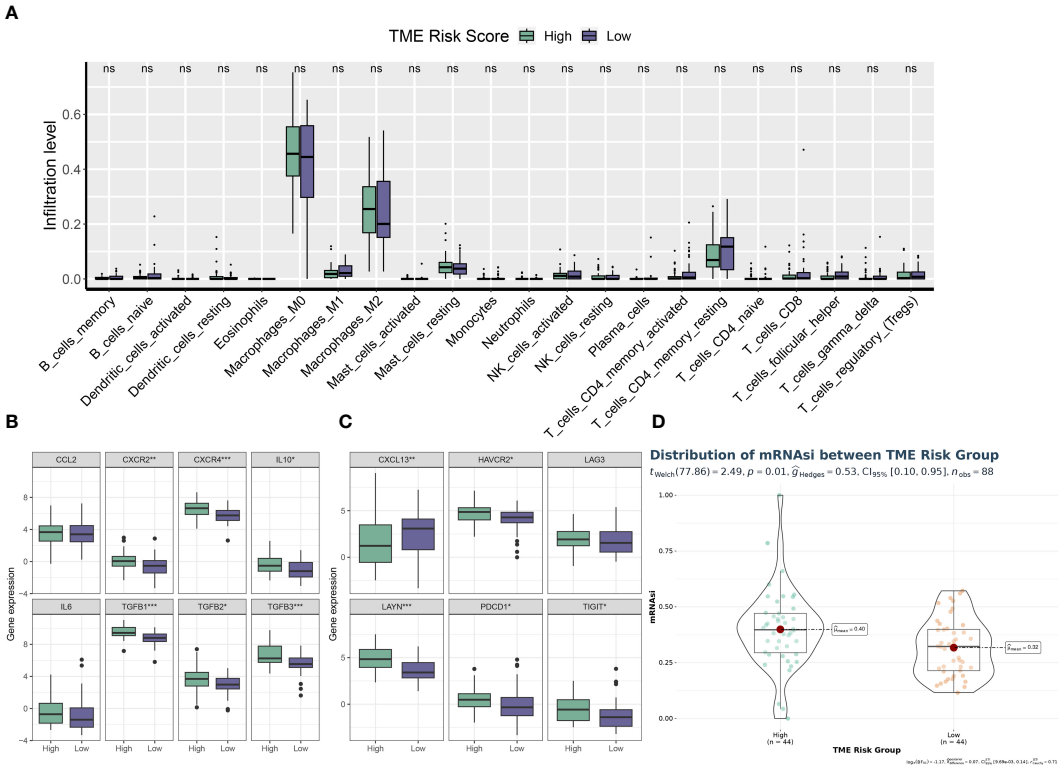

FIGURE 9
TME phenotypes between risk groups. **(A)** Box plot illustrating the distributions of 22 immune cell subsets determined by CIBERSORT between two risk groups. **(B, C)** Box plot illustrating the expression profiles of M2 polarization regulators **(B)** and TEXterm features **(C)** between two risk groups. **(D)** Violin plot displaying the mRNAsi index between two risk groups. * p<0.05; ** p<0.01; *** p<0.001; **** p<0.0001.

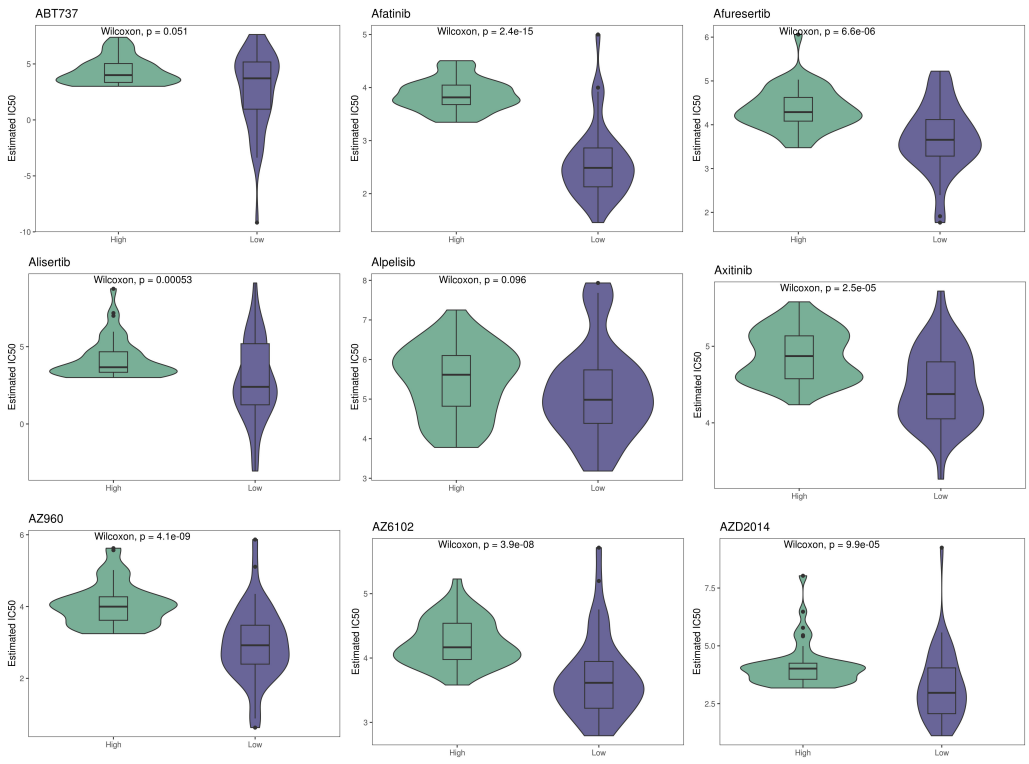

FIGURE 10
Therapeutic sensitivity between two risk groups.

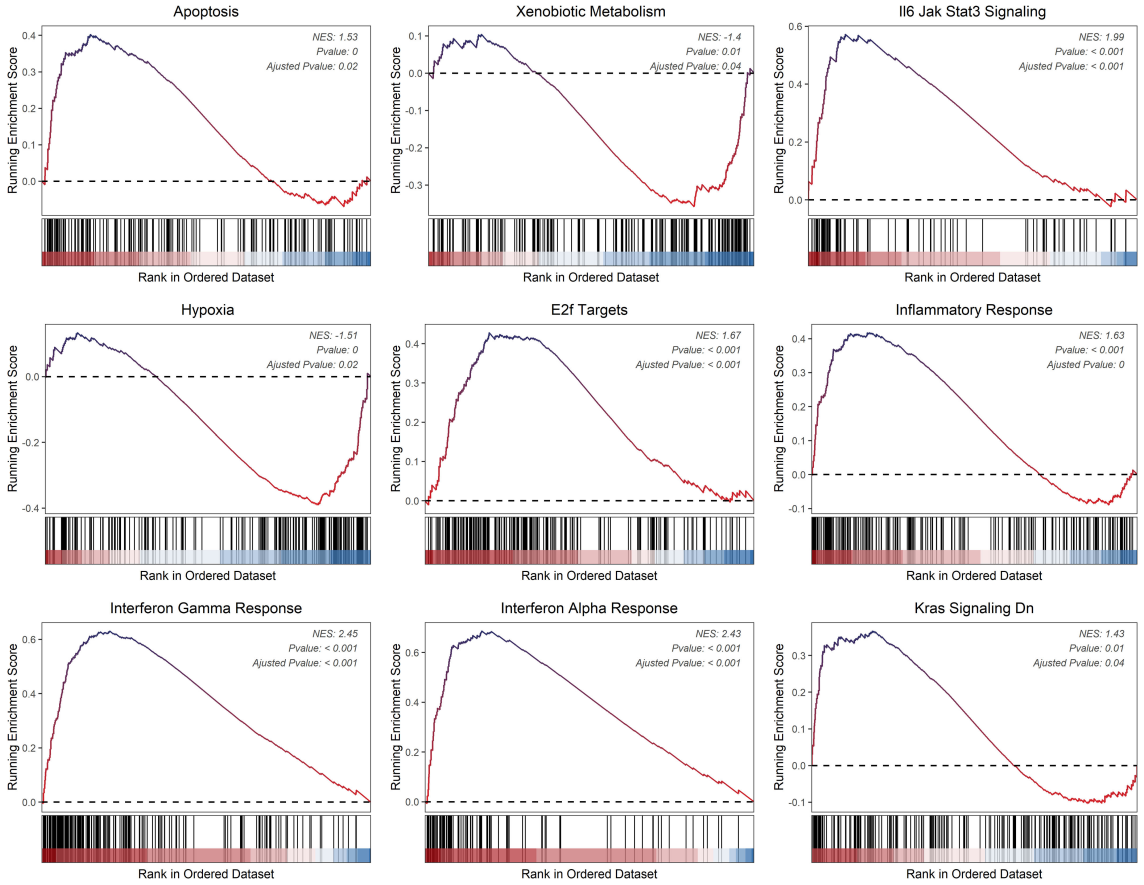

FIGURE 11
Dysregulated cancer hallmarks between two risk groups.

We conducted a multi-layered analysis using various types of transcriptome data downloaded from multiple public databases. We analyzed the expression differences of four TME-related gene sets between tumor and normal groups in the integrated bulk matrix obtained from the TARGET-OS and GTEx datasets. We performed unsupervised clustering analysis on tumor tissues, selecting k=2 as the optimal number based on matrix plots, CDF curves, and PAC scores. We calculated GSVA scores for four TME-related gene sets in the TARGET-OS dataset and conducted univariate Cox analysis. C2 had higher scores than C1 in most TME scoring items. The analysis revealed TMEScoreA_CIR and TMEscoreA_plus as prognostic risk factors. We explored the differences between the two clusters through Kaplan-Meier curves, distribution of clinical pathological information, analysis of immune cell infiltration, prediction of tumor immune escape, and abundance of immune inhibitory cells. The results showed that C1 had a poorer prognosis but was more relevant to OS treatment. We analyzed drug sensitivity in C1 and C2 using four drugs, finding that C2 was more sensitive to them, though this needs further validation. We identified DEGs between the clusters and performed GO enrichment analysis and GSEA.

Performing WGCNA on the TARGET-OS dataset, we obtained the optimal soft threshold power=3 to construct a co-expression network and partition gene modules. We identified the key module, MEbrown, and filtered critical genes with MM > 0.6 and GS > 0.3, then performed GO enrichment analysis. We used TARGET-OS as the training set and two GEO datasets as validation sets, defining two risk groups based on the median score of each dataset. Using LASSO and multiple regression analysis, we built a prognostic model and identified 11 genes: ALOX5AP, CD37, BIN2, C3AR1, HCLS1, ACSL5, CD209, FCGR2A, CORO1A, CD74, and CD163. Among these, ALOX5AP is a crucial enzyme that converts arachidonic acid to leukotrienes, serving as an important immunomodulatory lipid mediator. Diseases associated with ALOX5AP include stroke, ischemia, and myocardial infarction (26). Prior research also suggests widespread expression of ALOX5AP in 20 different types of epithelial cancer cell lines, implicating its potentially crucial role in influencing cancer patient prognosis (27). CD37, encoding a protein member of the transmembrane 4 superfamily, also known as the tetraspanin family, is associated with osteogenesis imperfecta, III-type, and mantle cell lymphoma, playing a critical role in regulating tumor onset and progression (28). CD37 serves as a significant immune marker in various immune cells (e.g., T cells, B cells, and macrophages), with high expression possibly indicating adequate filtration and immune competence in the tumor microenvironment (29). BIN2, encoding a cytoplasmic protein, influences podosome formation, movement, and phagocytosis through interactions with the cell membrane and cytoskeleton (30). Meanwhile the role of BIN2

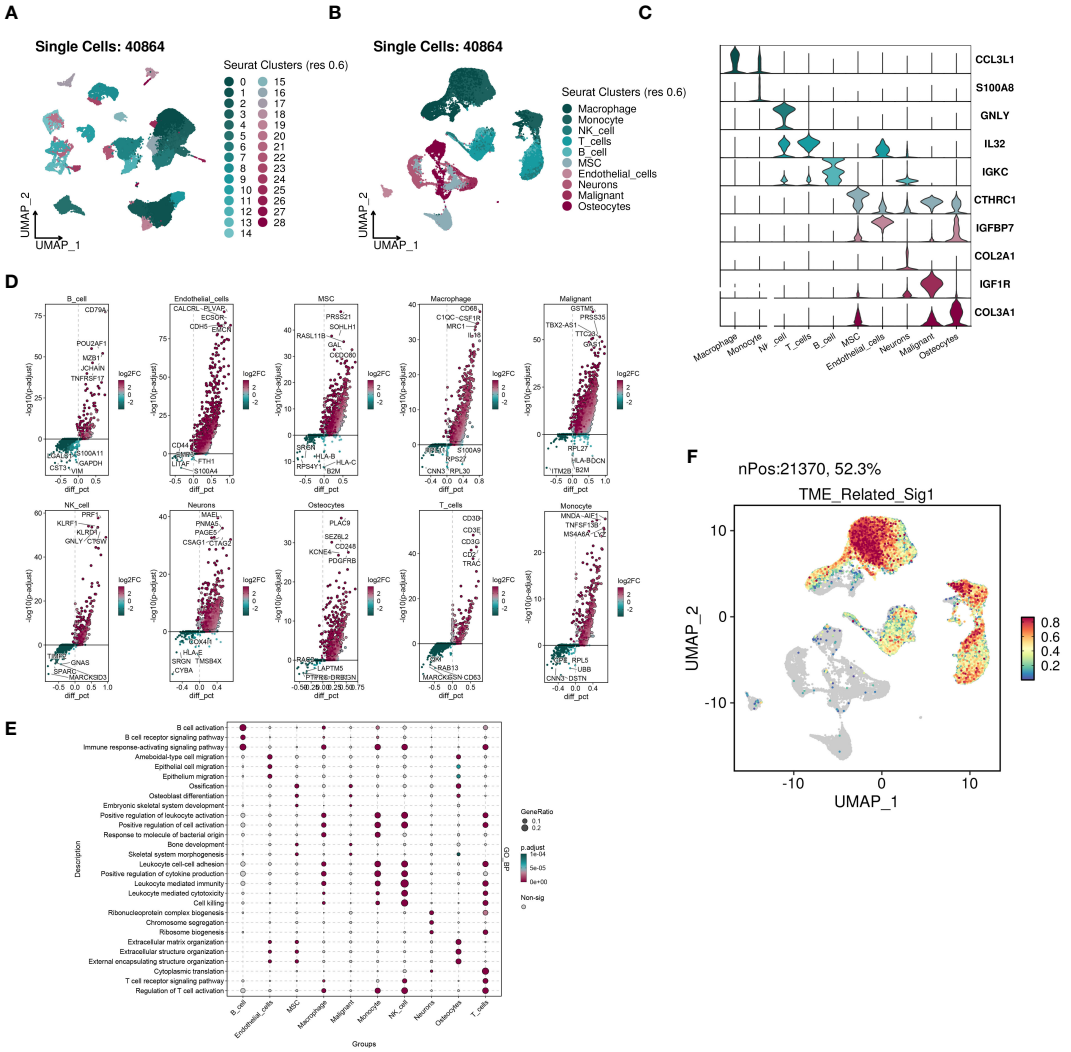

FIGURE 12
The highly activated TME-related signature in scRNA-seq datasets of OS. **(A)** UMAP visualization of 40864 cells from four public OS scRNA-seq cohorts. **(B)** 10 major cell types were manually annotated. **(C)** Vlnplots illustrating the expression values of cell type-specific markers. **(D)** Volcano plots illustrating the top five labeled markers upregulated (colored in red) or downregulated (colored in blue) in each cell cluster. **(E)** Dot plot showing the enriched GO_BP terms of each cell cluster. **(F)** The signature genes expression at single cell level determined by AddModuleScore() function in Seurat.

in cancer remains yet unclear, TCGA studies have observed an association between upregulated BIN2 and favorable survival outcomes in all cervical, endometrial, breast, and ovarian cancers (31). C3AR1, as the orphan G protein-coupled receptor for the allergic toxin C3a released during complement system activation, plays a crucial role in immune responses, particularly implicated in immune infiltration in sepsis (32). Endothelial C3AR1 regulates vascular inflammation in aging or neurodegenerative diseases (33). HCLS1, containing a Src homology 3 (SH3) domain, facilitates the activation of receptor tyrosine kinases (34). Levels of HCLS1 were linked to chronic lymphocytic leukemia, though its role in cancers, particularly OS, remains unclear. ACSL5, a mitochondrial enzyme, aids in the synthesis of long-chain fatty acyl-CoA and induces cellular apoptosis. Its predominant isoform in mitochondrial cardiolipin biosynthesis might also support cancer cell survival (35, 36). Previous studies suggest its crucial role in the malignant progression and metastasis of gliomas (37). CD209, also known as DC-SIGN, belongs to the C-type lectin superfamily primarily expressed in dendritic cells (38). CD209 binds Lewis antigens highly expressed in cancers, facilitating T-cell priming and initiating immune cascades (39). FCGR2A, a member of the immunoglobulin Fc receptor gene family found on various immune response cells, participates in immune surveillance and validation (40). Its association with the pharmacodynamics of monoclonal antibodies varies across different cancer types like colorectal, breast, and metastatic squamous cell carcinoma of the head and neck (41). CORO1A, encoding a member of the WD repeat protein family, is involved in multiple cellular processes, including cell cycle, apoptosis, signal transduction, and gene regulation (42). Previous studies identified CORO1A as a pro-proliferative target in breast cancer cells (42). CD74, also known as invariant chain, acts as an MHCII chaperone crucial in antigen presentation (43). Research

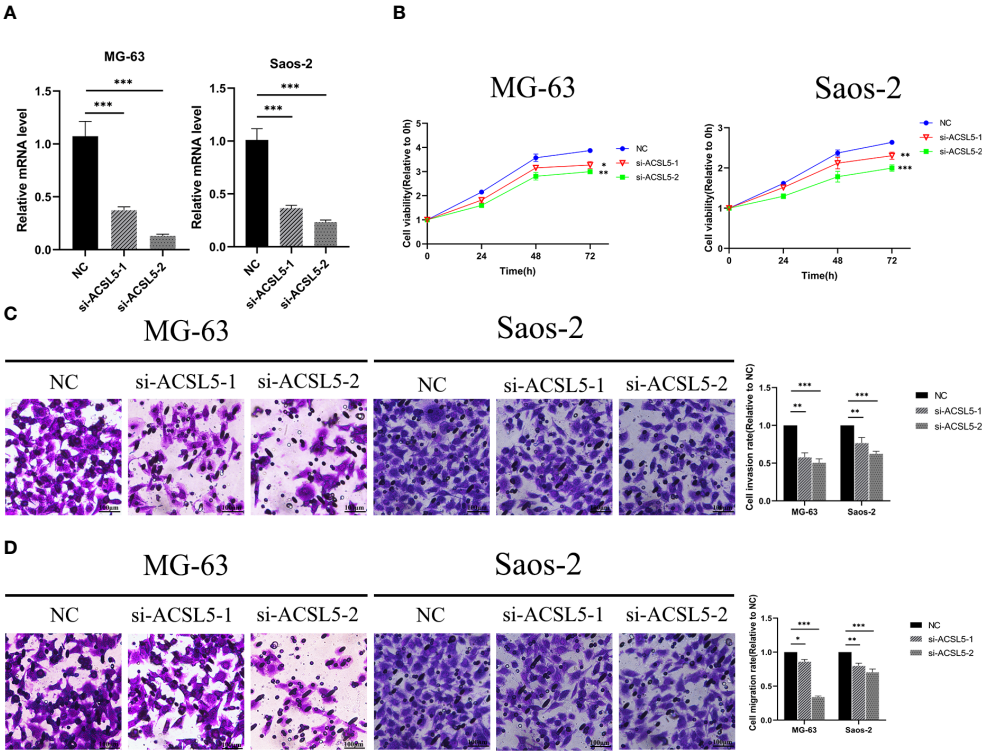

FIGURE 13
(A) The downregulation of ACSL5 expression in MG63 and Saos-2 cells was confirmed by RT-qPCR using two distinct siRNA sequences. **(B)** Differential knockdown efficacy of ACSL5 expression in MG-63 and Saos-2 cells was observed between the two siRNA sequences. **(C)** Following knockdown of ACSL5 using both sets of sequences, differential invasion capacities were observed in MG-63 and Saos-2 cells. **(D)** Subsequent to the knockdown of ACSL5 expression using both sets of sequences, differential migration capacities were observed in MG-63 and Saos-2 cells. * p<0.05; ** p<0.01; ****p<0.0001.

suggests its diverse roles within cells and the entire immune system, highlighting its potential as a therapeutic target for cancer and autoimmune diseases (44). CD163, an abundant endocytic receptor for various ligands, is particularly enriched in the inflammatory and tumor microenvironments with $CD163^+$ macrophages (45). Studies indicate CD163-positive M2-polarized macrophages as robust biomarkers for diagnosis and stratification of OS patients (46). We divided the cohorts into high and low-risk groups based on the

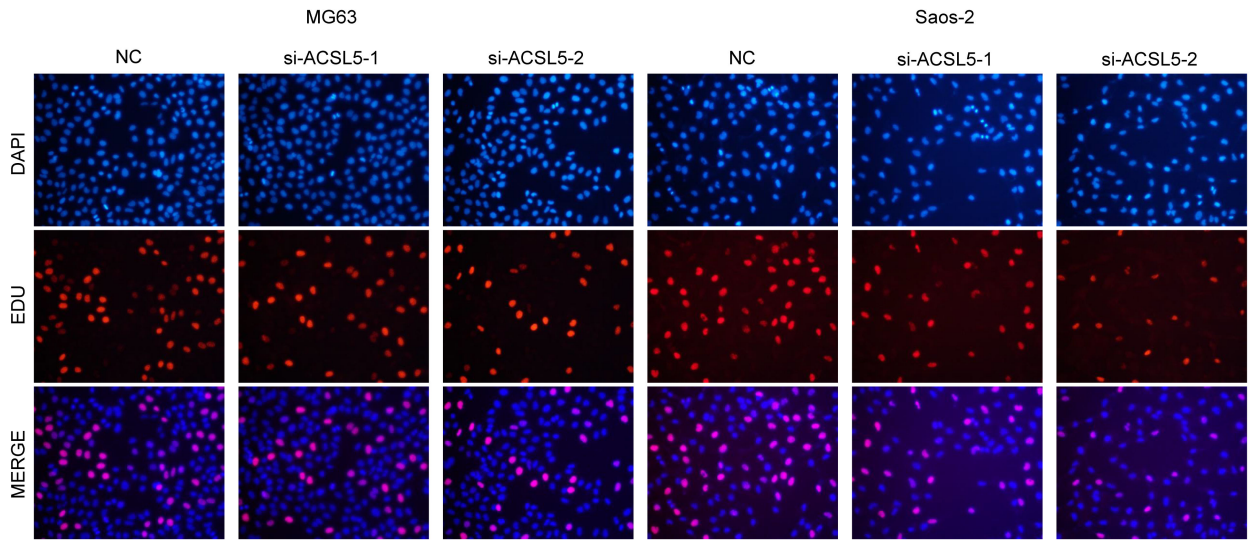

FIGURE 14
EdU assay between the control group and ACSL5 knockdown cells.

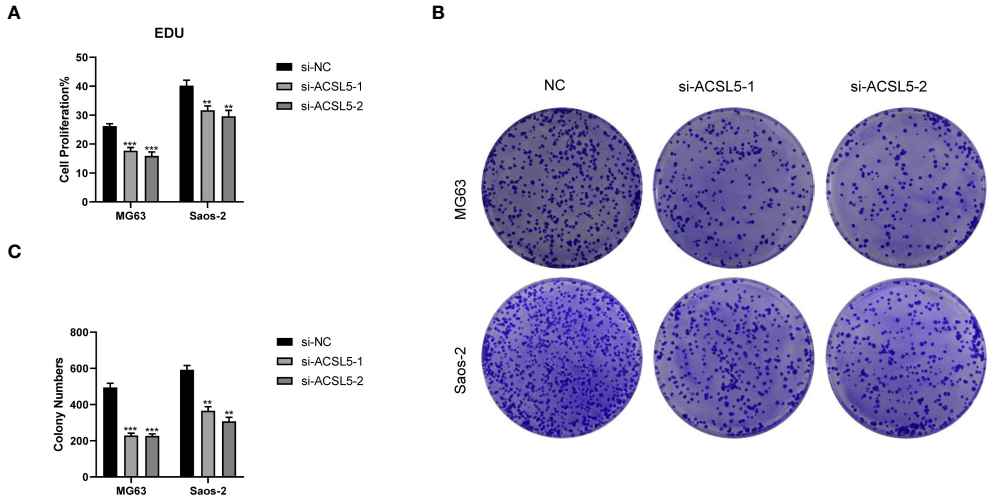

FIGURE 15
Colony formation experiments between the control group and ACSL5 knockdown cells. **(A)** The statistical data of the EDU assay. **(B, C)** The colon formation assay of ACSL5. ** p<0.01; *** p<0.001.

median scores of each dataset. Survival analysis showed a poorer prognosis for the high-risk group, while ROC curve analysis confirmed the model's strong performance at 1, 3, and 5 years.

Immune cell infiltration analysis identified relevant immune cell subtypes. Box plots illustrated differential expression of M2 and exhausted T cell markers between the two risk groups, with significantly higher expression observed in most of the high-risk group. Both markers are associated with tumor immune suppression, indicating a poorer immune microenvironment in the high-risk group (47). Violin plots depicted higher mRNAsi indices in the high-risk group. Sensitivity analysis to nine drugs indicated lower drug sensitivity in the high-risk group. Differential gene expression analysis between the two risk groups, followed by GSEA analysis of dysregulated pathways, revealed upregulation of numerous common tumor pathways in the high-risk group, suggesting activation of multiple tumor progression pathways and resistance to drug therapy and immune cell cytotoxicity. The malignant characteristics of tumors in the high-risk group are multifaceted and interrelated. Further exploration of tumor characteristics is necessary to develop targeted therapies for such patients. UMAP dimensionality reduction clustering of integrated single-cell data annotated ten cell subtypes based on cell-specific markers, with subsequent analysis of gene expression within each subtype. We annotated and identified malignant cells and calculated upregulated and downregulated genes in each subtype. GO_BP analysis showed significant pathway upregulation in certain cell subtypes. Using Seurat, we evaluated our prognostic model's activity in single-cell datasets, confirming its effectiveness.

ACSL5 belongs to an activating enzyme family of long-chain fatty acids (LCFAs), the role of which are not well understood. ACSL5 expression correlates with improved survival in lung cancer patients, and plasma EA levels predict immunotherapy success. Targeting ACSL5 may enhance immunotherapy by reprogramming antigen presentation (48). Research indicates that the protein PPARGC1A is linked to the development of hepatocellular carcinoma (HCC), although its exact functions and related pathways are not fully understood. PPARGC1A is under-expressed in HCC and correlates with a poorer prognosis. As regard to the underlying mechanisms, a PPARGC1A/BAMBI/ACSL5 axis is found to be responsive to hypoxia (49). In an effort to identify crucial biomarkers for pancreatic cancer prognosis, a study discovered a total of four genes, ACSL5, SLC44A4, LOX, and TOX3, showing correlation with PFS as indicated by qPCR and immunohistochemical staining. Further analysis revealed that differentiation status, tumor stage, LOX expression, and ACSL5 expression were independent factors predicting prognosis (50). In the context of OS, as one of ferroptosis-related genes, ACSL5 was integrated into a prognostic model for OS patient prognosis (51). However, the mechanic role of ACSL5 in the OS carcinogenesis remains to be further clarified. In our study, we validated that silencing ACSL5 (a pro-oncogene) via cell culture, siRNA transfection, RT-qPCR, cell proliferation assays, and cell migration and invasion assays reduced oncogenic behaviors like proliferation, migration, and invasion in OS cells.

5 Conclusion

This study conducted an in-depth analysis of the TME in OS, revealing two significantly distinct subgroups. Our prognostic model, based on eleven key genes (ALOX5AP, CD37, BIN2, C3AR1, HCLS1, ACSL5, CD209, FCGR2A, CORO1A, CD74, CD163), demonstrated good performance in predicting patient survival and disease progression. Additionally, we conducted immune analysis, drug sensitivity analysis, and gene enrichment analysis, providing new insights and theoretical foundations for the treatment and drug development of OS patients. Single cell sequencing analysis further revealed the expression profiles of cell subgroups, deepening our understanding of the immune microenvironment in OS. In summary, our study provides valuable insights and guidance for improving the prognosis of OS patients. It highlights key areas for optimizing treatment strategies and supports the development of more

effective drugs. By identifying crucial genes and pathways, our research lays the groundwork for targeted therapies and personalized medicine approaches in OS, ultimately aiming to enhance patient outcomes and survival rates.

Data availability statement

The datasets presented in this study can be found in online repositories. The names of the repository/repositories and accession number(s) can be found in the article/supplementary material.

Ethics statement

Ethical approval was not required for the studies on humans in accordance with the local legislation and institutional requirements because only commercially available established cell lines were used. Ethical approval was not required for the studies on animals in accordance with the local legislation and institutional requirements because only commercially available established cell lines were used.

Author contributions

SS: Conceptualization, Data curation, Writing – original draft. LZ: Conceptualization, Formal analysis, Investigation, Project administration, Writing – review & editing. XG: Conceptualization, Data curation, Writing – original draft.

Funding

The author(s) declare financial support was received for the research, authorship, and/or publication of this article. This study was supported by Natural Science Foundation of Shanxi Province, Grant/Award Number: 2021SF-241.

Conflict of interest

The authors declare that the research was conducted in the absence of any commercial or financial relationships that could be construed as a potential conflict of interest.

Publisher's note

All claims expressed in this article are solely those of the authors and do not necessarily represent those of their affiliated organizations, or those of the publisher, the editors and the reviewers. Any product that may be evaluated in this article, or claim that may be made by its manufacturer, is not guaranteed or endorsed by the publisher.

References

1. Valery PC, Laversanne M, Bray F. Bone cancer incidence by morphological subtype: a global assessment. *Cancer causes control CCC*. (2015) 26:1127–39. doi: 10.1007/s10552-015-0607-3

2. Kansara M, Teng MW, Smyth MJ, Thomas DM. Translational biology of osteosarcoma. *Nat Rev Cancer*. (2014) 14:722–35. doi: 10.1038/nrc3838

3. Simpson E, Brown HL. Understanding osteosarcomas. *JAAPA*. (2018) 31:15–9. doi: 10.1097/01.JAA.0000541477.24116.8d

4. Wittig JC, Bickels J, Priebat D, Jelinek J, Kellar-Graney K, Shmookler B, et al. Osteosarcoma: a multidisciplinary approach to diagnosis and treatment. *Am Fam Physician*. (2002) 65:1123–32.

5. Corre I, Verrecchia F, Crenn V, Redini F, Trichet V. The osteosarcoma microenvironment: A complex but targetable ecosystem. *Cells*. (2020) 9:976. doi: 10.3390/cells9040976

6. Mirabello L, Troisi RJ, Savage SA. International osteosarcoma incidence patterns in children and adolescents, middle ages and elderly persons. *Int J Cancer*. (2009) 125:229–34. doi: 10.1002/ijc.24320

7. Damron TA, Ward WG, Stewart A. Osteosarcoma, chondrosarcoma, and Ewing's sarcoma: National Cancer Data Base Report. *Clin orthopaedics related Res*. (2007) 459:40–7. doi: 10.1097/BLO.0b013e318059b8c9

8. Nie Z, Peng H. Osteosarcoma in patients below 25 years of age: An observational study of incidence, metastasis, treatment and outcomes. *Oncol Lett*. (2018) 16:6502–14. doi: 10.3892/ol

9. Fuchs B, Pritchard DJ. Etiology of osteosarcoma. *Clin orthopaedics related Res*. (2002) 397):40–52. doi: 10.1097/00003086-200204000-00007

10. Mirabello L, Troisi RJ, Savage SA. Osteosarcoma incidence and survival rates from 1973 to 2004: data from the Surveillance, Epidemiology, and End Results Program. *Cancer*. (2009) 115:1531–43. doi: 10.1002/cncr.24121

11. Nishida Y, Isu K, Ueda T, Nishimoto Y, Tsuchiya H, Wada T, et al. Osteosarcoma in the elderly over 60 years: a multicenter study by the Japanese Musculoskeletal Oncology Group. *J Surg Oncol*. (2009) 100:48–54. doi: 10.1002/jso.21287

12. Zhao X, Wu Q, Gong X, Liu J, Ma Y. Osteosarcoma: a review of current and future therapeutic approaches. *Biomed Eng Online*. (2021) 20:24. doi: 10.1186/s12938-021-00860-0

13. Cersosimo F, Lonardi S, Bernardini G, Telfer B, Mandelli GE, Santucci A, et al. Tumor-associated macrophages in osteosarcoma: from mechanisms to therapy. *Int J Mol Sci*. (2020) 21:5207. doi: 10.3390/ijms21155207

14. Bernthal NM, Federman N, Eilber FR, Nelson SD, Eckardt JJ, Eilber FC, et al. Long-term results (>25 years) of a randomized, prospective clinical trial evaluating chemotherapy in patients with high-grade, operable osteosarcoma. *Cancer*. (2012) 118:5888–93. doi: 10.1002/cncr.27651

15. Mahajan A, Woo SY, Kornguth DG, Hughes D, Huh W, Chang EL, et al. Multimodality treatment of osteosarcoma: radiation in a high-risk cohort. *Pediatr Blood Cancer*. (2008) 50:976–82. doi: 10.1002/pbc.21451

16. Gaspar N, Occean BV, Pacquement H, Bompas E, Bouvier C, Brisse HJ, et al. et al: Results of methotrexate-etoposide-ifosfamide based regimen (M-EI) in osteosarcoma patients included in the French OS2006/sarcome-09 study. *Eur J Cancer (Oxford Engl 1990)*. (2018) 88:57–66. doi: 10.1016/j.ejca.2017.09.036

17. Song XJ, Bi MC, Zhu QS, Liu XL. The emerging role of lncRNAs in the regulation of osteosarcoma stem cells. *Eur Rev Med Pharmacol Sci*. (2022) 26:966–74. doi: 10.26355/eurrev_202202_28006

18. Su H, Wang Y, Li H. RNA m6A methylation regulators multi-omics analysis in prostate cancer. *Front Genet*. (2021) 12 doi: 10.3389/FGENE.2021.768041

19. Zhou Y, Yang D, Yang Q, Lv X, Huang W, Zhou Z, et al. et al: Single-cell RNA landscape of intratumoral heterogeneity and immunosuppressive microenvironment in advanced osteosarcoma. *Nat Commun*. (2020) 11:6322. doi: 10.1038/s41467-020-20059-6

20. Wu S, Zhao K, Wang J, Liu N, Nie K, Qi L, et al. Recent advances of tanshinone in regulating autophagy for medicinal research. *Front Pharmacol*. (2023) 13 doi: 10.3389/fphar.2022.1059360

21. Jianfeng W, Yutao W, Jianbin B. Long non-coding RNAs correlate with genomic stability in prostate cancer: a clinical outcome and survival analysis. *Genomics*. (2021) 113(5):3141-51. doi: 10.1016/j.ygeno.2021.06.029

22. Qi L, Zhong F, Chen Y, Mao S, Yan Z, Ma Y. An integrated spectroscopic strategy to trace the geographical origins of emblic medicines: Application for the quality assessment of natural medicines. *J Pharm Anal*. (2020) 10(4):356-64. doi: 10.1016/j.jpha.2019.12.004

23. Wang J, An G, Peng X, Zhong F, Zhao K, Qi L, et al. Effects of three Huanglian-derived polysaccharides on the gut microbiome and fecal metabolome of high-fat diet/streptozocin-induced type 2 diabetes mice. *Int J Biol Macromol*. (2024) 273(Pt 1):133060. doi: 10.1016/j.ijbiomac.2024.133060

24. Zhao K, Wu X, Han G, Sun L, Zheng C, Hou H, et al. Phyllostachys nigra (Lodd. ex Lindl.) derived polysaccharide with enhanced glycolipid metabolism regulation and mice gut microbiome. *Int J Biol Macromol*. (2024) 257(Pt 1):128588. doi: 10.1016/j.ijbiomac.2023.128588

25. Zeng X, Wang S, Peng Z, Wang M, Zhao K, Xu BB, et al. Rapid screening and sensing of stearoyl-CoA desaturase 1 (SCD1) inhibitors from ginger and their efficacy in ameliorating non-alcoholic fatty liver disease. *Food Measure*. (2024). doi: 10.1007/s11694-024-02697-2

26. Li KL, Chen CY, Xu M, Zhu XQ, Yang XJ. ALOX5AP rs10507391 polymorphism and the risk of ischemic stroke in Caucasians: an update meta-analysis. *Cell Mol Biol (Noisy-le-Grand France)*. (2017) 63:137–40. doi: 10.14715/cmb/2017.63.10.22

27. Hong SH, Avis I, Vos MD, Martínez A, Treston AM, Mulshine JL. Relationship of arachidonic acid metabolizing enzyme expression in epithelial cancer cell lines to the growth effect of selective biochemical inhibitors. *Cancer Res*. (1999) 59:2223–8.

28. de Winde CM, Veenbergen S, Young KH, Xu-Monette ZY, Wang XX, Xia Y, et al. et al: Tetraspanin CD37 protects against the development of B cell lymphoma. *J Clin Invest*. (2016) 126:653–66. doi: 10.1172/JCI81041

29. Mao X, Song F, Jin J, Zou B, Dai P, Sun M, et al. Prognostic and immunological significance of an M1 macrophage-related gene signature in osteosarcoma. *Front Immunol*. (2023) 14:1202725. doi: 10.3389/fimmu.2023.1202725

30. Song X, Ji J, Gleason KJ, Yang F, Martignetti JA, Chen LS, et al. Insights into Impact of DNA Copy Number Alteration and Methylation on the Proteogenomic Landscape of Human Ovarian Cancer via a Multi-omics Integrative Analysis. *Mol Cell Proteomics MCP*. (2019) 18:S52–s65. doi: 10.1074/mcp.RA118.001220

31. Koboldt DC, Fulton RS, McLellan MD, Schmidt H, Kalicki-Veizer J, McMichael JF, et al. Comprehensive molecular portraits of human breast tumours. *Nature*. (2012) 490:61–70. doi: 10.1038/nature11412

32. Xu C, Xu J, Lu L, Tian W, Ma J, Wu M. Identification of key genes and novel immune infiltration-associated biomarkers of sepsis. *Innate Immun*. (2020) 26:666–82. doi: 10.1177/1753425920966380

33. Propson NE, Roy ER, Litvinchuk A, Köhl J, Zheng H. Endothelial C3a receptor mediates vascular inflammation and blood-brain barrier permeability during aging. *J Clin Invest*. (2021) 131:e140966. doi: 10.1172/JCI140966

34. Kitamura D, Kaneko H, Miyagoe Y, Ariyasu T, Watanabe T. Isolation and characterization of a novel human gene expressed specifically in the cells of hematopoietic lineage. *Nucleic Acids Res*. (1989) 17:9367–79.

35. van Rossum AG, Schuuring-Scholtes E, van Buuren-van Seggelen V, Kluin PM, Schuuring E. Comparative genome analysis of cortactin and HS1: the significance of the F-actin binding repeat domain. *BMC Genomics*. (2005) 6:15. doi: 10.1186/1471-2164-6-15

36. Zhang N, Wang H, Xie Q, Cao H, Wu F, Di Wu DB, et al. Identification of potential diagnostic and therapeutic target genes for lung squamous cell carcinoma. *Oncol Lett*. (2019) 18:169–80. doi: 10.3892/ol

37. Rossi Sebastiano M, Konstantinidou G. Targeting long chain acyl-coA synthetases for cancer therapy. *Int J Mol Sci*. (2019) 20:3624. doi: 10.3390/ijms20153624

38. Lin A, Yang H, Zhang J, Luo P. CD209 signaling pathway as a biomarker for cisplatin chemotherapy response in small cell lung cancer. *Genes Dis*. (2024) 11:101038. doi: 10.1016/j.gendis.2023.06.011

39. Kremsreiter SM, Kroell AH, Weinberger K, Boehm H. Glycan-lectin interactions in cancer and viral infections and how to disrupt them. *Int J Mol Sci*. (2021) 22:10577. doi: 10.3390/ijms221910577

40. He J, Yu L, Qiao Z, Yu B, Liu Y, Ren H. Genetic polymorphisms of FCGR2A, ORAI1 and CD40 are associated with risk of lung cancer. *Eur J Cancer Prev*. (2022) 31:7–13. doi: 10.1097/CEJ.0000000000000671

41. Li F, Teng H, Liu M, Liu B, Zhang D, Xu Z, et al. Prognostic value of immune-related genes in the tumor microenvironment of bladder cancer. *Front Oncol*. (2020) 10:1302. doi: 10.3389/fonc.2020.01302

42. He Y, Jiang Z, Chen C, Wang X. Classification of triple-negative breast cancers based on Immunogenomic profiling. *J Exp Clin Cancer Res CR*. (2018) 37:327. doi: 10.1186/s13046-018-1002-1

43. Hong WC, Lee DE, Kang HW, Kim MJ, Kim M, Kim JH, et al. CD74 promotes a pro-inflammatory tumor microenvironment by inducing S100A8 and S100A9 secretion in pancreatic cancer. *Int J Mol Sci*. (2023) 24:12993. doi: 10.3390/ijms241612993

44. Borghese F, Clanchy FI. CD74: an emerging opportunity as a therapeutic target in cancer and autoimmune disease. *Expert Opin Ther Targets*. (2011) 15:237–51. doi: 10.1517/14728222.2011.550879

45. Skytthe MK, Graversen JH, Moestrup SK. Targeting of CD163(+) macrophages in inflammatory and Malignant diseases. *Int J Mol Sci*. (2020) 21:5497. doi: 10.3390/ijms21155497

46. Gomez-Brouchet A, Illac C, Gilhodes J, Bouvier C, Aubert S, Guinebretiere JM, et al. CD163-positive tumor-associated macrophages and CD8-positive cytotoxic lymphocytes are powerful diagnostic markers for the therapeutic stratification of osteosarcoma patients: An immunohistochemical analysis of the biopsies fromthe French OS2006 phase 3 trial. *Oncoimmunology*. (2017) 6:e1331193. doi: 10.1080/2162402X.2017.1331193

47. Hu T, Wang Y, Wang X, Wang R, Song Y, Zhang L, et al. Construction and validation of an angiogenesis-related gene expression signature associated with clinical outcome and tumor immune microenvironment in glioma. *Front Genet*. (2022). 13. doi: 10.3389/fgene.2022.934683

48. Lai Y, Gao Y, Lin J, Liu F, Yang L, Zhou J, et al. et al: Dietary elaidic acid boosts tumoral antigen presentation and cancer immunity *via* ACSL5. *Cell Metab*. (2024) 36:822–38.e828. doi: 10.1016/j.cmet.2024.01.012

49. Zhang Q, Xiong L, Wei T, Liu Q, Yan L, Chen J, et al. et al: Hypoxia-responsive PPARGC1A/BAMBI/ACSL5 axis promotes progression and resistance to lenvatinib in hepatocellular carcinoma. *Oncogene*. (2023) 42:1509–23. doi: 10.1038/s41388-023-02665-y

50. Ma W, Li T, Wu S, Li J, Wang X, Li H. LOX and ACSL5 as potential relapse markers for pancreatic cancer patients. *Cancer Biol Ther*. (2019) 20:787–98. doi: 10.1080/15384047.2018.1564565

51. Huang H, Ye Z, Li Z, Wang B, Li K, Zhou K, et al. Employing machine learning using ferroptosis-related genes to construct a prognosis model for patients with osteosarcoma. *Front Genet*. (2023) 14:1099272. doi: 10.3389/fgene.2023.1099272

frontiers | Frontiers in Immunology

TYPE Mini Review
PUBLISHED 30 July 2024
DOI 10.3389/fimmu.2024.1444426

Check for updates

OPEN ACCESS

EDITED BY
Wantao Wu,
Central South University, China

REVIEWED BY
Xiaofei Liu,
Affiliated Hospital of Shandong University of Traditional Chinese Medicine, China
Shengze Yao,
Massachusetts General Hospital and Harvard Medical School, United States

*CORRESPONDENCE
Ke Xu
cqghxuke@cqu.edu.cn
Guanhu Yang
gy182915@ohio.edu
Shangke Huang
huangshangke001@swmu.edu.cn
Hao Chi
Chihao7511@163.com

†These authors have contributed equally to this work and share first authorship

RECEIVED 05 June 2024
ACCEPTED 16 July 2024
PUBLISHED 30 July 2024

CITATION
Yan Y, Su L, Huang S, He Q, Lu J, Luo H, Xu K, Yang G, Huang S and Chi H (2024) Circadian rhythms and breast cancer: unraveling the biological clock's role in tumor microenvironment and ageing.
Front. Immunol. 15:1444426.
doi: 10.3389/fimmu.2024.1444426

COPYRIGHT
© 2024 Yan, Su, Huang, He, Lu, Luo, Xu, Yang, Huang and Chi. This is an open-access article distributed under the terms of the Creative Commons Attribution License (CC BY). The use, distribution or reproduction in other forums is permitted, provided the original author(s) and the copyright owner(s) are credited and that the original publication in this journal is cited, in accordance with accepted academic practice. No use, distribution or reproduction is permitted which does not comply with these terms.

Circadian rhythms and breast cancer: unraveling the biological clock's role in tumor microenvironment and ageing

Yalan Yan[1†], Lanqian Su[1†], Shanshan Huang[1†], Qihui He[2], Jiaan Lu[1], Huiyan Luo[3], Ke Xu[3*], Guanhu Yang[4*], Shangke Huang[5*] and Hao Chi[1*]

[1]Clinical Medical College, Southwest Medical University, Luzhou, China, [2]Department of Paediatrics, Southwest Medical University, Luzhou, China, [3]Department of Oncology, Chongqing General Hospital, Chongqing University, Chongqing, China, [4]Department of Specialty Medicine, Ohio University, Athens, OH, United States, [5]Department of Oncology, The Affiliated Hospital, Southwest Medical University, Luzhou, China

Breast cancer (BC) is one of the most common and fatal malignancies among women worldwide. Circadian rhythms have emerged in recent studies as being involved in the pathogenesis of breast cancer. In this paper, we reviewed the molecular mechanisms by which the dysregulation of the circadian genes impacts the development of BC, focusing on the critical clock genes, brain and muscle ARNT-like protein 1 (BMAL1) and circadian locomotor output cycles kaput (CLOCK). We discussed how the circadian rhythm disruption (CRD) changes the tumor microenvironment (TME), immune responses, inflammation, and angiogenesis. The CRD compromises immune surveillance and features and activities of immune effectors, including CD8+ T cells and tumor-associated macrophages, that are important in an effective anti-tumor response. Meanwhile, in this review, we discuss bidirectional interactions: age and circadian rhythms, aging further increases the risk of breast cancer through reduced vasoactive intestinal polypeptide (VIP), affecting suprachiasmatic nucleus (SCN) synchronization, reduced ability to repair damaged DNA, and weakened immunity. These complex interplays open new avenues toward targeted therapies by the combination of clock drugs with chronotherapy to potentiate the immune response while reducing tumor progression for better breast cancer outcomes. This review tries to cover the broad area of emerging knowledge on the tumor-immune nexus affected by the circadian rhythm in breast cancer.

KEYWORDS

circadian rhythm, breast cancer, therapeutic targets in immunotherapy, aging, tumor microenvironment, clockwork therapy, tumor-immune interactions

1 Introduction

From gene expression and cellular metabolism to intricate biological behaviors, endogenous oscillations in organisms over approximately 24 hours are known as circadian rhythms. Disruptions in these rhythms increase the risk of various cancers (1, 2). In the breast, altered circadian gene expression affects breast biology, potentially promoting cancer (3). The coordination of intrinsic molecular clock networks between central and peripheral tissues maintains circadian rhythms. Core genes such as BMAL1 and CLOCK are positive transcription factors in circadian rhythms, which are involved in the regulation of immune cell function (4), and their overexpression promotes cancer cell proliferation and invasion (5, 6). Circadian rhythms also adjust the TME with tumor initiation and influence (7), and the tumor microenvironment is closely related to multiple stages of tumor initiation, progression, invasion, metastatic spread and growth (8). In this, proliferative and invasive behaviors are crucial processes.

Peripheral tissue rhythms are coordinated by the central clock in the SCN (9). Aging impairs SCN function, promoting age-related diseases (10). Breast cancer, an age-related disease, illustrates the complex interplay between circadian disruption, aging, and cancer risk. Circadian rhythm-related studies propose strategies for combining clock drugs and therapies to treat breast cancer.

This review outlines the role of circadian genes in breast cancer development, the impact of CRD on the TME, and the relationship between circadian rhythms, aging, and cancer risk. By synthesizing these findings, we aim to reveal the significant role of circadian rhythms in breast cancer pathogenesis and provide new treatment perspectives.

2 Exploring the relationship between circadian rhythms and breast cancer

2.1 Basis of circadian rhythms

The mammalian circadian system is multileveled and includes a central clock located in the hypothalamic SCN along with distributed peripheral clocks in the various tissues (11). (Figure 1A) The SCN nuclei maintain circadian rhythms, with a significant input pathway from environmental light signals (12). Light information is conveyed from the retina to the SCN via the retinal-hypothalamic pathway (13). Although peripheral clocks can

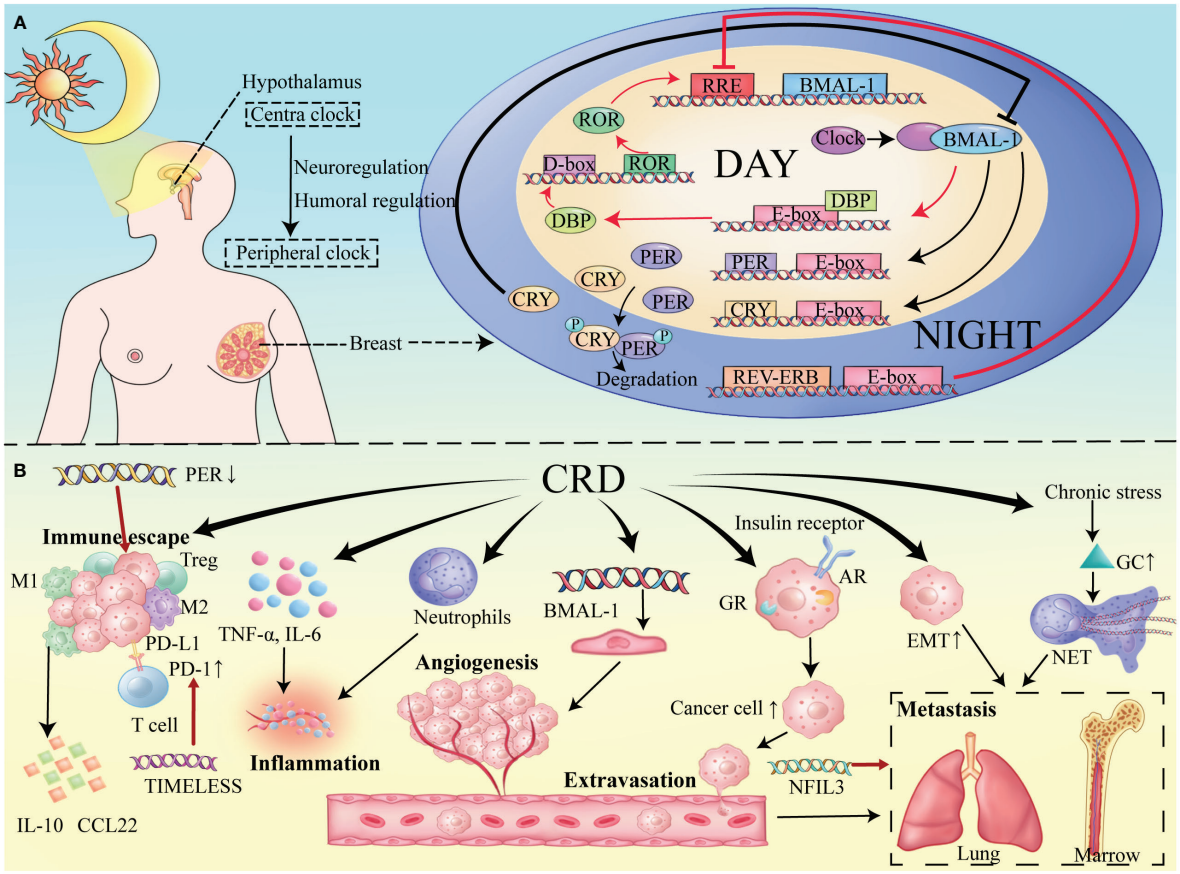

FIGURE 1
(A) Circadian Molecular Mechanism in Mammary Tissue. Main Loop (black lines): CLOCK-BMAL1 induces the expression of PER and CRY proteins. The main pathway for the production and maintenance of circadian rhythm. Secondary Loop (red lines): ROR and REV-ERB respectively promote and inhibit the production of BMAL1, thereby maintaining the stability of the main loop. **(B)** Impact of the tumor microenvironment on breast cancer under conditions of circadian rhythm disruption.

autonomously generate rhythms, synchronization with the central clock is essential for coherence (14). This synchronization occurs through neural and humoral pathways, maintaining consistent phase relationships within the circadian system (11).

At the molecular level, a complex network of transcription factors forms at the heart of the mammalian circadian clock, interacting through various transcriptional and translational feedback loops (TTFLs) that autoregulate activation and inhibition, thereby imposing the 24-hour cyclic rhythm on this process (15) (Figure 1A).

Within the primary loop of the circadian cycle, the positive regulators are heterodimers composed of BMAL1 and CLOCK transcription factors. During daylight hours, the CLOCK-BMAL1 complex binds to E-box regions in target genes, promoting their expression. These genes include negative regulators such as Period (PER) and Cryptochrome (CRY), which modulate the circadian rhythm. At night, PER and CRY form heterodimers, translocate to the nucleus, and inhibit CLOCK-BMAL1 activity, halting transcription (16, 17). Post-translational modifications then lead to PER and CRY degradation (18), allowing the cycle to restart once their levels are sufficiently reduced.

In addition to PER and CRY, the CLOCK-BMAL1 complex targets orphan nuclear receptors REV-ERBα and REV-ERBβ (19). These receptors are integral to forming a secondary feedback loop with RORα, RORβ, and RORγ (20). REV-ERB and ROR proteins compete for binding to the RRE elements in target gene promoters and enhancers, modulating transcription and ensuring the rhythmic expression of BMAL1 (21).

Other TTFLs include key transcription factors like DBP, which contribute to the stability of the circadian clock, maintaining oscillations even in constant conditions (22).

2.2 Circadian rhythm genes involved in breast cancer development

Circadian rhythms are regulated by a series of clock genes, which are strongly associated with the progression of breast cancer.

BMAL1 and CLOCK, as key transcription factors, are integral to breast cancer progression. Their overexpression correlates with increased tumor cell proliferation and invasion (5, 6). Notably BMAL1 regulates the involvement of Nrf2 in carcinogenesis, for example, its deletion downregulates the Nrf2-mediated antioxidant pathway and significantly increases the amount of IL-1β, which promotes cancer (5). Whereas, Nrf2 has both oncogenic and carcinogenic effects in breast cancer, and its oncogenic effects are achieved by binding to keap-1 to reduce Reactive Oxygen Species (ROS) and inhibit the pro-cancer effects of high levels of ROS (23). Furthermore, c-Myc can regulate cell proliferation (24), and is a key mediator between breast cancer cells and TME (25). And the target E-box sequence of CLOCK-NPAS2 (neuronal PAS domain protein 2)-BMAL1 complex is also a c-Myc cross site. Therefore, the core clock gene may regulate c-Myc expression to regulate cell proliferation (26).

Conversely, the PER and CRY genes act as negative regulator of circadian rhythms. Deletion of PER2 enhances breast cancer cell proliferation, likely due to decreased p53, increased c-Myc and increased CyclinD1 expression (18). PER2 is considered to be a tumor suppressor by inhibiting Epithelial-Mesenchymal Transition (EMT) and controlling cell proliferation; however, the ZnF704/SIN3A complex inhibits PER2 transcription, disrupts circadian rhythms, and exacerbates cancer cell invasion and metastasis (27). Recent studies have shown that CRY1 inhibits the growth of triple-negative breast cancer (TNBC) cells, which is associated with its inhibition of Pyruvate Dehydrogenase Kinase 1 (Pdk1) expression, Pyruvate Dehydrogenase (PDH) phosphorylation, and glucose depletion (28). In addition to this, CRY1 is involved in cellular DNA damage repair, and its depletion enhances DNA damage in cancer cells, whereas CRY1 expression is reduced in the presence of Yes-associated protein (YAP) silencing or TEA domain transcription factor (TEAD) inhibition (29). As for CRY2, it can exert an anti-proliferative effect on breast cancer cells because it may bind and inhibit the p65/p50 complex, thus inhibiting the nuclear factor-κB (NF-κB) pathway, but its acetylation in breast cancer impairs this function (30), the exact mechanism has yet to be studied. These findings underscore the complex relationship between circadian genes and breast cancer development.

Moreover, other circadian components are crucial. For instance, elevated expression of nuclear factor, interleukin 3 regulated (NFIL3) enhances TNBC cell proliferation and metastasis by inhibiting Nuclear Factor kappa B Inhibitor Alpha (NFκBIA) transcription and boosting NF-κB signaling (31). Similarly, TIM (TIMLESS) facilitates immune evasion by upregulating PD-1, which suppresses CD8+ T cell immunoreactivity (32). And hypomethylation of the TIM promoter correlates with advanced breast cancer (33). Overall, TIM is significantly associated with clinical prognosis across various cancers (34, 35) (Table 1).

2.3 TME in the context of CRD

CD8+ T cells, M1 macrophages, and neutrophils perform immune surveillance in the process of irruption through the stages of breast cancer. Meanwhile, suppressive cells, such as M2 macrophages, myeloid-derived suppressor cells, and regulatory T cells, have indispensable roles in the tumor microenvironment, creating a complex network of immune responses in the tumor (36). Cancer cells often have increased stemness, while T cells predominantly exhibit a regulatory or exhausted phenotype, and the macrophages a type M2 phenotype (37, 38).

Circadian clocks regulate the tumor microenvironment of breast cancer through complex mechanisms of immune cell type and activity, inflammation, angiogenesis, and tumor cell migration and invasion, all constituting central features of the breast cancer microenvironment (Figure 1B).

M2-type tumor-associated macrophages (TAMs) promote immune tolerance by producing anti-inflammatory cytokines, such as CCL22 and IL10 (39). Under conditions of CRD, both M1-type macrophages and M1/M2 ratios were reduced in the tumor, the proportion of regulatory T cells was increased, and myeloid cell infiltration (7, 40, 41). Shift in cytokine production balance from Th1-cytokines to Th2 cytokines (including IL-10)

TABLE 1 Circadian rhythm genes in breast cancer.

Character	Genes	Mechanism	Effect on breast cancer	reference
Positive	CLOCK-NPAS2-BMAL1	Control the expression of oncogene c-Myc	Regulates cell proliferation in breast cancer	(26)
	BMAL1	Direct regulation of Nrf2	Regulation of the Dual Role of Nrf2 in Breast Cancer	(5)
Negative	PER2	When deficient, p53 expression decreases, while the expression of c-Myc and its target cell Cyclin D1 increases	Promote proliferation of breast cancer cells	(18)
	CRY1	Inhibition of Pdk1 expression, PDH phosphorylation, and glucose consumption	Inhibition of TNBC cell growth	(28)
	CRY1	Overactivation of YAP and enhanced DNA damage response	Altered cell growth in breast cancer	(29)
	CRY2	Acetylation	The antiproliferative effect is diminished in breast cancer	(30)
Other	NFIL3	Inhibit the transcription of NEκBIA and enhance NF-κB signaling.	Promote TNBC cell proliferation and metastasis	(31)
	TIMELESS	Up-regulated the expression of PD-L1 and inhibited the immune activity of CD8T cells	Promotes immune evasion in breast cancer	(32)

(42). And dysregulated clock gene expression was positively correlated with the levels of T-cell incompetence markers such as programmed cell death protein 1, all of which promoted immune escape (15).

Inflammation is a crucial driver of tumor progression, promoting the upregulation of pro-inflammatory cytokines under chronic jet lag, such as TNF-α and IL-6, which modulate the disruption of circadian rhythms (43). CRD can worsen neutrophil-driven inflammation, further degrading the tumor microenvironment (44). Circadian rhythm genes also regulate angiogenesis. Endothelial cell formation, the starting point for angiogenesis, is affected by circadian genes like BMAL1 (45) which regulate the endothelial cell cycle and thus impact angiogenesis and tumor progression (46). In a spontaneous mouse model of breast cancer, circadian rhythm disruption promotes cancer cell spread and metastasis (47). This may be due to elevated expression of EMT-related genes under CRD conditions, making cancer cells more motile and invasive (48, 49). CRD-associated chronic stress releases glucocorticoids, forming neutrophil extracellular traps (NETs) that foster a metastasis-promoting environment (50, 51). Breast cancer frequently metastasizes to the bone and lungs (52, 53). Circulating tumor cell (CTC) exudation predominantly occurs during sleep (54), influenced by circadian-regulated hormone receptors, which increases CTC activity and impacts breast cancer progression (55, 56). An in-depth study of the finer and more specific mechanisms by which CRD regulates TME can help provide a clearer direction for research.

3 Exploring aging, circadian rhythms, and breast cancer risk

Circadian rhythms are crucial for regulating immune cell activity, immune responses, and inflammation (15). Breast cancer is an age-related disease, which significantly contributes to its risk factors. Evidence demonstrates that this relationship is bidirectional (57); in other words, aging through disruption of the circadian rhythm is accelerated, and vice versa (58). These interactions are closely linked to breast cancer progression.

Aging disrupts circadian rhythms in several ways. First, it weakens light signal entrainment and diminishes neuronal electrical activity and communication. Light transmission through the lens and pupil can decrease by up to 90% (59), leading to desynchronization within the central clock and peripheral clocks (60). Additionally, SCN neuronal activity declines with age, reducing the rhythmic amplitude and coherence of firing patterns, causing phase desynchronization (61). Disruption of the biological clock in aging mammals has been linked to significantly impaired interneuronal communication in the SCN. Although the total number of neurons within the SCN remains relatively constant during aging, there is a marked decrease in the subpopulation that secretes the neurotransmitter VIP (62). VIP is an important mediator of interneuronal coupling in the SCN, and their decrease leads to a reduction in cell-to-cell coupling and thus affects the synchronization of the SCN network (60). On the other hand, aging also affects the peripheral clock, but the exact mechanism of action remains unclear, one reason being that different tissues and organs change differently during aging (63).

Similarly, the circadian system influences aging. In drosophila and mice, system-wide knockouts of CLOCK genes (including BMAL1, clock, PER, etc.) produce an "accelerated aging" phenotype, suggesting that central and peripheral molecular clocks play an important role in aging (64). Alterations independent of the loss of circadian rhythms in behavior. It has also been proposed that Bmal1 also interacts with the nuclear factor-activated κ-light chain-enhanced (NF-κB) signaling system in B cells, and that knockdown of this gene leads to a chronic inflammatory state, which accelerates the senescence phenotype (58).

Aging is a significant risk factor for breast cancer development (65). The combination of increased endogenous and exogenous DNA damage (66) and reduced DNA repair capacity in aging cells raises the likelihood of mutations in critical mammary cell genes (67). For instance, mutations in BRCA1 and BRCA2 during aging can increase tumor development risk by 80% (68). Aging also weakens the immune system, reducing its ability to detect and eliminate cancerous cells, leading to tumorigenesis (69). This decline in immune function causes chronic inflammation (70), associated with various cancers, including breast cancer (71) and prostate cancer (72). Additionally, aging affects estrogen levels, crucial for breast growth and cancer progression (73). As individuals age, the proportion of adipocytes producing estrogen rises, leading to sustained high levels of estradiol. This, in turn, affects the expression of estrogen receptors and the behavior of cancer cells (74).

4 Conclusion and prospect

From the preceding discussion, it is evident that disruptions in circadian rhythms are strongly linked to the initiation and advancement of breast cancer. Consequently, we are proposing a pioneering therapeutic approach for breast cancer that leverages circadian rhythms. It is well-recognized that conventional breast cancer treatments primarily impede disease progression through various strategies: adjusting estrogen receptor levels, disrupting DNA and RNA synthesis in cancer cells, inhibiting cyclins, and specifically targeting the HER2 receptor. This novel method focuses on circadian rhythms, aiming to achieve therapeutic outcomes by correcting disrupted circadian rhythms at the cellular or molecular level. Moreover, this treatment offers significant advantages over traditional methods, including enhanced drug effectiveness, fewer side effects, and improved immune response (75). This emerging focus has garnered significant interest. There are two significant strategies being followed at present for the treatment of breast cancer based on circadian rhythm: 1) the administration of drugs either directly or indirectly acting on components of biological clocks, and 2) scheduling drug administration according to the circadian host's endogenous clock.

Clock drugs exert their anticancer effects both by the direct modulation of the circadian rhythm, such as through the biological clock by core circadian genes, and indirectly by the rhythm gene regulators. The latter method focuses on proteins that are involved in the phosphorylation or degradation of clock components, such as REV-ERB, ROAR, CRY1/2, CRA, and the casein kinase (CK) family (18), which is more straightforward and potent. For instance, CRY protein modulators inhibit breast cancer cell proliferation without affecting normal breast epithelial cells (76). These pharmaceutical interventions have brought new hope for breast cancer management (77). However, challenges remain due to limited human research on circadian gene expression in breast cancer (78) and the low specificity of clock drugs (1), affecting their clinical application.

Chronotherapy, which involves administering treatment at specific times aligned with circadian rhythms, enhances efficacy and reduces side effects, especially in cancer therapy by lowering toxicity and increasing drug effectiveness (79, 80). Experiments in rodents have shown that the timing of anticancer drugs can result in 2- to 10-fold differences in tolerance (81). Clinical trials, such as those using azithromycin and cisplatin in advanced ovarian cancer, have demonstrated increased survival rates (82). However, a study in rectal cancer found no significant benefit from clock-based drug administration (83). Thus, the evidence for routine clinical use of chronotherapy in cancer treatment remains inconclusive. Additionally, breast cancer chronotherapy faces challenges like the unclear oscillation mechanisms in breast tissues and the absence of effective methods to detect breast clock gene expression patterns (84). Future strategies must carefully consider drug timing design (26).

In addition, regarding the diagnosis and prognosis assessment of breast cancer, conducting research from the perspective of circadian rhythms, developing biomarkers related to circadian rhythms, and establishing a prognosis assessment system based on circadian rhythms … are all worthwhile research areas to explore.

Author contributions

YY: Writing – original draft, Writing – review & editing, Data curation. LS: Data curation, Writing – original draft, Writing – review & editing. SSH: Writing – original draft. QH: Writing – original draft. JL: Writing – original draft. HL: Writing – original draft. KX: Writing – original draft. GY: Supervision, Writing – original draft. SH: Funding acquisition, Supervision, Writing – original draft. HC: Supervision, Writing – original draft.

Funding

The author(s) declare financial support was received for the research, authorship, and/or publication of this article. This study was granted by the Science and Technology Strategic Cooperation Programs of Luzhou Municipal People's Government and Southwest Medical University (No.2023LZXNYDJ033).

Conflict of interest

The authors declare that the research was conducted in the absence of any commercial or financial relationships that could be construed as a potential conflict of interest.

Publisher's note

All claims expressed in this article are solely those of the authors and do not necessarily represent those of their affiliated organizations, or those of the publisher, the editors and the reviewers. Any product that may be evaluated in this article, or claim that may be made by its manufacturer, is not guaranteed or endorsed by the publisher.

References

1. Zhou L, Zhang Z, Nice E, Huang C, Zhang W, Tang Y. Circadian rhythms and cancers: the intrinsic links and therapeutic potentials. *J Hematol Oncol.* (2022) 15:21. doi: 10.1186/s13045-022-01238-y

2. Lee Y. Roles of circadian clocks in cancer pathogenesis and treatment. *Exp Mol Med.* (2021) 53:1529–38. doi: 10.1038/s12276-021-00681-0

3. Blakeman V, Williams JL, Meng QJ, Streuli CH. Circadian clocks and breast cancer. *Breast Cancer Res.* (2016) 18:89. doi: 10.1186/s13058-016-0743-z

4. Zeng Y, Guo Z, Wu M, Chen F, Chen L. Circadian rhythm regulates the function of immune cells and participates in the development of tumors. *Cell Death Discovery.* (2024) 10:199. doi: 10.1038/s41420-024-01960-1

5. Bevinakoppamath S, Ramachandra SC, Yadav AK, Basavaraj V, Vishwanath P, Prashant A. Understanding the emerging link between circadian rhythm, Nrf2 pathway, and breast cancer to overcome drug resistance. *Front Pharmacol.* (2021) 12:719631. doi: 10.3389/fphar.2021.719631

6. Sun C, Zhang H, Li Y, Yu Y, Liu J, Liu R, et al. Elucidation of clinical implications Arising from circadian rhythm and insights into the tumor immune landscape in breast cancer. *Heliyon.* (2024) 10:e27356. doi: 10.1016/j.heliyon.2024.e27356

7. Xuan W, Khan F, James CD, Heimberger AB, Lesniak MS, Chen P. Circadian regulation of cancer cell and tumor microenvironment crosstalk. *Trends Cell Biol.* (2021) 31:940–50. doi: 10.1016/j.tcb.2021.06.008

8. de Visser KE, Joyce JA. The evolving tumor microenvironment: From cancer initiation to metastatic outgrowth. *Cancer Cell.* (2023) 41:374–403. doi: 10.1016/j.ccell.2023.02.016

9. Sato T, Sato S. Circadian regulation of metabolism: commitment to health and diseases. *Endocrinology.* (2023) 164:bqad086. doi: 10.1210/endocr/bqad086

10. Buijink MR, Michel S. A multi-level assessment of the bidirectional relationship between aging and the circadian clock. *J Neurochem.* (2021) 157:73–94. doi: 10.1111/jnc.15286

11. Kramer A, Lange T, Spies C, Finger AM, Berg D, Oster H. Foundations of circadian medicine. *PloS Biol.* (2022) 20:e3001567. doi: 10.1371/journal.pbio.3001567

12. Meléndez-Fernández OH, Liu JA, Nelson RJ. Circadian rhythms disrupted by light at night and mistimed food intake alter hormonal rhythms and metabolism. *Int J Mol Sci.* (2023) 24:3392. doi: 10.3390/ijms24043392

13. Jang TW. Work-fitness evaluation for shift work disorder. *Int J Environ Res Public Health.* (2021) 18:1294. doi: 10.3390/ijerph18031294

14. Acosta-Rodríguez VA, Rijo-Ferreira F, Green CB, Takahashi JS. Importance of circadian timing for aging and longevity. *Nat Commun.* (2021) 12:2862. doi: 10.1038/s41467-021-22922-6

15. Wang C, Lutes LK, Barnoud C, Scheiermann C. The circadian immune system. *Sci Immunol.* (2022) 7:eabm2465. doi: 10.1126/sciimmunol.abm2465

16. Ruan W, Yuan X, Eltzschig HK. Circadian rhythm as a therapeutic target. *Nat Rev Drug Discovery.* (2021) 20:287–307. doi: 10.1038/s41573-020-00109-w

17. Damato AR, Herzog ED. Circadian clock synchrony and chronotherapy opportunities in cancer treatment. *Semin Cell Dev Biol.* (2022) 126:27–36. doi: 10.1016/j.semcdb.2021.07.017

18. Miro C, Docimo A, Barrea L, Verde L, Cernea S, Sojat AS, et al. Time" for obesity-related cancer: The role of the circadian rhythm in cancer pathogenesis and treatment. *Semin Cancer Biol.* (2023) 91:99–109. doi: 10.1016/j.semcancer.2023.03.003

19. Xiang S, Coffelt SB, Mao L, Yuan L, Cheng Q, Hill SM. Period-2: a tumor suppressor gene in breast cancer. *J Circadian Rhythms.* (2008) 6:4. doi: 10.1186/1740-3391-6-4

20. Honma S. The mammalian circadian system: a hierarchical multi-oscillator structure for generating circadian rhythm. *J Physiol Sci.* (2018) 68:207–19. doi: 10.1007/s12576-018-0597-5

21. Patke A, Young MW, Axelrod S. Molecular mechanisms and physiological importance of circadian rhythms. *Nat Rev Mol Cell Biol.* (2020) 21:67–84. doi: 10.1038/s41580-019-0179-2

22. Lin Y, He L, Cai Y, Wang X, Wang S, Li F. The role of circadian clock in regulating cell functions: implications for diseases. *MedComm (2020).* (2024) 5:e504. doi: 10.1002/mco2.504

23. Ghareghomi S, Habibi-Rezaei M, Arese M, Saso L, Moosavi-Movahedi AA. Nrf2 modulation in breast cancer. *Biomedicines.* (2022) 10:2688. doi: 10.3390/biomedicines10102668

24. Llombart V, Mansour MR. Therapeutic targeting of "undruggable" MYC. *EBioMedicine.* (2022) 75:103756. doi: 10.1016/j.ebiom.2021.103756

25. Gao FY, Li XT, Xu K, Wang RT, Guan XX. c-MYC mediates the crosstalk between breast cancer cells and tumor microenvironment. *Cell Commun Signal.* (2023) 21:28. doi: 10.1186/s12964-023-01043-1

26. Sancar A, Van Gelder RN. Clocks, cancer, and chronochemotherapy. *Science.* (2021) 371:eabb0738. doi: 10.1126/science.abb0738

27. Yang C, Wu J, Liu X, Wang Y, Liu B, Chen X, et al. Circadian rhythm is disrupted by ZNF704 in breast carcinogenesis. *Cancer Res.* (2020) 80:4114–28. doi: 10.1158/0008-5472.CAN-20-0493

28. Chiou YY, Lee CY, Yang HW, Cheng WC, Ji KD. Circadian modulation of glucose utilization via CRY1-mediated repression of Pdk1 expression. *J Biol Chem.* (2024) 300:105637. doi: 10.1016/j.jbc.2024.105637

29. Azzi A, Tao Z, Sun Y, Erb H, Guarino C, Wu X. The circadian clock protein Cryptochrome 1 is a direct target and feedback regulator of the Hippo pathway. *iScience.* (2023) 26:107449. doi: 10.1016/j.isci.2023.107449

30. Xia K, Li S, Yang Y, Shi X, Zhao B, Lv L, et al. Cryptochrome 2 acetylation attenuates its antiproliferative effect in breast cancer. *Cell Death Dis.* (2023) 14:250. doi: 10.1038/s41419-023-05762-8

31. Yang W, Li J, Zhang M, Yu H, Zhuang Y, Zhao L, et al. Elevated expression of the rhythm gene NFIL3 promotes the progression of TNBC by activating NF-κB signaling through suppression of NFKBIA transcription. *J Exp Clin Cancer Res.* (2022) 41:67. doi: 10.1186/s13046-022-02260-1

32. Dong X, Dai H, Lin Y, Sheng X, Li Y, Wang Y, et al. TIMELESS upregulates PD-L1 expression and exerts an immunosuppressive role in breast cancer. *J Transl Med.* (2023) 21:400. doi: 10.1186/s12967-023-04257-6

33. Nelson N, Lombardo J, Matlack L, Smith A, Hines K, Shi W, et al. Chronoradiobiology of breast cancer: the time is now to link circadian rhythm and radiation biology. *Int J Mol Sci.* (2022) 23:1331. doi: 10.3390/ijms23031331

34. Yang Y, Tang X, Lin Z, Zheng T, Zhang S, Liu T, et al. An integrative evaluation of circadian gene TIMELESS as a pan-cancer immunological and predictive biomarker. *Eur J Med Res.* (2023) 28:563. doi: 10.1186/s40001-023-01519-3

35. Vipat S, Moiseeva TN. The TIMELESS roles in genome stability and beyond. *J Mol Biol.* (2024) 436:168206. doi: 10.1016/j.jmb.2023.168206

36. Baxevanis CN, Fortis SP, Perez SA. The balance between breast cancer and the immune system: Challenges for prognosis and clinical benefit from immunotherapies. *Semin Cancer Biol.* (2021) 72:76–89. doi: 10.1016/j.semcancer.2019.12.018

37. Chung W, Eum HH, Lee HO, Lee KM, Lee HB, Kim KT, et al. Single-cell RNA-seq enables comprehensive tumour and immune cell profiling in primary breast cancer. *Nat Commun.* (2017) 8:15081. doi: 10.1038/ncomms15081

38. Pilipow K, Darwich A, Losurdo A. T-cell-based breast cancer immunotherapy. *Semin Cancer Biol.* (2021) 72:90–101. doi: 10.1016/j.semcancer.2020.05.019

39. Mehta AK, Kadel S, Townsend MG, Oliwa M, Guerriero JL. Macrophage biology and mechanisms of immune suppression in breast cancer. *Front Immunol.* (2021) 12:643771. doi: 10.3389/fimmu.2021.643771

40. Aiello I, Fedele MLM, Román F, Marpegan L, Caldart C, Chiesa JJ, et al. Circadian disruption promotes tumor-immune microenvironment remodeling favoring tumor cell proliferation. *Sci Adv.* (2020) 6. doi: 10.1126/sciadv.aaz4530

41. Tian R, Li Y, Shu M. Circadian regulation patterns with distinct immune landscapes in gliomas aid in the development of a risk model to predict prognosis and therapeutic response. *Front Immunol.* (2021) 12:797450. doi: 10.3389/fimmu.2021.797450

42. Samuelsson LB, Bovbjerg DH, Roecklein KA, Hall MH. Sleep and circadian disruption and incident breast cancer risk: An evidence-based and theoretical review. *Neurosci Biobehav Rev.* (2018) 84:35–48. doi: 10.1016/j.neubiorev.2017.10.011

43. Castanon-Cervantes O, Wu M, Ehlen JC, Paul K, Gamble KL, Johnson RL, et al. Dysregulation of inflammatory responses by chronic circadian disruption. *J Immunol.* (2010) 185:5796–805. doi: 10.4049/jimmunol.1001026

44. Hadadi E, Acloque H. Role of circadian rhythm disorders on EMT and tumour-immune interactions in endocrine-related cancers. *Endocr Relat Cancer.* (2021) 28:R67–r80. doi: 10.1530/ERC-20-0390

45. Astone M, Oberkersch RE, Tosi G, Biscontin A, Santoro MM. The circadian protein BMAL1 supports endothelial cell cycle during angiogenesis. *Cardiovasc Res.* (2023) 119:1952–68. doi: 10.1093/cvr/cvad057

46. Li D, Yu Q, Wu R, Tuo Z, Zhu W, Wang J, et al. Chronobiology of the tumor microenvironment: implications for therapeutic strategies and circadian-based interventions. *Aging Dis*. (2024) Online ahead of print. doi: 10.14336/AD.2024.0327

47. Riaz F, Zhang J, Pan F. Forces at play: exploring factors affecting the cancer metastasis. *Front Immunol*. (2024) 15:1274474. doi: 10.3389/fimmu.2024.1274474

48. Hadadi E, Taylor W, Li XM, Aslan Y, Villote M, Rivière J, et al. Chronic circadian disruption modulates breast cancer stemness and immune microenvironment to drive metastasis in mice. *Nat Commun*. (2020) 11:3193. doi: 10.1038/s41467-020-16890-6

49. Lee Y, Tanggono AS. Potential role of the circadian clock in the regulation of cancer stem cells and cancer therapy. *Int J Mol Sci*. (2022) 23:14181. doi: 10.3390/ijms232214181

50. Agorastos A, Olff M. Sleep, circadian system and traumatic stress. *Eur J Psychotraumatol*. (2021) 12:1956746. doi: 10.1080/20008198.2021.1956746

51. He XY, Gao Y, Ng D, Michalopoulou E, George S, Adrover JM, et al. Chronic stress increases metastasis via neutrophil-mediated changes to the microenvironment. *Cancer Cell*. (2024) 42:474–86.e12. doi: 10.1016/j.ccell.2024.01.013

52. Liang Y, Zhang H, Song X, Yang Q. Metastatic heterogeneity of breast cancer: Molecular mechanism and potential therapeutic targets. *Semin Cancer Biol*. (2020) 60:14–27. doi: 10.1016/j.semcancer.2019.08.012

53. Medeiros B, Allan AL. Molecular mechanisms of breast cancer metastasis to the lung: clinical and experimental perspectives. *Int J Mol Sci*. (2019) 20:2272. doi: 10.3390/ijms20092272

54. Diamantopoulou Z, Castro-Giner F, Schwab FD, Foerster C, Saini M, Budinjas S, et al. The metastatic spread of breast cancer accelerates during sleep. *Nature*. (2022) 607:156–62. doi: 10.1038/s41586-022-04875-y

55. Ball H, Nagrath S. Cancer cells spread aggressively during sleep. *Nature*. (2022) 607:33–4. doi: 10.1038/d41586-022-01639-6

56. Liu C, Guo L, Fu C. Circadian-rhythm-regulating hormones: Key factors to regulate breast cancer metastasis via circulating tumor cells. *MedComm (2020)*. (2022) 3:e189. doi: 10.1002/mco2.189

57. Miyano M, LaBarge MA. ELF5: A molecular clock for breast aging and cancer susceptibility. *Cancers (Basel)*. (2024) 16:431. doi: 10.3390/cancers16020431

58. Popa-Wagner A, Buga AM, Dumitrascu DI, Uzoni A, Thome J, Coogan AN. How does healthy aging impact on the circadian clock? *J Neural Transm (Vienna)*. (2017) 124:89–97. doi: 10.1007/s00702-015-1424-2

59. Farajnia S, Deboer T, Rohling JH, Meijer JH, Michel S. Aging of the suprachiasmatic clock. *Neuroscientist*. (2014) 20:44–55. doi: 10.1177/1073858413498936

60. Welz PS, Benitah SA. Molecular connections between circadian clocks and aging. *J Mol Biol*. (2020) 432:3661–79. doi: 10.1016/j.jmb.2019.12.036

61. Mattis J, Sehgal A. Circadian rhythms, sleep, and disorders of aging. *Trends Endocrinol Metab*. (2016) 27:192–203. doi: 10.1016/j.tem.2016.02.003

62. Panagiotou M, Michel S, Meijer JH, Deboer T. The aging brain: sleep, the circadian clock and exercise. *Biochem Pharmacol*. (2021) 191:114563. doi: 10.1016/j.bcp.2021.114563

63. Zhao J, Warman GR, Cheeseman JF. The functional changes of the circadian system organization in aging. *Ageing Res Rev*. (2019) 52:64–71. doi: 10.1016/j.arr.2019.04.006

64. Hood S, Amir S. The aging clock: circadian rhythms and later life. *J Clin Invest*. (2017) 127:437–46. doi: 10.1172/JCI90328

65. Mak JKL, McMurran CE, Kuja-Halkola R, Hall P, Czene K, Jylhävä J, et al. Clinical biomarker-based biological aging and risk of cancer in the UK Biobank. *Br J Cancer*. (2023) 129:94–103. doi: 10.1038/s41416-023-02288-w

66. Patel J, Baptiste BA, Kim E, Hussain M, Croteau DL, Bohr VA. DNA damage and mitochondria in cancer and aging. *Carcinogenesis*. (2020) 41:1625–34. doi: 10.1093/carcin/bgaa114

67. Huang R, Zhou PK. DNA damage repair: historical perspectives, mechanistic pathways and clinical translation for targeted cancer therapy. *Signal Transduct Target Ther*. (2021) 6:254. doi: 10.1038/s41392-021-00648-7

68. Patidar K, Panwar U, Vuree S, Sweta J, Sandhu MK, Nayarisseri A, et al. An In silico Approach to Identify High Affinity Small Molecule Targeting m-TOR Inhibitors for the Clinical Treatment of Breast Cancer. *Asian Pac J Cancer Prev*. (2019) 20:1229–41. doi: 10.31557/APJCP.2019.20.4.1229

69. Hong H, Ji M, Lai D. Chronic stress effects on tumor: pathway and mechanism. *Front Oncol*. (2021) 11:738252. doi: 10.3389/fonc.2021.738252

70. Ray D, Yung R. Immune senescence, epigenetics and autoimmunity. *Clin Immunol*. (2018) 196:59–63. doi: 10.1016/j.clim.2018.04.002

71. Bahiraee A, Ebrahimi R, Halabian R, Aghabozorgi AS, Amani J. The role of inflammation and its related microRNAs in breast cancer: A narrative review. *J Cell Physiol*. (2019) 234:19480–93. doi: 10.1002/jcp.28742

72. Oseni SO, Naar C, Pavlović M, Asghar W, Hartmann JX, Fields GB, et al. The molecular basis and clinical consequences of chronic inflammation in prostatic diseases: prostatitis, benign prostatic hyperplasia, and prostate cancer. *Cancers (Basel)*. (2023) 15:3110. doi: 10.3390/cancers15123110

73. Patel S, Homaei A, Raju AB, Meher BR. Estrogen: The necessary evil for human health, and ways to tame it. *BioMed Pharmacother*. (2018) 102:403–11. doi: 10.1016/j.biopha.2018.03.078

74. Dunneram Y, Greenwood DC, Cade JE. Diet, menopause and the risk of ovarian, endometrial and breast cancer. *Proc Nutr Soc*. (2019) 78:438–48. doi: 10.1017/S0029665118002884

75. Vaitaitis GM, Wagner DH. Are we aiming to miss in translational autoimmunity treatments? *F1000Res*. (2018) 7:1754. doi: 10.12688/f1000research.16894.2

76. Chun SK, Chung S, Kim HD, Lee JH, Jang J, Kim J, et al. A synthetic cryptochrome inhibitor induces anti-proliferative effects and increases chemosensitivity in human breast cancer cells. *Biochem Biophys Res Commun*. (2015) 467:441–6. doi: 10.1016/j.bbrc.2015.09.103

77. Sulli G, Lam MTY, Panda S. Interplay between circadian clock and cancer: new frontiers for cancer treatment. *Trends Cancer*. (2019) 5:475–94. doi: 10.1016/j.trecan.2019.07.002

78. Gutiérrez-Monreal MA, Treviño V, Moreno-Cuevas JE, Scott SP. Identification of circadian-related gene expression profiles in entrained breast cancer cell lines. *Chronobiol Int*. (2016) 33:392–405. doi: 10.3109/07420528.2016.1152976

79. Yang Y, Lindsey-Boltz LA, Vaughn CM, Selby CP, Cao X, Liu Z, et al. Circadian clock, carcinogenesis, chronochemotherapy connections. *J Biol Chem*. (2021) 297:101068. doi: 10.1016/j.jbc.2021.101068

80. Cardinali DP, Brown GM, Pandi-Perumal SR. Chronotherapy. *Handb Clin Neurol*. (2021) 179:357–70. doi: 10.1016/B978-0-12-819975-6.00023-6

81. Levi F, Schibler U. Circadian rhythms: mechanisms and therapeutic implications. *Annu Rev Pharmacol Toxicol*. (2007) 47:593–628. doi: 10.1146/annurev.pharmtox.47.120505.105208

82. Kobayashi M, Wood PA, Hrushesky WJ. Circadian chemotherapy for gynecological and genitourinary cancers. *Chronobiol Int*. (2002) 19:237–51. doi: 10.1081/CBI-120002600

83. Innominato PF, Giacchetti S, Moreau T, Smaaland R, Focan C, Bjarnason GA, et al. Prediction of survival by neutropenia according to delivery schedule of oxaliplatin-5-Fluorouracil-leucovorin for metastatic colorectal cancer in a randomized international trial (EORTC 05963). *Chronobiol Int*. (2011) 28:586–600. doi: 10.3109/07420528.2011.597532

84. Ohdo S, Koyanagi S, Matsunaga N. Chronopharmacological strategies focused on chrono-drug discovery. *Pharmacol Ther*. (2019) 202:72–90. doi: 10.1016/j.pharmthera.2019.05.018

frontiers | Frontiers in Immunology

TYPE Original Research
PUBLISHED 08 August 2024
DOI 10.3389/fimmu.2024.1440454

Check for updates

OPEN ACCESS

EDITED BY
Jiaheng Xie,
Central South University, China

REVIEWED BY
Huaping Xiao,
Mayo Clinic, United States
Xuemei Zhang,
North China University of Science and Technology, China

*CORRESPONDENCE
Guojun Lu
guojunlu@njmu.edu.cn
Qingyi Wei
qingyi.wei@duke.edu

RECEIVED 29 May 2024
ACCEPTED 22 July 2024
PUBLISHED 08 August 2024

CITATION
Lu G, Liu H, Wang H, Tang X, Luo S, Du M, Christiani DC and Wei Q (2024) Potentially functional variants of *INPP5D and EXOSC3* in immunity B cell-related genes are associated with non-small cell lung cancer survival. *Front. Immunol.* 15:1440454. doi: 10.3389/fimmu.2024.1440454

COPYRIGHT
© 2024 Lu, Liu, Wang, Tang, Luo, Du, Christiani and Wei. This is an open-access article distributed under the terms of the Creative Commons Attribution License (CC BY). The use, distribution or reproduction in other forums is permitted, provided the original author(s) and the copyright owner(s) are credited and that the original publication in this journal is cited, in accordance with accepted academic practice. No use, distribution or reproduction is permitted which does not comply with these terms.

Potentially functional variants of *INPP5D and EXOSC3* in immunity B cell-related genes are associated with non-small cell lung cancer survival

Guojun Lu[1,2,3]*, Hongliang Liu[2,3], Huilin Wang[2,3,4], Xiaozhun Tang[2,3,5], Sheng Luo[6], Mulong Du[7], David C. Christiani[7,8] and Qingyi Wei[2,3,9,10]*

[1]Department of Respiratory Medicine, Nanjing Chest Hospital, Affiliated Nanjing Brain Hospital, Nanjing Medical University, Nanjing, China, [2]Duke Cancer Institute, Duke University Medical Center, Durham, NC, United States, [3]Department of Population Health Sciences, Duke University School of Medicine, Durham, NC, United States, [4]Department of Respiratory Oncology, Guangxi Cancer Hospital, Guangxi Medical University Cancer Hospital, Nanning, China, [5]Department of Head and Neck Surgery, Guangxi Cancer Hospital, Guangxi Medical University Cancer Hospital, Nanning, China, [6]Department of Biostatistics and Bioinformatics, Duke University School of Medicine, Durham, NC, United States, [7]Departments of Environmental Health and Epidemiology, Harvard TH Chan School of Public Health, Boston, MA, United States, [8]Department of Medicine, Massachusetts General Hospital, Boston, MA, United States, [9]Department of Medicine, Duke University Medical Center, Durham, NC, United States, [10]Duke Global Health Institute, Duke University Medical Center, Durham, NC, United States

B cells are adaptive immune cells in the tumor microenvironment and play an important role in tumor development and metastasis. However, the roles of genetic variants of the immunity B cell-related genes in the survival of patients with non-small cell lung cancer (NSCLC) remain unknown. In the present study, we first evaluated associations between 10,776 single nucleotide polymorphisms (SNPs) in 220 immunity B cell-related genes and survival of NSCLC in a discovery dataset of 1,185 patients from the Prostate, Lung, Colorectal and Ovarian (PLCO) Cancer Screening Trial. We found that 369 SNPs were significantly associated with overall survival (OS) of NSCLC in multivariable Cox proportional hazards regression analysis ($P \leq 0.05$, Bayesian false discovery probability ≤ 0.80), of which 18 SNPs were validated in another independent genotyping dataset of 984 patients from the Harvard Lung Cancer Susceptibility (HLCS) Study. We then performed linkage disequilibrium (LD) analysis, followed by stepwise analysis with a multivariable Cox regression model. Finally, two independent SNPs, inositol polyphosphate-5-phosphatase D (*INPP5D*) rs13385922 C>T and exosome component 3 (*EXOSC3*) rs3208406 A>G, remained significantly associated withNSCLC OS with a combined hazards ratio (HR) of 1.14 (95% confidence

Abbreviations: AUC, receiver operating characteristic curve; BFDP, Bayesian false discovery probability; CI, confidence interval; DSS, disease special survival; eQTL, expression quantitative trait loci; *EXOSC3*, exosome component 3; GWAS, Genome-Wide Association Study; HWE, Hardy-Weinberg equilibrium; HLCS, Harvard Lung Cancer Susceptibility; HR, hazards ratio; *INPP5D*, inositol polyphosphate-5-phosphatase D; LD, linkage disequilibrium; LUAD, lung adenocarcinoma; LUSC, lung squamous cell carcinoma; MAF, minor allelic frequency; NSCLC, non-small cell lung cancer; PLCO, the Prostate, Lung, Colorectal and Ovarian Cancer Screening Trial; SNPs, single nucleotide polymorphisms; OS, overall survival; ROC, receiver operating characteristic; TCGA, the Cancer Genome Atlas.

interval = 1.06-1.23, $P = 2.41\times10^{-4}$) and 1.20 (95% confidence interval = 1.14-1.28, $P = 3.41\times10^{-9}$), respectively. Furthermore, NSCLC patients with the combination of unfavorable genotypes for these two SNPs were associated with a poor OS ($P_{trend} = 0.0002$) and disease-specific survival (DSS, $P_{trend} < 0.0001$) in the PLCO dataset. Expression quantitative trait loci (eQTL) analysis suggested that the *INPP5D* rs6782875 T allele was significantly correlated with elevated *INPP5D* mRNA expression levels in normal lung tissues and whole blood samples, while the *EXOSC3* rs3208406 G allele was significantly correlated with increased *EXOSC3* mRNA expression levels in normal lung tissues. Our data indicated that genetic variants in these immunity B cell-related genes may predict NSCLC survival possibly by influencing the gene expression.

KEYWORDS

non-small cell lung cancer, immunity B cell, single-nucleotide polymorphism, overall survival, tumor microenvironment

1 Introduction

Lung cancer is the leading cause of cancer-related deaths in the world. In 2023, there were nearly 238,340 new cases diagnosed with and 127,070 deaths from lung cancer in the United States (1). In 2022 the National Cancer Center of China reported that lung cancer was both the most common cancer and the leading cause of cancer deaths in China (2). Therefore, lung cancer remains a substantial economic burden for both patients and healthcare systems globally (3). Based on its histological types, lung cancer can be divided into small cell lung cancer and non-small cell lung cancer (NSCLC), with the latter accounting for approximately 85% of all lung cancer cases (4). In recent years, despite remarkable advancements in earlier detection and therapeutic strategies, such as targeted molecular therapy and immunotherapy, the 5-year survival rate of advanced lung cancer remains low at only about 21% (5). However, individual lung cancer patients may respond dramatically differently to the same treatment and present different survival rates, and genetic variation may be involved in cancer progression (6). As a result, identifying genetic variation such as single-nucleotide polymorphisms (SNPs) in key genes and pathways may provide some new insights into the strategy of treating lung cancer.

The tumor microenvironment (TME) is a complex ecosystem where cancer cells are surrounded by diverse immune cells, inflammatory cells, tumor-associated fibroblasts, and altered extracellular matrix (7). Accumulating evidence suggests that TME has an important role in tumor initiation, progression, and metastasis (8, 9). As the second in the number of adaptive immune cells in TME, B cells localize to tumor-associated tertiary lymphoid structures and then interact with peripheral T cells and antigen-presenting cells to play a critical role in both pro-tumorigenic and anti-tumorigenic immunity (10). B cells not only promote tumor growth by secreting suppressive cytokines like IL-10, promoting immune tolerance by PD-L1$^+$ B cells and producing proinflammatory cytokines such as IL-1β, but also inhibit tumor growth by secreting tumor-specific antibodies, serving as antigen-presenting cells themselves, and directly killing tumor cells (10–12). B cells were reported to be the second most common immune cell type with elevated expression levels in NSCLC tissues (13). A single-cell RNA-seq analysis indicated that plasma-like B cells inhibited tumor cell growth in the early stage and promoted cell growth in the advanced NSCLC (14). Moreover, the high percentage of naive-like B cells in tumor tissues of NSCLC patients was associated with a better prognosis (14, 15). However, the potential role played by genetic variants in immunity B cell-related genes in NSCLC progression has not been reported.

Genome-wide association studies (GWASs) have been used to dissect the genotype-phenotype associations, providing new insights into the understanding of associations between genetic variants and certain diseases (16). For example, Chen et al. reported that genetic variants in peroxisome-related genes predicted NSCLC survival by influencing gene regulation (17). Another study indicated that two genetic variants in the immune-activation pathway genes affected the prognosis of NSCLC patients by regulating corresponding gene expression (18). In the present study, we have hypothesized that genetic variants in immunity B cell-related genes are associated with NSCLC survival. To test this hypothesis, we performed a two-stage analysis, using available GWAS data to evaluate associations between genetic variants in immunity B cell-related genes and survival of NSCLC patients.

2 Materials and methods

2.1 Study populations

In the two-stage analysis, we first used the GWAS dataset of lung cancer patients of European ancestry from the Prostate, Lung,

Colorectal, and Ovarian cancer screening trial (PLCO) Cancer Screening Trial as the discovery. The PLCO enrolled approximately 155,000 participants aged 55-74 from 10 competitively selected screening centers across the United States between 1993 and 2001. Among all the participants, we extracted 1185 NSCLC patients (487 women and 698 men) with detailed personal information such as age, sex, smoking status, treatment history, and follow-up time for further survival analysis. Genotyping data were extracted from whole blood DNA samples genotyped using Illumina HumanHap240Sv1.0 and HumanHap550v3.0 platforms (dbGaP accession numbers: phs000093.v2.P2 and phs000336.v1.p1) (19, 20). The PLCO trial was approved by the National Cancer Institute and the institutional review boards of each involved center.

Then, we used another genotyping dataset from the Harvard University Lung Cancer Susceptibility (HLCS) study to validate the findings of the PLCO dataset. HLCS study included 984 histologically confirmed Caucasian NSCLC patients from the Massachusetts General Hospital (MGH) (21). The genomic blood DNA samples were used for genotyping by the Illumina Humanhap610-Quad array, and the genotyping data were subsequently imputed with the software MaCH based on the 1000 Genomes Project.

The use of the PLCO trial and HLCS study for experimentation was approved by the Internal Review Board of Duke University School of Medicine (Project #Pro00054575) and the dbGaP database (Project #6404). The characteristics of the two datasets are shown in Supplementary Table S1.

2.2 Gene selection and SNP imputation

We searched for the immunity B cell-related genes by using the keywords "B cell" and "immunity" from the Molecular Signature Database (http://www.gsea-msigdb.org/gsea/msigdb/human/search.jsp) (22). After excluding duplicated genes and genes on the X chromosome, 220 remaining genes were identified as candidate genes for further analyses (Supplementary Table S2). SNPs with ±2kb flanking regions of 220 immunity B cell-related genes were extracted from the PLCO trial and conducted using the Minimac4 based on the European data in the 1000 Genomes Project (phase 3). For the control quality, all the SNPs were extracted according to the following criteria: an imputation info score ≥ 0.3 (Supplementary Figure S1), a minor allele frequency (MAF) ≥ 5%, an individual call rate ≥ 95%, and the Hardy-Weinberg equilibrium *P*-value (HWE) ≥ 1×10^{-5}. Finally, a total of 10,776 SNPs (1,196 genotyped and 9,580 imputed) were obtained from the PLCO dataset for further analysis.

2.3 Statistical methods

In the PLCO dataset, to estimate the associations between 10,776 candidate SNPs and NSCLC survival in an additive genetic model, we first performed single-locus Cox proportional hazards regression analysis using the R package GenABEL package (23). The Cox regression analysis was performed with adjustment for clinical variables (including age, sex, smoking status, histologic subtype, tumor stage, chemotherapy, radiotherapy, and surgery) and the top four of the 10 principal components (PCs) in the discovery dataset (Supplementary Table S3). To filter out potential false-positive results, we employed a multiple testing correction by Bayesian false discovery probability (BFDP) with the threshold of 0.8 as recommended (24). We used a prior probability of 0.10 to detect an upper boundary hazards ratio (HR) of 3.0 for an association with variant genotypes or minor alleles of the SNPs with $P < 0.05$.

The identified SNPs from the PLCO GWAS dataset were validated using the GWAS dataset of the HLCS study in a multivariable Cox regression model. To combine the results of the two GWAS datasets, the inverse variance weighted meta-analysis was performed, using Cochran's Q-test and the heterogeneity statistic (I^2) to assess inter-study and determine the appropriate model. If no heterogeneity (Q-test $P > 0.10$ and $I^2 < 50\%$), the meta-analysis was performed with a fixed-effects model, otherwise with the random-effects model.

Linkage disequilibrium (LD) analysis was performed with Haploview 4.1. Two online bioinformatics tools, RegulomeDB (http://www.regulomedb.org/) and HaploReg v4.2 (https://pubs.broadinstitute.org/mammals/haploreg/haploreg.php), were used to predict the potentially functional SNPs (25, 26). Subsequently, to identify the associations between independent SNPs and NSCLC survival, we employed the multivariable stepwise Cox regression model with adjustment for demographic and clinical variables, the top four PCs, and 54 previously published SNPs from the same PLCO GWAS dataset. We also generated the Manhattan plots with Haploview4.1 and regional association plots with Locus Zoom (http://http://locuszoom.sph.umich.edu) to visualize the selected SNPs (27).

Subsequently, we employed the combined unfavorable genotypes to evaluate the cumulative effects of the two identified SNPs and the Kaplan-Meier (KM) survival curves to assess the survival probability. We also performed stratified analysis and evaluated inter-study heterogeneity to assess the associations between subgroups and survival as well as the combined effect of unfavorable genotypes that might be influenced by clinical characteristics. To evaluate predictive accuracy of the clinical models with the addition of the genetic variables, we constructed time-dependent area under the curve (AUC) and the receiver operating characteristic (ROC) curves using R (version 3.6.3) package "time ROC" and "survival" (28).

To explore the genotype-phenotype correlation between two identified SNPs and mRNA expression levels of their corresponding genes, we performed expression quantitative trait loci (eQTL) analyses with a linear regression model using data from two sources: lymphoblastoid cell lines in 373 European descendants from the 1,000 Genomes Project (Phase 3) and the genotype-tissue expression (GTEx) project (including 515 normal lung tissues and 670 whole blood samples) (29). To compare the mRNA expression among tumor tissue of lung adenocarcinoma (LUAD), lung squamous cell carcinoma (LUSC) and adjacent normal tissue with paired and unpaired *t*-tests, we downloaded the raw expression data

from the Cancer Genome Atlas (TCGA) database and performed the analyses on the online data platform UALCAN (https://ualcan.path.uab.edu/) (30), respectively. Finally, we assessed the correlations between the mRNA expression levels of two genes and NSCLC survival probability using the online survival analysis database Kaplan-Meier (http://kmplot.com/analysis/) (31). Unless specified otherwise, all statistical analyses were conducted with the SAS software 9.4 (SAS Institute, Cary, NC, USA).

3 Results

3.1 Associations between SNPs in the immunity B cell-related genes and the survival of NSCLC

The final analysis in the present study included 1185 NSCLC patients from the PLCO trial and 984 NSCLC patients from the HLCS study, and their clinical features are described in Supplementary Table S1. The study flow chart is depicted in Figure 1. After multiple testing corrections by BFDP (≤ 0.80), 369 SNPs out of the 10,776 SNPs in the immunity B cell-related genes were found to be statistically significantly associated with NSCLC overall survival (OS) ($P \leq 0.05$); then, these SNPs were further validated in the HLCS dataset. As a result, 18 SNPs in three genes (i.e., inositol polyphosphate-5-phosphatase D, *INPP5D*; complement factor I, *CFI*; and exosome component 3, *EXOSC3*) remained significant. While *EXOSC3* has only one SNP (i.e., rs3208406 in *EXOSC3*), further LD analyses of the remaining 17 SNPs with Haploview 4.1 software identified two SNPs (one in each of *INPP5D* and *CFI*) as the tagger SNPs (Supplementary Figure S2). The results of subsequent online functional prediction for these three SNPs are listed in Supplementary Table S4. *EXOSC3* rs3208406 A>G and *CFI* rs6836770 G>A may have an effect on enhancer histone marks, and the allele change in these three SNPs may alter protein motifs.

3.2 Identification the effect of independent SNPs on NSCLC OS in the PLCO trial

Because the HLCS replication dataset did not have the same genotyping data as the PLCO did, to identify the effect of independent SNPs on NSCLC OS, we first used the PLCO genotyping dataset to perform the stepwise multivariable Cox regression analysis. Next, we put the remaining significant SNPs into a post-stepwise multivariable model including 54 previously reported SNPs in the PLCO GWAS dataset. Finally, two SNPs (*INPP5D* rs13385922 C>T and *EXOSC3* rs3208406 A>G) remained significantly associated with NSCLC OS (P = 0.003 and 0.002, respectively) (Table 1). Moreover, the meta-analysis of the PLCO trial and HLCS study revealed that there was no interstudy heterogeneity across these two datasets, and the combined results are listed in Table 2. We also depicted Manhattan plots (Supplementary Figure S3) and regional association plots (Supplementary Figure S4) for these two significant SNPs.

As shown in Table 3, both *the INPP5D* rs13385922 *T* allele and *EXOSC3* rs3208406 G allele were significantly associated with OS (P_{trend} = 0.003 and 0.023, respectively) and disease-specific survival (DSS) (P_{trend} = 0.0005 and 0.003, respectively). Compared with those having the reference genotype in a dominant genetic model, NSCLC patients had a significantly poor survival associated with

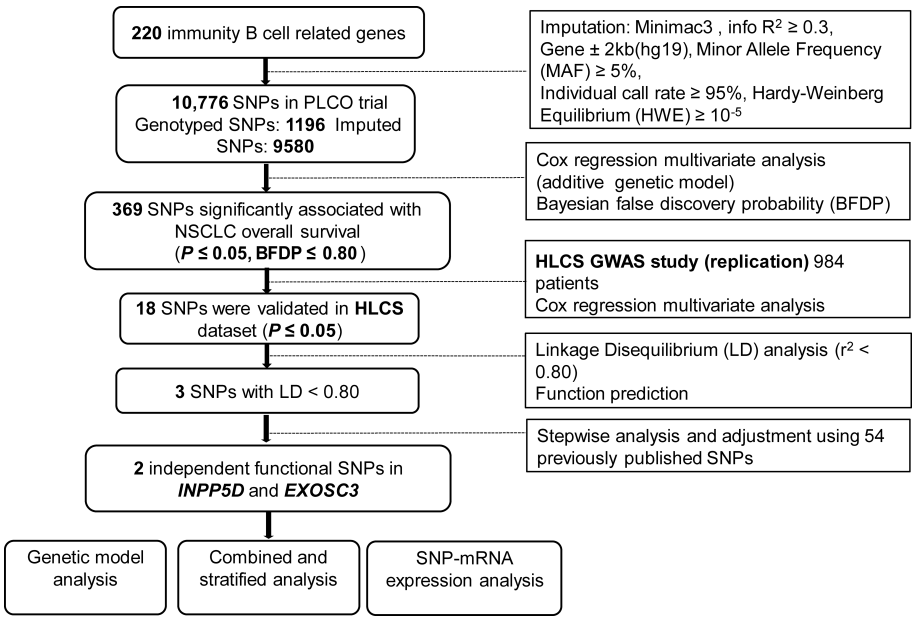

FIGURE 1
The flowchart of the present study. SNP, single-nucleotide polymorphism; PLCO, Prostate, Lung, Colorectal and Ovarian cancer screening trial; NSCLC, non-small cell lung cancer; HLCS, Harvard lung cancer susceptibility study; GWAS, Genome-Wide Association Study.

TABLE 1 Two independent SNPs in multivariable Cox proportional hazards regression analysis with adjustment for other covariates and 54 previously published SNPs in the PLCO dataset.

Variables	Category	Frequency	HR (95% CI) [a]	*P* [a]	HR (95% CI) [b]	*P* [b]
Age	Continuous	1185	1.03 (1.02-1.04)	<0.0001	1.05 (1.03-1.06)	<0.0001
Sex	Male	698	1.00		1.00	
	Female	487	0.81 (0.69-0.94)	0.006	0.65 (0.55-0.78)	<0.0001
Smoking status	Never	115	1.00		1.00	
	Current	423	1.67 (1.24-2.25)	0.0006	2.31 (1.67-3.19)	<0.0001
	Former	647	1.65 (1.25-2.18)	0.0004	2.26 (1.67-3.07)	<0.0001
Histology	AD	577	1.00		1.00	
	SC	285	1.14 (0.95-1.38)	0.166	1.13 (0.92-1.39)	0.246
	Others	323	1.31 (1.10-1.56)	0.002	1.46 (1.21-1.77)	0.0001
Stage	I-IIIA	655	1.00		1.00	
	IIIB-IV	528	2.76 (2.26-3.36)	<0.0001	3.98 (3.18-4.97)	<0.0001
Chemotherapy	No	639	1.00		1.00	
	Yes	538	0.59 (0.49-0.70)	<0.0001	0.47 (0.38-0.57)	<0.0001
Radiotherapy	No	762	1.00		1.00	
	Yes	415	0.93 (0.79-1.10)	0.417	1.10 (0.92-1.32)	0.291
Surgery	No	637	1.00		1.00	
	Yes	540	0.20 (0.16-0.26)	<0.0001	1.63 (1.23-2.15)	<0.0001
INPP5D rs13385922 C>T	CC/CT/TT	432/560/192	1.17 (1.06-1.30)	0.002	1.18 (1.06-1.32)	0.003
EXOSC3 rs3208406 A>G	AA/AG/GG	979/172/7	1.24 (1.04-1.49)	0.019	1.39 (1.13-1.71)	0.002

HR, hazards ratio; CI, confidence interval; SNP, single-nucleotide polymorphisms; PLCO, Prostate, Lung, Colorectal and Ovarian cancer screening trial; INPP5D, Inositol polyphosphate-5-phosphatase.

[a]Stepwise analysis included age, sex, smoking status, tumor stage, histology, chemotherapy, radiotherapy, surgery, PC1, PC2, PC3, PC4 and SNPs.

[b]54 published SNPs were used for post-stepwise adjustment: rs779901, rs3806116, rs199731120, rs10794069, rs1732793, rs225390, rs3788142, rs73049469, rs35970494, rs225388,rs7553295, rs1279590, rs73534533, rs677844, rs4978754, rs1555195, rs11660748, rs73440898, rs13040574, rs469783, rs36071574, rs7242481, rs1049493,rs1801701, rs35859010, rs1833970, rs254315, rs425904, rs35385129, rs4487030,rs60571065, rs13213007, rs115613985, rs9673682, rs2011404, rs7867814, rs2547235,rs4733124, rs11225211, rs11787670, rs67715745, rs922782, rs4150236, rs116454384, rs9384742, rs9825224, rs261083, rs76744140, rs6939623, rs113181986, rs2568847, rs10841847, rs2519996, rs36215.

INPP5D rs13385922 CT+TT (OS: HR = 1.22, 95% CI = 1.06-1.42, and $P = 0.008$; DSS: HR = 1.29, 95% CI = 1.10-1.51, and $P = 0.002$), and with *EXOSC3* rs3208406 AG+GG (OS: HR = 1.27, 95% CI = 1.05-1.55, and $P = 0.015$; DSS: HR = 1.37, 95% CI = 1.12-1.67, and $P = 0.002$). Additionally, we also depicted Kaplan-Meier survival curves for these results (Supplementary Figure S5).

3.3 Combined effect of two independent SNPs on NSCLC survival in the PLCO dataset

To assess the combined effect of these two independent SNPs on NSCLC survival, we combined unfavorable genotypes (*INPP5D* rs13385922 CT+TT and *EXOSC3* rs3208406 AG+GG) into a genetic score and divided all NSCLC patients into three groups (i.e., 0, 1, and 2) according to the number of unfavorable genotypes (NUGs). As shown in Table 3, an elevated NUG score was associated with a poor survival for both OS ($P_{trend} < 0.0002$) and DSS ($P_{trend} < 0.0001$). Furthermore, we dichotomized the NUGs and divided all NSCLC patients into low-unfavorable-genotypes group (0 NUGs) and high-unfavorable-genotypes group (1-2 NUGs). Compared with the 0 NUGs group, the 1-2 NUGs group had a significantly poorer survival for OS (HR = 1.34, 95% CI = 1.14-1.58, and $P = 0.0003$) and DSS (HR = 1.46, 95% CI = 1.23-1.73, and $P_{trend} < 0.0001$). We also depicted these results with Kaplan-Meier survival curves from a log-rank perspective (Figures 2A–D).

3.4 Stratified analysis for associations between NUGs and NSCLC survival

To assess the possible modification effect of NUGs on NSCLC survival by age, sex, smoking status, histology, tumor stage, chemotherapy, radiotherapy, and surgery, we further conducted stratified analysis in the PLCO trial. As shown in Supplementary Table S5, For the effects of both 0 and 1-2 NUG groups on NSCLC OS and DSS, no significant interactions were found between NUGs and age, sex, smoking status, histology, tumor stage, chemotherapy, radiotherapy, and surgery (all $P_{inter} > 0.05$).

TABLE 2 Associations of two independent SNPs with overall survival in both discovery and validation datasets from two previously published NSCLC GWASs.

SNP	Allele [a]	Gene	PLCO (n=1185)					Harvard (n=984)		Meta-analysis			
			BFDP	EAF	HR (95%CI) [b]	*P* [b]	EAF	HR (95%CI) [c]	*P* [c]	HR (95%CI) [d]	*P* [d]	P_{het} [e]	I^2
rs13385922	C>T	*INPP5D*	0.28	0.40	1.18 (1.06-1.30)	0.002	0.42	1.11 (1.00-1.22)	0.050	1.14 (1.06-1.23)	2.41×10^{-4}	0.376	0
rs3208406	A>G	*EXOSC3*	0.77	0.08	1.25 (1.04-1.50)	0.016	0.10	1.20 (1.02-1.41)	0.031	1.20 (1.14-1.28)	3.41×10^{-9}	0.669	0

EAF, effect allele frequency; HR, hazards ratio; CI, confidence interval.
[a]Reference>effect allele.
[b]Adjusted for age, sex, stage, histology, smoking status, chemotherapy, radiotherapy, surgery, PC1, PC2, PC3 and PC4.
[c]Adjusted for age, sex, stage, histology, smoking status, chemotherapy, radiotherapy, surgery, PC1, PC2, and PC3.
[d]Meta-analysis in the fix-effects model.
[e]P_{het}, P value for heterogeneity by Cochrane's Q test.

TABLE 3 Associations between two independent SNPs and survival of NSCLC in the PLCO trial.

Genotype	Frequency	OS [a]			DSS [a]		
		Death (%)	HR (95% CI)	*P*	Death (%)	HR (95% CI)	*P*
INPP5D rs13385922 C>T [b]							
CC	428	277 (64.72)	1.00		239 (55.84)	1.00	
CT	554	372 (67.15)	1.18 (1.01-1.39)	0.038	337 (60.83)	1.24 (1.05-1.47)	0.013
TT	192	139 (72.40)	1.36 (1.10-1.67)	0.004	132 (68.75)	1.44 (1.16-1.79)	0.001
Trend test				0.003			0.0005
Dominant							
CC	428	277 (64.72)	1.00		239 (55.84)	1.00	
CT+TT	**746**	**511 (68.50)**	**1.22 (1.06-1.42)**	**0.008**	**469 (62.87)**	**1.29 (1.10-1.51)**	**0.002**
EXOSC3 rs3208406 A>G [c]							
AA	970	649 (66.91)	1.00		575 (59.28)	1.00	
AG	171	119 (69.59)	1.29 (1.06-1.57)	0.013	113 (66.08)	1.37 (1.12-1.69)	0.002
GG	7	4 (57.14)	1.00 (0.37-2.67)	0.992	4 (57.14)	1.16 (0.43-3.12)	0.771
Trend test				0.023			0.003
Dominant							
AA	970	649 (66.91)	1.00		575 (59.28)	1.00	
AG+GG	**178**	**123 (69.10)**	**1.27 (1.05-1.55)**	**0.015**	**117 (65.73)**	**1.37 (1.12-1.67)**	**0.002**
NUG [d,e]							
0	350	220 (62.86)	1.00		183 (52.29)	1.00	
1	688	481 (69.91)	1.32 (1.12-1.56)	0.0009	443 (64.39)	1.43 (1.20-1.71)	<0.0001
2	109	70 (64.22)	1.50 (1.14-1.97)	0.003	65 (59.63)	1.67 (1.25-2.22)	0.0005
Trend test				0.0002			<0.0001
0	350	220 (62.86)	1.00		183 (52.29)	1.00	
1-2	797	551 (69.13)	1.34 (1.14-1.58)	0.0003	508 (63.74)	1.46 (1.23-1.73)	<0.0001

SNP, single nucleotide polymorphism; NSCLC, non-small cell lung cancer; PLCO, Prostate, Lung, Colorectal and Ovarian cancer screening trial; OS, overall survival; DSS, disease-specific survival; HR, hazards ratio; CI, confidence interval.
[a]Adjusted for age, sex, smoking status, histology, tumor stage, chemotherapy, surgery, radiotherapy and top four principal components.
[b]11 missing data were excluded.
[c]37 missing data were excluded.
[d]38 missing data were excluded.
[e]Unfavorable genotypes were INPP5D rs13385922 CT+TT and EXOSC3 rs3208406 AG+GG and their results are in bold.

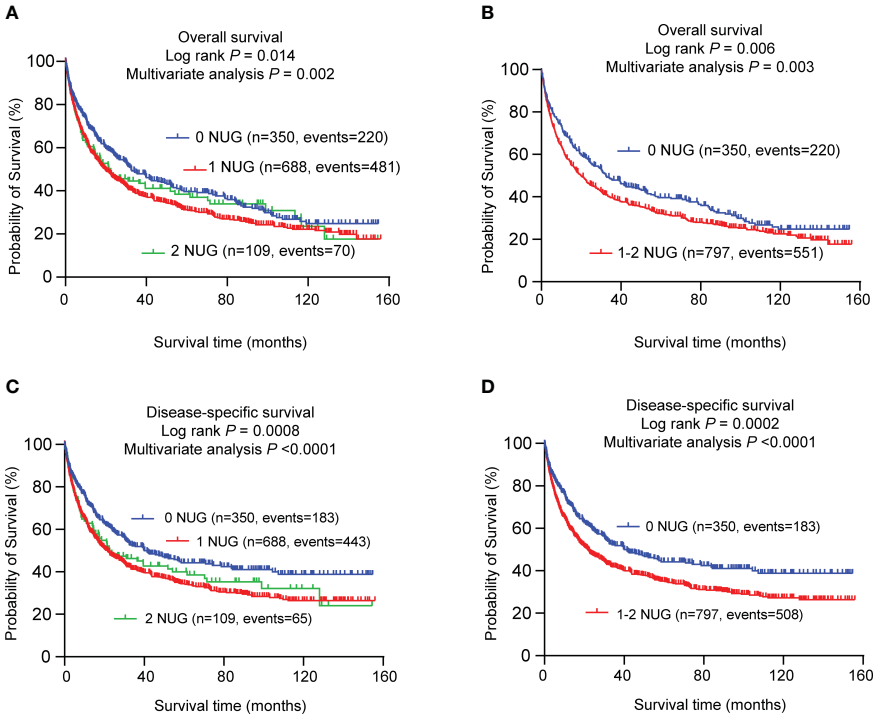

FIGURE 2
Prediction of survival with the combined unfavorable genotypes. Kaplan–Meier survival curves in the PLCO dataset for **(A)** OS with the combined unfavorable genotypes; **(B)** OS with the dichotomized groups of the NUGs; **(C)** DSS with the combined unfavorable genotypes; **(D)** DSS with dichotomized groups of the NUGs. #Unfavorable genotypes were *INPP5D* rs13385922 CT+TT and *EXOSC3* rs3208406 AG+GG. SNPs, single nucleotide polymorphism; NUG, number of unfavorable genotypes; PLCO, The Prostate, Lung, Colorectal and Ovarian Cancer Screening Trial.

3.5 Time-dependent AUC and ROC curves to predict NSCLC survival

To further evaluate the predictive role in survival of the two SNPs for OS and DSS, we performed the time-dependent AUC and ROC curves at the 12th,36th, and 60th month in the PLCO trial. Compared with the predictive model for clinical covariates including age, sex, smoking status, histology, tumor stage, chemotherapy, radiotherapy, surgery, and the four PCs, the predictive values before and after adding the two independent SNPs to the model were different. Time-dependent AUC for OS and DSS were shown in Supplementary Figures S6A, B. With the addition of the two SNPs, the AUC increased from 87.38% to 88.08% for OS (P = 0.020) and from 87.48% to 88.20% for DSS (P = 0.039) at 12th month (Supplementary Figures S6C, D). However, the predictive performance of AUC curves at the 36th and 60th month for both OS and DSS was not significantly improved (all P > 0.05, Supplementary Figures S6E–H).

3.6 The result of eQTL analysis

To explore the genotype-phenotype correlation, we first performed the eQTL analysis using genomic data of lymphoblastoid cell lines from the 373 European descendants in the 1000 Genomes Project. The results suggested that the *INPP5D* rs13385922 T allele was not associated with expression levels of *INPP5D* mRNA in the additive (P = 0.405, Supplementary Figure S7A), dominant model (P = 0.430, Supplementary Figure S7B), and recessive model (P = 0.586, Supplementary Figure S7C). We also employed an eQTL analysis using GTEx project data. The results suggested that the *INPP5D* rs13385922 T allele was significantly associated with high mRNA expression levels of *INPP5D* in both normal lung tissues (P = 0.001, Figure 3A) and whole blood samples (P = 1.67e-7, Figure 3B). Moreover, the *EXOSC3* rs3208406 G allele was associated with high mRNA expression levels of *EXOSC3* in the recessive model (P = 2e-05, Figure 3C), but not in the additive (P = 0.117, Supplementary Figure S7D) and dominant model (P = 0.557, Supplementary Figure S7E). In the GTEx project, the *EXOSC3* rs3208406 G allele was associated with mRNA expression levels of *EXOSC3* whole blood samples (P = 0.018, Figure 3D), but not in normal lung tissues (P = 0.105, Supplementary Figure S7F).

3.7 The analysis of mRNA expression and survival in NSCLC

To explore potential mechanisms of *INPP5D* and *EXOSC3* on NSCLC survival, we first evaluated the mRNA expression levels of these two genes using paired *t*-tests with data from the TCGA database and unpaired tests with the online UALCAN portal. Then, we used Kaplan-Meier Plotter web tool to estimate the associations between their mRNA expression levels and NSCLC survival. Compared with adjacent paired normal tissues, *INPP5D* mRNA

expression was significantly down-regulated in tissues from the combined LUSC and LUAD (P = 0.0007) (Figure 4A), and LUSC (P < 0.0001), but not from LUAD (P = 0.565) (Supplementary Figures S8A, B). Similar results were also observed for LUSC (P < 0.0001) and LUAD (P = 0.888) in the UALCAN database using unpaired tests (Supplementary Figures S8C, D). Furthermore, mRNA expression levels of *INPP5D* were not associated with OS of NSCLC (HR = 0.93, 95% CI: 0.83-1.05, log-rank P = 0.23) (Figure 4B). *EXOSC3* mRNA expression levels were significantly up-regulated in tissues from the combined LUSC + LUAD (Figure 4C), LUSC, and LUAD (Supplementary Figures S8E, F) (all P < 0.0001) than those in adjacent normal tissues using paired t-test. Similar results were also observed for LUSC and LUAD (all P < 0.0001) in the UALCAN database using unpaired tests (Supplementary Figures S8G, H). Moreover, high mRNA expression levels of *EXOSC3* were associated with a poor NSCLC OS (HR = 1.69, 95% CI: 1.45-1.96, log-rank P = 4e-12) (Figure 4D).

4 Discussion

In the present study, we evaluated the associations between 10,776 genetic variants in the 220 immunity B cell-related genes and NSCLC survival using available GWAS genotyping data from both PLCO trial and HLCS study. Our results indicated that the *INPP5D* rs13385922 C>T and *EXOSC3* rs3208406 A>G were significantly associated with a poor survival in the United States Caucasian populations. Our findings also suggested that the *INPP5D* rs13385922 variant T allele and *EXOSC3* rs3208406 variant G allele were associated with up-regulated mRNA expression levels of *INPP5D* and *EXOSC3* in the lymphoblastoid cell lines from the 1000 genomes project and the GTEx project, implying that these alleles may modulate mRNA expression and influence NSCLC survival. Our findings provided additional support for associations between genetic variants in the immunity B cell-related genes and survival of NSCLC patients.

B cells are the second most numerous adaptive immune cells in TME and may mediate both pro- and antitumorigenic effects in tumor development (32, 33). Within the tertiary lymphoid structures, B cells perform the function of antigen presentation and antibody production to focus immune responses, and the expression of B cells is associated with clinical outcomes in multiple cancer types (34, 35). However, up to now no studies have reported the association between functional genetic variants of immunity B cell-related genes and NSCLC survival. To the best of our knowledge, this is the first study to explore the role of genetic

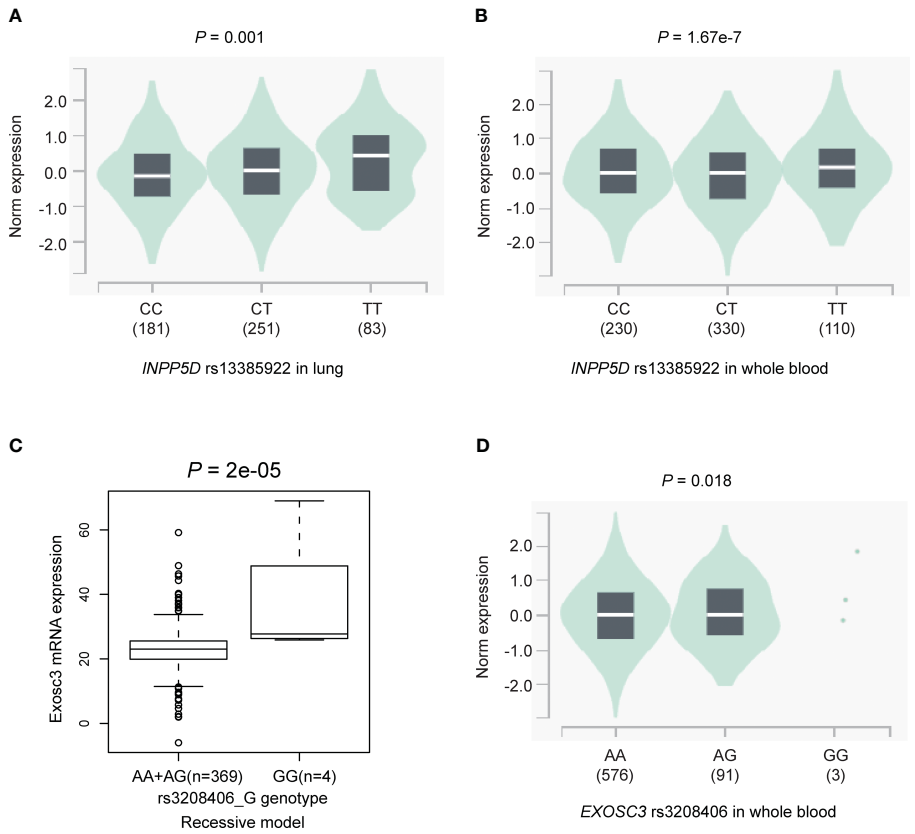

FIGURE 3
The results of the eQTL analysis. The *INPP5D* rs13385922 T allele was significantly associated with high mRNA expression levels of *INPP5D* in **(A)** normal lung tissues and **(B)** whole blood samples in the GTEx project; the *EXOSC3* rs3208406 G allele was associated with high mRNA expression levels of *EXOSC3* in **(C)** recessive model in the lymphoblastoid cell lines from the 1000 Genomes Project and **(D)** whole blood samples in the GTEx project. eQTL, expression quantitative trait loci.

variants of immunity B cell-related genes in predicting NSCLC survival. As a result, we identified two SNPs (i.e., *INPP5D* rs13385922 C>T and *EXOSC3* rs3208406 A>G) from immunity B cell-related genes that predicted the prognosis of NSCLC patients.

INPP5D, inositol polyphosphate-5-phosphatase D (all known as SHIP1), is located on chromosome 2 and composed of 1189 amino acids. *INPP5D* is a member of the inositol polyphosphate-5-phosphatase (*INPP5*) family and plays an important role in the immune system (36). A previous study reported that *INPP5D* can skew macrophage progenitors toward M1 macrophages and naive T cells to T helper 1 and T helper 17 cells; as a result, *INPP5D* is intricately linked to the activation of the immune system and plays a key role in the solid tumor eradication (37). Pulsatile *INPP5D* inhibition contributed to the enhancement of T and NK cell function and improved antitumor immunity and survival in mouse models of lymphoma and colon cancer (38). *INPP5D* has been shown to suppress the activity of PI3K/AKT/mTOR signaling pathway via reducing PI(3,4,5)P3 levels at the plasma membrane and promote cancer cell survival (39). In NSCLC, the expression of *INPP5D* was down-regulated in both tumor tissues and cell lines, and the overexpression of *INPP5D* suppressed cell growth, migration, and invasion by inactivating PI3K/AKT pathway (40). However, no report has investigated the role of the genetic variants of *INPP5D* in NSCLC survival. In the present study, for the first time, we found that the genetic variants of *INPP5D* were significantly associated with OS and DSS in NSCLC patients. The *INPP5D* rs13385922 T allele showed a significant unfavorable effect on NSCLC survival and an association with increased mRNA expression levels of *INPP5D*. However, the mRNA expression of *INPP5D* was not associated with NSCLC survival. We also found that the mRNA expression levels of *INPP5D* were down-regulated in LUSC but not in LUAD, suggesting tumor specificity between LUSC and LUAD. Moreover, the mRNA levels of *INPP5D* may also be possibly modulated by other factors, such as the regulation of RNA transcription and degradation. Nevertheless, the down-regulation of the *INPP5D* mRNA expression in NSCLC identified in the present study is in line with a previous study (40). Taken together, we concluded that *INPP5D* might be a potential tumor suppressor gene in NSCLC.

EXOSC3 (also known as exosome component 3) is located on chromosome 9 and composed of 275 amino acids. *EXOSC3* is one of the constituent elements of RNA exosomes, and mutations in

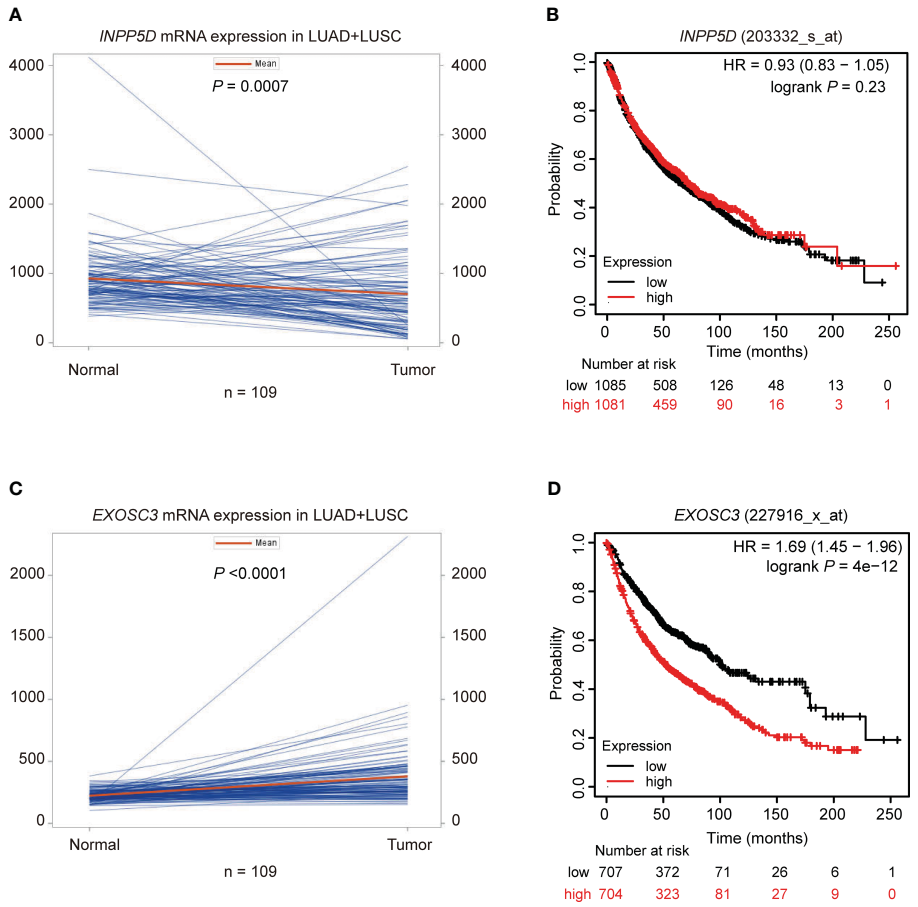

FIGURE 4
Paired mRNA expression and survival analyses in NSCLC. Paired *t*-test suggested that the mRNA expression of **(A)** *INPP5D* was down-regulated and **(C)** *EXOSC3* was up-regulated in NSCLC; survival analysis suggested that **(B)** mRNA expression levels of *INPP5D* were not associated with NSCLC survival; **(D)** high mRNA expression levels of *EXOSC3* were associated with a poor NSCLC survival.

EXOSC3 have been linked to pontocerebellar hypoplasia and spinal motor neuron degeneration (41). One study showed that exosc3-deficient B cells were impaired in the ability to undergo normal levels of somatic hypermutation and class switch recombination (42). Few studies have investigated the role of *EXOSC3* in cancer. A previous study showed that the protein expression of EXOSC3 was significantly up-regulated in pancreatic cancer tissue using protein-deep sequencing (43), but there were no published studies that explored the associations between genetic variants of *EXOSC3* and NSCLC survival. In the present study, our results suggest that the *EXOSC3* rs3208406 G allele may predict a reduced risk of survival for NSCLC patients and up-regulated the mRNA expression levels of *EXOSC3* in the 1000 Genomes Project and whole blood samples. Our findings on this SNP-mRNA correlation suggested that *EXOSC3* rs3208406 G may influence the prognosis of NSLCLC via modulating the mRNA expression of *EXOSC3*. However, functional experiments should be designed to explore the potential molecular mechanisms underlying the observed SNP-mRNA associations.

The observed SNP-survival associations in the present study suggested that genetic variants in the immunity B cell-related genes might be potential therapy targets for NSCLC. However, several methodological weaknesses in this study should be acknowledged. First, due to NSCLC patients in the two GWAS datasets were only limited to Caucasian descents, our findings may not be generalizable to other populations with different ethnicities. To address this gap, we will design replication study with other larger and independent populations from different races or geographic regions. Second, because the lack of detailed genotype data and clinical outcomes information in the HLCS study, we conducted the combined and stratified analyses with data only from the PLCO trial, and the results should be interpreted cautiously. Third, no further clinical information on nutrition status and details of treatment were available for further analysis. Moreover, although the two identified SNPs were identified to be associated with NSCLC survival, the potential mechanisms are not clear. Further experiments should be undertaken both *in vivo* and *in vitro* to better understand the mechanisms underlying the observed associations between two identified SNPs and NSCLC survival.

Data availability statement

Publicly available datasets were analyzed in this study. This data can be found here: dbGaP accession numbers: phs000093.v2.P2 and phs000336.v1.p1.

Ethics statement

The studies involving humans were approved by The PLCO trial was approved by the National Cancer Institute and the institutional review boards of each involved center. The use of the PLCO trial and HLCS study for experimentation was approved by the Internal Review Board of Duke University School of Medicine (Project #Pro00054575) and the dbGaP database (Project #6404). The studies were conducted in accordance with the local legislation and institutional requirements. Written informed consent for participation was not required from the participants or the participants' legal guardians/next of kin in accordance with the national legislation and institutional requirements.

Author contributions

GL: Conceptualization, Formal analysis, Funding acquisition, Methodology, Software, Writing – original draft. HL: Conceptualization, Data curation, Validation, Writing – original draft. HW: Formal analysis, Writing – original draft. XT: Formal analysis, Writing – original draft. SL: Methodology, Writing – review & editing. MD: Data curation, Formal analysis, Validation, Writing – original draft. DC: Funding acquisition, Methodology, Writing – review & editing. QW: Conceptualization, Funding acquisition, Methodology, Writing – review & editing.

Funding

The author(s) declare financial support was received for the research, authorship, and/or publication of this article. QW was supported by NIH grants 2R01 ES011740 and 1R01CA 131274 and also partly supported by the Duke Cancer Institute as part of the P30 Cancer Center Support Grant (Grant ID: NIH/NCI CA014236). The Harvard Lung Cancer Susceptibility Study was supported by NIH grants U01CA209414, CA092824, CA074386 and CA090578 to DC. GL was supported by Jiangsu Health International Exchange Program.

Acknowledgments

The authors thank all the participants of the PLCO Cancer Screening Trial. The authors also thank the National Cancer Institute for granting access to the data collected during the PLCO trial. It is important to note that the statements provided in this document solely reflect the perspectives of the authors and do not imply concurrence or endorsement by the National Cancer Institute. The authors would also like to acknowledge the dbGaP repository for providing valuable cancer genotyping datasets. The accession numbers for the lung cancer datasets are phs000336.v1.p1 and phs000093.v2.p2. A list of contributing investigators and funding agencies for those studies can be found in the Supplementary Data.

Conflict of interest

The authors declare that the research was conducted in the absence of any commercial or financial relationships that could be construed as a potential conflict of interest.

Publisher's note

All claims expressed in this article are solely those of the authors and do not necessarily represent those of their affiliated organizations, or those of the publisher, the editors and the reviewers. Any product that may be evaluated in this article, or claim that may be made by its manufacturer, is not guaranteed or endorsed by the publisher.

Supplementary material

The Supplementary Material for this article can be found online at: https://www.frontiersin.org/articles/10.3389/fimmu.2024.1440454/full#supplementary-material

References

1. Siegel RL, Miller KD, Wagle NS, Jemal A. Cancer statistics, 2023. *CA Cancer J Clin*. (2023) 73:17–48. doi: 10.3322/caac.21763

2. Han B, Zheng R, Zeng H, Wang S, Sun K, Chen R, et al. Cancer incidence and mortality in China, 2022. *Zhonghua Zhong Liu Za Zhi*. (2024) 46:221–31. doi: 10.3760/cma.j.cn112152-20240119-00035

3. Carbone DP, Gandara DR, Antonia SJ, Zielinski C, Paz-Ares L. Non-small-cell lung cancer: role of the immune system and potential for immunotherapy. *J Thorac Oncol*. (2015) 10:974–84. doi: 10.1097/JTO.0000000000000551

4. Liu X, Li R, Chen X, Yao J, Wang Q, Zhang J, et al. SYT7 is a key player in increasing exosome secretion and promoting angiogenesis in non-small-cell lung cancer. *Cancer Lett*. (2023) 577:216400. doi: 10.1016/j.canlet.2023.216400

5. Howlader N, Forjaz G, Mooradian MJ, Meza R, Kong CY, Cronin KA, et al. The effect of advances in lung-cancer treatment on population mortality. *N Engl J Med*. (2020) 383:640–9. doi: 10.1056/NEJMoa1916623

6. Wang S, Wang J, Bai Y, Wang Q, Liu L, Zhang K, et al. The genetic variations in DNA repair genes ERCC2 and XRCC1 were associated with the overall survival of advanced non-small-cell lung cancer patients. *Cancer Med*. (2016) 5:2332–42. doi: 10.1002/cam4.822

7. Yang E, Wang X, Gong Z, Yu M, Wu H, Zhang D. Exosome-mediated metabolic reprogramming: the emerging role in tumor microenvironment remodeling and its influence on cancer progression. *Signal Transduct Target Ther*. (2020) 5:242. doi: 10.1038/s41392-020-00359-5

8. de Visser KE, Joyce JA. The evolving tumor microenvironment: From cancer initiation to metastatic outgrowth. *Cancer Cell*. (2023) 41:374–403. doi: 10.1016/j.ccell.2023.02.016

9. Hinshaw DC, Shevde LA. The tumor microenvironment innately modulates cancer progression. *Cancer Res*. (2019) 79:4557–66. doi: 10.1158/0008-5472.CAN-18-3962

10. Downs-Canner SM, Meier J, Vincent BG, Serody JS. B cell function in the tumor microenvironment. *Annu Rev Immunol*. (2022) 40:169–93. doi: 10.1146/annurev-immunol-101220-015603

11. Anderson KG, Stromnes IM, Greenberg PD. Obstacles posed by the tumor microenvironment to T cell activity: A case for synergistic therapies. *Cancer Cell*. (2017) 31:311–25. doi: 10.1016/j.ccell.2017.02.008

12. Sarvaria A, Madrigal JA, Saudemont A. B cell regulation in cancer and anti-tumor immunity. *Cell Mol Immunol*. (2017) 14:662–74. doi: 10.1038/cmi.2017.35

13. Stankovic B, Bjørhovde HAK, Skarshaug R, Aamodt H, Frafjord A, Müller E, et al. Immune cell composition in human non-small cell lung cancer. *Front Immunol*. (2018) 9:3101. doi: 10.3389/fimmu.2018.03101

14. Chen J, Tan Y, Sun F, Hou L, Zhang C, Ge T, et al. Single-cell transcriptome and antigen-immunoglobin analysis reveals the diversity of B cells in non-small cell lung cancer. *Genome Biol*. (2020) 21:152. doi: 10.1186/s13059-020-02064-6

15. Diao XY, Wang F. Single-cell transcriptome analysis of tumor-infiltrating B cells reveals their clinical implications in non-small cell lung cancer. *Thorac cancer*. (2021) 12:5–7. doi: 10.1111/1759-7714.13719

16. Cusanovich DA, Caliskan M, Billstrand C, Michelini K, Chavarria C, De Leon S, et al. Integrated analyses of gene expression and genetic association studies in a founder population. *Hum Mol Genet*. (2016) 25:2104–12. doi: 10.1093/hmg/ddw061

17. Chen AS, Liu H, Wu Y, Luo S, Patz EFJr, Glass C, et al. Genetic variants in DDO and PEX5L in peroxisome-related pathways predict non-small cell lung cancer survival. *Mol Carcinog*. (2022) 61:619–28. doi: 10.1002/mc.23400

18. Bai Y, Zheng J, Cheng L, Liu Q, Zhao G, Li J, et al. Potentially functional genetic variants of VAV2 and PSMA4 in the immune-activation pathway and non-small cell lung cancer survival. *J Gene Med*. (2022) 24:e3447. doi: 10.1002/jgm.3447

19. Tryka KA, Hao L, Sturcke A, Jin Y, Wang ZY, Ziyabari L, et al. NCBI's database of genotypes and phenotypes: dbGaP. *Nucleic Acids Res*. (2014) 42:D975–979. doi: 10.1093/nar/gkt1211

20. Wong KM, Langlais K, Tobias GS, Fletcher-Hoppe C, Krasnewich D, Leeds HS, et al. The dbGaP data browser: a new tool for browsing dbGaP controlled-access genomic data. *Nucleic Acids Res*. (2017) 45:D819–d826. doi: 10.1093/nar/gkw1139

21. Zhai R, Yu X, Wei Y, Su L, Christiani DC. Smoking and smoking cessation in relation to the development of co-existing non-small cell lung cancer with chronic obstructive pulmonary disease. *Int J Cancer*. (2014) 134:961–70. doi: 10.1002/ijc.28414

22. Liberzon A, Birger C, Thorvaldsdóttir H, Ghandi M, Mesirov JP, Tamayo P. The Molecular Signatures Database (MSigDB) hallmark gene set collection. *Cell Syst*. (2015) 1:417–25. doi: 10.1016/j.cels.2015.12.004

23. Karssen LC, van Duijn CM, Aulchenko YS. The GenABEL Project for statistical genomics. *F1000Res*. (2016) 2016:5:914. doi: 10.12688/f1000research.8733.1

24. Park JH, Geum DI, Eisenhut M, van der Vliet HJ, Shin JI. Beaysian statistical methods in genetic association studies: Empirical examination of statistically non-significant Genome Wide Association Study (GWAS) meta-analyses in cancers: A systematic review. *Gene*. (2019) 685:170–8. doi: 10.1016/j.gene.2018.10.057

25. Dong S, Zhao N, Spragins E, Kagda MS, Li M, Assis P, et al. Annotating and prioritizing human non-coding variants with RegulomeDB v.2. *Nat Genet*. (2023) 55:724–6. doi: 10.1038/s41588-023-01365-3

26. Ward LD, Kellis M. HaploReg v4: systematic mining of putative causal variants, cell types, regulators and target genes for human complex traits and disease. *Nucleic Acids Res*. (2016) 44:D877–881. doi: 10.1093/nar/gkv1340

27. Boughton AP, Welch RP, Flickinger M, VandeHaar P, Taliun D, Abecasis GR, et al. LocusZoom.js: interactive and embeddable visualization of genetic association study results. *Bioinformatics*. (2021) 37:3017–8. doi: 10.1093/bioinformatics/btab186

28. Chambless LE, Diao G. Estimation of time-dependent area under the ROC curve for long-term risk prediction. *Stat Med*. (2006) 25:3474–86. doi: 10.1002/sim.2299

29. Human genomics. The Genotype-Tissue Expression (GTEx) pilot analysis: multitissue gene regulation in humans. *Science*. (2015) 348:648–60. doi: 10.1126/science.1262110

30. Chandrashekar DS, Karthikeyan SK, Korla PK, Patel H, Shovon AR, Athar M, et al. UALCAN: An update to the integrated cancer data analysis platform. *Neoplasia*. (2022) 25:18–27. doi: 10.1016/j.neo.2022.01.001

31. Győrffy B. Transcriptome-level discovery of survival-associated biomarkers and therapy targets in non-small-cell lung cancer. *Br J Pharmacol*. (2024) 181:362–74. doi: 10.1111/bph.16257

32. Wang SS, Liu W, Ly D, Xu H, Qu L, Zhang L. Tumor-infiltrating B cells: their role and application in anti-tumor immunity in lung cancer. *Cell Mol Immunol*. (2019) 16:6–18. doi: 10.1038/s41423-018-0027-x

33. Fridman WH, Petitprez F, Meylan M, Chen TW, Sun CM, Roumenina LT, et al. B cells and cancer: To B or not to B? *J Exp Med*. (2021) 218. doi: 10.1084/jem.20200851

34. Zheng M, Li YM, Liu ZY, Zhang X, Zhou Y, Jiang JL, et al. Prognostic landscape of tumor-infiltrating T and B cells in human cancer. *Front Immunol*. (2021) 12:731329. doi: 10.3389/fimmu.2021.731329

35. Laumont CM, Nelson BH. B cells in the tumor microenvironment: Multi-faceted organizers, regulators, and effectors of anti-tumor immunity. *Cancer Cell*. (2023) 41:466–89. doi: 10.1016/j.ccell.2023.02.017

36. Kerr WG. Inhibitor and activator: dual functions for SHIP in immunity and cancer. *Ann N Y Acad Sci*. (2011) 1217:1–17. doi: 10.1111/j.1749-6632.2010.05869.x

37. Hamilton MJ, Ho VW, Kuroda E, Ruschmann J, Antignano F, Lam V, et al. Role of SHIP in cancer. *Exp Hematol*. (2011) 39:2–13. doi: 10.1016/j.exphem.2010.11.002

38. Gumbleton M, Sudan R, Fernandes S, Engelman RW, Russo CM, Chisholm JD, et al. Dual enhancement of T and NK cell function by pulsatile inhibition of SHIP1 improves antitumor immunity and survival. *Sci Signal*. (2017) 10. doi: 10.1126/scisignal.aam5353

39. Fernandes S, Iyer S, Kerr WG. Role of SHIP1 in cancer and mucosal inflammation. *Ann N Y Acad Sci*. (2013) 1280:6–10. doi: 10.1111/nyas.12038

40. Fu Q, Huang Y, Ge C, Li Z, Tian H, Li Q, et al. SHIP1 inhibits cell growth, migration, and invasion in non–small cell lung cancer through the PI3K/AKT pathway. *Oncol Rep*. (2019) 41:2337–50. doi: 10.3892/or.2019.6990

41. Wan J, Yourshaw M, Mamsa H, Rudnik-Schöneborn S, Menezes MP, Hong JE, et al. Mutations in the RNA exosome component gene EXOSC3 cause pontocerebellar hypoplasia and spinal motor neuron degeneration. *Nat Genet*. (2012) 44:704–8. doi: 10.1038/ng.2254

42. Pefanis E, Wang J, Rothschild G, Lim J, Chao J, Rabadan R, et al. Noncoding RNA transcription targets AID to divergently transcribed loci in B cells. *Nature*. (2014) 514:389–93. doi: 10.1038/nature13580

43. Ansari D, Andersson R, Bauden MP, Andersson B, Connolly JB, Welinder C, et al. Protein deep sequencing applied to biobank samples from patients with pancreatic cancer. *J Cancer Res Clin Oncol*. (2015) 141:369–80. doi: 10.1007/s00432-014-1817-x

frontiers | Frontiers in Immunology

TYPE Original Research
PUBLISHED 09 August 2024
DOI 10.3389/fimmu.2024.1438364

Check for updates

OPEN ACCESS

EDITED BY
Wantao Wu,
Central South University, China

REVIEWED BY
Wenjian Hu,
Southwest Medical University, China
Zeyang Ding,
Huazhong University of Science and Technology, China
Jianbin Bi,
The First Hospital of China Medical University, China

*CORRESPONDENCE
Hong Cao
caohong9970@163.com

RECEIVED 25 May 2024
ACCEPTED 09 July 2024
PUBLISHED 09 August 2024

CITATION
Zhong Y, Cao H, Li W, Deng J, Li D and Deng J (2024) Investigating the impact of STING pathway activation on breast cancer treatment outcomes: development and validation of a prognostic model.
Front. Immunol. 15:1438364.
doi: 10.3389/fimmu.2024.1438364

COPYRIGHT
© 2024 Zhong, Cao, Li, Deng, Li and Deng. This is an open-access article distributed under the terms of the Creative Commons Attribution License (CC BY). The use, distribution or reproduction in other forums is permitted, provided the original author(s) and the copyright owner(s) are credited and that the original publication in this journal is cited, in accordance with accepted academic practice. No use, distribution or reproduction is permitted which does not comply with these terms.

Investigating the impact of STING pathway activation on breast cancer treatment outcomes: development and validation of a prognostic model

YangYan Zhong[1,2], Hong Cao[1,2*], Wei Li[1,2], Jian Deng[1,2], Dan Li[1,2] and JunJie Deng[1,2]

[1]The Second Affiliated Hospital, Department of Breast and Thyroid Surgery, Hengyang Medical School, University of South China, Hengyang, Hunan, China, [2]Clinical Research Center for Breast and Thyroid Disease Prevention and Control in Hunan Province, Hengyang Medical School, University of South China, Hengyang, Hunan, China

Introduction: Breast cancer (BRCA) is a significant cause of cancer-associated mortality across the globe. Current therapeutic approaches face challenges such as drug resistance and metastasis. Immune signaling is triggered by chromosomal instability (CIN) generates misplaced DNA structures that activate the cyclic GMP–AMP synthase–stimulator of interferon genes (cGAS-STING) pathway, triggering. Studies have linked STING activation to BRCA treatment.

Methods: The bulk RNA-seq data for patients with BRCA were collected from the TCGA-BRCA cohort, GSE20685, and GSE96058 cohorts. STING pathway-related genes (SRGs) were obtained from the Reactome database. Differentially expressed genes were analyzed using the limma package. Immune cell infiltration was analyzed using the IOBR package. Gene Ontology biological processes, Kyoto Encyclopedia of Genes and Genomes pathways, and cancer hallmark pathways were analyzed using the MSigDB database. Prognostic models were prepared using the least absolute shrinkage and selection operator and multiple-factor Cox regression analysis. Single-cell analysis was performed using the Seurat and SCP pipeline.

Results: The expression patterns and clinical relevance of SRGs were analyzed in patients with BRCA. Transcriptional differences in the SRGs were observed between normal and tumorous tissues, with global down-regulated STING1 and up-regulated TBK1 in BRCA tissue. Tumor tissues were classified through consensus clustering analysis into two distinct groups, with differences in clinical characteristics and immune infiltration. A prognostic model related to the

differences in STING pathway activity—high prognostic stratification potency—was developed and validated. Correlation analysis revealed suppressed overall immune activation in patients with BRCA having higher risk scores. Gemcitabine had a more favorable outcome in the low-risk group. The activity of the prognostic model at the single-cell level was confirmed through single-cell analysis, particularly in CD8 T cells and intratumor natural killer cells.

Conclusion: A STING pathway-related prognostic model developed and validated and the model could accurately predict BRCA patient outcomes. These findings have important implications for the personalized treatment and management of patients with BRCA.

KEYWORDS

breast cancer, STING, tumor microenvironment, single-cell analysis, prognosis

1 Introduction

The incidence of breast cancer (BRCA) has reached an approximately estimated mortality of 0.7 million across the globe (1). While several methods, such as mammectomy and chemoradiotherapy drugs, have been developed for the treatment and management of BRCA, there are still challenges to overcome. One such challenge is drug resistance, which restricts the ability of chemotherapy agents like doxorubicin (DOX) in suppressing BC progression (2). Besides drug resistance, metastasis is a major factor contributing to the poor prognosis of patients with BRCA (3). Understanding the inherent mechanisms that trigger BRCA development is crucial for developing effective treatments.

One key feature of cancer is chromosomal instability (CIN), which leads to the generation of misplaced DNA structures called micronuclei and chromatin bridges. These structures activate the cyclic GMP–AMP synthase–stimulator of interferon genes (cGAS-STING) pathway, triggering immune signaling and potentially eliminating cancer cells (4). However, cancers with high CIN often evade immune responses and exhibit metastatic behavior and poor outcomes. The cGAS-STING signaling pathway has attracted significant attention in cancer immunotherapy. In BRCA treatment, paclitaxel has been linked to the activation of the cGAS-STING pathway, implying that targeting this pathway may be a potentially novel therapeutic strategy (5, 6). Overall, understanding and manipulating the cGAS-STING pathway holds promise for improving BRCA treatment.

In this study, we developed a prognostic model based on the STING pathway-related dysregulated genes. We used the least absolute shrinkage and selection operator (LASSO) and multiple-factor regression analysis to select the genes of the most prognostic significance for the model construction. The model exhibited high prognostic stratification potential in the training set and was validated in two external datasets. In the high-risk group, enhanced expression of various STING pathway genes was observed. We found the association of higher risk scores with suppressed immune activation and altered immune cell infiltration. At single-cell resolution, a highly activated signature related to the STING pathway was identified in the CD8 T cells and intratumor NK cells. Our study provides extensive insights into the transcriptional changes, molecular subtypes, dysregulated pathways, and clinical implications of STING-pathway-related genes in BRCA.

2 Methods

2.1 Data origin

The bulk RNA-seq data for patients with BRCA were collected from The Cancer Genome Atlas Breast Invasive Carcinoma (TCGA-BRCA) cohort using the TCGAbiolinks R package, GSE20685 and GSE96058 cohorts using the GEOquery R package. These datasets contain single-cell RNA-seq (scRNA-seq) data for BRCA. We obtained single-cell RNA-seq (scRNA-seq) data for BRCA from three datasets from the Gene Expression Omnibus (GEO) database (https://www.ncbi.nlm.nih.gov/geo/). These datasets were chosen to comprehensively analyze gene expression patterns in BRCA across different research studies and omics.

2.2 Acquisition of STING-pathway-related gene sets

The STING-pathway-related genes (SRGs) were acquired from the R-HSA-3134800 of the Reactome database (https://curator.reactome.org/) to evaluate their effect on the STING pathway activity.

2.3 Differential gene analysis

Differential gene analysis was performed using the limma package with a significance threshold of adj.P.val. < 0.01 and fold change (|logFC|) > 1.

2.4 Analysis of immune cell infiltration

For this, the IOBR R package (https://github.com/IOBR/IOBR) was utilized. We employed the built-in tumor microenvironment (TME) analysis algorithms, namely CIBERSORT and ESITMATE, to examine the bulk RNA-seq dataset.

2.5 Identification of immune checkpoint genes (ICGs) and chemotherapy sensitivity

The immune checkpoint genes and chemotherapy sensitivity-related gene sets were retrieved from the literature (7).

2.6 Analysis of gene ontology-biological processes (GO-BP), Kyoto Encyclopedia of Genes and Genomes (KEGG), and cancer hallmarks

The MSigDB database (https://www.gsea-msigdb.org/gsea/msigdb/) was utilized for the analysis of GO-BP, KEGG pathways, and cancer hallmark pathways.

2.7 Mutation analysis and prediction of drug sensitivity

The mutation was analyzed using the maftool R package. The oncoPredict R package was employed to predict drug sensitivity based on gene expression levels. This package provides IC50 values for each drug, indicating drug effectiveness based on lower IC50 values.

2.8 Construction and validation of prognostic models

A prognostic model was constructed in the TCGA dataset, using LASSO and multiple-factor Cox regression analysis. The coefficients of each gene in the model have been visually represented using a lollipop plot, eliminating the need for separate formulas in the article and improving its aesthetic appeal.

2.9 Single-cell analysis

Single-cell analysis was carried out on the Seurat and SCP pipeline (https://github.com/zhanghao-njmu/SCP). Step1: Quality control: Cells with nFeature_RNA < 9000 and percent.mt < 25 were excluded from the analysis. Step2: Batch integration: The harmony R package was used for batch correction and integration of multiple samples. Step3: Annotation: SingleR was employed for the automatic annotation of cell types. Step4: Gene set scoring: The AddModuleScore() function, built-in within the Seurat R package, was used for scoring gene sets.

2.10 Cell culture

We obtained the human breast cancer cell lines, BT-549 and DU4475, from the ATCC. These cells were cultured in Dulbecco's Modified Eagle Medium (DMEM) (Gibco, Grand Island, NY, USA) supplemented with 10% fetal bovine serum (Gibco). The cells were maintained in a 5% CO2 atmosphere at 37 °C. To manipulate the expression of certain genes, we used overexpression plasmids (pcDNA3.1-TMEM31) and si-RNA, which were purchased from GenePharma (Suzhou, China). The transfection was performed using Lipofectamine® 3000 (Invitrogen; Thermo Fisher Scientific) according to the manufacturer's instructions.

2.11 Transwell assay

To conduct the Transwell assay, we added an appropriate number of cells in serum-free conditioned medium to the upper chamber. The cells were allowed to incubate at 37°C for 24 hours. Afterward, we removed the cells from the upper chamber and treated the invaded cells with 4% paraformaldehyde. We stained the cells with crystal violet and observed and counted them under a microscope.

2.12 Wound healing assay

For the wound healing assay, we seeded the cells in 6-well plates and allowed them to reach a sub-confluent state. After starving the cells in serum-free DMEM for 48 hours, we created a straight wound at the bottom of the plate using a sterile pipette tip. The cells were then cultured in a serum-free medium for 48 hours and observed at 0 and 48 hours using an inverted light microscope.

2.13 Cell viability and proliferation assay

To assess cell proliferation, we used a Cell Counting Kit-8 (CCK-8) assay obtained from Shanghai Yeasen Biotechnology Co., Ltd. In 96-well plates, we seeded 2,000 cells and added 10 µl of diluted CCK-8 solution. After incubating the cells with the CCK-8 reagent at 37°C for 1 hour in the dark, we measured the absorbance at 450 nm. Additionally, we detected cell proliferation using the BeyoClickTM EdU Cell proliferation kit, following the manufacturer's instructions from Beyotime Institute of Biotechnology. The cells were stained with Alexa Fluor 488 at room temperature for 30 minutes in the dark and observed using a fluorescence microscope. For cell cycle analysis, cells were fixed with ethanol at 4°C for 48 hours and subsequently stained with PI. Finally, flow cytometry (BD, NJ, USA) was used to evaluate cell cycle.

2.14 Statistical analysis

To perform bioinformatics analysis, we utilized R software (version 4.2.3). For statistical analysis of the experimental results, we used Prism 8 (Dotmatics) considering three replications. Two-group comparisons were conducted using unpaired t-tests. A statistically significant difference was defined as a P-value of less than 0.05. The results were presented with error bars indicating the mean ± standard deviation.

3 Results

3.1 Transcriptional differences of STING pathway-related genes in patients with breast cancer

The transcriptional changes and clinical relevance of SRGs in BRCA patients were examined. Next, the expression patterns of the 16 SRGs across different tissue types (Figure 1A), age populations (Figure 1B), and clinical stages (Figure 1C) in patients with BRCA in the TCGA dataset, and the somatic mutation status of these SRGs (Figure 1D). The expression of TREX1 was reduced either in the normal breast or tumorous tissues. Except for NLRP4 and TRIM21, the expressions of the remaining 13 genes between normal and tumorous tissues differed significantly. Of note, the expression of STING1 was down-regulated in the BRCA tissue, while that of TBK1 was enhanced. Moreover, the expression of three SRGs was significantly associated with differences in the age of patients. DDX41, DTX4, and NLRC3 were down-regulated in patients older than 65). However, the relevance of SRGs and clinical staging was not obvious. Among the 16 SRGs, the highest mutation rate was noted in PRKDC in the TCGA cohort.

3.2 Consensus clustering analysis of the TCGA-BRCA dataset using STING pathway-related genes

The expression levels of the 16 SRGs were used to perform an unsupervised clustering analysis using the ConsensusClusterPlus package to classify the tumor tissues from the TCGA dataset into

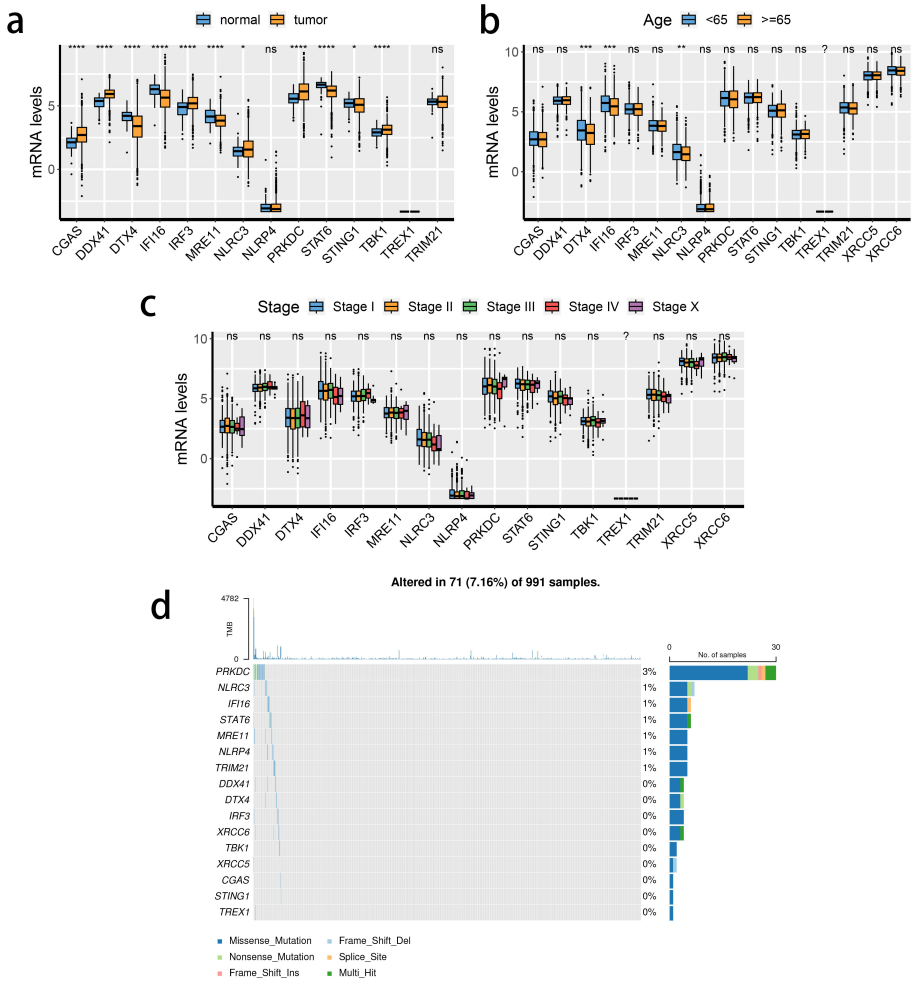

FIGURE 1
Transcriptional changes of STING pathway-related genes (SRGs) in breast cancer. **(A–C)** The expression patterns of 16 SRGs across tissue types **(A)**, age populations **(B)**, and stages **(C)**. **(D)** Somatic mutation of 16 SRGs.

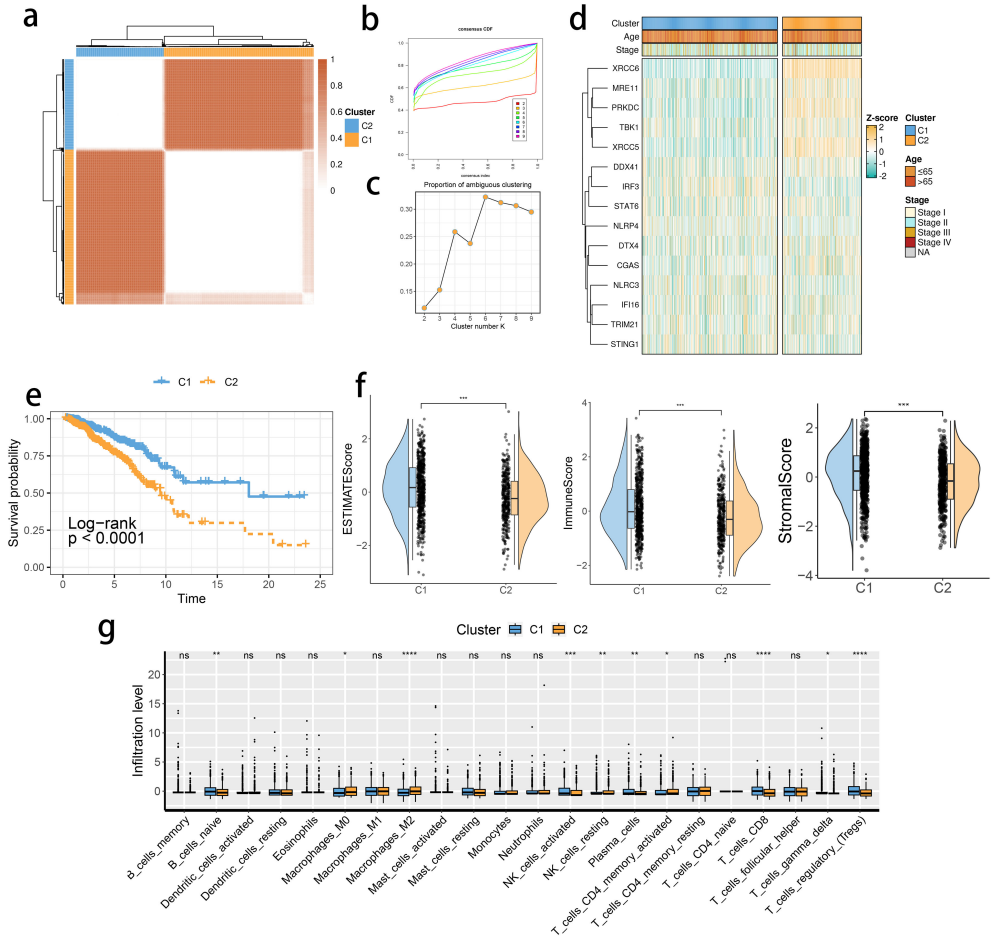

FIGURE 2
STING pathway-related genes (SRGs)-based molecular clusters with distinct prognosis and tumor microenvironment (TME) landscapes. **(A)** The consensus score matrix of tumor samples in The Cancer Genome Atlas Breast Invasive Carcinoma when the clustering number k = 2. The consensus score represents the intensity of interaction between two samples. **(B, C)** The cumulative distribution function (CDF) curves **(B)** and proportions of ambiguously clustered (PAC) scores **(C)** of the consensus matrix for each k. **(D)** Expression profiles of SRGs and clinicopathological characteristics between clusters. **(E)** Survival analysis between C1 and C2. **(F)** Differences in tumor microenvironment (TME) scores were determined by the ESTIMATE method between clusters. **(G)** Abundance of infiltrating immune cells between clusters. *p< 0.05, **p< 0.01, ***p< 0.001, ****p< 0.0001. ns, not significance.

two distinct groups, C1 and C2 (Figures 2A–C). Distinct expression differences in the 16 SRGs between two subclusters were found, highlighting most prominent difference in the XRCC6 expression (Figure 2D). We also observed a higher percentage of stage IV and elderly population in the C2 subgroup, which was consistent with survival analysis results and featured a significantly inferior prognosis of C2 (Figure 2E). All the three immune-associated evaluations displayed a similar pattern, indicating a more intensively activated TME in the C1 (Figure 2F). The immune differences of the two subclusters were further assessed by examining the immune infiltration (Figure 2G). M2 macrophages were in significantly higher abundance in the C2 subcluster, while another pivotal immunosuppressive cell type, namely Tregs, was highly abundant in the C1 BRCA tissue. Collectively, these results suggested M2 macrophages may potentially have a predominant role in shaping immunosuppressive TME in BRCA, rather than Tregs. A potential association between STING pathway activation and M2 infiltration is also suggested. We assessed the differences in the expression of the immune checkpoint inhibitors. The expression of CD276, PVR, and TDO2 were prominently up-regulated in C2 (Figure 3A), while AKR1C1 and MGMT were highly expressed in the C2 subgroup (Figure 3B), suggesting a potential difference in radiotherapy sensitivity in these two subgroups.

We found translational initiation and highly activated *de novo* AMP biosynthetic process within the C2 subgroup (Figure 4A). Moreover, a similar pattern of the cell cycle and RNA degradation was noted in the C2 group (Figure 4B). We focused on these functional differences and performed the Gene Set Enrichment Analysis, highlighting a consistent result (Figure 4C). Moreover, the mammalian target of rapamycin signaling, cell stemness, and regulation of actin were also differentially regulated in the two clusters (Figures 4D, E).

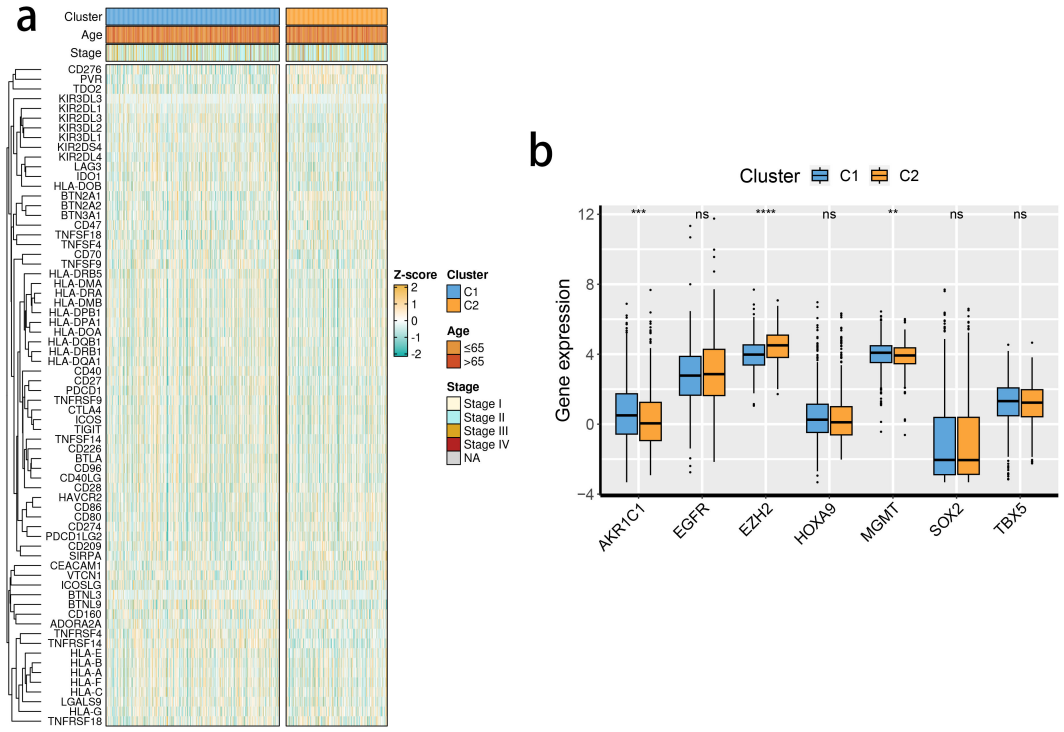

FIGURE 3
The expression profiles of immune checkpoint inhibitors and chemoradiotherapy sensitivity–related genes between clusters. **(A)** The immune checkpoint inhibitor mRNA expression levels in the 2 identified molecular subclusters. The expression intensity was normalized to the Z score value. **(B)** The chemoradiotherapy sensitivity–related genes mRNA expression levels in the 2 identified molecular subclusters.

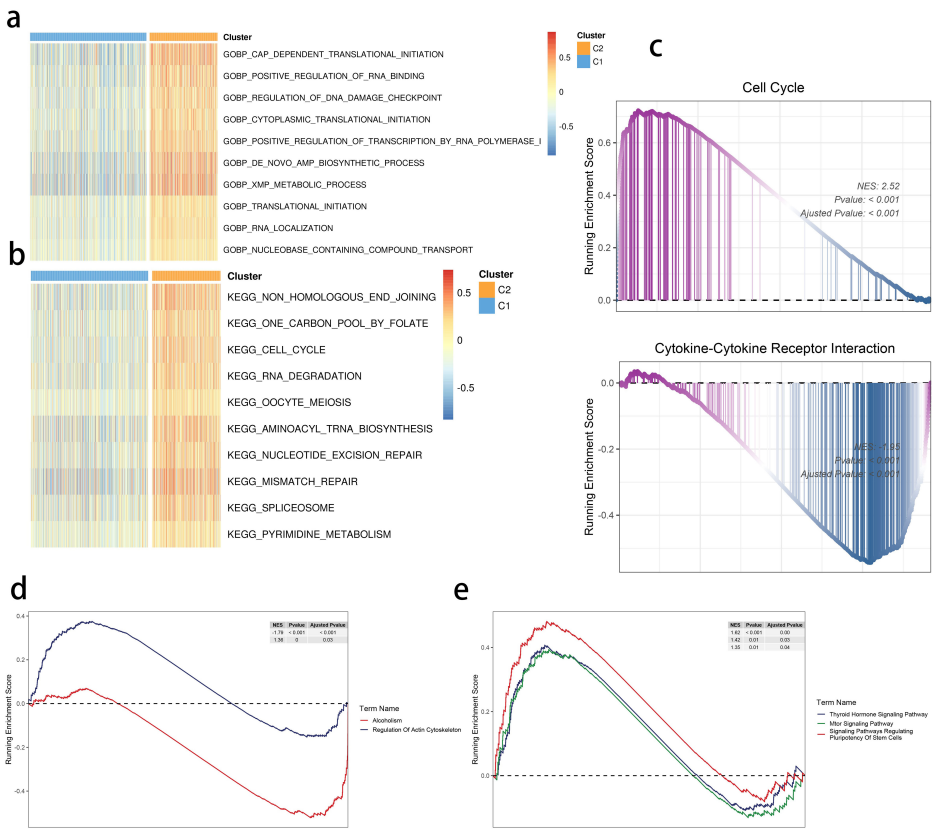

FIGURE 4
SRGs-based molecular clusters with dysregulated pathways and biological process. **(A, B)** GSVA of GO-BP **(A)** and KEGG (b) terms between 2 identified molecular subclusters. **(C)** GSEA of significant hallmarks enriched in SRG C2. **(D, E)** GSEA of significant dysregulated pathways enriched in SRG C2.

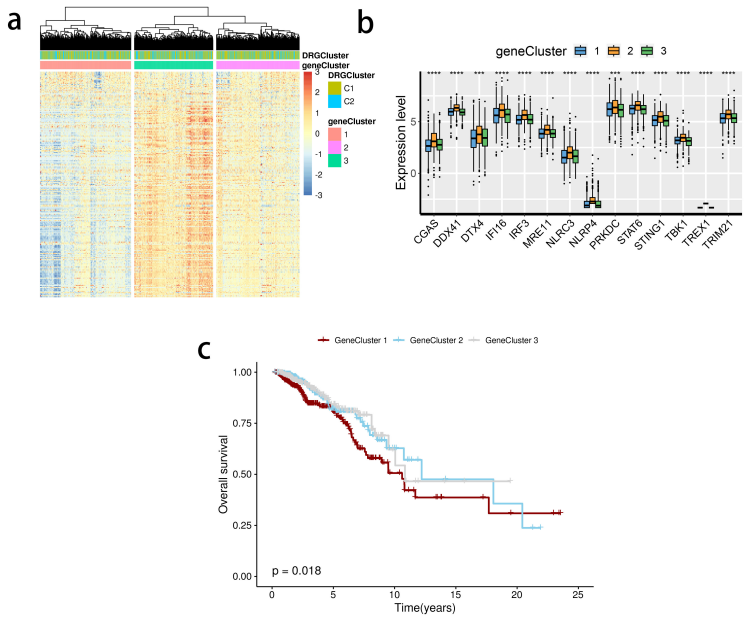

FIGURE 5
Detection of gene clusters related to the stimulator of interferon genes (STING) pathway. **(A)** The expression profiles of DEGs and the distribution of SRG clusters among gene clusters 1 to 3. **(B)** mRNA levels of 16 STING pathway-related genes between groups. **(C)** Survival analysis among three gene clusters. ns, not significance, **p< 0.01, ***p< 0.001, ****p< 0.0001.

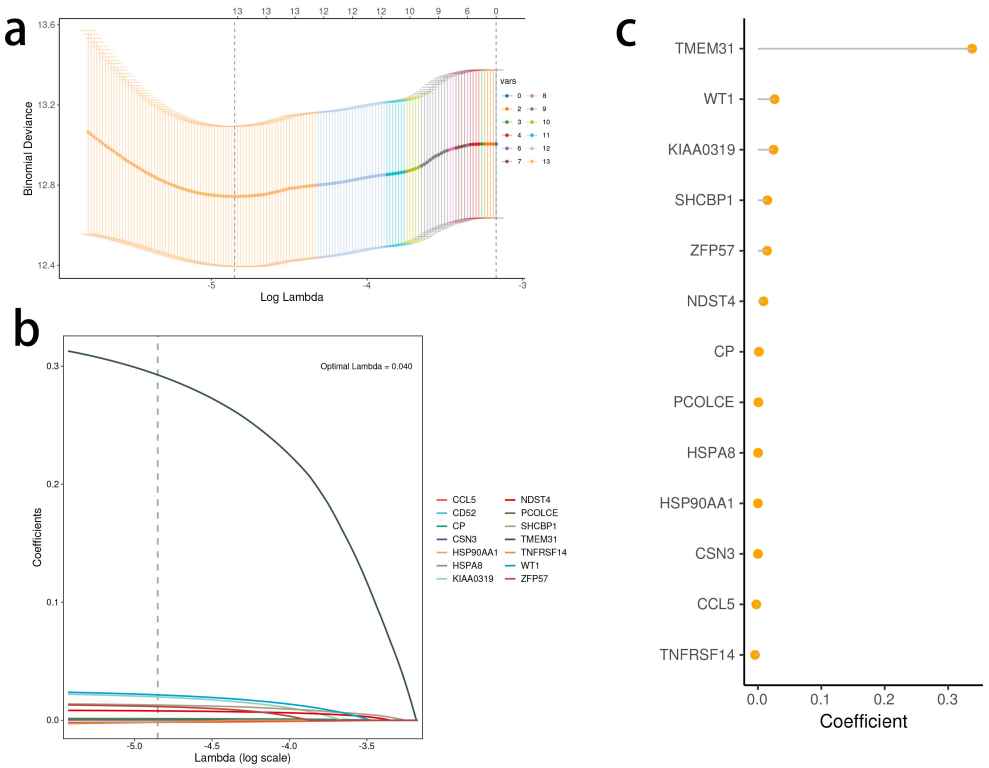

FIGURE 6
Development of the stimulator of interferon genes (STING) pathway-related prognostic model. **(A, B)** The selection of prognostic hub genes based on the optimal parameter λ that was obtained in the least absolute shrinkage and selection operator regression analysis. **(C)** Lollipop chart of the coefficients of signature genes determined by the multiCox regression analysis.

3.3 Detection of gene clusters related to the STING pathway

The limma package was used to detect differentially expressed genes (DEGs) between the C2 and C1 groups (Figure 5A), and a total of three subclusters were identified. The expression of the mentioned SRGs was markedly different between these groups (Figure 5B). Gene cluster 1 had the most inferior survival outcome (Figure 5C).

3.4 Development and validation of the STING pathway-related prognostic model

Based on the identified DEGs related to the STING pathway, we developed a prognostic model using LASSO and multiple-factor regression analyses (Figures 6A–C). The highest coefficient value was noted for TMEM31, followed by those of WT1 and KIAA0319. The prognostic model displayed high prognosis stratification potency in the training set (TCGA dataset, Figure 7A). The prognostic model was validated using two external GEO datasets (Figures 7B, C), highlighting an area under the ROC curve value > 0.7 at multiple time points. Consistent with our expectation, the C2 subgroup had a higher risk score value (Figure 7D). Subgroup 1 also was characterized by a higher value of risk score, in accordance with the inferior clinical outcome (Figure 7E). We determined the expression of 16 SRGs in the BRCA groups of different risk values. The high-risk group exhibited notable up-regulation of STING1 and TBK1 (Figure 7F).

3.5 Correlation analysis investigating tumor microenvironment from the perspective of the risk score value

We investigated the correlation between TME and risk score value to delineate the underlying mechanism of the strong prognosis stratification potency of our model. We found that higher risk score significantly suppressed the complement activation, immunoglobulin production, and phagocytosis, suggesting a significantly hampered immune activation in the patients with BRCA having higher risk scores (Figure 8A). All three immune evaluations consistently showed a similar result (Figure 8B). The expression of CCL5, CP, ZFP57, and TNFRSF14 were highly correlated with M1 macrophage infiltration, while negatively associated with M2 abundance (Figure 8C). Among the hub genes, TMEM31, featuring the highest coefficient value, was positively correlated with the expression of LAG3 and ICOSLG,

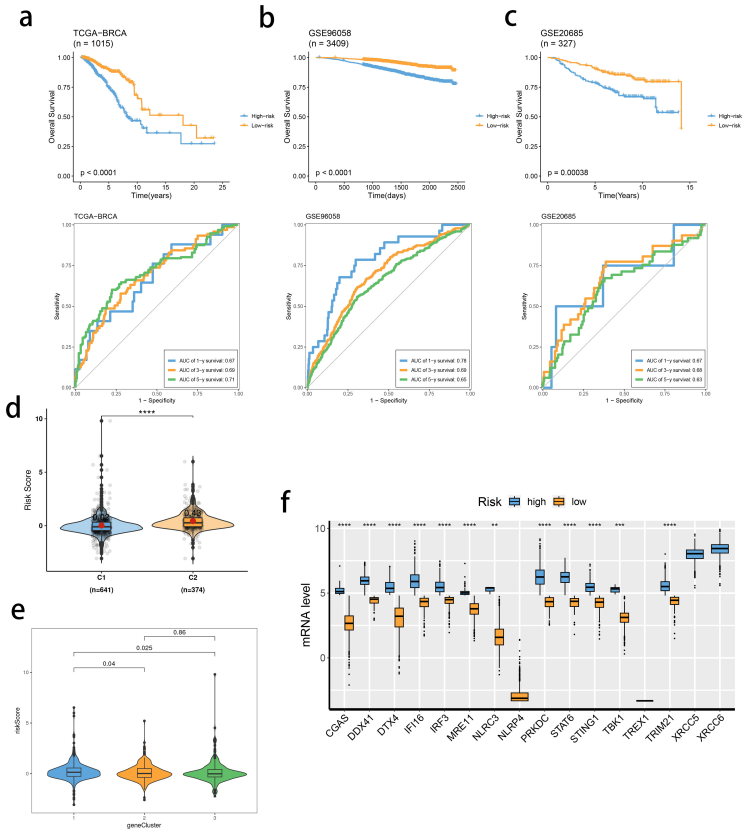

FIGURE 7
Validation of the stimulator of interferon genes (STING) pathway-related prognostic model. **(A–C)** Survival analysis and prognostic performance of the model in the three cohorts. **(D, E)** Distribution of risk scores between SRG clusters **(D)** and gene clusters **(E)**. **(F)** mRNA levels of 16 SRGs between risk groups. ns, not significance, **p< 0.01, ***p< 0.001, ****p< 0.0001.

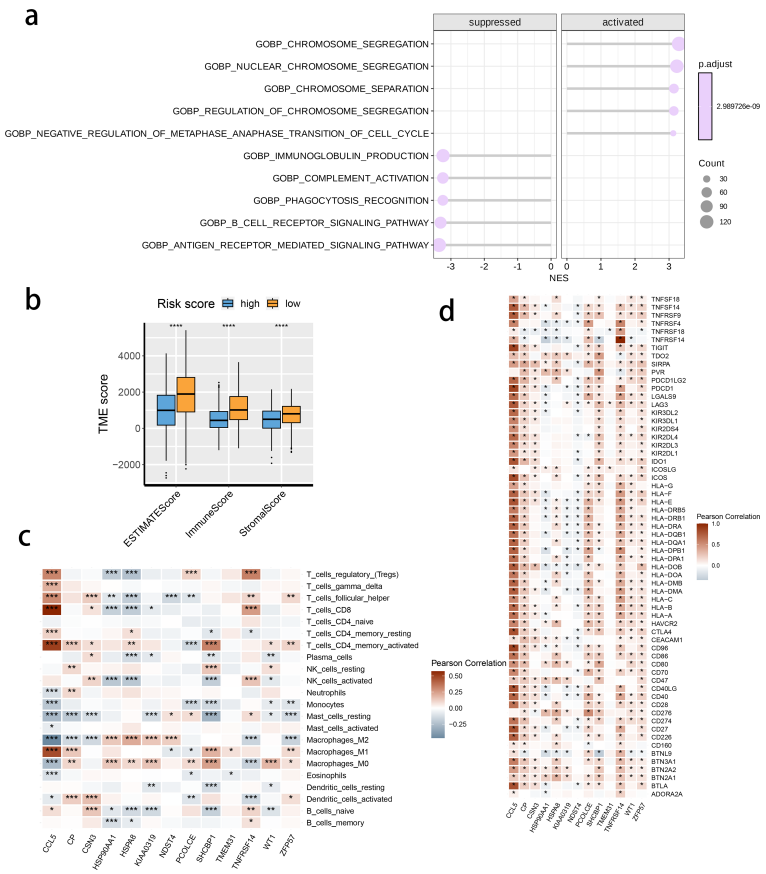

FIGURE 8
The correlation between the risk score and tumor microenvironment score. **(A)** The activated or suppressed hallmarks in the STING pathway-related genes (SRG) C2. **(B)** Differences in TME scores were determined by the ESTIMATE method between the two risk groups. **(C)** Correlations between the risk score and the abundance of immune cells. **(D)** Correlations between the risk score and the immune checkpoint genes.

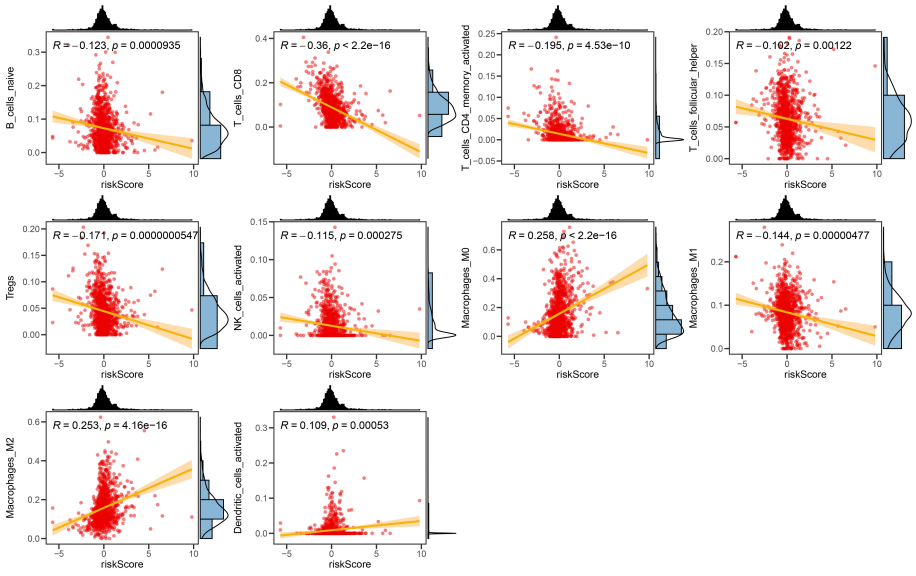

FIGURE 9
The correlation between the Risk score and immune cell sets. The scatter plots displaying the correlative relationship between the abundance of different infiltrated immune cells and risk score value.

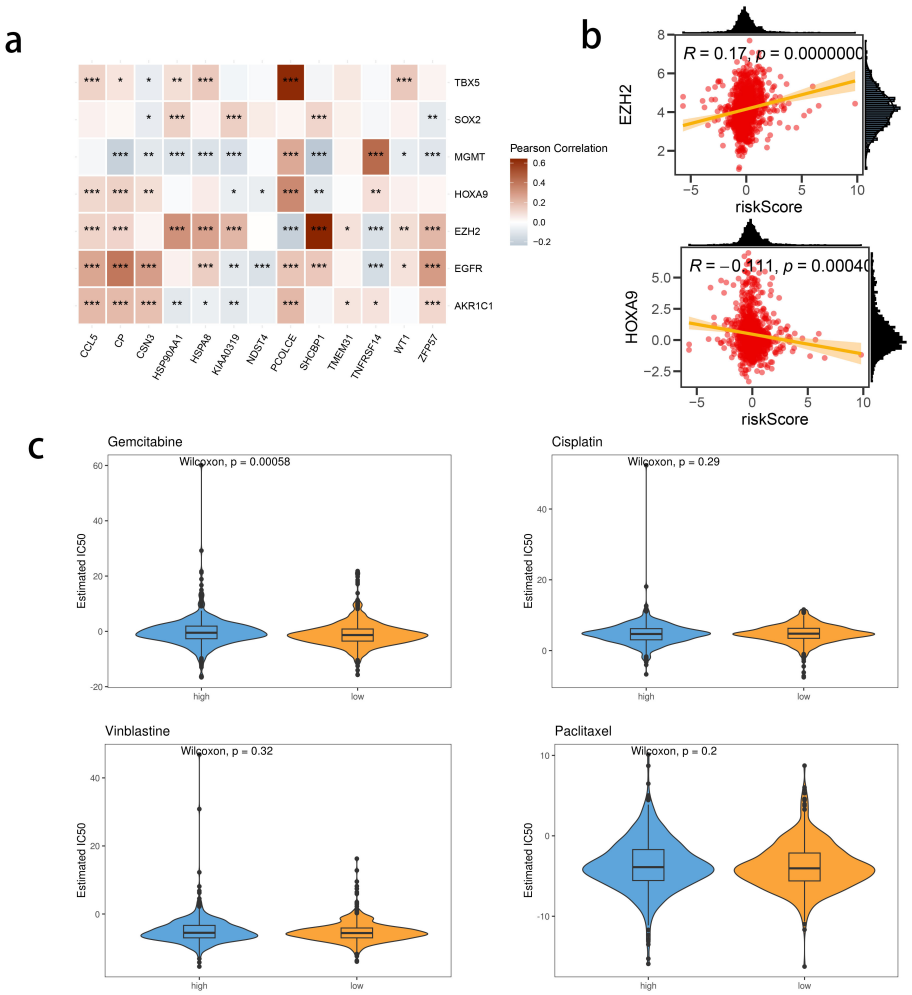

FIGURE 10
The correlation between risk score and chemotherapy sensitivity-related genes. **(A)** The correlations between prognostic model genes and chemotherapy sensitivity-related genes. **(B)** The correlations between the genes related to chemotherapy sensitivity and the Risk score. **(C)** Predicted IC50 between risk groups.

both immunosuppressive marker genes (Figure 8D). The infiltration of CD8, CD4, and B cells was distinctly decreased in the higher risk score, while M2 was positively correlated with the risk score (Figure 9). Among the hub genes, SHCBP1 had a high association with EZH2 expression, while PCOLCE was highly associated with TBX5 (Figure 10A), suggesting that these genes could act as potential novel biomarkers to assess the sensitivity to BRCA chemotherapy. Moreover, EZH2 exhibited a high correlation with risk value (Figure 10B). The high-risk group had a higher IC50 value for gemcitabine, suggesting a more favorable outcome in the low-risk group (Figure 10C).

3.6 A highly activated STING pathway-related signature in scRNA-seq datasets of breast cancer

The activity of the prognostic model was further investigated at the single-cell level, by analyzing three public single-cell RNA-seq datasets. We performed quality control, dimensionality reduction, and clustering analysis, and generated a total of 27 subclusters (Figures 11A, B), that were subsequently annotated into 12 main cell types (Figure 11C) in terms of the expression levels of marker genes as displayed in Figures 11D, E. The intratumor NK cells exhibited a highly activated STING pathway-related signature in the CD8 T cells, further supporting the clinical relevance of the prognostic model with BRCA TME (Figure 11F). -

3.7 A versatile role of TMEM31 in regulating BRCA proliferation and migration

In this study, we identified TMEM31 as the main risk factor in our prognosis model, hence we investigated the role of TMEM31 in regulating the proliferation and migration of BRCA cells. To examine the role of TMEM31 in mediating the migratory capability of DU4475 cells, we performed a wound healing assay, where we observed up-regulation of TMEM31 resulted in the enhanced migratory capability (Figure 12A). Additionally, up-regulation and down-regulation of TMEM31 prompted and

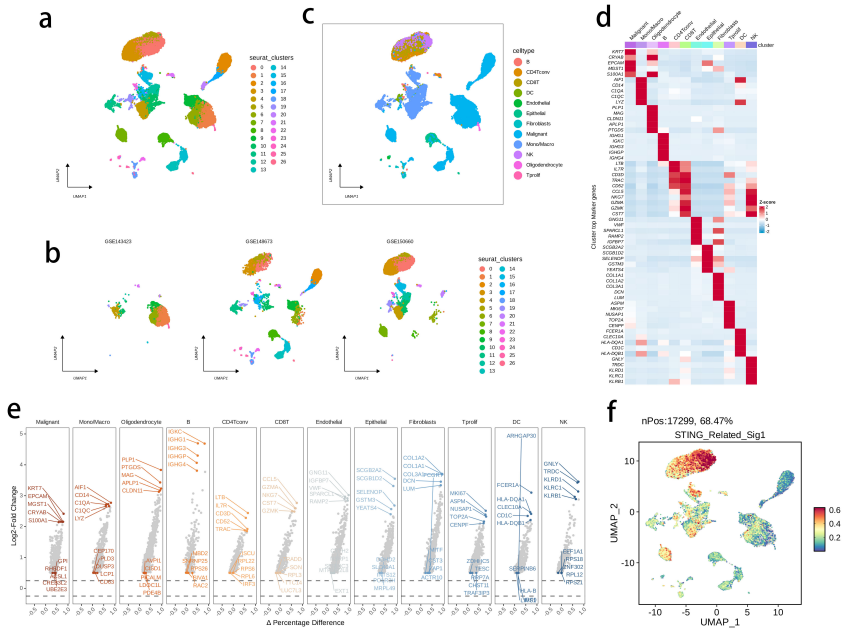

FIGURE 11
The highly activated STING pathway-related signature in single-cell RNA (scRNA)-seq datasets of BRCA. **(A, B)** UMAP visualization of cells from three public BRCA scRNA-seq cohorts. **(C)** 12 major cell types were annotated. **(D)** Heatmap showing the top five markers of each major cell set. **(E)** Volcano plots illustrating the downregulated and upregulated genes of each major cell set. **(D)** The expression of signature genes at single cell level was determined by the AddModuleScore() function in Seurat.

hampered the cell proliferation rate of DU4475, respectively (Figure 12B). Similarly, we conducted a wound healing assay and CCK8 analysis to explore the effects of up-regulation and down-regulation of TMEM31 on the migratory capability and proliferation rate of BT-549 cells, revealing similar results (Figures 12C, D). Furthermore, we further validated the role of TMEM31 in BRCA cells by conducting a colony formation assay. Both BT-549 and DU4475 cells were analyzed and showed that the loss or overexpression of TMEM31 affected their colony formation capability (Figures 13A, B). We further conducted the Transwell analysis to investigate the tridimensional migration regulated by TMEM31. In both the BT-549 and DU4475 cells, manipulating the levels of TMEM31 contributed to altered the transmembrane migration (Figure 13C). Additionally, we used the EDU assay to investigate the effects of TMEM31 on the proliferation (Figure 13D). We employed flow cytometry to evaluate whether the up-regulation and down-regulation of TMEM31 influenced the cell cycle progression of BT-549 and DU4475 cells (Figure 13E). We observed a higher proportion of G2/M cells in the BT-549 and DU4475 cells. Overall, our findings demonstrate the versatile role of TMEM31 in regulating the proliferation and migration of BRCA cells. These results provide valuable insights into the potential therapeutic targeting of TMEM31 in BRCA treatment.

4 Discussion

BRCA treatment strategies are evolving, with a focus on targeting STING activation triggered by DNA damage. One of the promising approaches for BRCA treatment involves targeting the nuclear receptor NR1D1 (REV-ERBα) to enhance antitumor immune responses. One study reported that deletion of Nr1d1 in mouse models resulted in increased tumor growth and metastasis, primarily driven by Nr1d1 loss in tumor cells. NR1D1 promotes cytosolic DNA fragment accumulation and activates cGAS-STING signaling, leading to increased production of type I interferons (IFNs) and immune chemokines (8). Ectonucleotide pyrophosphatase/phosphodiesterase 1 (ENPP1) drives BRCA growth and metastasis by suppressing the anti-tumoral immunity mediated by extracellular cGAMP-STING signaling. Inhibition of ENPP1 function slows tumor growth, prevents metastasis, and selectively blocks the cGAMP hydrolysis function of ENPP1, replicating the effects of complete ENPP1 knockout (9). JMJD8, an endoplasmic reticulum protein, inhibits the STING-mediated immune response in BRCA. JMJD8 competes with TBK1 for binding to STING, and prevents the formation of the STING-TBK1 complex, leading to reduced expression of type I IFN1 and IFN-stimulated genes. This immune evasion mechanism promotes breast tumorigenesis (10). Overexpression of DNA repair proteins in triple-negative BRCA can affect the efficacy of chemotherapy and sensitivity to DNA repair inhibitors (11). For example, IFI16 has shown promise in inducing a STING-mediated immune response in triple-negative breast cancer (BRCA). However, the cGAS-STING pathway induced by DNA repair activation is correlated with poor patient survival (12). These findings indicate a bidirectional role of the cGAS-STING pathway in BRCA, emphasizing the need to understand its regulation. One of the promising approaches for cancer therapy is the inhibition of DNA repair and promotion of DNA damage response (DDR) progression

10.3389/fimmu.2024.1438364

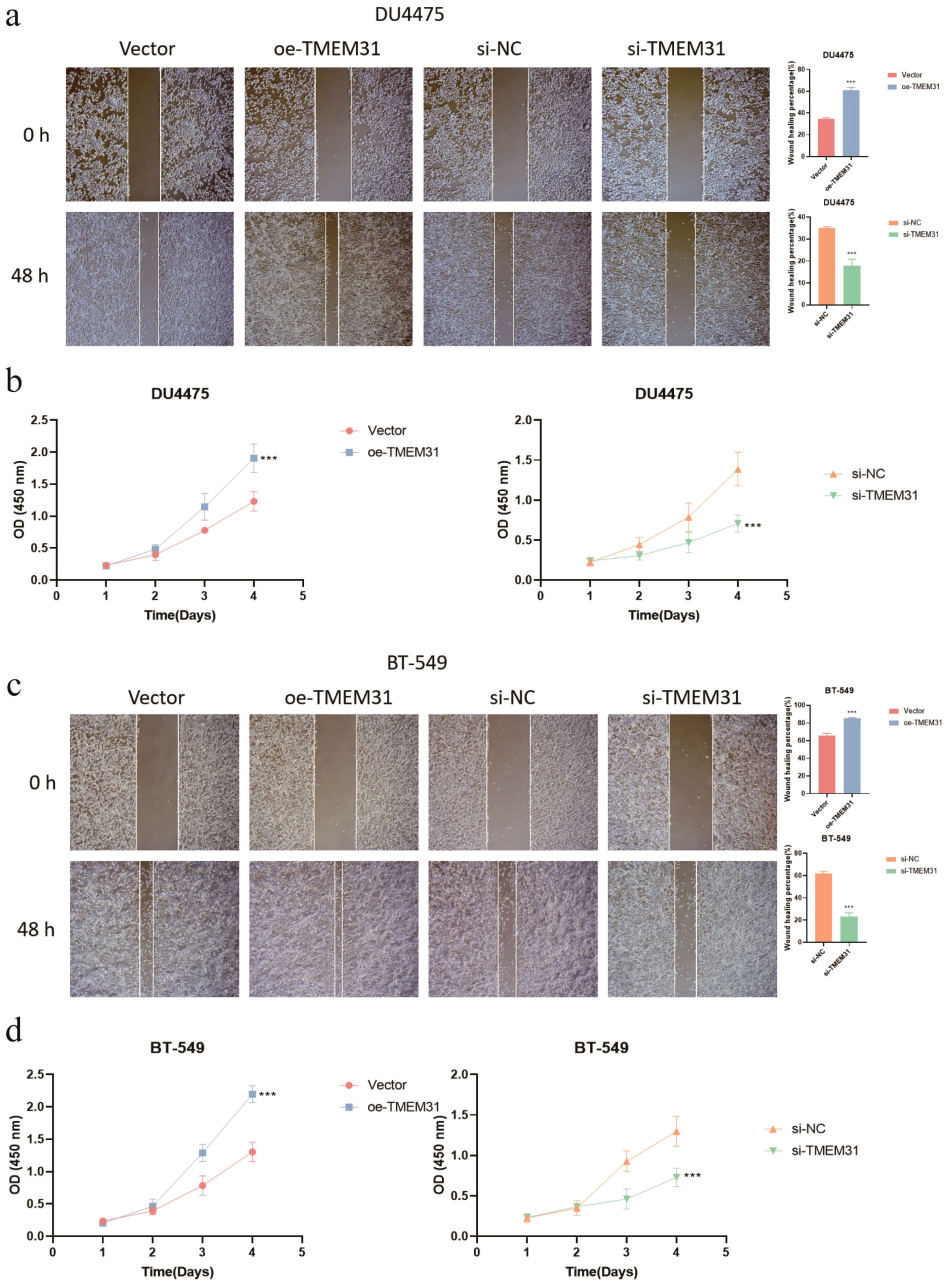

FIGURE 12
A versatile role of TMEM31 in regulating BRCA proliferation and migration. **(A)** The wound healing assay investigating whether the up-regulation and down-regulation of TMEM31 affected the migratory capability of the DU4475. **(B)** CCK8 analysis assessing the cell proliferation rate of DU4475 with up-regulation and down-regulation of TMEM31. **(C)** The wound healing assay investigating whether the up-regulation and down-regulation of TMEM31 affected the migratory capability of the BT-549. **(D)** The CCK8 analysis assessing whether the up-regulation and down-regulation of TMEM31 affected the proliferation rate of BT-549. (*p< 0.05, **p< 0.01, ***p< 0.001, ns, not significance.).

to activate the cGAS-STING pathway. PARP1 inhibitors and other DDR-targeting drugs have demonstrated efficacy in treating breast and ovarian cancers. Paclitaxel, a commonly used BRCA treatment, activates the cGAS-STING pathway through its effects on cell division. These findings highlight the potential of targeting the cGAS-STING pathway in BRCA cells.

In addition to its critical role in BRCA cancer cells, STING activation was also highly active in the TME. Elevated levels of tumor-infiltrating lymphocytes within the TME play a crucial role in treating BRCA (13). Differential analysis of tumor compartments in patients with triple-negative BRCA responsive to chemotherapy exhibit high levels of STING protein, indicating its presence in BRCA TME and its potential as a treatment target (14). Under the condition that the cGAS-STING pathway is activated within the BRCA TME, increased persistence of T helper/IL-17-producing CD8+ T -generated CAR-T cells is observed in the TME and enhanced tumor control (15). These reports support our observation that a highly active STING pathway-related signature was found in the CD8 T cells and intratumor NK

10.3389/fimmu.2024.1438364

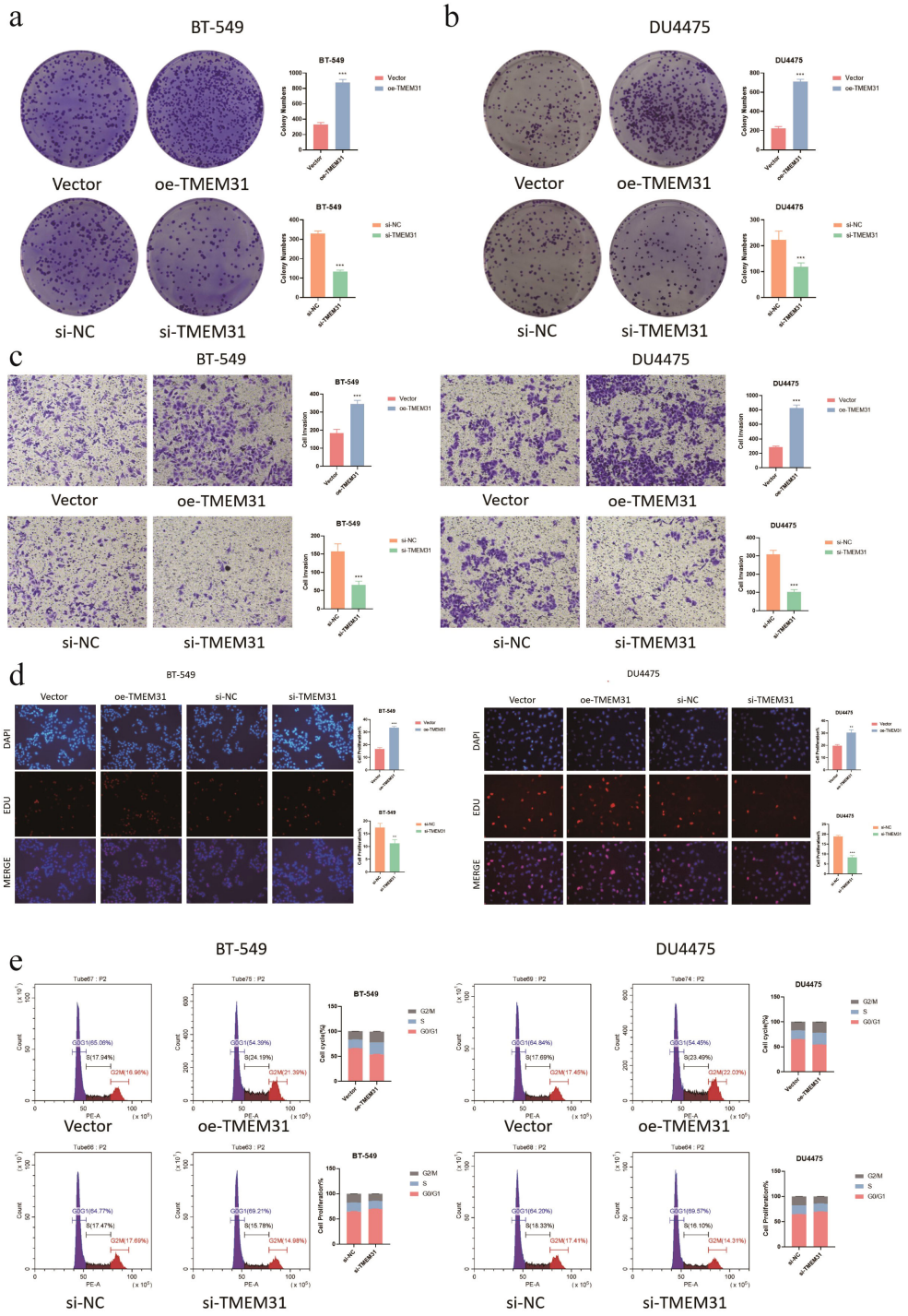

FIGURE 13
Further validation of TMEM31 in regulating BRCA proliferation and migration. **(A, B)** CFA analysis investigating whether the loss and overexpression of TMEM31 contributed to alteration in the colony formation capability of BT-549 (a) and DU4475 **(B)**. **(C)** Transwell analysis assessing the transmembrane migration of BT-549 and DU4475 with up-regulation and down-regulation of TMEM31, respectively. **(D, E)** The EDU assay investigating whether the up-regulation and down-regulation of TMEM31 affected the proliferation of the BT-549 and DU4475. **(D)** The flow cytometry assessing whether the up-regulation and down-regulation of TMEM31 affected the cell cycle progression of BT-549 and DU4475. (*p< 0.05, **p< 0.01, ***p< 0.001, ns, not significance.).

cells at single-cell resolution. The intra-tumoral DCs produce IFN-β upon induction by the STING protein, which initiates and recruits T cells into the TME. Consequently, STING agonists hold significant promise for reshaping the immunosuppressive TME by reversing its immunosuppressive nature and sensitizing BRCA to immunotherapy.

Rather than Tregs, M2 macrophages might have a predominant role in shaping immunosuppressive TME in BRCA, (16). CHI3L1,

secreted by M2 macrophages, promotes the metastasis of gastric and BRCA cells. CHI3L1 interacts with the interleukin-13 receptor α2 chain on the membrane of cancer cells, activating the mitogen-activated protein kinase signaling pathway. This leads to increased enhanced of matrix metalloproteinase genes, promoting tumor metastasis. CHI3L1 levels were also significantly higher in the serum of patients with gastric cancer and BRCA compared to healthy donors (17). The tumor-adipose microenvironment (TAME) is a novel microecosystem characterized by lipid metabolism dysfunction. The infiltration of M2-like macrophages in TAME is linked to poor survival in BRCA. Fatty acid transporters in TAME predict BRCA survival and are associated with macrophage function. Further, we identified lipid-associated macrophages (LAMs) in TAME expressing lipid metabolism genes and markers through scRNA sequencing and spatial transcriptomics. LAMs display an M2-like macrophage signature, lipid accumulation, and enhanced phagocytosis. Depleting LAMs in allograft cancer mouse models synergizes with anti-PD1 therapy. This defines a unique macrophage subtype in TAME with distinct clinical outcomes (18). Glycyrrhetinic acid (GA), a compound found in licorice, exhibits potential anti-cancer effects. In BRCA, GA inhibits the M2-like polarization of TAMs without affecting M1-like polarization. GA further reduces the expression of M2 markers and pro-angiogenic molecules in M2 macrophages, while promoting c-Jun N-terminal kinase 1/2 signaling. GA also suppresses tumor growth, angiogenesis, and lung metastasis in mice (19). Thus, these findings suggest that targeting M2 polarization could be an effective strategy in treating BRCA.

In our study, a higher IC50 value of gemcitabine in the high-risk group suggests a more favorable outcome in the low-risk group. Gemcitabine, a pyrimidine antimetabolite, has shown activity in metastatic BRCA singly as well as in combination regimens (20). Phase II trials have demonstrated the activity of gemcitabine in pretreated and unpretreated patients. In a Phase III trial, gemcitabine was inferior to epirubicin in elderly patients (21); however, when combined with taxanes like paclitaxel or docetaxel, gemcitabine showed high activity, improving response rate, the time to disease progression, quality of life, and survival (22). Currently, in a phase II trial, trilaciclib administered before gemcitabine plus carboplatin (GCb) improved overall survival in patients with metastatic TNBC. The ongoing phase III PRESERVE 2 trial is evaluating the efficacy and safety of trilaciclib when administered before GCb in patients with locally advanced unresectable or metastatic TNBC (23). This approach will potentially offer a new treatment strategy for patients with TNBC and potentially improve outcomes. In the case of advanced BRCA, gemcitabine monotherapy has not been reported to significantly improve patient survival. Singh et al. developed a combination regimen of gemcitabine with imiquimod and delivered using hyaluronic acid-based nanoparticles, to stimulate immune cells for anticancer activity. The combination showed enhanced anticancer effects *in vitro* as well as in a mouse model of BRCA. The findings suggest that imiquimod can enhance the efficacy of gemcitabine through the activation of immune cells to suppress tumors (24).

5 Conclusion

We developed and validated a STING pathway-related prognostic model that accurately predicts BRCA patient outcomes. These findings have important implications for the personalized treatment and management of BRCA patients.

Data availability statement

The datasets presented in this study can be found in online repositories. The names of the repository/repositories and accession number(s) can be found in the article/supplementary material.

Author contributions

YZ: Writing – original draft, Data curation. HC: Writing – review & editing, Funding acquisition. WL: Data curation, Writing – original draft. JD: Software, Writing – original draft. DL: Software, Writing – original draft. JJD: Formal Analysis, Writing – original draft.

Funding

The author(s) declare financial support was received for the research, authorship, and/or publication of this article. Clinical Research Center for Breast and Thyroid Disease Prevention and Control in Hunan Province, Grant/Award Number: 2018sk4001.

Conflict of interest

The authors declare that the research was conducted in the absence of any commercial or financial relationships that could be construed as a potential conflict of interest.

Publisher's note

All claims expressed in this article are solely those of the authors and do not necessarily represent those of their affiliated organizations, or those of the publisher, the editors and the reviewers. Any product that may be evaluated in this article, or claim that may be made by its manufacturer, is not guaranteed or endorsed by the publisher.

References

1. Sung H, Ferlay J, Siegel RL, Laversanne M, Soerjomataram I, Jemal A, et al. Global cancer statistics 2020: GLOBOCAN estimates of incidence and mortality worldwide for 36 cancers in 185 countries. *CA: Cancer J Clin*. (2021) 71:209–49. doi: 10.3322/caac.21660

2. Zangouei AS, Alimardani M, Moghbeli M. MicroRNAs as the critical regulators of Doxorubicin resistance in breast tumor cells. *Cancer Cell Int*. (2021) 21:213. doi: 10.1186/s12935-021-01873-4

3. Ishay-Ronen D, Diepenbruck M, Kalathur RKR, Sugiyama N, Tiede S, Ivanek R, et al. Gain fat-lose metastasis: Converting invasive breast cancer cells into adipocytes inhibits cancer metastasis. *Cancer Cell*. (2019) 35:17–32.e6. doi: 10.1016/j.ccell.2018.12.002

4. Jiang Y, Zhang J. Role of STING protein in breast cancer: mechanisms and therapeutic implications. *Med Oncol (Northwood London England)*. (2022) 40:30. doi: 10.1007/s12032-022-01908-4

5. Zhu C, Ma Q, Gong L, Di S, Gong J, Wang Y, et al. Manganese-based multifunctional nanoplatform for dual-modal imaging and synergistic therapy of breast cancer. *Acta biomaterialia*. (2022) 141:429–39. doi: 10.1016/j.actbio.2022.01.019

6. Qiu X, Qu Y, Guo B, Zheng H, Meng F, Zhong Z. Micellar paclitaxel boosts ICD and chemo-immunotherapy of metastatic triple negative breast cancer. *J Controlled release: Off J Controlled Release Society*. (2022) 341:498–510. doi: 10.1016/j.jconrel.2021.12.002

7. Chen H, Yang W, Li Y, Ma L, Ji Z. Leveraging a disulfidptosis-based signature to improve the survival and drug sensitivity of bladder cancer patients. *Front Immunol*. (2023) 14:1198878. doi: 10.3389/fimmu.2023.1198878

8. Ka NL, Park MK, Kim SS, Jeon Y, Hwang S, Kim SM, et al. NR1D1 stimulates antitumor immune responses in breast cancer by activating cGAS-STING signaling. *Cancer Res*. (2023) 83:3045–58. doi: 10.1158/0008-5472.CAN-23-0329

9. Wang S, Böhnert V, Joseph AJ, Sudaryo V, Skariah G, Swinderman JT, et al. ENPP1 is an innate immune checkpoint of the anticancer cGAMP-STING pathway in breast cancer. *Proc Natl Acad Sci United States America*. (2023) 120:e2313693120. doi: 10.1073/pnas.2313693120

10. Yi J, Wang L, Du J, Wang M, Shen H, Liu Z, et al. ER-localized JmjC domain-containing protein JMJD8 targets STING to promote immune evasion and tumor growth in breast cancer. *Dev Cell*. (2023) 58:760–78.e6. doi: 10.1016/j.devcel.2023.03.015

11. Lee KJ, Mann E, Wright G, Piett CG, Nagel ZD, Gassman NR. Exploiting DNA repair defects in triple negative breast cancer to improve cell killing. *Ther Adv Med Oncol*. (2020) 12:1758835920958354. doi: 10.1177/1758835920958354

12. Vasiyani H, Mane M, Rana K, Shinde A, Roy M, Singh J, et al. DNA damage induces STING mediated IL-6-STAT3 survival pathway in triple-negative breast cancer cells and decreased survival of breast cancer patients. *Apoptosis: an Int J programmed Cell Death*. (2022) 27:961–78. doi: 10.1007/s10495-022-01763-8

13. Ahn S, Chung YR, Seo AN, Kim M, Woo JW, Park SY. Changes and prognostic values of tumor-infiltrating lymphocyte subsets after primary systemic therapy in breast cancer. *PLoS One*. (2020) 15:e0233037. doi: 10.1371/journal.pone.0233037

14. Kulasinghe A, Monkman J, Shah ET, Matigian N, Adams MN, O'Byrne K. Spatial profiling identifies prognostic features of response to adjuvant therapy in triple negative breast cancer (TNBC). *Front Oncol*. (2021) 11:798296. doi: 10.3389/fonc.2021.798296

15. Xu N, Palmer DC, Robeson AC, Shou P, Bommiasamy H, Laurie SJ, et al. STING agonist promotes CAR T cell trafficking and persistence in breast cancer. *J Exp Med*. (2021) 218. doi: 10.1084/jem.20200844

16. Coexpressed Genes That Promote the Infiltration of M2 Macrophages in Melanoma Can Evaluate the Prognosis an Immunotherapy Outcome. *Journal of Immunology Research*. (2021). doi: 110.1155/2021/6664791

17. Chen Y, Zhang S, Wang Q, Zhang X. Tumor-recruited M2 macrophages promote gastric and breast cancer metastasis via M2 macrophage-secreted CHI3L1 protein. *J Hematol Oncol*. (2017) 10:36. doi: 10.1186/s13045-017-0408-0

18. Liu Z, Gao Z, Li B, Li J, Ou Y, Yu X, et al. Lipid-associated macrophages in the tumor-adipose microenvironment facilitate breast cancer progression. *Oncoimmunology*. (2022) 11:2085432. doi: 10.1080/2162402X.2022.2085432

19. Cheng Y, Zhong X, Nie X, Gu H, Wu X, Li R, et al. Glycyrrhetinic acid suppresses breast cancer metastasis by inhibiting M2-like macrophage polarization via activating JNK1/2 signaling. *Phytomedicine: Int J phytotherapy phytopharmacology*. (2023) 114:154757. doi: 10.1016/j.phymed.2023.154757

20. Hortobagyi GN. Gemcitabine in combination with vinorelbine for treatment of advanced breast cancer. *Clin Breast cancer*. (2002) 3 Suppl 1:34–8.

21. Conte P, Salvadori B, Donati S, Landucci E, Gennari A. Gemcitabine, epirubicin, and paclitaxel combinations in advanced breast cancer. *Semin Oncol*. (2001) 28:15–7. doi: 10.1016/S0093-7754(01)90273-8

22. Yardley DA. Gemcitabine plus paclitaxel in breast cancer. *Semin Oncol*. (2005) 32:S14–21. doi: 10.1053/j.seminoncol.2005.06.025

23. Goel S, Tan AR, Rugo HS, Aftimos P, Andrić Z, Beelen A, et al. Trilaciclib prior to gemcitabine plus carboplatin for metastatic triple-negative breast cancer: phase III PRESERVE 2. *Future Oncol (London England)*. (2022) 18:3701–11. doi: 10.2217/fon-2022-0773

24. Singh B, Maharjan S, Pan DC, Zhao Z, Gao Y, Zhang YS, et al. Imiquimod-gemcitabine nanoparticles harness immune cells to suppress breast cancer. *Biomaterials*. (2022) 280:121302. doi: 10.1016/j.biomaterials.2021.121302

frontiers | Frontiers in Immunology

TYPE Original Research
PUBLISHED 19 August 2024
DOI 10.3389/fimmu.2024.1434450

Check for updates

OPEN ACCESS

EDITED BY
Wantao Wu,
Central South University, China

REVIEWED BY
Jing Zhang,
University of South Dakota, United States
Luo Qiang,
Children's Hospital of Chongqing Medical University, China

*CORRESPONDENCE
Yining Zhang
zhangyn@zjcc.org.cn
Leilei Liang
liangleilei10006@163.com
Huarong Tang
tanghr@zjcc.org.cn

†These authors have contributed equally to this work and share first authorship

RECEIVED 17 May 2024
ACCEPTED 24 July 2024
PUBLISHED 19 August 2024

CITATION
Zhao F, Hong J, Zhou G, Huang T, Lin Z, Zhang Y, Liang L and Tang H (2024) Elucidating the role of tumor-associated ALOX5+ mast cells with transformative function in cervical cancer progression via single-cell RNA sequencing.
Front. Immunol. 15:1434450.
doi: 10.3389/fimmu.2024.1434450

COPYRIGHT
© 2024 Zhao, Hong, Zhou, Huang, Lin, Zhang, Liang and Tang. This is an open-access article distributed under the terms of the Creative Commons Attribution License (CC BY). The use, distribution or reproduction in other forums is permitted, provided the original author(s) and the copyright owner(s) are credited and that the original publication in this journal is cited, in accordance with accepted academic practice. No use, distribution or reproduction is permitted which does not comply with these terms.

Elucidating the role of tumor-associated ALOX5+ mast cells with transformative function in cervical cancer progression via single-cell RNA sequencing

Fu Zhao[1,2†], Junjie Hong[3†], Guangyao Zhou[4†], Tianjiao Huang[5], Zhiheng Lin[2], Yining Zhang[6*], Leilei Liang[1*] and Huarong Tang[1*]

[1]Department of Gynecological Radiotherapy, Zhejiang Cancer Hospital, Hangzhou, China, [2]Shandong University of Traditional Chinese Medicine, Jinan, China, [3]Department of Gynecological Oncology, Zhejiang Cancer Hospital, Hangzhou, China, [4]Department of Lung Cancer, Tianjin Lung Cancer Center, National Clinical Research Center for Cancer, Key Laboratory of Cancer Prevention and Therapy, Tianjin's Clinical Research Center for Cancer, Tianjin Medical University Cancer Institute and Hospital, Tianjin, China, [5]The First School of Clinical Medicine, Heilongjiang University of Traditional Chinese Medicine, Harbin, China, [6]Department of Clinical Laboratory, Zhejiang Cancer Hospital, Hangzhou, China

Background: Cervical cancer (CC) is the fourth most common malignancy among women globally and serves as the main cause of cancer-related deaths among women in developing countries. The early symptoms of CC are often not apparent, with diagnoses typically made at advanced stages, which lead to poor clinical prognoses. In recent years, numerous studies have shown that there is a close relationship between mast cells (MCs) and tumor development. However, research on the role MCs played in CC is still very limited at that time. Thus, the study conducted a single-cell multi-omics analysis on human CC cells, aiming to explore the mechanisms by which MCs interact with the tumor microenvironment in CC. The goal was to provide a scientific basis for the prevention, diagnosis, and treatment of CC, with the hope of improving patients' prognoses and quality of life.

Method: The present study acquired single-cell RNA sequencing data from ten CC tumor samples in the ArrayExpress database. Slingshot and AUCcell were utilized to infer and assess the differentiation trajectory and cell plasticity of MCs subpopulations. Differential expression analysis of MCs subpopulations in CC was performed, employing Gene Ontology, gene set enrichment analysis, and gene set variation analysis. CellChat software package was applied to predict cell communication between MCs subpopulations and CC cells. Cellular functional experiments validated the functionality of TNFRSF12A in HeLa and Caski cell lines. Additionally, a risk scoring model was constructed to evaluate the differences in clinical features, prognosis, immune infiltration, immune checkpoint, and functional enrichment across various risk scores. Copy number variation levels were computed using inference of copy number variations.

Result: The obtained 93,524 high-quality cells were classified into ten cell types, including T_NK cells, endothelial cells, fibroblasts, smooth muscle cells, epithelial cells, B cells, plasma cells, MCs, neutrophils, and myeloid cells. Furthermore, a total of 1,392 MCs were subdivided into seven subpopulations: C0 CTSG+ MCs, C1 CALR+ MCs, C2 ALOX5+ MCs, C3 ANXA2+ MCs, C4 MGP+ MCs, C5 IL32+

MCs, and C6 ADGRL4+ MCs. Notably, the C2 subpopulation showed close associations with tumor-related MCs, with Slingshot results indicating that C2 subpopulation resided at the intermediate-to-late stage of differentiation, potentially representing a crucial transition point in the benign-to-malignant transformation of CC. CNVscore and bulk analysis results further confirmed the transforming state of the C2 subpopulation. CellChat analysis revealed TNFRSF12A as a key receptor involved in the actions of C2 ALOX5+ MCs. Moreover, *in vitro* experiments indicated that downregulating the TNFRSF12A gene may partially inhibit the development of CC. Additionally, a prognosis model and immune infiltration analysis based on the marker genes of the C2 subpopulation provided valuable guidance for patient prognosis and clinical intervention strategies.

Conclusions: We first identified the transformative tumor-associated MCs subpopulation C2 ALOX5+ MCs within CC, which was at a critical stage of tumor differentiation and impacted the progression of CC. *In vitro* experiments confirmed the inhibitory effect of knocking down the TNFRSF12A gene on the development of CC. The prognostic model constructed based on the C2 ALOX5 +MCs subset demonstrated excellent predictive value. These findings offer a fresh perspective for clinical decision-making in CC.

KEYWORDS

single-cell RNA-sequencing, cervical cancer, tumor heterogeneity, prognosis, cancer immunotherapy

Introduction

Cervical cancer (CC) is among the most common malignancies, with the global statistics report for 2020 showing approximately 600,000 new cases of CC annually, leading to over 340,000 deaths. These figures place CC fourth in the incidence and mortality spectrum for women globally. More than 85% of these instances happen in countries with low and middle incomes, where the mortality rate is six times higher than in developed countries (1). The incidence and mortality rates of CC have declined in recent years because of enhanced early screening and wider administration of the HPV vaccine. However, there has been a rise in the incidence of CC among young women, indicating that it continues to be a significant public health concern (2). Furthermore, due to the atypical early symptoms of CC, most patients are diagnosed in advanced stages, posing significant challenges to treatment.

The primary method of treating locally advanced CC according to the 2024 NCCN recommendations is concurrent chemoradiotherapy (CCRT). Nevertheless, recurrence or metastasis affects about 50% of individuals following therapy (3). Research has indicated that the likelihood of cancer returning in patients with locally advanced CC stages IB-IIB after CCRT is between 10% and 20%, however it increases to 50% to 70% for stages IIB-IVA (4). In addition, the use of carboplatin and paclitaxel as adjuvant chemotherapy after radiation does not result in a substantial increase in overall survival (OS) or progression-free survival (5).

The progress in cancer treatment has been significant due to advancements in tumor immunology, immunotherapy, and molecular targeted therapies. Immune checkpoint blockade (ICB) therapy has been used to treat several solid cancers, such as lung cancer and melanoma, by targeting important molecules such CTLA-4, PD-L1, and PD-1. In addition, ICB therapy shows promising potential in cases of recurrent or metastatic CC. Studies suggest that ICB monotherapy increases OS by 3.5 months compared to chemotherapy alone. Furthermore, when ICB is combined with chemotherapy, with or without anti-angiogenic treatment, it can extend OS by almost one year (6). In addition, molecular targeted therapeutics are being investigated in the context of CC. *In vitro* studies have confirmed that pathways such as VEGF, EGFR/HER2, and PI3K/AKT/mTOR are strongly linked to a negative prognosis in CC patients (7). However, apart from Bevacizumab, the outcomes of phase II trials for other targeted therapies have not been encouraging, failing to progress to phase III trials (8). Moreover, immunotherapy and molecular targeted therapies struggle to sustain long-term efficacy in clinical settings due to tumor heterogeneity and the onset of primary or acquired drug resistance. Indeed, data indicate that more than 50% of patients initially responsive to ICB therapy exhibit disease progression within two years (9). Consequently, despite advances in immunotherapy, the treatment and survival outcomes for CC patients

continue to be worrisome, highlighting the need for new immunotherapeutic strategies.

Mast cells (MCs), widely distribute across all tissues, are known to secrete a plethora of vasoactive mediators and pro-inflammatory factors (10). MCs, which are a component of the innate immune system, play an important part in the manifestation of chronic inflammatory disorders that are linked to cancer. Furthermore, they are an essential component of the inflammatory milieu that controls the genesis and progression of tumors. Studies investigating the function of MCs in cancer have shown varied results: commonly, MCs appear to facilitate tumor cell growth, often enhancing the progression of cancers, including thyroid, gastric, and lung cancers. Nevertheless, in cases such as breast cancer, MCs have the ability to stimulate the attraction of immune cells, which might potentially have an anti-tumor effect (11). Furthermore, MCs may play a non-contributory role in tumors such as renal cell carcinoma, potentially acting as mere inert bystanders (12). Similarly, early studies investigating the association between MCs and CC have yielded contradictory results. Graham et al. observed a decrease in MC count with tumor progression (13) whereas another study found no significant difference in the number of MCs between grades I-III of cervical intraepithelial neoplasia, but a notable increase in MCs numbers in infiltrating CC suggested that MCs played a role in promoting the progression and dissemination of tumor around and within the cervix (14). Consequently, it is imperative to investigate the interactive mechanisms between CC and MCs.

In recent years, single-cell sequencing technology has come to be as a burgeoning technique, enabling multifaceted analysis at the single-cell resolution of the genome, proteome, epigenome, and spatial transcriptome (15–18). By elucidating the features, developmental trajectories, and underlying mechanisms of distinct cellular subgroups, it has furnished novel insights into the realm of tumor biology, facilitating the refinement of therapeutic strategies and propelling the progress of personalized medicine. The composition of CC tissue represents a complex ecosystem comprising diverse cellular subgroups, including immune cells, EPCs, and MCs (19). The tumor microenvironment (TME) and tumor heterogeneity have significant impacts on the onset (20), advancement and prognosis of CC. However, the full extent of MCs heterogeneity within the TME of CC remains incompletely elucidated (21). We thus seek to investigate the cellular heterogeneity within the tumor and expose its complex cellular states by using single-cell RNA sequencing (scRNA-seq) analysis on a CC dataset derived from the ArrayExpress database. It is our aspiration to offer fresh perspectives on the diagnosis, management, and prognosis of CC to improve patient outcomes and raise survival rates.

Method

Acquisition of single-cell data

The single-cell data for CC was acquired from the ArrayExpress database (https://www.ebi.ac.uk/arrayexpress/), under the dataset accession number E-MTAB-12305 (22). Bulk RNA sequencing data for CC was acquired from of the University of California Santa Cruz (UCSC, https://xena.ucsc.edu/) Xena. As we utilized publicly available database information in our study, ethical approval was not required.

Filtering and processing of the raw data

To analyze scRNA-seq data, we utilized R software (4.2.0) along with the "Seurat" software package (4.3.0) (23). To enhance the accuracy and reliability of the scRNA-seq data, we utilized the "DoubletFinder" software package (version 2.0.3) (24) for quality control, detection, and filtration of probable low-quality and aberrant cells (25, 26). The nFeature parameter must have a value within the range of 300 to 6000, whereas the nCount parameter must have a value within the range of 500 to 100,000. The proportion of genes related to red blood cells in the cell was less than 5% of the total number of genes. Furthermore, cells with mitochondrial gene expression exceeding 25% of the overall expression were excluded.

In order to analyze the filtered samples, we utilized the Seurat package's "NormalizeData" and "FindVariableFeatures" functions to normalize the data and identify the top 2000 genes with high variability (27–29). Afterwards, we utilized the "ScaleData" function to normalize the analyzed data and then addressed batch discrepancies among datasets by employing principal component analysis with the harmony R package (version 0.1.1) (30–32). Ultimately, we conducted dimensionality reduction and clustering using the most important 30 principal components.

The analysis of copy number variation (CNV) in scRNA-seq data was conducted using the inferCNV R package (version 1.6.0) obtained from the GitHub repository of the Broad Institute (https://github.com/broadinstitute/inferCNV). This software package enables the distinction between cancerous and healthy cells by analyzing the chromosomal locations and gene expression levels to determine copy number variations. Cells with high CNV scores were defined as Tumor-EPCs.

The identification of differentially expressed genes (DEGs) and cell types

We utilized the "FindClusters" and "FindNeighbors" functions in Seurat to carry out cell clustering (33). We used the Seurat function "FindAllMarkers" to detect DEGs in each cluster. Most of the identified marker genes for cell clusters were obtained from the CellMarker (http://xteam.xbio.top/CellMarker/), in addition to some citations from past research. Cell annotation was conducted through manual curation. Afterward, we utilized the UMAP technique to visualize the data.

Slingshot pseudotemporal analysis

Version 2.6.0 of the Slingshot software program was used to infer the cell lineage during the differentiation of the MCs subpopulations (34). The function "getLineages" was utilized to calculate the levels of cellular expression for every lineage.

Cellular stemness analysis

In order to assess the scores of gene sets in single-cell transcriptomic data, we employed the AUCell method. We utilized the AUCell package and employed the "AUCell_buildRankings" function to rank the stemness gene set based on the magnitude of scores.

Functional enrichment analysis

We conducted a functional analysis using the ClusterProfiler R software package based on Gene Ontology (GO) analysis and Kyoto Encyclopedia of Genes and Genomes (KEGG) (35–38). In order to perform gene set enrichment analysis (GSEA), we took into account the collective gene expression patterns within the gene sets. For this research, we employed the Molecular Signatures Database (MSigDB, https://www.gsea-msigdb.org/gsea/msigdb) to identify pathways that showed a significant enrichment (39–41).

Cell communication

The CellChat R package (version 1.6.1) (42) was utilized for quantitatively inferring and analyzing cellular interactions from scRNA-seq data. The "netVisual_diffInteraction" function was used to analyze variations in the strength of intercellular communication, while the "identifyCommunicationPatterns" function was utilized to determine the quantity of communication patterns. Scatter plots, heatmaps, and various visualization techniques were utilized to analyze the signals coming in and out of every cell visually (43).

The CellChat database (http://www.cellchat.org/) was subsequently utilized to identify signaling pathways and receptor pairings associated with specific types of MCs that are relevant to cancer. The "netVisual_bubble" function was employed to assess the probability of communication between ligand-receptor pairings regulated by distinct cell clusters and those originating from dissimilar cell clusters.

Development and validation of the prognostic prediction model

First, we filtered the most important prognostic genes using univariable Cox analysis and least absolute shrinkage and selection operator (LASSO) regression analysis (44–46). We next computed the hazard coefficients for every prognostic gene by multivariable Cox regression analysis (47–50). This enabled us to establish a risk scoring model (Risk score = $\sum_i^n Xi \times Yi$, where X represents the coefficient and Y represents the gene expression level) (51–53). On the basis of the optimal cutoff values that were determined by the "surv_cutpoint" function, we organized the data into groups. We analyzed the predictive results for various groups of patients by performing survival analysis on the risk scoring model we developed with the R package 'Survival' (version 3.3.1) and displaying the survival curves with the "ggsurvplot" function (54, 55). By plotting receiver operating characteristic (ROC) curves with the "timeROC" package (version 0.4.0), we evaluated the predictive model's accuracy (37, 56–59).

In addition, we performed a multivariable Cox regression analysis to validate the independent predictive value of the risk score. Furthermore, we created a nomogram to predict the OS at 1, 3, and 5 years. The accuracy of the nomogram's predictions was verified by the utilization of the C-index and calibration curves.

Immune microenvironment analysis

We utilized the CIBERSORT R package (version 0.1.0) to calculate immune-related scores for 22 immune cell types (60–62). Afterward, we utilized three different tools "CIBERSORT", "ESTIMATE", and "Xcell" to thoroughly assess the immune surroundings of the patients (63, 64). Additionally, we analyzed variations in levels of immune cell infiltration and the expression of genes related to immune checkpoints. We next ran correlation studies between OS, risk scores, immune cells, and model genes (65). We also evaluated the response to tumor immune therapy using Tumor Immune Dysfunction and Exclusion (TIDE, http://tide.dfci.harvard.edu) program.

Cell lines and cell culture

The HeLa and Caski cell lines were obtained from the Cell Resource Center at the Shanghai Institute for Biological Sciences, which is part of the Chinese Academy of Sciences. The cells were cultured individually in RPMI 1640 media supplemented with 10% fetal bovine serum (FBS) (Gibco BRL, USA), and 1% penicillin-streptomycin. The cell lines were cultivated under conventional conditions, with a temperature of 37°C and a 5% CO_2 atmosphere.

siRNA knockdown

RNA constructs (GenePharma, Suzhou, China) helped to knockdown TNFRSF12A. On a 6-well plate set at a 50% density, the cells were planted. They then underwent knockdown (si-TNFRSF12A-1 and si-TNFRSF12A-2) and negative control (si-NC) transfecting. Lipofectamine 3000RNAiMAX (Invitrogen, USA) was used for transfection under manufacturer directions. Every si-RNA (RIbbio, China) was transfected into cells. Supplementary Table S1 shows the siRNA sequence from 5' to 3'.

Cell viability assay

Transfected cell viability was assessed with the Cell Counting Kit-8 (CCK-8, A311-01, Vazyme) (66). The suspension of cells was placed in a 96-well dish with 5×10^3 cells in each well and left to incubate for 24 hours. Afterward, 10 microliters of CCK-8 labeling reagent were added to every well, followed by incubation of the plate at 37 degrees Celsius in a light-shielded setting for a duration of 2 hours. Cell viability was evaluated by measuring the absorbance at

450 nm over a period of four days. Mean optical density values were determined and graphically represented using a line graph.

Quantitative polymerase chain reaction (qPCR)

RNA extraction was performed using the Trizol reagent, and reverse transcription was carried out using the PrimeScript™ Kit. The qPCR reaction was conducted using SYBR Green premix (67). The primer sequences used were listed in Supplementary Table S1.

Wound-healing assay

The cells that had been successfully transfected with stable genetic material were placed in a 6-well plate and grown in a controlled environment within a cell culture incubator until they reached full coverage of the plate. With a sterile 200 μL plastic pipette tip, the cells in each culture well were delicately scraped and then rinsed with PBS to eliminate any cell debris. Afterwards, the cells were placed in a culture medium without serum and incubated. Photographs of the scratch injuries were taken at 0 hours and 48 hours, and the width of the scratches was quantified using the Image-J software. The wound healing percentage was determined by applying the formula: (the scratch area in 0-48 hours × 100)/the area in 0 hours.

Transwell assays

The cell migration capacity was evaluated using a Transwell test. The top compartment of a 24-well plate was covered with a matrix gel solution (BD Biosciences, USA), and the cell mixture was placed in the top compartment, while a culture medium containing 10% FBS was added to the bottom compartment. The plates were subsequently placed in a cell culture incubator and kept there for a duration of 48 hours. Following the removal of cells from the upper chamber, the surviving cells on the lower surface were treated with 4% paraformaldehyde for fixation and then stained with 0.1% crystal violet (Solarbio, China). The cells in five randomly selected fields of vision were quantified using an optical microscope.

5-Ethynyl-2′-deoxyuridine proliferation experiments

The HeLa and Caski cell lines that were transfected were placed into a 6-well cell culture plate with 5×10^3 cells in each well. Following a 24-hour incubation period at ambient temperature, the EdU working solution was introduced into the cell culture medium and left to incubate for 2 hours. Afterwards, the cells were rinsed twice with PBS and then treated with a 4% paraformaldehyde solution for 15 minutes to immobilize them. Next, the cells were subjected to treatment with glycine at a concentration of 2 mg/ml and 0.5% Triton X-100 for a duration of 15 minutes. Ultimately, the cells were subjected to a treatment involving the addition of 1 ml of 1X Apollo and 1 ml of 1X Hoechst staining reaction solution, which lasted for a duration of 30 minutes. Cell proliferation was assessed by capturing images using a fluorescence microscope.

Statistical analysis

We performed statistical analysis using the R software (version 4.2.0). The statistical significance of the data was determined by calculating the p-values. The levels of significance were marked with asterisks: $^*P < 0.05$, $^{**}P < 0.01$, $^{***}P < 0.001$, and $^{****}P < 0.0001$. "ns" was used to say that there was no significant difference.

Result

Single-cell analysis of the primary cell types in CC

We performed scRNA-seq analysis on 10 CC samples to explore the heterogeneity of cell types. Following quality assurance, a combined 93,524 cells were collected from 2 High Squamous Intraepithelial Lesion (H) specimens, 1 Metastatic Lymph Node (L) specimen, 4 Cervical Tumors (T) specimens, and 3 Normal Cervix (N) specimens. After batch effect removal, UMAP dimensionality reduction clustering was applied to high-quality cells to visualize distinct groupings (H: High Squamous Intraepithelial Lesion, L: Metastatic Lymph Node, T: Cervical Tumors, N: Normal Cervix) (Figure 1A). Using known marker genes for typical cell types, we annotated the 93,524 high-quality cells, resulting in 10 cell types: T_NK cells, endothelial cells (ECs), fibroblasts, smooth muscle cells (SMCs), epithelial cells (EPCs), B cells, plasma cells, MCs, neutrophils, and myeloid cells. The cell cycle distribution differences among these cell types were shown (Figure 1B). Our observation of MC infiltration in CC tissues primarily consisted of H and N clusters, leading us to hypothesize that MCs could be involved in the conversion of tumoral epithelium. The bar graph on the left illustrates the relative proportions of the ten distinct cell types across different tissue types (H, L, T, N), while the bar graph on the right showcases the relative proportions of different cell types at various stages of the cell cycle (Figure 1C).

In addition, an expression bubble plot was utilized to depict the expression levels of the top 5 marker genes for each cell type (Figure 1D). By examining the distribution patterns and levels of expression of nCount_RNA, nFeature_RNA, S.score, and G2M.score in various cell types, we may gain a deeper understanding of the differences between these cell types (Figures 1E, F). The violin plots demonstrate that the tumor group displays elevated amounts of nCount_RNA, nFeature_RNA, S.score, and G2M.score, suggesting a heightened cellular proliferation within this group (Figure 1G). The DEGs across the 10 cell types are illustrated in the UMAP plots (Figure 1H).

10.3389/fimmu.2024.1434450

Visualization of MCs subpopulations in CC

After performing dimensionality reduction and clustering, a total of 1392 CC-associated MCs were obtained. The UMAP plot illustrated the origins of the 10 samples and the removal of batch effects in CC cells (Figure 2A). We identified seven distinct subgroups of MCs and annotated them based on their respective cell marker genes: C0 CTSG+ MCs (555), C1 CALR+ MCs (371), C2 ALOX5+ MCs (207), C3 ANXA2+ MCs (98), C4 MGP+ MCs (84), C5 IL32+ MCs (39), and C6 ADGRL4+ MCs (38). Using the UMAP plot combined with pie charts depicting cell proportions, we showcased the distribution of these seven MCs subgroups across different groups

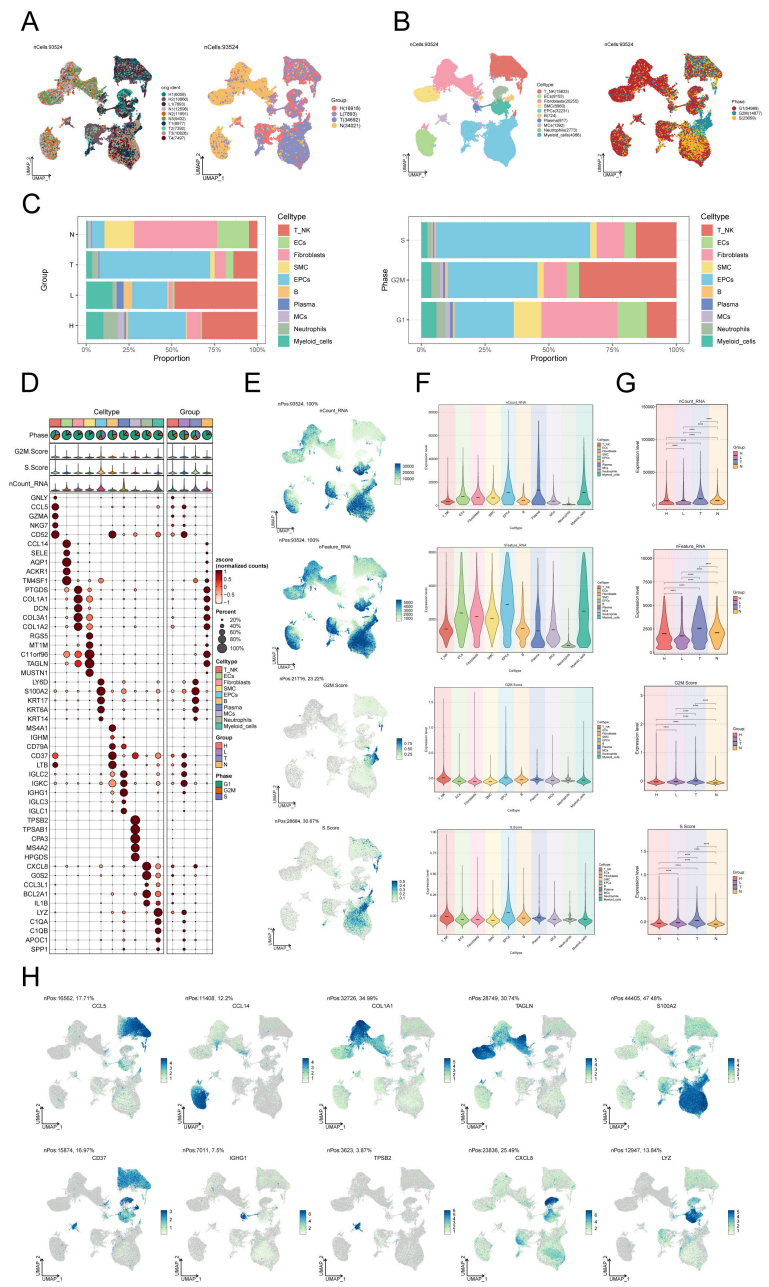

FIGURE 1
Single-cell landscape of CC. **(A)** The UMAP plots of the single cell spectrum depicted in this paper is presented. The plots exhibited distinguished coloration based on the sample source (on the left) and tissue type (on the right). **(B)** UMAP plot on the left annotated cell types (T_NK cells, ECs, SMCs, EPCs, B cells, plasma cells, MCs, neutrophils, and myeloid cells) based on known lineage-specific marker genes (represented by colors). On the right, the UMAP plot depicted the distribution of cells in different cell cycle phases (G1, G2M, S). **(C)** Bar graphs depicted the relative proportions of the ten distinct cell types across various tissue types (left) and cell cycle (right). **(D)** Bubble plot visually represented the expression levels of diverse marker genes according to annotated cell types. The coloration of the bubbles is determined by normalized data, while the size of the bubbles denotes the proportion of gene expression. **(E)** UMAP plots illustrated the distribution of nCount_RNA, nFeature_RNA, G2M.score, and S.score across ten distinct cell types within CC. **(F, G)** Violin plots depicted the expression levels of nCount_RNA, nFeature_RNA, G2M.score, and S.score across ten cell types **(F)** as well as various tissue types **(G)** in the context of CC. . ****$P < 0.0001$. **(H)** UMAP plots showed DEGs across distinct cell types in the context of CC.

(H, L, T, N) and cell cycle phases (G1, S, G2M) (Figure 2B). Among them, subgroups C0, C4 and C6 predominantly originated from normal tissues, while subgroups C1, C2, C3 and C5 had a higher proportion of tumor tissue representation. Subsequently, we utilized box plots to display the distribution of MCs from different tissue types within each subgroup (Figure 2C). The results revealed that Normal Cervix mainly clustered in subgroups C0, C4, and C6, while Cervical Tumors were predominantly concentrated in subgroup C1, with some presence in subgroups C2 and C3. High Squamous Intraepithelial cells were primarily distributed in subgroups C0, C1, and C2, with a smaller portion found in subgroup C3. A bar graph was employed to demonstrate the proportions of cell cycle phases across the different MCs subgroups of CC (Figure 2D), indicating no significant differences among the seven subgroups in terms of cell cycle distribution (G1, S, G2M).

We utilized inferCNV to identify chromosomal CNVs within cells, aiming to investigate the malignancy level of tumors and abnormal states of cells (68). This approach assists in distinguishing tumor cells from normal cells and identifying clusters of abnormal cells within tumor cells. The heatmap displays the CNV profiles of EPCs inferred using ECs as a reference (Supplementary Figure S1A). The results indicate the presence of abnormal chromosomal copy number amplifications or deletions in malignant EPCs of CC. In Supplementary Figure S1B, the inferred CNVs of each cell subpopulation are illustrated. Next, we employed UMAP plots to visualize the CNV scores, nCount_RNA, S.score, and G2M.score of the MCs subgroups. The results were presented using violin plots (Figures 2E, F). The C2 ALOX5+ MCs subgroup displayed the highest CNV score, indicating a greater occurrence of copy number variants in comparison to other subgroups. This suggests a possibly higher level of malignancy. On the other hand, the C3 ANXA2+ MCs subgroup displayed a higher nCount_RNA score, suggesting a relatively active cellular proliferation state. In Figure 2G, the top 5 marker genes' differential expression was highlighted within the MCs subgroups. The findings showed that the leading 5 marker genes in the C2 ALOX5+ MCs subgroup were similarly present in other MCs subgroups.

We ultimately employed bar graphs to exhibit the levels of marker genes expression in different subcategories (Figure 2H).

Slingshot analysis of proposed temporal trajectories of MCs subpopulations

To infer the lineage trajectory and pseudotime sequence of MCs, we employed slingshot analysis to assess the distribution of MCs differentiation trajectories across all MCs, visually represented through UMAP plots (Figure 3A). We found 3 cell lineage trajectories of the MCs subpopulations (Figures 3B, C). Lineage 1 followed the path C5 → C1 → C0 → C2 → C3; Lineage 2 followed the path C5 → C1 → C0 → C2 → C6; Lineage 3 followed the path C5 → C1 → C0 → C4. Slingshot analysis revealed that the differences among the three trajectories mainly reside in the middle to late stages. Combined with the analysis results depicted in Figure 2C, the C3 subpopulation was positioned at the end of Lineage1, predominantly present in CCs. On the other hand, although the C4 and C6 subpopulations were located at the ends of lineage3 and lineage2, respectively, they exhibited a significantly higher proportion in the normal cervix. Therefore, we inferred that lineage1 represents the differentiation line of MCs associated with the tumor. Moreover, we noted that both lineage1 and lineage2 pass through the C2 subpopulation at the late stage of differentiation, but with different endpoints. From this observation, we speculated that the C2 subpopulation likely plays a crucial role in the differentiation of tumor-associated MCs. Subsequently, Gene Ontology Biological Process (GO-BP) enrichment analysis was employed to validate the biological processes associated with the three lineage paths of MCs subpopulations (Figure 3D). The enrichment results indicated the following: C1: leukocyte immune, mediated immunity and lymphocyte antigen presentation; C2: cell-substrate, muscle; C3: smooth, proliferation; C4: humoral, tight, junction. The dynamic trends plot depicted the changes in expression levels and distribution patterns of marker genes for various subpopulations of MCs over three differentiation trajectories in pseudotime (Figure 3E).

Expression of stemness gene sets in MCs subpopulations

To examine the expression of stemness genes in distinct subgroups of MCs and comprehend their ability to differentiate, we employed a bubble plot to visually represent the variation in expression of stem cell genes across these subgroups. The results demonstrated the expression of stem cell genes CD44, CTNNB1, EPAS1, HIF1A, KDM5B, KLF4, and HIF1A in distinct tissue types and subpopulations of MCs, as shown in Figure 4A. Subsequently, we undertook further analysis to assess the variations in cellular stemness among different subpopulations (Figure 4B). The results demonstrated that C2 ALOX5+MCs exhibit a lower level of cell stemness, suggesting a higher degree of differentiation. The violin displayed the variations of cellular stemness across different cell cycles and tissue types (Figure 4C). The above findings suggested that the Normal Cervix tissue exhibits the highest level of cell stemness. Consequently, we could deduce that the remaining three tissue types may have undergo differentiation that originated from the Normal Cervix. Moreover, there was no significant disparity in cellular stemness between different cell cycles. Finally, the stemness genes with relatively elevated expression levels in Figure 3A were showcased in all MCs through UMAP plots and contour plots (Figure 4D).

Enrichment analysis of MCs subpopulations in CC

First, the differential gene expression patterns among the MCs subgroups were shown using volcano plots in Figure 5A.

To further demonstrate the enrichment of DEGs in biological processes, we performed GO-BP enrichment analysis on DEGs in the MCs subpopulations. Figure 5B displayed the top five enrichment entries for different MCs subgroups, revealing unique pathways of enrichment among the seven subgroups. The results demonstrated distinct enrichment pathways among the seven MCs subgroups. The C0 CTSG+ MCs subgroup was primarily associated with pathways such as cytoplasmic translation, negative regulation of ubiquitin protein ligase activity, positive regulation of signal transduction by

10.3389/fimmu.2024.1434450

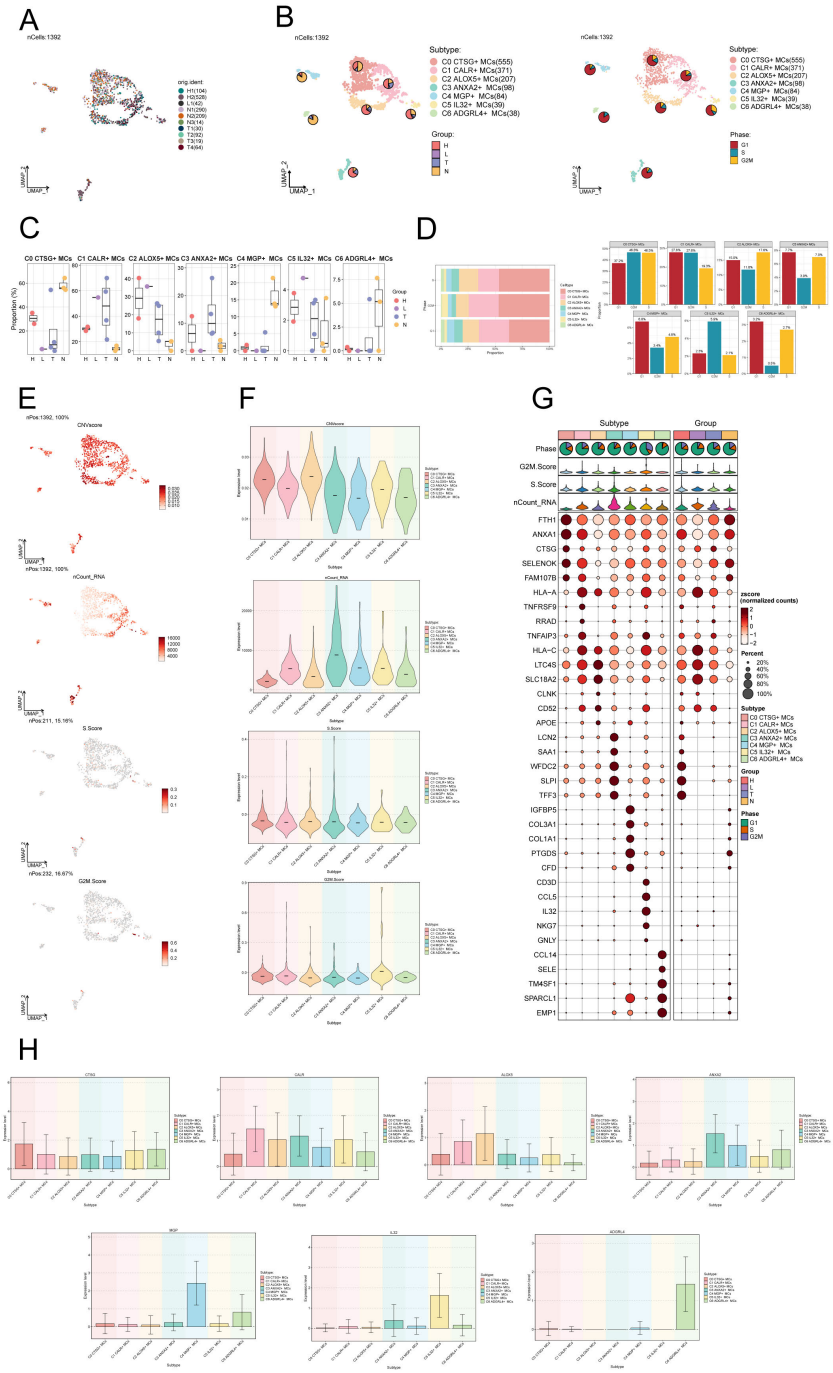

FIGURE 2
Visualization of MCs subpopulations in CC. **(A)** UMAP plot demonstrated the origin of the samples and the clustering of 1392 high-quality cells using the downscaling technique through the Seurat method. **(B)** The cells were annotated according to recognized lineage-specific marker genes (indicated by color): C0 represented CTSG+ MCs, C1 represented CALR+ MCs, C2 represented ALOX5+ MCs, C3 represented ANXA2+ MCs, C4 represented MGP+ MCs, C5 represented IL32+ MCs, and C6 represented ADGRL4+ MCs. A pie chart was employed to illustrate the MCs subpopulation in terms of tissue type and cell cycle. On the left side, the groups (H, L, T, N) were specified, while on the right side, the phases (G1, S, G2M) were delineated. **(C)** Box plots depicted the distribution of different tissue types among various subtypes of MCs. **(D)** Bar graph displayed the varying cell cycle occupancies of the seven cell subpopulations of MCs in CC. **(E)** UMAP plots exhibited the distribution of CNVscore, nFeature_RNA, S.score, and G2M.score across MCs subpopulations. **(F)** Violin plots demonstrated the expression levels of CNVscore, nFeature_RNA, S.score, and G2M.score across MCs subpopulations. **(G)** Bubble plot exemplified the differential expression of top5maker genes within MCs subpopulations and across distinct tissue types. The coloration of the bubbles signifies the level of gene expression, while the size reflects the proportionate percentage of gene expression within the subpopulations. **(H)** Bar graphs illustrated the expression levels of marker genes within each subgroup.

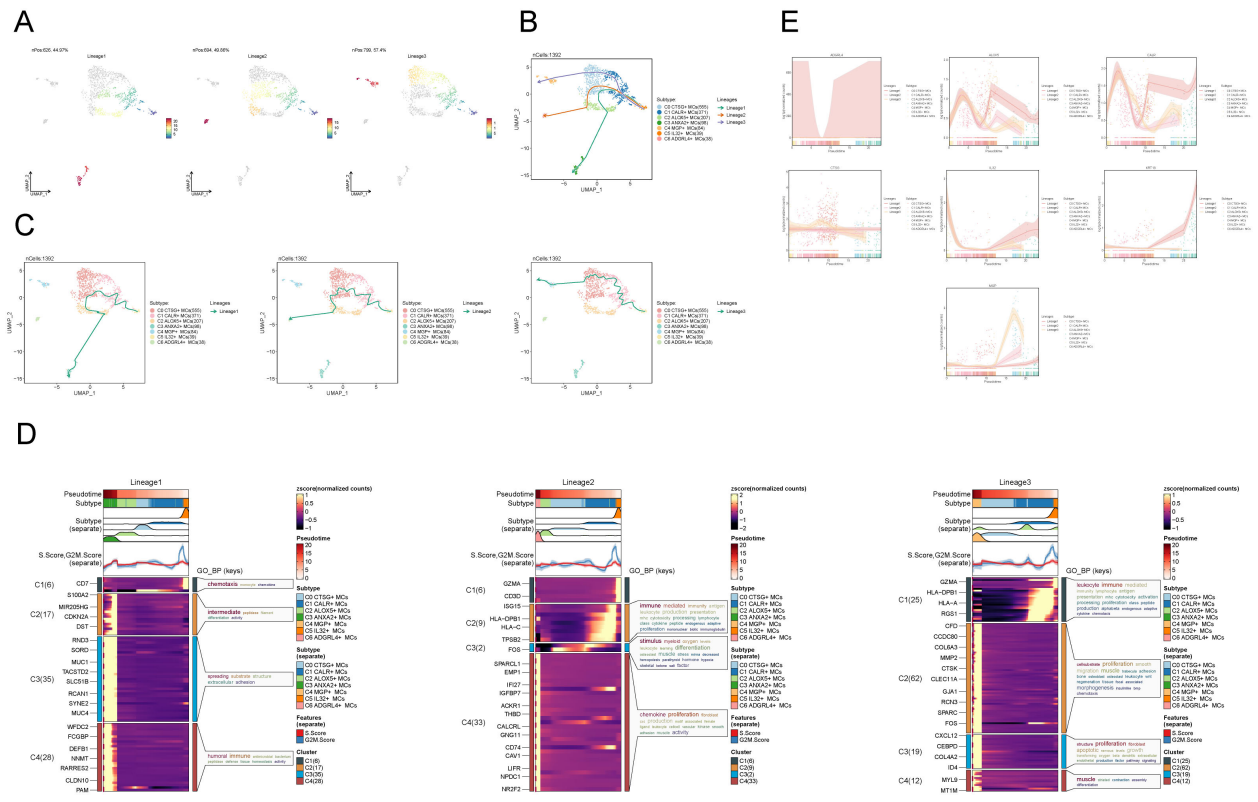

FIGURE 3
Slingshot analysis of proposed temporal trajectories of MCs subpopulations. **(A)** UMAP plots demonstrated the distribution of differentiation trajectories of MCs, fitted by slingshot, across the entire MCs population. Lineage1 nPos:626,44.97%, Lineage2 nPos:694,49.86%, Lineage3 nPos:799,57.4%. **(B, C)** UMAP plots showed the distribution of the three pseudotemporal trajectories of MCs in all MCs clusters. Solid lines indicate differentiation trajectories with arrows pointing to the direction of differentiation (from naive to mature). Lineage1: C5→C1→C0→C2→C3; Lineage2: C5→C1→C0→C2→C6; Lineage3:C5→C1→C0→C4. **(D)** The results of the GO-BP enrichment analysis confirmed the biological processes corresponding to the three pseudotemporal trajectories of MCs subpopulations. **(E)** Kinetic trend plot showcased the fluctuation and dispersion of marker gene expression in the MCs subpopulations along the three differentiation trajectories in pseudotime. The plot was color-coded according to cell type.

p53 class mediator. The C1 CALR+ MCs subgroup was enriched in pathways such as protein folding, regulation of immune effector process. The enrichment analysis conducted on the C2 ALOX5+ MCs subgroup revealed their close association with immune and inflammatory processes, including leukocyte mediated immunity, production of molecular mediator involved in inflammatory response, positive regulation of immune effector process. The C3 ANXA2+ MCs subgroup showed enrichment in pathways such as epidermis development, cell-cell junction organization. The C4 MGP+ MCs subgroup was enriched in pathways related to extracellular matrix organization, collagen fibril organization, and cell-substrate adhesion. The C5 IL32+ MCs subgroup mainly exhibited enrichment in pathways such as lymphocyte mediated immunity, leukocyte mediated cytotoxicity. The enrichment analysis of the C6 ADGRL4+ MCs subgroup revealed pathways related to regulation of angiogenesis, regulation of vasculature development, epithelial cell migration. Word cloud plots illustrate the enrichment results of DEGs in different pathways for the seven MCs subpopulations (Figure 5C). Additionally, the GSEA enrichment analysis results were visualized as bubble plots (Figure 5D).

Lastly, we conducted GSEA on the DEGs in the C2 subgroup of MCs, utilizing GO-BP terms. The results were depicted in Figure 5E. It was observed that the pathways associated with Regulation of lymphocyte-mediated immunity, Vesicle-mediated transport, Endocytosis and Regulated exocytosis were upregulated in the C2 subgroup. In contrast, the C2 subgroup exhibited downregulation of the pathways associated with the cellular response to stress and the response to hormone.

CellChat analysis among cell subtypes

To enhance our comprehension of the communication network among various cell types, decipher the intricacy of intercellular signaling, and investigate the functional and regulatory roles of cell subpopulations and crucial signaling pathways in physiological and disease processes, we utilized CellChat for the analysis and depiction of intercellular communication. Firstly, we constructed a communication network among all CC cells, including T_NK cells, ECs, fibroblasts, SMCs, EPCs, B cells, plasma cells, MCs, neutrophils, and myeloid cells. To determine the extent of cellular communication, we measured the quantity and intensity of these intercellular connections (shown by the thickness of the connecting lines). Higher numbers of intercellular contacts and higher levels of

10.3389/fimmu.2024.1434450

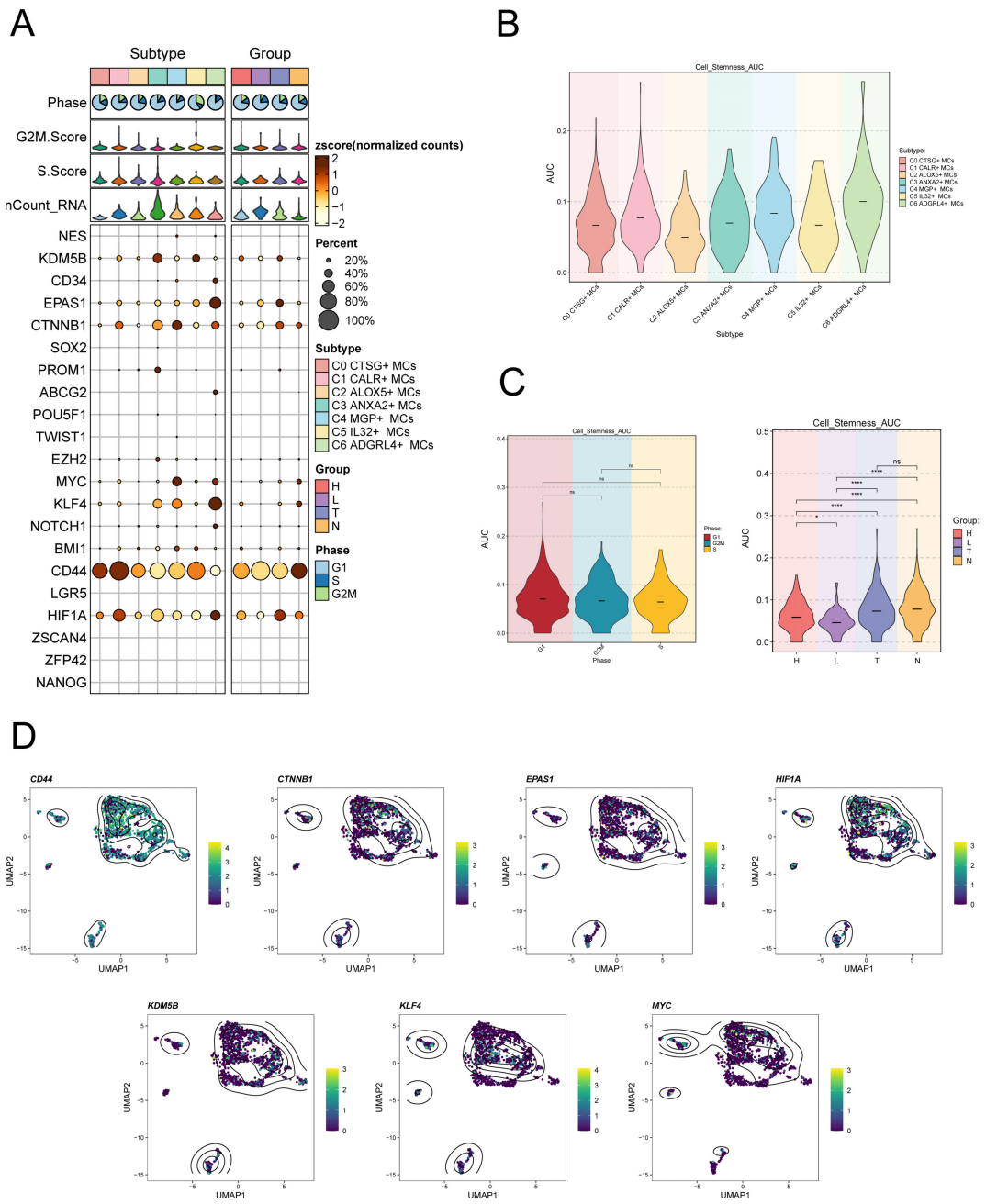

FIGURE 4
Expression of stemness gene sets in MCs subpopulations. **(A)** Bubble plot demonstrated the differential expression of stemness genes across various MCs subpopulations and tissue types. The size of the bubbles indicates gene expression score and the color represents the normalized data. **(B, C)** Violin plots demonstrated the AUC value of stemness genes in different MCs subpopulations **(B)**, cell cycle and tissue types **(C)**. *$P < 0.05$, and ****$P < 0.0001$ indicated a significant difference and "ns" indicated a non-significant difference. **(D)** UMAP plots showed the spatial arrangement of stemness genes among various subtypes of MCs, presented through the visualization of contour density.

communication intensity are shown by thicker lines (Figure 6A). To examine the coordination and interaction among several cell subtypes, we employed CellChat to detect overall communication patterns and important signaling components inside various cell clusters. This allowed us to establish connections among cell populations. As a result, we discovered three outgoing signal patterns (viewing cells as senders) and three incoming signal patterns (viewing cells as receivers) (Figure 6C). The results revealed that most outgoing signals from MCs were dominated by pattern 1, involving multiple signaling pathways such as TIGIT, TNF, SPP1, and TWEAK. The incoming signals from all tumor cells exhibited pattern 3, including but not limited to CD96, CEACAM, and AGRN signaling pathways.

Next, to identify the key incoming and outgoing signals associated with the C2 ALOX5+MCs subpopulation and other cell subpopulations, we also identified receptor-ligand signaling related to the communication pathways (Figures 6B, D). The results showed that as secretory cells, the ligands associated with

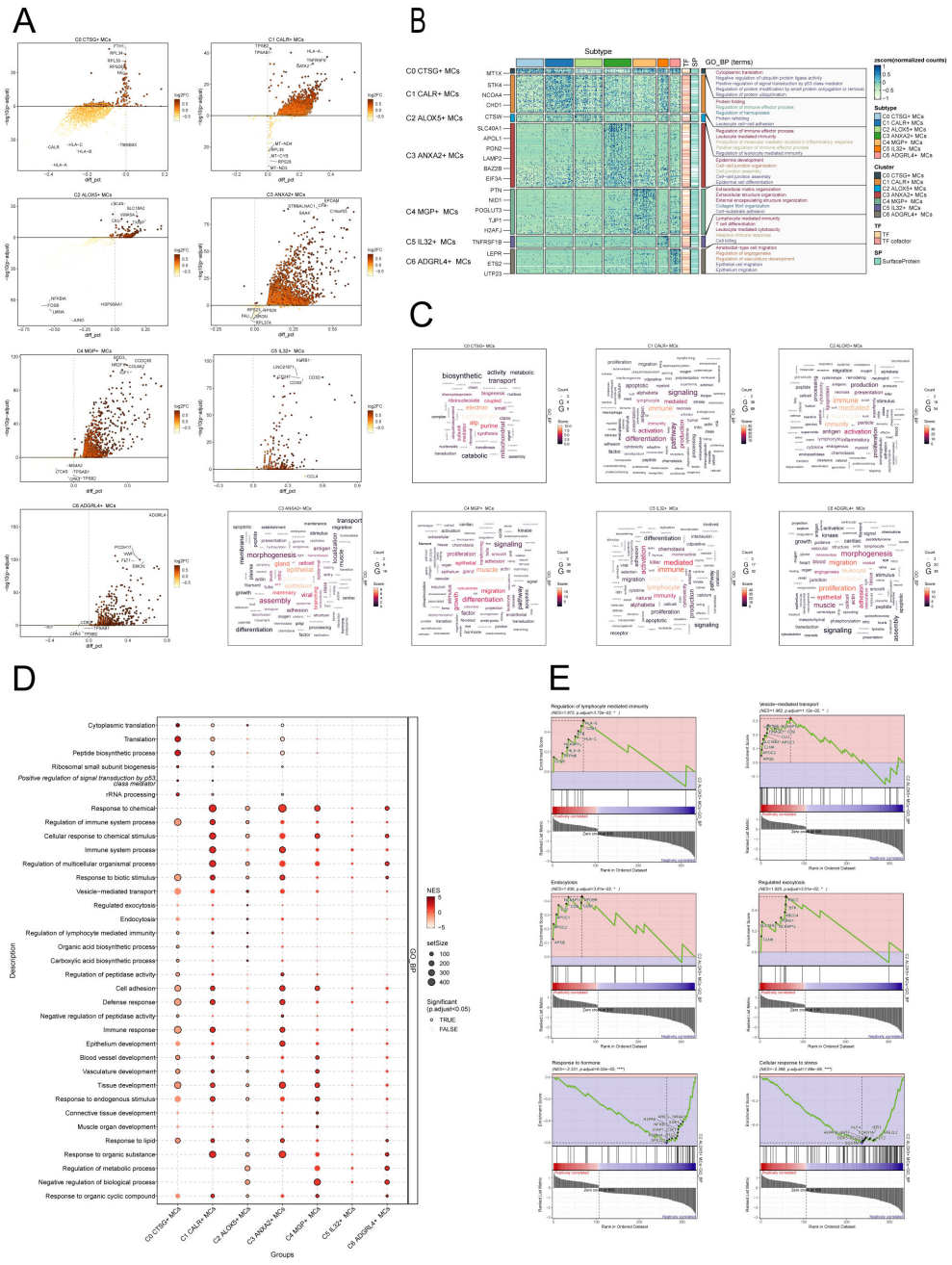

FIGURE 5
Enrichment analysis of MCs subpopulations in CC. **(A)** The volcanic plots provided descriptions of DEGs within each subgroup. **(B)** Heatmap showed the top5 enriched entries of GO-BP enrichment analysis for seven MCs subpopulations of differential genes. **(C)** Word cloud diagrams showed the results of GO-BP pathway in seven MCs subpopulations. **(D)** Based on the GO-BP entries, the results of enrichment analysis of differential genes in subpopulations of MCs were visualized using a bubble plot through GSEA. The size of the bubbles represents the number of genes enriched, while the color indicates the significance level. **(E)** The results of GSEA were presented, based on the GO-BP entries, showcasing the enriched pathways associated with differential genes in the C2 subpopulation of MCs.

the output of C2 ALOX5+MCs were mainly MIF, CD45, and TWEAK. Regarding the input pathways in target cells, the receptors associated with C2 ALOX5+MCs were primarily CD99, SELE, and SPP1, while the receptors related to tumor cells included TWEAK, CEACAM, and CD96. Figure 6E displayed a scatter plot that showcased the communication network analysis of pathways associated with tumor interaction, both in all cells and specifically within the C2 subgroup of MCs.

In addition, we chose C2 ALOX5+MCs as the source and tumor cells as the targets to study the interactions between MCs and tumor cells. The circular plot displayed the number (Figure 6F) and strength (Figure 6G) of cell-cell interactions between C2 ALOX5+MCs as the source and tumor cells as the targets. Combining the results from CellChat analyses, we found that the TWEAK signaling pathway exhibited strong interaction between ligands and receptors. The scatter plot revealed the cell-cell

10.3389/fimmu.2024.1434450

communication patterns of the TWEAK signaling pathway, emphasizing the significance of C2 CRYAB+MCs in this route (Figure 7A). Using the network centrality analysis of the TWEAK signaling network, we determined that the C2 MCs subpopulation had the highest level of importance as a sender in the TWEAK signaling pathway. Conversely, tumor cells were identified as the most significant receivers (Figures 7B, C). Significantly, the ligand-receptor pair TNFSF12 - TNFRSF12A was identified as a key element in the TWEAK communication network (Figures 7D, E). The circular and layered diagrams depicted the deduced network of cell-cell communication in TWEAK signaling (Figures 7F, G). All cell types identified in the CC tissue were examined as potential source cells for the TWEAK signaling pathway. The findings revealed that C1 CALR+MCs, C2 ALOX5+MCs, C3

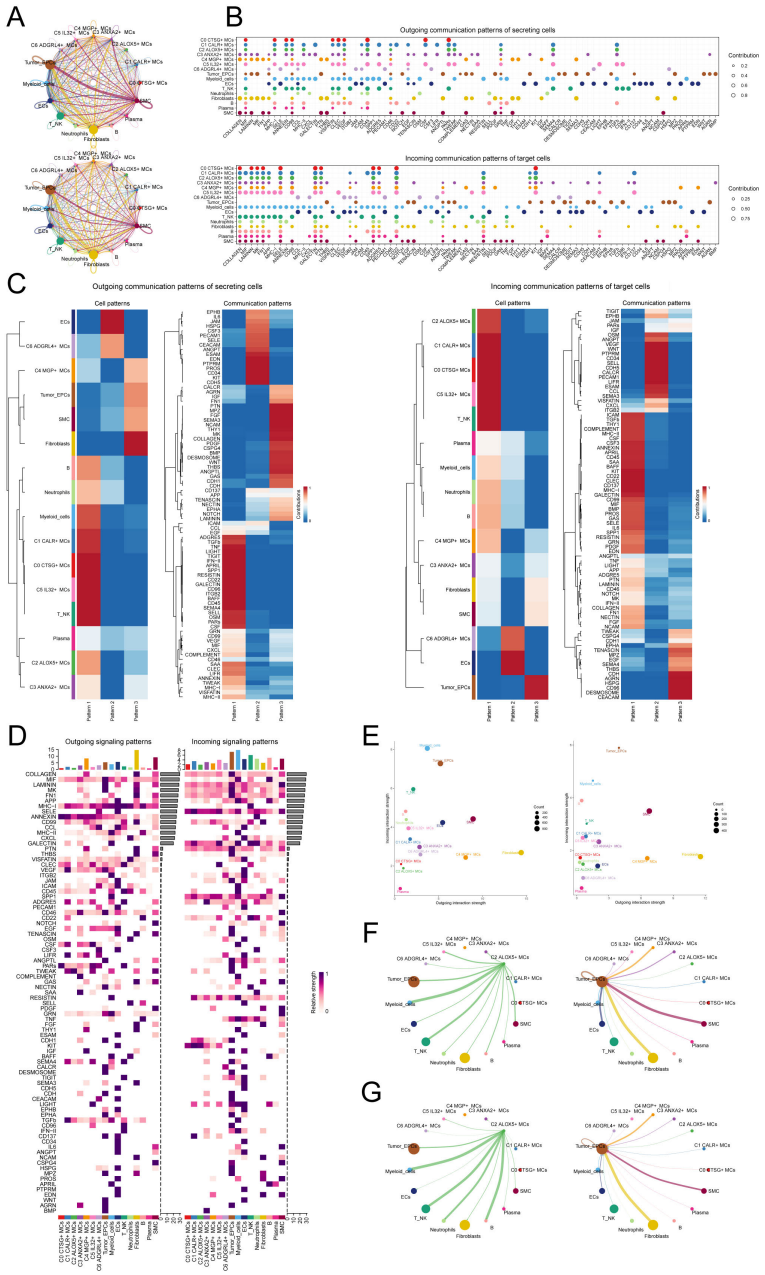

FIGURE 6
Presentation of CellChat results. **(A)** Circle plots depicted the number (top) and strength (bottom) of interactions among all cells in CC. **(B)** Dot plots showed the comparison of outgoing signaling patterns of secreting cells and incoming communication patterns of target cells. Higher contribution score implies the signaling pathway is more enriched in the corresponding cell group. **(C)** Heatmaps showed the outgoing communication patterns of secreting cells and incoming communication patterns of target cells, showing the correspondence between the inferred latent patterns and cell groups, as well as signaling pathways. **(D)** Heatmaps showed outgoing and incoming signal strength of all cell interactions in CC. **(E)** The scatter plot depicted the communication network analysis between all cells and the C2 subpopulation associated with tumor-related pathways, the color of the dots indicates different cells and the size of the dots indicates the number of cells. **(F, G)** Screening of the number **(F)** and strength **(G)** of cellular interactions circled plots with C2 ALOX5+ MCs as source and tumor as target.

ANXA2+MCs, C5 IL32+MCs, myeloid cells, fibroblasts, and SMCs are capable of targeting tumor cells by releasing TWEAK.

In vitro experimental validation of TNFSF12A

TNFRSF12A, also known as Tumor Necrosis Factor Receptor Superfamily Member 12A, was a part of the TNFR superfamily. It had a diverse function in controlling cellular growth, viability, migration and apoptosis (69–71). Recent research has highlighted the significant impact of TNFRSF12A on the development, advancement, and metastasis of different types of cancer in humans (72, 73). Nevertheless, the exact function of TNFRSF12A in CC had yet to be clarified. To this end, we conducted *in vitro* functional assays to determine the impact of TNFRSF12A on CC cells. For precision and consistency, we performed all tests on two CC cell lines (HeLa and CaSki). Initially, we assessed the baseline mRNA expression levels in these cell lines (Figure 8A). Knocking down TNFRSF12A in these cell lines resulted in a notable reduction in the viability of tumor cells, as seen by the CCK-8 test (Figures 8B, C). Moreover, a substantial reduction in cellular proliferation was confirmed by colony formation and EdU assays following the TNFRSF12A knockdown in both cell lines (Figures 8D, G). These results indicated that the silencing of TNFRSF12A reduced tumor cell activity and proliferation, thereby impeding tumor growth. Furthermore, scratch and Transwell assays demonstrated a significant decrease in the migratory and invasive abilities of the TNFRSF12A-knockdown tumor cells in contrast to the control group (Figures 8E, F). These investigations collectively affirmed the

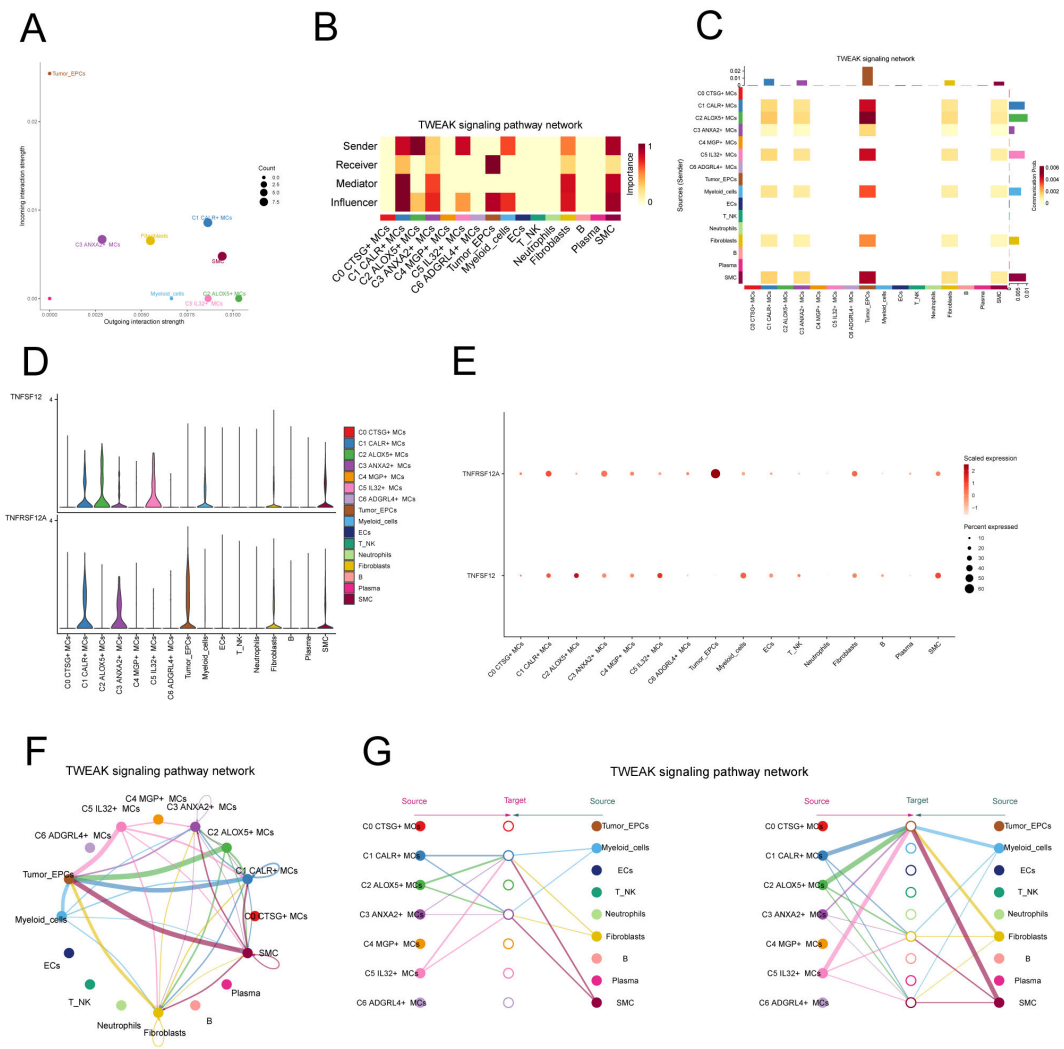

FIGURE 7
TWEAK signaling pathway. **(A)** Scatter plot of cellular communication patterns of TWEAK signaling pathway. The color of the dots indicates different cells and the size of the dots indicates the number of cells. **(B)** Heatmap showed the relative importance of each cell group based on the computed four network centrality measures of TWEAK signaling network. **(C)** Heatmap showed the centrality scores of TWEAK signaling pathways. **(D, E)** Violin and bubble plots demonstrated cellular interactions in the TWEAK signaling pathway. **(F, G)** Circle plot and hierarchical plot showed the inferred intercellular communication network for TWEAK signaling. The size of the circle is proportional to the number of cells in each cell group, and the edge width indicates the communication probability.

critical significance of the TNFRSF12A gene regulatory network in the etiology and metastatic capacity of CC.

Construction of a prognostic model associated with C2 ALOX5+ MCs score

In order to gain a deeper understanding of the key significance of MCs with high expression of ALOX5 in the prognosis of CC, and to offer more precise recommendations for clinical practice, we have created a risk scoring model. First, a univariate Cox regression analysis was conducted to identify the top 100 DEGs that are linked to C2 ALOX5+MCs. The study revealed 13 genes that had a significant correlation with prognosis (P<0.05) (Figure 9A). TINAGL1 and SLC5A3 exhibited a hazard ratio (HR > 1), signifying that these two genes are prognostic risk factors, whereas the other genes functioned as protective factors. To address the problem of multicollinearity among these genes, we conducted further selection using LASSO regression analysis. This led to the discovery of five genes that were shown to be linked with prognosis, as shown in Figure 9B. Afterwards, the coefficient values were computed using multivariable Cox regression analysis (Figure 9C).

Afterwards, using the expression levels and regression coefficients of the five chosen prognostic-related genes, we computed the ALOX5+MCs score for each patient using the following formula: ALOX5+MCs score = (0.24) × (TINAGL expression level) + (0.12) × (SLC45A3 expression level) + (-0.19) × (CD52 expression level) + (-0.21) × (PTPN6 expression level) + (-0.42) × (CLNK expression level). The ALOX5+MCs risk score (AMRS) was utilized to classify the participants into high-risk and low-risk groups, based on the optimal cutoff value. The curve plot and scatter plot illustrated the disparities in risk scores and survival rates between the two groups (Figure 9D), suggesting a link between higher AMRS and unfavorable prognosis. Furthermore, a heatmap illustrated the distinct patterns of gene expression employed in constructing the model (Figure 9E).

Figure 9F displayed the Kaplan-Meier curve showing the contrast in survival rates between the high AMRS group and the low AMRS group, supporting the conclusion of worse survival outcomes in the high AMRS group. The model's predictive accuracy was assessed by examining its sensitivity and specificity over 1, 3, and 5 years with ROC curves and AUC values (Figure 9G). The results indicated that the model had predictive value. Finally, survival analysis was performed on the five prognostic-related genes (TINAGL1, SLC45A3, PTPN6, CLNK, CD52) used in the model (Figure 9H), further confirming that SLC45A3 was risk factors associated with poorer prognosis in the high AMRS group, while CD52 was protective factors associated with better prognosis in the high AMRS group.

Nomogram construction and correlation analysis of risk scores and modeled genes

In order to confirm the autonomy of the AMRS as a predictive factor, we performed a multivariable Cox regression analysis that included the risk score along with clinical variables such as age, race, and tumor stages T, M, and N. The findings indicated that AMRS independently impacts patient prognosis as a risk factor (P< 0.05) (Figure 10A). To improve the accuracy of predicting patient survival rates, a nomogram was created using factors such as race, tumor stage, age, and risk score to forecast the likelihood of survival at 1, 3, and 5 years. The results indicated that the differences were most significant in the AMRS group (Figure 10B). Additionally, the Nomogram's prediction was confirmed by evaluating the C-index and ROC curves. The obtained AUC values were 0.837 (1 year), 0.786 (3 years), and 0.755 (5 years), confirming the accuracy of the model (Figures 10C, D). Similarly, the calibration curves demonstrated that the nomogram effectively predicted actual survival outcomes (Figures 10E–G). In addition, scatter plots were employed to examine the relationship between the five genes included in the model and the ALOX5+MCs score and OS (Figure 10H), as well as the variations in gene expression between the high AMRS and low AMRS groups (Figure 10I). Finally, the correlation analysis showed a positive association between TINAGL1, SLC45A3, and the risk score, and a negative correlation with OS. On the other hand, PTPN6, CLNK, and CD52 demonstrated a negative correlation with the risk score, and a positive correlation with OS. These findings were illustrated in Figures 10J, K.

Comparative examination of immune infiltration in groups with high and low scores of ALOX5+ MCs

To investigate the differences in immune cell composition across varying risk score categories of AMRS, we analyzed the presence of 22 immune cell types in CC patients from the TCGC database using the CIBERSORT algorithm, as shown in Figure 11A. Figure 11B displayed the percentages of 13 immune cell categories that showed variances between the two groups in box plots. The results indicated that the High AMRS group had a higher proportion of Macrophages M0, MCs activated, T cells CD4 memory resting, and Dendritic cells activated, while the Low AMRS group had higher proportions of T cells CD8, T cells CD4 activated, MCs resting, and Macrophages M1.

Subsequently, we evaluated the correlation between immune cells and AMRS, as shown in Figure 11C. The results demonstrated a significant positive correlation between AMRS and MCs activated, Macrophages M0, and a negative correlation with T cells CD8, MCs resting, among others. The heatmap visualized the correlation analysis between immune cells, the modeled genes, OS, and the risk score (Figure 11D), with results displayed in the figure. We further observed differences in the StromalScore, ImmuneScore, and ESTIMATEScore, as well as tumor purity between the High AMRS group and the Low AMRS group (Figure 11E). In particular, the High AMRS group exhibited lower scores across all three measures when compared to the Low AMRS group. The visualization of tumor purity (Figure 11F) indicated that the High AMRS group had higher tumor purity values than the Low AMRS group. The TIDE values between the two groups also exhibited differences (Figure 11G).

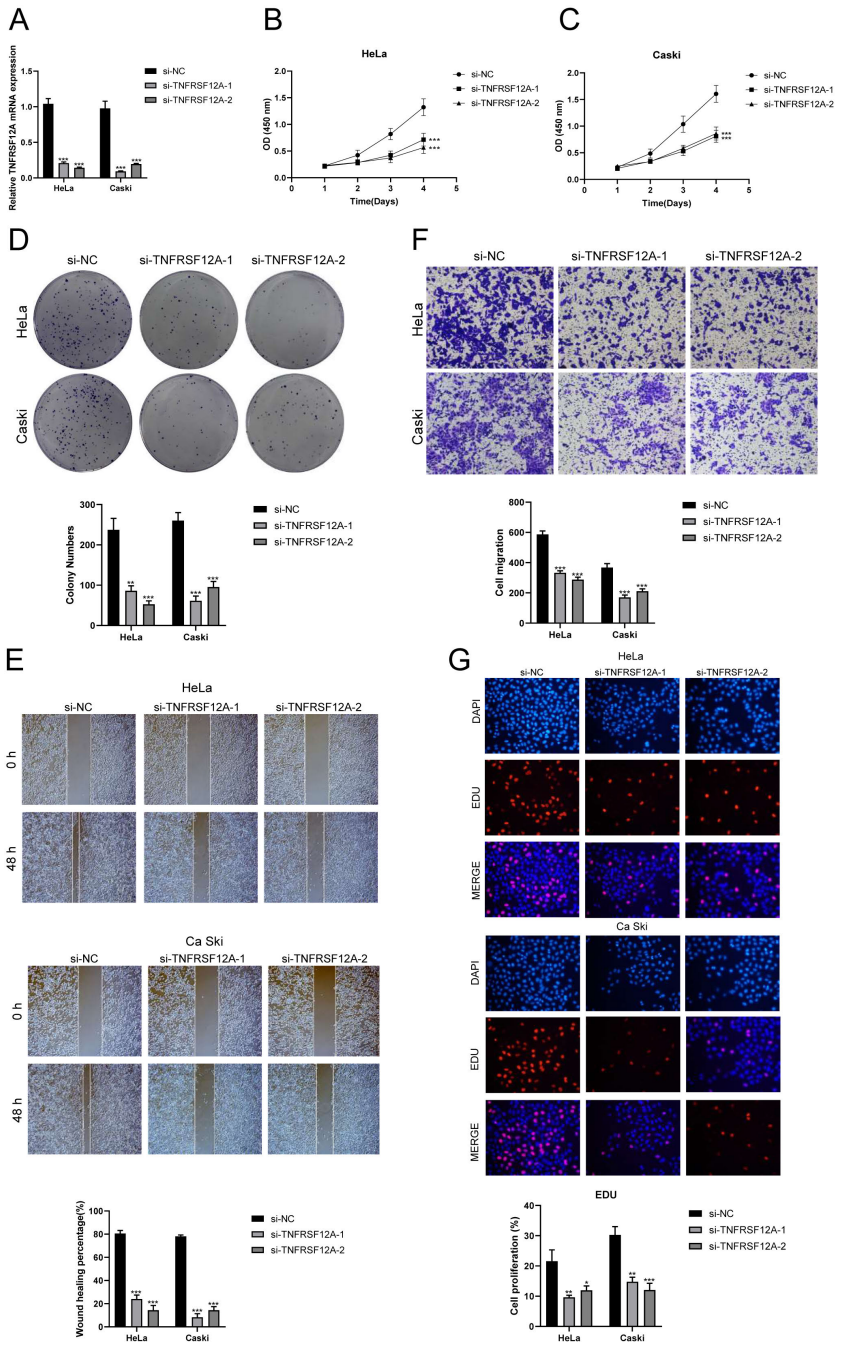

FIGURE 8
In vitro experimental validation of TNFSF12A. **(A)** The bar graph depicted the initial mRNA expression levels in Hela and Caski cell lines. **(B, C)** Cell viability was significantly diminished following the knockdown of TNFSF12A, as demonstrated by the CCK-8 assay. **(D)** The colony formation assay revealed that the number of colonies in cells with TNFSF12A knocked out was substantially lower compared to the si-NC group. **(E)** Scratch assays indicated that the knockdown of TNFSF12A markedly slowed the migration of Hela and Caski cells. **(F)** Transwell assays showed that the knockdown of the TNFSF12A gene significantly reduced the invasiveness of Hela and Caski cells. **(G)** EdU staining results suggested that the knockdown of the TNFSF12A gene inhibited the proliferation of Hela and Caski cells. *P< 0.05, **P< 0.01, and ***P< 0.001

The heatmap displayed in Figure 11H illustrated the differences in modeled genes, StromalScore, ImmuneScore, ESTIMATEScore, TumorPurity, and immune cell infiltration levels between the High AMRS group and the Low AMRS group, as calculated using CIBERSORT and Xcell algorithms. Furthermore, we compared the sensitivity of two immunotherapeutic drugs, CTLA4 and PD1, in the High AMRS group and the Low AMRS group using box plots (Figure 11I). The results showed that the sensitivity levels were generally lower in the High AMRS group compared to the Low AMRS group, particularly in the groups of CTLA4-neg/PD1-pos and CTLA4-pos/PD1-pos, with significant differences observed. The bubble plot (Figure 11J) displays the correlation between

10.3389/fimmu.2024.1434450

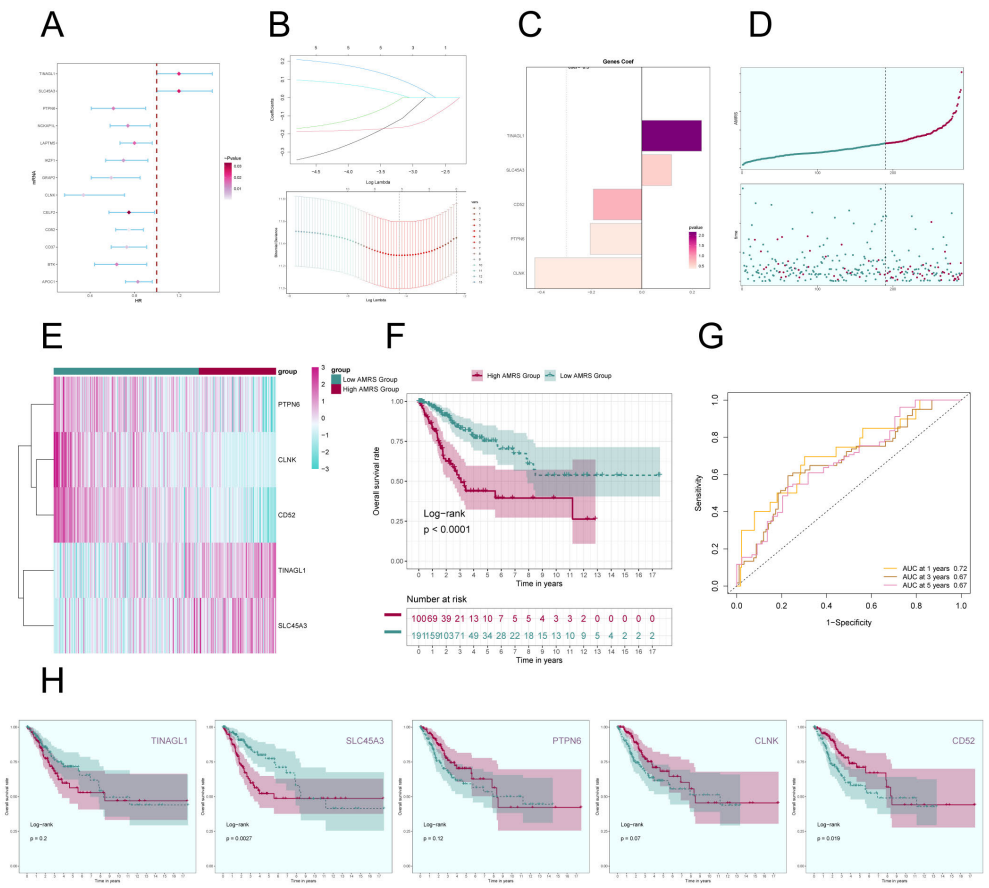

FIGURE 9
Construction of a prognostic model associated with C2 ALOX5+ MCs score. **(A)** Forest plot from univariate Cox regression analysis can be used to illustrate genes with statistically significant differences ($P<0.05$) (HR<1: protective factor, HR>1: risk factor). **(B)** Through LASSO regression analysis, five genes (non-zero regression coefficients) associated with prognosis were selected. The optimal parameter (lambda) was determined through ten-fold cross-validation (above), and the LASSO coefficient curve was determined by the optimal lambda (below). **(C)** Bar graph displayed the Coef values of the genes utilized for model construction. **(D)** Curve plots showed risk scores for the high AMRS group and the low AMRS group (top), and scatter plots showed survival status of both groups over time for survival/death events (bottom). AMRS: ALOX5+ MCs Risk Score. **(E)** Heatmap showed differential expression of modeled genes, with color scales based on normalized data. **(F)** Kaplan-Meier curves showed the survival difference between the high AMRS group and the low AMRS group. **(G)** The sensitivity and specificity of 1, 3, and 5-year outcomes were assessed through ROC curve and AUC values. **(H)** The Kaplan-Meier curves individually demonstrated the differences in survival among patients grouped based on the expression levels of five prognostic-related genes (TINAGL1, SLC45A3, PTPN6, CLNK, CD52).

immune checkpoint-related genes and the modeled genes, risk score, and OS. It indicates a strong positive correlation between PTPN6, CD52, CLNK, and most immune checkpoints, while SLC45A3 demonstrated a negative correlation with most immune checkpoints. Finally, the expression levels of immune checkpoint-related genes were analyzed, indicating higher expression in the majority of immune checkpoint-related genes in the Low AMRS group compared to the High AMRS group (Figure 11K).

Enrichment analysis

To delve deeper into the differences between the High AMRS group and the Low AMRS group, we analyzed DEGs and showcased the expression patterns of these unique genes through a volcano plot (Figure 12A). Afterwards, in order to obtain a more thorough comprehension of the biological importance and operational traits of the distinct genes, we utilized different enrichment techniques to examine the DEGs in each group. The results of the GO analysis unveiled a noteworthy enrichment of differential gene expression in pathways such as digestion, serine-type endopeptidase activity, serine hydrolase activity, among others (Figure 12C). The genes associated with these enriched terms are depicted in Figure 12B. Furthermore, the outcomes of the KEGG enrichment analysis were visually presented using a bar graph, affirming the significant associations between these differential genes and pathways such as Graft-versus-host disease, Antigen processing and presentation, Maturity onset diabetes of the young, and Natural killer cell mediated cytotoxicity (Figure 12D). Moreover, utilizing the enriched GO-BP terms as a basis, GSEA was conducted, and the results are illustrated in Figure 12E.

10.3389/fimmu.2024.1434450

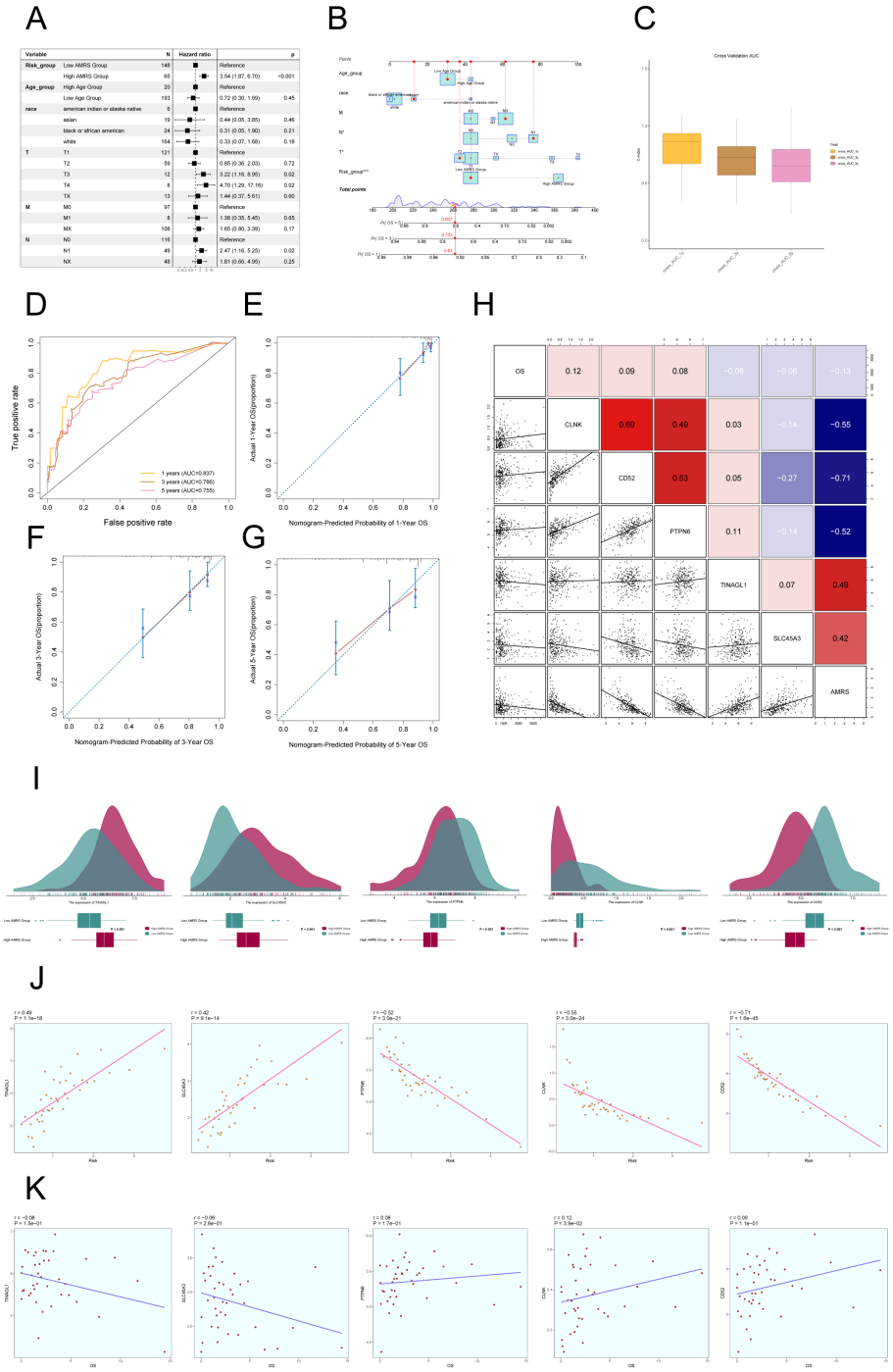

FIGURE 10
Construction of Risk Score Model for C2 ALOX5+MCs. **(A)** The Forest plot demonstrated the results of Multivariate Cox regression analysis integrating risk scores and clinical factors (age, race and tumor clinical stage T, M and N). **(B)** Nomogram showed the prediction of 1, 3, and 5-year of OS based on race, tumor clinical stage (T, M, and N), age, and risk score, with the most significant difference in the risk score group. **(C)** The box-line plot displayed visualizations of the C-index for cross-validation at 1, 3, and 5 years. **(D)** ROC curves showed nomogram AUC at 1,3,5 years. **(E–G)** Calibration curves validated the accuracy of the nomogram in predicting the 1-year, 3-year, and 5-year survival rates. **(H)** Heatmap and Scatter plots demonstrated the correlation between prognostic genes, OS, and genes used in model establishment. **(I)** Ridge and box plots showed the expression differences of prognosis-related genes in the high AMRS group and low AMRS group. High and low peaks indicate the patient density of patients with this gene expression. **(J)** The scatter plot illustrated the correlation between the risk scores and the genes utilized for model construction. **(K)** Scatter plot displayed the correlation analysis between the constructed model genes and the OS. *$P < 0.05$, and ***$P < 0.001$.

10.3389/fimmu.2024.1434450

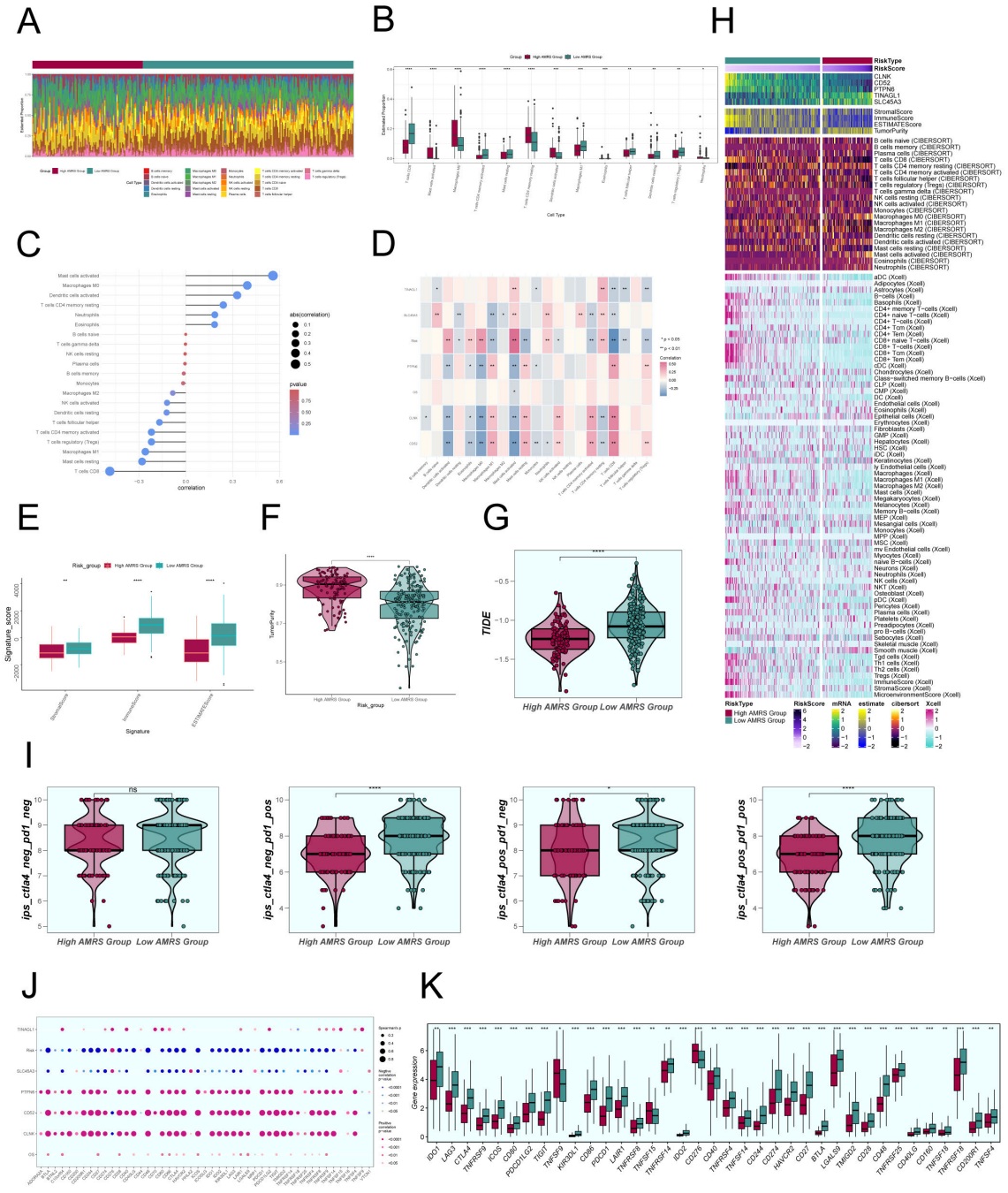

FIGURE 11
Comparative Analysis of Immune Infiltration between High and Low AMRS Groups. **(A)** Stacked bar graph illustrated the distribution of 22 immune cell types between the high and low AMRS groups. **(B)** Boxplots showed the estimated proportion of 13 immune cells types between the high AMRS group and the low AMRS group of CC patients. **(C)** Bar graph showed correlation between immune cells and risk scores. **(D)** Heatmap showed correlation analysis between immune cells and construct model genes, OS, and risk scores. **(E)** The differences in stromal score, immune score, and ESTIMATE score between the high and low AMRS groups of CC patients. **(F)** Boxplots showed the level of tumor purity between the high AMRS group and low AMRS group. *P<0.05, **P<0.01, ***P<0.001, and ****P< 0.0001 indicated a significant difference. **(G)** The differences in the levels of TIDE between the high and low AMRS groups. **(H)** Heatmap showed the difference in modeling genes, StromalScore, ImmuneScore, ESTIMATScore, TumorPurity, and the level of immune cell infiltration calculated using CIBERSORT, Xcell between the high and low AMRS groups. Color scales are based on standardized data. **(I)** Boxplots compared the sensitivity of two immunotherapeutic drugs, ctla4 and pd1, in the high and low AMRS groups. **(J)** Bubble plots showed correlations between modeled genes, risk scores, OS, and immune checkpoint-related genes. **(K)** Boxplots showed the expression levels of immune checkpoint-related genes in the high AMRS group and low AMRS group. Red: high AMRS group; Green: low AMRS group.

Discussion

Single-cell sequencing, as an emerging technology, has exhibited its unique advantage in uncovering tumor heterogeneity (74). In recent years, multiple studies utilized this technology to analyze various solid tumors, providing optimized guidance for clinical diagnosis and treatment strategies (75–77). MCs, as innate immune cells, played a role in both tumor suppression and promotion, with the effects varying depending on the cancer type (11, 78). Currently, there is ongoing controversy regarding the impact of MCs on CC. Research has indicated that the risk scores derived from prognostic models for CC may correlate with the infiltration of immune cells such as MCs (79). Additionally, MCs may facilitate the invasion and metastasis of CC cells by releasing histamine and cannabinoids (80). However, the mechanisms underlying the role of MCs in CC remain unclear. Consequently, we have undertaken an extensive investigation into this area. In this study, we employed single-cell sequencing technology to demonstrate the microenvironment landscape of CC, confirming the existence of immune cells, EPCs, and MCs as distinct cellular subgroups. Moreover, we observed that the histotype of MCs within cervical carcinomas was predominantly H-group, which is

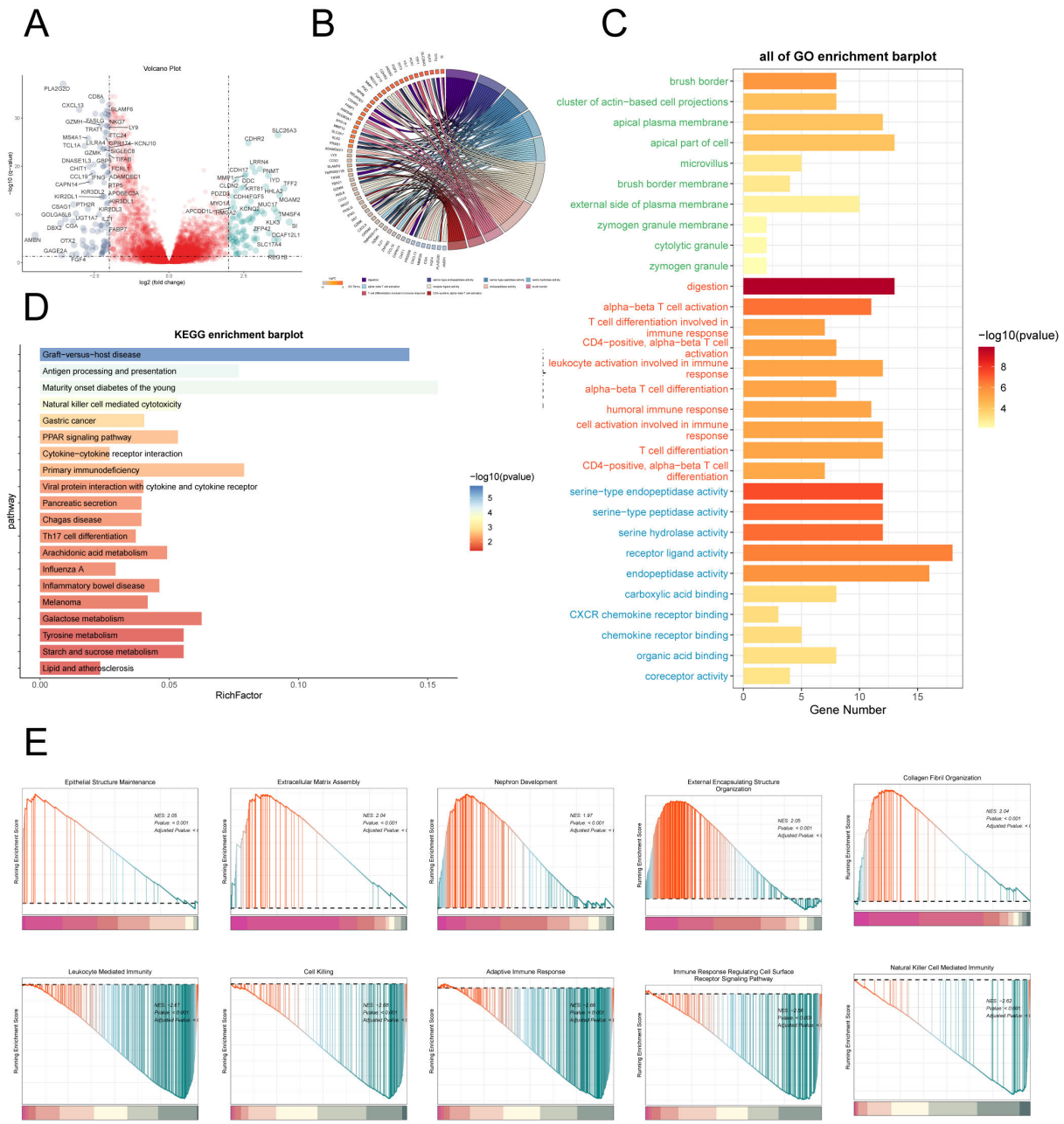

FIGURE 12
Enrichment analysis. **(A)** Volcano plot depicted differential gene distribution between the high AMRS group and low AMRS group. **(B, C)** Chord and bar graphs showed the results of GO Enrichment Analysis of differential genes in the high AMRS group and low AMRS group. **(D)** Bar graph showed the results of KEGG enrichment analysis of DEGs. **(E)** The GSEA was conducted to analyze the results of DEGs in the high and low AMRS groups.

commonly considered to be associated with an elevated risk of CC progression, leading us to surmise that MCs might be implicated in the progression of CC.

Subsequently, our analysis of MCs subgroups revealed a particular subset known as the C2 subgroup, characterized by significantly upregulated expression of arachidonate 5-lipoxygenase (ALOX5). ALOX5, a constituent of the lipoxygenase gene family, served a crucial function in both inflammation and malignancy. ALOX5 affected tumor occurrence and development through catalyzing the metabolism of arachidonic acid and was closely associated with poor prognosis in various malignant tumors (81–83). Enrichment analysis results revealed that subgroup C2 had a crucial impact on several biological processes, such as the regulation of immune effector processes, leukocyte-mediated immunity, the production of molecular mediators involved in inflammatory responses, the regulation of lymphocyte-mediated immunity, vesicle-mediated transport, and endocytosis. This demonstrated that subgroup C2 had a key role in immunity and inflammatory responses, and, according to previous studies, these biological processes were often closely associated with tumors (84–87). Moreover, our research discovered that the C2 subgroup had a higher proportion in the H and T-group compared to other subgroups, and relative to those subgroups, the C2 subgroup had a higher CNV score. Therefore, we hypothesized that the C2 subgroup possessed a higher degree of malignancy and may be correlated with the prognosis of CC.

Analysis results from Slingshot demonstrated that Lineage1 and Lineage2 represented the differentiation trajectories of tumor-associated MCs and normal cells, respectively, but their differentiation endpoints differed completely. The C2 subgroup was in the middle to late stages of both differentiation trajectories. We observed differences between the two trajectories after passing through the C2 subgroup, setting forth the hypothesis that the transformative effect of the C2 subgroup might be the reason for these differences. The C2 subgroup could potentially serve as a transformative MCs subset associated with tumor-related events, playing a pivotal role in the transition from benign to malignant states.

Considering the potential interactions between tumor cells and other cells, we conducted an analysis of intercellular communication involving the C2 subgroup. Research results demonstrated that the C2 subgroup interacted with tumor cells through the TWEAK signaling pathway. Its receptor, TNFSF12A, induced cell apoptosis and was associated with tumor cell migration and invasion (88, 89). To validate these findings, we conducted *in vitro* experiments on Hela and Caski cell lines, which revealed that the downregulation of TNFRSF12A suppressed CC tumor growth and migration, thereby confirming the critical role of the TNFRSF12A gene regulatory network in CC occurrence and metastatic potential and further supporting our hypotheses.

As controversies persist regarding the prognosis of CC patients in relation to MCs, we identified 13 genes associated with CC prognosis and constructed a risk scoring model. It is noteworthy that LASSO regression analysis identified five genes associated with prognosis, including TINAGL1 and SLC5A3 as risk factors, and CD52, PTPN6, and CLNK as protective factors. The coexistence of risk and protective factors among the prognosis-related genes led us to speculate that MCs of CC may induce the expression of these genes to promote tumor immune evasion and metastasis, exerting immunosuppressive effects. Protective genes were considered associated with a lower disease risk and generally indicative of a better prognosis. These findings suggest that the C2 subgroup may possess the potential to push the prognosis of CC towards either a poor or favorable outcome, serving as a crucial component in the transition between tumor malignancy and benign status, further validating our previous hypotheses. Utilizing external TCGA data, the prognostic significance of MCs infiltration was assessed, uncovering a link between elevated AMRS and reduced OS. Additionally, this finding was confirmed in a group of patients in a clinical setting.

Given the extensive presence of immune cells in the CC microenvironment, we conducted a comparison of this infiltration in different risk assessment categories. The high AMRS group showed elevated levels of immunosuppressive cells, as well as notable variations in matrix scores, immune scores, and ESTIMATE scores when compared to the low AMRS group. Our research indicated that individuals in the low AMRS category may have a higher chance of responding positively to anti-PD-1 treatment. It is worth mentioning that according to the immune checkpoint analysis results, we discovered that the TME of patients in the low AMRS group may contain a greater number of infiltrating T cells that express immune checkpoint-related proteins. Consequently, patients in this group may be more responsive to ICB therapy, whereas the high AMRS group may be resistant or unresponsive to ICB therapy, which is in accordance with our research. Further corroborating previous research, our findings support the conclusion that patients with advanced CC exhibit lower responsiveness to ICB therapy (6, 9). In summary, our comprehensive research findings suggest that C2 ALOX5+ MCs may be associated with the progression and malignant transformation of CC. Targeted studies on this subpopulation could potentially enhance the therapeutic efficacy for CC and pave the way for uncovering new therapeutic targets and mechanisms underlying the disease, thereby offering novel avenues for future intervention and treatment strategies.

Conclusion

Building on the single-cell characteristics of CC, we investigated the heterogeneity within the TME of CC. Further analysis of MCs subgroups identified the distinct presence of the C2 ALOX5+MCs subgroup in CC, suggesting its potential role as a tumor-associated MCs subgroup with transformative effects on immunity and inflammation. Importantly, coupled with CellChat analysis, we discovered that TNFRSF12A may facilitate the growth and migration of CC, a finding corroborated by *in vitro* experiments. These findings may unveil the crucial roles of TNFRSF12A in CC diagnosis, prognosis, and immune function, indicating its potential as a promising predictive marker and therapeutic target in CC patients. Subsequently, we developed a prognostic model to predict

the survival outcomes in CC patients and assessed immune infiltration in different risk groups, offering novel insights for patient prognosis and treatment guidance. However, despite the valuable insights provided by our analysis, the research was limited to a specific group of individuals for validation, which highlights the need for a larger and more diverse clinical sample as well as future prospective studies to ensure wider generalizability. In addition, our samples are derived from public databases, which may have inherent biases or limitations. It is crucial to acknowledge any potential biases associated with these choices and consider their impact on the generalizability of the research findings. Additionally, although our findings were validated *in vitro*, extrapolating these conclusions to the whole organism remains challenging, underscoring the need for *in vivo* experimentation. Finally, the prognostic models employed in our research necessitate refinement. We aim to gather more reliable data in the future to enable more comprehensive and precise investigations.

Data availability statement

The original contributions presented in the study are included in the article/Supplementary Material. Further inquiries can be directed to the corresponding authors.

Author contributions

FZ: Conceptualization, Data curation, Formal analysis, Investigation, Methodology, Project administration, Resources, Software, Validation, Visualization, Writing – original draft, Writing – review & editing. JH: Data curation, Formal analysis, Methodology, Project administration, Writing – review & editing. GZ: Data curation, Formal analysis, Software, Writing – review & editing. TH: Investigation, Writing – review & editing. ZL: Software, Writing – review & editing. YZ: Funding acquisition, Writing – review & editing. LL: Funding acquisition, Supervision, Writing – review & editing. HT: Funding acquisition, Supervision, Writing – review & editing.

Funding

The author(s) declare financial support was received for the research, authorship, and/or publication of this article. This research was supported Zhejiang Provincial Public Welfare Technology Applied Research Program No. LTGY23H160013. This research was supported by Zhejiang Provincial Medicine and Health Science and Technology Program (No. 2023KY071), the Zhejiang Provincial Medical and Health Science and Technology Plan (No. 2021KY574).

Conflict of interest

The authors declare that the research was conducted in the absence of any commercial or financial relationships that could be construed as a potential conflict of interest.

Publisher's note

All claims expressed in this article are solely those of the authors and do not necessarily represent those of their affiliated organizations, or those of the publisher, the editors and the reviewers. Any product that may be evaluated in this article, or claim that may be made by its manufacturer, is not guaranteed or endorsed by the publisher.

Supplementary material

The Supplementary Material for this article can be found online at: https://www.frontiersin.org/articles/10.3389/fimmu.2024.1434450/full#supplementary-material

SUPPLEMENTARY FIGURE 1
The analysis of CNV results. **(A)** Heatmap showed the inferCNV profiles of EPCs using ECs as a reference. The red color indicates copy number increase and the blue color indicates copy number decrease. **(B)** Heatmap showed the inferCNV for each MCs subpopulation using ECs as a reference. The red indicates copy number increase and the blue indicates copy number decrease.

References

1. Singh D, Vignat J, Lorenzoni V, Eslahi M, Ginsburg O, Lauby-Secretan B, et al. Global estimates of incidence and mortality of cervical cancer in 2020: a baseline analysis of the WHO Global Cervical Cancer Elimination Initiative. *Lancet Glob Health*. (2023) 11:e197–206. doi: 10.1016/S2214-109X(22)00501-0

2. Ferlay J, Colombet M, Soerjomataram I, Mathers C, Parkin DM, Pineros M, et al. Estimating the global cancer incidence and mortality in 2018: GLOBOCAN sources and methods. *Int J Cancer*. (2019) 144:1941–53. doi: 10.1002/ijc.31937

3. Abu-Rustum NR, Yashar CM, Arend R, Barber E, Bradley K, Brooks R, et al. NCCN guidelines(R) insights: cervical cancer, version 1.2024. *J Natl Compr Canc Netw*. (2023) 21:1224–33. doi: 10.6004/jnccn.2023.0062

4. Hong JH, Tsai CS, Lai CH, Chang TC, Wang CC, Chou HH, et al. Recurrent squamous cell carcinoma of cervix after definitive radiotherapy. *Int J Radiat Oncol Biol Phys*. (2004) 60:249–57. doi: 10.1016/j.ijrobp.2004.02.044

5. Mileshkin LR, Moore KN, Barnes EH, Gebski V, Narayan K, King MT, et al. Adjuvant chemotherapy following chemoradiotherapy as primary treatment for locally advanced cervical cancer versus chemoradiotherapy alone (OUTBACK): an international, open-label, randomised, phase 3 trial. *Lancet Oncol*. (2023) 24:468–82. doi: 10.1016/S1470-2045(23)00147-X

6. Song Z, Zou K, Zou L. Immune checkpoint blockade for locally advanced or recurrent/metastatic cervical cancer: An update on clinical data. *Front Oncol*. (2022) 12:1045481. doi: 10.3389/fonc.2022.1045481

7. Das S, Babu A, Medha T, Ramanathan G, Mukherjee AG, Wanjari UR, et al. Molecular mechanisms augmenting resistance to current therapies in clinics among cervical cancer patients. *Med Oncol*. (2023) 40:149. doi: 10.1007/s12032-023-01997-9

8. Longoria TC, Tewari KS. Pharmacologic management of advanced cervical cancer: antiangiogenesis therapy and immunotherapeutic considerations. *Drugs*. (2015) 75:1853–65. doi: 10.1007/s40265-015-0481-z

9. Zhou B, Gao Y, Zhang P, Chu Q. Acquired resistance to immune checkpoint blockades: the underlying mechanisms and potential strategies. *Front Immunol*. (2021) 12:693609. doi: 10.3389/fimmu.2021.693609

10. Theoharides TC, Valent P, Akin C. Mast cells, mastocytosis, and related disorders. *N Engl J Med*. (2015) 373:163–72. doi: 10.1056/NEJMra1409760

11. Varricchi G, Galdiero MR, Loffredo S, Marone G, Iannone R, Marone G, et al. Are mast cells MASTers in cancer? *Front Immunol*. (2017) 8:424. doi: 10.3389/fimmu.2017.00424

12. Tuna B, Yorukoglu K, Unlu M, Mungan MU, Kirkali Z. Association of mast cells with microvessel density in renal cell carcinomas. *Eur Urol*. (2006) 50:530–34. doi: 10.1016/j.eururo.2005.12.040

13. Graham RM, Graham JB. Mast cells and cancer of the cervix. *Surg Gynecol Obstet*. (1966) 123:3–09.

14. Cabanillas-Saez A, Schalper JA, Nicovani SM, Rudolph MI. Characterization of mast cells according to their content of tryptase and chymase in normal and neoplastic human uterine cervix. *Int J Gynecol Cancer*. (2002) 12:92–8. doi: 10.1111/ijg.2002.12.issue-1

15. Ma B, Qin L, Sun Z, Wang J, Tran LJ, Zhang J, et al. The single-cell evolution trajectory presented different hypoxia heterogeneity to reveal the carcinogenesis of genes in clear cell renal cell carcinoma: Based on multiple omics and real experimental verification. *Environ Toxicol*. (2024) 39:869–81. doi: 10.1002/tox.24009

16. Song G, Peng G, Zhang J, Song B, Yang J, Xie X, et al. Uncovering the potential role of oxidative stress in the development of periodontitis and establishing a stable diagnostic model *via* combining single-cell and machine learning analysis. *Front Immunol*. (2023) 14:1181467. doi: 10.3389/fimmu.2023.1181467

17. Wang J, Zuo Z, Yu Z, Chen Z, Meng X, Ma Z, et al. Single-cell transcriptome analysis revealing the intratumoral heterogeneity of ccRCC and validation of MT2A in pathogenesis. *Funct Integr Genomics*. (2023) 23:300. doi: 10.1007/s10142-023-01225-7

18. Sun Z, Wang J, Zhang Q, Meng X, Ma Z, Niu J, et al. Coordinating single-cell and bulk RNA-seq in deciphering the intratumoral immune landscape and prognostic stratification of prostate cancer patients. *Environ Toxicol*. (2024) 39:657–68. doi: 10.1002/tox.23928

19. Pfaffenzeller MS, Franciosi M, Cardoso AM. Purinergic signaling and tumor microenvironment in cervical Cancer. *Purinergic Signal*. (2020) 16:123–35. doi: 10.1007/s11302-020-09693-3

20. Xiong J, Chi H, Yang G, Zhao S, Zhang J, Tran LJ, et al. Revolutionizing anti-tumor therapy: unleashing the potential of B cell-derived exosomes. *Front Immunol*. (2023) 14:1188760. doi: 10.3389/fimmu.2023.1188760

21. Meacham CE, Morrison SJ. Tumour heterogeneity and cancer cell plasticity. *Nature*. (2013) 501:328–37. doi: 10.1038/nature12624

22. Li C, Liu D, Yang S, Hua K. Integrated single-cell transcriptome analysis of the tumor ecosystems underlying cervical cancer metastasis. *Front Immunol*. (2022) 13:966291. doi: 10.3389/fimmu.2022.966291

23. Stuart T, Butler A, Hoffman P, Hafemeister C, Papalexi E, Mauck WR, et al. Comprehensive integration of single-cell data. *Cell*. (2019) 177:1888–902. doi: 10.1016/j.cell.2019.05.031

24. McGinnis CS, Murrow LM, Gartner ZJ. DoubletFinder: doublet detection in single-cell RNA sequencing data using artificial nearest neighbors. *Cell Syst*. (2019) 8:329–37. doi: 10.1016/j.cels.2019.03.003

25. Lin Z, Li X, Shi H, Cao R, Zhu L, Dang C, et al. Decoding the tumor microenvironment and molecular mechanism: unraveling cervical cancer subpopulations and prognostic signatures through scRNA-Seq and bulk RNA-seq analyses. *Front Immunol*. (2024) 15:1351287. doi: 10.3389/fimmu.2024.1351287

26. Xing J, Cai H, Lin Z, Zhao L, Xu H, Song Y, et al. Examining the function of macrophage oxidative stress response and immune system in glioblastoma multiforme through analysis of single-cell transcriptomics. *Front Immunol*. (2023) 14:1288137. doi: 10.3389/fimmu.2023.1288137

27. Lin Z, Sui X, Jiao W, Chen C, Zhang X, Zhao J. Mechanism investigation and experiment validation of capsaicin on uterine corpus endometrial carcinoma. *Front Pharmacol*. (2022) 13:953874. doi: 10.3389/fphar.2022.953874

28. Liu P, Xing N, Xiahou Z, Yan J, Lin Z, Zhang J. Unraveling the intricacies of glioblastoma progression and recurrence: insights into the role of NFYB and oxidative phosphorylation at the single-cell level. *Front Immunol*. (2024) 15:1368685. doi: 10.3389/fimmu.2024.1368685

29. Di Z, Zhou S, Xu G, Ren L, Li C, Ding Z, et al. Single-cell and WGCNA uncover a prognostic model and potential oncogenes in colorectal cancer. *Biol Proced Online*. (2022) 24:13. doi: 10.1186/s12575-022-00175-x

30. Korsunsky I, Millard N, Fan J, Slowikowski K, Zhang F, Wei K, et al. Fast, sensitive and accurate integration of single-cell data with Harmony. *Nat Methods*. (2019) 16:1289–96. doi: 10.1038/s41592-019-0619-0

31. Zhou Y, Yang D, Yang Q, Lv X, Huang W, Zhou Z, et al. Single-cell RNA landscape of intratumoral heterogeneity and immunosuppressive microenvironment in advanced osteosarcoma. *Nat Commun*. (2020) 11:6322. doi: 10.1038/s41467-020-20059-6

32. Zhao Z, Luo Q, Liu Y, Jiang K, Zhou L, Dai R, et al. Multi-level integrative analysis of the roles of lncRNAs and differential mRNAs in the progression of chronic pancreatitis to pancreatic ductal adenocarcinoma. *BMC Genomics*. (2023) 24:101. doi: 10.1186/s12864-023-09209-4

33. Ge Q, Zhao Z, Li X, Yang F, Zhang M, Hao Z, et al. Deciphering the suppressive immune microenvironment of prostate cancer based on CD4+ regulatory T cells: Implications for prognosis and therapy prediction. *Clin Transl Med*. (2024) 14:e1552. doi: 10.1002/ctm2.1552

34. Street K, Risso D, Fletcher RB, Das D, Ngai J, Yosef N, et al. Slingshot: cell lineage and pseudotime inference for single-cell transcriptomics. *BMC Genomics*. (2018) 19:477. doi: 10.1186/s12864-018-4772-0

35. Lin Z, Fan W, Yu X, Liu J, Liu P. Research into the mechanism of intervention of SanQi in endometriosis based on network pharmacology and molecular docking technology. *Med (Baltimore)*. (2022) 101:e30021. doi: 10.1097/MD.0000000000030021

36. Yu G, Wang LG, Han Y, He QY. clusterProfiler: an R package for comparing biological themes among gene clusters. *Omics*. (2012) 16:284–87. doi: 10.1089/omi.2011.0118

37. Zhao Z, Li T, Dong X, Wang X, Zhang Z, Zhao C, et al. Untargeted metabolomic profiling of cuprizone-induced demyelination in mouse corpus callosum by UPLC-orbitrap/MS reveals potential metabolic biomarkers of CNS demyelination disorders. *Oxid Med Cell Longev*. (2021) 2021:7093844. doi: 10.1155/2021/7093844

38. Zhao ZJ, Zheng RZ, Wang XJ, Li TQ, Dong XH, Zhao CY, et al. Integrating lipidomics and transcriptomics reveals the crosstalk between oxidative stress and neuroinflammation in central nervous system demyelination. *Front Aging Neurosci*. (2022) 14:870957. doi: 10.3389/fnagi.2022.870957

39. Castanza AS, Recla JM, Eby D, Thorvaldsdottir H, Bult CJ, Mesirov JP. Extending support for mouse data in the Molecular Signatures Database (MSigDB). *Nat Methods*. (2023) 20:1619–20. doi: 10.1038/s41592-023-02014-7

40. Zhu C, Sun Z, Wang J, Meng X, Ma Z, Guo R, et al. Exploring oncogenes for renal clear cell carcinoma based on G protein-coupled receptor-associated genes. *Discovery Oncol*. (2023) 14:182. doi: 10.1007/s12672-023-00795-z

41. Tang C, Deng L, Luo Q, He G. Identification of oxidative stress-related genes and potential mechanisms in atherosclerosis. *Front Genet*. (2022) 13:998954. doi: 10.3389/fgene.2022.998954

42. Jin S, Guerrero-Juarez CF, Zhang L, Chang I, Ramos R, Kuan CH, et al. Inference and analysis of cell-cell communication using CellChat. *Nat Commun*. (2021) 12:1088. doi: 10.1038/s41467-021-21246-9

43. Zhang P, Wu X, Wang D, Zhang M, Zhang B, Zhang Z. Unraveling the role of low-density lipoprotein-related genes in lung adenocarcinoma: Insights into tumor microenvironment and clinical prognosis. *Environ Toxicol*. (2024). doi: 10.1002/tox.24230

44. Ding Y, Zhao Z, Cai H, Zhou Y, Chen H, Bai Y, et al. Single-cell sequencing analysis related to sphingolipid metabolism guides immunotherapy and prognosis of skin cutaneous melanoma. *Front Immunol*. (2023) 14:1304466. doi: 10.3389/fimmu.2023.1304466

45. Zheng R, Zhuang Z, Zhao C, Zhao Z, Yang X, Zhou Y, et al. Chinese admission warning strategy for predicting the hospital discharge outcome in patients with traumatic brain injury. *J Clin Med*. (2022) 11:974. doi: 10.3390/jcm11040974

46. Zhang P, Dong S, Sun W, Zhong W, Xiong J, Gong X, et al. Deciphering Treg cell roles in esophageal squamous cell carcinoma: a comprehensive prognostic and immunotherapeutic analysis. *Front Mol Biosci*. (2023) 10:1277530. doi: 10.3389/fmolb.2023.1277530

47. Lin Z, Sui X, Jiao W, Wang Y, Zhao J. Exploring the mechanism and experimental verification of puerarin in the treatment of endometrial carcinoma based on network pharmacology and bioinformatics analysis. *BMC Complement Med Ther*. (2022) 22:150. doi: 10.1186/s12906-022-03623-z

48. Zhao J, Jiao W, Sui X, Zou J, Wang J, Lin Z. Construction of a prognostic model of luteolin for endometrial carcinoma. *Am J Transl Res*. (2023) 15:2122–39.

49. Nie Q, Qin L, Yan W, Luo Q, Ying T, Wang H, et al. Predictive model of diabetes mellitus in patients with idiopathic inflammatory myopathies. *Front Endocrinol (Lausanne)*. (2023) 14:1118620. doi: 10.3389/fendo.2023.1118620

50. Liang L, Li J, Yu J, Liu J, Xiu L, Zeng J, et al. Establishment and validation of a novel invasion-related gene signature for predicting the prognosis of ovarian cancer. *Cancer Cell Int*. (2022) 22:118. doi: 10.1186/s12935-022-02502-4

51. Lin Z, Zou J, Sui X, Yao S, Lin L, Wang J, et al. Necroptosis-related lncRNA signature predicts prognosis and immune response for cervical squamous cell carcinoma and endocervical adenocarcinomas. *Sci Rep*. (2022) 12:16285. doi: 10.1038/s41598-022-20858-5

52. Zhao J, Zou J, Jiao W, Lin L, Wang J, Lin Z. Construction of N-7 methylguanine-related mRNA prognostic model in uterine corpus endometrial carcinoma based on multi-omics data and immune-related analysis. *Sci Rep*. (2022) 12:18813. doi: 10.1038/s41598-022-22879-6

53. Zou J, Lin Z, Jiao W, Chen J, Lin L, Zhang F, et al. A multi-omics-based investigation of the prognostic and immunological impact of necroptosis-related mRNA in patients with cervical squamous carcinoma and adenocarcinoma. *Sci Rep*. (2022) 12:16773. doi: 10.1038/s41598-022-20566-0

54. Jiang H, Yu D, Yang P, Guo R, Kong M, Gao Y, et al. Revealing the transcriptional heterogeneity of organ-specific metastasis in human gastric cancer using single-cell RNA Sequencing. *Clin Transl Med*. (2022) 12:e730. doi: 10.1002/ctm2.730

55. Lin Z, Fan W, Sui X, Wang J, Zhao J. Necroptosis-related lncRNA signatures for prognostic prediction in uterine corpora endometrial cancer. *Reprod Sci*. (2023) 30:576–89. doi: 10.1007/s43032-022-01023-9

56. Wang Y, Zhao ZJ, Kang XR, Bian T, Shen ZM, Jiang Y, et al. lncRNA DLEU2 acts as a miR-181a sponge to regulate SEPP1 and inhibit skeletal muscle differentiation and regeneration. *Aging (Albany Ny)*. (2020) 12:24033–56. doi: 10.18632/aging.v12i23

57. Zhao ZJ, Chen D, Zhou LY, Sun ZL, Wang BC, Feng DF. Prognostic value of different computed tomography scoring systems in patients with severe traumatic brain injury undergoing decompressive craniectomy. *J Comput Assist Tomogr*. (2022) 46:800–07. doi: 10.1097/RCT.0000000000001343

58. Zhao ZJ, Wei DP, Zheng RZ, Peng T, Xiao X, Li FS. The gene coexpression analysis identifies functional modules dynamically changed after traumatic brain injury. *Comput Math Methods Med*. (2021) 2021:5511598. doi: 10.1155/2021/5511598

59. Zheng RZ, Zhao ZJ, Yang XT, Jiang SW, Li YD, Li WJ, et al. Initial CT-based radiomics nomogram for predicting in-hospital mortality in patients with traumatic brain injury: a multicenter development and validation study. *Neurol Sci*. (2022) 43:4363–72. doi: 10.1007/s10072-022-05954-8

60. Newman AM, Liu CL, Green MR, Gentles AJ, Feng W, Xu Y, et al. Robust enumeration of cell subsets from tissue expression profiles. *Nat Methods*. (2015) 12:453–57. doi: 10.1038/nmeth.3337

61. Chi H, Gao X, Xia Z, Yu W, Yin X, Pan Y, et al. FAM family gene prediction model reveals heterogeneity, stemness and immune microenvironment of UCEC. *Front Mol Biosci*. (2023) 10:1200335. doi: 10.3389/fmolb.2023.1200335

62. Zhang P, Pei S, Zhou G, Zhang M, Zhang L, Zhang Z. Purine metabolism in lung adenocarcinoma: A single-cell analysis revealing prognostic and immunotherapeutic insights. *J Cell Mol Med*. (2024) 28:e18284. doi: 10.1111/jcmm.18284

63. Zhang P, Zhang H, Tang J, Ren Q, Zhang J, Chi H, et al. The integrated single-cell analysis developed an immunogenic cell death signature to predict lung adenocarcinoma prognosis and immunotherapy. *Aging (Albany Ny)*. (2023) 15:10305–29. doi: 10.18632/aging.v15i19

64. Sun W, Shen J, Liu J, Han K, Liang L, Gao Y. Gene signature and prognostic value of ubiquitin-specific proteases members in hepatocellular carcinoma and explored the immunological role of USP36. *Front Biosci (Landmark Ed)*. (2022) 27:190. doi: 10.31083/j.fbl2706190

65. Zhang L, Cui Y, Mei J, Zhang Z, Zhang P. Exploring cellular diversity in lung adenocarcinoma epithelium: Advancing prognostic methods and immunotherapeutic strategies. *Cell Prolif*. (2024):e13703. doi: 10.1111/cpr.13703

66. Yang H, Li Z, Zhu S, Wang W, Zhang J, Zhao D, et al. Molecular mechanisms of pancreatic cancer liver metastasis: the role of PAK2. *Front Immunol*. (2024) 15:1347683. doi: 10.3389/fimmu.2024.1347683

67. Li Y, Hu J, Wang M, Yuan Y, Zhou F, Zhao H, et al. Exosomal circPABPC1 promotes colorectal cancer liver metastases by regulating HMGA2 in the nucleus and BMP4/ADAM19 in the cytoplasm. *Cell Death Discovery*. (2022) 8:335. doi: 10.1038/s41420-022-01124-z

68. Zhao Z, Ding Y, Tran LJ, Chai G, Lin L. Innovative breakthroughs facilitated by single-cell multi-omics: manipulating natural killer cell functionality correlates with a novel subcategory of melanoma cells. *Front Immunol*. (2023) 14:1196892. doi: 10.3389/fimmu.2023.1196892

69. Cordido A, Nunez-Gonzalez L, Martinez-Moreno JM, Lamas-Gonzalez O, Rodriguez-Osorio L, Perez-Gomez MV, et al. TWEAK signaling pathway blockade slows cyst growth and disease progression in autosomal dominant polycystic kidney disease. *J Am Soc Nephrol*. (2021) 32:1913–32. doi: 10.1681/ASN.2020071094

70. Gupta RK, Miller J, Croft M. TNF-like weak inducer of apoptosis inhibition is comparable to IL-13 blockade in ameliorating atopic dermatitis inflammation. *Allergy*. (2024) 79:116–27. doi: 10.1111/all.15879

71. Wiley SR, Winkles JA. TWEAK, a member of the TNF superfamily, is a multifunctional cytokine that binds the TweakR/Fn14 receptor. *Cytokine Growth Factor Rev*. (2003) 14:241–49. doi: 10.1016/S1359-6101(03)00019-4

72. Fabris L, Cadamuro M, Fouassier L. Illuminate TWEAK/Fn14 pathway in intrahepatic cholangiocarcinoma: Another brick in the wall of tumor niche. *J Hepatol*. (2021) 74:771–74. doi: 10.1016/j.jhep.2020.12.019

73. Wei J, Li X, Xiang L, Song Y, Liu Y, Jiang Y, et al. Metabolomics and lipidomics study unveils the impact of polybrominated diphenyl ether-47 on breast cancer mice. *J Hazard Mater*. (2020) 390:121451. doi: 10.1016/j.jhazmat.2019.121451

74. Lei Y, Tang R, Xu J, Wang W, Zhang B, Liu J, et al. Applications of single-cell sequencing in cancer research: progress and perspectives. *J Hematol Oncol*. (2021) 14:91. doi: 10.1186/s13045-021-01105-2

75. Kumar V, Ramnarayanan K, Sundar R, Padmanabhan N, Srivastava S, Koiwa M, et al. Single-cell atlas of lineage states, tumor microenvironment, and subtype-specific expression programs in gastric cancer. *Cancer Discovery*. (2022) 12:670–91. doi: 10.1158/2159-8290.CD-21-0683

76. Puram SV, Tirosh I, Parikh AS, Patel AP, Yizhak K, Gillespie S, et al. Single-cell transcriptomic analysis of primary and metastatic tumor ecosystems in head and neck cancer. *Cell*. (2017) 171:1611–24. doi: 10.1016/j.cell.2017.10.044

77. Wu F, Fan J, He Y, Xiong A, Yu J, Li Y, et al. Single-cell profiling of tumor heterogeneity and the microenvironment in advanced non-small cell lung cancer. *Nat Commun*. (2021) 12:2540. doi: 10.1038/s41467-021-22801-0

78. Komi D, Redegeld FA. Role of mast cells in shaping the tumor microenvironment. *Clin Rev Allergy Immunol*. (2020) 58:313–25. doi: 10.1007/s12016-019-08753-w

79. Mei Y, Jiang P, Shen N, Fu S, Zhang J. Identification of miRNA-mRNA regulatory network and construction of prognostic signature in cervical cancer. *DNA Cell Biol*. (2020) 39:1023–40. doi: 10.1089/dna.2020.5452

80. Rudolph MI, Boza Y, Yefi R, Luza S, Andrews E, Penissi A, et al. The influence of mast cell mediators on migration of SW756 cervical carcinoma cells. *J Pharmacol Sci*. (2008) 106:208–18. doi: 10.1254/jphs.FP0070736

81. Marbach-Breitruck E, Rohwer N, Infante-Duarte C, Romero-Suarez S, Labuz D, Machelska H, et al. Knock-in mice expressing a 15-lipoxygenating Alox5 mutant respond differently to experimental inflammation than reported Alox5(-/-) mice. *Metabolites*. (2021) 11:698. doi: 10.3390/metabo11100698

82. Wang Y, Wang W, Sanidad KZ, Shih PA, Zhao X, Zhang G. Eicosanoid signaling in carcinogenesis of colorectal cancer. *Cancer Metastasis Rev*. (2018) 37:257–67. doi: 10.1007/s10555-018-9739-8

83. Yarla NS, Bishayee A, Sethi G, Reddanna P, Kalle AM, Dhananjaya BL, et al. Targeting arachidonic acid pathway by natural products for cancer prevention and therapy. *Semin Cancer Biol*. (2016) 40-41:48–81. doi: 10.1016/j.semcancer.2016.02.001

84. Banushi B, Joseph SR, Lum B, Lee JJ, Simpson F. Endocytosis in cancer and cancer therapy. *Nat Rev Cancer*. (2023) 23:450–73. doi: 10.1038/s41568-023-00574-6

85. Brena D, Huang MB, Bond V. Extracellular vesicle-mediated transport: Reprogramming a tumor microenvironment conducive with breast cancer progression and metastasis. *Transl Oncol*. (2022) 15:101286. doi: 10.1016/j.tranon.2021.101286

86. Kagi D, Ledermann B, Burki K, Zinkernagel RM , Hengartner H. Molecular mechanisms of lymphocyte-mediated cytotoxicity and their role in immunological protection and pathogenesis *in vivo*. *Annu Rev Immunol*. (1996) 14:207–32. doi: 10.1146/annurev.immunol.14.1.207

87. Xia L, Oyang L, Lin J, Tan S, Han Y, Wu N, et al. The cancer metabolic reprogramming and immune response. *Mol Cancer*. (2021) 20:28. doi: 10.1186/s12943-021-01316-8

88. Chicheportiche Y, Bourdon PR, Xu H, Hsu YM, Scott H, Hession C, et al. TWEAK, a new secreted ligand in the tumor necrosis factor family that weakly induces apoptosis. *J Biol Chem*. (1997) 272:32401–10. doi: 10.1074/jbc.272.51.32401

89. Johnston AJ, Murphy KT, Jenkinson L, Laine D, Emmrich K, Faou P, et al. Targeting of Fn14 prevents cancer-induced cachexia and prolongs survival. *Cell*. (2015) 162:1365–78. doi: 10.1016/j.cell.2015.08.031

frontiers | Frontiers in Immunology

TYPE Original Research
PUBLISHED 12 September 2024
DOI 10.3389/fimmu.2024.1460308

Check for updates

OPEN ACCESS

EDITED BY
Pengpeng Zhang,
Nanjing Medical University, China

REVIEWED BY
Xin Yu,
Baylor College of Medicine, United States
Kan Li,
Rutgers, The State University of New Jersey, United States
Yuquan Chen,
Monash University, Australia

*CORRESPONDENCE
Ke Xu
cqghxuke@cqu.edu.cn
Shangke Huang
huangshangke001@swmu.edu.cn
Jie Liu
123574514@qq.com

†These authors have contributed equally to this work

RECEIVED 05 July 2024
ACCEPTED 27 August 2024
PUBLISHED 12 September 2024

CITATION
Wang L, Zhou X, Yan H, Miao Y, Wang B, Gu Y, Fan W, Xu K, Huang S and Liu J (2024) Deciphering the role of tryptophan metabolism-associated genes ECHS1 and ALDH2 in gastric cancer: implications for tumor immunity and personalized therapy. *Front. Immunol.* 15:1460308. doi: 10.3389/fimmu.2024.1460308

COPYRIGHT
© 2024 Wang, Zhou, Yan, Miao, Wang, Gu, Fan, Xu, Huang and Liu. This is an open-access article distributed under the terms of the Creative Commons Attribution License (CC BY). The use, distribution or reproduction in other forums is permitted, provided the original author(s) and the copyright owner(s) are credited and that the original publication in this journal is cited, in accordance with accepted academic practice. No use, distribution or reproduction is permitted which does not comply with these terms.

Deciphering the role of tryptophan metabolism-associated genes ECHS1 and ALDH2 in gastric cancer: implications for tumor immunity and personalized therapy

Lexin Wang[1,2†], Xue Zhou[3†], Haisheng Yan[1,2†], Yaping Miao[1,2†], Binbin Wang[4], Yuheng Gu[3], Weining Fan[1,2], Ke Xu[5*], Shangke Huang[3*] and Jie Liu[6*]

[1]General Hospital of Ningxia Medical University, Department of Clinical Medicine, Yinchuan, Ningxia, China, [2]Ningxia Medical University, Department of Clinical Medicine, Yinchuan, Ningxia, China, [3]Department of Oncology, The Affiliated Hospital of Southwest Medical University, Luzhou, China, [4]Intensive Care Unit, Xichong People's Hospital, Nanchong, China, [5]Department of Oncology, Chongqing General Hospital, Chongqing University, Chongqing, China, [6]Department of General Surgery, Dazhou Central Hospital, Dazhou, China

Background: Tryptophan Metabolism-associated Genes (TMGs), such as ECHS1 and ALDH2, are crucial in cancer progression through immunosuppressive mechanisms, particularly in Gastric Cancer (GC). This study explores their effects on the Tumor Microenvironment (TME). Additionally, it examines their potential as novel immunotherapy targets.

Methods: We utilized single-cell and bulk transcriptomic technologies to analyze the heterogeneity of GC. Non-negative Matrix Factorization (NMF) clustering identified key TMGs, and extensive RNA-seq analyses were performed to pinpoint prognostic genes and potential immunotherapy targets. Furthermore, through PCR analyses we found that ECHS1 and ALDH2 gene expression plays a regulatory role in the migration, invasion and inflammatory factor in AGS and SNU-1 cell lines. The interference effect of si-ECHS1 and ad-ALDH2 was validated using cell scratch assay in AGS and SNU-1 cell line.

Results: We observed a statistically significant correlation between ECHS1 and ALDH2 expression and increased TME heterogeneity. Our findings also revealed that ECHS1 down-regulation and ALDH2 up-regulation contribute to reduced TME heterogeneity, decreased inflammation, and inhibited AGS and SNU-1 tumor cells migration and proliferation. GSVA enrichment analysis highlighted the NF-kappa B(NF-κB) signaling pathway as specifically regulated by TMGs. Furthermore,ECHS1 and ALDH2 modulated CD8+ and CD4+ T cell activities, impacting GC progression. *In vitro* experiments further solidified our conclusions by showcasing the inhibitory effects of Si-ECHS1 and ad-ALDH2 on the invasive and proliferative capabilities of AGS and SNU-1 cells. Moreover, Si-ECHS1 and ad-ALDH2 gene expression effectively reduced the expression of inflammatory factors IL-10,IL-7,CXCL8 and IL-6, leading to a remarkable alleviation of chronic inflammation and the heterogeneous nature of the TME.

Conclusion: This research highlights the importance of ECHS1 and ALDH2 in GC progression and immune modulation, suggesting that targeted therapies focusing on these genes offer promising avenues for personalized immunotherapy in GC. These findings hold potential for improving patient survival and quality of life. Future studies on the NF-κB signaling pathway's role in this context are warranted to further elucidate the mechanisms underlying TMG-mediated immune modulation in GC.

KEYWORDS

gastric cancer (GC), tryptophan metabolism-associated genes (TMGs), tumor microenvironment (TME), ALDH2, ECHS1

1 Introduction

GC is widely recognized as a major type of cancer that contributes to cancer-related deaths globally, with an increasing incidence each year (1–3). It ranks second in morbidity and mortality rates, trailing only behind lung cancer. Alarmingly, over 80% of patients are diagnosed with an advanced GC during initial treatment (4). Recent research underscores the critical role of understanding the TME in advancing immunotherapy for GC. Additionally, disruptions in the TME have been linked to alterations in immune responses and tryptophan metabolism (5). However, an abnormality in tryptophan metabolism leads to accelerated progression of GC and decreased patient survival (6–9). Hence, elucidating the interplay between tryptophan metabolism and the TME in GC is imperative. Studies published recently have shown that tumor cells can sustain cell proliferation and progression by adapting to the regulation of metabolic patterns to obtain essential nutrients from a nutrient-deficient environment. Furthermore, these cells can modify the tumor immune microenvironment (TIME) (10–13).

Tryptophan metabolism plays a crucial role in tumor cell activities and significantly regulates protein synthesis during cell proliferation. Emerging evidence supports that cancer, neurodegenerative disease, inflammatory bowel disease, and cardiovascular disease are significantly associated with the regulation of tryptophan metabolism (14–17). Recent research has shown that tryptophan metabolism, as an important nutrient *in vivo*, plays a significant role in the development of cancer due to its disorder. This is especially evident in cases of abnormal energy metabolism and nutrient provision (18). In breast cancer, we found that disordered tryptophan metabolism increases the tumor immune microenvironment (19). Additionally, tryptophan metabolism is primarily regulated by three rate-limiting enzymes: kynurenine monooxygenase (KMO), indoleamine 2,3-dioxygenase (IDO), and tryptophan 2,3-dioxygenase (TDO). These key regulatory enzymes offer therapeutic targets for several diseases, including tumors, shedding new light on disease treatment strategies. The metabolism of tryptophan also involves the kynuridine, 5-hydroxytryptamine, and indole pathways (20). This indicates that tryptophan metabolism pathways could potentially be key to inhibiting tumor growth. Studies have highlighted the significant role of tryptophan metabolism-related gene IDO2 in tumor progression and the immune response against tumors by influencing crucial metabolic pathways. However, the specific regulatory role of tryptophan metabolism in GC has not been thoroughly documented, and its role in the development of GC has not been reported.

As the bioinformatics technology constantly updated, it is a new breakthrough to explore the regulatory mechanism of TME in GC. RNA sequencing and single-cell transcriptome technology can well reveal the complex relationship between TME and GC, especially the discovery of cell communication and the regulation of transcription factors. For example, we also found the expression and function of ECHS1 and ALDH2 genes by bioinformatics technology.

The ECHS1 and ALDH2 genes are key members of the tryptophan metabolism family. In most cancers, the expression of ECHS1 is upregulated, including in non–small cell lung cancer, pancreatic cancer, and colon cancer (21–23). The expression of ECHS1 is correlated with lipid metabolism and metastasis. Additionally, we found that decreased expression of ALDH2 plays an important role in the activation of hepatocellular carcinoma carcinogenic pathways (24–26). It is particularly interesting that we have identified a crucial protein, ECHS1 and ALDH2, involved in regulating these genes, which is abnormally expressed in epithelial cells of GC, thereby accelerating epithelial carcinogenesis. However, there is still limited research on the role of TMGs in GC. The regulation of tryptophan metabolism could impact the progression of GC. Our study indicates that TMGs contribute to increasing heterogeneity in the TME of GC and enhance cell proliferation and invasion abilities. Moving forward, our research will focus on treating tryptophan metabolism as a strategy to mitigate the influence of the TME in GC.

2 Methods

2.1 Analysis of GEO and TCGA database progression

In our study, we targeted GC patients and healthy individuals as research subjects, utilizing data from the TCGA databases (https://www.cancer.gov/ccg/research/genome-sequencing/tcga) and GEO databases (https://www.ncbi.nlm.nih.gov/gds/). Specifically, we have focused on datasets of TCGA-STAD, GSE79973, GSE62254, GSE54129, GSE34942 and GSE5118986 for GC.

2.2 scRNA-seq data processing

For single-cell RNA sequencing (scRNA-seq) analysis, we obtained the 10× scRNA-seq dataset GSE163558 from the GEO database. We utilized "Seurat4.0" R package to integrate all samples. Quality control (QC) filters were applied using the following parameters, similar to what has been reported:(1) cells with <200 genes were excluded; and (2) cells with >30% mitochondrial RNA reads were excluded. Following normalization using the "LogNormalize" method, we conducted principal component analysis (PCA) on the top 2500 genes and applied uniform manifold approximation and projection (UMAP) for visualizing cell distribution (27, 28). Cell type identification was performed using specific gene markers. Subsequently, we used the "CellChat"R package for cell-cell communication analysis and network visualization. Subsequently, we identified markers to classify GC cell subsets for future analysis.

2.3 NMF classification of GC patients cluster in scRNA-seq

Non-negative matrix factorization (NMF) was carried to divide patients into different subtypes according to the following steps: 1) the univariate Cox regression analysis was performed to identify potential prognostic EDGs (P<0.05, logFC>1); 2) Performing sample clustering using the SNMF/R method was suitable for sparse data in scRNA-seq. This can be achieved using the "NMF" package.

2.4 Survival analysis

The effect of ECHS1 expression on the prognosis of GC patients was analyzed. This was conducted using the Kaplan-Meier plotter, a tool for the meta-analysis-based validation and discovery of biomarkers correlated with survival.

2.5 Identification of genes associated with TMGs

Two machine learning algorithms, Random Forest (RF) and Support Vector Machine Recursive Feature Elimination (SVM-RFE), were used to identify important biomarkers in tryptophan metabolism. The "randomForest" R package in R was used to implement the Random Forest technique. The validation set, used to fully analyze the utility of the identified biomarkers, was obtained from the GSE79973 dataset. Subsequently, the prediction ability of the algorithms was evaluated based on Receiver Operating Characteristic (ROC) curve analysis, and the area under the curve (AUC) was calculated.

2.6 Cell culture

AGS and SNU-1 cells, both sourced from Beijing, China, were cultured in a medium containing 10% FBS (fetal bovine serum) from Gibco, USA, at 37°C in a 5% CO2 atmosphere. After, we performed transfections with si-ECHS1 and ad-ALDH2, dividing the cells into distinct groups.

2.7 The expression of ALDH2 and ECHS1 by qRT-PCR in AGS and SNU-1 cells

Total RNA was extracted from AGS and SNU-1 cells using an RNA extraction kit provided by Aibotek Biotechnology Company, Wuhan. Subsequently, the mRNA expression levels were determined using primers. (Species of Human Origin) IL7 Forward Primer: TTGGACTTCCTCCCCTGATCC, reverse primer TCGATGCTGACCATTATAACAC; (Species of Human Origin) IL10 Forward Primer: GACTTTAAGGGTTACCTG GGTTG,Reverse Primer: TCACATGCGCCTTGATGTCTG; (Species of Human Origin) IL6 Forward Primer: TAGTCCTTC CTACCCCAATTTCC,Reverse Primer: TTGGTCCTTAGCCACT CCTTC; (Species of Human Origin) ECHS1 Forward Primer: CT GTTACTCCAGCAAGTTCT,Reverse Primer: TCACACATCATG GCAAGCTCA; (Species of Human Origin) CXCL8 Forward Primer: ACTGAGAGTGATTGAGAGTGGAC, Reverse Primer: AACCCTCTGCACCCAGTTTTC;(Species of Human Origin) ALDH2 Forward Primer: GGAATTTCCCGCTCCTGATG, Reverse Primer: CACATAGAGGGCGGTGAGG For reverse transcription of RNA into cDNA, we utilized the RNA reverse transcription kit from TaKaRa, Japan. At last, PCR signals $2^{-\Delta\Delta Ct}$ was used to calculate the expression of genes mRNA levels.

2.8 Tryptophan metabolism expression level

Tryptophan metabolism detection Assay following steps: 1) Add a certain dilution of the sample to be tested, 100 μ Incubate at 37°C for 1 hour in the reaction wells already coated; 2) Add fresh diluted calibration sample (diluted according to the instructions) to each reaction well for 100% μ L. Incubate at 37°C for 0.5-1 hour and wash three times; 3) Finally, add substrate solution to each reaction well for color development μ L. 37°C for 10-30 minutes. Within 30 minutes, measure cells tryptophan metabolism expression level, based on the absorbance value at 450nm to calculate the OD value.

2.9 SiRNA and adRNA transfection

Gene knockdown and overexpression fragment were carried out using the HiPerFect Transfection kit (Qiagen, Germany). AGS and SNU-1 cells were transfected with 5 nM si-ECHS1 and ad-ALDH2 following the protocol of manufacturer, and cells transfected with irrelevant non-targeting siRNA and adRNA, or were treated with sham transfection were used as negative control. The cells were cultured for another 24 h after transfection, and gene knockdown efficiency was measured by qRT-PCR.

2.10 Cell scratch

Seed AGS and SNU-1 cells onto the bottom of a six-well plate and mark scratch lines to create wounds. Remove the old culture medium and divide the cells into two groups: si-NC, ad-NC (negative control) and si-ECHS1 and ad-ALDH2. Place the plate in a 37°C, 5% CO2 cell culture incubator. At specified time points such as 0 hours and 48 hours, remove the cells from the plate and observe the width of the scratch at the same position under a microscope, taking pictures. Finally, use Image J software to analyze the distance of cell migration and the area of the scratch.

2.11 Statistical analysis

All data processing and statistical analysis were conducted using R software version 3.6.1 and GraphPad Prism. Student's t-test and One-way analysis of variance (ANOVA) were used to determine differences between groups, and a p-value<0.05 indicated statistical significance.

3 Results

3.1 The expression of TMGs entirety landscape in GC

The expression patterns of TMGs have been observed across a spectrum of cancer types. To delve deeper into the differential expression of TMGs in GC, we utilized scRNA-seq data from GSE163558, encompassing 3 GC patients and 1 normal individual. This analysis facilitated the identification of nine distinct cell clusters within the TME based on markers. Including T cells, monocytes, B cells, macrophages, plasma cells, epithelial cells, fibroblasts, mast cells, and stromal cells (Figures 1A, B). The transformation of epithelial cells is a pivotal element in the progression of advanced GC, with a particular emphasis on tryptophan metabolism. After isolating tumor cells, we performed comprehensive cell communication analysis and identified a robust correlation between GC epithelial cells and macrophages. This observation suggests the presence of extensive cross-talk and interactions between macrophages and epithelial cells within the TME (Figure 1C). Subsequently, we conducted a comprehensive analysis of the gene expression profiles of TMGs, and observed that STAT1, ALDH2, and ECHS1 were highly expressed in GC epithelial cells (Figure 1D).

3.2 Heterogeneity of tumor microenvironment in GC

To enhance our comprehension of the TME in GC, we discovered that each cell type manifests distinct receptor-ligand interactions, with epithelial cells notably prominent (Figure 2A). Epithelial cells are pivotal in dictating the intensity of outgoing interactions and are influenced by other cell types, which induces a shift from intracellular to extracellular functions. These interacting cell types encompass T cells, monocytes, B cells, macrophages, epithelial cells, fibroblasts, mast cells, and stromal cells (Figure 2B). Our analysis disclosed that HLA-A ligands, acting as crucial intermediaries, display differential expression patterns across various cell types within the TME, significantly impacting the regulation of epithelial cells (Figure 2C). Notably, the transcription factors FOXF1 and ZNF384 are implicated in the regulation of epithelial cell carcinogenesis at the protein transcription and translation levels (Figure 2D). Consequently, HLA-A ligands, through the modulation by FOXF1 and ZNF384, may facilitate the increased heterogeneity of the TME in GC.

3.3 Identification of key TMGs in GC

Our analysis revealed that TMGs are prominently expressed during the middle and late stages of GC, specifically STAT1, ALDH2, and ECHS1 (Figure 3A). We identified two distinct types of epithelial cells, designated as Epi-1 and Epi-2. Subsequently, a deeper examination of Epi-2 cells indicated that three genes, STAT1, ALDH2, and ECHS1, could be discerned through Non-negative Matrix Factorization (NMF) analysis (Figure 3B). By tSNE visualization of TMGs-related genes,STAT1, ALDH2, and ECHS1, we found that it were widely expressed GC epithelial cell (Figure 3C). Furthermore, KEGG enrichment analysis underscored the NF-κB signaling pathway as critically important for the progression of GC (the blue color represents the positive correlation enrichment) (Figure 3D). Additionally, metabolic analysis observed that the TMGs, STAT1, ALDH2, and ECHS1, were significantly enriched in pathways such as the TCA cycle, Glyoxylate and dicarboxylate metabolism, Pentose phosphate pathway, and tryptophan metabolism (red means highly enriched). This implies that the TMGs, STAT1, ALDH2, and ECHS1, could influence the TCA cycle and contribute to the reprogramming of energy metabolism via the NF-κB signaling pathways (Figure 3E).

3.4 The differential expression of TMGs in GC transcriptome

To corroborate our earlier findings, we examined the differential expression of TMGs ALDH2 and ECHS1 in the GC transcriptome, utilizing datasets from GSE79973 (Figure 4A). A subsequent

10.3389/fimmu.2024.1460308

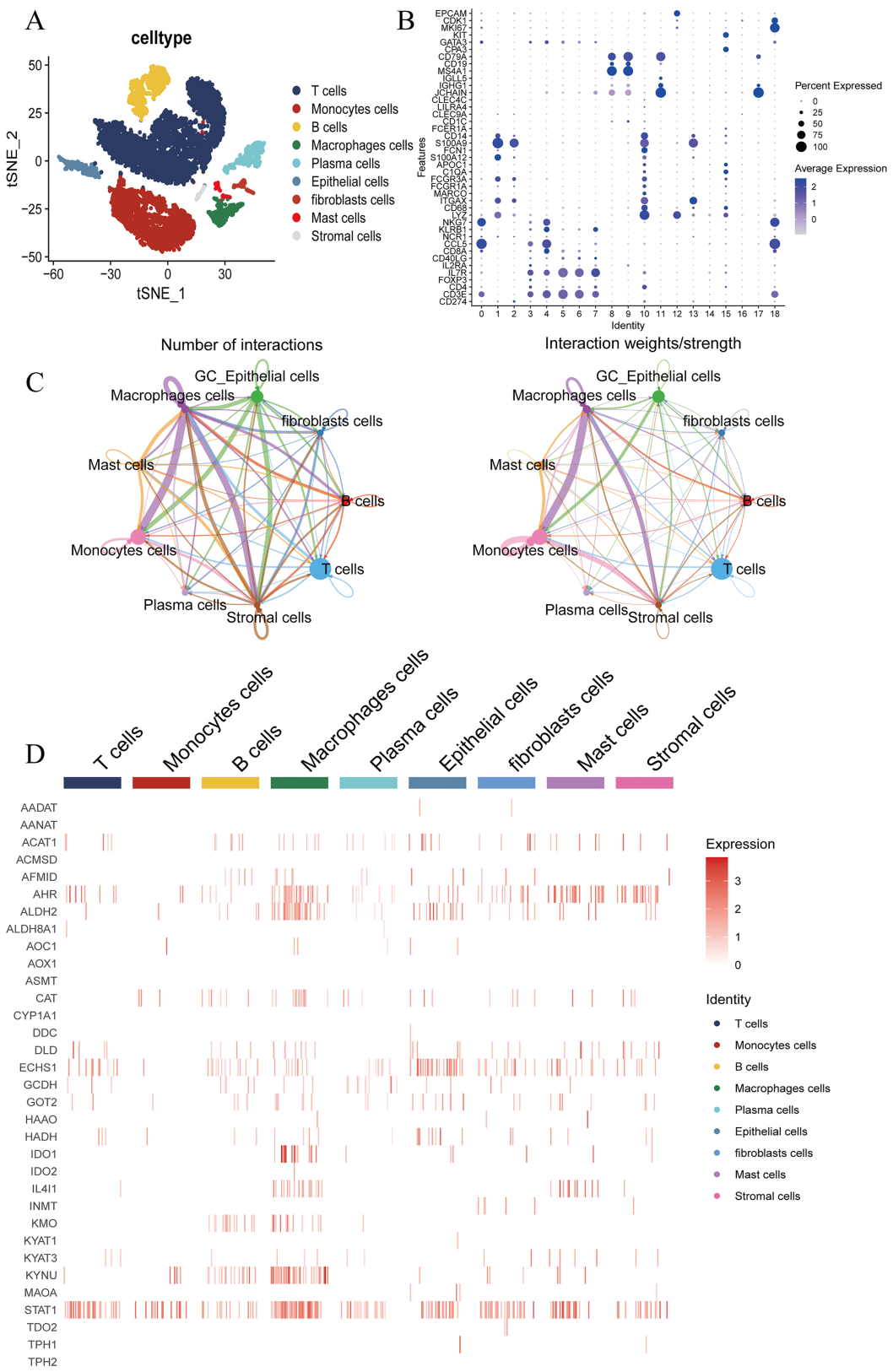

FIGURE 1
ScRNA-seq analysis of GC and normal groups. **(A, B)** Identification of TME cells type expression in GC including T cells, Monocytes cells, B cells, Macrophages cells, Plasma cells, Epithelial cells, Fibroblasts cells, Mast cells and Stromal cells in GSE163558. **(C)** The network diagram illustrates the interaction of key cell types in the GC. Each point represents a cell cluster, with the size of the point indicating the weight of that cluster in the network. The thickness of each line corresponds to its strength. **(D)** The expression of tryptophan metabolism family genes in key cell type of GC.

10.3389/fimmu.2024.1460308

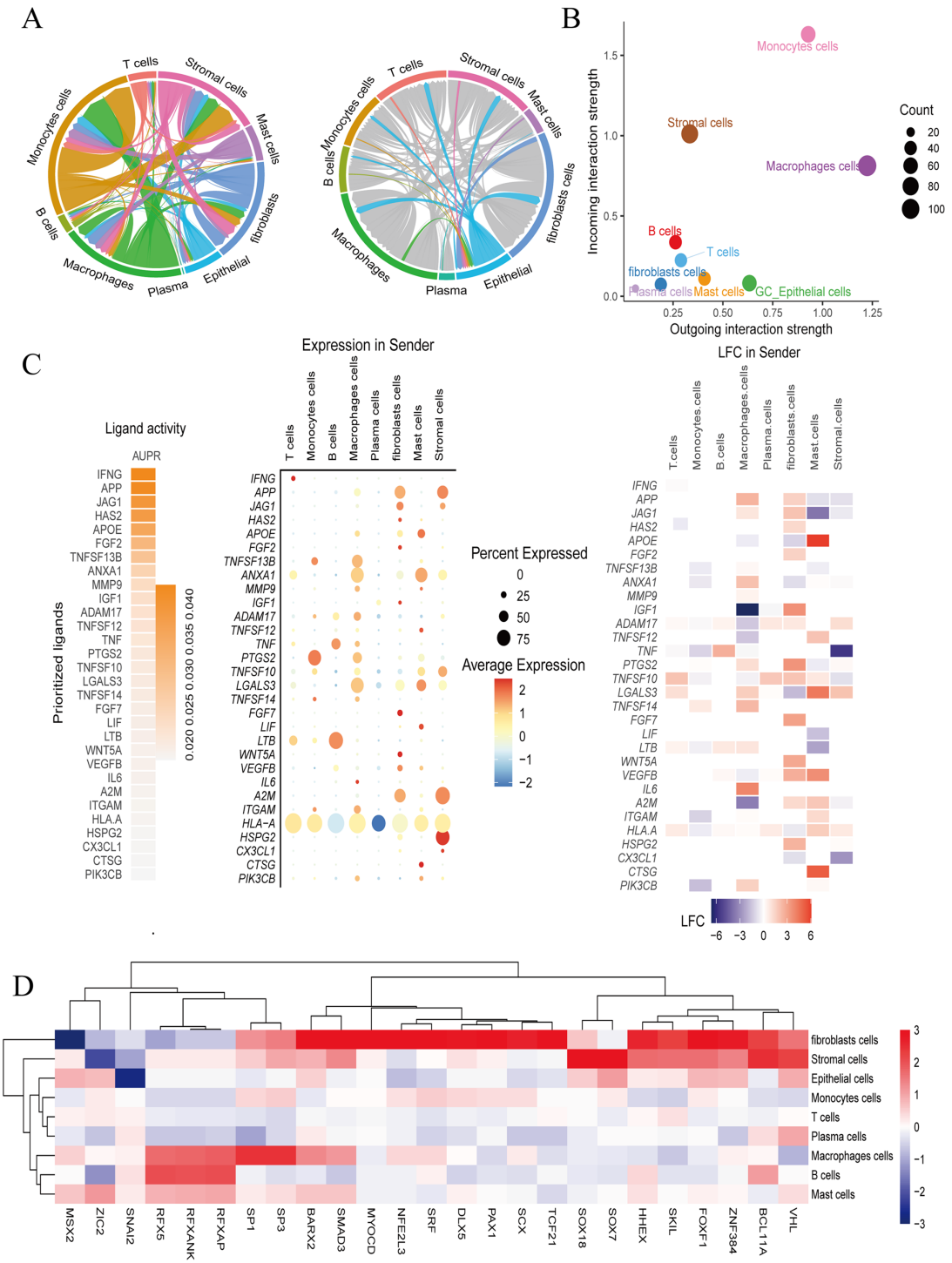

FIGURE 2
HLA-A ligands mediate a stronger tumor microenvironment regulated by FOXF1 and ZNF384. **(A, B)** The different expression of receptor-ligand in cell type. **(C)** The expression and function of HLA-A ligands in relation to the receptor on epithelial cells. Red indicates positive regulation, blue indicates negative regulation, and gray has no regulatory significance. **(D)** The expression of transcription factors varies among cell types. Red indicates positive regulation, blue indicates negative regulation, and gray has no regulatory significance.

correlation analysis between these genes in normal and GC tissues showed a robust correlation for the ECHS1 gene in tumor tissues, which was in stark contrast to the weak correlation observed in normal tissues. Conversely, the ALDH2 gene exhibited the opposite pattern (Figure 4B). We utilized the SVM-RFE technique to develop a machine learning algorithm model, evaluating its predictive accuracy. The model exhibited a high degree of accuracy in predicting GC, with an AUC of 0.950 at a minimum error value of 19 (Figures 4C, D). Furthermore, the calibration curve provided additional validation of the model's precision (Figure 4E).

10.3389/fimmu.2024.1460308

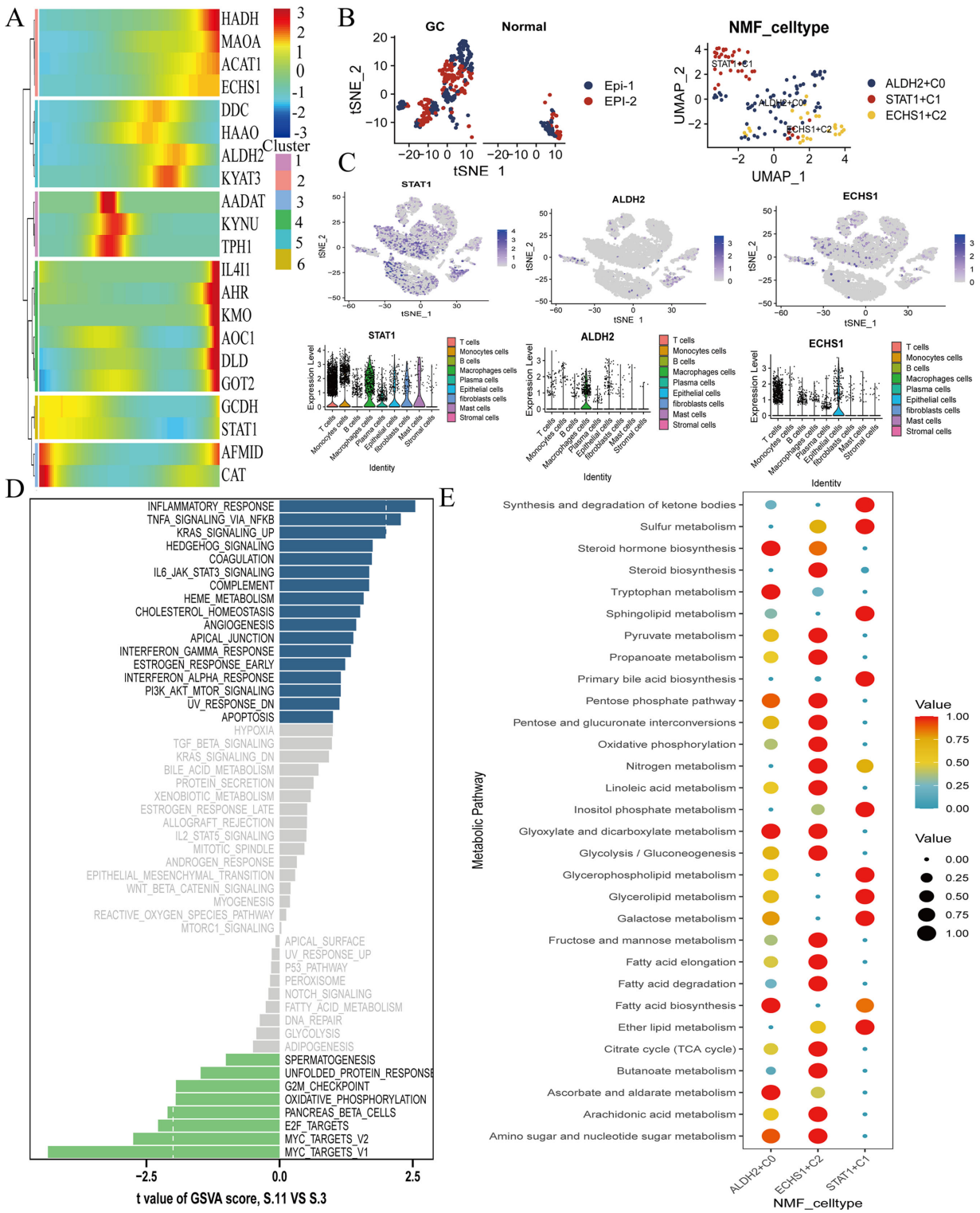

FIGURE 3
Identification of key tryptophan metabolism genes expression in GC. **(A)** The pseudo-time analysis the expression of TMGs-related genes, red indicates high expression and blue indicates low expression. **(B)**The process of extracting and visualizing epithelial cells through reclustering, which led to the identification of two distinct groups of epithelial cells, with epi-2 constituting the majority. The genes STAT1, ALDH2, and ECHS1 were specifically found to be expressed in the epi-2 group, as determined by NMF analysis. **(C)** The tSNE visualization displays the expression levels of STAT1, ALDH2, and ECHS1. **(D)** GSVA analysis highlights critical pathways in GC. **(E)**The tryptophan metabolism genes STAT1, ALDH2, and ECHS1 are significantly enriched in GC, with red indicating high expression levels.

10.3389/fimmu.2024.1460308

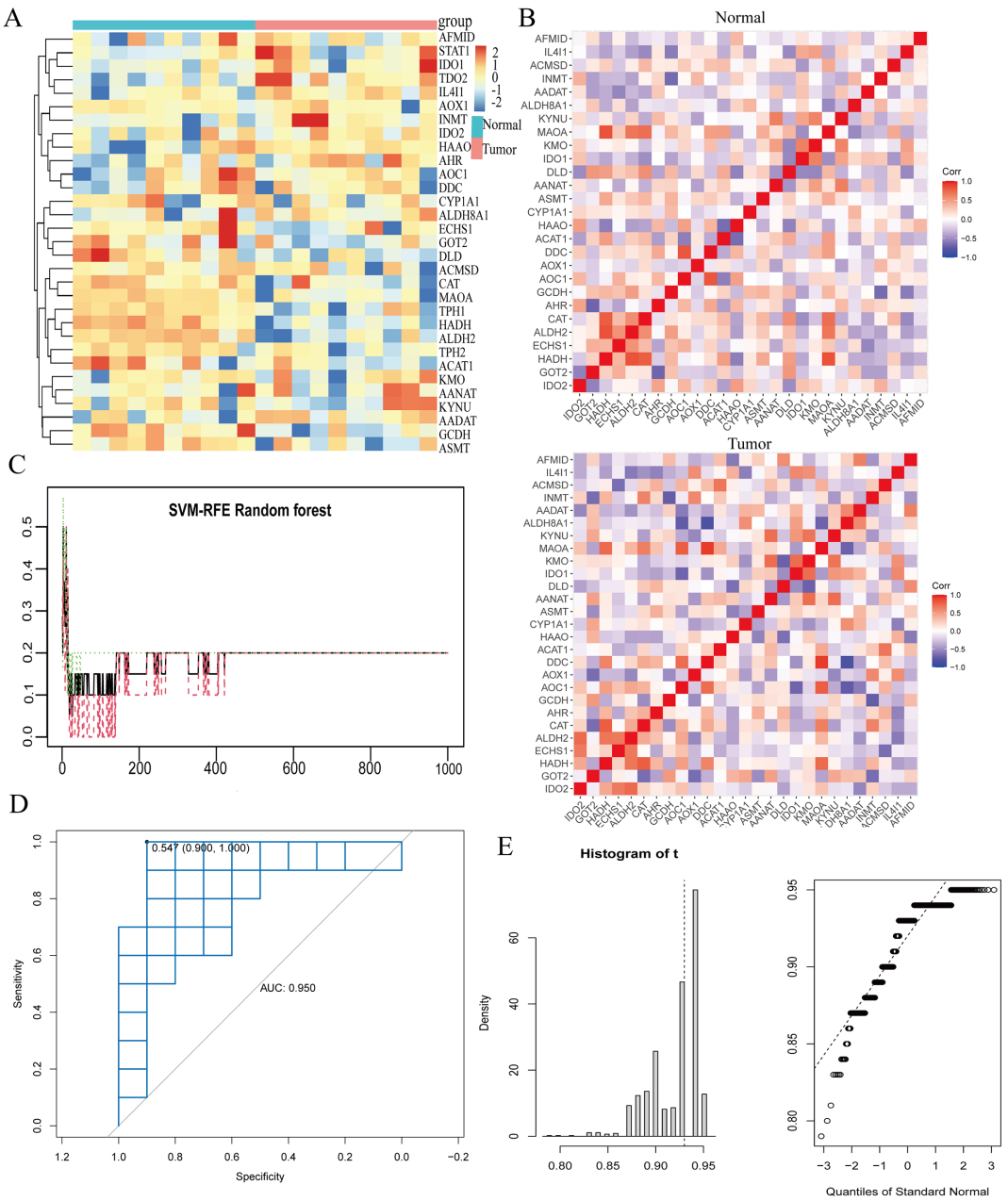

FIGURE 4
The SVM algorithm model was constructed for the tryptophan metabolism family genes. **(A)** The various expressions of tryptophan metabolism family genes in the GC transcriptome were analyzed. Red indicates high expression, blue indicates low expression. **(B)** The correlation of tryptophan metabolism family genes. The higher the correlation, the darker the color. **(C)** The SVM-RFE machine algorithm model was constructed in GSE79973. **(D, E)** ROC and calibration curve analysis of machine algorithm model predictive value in GSE79973. *, P<0.05,**, P<0.01, ***, P<0.001.

3.5 The ALDH2 and ECHS1 genes were promote the progression of GC

Additionally, we discovered that the expression levels of ALDH2 and ECHS1 provide a more practical approach for the prognosis and prediction of outcomes in GC. We employed the Random Forest (RF) model to identify key genes involved in tryptophan metabolism that may influence the progression of GC (Figure 5A). Our findings also indicated that ALDH2 and ECHS1 serve as risk factors, with their expression being indicative of a poor prognosis for GC patients (Figures 5B, C). Furthermore, the ALDH2 and ECHS1 genes were associated with the relative aggregation of inflammatory factors, suggesting that the activation of tryptophan metabolism is linked to the release of inflammatory mediators, including IL6, IL7, IL10, CXCL8, TGFB3, TGFB2, IFNG, and PDGFA proteins (Figure 5D). Collectively, the involvement of ALDH2 and ECHS1 in tryptophan metabolism was found to promote the release of inflammatory factors, thereby contributing to a poorer prognosis.

10.3389/fimmu.2024.1460308

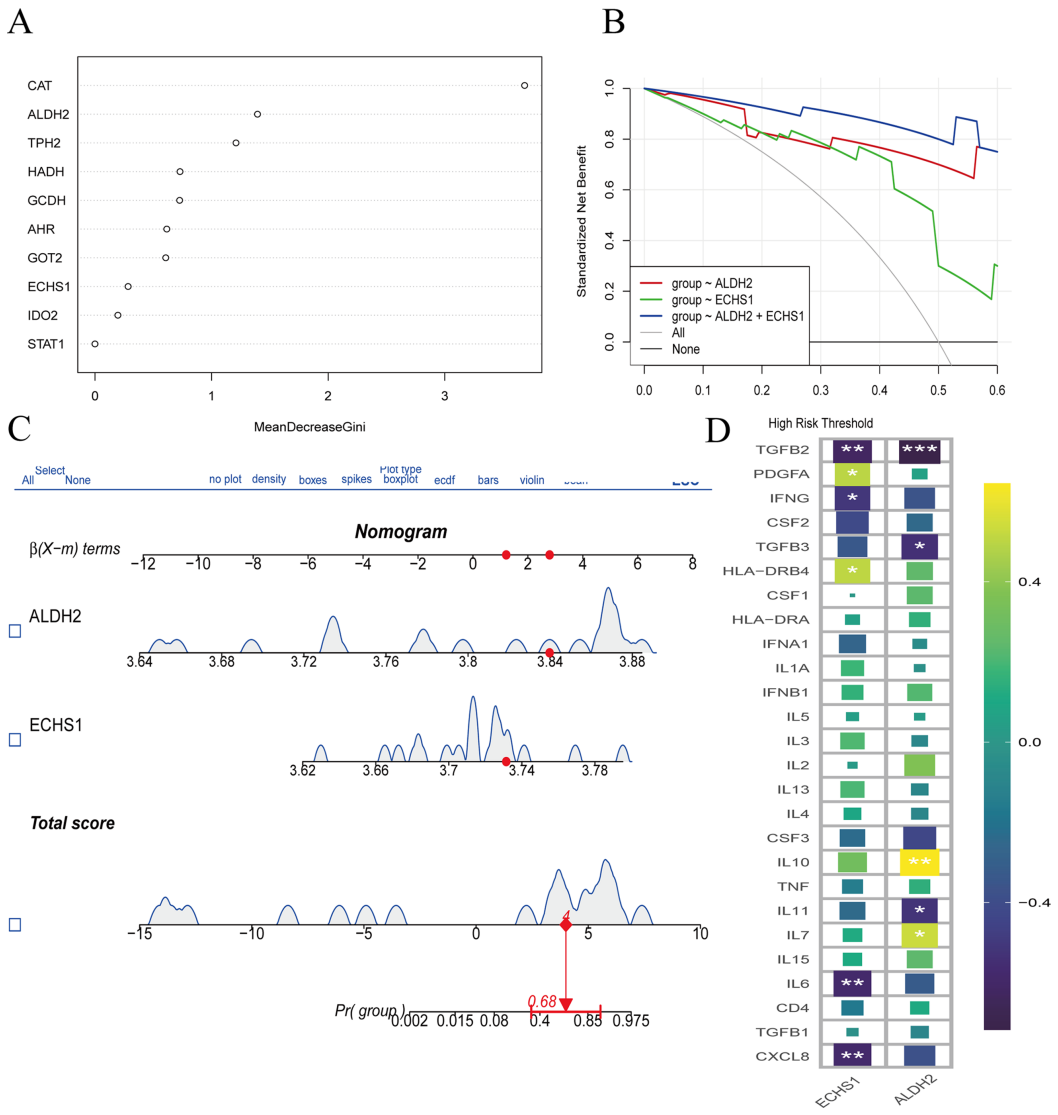

FIGURE 5
Transcriptomic analysis of tryptophan metabolic family genes expressed in GC and normal groups. The positive expression of tryptophan metabolism family genes were screened by svm algorithm. **(A)** RF model showed the top 10 tryptophan metabolic key genes in terms of importance. This graph is the MeanDecreaseGini coefficient graph, with MeanDecreaseGini values on the horizontal axis. The larger the MeanDecreaseGini value, the better the classification of categories. The vertical axis represents the expression of positive genes, arranged in descending order according to the MeanDecreaseGini coefficient. **(B, C)** Decision curve analysis (DCA) and nomogram predict the key gene expression in GC patients. **(D)** The correlation between the ALDH2 and ECHS1 genes and inflammation. *, P<0.05, **, P<0.01, ***, P<0.001.

3.6 ALDH2 and ECHS1 immunotherapy and prognosis by bulk transcriptome analysis in GC

We conducted an analysis to determine the correlation between ALDH2 and ECHS1 and the levels of various immune cells in GC. The findings revealed that ALDH2 was associated with disrupted immune levels, exhibiting a positive correlation with plasma cells, CD4+T cells, and NK cells, and a negative correlation with T-cells-CD8, Macrophages-M0, Macrophages-M1, and Macrophages-M2. In contrast, ECHS1 did not demonstrate any significant alterations in immune levels (Figure 6A). Furthermore, we employed the MCP counter to assess the immune infiltration score, which indicated that the expression of ALDH2 and ECHS1 influenced endothelial cell and monocyte cell function. Interestingly, these results aligned with our previous observations (Figure 6B). Subsequent analysis using bulk transcriptome data suggested that ALDH2 and ECHS1 may act as promoters of GC progression, while STAT1 could potentially function as a protective factor. Kaplan-Meier survival curves revealed that patients in the high-expression group of ECHS1 had significantly lower overall survival rates ($p<0.05$) (Figures 6E, C). Lastly, our findings indicated that the ALDH2 and ECHS1 proteins were associated with a better prognosis for GC when considering immunotherapy (ICB) (Figure 6D).

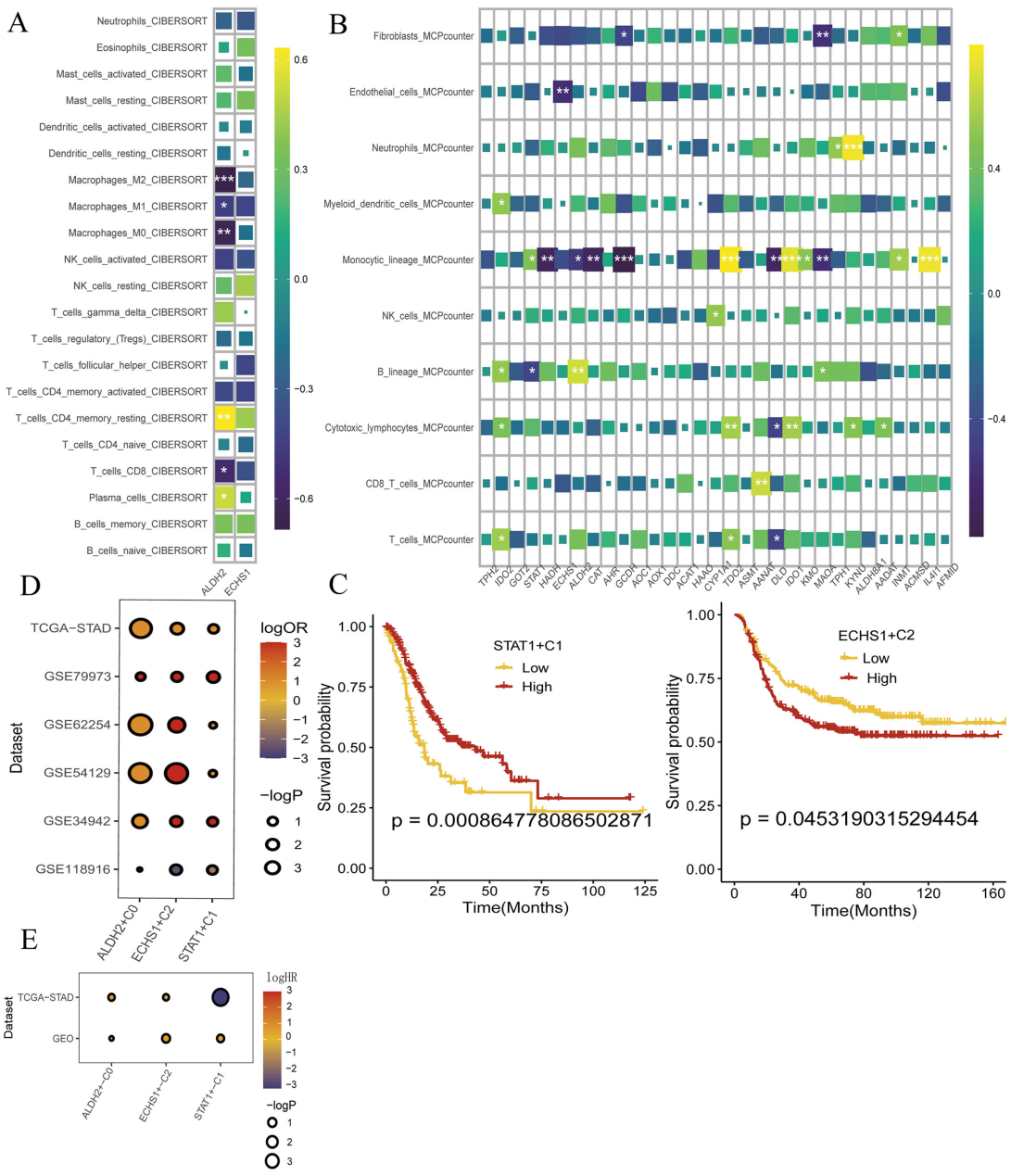

FIGURE 6
ALDH2 and ECHS1 ICB immunotherapy restrain the progress of GC. **(A, B)** Immune infiltration of ALDH2 and ECHS1 gene in GC. **(C)** To evaluate the key genes expression survival curves by Kaplan-Meier survival analysis. **(D)** Evaluation of the prognosis of ICB immunotherapy by TCGA-STAD, GSE79973, GSE62254, GSE54129, GSE34942 and GSE5118986. **(E)** bulk transcriptome analysis the expression of ALDH2 and ECHS1 and prognosis by TCGA-STAD, GSE54129 and GSE26253. *, P<0.05, **, P<0.01, ***, P<0.001.

3.7 TMGs related genes affect the release of inflammatory cytokines in TME

Chronic inflammation has always been an important factor in the complex TME.it stimulates vascular damage and epithelial tissue destruction. Our data demonstrated a decrease in the release of inflammatory mediators, including IL6, IL7, IL10, and CXCL8 (Figure 7).This also implies that inhibition of the expression of TMGs-related genes,ECHS1 and ALDH2, can regulate the expression of inflammatory factors and complex TME.

3.8 The down-regulated expression of ECHS1 and up-regulated expression ALDH2 decreased cell proliferation and migration in GC

Moreover, through the application of interference and overexpression techniques in the transfection of GC cells, we noted a reduction in ECHS1 expression following si-ECHS1 and an enhancement in ALDH2 expression via ad-ALDH2. Concurrently, the metabolism of tryptophan was down-regulated as a result of

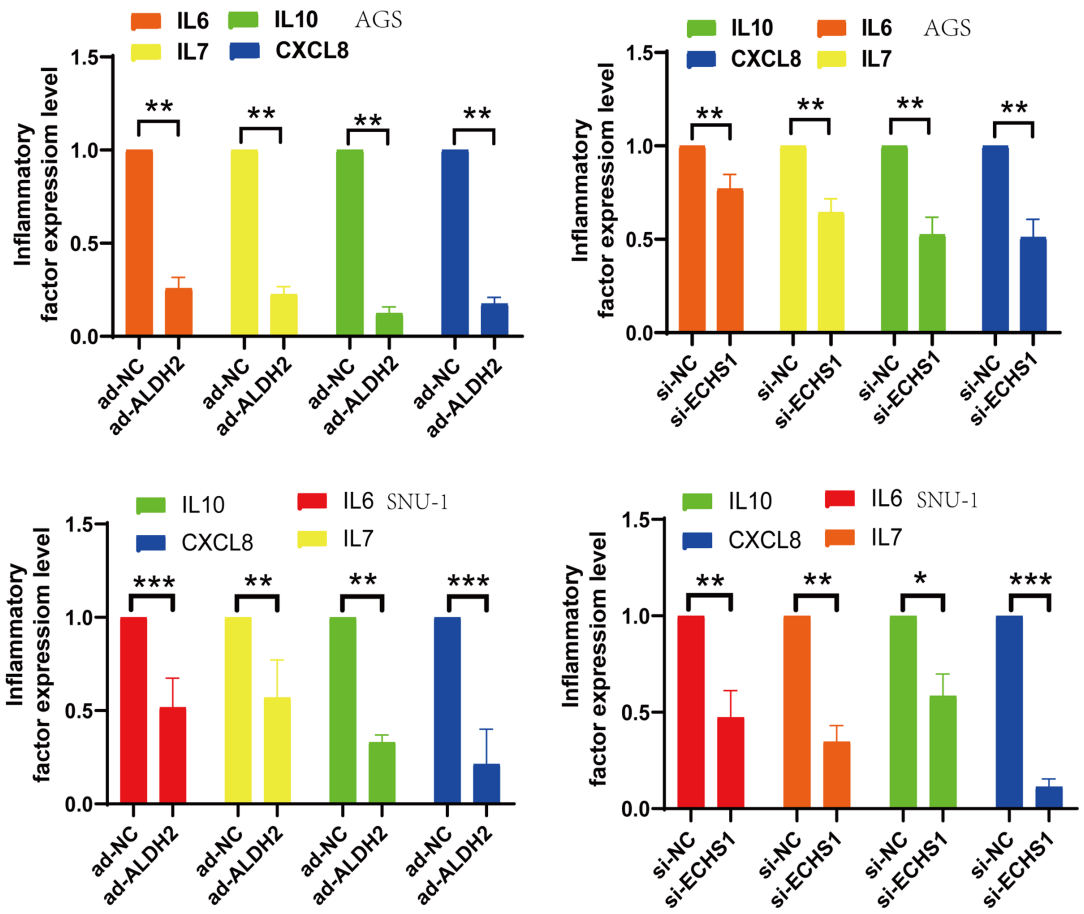

FIGURE 7
si-ECHS1 and ad-ALDH2 transfections were inhibition of inflammatory expression. The expression of IL6, IL7, IL10, CXCL8 by qPCR assay in AGS and SNU-1 cells. *, P<0.05, **, P<0.01, ***, P<0.001.

transfection with si-ECHS1 and ad-ALDH2 (Figures 8A, B). Additionally, si-ECHS1 and ad-ALDH2 were inhibited the proliferation and migration of GC cells (Figure 8B).

4 Discussion

This research highlights the importance of ECHS1 and ALDH2 in GC progression and immune modulation, suggesting that targeted therapies focusing on these genes offer promising avenues for personalized immunotherapy in GC. These findings hold potential for improving patient survival and quality of life. Future studies on the NF-κB signaling pathway's role in this context are warranted to further elucidate the mechanisms underlying TMG-mediated immune modulation in GC.

Recent studies have indicated that ALDH2 and ECHS1, as members of the TMGs, play a critical role in modulating immune responses in LUAD (29). It is worth noting that is famous for its cancer suppression characteristics of ALDH2 in LUAD and GC often lack of expression. This downregulation has been associated with increased cellular heterogeneity, leading to a more rapid tumor progression (25, 30). Furthermore, our findings reveal that the expression of ECHS1 is linked to various cancers, including colorectal cancer (31), hepatocellular carcinoma (32, 33), and breast cancer (34, 35), through its effects on metabolism and cell signaling pathways. These studies collectively suggest that the dysregulated expression of ALDH2 and ECHS1 can impair cellular functions, potentially contributing to the progression and worsening of gastric cancer.

In our current study, we have explored the correlation between TMGs (ALDH2 and ECHS1) and the progression of GC. Among these metabolites, ALDH2 and ECHS1 have been identified as particularly potent in preventing epithelial carcinogenesis. We observed an upregulation of ECHS1 and a downregulation of ALDH2 in GC cases. Notably, ALDH2 and ECHS1, derived from the clustering results in specific epithelial cells, were found to be significantly associated with molecular subtypes in tryptophan metabolism. Further analysis of various signaling pathways and immune-related attributes highlighted ALDH2 and ECHS1 as pivotal players in tryptophan metabolism, suggesting that the modulation of these genes could substantially influence the pathway's regulation. Additionally, we developed a prognostic

10.3389/fimmu.2024.1460308

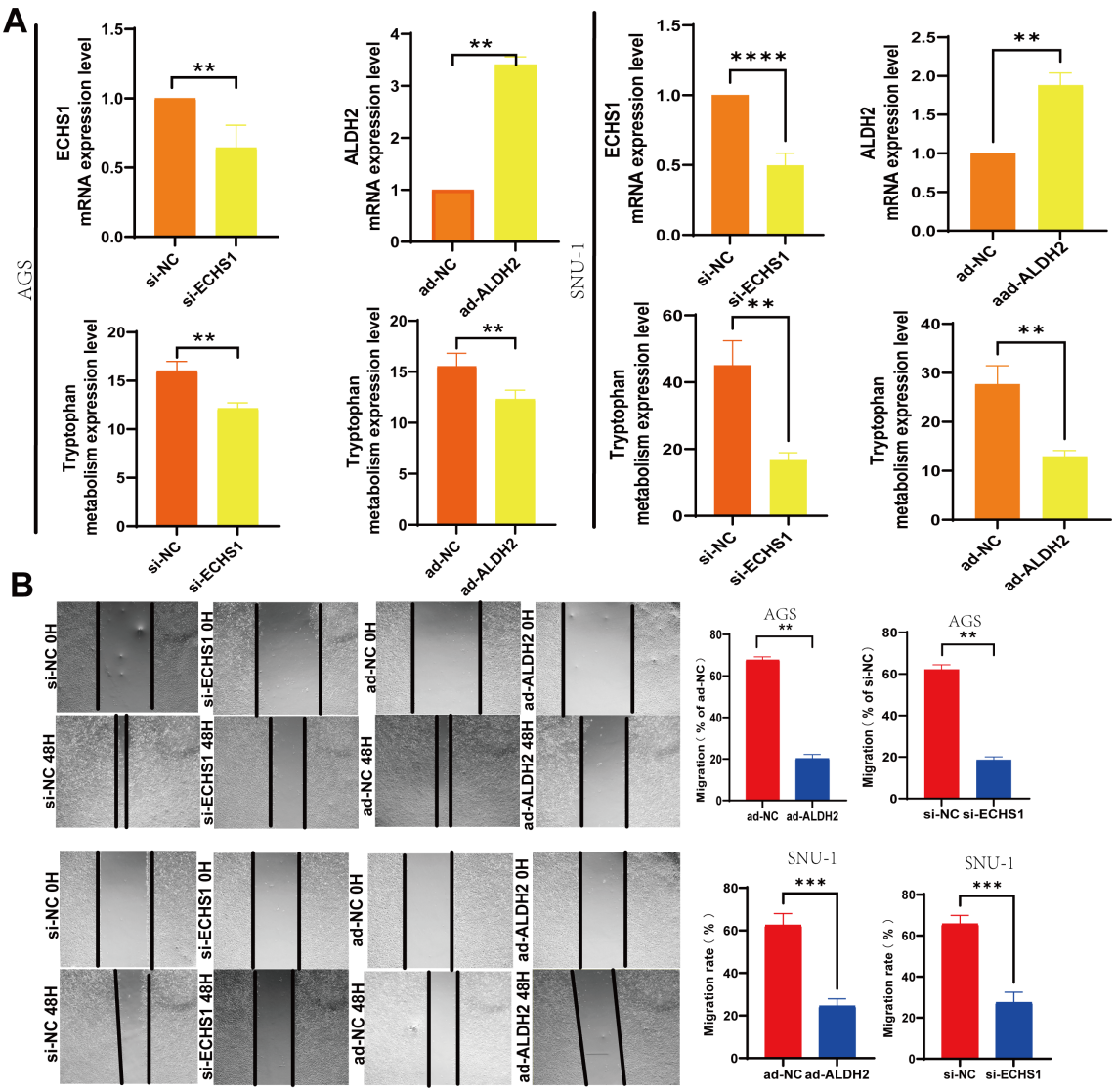

FIGURE 8
Low levels of tryptophan metabolism were effective in slowing the progression of GC. **(A)** The transfection of si-ECHS1 and ad-ALDH2 into AGS and SNU-1 cells influenced the expression of TMGs and tryptophan metabolism. **(B)** The influence of cell migration by the transfection of si-ECHS1 and ad-ALDH2 in AGS and SNU-1 cells. **, P<0.01, ***, P<0.001, ****, P<0.0001.

model that integrates both tryptophan metabolism and immune-related genes. Our data revealed that the expression of ECHS1 can lead to a poor prognosis in GC due to the impairment of CD8+ T cell and CD4+ T cell function. Moreover, ALDH2 and ECHS1 were found to regulate inflammation, including the expression of IL6, IL7, IL10, and CXCL8 proteins, and enhance TME heterogeneity through transcription factors ZNF384 and FOXF1, which is one of the significant causes of epithelial cell carcinogenesis in GC. Therefore, our data suggest that it can effectively predict the prognosis and immune therapy response of GC and guide personalized tryptophan metabolite-related targeted therapy.

Current research reports indicate that the NF-κB signaling pathways are pivotal in regulating both physiological and pathological processes. These pathways are implicated in responses to stimuli related to inflammation, immune response, and the heterogeneity of the TME (36). Several studies have demonstrated that the regulation of inflammation and natural aging is mediated by the NF-κB signaling pathways. Interestingly, our GSVA enrichment analysis revealed that the NF-κB signaling pathways specifically regulate TMGs, including IL6, IL7, IL10, and CXCL8 proteins (37, 38). Furthermore, we also discovered that the NF-κB signaling pathways are primarily involved in regulating and maintaining T cell function (39–41).

Our data indicate that the downregulated expression of ALDH2 contributes to a stronger immune invasion of CD8+ T cells and CD4+ T cells through the stimulation of NF-κB signaling pathways. However, ECHS1 did not exhibit changes in immune levels. Therefore, understanding the NF-κB signaling pathways is

particularly crucial for immune therapy and maintaining T cell function. Nevertheless, there remains significant scope for additional research to fully comprehend the complexities involved. The potential of immune therapy in treating various diseases has garnered increasing interest, particularly for its capacity to target cancerous or aberrant cells by enhancing the body's autoimmunity. Specifically, the study of ALDH2 and ECHS1 in immune therapy plays a crucial role in regulating GC. Additionally, the expression of ALDH2 and ECHS1 has a higher therapeutic value and can lead to improved survival outcomes through immune therapy. This can be achieved by utilizing samples from the TCGA and GEO databases. However, STAT1 appears to lack this therapeutic potential. In summary, ALDH2 and ECHS1, which are integral to tryptophan metabolism, serve as markers for prognostic prediction and viable targets for immunotherapy in GC patients.

It has been reported that chronic inflammation promotes the development of epithelial cancer, and the expression of ECHS1 and ALDH2 enhances the release of inflammatory factors, leading to a more robust TME. The release of inflammatory factors is likely associated with the NF-κB pathway. These findings suggest a dynamic cycle of chronic injury and repair, in which tryptophan metabolism plays a role. Importantly, interventions such as si-ECHS1 and ad-ALDH2 have been shown to significantly disrupt this dynamic cycle.

5 Conclusion

In conclusion, our study offers a new perspective for understanding the progression of the GC process (Figure 9). The TMGs- related genes ALDH2 and ECHS1 can contribute to TME heterogeneity and

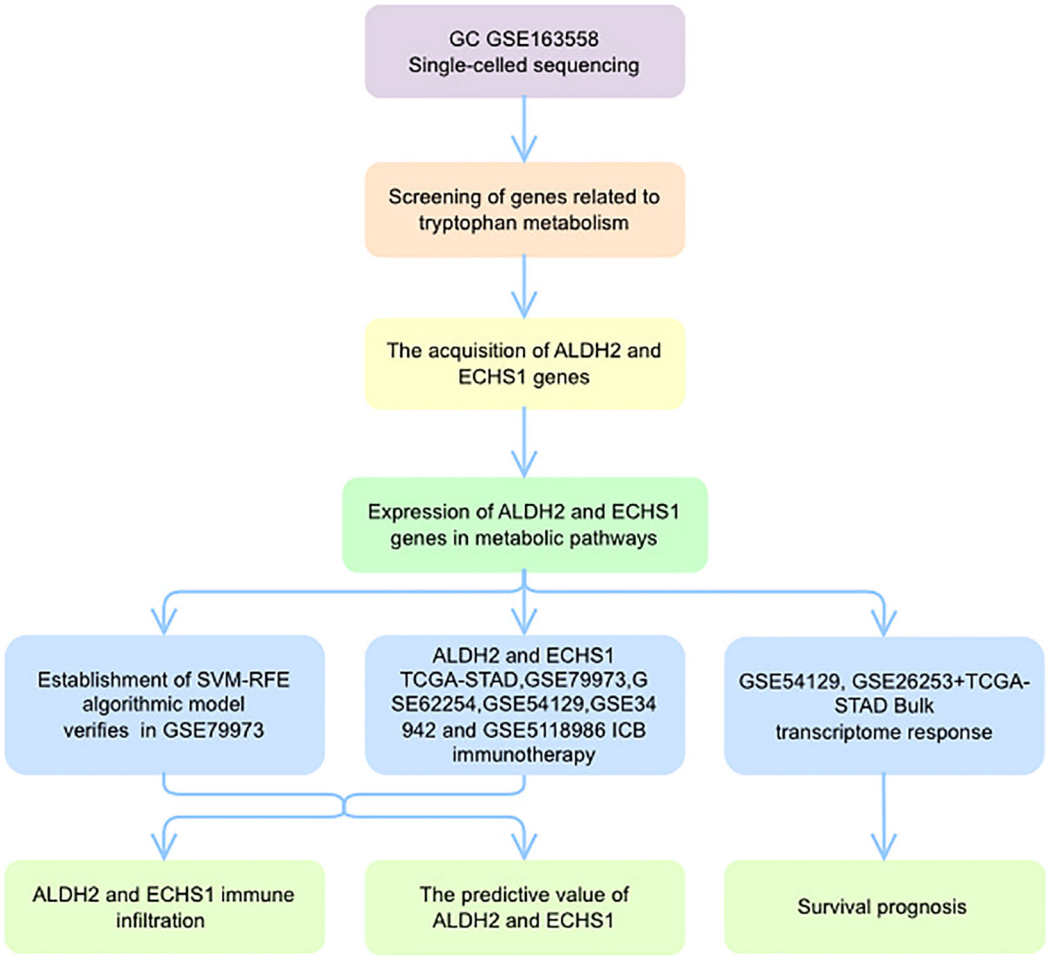

FIGURE 9
A global landscape of tryptophan metabolism analysis.

inflammation through the NF-κB signaling pathway. In addition, ALDH2 and ECHS1 may serve as novel tumor markers, providing a foundational basis for inhibiting GC progression. This study not only enhances our understanding of GC dynamics but also opens avenues for developing more effective therapeutic strategies.

Data availability statement

The original contributions presented in the study are included in the article/supplementary material. Further inquiries can be directed to the corresponding authors.

Ethics statement

Ethical approval was not required for the studies on humans in accordance with the local legislation and institutional requirements because only commercially available established cell lines were used.

Author contributions

LW: Data curation, Writing – original draft, Writing – review & editing. XZ: Writing – original draft, Writing – review & editing. HY: Writing – original draft, Writing – review & editing. LW: Writing – original draft, Writing – review & editing. BW: Writing – original draft, Writing – review & editing. YG: Writing – original draft, Writing – review & editing. YM: Writing – original draft, Writing – review & editing. WF: Writing – original draft, Writing – review & editing. KX: Writing – original draft, Writing – review & editing. SH: Writing – original draft, Writing – review & editing. JL: Writing – original draft, Writing – review & editing.

Funding

The author(s) declare financial support was received for the research, authorship, and/or publication of this article. This work was financially supported by grants from the National Natural Science Foundation of China(81860566,2022AAC03573), Dazhou Science and Technology Bureau project (21ZDYF0025, 21ZDYF0023), Sichuan Provincial Administration of Traditional Chinese Medicine project (2023MS141), Sichuan Medical Association Project (S21048), and The Doctoral Startup Fund of the Affiliated Hospital of Southwest Medical University (No. 19025).

Conflict of interest

The authors declare that the research was conducted in the absence of any commercial or financial relationships that could be construed as a potential conflict of interest.

Publisher's note

All claims expressed in this article are solely those of the authors and do not necessarily represent those of their affiliated organizations, or those of the publisher, the editors and the reviewers. Any product that may be evaluated in this article, or claim that may be made by its manufacturer, is not guaranteed or endorsed by the publisher.

References

1. Luo P, Chen G, Shi Z, Yang J, Wang X, Pan J, et al. Comprehensive multi-omics analysis of tryptophan metabolism-related gene expression signature to predict prognosis in gastric cancer. *Front Pharmacol.* (2023) 14:1267186. doi: 10.3389/fphar.2023.1267186

2. Mahajan S, Agashe D. Evolutionary jumps in bacterial GC content. *G3 (Bethesda).* (2022) 12. doi: 10.1093/g3journal/jkac108

3. Liu Y, Liang N, Xian Q, Zhang W. GC heterogeneity reveals sequence-structures evolution of angiosperm ITS2. *BMC Plant Biol.* (2023) 23:608. doi: 10.1186/s12870-023-04634-9

4. Chen XJ, Wei CZ, Lin J, Zhang RP, Chen GM, Li YF, et al. Prognostic significance of PD-L1 expression in gastric cancer patients with peritoneal metastasis. *Biomedicines.* (2023) 11:1–12. doi: 10.3390/biomedicines11072003

5. Jin X, Liu Z, Yang D, Yin K, Chang X. Recent progress and future perspectives of immunotherapy in advanced gastric cancer. *Front Immunol.* (2022) 13:948647. doi: 10.3389/fimmu.2022.948647

6. Wang X, Liu X, Dai H, Jia J. Peripheral blood nutrient indices as biomarkers for anti–PD–1 therapy efficacy and prognosis in patients with advanced gastric cancer. *Oncol Lett.* (2023) 26:397. doi: 10.3892/ol

7. Correia AS, Vale N. Tryptophan metabolism in depression: A narrative review with a focus on serotonin and kynurenine pathways. *Int J Mol Sci.* (2022) 23:1–17. doi: 10.3390/ijms23158493

8. van Zundert SKM, van Egmond NCM, van Rossem L, Willemsen SP, Griffioen PH, van Schaik RHN, et al. First trimester maternal tryptophan metabolism and embryonic and fetal growth: the Rotterdam Periconceptional Cohort (Predict Study). *Hum Reprod (Oxford England).* (2024) 39:912–22. doi: 10.1093/humrep/deae046

9. Pirzadeh M, Khalili N, Rezaei N. The interplay between aryl hydrocarbon receptor, H. pylori, tryptophan, and arginine in the pathogenesis of gastric cancer. *Int Rev Immunol.* (2022) 41:299–312. doi: 10.1080/08830185.2020.1851371

10. Li W, Ling L, Xiang L, Ding P, Yue W. Identification and validation of a risk model and molecular subtypes based on tryptophan metabolism-related genes to predict the clinical prognosis and tumor immune microenvironment in lower-grade glioma. *Front Cell Neurosci.* (2023) 17:1146686. doi: 10.3389/fncel.2023.1146686

11. Fu T, Dai LJ, Wu SY, Xiao Y, Ma D, Jiang YZ, et al. Spatial architecture of the immune microenvironment orchestrates tumor immunity and therapeutic response. *J Hematol Oncol.* (2021) 14:98. doi: 10.1186/s13045-021-01103-4

12. Ma G, Zhang Z, Li P, Zhang Z, Zeng M, Liang Z, et al. Reprogramming of glutamine metabolism and its impact on immune response in the tumor microenvironment. *Cell Commun Signal.* (2022) 20:114. doi: 10.1186/s12964-022-00909-0

13. Qin S, Xu Y, Yu S, Han W, Fan S, Ai W, et al. Molecular classification and tumor microenvironment characteristics in pheochromocytomas. *eLife.* (2024) 12. doi: 10.7554/eLife.87586

14. Li D, Yu S, Long Y, Shi A, Deng J, Ma Y, et al. Tryptophan metabolism: Mechanism-oriented therapy for neurological and psychiatric disorders. *Front Immunol.* (2022) 13:985378. doi: 10.3389/fimmu.2022.985378

15. Chen LM, Bao CH, Wu Y, Liang SH, Wang D, Wu LY, et al. Tryptophan-kynurenine metabolism: a link between the gut and brain for depression in inflammatory bowel disease. *J Neuroinflamm.* (2021) 18:135. doi: 10.1186/s12974-021-02175-2

16. Michaudel C, Danne C, Agus A, Magniez A, Aucouturier A, Spatz M, et al. Rewiring the altered tryptophan metabolism as a novel therapeutic strategy in inflammatory bowel diseases. *Gut.* (2023) 72:1296–307. doi: 10.1136/gutjnl-2022-327337

17. Ilie-Mihai RM, Stefan-van Staden RI, Magerusan L, Coros M, Pruneanu S. Enantioanalysis of tryptophan in whole blood samples using stochastic sensors-A screening test for gastric cancer. *Chirality.* (2020) 32:215–22. doi: 10.1002/chir.23155

18. Yao S, Yin X, Chen T, Chen W, Zuo H, Bi Z, et al. ALDH2 is a prognostic biomarker and related with immune infiltrates in HCC. *Am J Cancer Res*. (2021) 11:5319–37.

19. Chi H, Chen H, Wang R, Zhang J, Jiang L, Zhang S, et al. Proposing new early detection indicators for pancreatic cancer: Combining machine learning and neural networks for serum miRNA-based diagnostic model. *Front Oncol*. (2023) 13:1244578. doi: 10.3389/fonc.2023.1244578

20. Yao Q, Zhang X, Wang Y, Wang C, Wei C, Chen J, et al. Comprehensive analysis of a tryptophan metabolism-related model in the prognostic prediction and immune status for clear cell renal carcinoma. *Eur J Med Res*. (2024) 29:22. doi: 10.1186/s40001-023-01619-0

21. Li P, Xu W, Liu F, Zhu H, Zhang L, Ding Z, et al. The emerging roles of IDO2 in cancer and its potential as a therapeutic target. *BioMed Pharmacother*. (2021) 137:111295. doi: 10.1016/j.biopha.2021.111295

22. Hu T, Chen X, Lu S, Zeng H, Guo L, Han Y. Biological role and mechanism of lipid metabolism reprogramming related gene ECHS1 in cancer. *Technol Cancer Res Treat*. (2022) 21. doi: 10.1177/15330338221140655

23. Chi H, Huang J, Yan Y, Jiang C, Zhang S, Chen H, et al. Unraveling the role of disulfidptosis-related LncRNAs in colon cancer: a prognostic indicator for immunotherapy response, chemotherapy sensitivity, and insights into cell death mechanisms. *Front Mol Biosci*. (2023) 10:1254232. doi: 10.3389/fmolb.2023.1254232

24. Zhang S, Jiang C, Jiang L, Chen H, Huang J, Zhang J, et al. Uncovering the immune microenvironment and molecular subtypes of hepatitis B-related liver cirrhosis and developing stable a diagnostic differential model by machine learning and artificial neural networks. *Front Mol Biosci*. (2023) 10:1275897. doi: 10.3389/fmolb.2023.1275897

25. Lu T, Sun L, Fan Q, Yan J, Zhao D, Xu C, et al. Expression and clinical significance of ECHS1 in gastric cancer. *J Cancer*. (2024) 15:418–27. doi: 10.7150/jca.88604

26. Zhang S, Jiang C, Jiang L, Chen H, Huang J, Gao X, et al. Construction of a diagnostic model for hepatitis B-related hepatocellular carcinoma using machine learning and artificial neural networks and revealing the correlation by immunoassay. *Tumour Virus Res*. (2023) 16:200271. doi: 10.1016/j.tvr.2023.200271

27. Khan SU, Huang Y, Ali H, Ali I, Ahmad S, Khan SU, et al. Single-cell RNA sequencing (scRNA-seq): advances and challenges for cardiovascular diseases (CVDs). *Curr Probl Cardiol*. (2024) 49:102202. doi: 10.1016/j.cpcardiol.2023.102202

28. Takahashi H, Hisata K, Iguchi R, Kikuchi S, Ogasawara M, Satoh N. scRNA-seq analysis of cells comprising the amphioxus notochord. *Dev Biol*. (2024) 508:24–37. doi: 10.1016/j.ydbio.2024.01.003

29. Tran TO, Vo TH, Lam LHT, Le NQK. ALDH2 as a potential stem cell-related biomarker in lung adenocarcinoma: Comprehensive multi-omics analysis. *Comput Struct Biotechnol J*. (2023) 21:1921–9. doi: 10.1016/j.csbj.2023.02.045

30. Yao S, Gan C, Wang T, Zhang Q, Zhang M, Cheng H. High ALDH2 expression is associated with better prognosis in patients with gastric cancer. *Am J Cancer Res*. (2022) 12:5425–39.

31. Li R, Hao Y, Wang Q, Meng Y, Wu K, Liu C, et al. ECHS1, an interacting protein of LASP1, induces sphingolipid-metabolism imbalance to promote colorectal cancer progression by regulating ceramide glycosylation. *Cell Death Dis*. (2021) 12:911. doi: 10.1038/s41419-021-04213-6

32. Shihana F, Cholan PM, Fraser S, Oehlers SH, Seth D. Investigating the role of lipid genes in liver disease using fatty liver models of alcohol and high fat in zebrafish (Danio rerio). *Liver International: Off J Int Assoc Study Liver*. (2023) 43:2455–68. doi: 10.1111/liv.15716

33. Wang L, Qi Y, Wang X, Li L, Ma Y, Zheng J. ECHS1 suppresses renal cell carcinoma development through inhibiting mTOR signaling activation. *Biomed Pharmacother*. (2020) 123:109750. doi: 10.1016/j.biopha.2019.109750

34. Shi Y, Qiu M, Wu Y, Hai L. MiR-548-3p functions as an anti-oncogenic regulator in breast cancer. *BioMed Pharmacother*. (2015) 75:111–6. doi: 10.1016/j.biopha.2015.07.027

35. Muntean C, Tripon F, Bogliş A, Bănescu C. Pathogenic biallelic mutations in ECHS1 in a case with short-chain enoyl-coA hydratase (SCEH) deficiency-case report and literature review. *Int J Environ Res Public Health*. (2022) 19:1–15. doi: 10.3390/ijerph19042088

36. Yu H, Lin L, Zhang Z, Zhang H, Hu H. Targeting NF-κB pathway for the therapy of diseases: mechanism and clinical study. *Signal Transduct Target Ther*. (2020) 5:209. doi: 10.1038/s41392-020-00312-6

37. Shelby A, Pendleton C, Thayer E, Johnson GK, Xie XJ, Brogden KA. PD-L1 correlates with chemokines and cytokines in gingival crevicular fluid from healthy and diseased sites in subjects with periodontitis. *BMC Res Notes*. (2020) 13:532. doi: 10.1186/s13104-020-05376-9

38. Xue L, Wang C, Qian Y, Zhu W, Liu L, Yang X, et al. Tryptophan metabolism regulates inflammatory macrophage polarization as a predictive factor for breast cancer immunotherapy. *Int Immunopharmacol*. (2023) 125:111196. doi: 10.1016/j.intimp.2023.111196

39. Daniels MA, Luera D, Teixeiro E. NFκB signaling in T cell memory. *Front Immunol*. (2023) 14:1129191. doi: 10.3389/fimmu.2023.1129191

40. Rui R, Zhou L, He S. Cancer immunotherapies: advances and bottlenecks. *Front Immunol*. (2023) 14:1212476. doi: 10.3389/fimmu.2023.1212476

41. Chi H, Gao X, Xia Z, Yu W, Yin X, Pan Y, et al. FAM family gene prediction model reveals heterogeneity, stemness and immune microenvironment of UCEC. *Front Mol Biosci*. (2023) 10:1200335. doi: 10.3389/fmolb.2023.1200335

frontiers | Frontiers in Immunology

TYPE Original Research
PUBLISHED 12 September 2024
DOI 10.3389/fimmu.2024.1444222

Check for updates

OPEN ACCESS

EDITED BY
Wantao Wu,
Chongqing Medical University, China

REVIEWED BY
Xingyu He,
University of Cincinnati, United States
Dong Chen,
University of Duisburg-Essen, Germany
Donghui Jin,
Henan Provincial People's Hospital, China

*CORRESPONDENCE
Lin Gan
ganlindoctor@163.com
Hongda Li
lihd@cqmu.edu.cn
Ruochan Li
Ruochan Li@med.uni-muenchen.de

†These authors have contributed equally to this work

RECEIVED 05 June 2024
ACCEPTED 22 August 2024
PUBLISHED 12 September 2024

CITATION
Yang Q, Duan B, Yue J, Zhang D, Chen X, Shi M, Kan J, Li R, Li H and Gan L (2024) Causal effects and metabolites mediators between immune cell and risk of colorectal cancer: a Mendelian randomization study. *Front. Immunol.* 15:1444222. doi: 10.3389/fimmu.2024.1444222

COPYRIGHT
© 2024 Yang, Duan, Yue, Zhang, Chen, Shi, Kan, Li, Li and Gan. This is an open-access article distributed under the terms of the Creative Commons Attribution License (CC BY). The use, distribution or reproduction in other forums is permitted, provided the original author(s) and the copyright owner(s) are credited and that the original publication in this journal is cited, in accordance with accepted academic practice. No use, distribution or reproduction is permitted which does not comply with these terms.

Causal effects and metabolites mediators between immune cell and risk of colorectal cancer: a Mendelian randomization study

Qian Yang[1,2,3†], Bixia Duan[4†], Jian Yue[5†], Donglin Zhang[6†], Xueping Chen[1,7], Mengjia Shi[1], Jie Kan[1], Ruochan Li[6*], Hongda Li[3*] and Lin Gan[2*]

[1]Clinical Molecular Medicine Testing Center, The First Affiliated Hospital of Chongqing Medical University, Chongqing, China, [2]Chongqing Key Laboratory of Molecular Oncology and Epigenetics, The First Affiliated Hospital of Chongqing Medical University, Chongqing, China, [3]Institute for Brain Science and Disease, Key Laboratory of Major Brain Disease and Aging Research (Ministry of Education), Chongqing Medical University, Chongqing, China, [4]Department of Oncology, The Affiliated Yongchuan Hospital of Chongqing Medical University, Chongqing, China, [5]Department of Breast Surgery, Gaozhou People's Hospital, Gaozhou, China, [6]Department of General, Visceral, and Transplant Surgery, Ludwig-Maximilians-University Munich, Munich, Germany, [7]Biobank Center, The First Affiliated Hospital of Chongqing Medical University, Chongqing, China

Objective: The involvement of immune cells in colorectal cancer (CRC) and their interplay with metabolic disorders are yet to be fully elucidated. This study examines how peripheral immune cells, inferred genetically, affect CRC and investigates the intermediary roles of metabolites.

Methods: We employed a two-sample bidirectional Mendelian randomization (MR) approach to assess the causal influence of immune cells on CRC. Additionally, a two-step MR strategy was utilized to pinpoint potential metabolites that mediate this effect. Our analysis incorporated data from genome-wide association studies (GWAS), involving 731 immune cell types, 1,400 metabolites, and CRC outcomes. The primary method of analysis was randomized inverse variance weighting (IVW), supported by MR-Egger, weighted median, simple mode, and weighted mode analyses. Sensitivity checks were conducted using Cochran's Q test, MR-PRESSO test, MR-Egger regression intercept, and leave-one-out analysis.

Results: The study identified 23 immune cell types and 17 metabolites that are causally linked to CRC. Our mediation analysis highlighted that nine metabolites act as intermediaries in the relationship between nine specific immune cells and CRC risk. Notably, The ratios of Adenosine 5'-monophosphate (AMP) to aspartate and Retinol (Vitamin A) to linoleoyl-arachidonoyl-glycerol (18:2 to 20:4) were found to concurrently mediate the promoting effects of Myeloid DC %DC and BAFF-R on B cells in colorectal cancer (CRC). Moreover, iminodiacetate (IDA) was found to mediate the protective effect of $CD14^{+}$ $CD16^{-}$ monocytes on CRC, contributing 11.8% to this mediation. In contrast, IDA was also seen to decrease the protective effect of IgD^{+} CD38br %B cells on CRC risk, with a mediation effect proportion of -10.4%.

Conclusion: This study delineates a complex network involving immune cells, metabolites, and CRC, suggesting a multifaceted pathophysiological interaction. The identified causal links and mediation pathways underscore potential therapeutic targets, providing a foundation for interventions aimed at modulating immune responses to manage CRC.

KEYWORDS

immune cell, metabolites, Mendelian randomization, colorectal cancer, mediation analysis

1 Introduction

CRC is one of the most common malignancies of the digestive system, consistently showing high incidence rates in recent years. In 2022, there were over 1.92 million new cases and more than 900,000 deaths worldwide, with a 5-year survival rate of 65% (1, 2). The etiology of CRC is multifaceted, involving both genetic predispositions—such as Lynch syndrome (3) and inflammatory bowel disease (4)—and environmental influences, including lifestyle factors like smoking (5), excessive alcohol consumption (6), obesity (7), and gut microbiota composition (8). Immune cells are integral to the pathogenesis of CRC. Research has specifically implicated macrophages (9), dendritic cells (10), T cells (11), and NK cells (12) in the initiation and progression of CRC, with their precise mechanisms still needing clarification.

Multiple studies have reported that metabolic reprogramming within immune cells plays a critical role in tumor malignancy, influencing the effectiveness of anti-tumor responses (13). For example, inhibiting glycolysis in $CD8^+$ T cells not only enhances their memory function but also boosts their anti-tumor activity (14). Similarly, alterations in amino acid metabolism, particularly involving arginine and glutamine, significantly affect T cell viability and functionality, thereby modulating their capacity to combat tumors (15, 16). Curtailing cholesterol metabolism in $CD8^+$ T cells has also been shown to enhance their anti-tumor capabilities (17). However, a reduction in glycolysis in NK cells has been linked to accelerated lung cancer progression (18). These findings underscore the central role of immune cell metabolism in anti-tumor immunity. Moreover, additional studies suggest that targeting specific metabolic pathways, such as fatty acid metabolism in myeloid-derived suppressor cells (19), ketone metabolism in macrophages (20), and cholesterol efflux in macrophages (21), could profoundly influence tumor dynamics. These studies provide evidence from animal experiments and mechanistic insights into how metabolic reprogramming of immune cells influences tumor progression; however, evidence from large-scale human studies remains limited.

Mendelian randomization uses genetic variants as instrumental variables to assess causal relationships between exposures and outcomes, effectively simulating the conditions of a controlled experiment. This approach offers distinct advantages over both observational studies and randomized controlled trials (RCTs). Unlike observational studies, which are often plagued by confounding and reverse causation, Mendelian randomization leverages naturally occurring genetic variations that are randomly assigned and independent of the outcome, significantly reducing these biases. Compared to RCTs, which may be impractical due to ethical or economic limitations, Mendelian randomization provides a viable and efficient alternative for exploring causal relationships without the need for direct intervention (22).

Although recent Mendelian analyses have shown that metabolite-related SNPs can modulate the role of immune cells in the development of various cancers, including breast, pancreatic, and hepatocellular carcinoma (23–25), these studies have not fully addressed the complexities of immune cell involvement in colorectal cancer. Moreover, prior research about immune cells and colorectal cancer has primarily focused on mechanistic insights, lacking the perspective of large-scale genetic variation, which limits their ability to draw robust causal conclusions. Furthermore, while one Mendelian randomization study has explored the relationship between peripheral blood cell counts and colorectal cancer risk, identifying eosinophils and lymphocytes as potential contributors, this study examined only five leukocyte counts without delving into the specific roles of immune cell subtypes (26). Consequently, there still remains a gap in understanding the contribution of immune cells to colorectal cancer risk, particularly regarding the mediating role of metabolites.

In contrast, our study addresses these limitations by investigating the contribution of immune cells to colorectal cancer risk through a novel approach that integrates large-scale genetic variation and examines the mediating role of metabolites. This approach not only broadens the understanding of immune cell involvement in colorectal cancer but also provides new insights into the complex interplay between metabolites and immune cells, thereby filling a critical gap in the existing literature.

2 Methods

2.1 Study design

Our study aims to clarify the causal connections between immune cells and the risk of CRC through a detailed Mendelian

randomization analysis. Initially, we screened 731 immune cell traits for causal associations with CRC using a two-sample MR approach. Specific immune cells were then selected for further analysis, employing reverse MR to explore their potential mediation effects. To investigate the role of metabolites as mediators, a two-step MR strategy was utilized (27). Multiple sensitivity analyses were conducted to verify the robustness of our findings, as depicted in the study's design and progression in Figure 1.

2.2 Data sources of exposures, mediators, and outcomes

The data on exposures, mediators, and outcomes were obtained from GWAS, predominantly involving individuals of European ancestry. Immune cell data were derived from the dataset by Orrù V et al. (28), encompassing 731 immune cell traits from 3757 participants. The GWAS Catalog provided statistical summaries (accession numbers: GCST90001391-90002121, Supplementary Table 1). Metabolite data, including 1,091 metabolites and 309 metabolite ratios, organized into eight recognized pathways such as lipids, amino acids, and more, were also sourced from the GWAS Catalog (accession numbers: GCST90199621-90201020, Supplementary Table 2) (28). CRC data originated from a meta-analysis by Sakaue S et al. (29), which included 470,002 European participants, comprising 6,581 cases and 463,421 controls (GWAS Catalog accession number: GCST90018808).

2.3 SNP selection

For Mendelian randomization studies to be valid, the single nucleotide polymorphisms (SNPs) serving as instrumental variables (IVs) must meet three crucial criteria (Figure 2): (1) SNPs must be correlate with the exposure, (2) SNPs should have no association with confounding elements like age, sex, or lifestyle, and (3) SNPs must exclusively affect the outcome via the exposure. The first assumption can be tested by selecting genetic variants significantly associated with risk factors in GWAS. The validity of the second assumption can be assessed by examining whether genetic variants are associated with competing risk factors. The third assumption cannot be directly assessed but must be supported by biological knowledge (30). SNPs were chosen based on their association with immune cell traits at a genome-wide significance threshold of $P < 1 \times 10^{-5}$ (31, 32), the criteria used for selecting significant SNPs in the reverse Mendelian randomization analysis were $P < 5 \times 10^{-8}$; independence was verified by assessing linkage disequilibrium, selecting IVs with no linkage effects ($r^2 < 0.001$ within a 10,000 kb distance) (33). IVs were then screened from the CRC dataset to exclude any associated directly with the outcome and to remove palindromic SNPs. The strength of individual SNPs was determined by calculating the F-statistic, retaining those with an F-statistic greater than 10 (34). SNPs for immune cells and metabolites are listed in Supplementary Tables 3, 4.

2.4 Mendelian randomization and statistical analysis

A bidirectional two-sample MR analysis was performed using R (version 4.3.1) and the "TwoSampleMR" package to evaluate the link between immune cells and CRC. The impact on CRC risk was quantified as odds ratios (OR) with 95% confidence intervals (CI), considering a P-value < 0.05 as indicative of a significant causal connection. The main method employed was a random-effects inverse variance weighted (IVW) analysis, enhanced with MR-Egger, weighted median, simple mode, and weighted mode approaches to ensure result consistency.

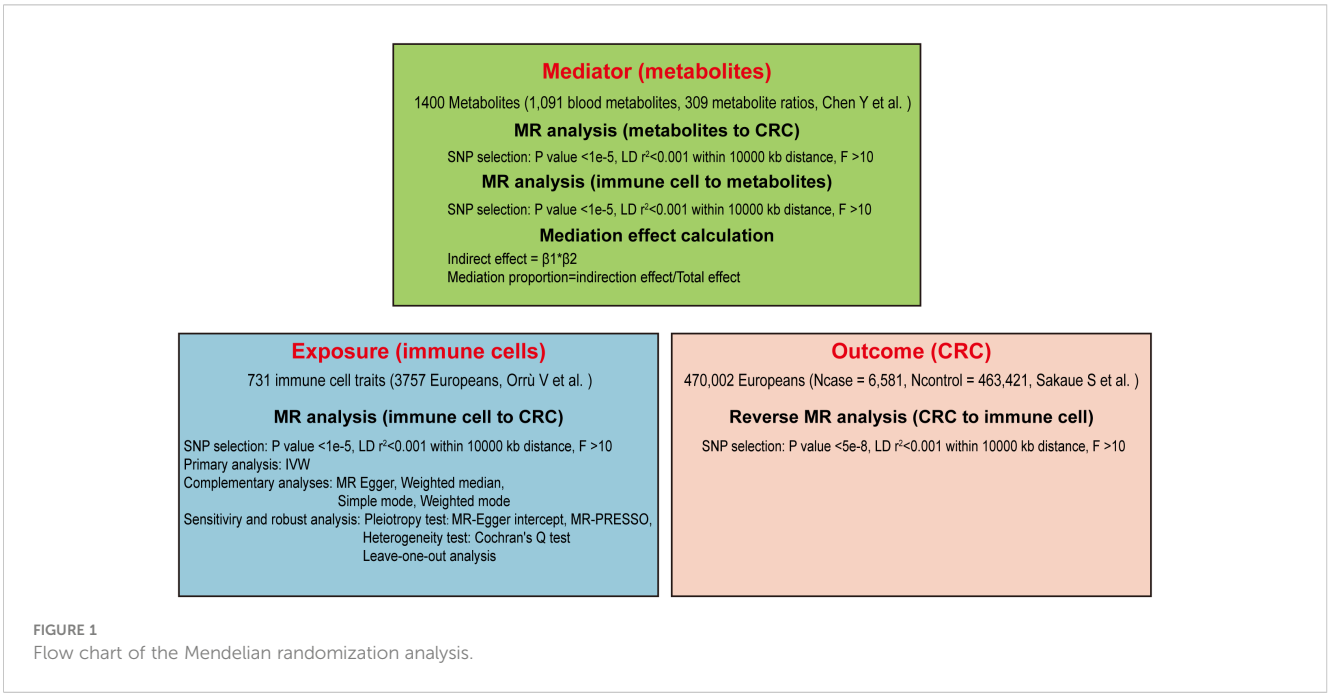

FIGURE 1
Flow chart of the Mendelian randomization analysis.

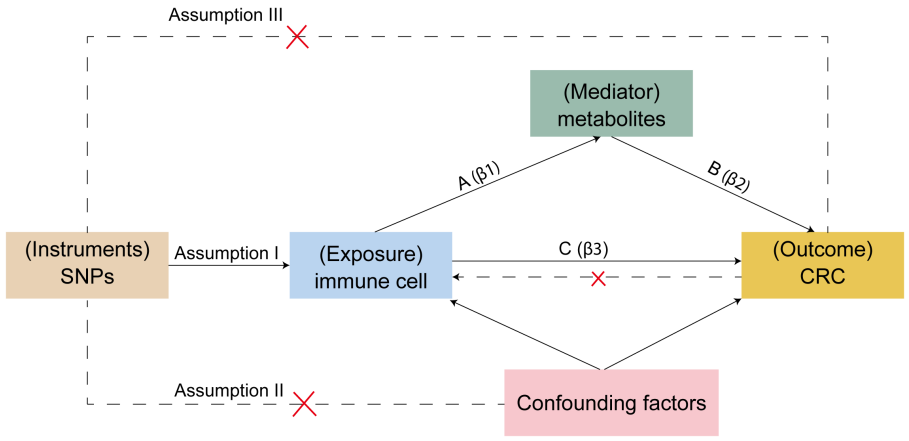

FIGURE 2
Mendelian randomization assumptions.

2.5 Sensitivity analysis

The primary assessment of the impact of immune cells on CRC employed the random-effects IVW method (35). Up to four MR methods, each with different assumptions regarding pleiotropy, were applied to generate effect estimates. Significant heterogeneity was identified through Cochran's Q test, with a *P*-value below 0.05 indicating its significance. Pleiotropy was assessed using the MR-PRESSO test and MR-Egger regression intercept, with *P*-values above 0.05 suggesting no pleiotropy. The robustness of our findings was further confirmed by a leave-one-out analysis, which assessed the impact of individual SNPs on the MR analysis.

2.6 Mediation analysis

A two-step MR approach was executed to investigate if an intermediate risk factor mediates the link between immune cells and CRC. First, we used bidirectional Mendelian randomization to identify 23 immune cells with a causal relationship to CRC out of 731 immune cells. The criteria for SNP selection included a significance threshold of $P < 1 \times 10^{-5}$, exclusion of SNPs in linkage disequilibrium ($r^2 < 0.001$ within a 10,000 kb distance), and removal of weak instruments ($F < 10$). Next, we applied the same criteria to identify 17 metabolites out of 1,400 with a causal relationship to CRC. We then used the 23 immune cell traits as exposure factors to identify significant mediators among the 17 metabolites, using the same SNP selection criteria. We employed the Inverse-Variance Weighted (IVW) method as the primary approach to estimate the effect of immune cells on metabolites (β1). The most significant metabolites associated with immune cell traits were then analyzed as mediators in the causal relationship with CRC. Ultimately, we identified the role of nine immune cell types in colorectal cancer risk, along with the mediating effects of nine metabolites. The direct effects β1 from immune cell traits to metabolites, β2 from metabolites to CRC, and the total effect β3 from immune cell traits to CRC were calculated. The mediating effect was defined as $\beta = \beta1 * \beta2$, and its proportion relative to the total effect was expressed as $R = (\beta/\beta3) * 100\%$ (36, 37).

3 Results

3.1 Two-sample Mendelian randomization analysis between immune cells and CRC

We assessed the causal relationships between 28 types of immune cells and CRC using a two-sample MR approach (Figure 3; Supplementary Table 5). Our analysis distinguished 14 immune cell types as protective and 14 as risk factors for CRC. Notably, immune cells such as IgD^+ $CD24^+$ %B cell, CD14 on $CD14^+$ $CD16^-$ monocytes, and IgD^- CD38br AC exhibited odds ratios (ORs) of 0.932 (95% CI: 0.881-0.986), 0.943 (95% CI: 0.900-0.988), and 0.946 (95% CI: 0.918-0.975), respectively, indicating their protective roles against CRC. Conversely, SSC-A on B cells, CD8 on $CD28^-$ CD8br, and CCR2 on $CD62L^+$ myeloid DC were identified as risk factors, with ORs of 1.073 (95% CI: 1.020-1.130), 1.054 (95% CI: 1.002-1.109), and 1.052 (95% CI: 1.007-1.100), respectively. Our analyses for heterogeneity and pleiotropy showed no significant findings, confirming the robustness of our results (Supplementary Table 6).

Further validation through reverse Mendelian randomization analysis on these 28 immune cell types revealed no significant findings for 23 of these types (Supplementary Table 7), which were subsequently analyzed for potential mediating effects.

3.2 Effect of metabolites on CRC

In our mediation analysis, we explored the effects of 1,400 metabolites on CRC using the IVW method. We identified eight

metabolites that demonstrated protective effects against CRC. Notably, IDA, an amino acid derivative, had a significant OR of 0.879 (95% CI: 0.797-0.969). Additionally, the ratio of retinol (Vitamin A) to linoleoyl-arachidonoyl-glycerol (18:2 to 20:4) showed a protective effect with an OR of 0.903 (95% CI: 0.857-0.951). Conversely, nine metabolites were identified as risk factors for CRC, including 3-carboxy-4-methyl-5-propyl-2-furanpropanoate (CMPF) and 1,2-dipalmitoyl-gpc (16:0/16:0), with ORs of 1.146 (95% CI: 1.039-1.264) and 1.133 (95% CI: 1.073-1.197), respectively (Figure 4; Supplementary Table 8). These findings highlight the complex relationship between specific metabolites and CRC and provide a basis for further mediation analysis. Analyses for heterogeneity and pleiotropy also indicated robustness (Supplementary Table 9).

3.3 Effect of immune cell traits on metabolites

Building on the previous identification of relationships between 23 immune cell traits and CRC, we examined the causal influence of these immune cell traits on 17 metabolites. Our analysis identified significant causal relationships for nine immune cells affecting nine metabolites (Figure 5; Supplementary Table 10). Notably, traits such as IgD$^-$ CD38dim %lymphocyte for Isovalerylcarnitine (C5), CD28 on secreting Treg for Glutarylcarnitine (c5-dc), and CD14 on CD14$^+$ CD16$^-$ monocytes for Iminodiacetate (IDA) had ORs of 1.035 (95% CI: 1.004-1.067), 1.040 (95% CI: 1.008-1.073), and 1.055 (95% CI: 1.001-1.112), respectively. The remaining immune cell traits exhibited protective effects on specific metabolites. Our

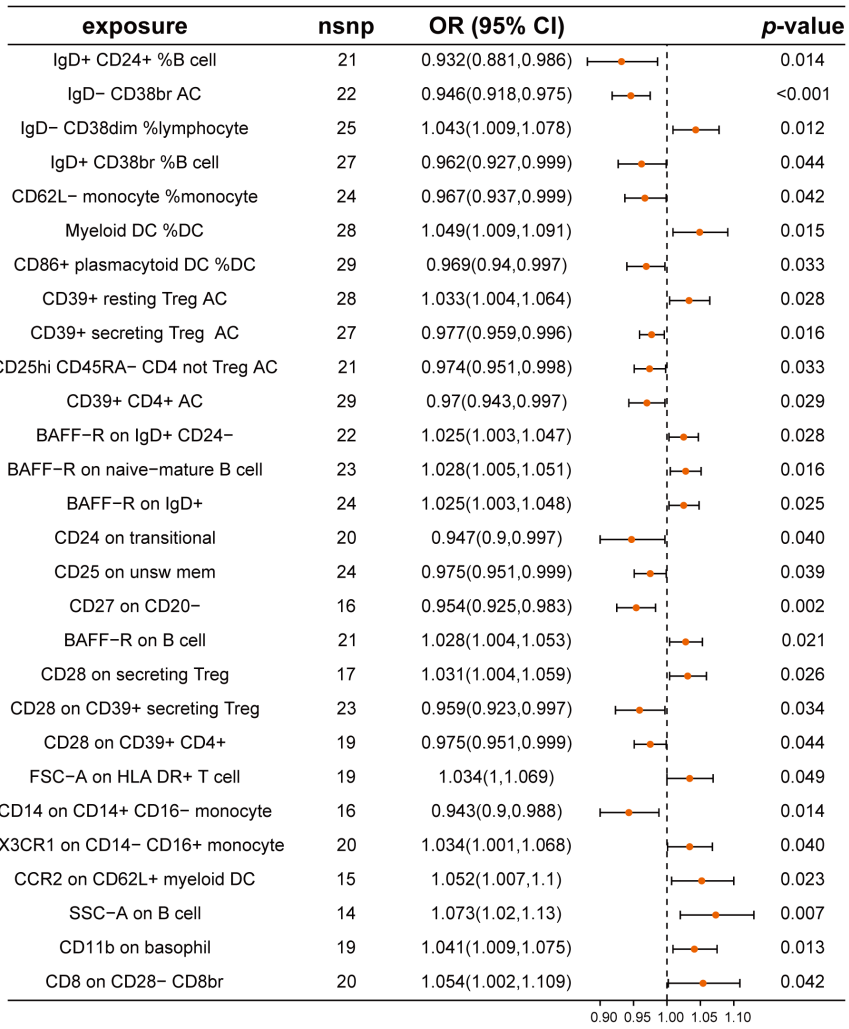

FIGURE 3
Mendelian randomization analysis between immune cells and CRC. This plot visualizes the association between immune cell and CRC. Each point denotes the Odds Ratio (OR) for the exposure. Horizontal lines represent the 95% confidence intervals. The vertical dashed line at OR=1 serves as a reference for no effect. OR > 1 indicates that immune cells are a risk factor for CRC, while OR < 1 indicates that immune cells are a protective factor for CRC.

10.3389/fimmu.2024.1444222

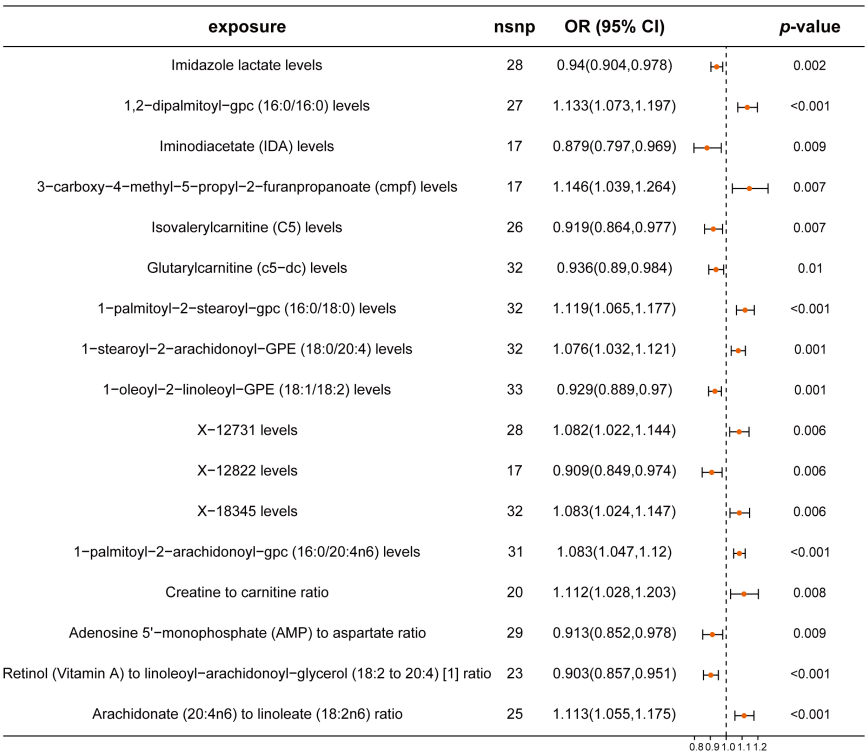

FIGURE 4
Forest plot of metabolites associated with CRC risk. This plot visualizes the association between metabolites and CRC. Each point denotes the Odds Ratio (OR) for the exposure. Horizontal lines represent the 95% confidence intervals. The vertical dashed line at OR=1 serves as a reference for no effect. OR > 1 indicates that metabolites are a risk factor for CRC, while OR < 1 indicates that metabolites are a protective factor for CRC.

analyses confirmed no significant pleiotropy or heterogeneity, reinforcing the reliability of these results (Supplementary Table 11).

3.4 Mediation analysis of immune cell traits, metabolites, and colorectal cancer

After identifying key mediators affecting CRC and the effects of immune cell traits on these mediators, we quantified the proportion of mediating effects. Comprehensive results can be found in Figure 6, Supplementary Table 12, leave-one-out plot was presented in Supplementary Figure 1. Notably, IgD^+ CD38br %B cell and CD14 on $CD14^+$ $CD16^-$ monocyte mediated their effects on CRC through IDA levels, with mediation proportions of -10.4% and 11.8%, respectively. Additionally, IgD^- CD38dim% lymphocyte and $CD62L^-$ monocyte %monocyte mediated their effects through isovalerylcarnitine (C5) levels, with mediation proportions of -6.86% and -14.7%, respectively. Furthermore, IgD^+ CD38br %B cell and BAFF-R on B cell mediated their effects through the Retinol (Vitamin A) to linoleoyl-arachidonoyl-glycerol (18:2 to 20:4) ratio, with mediation proportions of -8.84% and 11.4%, respectively.

4 Discussion

In this MR study examining the association between immune cells and CRC risk, we identified 23 immune cell types linked to CRC, with specific blood metabolites potentially acting as mediators. For example, The ratios of Adenosine 5'-monophosphate (AMP) to aspartate and Retinol (Vitamin A) to linoleoyl-arachidonoyl-glycerol (18:2 to 20:4) were found to concurrently mediate the promoting effects of Myeloid DC %DC and BAFF-R on B cells in colorectal cancer (CRC). IDA mediates the protective effect of $CD14^+$ $CD16^-$ monocytes on CRC risk with a mediation effect proportion of 11.8%. Conversely, IDA was also seen to decrease the protective effect of IgD^+ CD38br %B cells on CRC risk, with a mediation effect proportion of -10.4%. Additionally, $CD39^+$ resting Treg cells increase CRC risk through metabolites such as imidazole lactate, glutarylcarnitine (C5-DC), and 1-oleoyl-2-linoleoyl-GPE (18:1/18:2), with mediation proportions of 5.68%, 6.53%, and 7.07%, respectively. These results underscore the intricate interactions between specific immune cells, their associated metabolites, and their cumulative impact on CRC, highlighting the importance of understanding both direct and indirect effects of immune cell traits on CRC to develop targeted therapeutic strategies.

Immune cells hold significant prognostic value in colorectal cancer (CRC), with their plasticity within the tumor microenvironment (TME) leading to the expression of various phenotypes that either promote or inhibit tumor progression. Our study identifies four dendritic cell (DC) subsets associated with CRC development: Myeloid DC %DC and CCR2 on $CD62L^+$ myeloid DC are risk factors for CRC, while $CD86^+$ plasmacytoid DC %DC and $CD62L^-$ monocyte %monocyte serve as protective

10.3389/fimmu.2024.1444222

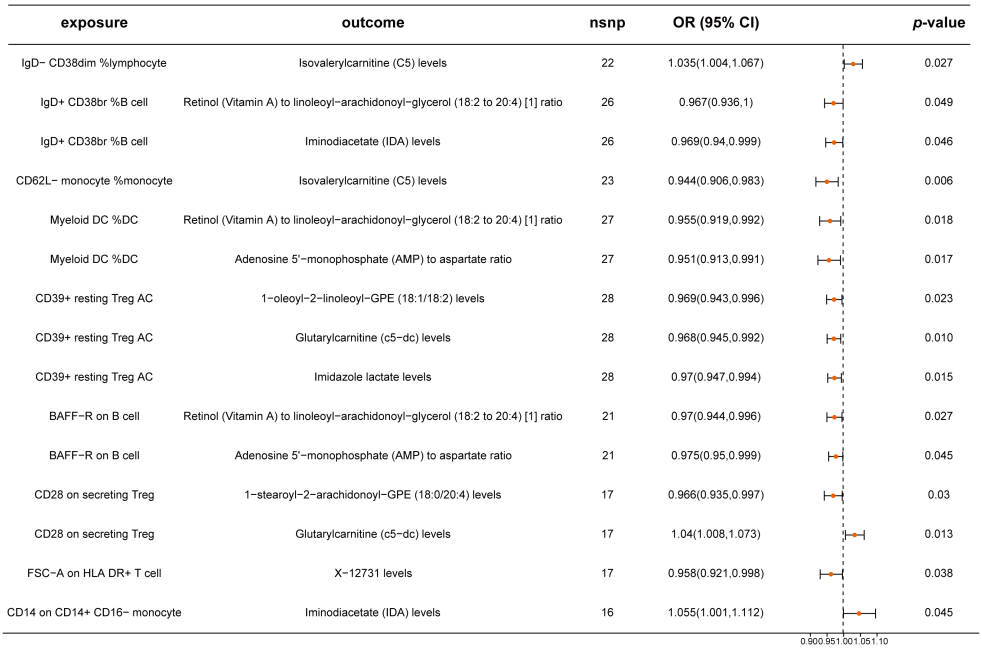

FIGURE 5
Mendelian randomization analysis between immune cells and metabolites. This plot visualizes the association between immune cells and metabolites. Each point denotes the Odds Ratio (OR) for the exposure. Horizontal lines represent the 95% confidence intervals. The vertical dashed line at OR=1 serves as a reference for no effect. OR > 1 indicates that immune cells are a risk factor for metabolites, while OR < 1 indicates that immune cells are a protective factor for metabolites.

factors. This aligns with findings by Gulubova MV, who reported that higher infiltration of $CD83^+$ DCs correlates with better prognosis in CRC patients (38). Conversely, Sandel MH observed that CD208-positive and CD1a-positive infiltrating dendritic cells are associated with shortened survival in CRC patients (39). Further mediation analysis in our study reveals that the ratios of Adenosine 5'-monophosphate (AMP) to aspartate and Retinol (Vitamin A) to linoleoyl-arachidonoyl-glycerol (18:2 to 20:4) mediate the promoting effects of Myeloid DC %DC on CRC. Additionally, Isovalerylcarnitine (C5) levels diminish the protective role of $CD62L^-$ monocyte %monocyte against CRC, suggesting that retinol metabolism, lipid metabolism, and leucine metabolism in DC cells impact CRC progression. Previous studies have highlighted the critical role of metabolic regulation in DC function. Alterations in cholesterol metabolism and mevalonate (MVA) signaling can affect DC function and consequently the immune response of CRC (40). The accumulation of lipid droplets can impede calreticulin exposure, thus preventing DC

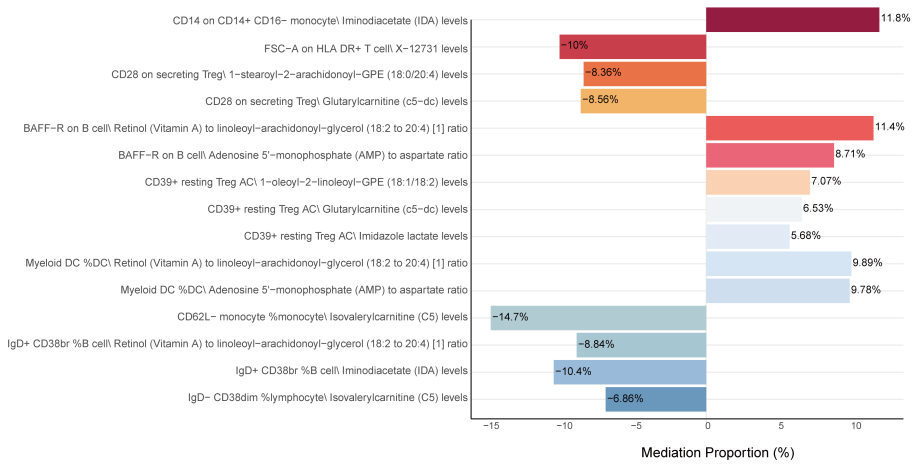

FIGURE 6
Mediation analysis of metabolites between immune cells and CRC. This figure shows the proportion of the mediation effect of each metabolite on the impact of various immune cells on CRC. A positive value indicates that the metabolite and immune cells have a consistent effect on CRC, while a negative value indicates that the metabolite and immune cells have opposite effects on CRC. The length of the bar represents the magnitude of the mediation effect.

maturation, delaying DC activation, and promoting CRC progression (41). However, reports on the impact of vitamin A and leucine metabolism in DC cells on CRC are lacking.

Our study also reveals differential impacts of B cell phenotypes on CRC. IgD^+ $CD24^+$ %B cells, IgD^- CD38br AC, and IgD^+ CD38br %B cells act as protective factors against CRC, while IgD^- CD38dim % lymphocyte, BAFF-R on IgD^+ $CD24^-$, BAFF-R on naive-mature B cell, BAFF-R on IgD^+, BAFF-R on B cell, and SSC-A on B cell are identified as risk factors. Mediation analysis further shows that Iminodiacetate (IDA) levels and Retinol (Vitamin A) to linoleoyl-arachidonoyl-glycerol (18:2 to 20:4) ratio attenuate the protective effect of IgD^+ CD38br %B cells on CRC, whereas Isovalerylcarnitine (C5) levels diminish the promoting effect of IgD^- CD38dim %lymphocyte. Besides, the ratios of Adenosine 5'-monophosphate (AMP) to aspartate and Retinol (Vitamin A) to linoleoyl-arachidonoyl-glycerol (18:2 to 20:4) mediate the promoting effects of BAFF-R on B cells in CRC. Our findings suggest that most B cells contribute to immune escape in CRC, consistent with previous reports indicating that certain regulatory B cell subsets, which preferentially metabolize leucine, can promote CRC progression (42). Lipid metabolites such as acylcarnitine enhance B cell-mediated anti-tumor immunity by promoting mitochondrial oxidative phosphorylation (43). Fundamental research indicates that inhibiting the conversion of B cells to IgA^+ cells may suppress CRC growth (44). In contrast, previous Mendelian randomization studies showed that IgD^+CD24^+ B cells are risk factors for glioblastoma (45), suggesting differences across tumor types and necessitating further experimental research to elucidate the roles of various immune cell phenotypes in CRC development and progression.

Moreover, we identified $CD39^+$ resting Treg cells and CD28 on secreting Treg cells as risk factors for CRC, consistent with previous findings that increased accumulation of Treg cells is often associated with CRC progression, metastasis, immune therapy failure, and poor prognosis (46–49). Additionally, our study found that Imidazole lactate levels, Glutarylcarnitine (C5-DC) levels, and 1-oleoyl-2-linoleoyl-GPE (18:1/18:2) levels mediate the promoting effect of $CD39^+$ resting Treg cells on CRC, while Glutarylcarnitine (C5-DC) levels and 1-stearoyl-2-arachidonoyl-GPE (18:0/20:4) levels attenuate the promoting effect of CD28 on secreting Treg cells. This suggests that amino acid metabolism and fatty acid oxidation may play roles in regulating Treg cells' impact on CRC. Previous research has shown that kynurenine can enhance tumor aggressiveness by upregulating PD-L1 expression on Treg cells, thus contributing to immune escape in CRC (50). Additionally, TI-Treg cells use lipid metabolism-driven oxidative phosphorylation (OXPHOS) to meet their energy needs and immune suppressive functions (51). Furthermore, high IDO expression in CRC cells and tryptophan depletion in the TME are associated with tumor immune escape and increased Treg infiltration in CRC (52). The above findings suggest that targeting amino acid and fatty acid metabolites of different Treg cell subtypes could offer a potential strategy for immune regulation in CRC.

Substantial evidence suggests that blood metabolites are closely linked to tumor malignancy. For instance, ketogenic diets rich in β-hydroxybutyrate can inhibit CRC cell growth (53), and α-ketoglutarate in the TME suppresses tumor growth (54). Beyond direct effects on tumor cells, metabolites like indole-3-propionic acid (IPA) regulate $CD8^+$ T cell stemness and enhance anti-PD-1 immunotherapy efficacy (55). Lactate in the TME also boosts $CD8^+$ T cell stemness and anti-tumor immunity (56), while gut microbiota-derived butyrate enhances chemotherapy efficacy by modulating $CD8^+$ T cell function (57), and indole-3-carboxylic acid (ICA) augments $CD8^+$ T cell functionality by inhibiting regulatory T cell differentiation (58). We identified 17 metabolites associated with CRC risk, with eight reducing and nine increasing CRC risk. Yet, there is no experimental evidence directly linking IDA, CMPF, or 1,2-dipalmitoyl-glycerophosphocholine to tumorigenesis.

This study leverages large-scale GWAS data to conduct two-sample, two-step, and mediation MR analyses, emphasizing the methodological rigor and efficiency of our approach. Our conclusions, founded on genetic instrumental variables and supported by extensive pleiotropy analyses, are reliable and minimally affected by horizontal pleiotropy or other confounding factors. However, the study has limitations, First, The MR-Egger and weighted median MR approaches might have lacked sufficient power to identify directional pleiotropy in the genetic instruments, if it existed (59). Second, Although MR can mitigate confounding effects from environmental and behavioral factors, residual confounding remains unavoidable. Third, notably the focus on European populations, which may limit the generalizability of the findings. Fourth, our reliance on summary-level data precludes detailed causal relationship analyses within specific subgroups, such as gender or cancer subtype. Despite these limitations, our comprehensive insights provide a solid foundation for understanding the complex dynamics at play and the potential for developing targeted therapeutic strategies based on these findings.

5 Conclusion

In conclusion, this study provides a comprehensive evaluation of the roles of circulating immune cells and blood metabolites in the development of CRC, uncovering significant abnormalities in the immune-metabolic network associated with this disease. Our findings open new avenues for understanding the pathogenesis of CRC and highlight the critical role of blood metabolites in mediating the relationship between immune cells and CRC. This enhanced understanding of CRC's pathological processes not only deepens our knowledge of the disease but also lays a theoretical foundation for the development of novel immunotherapeutic and metabolite-targeted interventions. These insights are pivotal for advancing CRC treatment strategies, emphasizing the necessity of further research to explore these complex biological interactions and their potential therapeutic applications.

Data availability statement

The original contributions presented in the study are included in the article/Supplementary Material. Further inquiries can be directed to the corresponding authors.

Ethics statement

The data for this study were obtained from publicly accessible databases, thereby eliminating the need for further ethical approval. The studies were conducted in accordance with the local legislation and institutional requirements. Written informed consent for participation was not required from the participants or the participants' legal guardians/next of kin in accordance with the national legislation and institutional requirements.

Author contributions

QY: Data curation, Formal analysis, Methodology, Resources, Software, Writing – original draft, Writing – review & editing. BD: Data curation, Formal analysis, Visualization, Writing – original draft, Writing – review & editing. JY: Data curation, Validation, Visualization, Writing – original draft, Writing – review & editing. DZ: Data curation, Formal analysis, Methodology, Writing – original draft, Writing – review & editing. XC: Data curation, Validation, Visualization, Writing – review & editing. MS: Data curation, Methodology, Validation, Writing – review & editing. JK: Validation, Visualization, Writing – review & editing. RL: Conceptualization, Project administration, Supervision, Validation, Writing – review & editing. HL: Conceptualization, Project administration, Supervision, Validation, Visualization, Writing – review & editing. LG: Conceptualization, Funding acquisition, Project administration, Supervision, Validation, Visualization, Writing – review & editing.

Funding

The author(s) declare financial support was received for the research, authorship, and/or publication of this article. This project was supported by the Science and Health joint medical research project in Fuling District, Chongqing (2022KWLH001).

Conflict of interest

The authors declare that the research was conducted in the absence of any commercial or financial relationships that could be construed as a potential conflict of interest.

The handling editor declared a shared parent affiliation, though no other collaboration, with several of the authors QY, BD, XC, MS, JK, HL, LG at the time of the review.

Publisher's note

All claims expressed in this article are solely those of the authors and do not necessarily represent those of their affiliated organizations, or those of the publisher, the editors and the reviewers. Any product that may be evaluated in this article, or claim that may be made by its manufacturer, is not guaranteed or endorsed by the publisher.

Supplementary material

The Supplementary Material for this article can be found online at: https://www.frontiersin.org/articles/10.3389/fimmu.2024.1444222/full#supplementary-material

SUPPLEMENTARY FIGURE 1
Leave-one-out plots for the mediation analysis.

References

1. Bray F, Laversanne M, Sung H, Ferlay J, Siegel RL, Soerjomataram I, et al. Global cancer statistics 2022: GLOBOCAN estimates of incidence and mortality worldwide for 36 cancers in 185 countries. *CA Cancer J Clin*. (2024) 74:229–63. doi: 10.3322/caac.21834

2. Siegel RL, Miller KD, Wagle NS, Jemal A. Cancer statistics, 2023. *CA Cancer J Clin*. (2023) 73:17–48. doi: 10.3322/caac.21763

3. Chung DC, Rustgi AK. The hereditary nonpolyposis colorectal cancer syndrome: genetics and clinical implications. *Ann Intern Med*. (2003) 138:560–70. doi: 10.7326/0003-4819-138-7-200304010-00012

4. Jess T, Rungoe C, Peyrin-Biroulet L. Risk of colorectal cancer in patients with ulcerative colitis: a meta-analysis of population-based cohort studies. *Clin Gastroenterol Hepatol*. (2012) 10:639–45. doi: 10.1016/j.cgh.2012.01.010

5. Botteri E, Borroni E, Sloan EK, Bagnardi V, Bosetti C, Peveri G, et al. Smoking and colorectal cancer risk, overall and by molecular subtypes: A meta-analysis. *Am J Gastroenterol*. (2020) 115:1940–9. doi: 10.14309/ajg.0000000000000803

6. Fedirko V, Tramacere I, Bagnardi V, Rota M, Scotti L, Islami F, et al. Alcohol drinking and colorectal cancer risk: an overall and dose-response meta-analysis of published studies. *Ann Oncol*. (2011) 22:1958–72. doi: 10.1093/annonc/mdq653

7. Kyrgiou M, Kalliala I, Markozannes G, Gunter MJ, Paraskevaidis E, Gabra H, et al. Adiposity and cancer at major anatomical sites: umbrella review of the literature. *BMJ*. (2017) 356:j477. doi: 10.1136/bmj.j477

8. Wong CC, Yu J. Gut microbiota in colorectal cancer development and therapy. *Nat Rev Clin Oncol*. (2023) 20:429–52. doi: 10.1038/s41571-023-00766-x

9. Fang M, Li Y, Huang K, Qi S, Zhang J, Zgodzinski W, et al. IL33 promotes colon cancer cell stemness via JNK activation and macrophage recruitment. *Cancer Res*. (2017) 77:2735–45. doi: 10.1158/0008-5472.CAN-16-1602

10. Kießler M, Plesca I, Sommer U, Wehner R, Wilczkowski F, Müller L, et al. Tumor-infiltrating plasmacytoid dendritic cells are associated with survival in human colon cancer. *J Immunother Cancer*. (2021) 9:e001813. doi: 10.1136/jitc-2020-001813

11. Sundström P, Stenstad H, Langenes V, Ahlmanner F, Theander L, Ndah TG, et al. Regulatory T cells from colon cancer patients inhibit effector T-cell migration through an adenosine-dependent mechanism. *Cancer Immunol Res*. (2016) 4:183–93. doi: 10.1158/2326-6066.CIR-15-0050

12. Toffoli EC, van Vliet AA, Verheul HWM, van der Vliet HJ, Tuynman J, Spanholtz J, et al. Allogeneic NK cells induce monocyte-to-dendritic cell conversion, control tumor growth, and trigger a pro-inflammatory shift in patient-derived cultures

of primary and metastatic colorectal cancer. *J Immunother Cancer*. (2023) 11:e007554. doi: 10.1136/jitc-2023-007554

13. Leone RD, Powell JD. Metabolism of immune cells in cancer. *Nat Rev Cancer*. (2020) 20:516–31. doi: 10.1038/s41568-020-0273-y

14. Sukumar M, Liu J, Ji Y, Subramanian M, Crompton JG, Yu Z, et al. Inhibiting glycolytic metabolism enhances CD8$^+$ T cell memory and antitumor function. *J Clin Invest*. (2013) 123:4479–88. doi: 10.1172/JCI69589

15. Geiger R, Rieckmann JC, Wolf T, Basso C, Feng Y, Fuhrer T, et al. L-arginine modulates T cell metabolism and enhances survival and anti-tumor activity. *Cell*. (2016) 167:829–42.e13. doi: 10.1016/j.cell.2016.09.031

16. Nabe S, Yamada T, Suzuki J, Toriyama K, Yasuoka T, Kuwahara M, et al. Reinforce the antitumor activity of CD8$^+$ T cells via glutamine restriction. *Cancer Sci*. (2018) 109:3737–50. doi: 10.1111/cas.13827

17. Yang W, Bai Y, Xiong Y, Zhang J, Chen S, Zheng X, et al. Potentiating the antitumour response of CD8($^+$) T cells by modulating cholesterol metabolism. *Nature*. (2016) 531:651–5. doi: 10.1038/nature17412

18. Cong J, Wang X, Zheng X, Wang D, Fu B, Sun R, et al. Dysfunction of natural killer cells by FBP1-induced inhibition of glycolysis during lung cancer progression. *Cell Metab*. (2018) 28:243–55.e5. doi: 10.1016/j.cmet.2018.06.021

19. Hossain F, Al-Khami AA, Wyczechowska D, Hernandez C, Zheng L, Reiss K, et al. Inhibition of fatty acid oxidation modulates immunosuppressive functions of myeloid-derived suppressor cells and enhances cancer therapies. *Cancer Immunol Res*. (2015) 3:1236–47. doi: 10.1158/2326-6066.CIR-15-0036

20. Zhu C-X, Yan K, Chen L, Huang RR, Bian ZH, Wei HR, et al. Targeting OXCT1-mediated ketone metabolism reprograms macrophages to promote antitumor immunity via CD8$^+$ T cells in hepatocellular carcinoma. *J Hepatol*. (2024) S0168-8278(24)00342-8. doi: 10.1016/j.jhep.2024.05.007

21. Goossens P, Rodriguez-Vita J, Etzerodt A, Masse M, Rastoin O, Gouirand V, et al. Membrane cholesterol efflux drives tumor-associated macrophage reprogramming and tumor progression. *Cell Metab*. (2019) 29:1376–89.e4. doi: 10.1016/j.cmet.2019.02.016

22. Sekula P, Del Greco MF, Pattaro C, Köttgen A. Mendelian randomization as an approach to assess causality using observational data. *J Am Soc Nephrol*. (2016) 27:3253–65. doi: 10.1681/ASN.2016010098

23. Ming R, Wu H, Liu H, Zhan F, Qiu X, Ji M. Causal effects and metabolites mediators between immune cell and risk of breast cancer: a Mendelian randomization study. *Front In Genet*. (2024) 15:1380249. doi: 10.3389/fgene.2024.1380249

24. Zhang K, Zhu J, Wang P, Chen Y, Wang Z, Ge X, et al. Plasma metabolites as mediators in immune cell-pancreatic cancer risk: insights from Mendelian randomization. *Front Immunol*. (2024) 15:1402113. doi: 10.3389/fimmu.2024.1402113

25. Zhu X, Qiu Z, Yang M, Yang J, Kong L, Li L, et al. Causal associations of BAFF-R on IgD$^+$ CD24- B cell immune cell trait with hepatocellular carcinoma and the mediating role of phenylacetylglutamate levels: a Mendelian randomization study. *J Cancer*. (2024) 15:4591–603. doi: 10.7150/jca.96059

26. Constantinescu A-E, Bull CJ, Jones N, Mitchell R, Burrows K, Dimou N, et al. Circulating white blood cell traits and colorectal cancer risk: A Mendelian randomisation study. *Int J Cancer*. (2024) 154:94–103. doi: 10.1002/ijc.34691

27. Carter AR, Sanderson E, Hammerton G, Richmond RC, Davey Smith G, Heron J, et al. Mendelian randomisation for mediation analysis: current methods and challenges for implementation. *Eur J Epidemiol*. (2021) 36:465–78. doi: 10.1007/s10654-021-00757-1

28. Orrù V, Steri M, Sidore C, Marongiu M, Serra V, Olla S, et al. Complex genetic signatures in immune cells underlie autoimmunity and inform therapy. *Nat Genet*. (2020) 52:1036–45. doi: 10.1038/s41588-020-0684-4

29. Sakaue S, Kanai M, Tanigawa Y, Karjalainen J, Kurki M, Koshiba S, et al. A cross-population atlas of genetic associations for 220 human phenotypes. *Nat Genet*. (2021) 53:1415–24. doi: 10.1038/s41588-021-00931-x

30. Larsson SC, Butterworth AS, Burgess S. Mendelian randomization for cardiovascular diseases: principles and applications. *Eur Heart J*. (2023) 44:4913–24. doi: 10.1093/eurheartj/ehad736

31. Xiang Y, Zhang C, Wang J, Cheng Y, Wang L, Tong Y, et al. Identification of host gene-microbiome associations in colorectal cancer patients using mendelian randomization. *J Transl Med*. (2023) 21:535. doi: 10.1186/s12967-023-04335-9

32. Ni J-J, Li X-S, Zhang H, Xu Q, Wei XT, Feng GJ, et al. Mendelian randomization study of causal link from gut microbiota to colorectal cancer. *BMC Cancer*. (2022) 22:1371. doi: 10.1186/s12885-022-10483-w

33. Cao J, Wang Z, Zhu M, Huang Y, Jin Z, Xiong Z. Low-density lipoprotein cholesterol and risk of hepatocellular carcinoma: a Mendelian randomization and mediation analysis. *Lipids Health Dis*. (2023) 22:110. doi: 10.1186/s12944-023-01877-1

34. Pierce BL, Ahsan H, Vanderweele TJ. Power and instrument strength requirements for Mendelian randomization studies using multiple genetic variants. *Int J Epidemiol*. (2011) 40:740–52. doi: 10.1093/ije/dyq151

35. Yun Z, Guo Z, Li X, Shen Y, Nan M, Dong Q, et al. Genetically predicted 486 blood metabolites in relation to risk of colorectal cancer: A Mendelian randomization study. *Cancer Med*. (2023) 12:13784–99. doi: 10.1002/cam4.6022

36. VanderWeele TJ. Mediation analysis: A practitioner's guide. *Annu Rev Public Health*. (2016) 37:17–32. doi: 10.1146/annurev-publhealth-032315-021402

37. Dai H, Hou T, Wang Q, Hou Y, Wang T, Zheng J, et al. Causal relationships between the gut microbiome, blood lipids, and heart failure: a Mendelian randomization analysis. *Eur J Prev Cardiol*. (2023) 30:1274–82. doi: 10.1093/eurjpc/zwad171

38. Gulubova MV, Ananiev JR, Vlaykova TI, Yovchev Y, Tsoneva V, Manolova IM. Role of dendritic cells in progression and clinical outcome of colon cancer. *Int J Colorectal Dis*. (2012) 27:159–69. doi: 10.1007/s00384-011-1334-1

39. Sandel MH, Dadabayev AR, Menon AG, Morreau H, Melief CJ, Offringa R, et al. Prognostic value of tumor-infiltrating dendritic cells in colorectal cancer: role of maturation status and intratumoral localization. *Clin Cancer Research: an Off J Am Assoc For Cancer Res*. (2005) 11:2576–82. doi: 10.1158/1078-0432.CCR-04-1448

40. Yang J, Pan X, Zhang J, Ma S, Zhou J, Jia Z, et al. Reprogramming dysfunctional dendritic cells by a versatile metabolism nano-intervenor for enhancing cancer combinatorial immunotherapy. *Nano Today*. (2022) 46:101618. doi: 10.1016/j.nantod.2022.101618

41. Cotte AK, Aires V, Fredon M, Limagne E, Derangère V, Thibaudin M, et al. Lysophosphatidylcholine acyltransferase 2-mediated lipid droplet production supports colorectal cancer chemoresistance. *Nat Commun*. (2018) 9:322. doi: 10.1038/s41467-017-02732-5

42. Wang Z, Lu Z, Lin S, Xia J, Zhong Z, Xie Z, et al. Leucine-tRNA-synthase-2-expressing B cells contribute to colorectal cancer immunoevasion. *Immunity*. (2022) 55:1067–81.e8. doi: 10.1016/j.immuni.2022.04.017

43. Zhang Z, Xu X, Zhang D, Zhao S, Wang C, Zhang G, et al. Targeting Erbin-mitochondria axis in platelets/megakaryocytes promotes B cell-mediated antitumor immunity. *Cell Metab*. (2024) 36:541–56.e9. doi: 10.1016/j.cmet.2023.12.020

44. Zhong Z, Zhang H, Nan K, Zhong J, Wu Q, Lu L, et al. Fasting-mimicking diet drives antitumor immunity against colorectal cancer by reducing igA-producing cells. *Cancer Res*. (2023) 83:3529–43. doi: 10.1158/0008-5472.CAN-23-0323

45. Huang M, Liu Y, Peng J, Cheng Y. Causal effects of immune cells in glioblastoma: a Bayesian Mendelian Randomization study. *Front Neurol*. (2024) 15:1375723. doi: 10.3389/fneur.2024.1375723

46. Chang L-Y, Lin Y-C, Mahalingam J, Huang CT, Chen TW, Kang CW, et al. Tumor-derived chemokine CCL5 enhances TGF-β-mediated killing of CD8($^+$) T cells in colon cancer by T-regulatory cells. *Cancer Res*. (2012) 72:1092–102. doi: 10.1158/0008-5472.CAN-11-2493

47. Brudvik KW, Henjum K, Aandahl EM, Bjørnbeth BA, Taskén K. Regulatory T-cell-mediated inhibition of antitumor immune responses is associated with clinical outcome in patients with liver metastasis from colorectal cancer. *Cancer Immunology Immunotherapy: CII*. (2012) 61:1045–53. doi: 10.1007/s00262-011-1174-4

48. Katz SC, Bamboat ZM, Maker AV, Shia J, Pillarisetty VG, Yopp AC, et al. Regulatory T cell infiltration predicts outcome following resection of colorectal cancer liver metastases. *Ann Surg Oncol*. (2013) 20:946–55. doi: 10.1245/s10434-012-2668-9

49. Chaput N, Louafi S, Bardier A, Charlotte F, Vaillant JC, Ménégaux F, et al. Identification of CD8$^+$CD25$^+$Foxp3$^+$ suppressive T cells in colorectal cancer tissue. *Gut*. (2009) 58:520–9. doi: 10.1136/gut.2008.158824

50. Deng B, Yang B, Chen J, Wang S, Zhang W, Guo Y, et al. Gallic acid induces T-helper-1-like Treg cells and strengthens immune checkpoint blockade efficacy. *J Immunother Cancer*. (2022) 10:e004037. doi: 10.1136/jitc-2021-004037

51. Michalek RD, Gerriets VA, Jacobs SR, Macintyre AN, MacIver NJ, Mason EF, et al. Cutting edge: distinct glycolytic and lipid oxidative metabolic programs are essential for effector and regulatory CD4$^+$ T cell subsets. *J Immunol*. (2011) 186:3299–303. doi: 10.4049/jimmunol.1003613

52. Brandacher G, Perathoner A, Ladurner R, Schneeberger S, Obrist P, Winkler C, et al. Prognostic value of indoleamine 2,3-dioxygenase expression in colorectal cancer: effect on tumor-infiltrating T cells. *Clin Cancer Research: an Off J Am Assoc For Cancer Res*. (2006) 12:1144–51. doi: 10.1158/1078-0432.CCR-05-1966

53. Dmitrieva-Posocco O, Wong AC, Lundgren P, Golos AM, Descamps HC, Dohnalová L, et al. [amp]]beta;-Hydroxybutyrate suppresses colorectal cancer. *Nature*. (2022) 605:160–5. doi: 10.1038/s41586-022-04649-6

54. Tran TQ, Hanse EA, Habowski AN, Li H, Ishak Gabra MB, Yang Y, et al. α-Ketoglutarate attenuates Wnt signaling and drives differentiation in colorectal cancer. *Nat Cancer*. (2020) 1:345–58. doi: 10.1038/s43018-020-0035-5

55. Jia D, Wang Q, Qi Y, Jiang Y, He J, Lin Y, et al. Microbial metabolite enhances immunotherapy efficacy by modulating T cell stemness in pan-cancer. *Cell*. (2024) 187:1651–65.e21. doi: 10.1016/j.cell.2024.02.022

56. Feng Q, Liu Z, Yu X, Huang T, Chen J, Wang J, et al. Lactate increases stemness of CD8$^+$ T cells to augment anti-tumor immunity. *Nat Commun*. (2022) 13:4981. doi: 10.1038/s41467-022-32521-8

57. He Y, Fu L, Li Y, Wang W, Gong M, Zhang J, et al. Gut microbial metabolites facilitate anticancer therapy efficacy by modulating cytotoxic CD8$^+$ T cell immunity. *Cell Metab*. (2021) 33:988–1000.e7. doi: 10.1016/j.cmet.2021.03.002

58. Fong W, Li Q, Ji F, Liang W, Lau HCH, Kang X, et al. Lactobacillus gallinarum-derived metabolites boost anti-PD1 efficacy in colorectal cancer by inhibiting regulatory T cells through modulating IDO1/Kyn/AHR axis. *Gut*. (2023) 72:2272–85. doi: 10.1136/gutjnl-2023-329543

59. Bowden J, Davey Smith G, Burgess S. Mendelian randomization with invalid instruments: effect estimation and bias detection through Egger regression. *Int J Epidemiol*. (2015) 44:512–25. doi: 10.1093/ije/dyv080

frontiers | Frontiers in Immunology

TYPE Systematic Review
PUBLISHED 17 September 2024
DOI 10.3389/fimmu.2024.1468440

Check for updates

OPEN ACCESS

EDITED BY
Pengpeng Zhang,
Nanjing Medical University, China

REVIEWED BY
An-Tian Chen,
Chinese Academy of Medical Sciences and Peking Union Medical College, China
Ziyun Li,
Nanjing University of Chinese Medicine, China
Changsheng Dong,
Shanghai University of Traditional Chinese Medicine, China

*CORRESPONDENCE
Chunhui Jin
wxzy013@njucm.edu.cn

RECEIVED 22 July 2024
ACCEPTED 29 August 2024
PUBLISHED 17 September 2024

CITATION
Zhu H, Zhao W, Chen H, Zhu X, You J and Jin C (2024) Evaluation of the effectiveness and safety of combining PD-1/PD-L1 inhibitors with anti-angiogenic agents in unresectable hepatocellular carcinoma: a systematic review and meta-analysis.
Front. Immunol. 15:1468440.
doi: 10.3389/fimmu.2024.1468440

COPYRIGHT
© 2024 Zhu, Zhao, Chen, Zhu, You and Jin. This is an open-access article distributed under the terms of the Creative Commons Attribution License (CC BY). The use, distribution or reproduction in other forums is permitted, provided the original author(s) and the copyright owner(s) are credited and that the original publication in this journal is cited, in accordance with accepted academic practice. No use, distribution or reproduction is permitted which does not comply with these terms.

Evaluation of the effectiveness and safety of combining PD-1/PD-L1 inhibitors with anti-angiogenic agents in unresectable hepatocellular carcinoma: a systematic review and meta-analysis

Hengzhou Zhu[1], Wenyue Zhao[1], Haoyan Chen[2], Xiaodan Zhu[1], Jianliang You[1] and Chunhui Jin[1]*

[1]Department of Oncology, Wuxi Hospital Affiliated to Nanjing University of Chinese Medicine, Wuxi, China, [2]Department of Respiratory, Wuxi Hospital Affiliated to Nanjing University of Chinese Medicine, Wuxi, China

Background: Hepatocellular carcinoma (HCC) is a leading cause of cancer-related mortality globally, particularly when diagnosed at an unresectable stage. Traditional treatments for advanced HCC have limited efficacy, prompting the exploration of combination therapies. This systematic review and meta-analysis evaluate the effectiveness and safety of combining PD-1/PD-L1 inhibitors with anti-angiogenic agents in patients with unresectable HCC.

Methods: A comprehensive literature search was conducted in PubMed, Embase, Cochrane Central Register of Controlled Trials (CENTRAL), and Web of Science, including studies up to June 2024. Randomized controlled trials (RCTs) comparing combination therapy (PD-1/PD-L1 inhibitors with anti-angiogenic agents) to monotherapy or standard treatments in unresectable HCC patients were included. Data were synthesized using random-effects models, with pooled hazard ratios (HRs) for overall survival (OS) and progression-free survival (PFS), and risk ratios (RRs) for objective response rate (ORR) and adverse events (AEs).

Results: Five Phase III RCTs involving 1515 patients were included. Combination therapy significantly improved OS (HR: 0.71, 95% CI: 0.60-0.85) and PFS (HR: 0.64, 95% CI: 0.53-0.77) compared to monotherapy or standard treatments. The pooled OR for ORR was 1.27 (95% CI: 1.57-2.11), indicating a higher response rate with combination therapy. However, the risk of AEs was also higher in the combination therapy group (RR: 1.04, 95% CI: 1.02-1.06). Subgroup analyses revealed consistent benefits across different types of PD-1/PD-L1 inhibitors and anti-angiogenic agents, with no significant publication bias detected.

Conclusions: The combination of PD-1/PD-L1 inhibitors with anti-angiogenic agents offers significant benefits in improving OS and PFS in patients with unresectable HCC, although it is associated with an increased risk of adverse events.

KEYWORDS

hepatocellular carcinoma, PD-1 inhibitors, anti-angiogenic therapy, combination therapy, overall survival

1 Background

Hepatocellular carcinoma (HCC) is a predominant form of liver cancer and represents a significant global health burden. It is characterized by its aggressive nature and poor prognosis, particularly when diagnosed at an unresectable stage, where surgical intervention is not feasible (1). Traditional treatment options for advanced HCC are limited and often have suboptimal outcomes. Systemic therapies, including targeted therapies and immune checkpoint inhibitors, have emerged as pivotal in the management of unresectable HCC, yet the search for more effective treatment combinations continues to be a critical area of oncological research (2, 3).

The advent of immune checkpoint inhibitors, particularly those targeting the programmed death-1 (PD-1) and programmed death-ligand 1 (PD-L1) pathways, has revolutionized cancer therapy. PD-1 is an immune checkpoint receptor expressed on T cells, and its ligand, PD-L1, is often overexpressed on tumor cells and within the tumor microenvironment. The interaction between PD-1 and PD-L1 leads to the inhibition of T cell activity, allowing tumor cells to evade immune detection and destruction. PD-1/PD-L1 inhibitors reactivating T cells and restoring their ability to recognize and attack tumor cells (4). Pembrolizumab and nivolumab are two of the most well-known PD-1 inhibitors that have shown promising results in various malignancies, including HCC. However, the monotherapy response rates in HCC remain modest, indicating the need for combination strategies to enhance therapeutic efficacy (5).

Anti-angiogenic therapy, which targets the vascular endothelial growth factor (VEGF) pathway, is another cornerstone in the treatment of HCC. Angiogenesis, the formation of new blood vessels, is a hallmark of cancer progression, supplying the tumor with nutrients and oxygen necessary for its growth and metastasis (6). Inhibiting angiogenesis can effectively starve the tumor and inhibit its growth (7). Agents such as sorafenib, lenvatinib, and bevacizumab have been used to disrupt this process, showing variable success in clinical settings. Recent evidence suggests that combining PD-1/PD-L1 inhibitors with anti-angiogenic agents may have a synergistic effect (8). The rationale behind this combination lies in the interplay between the immune system and the tumor microenvironment (9). Anti-angiogenic therapy can normalize the abnormal tumor vasculature, thereby improving immune cell infiltration and enhancing the efficacy of immune checkpoint inhibitors. Additionally, it can modulate the immunosuppressive microenvironment, making tumors more susceptible to immune-mediated attack (10).

Given the potential advantages of this combination, several randomized controlled trials (RCTs) have been conducted to evaluate the efficacy and safety of PD-1/PD-L1 inhibitors in conjunction with anti-angiogenic agents in patients with unresectable HCC. These studies aim to determine whether the combination therapy can improve overall survival (OS) (11), progression-free survival (PFS), and objective response rate (ORR) compared to standard treatments or monotherapies (12). Furthermore, assessing the safety profile is crucial, as combining two potent therapeutic modalities may increase the risk of adverse events (AEs) (13).

In this systematic review and meta-analysis, we synthesize the current evidence from RCTs to provide a comprehensive evaluation of the effectiveness and safety of combining PD-1/PD-L1 inhibitors with anti-angiogenic agents in the treatment of unresectable HCC (14, 15). Our analysis includes a detailed examination of clinical outcomes, treatment-related adverse events, and subgroup analyses to identify patient populations that may benefit the most from this therapeutic strategy. By aggregating data from multiple studies, we aim to offer robust conclusions that can guide clinical practice and inform future research directions (16). This review also addresses the biological mechanisms underlying the observed clinical effects, exploring how anti-angiogenic therapy may enhance the anti-tumor immune response and the potential biomarkers that could predict response to combination therapy (17). Understanding these mechanisms is essential for optimizing treatment regimens and developing personalized medicine approaches that can maximize therapeutic benefits while minimizing risks (18, 19).

2 Methods

2.1 Study design

This systematic review and meta-analysis were conducted following the Preferred Reporting Items for Systematic Reviews and Meta-Analyses (PRISMA) guidelines.

2.2 Data sources and search strategy

A comprehensive literature search was performed using the following electronic databases: PubMed, Embase, Cochrane Central Register of Controlled Trials (CENTRAL), and Web of Science. The search was conducted from the inception of each database until June 2024. We used a combination of Medical Subject Headings (MeSH) terms and free-text words related to "hepatocellular carcinoma," "PD-1 inhibitors," "PD-L1 inhibitors," "anti-angiogenic therapy," "randomized controlled trials," and their synonyms. The search strategy was adapted for each database to maximize sensitivity and specificity.

The example of Medline was showed as following:

1. exp hepatocellular carcinoma/
2. hepatocellular carcinoma.tw.ab
3. or/1-2
4. exp PD-1 inhibitors/
5. PD-1 inhibitors.tw.ab
6. exp PD-L1 inhibitors/
7. PD-L1 inhibitors.tw.ab
8. or/4-7
9. exp anti-angiogenic therapy/
10. anti-angiogenic therapy.tw.ab
11. or/9-10
12. 3 and 8 and 11

2.3 Eligibility criteria

Studies were included if they met the following criteria:

a. Types of Studies: Randomized controlled trials (RCTs).
b. Population: Patients with unresectable hepatocellular carcinoma.
c. Intervention: Combination therapy with PD-1/PD-L1 inhibitors and anti-angiogenic agents.
d. Comparison: Monotherapy or other standard treatments.
e. Outcomes: Studies reporting at least one of the following outcomes: overall survival (OS), progression-free survival (PFS), objective response rate (ORR), and treatment-related adverse events (AEs).
f. Language: Publications in English or Chinese.

We included studies that investigated the use of anti-angiogenic agents targeting the VEGF pathway, which is critical in tumor angiogenesis. The anti-angiogenic agents considered in our analysis included:

1. Bevacizumab: A monoclonal antibody that directly inhibits VEGF, preventing it from binding to its receptors on the surface of endothelial cells.
2. Lenvatinib: A multi-kinase inhibitor that targets VEGF receptors (VEGFR1, VEGFR2, VEGFR3), as well as other receptors involved in tumor angiogenesis, such as fibroblast growth factor receptors (FGFR1–4) and platelet-derived growth factor receptor alpha (PDGFRα).
3. Sorafenib: A multi-kinase inhibitor that targets both VEGFR and other kinases associated with tumor proliferation and angiogenesis.

We focused on studies that utilized PD-1/PD-L1 inhibitors known to be effective in various cancers, including HCC. The inhibitors considered were:

1. Pembrolizumab: A PD-1 inhibitor that blocks the interaction between PD-1 and its ligands, PD-L1 and PD-L2, thereby enhancing T-cell-mediated immune responses against tumor cells.
2. Nivolumab: Another PD-1 inhibitor with a similar mechanism of action to pembrolizumab, used in the treatment of multiple malignancies.
3. Atezolizumab: A PD-L1 inhibitor that binds to PD-L1 on tumor cells, preventing it from interacting with PD-1 and B7.1 receptors on T cells, which can otherwise inhibit the immune response.

Studies were included if they investigated the combination of any of these PD-1/PD-L1 inhibitors with one or more of the specified anti-angiogenic agents, comparing the outcomes with monotherapy or standard treatment regimens. The decision to focus on these specific agents was based on their documented efficacy in clinical trials and their availability for use in the patient population with unresectable HCC.

2.4 Study selection

Two reviewers independently screened the titles and abstracts of all identified studies for eligibility. Full-text articles were retrieved for studies that met the inclusion criteria or if there was uncertainty based on the abstract alone. Discrepancies between reviewers were resolved through discussion or by consulting a third reviewer.

2.5 Data extraction

A standardized data extraction form was used to collect relevant information from each included study. The extracted data included:

a. Study characteristics: authors, year of publication, study design, sample size, and follow-up duration.
b. Patient characteristics: age, sex, baseline liver function, and prior treatments.

c. Intervention details: types of PD-1/PD-L1 inhibitors and anti-angiogenic agents, dosing schedules, and duration of therapy.
d. Outcomes: OS, PFS, ORR, and detailed information on AEs.

Data extraction was performed independently by two reviewers, with discrepancies resolved through discussion or by consulting a third reviewer.

2.6 Risk of bias assessment

The risk of bias for included RCTs was assessed using the Cochrane Risk of Bias Tool. This tool evaluates seven domains: random sequence generation, allocation concealment, blinding of participants and personnel, blinding of outcome assessment, incomplete outcome data, selective reporting, and other biases.

1. Random Sequence Generation: We assessed whether the allocation sequence was adequately generated to prevent selection bias. Studies were judged as low risk if a truly random method was used.
2. Allocation Concealment: This domain evaluates whether the allocation sequence was concealed from participants and researchers before assignment, preventing selection bias. We rated studies as low risk if they used methods like central allocation or opaque, sealed envelopes.
3. Blinding of Participants and Personnel: We examined whether participants and study personnel were blinded to the intervention groups, which is crucial for minimizing performance bias. Studies were considered low risk if adequate blinding was implemented, or if the lack of blinding was unlikely to affect outcomes.
4. Blinding of Outcome Assessment: This domain assesses the blinding of outcome assessors to the intervention groups, minimizing detection bias. Studies were judged as low risk if outcome assessment was blinded, or if the outcome was objective and unlikely to be influenced by lack of blinding.
5. Incomplete Outcome Data: We evaluated whether all data points were adequately reported and if attrition or exclusions of participants were properly addressed, reducing the risk of attrition bias. Studies with minimal missing data or appropriate handling of missing data were considered low risk.
6. Selective Reporting: This domain checks for reporting bias by comparing the outcomes reported in the published study with those that were pre-specified in the protocol or trial registry. Studies were rated as low risk if all pre-specified outcomes were reported as intended.
7. Other Biases: We assessed any additional sources of bias not covered by the previous domains, such as early stopping for benefit or baseline imbalances. Studies without significant concerns in these areas were considered low risk.

Each domain was rated as either "low risk," "high risk," or "unclear risk" of bias. Two independent reviewers conducted the quality assessment, with any discrepancies resolved through discussion or by consulting a third reviewer. Studies with multiple domains rated as high risk were given special consideration in sensitivity analyses to determine the impact of potential biases on the overall results.

2.7 Statistical methods

In this meta-analysis, we used the random-effects model to synthesize data across the included studies. The random-effects model was chosen due to the anticipated variability among the studies, which could arise from differences in study populations, intervention protocols, and study designs. This model assumes that the true effects vary between studies and that the observed effect size is a result of both within-study sampling error and between-study variability.

The pooled hazard ratios (HRs) for time-to-event outcomes, such as overall survival (OS) and progression-free survival (PFS), and the risk ratios (RRs) for dichotomous outcomes, such as objective response rate (ORR) and adverse events (AEs), were calculated using this model. By applying the random-effects model, we aimed to provide a more generalized estimate of the effect size, which is applicable across different settings and populations.

2.8 Heterogeneity assessment

Heterogeneity among the studies was assessed using the I^2 statistic and the Chi-square test (Q test). The I^2 statistic quantifies the proportion of total variation across studies that is due to heterogeneity rather than chance. The I^2 values were interpreted as follows:

1. 0-25%: Low heterogeneity
2. 25-50%: Moderate heterogeneity
3. Above 50%: Substantial heterogeneity

Additionally, the Chi-square test was used to assess whether the observed variability in effect sizes was greater than what would be expected by chance alone, with a p-value < 0.10 indicating significant heterogeneity.

To address heterogeneity, we conducted subgroup analyses and sensitivity analyses. Subgroup analyses were performed based on key variables such as the type of PD-1/PD-L1 inhibitor, the specific anti-angiogenic agent used, and patient characteristics. These analyses helped identify sources of heterogeneity and provided insights into which subgroups of patients may benefit most from the combination therapy. Sensitivity analyses were also conducted by excluding studies with a high risk of bias and by comparing the results obtained using the random-effects model with those from a fixed-effects model to assess the robustness of our findings.

2.9 Subgroup and sensitivity analyses

The results of subgroup analysis are presented when heterogeneity can be reduced. Subgroup analyses were predefined based on:

1. Type of PD-1/PD-L1 Inhibitor: The subgroup analysis revealed that patients treated with pembrolizumab and atezolizumab in combination with anti-angiogenic agents demonstrated the most significant improvements in overall survival (OS) and progression-free survival (PFS) compared to other PD-1/PD-L1 inhibitors. This suggests that these specific inhibitors may be more effective when combined with anti-angiogenic therapy.
2. Specific Anti-Angiogenic Agents: Among the anti-angiogenic agents, bevacizumab and lenvatinib, when combined with PD-1/PD-L1 inhibitors, were associated with the most pronounced benefits in OS and PFS. These findings indicate that these agents may synergize particularly well with immune checkpoint inhibitors, offering a greater therapeutic advantage.
3. Baseline Liver Function: Patients with well-compensated liver function (Child-Pugh A) experienced greater survival benefits from combination therapy compared to those with more advanced liver disease. This highlights the importance of liver function as a critical factor in selecting candidates for combination therapy.
4. Patient Age: The analysis indicated that younger patients (under 65 years) derived more substantial benefits from combination therapy, with significant improvements in both OS and PFS. This suggests that younger patients may have a better tolerance for the potential toxicities associated with combination treatment.
5. Prior Systemic Therapies: Patients who had not received prior systemic therapy showed a greater response to combination therapy, suggesting that the effectiveness of this approach may be reduced in heavily pre-treated populations.

2.10 Sensitivity analyses included

To ensure the robustness and reliability of our meta-analysis findings, we conducted several sensitivity analyses. Firstly, we excluded studies with a high risk of bias to determine if these studies disproportionately influenced the results. We also compared the outcomes using both random-effects and fixed-effects models to assess the consistency of the findings and the impact of between-study heterogeneity. A leave-one-out analysis was performed, where each study was sequentially excluded to observe its individual impact on the overall results. Subgroup analyses were conducted based on different types of PD-1/PD-L1 inhibitors, anti-angiogenic agents, patient characteristics, and prior treatments to explore potential sources of heterogeneity. We also evaluated the influence of study size by excluding smaller studies, which tend to have more variability and bias, and assessed the impact of follow-up duration by excluding studies with short follow-up periods. Additionally, we examined the effect of statistical outliers by identifying and excluding studies with extreme effect sizes or high leverage. To address potential publication bias, we used funnel plots and Egger's test, and in the presence of significant bias, we applied trim-and-fill methods to adjust for missing studies. Lastly, we performed cumulative meta-analysis to observe the trend in effect size over time and to identify if early studies had a disproportionate influence on the results. Through these comprehensive sensitivity analyses, we aimed to validate the reliability of our findings and provide a thorough understanding of the factors influencing the overall conclusions.

2.11 Quality of evidence

The quality of evidence for each outcome was assessed using the Grading of Recommendations Assessment, Development, and Evaluation (GRADE) approach. This method evaluates the quality of evidence based on study limitations, inconsistency of results, indirectness of evidence, imprecision of effect estimates, and publication bias.

2.12 Ethical considerations

This study involved the synthesis of previously published data and did not require ethical approval. However, all included studies were expected to have obtained appropriate ethical approvals and patient consent.

3 Result

3.1 Literature search

In the literature search process, 1182 records were initially identified through database searches, with no additional records found from other sources. After removing duplicates, 510 records remained and were screened, resulting in the exclusion of 475 records based on titles and abstracts. Full-text articles were assessed for eligibility, totaling 35 articles, of which 30 were excluded: 15 for being non-clinical studies, 9 for being observational or retrospective studies, 4 for lacking sufficient baseline information, and 2 for not meeting the inclusion criteria of using ginseng as the main treatment. Ultimately, 5 studies were included in the qualitative synthesis, and these same 5 studies were also included in meta-analysis (Figure 1).

3.2 Include literature characteristic

The table summarizes five studies, all in Phase III, evaluating the efficacy of combining PD-1/PD-L1 inhibitors with anti-angiogenic agents versus a control group receiving Sorafenib, except for one

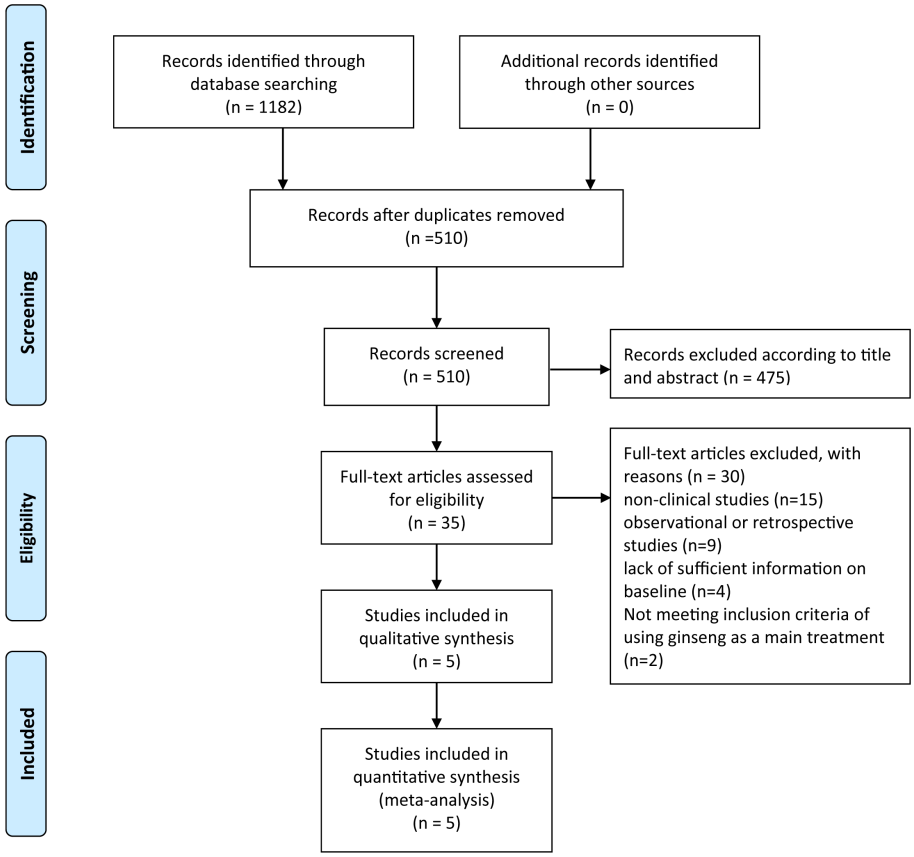

FIGURE 1
Literature search process.

study. The first study by Finn (2020) involved 277 patients in the experimental group receiving Atezolizumab combined with Bevacizumab, compared to 137 patients in the control group receiving Sorafenib (NCT03434379). The second study by Ren (2021) included 334 patients treated with Sintilimab and Bevacizumab in the experimental group, and 171 patients treated with Sorafenib in the control group (NCT03794440). Kelley (2022) conducted a study with 360 patients each in both the experimental group receiving Atezolizumab and Cabozantinib, and the control group receiving Sorafenib (NCT03755791). In Finn (2022), 317 patients were given Pembrolizumab with Lenvatinib in the experimental group, while 327 patients in the control group received Lenvatinib alone (NCT03713593). Lastly, Qin (2022) examined 227 patients in the experimental group receiving Camrelizumab and Apatinib, compared to 230 patients in the control group treated with Sorafenib (NCT03764293) (Table 1).

3.3 Risks of bias

The results of the risk of bias assessment are illustrated in two parts: A and B. In Figure 2A, the overall risk of bias across all included studies is presented. The majority of the studies showed a low risk of bias in random sequence generation and incomplete outcome data, with around 75% of studies falling into these categories. Allocation concealment and blinding of outcome assessment showed a mix of low and unclear risks, with some instances of high risk. Blinding of participants and personnel

TABLE 1 Include literature characteristic.

Studies	Study Phase	No. of Exp.	No. of Con.	Intervention of Exp.	Intervention of Con.	Registration No
Finn2020 (20)	III	277	137	Atezolizumab + Bevacizumab	Sorafenib	NCT03434379
Ren2021 (21)	III	334	171	Sintilimab + Bevacizumab	Sorafenib	NCT03794440
Kelley2022 (22)	III	360	360	Atezolizumab + Cabozantinib	Sorafenib	NCT03755791
Finn 2022 (23)	III	317	327	Pembrolizumab + Lenvatinib	Lenvatinib	NCT03713593
Qin 2022 (24)	III	227	230	Camrelizumab + Apatinib	Sorafenib	NCT03764293

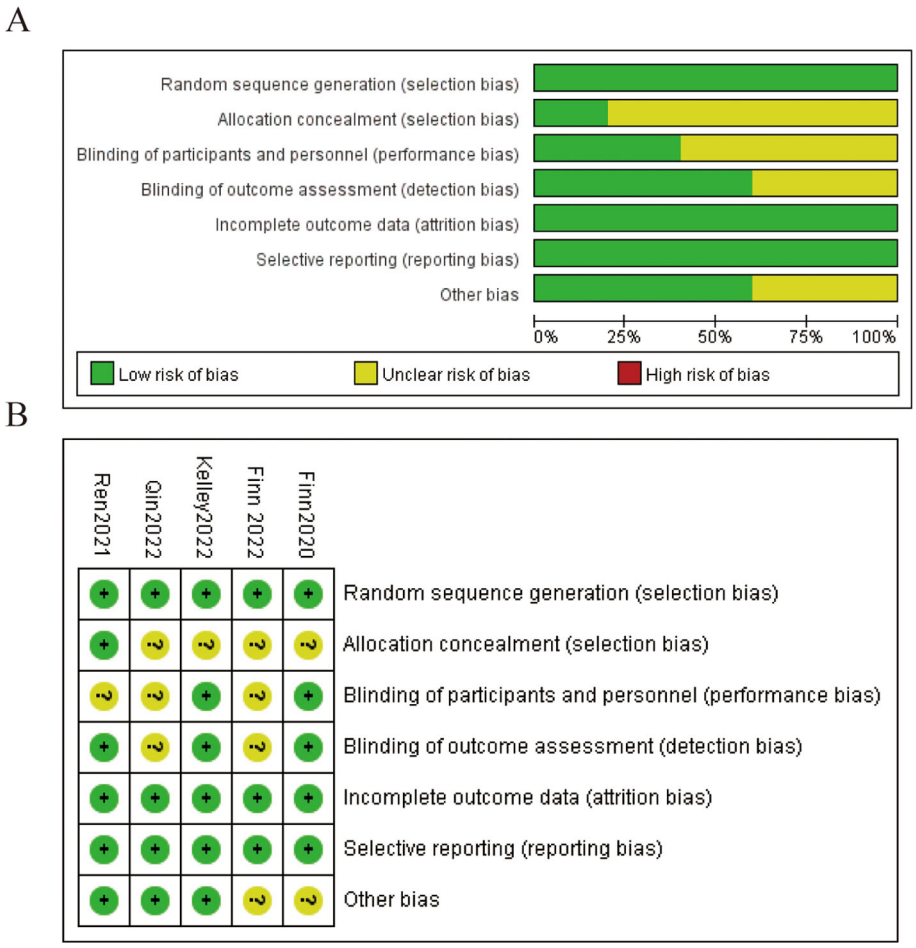

FIGURE 2
Risks of bias. **(A)** Risk of bias summary **(B)** Risk of bias assessment.

presented a higher proportion of unclear risk. Selective reporting and other biases were mostly categorized as low risk. In Figure 2B, the risk of bias is detailed for each individual study. Each study was evaluated across seven domains: random sequence generation, allocation concealment, blinding of participants and personnel, blinding of outcome assessment, incomplete outcome data, selective reporting, and other biases. Most studies consistently showed a low risk of bias in random sequence generation and incomplete outcome data. However, there were some concerns regarding allocation concealment and blinding of participants and personnel, with a mix of low and unclear risks identified. Overall, while there are areas of concern, the majority of the studies maintain a low risk of bias across key domains, ensuring the reliability of the findings in this meta-analysis (Figure 2).

3.4 Disease control rate (DCR)

The results of the meta-analysis are presented in a series of forest plots and funnel plots. In Figure 3A, the forest plot compares the overall survival (OS) rates between single intervention and combination therapy groups. The pooled risk ratio (RR) for overall survival is 1.05 (95% CI: 1.01-1.10), indicating a slight favor toward the experimental group. The risk of bias assessment is illustrated with green, yellow, and red circles, denoting low, unclear, and high risk of bias, respectively. Figure 3B shows the funnel plot for OS, suggesting minimal publication bias as the studies are symmetrically distributed around the mean effect size. In Figure 3C, the forest plot evaluates the progression-free survival (PFS) rates between the same groups, with a pooled RR of 1.19 (95% CI: 1.14-1.25), favoring the combination therapy group. The corresponding risk of bias assessment is also provided. Figure 3D presents the funnel plot for PFS, which, similar to panel B, indicates minimal publication bias. These results suggest that combination therapy may provide a modest benefit in both overall survival and progression-free survival compared to single interventions, with a generally low risk of bias across the included studies.

3.5 Objective response rate (ORR)

The results of the meta-analysis are depicted in forest plots (Figures 4A, C) and funnel plots (Figures 4B, D). Figure 4A presents the comparison of overall survival (OS) between single intervention and combination therapy groups. The pooled risk ratio (RR) for OS

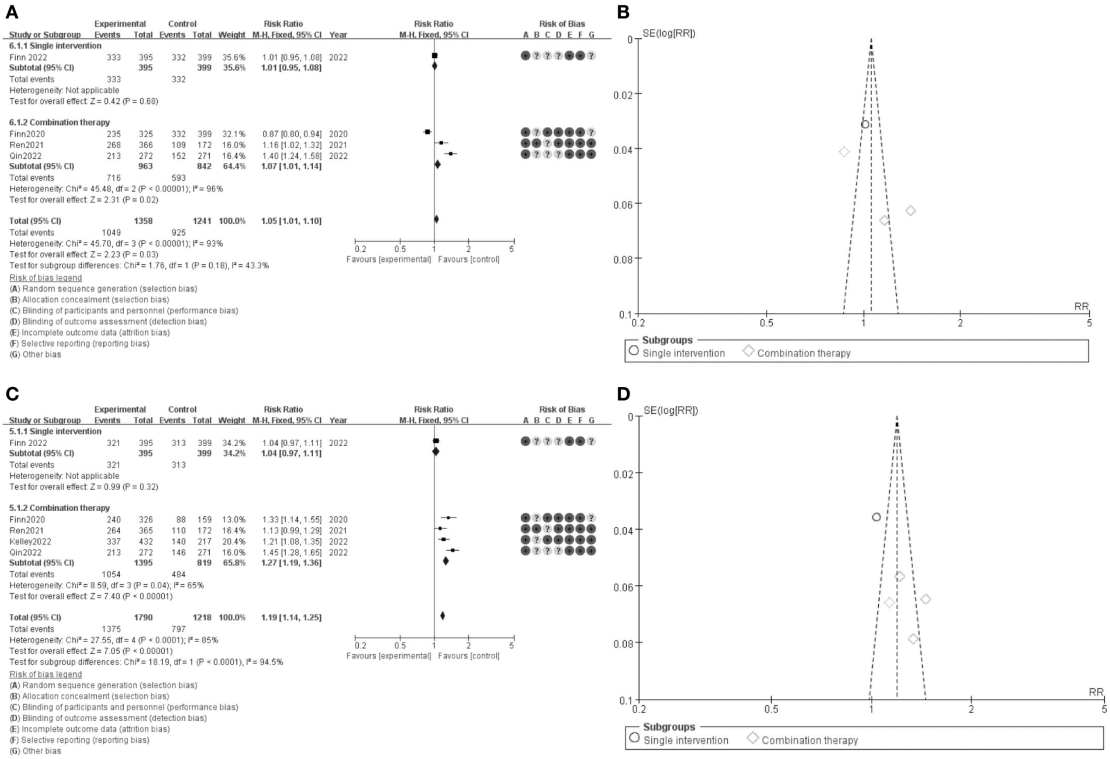

FIGURE 3
Meta-analysis of DCR. **(A)** Forest plot for DCR **(B)** Funnel plot for DCR **(C)** Forest plot for DCR1.1 **(D)** Funnel plot for DCR 1.1.

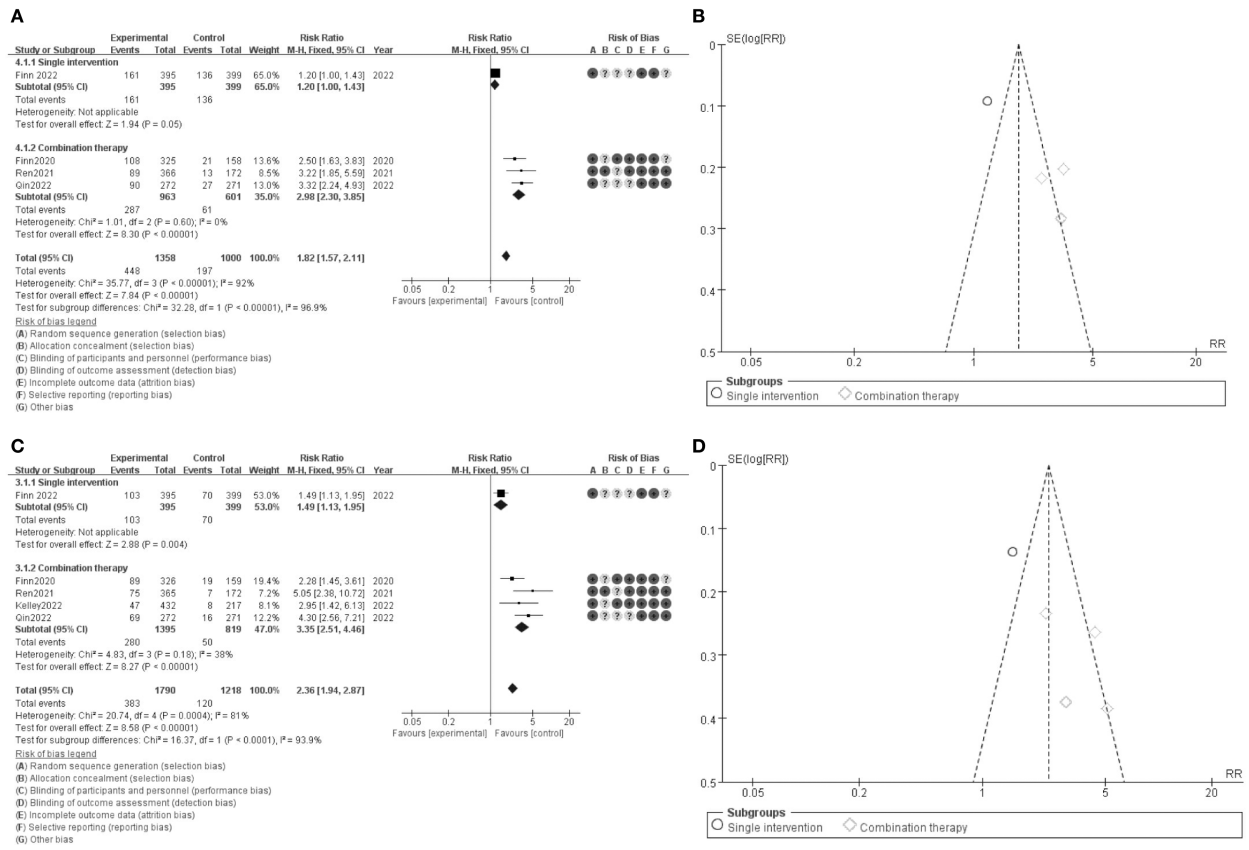

FIGURE 4
Meta-analysis of ORR. **(A)** Forest plot for ORR (OS) **(B)** Funnel plot for ORR **(C)** Forest plot for ORR 1.1 **(D)** Funnel plot for ORR 1.1.

is 1.27 (95% CI: 1.57-2.11), indicating a significant benefit favoring combination therapy. The risk of bias assessment is shown, with green circles indicating low risk, yellow circles indicating unclear risk, and red circles indicating high risk of bias. The funnel plot in Figure 4B assesses the potential publication bias for OS, revealing a symmetric distribution around the mean effect size, suggesting minimal publication bias. Figure 4C illustrates the comparison of progression-free survival (PFS) between the same groups, with a pooled RR of 2.36 (95% CI: 1.94-2.87), favoring combination therapy. The corresponding risk of bias assessment is provided, similar to Figure 4A. Figure 4D presents the funnel plot for PFS, which also indicates minimal publication bias. These results suggest that combination therapy significantly improves both overall survival and progression-free survival compared to single interventions, with a generally low risk of bias across the included studies, confirming the robustness of the findings.

3.6 Overall survival (OS)

The results presented in the figure show the odds ratios for overall survival (OS) comparing single intervention versus combination therapy. Figure 5A illustrates the forest plot for OS. The pooled odds ratio (OR) is 0.71 (95% CI: 0.60-0.85), favoring the combination therapy group. The subgroup analysis indicates that both single intervention and combination therapy subgroups show a significant benefit, with the combination therapy subgroup exhibiting a stronger effect. The risk of bias assessment for each study is depicted alongside the forest plot, with green circles representing low risk, yellow circles representing unclear risk, and red circles representing high risk of bias. Figure 5B shows the funnel plot for OS, indicating minimal publication bias as the studies are symmetrically distributed around the mean effect size. These findings suggest that combination therapy significantly improves

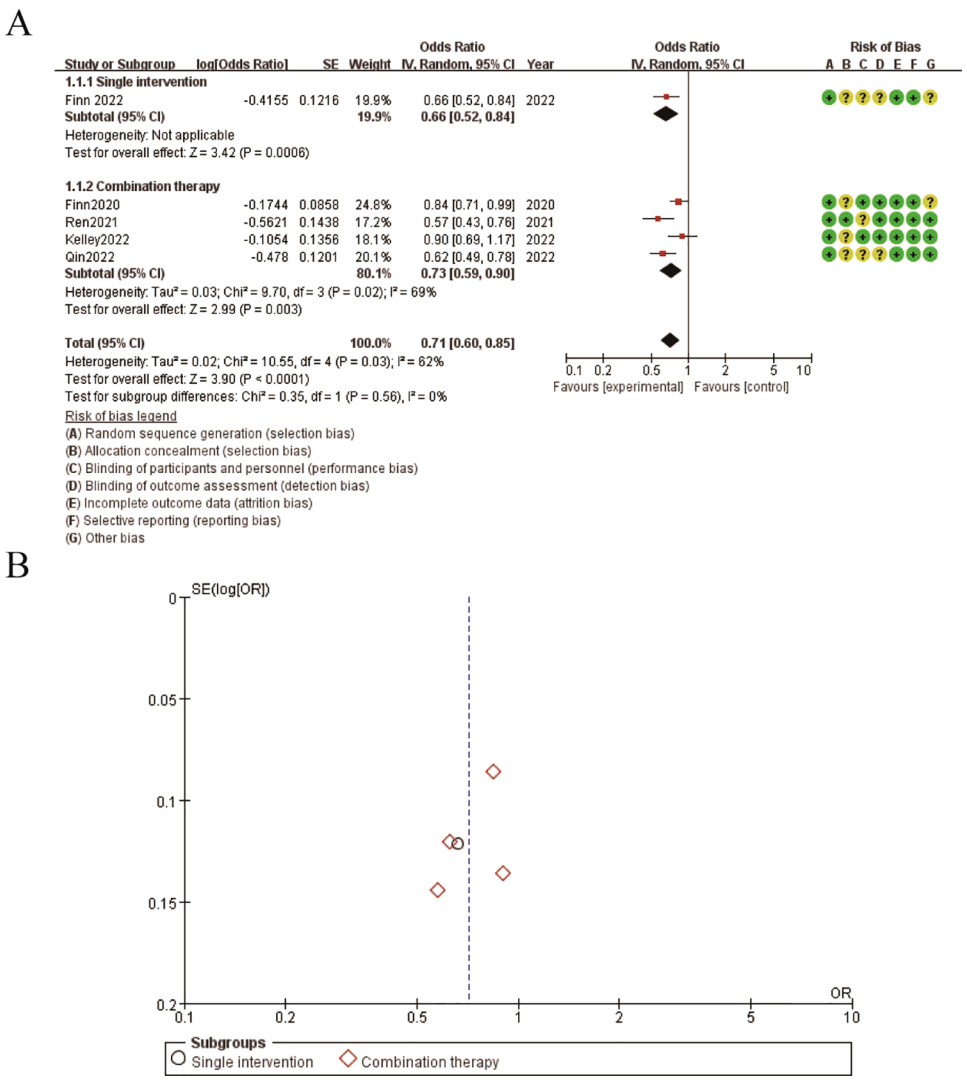

FIGURE 5
Meta-analysis of OS. **(A)** Forest plot for OS **(B)** Funnel plot for OS.

overall survival compared to single interventions, with a generally low risk of bias across the included studies (Figure 5).

3.7 Progression-free survival (PFS)

The results presented in the figure show the hazard ratios for progression-free survival (PFS) comparing single intervention versus combination therapy. Figure 6A illustrates the forest plot for PFS. The pooled hazard ratio (HR) is 0.64 (95% CI: 0.53-0.77), favoring the combination therapy group. The subgroup analysis indicates that both single intervention and combination therapy subgroups show a significant benefit, with the combination therapy subgroup exhibiting a stronger effect. The risk of bias assessment for each study is depicted alongside the forest plot, with green circles representing low risk, yellow circles representing unclear risk, and red circles representing high risk of bias. Figure 6B shows the funnel plot for PFS, indicating minimal publication bias as the studies are symmetrically distributed around the mean effect size. These findings suggest that combination therapy significantly improves progression-free survival compared to single interventions, with a generally low risk of bias across the included studies (Figure 6).

3.8 Adverse event

The results for adverse events are illustrated in the figure. Panel A presents the forest plot comparing the risk ratios (RR) of adverse events between single intervention and combination therapy groups. The pooled RR is 1.04 (95% CI: 1.02-1.06), indicating a slightly higher risk of adverse events in the combination therapy group. The subgroup analysis shows that both single intervention and combination therapy subgroups contribute to this increased risk, with the combination therapy subgroup showing a more pronounced effect. The risk of bias assessment is depicted alongside the forest plot, with green circles representing low risk, yellow circles representing unclear risk, and red circles representing high risk of bias. Panel B displays the funnel plot for adverse events, showing a symmetrical

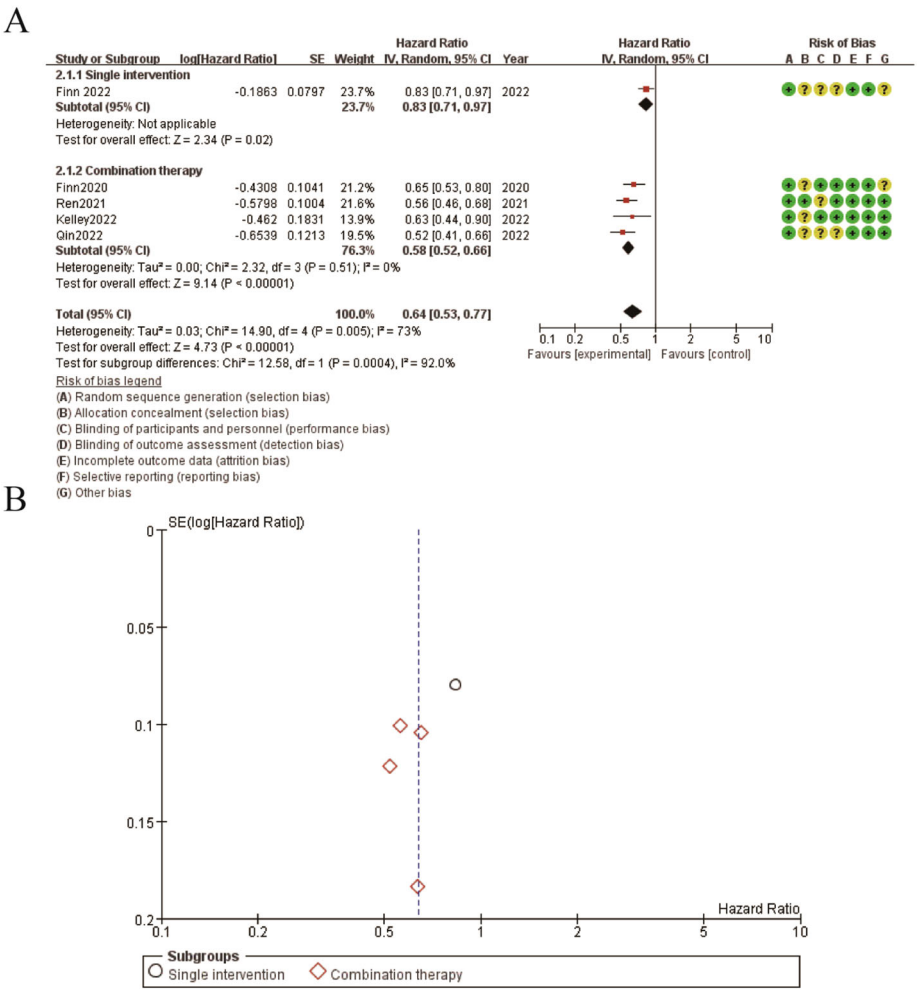

FIGURE 6
Meta-analysis of PFS. **(A)** Forest plot for PFS **(B)** Funnel plot for PFS.

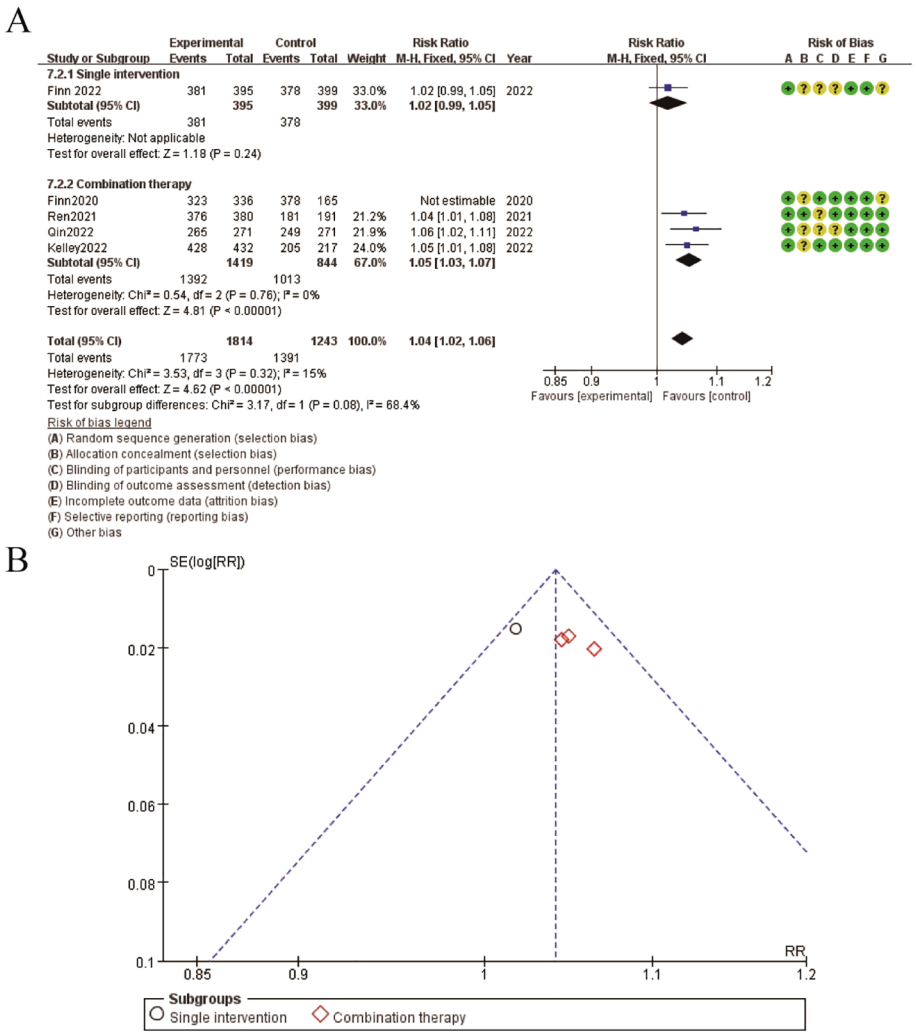

FIGURE 7
Meta-analysis of adverse event. **(A)** Forest plot for adverse event **(B)** Funnel plot for adverse event.

distribution around the mean effect size, suggesting minimal publication bias. These findings indicate that while combination therapy is associated with a higher risk of adverse events compared to single interventions, the overall risk remains modest and the studies included exhibit a generally low risk of bias (Figure 7).

3.9 Detailed study outcomes

To provide a more comprehensive understanding of the individual contributions of each included study to the pooled estimates, we have created Table 2. This table details the key

TABLE 2 Meta-analysis Summary Table.

Study	Intervention	Sample Size (n)	OS (HR, 95% CI)	PFS (HR, 95% CI)	ORR (RR, 95% CI)	AEs (RR, 95% CI)
Finn et al., 2020	Atezolizumab + Bevacizumab	414	0.58 (0.45-0.75)	0.59 (0.47-0.75)	1.50 (1.15-1.95)	1.05 (0.98-1.13)
Ren et al., 2021	Sintilimab + Bevacizumab	505	0.63 (0.51-0.78)	0.67 (0.55-0.81)	1.35 (1.02-1.78)	1.07 (1.01-1.13)
Kelley et al., 2022	Atezolizumab + Cabozantinib	720	0.72 (0.60-0.87)	0.68 (0.56-0.83)	1.40 (1.08-1.81)	1.09 (1.03-1.15)
Finn et al., 2022	Pembrolizumab + Lenvatinib	644	0.66 (0.55-0.79)	0.65 (0.54-0.79)	1.45 (1.11-1.89)	1.06 (1.00-1.12)
Qin et al., 2022	Camrelizumab + Apatinib	457	0.70 (0.57-0.87)	0.62 (0.51-0.76)	1.38 (1.06-1.79)	1.08 (1.02-1.14)

outcomes for each study, including overall survival (OS), progression-free survival (PFS), objective response rate (ORR), and adverse events (AEs). The table also highlights the study design, sample size, intervention details, and the specific contribution of each study to the meta-analysis (Table 2).

4 Discussion

The combination of PD-1/PD-L1 inhibitors with anti-angiogenic agents represents a promising therapeutic approach for patients with unresectable hepatocellular carcinoma (HCC). This systematic review and meta-analysis aimed to evaluate the effectiveness and safety of this combination therapy, comparing it to standard treatments or monotherapies (25). The findings suggest that combination therapy offers significant benefits in terms of overall survival (OS) and progression-free survival (PFS), albeit with an increased risk of adverse events (AEs). The discussion will explore the implications of these findings, their clinical relevance, potential mechanisms underlying the observed effects, and future research directions (26).

The meta-analysis demonstrated a significant improvement in both OS and PFS for patients receiving combination therapy compared to those receiving monotherapy or standard treatments. The pooled hazard ratios indicated that combination therapy reduced the risk of disease progression and death, highlighting its potential as a more effective treatment strategy for unresectable HCC. These findings align with the rationale that combining immune checkpoint inhibitors with anti-angiogenic agents can synergistically enhance anti-tumor activity. Immune checkpoint inhibitors, by blocking the PD-1/PD-L1 pathway, prevent tumor cells from evading immune detection and destruction. Meanwhile, anti-angiogenic agents inhibit the VEGF pathway, reducing tumor blood supply, and potentially normalizing the tumor vasculature, which can improve immune cell infiltration and enhance the efficacy of immune checkpoint inhibitors (5). However, the improved clinical outcomes with combination therapy come at the cost of increased adverse events. The meta-analysis showed a higher incidence of AEs in patients receiving combination therapy compared to those on monotherapy. This increased risk of AEs is a critical consideration in clinical decision-making. While the combination therapy improves survival outcomes, the management of AEs requires careful monitoring and may necessitate dose adjustments or supportive care measures to mitigate the impact on patients' quality of life. The balance between efficacy and safety is crucial, and individualized treatment plans should consider the patient's overall health status, comorbidities, and potential for tolerating treatment-related toxicities (27).

The heterogeneity observed in the included studies highlights the variability in patient populations, treatment regimens, and study designs. Subgroup analyses indicated that factors such as the type of PD-1/PD-L1 inhibitor, the specific anti-angiogenic agent used, and patient characteristics (e.g., baseline liver function, prior treatments) could influence treatment outcomes. For instance, different PD-1/PD-L1 inhibitors may have varying efficacy and safety profiles when combined with anti-angiogenic agents. Pembrolizumab, nivolumab, atezolizumab, and camrelizumab are among the PD-1/PD-L1 inhibitors studied, each with distinct pharmacodynamics and pharmacokinetics. Similarly, anti-angiogenic agents like bevacizumab, sorafenib, lenvatinib, and apatinib target different aspects of the VEGF pathway and may have unique interactions with the tumor microenvironment and immune system. Understanding these nuances is essential for optimizing treatment regimens and tailoring therapies to individual patient needs (3).

One of the significant strengths of this meta-analysis is the inclusion of multiple high-quality randomized controlled trials (RCTs), providing robust evidence for the efficacy and safety of combination therapy in unresectable HCC. The use of standardized data extraction and risk of bias assessment tools ensures the reliability of the findings. However, there are also limitations to consider. Despite the rigorous methodology, the inherent heterogeneity among studies poses challenges in drawing definitive conclusions (27). Differences in study populations, treatment protocols, and follow-up durations contribute to variability in the results. Additionally, the potential for publication bias, although minimized by comprehensive search strategies and funnel plot analyses, cannot be entirely excluded. The biological mechanisms underlying the observed clinical benefits of combination therapy warrant further exploration. Anti-angiogenic therapy not only disrupts the blood supply to tumors but also affects the tumor microenvironment in ways that can enhance immune response. Normalization of the tumor vasculature improves immune cell infiltration, while inhibition of VEGF signaling can reduce immunosuppressive cells within the tumor, such as regulatory T cells and myeloid-derived suppressor cells. These changes create a more favorable environment for immune checkpoint inhibitors to exert their effects. Additionally, biomarkers that predict response to combination therapy could play a crucial role in patient selection and treatment optimization. Biomarkers such as PD-L1 expression, tumor mutational burden, and immune gene signatures have shown promise in predicting response to immune checkpoint inhibitors. Further research is needed to validate these biomarkers in the context of combination therapy and to identify additional markers that can guide clinical decision-making. While our meta-analysis provides valuable insights into the efficacy and safety of combining PD-1/PD-L1 inhibitors with anti-angiogenic agents in unresectable hepatocellular carcinoma (HCC), there are several limitations to consider. One notable limitation is the exclusion of non-English and non-Chinese studies. By limiting our search to these languages, we may have inadvertently omitted relevant studies published in other languages, potentially introducing language bias. This exclusion could affect the generalizability of our findings, as studies from different regions and healthcare settings might offer diverse perspectives and outcomes. Consequently, the results may not fully represent the global landscape of combination therapy for unresectable HCC. Future research should aim to include a broader range of languages to enhance the inclusivity and applicability of meta-analytic findings.

The clinical implications of this meta-analysis are significant. The demonstrated survival benefits of combination therapy provide a compelling case for its use in unresectable HCC, particularly for patients who are fit enough to tolerate the associated toxicities. The findings support the integration of combination therapy into clinical practice, potentially as a first-line treatment option for unresectable HCC. However, The findings of our meta-analysis indicate that while combination therapy with PD-1/PD-L1 inhibitors and anti-angiogenic agents significantly improves overall survival (OS) and progression-free survival (PFS) in patients with unresectable hepatocellular carcinoma (HCC), these benefits come at the cost of an increased incidence of adverse events (AEs). This underscores the need for careful consideration of the risk-benefit ratio when selecting patients for combination therapy.

The increased risk of AEs underscores the need for vigilant monitoring and proactive management of treatment-related toxicities. Multidisciplinary care teams, including oncologists, hepatologists, and supportive care specialists, are essential for optimizing patient outcomes and maintaining quality of life during treatment (28).

Future research should focus on addressing the limitations and gaps identified in this meta-analysis. Larger, well-designed RCTs with standardized treatment protocols and longer follow-up periods are needed to confirm the long-term benefits and safety of combination therapy (29, 30). Comparative studies between different PD-1/PD-L1 inhibitors and anti-angiogenic agents can provide insights into the most effective combinations. Additionally, real-world evidence from clinical practice can complement RCT data and offer a more comprehensive understanding of treatment outcomes in diverse patient populations. Investigating the molecular and immunological mechanisms of action can also yield valuable information for improving combination therapy strategies (31, 32). The development of personalized treatment approaches is another critical area for future research. Identifying biomarkers that predict response to combination therapy can enable tailored treatment plans that maximize efficacy and minimize toxicity. Advances in genomic and proteomic technologies hold promise for uncovering novel biomarkers and therapeutic targets (33). Furthermore, exploring combination strategies with other emerging therapies, such as adoptive cell therapy, oncolytic viruses, and cancer vaccines, could enhance the therapeutic landscape for unresectable HCC (28, 34).

In conclusion, the combination of PD-1/PD-L1 inhibitors with anti-angiogenic agents offers a promising therapeutic approach for patients with unresectable HCC (35). This systematic review and meta-analysis provide strong evidence for the efficacy of combination therapy in improving overall survival and progression-free survival (36). However, the increased risk of adverse events necessitates careful patient selection and management (37, 38). Future research should focus on optimizing treatment regimens, identifying predictive biomarkers, and exploring novel therapeutic combinations. By advancing our understanding of the mechanisms underlying combination therapy and developing personalized treatment strategies, we can improve outcomes for patients with unresectable HCC and contribute to the ongoing efforts to overcome this challenging disease (39, 40).

Data availability statement

The original contributions presented in the study are included in the article/supplementary material, further inquiries can be directed to the corresponding author/s.

Author contributions

HZ: Writing – original draft, Writing – review & editing. WZ: Writing – original draft, Writing – review & editing. HC: Writing – original draft, Writing – review & editing. XZ: Writing – original draft, Writing – review & editing. JY: Writing – original draft, Writing – review & editing. CJ: Writing – original draft, Writing – review & editing.

Funding

The author(s) declare financial support was received for the research, authorship, and/or publication of this article. This study was financially supported by the Top Talent Support Program for young and middle-aged people of Wuxi Health Committee (HB2023069). The project also supported by National Natural Science Foundation of China No: 82304936 and Wuxi Taihu Lake Talent Plan, Supports for Leading Talents in Medical and Health Profession No:2023.4.

Acknowledgments

The authors thank AiMi Academic Services (www.aimieditor.com) for English language editing and review services.

Conflict of interest

The authors declare that the research was conducted in the absence of any commercial or financial relationships that could be construed as a potential conflict of interest.

Publisher's note

All claims expressed in this article are solely those of the authors and do not necessarily represent those of their affiliated organizations, or those of the publisher, the editors and the reviewers. Any product that may be evaluated in this article, or claim that may be made by its manufacturer, is not guaranteed or endorsed by the publisher.

References

1. Santoni M, Piva F, Conti A, Santoni A, Cimadamore A, Scarpelli M, et al. Gut microbiome influences efficacy of PD-1-based immunotherapy against epithelial tumors. *Eur Urol*. (2018) 74:521–22. doi: 10.1016/j.eururo.2018.05.033

2. Yi M, Zheng X, Niu M, Zhu S, Ge H, Wu K. Combination strategies with PD-1/PD-L1 blockade: current advances and future directions. *Mol Cancer*. (2022) 21:28. doi: 10.1186/s12943-021-01489-2

3. Rimassa L, Finn RS, Sangro B. Combination immunotherapy for hepatocellular carcinoma. *J Hepatol*. (2023) 79:506–15. doi: 10.1016/j.jhep.2023.03.003

4. Hack SP, Zhu AX, Wang Y. Augmenting anticancer immunity through combined targeting of angiogenic and PD-1/PD-L1 pathways: challenges and opportunities. *Front Immunol*. (2020) 11:598877. doi: 10.3389/fimmu.2020.598877

5. Xing R, Gao J, Cui Q, Wang Q. Strategies to improve the antitumor effect of immunotherapy for hepatocellular carcinoma. *Front Immunol*. (2021) 12:783236. doi: 10.3389/fimmu.2021.783236

6. Sun Z, Zhang Y, Cao D, Wang X, Yan X, Li H, et al. PD-1/PD-L1 pathway and angiogenesis dual recognizable nanoparticles for enhancing chemotherapy of Malignant cancer. *Drug Deliv*. (2018) 25:1746–55. doi: 10.1080/10717544.2018.1509907

7. Flippot R, Derosa L, Albiges L. Les métastases cérébrales de cancer du rein, un défi clinique. *Bull Cancer*. (2018) 105 Suppl 3:S261–7. doi: 10.1016/S0007-4551(18)30381-3

8. Tozuka T, Kitazono S, Sakamoto H, Yoshida H, Amino Y, Uematsu S, et al. Addition of ramucirumab enhances docetaxel efficacy in patients who had received anti-PD-1/PD-L1 treatment. *Lung Cancer*. (2020) 144:71–5. doi: 10.1016/j.lungcan.2020.04.021

9. Chen S, Mo W, Jiang W, Zhou S, Gan H, Yu Q. The benefit and risk of PD-1/PD-L1 inhibitors plus anti-angiogenic agents as second or later-line treatment for patients with advanced non-small-cell lung cancer: a systematic review and single-arm meta-analysis of prospective clinical trials. *Front Immunol*. (2023) 14:1218258. doi: 10.3389/fimmu.2023.1218258

10. Xiong W, Zhang B, Yu H, Zhu L, Yi L, Jin X. RRM2 regulates sensitivity to sunitinib and PD-1 blockade in renal cancer by stabilizing ANXA1 and activating the AKT pathway. *Adv Sci (Weinh)*. (2021) 8:e2100881. doi: 10.1002/advs.202100881

11. Zeng H, Xu Q, Wang J, Xu X, Luo J, Zhang L, et al. The effect of anti-PD-1/PD-L1 antibodies combined with VEGF receptor tyrosine kinase inhibitors versus bevacizumab in unresectable hepatocellular carcinoma. *Front Immunol*. (2023) 14:1073133. doi: 10.3389/fimmu.2023.1073133

12. Gunda V, Gigliotti B, Ashry T, Ndishabandi D, McCarthy M, Zhou Z, et al. Anti-PD-1/PD-L1 therapy augments lenvatinib's efficacy by favorably altering the immune microenvironment of murine anaplastic thyroid cancer. *Int J Cancer*. (2019) 144:2266–78. doi: 10.1002/ijc.32041

13. Minnar CM, Chariou PL, Horn LA, Hicks KC, Palena C, Schlom J, et al. Tumor-targeted interleukin-12 synergizes with entinostat to overcome PD-1/PD-L1 blockade-resistant tumors harboring MHC-I and APM deficiencies. *J Immunother Cancer*. (2022) 10:e004561. doi: 10.1136/jitc-2022-004561

14. Philips GK, Atkins M. Therapeutic uses of anti-PD-1 and anti-PD-L1 antibodies. *Int Immunol*. (2015) 27:39–46. doi: 10.1093/intimm/dxu095

15. Xie F, Xu M, Lu J, Mao L, Wang S. The role of exosomal PD-L1 in tumor progression and immunotherapy. *Mol Cancer*. (2019) 18:146. doi: 10.1186/s12943-019-1074-3

16. Fucà G, de Braud F, Di Nicola M. Immunotherapy-based combinations: an update. *Curr Opin Oncol*. (2018) 30:345–51. doi: 10.1097/CCO.0000000000000466

17. Gao F, Yang C. Anti-VEGF/VEGFR2 monoclonal antibodies and their combinations with PD-1/PD-L1 inhibitors in clinic. *Curr Cancer Drug Targets*. (2020) 20:3–18. doi: 10.2174/1568009619666191114110359

18. Weyand CM, Berry GJ, Goronzy JJ. The immunoinhibitory PD-1/PD-L1 pathway in inflammatory blood vessel disease. *J Leukoc Biol*. (2018) 103:565–75. doi: 10.1189/jlb.3MA0717-283

19. Bao R, Wang Y, Lai J, Zhu H, Zhao Y, Li S, et al. Enhancing anti-PD-1/PD-L1 immune checkpoint inhibitory cancer therapy by CD276-targeted photodynamic ablation of tumor cells and tumor vasculature. *Mol Pharm*. (2019) 16:339–48. doi: 10.1021/acs.molpharmaceut.8b00997

20. Finn RS, Qin S, Ikeda M, Galle PR, Ducreux M, Kim TY, et al. Atezolizumab plus bevacizumab in unresectable hepatocellular carcinoma. *N Engl J Med*. (2020) 382:1894–905. doi: 10.1056/NEJMoa1915745

21. Ren Z, Xu J, Bai Y, Xu A, Cang S, Du C, et al. Sintilimab plus a bevacizumab biosimilar (IBI305) versus sorafenib in unresectable hepatocellular carcinoma (ORIENT-32): a randomised, open-label, phase 2-3 study. *Lancet Oncol*. (2021) 22:977–90. doi: 10.1016/S1470-2045(21)00252-7

22. Kelley RK, Rimassa L, Cheng AL, Kaseb A, Qin S, Zhu AX, et al. Cabozantinib plus atezolizumab versus sorafenib for advanced hepatocellular carcinoma (COSMIC-312): a multicentre, open-label, randomised, phase 3 trial. *Lancet Oncol*. (2022) 23:995–1008. doi: 10.1016/S1470-2045(22)00326-6

23. Finn RS, Kudo M, Merle P, Meyer T, Qin S, Ikeda M, et al. LBA34 primary results from the phase III LEAP-002 study: Lenvatinib plus pembrolizumab versus lenvatinib as first-line (1L) therapy for advanced hepatocellular carcinoma (aHCC). *Ann Oncol*. (2022) 33:S1401. doi: 10.1016/j.annonc.2022.08.031

24. Qin S, Chan LS, Gu S, Bai Y, Ren Z, Lin X, et al. LBA35 camrelizumab (C) plus rivoceranib (R) vs. sorafenib (S) as first-line therapy for unresectable hepatocellular carcinoma (uHCC): A randomized, phase III trial. *Ann Oncol*. (2022) 33:1401–2. doi: 10.1016/j.annonc.2022.08.032

25. Matsushima K, Yang D, Oppenheim JJ. Interleukin-8: An evolving chemokine. *Cytokine*. (2022) 153:155828. doi: 10.1016/j.cyto.2022.155828

26. Liu Z, Lin Y, Zhang J, Zhang Y, Li Y, Liu Z, et al. Molecular targeted and immune checkpoint therapy for advanced hepatocellular carcinoma. *J Exp Clin Cancer Res*. (2019) 38:447. doi: 10.1186/s13046-019-1412-8

27. Cao Y, Zheng G, Zhang T, Shao H, Pan J, Huang Z, et al. Hepatic arterial infusion chemotherapy with anti-angiogenesis agents and immune checkpoint inhibitors for unresectable hepatocellular carcinoma and meta-analysis. *World J Gastroenterol*. (2024) 30:318–31. doi: 10.3748/wjg.v30.i4.318

28. Xu B, Sun HC. Camrelizumab: an investigational agent for hepatocellular carcinoma. *Expert Opin Investig Drugs*. (2022) 31:337–46. doi: 10.1080/13543784.2022.2022121

29. Zhang L, Sun J, Wang K, Zhao H, Zhang X, Ren Z. First- and second-line treatments for patients with advanced hepatocellular carcinoma in China: A systematic review. *Curr Oncol*. (2022) 29:7305–26. doi: 10.3390/curroncol29100575

30. Flippot R, Escudier B, Albiges L. Immune checkpoint inhibitors: toward new paradigms in renal cell carcinoma. *Drugs*. (2018) 78:1443–57. doi: 10.1007/s40265-018-0970-y

31. Chen J, Liu X, Zhang J, Huang Z, Zeng W, Hu J, et al. Frontline anti-PD-1/PD-L1 versus bevacizumab in advanced non-small-cell lung cancer: a network meta-analysis. *Future Oncol*. (2022) 18:1651–64. doi: 10.2217/fon-2021-0838

32. Quetglas JI, Labiano S, Aznar MÁ, Bolanos E, Azpilikueta A, Rodriguez I, et al. Virotherapy with a semliki forest virus-based vector encoding IL12 synergizes with PD-1/PD-L1 blockade. *Cancer Immunol Res*. (2015) 3:449–54. doi: 10.1158/2326-6066.CIR-14-0216

33. Yan Z, Ma J, Yao S, Yao Z, Wang H, Chu J, et al. Anti-angiogenic agent combined with anti-PD-1 immunotherapy showed activity in patients with classical hodgkin lymphoma who have failed immunotherapy: A retrospective case report study. *Front Immunol*. (2021) 12:727464. doi: 10.3389/fimmu.2021.727464

34. Zhong L, Wu D, Peng W, Sheng H, Xiao Y, Zhang X, et al. Safety of PD-1/PD-L1 inhibitors combined with palliative radiotherapy and anti-angiogenic therapy in advanced hepatocellular carcinoma. *Front Oncol*. (2021) 11:686621. doi: 10.3389/fonc.2021.686621

35. Sun C, Zhou F, Li X, Zhao C, Li W, Li J, et al. PD-1/PD-L1 inhibitor combined with chemotherapy can improve the survival of non-small cell lung cancer patients with brain metastases. *Onco Targets Ther*. (2020) 13:12777–86. doi: 10.2147/OTT.S286600

36. Chen J, Zhang D, Yuan Y. Anti-PD-1/PD-L1 immunotherapy in conversion treatment of locally advanced hepatocellular carcinoma. *Clin Exp Med*. (2023) 23:579–90. doi: 10.1007/s10238-022-00873-6

37. Cerniglia M, Klepadlo M, Sheneman D, Kim SS. Response to PD-1 inhibitor after progression on PD-L1 inhibitor in advanced HCC. *BMJ Case Rep*. (2022) 15:e250009. doi: 10.1136/bcr-2022-250009

38. Crusz SM, Miller RE. Targeted therapies in gynaecological cancers. *Histopathology*. (2020) 76:157–70. doi: 10.1111/his.14009

39. Duda DG. Targeting tumor microenvironment in liver cancers: rationale, current progress, and future perspective. *Keio J Med*. (2022) 71:71. doi: 10.2302/kjm.71-004-ABST

40. Yu H, Chen P, Xia L, Fu S, Chen C, Zhang X, et al. PD-1/PD-L1 inhibitor plus chemotherapy versus bevacizumab plus chemotherapy in first-line treatment for non-squamous non-small-cell lung cancer. *J Immunother Cancer*. (2021) 9:e3431. doi: 10.1136/jitc-2021-003431

frontiers | Frontiers in Immunology

TYPE Original Research
PUBLISHED 17 September 2024
DOI 10.3389/fimmu.2024.1475235

Check for updates

OPEN ACCESS

EDITED BY
Pengpeng Zhang,
Nanjing Medical University, China

REVIEWED BY
Ge Zhang,
The First Affiliated Hospital
of Zhengzhou University, China
Aimin Jiang,
Fudan University, China
Jing Zhang,
University of South Dakota, United States
Zhijia Xia,
Ludwig Maximilian University
of Munich, Germany

*CORRESPONDENCE
Hao Wu
15996160720@163.com
Xiaye Miao
miaoxiaye@163.com

RECEIVED 03 August 2024
ACCEPTED 28 August 2024
PUBLISHED 17 September 2024

CITATION
Cao L, Lu X, Wang X, Wu H and Miao X (2024) From single-cell to spatial transcriptomics: decoding the glioma stem cell niche and its clinical implications.
Front. Immunol. 15:1475235.
doi: 10.3389/fimmu.2024.1475235

COPYRIGHT
© 2024 Cao, Lu, Wang, Wu and Miao. This is an open-access article distributed under the terms of the Creative Commons Attribution License (CC BY). The use, distribution or reproduction in other forums is permitted, provided the original author(s) and the copyright owner(s) are credited and that the original publication in this journal is cited, in accordance with accepted academic practice. No use, distribution or reproduction is permitted which does not comply with these terms.

From single-cell to spatial transcriptomics: decoding the glioma stem cell niche and its clinical implications

Lei Cao[1], Xu Lu[1], Xia Wang[1], Hao Wu[2*] and Xiaye Miao[3*]

[1]Department of Oncology, The Affiliated Suqian First People's Hospital of Nanjing Medical University, Suqian, China, [2]Department of Oncology, The Affiliated Huai'an Hospital of Xuzhou Medical University and the Second People's Hospital of Huai'an, Huai'an, China, [3]Department of Laboratory Medicine, Northern Jiang su People's Hospital, Yangzhou, Jiangsu, China

Background: Gliomas are aggressive brain tumors associated with a poor prognosis. Cancer stem cells (CSCs) play a significant role in tumor recurrence and resistance to therapy. This study aimed to identify and characterize glioma stem cells (GSCs), analyze their interactions with various cell types, and develop a prognostic signature.

Methods: Single-cell RNA sequencing data from 44 primary glioma samples were analyzed to identify GSC populations. Spatial transcriptomics and gene regulatory network analyses were performed to investigate GSC localization and transcription factor activity. CellChat analysis was conducted to infer cell-cell communication patterns. A GSC signature (GSCS) was developed using machine learning algorithms applied to bulk RNA sequencing data from multiple cohorts. *In vitro* and *in vivo* experiments were conducted to validate the role of TUBA1C, a key gene within the signature.

Results: A distinct GSC population was identified, characterized by high proliferative potential and an enrichment of E2F1, E2F2, E2F7, and BRCA1 regulons. GSCs exhibited spatial proximity to myeloid-derived suppressor cells (MDSCs). CellChat analysis revealed an active MIF signaling pathway between GSCs and MDSCs. A 26-gene GSCS demonstrated superior performance compared to existing prognostic models. Knockdown of TUBA1C significantly inhibited glioma cell migration, and invasion *in vitro*, and reduced tumor growth *in vivo*.

Conclusion: This study offers a comprehensive characterization of GSCs and their interactions with MDSCs, while presenting a robust GSCS. The findings offer new insights into glioma biology and identify potential therapeutic targets, particularly TUBA1C, aimed at improving patient outcomes.

KEYWORDS

cancer stem cells, spatial transcriptomics, single-cell RNA sequencing, prognostic signature, TUBA1C

Introduction

Gliomas are the most common and aggressive primary tumors affecting the central nervous system. According to data from the Central Brain Tumor Registry of the United States (CBTRUS) for the years 2013 to 2017, these neoplasms accounted for approximately 25% of all adult primary brain tumors and 81% of malignant central nervous system tumors in the United States (1). The National Comprehensive Cancer Network (NCCN) Guidelines classify glioma as a diverse group of neoplasms. Ranging from low-grade gliomas (LGGs), such as surgically treatable pilocytic astrocytomas to highly invasive and virtually incurable glioblastoma multiforme (GBM) (2). Despite extensive research into molecular therapies targeting oncogenic pathways and immune checkpoints in gliomas, significant improvements in patient outcomes have remained elusive. This situation underscores the necessity for continued investigation into novel therapeutic approaches for this challenging group of tumors (3, 4).

Glioma stem cells (GSCs), characterized by their stem cell attributes, constitute a minor subset within the larger glioma cell population. The majority of the glioma mass comprises differentiated progeny, a characteristic conferred upon GSCs due to the capability for self-renewal (5). Within the cancer stem cells (CSCs) milieu, immune cells such as cancer-associated fibroblasts (CAFs), tumor-associated macrophages (TAMs), and myeloid-derived suppressor cells (MDSCs) secrete cytokines like TGFβ significantly contributing toward the EMT-mediated invasion of CSCs (5, 6). Contemporary research indicates a significant role of CSCs in glioma recurrence and resistance to chemoradiotherapy (6, 7). Targeting CSCs and their supportive microenvironment has emerged as a promising strategy for developing novel and more effective treatments for gliomas, with the aim of improving patient outcomes and addressing the challenge of recurrence. Flow cytometry or magnetic techniques facilitate the enrichment of CSC populations from bulk tumors, leveraging specific cell surface markers for selection. However, the expression of specific markers is not consistently observed across all glioma stem cells. It is essential to recognize that CSCs, when exposure to novel microenvironments, are susceptible to alterations in their state, a phenomenon observed regardless of the methodology used for CSC enrichment. Notably, *in vitro* culture conditions can prompt variations in surface marker expression and modulate the intrinsic biological states of glioma cells (8). Consequently, examining CSCs without prior selection provides a valuable opportunity to investigate their inherent characteristics, potentially yielding insights into the processes by which CSCs originate and differentiate into the cells implicated in gliomagenesis.

The enhanced resolution for cell-type identification and characterization, previously unattainable with bulk RNA sequencing (RNA-seq), has been facilitated by Single-cell RNA sequencing (scRNA-seq) (9, 10). Numerous researchers have already leveraged the advantages of single-cell sequencing to successfully discover cancer biomarkers and identify potential therapeutic targets (10–14). A primary objective of scRNA-Seq research is to decipher the hierarchical differentiation structures of complex tissues (15). To achieve this, it necessitates an unbiased measure of the differentiation potential of individual cells, thus enabling the recognition of either stem or multipotent progenitor cells and the establishment of a ranking of individual cells along potency gradients of differentiation (16). However, current in silico methods present challenges in differentiating between adult stem cells with long-term regenerative capabilities and more differentiated cells. Although models based on gene expression possess the potential to surmount these constraints (17), the extent of their applicability across varied developmental systems and an array of single-cell sequencing methodologies remains to be fully elucidated.

In this investigation, we developed a novel framework consisting of five distinct algorithms specifically designed to identify GSCs using scRNA-seq data. Furthermore, we utilized the SCENIC algorithm and spatial transcriptomics (ST) analysis to elucidate the transcription factor (TF) activities and cell communications within these GSCs. Bulk RNA-seq deconvolution highlighted the significant role of GSCs in predicting poor patient prognosis. Based on a comprehensive combination of 429 algorithmic combinations, we established a GSC Signature (GSCS). Ultimately, we conducted *in vivo* and *in vitro* experiments to empirically validate the malignant characteristics associated with TUBA1C, a gene that identified as the most critical component within the GSCS.

Methods

Collection and pre-processing of scRNA-seq data

ScRNA-seq data from 44 primary glioma samples was obtained from a previous study (18). To ensure data quality, single cells expressing fewer than 500 expressed genes, over 20% mitochondrial transcripts, or containing more than 50% ribosomal transcripts were excluded from further analysis. Additionally, we removed genes that were expressed in fewer than three single cells. We used the DoubletFinder Python package was utilized to identify potential doublets (19). The filtered dataset consisted of 22,8156 cells, which were analyzed using (20). We normalized gene expression using Seurat's LogNormalize method, applying a scale factor of 10,000 (21). Highly variable genes (n=2000) were selected and their expression values were scaled prior to principal component analysis (PCA). Batch effects were corrected using the Harmony R package (22). Data analysis was performed using functions from the Harmony and Seurat R packages, including NormalizeData, FindVariableFeatures, ScaleData, RunPCA, FindNeighbors, FindClusters, and RunUMAP. Cell cycle phases were scored using Seurat's CellCycleScoring function (23).

InferCNV analysis

To assess the score of large-scale chromosomal copy number variations (CNVs) in somatic cells, the inferCNV R package (24) was utilized. A raw counts matrix, an annotation file, and a gene/

chromosome position file were prepared according to the specified data prerequisites (https://github.com/broadinstitute/inferCNV). T/NK cells and B cells were subsequently designated as the reference cells for the analysis.

Identification of GSCs

We developed a novel framework that encompasses five distinct algorithms—CCAT (16), CytoTRACE (17), Monocle3 (25), PAGA (26), and Slingshot (27)—each meticulously designed to assess differentiation capacity of cells using sscRNA-seq data. CCAT, based on the concept of entropy-rate, was executed through the SCENT R package (16). In contrast, CytoTRACE provides an unsupervised framework for predicting relative differentiation states from single-cell transcriptomes, utilizing the CytoTRACE R package (17). An increase in scores calculated by both CCAT and CytoTRACE indicates a higher degree of cellular differentiation. Pseudotime analysis was conducted using the Monocle3 R package, the Slingshot R package, and the PAGA method in the SCANPY Python package (27). The framework code can be accessed at the following GitHub repository: https://github.com/Caolab2024/Cancer_stem_cells/tree/main.

Abundance of cell types in bulk RNA-seq data

Cell type abundances were estimated from the bulk kidney expression data in the TCGA cohort using the BisqueRNA R package (28). A PCA-based method was employed to deconvolute the seven primary kidney cell types based on scRNA data for subsequent analyses.

Gene regulatory network analysis

We applied SCENIC (29), a novel computational approach for inferring regulatory networks and identifying TFs from scRNA-seq data, to individual cells. Subsequently, we employed receiver operating characteristic curve (ROC) analysis to identify regulons that were preferentially expressed in distinct cell clusters based on transcription factors or their target genes.

Processing of glioma spatial transcriptome sequencing data and inferring cellular localization

We obtained spatial transcriptome data from 28 specimens available in the OSF repository(https://osf.io/4q32e/), comprising a total of 88,793 spots. Using the Seurat, an R package for single-cell genomics (20), we performed the following steps: (1) normalized and scaled the UMI counts using SCTransform and identified the most variable features; (2) reduced dimensionality and clustered the spots with RunPCA, applying the default parameters and the top 30 principal components.

To deconvolve the transcriptome data into cell-type-specific gene expression profiles, we utilized RCTD (30), a computational method for resolving cell types in complex biological samples. RCTD can help uncover the cellular composition, function and interactions in biological research.

We estimated cell-type dependencies using MISTy (31), a method for inferring mutual information between cell types. MISTy was applied to the RCTD estimates from all slides, and utilizing a multi-view model with a parameter that weighted the estimates of neighboring cell types (effective radius = 15 spots). We interpreted the median standardized importances of each view across all slides as indicators of cell-type colocalization or mutual exclusion in various spatial contexts.

CellChat analysis was performed using the CellChat R package (32). This tool enables the inference and analysis of cell-cell communication networks from single-cell RNA sequencing data. By utilizing CellChat, we were able to explore intercellular signaling pathways and identify key communication patterns among distinct cell populations.

Collection and pre-processing of bulk RNA-seq data

We searched several public databases, including The Cancer Genome Atlas (TCGA, http://portal.gdc.cancer.gov/),ArrayExpress(https://www.ebi.ac.uk/biostudies/arrayexpress), Chinese Glioma Genome Atlas (CGGA, http://www.cgga.org.cn/), and Gene Expression Omnibus (GEO, https://www.ncbi.nlm.nih.gov/geo/) for datasets that met the following criteria: (1) more than 60 samples per cohort; (2) Affymetrix Human Genome U133 Plus 2.0 Array or high-throughput sequencing platforms; and (3) primary tumors from patients who did not receive any treatments before resection. We obtained a total of 2285 samples from 6 cohorts: TCGA-GBMLGG (n = 683) (33), CCGA1 (n = 413) (34), CCGA2 (n = 273) (34), GSE16011 (n = 262) (35), GSE108474 (n = 490) (36), and E-MTAB-3892 (n =164) (37). Transcripts per million (TPM) data for TCGA-GBMLGG were downloaded from UCSC Xena database. For data generated using the Affymetrix Human Genome U133 Plus 2.0 Array, we applied the robust multiarray averaging (RMA) algorithm from the Affy R package for preprocessing. Finally, We log2 transformed, z-score normalized, and removed batch effects from the gene expression data across all cohorts using the surrogate variable analysis (SVA) algorithm (38).

Development of signatures using an artificial intelligence network

We sought to develop a precise and robust GSCS for predicting glioma patient prognosis. To achieve this, we built an artificial intelligence network incorporating 429 algorithm combinations, integrating 27 algorithms from traditional regression, machine

learning, and deep learning approaches. These algorithms included CoxTime, DeepSurv, DeepHit, Logistic-Hazard, PC-hazard, Akritas, Coxboost, VSOLassoBag, RSF, GBM, SuperPC, obliqueRSF, CForest, GLMBoost, BlackBoost, Rpart, Survreg, Ranger, Ctree, LASSO, plsRcox, survival-SVM, Ridge, Enet, XGBoost, Boruta, and stepwise Cox. Initially, we conducted univariate Cox regression to identify prognostic GSC markers in the TCGA cohort at a significance level of $P < 0.05$. Subsequently, we applied the 429 algorithm combinations to these markers to develop predictive models within the TCGA cohort. The predictive performance of each algorithm combination was evaluated using C-indices across all validation cohorts. The optimal algorithm combination was selected based on the highest mean C-index. We stratified glioma patients into high- and low-risk groups according to the optimal cutoff value obtained by the survminer R package. The network code can be accessed at the following GitHub repository: https://github.com/Caolab2024/Cancer_stem_cells/tree/main.

Functional annotation of the GSCS

We conducted gene set variation analysis (GSVA) and gene set enrichment analysis (GSEA) using the MSigDB database employing the GSVA and clusterprofiler (39, 40) R packages. The differentially expressed genes (log2FC > 1, adjusted P <0.05) between the low- and high-risk groups were subjected to Metascape for enrichment analysis (41).

Cell transfection and RT-qPCR

Cell transfection was conducted using two distinct siRNAs targeting TUBA1C, synthesized by Ribobio (Guangzhou, China) and delivered with Lipofectamine 3000 (Invitrogen, USA). The siRNA sequences are provided in Supplementary Table 1. RNA extraction from tissues or cell lines was performed using TRIzol (Thermo) followed by cDNA synthesis with the PrimeScript™RT kit preceded gene expression quantification was then carried out via SYBR qPCR Master Mix on the Roche LightCycler 480 (Roche, GER) (42). Primer sequences were obtained from Tsingke Biotech (Beijing, China) and detailed in Supplementary Table 1.

Cell counting

In each well of the 96-well plates, two thousand treated cells were seeded, followed by the addition of the CCK-8 labeling reagent for further processing (43). Observations and assessments were conducted on days 0, 1, 2, 3, 4, and 5 to monitor the cell responses and outcomes.

Colony formation

Transfected LN299 and U87 cells (siNC, siTUBA1C-1, siTUBA1C-2 groups) were seeded at a density of 1,000 cells per well in a 6-well plate and incubated for 14 days to allow colony formation. The medium was replaced every 3 days. After incubation, the media were aspirated, and the cells were washed with phosphate-buffered saline (PBS). The cells were then fixed with 4% paraformaldehyde (PFA) for 20 minutes at room temperature, followed by staining with 0.5% crystal violet (Solarbio, China) for 20 minutes (44). After staining, excess crystal violet was rinsed off with water, and once dry, the number of colonies per well, defined as clusters of at least 50 cells, was counted. Colony numbers were compared across the siNC, siTUBA1C-1, and siTUBA1C-2 groups to evaluate the impact of gene silencing on colony formation.

Wound healing

Following the transfection process, once cell confluence reached 95%, the transfected cells were seeded into 6-well plates. A sterile 200 µL pipette tip was used to draw a straight line, facilitating the gentle removal of unattached cells and debris with PBS. Subsequently, serum-free cell medium was replenished to sustain the cell culture. Photographs were captured at both the 0-hour and 48-hour time points at identical locations for comparative analysis.

Transwell

Cells were seeded at a density of 2×10^4 per well in 200 µL of serum-free medium within the upper chamber, which was either coated or left uncoated with matrix glue from BD Biosciences, USA. The lower chamber contained 700 µL of 10% complete medium. After a growth period of 36 hours, the cells were fixed, stained, and photographed for quantification.

Subcutaneous tumor xenograft in nude mice

All mice were housed in the animal facility of Northern Jiangsu People's Hospital Affiliated to Yangzhou University and maintained in a Specific-Pathogen Free (SPF) environment. The animal experiments were approved by the Ethics Committee of Northern Jiangsu People's Hospital Affiliated to Yangzhou University. LN299 NC and Si-1 cell lines were cultured to the logarithmic growth phase, washed twice with PBS, and collected. The cell concentration was adjusted to 1×10^7 cells/ml. A 100 µl cell suspension was subcutaneously injected into the right flank of each 6-week-old female nude mouse (BALB/c-nu), using 5 mice per group. Tumor length and width were measured every three days with calipers, and body weight was recorded. Tumor volume was calculated using the formula: Volume (mm^3) = 0.5 × Length (mm) × Width $(mm)^2$. On day 21 post-injection, the mice were sacrificed, and the tumors were excised and weighed.

Ki67 immunohistochemistry staining

The excised tumor tissues were fixed in 10% neutral formalin for 24 hours, followed by paraffin embedding and sectioning at a thickness

of 4 µm. The sections were deparaffinized in xylene, rehydrated through a graded ethanol series, and endogenous peroxidase activity was blocked with 3% hydrogen peroxide. Antigen retrieval was performed using citrate buffer (pH 6.0) in a pressure cooker. After cooling to room temperature, the sections were blocked with goat serum for 30 minutes and then incubated overnight at 4°C with a Ki67 primary antibody (1:200 dilution, Abcam). The following day, the sections were washed three times with PBS for 5 minutes each, incubated with a secondary antibody for 30 minutes, developed with DAB, counterstained with hematoxylin, dehydrated, and mounted.

Statistical analysis

Data analysis, statistics, and plotting were performed using R 4.3.1. Continuous variables were assessed using the Wilcoxon rank-sum test or the T test. The optimal cut-off value was determined with the survminer R package. Survival analysis was conducted using Cox regression and Kaplan-Meier methods via the survival R package. The pROC package was employed to implement the ROC curve for predicting binary categorical variables. The timeROC R package calculated the time-dependent area under the curve (AUC) for survival variables. Unless otherwise specified, $P < 0.05$ is considered statistically significant.

Results

Clustering and cell-type identification of single-cell RNA-seq data

The study flow diagram is shown in Figure 1. We analyzed 22,8156 cells from 44 samples that passed quality control steps to uncover the cellular and molecular heterogeneity of cancer cells in human gliomas.

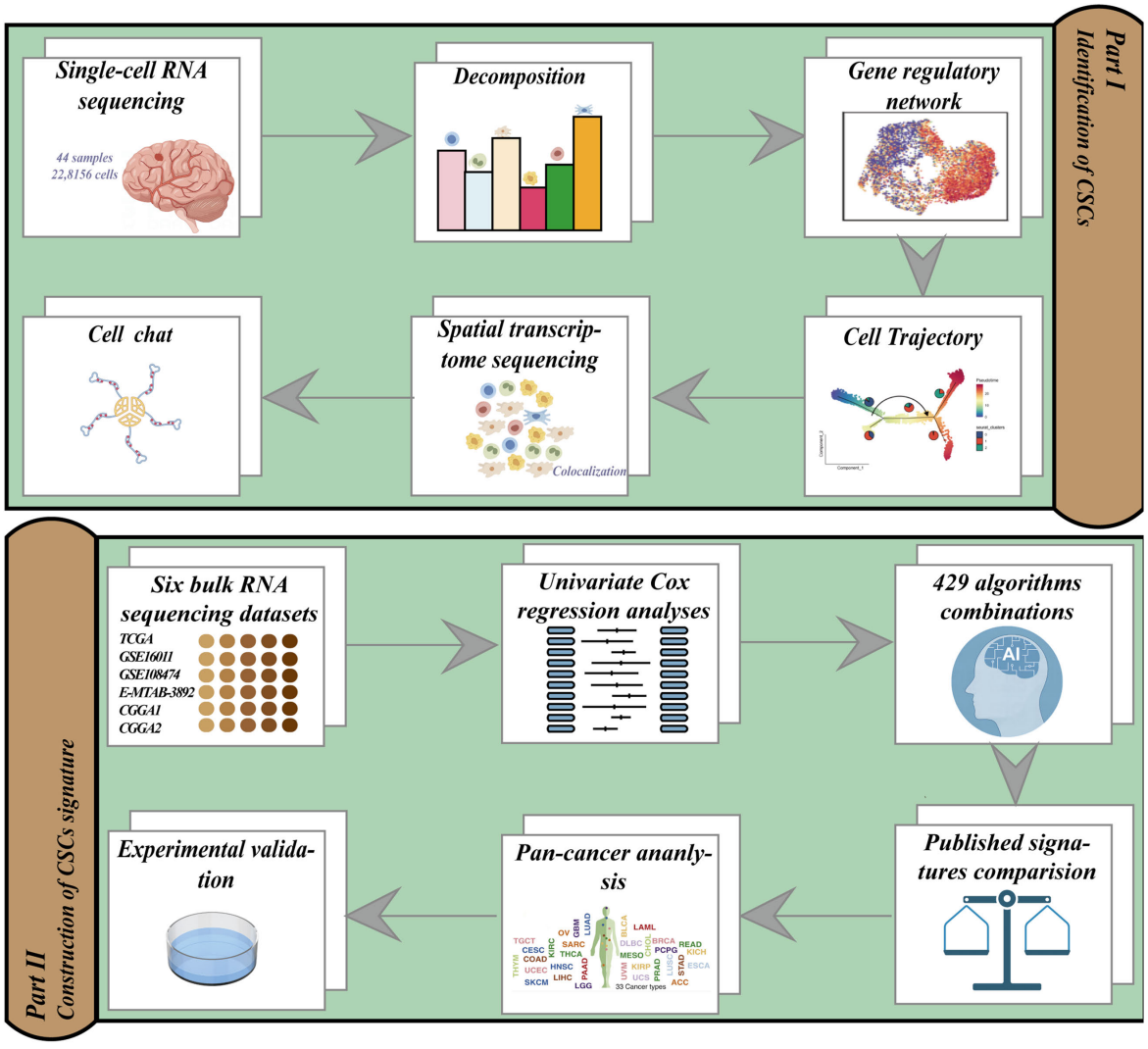

FIGURE 1
An illustration of the general workflow adopted in this study.

10.3389/fimmu.2024.1475235

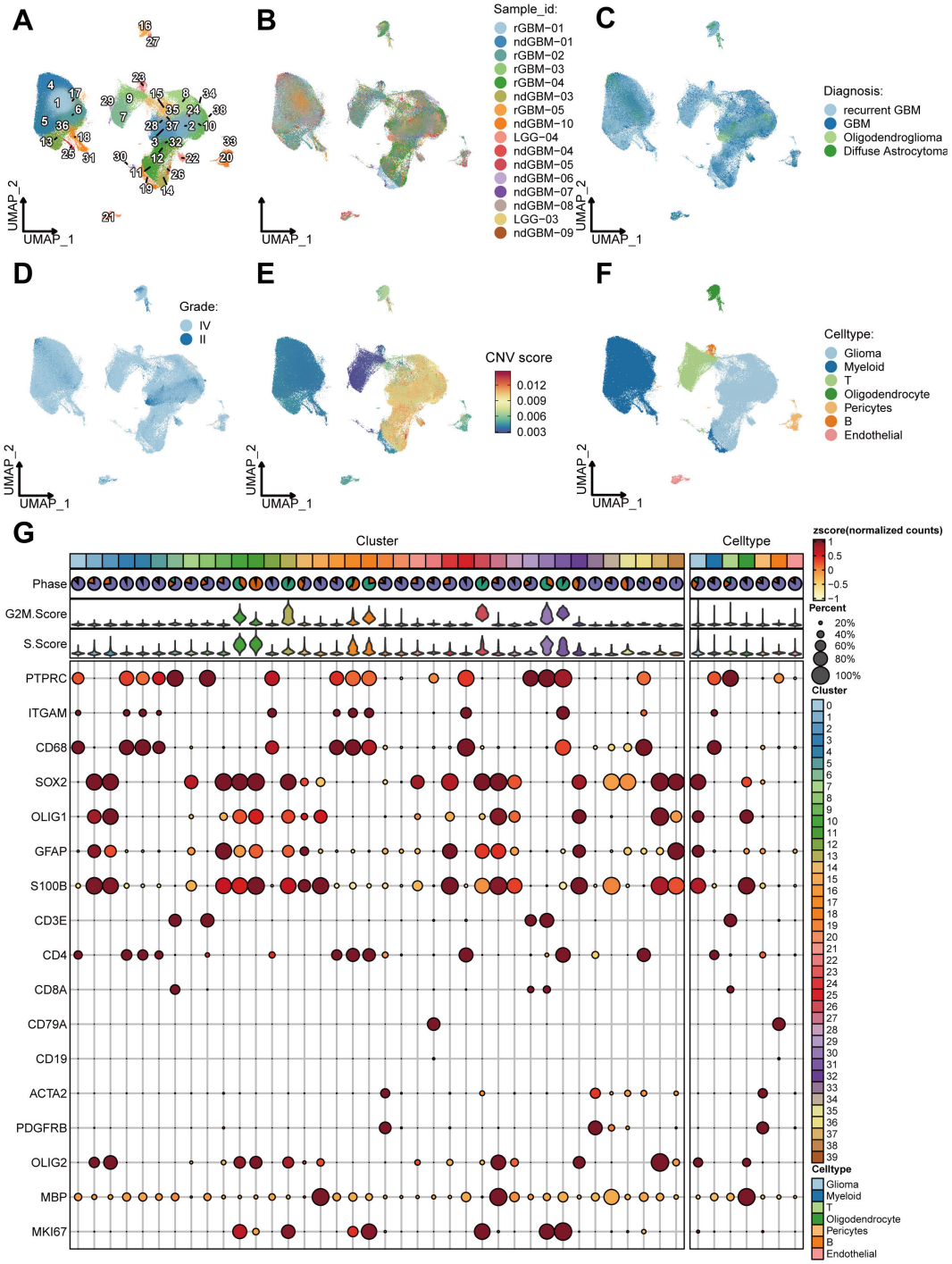

FIGURE 2
Clustering and cell-type identification of single-cell RNA-seq data. **(A–F)** UMAP projections of 228,156 aggregate single cells from 44 primary glioma samples showing the composition of different cell types in human gliomas. UMAP projections are shown by cluster numbers **(A)**, by the patient **(B)**, by pathological type **(C)**, by grade **(D)**, by Copy Number Variation (CNV) score **(E)** and by cell types **(F)**. **(G)** Dot plot showing marker gene expression and cell cycle score for different cell types.

Unsupervised clustering identified 38 clusters with distinct gene expression patterns (Figures 2A–D). InferCNV analysis was employed to distinguish malignant and non-malignant cells based on the CNV score (Figure 2E). Each cluster was assigned to a cell type using InferCNV analysis and marker gene expression (Figures 2F, G).

Identification and characterization of glioma stem cells

After conducting additional dimensionality reduction and clustering of glioma cells, our bespoke analytical framework

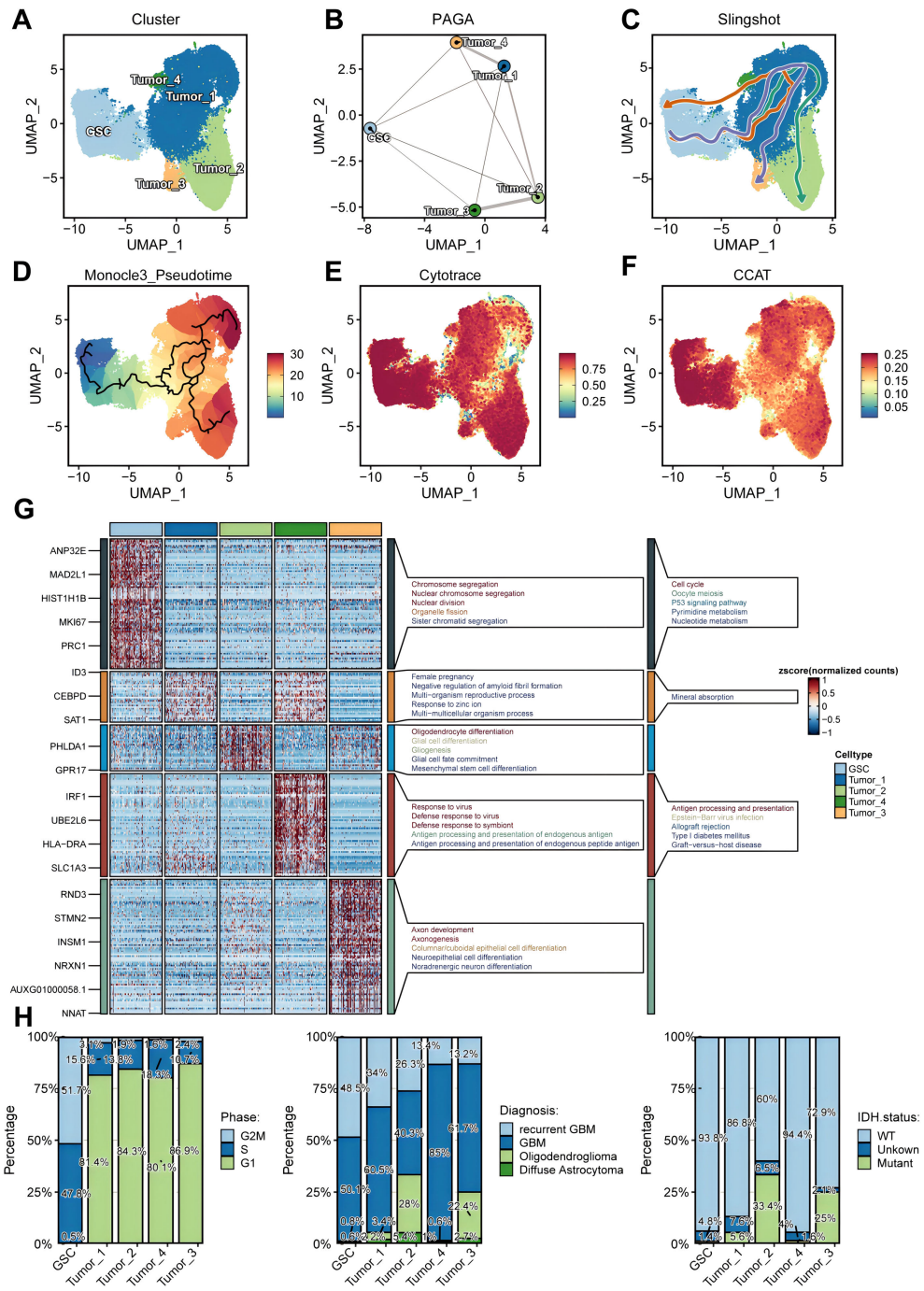

FIGURE 3
Identification and characterization of glioma stem cells (GSCs). **(A)** UMAP projections of 92,014 aggregate glioma cells are shown by cell annotation. **(B–D).** Trajectory inference using PAGA **(B)**, Slingshot **(C)**, and Monocle3 **(D)**. **(E, F)** UMAP projections of 92,014 aggregate glioma cells are shown by Cytotrace score **(E)** and CCAT score **(F)**. **(G)** Marker genes and Kyoto Encyclopedia of Genes and Genomes (KEGG)/Gene Ontology (GO) enrichment analysis for each glioma cell subpopulations. **(H)** Differential distribution of glioma cell subsets across cell cycle phases (left), histopathological classifications (middle), and IDH mutation status (right).

enabled us to pinpoint GSCs, as indicated in Figure 3A. Utilizing the PAGA algorithm, we demonstrated the differential potential of GSCs as they evolve into various tumor cell subpopulations (Figure 3B). Analyses integrating Monocle3 and the Slingshot algorithm further elucidated the fundamental role that GSCs subpopulations play as the origin of tumoral evolution (Figures 3C, D). Both the CCAT and CytoTRACE algorithms highlighted the pronounced stem-like qualities inherent within GSCs (Figures 3E, F). Then, we performed a comprehensive enrichment analysis of the highly expressed marker genes across various tumor subpopulations, utilizing the Kyoto Encyclopedia of Genes and Genomes (KEGG) and Gene Ontology (GO) databases.

Our findings revealed significant enrichment of GSC marker genes within pathways associated with cell proliferation, particularly those involving the cell cycle (Figure 3G). To further elucidate the proliferative capacity of GSCs, we conducted a detailed assessment of their cell cycle profiles, which demonstrated a predominant presence in the G2M and S phases (Figure 3H). This observation underscores the pivotal role of proliferation in the maintenance of stemness (45). Moreover, our analysis uncovered a striking prevalence of GSCs within samples of higher malignancy, including recurrent GBM, and gliomas with wild-type (WT) IDH (Figure 3H).

GSCs correlated with unfavorable prognosis

Utilizing bulk RNA-seq data from the TCGA cohort, we evaluated the prognostic significance of five distinct tumor cell populations. Initially, we identified cell-type-specific marker genes at the single-cell level, characterized by a log2 fold change exceeding 1 and an adjusted P below 0.05, and proceeded to determine their hazard ratios (HRs) based on overall survival (OS), progression-free interval (PFI), disease-specific survival (DSS), and disease free interval (DFI) within the TCGA cohort. Our observations revealed that GSC marker genes exhibited the most elevated HRs for OS, PFI, DFI, and DSS (Figures 4A–D). We ascertained that these GSCs constitute independent prognostic indicators for OS, PFI, and DSS ($P < 0.05$) (Figures 4E–G). Nevertheless, GSCs did not emerge as independent risk factors for DFI, a finding potentially attributable to the paucity of DFI data (Figure 4H). Kaplan-Meier analysis further demonstrated that a higher abundance of GSCs was associated with adverse outcomes across OS, PFI, DFI, and DSS ($P < 0.05$) (Figures 4I–L). Moreover, the area under the curve (AUC) values for the prediction of OS, PFI, DSS, and DFI consistently surpassed 0.7 (Figures 4I–L), underscoring the formidable prognostic predictive power of GSCs.

Unique TF profile associated with GSCs

As previous studies (46) showed, TFs are key for cell fate specification. Each cell type exhibited a unique TFs pattern (Figure 5A). Strong enrichment was in E2F1, E2F2, E2F7, and BRCA1 regulon activity in GSCs (Figure 5B). Figure 5C displays the expression patterns of these four TFs, which correlated with worse prognosis in glioma patients from the TCGA cohort ($P < 0.05$) (Figure 5D). These findings indicated that the four TFs might be essential for maintaining the stemness of GSCs.

Spatial transcriptomics of glioma reveals cellular localization

We reduced the dimensionality and clustered the spatial transcriptome data, identified the predominant cell types at each spot based on the back-convolutional via the scRNA-seq reference data, and chose the two samples with the highest GSCs abundance for the next step in the analysis (Figures 6A, B). Based on MISTy results, GSCs had a close spatial location to myeloid-derived suppressor cells (MDSCs) (Figure 6C). Then, we found that the MIF pathway was active between GSCs and MDSCs (Figure 6D). This result confirmed the previous conclusion that GSCs activate MDSCs to suppress immune responses by secreting MIF (47).

Construction of the GSCS

To further quantify the abundance of GSCs using key genes and improve the ability to predict prognosis in gliomas, we developed a GSCS on a novel artificial intelligence network. We first performed univariate Cox analysis to select the most specific GSCs marker (log2 fold change > 1, adjusted $P = 0$) with prognostic value ($P < 0.05$). We then fitted 429 algorithm combinations on the TCGA cohort and computed the C-index for each combination on the validation cohorts. The combination of VSOLassoBag and RSF had the highest mean C-index of 0.764 (Figure 7A). VSOLassoBag identified 26 genes, which were used by RSF to construct the GSCS (Supplementary Figures 1A, B). We stratified glioma patients into high- and low-risk groups based on the optimal cutoff from the TCGA cohort. Our results showed that the high-risk group had significantly worse OS than the low-risk group in all cohorts ($P < 0.05$) (Figures 7B–G). Moreover, time-dependent ROC curves demonstrated the robust and stable performance of the GSCS in the all cohorts (Figures 7B–G).

Comparison of prognostic signatures

The GSCS outperformed age, grade, gender, IDH status, MGMT promoter status, karnofsky score (KPS), 1p/19q co-deletion,TP53 protein expression, and recurrent status in terms of the C-index across the all cohorts (Figure 8A). We also compared the GSCS with other pulished signatures in the TCGA, GSE108474, GSE16011, E-MTAB-3892, CGCA1 and CGCA2 cohorts (Figures 8B–H). The GSCS had the highest C-index among all signatures in the all cohorts.

The GSCS exhibited a generalizability signature in pan-cancer

We calculated the GSCS score for 33 cancers from the TCGA (Figure 9A) and divided them into High-risk and Low-risk groups. We observed that high GSCS scores correlated with worse prognosis across all 15 cancers ($P < 0.05$) (Figure 9B). These results suggest that GSCS may also be a key factor affecting the prognosis of various other cancers.

Potential biological peculiarities of the GSCS

To explore the biological mechanisms underlying the association between GSCS and proliferative features, we performed pathway analysis on the GSCS score. We found that the score is strongly correlated with several tumorigenic pathways,

10.3389/fimmu.2024.1475235

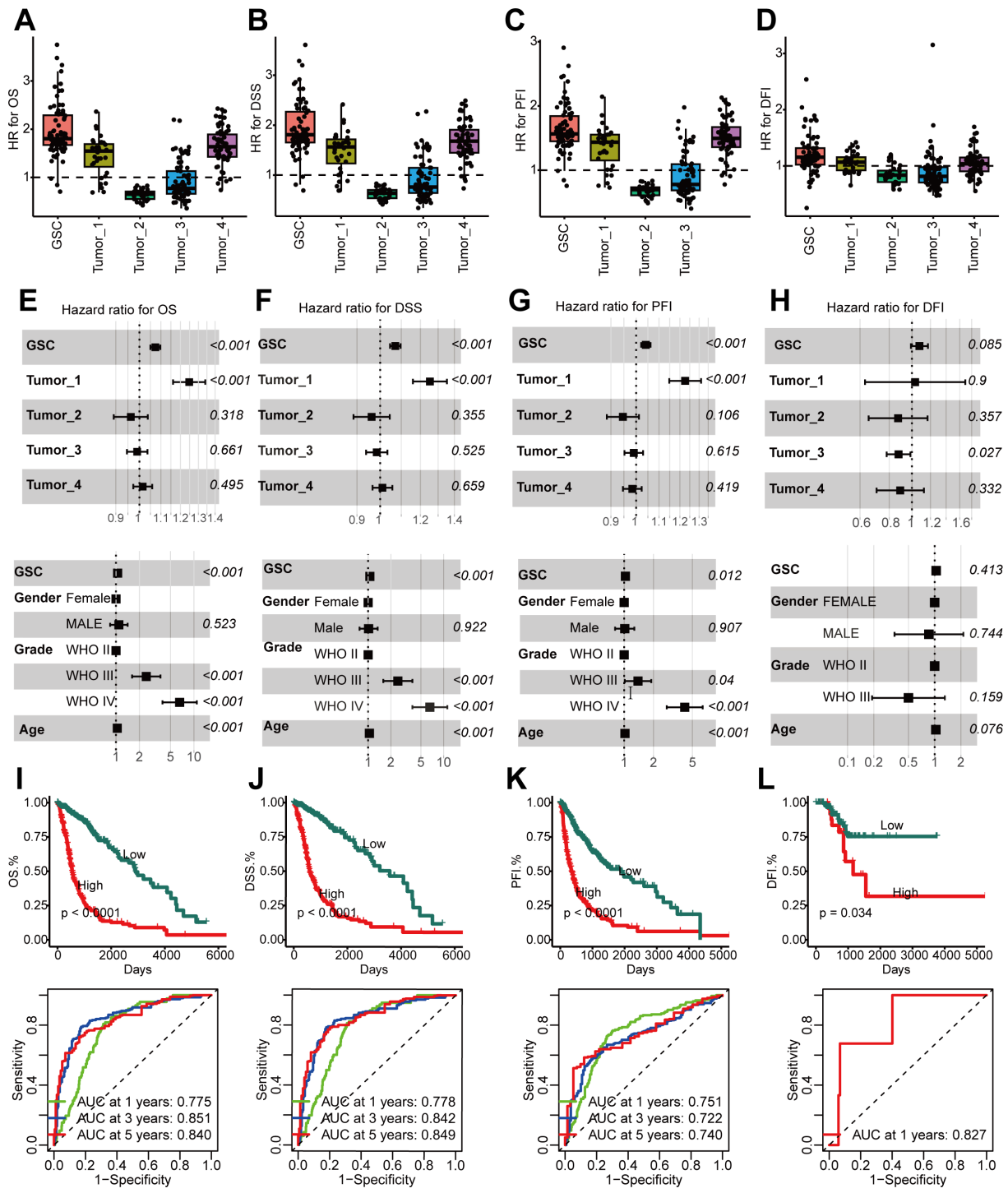

FIGURE 4
Higher GSCs abundance in glioma, linked with poor prognosis. **(A–D)** GSCs abundance's association with poor overall survival (OS) **(A)**, disease-specific survival (DSS) **(B)**, progression-free interval (PFI) **(C)**, and disease free interval (DFI) **(D)** manifested through HR values for cell type marker genes from Cox proportional hazards regression. Each dot is a gene, with HR value on x-axis and cell type on y-axis. **(E–H).** Multivariate Cox analyses to identify the risk factors in OS **(E)**, DSS **(F)**, PFI **(G)**, DFI **(H)**. **(I–L)**. Time-dependent receiver operating characteristic (ROC) analysis (top) and Kaplan-Meier (KM) curves (below) of the GSCs abundance in OS **(I)**, DSS **(J)**, PFI **(K)**, DFI **(L)**.

such as the G2M DNA replication checkpoint, angiogenesis, E2F targets, and epithelial-mesenchymal transition (EMT) ($P < 0.05$) (Figure 10A). We also observed significant differences in proliferation-related pathways between the two risk groups ($P < 0.05$) (Figure 10B). The DEGs between the low- and high-risk groups were enriched in immune-related and proliferation-related pathways ($P < 0.05$) (Figure 10C). Furthermore, GSEA of kyoto encyclopedia of genes and genomes (KEGG) terms revealed that the high-risk group was enriched for ecm-receptor interaction, cell cycle, P53 signaling pathway, and DNA replication ($P < 0.05$)

10.3389/fimmu.2024.1475235

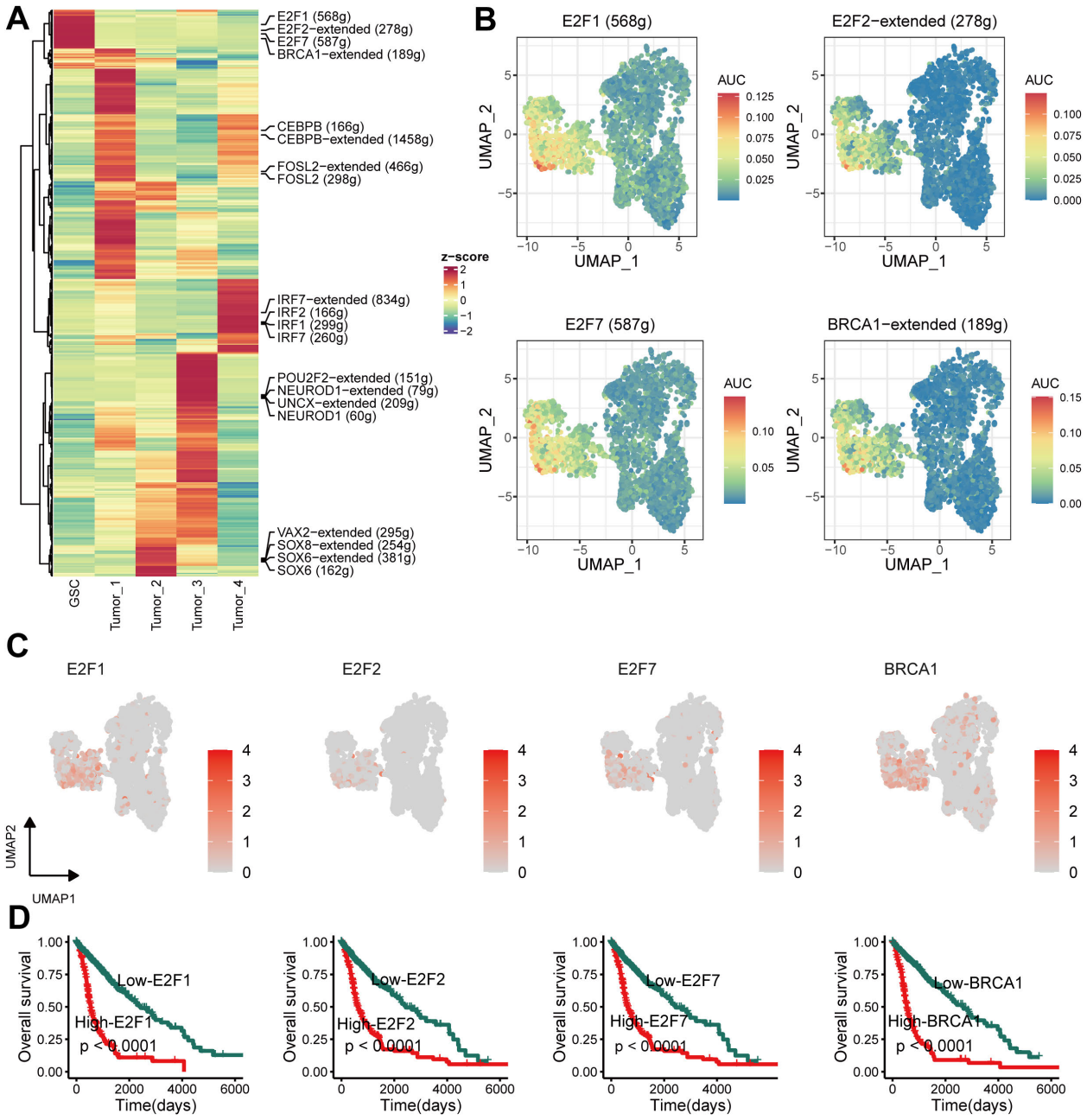

FIGURE 5
Unique transcription factor (TF) activity associated with GSCs. **(A)** Heatmap showing differences in TF activity scored by SCENIC. **(B)** TF activity of E2F1, E2F2, E2F7 and BRCA1 projected on UMAP. **(C)** TF expression of E2F1, E2F2, E2F7 and BRCA1 projected on UMAP. **(D)** Kaplan–Meier survival curves for E2F1, E2F2, E2F7 and BRCA1.

(Figure 10D). These findings also demonstrated the critical role of proliferation in maintaining stemness (48).

The silence of the TUBA1C inhibits the malignant biological behavior of glioma cells

To investigate the key role of TUBA1C in the pathogenesis of glioma, we selected the LN299 and U87 glioma cell lines as research subjects and used targeted siRNA-mediated knockdown technology to regulate the expression of TUBA1C (Figure 11A). We evaluated the impact of TUBA1C knockdown on the viability of glioma cells using the CCK-8 assay. The experimental results showed that the OD value of glioma cells decreased significantly after TUBA1C expression was silenced (Figures 11B, C). To further investigate the impact of TUBA1C suppression on the migration and invasion ability of glioma cells, we conducted in-depth analyses. Using the Transwell migration and invasion assay, we observed that the invasion and migration ability of glioma cells were significantly reduced after TUBA1C knockdown (Figures 11D–F).

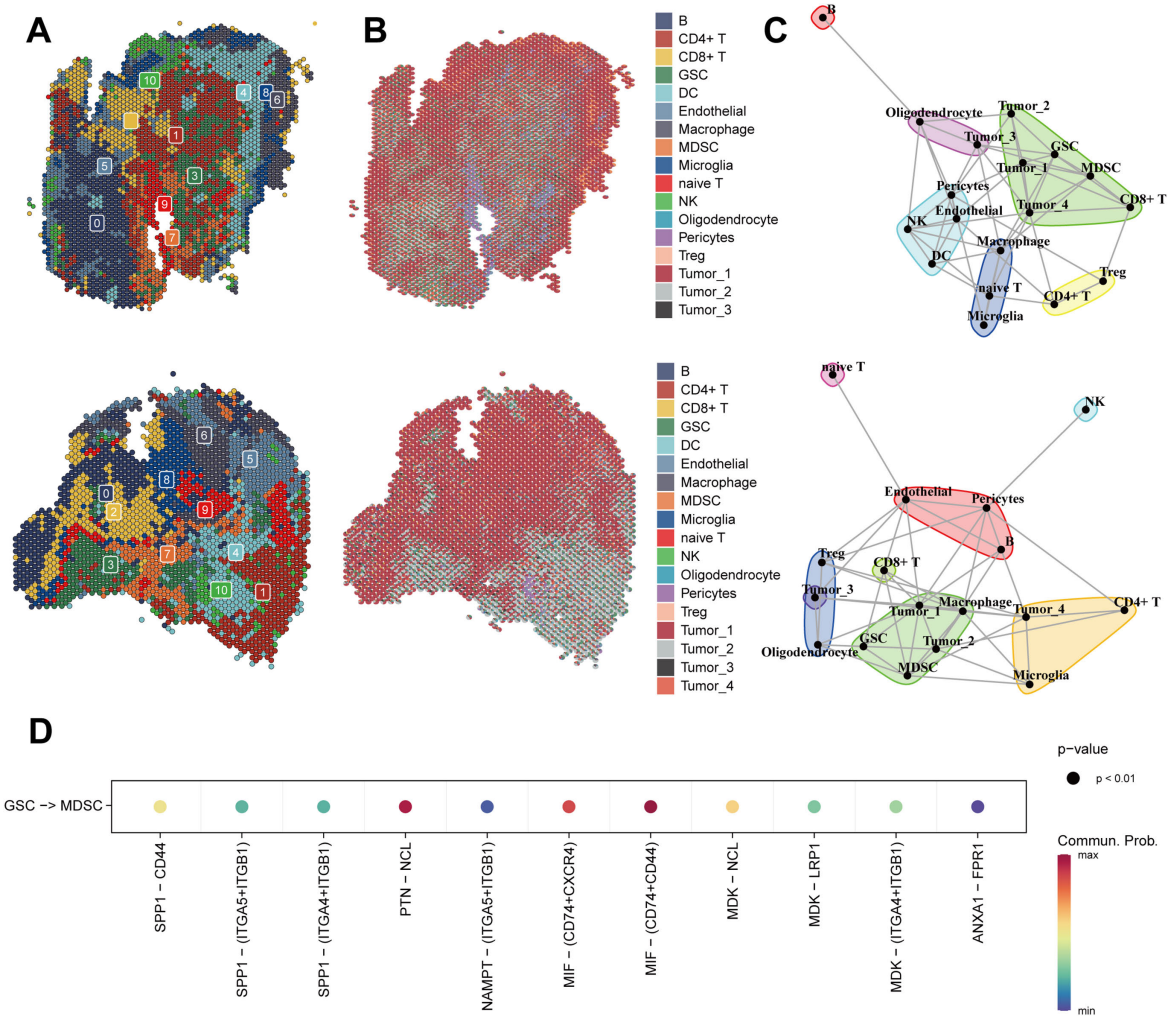

FIGURE 6
Spatial transcriptomics of glioma reveals cellular localization and cell communication. **(A)** Spatial Transcriptomics-based UMAP clustering of sample 1 (**top**) and sample 2 (**below**). **(B)** Spatial localization of individual clusters in the sample 1 (**top**) and sample 2 (**below**). **(C)** The spatial distribution of different cell-types in the spatial transcriptomics reference calculated by RCTD in the sample 1 (**top**) and sample 2 (**below**). **(D)** MIF signaling pathway from CellChat results.

Clonogenic assays confirmed that the proliferation ability of glioma cells was weakened after TUBA1C knockdown (Figures 11G, H). The wound healing experiment provided quantitative data, showing that TUBA1C knockdown significantly slowed the wound healing process, indicating that cell migration ability was significantly inhibited (Figures 11I, J). Taken together, we have revealed the key role of TUBA1C in promoting the proliferation, migration, and invasion of glioma cells. This discovery underscores the importance of TUBA1C as a potential therapeutic target in glioma treatment and may provide new ideas and methods for future glioma treatment.

Silencing TUBA1C inhibits subcutaneous tumor growth *in vivo*

We injected LN299 cell lines transfected with either TUBA1C-NC or TUBA1C-Si-1 subcutaneously into nude mice and dynamically observed the body weight and tumor growth of the mice. Through qPCR analysis, we compared the differences in TUBA1C expression between the two groups and confirmed the effectiveness of gene silencing in the xenograft tumors (Supplementary Figure 2). The results indicated that, compared to the NC group, the tumor weight and volume were significantly reduced in the Si-1 group mice, while there was no significant difference in body weight between the groups (Figures 12A–D). Immunohistochemical analysis of the mouse tissues showed that the percentage of Ki67 positive cells in the tumor tissues of the Si-1 group mice was also significantly reduced, suggesting that Si-1 treatment effectively inhibits tumor growth and cell proliferation (Figures 12E, F). In summary, these results highlight the potential of TUBA1C as a therapeutic target in glioma treatment strategies.

Discussion

Treatment for gliomas has remained unchanged since 2005, involving surgical resection, radiation and concurrent and adjuvant

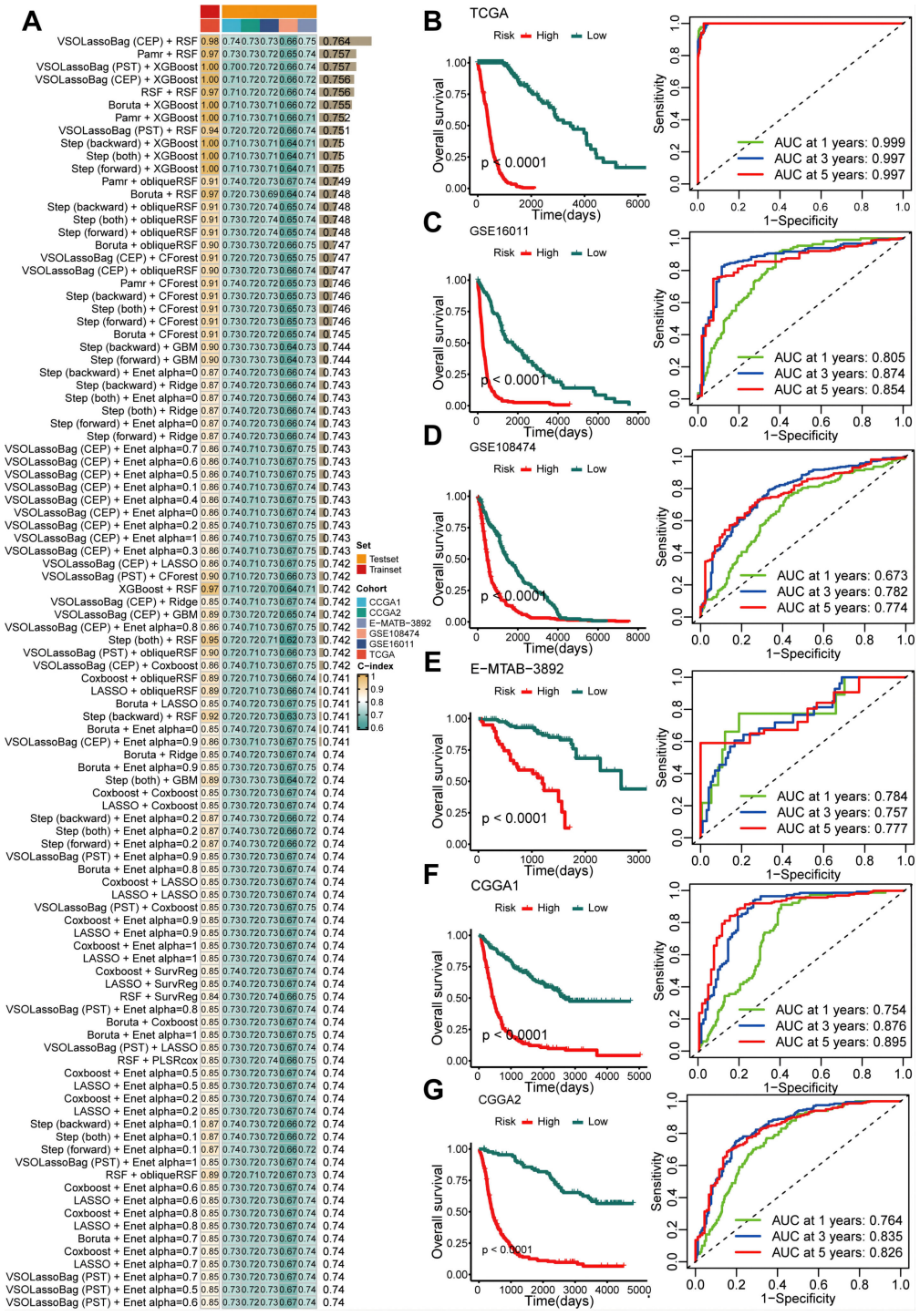

FIGURE 7
An artificial intelligence network was utilized to develop and validate a consensus GSC signature (GSCS). **(A)** A total of 429 prediction models were developed using a 10-fold cross-validation framework, and the C-index of each model was computed across all datasets. **(B–G).** Kaplan-Meier curves and ROC curves of OS according to the GSCS in the **(B)** TCGA, **(C)** GSE16011, **(D)** GSE108474, **(E)** E-MTAB-3892, **(F)** CGG1, and **(G)** CGGA2.

TMZ (49). Adjuvant TMZ marginally increased survival time for adults with gliomas; however, this agent has caused systemic toxicities and decreased the quality of life for patients (49, 50). Moreover, many tumors exhibit primary or acquired resistance to temozolomide (51). The anti-angiogenic antibody bevacizumab, which neutralizes VEGF, was approved for recurrent gliomas and increased PFS in patients (52). However, subsequent trials showed no improvement in OS for newly diagnosed patients (53). While bevacizumab normalized the tumor blood vessels and reduced symptoms such as oedema, it does not extend lifespan (54). Gliomas are widely infiltrative and resistant to standard therapies, remaining non-curative. Therefore, new therapeutic options are

10.3389/fimmu.2024.1475235

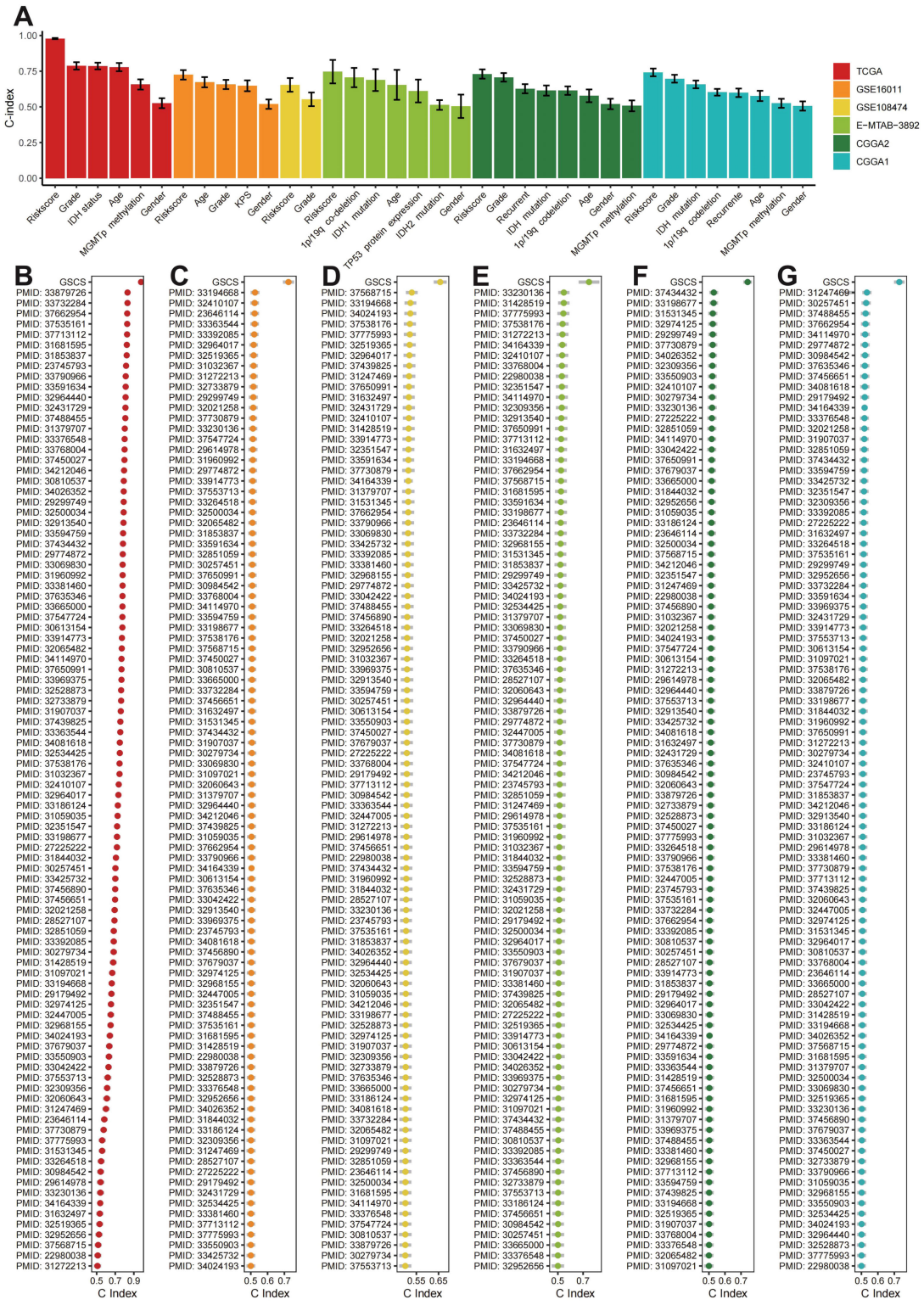

FIGURE 8
(A) The C-index of the GSCS and other models developed in the **(B)** TCGA, **(C)** GSE16011, **(D)** GSE108474, **(E)** E-MTAB-3892, **(F)** CGCA1, and **(G)** CGCA2.

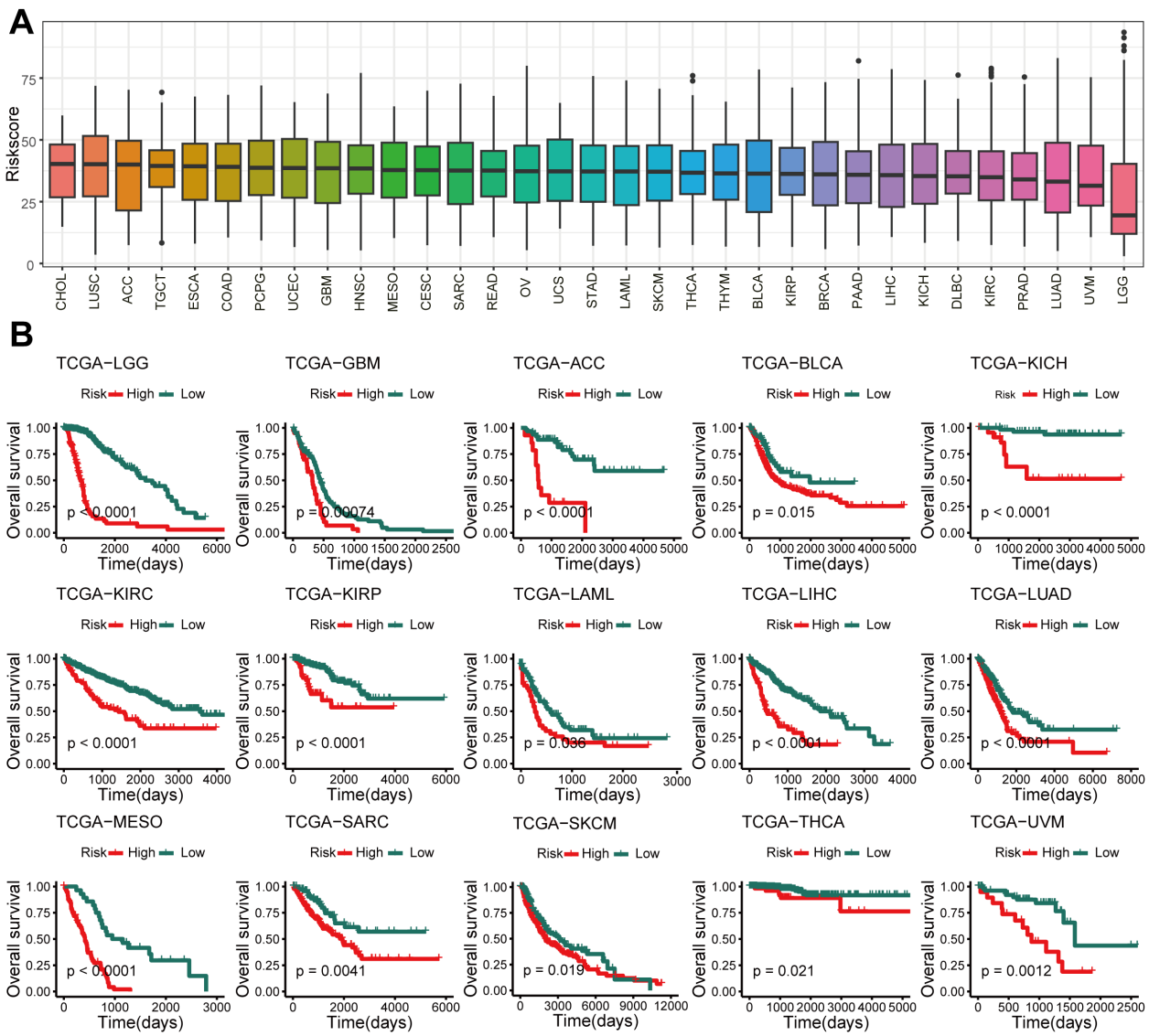

FIGURE 9
Pan-cancer of GSCS. **(A)** GSCS score for 33 cancers in the TCGA database. **(B)** Kaplan-Meier curves of OS according to the GSCS in the TCGA database.

urgently needed. In this work, based on integrated analysis of scRNA, bulk RNA sequencing, ST and machine learning algorithms, we identified and characterized GSC and developed a GSCS based on maker genes from the GSC as a predictive model for glioma patient outcomes.

We identified a glioma cell type, GSCs, that demonstrate a predominant presence in the G2M and S phases of the cell cycle. Furthermore, we observed a strong enrichment of E2F1, E2F2, E2F7, and BRCA1 regulons in GSCs. These four TFs are implicated in proliferation and DNA repair, indicating the high proliferative potential of this subcluster. Previous studies have shown that these TFs regulate stemness (55, 56). Additionally, GSCs were enriched with genes previously linked to poor glioma outcomes, such as CENPF (57), TOP2A (58), NUSAP1 (59), PTTG1 (60), UBE2C (61), and UBE2S (62). Unlike previous studies that focused on individual glioma genes, we employed a single-cell decomposition approach to reveal the association of the GSC type proportion and reduced survival. Moreover, the GSCs encompass not only encompasses known glioma genes, but also novel targets, such as HMGN2, TUBB4B, and ARL6IP1, that warrant further investigation. In summary, our research confirms the role of previously known genes in glioma GSCs while also identifying novel targets and TF regulators that can enhance our understanding of this complex disease. With further investigation, these discoveries could pave the way for developing more effective therapeutic strategies for glioma patients.

We aimed to enhance our understanding of the factors affecting survival in glioma patients, given their poor prognosis. Our findings suggest that GSCs could serve as useful biomarker for guiding treatment and predicting outcomes. Current prognostic tools for glioma primarily rely on factors such as WHO grade, IDH mutations, 1p/19q codeletion, MGMT promoter methylation, TERT

10.3389/fimmu.2024.1475235

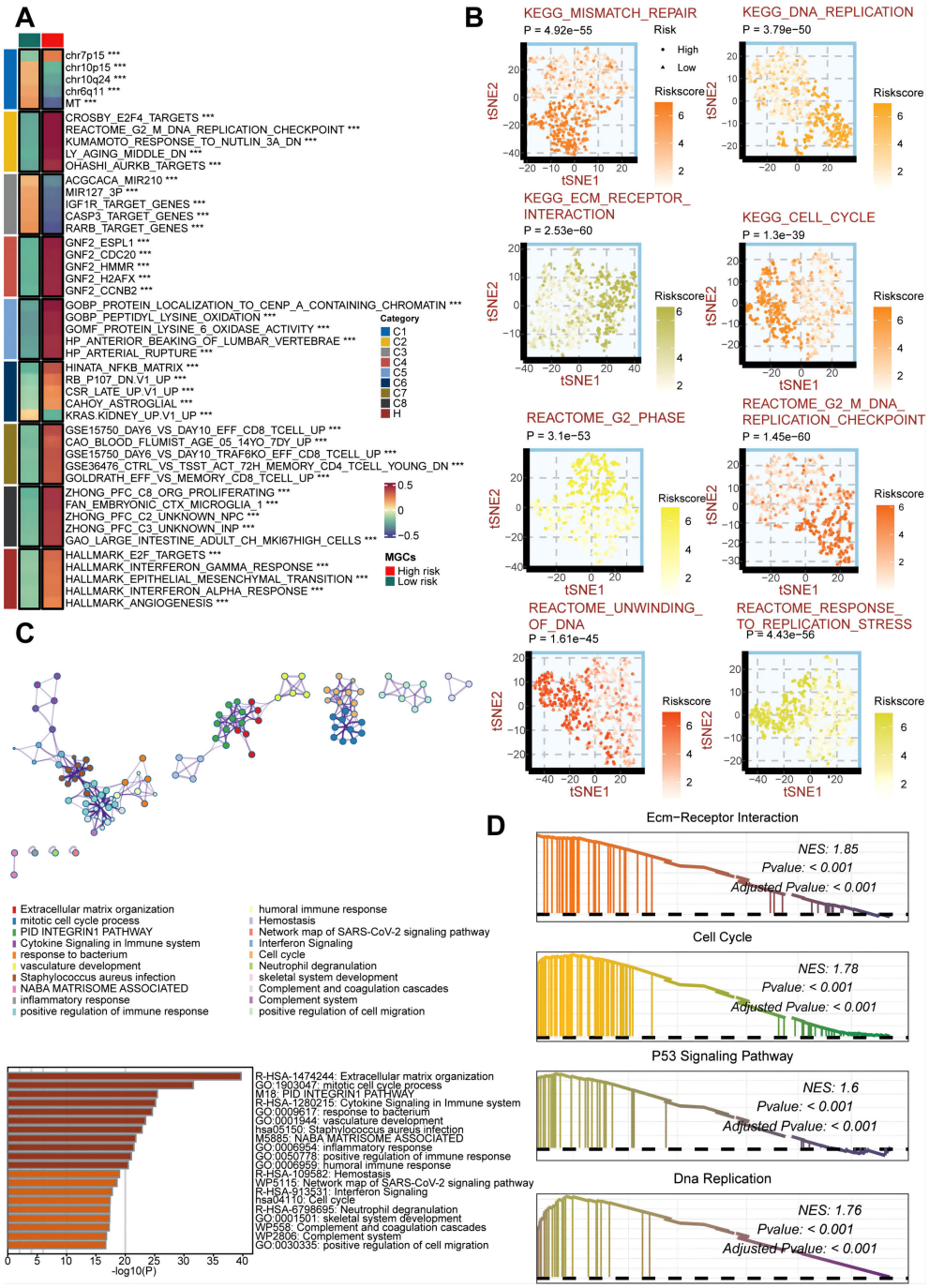

FIGURE 10
Biological peculiarities of the GSCS in the TCGA cohort. **(A)** MsigDB-based gene set variation analysis (GSVA) delineated the biological attributes of two risk groups. **(B)** t-Distributed Stochastic Neighbor Embedding (t-SNE) plots of kyoto encyclopedia of genes and genomes (KEGG) and reactome terms delineated the differences in pathway activity in the two risk groups. **(C)** Metascape-based enrichment analysis of differentially expressed genes between two risk groups. **(D)** Gene set enrichment analysis (GSEA) of KEGG terms for the GSCS. ***p < 0.001.

promoter mutations and EGFR amplification (63). Cell type markers can aid in comprehend cancer biology and supplement existing clinical practices. The marker genes associated with GSCs may pave the way for new expression-based prognostic technologies. As RNA sequencing technology has matured and clinical laboratories can now detect gene expression patterns with prognostic value (64). We developed an integrative pipeline to construct a GSCS using the expression profiles of GSCs marker genes. We validated this signature in six independent cohorts and confirmed that the best model is a combination of VSOLassoBag and RSF. The algorithm combinations eliminated low-value features, optimized the model, and enhanced its generalization ability (65). The GSCS performed well in predicting outcomes across all

10.3389/fimmu.2024.1475235

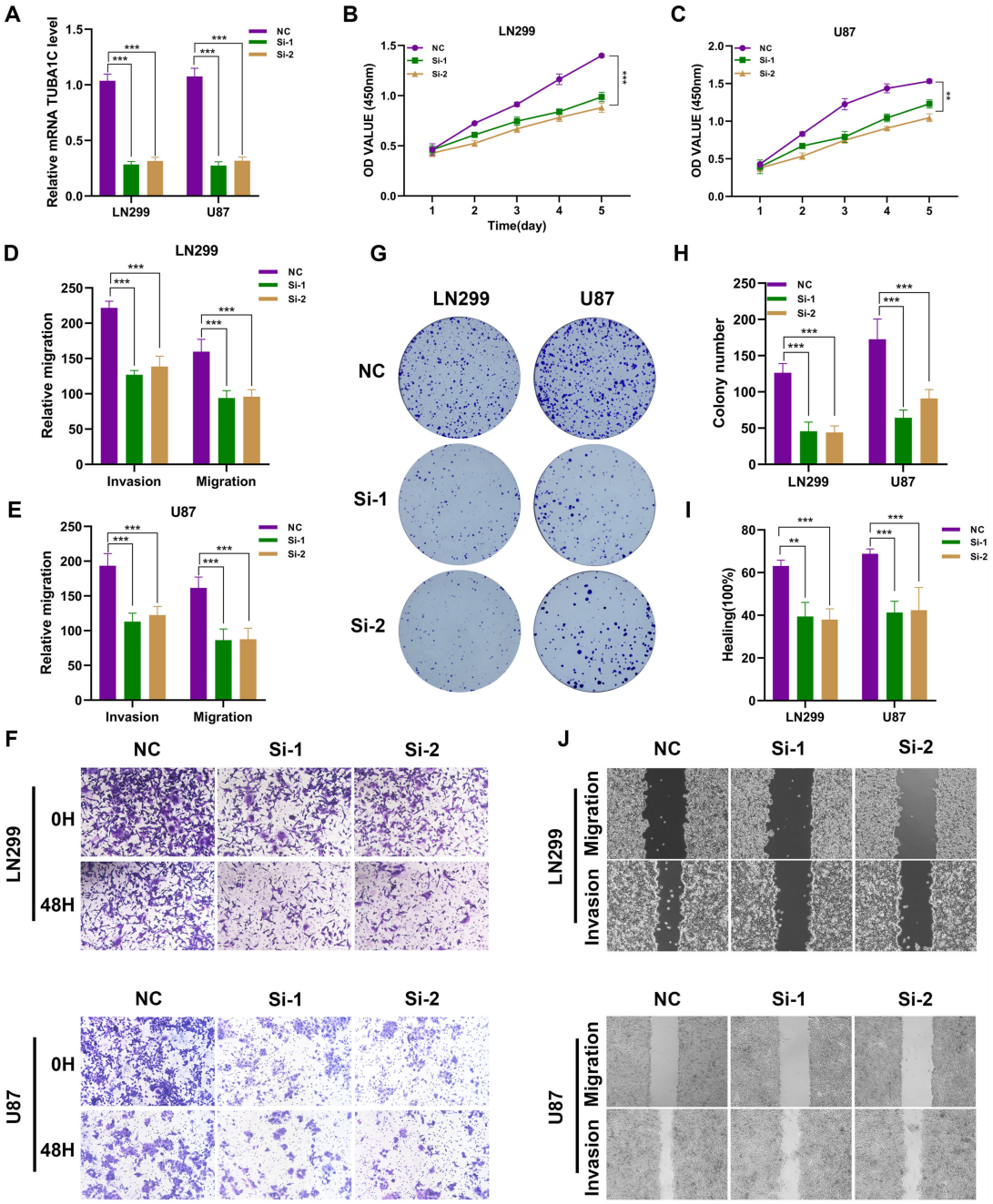

FIGURE 11
Silencing of TUBA1C Inhibits the Malignant Biological Behavior of Glioma Cells. **(A)** Schematic representation of the targeted siRNA-mediated knockdown of TUBA1C in LN299 and U87 glioma cell lines. **(B, C)** CCK-8 assay results showing a significant decrease in OD values of glioma cells following TUBA1C knockdown, indicating reduced cell viability. The results are presented as the mean ± SD of three independent experiments. **(D–F)** Transwell migration and invasion assays demonstrating a significant reduction in the migration and invasion abilities of glioma cells after TUBA1C knockdown. Quantitative analysis showed a significant decrease in the number of migrated and invaded cells. **(G, H)** Clonogenic assays confirming that the proliferation capacity of glioma cells is weakened upon TUBA1C knockdown. The number of colonies formed was significantly reduced compared to the control group. **(I, J).** Wound healing assays showing quantitative data that TUBA1C knockdown significantly slows the wound healing process, indicating a marked inhibition of cell migration capability. Wound closure percentage was significantly lower in TUBA1C knockdown cells. **p < 0.01; ***p < 0.001.

six cohorts, as shown by ROC and C-index analyses, indicating its potential clinical utility. To maximize the clinical utility of the GSCS, future research should focus on integrating this biomarker into routine diagnostic workflows. Investigating its application in personalized treatment plans could enhance therapeutic decision-making, particularly for patients with varying glioma subtypes. Additionally, exploring the GSCS in conjunction with existing prognostic factors may lead to more refined risk stratification models. Longitudinal studies assessing the signature's predictive power in response to specific therapies will be crucial. Furthermore, expanding the

10.3389/fimmu.2024.1475235

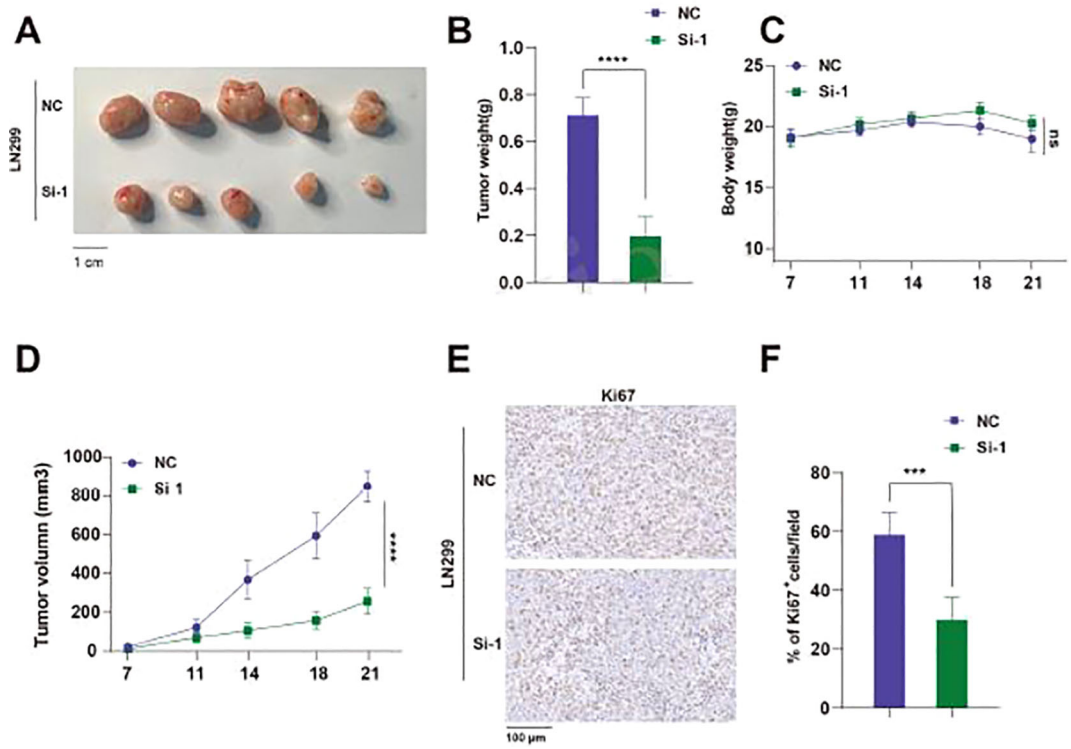

FIGURE 12
Knockdown of TUBA1C Inhibits Subcutaneous Tumor Growth *In Vivo*. **(A)** Representative images of tumors from mice, showing the tumor size comparison between the NC group and the Si-1 group. Scale bar: 1 cm. **(B)** Comparison of tumor weights between NC and Si-1 groups of mice. **(C)** Body weight changes during the experiment, showing no significant difference between the two groups. **(D)** Tumor volume growth curves, showing that the tumor volume in Si-1 group mice was significantly smaller than that in the NC group. **(E)** Ki67 immunohistochemistry images showing Ki67 positive cells in tumors from NC and Si-1 groups. **(F)** Comparison of the percentage of Ki67 positive cells per field. ****p < 0.0001.

signature's validation across diverse populations and treatment settings will strengthen its relevance and applicability in clinical practice, ultimately improving patient outcomes.

Based on the RSF algorithm, TUBA1C was identified as the most significant gene in GSCS. TUBA1C is an isoform of α-tubulin that has been shown to play a critical role in the cell cycle and immune microenvironment of lung adenocarcinoma (LUAD). Elevated TUBA1C expression correlates with poor outcomes and with tumor-infiltrating immune cells (TIICs) in LUAD (66). Additionally, TUBA1C is upregulated in hepatocellular carcinoma (HCC) and pancreatic ductal adenocarcinoma (PDAC), where it predicts poor prognosis and enhances cell proliferation and migration (67, 68). Furthermore, a prior study indicated that TUBA1C was statistically associated with the expression of RP11-480I12.5 in breast cancer (BRCA) and demonstrated prognostic significance (69). TUBA1C has also been shown to promote aerobic glycolysis and cell growth via upregulation of YAP expression, thereby contributing to BRCA development. Our findings further revealed that TUBA1C knockdown significantly inhibited the malignant biological behaviors of glioma cells, demonstrating that TUBA1C is a promising target for the treatment of glioma.

This study has advanced our understanding of GSCs and their clinical relevance; however, we acknowledge several limitations. First, the cohorts exhibited had heterogeneity due to different in sequencing or microarray platforms. We harmonized the data using standard normal transformation, which was only partially effective. Second, we relied on retrospective samples, necessitating future validation in a prospective, large cohort. Third, we should conduct more in-depth and detailed molecular biology studies in both *in vivo* and *in vitro* experiments to uncover the molecular mechanisms of tumor recurrence and identify new therapeutic targets.

Conclusion

This study provides a comprehensive characterization of GSCs through integrated analysis of single-cell RNA sequencing, spatial transcriptomics, and machine learning approaches. We identified a distinct GSC population with high proliferative potential and developed a novel 26-gene GSCS that exhibits robust prognostic value across multiple cohorts. The signature demonstrated pan-cancer prognostic ability and an association with critical tumorigenic pathways. We validated the functional significance of TUBA1C, a key component of our signature, through *in vitro* and *in vivo* experiments. Silencing TUBA1C significantly inhibited glioma cell proliferation, migration, and invasion, as well as tumor growth in xenograft models. This study

enhances our understanding of glioma biology and provides a clinically relevant prognostic tool and potential therapeutic targets.

Data availability statement

The datasets presented in this study can be found in online repositories. The names of the repository/repositories and accession number(s) can be found in the article/Supplementary Material. The Raw data is available at: https://www.jianguoyun.com/p/DWH4qUEQ45m7Cxih8NwFIAA.

Ethics statement

The animal study was approved by The Ethics Committee Northern Jiangsu People's Hospital Affiliated to Yangzhou University. The study was conducted in accordance with the local legislation and institutional requirements.

Author contributions

LC: Funding acquisition, Methodology, Software, Visualization, Writing – original draft, Writing – review & editing. XL: Software, Visualization, Writing – review & editing. XW: Software, Validation, Writing – review & editing. HW: Conceptualization, Data curation, Methodology, Writing – original draft, Writing – review & editing. XM: Conceptualization, Data curation, Methodology, Writing – original draft, Writing – review & editing.

Funding

The author(s) declare financial support was received for the research, authorship, and/or publication of this article. This research was supported by the Suqian Sci&Tech Program (Grant No. 32B0301).

Conflict of interest

The authors declare that the research was conducted in the absence of any commercial or financial relationships that could be construed as a potential conflict of interest.

Publisher's note

All claims expressed in this article are solely those of the authors and do not necessarily represent those of their affiliated organizations, or those of the publisher, the editors and the reviewers. Any product that may be evaluated in this article, or claim that may be made by its manufacturer, is not guaranteed or endorsed by the publisher.

Supplementary material

The Supplementary Material for this article can be found online at: https://www.frontiersin.org/articles/10.3389/fimmu.2024.1475235/full#supplementary-material

SUPPLEMENTARY FIGURE 1
(A) Determination of the number of trees by minimizing error. **(B)** Variable importance of the top 26 genes determined using the random survival forest (RSF) algorithm.

SUPPLEMENTARY FIGURE 2
Relative TUBA1C mRNA expression levels in xenograft tumors from si-NC and si-LN299 groups. qPCR analysis revealed that TUBA1C expression was significantly reduced in the si-LN299 group compared to the si-NC group. ***$p < 0.001$.

References

1. Ostrom QT, Patil N, Cioffi G, Waite K, Kruchko C, Barnholtz-Sloan JS. CBTRUS statistical report: primary brain and other central nervous system tumors diagnosed in the United States in 2013-2017. *Neuro Oncol.* (2020) 22:iv1–iv96. doi: 10.1093/neuonc/noaa200

2. Nabors LB, Portnow J, Ahluwalia M, Baehring J, Brem H, Brem S, et al. Central nervous system cancers, version 3.2020, NCCN clinical practice guidelines in oncology. *J Natl Compr Canc Netw.* (2020) 18:1537–70. doi: 10.6004/jnccn.2020.0052

3. Wang X, Guo G, Guan H, Yu Y, Lu J, Yu J. Challenges and potential of PD-1/PD-L1 checkpoint blockade immunotherapy for glioblastoma. *J Exp Clin Cancer Res.* (2019) 38:87. doi: 10.1186/s13046-019-1085-3

4. Choma CT, Kaplan H. Bacillus thuringiensis crystal protein: effect of chemical modification of the cysteine and lysine residues. *J Invertebr Pathol.* (1992) 59:75–80. doi: 10.1016/0022-2011(92)90114-J

5. Suvà ML, Tirosh I. The glioma stem cell model in the era of single-cell genomics. *Cancer Cell.* (2020) 37:630–6. doi: 10.1016/j.ccell.2020.04.001

6. Prieto-Vila M, Takahashi RU, Usuba W, Kohama I, Ochiya T. Drug resistance driven by cancer stem cells and their niche. *Int J Mol Sci.* (2017) 18. doi: 10.3390/ijms18122574

7. Schulz A, Meyer F, Dubrovska A, Borgmann K. Cancer stem cells and radioresistance: DNA repair and beyond. *Cancers (Basel).* (2019) 11. doi: 10.3390/cancers11060862

8. Gisina A, Kholodenko I, Kim Y, Abakumov M, Lupatov A, Yarygin K. Glioma stem cells: novel data obtained by single-cell sequencing. *Int J Mol Sci.* (2022) 23. doi: 10.3390/ijms232214224

9. Ye B, Wang Q, Zhu X, Zeng L, Luo H, Xiong Y, et al. Chen T et al: Single-cell RNA sequencing identifies a novel proliferation cell type affecting clinical outcome of pancreatic ductal adenocarcinoma. *Front Oncol.* (2023) 13:1236435. doi: 10.3389/fonc.2023.1236435

10. Ye B, Hongting G, Zhuang W, Chen C, Yi S, Tang X, et al. Deciphering lung adenocarcinoma prognosis and immunotherapy response through an AI-driven stemness-related gene signature. *J Cell Mol Med.* (2024) 28:e18564. doi: 10.1111/jcmm.18564

11. Zhang P, Dong S, Sun W, Zhong W, Xiong J, Gong X, et al. Deciphering Treg cell roles in esophageal squamous cell carcinoma: a comprehensive prognostic and immunotherapeutic analysis. *Front Mol Biosci.* (2023) 10:1277530. doi: 10.3389/fmolb.2023.1277530

12. Zhang L, Cui Y, Mei J, Zhang Z, Zhang P. Exploring cellular diversity in lung adenocarcinoma epithelium: Advancing prognostic methods and immunotherapeutic strategies. *Cell Prolif.* (2024) 2024:e13703. doi: 10.1111/cpr.13703

13. Zhang P, Pei S, Zhou G, Zhang M, Zhang L, Zhang Z. Purine metabolism in lung adenocarcinoma: A single-cell analysis revealing prognostic and immunotherapeutic insights. *J Cell Mol Med.* (2024) 28:e18284. doi: 10.1111/jcmm.18284

14. Ye B, Ji H, Zhu M, Wang A, Tang J, Liang Y, et al. Single-cell sequencing reveals novel proliferative cell type: a key player in renal cell carcinoma prognosis and therapeutic response. *Clin Exp Med*. (2024) 24:167. doi: 10.1007/s10238-024-01424-x

15. Rozenblatt-Rosen O, Stubbington MJT, Regev A, Teichmann SA. The Human Cell Atlas: from vision to reality. *Nature*. (2017) 550:451–3. doi: 10.1038/550451a

16. Teschendorff AE, Maity AK, Hu X, Weiyan C, Lechner M. Ultra-fast scalable estimation of single-cell differentiation potency from scRNA-Seq data. *Bioinformatics*. (2021) 37:1528–34. doi: 10.1093/bioinformatics/btaa987

17. Gulati GS, Sikandar SS, Wesche DJ, Manjunath A, Bharadwaj A, Berger MJ, et al. Single-cell transcriptional diversity is a hallmark of developmental potential. *Science*. (2020) 367:405–11. doi: 10.1126/science.aax0249

18. Abdelfattah N, Kumar P, Wang C, Leu JS, Flynn WF, Gao R, et al. Single-cell analysis of human glioma and immune cells identifies S100A4 as an immunotherapy target. *Nat Commun*. (2022) 13:767. doi: 10.1038/s41467-022-28372-y

19. McGinnis CS, Murrow LM, Gartner ZJ. DoubletFinder: doublet detection in single-cell RNA sequencing data using artificial nearest neighbors. *Cell Syst*. (2019) 8:329–337.e324. doi: 10.1016/j.cels.2019.03.003

20. Satija R, Farrell JA, Gennert D, Schier AF, Regev A. Spatial reconstruction of single-cell gene expression data. *Nat Biotechnol*. (2015) 33:495–502. doi: 10.1038/nbt.3192

21. Song G, Peng G, Zhang J, Song B, Yang J, Xie X, et al. Uncovering the potential role of oxidative stress in the development of periodontitis and establishing a stable diagnostic model via combining single-cell and machine learning analysis. *Front Immunol*. (2023) 14:1181467. doi: 10.3389/fimmu.2023.1181467

22. Korsunsky I, Millard N, Fan J, Slowikowski K, Zhang F, Wei K, et al. Fast, sensitive and accurate integration of single-cell data with Harmony. *Nat Methods*. (2019) 16:1289–96. doi: 10.1038/s41592-019-0619-0

23. Tirosh I, Izar B, Prakadan SM, Wadsworth MH 2nd, Treacy D, Trombetta JJ, et al. Dissecting the multicellular ecosystem of metastatic melanoma by single-cell RNA-seq. *Science*. (2016) 352:189–96. doi: 10.1126/science.aad0501

24. Patel AP, Tirosh I, Trombetta JJ, Shalek AK, Gillespie SM, Wakimoto H, et al. Single-cell RNA-seq highlights intratumoral heterogeneity in primary glioblastoma. *Science*. (2014) 344:1396–401. doi: 10.1126/science.1254257

25. Cao J, Spielmann M, Qiu X, Huang X, Ibrahim DM, Hill AJ, et al. The single-cell transcriptional landscape of mammalian organogenesis. *Nature*. (2019) 566:496–502. doi: 10.1038/s41586-019-0969-x

26. Wolf FA, Hamey FK, Plass M, Solana J, Dahlin JS, Göttgens B, et al. PAGA: graph abstraction reconciles clustering with trajectory inference through a topology preserving map of single cells. *Genome Biol*. (2019) 20:59. doi: 10.1186/s13059-019-1663-x

27. Street K, Risso D, Fletcher RB, Das D, Ngai J, Yosef N, et al. Slingshot: cell lineage and pseudotime inference for single-cell transcriptomics. *BMC Genomics*. (2018) 19:477. doi: 10.1186/s12864-018-4772-0

28. Jew B, Alvarez M, Rahmani E, Miao Z, Ko A, Garske KM, et al. Accurate estimation of cell composition in bulk expression through robust integration of single-cell information. *Nat Commun*. (2020) 11:1971. doi: 10.1038/s41467-020-15816-6

29. Aibar S, González-Blas CB, Moerman T, Huynh-Thu VA, Imrichova H, Hulselmans G, et al. SCENIC: single-cell regulatory network inference and clustering. *Nat Methods*. (2017) 14:1083–6. doi: 10.1038/nmeth.4463

30. Cable DM, Murray E, Zou LS, Goeva A, Macosko EZ, Chen F, et al. Robust decomposition of cell type mixtures in spatial transcriptomics. *Nat Biotechnol*. (2022) 40:517–26. doi: 10.1038/s41587-021-00830-w

31. Wu Y, Yang S, Ma J, Chen Z, Song G, Rao D, et al. Spatiotemporal immune landscape of colorectal cancer liver metastasis at single-Cell level. *Cancer Discovery*. (2022) 12:134–53. doi: 10.1158/2159-8290.CD-21-0316

32. Sun Z, Wang J, Zhang Q, Meng X, Ma Z, Niu J, et al. Coordinating single-cell and bulk RNA-seq in deciphering the intratumoral immune landscape and prognostic stratification of prostate cancer patients. *Environ Toxicol*. (2024) 39:657–68. doi: 10.1002/tox.23928

33. Brennan CW, Verhaak RG, McKenna A, Campos B, Noushmehr H, Salama SR, et al. The somatic genomic landscape of glioblastoma. *Cell*. (2013) 155:462–77. doi: 10.1016/j.cell.2013.09.034

34. Zhao Z, Zhang KN, Wang Q, Li G, Zeng F, Zhang Y, et al. Chinese glioma genome atlas (CGGA): A comprehensive resource with functional genomic data from chinese glioma patients. *Genomics Proteomics Bioinf*. (2021) 19:1–12. doi: 10.1016/j.gpb.2020.10.005

35. Gravendeel LA, Kouwenhoven MC, Gevaert O, de Rooi JJ, Stubbs AP, Duijm JE, et al. Intrinsic gene expression profiles of gliomas are a better predictor of survival than histology. *Cancer Res*. (2009) 69:9065–72. doi: 10.1158/0008-5472.CAN-09-2307

36. Gusev Y, Bhuvaneshwar K, Song L, Zenklusen JC, Fine H, Madhavan S. The REMBRANDT study, a large collection of genomic data from brain cancer patients. *Sci Data*. (2018) 5:180158. doi: 10.1038/sdata.2018.158

37. Kamoun A, Idbaih A, Dehais C, Elarouci N, Carpentier C, Letouzé E, et al. Integrated multi-omics analysis of oligodendroglial tumours identifies three subgroups of 1p/19q co-deleted gliomas. *Nat Commun*. (2016) 7:11263. doi: 10.1038/ncomms11263

38. Leek JT, Johnson WE, Parker HS, Jaffe AE, Storey JD. The sva package for removing batch effects and other unwanted variation in high-throughput experiments. *Bioinformatics*. (2012) 28:882–3. doi: 10.1093/bioinformatics/bts034

39. Yu G, Wang LG, Han Y, He QY. clusterProfiler: an R package for comparing biological themes among gene clusters. *Omics*. (2012) 16:284–7. doi: 10.1089/omi.2011.0118

40. Zhang S, Jiang C, Jiang L, Chen H, Huang J, Gao X, et al. Construction of a diagnostic model for hepatitis B-related hepatocellular carcinoma using machine learning and artificial neural networks and revealing the correlation by immunoassay. *Tumour Virus Res*. (2023) 16:200271. doi: 10.1016/j.tvr.2023.200271

41. Zhou Y, Zhou B, Pache L, Chang M, Khodabakhshi AH, Tanaseichuk O, et al. Metascape provides a biologist-oriented resource for the analysis of systems-level datasets. *Nat Commun*. (2019) 10:1523. doi: 10.1038/s41467-019-09234-6

42. Ma B, Qin L, Sun Z, Wang J, Tran LJ, Zhang J, et al. The single-cell evolution trajectory presented different hypoxia heterogeneity to reveal the carcinogenesis of genes in clear cell renal cell carcinoma: Based on multiple omics and real experimental verification. *Environ Toxicol*. (2024) 39:869–81. doi: 10.1002/tox.24009

43. Zhang H, Xia T, Xia Z, Zhou H, Li Z, Wang W, et al. KIF18A inactivates hepatic stellate cells and alleviates liver fibrosis through the TTC3/Akt/mTOR pathway. *Cell Mol Life Sci*. (2024) 81:96. doi: 10.1007/s00018-024-05114-5

44. Zhu C, Sun Z, Wang J, Meng X, Ma Z, Guo R, et al. Exploring oncogenes for renal clear cell carcinoma based on G protein-coupled receptor-associated genes. *Discovery Oncol*. (2023) 14:182. doi: 10.1007/s12672-023-00795-z

45. Kildisiute G, Kalyva M, Elmentaite R, van Dongen S, Thevanesan C, Piapi A, et al. Transcriptional signals of transformation in human cancer. *Genome Med*. (2024) 16:8. doi: 10.1186/s13073-023-01279-z

46. Chen K, Ma Y, Liu X, Zhong X, Long D, Tian X, et al. Single-cell RNA-seq reveals characteristics in tumor microenvironment of PDAC with MSI-H following neoadjuvant chemotherapy with anti-PD-1 therapy. *Cancer Lett*. (2023) 576:216421. doi: 10.1016/j.canlet.2023.216421

47. Otvos B, Silver DJ, Mulkearns-Hubert EE, Alvarado AG, Turaga SM, Sorensen MD, et al. Cancer stem cell-Secreted macrophage migration inhibitory factor stimulates myeloid derived suppressor cell function and facilitates glioblastoma immune evasion. *Stem Cells*. (2016) 34:2026–39. doi: 10.1002/stem.2393

48. Jiang H, Wei H, Wang H, Wang Z, Li J, Ou Y, et al. Zeb1-induced metabolic reprogramming of glycolysis is essential for macrophage polarization in breast cancer. *Cell Death Dis*. (2022) 13:206. doi: 10.1038/s41419-022-04632-z

49. Stupp R, Mason WP, van den Bent MJ, Weller M, Fisher B, Taphoorn MJ, et al. Radiotherapy plus concomitant and adjuvant temozolomide for glioblastoma. *N Engl J Med*. (2005) 352:987–96. doi: 10.1056/NEJMoa043330

50. Stupp R, Hegi ME, Mason WP, van den Bent MJ, Taphoorn MJ, Janzer RC, et al. Effects of radiotherapy with concomitant and adjuvant temozolomide versus radiotherapy alone on survival in glioblastoma in a randomised phase III study: 5-year analysis of the EORTC-NCIC trial. *Lancet Oncol*. (2009) 10:459–66. doi: 10.1016/S1470-2045(09)70025-7

51. Singh N, Miner A, Hennis L, Mittal S. Mechanisms of temozolomide resistance in glioblastoma - a comprehensive review. *Cancer Drug Resist*. (2021) 4:17–43. doi: 10.20517/cdr.2020.79

52. Vredenburgh JJ, Desjardins A, Herndon JE2nd, Dowell JM, Reardon DA, Quinn JA, et al. Phase II trial of bevacizumab and irinotecan in recurrent Malignant glioma. *Clin Cancer Res*. (2007) 13:1253–9. doi: 10.1158/1078-0432.CCR-06-2309

53. Gilbert MR, Dignam JJ, Armstrong TS, Wefel JS, Blumenthal DT, Vogelbaum MA, et al. A randomized trial of bevacizumab for newly diagnosed glioblastoma. *N Engl J Med*. (2014) 370:699–708. doi: 10.1056/NEJMoa1308573

54. Tamura R, Tanaka T, Miyake K, Tabei Y, Ohara K, Sampetrean O, et al. Histopathological investigation of glioblastomas resected under bevacizumab treatment. *Oncotarget*. (2016) 7:52423–35. doi: 10.18632/oncotarget.v7i32

55. Xie D, Pei Q, Li J, Wan X, Ye T. Emerging role of E2F family in cancer stem cells. *Front Oncol*. (2021) 11:723137. doi: 10.3389/fonc.2021.723137

56. Kim H, Lin Q, Yun Z. BRCA1 regulates the cancer stem cell fate of breast cancer cells in the context of hypoxia and histone deacetylase inhibitors. *Sci Rep*. (2019) 9:9702. doi: 10.1038/s41598-019-46210-y

57. Zhang M, Zhang Q, Bai J, Zhao Z, Zhang J. Transcriptome analysis revealed CENPF associated with glioma prognosis. *Math Biosci Eng*. (2021) 18:2077–96. doi: 10.3934/mbe.2021107

58. Yang H, Liu X, Zhu X, Zhang M, Wang Y, Ma M, et al. GINS1 promotes the proliferation and migration of glioma cells through USP15-mediated deubiquitination of TOP2A. *iScience*. (2022) 25:104952. doi: 10.1016/j.isci.2022.104952

59. Zhao Y, He J, Li Y, Lv S, Cui H. NUSAP1 potentiates chemoresistance in glioblastoma through its SAP domain to stabilize ATR. *Signal Transduct Target Ther*. (2020) 5:44. doi: 10.1038/s41392-020-0137-7

60. Genkai N, Homma J, Sano M, Tanaka R, Yamanaka R. Increased expression of pituitary tumor-transforming gene (PTTG)-1 is correlated with poor prognosis in glioma patients. *Oncol Rep*. (2006) 15:1569–74. doi: 10.3892/or

61. Guo L, Ding Z, Huang N, Huang Z, Zhang N, Xia Z. Forkhead Box M1 positively regulates UBE2C and protects glioma cells from autophagic death. *Cell Cycle*. (2017) 16:1705–18. doi: 10.1080/15384101.2017.1356507

62. Hu L, Li X, Liu Q, Xu J, Ge H, Wang Z, et al. UBE2S, a novel substrate of Akt1, associates with Ku70 and regulates DNA repair and glioblastoma multiforme resistance to chemotherapy. *Oncogene*. (2017) 36:1145–56. doi: 10.1038/onc.2016.281

63. Aquilanti E, Miller J, Santagata S, Cahill DP, Brastianos PK. Updates in prognostic markers for gliomas. *Neuro Oncol*. (2018) 20:vii17–26. doi: 10.1093/neuonc/noy158

64. Byron SA, Van Keuren-Jensen KR, Engelthaler DM, Carpten JD, Craig DW. Translating RNA sequencing into clinical diagnostics: opportunities and challenges. *Nat Rev Genet*. (2016) 17:257–71. doi: 10.1038/nrg.2016.10

65. Ye B, Li Z, Wang Q. A novel artificial intelligence network to assess the prognosis of gastrointestinal cancer to immunotherapy based on genetic mutation features. *Front Immunol*. (2024) 15:1428529. doi: 10.3389/fimmu.2024.1428529

66. Bian T, Zheng M, Jiang D, Liu J, Sun H, Li X, et al. Prognostic biomarker TUBA1C is correlated to immune cell infiltration in the tumor microenvironment of lung adenocarcinoma. *Cancer Cell Int*. (2021) 21:144. doi: 10.1186/s12935-021-01849-4

67. Albahde MAH, Zhang P, Zhang Q, Li G, Wang W. Upregulated expression of TUBA1C predicts poor prognosis and promotes oncogenesis in pancreatic ductal adenocarcinoma via regulating the cell cycle. *Front Oncol*. (2020) 10:49. doi: 10.3389/fonc.2020.00049

68. Wang J, Chen W, Wei W, Lou J. Oncogene TUBA1C promotes migration and proliferation in hepatocellular carcinoma and predicts a poor prognosis. *Oncotarget*. (2017) 8:96215–24. doi: 10.18632/oncotarget.v8i56

69. Lou W, Ding B, Zhong G, Yao J, Fan W, Fu P. RP11-480I12.5-004 promotes growth and tumorigenesis of breast cancer by relieving miR-29c-3p-mediated AKT3 and CDK6 degradation. *Mol Ther Nucleic Acids*. (2020) 21:916–31. doi: 10.1016/j.omtn.2020.07.022

frontiers | Frontiers in Immunology

TYPE Original Research
PUBLISHED 24 September 2024
DOI 10.3389/fimmu.2024.1475206

Check for updates

OPEN ACCESS

EDITED BY
Pengpeng Zhang,
Nanjing Medical University, China

REVIEWED BY
Dechao Feng,
University College London, United Kingdom
Jindong Xie,
Sun Yat-sen University Cancer Center (SYSUCC), China
Jinghao Sheng,
Zhejiang University, China

*CORRESPONDENCE
Ying Xia
xiaying008@163.com
Jun Peng
xypengjun@126.com
Changfeng Miao
miaochangfeng@hunnu.edu.cn
Qisheng Luo
1917@ymcn.edu.cn

RECEIVED 03 August 2024
ACCEPTED 30 August 2024
PUBLISHED 24 September 2024

CITATION
Chen Z, Liu C, Zhang C, Xia Y, Peng J, Miao C and Luo Q (2024) Machine learning-based discovery of UPP1 as a key oncogene in tumorigenesis and immune escape in gliomas. *Front. Immunol.* 15:1475206. doi: 10.3389/fimmu.2024.1475206

COPYRIGHT
© 2024 Chen, Liu, Zhang, Xia, Peng, Miao and Luo. This is an open-access article distributed under the terms of the Creative Commons Attribution License (CC BY). The use, distribution or reproduction in other forums is permitted, provided the original author(s) and the copyright owner(s) are credited and that the original publication in this journal is cited, in accordance with accepted academic practice. No use, distribution or reproduction is permitted which does not comply with these terms.

Machine learning-based discovery of UPP1 as a key oncogene in tumorigenesis and immune escape in gliomas

Zigui Chen[1], Chao Liu[2], Chunyuan Zhang[3,4], Ying Xia[1*], Jun Peng[1*], Changfeng Miao[5*] and Qisheng Luo[3,4*]

[1]Department of Neurosurgery, Haikou Affiliated Hospital of Central South University Xiangya School of Medicine, Haikou, China, [2]Department of Neurosurgery, Central Hospital of Zhuzhou, Zhuzhou, Hunan, China, [3]Department of Neurosurgery, Affiliated Hospital of Youjiang Medical University for Nationalities, Baise, Guangxi, China, [4]Guangxi Engineering Research Center for Biomaterials in Bone and Joint Degenerative Diseases, Baise, Guangxi, China, [5]Department of Neurosurgery Second Branche, Hunan Provincial People's Hospital (The First Affiliated Hospital of Hunan Normal University), Changsha, Hunan, China

Introduction: Gliomas are the most common and aggressive type of primary brain tumor, with a poor prognosis despite current treatment approaches. Understanding the molecular mechanisms underlying glioma development and progression is critical for improving therapies and patient outcomes.

Methods: The current study comprehensively analyzed large-scale single-cell RNA sequencing and bulk RNA sequencing of glioma samples. By utilizing a series of advanced computational methods, this integrative approach identified the gene UPP1 (Uridine Phosphorylase 1) as a novel driver of glioma tumorigenesis and immune evasion.

Results: High levels of UPP1 were linked to poor survival rates in patients. Functional experiments demonstrated that UPP1 promotes tumor cell proliferation and invasion and suppresses anti-tumor immune responses. Moreover, UPP1 was found to be an effective predictor of mutation patterns, drug response, immunotherapy effectiveness, and immune characteristics.

Conclusions: These findings highlight the power of combining diverse machine learning methods to identify valuable clinical markers involved in glioma pathogenesis. Identifying UPP1 as a tumor growth and immune escape driver may be a promising therapeutic target for this devastating disease.

KEYWORDS

UPP1, glioma, immunotherapy, machine learning, single-cell sequencing

Introduction

Gliomas are the most common and aggressive type of primary brain tumor, with a poor prognosis despite current treatment approaches. Understanding the molecular mechanisms underlying glioma development and progression is critical for improving therapies and patient outcomes (1). Recent advances in single-cell sequencing (scRNA-seq) have provided unprecedented resolution into the cellular heterogeneity of gliomas, revealing diverse populations of tumor, immune, and stromal cells (2, 3). At the same time, bulk tumor sequencing has identified key driver mutations and signaling pathways dysregulated in gliomas (4, 5). However, integrating single-cell and bulk tumor data to identify critical genes and pathways remains an important challenge.

Immune evasion is a key hallmark of cancer, where tumor cells are able to avoid detection and destruction by the body's immune system. Understanding the mechanisms of immune evasion in cancer is crucial for the development of effective immunotherapies, which aim to overcome these immune evasion strategies and reactivate the body's immune system to recognize and eliminate cancer cells (6).

In this study, we utilized diverse machine learning methods to comprehensively analyze scRNA-seq and bulk RNA sequencing of glioma samples (7). Through a series of advanced computational techniques, this integrative approach identified UPP1 (Uridine Phosphorylase 1) as a novel driver of glioma tumorigenesis and immune evasion. High UPP1 expression was linked to poor patient survival. Functional experiments revealed that UPP1 promotes tumor cell proliferation and invasion while suppressing anti-tumor immune responses. Additionally, UPP1 effectively predicted mutation characteristics, drug response, immunotherapy response, and immune features. These findings highlight the power of integrating single-cell and bulk tumor data from over 3,000 samples to identify critical genes involved in glioma pathogenesis. Identifying UPP1 as a tumor growth and immune escape driver suggests it may be a promising therapeutic target for this devastating disease.

Materials and methods

Data collection and processing

The scRNA-seq data of human glioblastoma (GBM) samples were obtained from the Single Cell Portal platform (SCP50 and SCP393) and processed using Smart-seq2. The bulk-sequencing data of human glioma samples were obtained from the TCGA (The Cancer Genome Atlas), CGGA (Chinese Glioma Genome Atlas), and GEO (Gene Expression Omnibus) databases. The current study included over 3,000 samples. The raw data from the GEO database was generated using the Affymetrix and Agilent platforms. The robust multichip average (RMA) technique accomplished the background correction and normalization. The RNA-sequencing data were obtained from the TCGA and CGGA data sites. Transcripts per kilobase million (TPM) values were created by converting the fragments per kilobase million (FPKM) values into values with a signal strength comparable to the RMA-processed values.

Computational analysis

Uniform Manifold Approximation and Projection (UMAP) function from the R package Seurat was used to depict the microenvironment cells in the scRNA-seq data. Differentially expressed genes (DEGs) between the immune cells and neoplastic cells were identified. 182 immune escape (IE) pathway genes were collected (8). Weighted Correlation Network Analysis (WGCNA) was performed on the TCGA glioma dataset to determine the IE-related genes (9). Soft threshold settings were established to ensure a scale-free topology network and generate a TOM matrix. A power of $\beta = 10$ was used as the parameter. Blue module genes were extracted for subsequent analysis. The intersected genes between IE-related genes and DEGs were identified. Univariate Cox regression analysis was performed on intersected genes. Machine learning, RSF (Random Survival Forests) analysis (10), was performed on prognostic intersected genes. Machine learning, LASSO (Least Absolute Shrinkage and Selection Operator) regression analysis (11), was further performed on prognostic intersected genes. The R package survminer was used to create the survival curves of UPP1-related groups. Gene Set Enrichment Analysis (GSEA) was performed on UPP1. The R package oncoPredict was used to predict drug responses related to UPP1 (12). GISTIC 2.0 analysis was performed on UPP1 (13). The R packages maftools was used to generate the mutation landscape (14). The R package ComplexHeatmap was used to generate a heatmap of the immune infiltrating cells calculated by TIMER, MCPcounter, and ssGSEA (15–18) related to UPP1. The R package ComplexHeatmap was also to create a heatmap of the immune modulators related to UPP1.

In vitro validation on UPP1

The glioma cell lines U251 and LN229 and microglia cell line HMC3 were purchased from iCell. Two siRNA sequences of UPP1 (Forward AGGCAGAGUUUGAGCAGAUTT; Forward UCAAGAAGAAACUGAGCAATT) were used to silence the expression of UPP1. Total RNA was extracted from siRNA-transfected glioma cells. The extracted RNA was then reverse-transcribed into cDNA using a reverse transcriptase enzyme. Next, the cDNA was used as a qPCR amplification template. Gene-specific primers were used to measure the abundance of target gene transcripts. The qPCR reaction was monitored in real-time, allowing for precise quantification of mRNA levels. Relative expression was calculated using the 2^-ΔΔCt method, with normalization to endogenous control genes. The EdU assay was employed to assess cell proliferation. Glioma cells were incubated with the thymidine analog EdU, which gets incorporated into the DNA of proliferating cells during S-phase. The stained cells were then analyzed by microscopy. The percentage of EdU-positive cells reflects the fraction of proliferating cells in the population, providing a quantitative measure of cell proliferation. The Transwell assay was used to evaluate the migratory capabilities of glioma cells. Cells were seeded onto the top chamber of a Transwell plate with a porous membrane. Cells that migrated through the porous membrane to the bottom chamber were

quantified. The Co-culture Transwell assay was used to evaluate the migratory capabilities of macrophages. Macrophages were seeded onto the top chamber of a Transwell plate, and glioma cells were seeded onto the down chamber of a Transwell plate. Cells that migrated through the porous membrane to the bottom chamber were quantified.

Statistical analysis

All statistical analyses were conducted with R. Student's t-test and wilcoxon test were used to compare normally distributed variables and non-normally distributed data between the two groups, respectively. $P < 0.05$ was considered statistically significant.

Results

The scRNA-seq analysis for malignant markers

The microenvironment cells (astrocyte, oligodendrocyte, macrophage, microglial cell, neoplastic, neural stem cell, neuron, T cell, etc.) in GBM are shown in Figure 1A. The major types of immune cells (macrophage, microglial cell, T cell) and neoplastic cells in GBM are shown in Figure 1B. The immune cells and neoplastic cells in GBM are shown in Figures 1C, D. DEGs between the immune cells and neoplastic cells are shown in Figure 1D.

WGCNA for IE-related markers

ssGSEA was performed on IE pathway genes to calculate the IE score. Scale-free topology model fit and mean connectivity are shown in Figure 2A. WGCNA-based gene models in the glioma dataset are shown in Figure 2B. Correlation between gene modules and IE score showed that the blue module was the most correlated among the nine gene modules (Figure 2C). Gene significance is significantly associated with module membership in the blue module (Figure 2D).

Machine learning for potent markers

The high IE group is related to worse survival (Figure 3A). 69 intersected genes between IE-related genes and malignant genes are identified (Figure 3B). Univariate Cox regression analysis on intersected genes showed that 21 genes were hazardous (Figure 3C). RSF analysis was performed for dimension reduction of prognostic intersected genes, which came to CD151, EFEMP2, PLS3, TMSB10, and UPP1 (Figure 3D). LASSO regression analysis was further performed for dimension reduction of prognostic intersected genes, which also came to CD151, EFEMP2, PLS3, TMSB10, and UPP1 (Figure 3E).

Prognostic value of UPP1

Univariate and multivariate Cox regression analysis on UPP1 and clinical factors (age, gender, IDH, 1p19q, MGMT) showed that UPP1 was an independent prognostic factor (Figure 4A). The high UPP1 group was related to worse survival (Figure 4B). Univariate Cox regression analysis on UPP1 in different glioma datasets showed that UPP1 was a hazardous marker (Figure 4C). The high UPP1 group was related to worse survival in different glioma datasets (Figure 4D).

In vitro validation on UPP1

Given the potential prognostic value of UPP1, experimental validation was performed. RT-qPCR assay showed that UPP1 expression was significantly suppressed in siRNA-transfected groups in U251 (Figure 5A) and LN229 (Figure 5B) cells. EdU assay showed that the proliferated glioma cells were significantly reduced in siRNA-transfected groups in U251 and LN229 cells (Figures 5C, F). Transwell assay shows the migrated glioma cells were significantly reduced in siRNA-transfected groups in U251 and LN229 cells (Figures 5D, F). Co-culture Transwell assay showed the migrated macrophages were significantly reduced in siRNA-transfected groups in U251 and LN229 cells (Figures 5E, F).

Functional annotations of UPP1

GSEA on UPP1 was performed, and immune pathways such as cytokine, chemokine, T cell activation, and macrophage activation were significantly enriched (Figure 6A). This indicates that UPP1 is intimately linked to the regulation of the tumor immune microenvironment. Drug prediction of UPP1 revealed that Dasatinib, Temozolomide, AZD5582, Fludarabine, AZD3759, and AZD8186 in the low UPP1 group had significantly higher drug sensitivity (Figure 6B).

Immunological features of UPP1

UPP1 was significantly associated with immune modulators CD274, CD276, CD28, and ICOSLG (Figure 7A). This suggests that UPP1 may contribute to immune evasion by modulating the expression of these immune checkpoint molecules. Besides, UPP1 was significantly associated with immune cells DCs, B cells, T cells, MDSCs, Tregs, and macrophages (Figure 7B). This indicates that UPP1 may play a role in shaping the composition and function of the tumor immune microenvironment.

10.3389/fimmu.2024.1475206

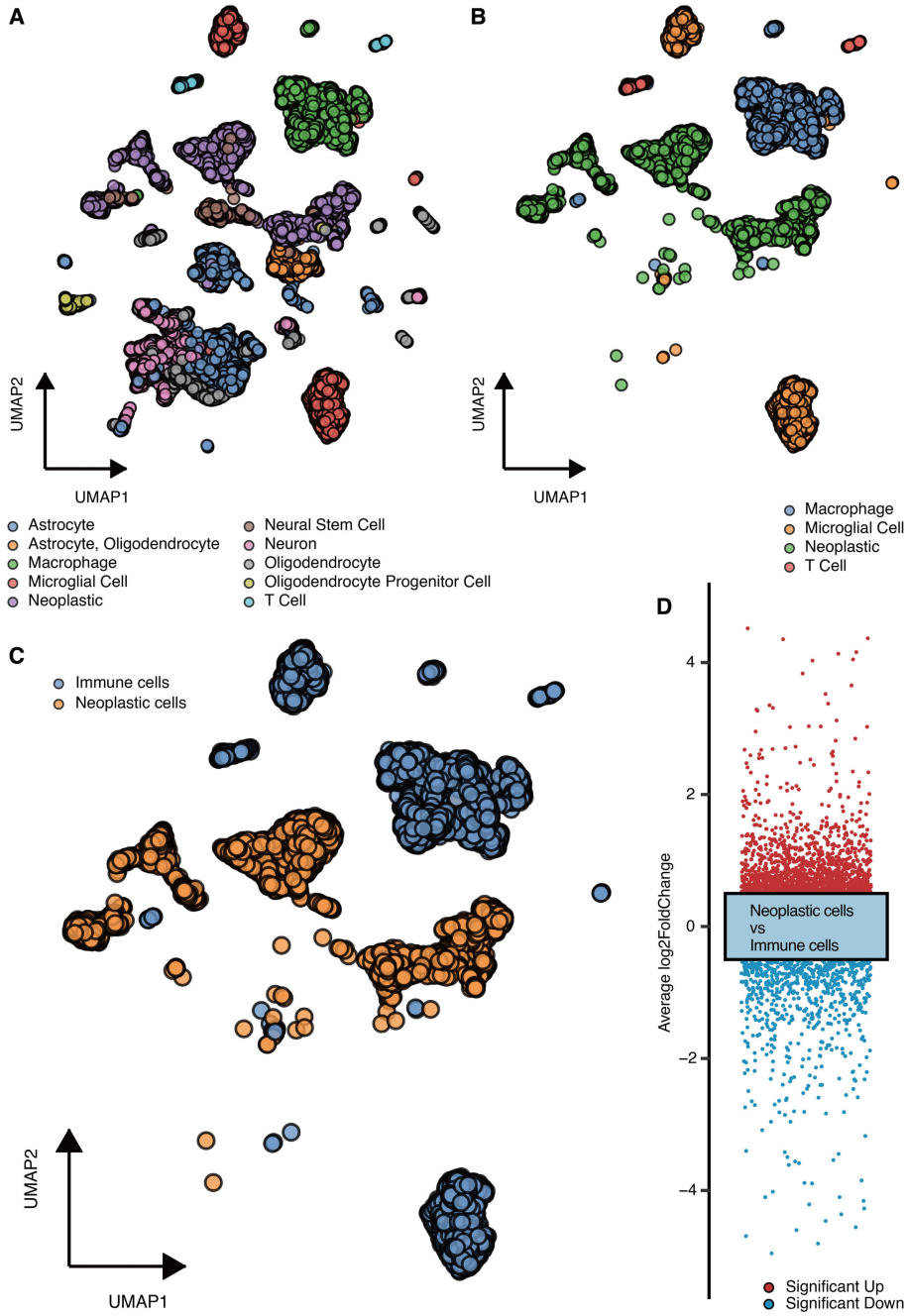

FIGURE 1
scRNA-seq analysis for malignant genes. **(A)** UMAP shows the microenvironment cells. **(B)** UMAP shows the major types of immune cells and neoplastic cells. **(C)** UMAP shows the immune cells and neoplastic cells. **(D)** DEGs between the immune cells and neoplastic cells.

Immunotherapy response prediction of UPP1

ROC curves of UPP1 in four immunotherapy cohorts showed that UPP1 could effectively predict immunotherapy responses (Figure 8A). Besides, the high UPP1 group was associated with better survival in four immunotherapy cohorts (Figure 8B).

Mutation characteristics of UPP1

The mutation landscape in the high UPP1 group is shown in Figure 9A, in which EGFR and PTEN were highly mutated. The mutation landscape in the low UPP1 group is shown in Figure 9B, in which TP53 and IDH were highly mutated. Differentially expressed mutation genes in the high and low UPP1 groups are shown in Supplementary Figure 1A, in which IDH was the top-

10.3389/fimmu.2024.1475206

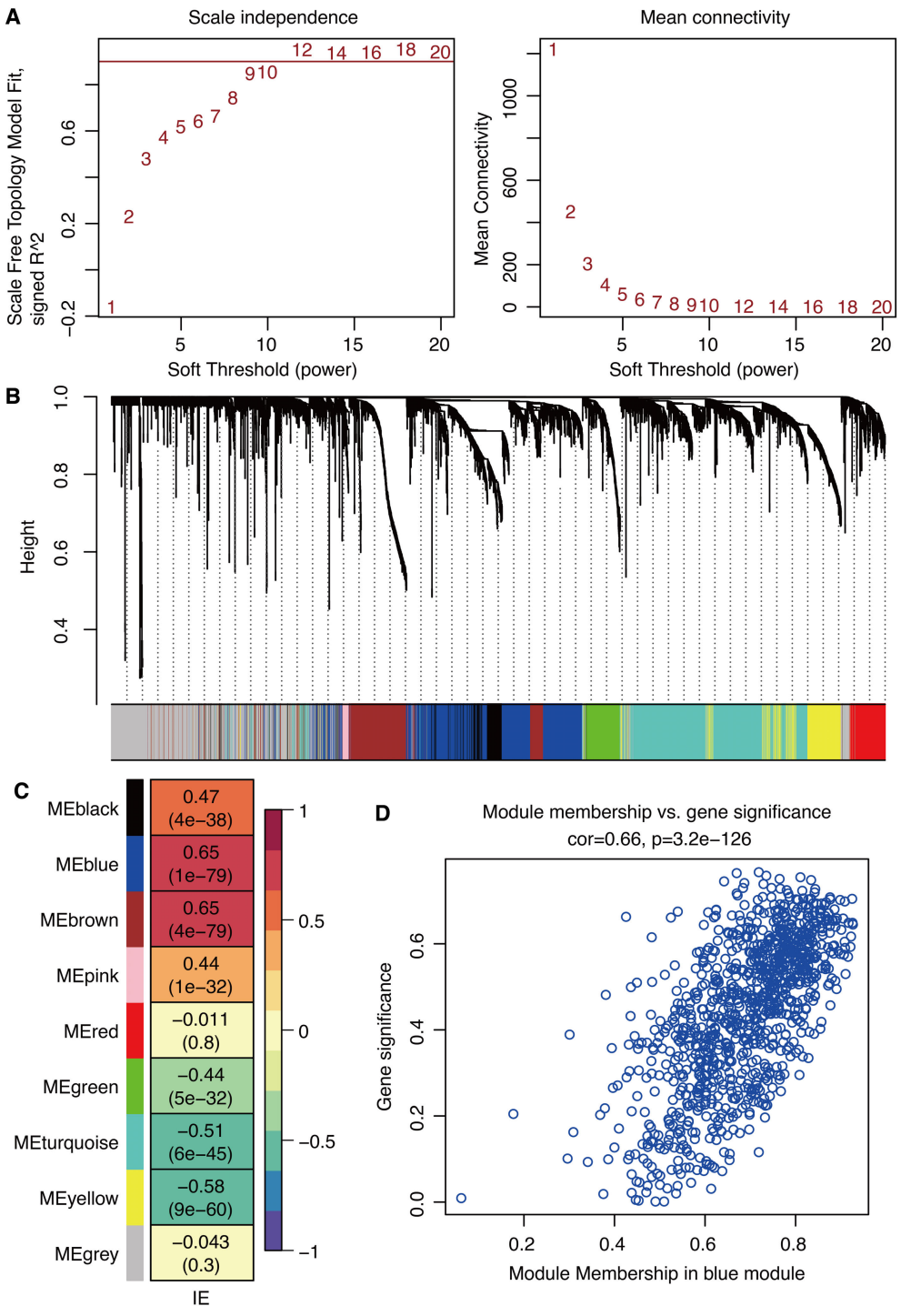

FIGURE 2
WGCNA for IE-related genes. **(A)** Scale-free topology model fit and mean connectivity. **(B)** Waterfall plot shows the gene models. **(C)** Correlation between gene modules and immune escape. **(D)** Correlation between gene significance and module membership.

ranked mutated gene in the low UPP1 group. Mutually mutated gene pairs in the high UPP1 group are shown in Supplementary Figure 1B. Mutually mutated gene pairs in the low UPP1 group are shown in Supplementary Figure 1C.

Pan-cancer analysis of UPP1

UPP1 expression was significantly higher in tumor and normal tissues in most cancer types (Supplementary Figure 2A). Univariate

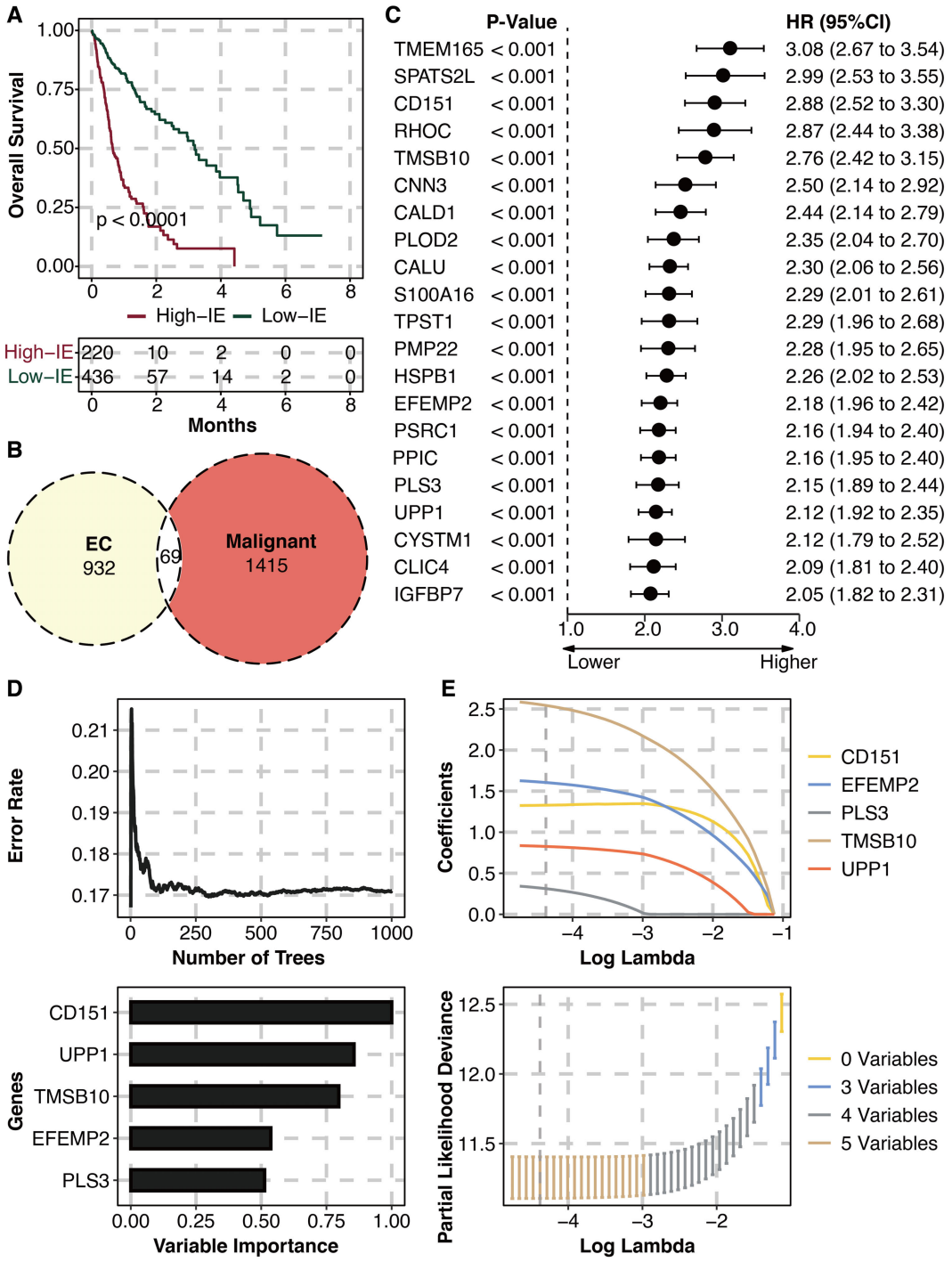

FIGURE 3
Machine learning for potent genes. **(A)** Survival plot shows the survival outcomes in the high and low IE groups. **(B)** Intersected genes between IE-related genes and malignant genes. **(C)** Univariate Cox regression analysis on intersected genes. **(D)** RSF analysis on prognostic intersected genes. **(E)** LASSO regression analysis on prognostic intersected genes.

Cox regression analysis of UPP1 confirmed that UPP1 was a hazardous marker in most cancer types (Supplementary Figure 2B).

Discussion

The rapid advancement of high-throughput genomic and molecular profiling technologies has generated vast amounts of complex biological data in cancer research. This data deluge has necessitated the development of sophisticated computational approaches to extract meaningful insights and patterns from the data (19). Machine learning, a field of artificial intelligence, has emerged as a powerful tool to tackle these challenges in cancer research. Machine learning models can analyze multi-omics data, such as genomics, transcriptomics, and proteomics, to identify

10.3389/fimmu.2024.1475206

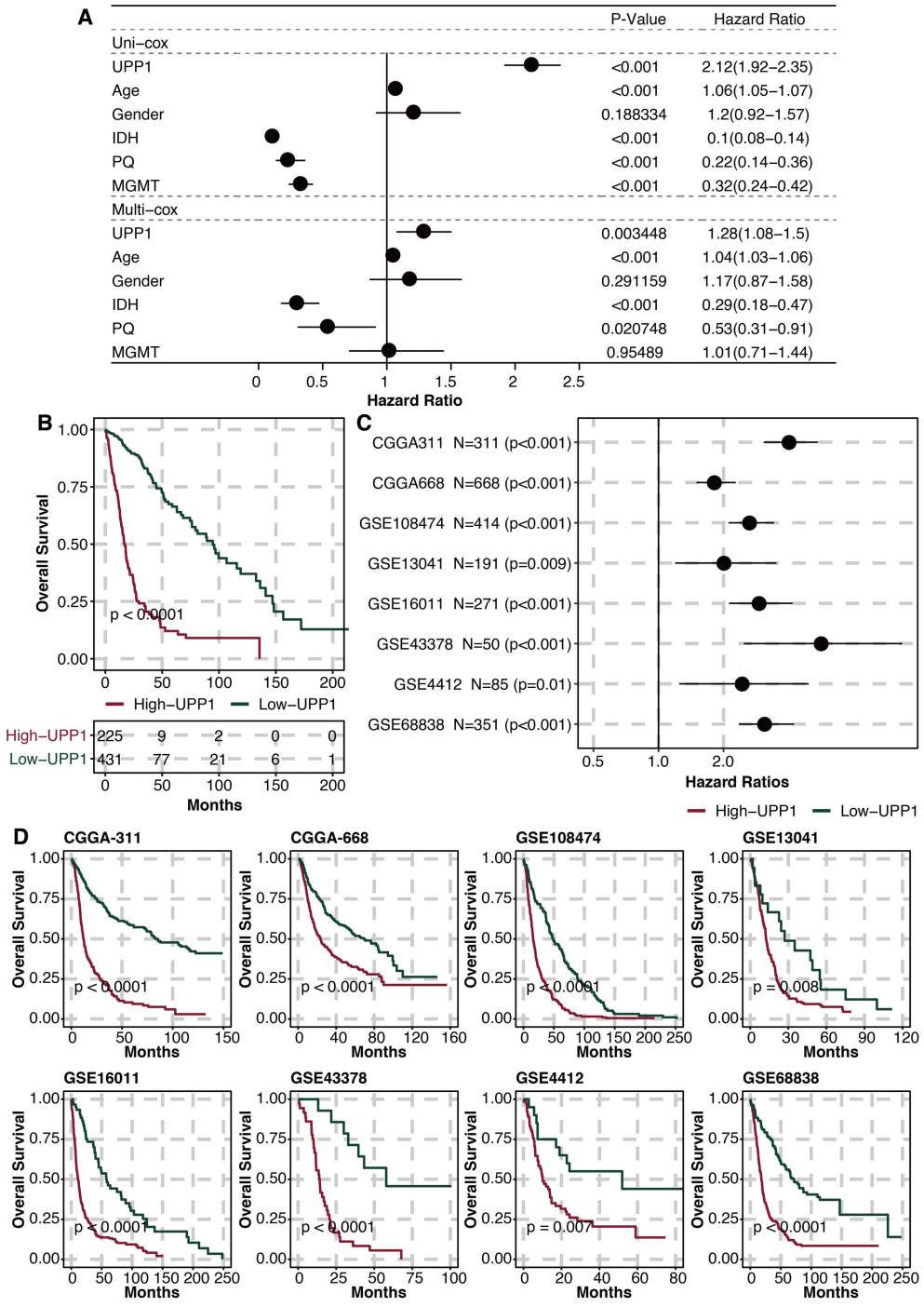

FIGURE 4
Prognostic value of UPP1. **(A)** Univariate and multivariate Cox regression analysis on UPP1 and clinical factors. **(B)** Survival plot shows the survival outcomes in the high and low UPP1 groups. **(C)** Univariate Cox regression analysis on UPP1 in different glioma datasets. **(D)** Survival plot shows the survival outcomes in the high and low UPP1 groups in different glioma datasets.

robust molecular biomarkers predictive of cancer risk, prognosis, or treatment response (20). This can help guide the development of personalized cancer diagnostics and therapeutics. Our integrative analysis of single-cell and bulk tumor sequencing data by machine learning identified the gene UPP1 as a critical driver of glioma tumorigenesis and immune evasion. UPP1 encodes the enzyme uridine phosphorylase 1, which catalyzes the reversible phosphorolysis of uridine and 2'-deoxyuridine (21). It plays a significant role in the ubiquitin-proteasome system, which is essential for maintaining cellular homeostasis by regulating protein turnover. In the context of cancer, UPP1 is involved in various aspects of cancer development and progression, including

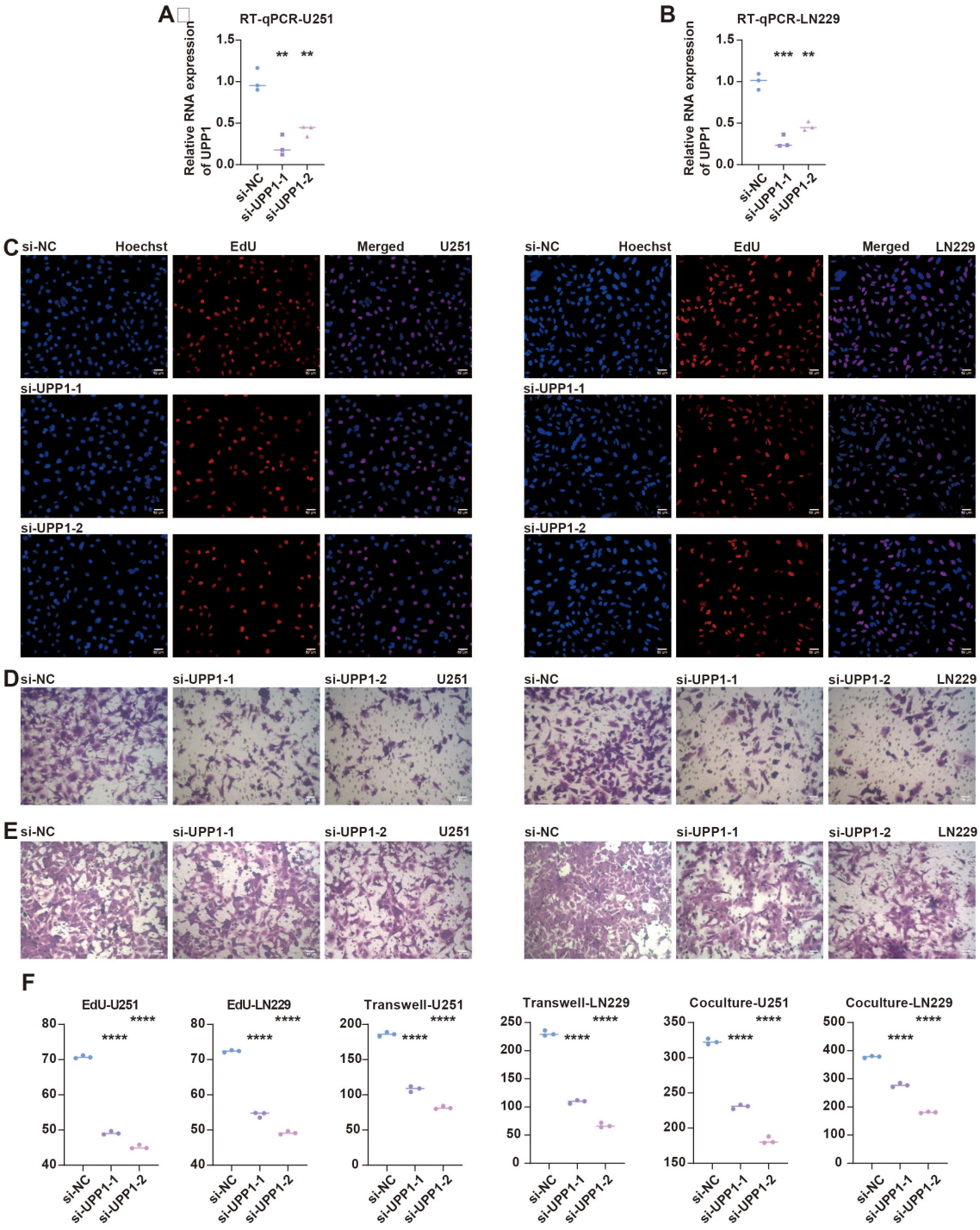

FIGURE 5
In vitro validation on UPP1. **(A)** RT-qPCR assay shows the RNA expression of UPP1 in different groups in U251 cells. **(B)** RT-qPCR assay shows the RNA expression of UPP1 in different groups in LN229 cells. **(C)** EdU assay shows the proliferated glioma cells in different groups in U251 and LN229 cells. **(D)** Transwell assay shows the migrated glioma cells in different groups in U251 and LN229 cells. **(E)** Co-culture Transwell assay shows the migrated macrophages in different groups in U251 and LN229 cells. **(F)** Statistical analysis of RT-qPCR, EdU, and Transwell assays in U251 cells. **(G)** Statistical analysis of RT-qPCR, EdU, and Transwell assays in LN229 cells. **, $P < 0.01$; ***, $P < 0.001$; ****, $P < 0.0001$.

regulation of protein homeostasis, cell cycle regulation, apoptosis and survival, angiogenesis and metastasis, and immune evasion (22).

Elevated expression of UPP1 was associated with significantly worse patient survival across multiple independent glioma cohorts. Functional studies demonstrated that silencing UPP1 in glioma cell lines reduced tumor cell proliferation and invasion, enhancing anti-tumor immune responses through increased cell recruitment and activation of macrophages. These results indicate that UPP1 plays a dual role in promoting intrinsic tumor growth and

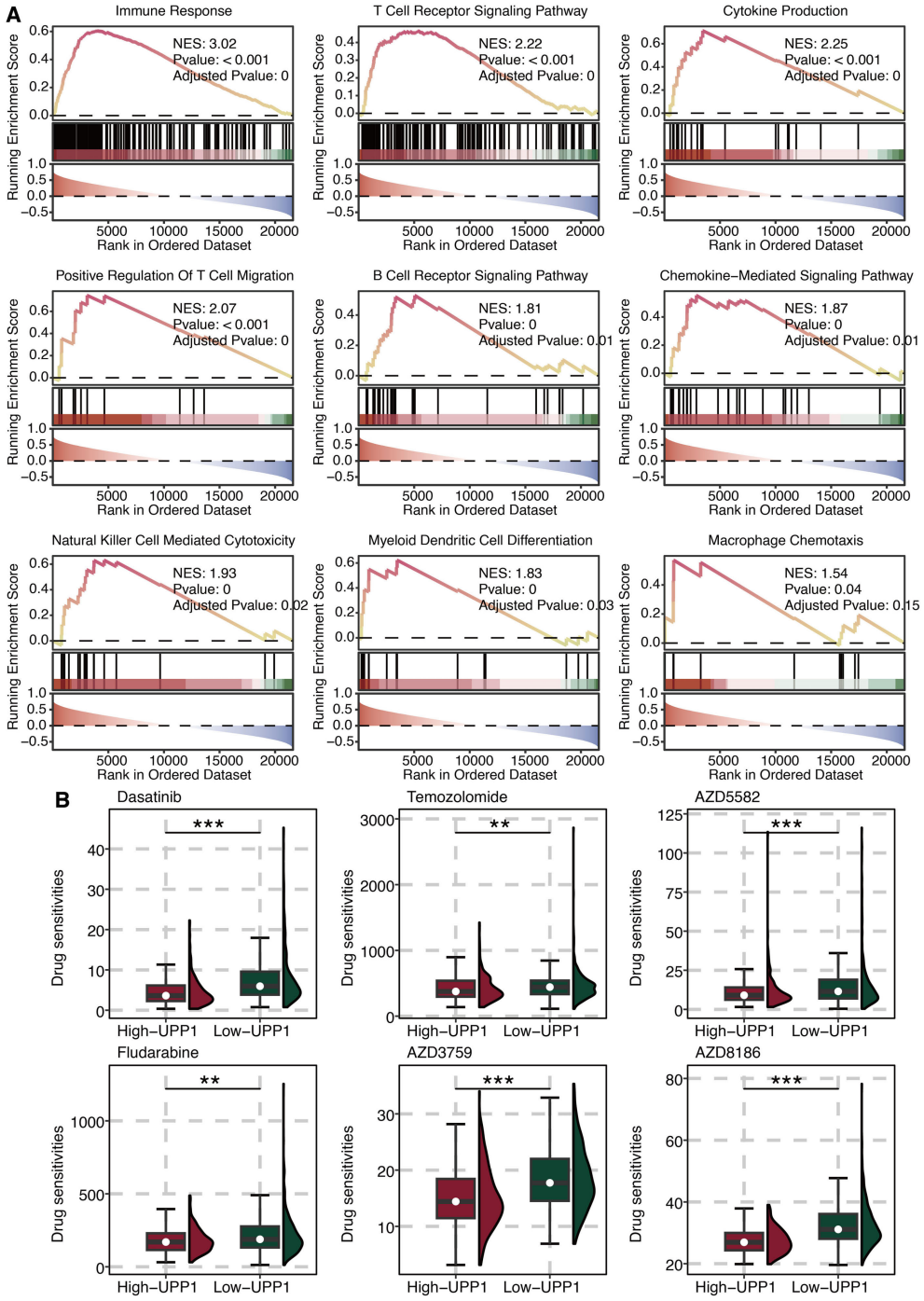

FIGURE 6
Functional annotation of UPP1. **(A)** GSEA on UPP1. **(B)** Drug prediction of UPP1. **, P < 0.01; ***, P < 0.001.

immunosuppression within the glioma microenvironment. UPP1 plays a significant role in modulating macrophage activity through several potential mechanisms: UPP1 is involved in the ubiquitin-proteasome pathway, where it tags dysfunctional proteins for degradation. By regulating protein turnover, UPP1 helps maintain macrophage homeostasis, ensuring that only functional proteins are present for critical immune responses. UPP1 can influence the production of pro-inflammatory cytokines. By degrading specific proteins involved in inflammatory signaling pathways, UPP1 may help fine-tune the macrophage response to pathogens and tissue damage, preventing excessive inflammation that could lead to tissue injury. Macrophages play a crucial role in antigen presentation. UPP1 may facilitate the processing of antigens by regulating the degradation of precursor proteins, thus enhancing the ability of

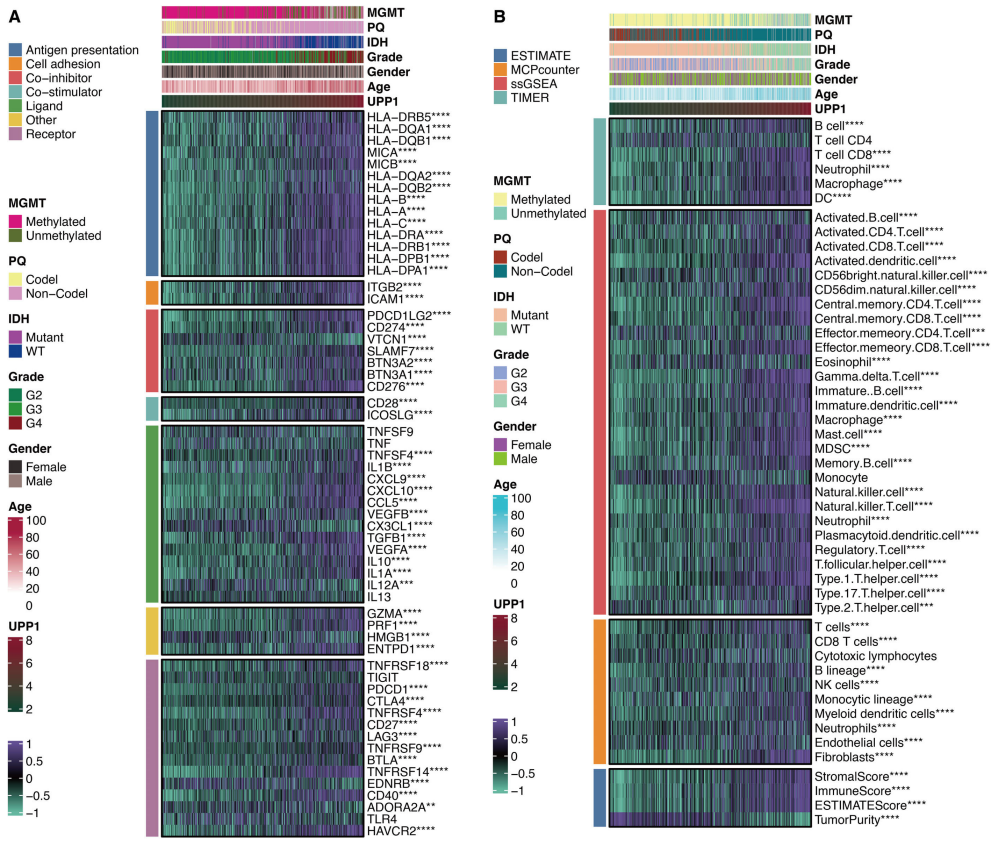

FIGURE 7
Immune features of UPP1. **(A)** Correlation between UPP1 and immune modulators. **(B)** Correlation between UPP1 and immune cells. **, P < 0.01; ***, P < 0.001; ****, P < 0.0001.

macrophages to present antigens to T cells and initiate adaptive immune responses. UPP1 can affect the expression of surface receptors involved in phagocytosis. By regulating the turnover of these receptors, UPP1 may enhance or diminish the macrophage's ability to engulf and eliminate pathogens or debris. In response to environmental stress, UPP1 can help macrophages adapt by managing the levels of proteins involved in stress responses. This may enhance macrophage survival and functionality under adverse conditions, such as during infection or inflammation. UPP1 may interact with various signaling pathways, such as NF-kB and MAPK pathways, which are critical for macrophage activation and function. By modulating these pathways, UPP1 can influence macrophage differentiation, activation, and effector functions.

The identification of UPP1 as a driver of glioma malignancy is notable, as the role of this enzyme in cancer pathogenesis has been relatively unexplored. Previous studies have primarily focused on the potential utility of UPP1 as a target for cancer chemotherapy, given its involvement in the metabolism of nucleoside analogs (23, 24). Our findings suggest a more fundamental role for UPP1 in regulating core tumorigenic processes, including cell proliferation, migration, and immune evasion.

Mechanistically, UPP1 may promote glioma progression through several potential pathways. At the metabolic level, UPP1-mediated catabolism of nucleosides could influence nucleotide biosynthesis, DNA repair, and other proliferation-associated processes (25). UPP1 has also been linked to regulating inflammatory signaling cascades, which could modulate the anti-tumor immune response (26, 27). Through the PI3K/AKT/mTOR pathway, UPP1 overexpression also increases the production of PD-L1, which aids in inhibiting CD8+ T cells and shapes the immunosuppressive nature of the TME (27). Further investigation is needed to fully elucidate the downstream effectors of UPP1 that drive its pro-tumorigenic and immunosuppressive functions. It is hypothesized that PP1's role in nucleotide metabolism allows cancer cells to adapt their energy production and biosynthetic pathways, enhancing their survival and competitive advantage in nutrient-poor environments.

In addition to its prognostic significance, our analysis indicates that UPP1 expression levels could be a useful biomarker to predict other clinically relevant tumor characteristics. High UPP1 was associated with specific genomic alterations, drug response profiles, and immune infiltration patterns. The differential mutation patterns observed in the high UPP1 and low UPP1 groups may provide insights into the potential mechanisms by which UPP1 expression influences cancer biology. For example, the interplay between UPP1 and the deubiquitination of key oncogenic or tumor suppressor proteins, such as those encoded by EGFR, PTEN, TP53, and IDH, may be an important factor in cancer development (28). This suggests that UPP1 could be a versatile

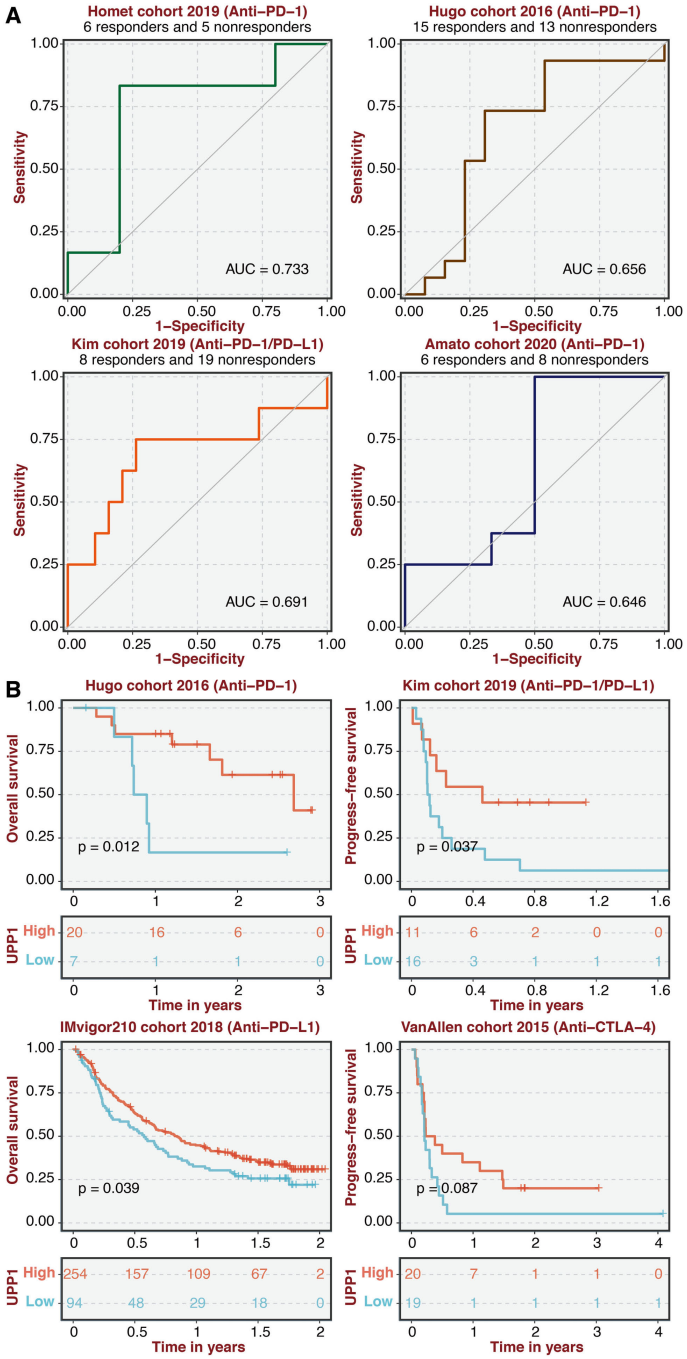

FIGURE 8
Immunotherapy prediction of UPP1. **(A)** ROC curves of UPP1 in four immunotherapy cohorts. **(B)** Survival plot shows the survival outcomes in the high and low UPP1 groups in four immunotherapy cohorts.

marker to help guide personalized treatment approaches for glioma patients. Notably, the expression level of UPP1 could be used as a biomarker to predict the sensitivity of cancer cells to certain drugs, such as Dasatinib, Temozolomide, AZD5582, Fludarabine, AZD3759, and AZD8186. Understanding the relationship between UPP1 expression and drug sensitivity could help develop personalized treatment strategies where the choice of drug therapy is based on the UPP1 status of the cancer (29, 30). In addition, the ability of UPP1 to predict immunotherapy responses and its association with better survival in immunotherapy-treated patients suggest a complex interplay between UPP1 and anti-tumor immunity. While high UPP1 expression was generally associated with immune suppression, the improved outcomes in the immunotherapy cohorts indicate that the heightened immune response elicited by immunotherapy can overcome the suppressive effects of UPP1.

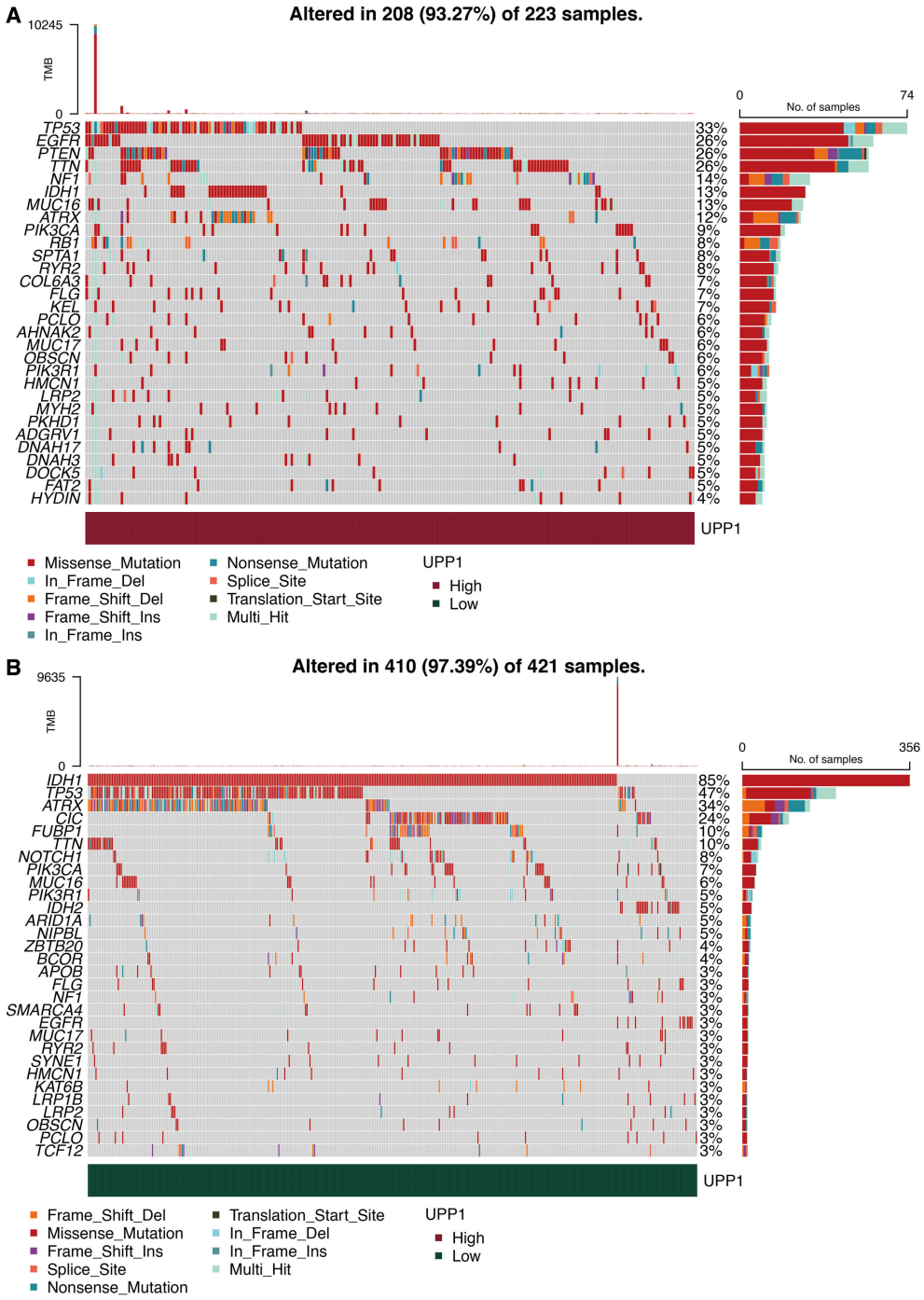

FIGURE 9
Mutation characteristics of UPP1. **(A)** Mutation landscape in high UPP1 group. **(B)** Mutation landscape in low UPP1 group.

In conclusion, our study has uncovered a previously unappreciated role for the metabolic enzyme UPP1 as a driver of glioma malignancy. Targeting UPP1 or its downstream effectors may represent a promising therapeutic strategy for this devastating disease. Further research is needed to elucidate the precise molecular mechanisms by which UPP1 drives tumor progression and immune evasion. Investigating the downstream signaling pathways and regulatory networks of UPP1 could uncover additional therapeutic vulnerabilities. Besides, the role of UPP1 in tumorigenesis and immune evasion identified in this study may not be limited to glioma. Investigating the potential implications of UPP1 in other cancer types could uncover broader therapeutic applications. There are also some limitations of the study. While UPP1 shows promise as a therapeutic target, the study does not provide a detailed analysis of potential resistance mechanisms or how targeting UPP1 could interact with existing therapies. Besides,

a real-world cohort is expected to confirm the prognostic roles of UPP1.

Data availability statement

The original contributions presented in the study are included in the article/Supplementary Material. Further inquiries can be directed to the corresponding authors.

Ethics statement

Ethical approval was not required for the studies on humans in accordance with the local legislation and institutional requirements because only commercially available established cell lines were used. Ethical approval was not required for the studies on animals in accordance with the local legislation and institutional requirements because only commercially available established cell lines were used.

Author contributions

ZC: Writing – original draft, Methodology, Funding acquisition, Formal analysis, Data curation. CL: Writing – original draft, Data curation. CZ: Writing – original draft, Formal analysis. YX: Writing – review & editing, Supervision, Funding acquisition. JP: Writing – review & editing, Supervision, Funding acquisition. CM: Writing – review & editing, Supervision, Funding acquisition. QL: Writing – review & editing, Visualization, Supervision, Investigation, Funding acquisition.

Funding

The author(s) declare financial support was received for the research, authorship, and/or publication of this article. Project supported by Hainan Province Clinical Medical Research Center (grant no. LCYX202410, LCYX202309) and the Hainan Province Clinical Medical Center (grant no. 0202068). National Natural Science Foundation of China (grant no. 82360259). Natural Science Foundation of Hunan Province (grant no. 2024JJ9290).

Conflict of interest

The authors declare that the research was conducted in the absence of any commercial or financial relationships that could be construed as a potential conflict of interest.

Publisher's note

All claims expressed in this article are solely those of the authors and do not necessarily represent those of their affiliated organizations, or those of the publisher, the editors and the reviewers. Any product that may be evaluated in this article, or claim that may be made by its manufacturer, is not guaranteed or endorsed by the publisher.

Supplementary material

The Supplementary Material for this article can be found online at: https://www.frontiersin.org/articles/10.3389/fimmu.2024.1475206/full#supplementary-material

SUPPLEMENTARY FIGURE 1
Mutation characteristics of UPP1. **(A)** Differentially expressed mutation genes in the high and low UPP1 groups. **(B)** Mutually mutated gene pairs in high UPP1 group. **(C)** Mutually mutated gene pairs in low UPP1 group.

SUPPLEMENTARY FIGURE 2
Pan-cancer analysis of UPP1. **(A)** Vlnplot shows the expression of UPP1 in tumor and normal tissues in pan-cancer. **(B)** Univariate Cox regression analysis of UPP1 in pan-cancer.

References

1. Reifenberger G, Wirsching HG, Knobbe-Thomsen CB, Weller M. Advances in the molecular genetics of gliomas - implications for classification and therapy. *Nat Rev Clin Oncol*. (2017) 14:434–52. doi: 10.1038/nrclinonc.2016.204

2. Jain S, Rick JW, Joshi RS, Beniwal A, Spatz J, Gill S, et al. Single-cell RNA sequencing and spatial transcriptomics reveal cancer-associated fibroblasts in glioblastoma with protumoral effects. *J Clin Invest*. (2023) 133(5):e147087. doi: 10.1172/JCI147087

3. Ochocka N, Segit P, Walentynowicz KA, Wojnicki K, Cyranowski S, Swatler J, et al. Single-cell RNA sequencing reveals functional heterogeneity of glioma-associated brain macrophages. *Nat Commun*. (2021) 12:1151. doi: 10.1038/s41467-021-21407-w

4. Hoogstrate Y, Draaisma K, Ghisai SA, van Hijfte L, Barin N, de Heer I, et al. Transcriptome analysis reveals tumor microenvironment changes in glioblastoma. *Cancer Cell*. (2023) 41:678–92.e7. doi: 10.1016/j.ccell.2023.02.019

5. Yang K, Wu Z, Zhang H, Zhang N, Wu W, Wang Z, et al. Glioma targeted therapy: insight into future of molecular approaches. *Mol Cancer*. (2022) 21:39. doi: 10.1186/s12943-022-01513-z

6. Jhunjhunwala S, Hammer C, Delamarre L. Antigen presentation in cancer: insights into tumour immunogenicity and immune evasion. *Nat Rev Cancer*. (2021) 21:298–312. doi: 10.1038/s41568-021-00339-z

7. Zhang J, Wang Z, Zhang X, Dai Z, Zhi-Peng W, Yu J, et al. Large-scale single-cell and bulk sequencing analyses reveal the prognostic value and immune aspects of CD147 in pan-cancer. *Front Immunol*. (2022) 13:810471. doi: 10.3389/fimmu.2022.810471

8. Jia HR, Li WC, Wu L. The prognostic value of immune escape-related genes in lung adenocarcinoma. *Transl Cancer Res*. (2024) 13:2647–61. doi: 10.21037/tcr-23-2295

9. Langfelder P, Horvath S. WGCNA: an R package for weighted correlation network analysis. *BMC Bioinf*. (2008) 9:559. doi: 10.1186/1471-2105-9-559

10. Rigatti SJ. Random forest. *J Insur Med*. (2017) 47:31–9. doi: 10.17849/insm-47-01-31-39.1

11. Tibshirani R. The lasso method for variable selection in the Cox model. *Stat Med*. (1997) 16:385–95. doi: 10.1002/(SICI)1097-0258(19970228)16:4<385::AID-SIM380>3.0.CO;2-3

12. Maeser D, Gruener RF, Huang RS. oncoPredict: an R package for predicting in vivo or cancer patient drug response and biomarkers from cell line screening data. *Brief Bioinform*. (2021) 22(6):bbab260. doi: 10.1093/bib/bbab260

13. Mermel CH, Schumacher SE, Hill B, Meyerson ML, Beroukhim R, Getz G. GISTIC2.0 facilitates sensitive and confident localization of the targets of focal somatic

copy-number alteration in human cancers. *Genome Biol*. (2011) 12:R41. doi: 10.1186/gb-2011-12-4-r41

14. Mayakonda A, Lin DC, Assenov Y, Plass C, Koeffler HP. Maftools: efficient and comprehensive analysis of somatic variants in cancer. *Genome Res*. (2018) 28:1747–56. doi: 10.1101/gr.239244.118

15. Becht E, Giraldo NA, Lacroix L, Buttard B, Elarouci N, Petitprez F, et al. Estimating the population abundance of tissue-infiltrating immune and stromal cell populations using gene expression. *Genome Biol*. (2016) 17:218. doi: 10.1186/s13059-016-1070-5

16. Charoentong P, Finotello F, Angelova M, Mayer C, Efremova M, Rieder D, et al. Pan-cancer immunogenomic analyses reveal genotype-immunophenotype relationships and predictors of response to checkpoint blockade. *Cell Rep*. (2017) 18:248–62. doi: 10.1016/j.celrep.2016.12.019

17. Li T, Fan J, Wang B, Traugh N, Chen Q, Liu JS, et al. TIMER: A web server for comprehensive analysis of tumor-infiltrating immune cells. *Cancer Res*. (2017) 77: e108–e10. doi: 10.1158/0008-5472.CAN-17-0307

18. Li X, Dai Z, Wu X, Zhang N, Zhang H, Wang Z, et al. The comprehensive analysis identified an autophagy signature for the prognosis and the immunotherapy efficiency prediction in lung adenocarcinoma. *Front Immunol*. (2022) 13:749241. doi: 10.3389/fimmu.2022.749241

19. Reuter JA, Spacek DV, Snyder MP. High-throughput sequencing technologies. *Mol Cell*. (2015) 58:586–97. doi: 10.1016/j.molcel.2015.05.004

20. Swanson K, Wu E, Zhang A, Alizadeh AA, Zou J. From patterns to patients: Advances in clinical machine learning for cancer diagnosis, prognosis, and treatment. *Cell*. (2023) 186:1772–91. doi: 10.1016/j.cell.2023.01.035

21. Wang X, Wang Z, Huang R, Lu Z, Chen X, Huang D. UPP1 promotes lung adenocarcinoma progression through epigenetic regulation of glycolysis. *Aging Dis*. (2022) 13:1488–503. doi: 10.14336/AD.2022.0218

22. Strefeler A, Blanco-Fernandez J, Jourdain AA. Nucleosides are overlooked fuels in central carbon metabolism. *Trends Endocrinol Metab*. (2024) 35:290–9. doi: 10.1016/j.tem.2024.01.013

23. Zhao Y, Feng X, Chen Y, Selfridge JE, Gorityala S, Du Z, et al. 5-fluorouracil enhances the antitumor activity of the glutaminase inhibitor CB-839 against PIK3CA-mutant colorectal cancers. *Cancer Res*. (2020) 80:4815–27. doi: 10.1158/0008-5472.CAN-20-0600

24. Nwosu ZC, Ward MH, Sajjakulnukit P, Poudel P, Ragulan C, Kasperek S, et al. Uridine-derived ribose fuels glucose-restricted pancreatic cancer. *Nature*. (2023) 618:151–8. doi: 10.1038/s41586-023-06073-w

25. Bhasin N, Alleyne D, Gray OA, Kupfer SS. Vitamin D regulation of the uridine phosphorylase 1 gene and uridine-induced DNA damage in colon in african americans and european americans. *Gastroenterology*. (2018) 155:1192–204.e9. doi: 10.1053/j.gastro.2018.06.049

26. Lai K, Song C, Gao M, Deng Y, Lu Z, Li N, et al. Uridine alleviates sepsis-induced acute lung injury by inhibiting ferroptosis of macrophage. *Int J Mol Sci*. (2023) 24 (6):5093. doi: 10.3390/ijms24065093

27. Li Y, Jiang M, Aye L, Luo L, Zhang Y, Xu F, et al. UPP1 promotes lung adenocarcinoma progression through the induction of an immunosuppressive microenvironment. *Nat Commun*. (2024) 15:1200. doi: 10.1038/s41467-024-45340-w

28. Weng JY, Salazar N. DNA methylation analysis identifies patterns in progressive glioma grades to predict patient survival. *Int J Mol Sci*. (2021) 22(3):1020. doi: 10.3390/ijms22031020

29. Okumura M, Iwakiri T, Yoshikawa N, Nagatomo T, Ayabe T, Tsuneyoshi I, et al. Hepatocyte growth factor enhances antineoplastic effect of 5-fluorouracil by increasing UPP1 expression in hepG2 cells. *Int J Mol Sci*. (2022) 23(16):9108. doi: 10.3390/ijms23169108

30. Du W, Tu S, Zhang W, Zhang Y, Liu W, Xiong K, et al. UPP1 enhances bladder cancer progression and gemcitabine resistance through AKT. *Int J Biol Sci*. (2024) 20:1389–409. doi: 10.7150/ijbs.83774

frontiers | Frontiers in Immunology

TYPE Original Research
PUBLISHED 04 October 2024
DOI 10.3389/fimmu.2024.1449251

Check for updates

OPEN ACCESS

EDITED BY
Pengpeng Zhang,
Nanjing Medical University, China

REVIEWED BY
Baosheng Li,
Shandong Cancer Hospital, China
Shuanghu Yuan,
Anhui Provincial Hospital, China
Wei Deng,
Capital Medical University, China

*CORRESPONDENCE
Yong Zhang
doctorzzb@163.com
Zhongbao Zhou
346894383@qq.com

RECEIVED 14 June 2024
ACCEPTED 19 September 2024
PUBLISHED 04 October 2024

CITATION
Liu R, Ma J, Zhang Y and Zhou Z (2024) Integrated transcriptome analysis of CSE1L regarding poor prognosis and immune infiltration in bladder urothelial carcinoma and experimental verification.
Front. Immunol. 15:1449251.
doi: 10.3389/fimmu.2024.1449251

COPYRIGHT
© 2024 Liu, Ma, Zhang and Zhou. This is an open-access article distributed under the terms of the Creative Commons Attribution License (CC BY). The use, distribution or reproduction in other forums is permitted, provided the original author(s) and the copyright owner(s) are credited and that the original publication in this journal is cited, in accordance with accepted academic practice. No use, distribution or reproduction is permitted which does not comply with these terms.

Integrated transcriptome analysis of CSE1L regarding poor prognosis and immune infiltration in bladder urothelial carcinoma and experimental verification

Runze Liu[1], Jiayi Ma[2], Yong Zhang[1]* and Zhongbao Zhou[1]*

[1]Department of Urology, Beijing Tiantan Hospital, Capital Medical University, Beijing, China, [2]Beijing National Day School, Beijing, China

Background: Bladder urothelial carcinoma (BLCA) is one of the most prevalent tumors globally, with its incidence rising notably in developed countries, significantly affecting human health. CSE1L encodes a protein that is involved in various cellular processes and plays a critical role in cancer initiation and progression. However, its role in BLCA remains underexplored.

Methods: CSE1L expression in BLCA was analyzed using TCGA data and validated by qRT-PCR and Western blot in clinical samples. Survival analysis and Cox regression models were used to evaluate its prognostic value. Functional enrichment and protein interaction analyses were performed, and immune cell infiltration was assessed using CIBERSORT. Drug sensitivity was analyzed using GDSC data. *In vitro* assays evaluated the effects of CSE1L knockdown on cell proliferation, migration, and invasion.

Results: CSE1L was found to be significantly overexpressed in BLCA tissues compared to normal tissues. High CSE1L expression was associated with poor overall survival and unfavorable clinicopathological features. Functional enrichment analysis revealed that DEGs related to CSE1L were involved in cell cycle regulation and immune-related pathways. Immune infiltration analysis indicated a significant correlation between CSE1L expression and various immune cell types, particularly T cells and macrophages. Drug sensitivity analysis identified several chemotherapeutic agents, including MG-132, Palbociclib, and Nutlin-3a, which were more effective in the low-CSE1L expression group, while the high-CSE1L expression group showed sensitivity to drugs like S-Trityl-L-cysteine, Bleomycin, and Cisplatin. *In vitro* knockdown of CSE1L in BLCA cell lines inhibited cell proliferation, migration, and invasion.

Conclusions: The overexpression of CSE1L is associated with the progression and poor prognosis of bladder cancer, suggesting it could be a promising target for bladder cancer in the future.

KEYWORDS

CSE1L, bladder urothelial carcinoma, prognosis, therapeutic target, immune infiltration

Introduction

Bladder urothelial carcinoma (BLCA) remains a significant global health concern, ranking 9th in incidence and 13th in cancer-related deaths worldwide (1). Treatment options for BLCA depend on various factors, including tumor stage, grade, and patient characteristics. Transurethral resection of bladder tumor (TURBT) is the standard treatment for non-muscle-invasive bladder cancer (NMIBC). For muscle-invasive bladder cancer (MIBC), radical cystectomy, with or without neoadjuvant chemotherapy, is often recommended (2, 3). Despite advances in understanding BLCA, challenges persist, including tumor heterogeneity, risk stratification, and treatment response prediction. Additionally, the identification of novel biomarkers, genetic alterations, and therapeutic targets holds promise for personalized medicine approaches.

CSE1L (chromosome segregation 1-like protein), also known as CAS (cellular apoptosis susceptibility protein), encodes a protein involved in various cellular processes and is found in humans and many other organisms. CSE1L is primarily recognized for its role in nucleocytoplasmic transport, the process by which molecules such as proteins and RNA move between the nucleus and the cytoplasm of a cell (4). CSE1L functions as part of the nuclear pore complex (NPC), serving as a gateway for the transport of molecules in and out of the nucleus (5). Additionally, CSE1L has been implicated in other cellular functions, including cell cycle regulation, cell division, and apoptosis (6, 7). Research on the CSE1L gene and protein has highlighted its importance in maintaining cellular homeostasis and its potential involvement in disease. Dysregulation of regulatory mechanisms can lead to aberrant CSE1L expression, contributing to developmental defects or disease progression (8). Further research is needed to deepen our understanding of the precise mechanisms by which CSE1L exerts its functions in development and disease. Unraveling the upstream regulators and downstream targets of CSE1L will provide insights into its molecular networks and potential therapeutic targets. Additionally, investigating the utility of CSE1L as a diagnostic or prognostic marker in BLCA may open avenues for personalized medicine approaches.

The present study aimed to explore the correlation between CSE1L and BLCA and identify potential biomarkers for this disease. The prognostic value of CSE1L expression was analyzed using survival analysis, and its correlation between CSE1L expression and clinicopathological characteristics in BLCA patients was examined.

Materials and methods

Data acquisition

Gene expression profile data and clinical information were collected from the TCGA-BLCA project, specifically utilizing the HTSeq-FPKM workflow. The data were sourced from the TCGA database (https://portal.gdc.cancer.gov/). To ensure a comprehensive analysis, RNA-seq data lacking clinical information were excluded, resulting in a total of 431 cases. These cases included both BLCA specimens and adjacent non-tumor specimens. Any unavailable or unknown clinical features were treated as missing values in the analysis.

Survival analysis and construction of nomogram

Survival analyses of CSE1L were conducted using the R package *survival*. Patients were divided into low and high CSE1L expression groups. Univariate and multivariate Cox regression analyses of the clinical characteristics were used to establish a risk score as an independent prognostic predictor. To accurately estimate each patient's prognosis, a nomogram was constructed based on the risk score and conventional clinical characteristics, including age, gender, stage, and TNM classification. The nomogram was then evaluated using calibration curves.

GO and KEGG enrichment analyses

The *clusterProfiler* R package was used to identify significantly differentially expressed genes (DEGs) between BLCA samples and normal samples using an unpaired t-test. The Benjamini-Hochberg method was applied to adjust the threshold value, with an adjusted $P < 0.05$ and $|\log FC| > 1$. Gene Ontology (GO) analysis revealed that these genes were associated with a diverse range of functional categories, including biological process and molecular function. Additionally, Kyoto Encyclopedia of Genes and Genomes (KEGG) enrichment analyses of DEGs were conducted using the Database for Annotation, Visualization, and Integrated Discovery (DAVID) online tools (https://david.ncifcrf.gov/), with a P-value cut-off criterion of <0.05.

Composition of invasive immune cells in BLCA

The marker genes for 24 immune cell types were identified based on a literature review. The infiltration of these immune cells in BLCA was analyzed using the CIBERSORT algorithm and single-sample Gene Set Enrichment Analysis(ssGSEA) (9). The correlation between CSE1L expression and immune cell infiltration was assessed using the Wilcoxon method.

Protein-protein interaction networks

The Pearson method was applied to calculate the correlation coefficient, with an adjusted $|Cor| \geq 0.3$ and $P \leq 0.05$. A protein-protein interaction (PPI) network was constructed using the STRING database (https://string-db.org) based on the intersection of genes between the screened DEGs and CSE1L-correlation genes. Subsequently, Gene Ontology Biological Process (GO-BP) enrichment analysis was performed on intersection genes, and the PPI network was annotated.

Drug sensitivity analysis

Based on the Genomics of Drug Sensitivity in Cancer (GDSC, https://www.cancerrxgene.org/), we used the R package *prophytic* to predict the drug sensitivity of each tumor sample. The estimated half-maximal inhibitory concentration (IC50) of each compound was calculated. Representative drugs were then selected for Spearman correlation analysis.

Patient samples

We collected BLCA tissues and matched normal bladder tissues from BLCA patients who underwent TURBT in the Urology Department of Beijing Tiantan Hospital, Capital Medical University, between February 2024 and May 2024. During the operation, the surgical specimens were promptly immersed in liquid nitrogen and stored at -80°C for subsequent use. All participants provided informed consent by signing the required form, and the project was approved by the Ethics Committee of Beijing Tiantan Hospital, Capital Medical University [KY2024-005-01].

Cell lines and cell culture

The human normal urothelial cell line (SV-HUC-1) and BLCA cell lines (5637 and T24) were purchased from the Cell Bank of the Chinese Academy of Sciences. SV-HUC-1 cells were cultured in F-12K medium (Gibco), while T24 and 5637 cells were cultured in RPMI-1640 medium (Gibco). The medium was supplemented with 10% fetal bovine serum (FBS) and 1% penicillin and streptomycin. All cells were incubated at 37°C in a humidified environment with 5% carbon dioxide.

Transfection

Small interfering CSE1L RNA (siR-CSE1L) and its corresponding negative control siRNAs (NC) were synthesized by General Biol Company (China). NC and siR-CSE1L were transfected into BLCA cell lines using Lipofectamine 3000 (Invitrogen, USA). All primer sequences are listed in Table 1.

RNA extraction, reverse transcription, and quantitative real-time PCR

Total RNA was extracted from freshly frozen tissues or bladder cancer cell lines using QIAGEN/74136/RNeazy Plus Mini Kit. Reverse transcription was then performed using the Vazyme/R312-02/HiScript III 1st Strand cDNA Synthesis Kit (+gDNA wiper). Subsequently, qRT-PCR was carried out using Vazyme/Q712-03/Taq Pro Universal SYBR qPCR Master Mix. The housekeeping gene GAPDH was used as an internal reference, and the relative expression level of the target gene was calculated using the $2-\Delta\Delta CT$ method. Each experiment was performed in three replicates, and the primer sequences used are provided in Table 1.

Western blot

Protein extraction and Western blotting were performed as follows. Tumor tissue was cut into small pieces, each weighing approximately 30mg, and placed in 500 µL RIPA lysis buffer (pre-added with protease and phosphatase inhibitors). A sample of 20 µg of protein was then loaded onto an SDS- PAGE gel and run under standard conditions, with the same volume of culture medium used as a control. The proteins were transferred to a PVDF membrane using iBlot 2 system following the standard protocol. The membrane was blocked with 5% nonfat milk in TBST and incubated for 1 hour at room temperature, then incubated overnight at 4°C with agitation in a solution containing the primary antibody diluted to the recommended concentration in

TABLE 1 Primer sequences used in this research.

Name	Sequence (5′->3′)
GAPDH (human)-F	GTCTCCTCTGACTTCAACAGCG
GAPDH (human)-R	ACCACCCTGTTGCTGTAGCCAA
CSE1L(human)-F	GAACGGCTCTTTACTATGCGAGG
CSE1L(human)-R	CTGAAGAGCCAGGAAGTGTGAG
Si-CSE1L 1	GGATAATGTTATCAAAGTA
Si-CSE1L 2	CGACGGTATCAAATATATT

TBST. After washing the blot in TBST three to four times for 5 minutes each at room temperature, the membrane was incubated with a horseradish peroxidase (HRP)-conjugated secondary antibody, diluted to the recommended concentration, for 1 hour at room temperature. Protein bands were visualized using a Clinx Gel Documentation and Analysis instrument, while ImageJ was used for the analysis of the gray values of the bands.

Cell counting kit-8 assay

5637 and T24 cells transfected with NC and siR-CSE1L were plated in 96-well plates at a density of 5×10^3 cells per well. The cells were pre-cultured in a CO_2 incubator at 37°C for 24 hours. CCK-8 reagent was added at 24, 48, 72 and 96 hours. After a 2-hour incubation at 37°C, absorbance at 450nm was measured using a spectrophotometer.

Cell migration assay

Cells were seeded at a density of 2×10^5 cells per well in a 6-well plate and cultured for 24 hours until they adhered. A P200 pipette tip was used to create a vertical scratch. The cells were then washed three times with PBS to remove the dislodged cells, and images were captured immediately using a microscope (0h point). Afterward, serum-free medium was added, and the cells were incubated for an additional 12 hours before capturing images at the same locations. The results were analyzed using ImageJ software, with the wound healing area as an indicator of cell migration.

Transwell invasion assay

For the cell invasion assay, the transwell plate with an 8-mm diameter polycarbonate membrane was used. The membrane in the upper chamber was coated with a layer of Matrigel diluted in medium, and the cells were resuspended in serum-free medium. The lower chamber was filled with complete medium. After incubation at 37°C in a humidified atmosphere with 5% carbon dioxide for 24-72 hours, the cells on the lower surface of the membrane were fixed with 100% methanol, stained with 0.1% crystal violet for 15-30 minutes, and counted under the microscope.

Statistical analysis

The associations between clinical factors and CSE1L were analyzed using various statistical tests, including the Wilcoxon rank-sum test and logistic regression, and the t-test for numerical variables. The chi-square test was also employed for categorical data. Prognostic data were obtained from TCGA, and Cox regression analyses, along with the Kaplan-Meier method, were used to evaluate prognostic factors. In all tests, P value <0.05 was considered statistically significant.

Results

CSE1L expression in pan–cancer and BLCA

First, pan-cancer analyses were conducted to compare the CSE1L expression between tumor samples and their corresponding normal samples, using the Wilcoxon rank-sum test. Most human cancers, including BLCA, BRCA, CESC, CHOL, COAD, ESCA, HNSC, KICH, KIRC, KIRP, LIHC, LUAD, LUSC, READ, STAD and UCEC exhibit overexpression of CSE1L. In BLCA, a significant increase in CSE1L expression was observed in tumors compared to normal tissues ($p < 0.05$) (Figure 1A). Next, we compared the expression of CSE1L in 19 normal samples and 412 BLCA samples from the TCGA-BLCA dataset. CSE1L expression was significantly high in cancer samples, with a median level of 6.924 and 6.211 in tumor and normal tissues, respectively ($p < 0.001$) (Figure 1B). Subsequently, we grouped the samples based on high- and low-CSE1L expression groups, analyzed the DEGs, and generated heatmaps (Figures 1B, C).

CSE1L could be an independent prognostic factor for BLCA

Clinical data and gene expression data for 412 BLCA samples were downloaded from TCGA database. We investigated the clinicopathological characteristics of BLCA patients with differential CSE1L expression. As shown in Table 2, compared with the low-CSE1L group, patients in the high-CSE1L group exhibited a higher proportion of histologic grade ($P < 0.001$), and worse primary therapy outcome ($P = 0.003$). There was also a significant correlation between CSE1L levels and smoking status ($P = 0.013$) as well as overall survival (OS) ($P < 0.001$). To explore the correlation between CSE1L expression and BLCA prognosis, we compared the survival rates of high-and low-CSE1L expression groups using Kaplan-Meier analysis. The results showed that high CSE1L expression was significantly associated with poor OS in BLCA patients (P=0.002) (Figure 2C).

A nomogram model was constructed using multivariate Cox regression based on the relative expression of the key gene CSE1L and its main clinical observation indicators. The results indicate that CSE1L is an independent prognostic factor in patients with BLCA, with the prognosis worsening as the risk score increased (Figure 2A). The calibration curve demonstrated that the actual OS values were consistent with those predicted by the nomogram, with an overall concordance index of 0.704 (Figure 2B).

Functional enrichment and analyses

We performed DEGs analysis using data from the TCGA cohort. The GO enrichment for DEGs showed that they were primarily associated with chromosome activity, the cell cycle, and mitosis (Figures 3A, C). The Kyoto Encyclopedia of Genes and Genomes (KEGG) enrichment analysis indicated significant

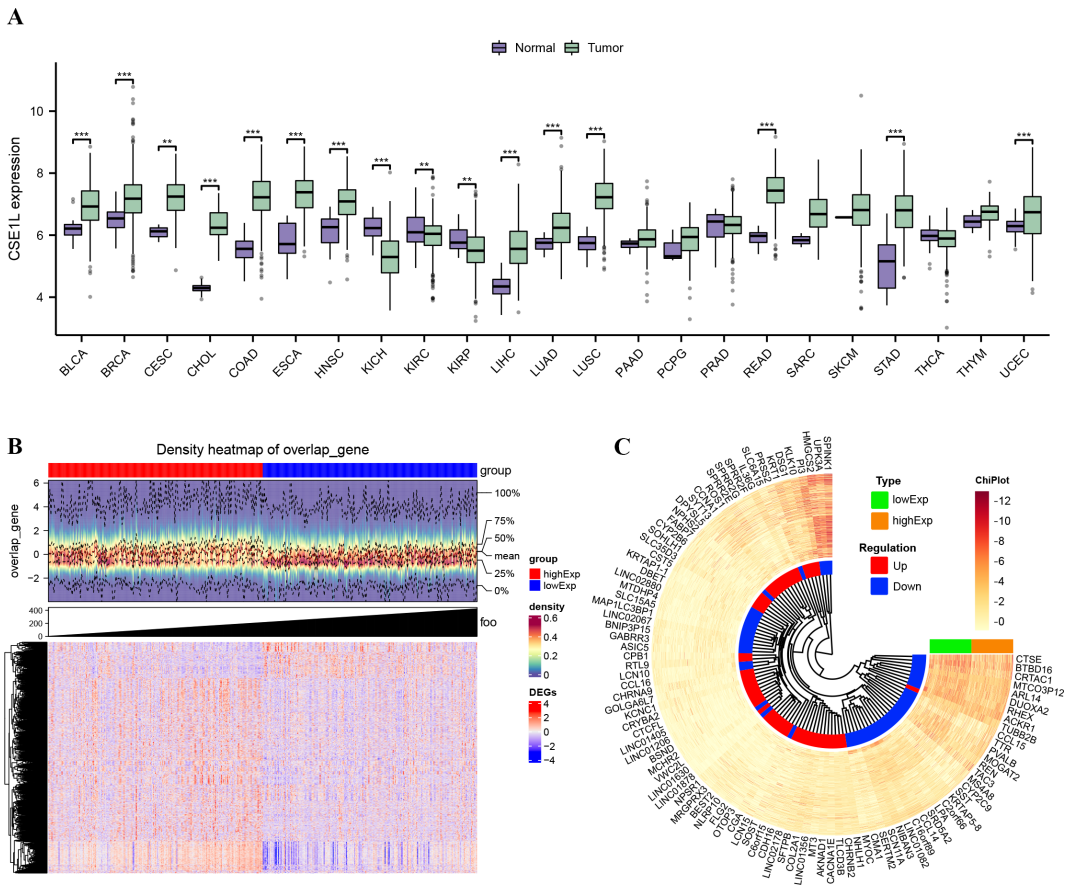

FIGURE 1
CSE1L expression in TCGA database and DEGs. **(A)** The mRNA expression levels of CSE1L in pan-cancer; **(B)** Density heatmap of DEGs; **(C)** Heatmap of top 100 DEGs. **p < 0.01; ***p < 0.001.

enrichment in pathways related to cell cycle, systemic lupus erythematosus, retinol metabolism, motor proteins, neutrophil extracellular trap formation, alcoholism, and amoebiasis (Figure 3B). Figure 3D illustrates the DEGs enriched in corresponding pathways. Overall, the functions of DEGs are significantly related to the cell cycle.

PPI network analysis

PPI network analysis is essential for studying the pathway involved in tumor development. To better understand the potential biological functions of CSE1L in BLCA, gene correlations were assessed using Pearson correlation analysis. Using the STRING database, we constructed a PPI network. Based on the intersecting genes, we performed Gene Ontology Biological Process (GO-BP) enrichment analysis and classified their functions into seven categories for PPI network annotation. The inner circle in the PPI network represents the regulation of gene expression, while the outer circle indicates the different functions of the gene/protein (Figure 4).

Correlation between CSE1L expression and immune infiltration

First, the CIBERSORT method was used to assess the infiltration of 22 different immune cell types in BLCA. The Wilcoxon method was employed to explore differences in immune cell infiltration between the high- and low-CSE1L expression groups. Our analysis revealed that CSE1L expression primarily affected T cells, macrophages, and mast cells (Figure 5A). We further analyzed the correlation between CSE1L expression and immune infiltration. As illustrated in Figure 5B, CSE1L expression was positively correlated with the CD4 memory-activated T cells, M0 macrophages, M1 macrophages, and resting NK cells, while it was negatively correlated with the infiltration level of regulatory Tregs and plasma cells. Next, we used ssGSEA to determine the infiltration of different immune cell types in BLCA. Spearman analysis was conducted to investigate the relationship between CSE1L expression and immune cell infiltration. Our analysis revealed that CSE1L expression was negatively correlated with the pDCs and CD56bright NK cells and positively correlated with the infiltration of Th2 cells (Figure 5C).

10.3389/fimmu.2024.1449251

TABLE 2 Clinical pathological characteristics of the patients.

Characteristics	Low expression of CSE1L	High expression of CSE1L	P value
n	206	206	
Pathologic T stage, n (%)			0.939
T1&T2	64 (16.9%)	59 (15.6%)	
T3	98 (25.9%)	98 (25.9%)	
T4	30 (7.9%)	29 (7.7%)	
Pathologic N stage, n (%)			0.682
N0	119 (32.3%)	119 (32.3%)	
N1	21 (5.7%)	25 (6.8%)	
N2&N3	45 (12.2%)	39 (10.6%)	
Pathologic M stage, n (%)			0.248
M0	109 (51.4%)	92 (43.4%)	
M1	4 (1.9%)	7 (3.3%)	
Pathologic stage, n (%)			0.824
Stage I&Stage II	68 (16.6%)	65 (15.9%)	
Stage III	68 (16.6%)	74 (18%)	
Stage IV	69 (16.8%)	66 (16.1%)	
Primary therapy outcome, n (%)			**0.003**
CR	133 (37.5%)	100 (28.2%)	
PR	13 (3.7%)	9 (2.5%)	
SD	9 (2.5%)	21 (5.9%)	
PD	27 (7.6%)	43 (12.1%)	
Gender, n (%)			0.823
Male	153 (37.1%)	151 (36.7%)	
Female	53 (12.9%)	55 (13.3%)	
Age, n (%)			0.691
<= 70	114 (27.7%)	118 (28.6%)	
> 70	92 (22.3%)	88 (21.4%)	
Histologic grade, n (%)			< 0.001
Low grade	19 (4.6%)	2 (0.5%)	
High grade	186 (45.5%)	202 (49.4%)	
Lymphovascular invasion, n (%)			0.082
No	57 (20.3%)	72 (25.6%)	
Yes	83 (29.5%)	69 (24.6%)	
Smoker, n (%)			**0.013**
No	66 (16.5%)	43 (10.8%)	
Yes	135 (33.8%)	155 (38.8%)	
OS event, n (%)			< 0.001
Alive	132 (32%)	98 (23.8%)	
Dead	74 (18%)	108 (26.2%)	

(Continued)

TABLE 2 Continued

Bold values indicate P < 0.05, representing statistically significant differences.

Drug sensitivity analysis

We conducted a chemosensitivity analysis of the TCGA dataset using the GDSC database through the R software package *prophytic*. The relationship between CSE1L expression levels and drug sensitivity was explored by calculating the correlation between the half-maximal inhibitory concentration (IC50) of chemotherapeutic drugs and CSE1L expression. A total of 70 drugs with IC50 values significantly correlated with CSE1L expression ($p < 0.05$) were identified. The results showed that the low CSE1L expression group was more sensitive to MG-132, Palbociclib (PD-0332991), Nutlin-3a, and Selumetinib (AZD6244), while the high CSE1L expression group was more sensitive to S-Trityl-L-cysteine (NSC 83265), Bleomycin, BAY 61-3606, and Cisplatin. These findings have implications for selecting specific medications based on anti-tumor drug sensitivity (Spearman $|Cor| > 0.2$ and $p < 0.05$, Figures 6A–H).

CSE1L expression in BLCA tissues and cell lines

We collected tumor tissues and adjacent normal tissues from six pairs of BLCA patients for qRT-PCR and Western blot validation. The results revealed a significantly elevated expression level of CSE1L mRNA in the tumor tissues (Figures 7A, B). This finding was similarly confirmed in BLCA cell lines. Compared to the normal urothelial cell line SV-HUC1, CSE1L mRNA expression was significantly elevated in all BLCA cell lines tested (Figure 7C: 5637, $P < 0.01$; T24, $P < 0.001$).

CSE1L exerted a promoting effect on BLCA *in vitro*

To explore the biological functions of CSE1L in BLCA, we transfected 5637 and T24 cell lines with siR-CSE1L and a negative control (NC) separately. Knockdown efficiency was validated by qRT-PCR, which demonstrated a significant decrease in CSE1L expression at the mRNA level (Figure 8D). We then assessed the impact of CSE1L on the migration and invasion of BLCA cells using wound healing and

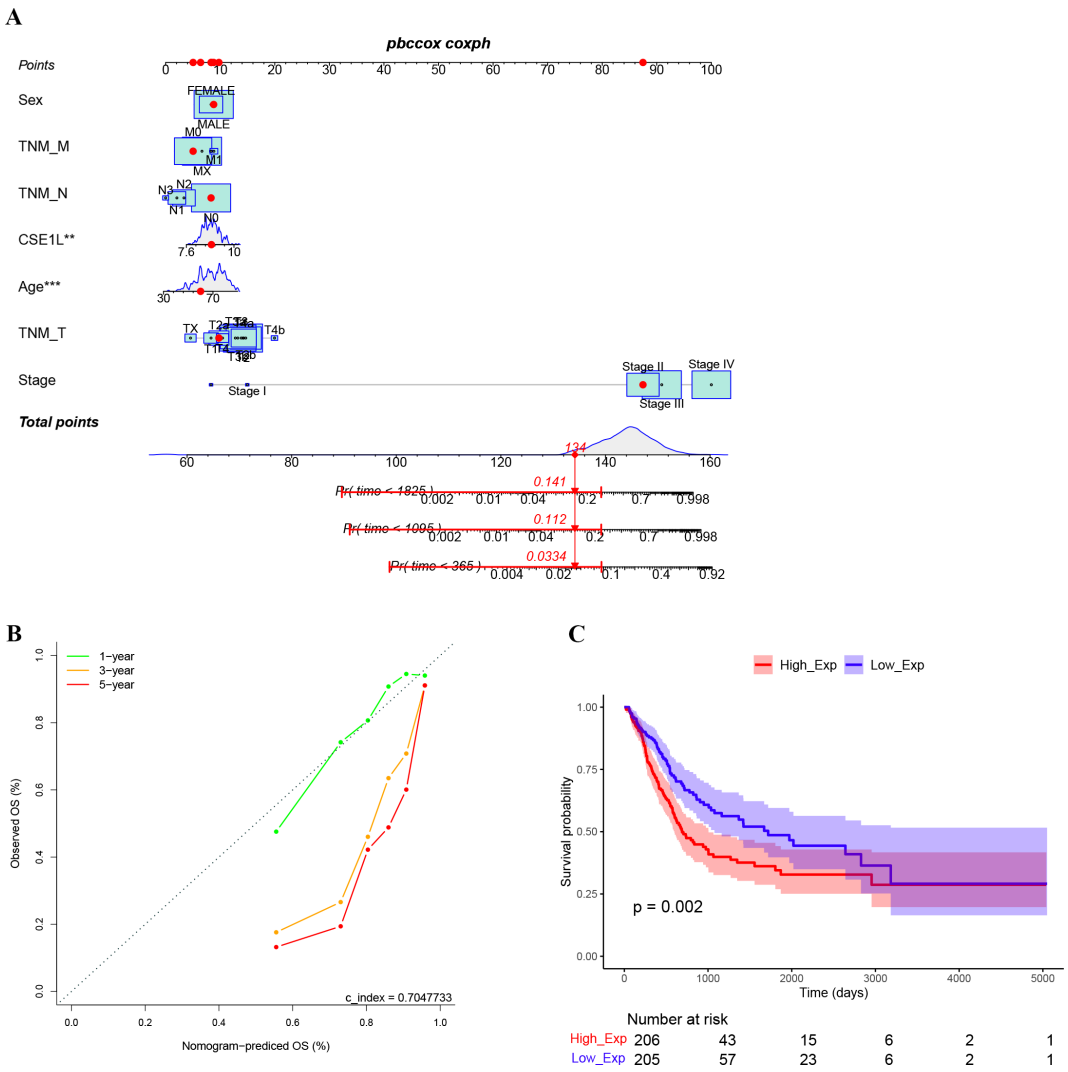

FIGURE 2
High expression of CSE1L indicates worse prognosis. **(A)** The nomogram to estimate the 1-, 3-, and 5-year OS of bladder cancer patients. **(B)** The calibration curves of actual values and predicted values provided by the nomogram. **(C)** Kaplan-Meier survival curves indicated that bladder cancer patients with high CASE1L mRNA expression had a shorter OS.

transwell invasion assay. The wound healing assay indicated a significant reduction in the migration ability of 5637 and T24 cells after CSE1L knockdown (Figures 8A, E). Similarly, the transwell invasion assay showed a decrease in the invasive ability of BLCA cells as CSE1L expression was downregulated (Figures 8B, F). These results indicate that CSE1L promotes the migration and invasion of BLCA cells *in vitro*. Additionally, we investigated the effect of CSE1L on the proliferation of BLCA cells using CCK-8 assay. The CCK-8 assay showed that silencing CSE1L significantly attenuated the proliferation of 5637 and T24 cells (Figure 8C). In summary, these findings suggest that CSE1L promotes the development of BLCA *in vitro*.

Discussion

Bladder cancer is the fifth most common cancer worldwide, characterized by a high incidence, poor prognosis, and a significant likelihood of recurrence. Currently, surgical resection is the most effective treatment (10). However, due to the high recurrence rate and substantial heterogeneity of bladder tumors, there is an urgent need for new molecular markers to predict patient survival in this disease.

In 1995, Brinkmann et al. first isolated a CSE1L-DNA fragment in breast cancer cells (11). CSE1L is the human homolog of the yeast gene CSE1, encoding a protein distributed in the cell nucleus and cytoplasm (12). The gene is located on 20q13, a site frequently amplified in various cancers and associated with genetic instability (13). CSE1L has been found to be involved in apoptosis, proliferation, survival, nuclear-cytoplasmic transport, and cancer metastasis (6, 14, 15). Additionally, CSE1L is a novel micro-vesicle membrane protein that may serve as a potential target for the development of efficient antibody-drug conjugates (ADCs) for cancer therapy (16).

As a key factor in the nuclear transport pathway, CSE1L participates in nucleocytoplasmic transport, a crucial process in

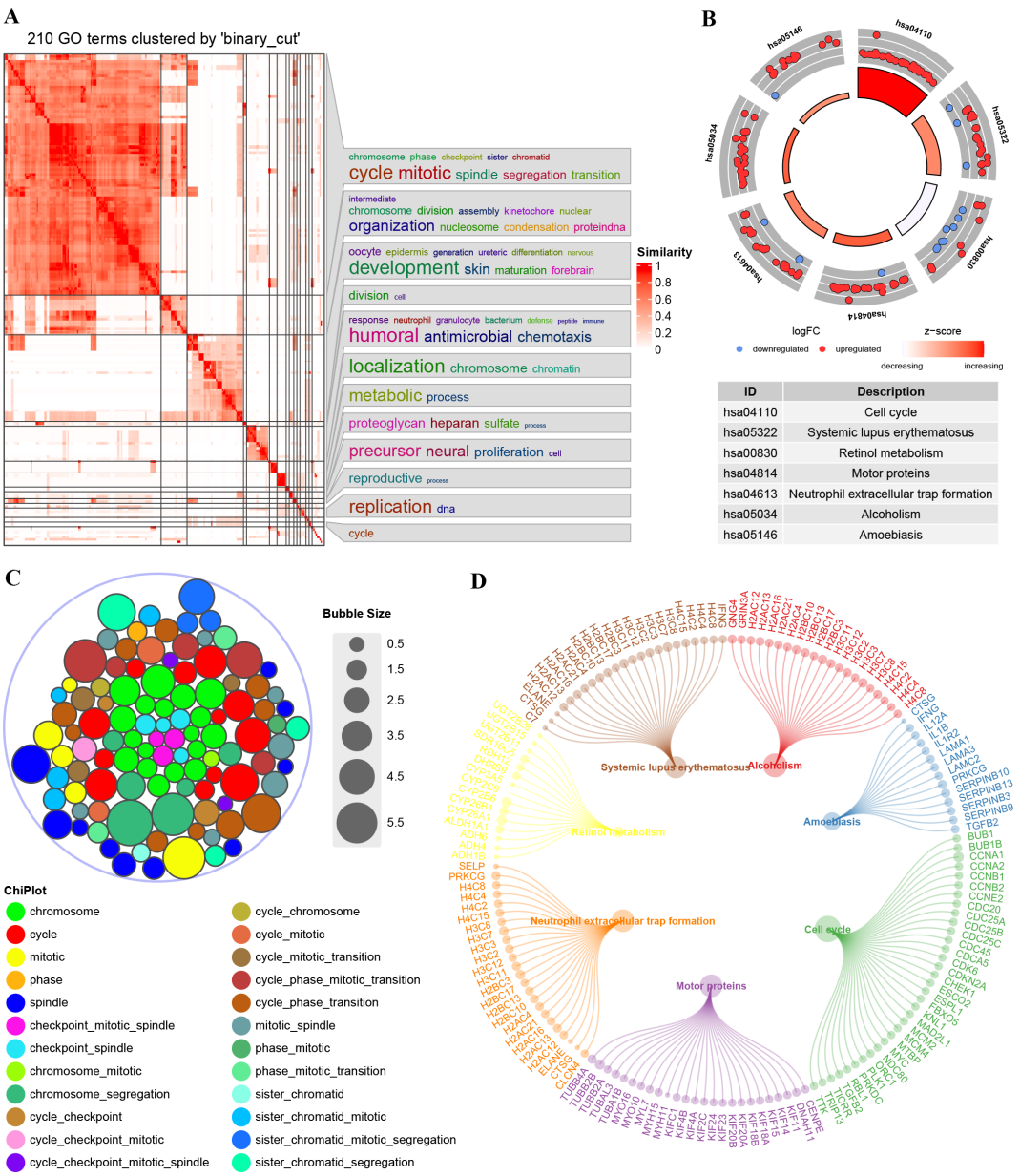

FIGURE 3
Enrichment plots from GO-KEGG analysis. **(A)** GO enrichment semantic similarity matrix. **(B)** Stacked chart of GO terms; **(C)** KEGG enrichment significance and the descriptions of each corresponding pathway. **(D)** DEGs enriched under the corresponding pathways.

tumor growth and development. Consequently, it may have applications in clinical diagnosis and treatment. Moreover, CSE1L expression is associated with tumor progression in various types of cancers. However, the clinical significance and biological functions of CSE1L in bladder cancer remain unclear. In this study, CSE1L was found to promote the initiation and progression of tumors. Evidence from the Kaplan-Meier plotter and nomogram analyses indicated that CSE1L possesses both diagnostic and prognostic value in distinguishing bladder cancer patients from healthy individuals. Furthermore, it was revealed that high CSE1L expression is associated with poor prognosis.

Based on the differentially expressed genes we screened and CSE1L-related genes, a PPI network was constructed. GO-BP enrichment analysis was performed on the intersecting genes, categorizing their functions into seven group: cell composition, cell cycle, enzymatic activity, metabolize, protein modifications, signaling and others. Genes that primarily interact with CSE1L include AURKA, NUP155, BIRC5, and TPX2. Interestingly, many of these genes are associated with unfavorable patient prognosis. Our study also revealed that CSE1L expression in bladder cancer is correlated with the type and density of infiltrating immune cells. The degree of infiltration of various immune cells, including T cells and macrophages, was significantly correlated with the CSE1L expression. CSE1L is believed to play a role in nucleus-to-cytoplasmic transport, chromosome separation during mitosis, proliferation, and apoptosis. In our study, the decrease in

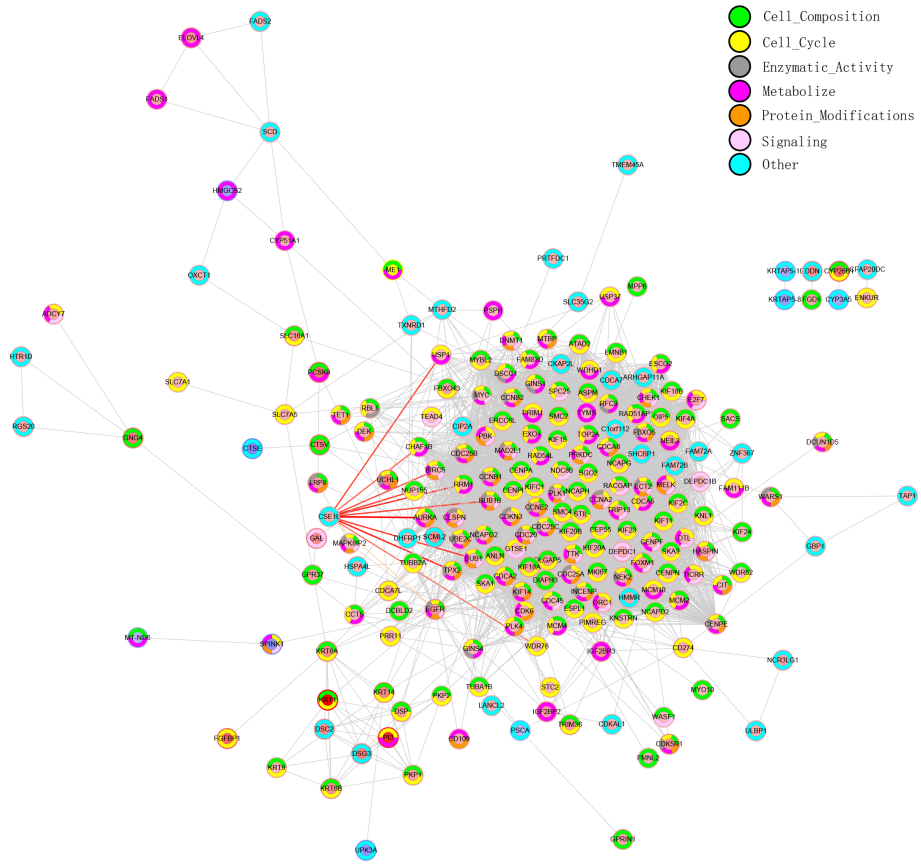

FIGURE 4
Protein-protein interaction (PPI) network of the intersecting genes.

immune infiltration of regulatory T cells may be due to the high expression of CSE1L in these cells, leading to their apoptosis. The relationship between CSE1L expression and immune regulatory cells warrants further investigation.

Previous studies have shown that the expression of CSE1L is positively correlated with the immune checkpoint molecules PD-L1 (CD274) and PDL2 (PDCD1LG2). Progression-free survival (PFS) was significantly shorter in patients with high CSE1L expression compared to those with low expression, suggesting that CSE1L expression may affect the therapeutic efficacy of PD-1 monoclonal antibodies (17). Studies have also indicated that PD-L1 protein levels are reduced following CSE1L silencing (18). Additionally, Lee et al. found that serum phospho-CSE1L could be used for early detection of tumor-targeted therapy efficacy and to monitor secondary resistance in mouse tumor xenograft models. The CSE1L high expression group was more sensitive to S-Trityl-L-cysteine (NSC 83265), Bleomycin, BAY 61-3606, and Cisplatin, while the CSE1L low expression group was more sensitive to MG-132, Palbociclib (PD-0332991), Nutlin-3a, and Selumetinib (AZD6244). Notably, Nutlin-3a, which inhibits the MDM2-p53 interaction and stabilizes p53 protein, induces autophagy and apoptosis. In future studies, we will verify these findings using a larger cancer cell panel and *in vivo* animal models.

In this study, a series of experiments was conducted to elucidate the biological functions of CSE1L in bladder tumor cells. We found that silencing CSE1L expression in bladder cancer cells inhibited cell proliferation and reduced cell invasion and migration. CSE1L promotes tumor progression by enhancing cell proliferation and contributing to drug resistance. These findings align with our understanding of CSE1L's impact on cancer cell growth and are consistent with previous studies.

Multiple potential underlying mechanisms of CSE1L action have been documented in various types of cancer. Studies have proposed that CSE1L interacts with the cAMP/PKA and RAS/ERK signaling pathways in melanoma. According to Jiang et al., the phosphorylation of CSE1L is regulated by extracellular signal-regulated kinase (ERK) (19, 20). Notably, CSE1L promotes melanin formation and melanoma progression by influencing the expression and phosphorylation of CREB (cAMP response element binding protein) and MITF (microphthalmia-associated transcription factor) (20). The PKA signaling pathway induces CREB phosphorylation, thereby prompting MITF expression. Furthermore, the PKA pathway also interacts with the MAPK/ERK pathway, leading to ERK activation. ERK, in turn, interacts with CSE1L, facilitating the phosphorylation of MITF (21). In gastric cancer, CSE1L inhibition has been shown to activate the PI3K/AKT/mTOR and MEK/ERK pathways by downregulation of MITF and GPNMB (15). In pancreatic cancer, CSE1L may regulate proliferation through the AKT signaling pathway (22). In lung cancer, CSE1L interacts with p65 and regulates MAPK signaling (23, 24). CSE1L could also promotes the proliferative and migratory abilities in oral cancer by positively regulating MITF and

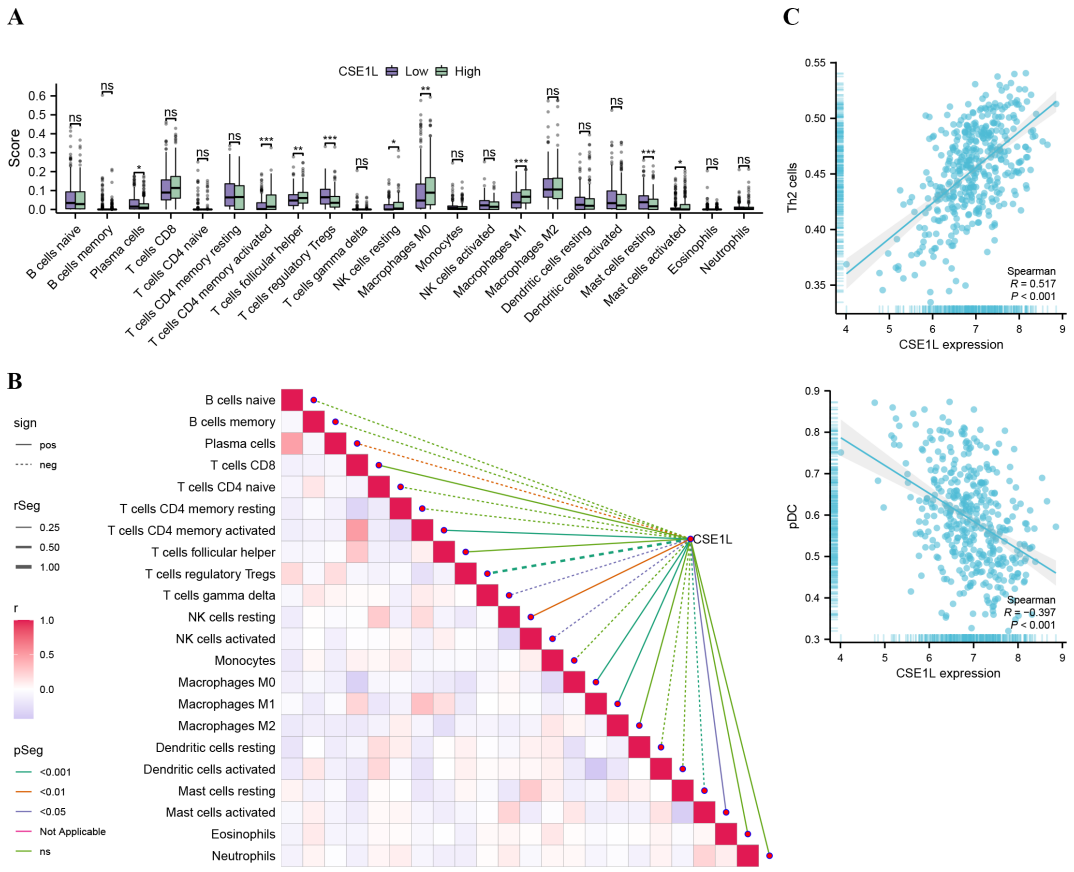

FIGURE 5
Association analysis of CSE1L gene expression and immune infiltration **(A)** Comparison of immune cells between high- and low-CSE1L expression groups (*P<0.05, **P<0.01, ***P<0.001.). **(B)** Immuno-infiltration correlation heat map and association with CSE1L gene expression **(C)** Correlation between CSE1L expression and Th2, pDC based on ssGSEA.

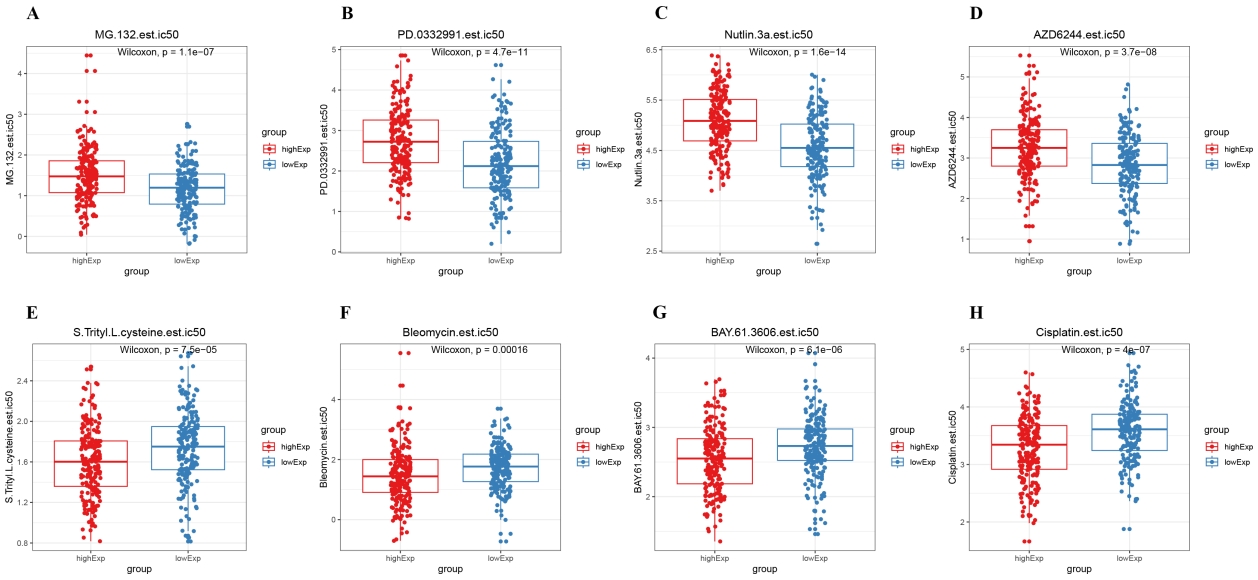

FIGURE 6
Drug sensitivity analysis. **(A–H)** There were significant differences in IC50 between the high and low CSE1L expression groups.

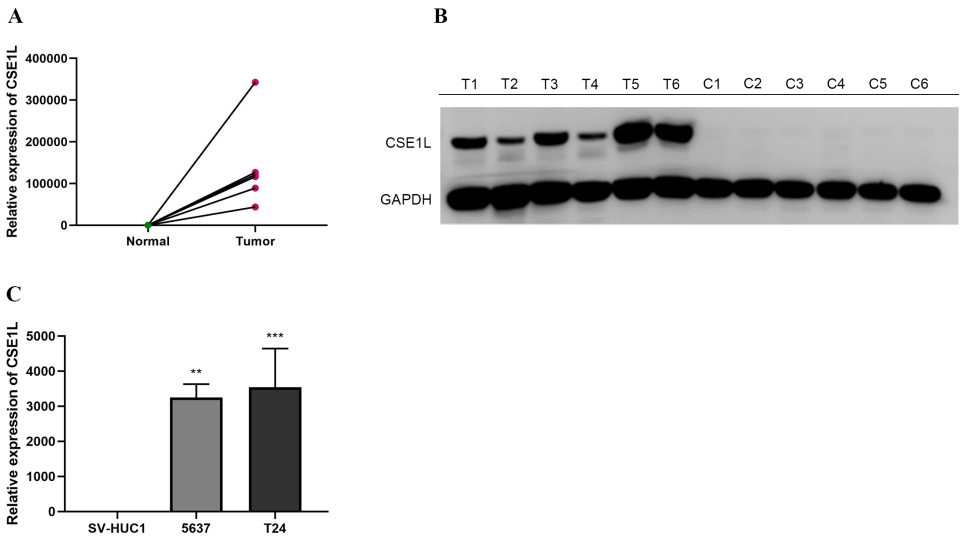

FIGURE 7
mRNA expression levels of CSE1L in BLCA tissues and cell lines. **(A, B)** mRNA expression levels of CSE1L in BLCA tissues; **(C)** mRNA expression levels of CSE1L in BLCA cell lines. (**p < 0.01, ***P < 0.001).

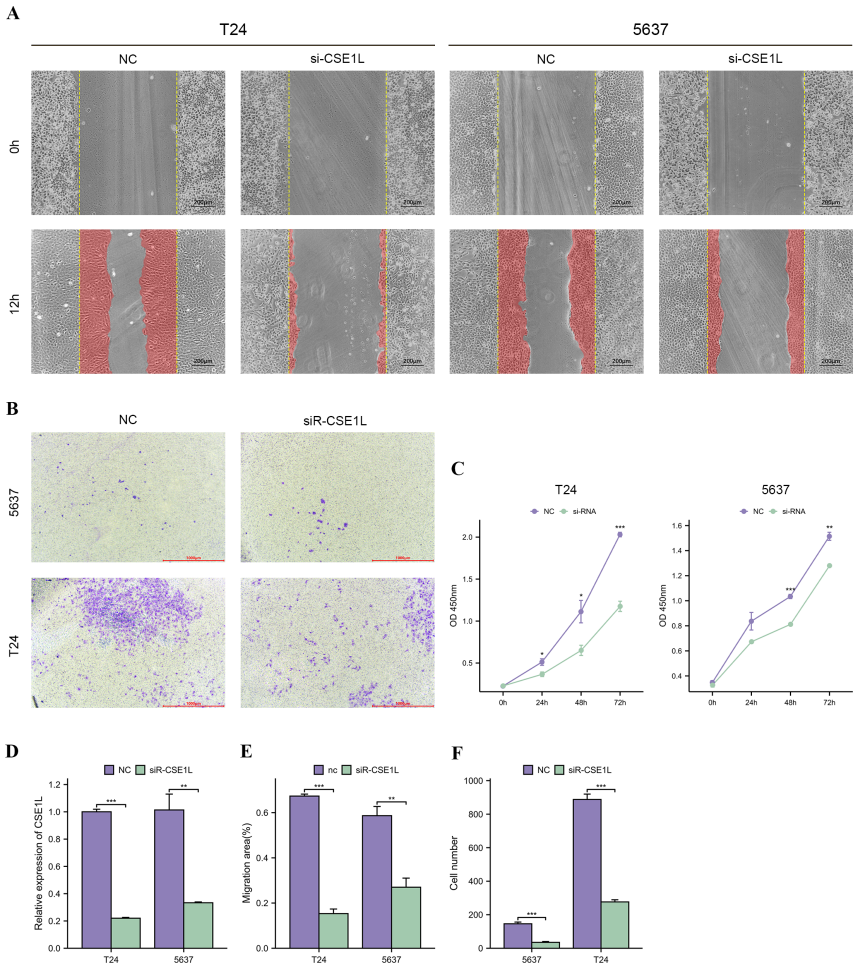

FIGURE 8
CSE1L promotes bladder cancer cells proliferation, migration and invasion *in vitro*. **(A, E)** Wound healing assay indicated that knockdown of CSE1L reduced the migratory ability of bladder cancer cells; **(B, F)** Transwell invasion assay indicated that knockdown of CSE1L reduced the invasive activity of bladder cancer cells; **(C)** CCK-8 assay indicated that knockdown of CSE1L reduced the proliferation ability of bladder cancer cells; **(D)** The mRNA expression level of CSE1L measured by qRT-PCR after cell transfection. *p < 0.05; **p < 0.01; ***p < 0.001.

activating the Akt/mTOR pathway (25). In osteosarcoma cells, CSE1L, a positive regulator of MSH6 protein, is associated with poor patient prognosis. A rescue study suggested that the inhibitory effect of CSE1L knockdown on osteosarcoma cell growth could be reversed by overexpression of MSH6 (26). Current research has investigated whether CSE1L can be used to predict the prognosis of bladder cancer (BLCA) and provide treatment recommendations. However, this study had several limitations. First, due to the lack of additional data sources, the study may be subject to bias. Second, prospective studies are needed to validate our findings. Third, the stability and accuracy of CSE1L as a prognostic marker must be verified using data from other sources. Fourth, the molecular mechanisms by which CSE1L influences the development and progression of BLCA require further exploration through basic experiments.

Conclusions

The expression level of CSE1L is upregulated in BLCA cells and is correlated with tumor progression, poor prognosis, and immune infiltration in bladder cancer. *In vitro* experiments demonstrated that the proliferation, migration, and invasion of BLCA cells can be inhibited by knocking down CSE1L expression.

Data availability statement

The original contributions presented in the study are included in the article/supplementary materials. Further inquiries can be directed to the corresponding authors.

Ethics statement

The studies involving humans were approved by IRB of Beijing Tiantan Hospital, Capital Medical University {KY2024-005-01}. The studies were conducted in accordance with the local legislation and institutional requirements. The human samples used in this study were acquired from primarily isolated as part of your previous study for which ethical approval was obtained. Written informed consent for participation was not required from the participants or the participants' legal guardians/next of kin in accordance with the national legislation and institutional requirements.

Author contributions

RL: Data curation, Formal analysis, Investigation, Resources, Writing – original draft, Writing – review & editing. ZZ: Investigation, Methodology, Validation, Writing – review & editing. JM: Resources, Software, Writing – review & editing. YZ: Conceptualization, Investigation, Project administration, Supervision, Writing – review & editing.

Funding

The author(s) declare financial support was received for the research, authorship, and/or publication of this article. This study was supported by the National Nature Science Foundation of China (Grant No.82270782).

Acknowledgments

Thanks to Dr. Ning and Dr. Zhai for their technical support and guidance for this study.

Conflict of interest

The authors declare the research was conducted in the absence of any commercial or financial relationships that could be construed as a potential conflict of interest.

The reviewer WD declared a shared parent affiliation, with no collaboration, with the authors to the handling editor at the time of the review.

Publisher's note

All claims expressed in this article are solely those of the authors and do not necessarily represent those of their affiliated organizations, or those of the publisher, the editors and the reviewers. Any product that may be evaluated in this article, or claim that may be made by its manufacturer, is not guaranteed or endorsed by the publisher.

References

1. Sung H, Ferlay J, Siegel RL, Laversanne M, Soerjomataram I, Jemal A, et al. Global cancer statistics 2020: GLOBOCAN estimates of incidence and mortality worldwide for 36 cancers in 185 countries. *CA Cancer J Clin*. (2021) 71:209–49. doi: 10.3322/caac.21660

2. Babjuk M, Burger M, Capoun O, Cohen D, Comperat EM, Dominguez Escrig JL, et al. European association of urology guidelines on non-muscle-invasive bladder cancer (Ta, T1, and carcinoma in situ). *Eur Urol*. (2022) 81:75–94. doi: 10.1016/j.eururo.2021.08.010

3. Witjes JA, Bruins HM, Cathomas R, Comperat EM, Cowan NC, Gakis G, et al. European association of urology guidelines on muscle-invasive and metastatic bladder cancer: summary of the 2020 guidelines. *Eur Urol*. (2021) 79:82–104. doi: 10.1016/j.eururo.2020.03.055

4. Cole CN, Scarcelli JJ. Transport of messenger RNA from the nucleus to the cytoplasm. *Curr Opin Cell Biol*. (2006) 18:299–306. doi: 10.1016/j.ceb.2006.04.006

5. Beck M, Hurt E. The nuclear pore complex: understanding its function through structural insight. *Nat Rev Mol Cell Biol*. (2017) 18:73–89. doi: 10.1038/nrm.2016.147

6. Behrens P, Brinkmann U, Wellmann A. CSE1L/CAS: its role in proliferation and apoptosis. *Apoptosis*. (2003) 8:39–44. doi: 10.1023/A:1021644918117

7. Jiang MC. CAS (CSE1L) signaling pathway in tumor progression and its potential as a biomarker and target for targeted therapy. *Tumour Biol*. (2016) 37:13077–90. doi: 10.1007/s13277-016-5301-x

8. Nagashima S, Maruyama J, Honda K, Kondoh Y, Osada H, Nawa M, et al. CSE1L promotes nuclear accumulation of transcriptional coactivator TAZ and enhances invasiveness of human cancer cells. *J Biol Chem*. (2021) 297:100803. doi: 10.1016/j.jbc.2021.100803

9. Chen B, Khodadoust MS, Liu CL, Newman AM, Alizadeh AA. Profiling tumor infiltrating immune cells with CIBERSORT. *Methods Mol Biol*. (2018) 1711:243–59. doi: 10.1007/978-1-4939-7493-1_12

10. Tran L, Xiao JF, Agarwal N, Duex JE, Theodorescu D. Advances in bladder cancer biology and therapy. *Nat Rev Cancer*. (2021) 21:104–21. doi: 10.1038/s41568-020-00313-1

11. Brinkmann U, Brinkmann E, Gallo M, Pastan I. Cloning and characterization of a cellular apoptosis susceptibility gene, the human homologue to the yeast chromosome segregation gene CSE1. *Proc Natl Acad Sci USA*. (1995) 92:10427–31. doi: 10.1073/pnas.92.22.10427

12. Scherf U, Pastan I, Willingham MC, Brinkmann U. The human CAS protein which is homologous to the CSE1 yeast chromosome segregation gene product is associated with microtubules and mitotic spindle. *Proc Natl Acad Sci USA*. (1996) 93:2670–4. doi: 10.1073/pnas.93.7.2670

13. Tanaka T, Ohkubo S, Tatsuno I, Prives C. hCAS/CSE1L associates with chromatin and regulates expression of select p53 target genes. *Cell*. (2007) 130:638–50. doi: 10.1016/j.cell.2007.08.001

14. Dong Q, Li X, Wang CZ, Xu S, Yuan G, Shao W, et al. Roles of the CSE1L-mediated nuclear import pathway in epigenetic silencing. *Proc Natl Acad Sci USA*. (2018) 115:E4013–E22. doi: 10.1073/pnas.1800505115

15. Li Y, Yuan S, Liu J, Wang Y, Zhang Y, Chen X, et al. CSE1L silence inhibits the growth and metastasis in gastric cancer by repressing GPNMB via positively regulating transcription factor MITF. *J Cell Physiol*. (2020) 235:2071–9. doi: 10.1002/jcp.v235.3

16. Liao CF, Lin SH, Chen HC, Tai CJ, Chang CC, Li LT, et al. CSE1L, a novel microvesicle membrane protein, mediates Ras-triggered microvesicle generation and metastasis of tumor cells. *Mol Med*. (2012) 18:1269–80. doi: 10.2119/molmed.2012.00205

17. Li H, Wang L, Ruan Z, Li X, Yang Y, Fang J, et al. CSE1L as a prognostic biomarker associated with pan cancer immune infiltration and drug sensitivity. *Expert Rev Clin Immunol*. (2024) 20(9):1113–25. doi: 10.1080/1744666X.2024.2356747

18. Liu W, Zhou Z, Li Y, Xu J, Shen Y, Luo S, et al. CSE1L silencing impairs tumor progression via MET/STAT3/PD-L1 signaling in lung cancer. *Am J Cancer Res*. (2021) 11:4380–93.

19. Lee WR, Shen SC, Shih YH, Chou CL, Tseng JT, Chin SY, et al. Early decline in serum phospho-CSE1L levels in vemurafenib/sunitinib-treated melanoma and sorafenib/lapatinib-treated colorectal tumor xenografts. *J Transl Med*. (2015) 13:191. doi: 10.1186/s12967-015-0553-6

20. Lee WR, Shen SC, Wu PR, Chou CL, Shih YH, Yeh CM, et al. CSE1L Links cAMP/PKA and Ras/ERK pathways and regulates the expressions and phosphorylations of ERK1/2, CREB, and MITF in melanoma cells. *Mol Carcinog*. (2016) 55:1542–52. doi: 10.1002/mc.v55.11

21. Levy C, Khaled M, Fisher DE. MITF: master regulator of melanocyte development and melanoma oncogene. *Trends Mol Med*. (2006) 12:406–14. doi: 10.1016/j.molmed.2006.07.008

22. Zhang X, Zhang X, Mao T, Xu H, Cui J, Lin H, et al. CSE1L, as a novel prognostic marker, promotes pancreatic cancer proliferation by regulating the AKT/mTOR signaling pathway. *J Cancer*. (2021) 12:2797–806. doi: 10.7150/jca.54482

23. Lin HC, Li J, Cheng DD, Zhang X, Yu T, Zhao FY, et al. Nuclear export protein CSE1L interacts with P65 and promotes NSCLC growth via NF-kappaB/MAPK pathway. *Mol Ther Oncolytics*. (2021) 21:23–36. doi: 10.1016/j.omto.2021.02.015

24. Duan L, Tadi MJ, Maki CG. CSE1L is a negative regulator of the RB-DREAM pathway in p53 wild-type NSCLC and can be targeted using an HDAC1/2 inhibitor. *Sci Rep*. (2023) 13:16271. doi: 10.1038/s41598-023-43218-3

25. Wang YS, Peng C, Guo Y, Li Y. CSE1L promotes proliferation and migration in oral cancer through positively regulating MITF. *Eur Rev Med Pharmacol Sci*. (2020) 24:5429–35. doi: 10.26355/eurrev_202005_21327

26. Cheng DD, Lin HC, Li SJ, Yao M, Yang QC, Fan CY. CSE1L interaction with MSH6 promotes osteosarcoma progression and predicts poor patient survival. *Sci Rep*. (2017) 7:46238. doi: 10.1038/srep46238

frontiers | Frontiers in Immunology

TYPE Original Research
PUBLISHED 17 October 2024
DOI 10.3389/fimmu.2024.1484226

Check for updates

OPEN ACCESS

EDITED BY
Pengpeng Zhang,
Nanjing Medical University, China

REVIEWED BY
Lei Yin,
Shanghai Jiaotong University School of Medicine, China
Guangyan Zhangyuan,
Shanghai Jiao Tong University, China

*CORRESPONDENCE
Xiumei Wang
hrbwangmei@163.com

†The authors have contributed equally to this work and share first authorship

RECEIVED 21 August 2024
ACCEPTED 24 September 2024
PUBLISHED 17 October 2024

CITATION
Yao L, Liu L, Xu W, Xi H, Lin S, Piao G, Liu Y, Guo J and Wang X (2024) mRNA-seq-based analysis predicts: AEG-1 is a therapeutic target and immunotherapy biomarker for pan-cancer, including OSCC. *Front. Immunol.* 15:1484226. doi: 10.3389/fimmu.2024.1484226

COPYRIGHT
© 2024 Yao, Liu, Xu, Xi, Lin, Piao, Liu, Guo and Wang. This is an open-access article distributed under the terms of the Creative Commons Attribution License (CC BY). The use, distribution or reproduction in other forums is permitted, provided the original author(s) and the copyright owner(s) are credited and that the original publication in this journal is cited, in accordance with accepted academic practice. No use, distribution or reproduction is permitted which does not comply with these terms.

mRNA-seq-based analysis predicts: AEG-1 is a therapeutic target and immunotherapy biomarker for pan-cancer, including OSCC

Lihong Yao†, Lixue Liu†, Wanqiu Xu, Hualei Xi, Song Lin, Guiyan Piao, Ying Liu, Jinrong Guo and Xiumei Wang*

Department of Stomatology, The Second Affiliated Hospital of Harbin Medical University, Harbin, Heilongjiang, China

Background: The aberrant expression of AEG-1 is significantly correlated with tumorigenesis, development, neurodegeneration and inflammation. However, the relationship between AEG-1 expression and immune infiltration in OSCC, as well as other tumor types, has yet to be comprehensively analyzed.

Methods: The expression levels, prognostic and clinicopathological characteristics, mutation patterns and methylation landscapes of AEG-1 in various tumors were obtained from multiple databases, including TIMER, GEPIA, HPA, TCGA, UALCAN, cBioPortal, SMART and TISIDB, in addition to single-cell RNA-seq data. The integration of these datasets facilitated the elucidation of the relationships among pan-cancer cellular heterogeneity, immune infiltration and AEG-1 expression levels. *In vitro* experiments created AEG-1 overexpressing cell lines, and mRNA-seq analyzed AEG-1-related differential genes in OSCC. RT-PCR validated these findings *in vivo* using xenograft tumors. Tumor cell lines were developed to study AEG-1's effects through H&E, Masson, and PAS staining. Immunohistochemistry examined AEG-1-related gene expression patterns.

Results: Our analysis demonstrated that AEG-1 is highly expressed across various cancer types and is associated with tumor grade and patient prognosis. Additionally, AEG-1 amplification was observed in multiple cancers. Notably, we identified a significant elevation of AEG-1 expression in OSCC, which strongly correlated with patient prognosis and immune infiltration. Through mRNA-seq analysis of differentially expressed genes and immune-related gene sets, we identified a strong correlation between AEG-1 and immune infiltration markers such as LCP2, CD247, HLA-DPA1, HLA-DRA, HLA-DRB1, CIITA and CD74 in OSCC. Additionally, AEG-1 was found to regulate Th1/Th2 immune homeostasis, promote glycogen accumulation, and contribute to tumor fibrosis.

Conclusion: In conclusion, AEG-1 significantly correlates with prognosis and immune infiltration across various cancer types and holds potential as a novel prognostic immune biomarker for OSCC. This finding may facilitate the identification of patients who are most likely to benefit from adjuvant immunotherapy.

KEYWORDS

AEG-1, pan-cancer, OSCC, immune infiltration, mRNA-seq

1 Introduction

The immune system constitutes the organism's primary defense mechanism against pathogenic invasion, tasked with the detection and elimination of foreign bodies and pathogenic microorganisms. Nonetheless, hyperactivity of the immune system can result in deleterious effects on the organism's organs and tissues (1, 2). Furthermore, the immune system exhibits an antagonistic role in tumorigenesis (3).

Oral squamous cell carcinoma (OSCC) constitutes a significant subset of head and neck squamous cell carcinoma (HNSCC) and continues to be among the most fatal malignancies worldwide (4). The condition exhibits a high prevalence, mortality rate, and teratogenicity, collectively posing a substantial threat to human life and health (5). An increasing body of research has demonstrated that tumor development can be regulated by various genes, proteins, and molecular compounds, enabling tumor cells to evade immune responses, immune surveillance, and develop resistance to chemotherapy. Immunotherapy for tumors aims at modulating various immune processes and critical checkpoints, such as cytotoxic T-lymphocyte-associated antigen-4 (CTLA4) and the programmed death protein 1 (PD-1) along with its ligand (PD-L1) (6, 7). However, only a limited subset of patients derive clinical benefit from these treatments. In the context of clinical pharmacotherapy, the four-year survival outcomes associated with drug K (pembrolizumab) in patients with HNSCC signify a substantial advancement in the application of immunotherapy for recurrent or metastatic HNSCC. This breakthrough has garnered significant attention towards HNSCC within the broader scientific community and represents a noteworthy advancement in oncology. However, the overall survival rate for patients with OSCC has not shown substantial improvement, with the 5-year survival rate persisting below 50% (8, 9). Consequently, it is crucial to identify novel immunotherapeutic targets capable of overcoming tumor resistance and eliciting a robust immune response to eradicate tumor cells, thereby enhancing patient survival and quality of life.

The Astrocyte Elevated Gene-1 (AEG-1), also referred to as MTDH or LYRIC (10), is located on chromosome 8q22.20 (11) and is characterized by rapid subtraction hybridization (RaSH). AEG-1 was initially identified in primary human fetal astrocytes (PHFAs) through RaSH as an inducible gene for HIV-, gp120-, and tumor necrosis factor-α (TNF-α) (12–17). Its primary localization site has been identified as the endoplasmic reticulum (ER). AEG-1 is markedly overexpressed in various cancers, facilitating several oncogenic characteristics such as proliferation, invasion, metastasis, angiogenesis, and chemoresistance (18). Additionally, it is regulated by miRNAs (19). These pathways, including phosphatidylinositol-3-kinase/AKT (PI3K/AKT), NF-κB, mitogen-activated protein kinase (MAPK), and Wnt signaling, mediate the oncogenic function of AEG-1 and regulate angiogenesis and drug resistance. Nevertheless, the relationship between these factors and tumor immune cell infiltration remains to be fully elucidated.

In this context, we performed an analytical study utilizing public databases and mRNA-seq data to thoroughly investigate the role of AEG-1 in OSCC compared to other tumor types. Our research specifically involved mRNA expression profiling, prognostic value analysis, differential expression gene ontology analysis, and examination of correlations with tumor-infiltrating immune cells. This approach aimed to elucidate the relationship between AEG-1 expression, favorable overall survival in OSCC, and the positive modulation of the immune response in OSCC. These findings suggest that AEG-1 expression could function as a prognostic indicator and a critical biomarker for informing therapeutic strategies in patients with OSCC.

2 Materials and methods

2.1 AEG-1 gene expression analysis

The TIMER database (https://cistrome.shinyapps.io/timer/) (20)is an analytical network about the infiltration of tumor-infiltrating immune cells (21). In addition to evaluating the infiltration levels of tumor-infiltrating immune cells, the database also examines gene expression disparities between tumor tissues and normal tissues. Given that the TIMER database exclusively incorporates TCGA data and does not provide exhaustive coverage of specific tumor types, we performed a supplementary search utilizing both TCGA and GTEx data through the GEPIA database (http://gepia.cancer-pku.cn) (22) to identify tumors not represented

in TIMER. To determine significant differences, we utilized the Wilcoxon test. Additionally, the expression level of the AEG-1 protein in HNSC was analyzed using data from HPA database (https://www.proteinatlas.org/) (23).

2.2 Prognostic and clinicopathological characterization of AEG-1

Clinical data for 33 tumor types were obtained from the TCGA database. Four survival outcomes were chosen for analysis: overall survival (OS) (24), disease-free survival (DFS) (25), disease-specific survival (DSS) (26), and progression-free survival (PFS) (24). The aim was to determine the association between AEG-1 expression and the prognosis of these 33 cancers. Cox regression analysis was employed, and the results were visualized using a forest plot. The UALCAN database (ualcan.path.uab.edu/analysis) (27) serves as a comprehensive, user-friendly, and interactive web resource for the analysis of cancer-related omics data, offering access to publicly available datasets such as TCGA, MET500, CPTAC, and CBTTC. This database investigated the correlation between AEG-1 expression and various clinical parameters, including age, gender, weight, and tumor grading, in patients diagnosed with HNSC.

2.3 Mutation analysis of AEG-1

The cBioPortal (https://www.cbioportal.org/) (28) is a web-based platform to analyze oncogenomic characterization of the AEG-1 gene. The database was employed to investigate the mutation frequency of AEG-1.

2.4 AEG-1 with TMB, MSI, and DNA methylation analysis

Tumor mutation burden (TMB) (29), defined as the total number of somatic cell-based coding errors, including base substitutions and insertion-based errors per million bases, is the most recent biomarker for evaluating the efficacy of PD-1 antibodies and their impact on tumors. Microsatellite instability (MSI) (30) represents a phenomenon wherein a microsatellite allele at a specific locus in a tumor arises due to the insertion or deletion of a repetitive unit, as compared to normal tissue. This marker is clinically significant due to functional defects in DNA mismatch repair mechanisms within tumor tissues.

DNA methylation constitutes a chemical alteration of DNA, characterized by the covalent attachment of a methyl group to the 5-carbon position of cytosine within a CpG dinucleotide, a process facilitated by DNA methyltransferase (31). This epigenetic modification induces alterations in chromatin structure, DNA conformation, DNA stability, and the interaction of DNA with proteins, thereby modulating gene expression. Employing the SMART (http://www.bioinfo-zs.com/smart) tool, we analyzed AEG-1 DNA methylation in tumor samples (32).

2.5 Correlation of AEG-1 with tumor immunity

The TISIDB database (http://cis.hku.hk/TISIDB/index.php) (33) encompasses ten principal sections dedicated to the analysis of the relationships between tumor immune cell infiltration, immunochemokines, lymphocytes, immunosuppressants, immune activators, and immune molecule subtypes. Using TISIDB, the correlation between AEG-1 and tumor immune cell infiltration and immune molecular subtypes was systematically investigated.

2.6 AEG-1 single-cell analysis

The CancerSEA database (http://biocc.hrbmu.edu.cn/CancerSEA/) (34) constitutes the inaugural specialized repository dedicated to comprehensively elucidating the diverse functional states of cancer cells at single-cell resolution. This resource enables the analysis of a broad spectrum of relevant cellular functions, including angiogenesis, cell cycle regulation, DNA damage response, epithelial-to-mesenchymal transition (EMT), inflammation, metastasis, gene silencing, apoptosis, differentiation, DNA repair, hypoxia, invasion, proliferation, and sensitization. The influence of AEG-1 on the biological functions of various cancer cell types was investigated using this database.

2.7 Cell culture and plasmid transfection

The SCC15 cell line was utilized in this study, maintained in DMEM basal medium supplemented with 10% FBS and 1% double-antibody. This approach ensured optimal growth and experimental conditions for all cell lines. Furthermore, routine monitoring for mycoplasma contamination was conducted before initiating any experimental procedures. Shanghai Gikai constructed the AEG-1 overexpressing lentivirus, the viral titer was adjusted by the lentivirus transfection manual, and puromycin selection was employed. The cell lines utilized in this study were provided by Xiu-Mei Wang, a member of our research group (35).

2.8 Quantitative real-time PCR

Total RNA was extracted utilizing TRIzol reagent (TAKARA, Japan). cDNA synthesis was performed using PrimeScript RT kit with gDNA Eraser (TAKARA, Japan). The expression level of the gene was quantified by real-time fluorescence quantitative PCR(RT-PCR) using SYBR Premix Ex Taq (TAKARA, Japan). The relative expression of mRNA was calculated using the 2 ΔΔCt method and normalized to the reference gene to correct for non-specific experimental variation (Supplementary Table 1).

2.9 mRNA-seq and bioinformatics analysis

Cell samples were meticulously gathered for mRNA-seq analysis after successfully constructing the AEG-1 overexpression SCC15 cell line. This component of the experiment was conducted by LC-Biotechnology Company. The data were analyzed using the company's UNIKAWA Cloud Platform Interactive System. Per your request, the raw sequencing results have been uploaded to NutCloud (https://www.jianguoyun.com/c/sd/19a6ec9/4185bef735a28a76). Following genomic localization, the highly regarded Stringtie software (version 1.3.0) was employed to generate and annotate fragment per kilobase per million exons (FPKM) values. The threshold for statistical significance was set at a p-value corresponding to a false discovery rate (FDR) of 0.05. This resulted in the categorization of mRNAs exhibiting a 2-fold change as differentially expressed. Two groups of differentially expressed genes (DEGs) were subjected to enrichment analysis using the Gene Ontology (GO) and the Kyoto Encyclopedia of Genes and Genomes (KEGG). The immune infiltration gene set was obtained from the Immpot database; the intersection set was taken through the Venny database (https://bioinfogp.cnb.csic.es/tools/venny/index.html) (34) and the STRING database (https://cn.string-db.org/cgi/INPUT) (36) for protein network interactions. The gene clusters obtained from Cytoscape (37) were again analyzed for GO and KEGG enrichment by applying the INPUT2.0 database.

2.10 Protein-protein interaction docking analysis

Protein docking is a computational method to predict the interactions and mutual recognition between proteins. ZDOCK is a rigid-body protein docking algorithm that utilizes the Fast Fourier Transform Correlation technique. In contrast, RDOCK is an energy optimization process based on the CHARMm force field. RDOCK is employed to refine the binding conformations of protein-protein complexes identified by ZDOCK and to evaluate these conformations using an energy-scoring function.

2.11 Apoptosis staining

The cells were inoculated into 96-well plates at a predetermined concentration and cultured for 24 hours. Following incubation, the medium was removed, and the cells were washed twice with phosphate-buffered saline (PBS). Subsequently, the cells were stained according to the protocol provided by the Wanlei Annexin V-FITC/PI Apoptosis Detection Kit. The stained cells were then examined and imaged using a fluorescence-inverted microscope. The excitation wavelength for Annexin V-FITC was 488 nm, and the emission wavelength was 530 nm, resulting in green fluorescence. The excitation wavelength of propidium iodide is 488 nm, and the emission wavelength is 630 nm, resulting in red fluorescence.

2.12 Construction of xenograft tumors

Female BALB/c mice, aged between four and six weeks, were procured from the Beijing Viton Lever Laboratory Animal Center. To establish the xenograft tumor model, 1×10^7 SCC15 cells and overexpressing AEG-1 were subcutaneously injected into the dorsal abdomen of the mice. Before the initiation of the study, a qualified veterinarian verified the health status of each mouse. The mice were housed in a controlled environment featuring a 12-hour light/dark cycle and provided ad libitum access to food and water. The subjects were randomly allocated into two groups: a control group (CTRL) and an experimental group (OV) comprising five mice. One month following the initiation of the study, all mice were humanely euthanized, and tumor tissues were harvested for further analysis. The animal experiments were conducted with the approval of the Ethics Committee of the Second Hospital of Harbin Medical University (YJSDW2023-121).

2.13 H&E staining

Tumor tissues were immersed in 4% PFA and fixed at room temperature. After 24 hours, the tissues were dehydrated using a tissue processor. Subsequently, the tissues were embedded in paraffin wax and sectioned into continuous thin slices 4μm thick. The sections were then baked in an oven at 60°C for 1h, followed by a dewaxing procedure to remove residual wax. Following hydrochloric acid-alcohol differentiation, the samples were rinsed with distilled water and stained with hematoxylin for 5min and eosin for 2min. The sections were then mounted using neutral gum, examined microscopically, and photographed for documentation.

2.14 PAS staining

The slices should be subjected to baking at 60°C for 1h. A dewaxing process and subsequent washing with distilled water should follow this. After that, staining should be conducted using the protocol specified in the PAS kit supplied by BASO. Subsequently, the slices should be sealed with neutral resin, observed under a microscope, and photographed.

2.15 Masson staining

The tissue sections were subjected to a baking process at 60°C for 1h, then dewaxed with water and washed with distilled water. Staining was performed using the protocol outlined in the Masson Staining Kit (Solebel). Post-staining, the sections were sealed with neutral resin, examined microscopically, and documented through photomicrography.

2.16 Immunohistochemical staining

Antigen retrieval was performed using an autoclave following the dewaxing of tissue sections in water. The sections were then allowed to return to room temperature and treated with 3% hydrogen peroxide for 10min. 3%BSA was applied to block non-specific binding sites. The sections were then incubated overnight with the primary antibody at 4°C (Supplementary Table 2). The following day, the sections were incubated with the secondary antibody at ambient temperature for one hour. Positive signals were visualized in brown using DAB as a chromogenic substrate. The nuclei were counterstained with hematoxylin for 4min. After that, the sections were mounted with a neutral dendrimer, examined under a microscope, and photographed for documentation.

2.17 Statistical methods

The statistical analysis and generation of figures were conducted using the R language, version 4.0.2, and GraphPad Prism 9.0. In cases where the objective is to compare continuous variables between two groups, the decision between the Student *t*-test and the Mann-Whitney test is contingent upon the specific conditions at hand. In the case of multiple groups, either one-way ANOVA or the Kruskal-Wallis test with subsequent multiple comparisons was employed, contingent on the circumstances. The prognostic significance of categorical variables was determined using the log-rank test. The threshold for statistical significance was set at a *P*-value.

3 Results

3.1 Expression of AEG-1 in tumors and its prognostic value

To investigate the expression of AEG-1 in tumors, we analyzed the expression of AEG-1 mRNA in 33 cancer types using the TIMER database. The results indicated that AEG-1 was highly expressed in Breast invasive carcinoma (BRCA), Cholangio carcinoma (CHOL), Colon adenocarcinoma (COAD), Esophageal carcinoma (ESCA), HNSC, Kidney Renal Clear Cell Carcinoma (KIRC), Liver hepatocellular carcinoma (LIHC), Lung adenocarcinoma (LUAD), Lung squamous cell carcinoma (LUSC), Rectum adenocarcinoma (READ), and Stomach adenocarcinoma (STAD), and exhibited low expression in Thyroid carcinoma (THCA) and Uterine Corpus Endometrial Carcinoma (UCEC) (Figure 1A). Due to the unavailability of normal tissue controls for Cervical squamous cell carcinoma (CESC), Lymphoid Neoplasm Diffuse Large B-cell Lymphoma (DLBC), Glioblastoma Multiforme (GBM), Acute Myeloid Leukemia (LAML), Brain Lower Grade Glioma (LGG), Ovarian serous cystadenocarcinoma (OV), Pancreatic adenocarcinoma (PAAD), Pheochromocytoma and Paraganglioma (PCPG), Sarcoma (SARC), Testicular Germ Cell Tumors (TGCT), Thymoma (THYM), and Uterine Carcinosarcoma (UCS) in the TIMER database, we conducted an additional search in the GEPIA database. Notably, AEG-1 exhibited high expression levels in LGG, PAAD, and THYM. However, no significant correlation was observed for CESC, LAML, OV, PCPG, SARC, TGCT, and UCS (Figures 1B, C). This evidence suggests that the abnormal expression of AEG-1 plays a role in tumorigenesis, with predominantly deleterious effects.

The prognosis is influenced by the tumor type, the patient's physical condition, the accessibility of suitable therapeutic interventions, and the promptness with which these interventions are administered. This study investigated the prognostic significance of AEG-1 and various tumors utilizing the GEPIA and Home for Researchers databases. We found that AEG-1 was associated with tumor grade (Figure 1D), negatively correlated with overall OS and DFS in tumor patients (Figure 1E), and was associated with OS in LGG, PAAD, Kidney Chromophobe (KICH), and KIRC, DFS in PAAD and Kidney renal papillary cell carcinoma (KIRP), and DFS in LGG, PAAD, and KIRC. KIRP, DFS in LGG, PAAD, STAD, COAD, Bladder Urothelial Carcinoma (BLCA), KIRC, KIRP, Uveal Melanoma (UVM), and Mesothelioma (MESO), and PFS in LGG, PAAD, STAD, BLCA, KICH, KIRP, UVM, and Adrenocortical carcinoma (ACC) (Supplementary Figure 1), and DMFS, RFS, and DSS in breast, lung, and eye cancers (Supplementary Figure 2). AEG-1 may become a novel tumor prognostic assessment index.

3.2 AEG-1 gene alterations in HNSC and other cancers

Our investigation demonstrated that AEG-1 exhibits a significant positive correlation with TMB and a negative correlation with THCA and UVM in BRCA, LAML, LGG, LUAD, LUSC, Prostate adenocarcinoma (PRAD), and STAD (Figure 2A). AEG-1 was positively correlated with MSI in COAD, KIRC, READ, STAD, TGCT, and UCEC. It is negatively correlated in DLBC, LGG, LUAD, PCPG, and PRAD (Figure 2B).

We also discussed the genetic alterations of AEG-1 in pan-cancer using the cBioPortal database. The frequency of AEG-1 deletion was highest in BRCA (9.23%), which was mainly an amplification mutation, and the mutation was highest in UCEC (3.07), and the second and third highest frequencies of AEG-1 were found in CESC (2.69%) and COAD (2.53%) (Figure 2C). Meanwhile, we examined the DNA methylation levels of various tumors. The results showed that the methylation levels of KIRC, LUSC, PAAD, PRAD, and SARC were higher than those of normal tissues, and the methylation levels of BLCA, BRCA, HNSC, LIHC, THCA, and UCEC were lower than those of normal tissues (Figure 3A). Next, DNA methylation level and

10.3389/fimmu.2024.1484226

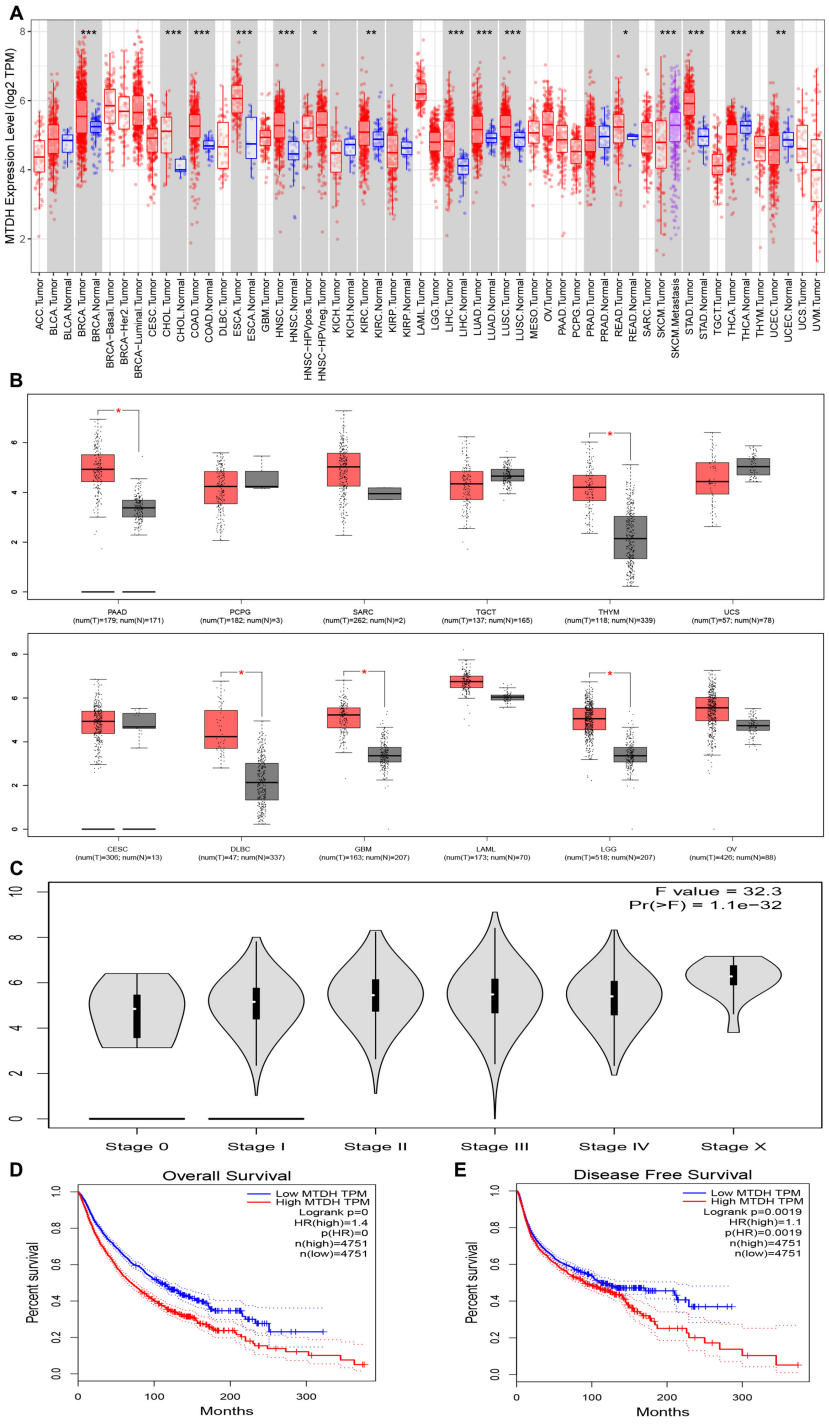

FIGURE 1
AEG-1 expression in pan-cancer from different databases. **(A)** AEG-1 expression in pan-cancer in TIMER. **(B)** AEG-1expression in PAAD, PCPG, SARC, TGCT, THYM, UCS, CESE, DLBC, GBM, LAML, LGG, and OV from the GEPIA database. **(C)** Correlation between AEG-1 and tumor grading. **(D, E)** Correlation between AEG-1 and patients' overall survival (OS) and disease-free survival (DFS). (*, P<0.05; **, P<0.01; ***, P<0.001.).

survival analysis were performed for each CpG site of AEG-1 using SMART (Figure 3B). AEG-1 was found to have 14 methylation probes, such as cg19506380, cg07402337, cg01873391, cg19251280, cg04464219, cg10290527, cg00161931, cg17335114, cg25544073, cg08874788, cg21225450, cg21206266, cg05237543, cg00265490.

3.3 Correlation of AEG-1 with tumor immune cell infiltration, immune subtypes, and molecular subtypes

Tumor-infiltrating immune cells are infiltrating immune cells isolated from tumor tissue. A successful anti-tumor immune

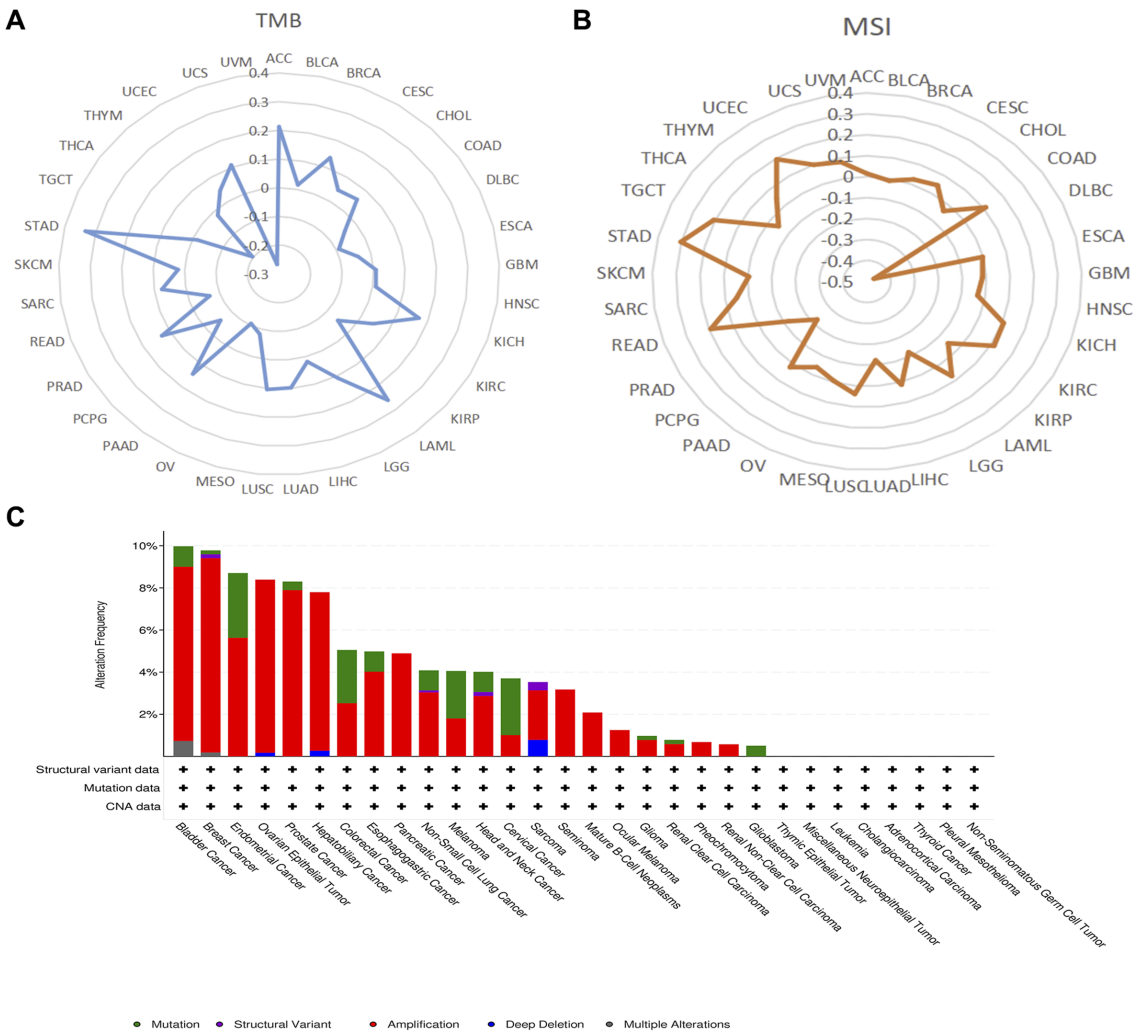

FIGURE 2
The correlation of AEG-1 expression with TMB **(A)**, MSI **(B)**, and genetic alterations of AEG-1 in pan-cancer using the cBioPortal database **(C)**.

response requires the presence, activation, and co-stimulation of all lymphoid-like components of the immune system, including various populations of T cells, B cells, DCs, NK cells, MDSCs, neutrophils, and macrophages. Our analysis showed that AEG-1 was associated with immune cell infiltration in various cancers, from T cell NK to CD^{4+}Th1 and T cell CD^{4+}Th2 (Supplementary Figure 3A). We also evaluated the association of AEG-1 with stromal scores, microenvironment scores, and immune scores in 33 cancers. We found that AEG-1 was associated with ACC, BLCA, BRCA, DLBC, LGG, LIHC, LUAD, LUSCPRAD, READ, SARC, STAD, THCA, THYM, UCEC, and UVM were positively correlated with stromal scores and negatively correlated with stromal scores in TGCT, in ACC, BRCA, CESC, ESCA, HNSC, LIHC, LUAD, LUSC, SARC, Skin Cutaneous Melanoma (SKCM), STAD, TGCT, THCA, and UCEC were positively correlated with microenvironment scores and negatively correlated with UVM; positively correlated with immune scores in CESC, ESCA, HNSC, KIRP, LUAD, LUSC, SARC, SKCM, STAD, TGCT, THCA, UCEC, and negatively correlated in LGG, PCPG, PRAD, UVM. There was no correlation with a stromal score, microenvironment score, and immunity score in CHOL, COAD, GBM, KICH, KIRC, LAML, MESO, OV, PAAD, and UCS.

Furthermore, our analysis revealed that AEG-1 is correlated with the immune subtypes of BLCA, BRCA, COAD, GBM, KIRC, LIHC, LUSC, OV, SKCM, STAD, TGCT, and UCEC (Supplementary Figure 3B), as well as with the molecular subtypes of BRCA, COAD, HNSC, KIRP, LGG, OV, and STAD (Supplementary Figure 3C). These findings unequivocally suggest that AEG-1 is intricately linked to tumor immunity.

To further investigate the potential role of AEG-1 in tumors, we examined the function of AEG-1 at the single-cell level using CancerSEA (Supplementary Figure 4). The results showed that AEG-1 was negatively correlated with metastasis, differentiation, proliferation, inflammation, EMT, and angiogenesis in AML, DNA damage in LUAD, apoptosis in MEL, and invasion in OV, and positively correlated with stemness in MEL.

10.3389/fimmu.2024.1484226

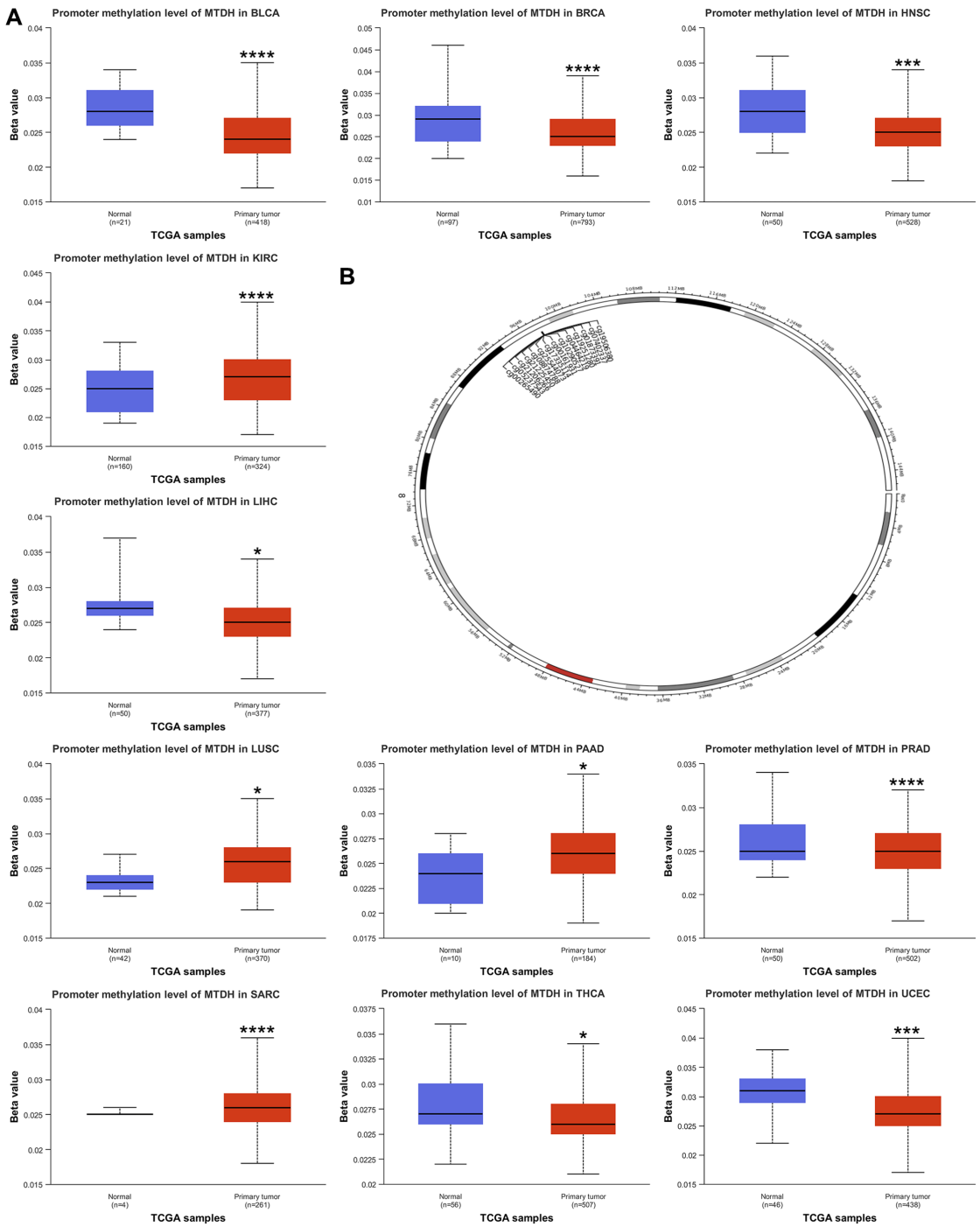

FIGURE 3
Relationship of AEG-1 with methylation. **(A)** Promoter methylation level of BLCA, BRCA, HNSC, KIRC, LIHC, LUSC, PAAD, PRAD, SARC, THCA and UCEC. **(B)** Chromosomal distribution of the methylation probes associated with AEG-1. (*, $P<0.05$; ***, $P<0.001$; ****, $P<0.0001$.).

3.4 Expression, clinical characteristics, correlation and immune cell infiltration of AEG-1 in HNSC

It is established that AEG-1 is closely associated with HNSC, but its correlation with immune cell infiltration in HNSC has not been investigated. Our study confirmed that AEG-1 was highly expressed in OSCC by HPA (Figure 4A); UALCAN discussed the correlation between AEG-1 and clinical characteristics of HNSC and found that AEG-1 was with higher correlation with females than males, and closer correlation with age, body weight, and grading with increasing (Figure 4B). Additionally, AEG-1 demonstrated a correlation with

10.3389/fimmu.2024.1484226

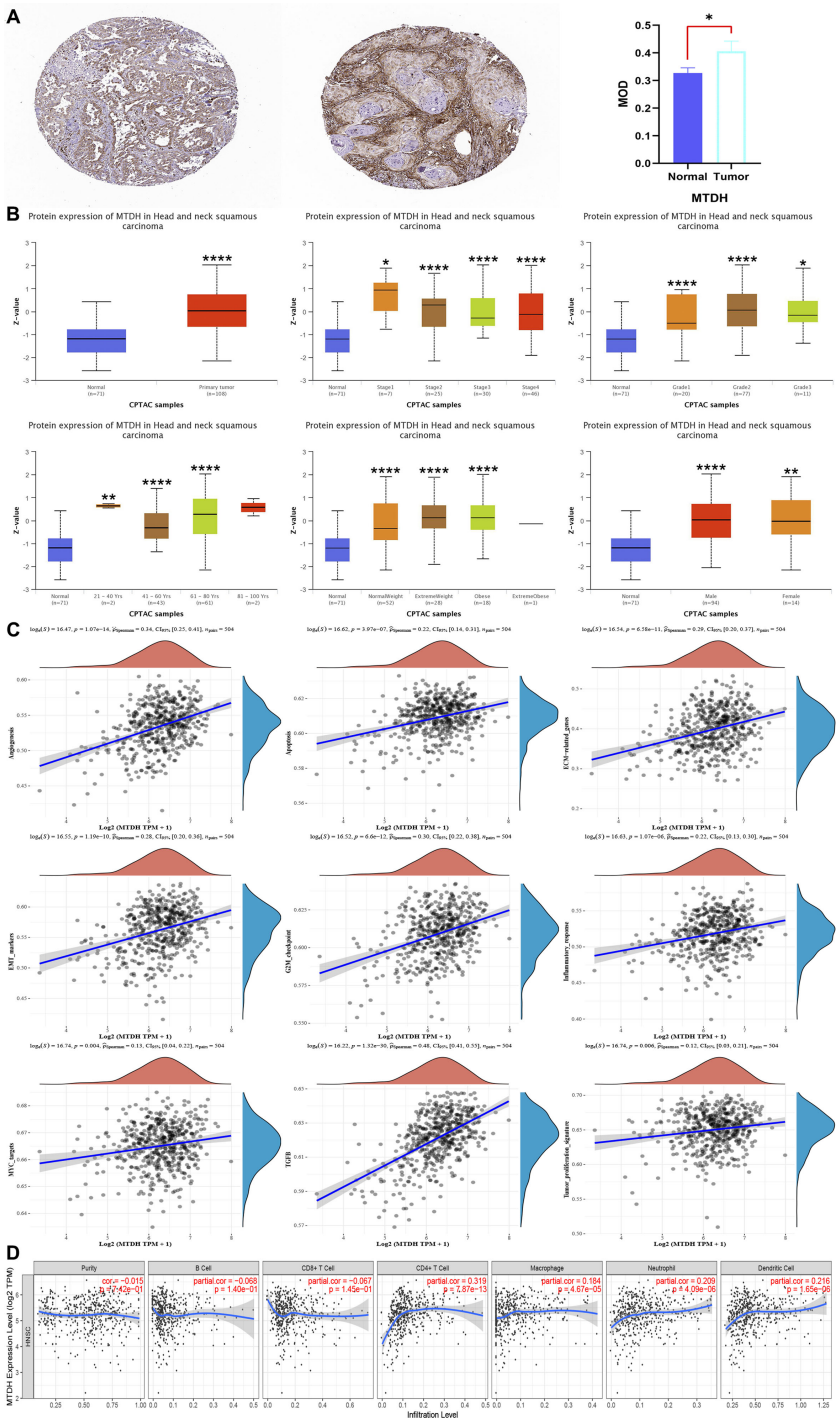

FIGURE 4
AEG-1 expression, clinical features, correlation and immune cell infiltration in HNSC. **(A)** AEG-1 expression in HNSC from the HPA database, normal tissue on the left, HNSC tissue in the middle and quantitative analysis on the right. **(B)** AEG-1 was correlated with HNSC patients' grading, staging, age weight and gender correlation. **(C)** Correlation of AEG-1 with angiogenesis, apoptosis, EMC-related genes, EMT markers, G2M checkpoints, immune response, MYC markers, and tumor proliferation in HNSC. **(D)** Correlation of AEG-1 with immune infiltration of HNSC. n=5. (*, *P*<0.05; **, *P*<0.01; ****, *P*<0.0001.).

angiogenesis, apoptosis, extracellular matrix-related genes, epithelial-mesenchymal transition markers, G2/M checkpoints, immune response, MYC markers, and tumor proliferation in HNSC (Figure 4C).

We also explored the correlation between AEG-1 and immune cell infiltration in HNSC through the TIMER database, and AEG-1 was correlated with CD^{4+} T cells (*P*=7.87e-13), macrophage (*P*=4.67e-05), neutrophil (*P*=4.09e-06), and DCs (*P*=1.65e-06) were significantly positively correlated, with no correlation with B cell and CD^{8+} T cell (Figure 4D). In addition, we analysed other immune-related cells (Supplementary Table 3). To further explore the correlation of AEG-1

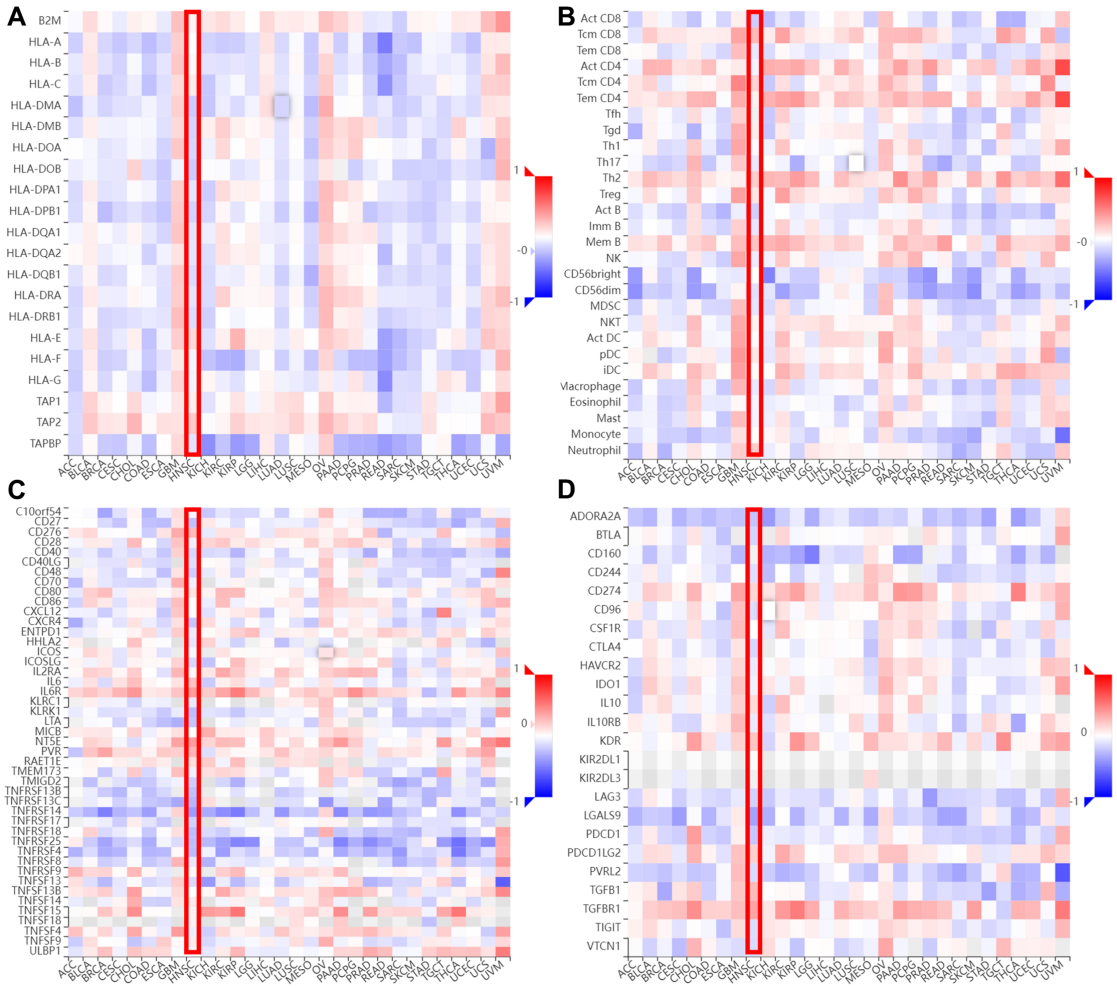

FIGURE 5
The relevance between AEG-1 and chemokines in different cancer types. **(A)**The relevance between AEG-1 methylation status and MHC molecules. **(B)** The relevance between AEG-1 methylation status and Lymphocyte. **(C)** The relevance between AEG-1 methylation status and Immunostimulator. **(D)** The relevance between AEG-1 methylation status and Immunoinhibitor.

with immune molecules, immunostimulatory molecules, immunosuppressive molecules, immunochemokines, and lymphocytes, we also searched by TSIDB (Figures 5A–D). We found that it was correlated with tumor immunotherapy targets BTLA, CTLA4, HAVCR2, LAG3, PDCD1, and TIGIT in HNSC; ICOS were all significantly correlated.

3.5 Identification and analysis of differentially expressed genes associated with AEG-1 in OSCC

To further elucidate the correlation between AEG-1 and immune cell infiltration in OSCC, we engineered OSCC cell lines with overexpressed AEG-1. Our findings indicate that AEG-1 overexpression enhances the expression of SCC15 migration markers while inhibiting apoptosis (Figure 6A). Additionally, mRNA-seq analysis revealed 1016 differentially expressed genes, comprising 413 up-regulated and 603 down-regulated genes (Figures 6B–D). We also performed GO enrichment analysis and found that AEG-1 was mainly localized in the extracellular matrix and cell membrane and was involved in biological processes such as cell adhesion, type I interferon signaling pathway, neurotransmitter secretion, viral defense, IFN-γ-mediated signaling pathway, angiogenesis, and immune response, angiogenesis, and immune response, and possessed 2'-5'-oligomeric adenosine monophosphate synthetase activity, peptidase inhibitor activity, transmembrane protein transporter activity, small molecule binding, CD4 receptor binding, iron ion binding, and calcium ion binding (Figure 7A). At the same time, KEGG was mainly enriched in cytokine-cytokine receptor interaction, Legionnaires' disease, ECM receptor interaction, NOD-like receptor signaling pathway, PI3K-Akt signaling pathway, ferroptosis and MAPK signaling pathway, and other signaling pathways (Figure 7B). GSEA enrichment analysis revealed that AEG-1 was highly associated with IFN-γ, DNA methylation, and programmed cell death in OSCC (Figure 7C).

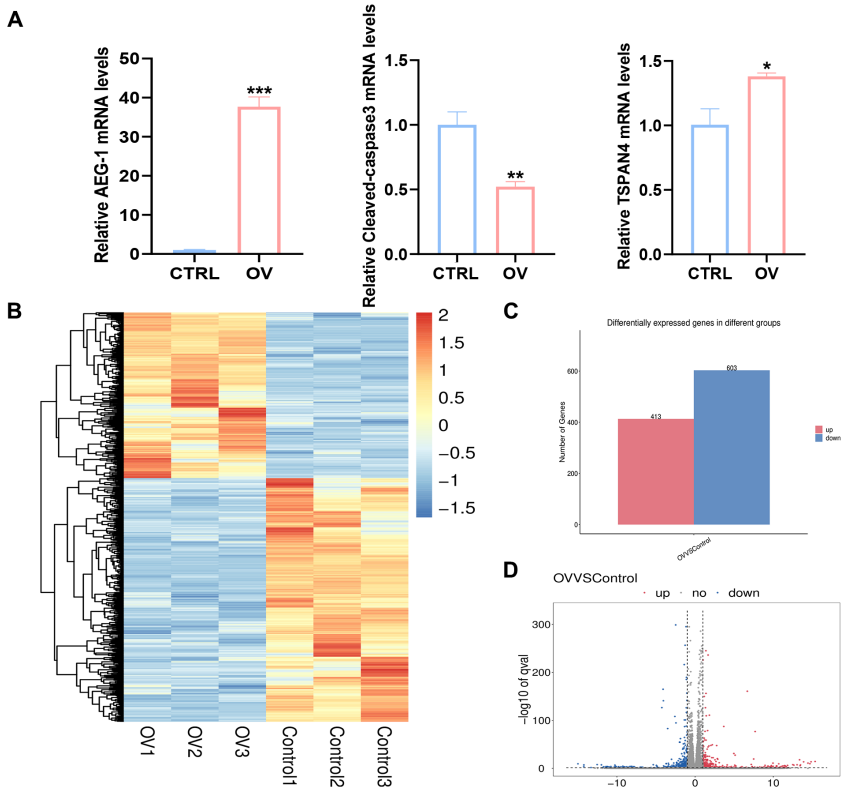

FIGURE 6
AEG-1 transcriptomic analysis after overexpression. **(A)** RT-PCR to detect the correlation of AEG-1 with Caspase3, TSPAN4 **(B)** Heatmap of Hierarchical clustering analysis of changed mRNAs. **(C, D)** mRNAs differentially expressed between CTRL and OV group. (*, $P<0.05$; **, $P<0.01$; ***, $P<0.001$.).

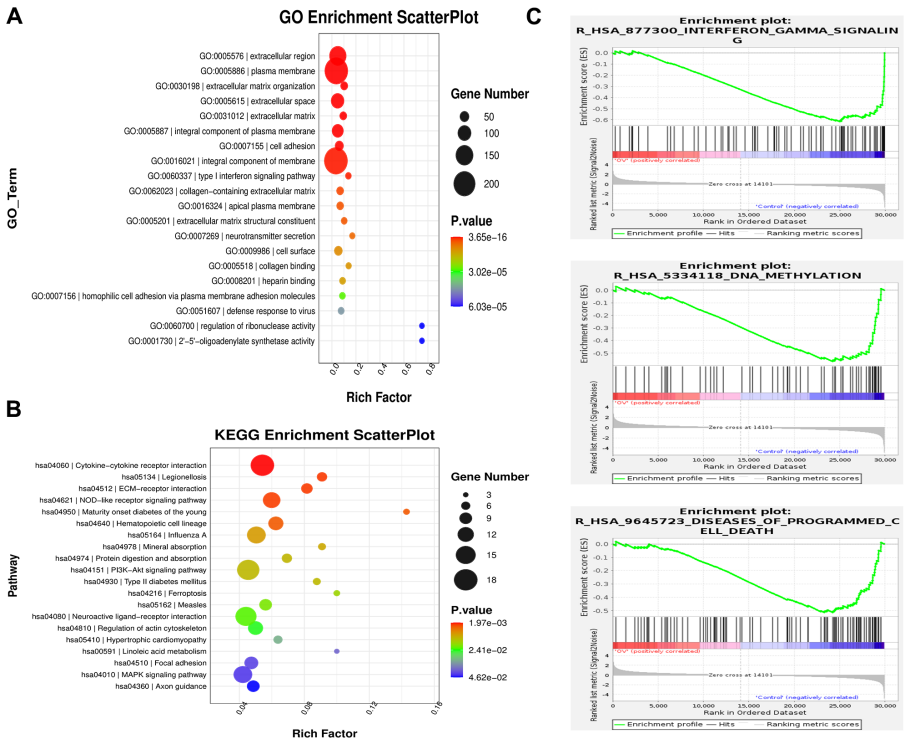

FIGURE 7
AEG-1-related gene enrichment analysis. **(A)** GO analysis of the AEG-1 binding proteins. **(B)** KEGG analysis of the AEG-1 binding proteins. **(C)** GSEA analysis of the AEG-1 binding proteins.

10.3389/fimmu.2024.1484226

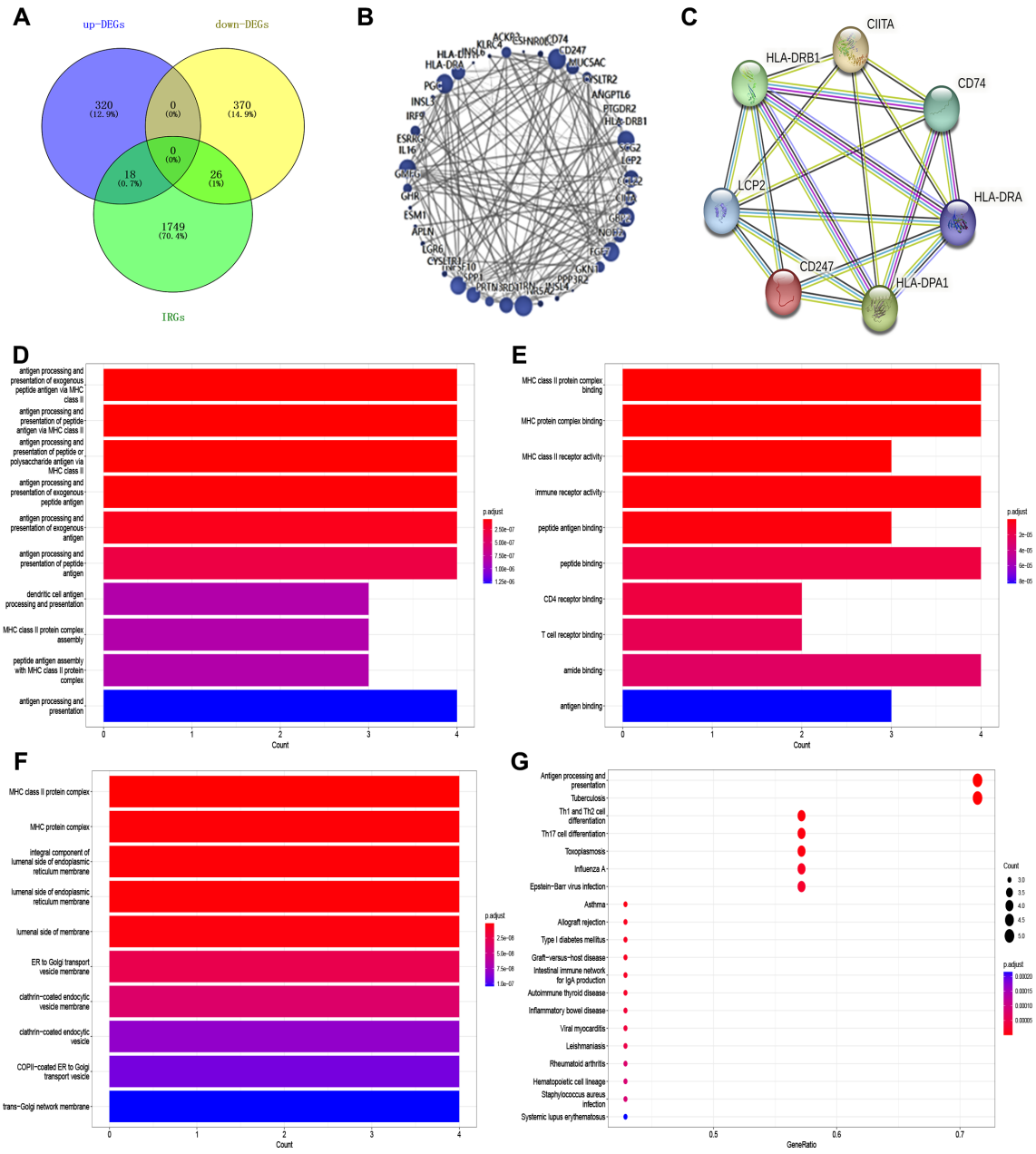

FIGURE 8
AEG-1 is associated with immune-related factors in OSCC. **(A)** Venn's plot to obtain the intersecting genes of AEG-1 overexpressed differential genes with the set of immune-related genes. **(B)** Intersected genes were subjected to PPI. **(C)** Gene clusters were obtained by Cytoscape. **(D)** GO analysis (biological process) of the AEG-1 binding proteins. **(E)** GO analysis (cellular component) of the AEG-1 binding proteins. **(F)** GO analysis (molecular function) of the AEG-1 binding proteins. **(G)** KEGG analysis of the AEG-1 binding proteins.

3.6 AEG-1-related expression of differential genes in OSCC is associated with immune cell infiltration

We acquired the immune cell infiltration gene set, comprising 1,793 genes, from the Immpot database. Subsequently, we enriched this gene set with differentially expressed genes identified through transcriptomic analysis, resulting in 44 differential genes, of which 18 were up-regulated, and 26 were down-regulated (Figure 8A). Concurrently, we conducted PPI analysis using STRING on these 44 differential genes (Figure 8B). Further Cytoscape enrichment analysis identified 7 vital differential genes: LCP2, CD247, HLA-DPA1, HLA-DRA, HLA-DRB1, CIITA and CD74 (Figure 8C). Subsequently, the seven differential genes were subjected to GO and KEGG enrichment analyses, revealing significant associations with Th1/Th2 cells, Th17 cells, and other immune cell types (Figures 8D–G). To elucidate the interaction between AEG-1 and the seven differential genes, we conducted a protein-protein docking analysis using ZDOCK, which allowed us to determine the binding energies of AEG-1 with each of the seven differential

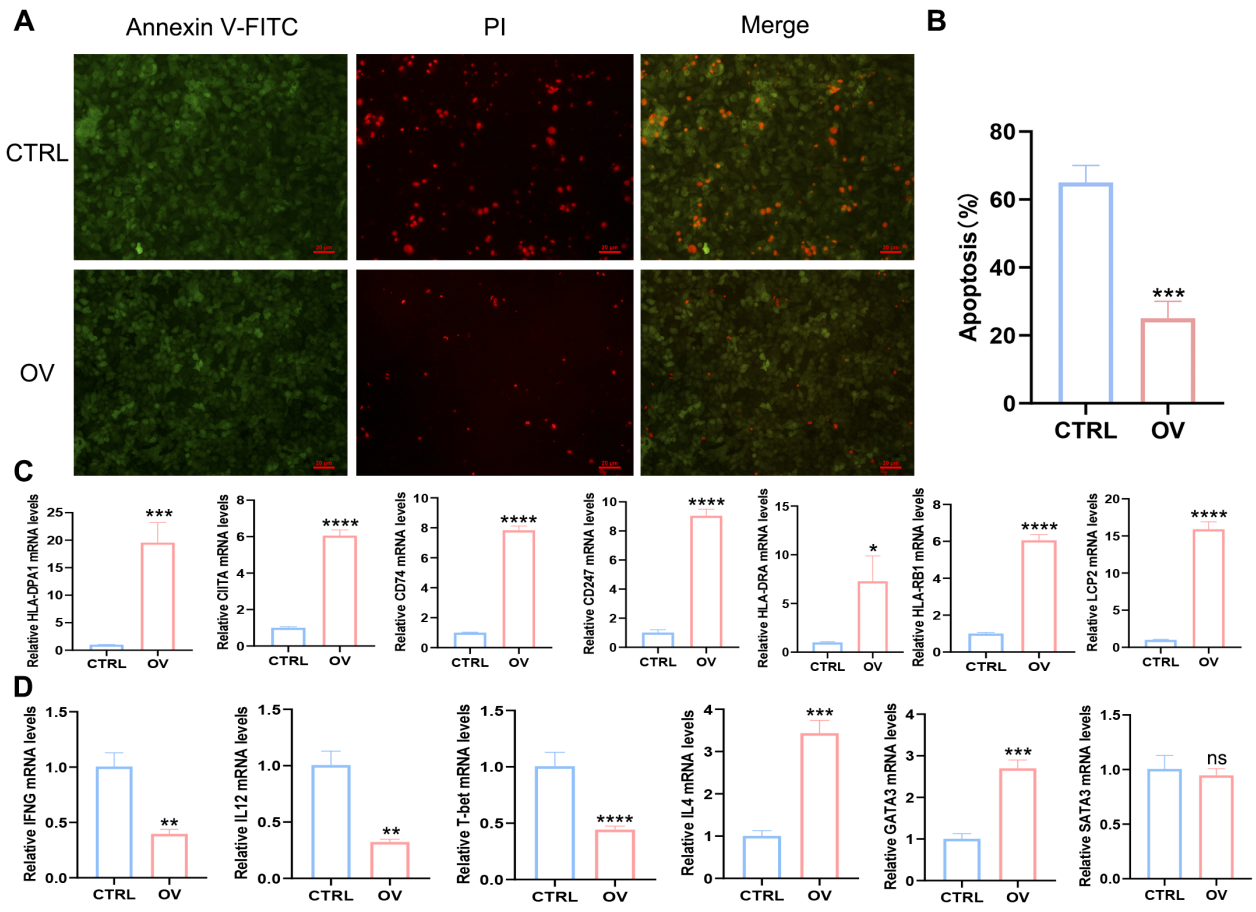

FIGURE 9
AEG-1 is associated with immunity and regulates Th1/Th2 immune homeostasis. **(A, B)** Apoptosis staining to explore the effect of AEG-1 on apoptosis. **(C)** RT-PCR to detect the correlation of AEG-1 with LCP2, CD247, HLA-DPA1, HLA-DRA, HLA-DRB1, CIITA, and CD74. **(D)** RT-PCR was performed to detect the correlation between AEG-1 and Th1-associated factors IFNG, IL12 and T-bet, and Th2-associated factors IL4, GATA3 and STAT3. (ns, $P>0.05$; *, $P<0.05$; **, $P<0.01$; ***, $P<0.001$; ****, $P<0.0001$.).

genes (Supplementary Figure 5). These findings suggest that AEG-1 may serve as an immune prognostic marker for OSCC.

3.7 AEG-1 is associated with OSCC immunity and affects Th1/Th2 immune balance

Our study demonstrated that AEG-1 induces apoptosis in SCC15 cells, as evidenced by apoptosis staining (Figures 9A, B). RT-PCR analysis further revealed that SCC15 cells overexpressing AEG-1 exhibited a strong association with immune-related factors, including HLA-DPA1, CIITA, CD74, CD247, HLA-DRA, LCP2, and HLA-DRB1 (Figure 9C). Additionally, AEG-1 overexpression promoted the expression of Th2-related factors IL4 and GATA3 while inhibiting the expression of Th1-related factors IFN-γ, IL12, and T-bet (Figure 9D).

The *in vivo* establishment of xenograft tumors and PAS and Masson's staining demonstrated that AEG-1 promotes tumor growth(Supplementary Figure 6), significantly enhanced glycogen accumulation and fibrosis within tumor tissues compared to the control group (Figure 10A). Furthermore, IHC analysis revealed an up-regulation of immune-related factors HLA-DPA1 and CIITA in tumor tissues overexpressing AEG-1 (Figures 10B–D).

4 Discussion

AEG-1, an HIV- and TNF-α-inducible gene (18) in PHFAs, is predominantly localized in the endoplasmic reticulum and is implicated in the initiation, progression, and metastasis of breast (38), gastric (39), liver (8), and OSCC. This study reveals the gene expression, prognosis, alteration, immune infiltration, and DNA methylation of AEG-1 in pan-cancer, elucidating its development and prospective role. This was accomplished by utilizing the TIMER, GEPIA, and TISIDB databases derived from the TCGA, GTEx, and UALCAN repositories.

The findings of our study demonstrate that AEG-1 is markedly expressed in 16 types of cancers, whereas its expression is low in THCA and UCEC. This differential expression implies that AEG-1

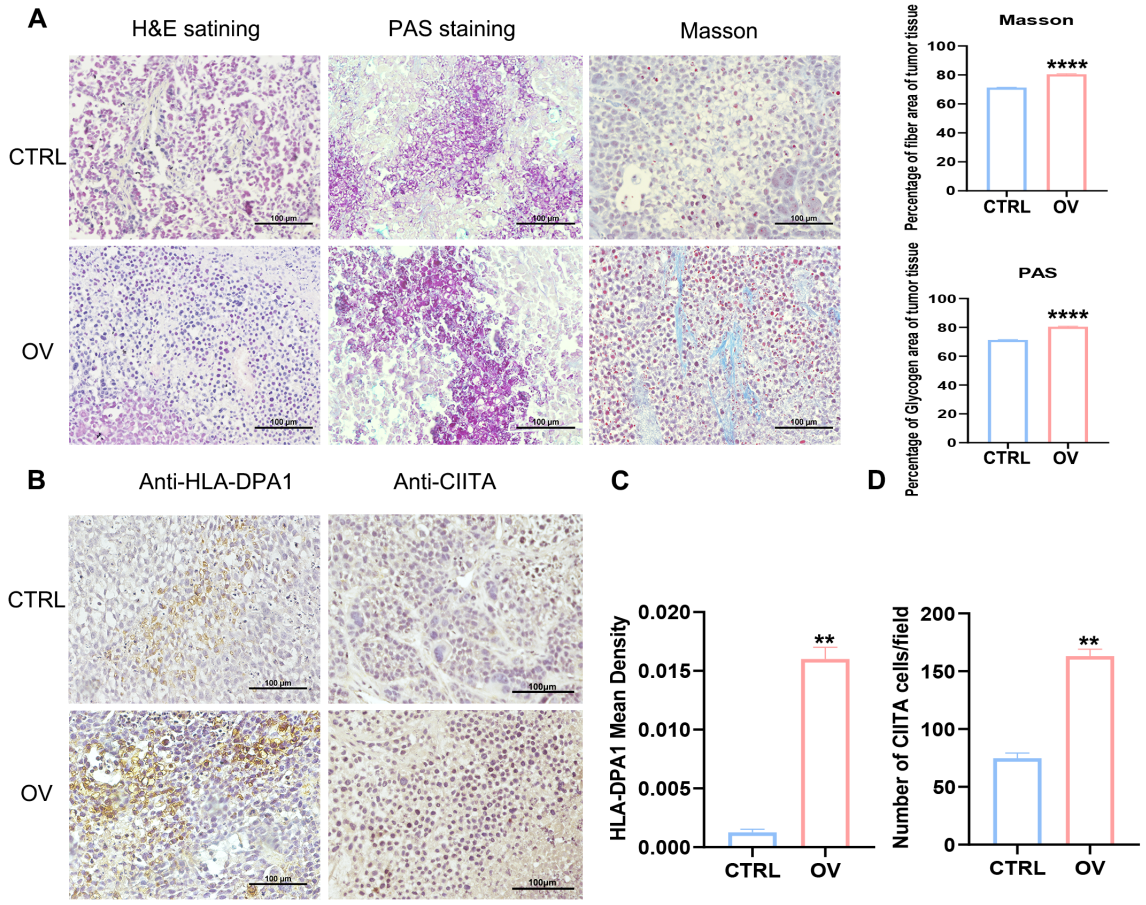

FIGURE 10
AEG-1 affects tumor immunity. **(A)** The effect of AEG-1 on tumors was explored by H&E staining, PAS staining and Masson staining. **(B–D)** Immunohistochemistry probed the correlation of AEG-1 with immune-related factors HLA-DPA1 and CIITA in tumor tissues. n=3. (**, *P*<0.01; ****, *P*<0.0001.).

may have varying functional roles across tumor types. Furthermore, AEG-1 expression is associated with OS, DFS, DSS and PFS in PAAD, suggesting its potential as a prognostic biomarker for PAAD. Additionally, prior research by our group has established that AEG-1 is significantly expressed in OSCC.

Furthermore, AEG-1 has been demonstrated to enhance the proliferation, migration, invasion, and EMT of OSCC. However, the association between AEG-1 and immune infiltration in OSCC remains inadequately understood. Consequently, this study aims to elucidate the relationship between AEG-1 and immune infiltration in both OSCC and pan-cancer contexts.

The current biomarkers associated with the efficacy of immunotherapy encompass but are not limited to, PD-L1 expression, MSI status, TMB, Epstein-Barr virus (EBV) infection status, and tumor-infiltrating lymphocytes (TILs). Our study identified a significant correlation between AEG-1 and TMB and MSI across various tumor types in a pan-cancer analysis. Notably, AEG-1 exhibited a positive association with both TMB and MSI in STAD, indicating that AEG-1 may serve as a potential immunotherapeutic biomarker for STAD. Furthermore, analyses of tumor immune cell infiltration, immunosubtyping, and molecular subtyping revealed that AEG-1 was negatively correlated with T cell NK in 27 out of 33 cancers, positively correlated with Th2 in 27 cancers, and negatively correlated with Th1 in 29 cancers. It can thus be postulated that AEG-1 may impede the secretion of Th2-associated factors by promoting the secretion of Th2-related factors, which in turn inhibits Th1 differentiation and attenuates T cell NK's ability to regulate the recruitment and function of other immune cells through the secretion of cytokines, thus exerting a pro-tumorigenic effect.

Furthermore, we examined the association between AEG-1 and immune cell infiltration in OSCC. Our findings indicated that AEG-1 is correlated with several clinical parameters in HNSC patients, including OS, gender, age, body weight, tumor grade, and stage. Additionally, AEG-1 was found to be associated with various biological processes, such as angiogenesis, apoptosis, ECM-related genes, EMT markers, G2/M checkpoints, immune response, MYC markers, tumor proliferation, and TGF-β signaling. Furthermore, an analysis utilizing the TSIDB database uncovered a significant correlation between AEG-1 and several key factors, including the tumor-promoting cell Th2, immune activator IL6, CXCR4,

immunosuppressants CTLA4, IL1, IDO1, LAG3, PDCD1, TGFB1, and the DHC molecule HLA-DPA1. These findings support the hypothesis that AEG-1 is integral to the immunotherapy of HNSC.

Research indicates that excessive glycogen accumulation, resulting from liquid-liquid phase separation, leads to the inactivation of the Hippo pathway (40). This inactivation inhibits cellular carcinogenesis and concurrently enhances the activity of the downstream proto-oncoprotein YAP, thereby promoting tumor development. Additionally, fibrosis within tumors represents the body's response to malignancy and further contributes to tumor growth and metastasis. We developed a nude mouse tumor model through the establishment of an OSCC cell line with overexpression of AEG-1. Our findings indicate that AEG-1 facilitates glycogen accumulation and fibrosis within tumors, thereby providing compelling evidence that AEG-1 plays a significant role in promoting tumorigenesis and tumor progression.

DCs constitute a distinct class of immune cells distributed across various organs. They are classified as antigen-presenting cells owing to their capacity to present antigens—molecular structures characteristic of organ cells—to T cells, thereby initiating an immune response. Within the tumor microenvironment, dendritic cells perform the functions of antigen uptake, processing, and presentation, which subsequently activates the T-cell-mediated immune response targeting tumor cells. Due to their involvement in tumorigenesis and progression, DCs have been extensively utilized in tumor immunotherapy (41). Furthermore, dendritic cells facilitate the proliferation and maturation of B lymphocytes and activate Th cells and NK cells, thereby enhancing immune function through multiple pathways (42). Our study identified a significant correlation between AEG-1 and immune-related genes, including HLA-DPA1, CIITA, HLA-DRB1, CD74, HLA-DRA, LCP2, and CD247. This association was elucidated through an integrative approach combining mRNA-seq and biosignature analysis. HLA-DPA1, CIITA, HLA-DRB1, and HLA-DRA have been identified as critical markers for dendritic cells (DCs). CD74 and LCP2 serve as markers for lymphocytes, whereas CD247 is indicative of natural killer (NK) cells. Consequently, it can be hypothesized that AEG-1 influences immune function through multiple pathways, including the modulation of B lymphocyte proliferation and maturation, as well as the regulation of Th cell and NK cell activation via DC surface markers. Therefore, AEG-1 emerges as a potential novel target for immunotherapy in OSCC.

In recent years, a growing body of evidence has demonstrated that T-cell immunity, activated by DC vaccines (43), plays a pivotal role in the anti-tumor response and is being investigated for its potential across a spectrum of clinical applications, including melanoma, renal cancer, prostate cancer, bladder cancer, gastrointestinal tumors, gynecological tumors, and endocrine tumors, among others. These studies have indicated that DC vaccines can reduce tumor recurrence rates and enhance patient survival outcomes. The data from a real-world study of Provenge (sipuleucel-T), the first dendritic cell vaccine approved in the United States, has been published. This study examined the survival outcomes of patients with metastatic castration-resistant prostate cancer (mCRPC) who received the cancer therapeutic vaccine Provenge in conjunction with oral medication in a real-world clinical setting. The findings indicated a 45% reduction in mortality risk among prostate cancer patients, alongside an extension in OS by 14.5 months. In summary, AEG-1 is closely linked to DC and disrupts immune function through multiple mechanisms. Consequently, a DC-based vaccine may represent a promising therapeutic strategy for OSCC.

Data availability statement

The original contributions presented in the study are included in the article/Supplementary Materials, further inquiries can be directed to the corresponding author.

Ethics statement

The animal study was approved by the approval of the Ethics Committee of the Second Hospital of Harbin Medical University. The study was conducted in accordance with the local legislation and institutional requirements.

Author contributions

LY: Writing – review & editing, Writing – original draft, Visualization, Validation, Supervision, Software, Resources, Project administration, Methodology, Investigation, Funding acquisition, Formal analysis, Data curation, Conceptualization. LL: Writing – review & editing, Writing – original draft, Visualization, Validation, Supervision, Software, Resources, Project administration, Methodology, Investigation, Funding acquisition, Formal analysis, Data curation, Conceptualization. WX: Writing – review & editing, Writing – original draft, Investigation. HX: Writing – original draft, Investigation, Formal analysis, Data curation. SL: Writing – review & editing, Writing – original draft, Investigation, Formal analysis, Data curation. GP: Writing – review & editing, Writing – original draft, Investigation. YL: Writing – review & editing, Writing – original draft, Investigation. JG: Writing – review & editing, Writing – original draft, Investigation. XW: Writing – review & editing, Writing – original draft, Supervision, Resources, Project administration, Funding acquisition.

Funding

The author(s) declare that financial support was received for the research, authorship, and/or publication of this article. This work was financially supported by the Central Support for the Reform and Development of Local Universities Project investigated the

influence and mechanism of PLP1 point mutation on the occurrence of neurological diseases. Funding for the Reserve Leader of Provincial Leading Talent Echelon (0401-21992139923).

Acknowledgments

We thank LC-Bio Technologies for the data analysis.

Conflict of interest

The authors declare that the research was conducted in the absence of any commercial or financial relationships that could be construed as a potential conflict of interest.

Publisher's note

All claims expressed in this article are solely those of the authors and do not necessarily represent those of their affiliated organizations, or those of the publisher, the editors and the reviewers. Any product that may be evaluated in this article, or claim that may be made by its manufacturer, is not guaranteed or endorsed by the publisher.

Supplementary material

The Supplementary Material for this article can be found online at: https://www.frontiersin.org/articles/10.3389/fimmu.2024.1484226/full#supplementary-material

References

1. Silva JF, Olivon VC, Mestriner FLAC, Zanotto CZ, Tostes RC. Acute increase in O-glcNAc improves survival in mice with LPS-induced systemic inflammatory response syndrome. *Front Physiol*. (2020) 10:1614. doi: 10.3389/fphys.2019.01614

2. Li F, Tian Z. The liver works as a school to educate regulatory immune cells. *Cell Mol Immunol*. (2013) 10:292–302. doi: 10.1038/cmi.2013.7

3. Yuan J, Wang Y, Cao Y, Yue S, Li X, K. S. Retracted] application of nanoparticles in diagnosis and treatment of pancreatic cancer. *Bioinorg Chem Appl*. (2022) 2022:7803001. doi: 10.1155/2022/7803001

4. You Y, Tian Z, Du Z, Wu K, Xu G, Dai M, et al. M1-like tumor-associated macrophages cascade a mesenchymal/stem-like phenotype of oral squamous cell carcinoma *via* the IL6/Stat3/THBS1 feedback loop. *J Exp Clin Cancer research: CR*. (2022) 41:10. doi: 10.1186/s13046-021-02222-z

5. Zhao W, Cui Y, Liu L, Qi X, Liu J, Ma S, et al. Splicing factor derived circular RNA circUHRF1 accelerates oral squamous cell carcinoma tumorigenesis *via* feedback loop. *Cell Death differentiation*. (2020) 27:27. doi: 10.1038/s41418-019-0423-5

6. Davis CM, Lewis KD. Brief overview: cemiplimab for the treatment of advanced basal cell carcinoma: PD-1 strikes again. *Ther Adv Med Oncol*. (2022) 14:17588359211066147. doi: 10.1177/17588359211066147

7. Veigas F, Mahmoud YD, Merlo J, Rinflerch A, Girotti MR. Immune checkpoints pathways in head and neck squamous cell carcinoma. *Cancers (Basel)*. (2021) 13:1018. doi: 10.3390/cancers13051018

8. Xia X, Du R, Zhao L, Sun W, Wang X. Expression of AEG-1 and microvessel density correlate with metastasis and prognosis of oral squamous-cell carcinoma. *Hum Pathol*. (2014) 45:858–65. doi: 10.1016/j.humpath.2013.08.030

9. Jiaqin Y, Junhui Z, Xudong Z, Xin L, Ling L, Zhaoming L, et al. AEG-1 is involved in hypoxia-induced autophagy and decreases chemosensitivity in T-cell lymphoma. *Mol Med*. (2018) 24:35–. doi: 10.1186/s10020-018-0033-6

10. Jeyamohan S, Kannan M, Kannan R, Rajasekaran N, Antony JVA. Dysregulation of miR-375/AEG-1 axis by human papillomavirus 16/18-E6/E7 promotes cellular proliferation, migration, and invasion in cervical cancer. *Front Oncol*. (2019) 9:847–. doi: 10.3389/fonc.2019.00847

11. Liu Y, Wei G, Ma Q, Han Y. Knockdown of long noncoding RNA TP73-AS1 suppresses the Malignant progression of breast cancer cells in vitro through targeting miRNA-125a-3p/metadherin axis. *Thorac Cancer*. (2020) 11:394–407. doi: 10.1111/1759-7714.13283

12. Fanling M, Yao W, Xin J, Hongtao S. AEG-1 as a predictor of sensitivity to neoadjuvant chemotherapy in advanced epithelial ovarian cancer. *Onco Targets Ther*. (2016) 9:2385–92. doi: 10.2147/OTT.S102648

13. Chen Y, Pekarskaya O, Chao W, Volsky DJ, Fisher PB, Su ZZ, et al. Identification and cloning of human astrocyte genes displaying elevated expression after infection with HIV-1 or exposure to HIV-1 envelope glycoprotein by rapid subtraction hybridization, RaSH. *Oncogene*. (2002) 21:3592–602. doi: 10.1038/sj.onc.1205445

14. Kang DC, Su ZZ, Sarkar D, Emdad L. Cloning and characterization of HIV-1-inducible astrocyte elevated gene-1, AEG-1. *Gene*. (2005) 353:8–15. doi: 10.1016/j.gene.2005.04.006

15. Brown DM, Ruoslahti E. Metadherin, a cell surface protein in breast tumors that mediates lung metastasis. *Cancer Cell*. (2004) 5:365–74. doi: 10.1016/S1535-6108(04)00079-0

16. Britt DE, Yang DF, Yang DQ, Flanagan D, Callanan H, Lim YP, et al. Identification of a novel protein, LYRIC, localized to tight junctions of polarized epithelial cells. *Exp Cell Res*. (2004) 300:134–48. doi: 10.1016/j.yexcr.2004.06.026

17. Sutherland HGE, Lam YW, Briers S, Lamond AI, Bickmore WA. 3D3/lyric: a novel transmembrane protein of the endoplasmic reticulum and nuclear envelope, which is also present in the nucleolus. *Exp Cell Res*. (2004) 294:94–105. doi: 10.1016/j.yexcr.2003.11.020

18. Sriramulu S, Sun XF, Malayaperumal S, Ganesan H, Pathak S. Emerging role and clinicopathological significance of AEG-1 in different cancer types: A concise review. *Cells*. (2021) 10:1497. doi: 10.3390/cells10061497

19. Amirhosein M, Faezeh TG, Iman ZM, Moghbeli M. MicroRNA-495: a therapeutic and diagnostic tumor marker. *J Mol Histol*. (2023) 54:559–78. doi: 10.1007/s10735-023-10159-0

20. Chen W, Dai X, Chen Y, Tian F, Zhang Y, Zhang Q, et al. Significance of STAT3 in immune infiltration and drug response in cancer. *Biomolecules*. (2020) 10:834. doi: 10.3390/biom10060834

21. Zheng W, Bai X, Zhou Y, Yu L, Ji D, Zheng Y, et al. Transcriptional ITPR3 as potential targets and biomarkers for human pancreatic cancer. *Aging*. (2022) 14:4425–44. doi: 10.18632/aging.204080

22. Xin-Yue G, Yang J, Ming-Qi L, Peng H, Yan-Long L, Bin-Bin C. Over-expression of EGFR regulated by RARA contributes to 5-FU resistance in colon cancer. *Aging*. (2020) 12:156–77. doi: 10.18632/aging.102607

23. Zhou X, Zhang B, Zheng G, Zhang Z, Wu J, Du K, et al. Novel necroptosis-related gene signature for predicting early diagnosis and prognosis and immunotherapy of gastric cancer. *Cancers (Basel)*. (2022) 14:3891. doi: 10.3390/cancers14163891

24. Gijtenbeek RGP, Jong KD, Venmans BJW, Vollenhoven FHMV, Brinke AT, Wekken AJVD, et al. Best first-line therapy for patients with advanced non-small cell lung cancer, performance status 2 without a targetable mutation or with an unknown mutation status. *Cohrane Database Systematic Rev*. (2019) 8:CD013382. doi: 10.1002/14651858.CD013382

25. Shen Z, Zhang J, Chen H, Wang W, Xu W, Lu X, et al. Does pre-operative biliary drainage influence long-term survival in patients with obstructive jaundice with resectable pancreatic head cancer? *Front Oncol*. (2020) 10. doi: 10.3389/fonc.2020.575316

26. Talvitie E-M, Vilhonen H, Kurki S, Karlsson A, Orte K, Almangush A, et al. High tumor mutation burden predicts favorable outcome among patients with aggressive histological subtypes of lung adenocarcinoma: A population-based single-institution study. *Neoplasia*. (2020) 22:333–42. doi: 10.1016/j.neo.2020.05.004

27. Xi X, Liu N, Wang Q, Chu Y, Yin Z, Ding Y, et al. ACT001, a novel PAI-1 inhibitor, exerts synergistic effects in combination with cisplatin by inhibiting PI3K/AKT pathway in glioma. *Cell Death Dis*. (2019) 10:757. doi: 10.1038/s41419-019-1986-2

28. Wang M, Qiao X, Cooper T, Pan W, Wang X. HPV E7-mediated NCAPH ectopic expression regulates the carcinogenesis of cervical carcinoma *via* PI3K/AKT/SGK pathway. *Cell Death Dis*. (2020) 11:1049. doi: 10.1038/s41419-020-03244-9

29. Guo X, Chen S, Wang S, Zhang H, Yin F, Guo P, et al. CircRNA-based cervical cancer prognosis model, immunological validation and drug prediction. *Curr Oncol*. (2022) 29:7994–8018. doi: 10.3390/curroncol29110633

30. Liu J, Wang Y, Yin J, Yang Y, Geng R, Zhong Z, et al. Pan-cancer analysis revealed SRSF9 as a new biomarker for prognosis and immunotherapy. *J Oncol*. (2022) 2022:3477148. doi: 10.1155/2022/3477148

31. Pervaiz T. Demethylation alters transcriptome profiling of buds and leaves in 'Kyoho' grape. *BMC Plant Biol*. (2020) 20:544. doi: 10.1186/s12870-020-02754-0

32. He L, Peng X, Cao H, Yang K, Xiang L, Li R, et al. The ntSPL gene family in nicotiana tabacum: genome-wide investigation and expression analysis in response to cadmium stress. *Genes*. (2023) 14:183. doi: 10.3390/genes14010183

33. Luo L, Zhang Z, Weng Y, Zeng J. Ferroptosis-related gene GCLC is a novel prognostic molecular and correlates with immune infiltrates in lung adenocarcinoma. *Cells*. (2022) 11:3371. doi: 10.3390/cells11213371

34. Song Y, Ma R. Identifying the potential roles of PBX4 in human cancers based on integrative analysis. *Biomolecules*. (2022) 12:822. doi: 10.3390/biom12060822

35. Wang Y, Wang T, Sun Y, Sun W, Wang X. Astrocyte elevated gene-1 promotes tumour growth and invasion by inducing EMT in oral squamous cell carcinoma. *Sci Rep*. (2017) 7:15447. doi: 10.1038/s41598-017-15805-8

36. Zhao X, Zhang X, Zhang Z, Liu Z, He Q. Comprehensive circular RNA expression profiling constructs a ceRNA network and identifies hsa_circ_0000673 as a novel oncogene in distal cholangiocarcinoma. *Aging*. (2020) 12:23251–74. doi: 10.18632/aging.104099

37. Zhang Y, Fu Y, Zheng Y, Wen Z, Wang C. Identification of differentially expressed mRNA and the Hub mRNAs modulated by lncRNA Meg3 as a competing endogenous RNA in brown adipose tissue of mice on a high-fat diet. *Adipocyte*. (2020) 9:346–58. doi: 10.1080/21623945.2020.1789283

38. Lee SJ, Choi KM, Bang G, Park SG, Kim JY. Identification of nucleolin as a novel AEG-1-interacting protein in breast cancer *via* interactome profiling. *Cancers (Basel)*. (2021) 13:2842. doi: 10.3390/cancers13112842

39. Banerjee I, Fisher PB, Sarkar D. Astrocyte elevated gene-1 (AEG-1): A key driver of hepatocellular carcinoma (HCC). *Adv Cancer Res*. (2021) 152(2021):329–81. doi: 10.1016/bs.acr.2021.05.003

40. Liu Q, Li J, Zhang W, Xiao C, Zhang S, Nian C, et al. Glycogen accumulation and phase separation drives liver tumor initiation. *Cell*. (2021) 184:5559–76 e19. doi: 10.1016/j.cell.2021.10.001

41. Hu X, Zhu H, Chen B, He X, Shen Y, Zhang X, et al. Tubulin alpha 1b is associated with the immune cell infiltration and the response of HCC patients to immunotherapy. *Diagnostics*. (2022) 12:858. doi: 10.3390/diagnostics 12040858

42. Kim K. Engineering therapeutic strategies in cancer immunotherapy *via* exogenous delivery of toll-like receptor agonists. *Pharmaceutics*. (2021) 13:1374. doi: 10.3390/pharmaceutics13091374

43. Zhang G, Liao Y, Pan X, Zhang X. Exosomes from HPV-16 E7-pulsed dendritic cells prevent the migration, M1 polarization, and inflammation of macrophages in cervical cancer by regulating catalase 2 (CAT2). *Ann Trans Med*. (2022) 10:217. doi: 10.21037/atm-21-6998

frontiers | Frontiers in Oncology

TYPE Original Research
PUBLISHED 21 October 2024
DOI 10.3389/fonc.2024.1488118

Check for updates

OPEN ACCESS

EDITED BY
Pengpeng Zhang,
Nanjing Medical University, China

REVIEWED BY
Luo Qiang,
Children's Hospital of Chongqing Medical University, China
Zhaokai Zhou,
First Affiliated Hospital of Zhengzhou University, China

*CORRESPONDENCE
Jun Ma
drmajun234@163.com
Wei Li
power8446@163.com

RECEIVED 29 August 2024
ACCEPTED 19 September 2024
PUBLISHED 21 October 2024

CITATION
Teng B, Zhang X, Ge M, Miao M, Li W and Ma J (2024) Personalized three-year survival prediction and prognosis forecast by interpretable machine learning for pancreatic cancer patients: a population-based study and an external validation.
Front. Oncol. 14:1488118.
doi: 10.3389/fonc.2024.1488118

COPYRIGHT
© 2024 Teng, Zhang, Ge, Miao, Li and Ma. This is an open-access article distributed under the terms of the Creative Commons Attribution License (CC BY). The use, distribution or reproduction in other forums is permitted, provided the original author(s) and the copyright owner(s) are credited and that the original publication in this journal is cited, in accordance with accepted academic practice. No use, distribution or reproduction is permitted which does not comply with these terms.

Personalized three-year survival prediction and prognosis forecast by interpretable machine learning for pancreatic cancer patients: a population-based study and an external validation

Buwei Teng[1], Xiaofeng Zhang[1], Mingshu Ge[1], Miao Miao[1], Wei Li[1]* and Jun Ma[2]*

[1]Department of Hepatobiliary Surgery, The Affiliated Lianyungang Hospital of Xuzhou Medical University/The First People's Hospital of Lianyungang, Lianyungang, China, [2]Department of Imaging, The Affiliated Huai'an Hospital of Xuzhou Medical University and the Second People's Hospital of Huai'an, Huai'an, China

Purpose: The overall survival of patients with pancreatic cancer is extremely low. We aimed to establish machine learning (ML) based model to accurately predict three-year survival and prognosis of pancreatic cancer patients.

Methods: We analyzed pancreatic cancer patients from the Surveillance, Epidemiology, and End Results (SEER) database between 2000 and 2021. Univariate and multivariate logistic analysis were employed to select variables. Recursive Feature Elimination (RFE) method based on 6 ML algorithms was utilized in feature selection. To construct predictive model, 13 ML algorithms were evaluated by area under the curve (AUC), area under precision-recall curve (PRAUC), accuracy, sensitivity, specificity, precision, cross-entropy, Brier scores and Balanced Accuracy (bacc) and F Beta Score (fbeta). An optimal ML model was constructed to predict three-year survival, and the predictive results were explained by SHapley Additive exPlanations (SHAP) framework. Meanwhile, 101 ML algorithm combinations were developed to select the best model with highest C-index to predict prognosis of pancreatic cancer patients.

Results: A total of 20,064 pancreatic cancer patients from SEER database was consecutively enrolled. We utilized eight clinical variables to establish prediction model for three-year survival. CatBoost model was selected as the best prediction model, and AUC was 0.932 [0.924, 0.939], 0.899 [0.873, 0.934] and 0.826 [0.735, 0.919] in training, internal test and external test sets, with 0.839 [0.831, 0.847] accuracy, 0.872 [0.858, 0.887] sensitivity, 0.803 [0.784, 0.825] specificity and 0.832 [0.821, 0.853] precision. Surgery type had the greatest effects on three-year survival according to SHAP results. For prognosis prediction, "RSF+GBM" algorithm was the best prognostic model with C-index of 0.774, 0.722 and 0.674 in training, internal test and external test sets.

Conclusions: Our ML models demonstrate excellent accuracy and reliability, offering more precise personalized prognostic prediction to pancreatic cancer patients.

KEYWORDS

machine learning, pancreatic cancer, three-year survival, prognosis prediction, SEER

Introduction

Pancreatic cancer is a highly lethal disease with a dismal prognosis, and the 5-year survival rate is merely 9% (1). Only 1% of patients survive for 3 years or more after diagnosis of metastatic pancreatic cancer, while the incidence continues to climb steadily. Surgical resection is the only potential curative treatment, yet only a small proportion of pancreatic cancer patients are eligible for surgery at the time of initial diagnosis (2). This is largely because pancreatic cancer often lacks symptoms in its early stages, leading to most cases being diagnosed at an advanced stage (3). While some individuals may detect the disease through routine physical examinations and undergo early surgery, many patients still experience relapse and ultimately succumb to the disease (4). The treatment of pancreatic cancer mainly includes surgical resection, radiotherapy, chemotherapy and targeted therapy, but the overall efficacy is limited due to its high aggressiveness and the norm of late detection. Novel drugs targeting the KRAS gene, such as sotorasib and adagrasib, have demonstrated efficacy and tolerability in treating solid tumors, including pancreatic cancer, in clinical trials (5). Consequently, it is critical to promptly and early identify pancreatic cancer patients at high risk to optimize their treatment and improve prognosis. And exploring the prognostic risk factors for pancreatic cancer patients is crucial to assess their survival prospects.

Several biomarkers for prognosis prediction in pancreatic cancer have been identified in recent years, including CA19-9, circulating tumor DNA (ctDNA), microRNAs (miRNAs), and tumor mutational burden (TMB) (6). However, CA19-9 is not specific to pancreatic cancer and can be elevated in other conditions such as cholangitis, leading to false positives. Meanwhile, ctDNA analysis is limited by the low abundance of tumor DNA in the bloodstream, particularly in early-stage cancers, which may result in false negatives. And the clinical application of miRNAs is still in the early stages, and their stability in circulation poses challenges for reliable detection (7). Furthermore, TMB's predictive value is still under investigation, and its utility may vary depending on the genetic landscape of the tumor and the therapeutic context (8). Recently, nomogram based on Cox model has been widely utilized in cancer prognosis prediction, but its sensitivity and specificity may be insufficient, calling an urgent need for predicting prognosis more accurately and specifically. Machine learning (ML) approach, a subset of artificial intelligence, has become increasingly popular due to its ability to handle complex, non-linear relationships, particularly effective with vast datasets and loosely structured information (9). With the advent of big data analytics and ML, new approaches for screening risk factors affecting prognosis have become feasible. Several predictive models leveraging these technologies have shown excellent performance and are increasingly being integrated into clinical settings (10, 11), while there is no ML-based sophisticated model to predict prognosis in pancreatic cancer so far, necessitating development and validation of a novel ML model.

The Surveillance, Epidemiology, and End Results (SEER) database (https://seer.cancer.gov/) is particularly valuable in this context, which encompasses a wide range of patient data, offering comprehensive clinicopathological statistics and follow-up information. This rich, real-world database is an ideal resource for developing and testing ML models in the medical field. However, it appears that there is still a gap in research specifically focused on developing models for three-year survival prediction and prognosis forecast of pancreatic cancer patients. Our study was committed to firstly developing and validating predictive and prognostic models utilizing multiple ML algorithms. This approach leverages extensive population data and the capabilities of ML, which is competent in providing personalized predictive tools that assist clinicians in effectively assessing the risk and prognosis of pancreatic cancer patients.

Materials and methods

Data source and characteristics

Clinicopathological data of patients with site recode ICD-O-3/WHO 2008 "pancreas" and AYA site recode 2020 Revision "9.3.9.2 Pancreas – adenocarcinoma" between 2000 and 2021 was retrieved from the SEER database. Additionally, clinicopathological information of pancreatic The First People's Hospital of Lianyungang (2015–2024) was retrospectively collected through electronic medical record system. The study was conducted according to the guidelines of the Declaration of Helsinki and was approved by the Ethics Committee of The First People's Hospital of Lianyungang (protocol code: KY-20210910004, approved on 2021-09-10). Informed consent was obtained from

all subjects involved in this study. Inclusion criteria comprised individuals with ICD-O-3/WHO 2008 "pancreas" and AYA site recode 2020 Revision "9.3.9.2 Pancreas – adenocarcinoma" which are older than 18 years old. Exclusion criteria comprised patients lacking follow-up information of survival months and death cause, not diagnosed with positive histology, no surgery information, not first malignant tumor, without TNM stage or grade details. In SEER database, metastasis is characterized by spreading to distant organs during the initial cancer diagnosis. And we define the outcome of predictive model as three-year survival, indicating that patients are still alive at the timepoint of 36 months follow-up. The positive outcome was death of patient in three-year follow-up.

Extracted data were gathered on demographic data (age, gender, race, marital status household location and income), cancer characteristics (pathological grade, summary stage, TNM stage, tumor size, tumor primary location, pathology, metastasis information), therapeutic information (surgery, lymph node surgery, positive lymph node, radiotherapy, chemotherapy) and follow-up information (overall and cancer-specific survival status, survival months). Two continuous variables, age and tumor size, were divided into categorical variables. The age was split into five groups: "<50", "50-59", "60-69", "70-79" and ">=80". The tumor size was split into "<2cm", "2-3.9cm", "4-5.9cm", "6-7.9cm", ">8cm" and "Unknown". "Metastasis" was defined as "yes" with metastasis either in brain, bone, liver, lung, and distant lymph nodes, as well as tumor categorized as M1 stage. The missing rate for each categorical variable is calculated and reported. For those classified data that is unknown, we classify its missing value into the "unknown" category. This processing ensures data integrity and avoids information loss due to missing data. We determined the minimum sample size needed for an external validation cohort by formula of Riley et al. (12).

Establishment and validation of predictive model for three-year survival

In the preliminary analysis, variables with $P < 0.05$ in the univariate and multivariate logistic analysis in the training set were included for the feature selection process. Subsequently, we employed Recursive Feature Elimination (RFE) method based on 6 ML algorithms, involving categorical boosting (CatBoost), random forest (RF), support vector machine (SVM), extreme gradient boosting (XGB), decision tree (DT) and gradient boosting machine (GBM), combined with 5-fold cross-validation, to sift through the clinical features. RFE works by building a model and identifying the most significant features in feature selection phase. This selection process is then iteratively repeated on the subset of remaining features until all features have been evaluated and ranked (13). Then Robust rank aggregation (RRA) algorithm was utilized to integrate the rank of variable importance from six ML algorithms utilized in RFE method to obtain a comprehensive ranking of all variables (14). We set random seed as "2024" in our analysis. In model development phase, we applied 13 ML algorithms, including CatBoost, RF, SVM, XGB, DT, GBM, k-nearest neighbor (KNN), logistic regression (LR), naive bayes classifier (NBC), linear discriminant analysis (LDA), quadratic discriminant analysis (QDA), neural network (NNET) and generalized linear model (GLM) to predict three-year survival via "mlr3" R package (15). This approach allows us to compare the performance of various models and select the best predictive model. To tackle the issue of class imbalance, which could significantly skew performance metrics, we implemented the Synthetic Minority Over-sampling Technique (SMOTE) for training our model (16). We further refined our approach by employing nested resampling, which involved a two-tiered k-fold cross-validation process: one for optimizing model hyperparameters and another nested within it for model selection. Meanwhile, we utilized a 1000-evaluation random search across a 5-fold cross-validation framework, repeated five times for each model. Subsequently, area under the curve (AUC), area under precision-recall curve (PRAUC), accuracy, sensitivity, specificity, precision, cross-entropy, Brier scores and Balanced Accuracy (bacc) and F Beta Score (fbeta) were calculated to select the best ML model. Internal validation was carried out through 5-fold cross-validation. Precision-recall curve (PRC) was employed to evaluate the performance of classification models in handling imbalanced datasets. Calibration curve was utilized to appraise model's discriminative ability, and decision curve analysis (DCA) was applied to verify the clinic benefit of ML model via "runway" R package (https://github.com/ML4LHS/runway/). We set the selection criteria of our best model: highest AUC, highest PRAUC, and lowest Brier score, while also ensuring a good calibration curve, as well as outperforming balanced accuracy and F Beta Score. To quantify the impact of each variable, we calculated its mean contribution to the AUC as a percentage relative to the full model via "DALEX" R package (17). SHapley Additive exPlanations (SHAP) value were used to explain the best model predictions and to interpret the black-box ML model via "shapviz" R package (https://github.com/ModelOriented/shapviz) (18).

Prognostic model based on integrative machine learning algorithms

Univariate and multivariate cox analysis were employed to define clinical variables with significant prognosis value in overall survival (OS). We integrated 10 ML algorithms involving random survival forest (RSF), elastic network (Enet), Lasso, Ridge, stepwise Cox, CoxBoost, partial least squares regression for Cox (plsRcox), supervised principal components (SuperPC), GBM and survival support vector machine (survival-SVM) to predict prognosis (in terms of OS) of pancreatic cancer patients. Altogether 101 prognostic ML algorithm combinations were trained in the training cohort, to develop the prognostic ML model according to the leave-one-out cross-validation (LOOCV) framework. Models with <3 clinical variable were removed. Subsequently, the concordance index (C-index) of every ML combination in training, testing and external validation cohorts was obtained (19). The top five ML combinations yielding the highest average C-index across three cohorts were selected for model evaluation via k-fold cross-validation, to mitigate overfitting and ensure the robustness and generalizability of model. Logarithmic loss, recall

and decision calibration were utilized to select the best prognostic ML combination via "mlr3proba" R package (20). We incorporated variables from various feature selection patterns to compute risk scores using a linear combination function for each prognostic ML combination. The median risk score from the training cohort was chosen as the threshold to categorize patients in training, testing and external validation cohorts into high or low-risk groups. We utilized the Kaplan-Meier (KM) survival analysis and the log-rank test on these groups, using the "survival" and "survminer" R packages. AUC, time-dependent receiver operating characteristic (ROC) curves, calibration curves and DCA were employed to evaluate the precision, discrimination and clinical benefit of the model.

Results

Demographic composition and clinical baseline information

In the predictive model for three-year survival, a total of 20064 pancreatic cancer patients from SEER database and 103 patients from The First People's Hospital of Lianyungang were included. We divided patients from SEER database randomly into training and internal validation sets in a 7:3 ratio, respectively. And pancreatic cancer patients from The First People's Hospital of Lianyungang were assigned as the external validation set. In the trainset from SEER database, 2579 cases (18.3%) were alive at three-year follow-up, while 11548 cases (81.7%) did not. Detailed clinical information regarding the training and validation sets to predict three-year survival can be found in Table 1. For the outcomes (in terms of OS) of prognostic model, 13157 cases (93.1%) were dead at the time of follow-up, while 970 cases (6.87%) were alive (Table 1). In the training, internal validation and external validation sets, the median follow-up time was 12.0 [5.00;26.0], 12.0 [5.00;27.0] and 16.0 [6.00;30.5] (Table 1). The specific selection process of patients from SEER database is shown in Figure 1.

Feature selection for the predictive model

We utilized "autoplot" function in "mlr3" R package to visualized the correlation coefficients of the baseline characteristics with three-year survival, which revealed that "AJCC stage" had the most significant correlation with three-year survival (Figure 2A). Based on our clinical experiences, we selected 24 variables for the logistic regression analysis (Table 2), while the variable with a correlation coefficient > 0.6 was removed. Subsequently, we performed univariate and multivariate logistic regression analysis in the training cohort to find the effective variables to predict three-year survival, which revealed that "Age" (OR 1.67(1.35-2.06)), "Marital_Status" (OR 1.27 (1.14-1.42)), "Household_Income" (OR 0.75(0.68-0.83)), "Histology" (OR 0.5(0.43-0.59)), "Grade" (OR 2.4(1.59-3.72)), "Summary_Stage" (OR 3.12(2.27-4.31)), "Tumor_Size" (OR 2.63(2.08-3.34)), "AJCC_Stage" (OR 1.59(1.09-2.35)), "Surgery_Type" (OR 0.15(0.11-0.2)), "Radiotherapy" (OR 0.79(0.72-0.87)), "Chemotherapy" (OR 0.57(0.52-0.64)), "Lung_Metastasis" (OR 0.2(0.06-0.99)), "M_Stage" (OR 1.26(1.07-1.48)) were significantly powerful to predict three-year survival ($P < 0.05$, Table 2). The correlation analysis between the variables and three-year survival showed that "AJCC_stage" is the most influential factor (Figure 2B). Due to high correlation between "AJCC_stage" and "Summary_Stage", we only choose "AJCC_stage" in the following analysis. Afterwards, we utilized Recursive Feature Elimination (RFE) method based on six ML algorithms (GBM, SVM, RF, DT, XGB and CatBoost), combined with 5-fold cross-validation, to sift through the clinic features (Figures 2C–H). Feature selection based on RFE found that the optimal selection was according to GBM algorithm, remaining 12 variables, with the highest AUC (0.819, Figure 2C). We utilized RRA algorithm to obtain the comprehensive ranking of the clinic variables in six ML algorithms, with the "AJCC_stage" considered most important (Supplementary Table 1). We finally select eight variables with frequencies more than 4, which indicates that these variables are important in most of the ML selection process, into the following procedures of model development (Supplementary Table 1).

Development and validation of predictive model for three-year survival

To establish a precise model to predict three-year survival, we utilized the eight variables ("AJCC_Stage", "Chemotherapy", "Age", "Grade", "Lung_Metastasis", "M_Stage", "Surgery_Type", "Tumor_Size") selected by RFE and RRA. A total of 13 ML models, comprising CatBoost, RF, SVM, XGB, DT, GBM, KNN, LR, NBC, LDA, QDA, NNET and GLM algorithms, were developed by incorporating the above selection of eight variables in the training set. Hyperparameters were fine-tuned by performing 5-cross validation and random searches. Then we evaluated the 13 ML models in the internal validation and external validation cohorts, respectively. Finally, ROC curves analysis found that CatBoost model had the highest AUC in the training (0.932 [0.924, 0.939]), internal validation (0.899 [0.873, 0.934]) and external validation (0.826 [0.735, 0.919]) cohorts (Figures 3A, 4A, 5A). CatBoost model has the accuracy of 0.839 [0.831, 0.847], sensitivity of 0.872 [0.858, 0.887], specificity of 0.803 [0.784, 0.825] and precision of 0.832 [0.821, 0.853]. After grid search in hyperparameter tuning, the best hyperparameter metric of CatBoost was depth, 5; learning_rate, 0.01678325; iterations, 548; l2_leaf_reg, 7.409126. The precision-recall curves (PRC) revealed that CatBoost model was powerful in handling imbalanced datasets (Figures 3B, 4B, 5B). Calibration plots showed that CatBoost algorithm had the best fitting ability and could accurately predict three-year survival (Figures 3C, 4C, 5C). This indicates that the model's probability estimates are reliable and well-calibrated, as it ensures that the risk estimates provided by the model can be trusted to reflect the true likelihood of patient outcomes. DCA curves suggested that CatBoost algorithm had the best clinical application value and could effectively help predict three-year survival (Figures 3D, 4D, 5D). This implies that using the CatBoost model to guide clinical decision-making would result in more effective identification of patients who are likely to benefit from certain interventions, such as more aggressive treatment or

10.3389/fonc.2024.1488118

TABLE 1 Clinicopathological characteristics of patients with pancreatic cancer in the training, internal validation and external validation cohorts.

	Training Cohort N=14127	Validation Cohort N=5937	External Validation Cohort N=103	p.overall
Sex				**0.997**
Male				
Female	7162 (50.7%)	3013 (50.7%)	52 (50.5%)	
Age				**0.046**
<50	1048 (7.42%)	419 (7.06%)	11 (10.7%)	
50-59	2928 (20.7%)	1223 (20.6%)	21 (20.4%)	
60-69	4567 (32.3%)	1963 (33.1%)	17 (16.5%)	
70-79	3936 (27.9%)	1654 (27.9%)	38 (36.9%)	
>=80	1648 (11.7%)	678 (11.4%)	16 (15.5%)	
Race				**<0.001**
White	11343 (80.3%)	4772 (80.4%)	0 (0.00%)	
Black	1558 (11.0%)	641 (10.8%)	0 (0.00%)	
Other	1226 (8.68%)	524 (8.83%)	103 (100%)	
Marital_Status				**0.378**
Married	8571 (60.7%)	3614 (60.9%)	69 (67.0%)	
Unmarried	1782 (12.6%)	720 (12.1%)	14 (13.6%)	
Widowed or divorced	3365 (23.8%)	1418 (23.9%)	20 (19.4%)	
Unknown	409 (2.90%)	185 (3.12%)	0 (0.00%)	
Year_of_Diagnosis				**<0.001**
2000-2010	7649 (54.1%)	3221 (54.3%)	78 (75.7%)	
2011-2020	6478 (45.9%)	2716 (45.7%)	25 (24.3%)	
Household_Location				**0.684**
Rural	1587 (11.2%)	656 (11.0%)	9 (8.74%)	
Urban	12540 (88.8%)	5281 (89.0%)	94 (91.3%)	
Household_Income				**<0.001**
<$70,000	4765 (33.7%)	1974 (33.2%)	9 (8.74%)	
>=$70,000	9362 (66.3%)	3963 (66.8%)	94 (91.3%)	
Tumor_Primary_Site				**0.519**
Pancreas Head	9330 (66.0%)	3924 (66.1%)	63 (61.2%)	
Pancreas Body or Tail	2910 (20.6%)	1259 (21.2%)	24 (23.3%)	
Other	1887 (13.4%)	754 (12.7%)	16 (15.5%)	
Histology				**0.633**
Adenomas and adenocarcinomas	9285 (65.7%)	3940 (66.4%)	73 (70.9%)	
Ductal and lobular neoplasms	3769 (26.7%)	1586 (26.7%)	23 (22.3%)	
Cystic, mucinous and serous neoplasms	854 (6.05%)	329 (5.54%)	6 (5.83%)	
Other	219 (1.55%)	82 (1.38%)	1 (0.97%)	

(Continued)

10.3389/fonc.2024.1488118

TABLE 1 Continued

	Training Cohort N=14127	Validation Cohort N=5937	External Validation Cohort N=103	p.overall
Grade				0.629
Well differentiated I	1673 (11.8%)	709 (11.9%)	13 (12.6%)	
Moderately differentiated II	6606 (46.8%)	2783 (46.9%)	48 (46.6%)	
Poorly differentiated III	5645 (40.0%)	2376 (40.0%)	39 (37.9%)	
Undifferentiated anaplastic IV	203 (1.44%)	69 (1.16%)	3 (2.91%)	
Summary_Stage				0.186
Localized	1341 (9.49%)	533 (8.98%)	16 (15.5%)	
Regional	8635 (61.1%)	3636 (61.2%)	57 (55.3%)	
Distant	4151 (29.4%)	1768 (29.8%)	30 (29.1%)	
AJCC_Stage				0.360
I	1341 (9.49%)	533 (8.98%)	16 (15.5%)	
II	8000 (56.6%)	3392 (57.1%)	54 (52.4%)	
III	1448 (10.2%)	590 (9.94%)	10 (9.71%)	
IV	3338 (23.6%)	1422 (24.0%)	23 (22.3%)	
T_Stage				0.459
T1	633 (4.48%)	284 (4.78%)	7 (6.80%)	
T2	2352 (16.6%)	964 (16.2%)	22 (21.4%)	
T3	8764 (62.0%)	3718 (62.6%)	56 (54.4%)	
T4	2378 (16.8%)	971 (16.4%)	18 (17.5%)	
N_Stage				0.758
N0	6526 (46.2%)	2776 (46.8%)	47 (45.6%)	
N1	7601 (53.8%)	3161 (53.2%)	56 (54.4%)	
M_Stage				0.839
M0	10789 (76.4%)	4515 (76.0%)	80 (77.7%)	
M1	3338 (23.6%)	1422 (24.0%)	23 (22.3%)	
Tumor_Size				0.297
<2cm	1084 (7.67%)	472 (7.95%)	11 (10.7%)	
2-3.9cm	6743 (47.7%)	2798 (47.1%)	47 (45.6%)	
4-5.9cm	3896 (27.6%)	1657 (27.9%)	29 (28.2%)	
6-7.9cm	1050 (7.43%)	427 (7.19%)	10 (9.71%)	
>8cm	470 (3.33%)	211 (3.55%)	6 (5.83%)	
Unknown	884 (6.26%)	372 (6.27%)	0 (0.00%)	
Surgery_Type				0.180
No Surgery	5646 (40.0%)	2408 (40.6%)	41 (39.8%)	
Local or partial pancreatectomy	6947 (49.2%)	2829 (47.7%)	48 (46.6%)	
Total pancreatectomy	1534 (10.9%)	700 (11.8%)	14 (13.6%)	
Lymph_Nodes_Surgery				0.743
No or biopsy only	5696 (40.3%)	2441 (41.1%)	42 (40.8%)	

(Continued)

TABLE 1 Continued

	Training Cohort N=14127	Validation Cohort N=5937	External Validation Cohort N=103	p.overall
Lymph_Nodes_Surgery				0.743
1-3 regional lymph nodes removed	787 (5.57%)	342 (5.76%)	7 (6.80%)	
4 or more regional lymph nodes removed	7644 (54.1%)	3154 (53.1%)	54 (52.4%)	
Regional_Lymph_Nodes				0.676
No nodes were examined	5302 (37.5%)	2277 (38.4%)	38 (36.9%)	
Negative	3059 (21.7%)	1267 (21.3%)	25 (24.3%)	
Positive	5729 (40.6%)	2384 (40.2%)	40 (38.8%)	
Unknown	37 (0.26%)	9 (0.15%)	0 (0.00%)	
Chemotherapy				0.911
None/Unknown	4666 (33.0%)	1945 (32.8%)	35 (34.0%)	
Yes	9461 (67.0%)	3992 (67.2%)	68 (66.0%)	
Radiation				0.328
None/Unknown	9995 (70.8%)	4174 (70.3%)	79 (76.7%)	
Yes	4132 (29.2%)	1763 (29.7%)	24 (23.3%)	
Metastasis				0.940
No	5859 (41.5%)	2465 (41.5%)	41 (39.8%)	
Yes	8268 (58.5%)	3472 (58.5%)	62 (60.2%)	
Bone_Metastasis				0.804
No	7530 (53.3%)	3180 (53.6%)	54 (52.4%)	
Yes	97 (0.69%)	47 (0.79%)	0 (0.00%)	
Unknown	6500 (46.0%)	2710 (45.6%)	49 (47.6%)	
Brain_Metastasis				0.485
No	7620 (53.9%)	3227 (54.4%)	54 (52.4%)	
Yes	5 (0.04%)	0 (0.00%)	0 (0.00%)	
Unknown	6502 (46.0%)	2710 (45.6%)	49 (47.6%)	
Liver_Metastasis				0.492
No	6381 (45.2%)	2667 (44.9%)	48 (46.6%)	
Yes	1264 (8.95%)	569 (9.58%)	6 (5.83%)	
Unknown	6482 (45.9%)	2701 (45.5%)	49 (47.6%)	
Lung_Metastasis				0.778
No	7288 (51.6%)	3073 (51.8%)	51 (49.5%)	
Yes	329 (2.33%)	154 (2.59%)	3 (2.91%)	
Unknown	6510 (46.1%)	2710 (45.6%)	49 (47.6%)	
Survival_Months	12.0 [5.00;26.0]	12.0 [5.00;27.0]	16.0 [6.00;30.5]	0.605
Vital_Status				0.848
Alive	970 (6.87%)	421 (7.09%)	7 (6.80%)	
Dead	13157 (93.1%)	5516 (92.9%)	96 (93.2%)	

(Continued)

TABLE 1 Continued

	Training Cohort N=14127	Validation Cohort N=5937	External Validation Cohort N=103	p.overall
Cancer_Specific_Death				0.440
Not cancer specific death	1823 (12.9%)	799 (13.5%)	11 (10.7%)	
Dead due to bladder cancer	12304 (87.1%)	5138 (86.5%)	92 (89.3%)	
Other_Cause_Death				0.430
Not other cause death	13274 (94.0%)	5559 (93.6%)	99 (96.1%)	
Dead due to other cause	853 (6.04%)	378 (6.37%)	4 (3.88%)	
Three_Year_Survival				0.911
Alive	2579 (18.3%)	1097 (18.5%)	18 (17.5%)	
Dead	11548 (81.7%)	4840 (81.5%)	85 (82.5%)	

intensive monitoring. The accuracy, sensitivity, specificity, precision, cross-entropy, Brier scores, Balanced Accuracy (bacc) and F Beta Score (fbeta) of the 13 ML models were calculated to comprehensively evaluate the model performance, which revealed that CatBoost model was robust in predicting three-year survival (Figures 3E, 4E, 5E). The results of tenfold cross-validation indicated that CatBoost exhibited the best performance (Figure 3F). Confusion matrix displayed the outstanding

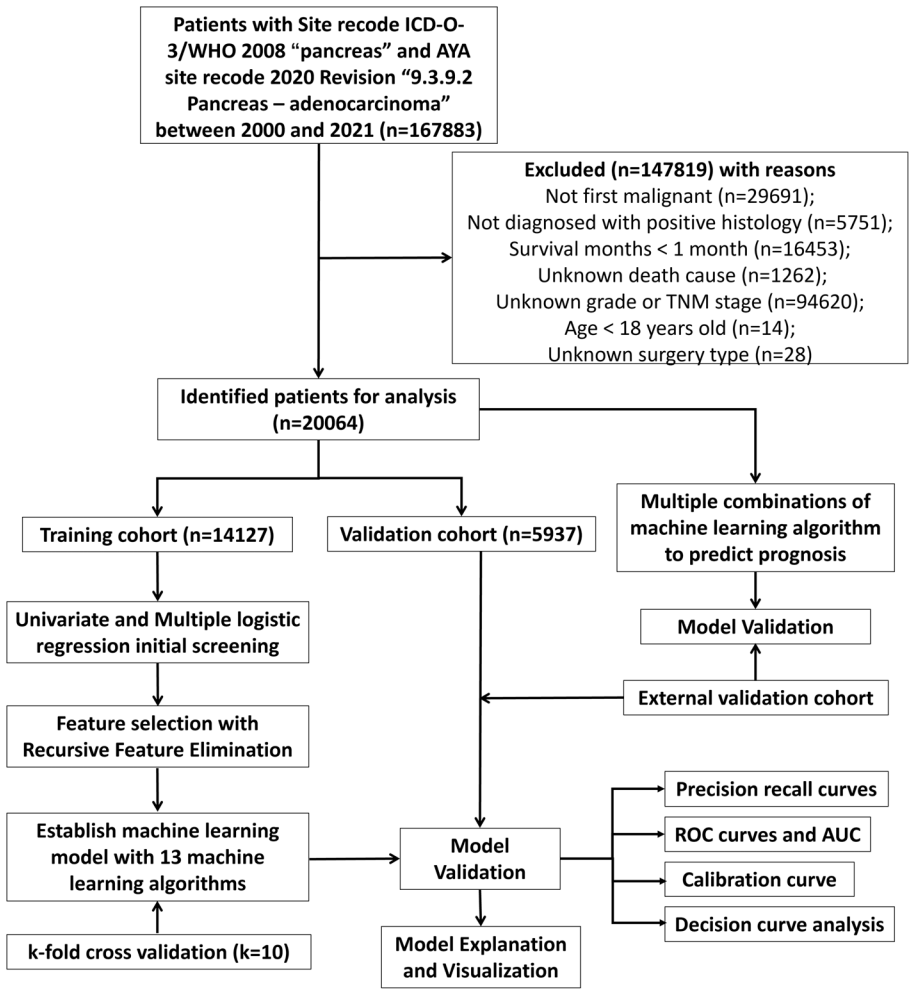

FIGURE 1
The workflow diagram for study design and patient screening.

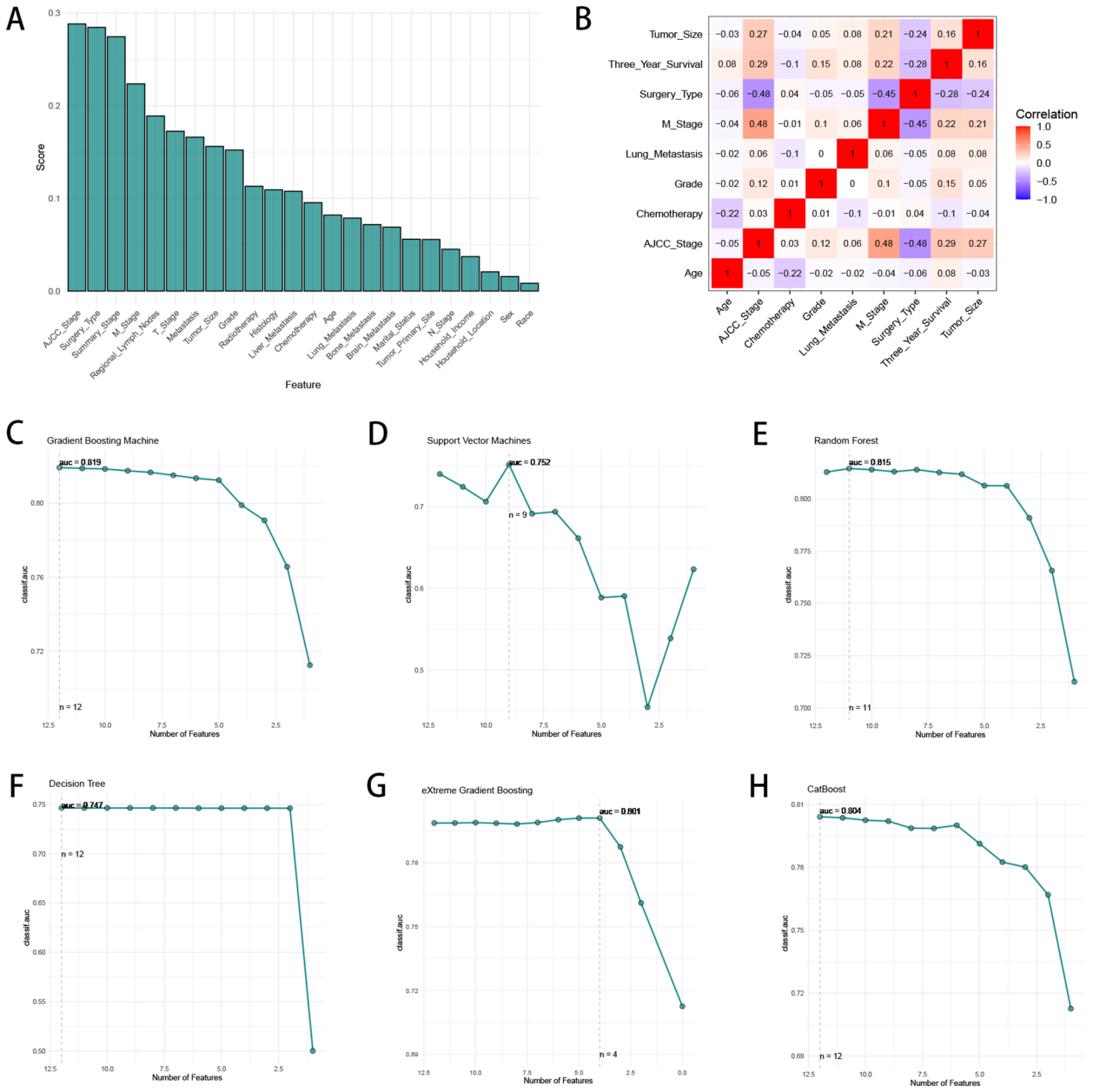

FIGURE 2
The process of feature selection. **(A)** The correlation coefficients of the baseline characteristics with three-year survival. **(B)** The heatmap of Spearman's correlation analysis of the clinic variables with three-year survival. The correlation index ranges from -1.0 to 1.0, with a brighter color indicating a stronger correlation. **(C–H)** Feature selection process with Recursive Feature Elimination (RFE) method based on six ML algorithms (GBM, SVM, RF, DT, XGB and CatBoost).

predictive ability of CatBoost in the internal validation and external validation cohorts (Figures 4F, 5F). Therefore, CatBoost was chosen as the best model for the next step.

Model interpretation

We calculated the feature importance rankings of each ML models and illustrated eight of them, including CatBoost, GBM, GLM, NB, KNN, RF, NNET and SVM (Figure 6A). The importance scores were determined by leveraging the inherent attributes of various ML algorithms, which revealed that the risk factors most associated with three-year survival were "Surgery Type", "AJCC Stage" and "M Stage". Subsequently, we utilized SHAP framework to interpret CatBoost model. We illustrated all of the risk factors evaluated by the mean absolute SHAP value, which revealed that "Surgery Type" was the most impactful variable (Figure 6B). Besides, beeswarm plot elucidated the influence of various risk factors on three-year survival (Figure 6C). The y-axis denotes the magnitude of the risk factors, while the x-axis represents their impact on the model's output, specifically three-year survival, as measured by the SHAP value. It was observed that no surgery,

TABLE 2 Univariate and multivariate logistics analysis of pancreatic cancer patients for 3-year survival in the training cohort.

Variable	Univariable logistic analysis		Multivariate logistic analysis	
term	OR (95%CI)	p.value	OR (95%CI)	p.value
Sex: Male	Reference			
Female	0.92 (0.85-1)	0.064	\	\
Age: <50	Reference			
50-59	1.12 (0.95-1.33)	0.185	1.05 (0.89-1.24)	0.568
60-69	1.15 (0.98-1.35)	0.089	1.18 (1.01-1.39)	0.04
70-79	1.51 (1.28-1.79)	<0.001	1.41 (1.19-1.66)	<0.001
>=80	2.46 (1.99-3.05)	<0.001	1.67 (1.35-2.06)	<0.001
Race: White	Reference			
Black	1.15 (1-1.33)	0.047	1.01 (0.88-1.16)	0.898
Other	1.02 (0.87-1.19)	0.841	1.04 (0.9-1.2)	0.604
Marital_Status: Married	Reference			
Unmarried	1.21 (1.06-1.38)	0.006	1.18 (1.03-1.34)	0.015
Widowed or divorced	1.47 (1.32-1.64)	<0.001	1.27 (1.14-1.42)	<0.001
Unknown	1.21 (0.94-1.59)	0.154	1.3 (1.02-1.68)	0.038
Household_Income: <$70,000	Reference			
>=$70,000	0.81 (0.74-0.89)	<0.001	0.75 (0.68-0.83)	<0.001
Household_Location: Rural				
Urban	0.84 (0.73-0.96)	0.014	0.94 (0.81-1.08)	0.386
Tumor_Primary_Site: Pancreas Head	Reference			
Pancreas Body or Tail	1.27 (1.14-1.42)	<0.001	0.91 (0.79-1.05)	0.191
Other	1.51 (1.31-1.73)	<0.001	1.05 (0.91-1.21)	0.488
Histology: Adenomas and adenocarcinomas	Reference			
Ductal and lobular neoplasms	0.55 (0.5-0.6)	<0.001	1.05 (0.96-1.15)	0.3
Cystic, mucinous and serous neoplasms	0.41 (0.35-0.48)	<0.001	0.5 (0.43-0.59)	<0.001
Other	0.92 (0.64-1.34)	0.642	0.86 (0.62-1.2)	0.359
Grade: Well differentiated I	Reference			
Moderately differentiated II	1.56 (1.38-1.76)	<0.001	1.77 (1.57-2)	<0.001
Poorly differentiated III	3.12 (2.73-3.56)	<0.001	2.75 (2.41-3.14)	<0.001
Undifferentiated anaplastic IV	2.97 (1.97-4.68)	<0.001	2.4 (1.59-3.72)	<0.001
Summary_Stage: Localized	Reference			
Regional	2.55 (2.26-2.87)	<0.001	1.74 (1.31-2.3)	<0.001
Distant	15.52 (12.92-18.72)	<0.001	3.12 (2.27-4.31)	<0.001
AJCC_Stage: I	Reference			
II	2.34 (2.07-2.64)	<0.001	1.11 (0.89-1.39)	0.336
III	8.99 (7.19-11.33)	<0.001	1.17 (0.93-1.48)	0.179
IV	24.81 (19.71-31.56)	<0.001	1.59 (1.09-2.35)	0.018

(Continued)

TABLE 2 Continued

Variable	Univariable logistic analysis		Multivariate logistic analysis	
term	OR (95%CI)	p.value	OR (95%CI)	p.value
T_Stage: T1	Reference			
T2	3.5 (2.9-4.22)	<0.001	1.11 (0.89-1.38)	0.374
T3	3.33 (2.83-3.93)	<0.001	1.17 (0.92-1.47)	0.196
T4	15.41 (12.14-19.67)	<0.001	1.59 (1.03-2.54)	0.051
N_Stage: N0	Reference			
N1	1.26 (1.16-1.38)	<0.001	1.1 (0.86-1.41)	0.448
M_Stage: M0	Reference			
M1	10.69 (8.7-13.32)	<0.001	1.26 (1.07-1.48)	0.005
Tumor_Size: <2cm	Reference			
2-3.9cm	2.75 (2.4-3.15)	<0.001	1.74 (1.5-2.02)	<0.001
4-5.9cm	4.57 (3.92-5.32)	<0.001	2.19 (1.85-2.59)	<0.001
6-7.9cm	5.8 (4.62-7.32)	<0.001	2.63 (2.08-3.34)	<0.001
>8cm	3.62 (2.77-4.79)	<0.001	1.63 (1.22-2.19)	0.001
Unknown	9.43 (7.13-12.67)	<0.001	1.72 (1.3-2.3)	<0.001
Surgery_Type: No Surgery	Reference			
Local or partial pancreatectomy	0.07 (0.06-0.08)	<0.001	0.15 (0.11-0.2)	<0.001
Total pancreatectomy	0.08 (0.06-0.09)	<0.001	0.15 (0.12-0.21)	<0.001
Lymph_Nodes_Surgery: No or biopsy only	Reference			
1-3 regional lymph nodes removed	0.14 (0.11-0.17)	<0.001	1.09 (0.76-1.54)	0.652
4 or more regional lymph nodes removed	0.09 (0.08-0.11)	<0.001	0.74 (0.53-1.02)	0.067
Regional_Lymph_Nodes: No nodes were examined	Reference			
Negative	0.06 (0.05-0.07)	<0.001	0.75 (0.51-1.12)	0.158
Positive	0.14 (0.12-0.17)	<0.001	1.28 (0.88-1.86)	0.196
Unknown	0.19 (0.09-0.52)	<0.001	0.53 (0.21-1.54)	0.205
Chemotherapy: None/Unknown	Reference			
Yes	0.57 (0.51-0.63)	<0.001	0.57 (0.52-0.64)	<0.001
Radiotherapy: None/Unknown	Reference			
Yes	0.55 (0.5-0.6)	<0.001	0.79 (0.72-0.87)	<0.001
Metastasis: No	Reference			
Yes	2.37 (2.17-2.58)	<0.001	0.9 (0.6-1.4)	0.633
Bone_Metastasis: No	Reference			
Yes	12.58 (3.98-76.41)	<0.001	2.29 (0.68-14.29)	0.262
Unknown	1.46 (1.34-1.59)	<0.001	0.83 (0.05-21.63)	0.919
Brain_Metastasis: No	Reference			
Yes	2.92 (0-NA)	0.908	1766.26 (0-NA)	0.958
Unknown	1.44 (1.32-1.57)	<0.001	0.96 (0.06-25.1)	0.984

(Continued)

TABLE 2 Continued

Variable	Univariable logistic analysis		Multivariate logistic analysis	
term	OR (95%CI)	p.value	OR (95%CI)	p.value
Liver_Metastasis: No	Reference			
Yes	10 (7.34-14.05)	<0.001	1.03 (0.58-1.79)	0.930
Unknown	1.75 (1.6-1.91)	<0.001	4.39 (0.42-24.26)	0.150
Lung_Metastasis: No	Reference			
Yes	9.75 (5.33-20.47)	<0.001	1.06 (0.51-2.44)	0.877
Unknown	1.51 (1.38-1.64)	<0.001	0.2 (0.06-0.99)	0.023

higher grade, older age, have lung metastasis, no chemotherapy, higher AJCC stage and M1 stage are associated with an increased likelihood of death in three-year follow-up. To illustrate the model's interpretability, we highlighted two representative cases. SHAP values were used to understand the impact of each feature on the model's prediction. In our study, lower SHAP values indicate a higher likelihood of three-year survival, while higher SHAP values suggest a higher probability of death within the three-year follow-up. We chose median value (0.0962) as the cut-off point for predicting the low or high probability of three-year survival. For instance, the first patient with three-year survival had a lower SHAP value and a prediction score of 0.0276, indicating a higher likelihood of three-year survival (Figure 6D). In contrast, the second patient without three-year survival showed a higher SHAP value and a prediction score of 0.187, suggesting a higher probability of death in three-year follow-up (Figure 6E).

Prognostic model establishment and performance

To explore the prognostic values of multiple variables, we performed univariate and multivariate Cox analysis to found that "Sex" (HR 0.934(0.907-0.963)), "Race" (HR 1.071(1.022-1.123)), "Age" (HR 1.19(1.119-1.264)), "Marital_Status" (HR 1.137(1.086-1.191)), "Household_Income" (HR 0.866(0.837-0.896)), "Household_Location" (HR 0.945(0.899-0.993)), "Tumor_Primary_Site" (HR 0.946(0.91-0.983)), "Histology" (HR 0.706(0.66-0.755)), "Grade" (HR 1.334(1.271-1.401)), "Tumor_Size" (HR 1.325(1.238-1.417)), "AJCC_Stage" (HR 0.712 (0.643-0.789)), "T_Stage" (HR 1.127(1.024-1.242)), "Surgery_Type" (HR 0.491(0.45-0.535)), "Lymph_Nodes_Surgery" (HR 0.846 (0.761-0.94)), "Regional_Lymph_Nodes" (HR 0.709(0.65-0.774)), "Radiotherapy" (HR 0.905(0.873-0.938)), "Chemotherapy" (HR 0.582(0.562-0.602)), "Bone_Metastasis" (HR 1.196(1.006-1.422)), "Liver_Metastasis" (HR 1.338(1.224-1.463)), "Lung_Metastasis" (HR 1.338(1.224-1.463)) and "Metastasis" (HR 0.781(0.709-0.861)) were independent prognosis variables for predicting OS in pancreatic cancer patients ($P < 0.05$, Table 3). Incorporating these clinical variables, 101 prognostic ML algorithm combinations were constructed via LOOCV framework. The C-index of each ML combination was calculated in training, internal validation and external validation datasets (Figure 7A). Among top five ML combinations with highest C-index across three cohorts, logarithmic loss, recall and decision calibration were calculated to assess the model performances, discovering the well calibration and precision of "RSF+GBM" model (Supplementary Figure 1). The best ML model combination was "RSF+GBM", which was established based on RSF algorithm in feature selection (Figure 7B), and GBM algorithm in model construction (Figure 7C), with the highest average C-index (0.723) across three datasets (Figure 7A). Finally, a 20-variable "RSF+GBM" prognostic ML model was accordingly established to predict OS of pancreatic patients, with "Surgery Type" being the most significant variable both in the feature importance visualization of RSF and GBM model (Figures 7B, C). ROC curves of 1-, 3- and 5-year OS showed well specificity of "RSF+GBM" model (Figure 7D). Time dependent ROC curves indicated that the curve of "RSF+GBM" model was upper than other curves at most of the time points, indicating that "RSF+GBM" model remarkably outperformed conventional clinical variables in capability of discrimination and prediction (Figure 7E). Calibration curves (Figure 7F) and DCA curves (Figure 7G) showed that "RSF+GBM" model is well-behaved in accuracy and clinical benefit. Based on risk scores calculated by GBM algorithm, we utilized the median risk score to divide patients in the training, internal validation and external validation cohorts into low-risk and high-risk groups, respectively. Obliviously, the low-risk group owned a relatively longer OS than the high-risk group in the training, internal validation and external validation cohorts, respectively (Figure 7H). The K-M curves validated the capability of risk stratification of "RSF+GBM" model. All these metrics collectively indicated that "RSF+GBM" model demonstrated stability and robustness in model performances. In conclusion, we have successfully developed a "RSF+GBM" model to predict OS in pancreatic cancer patients, which outperforming other models and was well behaved in model performances.

Discussion

Pancreatic cancer is among the most invasive and deadly malignancies, with projections suggesting it could become the

10.3389/fonc.2024.1488118

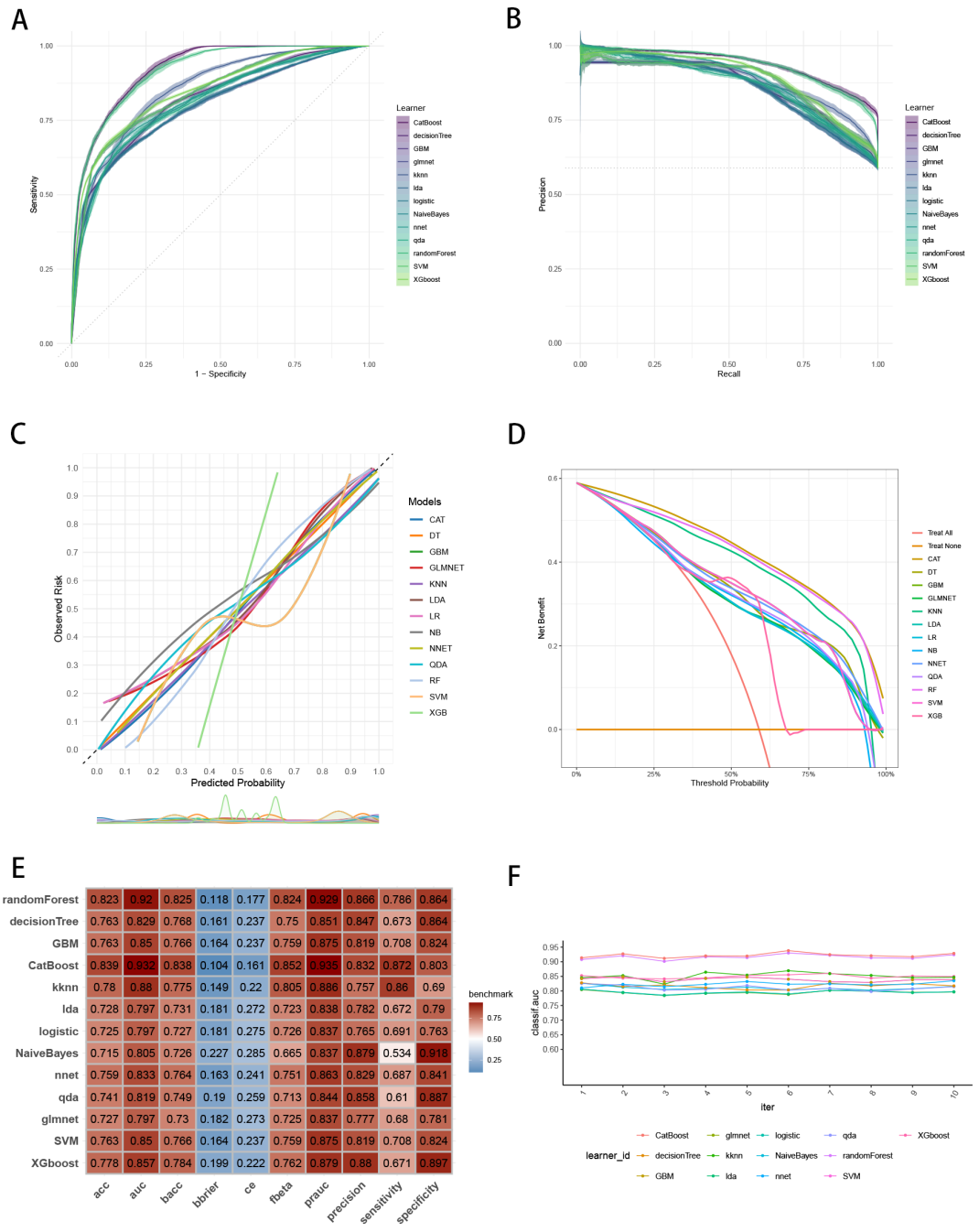

FIGURE 3
Establishment and evaluation of the ML models in the training set. **(A)** ROC curves of different ML models in the training set. **(B)** PR curves of different ML models in the training set. **(C)** Calibration curves of different ML models in the training set. **(D)** DCA curves of different ML models in the training set. **(E)** The performance of 13 ML models in terms of AUC, PRAUC, accuracy, sensitivity, specificity, precision, cross-entropy, Brier scores and Balanced Accuracy (bacc) and F Beta Score (fbeta) in the training set. **(F)** Ten-fold cross-validation results of different ML models in the training set. ML, machine learning; CAT, categorical boosting; LR, logistic regression; DT, decision tree; RF, random forest; XGB, extreme gradient boosting; GBM, gradient boosting machine; NB, Naive Bayes; LDA, linear discriminant analysis; QDA, quadratic discriminant analysis; NNET, neural network; GLMNET, generalized linear models with elastic net regularization; SVM, support vector machine; KNN, k-nearest neighbor.

second leading cause of cancer-related deaths by 2030 (21). Although radical surgery offers a chance for a cure, high rates of postoperative recurrence and mortality remain a significant concern (22). Given these challenges, accurately predicting survival rates and identifying prognostic risk factors is of critical importance for pancreatic cancer patients. In this study, we focused on developing novel predictive and prognostic ML models to early predict three-year survival, and to forecast the prognosis of pancreatic cancer patients. By gathering clinical data on several key variables and establishing ML models via benchmark framework, we were able to calculate risk scores related to prediction and prognosis, enabling us to precisely predict the

10.3389/fonc.2024.1488118

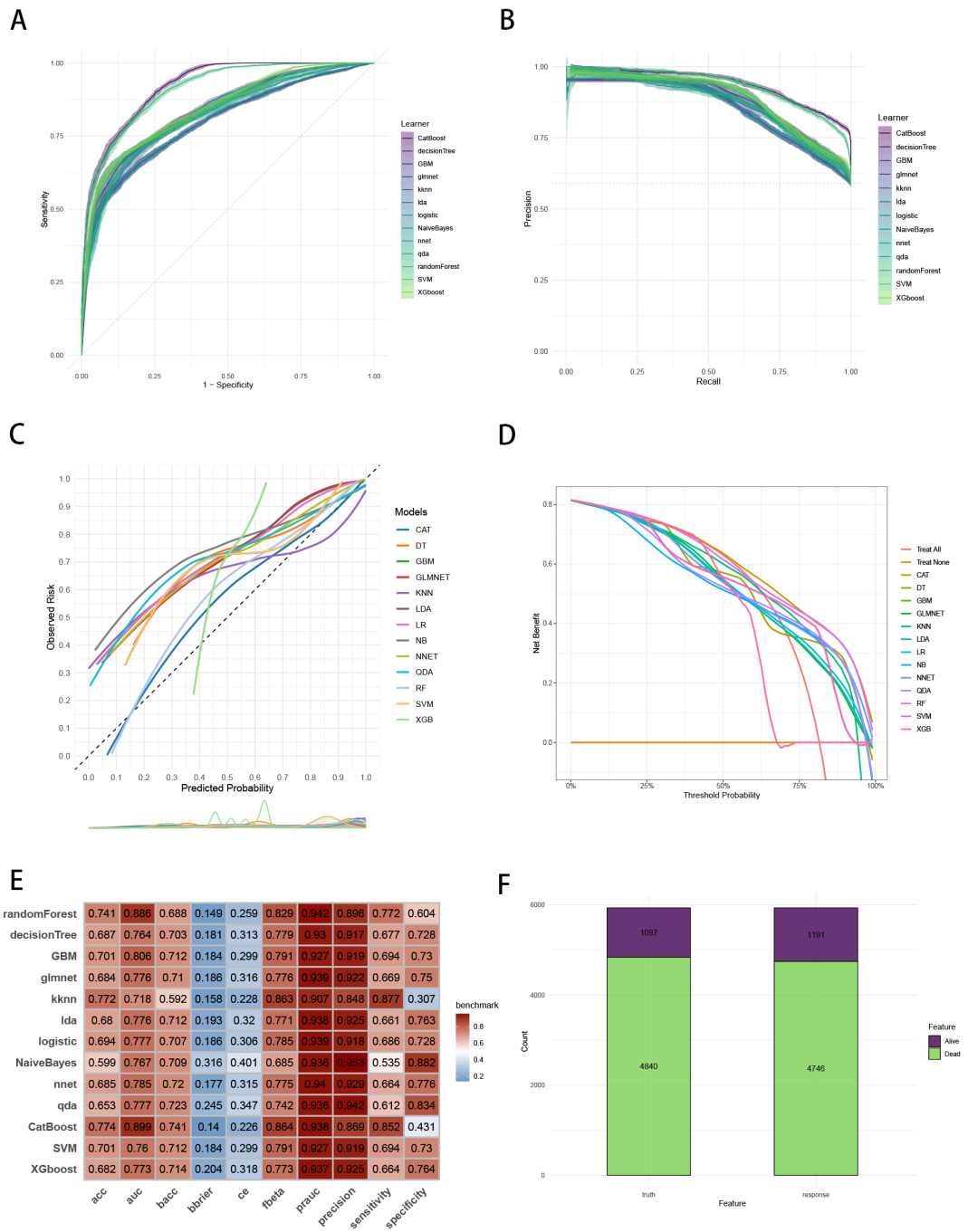

FIGURE 4
Evaluation of the ML models in the internal validation set. **(A)** ROC curves of different ML models in the internal validation set. **(B)** PR curves of different ML models in the internal validation set. **(C)** Calibration curves of different ML models in the internal validation set. **(D)** DCA curves of different ML models in the internal validation set. **(E)** The performance of 13 ML models in terms of AUC, PRAUC, accuracy, sensitivity, specificity, precision, cross-entropy, Brier scores and Balanced Accuracy (bacc) and F Beta Score (fbeta) in the internal validation set. **(F)** Confusion matrix of the best ML model in the internal validation set. ML, machine learning; CAT, categorical boosting; LR, logistic regression; DT, decision tree; RF, random forest; XGB, extreme gradient boosting; GBM, gradient boosting machine; NB, Naive Bayes; LDA, linear discriminant analysis; QDA, quadratic discriminant analysis; NNET, neural network; GLMNET, generalized linear models with elastic net regularization; SVM, support vector machine; KNN, k-nearest neighbor.

probability of three-year survival and the prognosis of patients. The model analyzes various clinical and demographic features to provide a risk score for three-year survival and prognosis, which helps clinicians determine the intensity and type of treatment required for each patient, outperforming the existing models without ML algorithms (23, 24).

The clinical importance of this work lies in its potential to enhance patient management and treatment planning for those

10.3389/fonc.2024.1488118

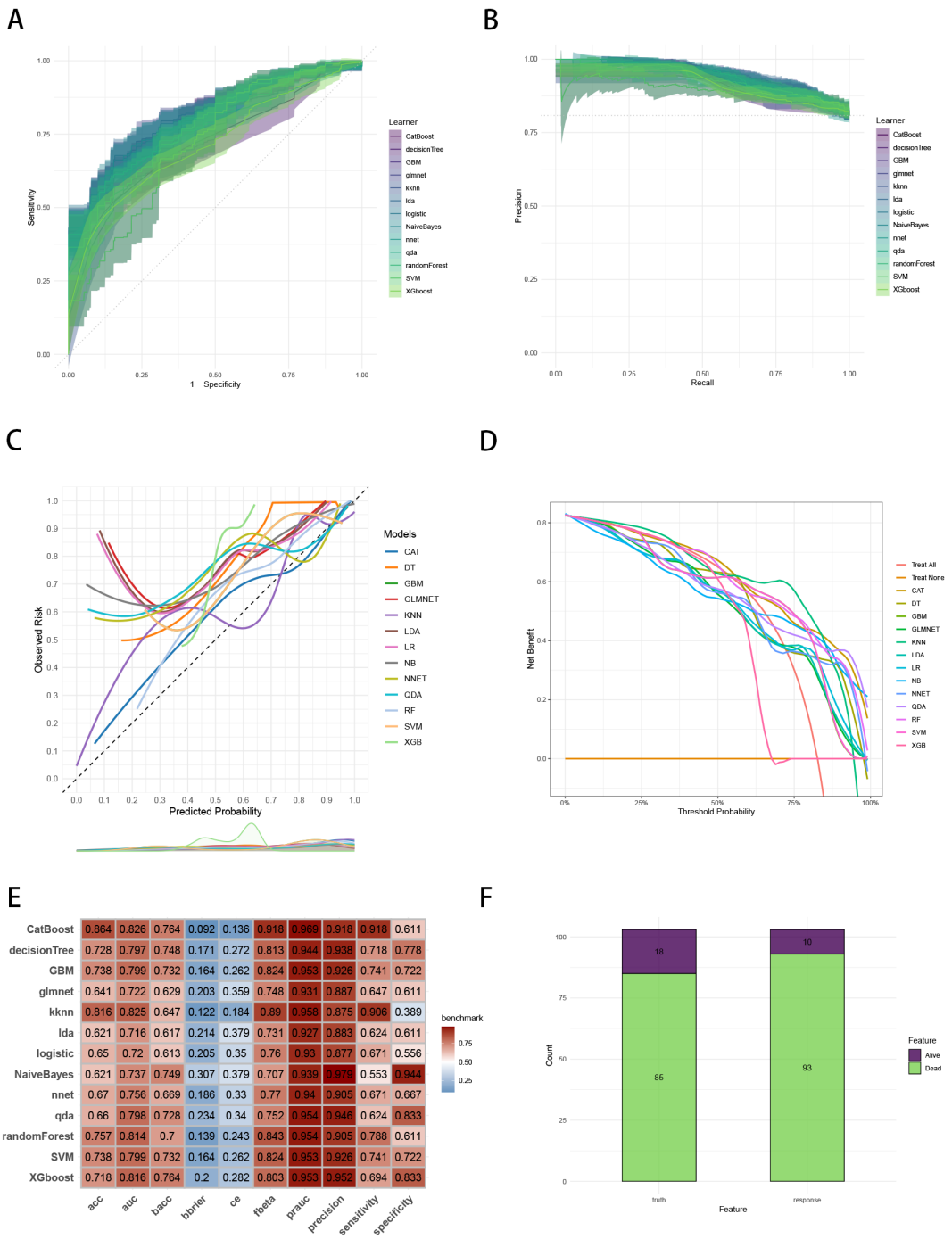

FIGURE 5
Evaluation of the ML models in the external validation set. **(A)** ROC curves of different ML models in the external validation set. **(B)** PR curves of different ML models in the external validation set. **(C)** Calibration curves of different ML models in the external validation set. **(D)** DCA curves of different ML models in the external validation set. **(E)** The performance of 13 ML models in terms of AUC, PRAUC, accuracy, sensitivity, specificity, precision, cross-entropy, Brier scores and Balanced Accuracy (bacc) and F Beta Score (fbeta) in the external validation set. **(F)** Confusion matrix of the best ML model in the external validation set. ML, machine learning; CAT, categorical boosting; LR, logistic regression; DT, decision tree; RF, random forest; XGB, extreme gradient boosting; GBM, gradient boosting machine; NB, Naive Bayes; LDA, linear discriminant analysis; QDA, quadratic discriminant analysis; NNET, neural network; GLMNET, generalized linear models with elastic net regularization; SVM, support vector machine; KNN, k-nearest neighbor.

diagnosed with pancreatic cancer. By providing an accurate risk stratification tool, our model can significantly aid clinicians in making more informed, personalized treatment decisions. For instance, patients identified as high-risk for three-year mortality could be prioritized for aggressive surgical interventions, adjuvant therapies, and closer post-operative monitoring, which may improve their chances of survival. Conversely, patients deemed low-risk could benefit from less intensive treatments, thereby

10.3389/fonc.2024.1488118

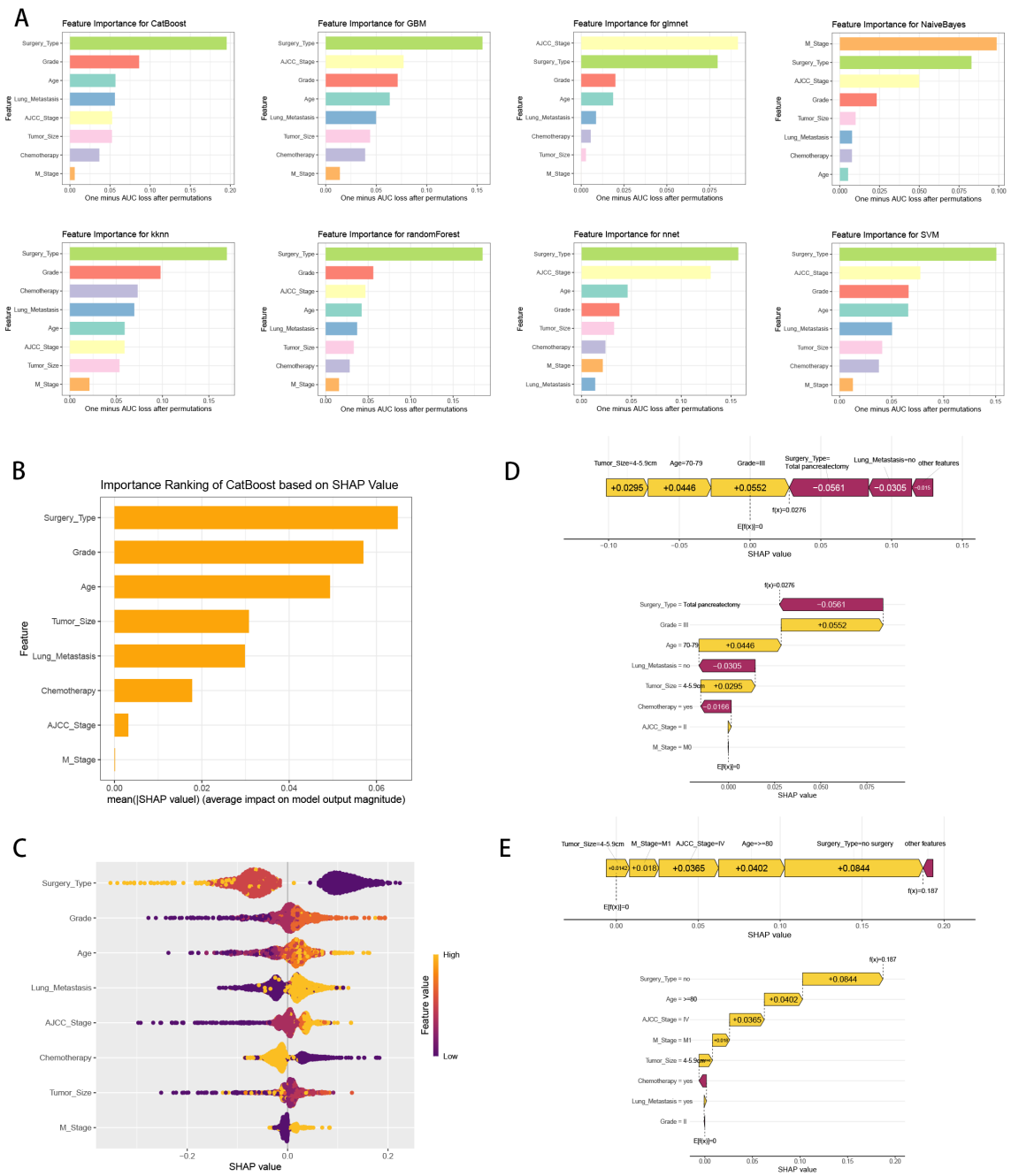

FIGURE 6
ML model interpretation. **(A)** Importance ranking of features in eight ML prediction algorithms (CatBoost, GBM, GLM, NB, KNN, RF, NNET and SVM). **(B)** The importance ranking of different variables according to the mean (|SHAP value|) using the optimal CatBoost model. **(C)** The importance ranking of different risk factors with stability and interpretation using the optimal CatBoost model. The higher SHAP value of a feature is given, the higher risk of distant metastasis the patient would have. The yellow part in feature value represents higher value. **(D)** SHAP value explanation in a classical sample with three-year survival. **(E)** SHAP value explanation in a classical sample without three-year survival.

avoiding the potential side effects and complications associated with overtreatment. Additionally, the model's predictions can help the selection of adjuvant therapies, the frequency of follow-up visits, and the need for additional laboratory tests. By integrating the prediction model into clinical workflows, we enable data-driven decision-making that optimizes patient outcomes and resource allocation. As a result, it helps in standardizing care across different healthcare providers and institutions, potentially reducing variability in treatment approaches and outcomes for pancreatic cancer patients.

Moreover, the highlight of our study lies in showcasing how interpretable ML algorithms, particularly through the use of SHAP values, can effectively decipher key factors contributing to predict three-year survival. CatBoost algorithm is a gradient boosting framework based on the symmetric decision tree (oblivious trees) algorithm, which boasts high accuracy and requires fewer

TABLE 3 Univariate and multivariate cox regression analysis of pancreatic cancer patients for overall survival in the training cohort.

Variable	Univariable cox analysis		Multivariate cox analysis	
term	HR (95%CI)	p.value	HR (95%CI)	p.value
Sex: Male	Reference			
Female	0.96 (0.94-0.99)	0.012	0.934 (0.907-0.963)	<0.001
Age: <50	Reference			
50-59	1.09 (1.02-1.16)	0.008	1.114 (1.045-1.188)	0.001
60-69	1.12 (1.06-1.19)	<0.001	1.19 (1.119-1.264)	<0.001
70-79	1.33 (1.25-1.41)	<0.001	1.412 (1.326-1.502)	<0.001
>=80	1.76 (1.64-1.88)	<0.001	1.598 (1.487-1.717)	<0.001
Race: White	Reference			
Black	1.12 (1.07-1.18)	<0.001	1.071 (1.022-1.123)	0.004
Other	0.96 (0.91-1.01)	0.121	1.022 (0.97-1.077)	0.41
Marital_Status: Married	Reference			
Unmarried	1.11 (1.06-1.16)	<0.001	1.137 (1.086-1.191)	<0.001
Widowed or divorced	1.23 (1.19-1.27)	0	1.162 (1.121-1.206)	<0.001
Unknown	1.07 (0.98-1.16)	0.151	1.07 (0.981-1.167)	0.126
Household_Income: <$70,000	Reference			
>=$70,000	0.89 (0.87-0.92)	<0.001	0.866 (0.837-0.896)	<0.001
Household_Location: Rural				
Urban	0.91 (0.87-0.95)	<0.001	0.945 (0.899-0.993)	0.025
Tumor_Primary_Site: Pancreas Head	Reference			
Pancreas Body or Tail	1.17 (1.13-1.21)	<0.001	0.946 (0.91-0.983)	0.005
Other	1.3 (1.25-1.36)	<0.001	1.004 (0.96-1.051)	0.858
Histology: Adenomas and adenocarcinomas	Reference			
Ductal and lobular neoplasms	0.71 (0.68-0.73)	<0.001	1.022 (0.986-1.059)	0.236
Cystic, mucinous and serous neoplasms	0.59 (0.55-0.63)	0	0.706 (0.66-0.755)	<0.001
Other	0.89 (0.79-1)	0.05	0.876 (0.776-0.988)	0.032
Grade: Well differentiated I	Reference			
Moderately differentiated II	1.25 (1.2-1.32)	<0.001	1.334 (1.271-1.401)	<0.001
Poorly differentiated III	1.74 (1.66-1.83)	<0.001	1.718 (1.635-1.806)	<0.001
Undifferentiated anaplastic IV	1.74 (1.53-1.99)	<0.001	1.485 (1.302-1.694)	<0.001
Summary_Stage: Localized	Reference			
Regional	1.62 (1.53-1.71)	<0.001	1.847 (1.641-2.079)	<0.001
Distant	3.78 (3.56-4)	<0.001	2.136 (1.935-2.357)	<0.001
AJCC_Stage: I	Reference			
II	1.56 (1.48-1.65)	<0.001	0.712 (0.643-0.789)	<0.001
III	2.76 (2.58-2.95)	<0.001	0.762 (0.687-0.846)	<0.001
IV	4.59 (4.32-4.88)	<0.001	NA (NA-NA)	NA

(Continued)

TABLE 3 Continued

Variable	Univariable cox analysis		Multivariate cox analysis	
term	HR (95%CI)	p.value	HR (95%CI)	p.value
T_Stage: T1	Reference			
T2	2 (1.84-2.17)	<0.001	1.066 (0.969-1.172)	0.19
T3	1.85 (1.72-2)	<0.001	1.127 (1.024-1.242)	0.015
T4	3.4 (3.13-3.69)	<0.001	1.15 (1.029-1.285)	0.014
N_Stage: N0	Reference			
N1	1.05 (1.02-1.08)	0.002	1.036 (0.988-1.087)	0.148
M_Stage: M0	Reference			
M1	1.96 (1.9-2.02)	<0.001	1.017 (0.962-1.075)	0.553
Tumor_Size: <2cm	Reference			
2-3.9cm	1.6 (1.51-1.7)	<0.001	1.325 (1.238-1.417)	<0.001
4-5.9cm	2.12 (1.99-2.25)	<0.001	1.514 (1.41-1.625)	<0.001
6-7.9cm	2.46 (2.28-2.65)	<0.001	1.722 (1.581-1.875)	<0.001
>8cm	2.22 (2.02-2.44)	<0.001	1.629 (1.467-1.808)	<0.001
Unknown	3.01 (2.78-3.26)	<0.001	1.439 (1.318-1.572)	<0.001
Surgery_Type: No Surgery	Reference			
Local or partial pancreatectomy	0.31 (0.3-0.32)	<0.001	0.491 (0.45-0.535)	<0.001
Total pancreatectomy	0.33 (0.31-0.34)	<0.001	0.507 (0.462-0.556)	<0.001
Lymph_Nodes_Surgery: No or biopsy only	Reference			
1-3 regional lymph nodes removed	0.41 (0.38-0.44)	<0.001	0.991 (0.888-1.105)	0.868
4 or more regional lymph nodes removed	0.33 (0.32-0.35)	<0.001	0.846 (0.761-0.94)	0.002
Regional_Lymph_Nodes: No nodes were examined	Reference			
Negative	0.25 (0.24-0.27)	<0.001	0.709 (0.65-0.774)	<0.001
Positive	0.41 (0.39-0.42)	<0.001	1.03 (0.941-1.128)	0.524
Unknown	0.71 (0.53-0.94)	0.018	0.914 (0.682-1.225)	0.547
Chemotherapy: None/Unknown	Reference			
Yes	0.65 (0.63-0.67)	<0.001	0.582 (0.562-0.602)	<0.001
Radiotherapy: None/Unknown	Reference			
Yes	0.69 (0.67-0.71)	<0.001	0.905 (0.873-0.938)	<0.001
Metastasis: No	Reference			
Yes	1.58 (1.54-1.63)	<0.001	0.781 (0.709-0.861)	<0.001
Bone_Metastasis: No	Reference			
Yes	2.82 (2.39-3.33)	<0.001	1.196 (1.006-1.422)	0.042
Unknown	1.19 (1.16-1.23)	<0.001	1.186 (0.636-2.21)	0.591
Brain_Metastasis: No	Reference			
Yes	5.37 (2.23-12.9)	<0.001	1.822 (0.747-4.446)	0.187
Unknown	1.18 (1.15-1.22)	<0.001	0.909 (0.498-1.659)	0.756

(Continued)

TABLE 3 Continued

Variable	Univariable cox analysis		Multivariate cox analysis	
term	HR (95%CI)	p.value	HR (95%CI)	p.value
Liver_Metastasis: No	Reference			
Yes	2.99 (2.84-3.15)	<0.001	1.338 (1.224-1.463)	<0.001
Unknown	1.34 (1.3-1.39)	<0.001	1.753 (1.27-2.419)	0.001
Lung_Metastasis: No	Reference			
Yes	2.77 (2.52-3.04)	<0.001	1.338 (1.224-1.463)	<0.001
Unknown	1.22 (1.19-1.26)	<0.001	1.753 (1.27-2.419)	0.001

parameters, making it efficient and effective in handling categorical features (25). CatBoost's performance rivals that of other advanced machine learning algorithms, demonstrating its superiority in many applications. But the black-box feature of CatBoost model necessitated its interpretation and explanation with vivid figures. CatBoost's SHAP summary plots and force maps serve as valuable tools, offering clinicians a visual and intuitive means to understand and identify the critical features influencing three-year survival, which not only elucidates the pivotal risk factors but also improves the interpretability of ML models in clinical settings. Meanwhile, several advanced ML techniques, including feature selection through RFECV, hyperparameter optimization with GridSearchCV, and addressing sample imbalance using SMOTE oversampling, had significantly enhanced the prediction accuracy for the probability of three-year survival. Overall, our precise ML prediction model allowed clinicians to schedule personalized treatment plans, helping them tailor therapy methods in time and enhance prognosis of pancreatic cancer patients.

Researchers have previously shown that old age, high histological grade, large tumor size, AJCC stage, surgery type and metastasis are associated with poorer long-term survival outcomes for pancreatic cancer patients (26, 27). In clinical practice, serum CA199 and CEA levels are commonly used biomarkers in pancreatic cancer, and high levels of CA199 are generally associated with a worse prognosis. Meanwhile, the methylation status of NPTX2, BMP3 and SPARC genes plays an important role in the prognosis of pancreatic cancer. Researchers suggest that methylation of these genes could be used as non-invasive biomarkers to assess prognosis and monitor disease progression in patients with pancreatic cancer (28). In our analysis, we performed univariate and multivariate logistic and cox regression analyses to discover important predictive factors for three-year survival, as well as independent risk factors for prognosis. Based on clinical variables which can be easily obtained during clinical practices, we succeeded in constructing a powerful CatBoost model to early predict three-year survival.

In our research, we observed that patients with pancreatic cancer who undergo surgical resection demonstrated significantly improved survival rates, as supported by Hester et al.'s analysis of the National Cancer Database (29). However, surgery alone is often insufficient for achieving long-term survival, with median survival times typically ranging between 8 to 10 months, frequently accompanied by tumor recurrence (30). Chemotherapy, both as a neoadjuvant (preoperative) and adjuvant (postoperative) treatment, has been identified through logistic and cox regression analyses as a key independent factor in enhancing patient survival. Specifically, adjuvant chemotherapy has been shown to double median survival rates compared to patients who do not receive it, while neoadjuvant chemotherapy improves overall survival and increases the likelihood of R0 resection, making it a valuable treatment option (31). Additionally, age is an independent risk factor, with older patients exhibiting lower survival rates, likely due to diminished immunity and physical decline, which is also common in other types of cancer. Moreover, we found that race does play a role in pancreatic cancer prognosis. African Americans have a higher rate of pancreatic cancer than other racial groups, and their overall survival rate is lower. This difference may be related to a variety of factors, including socioeconomic status, access to and quality of health care, and genetic and environmental factors (32).

Gender can influence the prognosis of pancreatic cancer, though the impact is complex and varies depending on several factors (33). Our analysis results show that women generally have a slightly better overall survival (OS) compared to men. This improved survival in women has also been observed in studies analyzing the outcomes of both standard treatments and more aggressive chemotherapy regimens like FOLFIRINOX (34). Moreover, our analysis displayed that metastasis in pancreatic cancer significantly affected prognosis, with different metastatic sites influencing survival outcomes differently (35). Common sites of distant metastasis in pancreatic cancer include the peritoneum and liver, followed by the lungs, bones, and other organs (36). Liver metastasis is the most common and is associated with the poorest prognosis, often due to the liver's role in filtering blood and its involvement in the metabolism of cancer drugs. Lung metastasis, while also serious and crucial, generally presents a slightly better prognosis compared to liver involvement. Peritoneal metastasis reflects a more extensive spread of the disease within the abdominal cavity. This type of metastasis is particularly challenging because it often leads to complications such as ascites (the accumulation of fluid in the abdomen), which can be difficult to manage and severely impacts the patient's quality of life. Overall,

10.3389/fonc.2024.1488118

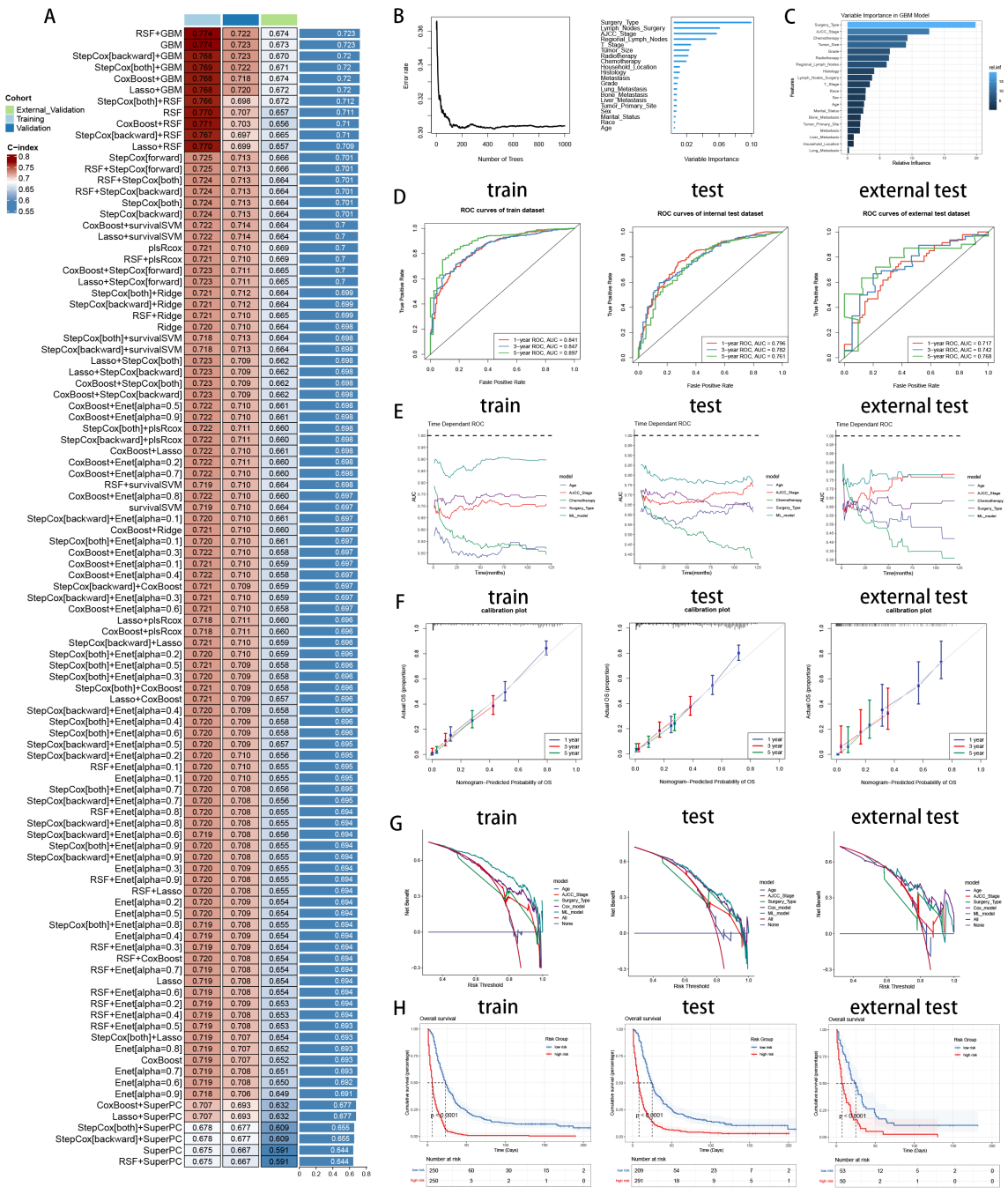

FIGURE 7
Establishment and validation of prognostic model for pancreatic cancer patients. **(A)** A total of 101 kinds of prognostic models via a leave-one-out cross-validation framework and further calculated the C-index of each model. **(B)** Feature selection process by RSF algorithm. **(C)** Model construction by GBM algorithm and visualization of feature importance. **(D)** ROC curves of ML model in training, internal validation and external validation cohorts. **(E)** Time dependent AUC values of ML model in training, internal validation and external validation cohorts. **(F)** Calibration curves of ML model in training, internal validation and external validation cohorts. **(G)** DCA curves of ML model in training, internal validation and external validation cohorts. **(H)** K-M curves of low-risk and high-risk groups divided by ML model in training, internal validation and external validation cohorts. Left: training cohort, Middle: internal validation cohort, Right: external validation cohort.

the presence of metastasis generally indicates an advanced disease and a poor prognosis, due to the difficulty of achieving complete surgical resection and the challenges in effectively targeting metastatic sites with systemic therapies.

While this study boasts certain strengths, it also faces multiple limitations. Firstly, we calculated the needed sample size for our external validation set, but we were unable to gather a large enough external validation set due to the limited number of patients with complete follow-up information. Although we recognize that large sample sizes improve the reliability of model evaluations, we have tried to collect the largest sample size available in the current research environment. Despite the small set of external

validations, we maximize the reliability of validation by using a 10-fold cross-validation approach to assess the model's ability to generalize. In future studies, we plan to increase the sample size of the external validation set, thereby further verifying the universality and reliability of the model. Secondly, our study relies on retrospective datasets sourced from the SEER database, causing possibility of selection bias. Meanwhile, the inconsistent data collection across multiple hospitals, as well as the retrospective study design, led to some missing clinical feature data. Thirdly, the absence of some key clinicopathological parameters is noted, due to the unavailability of image data and laboratory test indicators from the SEER database. The study predominantly utilizes baseline characteristics and routine clinical data as variables, without some important indicators such as CA199, CEA and KRAS gene mutation. To enhance the model's predictive accuracy and identify risk factors, a broad range of features was included, which somewhat complicates its practical application in a clinical setting. Finally, the model has yet to be implemented in clinical practice, thus necessitating prospective, multicenter, and large-scale validations to fully ascertain its generalizability in the future.

Conclusions

In this study, we developed a CatBoost predictive model based on ML benchmark framework, to more accurately predict three-year survival for pancreatic cancer patients, surpassing traditional models in effectiveness and performances. We successfully identified significant predictive factors for three-year survival of pancreatic cancer. Meanwhile, we establish a GBM prognostic model to predict prognosis of pancreatic cancer patients for achieving personalized medicine. This research laid a foundation for future efforts aimed at enhancing three-year survival prediction and prognosis forecasting, which could help clinicians in decision making and therapy plan tailoring.

Data availability statement

The raw data supporting the conclusions of this article will be made available by the authors, without undue reservation.

Ethics statement

The studies involving humans were approved by Ethics Committee of The First People's Hospital of Lianyungang. The studies were conducted in accordance with the local legislation and institutional requirements. Written informed consent for participation was not required from the participants or the participants' legal guardians/next of kin in accordance with the national legislation and institutional requirements. Written informed consent was obtained from the individual(s) for the publication of any potentially identifiable images or data included in this article.

Author contributions

BT: Data curation, Formal analysis, Investigation, Methodology, Validation, Visualization, Writing – original draft. XZ: Data curation, Formal analysis, Investigation, Methodology, Validation, Visualization, Writing – original draft. MG: Data curation, Formal analysis, Writing – original draft. MM: Data curation, Formal analysis, Writing – original draft. WL: Conceptualization, Investigation, Supervision, Writing – review & editing. JM: Conceptualization, Investigation, Supervision, Writing – review & editing.

Funding

The author(s) declare that no financial support was received for the research, authorship, and/or publication of this article.

Acknowledgments

We are grateful to the Surveillance, Epidemiology, and End Results (SEER) database for providing data.

Conflict of interest

The authors declare that the research was conducted in the absence of any commercial or financial relationships that could be construed as a potential conflict of interest.

Publisher's note

All claims expressed in this article are solely those of the authors and do not necessarily represent those of their affiliated organizations, or those of the publisher, the editors and the reviewers. Any product that may be evaluated in this article, or claim that may be made by its manufacturer, is not guaranteed or endorsed by the publisher.

Supplementary material

The Supplementary Material for this article can be found online at: https://www.frontiersin.org/articles/10.3389/fonc.2024.1488118/full#supplementary-material

References

1. Siegel RL, Miller KD, Wagle NS, Jemal A. Cancer statistics, 2023. *CA Cancer J Clin*. (2023) 73:17–48. doi: 10.3322/caac.21763

2. Vincent A, Herman J, Schulick R, Hruban RH, Goggins M. Pancreatic cancer. *Lancet*. (2011) 378:607–20. doi: 10.1016/S0140-6736(10)62307-0

3. Gillen S, Schuster T, Meyer Zum Büschenfelde C, Friess and J. Kleeff H. Preoperative/neoadjuvant therapy in pancreatic cancer: a systematic review and meta-analysis of response and resection percentages. *PLoS Med*. (2010) 7:e1000267. doi: 10.1371/journal.pmed.1000267

4. Zhao Z, Liu W. Pancreatic cancer: A review of risk factors, diagnosis, and treatment. *Technol Cancer Res Treat*. (2020) 19:1533033820962117. doi: 10.1177/1533033820962117

5. He Q, Liu Z, Wang J. Targeting KRAS in PDAC: A new way to cure it? *Cancers (Basel)*. (2022) 14(20):4982. doi: 10.3390/cancers14204982

6. Tempero MA, Malafa MP, Chiorean EG, Czito B, Scaife C, Narang AK, et al. Pancreatic adenocarcinoma, version 1.2019. *J Natl Compr Canc Netw*. (2019) 17:202–10. doi: 10.6004/jnccn.2019.0014

7. Mitchell PS, Parkin RK, Kroh EM, Fritz BR, Wyman SK, Pogosova-Agadjanyan EL, et al. Circulating microRNAs as stable blood-based markers for cancer detection. *Proc Natl Acad Sci U S A*. (2008) 105:10513–8. doi: 10.1073/pnas.0804549105

8. Chalmers ZR, Connelly CF, Fabrizio D, Gay L, Ali SM, Ennis R, et al. Analysis of 100,000 human cancer genomes reveals the landscape of tumor mutational burden. *Genome Med*. (2017) 9:34. doi: 10.1186/s13073-017-0424-2

9. Collins GS, Dhiman P, Andaur Navarro CL, Ma J, Hooft L, Reitsma JB, et al. Protocol for development of a reporting guideline (TRIPOD-AI) and risk of bias tool (PROBAST-AI) for diagnostic and prognostic prediction model studies based on artificial intelligence. *BMJ Open*. (2021) 11:e048008. doi: 10.1136/bmjopen-2020-048008

10. Pera M, Gibert J, Gimeno M, Garsot E, Eizaguirre E, Miró M, et al. Machine learning risk prediction model of 90-day mortality after gastrectomy for cancer. *Ann Surg*. (2022) 276:776–83. doi: 10.1097/SLA.0000000000005616

11. Zhuang D, Li T, Xie H, Sheng J, Chen X, Li X, et al. A dynamic nomogram for predicting intraoperative brain bulge during decompressive craniectomy in patients with traumatic brain injury: a retrospective study. *Int J Surg*. (2023) 110(2):909–20. doi: 10.1097/JS9.0000000000001348

12. Riley RD, Debray TPA, Collins GS, Archer L, Ensor J, van Smeden M, et al. Minimum sample size for external validation of a clinical prediction model with a binary outcome. *Stat Med*. (2021) 40:4230–51. doi: 10.1002/sim.v40.19

13. Wang K, Tian J, Zheng C, Yang H, Ren J, Liu Y, et al. Interpretable prediction of 3-year all-cause mortality in patients with heart failure caused by coronary heart disease based on machine learning and SHAP. *Comput Biol Med*. (2021) 137:104813. doi: 10.1016/j.compbiomed.2021.104813

14. Kolde R, Laur S, Adler P, Vilo J. Robust rank aggregation for gene list integration and meta-analysis. *Bioinformatics*. (2012) 28:573–80. doi: 10.1093/bioinformatics/btr709

15. Lang M, Binder M, Richter J, Schratz P, Pfisterer F, Coors S, et al. mlr3: A modern object-oriented machine learning framework in R. *J Open Source Software*. (2019) 4:1903. doi: 10.21105/joss.01903

16. Wang K, Tian J, Zheng C, Yang H, Ren J, Li C, et al. Improving risk identification of adverse outcomes in chronic heart failure using SMOTE+ENN and machine learning. *Risk Manag Healthc Policy*. (2021) 14:2453–63. doi: 10.2147/RMHP.S310295

17. Biecek P. Dalex: Explainers for complex predictive models in R. *J Mach Learn Res*. (2018) 19:1–5. doi: 10.5555/3291125.3309646

18. Lo YT, Liao JC, Chen MH, Chang CM, Li CT. Predictive modeling for 14-day unplanned hospital readmission risk by using machine learning algorithms. *BMC Med Inform Decis Mak*. (2021) 21:288. doi: 10.1186/s12911-021-01639-y

19. Liu Z, Liu L, Weng S, Guo C, Dang Q, Xu H, et al. Machine learning-based integration develops an immune-derived lncRNA signature for improving outcomes in colorectal cancer. *Nat Commun*. (2022) 13:816. doi: 10.1038/s41467-022-28421-6

20. Sonabend R, Király FJ, Bender A, Bischl B, Lang M. mlr3proba: an R package for machine learning in survival analysis. *Bioinformatics*. (2021) 37:2789–91. doi: 10.1093/bioinformatics/btab039

21. Rahib L, Smith BD, Aizenberg R, Rosenzweig AB, Fleshman JM, Matrisian LM. Projecting cancer incidence and deaths to 2030: the unexpected burden of thyroid, liver, and pancreas cancers in the United States. *Cancer Res*. (2014) 74:2913–21. doi: 10.1158/0008-5472.CAN-14-0155

22. Fatima J, Schnelldorfer T, Barton J, Wood CM, Wiste HJ, Smyrk TC, et al. Pancreatoduodenectomy for ductal adenocarcinoma: implications of positive margin on survival. *Arch Surg*. (2010) 145:167–72. doi: 10.1001/archsurg.2009.282

23. You K, Lei K, Wang X, Hu R, Zhang H, Xu J, et al. A novel nomogram based on the number of positive lymph nodes can predict the overall survival of patients with pancreatic head cancer after radical surgery. *World J Surg Oncol*. (2024) 22:241. doi: 10.1186/s12957-024-03519-x

24. Peng W, Yu X, Yang R, Nie S, Jian X, Zeng P. Construction and validation of a nomogram for cancer specific survival of postoperative pancreatic cancer based on the SEER and China database. *BMC Gastroenterol*. (2024) 24:104. doi: 10.1186/s12876-024-03180-4

25. Zhang C, Chen X, Wang S, Hu J, Wang C, Liu X. Using CatBoost algorithm to identify middle-aged and elderly depression, national health and nutrition examination survey 2011-2018. *Psychiatry Res*. (2021) 306:114261. doi: 10.1016/j.psychres.2021.114261

26. Zhang W, Ji L, Wang X, Zhu S, Luo J, Zhang Y, et al. Nomogram predicts risk and prognostic factors for bone metastasis of pancreatic cancer: A population-based analysis. *Front Endocrinol (Lausanne)*. (2021) 12:752176. doi: 10.3389/fendo.2021.752176

27. Li Q, Feng Z, Miao R, Liu X, Liu C, Liu Z. Prognosis and survival analysis of patients with pancreatic cancer: retrospective experience of a single institution. *World J Surg Oncol*. (2022) 20:11. doi: 10.1186/s12957-021-02478-x

28. García-Ortiz MV, Cano-Ramírez P, Toledano-Fonseca M, Cano MT, Inga-Saavedra E, Rodríguez-Alonso RM, et al. Circulating NPTX2 methylation as a non-invasive biomarker for prognosis and monitoring of metastatic pancreatic cancer. *Clin Epigenet*. (2023) 15:118. doi: 10.1186/s13148-023-01535-4

29. Hester CA, Augustine MM, Choti MA, Mansour JC, Minter RM, Polanco PM, et al. Comparative outcomes of adenosquamous carcinoma of the pancreas: An analysis of the National Cancer Database. *J Surg Oncol*. (2018) 118:21–30. doi: 10.1002/jso.v118.1

30. Groot VP, Rezaee N, Wu W, Cameron JL, Fishman EK, Hruban RH, et al. Patterns, timing, and predictors of recurrence following pancreatectomy for pancreatic ductal adenocarcinoma. *Ann Surg*. (2018) 267:936–45. doi: 10.1097/SLA.0000000000002234

31. Luo G, Fan Z, Gong Y, Jin K, Yang C, Cheng H, et al. Characteristics and outcomes of pancreatic cancer by histological subtypes. *Pancreas*. (2019) 48:817–22. doi: 10.1097/MPA.0000000000001338

32. Jiang Z, Zheng X, Li M, Liu M. Improving the prognosis of pancreatic cancer: insights from epidemiology, genomic alterations, and therapeutic challenges. *Front Med*. (2023) 17:1135–69. doi: 10.1007/s11684-023-1050-6

33. Pijnappel EN, Schuurman M, Wagner AD, de Vos-Geelen J, van der Geest LGM, de Groot JB, et al. Sex, gender and age differences in treatment allocation and survival of patients with metastatic pancreatic cancer: A nationwide study. *Front Oncol*. (2022) 12:839779. doi: 10.3389/fonc.2022.839779

34. Kim J, Ji E, Jung K, Jung IH, Park J, Lee JC, et al. Gender differences in patients with metastatic pancreatic cancer who received FOLFIRINOX. *J Pers Med*. (2021) 11(2):83. doi: 10.3390/jpm11020083

35. Usón PLSJ, Tolentino FDS, Santos VM, Rother ET, Maluf FC. The impact of metastatic sites in advanced pancreatic adenocarcinoma, systematic review and meta-analysis of prospective randomized studies. *PLoS One*. (2020) 15:e0230060. doi: 10.1371/journal.pone.0230060

36. He C, Huang X, Zhang Y, Lin X, Li S. The impact of different metastatic patterns on survival in patients with pancreatic cancer. *Pancreatology*. (2021) 21:556–63. doi: 10.1016/j.pan.2021.01.014

frontiers | Frontiers in Immunology

TYPE Review
PUBLISHED 28 October 2024
DOI 10.3389/fimmu.2024.1485628

Check for updates

OPEN ACCESS

EDITED BY
Wantao Wu,
Chongqing Medical University, China

REVIEWED BY
Weijie Sun,
First Affiliated Hospital of Bengbu Medical University, China
Ping'An Ding,
Fourth Hospital of Hebei Medical University, China

*CORRESPONDENCE
Sinian Liu
263709268@qq.com
Zhongqiu Yang
yangzhongqiu2008@163.com
Xiaowei Tang
solitude5834@hotmail.com

†These authors share first authorship

RECEIVED 24 August 2024
ACCEPTED 08 October 2024
PUBLISHED 28 October 2024

CITATION
Su L, Yue Y, Yan Y, Sun J, Meng L, Lu J, Zhang L, Liu J, Chi H, Liu S, Yang Z and Tang X (2024) Extracellular vesicles in hepatocellular carcinoma: unraveling immunological mechanisms for enhanced diagnosis and overcoming drug resistance. *Front. Immunol.* 15:1485628. doi: 10.3389/fimmu.2024.1485628

COPYRIGHT
© 2024 Su, Yue, Yan, Sun, Meng, Lu, Zhang, Liu, Chi, Liu, Yang and Tang. This is an open-access article distributed under the terms of the Creative Commons Attribution License (CC BY). The use, distribution or reproduction in other forums is permitted, provided the original author(s) and the copyright owner(s) are credited and that the original publication in this journal is cited, in accordance with accepted academic practice. No use, distribution or reproduction is permitted which does not comply with these terms.

Extracellular vesicles in hepatocellular carcinoma: unraveling immunological mechanisms for enhanced diagnosis and overcoming drug resistance

Lanqian Su[1†], Yuxin Yue[2†], Yalan Yan[1†], Jianming Sun[3†], Lanxin Meng[1], Jiaan Lu[1], Lanyue Zhang[1], Jie Liu[3], Hao Chi[1], Sinian Liu[4*], Zhongqiu Yang[3*] and Xiaowei Tang[5*]

[1]School of Clinical Medicine, The Affiliated Hospital of Southwest Medical University, Luzhou, China, [2]Department of Pediatrics, Southwest Medical University, Luzhou, China, [3]Department of General Surgery, Dazhou Central Hospital, Dazhou, China, [4]Department of Pathology, Xichong People's Hospital, Nanchong, China, [5]Department of Gastroenterology, The Affiliated Hospital of Southwest Medical University, Luzhou, China

Current research is focused on utilizing EVs as a biopsy tool to improve the diagnostic accuracy of HCC, reduce surgical risk, and explore their potential in modulating drug resistance and advancing immunotherapeutic strategies. Extracellular vesicles (EVs) have been increasingly recognized as important non-invasive biomarkers in hepatocellular carcinoma (HCC) due to the presence of a variety of biomolecules within them, such as proteins and RNAs, etc. EVs play a key role in the early detection, diagnosis, treatment, and prognostic monitoring of HCC. These vesicles influence the development of HCC and therapeutic response in a variety of ways, including influencing the tumor microenvironment, modulating drug resistance, and participating in immune regulatory mechanisms. In addition, specific molecules such as miRNAs and specific proteins in EVs are regarded as potential markers for monitoring treatment response and recurrence of HCC, which have certain research space and development prospects. In this paper, we summarize the aspects of EVs as HCC diagnostic and drug resistance markers, and also discuss the questions that may be faced in the development of EVs as markers.

KEYWORDS

extracellular vesicles, hepatocellular carcinoma, tumor marker, diagnosis, drug resistance

1 Introduction

As a non-invasive biomarker, extracellular vesicles (EVs) contain a variety of biomolecules that may play an important role in the early detection diagnosis, precise treatment, and prognostic monitoring of HCC (1–3). The adoption of EV as a biomarker for HCC may improve diagnostic accuracy, enhance therapeutic efficacy, and improve prognostic outcomes (4). Currently, such innovative markers have attracted extensive scientific attention (5–8).

This is a heterogeneous group of lipid bilayer boundary particles actively secreted by cells into their surroundings (9), which are divided into three main subtypes: microvesicles/extranuclear granular bodies (Ectosomes) (100-500 nm), Exosomes (30-150 nm), and Apoptotic Bodies (500-2000 nm) (10). They are carriers of a wide range of bioactive molecules originating from the mother cell, including lipids (phosphatidylserine, etc.), RNAs (long non-coding RNAs, mRNAs, etc.), carbohydrates (glycoproteins, glycolipids), and proteins (growth factors, tumor suppressors, enzymes, membrane-integrating proteins, etc.) (11). They are widely distributed in various biological fluids with different sizes, cellular sources of secretion, biological functions and release pathways (12). Meanwhile, EVs play an important role in controlling the tumor microenvironment (TME), and they can control the development of certain cancers, immune escape, angiogenesis, tumor metastasis, proliferation and migration, etc. (Figure 1A).

EV secretion is an emerging mechanism by which tumor cells communicate with their surroundings (13). In a variety of cancers, EV can transfer a variety of molecular to the target organ, creating a microenvironment conducive to tumor cell colonization and growth by regulating local cell function, inducing the transformation of mesenchymal cells into fibroblasts (CAF) with pro-tumorigenic properties or directly transforming resident cells into tumor-supportive cells (14, 15). In HCC, EVs can be derived from tumor cells versus non-tumor cells. Since EVs can carry different molecules, and these biomarkers can provide specific information on tumor type, subtype, genetic variation, and drug sensitivity, and the secretion, composition, and functional status of EVs change dynamically with tumor progression, metastasis, the development of drug resistance, and other pathological processes, EVs can be used as a carrier of biomarkers for liver cancer (7, 16).

Through the technical means of liquid biopsy, DNA and RNA in EVs with the help of finer molecular profiling (17), can provide valuable information about early detection, therapeutic monitoring and prognostic assessment of hepatocellular carcinoma (HCC) (18). Exosomes carry genetic information consistent with their parent cells, including DNA fragments, mRNA, miRNA, lncRNA, and others. Detection and analysis of these molecular cargoes provide new methods for non-invasive and precise tumor diagnosis. For example, some experiments have shown that DNA carried by exosomes can be examined by digital PCR (dPCR) or next-generation sequencing (NGS), and that the gene mutation profile

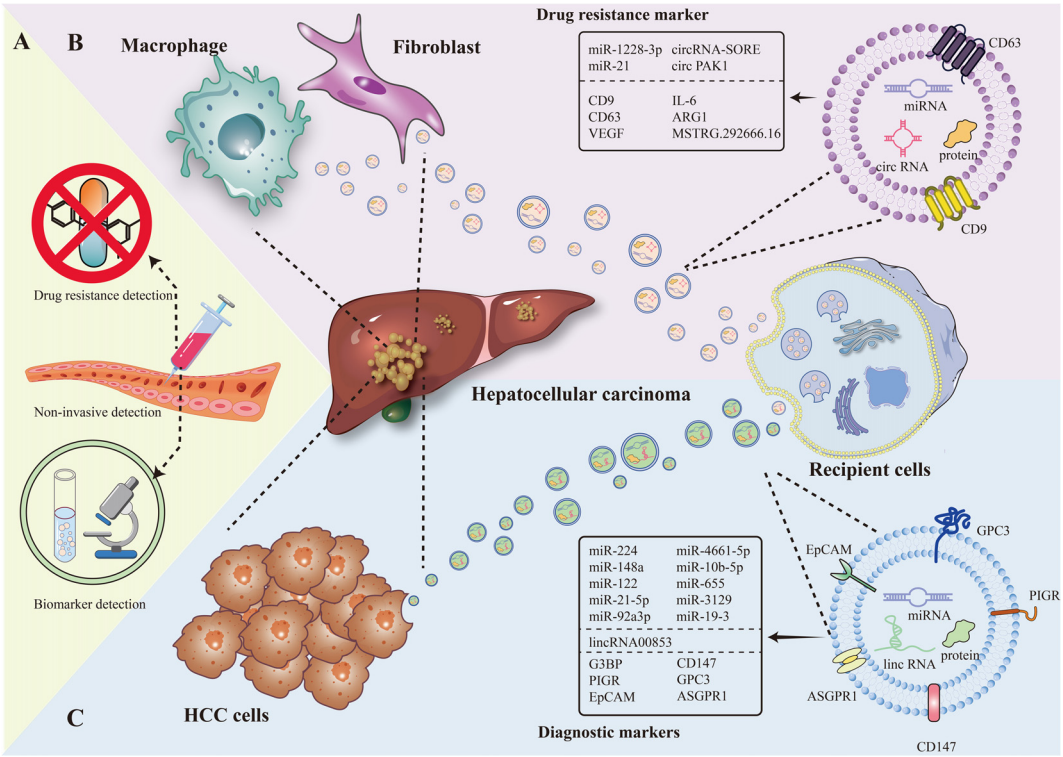

FIGURE 1
The figure present EV as a marker for diagnosis and drug resistance in HCC in terms of non-invasive testing, EV of tumor cell origin, and EV of immune cell origin. **(A)** Diagnostic markers and resistance markers by non-invasive testing. **(B)** Macrophage, fibroblast-derived EV as drug resistance markers in HCC. **(C)** Hepatocellular carcinoma cell-derived EV as a diagnostic marker in HCC.

of cells can be recognized in the presence of low DNA concentrations (19).

2 EV as a biomarker for the diagnosis of HCC

In the past, extracellular vesicles (EV) have (20, 21) become another novel marker for diagnosis by virtue of its special composition (e.g., carrying various types of biomolecules including DNA, RNA, metabolic substances, etc.) and biological functions (involved in inter-cellular communication and cancer progression, etc.) (22). Compared with the low positive rate of traditional direct detection of mi-RNA and protein, EV for diagnosis has more natural advantages: it is widely distributed and can be detected in the blood and other biological fluids of cancer patients; it carries a wide range of tumor-associated molecules, which can specifically reflect the tumor situation. Moreover, EV can protect the nucleic acids within it from decomposition, and EV is highly correlated with the state of its parental cells and can inherit the expression of parental cell traits (23). In addition, the use of EV as a biopsy tool in the diagnostic process can reduce the risk of cancer cell dissemination and infection (24) (Figure 1B).

Some data studies have shown that the area under the curve (AUC) of the summarized subject work characteristics (SROC) is 0.88, which may indicate that EV is highly conservative as an early diagnostic marker (25). Meanwhile, subgroup analysis showed that the use of small EV as a biomarker was more accurate ($p < 0.001$) in serum-based neurological cancer samples (26). In addition, a team of researchers retrieved a total of 3993 records related to HCC by analyzing relevant literature in various databases and screened 18 studies for diagnostic analysis. The results showed that the combined sensitivity of exosomal miRNA amounted to 0.86, which increased to 0.89 when exosomal RNA was used in combination with AFP for diagnostic purposes (27). Various types of studies have demonstrated the greater diagnostic ability and sensitivity of EV (28).

Extraction and purification techniques for EV have been advancing, and the exosome extraction methods currently in use are ultracentrifugation and total exosome isolation kits, among others (29). In terms of testing technologies, emerging technologies such as nano-flow cytometry and super-resolution microscopy have emerged. The former nano-flow cytometry provides high-throughput characterization of exosomes (30), and the latter ultra-high-resolution microscopy provides high-resolution structural information (31), which has become a more precise and efficient tool for exosome research. The importance of exosomes in the diagnostic field is gradually emerging as the RNA and protein content and classes in exosomes are further investigated using cutting-edge technologies.

2.1 RNA sorting

The RNA components expressed by exosomes differ between HCC patients and healthy individuals (32–34). Taking miR-224 as an example, several studies demonstrated that its expression level in HCC tissues was significantly higher than that in normal controls (35), suggesting that miR-224 may serve as a potential biomarker for hepatocellular carcinoma. Further validation revealed that the expression of miR-224-containing exosomes was also higher in HepG2 and SKHEP1 hepatocellular carcinoma cell lines compared with normal controls (35). And this high expression of miR-224 was associated with larger tumor volumes and advanced stages of disease (35). From hepatocellular carcinoma cells to sera of hepatocellular carcinoma patients, in conclusion, differential expression of miR-224-containing exosomes may provide more informative support for early noninvasive diagnosis and prediction of HCC.

The diagnostic performance of exosome-derived miRNA as a diagnostic marker for HCC was higher than that of conventional HCC markers. In the HCC group, the area under the curve of miR-148a from serum exosomes was higher than that of alpha-fetoprotein (36). Not only that, some of the mi-RNAs carried by EV had high specificity and sensitivity on HCC. For example, the prediction of HCC using miR-224 had a sensitivity of 92.5%, a specificity of 90%, and an accuracy of 0.94, which was higher than the sensitivity of AFP (37).

In addition to miR-224, there are other EV-carrying miRNAs that have been suggested as biomarkers of early potentiality. For example, miR-21-5p, miR-92a3p, miR-4661-5p, miR-10b-5p, miR-655, miR-3129, miR-19-3 (38–44) and others.

Furthermore, at the level of tumor heterogeneity, RNA and protein cargoes in EVs secreted by different subpopulations of HCC cells reflect tumor suppressive and metastatic potentials, and these molecules reveal phenotypic differences between different subpopulations of HCC cells. Taking miR-122 as an example, it was demonstrated that deletion of miR-122 resulted in increased cell migration and invasion, and conversely, restoration of miR-122 reversed this phenotype (45). This suggests that miR-122 is a marker of hepatocyte-specific differentiation, and that there are differences in the levels of miR-122 in EVs secreted by different subpopulations of HCC cells, which affects tumor suppression and metastatic potential, and can be used to distinguish between different subtypes of HCC.

miRNAs have a clear biological mechanism and a broad research base, however, other RNAs contained within EV, such as highly stable circRNAs and tsRNAs, as well as lincRNAs, which have complex regulatory capabilities and specific expression, have been less studied for possible use as biomarkers. For example, the demonstration of a cohort experiment showed that lincRNA00853 in serum-derived EV showed a high degree of specificity in patients with primary hepatocellular carcinoma (HCC), whereas another scientific team observed differential changes in lincRNA by controlling themselves before and after resection of the tumor (46).Thus, there is an opportunity for lincRNA to be used as a diagnostic marker for early HCC, especially in patients with early-stage tumors who have negative AFP test results (46).

2.2 Protein sorting

Previously, the conventional protein-based marker in clinical HCC diagnosis was AFP, which has a sensitivity between 60% and

70% and a specificity of 90% (47). Using a simplified HCC-derived EV surface protein assay (SPA) test, the possibility of utilizing EV-loaded proteins as novel markers was identified, which possessed higher sensitivity and specificity, providing new ideas for the use of proteins in diagnosis (48). For example, tumor cells derived from hepatocellular carcinoma secreted elevated levels of RasGAP SH3 structural domain binding protein (G3BP) and polymeric immunoglobulin receptor (PIGR) contained in EVs. In addition, proteomic profiles constructed by mass spectrometry also demonstrated differential expression of a variety of proteins between different groups (49). These differential expressions provide a basis for the use of protein-carrying EVs as biomarkers. In addition, some EV piggybacked proteins can be used to differentiate early HCC from cirrhosis, including EpCAM, CD147, GPC3 and ASGPR1 (48).

3 EV from different cellular sources

Systemic drugs including multikinase inhibitors such as sorafenib and lenvatinib are widely used in the treatment of HCC (3, 50–52). However, after drug application, the dynamics of the cancer cells and the cells in the TME change, and relevant measures are rapidly adopted to relieve the stress generated by cancer treatment. Ultimately this leads to mechanisms of resistance to tumor therapy and provides new therapeutic targets. Tumor cell-derived EV promotes cancer progression by transferring aggressive and drug-resistant phenotypes to other cancer cells (23), and EV is involved in a key metastatic pathway for the development of drug resistance and is a promising liquid biopsy marker, so here we discuss the role of EV produced by various types of cells in HCC tissues in the regulation of drug resistance, and explore whether EV carrying different types of molecules can serve as a mechanism for the development of drug resistance. Therefore, we herein discuss the role of EVs produced by various types of cells in HCC tissues in the regulation of drug resistance, and explore whether EVs carrying different types of molecules can be used as markers for monitoring the development of drug resistance as well as references for precision medicine, in order to provide more strategies for the treatment of HCC.

3.1 Mechanisms of HCC drug resistance

Drug resistance in HCC may exist prior to drug administration and can manifest or be enhanced after treatment with the same drug. Although anticancer drugs have multiple targets on HCC, these targets are affected by genetic polymorphisms and heterogeneity, leading to resistance and treatment failure (53). The development of resistance in HCC involves altered cell transduction signaling pathways, dysregulated apoptosis, and the tumor microenvironment (54) (Table 1).

Typical cellular pathways include the PI3K/AKT pathway (65), MAP/ERK pathway (66), and others. Alterations in these pathways simultaneously activate cancer cell survival and dysregulation of apoptosis. Taking the PI3K/AKT pathway as an example, activation of AKT by PI3K promotes cell survival by inhibiting programmed cell death. At the same time, AKT helps cancer cells avoid death in the presence of drug-induced apoptosis by inactivating pro-apoptotic factors (67).When EV-carried factors activate the PI3K/AKT/mTOR pathway, drug-resistant cells are less sensitive to apoptosis induced by sorafenib action, and in these drug-resistant cells, phosphorylated AKT, and tumor suppressor phosphatases are down-regulated, leading to drug resistance (68). The tumor microenvironment consists of cells, extracellular matrix, and signaling molecules. Immune cells release EVs representing the

TABLE 1 Biomarkers carried by EVs from different parental cell sources.

EV Source	Biomarker	Drug Resistance Receptor Cell	Mechanisms	Effecttion	Reference
M2-TAM	VEGF, IL-6, ARG1	Hepatocellular Carcinoma Cell	Stimulation of vascular growth of tumour tissue, enhancement of tumour invasiveness, suppression of tumour immunity	Promotion	(55–57)
CAF	miR-1228-3p	Hepatocellular Carcinoma Cell	Activation of PLAC8-mediated PI3K/Akt signalling pathway	Promotion	(58)
Hepatocellular Carcinoma Cell	miR-21	Normal Hepatic Stellate Cell	Down-regulation of oncogene PTEN and up-regulation of PI3K/AKT	Promotion	(59)
Hepatocellular Carcinoma Cell	circRNA-SORE	Specific Sensitive Hepatocellular Carcinoma Cells	Blocking PRP19-catalysed breakdown of the key cancer protein YBX1	Promotion	(60)
Hepatocellular Carcinoma Cell	circPAK1	Hepatocellular Carcinoma Cell	Inhibition of the Hippo signalling pathway	Promotion	(61)
HepG2 Cell	miR-774	Low Level MiR-744 Level Cells	Targeted PAX2	Inhibition	(62)
Hepatocellular Carcinoma Cell	CD9, CD63	Hepatocellular Carcinoma Cell	Activation of the HGF/c-Met/Akt signalling pathway	Promotion	(63)
M1-TAM	–	Hepatocyte	Blunt targeting of hepatocyte sensitivity	Promotion	(64)

expression of parental cellular molecules, which exert an immunomodulatory function on the disease progression process. After the action of sorafenib, the redevelopment of HCC is promoted, and the mechanism of redevelopment is related to tumor-associated neutrophil infiltration and the release of cytokines (69). On the one hand, they exacerbate tumor inflammation by driving angiogenesis (70), remodeling the extracellular matrix, and suppressing the immune response. On the other hand, they exert antitumor effects by directly attacking tumor cells or by modulating drug-resistant cell networks of antitumor cells (71).

3.2 Tumor cells and mesenchymal cells

3.2.1 RNA sorting

Numerous studies have shown that in HCC tissues, different types of cells release exosomes (EVs) that are piggybacked with specific RNAs, and this leads to a degree of resistance to multikinase inhibitors (72, 73) (Figure 1C).

EVs derived from tumor-associated fibroblasts (CAF) also enhance the resistance of HCC to sorafenib treatment. On the one hand, these fibroblasts, after being activated by HCC cell-derived EVs carrying miR-21, produced CAF-EVs containing miR-1228-3p, which enhanced HCC resistance by targeting PLAC8 and activating the PI3K/Akt signaling pathway (58). HCC cells containing miR - 21, on the other hand, the source of EVs by converting normal hepatic stellate cells to CAF, cut tumor suppressor gene PTEN, which make the PI3K/AKT signaling pathway increases (59). Activation of the AKT signaling pathway inhibits autophagy, leading to acquired resistance to sorafenib, a critical step in miR-21-mediated resistance to sorafenib in HCC patients (74).

In addition, cancer cells that have developed drug resistance also produce corresponding EVs to further regulate the development of drug resistance. Taking sorafenib-resistant cells as an example, the EVs produced by them contain circRNA-SORE. circRNA-SORE is transmitted to specific sensitive cells, which can prevent the breakdown of YBX1, a key cancer protein catalyzed by PRP19, and then inhibit the activation of related downstream factors (e.g., AKT, Raf1, ERK, etc.), thus spreading the resistance generated by chemotherapeutic drugs. And a research team demonstrated that silencing circRNA-SORE by injecting siRNA can greatly overcome sorafenib resistance (60). Similarly, lenvatinib-resistant cells induce drug resistance in recipient cells via EV-delivered circPAK1, which works by inhibiting the Hippo signaling pathway, the role of Hippo channels in inhibiting cell growth, proliferation, promoting apoptosis and regulating hepatocytes is critical for tumor suppression, and dysregulation of the Hippo signaling pathway leads to uncontrolled cell proliferation (75). Therefore, it promotes the resistance of receptor cells to lenvatinib drug (61). The above process also demonstrates the transfer of drug resistance from drug-resistant cancer cells to other cancer cells at the level of extracellular vesicles.

3.2.2 Protein sorting

Studies have shown that exosomes containing protein factors can modulate drug resistance in hepatocellular carcinoma (HCC) by activating specific signaling pathways.

Researchers explored the role of exosomes in sorafenib resistance using a subcutaneous tumor transplantation model in thymus-free mice. They found that exosomes enriched with CD9 and CD63 markers promoted resistance to sorafenib by activating the HGF/c-Met/Akt signaling pathway and inhibiting sorafenib-induced apoptosis, enhancing the manifestation of resistance (63). Activation of the HGF/c-Met axis is also one of the causes of resistance to Renvastinib in patients (76).Activation of this pathway resulted in the following resistance effects: HGF attenuated the anti-proliferative, pro-apoptotic, and anti-invasive functions of lenvatinib in HCC cells with high c-MET expression (77). It can be hypothesized that if the activation status of the HGF/c-Met/Akt pathway is monitored in the clinic, the potential resistance of patients to sorafenib or lenvatinib can be predicted, leading to the development of individualized and precise treatment strategies.

3.3 Tumor cells and immune cells

The tumor microenvironment (TME) is complex and evolving. In addition to stromal cells, fibroblasts and endothelial cells, the TME includes innate and adaptive immune cells. There is a causal relationship between these immune cells and hepatocellular carcinoma (78). Mechanistically, cytokines within the TME manipulate immune function, ultimately leading to a diminished immune response that directs tumor progression (79). Tumor cell-derived EVs and immune cell-derived EVs are able to interact with each other and together play a role in tumor cell resistance (80, 81). For example, it was experimentally demonstrated that miR-21 transfer carried by tumor-associated macrophage-derived EVs conferred drug resistance in gastric cancer ce.

3.3.1 Macrophage-derived EVs

Macrophage-derived EVs have multiple functions, depending on the various phenotypes of the parental cells, and carry LncRNAs capable of regulating the tumor microenvironment and participating in tumor pathogenesis (82). Excessive insulin levels were found to be significantly associated with an increased risk of hepatocellular carcinoma (83). Exos in pro-inflammatory M1-like macrophage-derived EVs blunts insulin sensitivity in target cells (64), which may be one of the reasons for the dysfunction of insulin signaling pathway in hepatocytes, thus helping hepatocellular carcinoma cells to build up resistance to drugs associated with insulin-sensitizing therapies.

M2 tumor-associated macrophages (M2-TAM) contribute to tumor development through multiple mechanisms, including stimulation of tumor tissue vascular growth, enhancement of tumor invasiveness, and suppression of tumor immunity (55–57, 84). The above mechanisms are realized through their release of EVs enriched with factors such as VEGF, IL-6, and ARG1 (85).

In particular, EVs released by M2-TAM not only play the role of transmitting information and regulating gene expression in the tumor microenvironment, but also influence the behavior and therapeutic response of cancer cells through complex mechanisms. Cutting from the gene expression perspective, these exosomes affect gene expression in cancer cells through two main pathways (86). One is that EVs released by M2-TAM can increase the levels of specific competing endogenous RNAs (ceRNAs). For example, it was found that M2-TAM-derived EV containing MSTRG.292666.16 could significantly increase the level of miR-6386-5p. ceRNAs indirectly increase the expression of target genes by binding to miRNAs and decreasing their inhibition. It promotes the proliferation and survival of tumor cells, thus enhancing resistance to chemotherapeutic drugs. Secondly, it directly regulates the expression of specific genes to enhance the resistance of tumor cells to chemotherapeutic drugs (87). Using known resistance mechanisms, intervention by targeting components in the context of personalized therapy by monitoring EVs containing STRG.292666.16 can be aligned with the goal of precision therapy (88).

3.3.2 Treg cell-derived EVs

Treg (regulatory T) cells are key mediators of tumor-associated immunosuppression (89). Treg cell-derived EVs may represent a fine-grained intercellular exchange apparatus with the ability to modulate the immune response, thereby creating a tolerogenic microenvironment in a cell-free manner. Mechanisms by which Treg cell-derived EVs may mediate immune response include miRNA-induced gene silencing and surface proteins and enzyme delivery. It was found that secretion of EV by CD8 Treg cells stimulated a significant decrease in CD8 T cell responses and protective anti-tumor immunity, while secretion of exosomes by CD8 Treg cells was also able to suppress DC-induced CD8 cytotoxic T lymphocyte (CTL) responses (90, 91). These vesicles were demonstrated to be able to suppress the immune response, thus enabling tumor cells to develop drug resistance (92, 93).

4 Conclusion and prospect

Extracellular vesicles (EVs) are gaining attention from the research community as potential biomarkers for the diagnosis and recurrence detection of hepatocellular carcinoma (HCC) (94). EVs as markers also have certain practical difficulties. For example, in terms of standardization, there is a lack of a unified standardized process for purification and isolation, purification and characterization of EVs, the number of target exosomes required is much higher than can now be efficiently produced, and differences in standards and techniques among different laboratories can lead to poor reproducibility and comparability of results (95). If the problem of poor reproducibility and comparability is to be solved in the future, more precise isolation and identification techniques will need to be developed, and exosomes will need to be more finely characterized by emerging means. In terms of samples, the complexity of clinical samples also increases the difficulty of testing. Serum or plasma contains a large number of non-EV components that may interfere with the isolation and detection of EVs, thus affecting the accuracy of the results (96). When selecting substances carried or embedded in EVs as markers, they will face low abundance of markers, which is difficult to detect and identify (97). The development of internationally recognized standardized protocols would provide some assurance of the reproducibility and consistency of EVs study results. As for drug resistance, the limited understanding of the biological mechanisms of EVs in hepatocellular carcinoma drug resistance limits their development and application as diagnostic markers. More basic studies are needed to go deeper, and these basic studies can be combined with multidisciplinary and multi-omics to delve into the specific mechanisms of the role of EVs in HCC. For example, transcriptomics could be combined to study how mRNAs carried in EVs affect drug resistance by influencing gene expression in recipient cells. Machine learning and neural networks can also be used to construct a diagnostic model for hepatitis B-related hepatocellular carcinoma (98, 99). In addition, immune cell-derived EVs can be used as diagnostic tools and preventive strategies at the level of potential biomarkers, e.g., for the development of vaccines, making targeted drugs, etc. Despite the promising research on EVs as biomarkers for hepatocellular carcinoma, they are still at a relatively early stage, and more large-scale clinical studies are needed to validate their specificity, sensitivity and assess the long-term safety and efficacy of EVs in the treatment of HCC, as well as to establish a more standardized detection method (100).

Author contributions

LS: Conceptualization, Data curation, Visualization, Writing – original draft. YYu: Data curation, Writing – original draft. YYa: Conceptualization, Data curation, Writing – original draft. JS: Writing – original draft. LM: Writing – original draft. JLu: Writing – original draft. LZ: Writing – original draft. JLi: Writing – original draft. HC: Conceptualization, Writing – original draft, Writing – review & editing. SL: Conceptualization, Writing – original draft, Writing – review & editing. ZY: Conceptualization, Writing – original draft, Writing – review & editing. XT: Conceptualization, Writing – original draft, Writing – review & editing.

Funding

The author(s) declare that financial support was received for the research, authorship, and/or publication of this article. This study was funded by The Xinglin Scholar Research Premotion Project of Chengdu University of TCM (Grant No. YYZX2022176), The project of Hubei Chen Xiaoping Science and Technology Development Foundation (CXPJJH123003-008), and The project of Sichuan Medical Association (Q23095).

Conflict of interest

The authors declare that the research was conducted in the absence of any commercial or financial relationships that could be construed as a potential conflict of interest.

Publisher's note

All claims expressed in this article are solely those of the authors and do not necessarily represent those of their affiliated organizations, or those of the publisher, the editors and the reviewers. Any product that may be evaluated in this article, or claim that may be made by its manufacturer, is not guaranteed or endorsed by the publisher.

References

1. Nimitrungtawee N, Inmutto N, Chattipakorn SC, Chattipakorn N. Extracellular vesicles as a new hope for diagnosis and therapeutic intervention for hepatocellular carcinoma. *Cancer Med*. (2021) 10:8253–71. doi: 10.1002/cam4.v10.23

2. Qi X, Chen S, He H, Wen W, Wang H. The role and potential application of extracellular vesicles in liver cancer. *Sci China Life Sci*. (2021) 64:1281–94. doi: 10.1007/s11427-020-1905-7

3. Li H, Wu Z, Chen J, Su K, Guo L, Xu K, et al. External radiotherapy combined with sorafenib has better efficacy in unresectable hepatocellular carcinoma: a systematic review and meta-analysis. *Clin Exp Med*. (2023) 23:1537–49. doi: 10.1007/s10238-022-00972-4

4. D'Agnano I, Berardi AC. Extracellular vesicles, a possible theranostic platform strategy for hepatocellular carcinoma-an overview. *Cancers (Basel)*. (2020) 12:261. doi: 10.3390/cancers12020261

5. Abhange K, Kitata RB, Zhang J, Wang YT, Gaffrey MJ, Liu T, et al. In-depth proteome profiling of small extracellular vesicles isolated from cancer cell lines and patient serum. *J Proteome Res*. (2024) 23:386–96. doi: 10.1021/acs.jproteome.3c00614

6. Borhani A, Luu H, Mohseni A, Xu Z, Shaghaghi M, Tolosa C, et al. Screening for exclusion of high-risk bleeding features of esophageal varices in cirrhosis through CT and MRI. *Clin Imag*. (2024) 110:110168. doi: 10.1016/j.clinimag.2024.110168

7. Li X, Liu Y, Fan Y, Tian G, Shen B, Zhang S, et al. Advanced nanoencapsulation-enabled ultrasensitive analysis: unraveling tumor extracellular vesicle subpopulations for differential diagnosis of hepatocellular carcinoma via DNA cascade reactions. *ACS Nano*. (2024) 18:11389–403. doi: 10.1021/acsnano.4c01310

8. Yan R, Chen H, Selaru FM. Extracellular vesicles in hepatocellular carcinoma: progress and challenges in the translation from the laboratory to clinic. *Med (Kaunas)*. (2023) 59:1599. doi: 10.3390/medicina59091599

9. van de Wakker SI, Meijers FM, Sluijter JPG, Vader P. Extracellular vesicle heterogeneity and its impact for regenerative medicine applications. *Pharmacol Rev*. (2023) 75:1043–61. doi: 10.1124/pharmrev.123.000841

10. Li M, Zeringer E, Barta T, Schageman J, Cheng A, Vlassov AV. Analysis of the RNA content of the exosomes derived from blood serum and urine and its potential as biomarkers. *Philos Trans R Soc Lond B Biol Sci*. (2014) 369:20130502. doi: 10.1098/rstb.2013.0502

11. Jin Y, Xing J, Xu K, Liu D, Zhuo Y. Exosomes in the tumor microenvironment: Promoting cancer progression. *Front Immunol*. (2022) 13:1025218. doi: 10.3389/fimmu.2022.1025218

12. Tan M, Ge Y, Wang X, Wang Y, Liu Y, He F, et al. Extracellular vesicles (EVs) in tumor diagnosis and therapy. *Technol Cancer Res Treat*. (2023) 22:15330338231171463. doi: 10.1177/15330338231171463

13. Bonner SE, Willms E. Intercellular communication through extracellular vesicles in cancer and evolutionary biology. *Prog Biophys Mol Biol*. (2021) 165:80–7. doi: 10.1016/j.pbiomolbio.2021.08.006

14. Guo Y, Ji X, Liu J, Fan D, Zhou Q, Chen C, et al. Effects of exosomes on pre-metastatic niche formation in tumors. *Mol Cancer*. (2019) 18:39. doi: 10.1186/s12943-019-0995-1

15. Gong X, Chi H, Strohmer DF, Teichmann AT, Xia Z, Wang Q. Exosomes: A potential tool for immunotherapy of ovarian cancer. *Front Immunol*. (2022) 13:1089410. doi: 10.3389/fimmu.2022.1089410

16. Chen W, Zhang F, Xu H, Hou X, Tang D. Prospective analysis of proteins carried in extracellular vesicles with clinical outcome in hepatocellular carcinoma. *Curr Genomics*. (2022) 23:109–17. doi: 10.2174/1389202923666220304125458

17. San Lucas FA, Allenson K, Bernard V, Castillo J, Kim DU, Ellis K, et al. Minimally invasive genomic and transcriptomic profiling of visceral cancers by next-generation sequencing of circulating exosomes. *Ann Oncol*. (2016) 27:635–41. doi: 10.1093/annonc/mdv604

18. Li S, Yi M, Dong B, Tan X, Luo S, Wu K. The role of exosomes in liquid biopsy for cancer diagnosis and prognosis prediction. *Int J Cancer*. (2021) 148:2640–51. doi: 10.1002/ijc.v148.11

19. Bettegowda C, Sausen M, Leary RJ, Kinde I, Wang Y, Agrawal N, et al. Detection of circulating tumor DNA in early- and late-stage human Malignancies. *Sci Transl Med*. (2014) 6:224ra24. doi: 10.1126/scitranslmed.3007094

20. Lee YT, Tran BV, Wang JJ, Liang IY, You S, Zhu Y, et al. The role of extracellular vesicles in disease progression and detection of hepatocellular carcinoma. *Cancers (Basel)*. (2021) 13:3076. doi: 10.3390/cancers13123076

21. Théry C, Witwer KW, Aikawa E, Alcaraz MJ, Anderson JD, Andriantsitohaina R, et al. Minimal information for studies of extracellular vesicles 2018 (MISEV2018): a position statement of the International Society for Extracellular Vesicles and update of the MISEV2014 guidelines. *J Extracell Vesicles*. (2018) 7:1535750. doi: 10.1080/20013078.2018.1535750

22. Lapitz A, Arbelaiz A, Olaizola P, Aranburu A, Bujanda L, Perugorria MJ, et al. Extracellular vesicles in hepatobiliary Malignancies. *Front Immunol*. (2018) 9:2270. doi: 10.3389/fimmu.2018.02270

23. Vasconcelos MH, Caires HR, Ābols A, Xavier CPR, Linē A. Extracellular vesicles as a novel source of biomarkers in liquid biopsies for monitoring cancer progression and drug resistance. *Drug Resist Updat*. (2019) 47:100647. doi: 10.1016/j.drup.2019.100647

24. Buscail E, Alix-Panabières C, Quincy P, Cauvin T, Chauvet A, Degrandi O, et al. High clinical value of liquid biopsy to detect circulating tumor cells and tumor exosomes in pancreatic ductal adenocarcinoma patients eligible for up-front surgery. *Cancers (Basel)*. (2019) 11:1656. doi: 10.3390/cancers11111656

25. Godoy P, Widera A, Schmidt-Heck W, Campos G, Meyer C, Cadenas C, et al. Gene network activity in cultivated primary hepatocytes is highly similar to diseased mammalian liver tissue. *Arch Toxicol*. (2016) 90:2513–29. doi: 10.1007/s00204-016-1761-4

26. Liu SY, Liao Y, Hosseinifard H, Imani S, Wen QL. Diagnostic role of extracellular vesicles in cancer: A comprehensive systematic review and meta-analysis. *Front Cell Dev Biol*. (2021) 9:705791. doi: 10.3389/fcell.2021.705791

27. Tiyuri A, Baghermanesh SS, Davatgaran-Taghipour Y, Eslami SS, Shaygan N, Parsaie H, et al. Diagnostic accuracy of serum derived exosomes for hepatocellular carcinoma: a systematic review and meta-analysis. *Expert Rev Mol Diagn*. (2023) 23:971–83. doi: 10.1080/14737159.2023.2260306

28. Zhao R, Zhang Y, Zhang X, Yang Y, Zheng X, Li X, et al. Exosomal long noncoding RNA HOTTIP as potential novel diagnostic and prognostic biomarker test for gastric cancer. *Mol Cancer*. (2018) 17:68. doi: 10.1186/s12943-018-0817-x

29. Yu XL, Wu MR, Abdul M, Liu X, Zhang S, Xu Z, et al. Comparison of two methods for extracting exosomes from the nucleus accumbens in mice. *Neurosci Lett*. (2023) 796:137017. doi: 10.1016/j.neulet.2022.137017

30. Zhang H, Freitas D, Kim HS, Fabijanic K, Li Z, Chen H, et al. Identification of distinct nanoparticles and subsets of extracellular vesicles by asymmetric flow field-flow fractionation. *Nat Cell Biol*. (2018) 20:332–43. doi: 10.1038/s41556-018-0040-4

31. Choi D, Montermini L, Jeong H, Sharma S, Meehan B, Rak J. Mapping subpopulations of cancer cell-derived extracellular vesicles and particles by nano-flow cytometry. *ACS Nano*. (2019) 13:10499–511. doi: 10.1021/acsnano.9b04480

32. Augello G, Cusimano A, Cervello M, Cusimano A. Extracellular vesicle-related non-coding RNAs in hepatocellular carcinoma: an overview. *Cancers (Basel)*. (2024) 16:1415. doi: 10.3390/cancers16071415

33. Ferro A, Saccu G, Mattivi S, Gaido A, Herrera Sanchez MB, Haque S, et al. Extracellular vesicles as delivery vehicles for non-coding RNAs: potential biomarkers for chronic liver diseases. *Biomolecules*. (2024) 14:277. doi: 10.3390/biom14030277

34. Son JA, Weon JH, Baek GO, Ahn HR, Choi JY, Yoon MG, et al. Circulating small extracellular vesicle-derived splicing factor 3b subunit 4 as a non-invasive diagnostic biomarker of early hepatocellular carcinoma. *J Exp Clin Cancer Res*. (2023) 42:288. doi: 10.1186/s13046-023-02867-y

35. Cui Y, Xu HF, Liu MY, Xu YJ, He JC, Zhou Y, et al. Mechanism of exosomal microRNA-224 in development of hepatocellular carcinoma and its diagnostic and prognostic value. *World J Gastroenterol*. (2019) 25:1890–8. doi: 10.3748/wjg.v25.i15.1890

36. Wang Y, Zhang C, Zhang P, Guo G, Jiang T, Zhao X, et al. Serum exosomal microRNAs combined with alpha-fetoprotein as diagnostic markers of hepatocellular carcinoma. *Cancer Med*. (2018) 7:1670–9. doi: 10.1002/cam4.2018.7.issue-5

37. Amr KS, Elmawgoud Atia HA, Elazeem Elbnhawy RA, Ezzat WM. Early diagnostic evaluation of miR-122 and miR-224 as biomarkers for hepatocellular carcinoma. *Genes Dis*. (2017) 4:215–21. doi: 10.1016/j.gendis.2017.10.003

38. Boonkaew B, Satthawiwat N, Pinjaroen N, Chuaypen N, Tangkijvanich P. Circulating extracellular vesicle-derived microRNAs as novel diagnostic and prognostic biomarkers for non-viral-related hepatocellular carcinoma. *Int J Mol Sci*. (2023) 24:16043. doi: 10.3390/ijms242216043

39. Cabiati M, Salvadori C, Basta G, Del Turco S, Aretini P, Cecchettini A, et al. miRNA and long non-coding RNA transcriptional expression in hepatocellular

carcinoma cell line-secreted extracellular vesicles. *Clin Exp Med*. (2022) 22:245–55. doi: 10.1007/s10238-021-00744-6

40. Cho HJ, Baek GO, Seo CW, Ahn HR, Sung S, Son JA, et al. Exosomal microRNA-4661-5p-based serum panel as a potential diagnostic biomarker for early-stage hepatocellular carcinoma. *Cancer Med*. (2020) 9:5459–72. doi: 10.1002/cam4.v9.15

41. Cho HJ, Eun JW, Baek GO, Seo CW, Ahn HR, Kim SS, et al. Serum exosomal microRNA, miR-10b-5p, as a potential diagnostic biomarker for early-stage hepatocellular carcinoma. *J Clin Med*. (2020) 9:281. doi: 10.3390/jcm9010281

42. Gyöngyösi B, Végh ÉChecktae, Járay B, Székely E, Fassan M, Bodoky G, et al. Pretreatment microRNA level and outcome in sorafenib-treated hepatocellular carcinoma. *J Histochem Cytochem*. (2014) 62:547–55. doi: 10.1369/0022155414537277

43. Qu Z, Wu J, Wu J, Ji A, Qiang G, Jiang Y, et al. Exosomal miR-665 as a novel minimally invasive biomarker for hepatocellular carcinoma diagnosis and prognosis. *Oncotarget*. (2017) 8:80666–78. doi: 10.18632/oncotarget.20881

44. Sorop A, Iacob R, Iacob S, Constantinescu D, Chitoiu L, Fertig TE, et al. Plasma Small Extracellular Vesicles Derived miR-21-5p and miR-92a-3p as Potential Biomarkers for Hepatocellular Carcinoma Screening. *Front Genet*. (2020) 11:712. doi: 10.3389/fgene.2020.00712

45. Coulouarn C, Factor VM, Andersen JB, Durkin ME, Thorgeirsson SS. Loss of miR-122 expression in liver cancer correlates with suppression of the hepatic phenotype and gain of metastatic properties. *Oncogene*. (2009) 28:3526–36. doi: 10.1038/onc.2009.211

46. Kim SS, Baek GO, Ahn HR, Sung S, Seo CW, Cho HJ, et al. Serum small extracellular vesicle-derived LINC00853 as a novel diagnostic marker for early hepatocellular carcinoma. *Mol Oncol*. (2020) 14:2646–59. doi: 10.1002/1878-0261.12745

47. Tzartzeva K, Obi J, Rich NE, Parikh ND, Marrero JA, Yopp A, et al. Surveillance imaging and alpha fetoprotein for early detection of hepatocellular carcinoma in patients with cirrhosis: A meta-analysis. *Gastroenterology*. (2018) 154:1706–18.e1. doi: 10.1053/j.gastro.2018.01.064

48. Sun N, Zhang C, Lee YT, Tran BV, Wang J, Kim H, et al. HCC EV ECG score: An extracellular vesicle-based protein assay for detection of early-stage hepatocellular carcinoma. *Hepatology*. (2023) 77:774–88. doi: 10.1002/hep.32692

49. Arbelaiz A, Azkargorta M, Krawczyk M, Santos-Laso A, Lapitz A, Perugorria MJ, et al. Serum extracellular vesicles contain protein biomarkers for primary sclerosing cholangitis and cholangiocarcinoma. *Hepatology*. (2017) 66:1125–43. doi: 10.1002/hep.29291

50. da Fonseca LG, Reig M, Bruix J. Tyrosine kinase inhibitors and hepatocellular carcinoma. *Clin Liver Dis*. (2020) 24:719–37. doi: 10.1016/j.cld.2020.07.012

51. Jiang X, Wang P, Su K, Li H, Chi H, Wang F, et al. Camrelizumab combined with transcatheter arterial chemoembolization and sorafenib or lenvatinib for unresectable hepatocellular carcinoma: A multicenter, retrospective study. *Ann Hepatol*. (2024) 101578:101587. doi: 10.3389/fimmu.2022.972503

52. Su K, Guo L, Ma W, Wang J, Xie Y, Rao M, et al. PD-1 inhibitors plus anti-angiogenic therapy with or without intensity-modulated radiotherapy for advanced hepatocellular carcinoma: A propensity score matching study. *Front Immunol*. (2022) 13:972503. doi: 10.3389/fimmu.2022.972503

53. Zhuang M, Zhang X, Li LU, Wen L, Qin J. Tmem39b promotes tumor progression and sorafenib resistance by inhibiting ferroptosis in hepatocellular carcinoma. *Oncol Res*. (2024) 32:1347–57. doi: 10.32604/or.2024.046170

54. Ladd AD, Duarte S, Sahin I, Zarrinpar A. Mechanisms of drug resistance in HCC. *Hepatology*. (2024) 79:926–40. doi: 10.1097/HEP.0000000000000237

55. Becker A, Thakur BK, Weiss JM, Kim HS, Peinado H, Lyden D. Extracellular vesicles in cancer: cell-to-cell mediators of metastasis. *Cancer Cell*. (2016) 30:836–48. doi: 10.1016/j.ccell.2016.10.009

56. Dallavalasa S, Beeraka NM, Basavaraju CG, Tulimilli SV, Sadhu SP, Rajesh K, et al. The role of tumor associated macrophages (TAMs) in cancer progression, chemoresistance, angiogenesis and metastasis - current status. *Curr Med Chem*. (2021) 28:8203–36. doi: 10.2174/0929867328666210720143721

57. Pavlyukov MS, Yu H, Bastola S, Minata M, Shender VO, Lee Y, et al. Apoptotic cell-derived extracellular vesicles promote Malignancy of glioblastoma via intercellular transfer of splicing factors. *Cancer Cell*. (2018) 34:119–35.e10. doi: 10.1016/j.ccell.2018.05.012

58. Zhang Y, Pan Q, Shao Z. Extracellular vesicles derived from cancer-associated fibroblasts carry tumor-promotive microRNA-1228-3p to enhance the resistance of hepatocellular carcinoma cells to sorafenib. *Hum Cell*. (2023) 36:296–311. doi: 10.1007/s13577-022-00800-7

59. Zhou Y, Ren H, Dai B, Li J, Shang L, Huang J, et al. Correction: Hepatocellular carcinoma-derived exosomal miRNA-21 contributes to tumor progression by converting hepatocyte stellate cells to cancer-associated fibroblasts. *J Exp Clin Cancer Res*. (2022) 41:359. doi: 10.1186/s13046-022-02575-z

60. Xu J, Ji L, Liang Y, Wan Z, Zheng W, Song X, et al. CircRNA-SORE mediates sorafenib resistance in hepatocellular carcinoma by stabilizing YBX1. *Signal Transduct Target Ther*. (2020) 5:298. doi: 10.1038/s41392-020-00375-5

61. Hao X, Zhang Y, Shi X, Liu H, Zheng Z, Han G, et al. CircPAK1 promotes the progression of hepatocellular carcinoma via modulation of YAP nucleus localization by interacting with 14-3-3ζ. *J Exp Clin Cancer Res*. (2022) 41:281. doi: 10.1186/s13046-022-02494-z

62. Wang G, Zhao W, Wang H, Qiu G, Jiang Z, Wei G, et al. Exosomal MiR-744 inhibits proliferation and sorafenib chemoresistance in hepatocellular carcinoma by targeting PAX2. *Med Sci Monit*. (2019) 25:7209–17. doi: 10.12659/MSM.919219

63. Qu Z, Wu J, Wu J, Luo D, Jiang C, Ding Y. Exosomes derived from HCC cells induce sorafenib resistance in hepatocellular carcinoma both in *vivo* and in vitro. *J Exp Clin Cancer Res*. (2016) 35:159. doi: 10.1186/s13046-016-0430-z

64. Ying W, Riopel M, Bandyopadhyay G, Dong Y, Birmingham A, Seo JB, et al. Adipose tissue macrophage-derived exosomal miRNAs can modulate *in vivo* and *in vitro* insulin sensitivity. *Cell*. (2017) 171:372–84.e12. doi: 10.1016/j.cell.2017.08.035

65. Zulehner G, Mikula M, Schneller D, van Zijl F, Huber H, Sieghart W, et al. Nuclear beta-catenin induces an early liver progenitor phenotype in hepatocellular carcinoma and promotes tumor recurrence. *Am J Pathol*. (2010) 176:472–81. doi: 10.2353/ajpath.2010.090300

66. Caruso S, Calatayud AL, Pilet J, La Bella T, Rekik S, Imbeaud S, et al. Analysis of liver cancer cell lines identifies agents with likely efficacy against hepatocellular carcinoma and markers of response. *Gastroenterology*. (2019) 157:760–76. doi: 10.1053/j.gastro.2019.05.001

67. Buontempo F, Ersahin T, Missiroli S, Senturk S, Etro D, Ozturk M, et al. Inhibition of Akt signaling in hepatoma cells induces apoptotic cell death independent of Akt activation status. *Invest New Drugs*. (2011) 29:1303–13. doi: 10.1007/s10637-010-9486-3

68. Chen KF, Chen HL, Tai WT, Feng WC, Hsu CH, Chen PJ, et al. Activation of phosphatidylinositol 3-kinase/Akt signaling pathway mediates acquired resistance to sorafenib in hepatocellular carcinoma cells. *J Pharmacol Exp Ther*. (2011) 337:155–61. doi: 10.1124/jpet.110.175786

69. Tecchio C, Scapini P, Pizzolo G, Cassatella MA. On the cytokines produced by human neutrophils in tumors. *Semin Cancer Biol*. (2013) 23:159–70. doi: 10.1016/j.semcancer.2013.02.004

70. Tazzyman S, Niaz H, Murdoch C. Neutrophil-mediated tumor angiogenesis: subversion of immune responses to promote tumor growth. *Semin Cancer Biol*. (2013) 23:149–58. doi: 10.1016/j.semcancer.2013.02.003

71. Jaillon S, Ponzetta A, Di Mitri D, Santoni A, Bonecchi R, Mantovani A. Neutrophil diversity and plasticity in tumor progression and therapy. *Nat Rev Cancer*. (2020) 20:485–503. doi: 10.1038/s41568-020-0281-y

72. Fan FM, Fleishman JS, Chen J, Chen ZS, Dong HH. New insights into the mechanism of resistance to lenvatinib and strategies for lenvatinib sensitization in hepatocellular carcinoma. *Drug Discovery Today*. (2024) 29:104069. doi: 10.1016/j.drudis.2024.104069

73. Uyulgan S, Köse SN, Kıpçak A, Başkan Y, Dağlar G, Karagonlar ZF, et al. Thyroid hormone T3 augments the cytotoxicity of sorafenib in Huh7 hepatocellular carcinoma cells by suppressing AKT expression. *J Cancer Res Ther*. (2024) 20:755–62. doi: 10.4103/jcrt.jcrt_2106_22

74. He C, Dong X, Zhai B, Jiang X, Dong D, Li B, et al. MiR-21 mediates sorafenib resistance of hepatocellular carcinoma cells by inhibiting autophagy via the PTEN/Akt pathway. *Oncotarget*. (2015) 6:28867–81. doi: 10.18632/oncotarget.v6i30

75. Liu Q, Liu X, Song G. The hippo pathway: A master regulatory network important in cancer. *Cells*. (2021) 10:1416. doi: 10.3390/cells10061416

76. Fu R, Jiang S, Li J, Chen H, Zhang X. Activation of the HGF/c-MET axis promotes lenvatinib resistance in hepatocellular carcinoma cells with high c-MET expression. *Med Oncol*. (2020) 37:24. doi: 10.1007/s12032-020-01350-4

77. Tang Z, He J, Zou J, Yu S, Sun X, Qin L. Cisplatin-resistant HepG2 cell-derived exosomes transfer cisplatin resistance to cisplatin-sensitive cells in HCC. *PeerJ*. (2021) 9:e11200. doi: 10.7717/peerj.11200

78. Tang J, Zhang S, Jiang L, Liu J, Xu J, Jiang C, et al. Causal relationship between immune cells and hepatocellular carcinoma: a Mendelian randomization study. *J Cancer*. (2024) 15:4219–31. doi: 10.7150/jca.96744

79. Hinshaw DC, Shevde LA. The tumor microenvironment innately modulates cancer progression. *Cancer Res*. (2019) 79:4557–66. doi: 10.1158/0008-5472.CAN-18-3962

80. Xiong J, Chi H, Yang G, Zhao S, Zhang J, Tran LJ, et al. Revolutionizing anti-tumor therapy: unleashing the potential of B cell-derived exosomes. *Front Immunol*. (2023) 14:1188760. doi: 10.3389/fimmu.2023.1188760

81. He S, Su L, Hu H, Liu H, Xiong J, Gong X, et al. Immunoregulatory functions and therapeutic potential of natural killer cell-derived extracellular vesicles in chronic diseases. *Front Immunol*. (2023) 14:1328094. doi: 10.3389/fimmu.2023.1328094

82. Yang P, Peng Y, Feng Y, Xu Z, Feng P, Cao J, et al. Immune cell-derived extracellular vesicles - new strategies in cancer immunotherapy. *Front Immunol*. (2021) 12:771551. doi: 10.3389/fimmu.2021.771551

83. Bowker SL, Majumdar SR, Veugelers P, Johnson JA. Increased cancer-related mortality for patients with type 2 diabetes who use sulfonylureas or insulin. *Diabetes Care*. (2006) 29:254–8. doi: 10.2337/diacare.29.02.06.dc05-1558

84. Deng J, Ke H. Overcoming the resistance of hepatocellular carcinoma to PD-1/PD-L1 inhibitor and the resultant immunosuppression by CD38 siRNA-loaded extracellular vesicles. *Oncoimmunology*. (2023) 12:2152635. doi: 10.1080/2162402X.2022.2152635

85. Zhou J, Che J, Xu L, Yang W, Zhou W, Zhou C. Tumor-derived extracellular vesicles containing long noncoding RNA PART1 exert oncogenic effect in hepatocellular carcinoma by polarizing macrophages into M2. *Dig Liver Dis*. (2022) 54:543–53. doi: 10.1016/j.dld.2021.07.005

86. Mantovani A, Allavena P. The interaction of anticancer therapies with tumor-associated macrophages. *J Exp Med*. (2015) 212:435–45. doi: 10.1084/jem.20150295

87. Wan X, Xie B, Sun H, Gu W, Wang C, Deng Q, et al. Exosomes derived from M2 type tumor-associated macrophages promote osimertinib resistance in non-small cell lung cancer through MSTRG.292666.16-miR-6836-5p-MAPK8IP3 axis. *Cancer Cell Int*. (2022) 22:83. doi: 10.1186/s12935-022-02509-x

88. Su L, Luo H, Yan Y, Yang Z, Lu J, Xu D, et al. Exploiting gender-based biomarkers and drug targets: advancing personalized therapeutic strategies in hepatocellular carcinoma. *Front Pharmacol*. (2024) 15:1433540. doi: 10.3389/fphar.2024.1433540

89. Wang Z, He L, Li W, Xu C, Zhang J, Wang D, et al. GDF15 induces immunosuppression via CD48 on regulatory T cells in hepatocellular carcinoma. *J Immunother Cancer*. (2021) 9. doi: 10.1136/jitc-2021-002787

90. Rojas C, Campos-Mora M, Cárcamo I, Villalón N, Elhusseiny A, Contreras-Kallens P, et al. T regulatory cells-derived extracellular vesicles and their contribution to the generation of immune tolerance. *J Leukoc Biol*. (2020) 108:813–24. doi: 10.1002/JLB.3MR0420-533RR

91. Sullivan JA, Tomita Y, Jankowska-Gan E, Lema DA, Arvedson MP, Nair A, et al. Treg-cell-derived IL-35-coated extracellular vesicles promote infectious tolerance. *Cell Rep*. (2020) 30:1039–51.e5. doi: 10.1016/j.celrep.2019.12.081

92. Kobayashi S, Kondo N, Tomiyama T, Nakamura N, Masuda M, Matsumoto Y, et al. Intravenous injection of tumor extracellular vesicles suppresses tumor growth by reducing the regulatory T cell phenotype. *Cancer Immunol Immunother*. (2023) 72:3651–64. doi: 10.1007/s00262-023-03517-0

93. Korutla L, Hoffman JR, Rostami S, Hu R, Korutla V, Markmann C, et al. Circulating T cell specific extracellular vesicle profiles in cardiac allograft acute cellular rejection. *Am J Transpl*. (2024) 24:419–35. doi: 10.1016/j.ajt.2023.10.021

94. Juratli MA, Pollmann NS, Oppermann E, Mohr A, Roy D, Schnitzbauer A, et al. Extracellular vesicles as potential biomarkers for diagnosis and recurrence detection of hepatocellular carcinoma. *Sci Rep*. (2024) 14:5322. doi: 10.1038/s41598-024-55888-8

95. Gardiner C, Di Vizio D, Sahoo S, Théry C, Witwer KW, Wauben M, et al. Techniques used for the isolation and characterization of extracellular vesicles: results of a worldwide survey. *J Extracell Vesicles*. (2016) 5:32945. doi: 10.3402/jev.v5.32945

96. Kurian TK, Banik S, Gopal D, Chakrabarti S, Mazumder N. Elucidating methods for isolation and quantification of exosomes: A review. *Mol Biotechnol*. (2021) 63:249–66. doi: 10.1007/s12033-021-00300-3

97. Millioni R, Tolin S, Puricelli L, Sbrignadello S, Fadini GP, Tessari P, et al. High abundance proteins depletion vs low abundance proteins enrichment: comparison of methods to reduce the plasma proteome complexity. *PloS One*. (2011) 6:e19603. doi: 10.1371/journal.pone.0019603

98. Zhang S, Jiang C, Jiang L, Chen H, Huang J, Gao X, et al. Construction of a diagnostic model for hepatitis B-related hepatocellular carcinoma using machine learning and artificial neural networks and revealing the correlation by immunoassay. *Tumor Virus Res*. (2023) 16:200271. doi: 10.1016/j.tvr.2023.200271

99. Zhang S, Jiang C, Jiang L, Chen H, Huang J, Zhang J, et al. Uncovering the immune microenvironment and molecular subtypes of hepatitis B-related liver cirrhosis and developing stable a diagnostic differential model by machine learning and artificial neural networks. *Front Mol Biosci*. (2023) 10:1275897. doi: 10.3389/fmolb.2023.1275897

100. Wang J, Wang X, Zhang X, Shao T, Luo Y, Wang W, et al. Extracellular vesicles and hepatocellular carcinoma: opportunities and challenges. *Front Oncol*. (2022) 12:884369. doi: 10.3389/fonc.2022.884369

frontiers | Frontiers in Immunology

TYPE Review
PUBLISHED 28 October 2024
DOI 10.3389/fimmu.2024.1454720

Check for updates

OPEN ACCESS

EDITED BY
Pengpeng Zhang,
Nanjing Medical University, China

REVIEWED BY
Dainius Characiejus,
Vilnius University, Lithuania
Longchao Liu,
Chinese Academy of Sciences (CAS), China

*CORRESPONDENCE
Gebin Li
ligebin@cau.edu.cn
Shuaiyu Wang
wangshuaiyu2016@cau.edu.cn

†These authors have contributed equally to this work and share last authorship

RECEIVED 25 June 2024
ACCEPTED 27 September 2024
PUBLISHED 28 October 2024

CITATION
Wang Z, Zou X, Wang H, Hao Z, Li G and Wang S (2024) Companion diagnostics and predictive biomarkers for PD-1/PD-L1 immune checkpoint inhibitors therapy in malignant melanoma.
Front. Immunol. 15:1454720.
doi: 10.3389/fimmu.2024.1454720

COPYRIGHT
© 2024 Wang, Zou, Wang, Hao, Li and Wang. This is an open-access article distributed under the terms of the Creative Commons Attribution License (CC BY). The use, distribution or reproduction in other forums is permitted, provided the original author(s) and the copyright owner(s) are credited and that the original publication in this journal is cited, in accordance with accepted academic practice. No use, distribution or reproduction is permitted which does not comply with these terms.

Companion diagnostics and predictive biomarkers for PD-1/PD-L1 immune checkpoint inhibitors therapy in malignant melanoma

Zeping Wang[1], Xiaojing Zou[1], Haiyan Wang[2], Zhihui Hao[1,3,4], Gebin Li[1*†] and Shuaiyu Wang[1,3,4*†]

[1]College of Veterinary Medicine, China Agricultural University, Beijing, China, [2]Beijing Biomedical Science and Technology Center, Zhaofenghua Biotechnology (Nanjing) Company Limited, Beijing, China, [3]Key Biology Laboratory of Chinese Veterinary Medicine, Ministry of Agriculture and Rural Affairs, Beijing, China, [4]National Center of Technology Innovation for Medicinal Function of Food, National Food and Strategic Reserves Administration, Beijing, China

Programmed cell death receptor 1 (PD-1), when bound to the ligand programmed death-ligand 1 (PD-L1), can suppress cellular immunity and play a critical role in the initiation and development of cancer. Immune drugs targeting these two sites have been developed for different cancers, including malignant melanoma. The accompanying diagnostic method has been approved by the FDA to guide patient medication. However, the method of immunohistochemical staining, which varies widely due to the antibody and staining cut-off values, has certain limitations in application and does not benefit all patients. Increasing researches begin to focus on new biomarkers to improve objective response rates and survival in cancer patients. In this article, we enumerated three major groups, including tumour microenvironment, peripheral circulation, and gene mutation, which covered the current main research directions. In the future, we hope those biomarkers may be used to guide the treatment of patients with malignant melanoma.

KEYWORDS

PD-1, PD-L1, biomarkers, CDx, immunotherapy

1 Introduction

As aging population keeps growing, deaths and disability-adjusted life years (DALYs) due to non-communicable diseases (NCDs) are ticking up. According to the latest report from the World Health Organization (WHO), the number of people killed by NCDs in 2019 rose by 28% as compared to 2000, with cancer being the second cause of death (9.3 million) (1). Melanoma is caused by malignant transformation of melanocytes, with a high

incidence across the world. It is the fifth, sixth most common cancer in men, women respectively (2). Before the advent of cancer immunotherapy, metastatic melanoma (MM) had a poor survival prognosis. Nowadays, there are several immunotherapy options for MM, such as anti-PD-1 and anti-cytotoxic T-lymphocyte-associated protein 4 (CTLA4) antibody therapy, which represent desirable efficacy (3, 4).

Programmed cell death protein 1(PD-1) is an important immunosuppressive apoptotic process. It regulates the immune system and promotes self-tolerance by down-regulating the immune system's response to the body's cells and by suppressing T cell activity. Programmed cell death 1 ligand 1 (PD-L1) is often overexpressed in tumour cells and is an apoptotic process to bind to PD-1 *in vivo*, signaling immunosuppression and reducing T cell proliferation and activation, which suggests that the PD-1/PD-L1 pathway is a mechanism of tumour immune escape (5, 6). PD-L1 expression is upregulated on tumour cells or tumour microenvironments such as tumour-infiltrating lymphocyte, and decreases T cell activity by binding to PD-1 on tumour antigen-specific T cell (5, 7, 8). Blocking the PD-1/PD-L1 pathway with anti-PD-1 or anti-PD-L1 antibodies can restore multiple effector functions of T cell (9), which in turn can alleviate cancer progression (10).

Despite the promising potential of immunotherapy, only a small proportion of patients achieve durable responses to monotherapy, and therefore predictive biomarkers are used for the prognosis of immunotherapy (11). Companion diagnostic (CDx) is an *in vitro* diagnostic technique associated with targeted drugs, which selects the most suitable drug groups and target therapy by measuring the expression levels of biomarkers in the body. The Food and Drug Administration (FDA) has approved several CDx methods for PD-1 immunotherapy, such as the use of PD-L1 22C3 monoclonal antibody for immunohistochemical staining of tumour tissue from patients with non-small-cell lung carcinoma (NSCLC). Patients with Tumour Proportion Score (TPS) higher than 50% can be treated with targeted immunotherapy with PD-1 monoclonal antibody. With the advancement of the research, the CDx method of detecting PD-L1 expression in tumour tissue is not of the greatest benefit to patients. Because of differences in sampling sites, some PD-L1-negative patients may still benefit from PD-1 immunotherapy (12). To date, many patients benefit greatly from guided therapy with CDx, but we are still looking forward to the discovery of additional diagnostic methods and biomarkers to improve the objective response rate (ORR) of patients to immunotherapy. There are several biomarkers associated with the response to anti-PD-1/anti-PD-L1 therapy including T cell infiltration, mutant genome, circulating extracellular vesicles, and circulating soluble PD-L1 expression, etc. In addition, we expect RT-PCR to replace IHC as a CDx method for cancer patients.

This review will summarize the CDx approaches and prospective biomarkers associated with PD-1/PD-L1 immunotherapy for malignant melanoma, providing the latest advances in melanoma immunotherapy and new strategies for future development of cancer therapy.

2 PD-1/PD-L1 immunotherapy and malignant melanoma

Activation of the PD-1/PD-L1 signalling pathway can suppress cellular immunity in cancer patients, thus maintaining tumour immune tolerance. Modern research has shown that T cell activation depends primarily on dual signals, with the first being major histocompatibility complex (MHC) antigen presentation that binds to the T-cell receptor (TCR), and the second signal consisting of a costimulatory signal and a coinhibitory signal (13).

The combination of PD-1 expressed on T cell surface and PD-L1 expressed on tumour cell or antigen presenting cell surface can effectively inhibit T cell activation, reduce cytokine production and even cause T cell death (Figure 1). Activation of the PD-1/PD-L1 signalling pathway in normal organisms is primarily to reduce ineffective or deleterious immune responses and maintain immune tolerance. However, its negative effects on immunity can lead to immune escape by tumour cells (14), which is known as the "adaptive immune mechanism" of tumour cells (15). Tumour cell expressed PD-L1 binds to its receptor to act as a pro-cancer factor, activating proliferation and survival signalling pathways (16).

As the PD-1/PD-L1 pathway mediated immunosuppression is reversible, blocking PD-1/PD-L1 signalling therapy represents a breakthrough in tumour immunotherapy. This technique has been used in preclinical trials and clinical stages for the treatment of various malignant tumours. FDA approved the use of PD-1/PD-L1 immunotherapies for patients with malignant melanoma, including pembrolizumab, nivolumab, and atezolizumab, without specific CDx regimen for melanoma patients. There are enough clinical data to demonstrate the efficacy of PD-1/PD-L1 immunotherapy in patients with melanoma.

Pembrolizumab is the first monoclonal antibody anti-PD-1 drug FDA-approved and is generally used in patients with advanced melanoma or as an adjuvant therapy after surgery. In a Phase I trial (KEYNOTE-001), pembrolizumab had an antitumour effect in patients with locally advanced or MM (17). A randomized, controlled, phase III trial (KEYNOTE-006) revealed that pembrolizumab prolonged progression-free survival (PFS) and overall survival (OS) in patients with advanced melanoma as compared with the monoclonal antibody anti-CTLA-4 drug ipilimumab, and the incidence of high-grade adverse reactions was low (18). These trials demonstrated durable benefits with pembrolizumab in the majority of patients, with one study evaluating pembrolizumab's durable benefits for the KEYNOTE-001 and KEYNOTE-006 trials and assessment of stable disease (SD) at week 12 or week 24. As for melanoma patients with partial response (PR) or complete response (CR), the earlier the CR outcome, the better the prognosis (19). This indicates the need for regular assessment of patient response during treatment to predict subsequent treatment progress. Patients with completely resected stage III melanoma were randomly assigned to pembrolizumab (505 patients) or placebo (3 patients) for 1 year, and relapse free survival and drug safety were assessed. The results showed that pembrolizumab, as an adjunct therapy after surgery for high-risk stage III melanoma, offered more benefits to patients than placebo, without new toxic side effects (20).

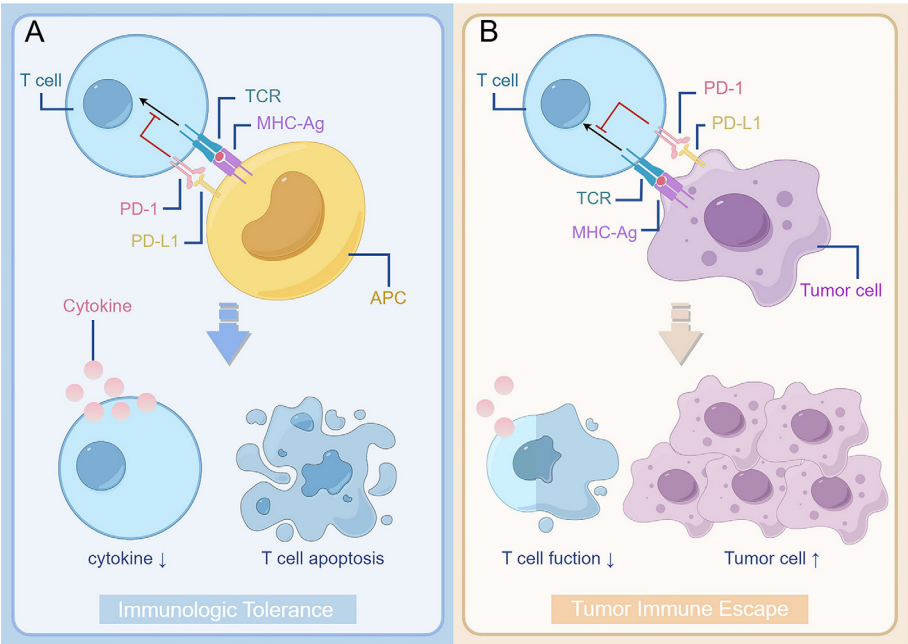

FIGURE 1
The interaction between PD-1 and PD-L1 reduces T cell function and plays a role in promoting the development of tumour. **(A)** Binding of PD-1 on the surface of T cells to PD-L1 on the surface of antigen-presenting cells results in suppression of T cell function, such as reduced cytokine secretion and apoptosis. It forms immunologic tolerance and reduces ineffective or harmful immune responses in normal organisms. **(B)** However, as binding of PD-1 on the surface of T cell to PD-L1 on the surface of tumour cells takes place in the tumour patient body, it can cause the tumour cell's immunity escape. The decrease of T cell function leads to the proliferation of tumour cells. TCR, T cell receptor; MHC, major histocompatibility complex; APC, antigen-presenting cells; PD-1, programmed cell death protein 1; PD-L1, programmed cell death 1 ligand 1.

Nivolumab, a human-derived IgG4, was found to have excellent anti-solid tumour activity and safety in a phase I trial (21). During 18 months of follow-up, nivolumab showed a higher 12-month recurrence-free survival rate (70.5%: 60.8%) and a lower rate of adverse events (3.4%: 14.4%) than ipilimumab (22). In a phase III, randomized, double-blind trial (Checkmate 066) of patients with untreated MM without v-raf murine sarcoma viral oncogene homolog B1 (BRAF) mutations, nivolumab was found to have a much higher ORR and OS than dacarbazine, and the incidence of adverse events was lower (23).

Atezolizumab, an anti-PD-L1 monoclonal antibody, was first approved as a monotherapy or combination therapy for patients with urothelial, lung, or breast cancer. In a phase I trial, atezolizumab demonstrated desirable anti-metastatic melanoma efficacy (ORR = 30.2%) and a long duration of response, with a median response period of up to 62 months (24). atezolizumab is often used as a member of adjuvant or combination therapy, and in a phase I study the combination safety and clinical activity of the MEK inhibitor cobimetinib with the anti-PD-L1 antibody atezolizumab was available regardless of Kirsten rat sarcoma viral oncogene homologue (KRAS)/BRAF status (25). A phase III trial showed that the combination of cobimetinib-vemurafenib with atezolizumab was more effective than placebo in BRAFV600 mutation-positive unresectable or advanced melanoma with no greater risk of adverse effects (26).

Pembrolizumab or nivolumab is often used in combination with CTLA-4 immune checkpoint inhibitors, and its clinical benefit in patients with metastatic or advanced melanoma has been noted in numerous literature. In a phase II clinical trial (Checkmate 069), 142 patients with untreated advanced melanoma were randomly assigned in a 2:1 ratio to compare the efficacy of nivolumab plus ipilimumab combination with that of ipilimumab monotherapy; clinical ORR improved significantly in patients receiving combination therapy, but the incidence of adverse events increased (27). nivolumab demonstrated desirable clinical response to combination and monotherapy in the phase III clinical trial (Checkmate 067), where patients were followed for an additional 6.5 years, and the longest progression-free survival and median OS were found to be 27.6 months and 72.1 months in the combination group, respectively (28). It was precisely because of the increased incidence of adverse events with combination therapy that patients with cancer were generally treated with PD-1/PD-L1 monotherapy, followed by ipilimumab as second-line therapy when treatment failed. One study recruited patients with melanoma who had failed PD-1/PD-L1 immunotherapy to pembrolizumab in combination with low-dose ipilimumab, with an ORR of 29%, a median survival time (MST) of 16.6 months, and a 3% rate of adverse events (29). Whether it is monotherapy, sequential administration, or combination therapy, the recommendations of oncologists must be strictly followed in order to achieve greater clinical benefits for patients.

3 Companion diagnostics of PD-1/PD-L1

CDx is an *in vitro* Companion Diagnostic Devices associated with targeted drugs, and the FDA issued guidelines for CDx in 2014 to help screen specific groups of patients who could benefit from the treatment product, to improve the prognosis of treatment and reduce medical expenditure (30). There is substantial clinical evidence that the higher the level of PD-L1 expression by tumour cells or tumour-infiltrating lymphocyte, the higher the clinical response rate for patients using PD-1/PD-L1 immunotherapy. It is suggested that PD-L1 CDx plays an important role in guiding the use of antibody in tumour immunotherapy, improving the accuracy of tumour pathological detection and prognostic assessment, and the development of PD-L1 CDx reagents is the inevitable trend of immune checkpoint targeted therapy in the future. FDA-approved CDx methods for PD-1/PD-L1 immunotherapy are listed in Table 1.

Immunohistochemistry (IHC) is an effective and commonly used method to evaluate the expression of PD-L1 in tumour tissues. It is widely used in many kinds of tumours, including NSCLC, MM and so on, to identify or aid in the prediction of patients who may benefit from immunotherapy. The principle is to use antigen-antibody specific binding, through chemical reaction to make the color reagent labeled antibody to determine the tissue-cell antigen, its location, qualitative and relative quantitative study. Currently, the FDA has approved tests for PD-1/PD-L1 concomitant diagnostic with anti-PD-L1 monoclonal antibody 22C3,28-8, SP142, and SP263 to guide clinical use of pembrolizumab, nivolumab, and atezolizumab, respectively.

In a phase I study of pembrolizumab in patients with advanced NSCLC, the ORR was 19.4%. However, when patients were grouped using the concomitant diagnostic, the ORR with pembrolizumab increased to 45.2% in patients with TPS greater than 50% (32). In another study of clinical efficacy of pembrolizumab in combination with a CDx in patients with NSCLC, the ORR was 52% was found for patients with TPS greater than 50% (33). Similar results were seen in patients with PD-L1-positive melanoma, where ORR, MST, and OS were significantly higher than in patients with PD-L1-negative melanoma (34).

Although the advent of CDx benefits numerous patients, IHC still has many limitations: the IHC protocol for PD-L1 detection varies greatly due to the difference of antibody and staining threshold (35); the interchangeable detection method and PD-L1 positive cut-off criterion may lead to the discordance of PD-L1 status classification in some patients; the limitations of the current IHC methods for assessing PD-L1 expression in terms of reproducibility and sampling variability are illustrated (36). Current detection of PD-L1 focuses on biopsy samples, which are not representative of the entire tumour, and studies have found that in a substantial proportion of patients, the PD-L1 positive rate in biopsy samples is lower than that in surgical resection samples, leading to false-negative results and patients misdiagnosis (37). Moreover, IHC results need to be evaluated by a pathologist, which is subjective. In a study that used multiple PD-L1 IHC to detect tumour specimens, 22C3 was the most sensitive monoclonal antibody, followed by 28-8 and finally SP-142. This shows the problem that if the physician selects only one IHC test, the PD-L1 status of the patient's tumour sample in the results may not be accurate. This may be related to the differences in the number, size and accessibility of specific epitopes recognized by different antibodies (38).

In view of the limitations of PD-L1 IHC detection, we need a more convenient and accurate CDx method. As research advances, molecular diagnosis will become the fastest growing and most profitable field, including real-time PCR, *in situ* hybridization and

TABLE 1 FDA approvals of companion diagnostic assays for PD-1/PD-L1 immunotherapy.

Drug	Diagnostic name	Manufacturer	Biomarkers	Grant date and indication sample type
Keytrud (Pembrolizumab)	PD-L1 IHC 22C3 pharmDx	Dako	PD-L1 protein expression (Any staining intensity, TPS <50% or ≥50%)	2015, NSCLC 2018, Cervical Cancer 2019, HNSCC 2019, ESCC 2020, TNBC
	FoundationOne CDx	Foundation Medicine	TMB ≥10 mutations per megabase	2020, Solid Tumours
Libtayo (Cemiplimab-rwlc)	PD-L1 IHC 22C3 pharmDx	Dako	PD-L1 protein expression (TPS ≥50%)	2021, NSCLC
Opdivo (Nivolumab) in combination with Yervoy (Ipilimumab)	PD-L1 IHC 28-8 pharmDx	Dako	PD-L1 protein expression (Tumour cell staining ≥1%)	2020, NSCLC
Tecentriq (Atezolizumab)	Ventana PD-L1 (SP142) Assay	Ventana	PD-L1 protein expression (IC ≥5%) PD-L1 protein expression (TC ≥50 or IC ≥10%)	2016, Urothelial Carcinoma 2018, NSCLC
	Ventana PD-L1 (SP263) Assay		PD-L1 protein expression	2021, NSCLC

PD-L1, programmed cell death 1 ligand 1; IHC, immunohistochemistry; CDx, companion diagnostic; TPS, Tumour Proportion Score; TMB, tumour mutation burden; IC, immune cells; TC, tumour cells; NSCLC, non-small cell lung cancer; HNSCC, head and neck squamous cell carcinoma; ESCC, esophageal squamous cell carcinoma; TNBC, triple-negative breast cancer. Information was collected from the "List of Cleared or Approved Companion Diagnostic Devices (*in vitro* and Imaging Tools)" (31).

new generation sequencing technology. The expression level of PD-L1 mRNA in peripheral blood of patients with gastrointestinal cancer by qRT-PCR was compared with that by PD-L1 IHC in paired tumour tissues, but it was not statistically significant. However, it was found that gastric cancer patients with high expression of PD-L1 in blood had better response to immunotherapy (35). Similar trials were conducted in patients with non-metastatic renal clear cell carcinoma and patients with primary NSCLC, both of which used tumour tissue from patients to compare the concordance of the qRT-PCR method with the IHC method. The results showed high consistency between the two methods, but they were also related to the selection of anti-PD-L1 monoclonal antibody (39, 40). Compared with IHC, qRT-PCR is a simple, accurate, easy-to-use, time-and cost-saving, semi-quantitative method that does not depend on the evaluation of observers and is expected to be a new CDx method for melanoma patients (41).

4 Prospective biomarkers for PD-1/PD-L1 immunotherapy

Currently, PD-L1 levels in tumour tissue are a commonly used marker to predict the efficacy of PD-1/PD-L1 immunotherapy. However, studies have shown that, no matter the patient's tumour tissue expresses PD-L1 or not, they can equally benefit from immunotherapy. This illustrates the importance of finding novel and effective biomarkers that predict the efficacy of PD-1/PD-L1 inhibitors, as well as the need for innovation in CDx assays (42). In addition to PD-L1 expression status, the biomarkers were classified into tumour microenvironment biomarkers, peripheral circulation biomarkers and gene mutations according to their characteristics (Figure 2), as discussed below.

4.1 Tumour microenvironment biomarkers

The internal environment in which tumour cells are produced and live is called the tumour microenvironment (TME), including haematopoietic cells, fibroblasts, blood and lymphatic endothelial cells, as well as the surrounding extracellular matrix and soluble factors they produce. It is characterized by hypoxia, chronic inflammation and immunosuppression, which forms a very complex network of mechanisms. It plays an important role in the development of tumour. Biomarkers associated with PD-1/PD-L1 immunotherapy include PD-L2, human endogenous retrovirus-H long repeat-associating 2 (HHLA2), CD8+ T cells, B-cell receptor (BCR), tumour-associated macrophage (TAM), collagen alpha-1 (III) (COL3A1), phosphatase and tensin homolog deleted on chromosome 10 (PTEN), epidermal growth factor receptor (EGFR), mouse double minute 2 homolog (MDM2), fibroblast growth factor receptor (FGFR), serine/threonine kinase 11 (STK11), interferon-γ (IFN-γ), Janus kinases 1/2 (JAK1/2), β2-microglobulin (B2M), cancer-associated fibroblasts (CAFs), S100A8/A9 and so on (Table 2).

PD-L2 is another important ligand in PD-1/PD-L1 signalling pathway, which can bind to PD-1 to suppress cellular immunity. Moreover, PD-L2 has stronger affinity than PD-L1. This is because the tryptophan side chain of PD-L2 is exposed to the surface of the protein and can interact with PD-1, while the corresponding structure of PD-L1 is hidden in the hydrophobic core of the protein (65). In a study in 147 patients with metastatic melanoma, expressions of both PD-L1 and PD-L2 correlated significantly with increasing densities of immune cells in the tumour specimens and with immunocytes. Patients with positive PD-L2 expression had significantly prolonged OS regardless of 5% or 20% expression levels. Patients whose tumours were double positive for PD-L1 and PD-L2 had better OS than patients with tumours that were not double positive. PD-L2, alone or in combination with PD-L1, may predict clinical outcomes in patients with MM (43). In an epigenetic study of PD-L2, DNA promoter hypomethylation and high mRNA expression were strong predictors of prolonged OS. Low PD-L2 DNA methylation and high PD-L2 mRNA expression in pre-treatment melanoma samples from anti-PD-1-treated patients predicted longer progression-free survival. PD-L2 DNA methylation and mRNA expression also correlated with TILs and IFN-γ signature. The IFN-γ-induced PD-L2 expression in melanoma cells is controlled by the extent of DNA methylation in the PD-L2 promoter region (44).

HHLA2 is a specific molecule in TME ubiquitously and highly expresses in many cancers and belongs to the B7 family. A study suggested that the OS and PFS was significantly longer in skin cutaneous melanoma (SKCM) patients with higher HHLA2 expression levels. The immune infiltration levels and TME scores were obviously higher in the HHLA2 high group. For immunotherapy patients, responders had significantly higher HHLA2 expression levels than non-responders. The ORR was 50% in HHLA2-positive patients and 14.3% in negative patients (45).

Tumor-infiltrating lymphocytes (TILs) exist in the TME, and its components include cytotoxic T cells, regulatory T cells, B cells, etc. They can directly or indirectly participate in the immune response, affect tumour growth and treatment response. The presence of TILs is critical for immunotherapy, no matter it is TILs treatment that returns to the patient *in vivo* after direct extraction of amplification, or treatment that restores T cell function through immune checkpoint inhibitors; the effect is influenced by the number and functionality of TILs. A combination of PD-L1 and TILs statuses may lead to a more accurate prognosis than a single PD-L1-level status. Tumours have been divided into four distinct subgroups according to PD-L1 and TILs status, and patients with positive PD-L1 expression and high TILs levels are considered to have adaptive immune resistance (66).

The CD8+ T cells play a critical role in tumour control, particularly in melanoma. In a Korean study involving 63 patients with melanoma, patients with positive PD-L1 expression and low levels of CD8+ TILs had a worse prognosis (46). Studies have demonstrated that the higher the density of CD8+ T cells at baseline in metastatic melanoma, the better the prognosis of PD-1 immunotherapy (47). A subset of antigen-experienced CD8+ T cells become resident within tissue environments, facilitated by local cytokines. Tissue-resident CD8+ T cells are characterized by

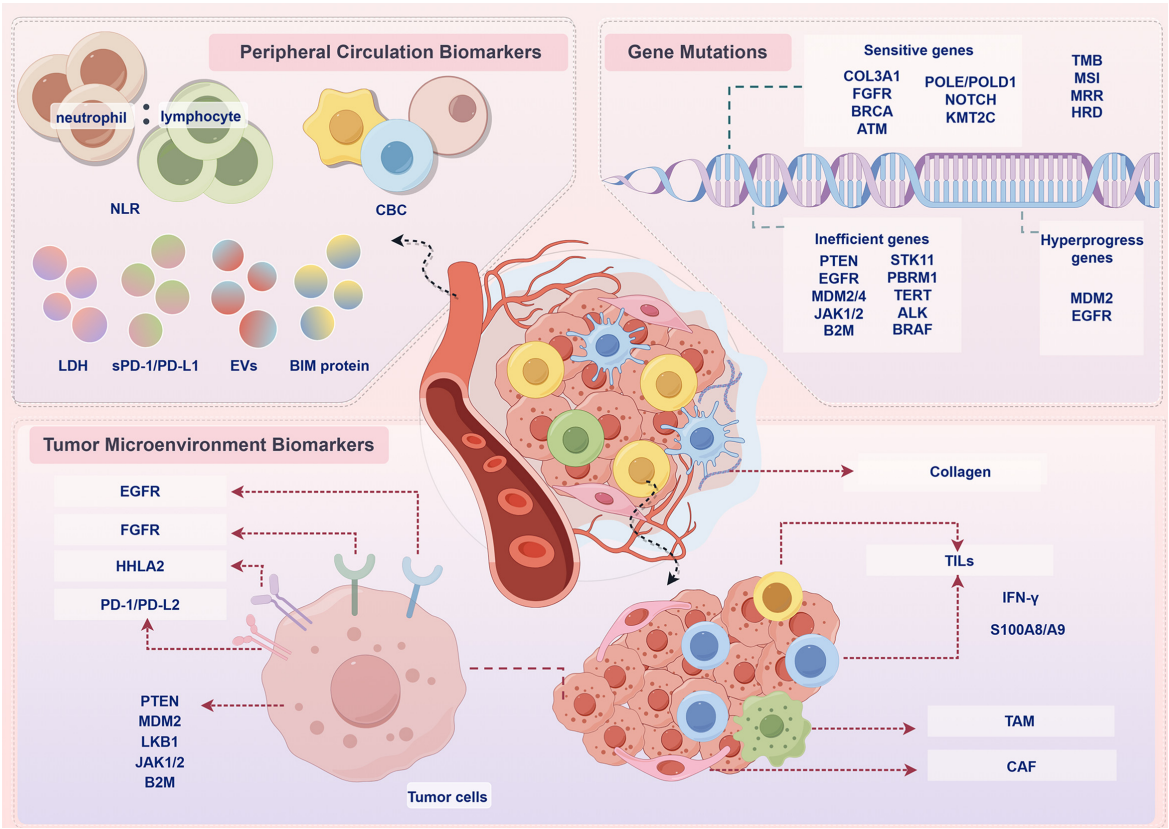

FIGURE 2
Prospective biomarkers for PD-1/PD-L1 immunotherapy. In addition to PD-L1 expression status, the biomarkers were classified into peripheral circulation biomarkers, tumour microenvironment biomarkers, gene mutations according to their characteristics. NLR, neutrophil-to-lymphocyte ratio; CBC, complete blood count; LDH, lactate dehydrogenase; EVs, extracellular vesicles; BIM, BCL-2 interacting mediator of cell death; COL3A1, collagen alpha-1 (III) gene; FGFR, fibroblast growth factor receptor; BRCA, breast cancer susceptibility gene; ATM, ataxia telangiectasia-mutated gene; POLE, polymerase epsilon; POLD, DNA polymerase delta; PTEN, phosphatase and tensin homolog deleted on chromosome 10; EGFR, epidermal growth factor receptor; MDM2, mouse double minute 2 homolog; JAK, Janus kinase; B2M, β2-microglobulin; STK11, serine/threonine kinase 11; PBRM1, polybromo 1; TERT, telomerase reverse transcriptase; ALK, anaplastic lymphoma kinase; BRAF, v-raf murine sarcoma viral oncogene homolog B1; TMB, tumour mutational burden; MSI, microsatellite instability; MRR, DNA mismatch repair; HRD, homologous recombination deficiency; HHLA2, human endogenous retrovirus-H long repeat-associating 2; PD-L2, programmed cell death 1 ligand 2; LKB1 liver kinase B1; TILs, tumor-infiltrating lymphocytes; TAM, tumour-associated macrophage; CAFs, cancer-associated fibroblast; IFN-γ, interferon-γ.

the constitutive expression of CD69 and CD103. A study of advanced stage MM patients being treated with anti–PD-1 monotherapy showed that tumor-resident CD8+ T-cell numbers were more prognostic than total CD8+ T cells in metastatic melanoma. The increased presence of tumor-resident CD8+ T cells was strongly associated with better melanoma-specific survival in untreated patients (48).

The B cells also play an important role in anti-tumor immunity in TME. A genomic analysis of immune cell infiltrates across 11 tumour types showed that high expression of T-cell and B-cell signatures predicted improved OS in melanoma. B-cell gene signature expression was more statistically significantly associated with improved OS than T-cell gene signature expression. Decreased BCR gene segment diversity was associated with improved survival in melanoma (HR = 2.67) (49).

TAM is considered to play an important role in tumour growth, progression and metastasis. Macrophages can be divided into M1 and M2 subtypes according to the cell phenotype. M1 subtype macrophages have anti-cancer effects, while M2 subtype macrophages can promote tumour development. Different subtypes of macrophages influence the prognosis of cancer patients and their response to immunotherapy (50). In melanoma, high-density macrophages are often suggestive of a poor prognosis, which may be related to the fact that melanoma exosomes can stimulate TAM polarization, promoting tumour growth and metastasis (67).

The TILs can also be altered by gene mutations or increased receptor expression in some tumour cells or other cells in TME. COL3A1 gene encodes alpha 1 chain of type III collagen, which is an extracellular matrix protein and a major structural component in hollow organs such as large blood vessels (68). The alterations in COL3A1 have been demonstrated to be associated with melanoma metastasis. A study of 631 melanoma patients who received blockade therapy of immune checkpoints showed that patients with COL3A1 mutations showed a significantly improved OS and PFS compared with patients without such mutations. The COL3A1-mutated tumours exhibited an elevated ORR and disease control rates. CD8+ T cells, activated CD4+ memory T cells, and resting NK cells infiltrated tumours of patients with COL3A1 mutations. Furthermore, the

TABLE 2 Biomarkers in the TME.

Classification	Biomarkers	Drug	Results	Reference
Tumour microenvironment biomarkers	PD-L2	Nivolumab, ipilimumab	Patients with positive PD-L2 expression or low PD-L2 DNA methylation and high PD-L2 mRNA expression achieved higher OS and PFS.	(43, 44)
	HHLA2	Immune-checkpoint inhibitor	Responders had significantly higher HHLA2 expression levels than non-responders. The ORR was 50% in HHLA2-positive patients and 14.3% in negative patients.	(45)
	CD8+ T cells	Pembrolizumab	Patients with positive PD-L1 expression and higher levels of CD8+ TILs had a better prognosis. The increased presence of CD8+ T cells tumor-resident is strongly associated with better melanoma-specific survival.	(46–48)
	BCR	None	Decreased BCR gene segment diversity was associated with improved survival in melanoma.	(49)
	TAM	None	Patients with MM of higher TAM levels usually indicate a poor prognosis.	(50)
	COL3A1	Immune-checkpoint inhibitor	Patients with COL3A1 mutations showed a significantly improved OS and PFS compared with patients without such mutations	(51)
	PTEN	PD-1/PD-L1 inhibitor	Loss of PTEN in MM patients increases tumour resistance to immunotherapy. Patients with MM with PTEN hypermethylation had shorter survival.	(52, 53)
	EGFR	Pembrolizumab, nivolumab	Patients with high baseline EGFR expression had a significantly higher relapse rate than those with low EGFR expression.	(54)
	MDM2	Immune-checkpoint inhibitor	Patients with MDM2/MDM4 amplification developed TTF <2 months and showed a clearly accelerated rate of tumor growth compared to that before treatment.	(55)
	FGFR	Immune-checkpoint inhibitor	Patients with FGFR mutations had better median-OS than those without (60.00 vs. 31.00 months).	(56)
	STK11	Immune-checkpoint inhibitor	Mutations or phenotypic defects in STK11 have been significantly associated with immunotherapy resistance in patients with metastatic melanoma.	(57, 58)
	IFN-γ	Atezolizumab, pembrolizumab	Expression of IFN-γ and IFN-γ-inducible genes was elevated in tumors before treatment in responding patients.	(59, 60)
	JAK1/2, B2M	PD-1 inhibitor	Patients with MM harboring JAK1/2-inactivating and B2M-truncating mutations did not respond to anti-PD-1 drugs.	(61, 62)
	CAF	PD-1 inhibitor	CAF significantly impaired the generation of melanoma-specific T-cell responses and compromise the efficacy of anti-PD-1 checkpoint inhibition.	(63)
	S100A8/A9	Pembrolizumab	Patients with high baseline S100A8/A9 showed significantly impaired survival compared to patients with low baseline S100A8/A9.	(64)

PD-L2, programmed cell death 1 ligand 2; OS, overall survival; PFS, progression-free survival; HHLA2, human endogenous retrovirus-H long repeat-associating 2; ORR, objective response rate; BCR, B-cell receptor; TAM, Tumour-associated macrophage; MM, metastatic melanoma; COL3A1, collagen alpha-1 (III); PTEN, phosphatase and tensin homolog deleted on chromosome 10; MDM2, mouse double minute 2 homolog; TTF, time-to-treatment failure; FGFR, fibroblast growth factor receptor; STK11, serine/threonine kinase 11; IFN-γ, interferon-γ; JAK1/2, Janus kinases 1/2; B2M, β2-microglobulin; CAF, cancer-associated fibroblast.

COL3A1 mutant tumours exhibited increased infiltration of pro-inflammatory M1 macrophages and decreased infiltration of immune-suppressive M2 macrophages. The favourable genomic traits and the immune microenvironment may underlie the better immunotherapy response of COL3A1 mutations (51).

The phosphoinositide 3-kinase (PI3K) pathway plays a critical role in cancer by regulating several critical cellular processes, including proliferation and survival. One of the most common ways that this pathway is activated in cancer is by loss of expression of the tumour suppressor PTEN, which is a lipid phosphatase that dampens the

activity of PI3K signalling. Loss of PTEN occurs in up to 30% of melanomas. A study of preclinical models demonstrated that loss of PTEN promoted resistance to immunotherapy in melanoma by reducing CD8+ TILs (52). The methylation of the PTEN gene leads to its inactivation. In a review of the methylation levels of the PTEN gene in 158 Korean melanoma patients, it was found that the PTEN hypomethylated subgroup had a relatively longer survival, whereas the PTEN hypomethylated subgroup had a shorter survival, indicating significant difference between them ($p = 0.017$) (53).

EGFR is a growth factor receptor that induces cell differentiation and proliferation upon activation through the binding of one of its ligands. EGFR activation is associated with upregulation of PD-1, PD-L1 and CTLA-1, which can drive immune escape. EGFR is frequently expressed at elevated levels in different forms of cancer and expression often correlates positively with cancer progression and poor prognosis (69). PD-1 immunotherapy is not recommended for patients with EGFR-mutant cancers, and available data suggest that immunotherapy is ineffective in patients with EGFR mutations and even presents a risk of explosive progression. One study included 137 treatment-naive patients treated with adjuvant pembrolizumab or nivolumab. Patients with high baseline EGFR expression had a significantly higher relapse rate than those with low EGFR expression. Patients with high EGFR expression had significantly worse outcomes, and the median relapse-free survival for these patients was 3 months; for patients with low EGFR expression, the median relapse-free survival was not reached. It identified EGFR expression in therapy-naive metastatic tissue as a potential negative predictive factor for immunotherapy (54).

MDM2 is a negative regulator of the tumour suppressor p53 and is often highly expressed in solid tumours. p53 protein is a tumour suppressor, which plays a role in regulating cell growth cycle. For T cells it was shown that MDM2 inhibition can induce production of tumour necrosis factor α and IFN-γ, whereas in melanoma cells MDM2 inhibition induces interleukin-15 (IL-15) production. IL-15 serves as an activator of anti-tumor CD8+ T cells and natural killer cells. MDM2 amplification is found in about 7% of cancers; it inhibits the p53 tumour suppressor. MDM4 is a homolog of MDM2 that interacts with it and also inhibits p53 (70). A study of 155 patients who received immunotherapy identified that those with melanoma were more likely to develop time-to-treatment failure (TTF) <2 months compared with patients with other tumours. Patients with MDM2/MDM4 amplification were taken off immunotherapy in less than two months, and four showed a clearly accelerated rate of tumour growth compared to that before treatment. In that study, EGFR alterations was also described as a high risk factor. Among 10 patients with EGFR alterations, eight had a TTF <2 months (55).

The FGFR family consists of four highly conserved transmembrane receptors, FGFR1-4, which play key roles in embryonic development, proliferation, angiogenesis, and tumour metastasis. FGFR is mutated across numerous cancers, triggering the FGFR signalling pathway, hence promoting tumour progression (71). Melanoma had the highest mutation frequency of 22.05% among 27 cancers. In the immune checkpoint inhibitors-treated cohort, patients with FGFR mutations had better survival than those without (median OS: 60.00 vs. 31.00 months). The ORR was higher for patients harbouring FGFR mutations (55.56%) compared to wild-type patients (22.40%). FGFR mutant melanoma tended to exhibit an enhanced anti-tumor and inflammatory tumour immune microenvironment, which synergistically promotes inflammatory to activate immune cells to kill cancer cells (56).

The STK11 gene codes for liver kinase B1, a highly conserved serine/threonine kinase, is implicated as a tumour suppressor in epithelial cancer invasion and metastasis. For the STK11-deficient population, the efficacy of immunotherapy was significantly reduced. This may be related to the fact that STK11 deficiency leads to T cell suppression, resulting in reduced numbers of tumour-infiltrating lymphocyte and decreased expression of PD-L1 in tumours (72). Mutations in STK11 have been reported to be significantly associated with immunotherapy resistance in patients with MM (57). But in addition to mutation status, the phenotypic classification of STK11 is also important for survival prognosis. Among the patients whose mutation status was not consistent with the phenotype classification, the immunotherapy efficacy was significantly worse in the patients without STK11 mutation but with defective phenotype than in the patients with STK11 mutation but with normal phenotype (58).

TILs produce cytokines such as IL-2 and IFN-γ, which play an important role in the activation and proliferation of TILs. IFN-γ can induce PD-L1 expression in tumour cells and macrophages, suggesting that IFN-γ may be an important factor in inducing PD-L1 expression in the TME. IFN-γ signalling and the associated biology of T cell cytolytic activity, antigen presentation, and chemokine production are important components of a PD-1 checkpoint blockade–responsive immune microenvironment in melanoma. In a phase I study of atezolizumab for patients with advanced melanoma, elevated expression of IFN-γ as well as IFN-γ-inducible genes (for example, indoleamine 2,3 dioxygenase 1 [IDO1] and C-x-C motif chemokine ligand 9 [CXCL9]) in pre-treatment tumours were demonstrated in responding patients (59). A study analyzed gene expression profiles using RNA from baseline tumour samples of pembrolizumab-treated patients. To examine immune-related gene expression signatures associated with pembrolizumab response in patients with metastatic melanoma. Many of the top-ranked genes were directly linked to IFN-γ signalling and showed correlation with the expression of IFN-γ. A 10-gene "preliminary IFN-γ" signature was constructed that was able to separate responders and nonresponders to pembrolizumab among the 19 pilot data patients with melanoma (60).

IFN-γ through the interferon gamma receptor, the Janus kinases JAK1 and JAK2 and the signal transducers and activators of transcriptions (STATs) results in the expression of a large number of interferon-stimulated genes and lead to beneficial anti-tumor effects. The melanoma cell lines that had JAK1/2 homozygous loss of function mutations did not respond to IFN-γ. β2-microglobulin (B2M) is an important subunit of MHC class I which exerts substantive biological functions in tumourigenesis and immune control. Acquired resistance to PD-1 blockade in patients with advanced melanoma can be associated with loss-of-function mutations with loss of heterozygosity in JAK1/2 or in B2M. Two cancer patients with higher TMB but JAK1/2-inactivating mutations did not respond to PD-1 immunotherapy (62). Sequencing of the genes of four other drug-resistant MM patients revealed that mutations in their JAK1/2 or B2M genes were a major cause of drug resistance (61).

Cancer-associated fibroblasts (CAFs) contribute to the development of a physical barrier that interferes with immune cell infiltration, directly inhibiting T-cell trafficking, and expressing an array of factors, including C-C motif ligand 2 (CCL2), that contribute to the establishment of an immunotolerant TME. A preclinical study suggested that melanoma-associated fibroblasts (MAFs), significantly impair the generation of melanoma-specific T-cell responses and compromise the efficacy of anti-PD-1 checkpoint inhibition (63).

S100A8/A9 is a member of the damage-associated molecular pattern (DAMP) (also known as alarmins) that is released upon cell stress or damage promoting thereby an inflammation. The inflammation-associated S100A8 and S100A9 have been identified to attract melanoma cells and described as a critical factor for recruitment of myeloid-derived suppressor cells (MDSCs) and stimulation of their immunosuppressive functions in the TME (73). In a study of patients with advanced melanoma revealed an exclusive and abundant expression of S100A8/A9 in cells of the TME, mainly granulocytes. High numbers of S100A8/A9 expressing cells in melanomas would translate into elevated S100A8/A9 serum levels. Patients with high baseline S100A8/A9 >5.5 mg/l showed significantly impaired survival compared to patients with low baseline S100A8/A9 in two independent cohorts of patients treated with pembrolizumab (HR 5.37,10.70) (64).

4.2 Peripheral circulation biomarkers

Circulating biomarkers are molecules that can be detected in the blood after release, including sugars, cholesterol, proteins, and even intact cells. They can be measured objectively, and some of them can be used as indicators of tumour progression. Circulating biomarkers associated with PD-1/PD-L1 immunotherapy include lactate dehydrogenase (LDH), neutrophil-to-lymphocyte ratio (NLR), soluble PD-L1 (sPD-L1), soluble PD-1 (sPD-1), BCL-2 interacting mediator of cell death (BIM), relative lymphocyte and eosinophil granulocyte counts, and circulating extracellular vesicles (EVs) (Table 3).

LDH is a kind of NAD-dependent kinases, which can catalyze the oxidation reaction between pyruvate and lactic acid. During the growth, invasion and metastasis of tumour cells, serum LDH level may increase. LDH can be a good predictive biomarker for patients with malignant melanoma. Evidence have shown that patients with higher-than-normal serum LDH levels at baseline generally have a worse prognosis and that patients with higher-than-normal serum LDH levels at 2 times the upper limit are less likely to benefit in the long term from ipilimumab treatment (74). Patients with elevated serum LDH levels during the first two weeks of PD-1 immunotherapy had shorter survival (75). The rapid growth and proliferation of tumour cells may result in impairment of surrounding normal tissues, which can also be destroyed during their invasion and metastasis, allowing LDH to be released into the blood. Fast-growing tumour tissue usually gets its energy from glycolysis and also produces a lot of LDH. Elevated levels of LDH in the blood can lead to a decrease in the pH of the TME, which negatively affects the function of the lymphocyte and the efficacy of the immune response (85).

The higher the baseline NLR level in cancer patients, the worse the prognosis. An elevated NLR ratio usually indicates increased neutrophil, reflecting a state of systemic inflammation. The inflammatory reaction can promote the proliferation and survival of tumour cells, as well as the formation and metastasis of blood vessels. In particular, increased neutrophil can suppress adaptive immune responses in the TME, while decreased lymphocyte counts

TABLE 3 Biomarkers in the peripheral circulation.

Classification	Biomarkers	Drug	Results	Reference
Peripheral circulation biomarkers	LDH	Ipilimumab	Patients with baseline serum LDH concentrations more than 2 times the upper limit of normal and those with elevated serum LDH levels during the first two weeks of immunotherapy showed a significantly shorter OS.	(74, 75)
	NLR	Ipilimumab	Patients with NLR ≥5 showed a lower OS.	(76–78)
	sPD-L1	Ipilimumab, pembrolizumab	Patients with moderate to low baseline serum sPD-L1 levels and those with reduced serum sPD-L1 levels during immunotherapy showed better clinical responses.	(79)
	sPD-1	Nivolumab	Patients with elevated serum sPD-1 levels during immunotherapy showed a better prognosis.	(80)
	BIM	Pembrolizumab	Patients with higher expression of BIM protein on CD8+ T cells in peripheral blood responded better to immunotherapy.	(81)
	Relative lymphocyte and eosinophil granulocyte counts	Nivolumab, pembrolizumab	Higher levels of lymphocyte and eosinophil granulocyte at baseline are associated with better outcomes. An increase in the number of absolute eosinophil granulocyte and a decrease in the number of relative lymphocyte showed a worse prognosis after immunotherapy.	(82, 83)
	Circulating EVs	Nivolumab, pembrolizumab	Patients with higher levels of circulating EVs had a poor prognosis.	(84)

LDH, lactate dehydrogenase; NLR, neutrophil-to-lymphocyte ratio; sPD-L1, soluble PD-L1; sPD-1, soluble PD-1; BIM, BCL-2 interacting mediator of cell death; EVs, extracellular vesicles.

indicate a state of immunosuppression (86). Studies have shown greater improvement in PFS and OS with ipilimumab in melanoma patients with baseline NLR <5 than patients with baseline NLR ≥5 (76). The NLR of 5 was considered a cutoff point, and NLR ≥5 was an independent prognostic risk indicator in the multivariate analysis model, indicating poor OS (77). In a retrospective study, which was more focused than ever on the analysis of the association of pre-treatment peripheral blood NLR with survival and response rates in patients treated with immune checkpoint inhibitors, the distribution of NLR in different cancer species was investigated, which was consistent with the predictive value. Using the NLR as an independent cohort predictor, high NLR was observed to be associated with significantly worse OS as well as lower response rates (17% vs. 28%) and clinical benefit (26% vs. 41%) (78).

Soluble PD-L1 is associated with a poor prognosis in many tumours, which may be related to its production mechanism. The serum sPD-L1 of the patient has multiple sources of production, including the intrinsic splicing of secretory cells, pre-tumour inflammatory response and anti-tumour immune response. Several melanoma cell lines have been found to secrete PD-L1 splice variants lacking transmembrane structure, namely sPD-L1 variants. It can inhibit T cell activation and proliferation. The higher circulating sPD-L1 levels at tumour baseline may represent the greater tumour burden of the patient, increased aberrant splicing activity in tumour cells, or decreased anti-tumour immunity, leading to a poor response to immunotherapy. However, response to immune checkpoint inhibitors was the highest in patients with a moderate increase in sPD-L1 at baseline (79). Similar to sPD-L1, sPD-1 is a shear variant formed by the removal of the transmembrane structure by the full-length PD-1. Soluble PD-1 can block PD-1/PD-L1 pathway by binding membrane PD-L1 competitively, enhance T cell immunity and exert its anti-tumour effect (87). The presence of progressive or stable disease was associated with increased sPD-L1 when nivolumab was used to treat renal cell carcinoma (RCC) and melanoma. In patients in remission, circulating sPD-L1 levels were stable or decreased (88). For patients with advanced melanoma, incremental levels of serum sPD-1 during treatment were a good biomarker for the combination of nivolumab and ipilimumab, but it was not associated with the treatment effect of pembrolizumab (80).

The BIM gene (BCL2L11 gene) is responsible for encoding the BIM protein in the BCL2 protein family, whose function is to induce apoptosis by binding to anti-apoptotic proteins of other BCL2 families through a highly conserved BH3 domain. Melanoma is known to upregulate the BIM protein level of anti-cancer T cells through PD-1/PD-L1 signalling pathway, inducing T cells apoptosis and achieving the goal of immune evasion. Because BIM levels at tumour baseline can reflect the intensity of the PD-1/PD-L1 signalling pathway in tumour patients, and the method of detecting BIM levels is simpler than the ICH method for assessing PD-L1 expression, T-cell BIM level is expected to be a predictive biomarker. Studies have demonstrated higher levels of BIM in CD8+ T cells in the peripheral blood of patients who respond to anti-PD-1 therapy (81). In addition, repeated assessment of T-cell BIM levels during treatment provides greater flexibility in determining drug efficacy and discontinuation time. In general, a decrease in BIM levels on treatment predicts a desirable response to immune checkpoint inhibitors in patients, as this implies that immunotherapy may have successfully blocked the PD-1/PD-L1 pathway. If BIM levels remain or increase during treatment, this may represent resistance or a false progression (89).

Circulating complete blood count is an objective method that allows us to visualize the blood changes of cancer patients before and after immunotherapy. Its role in tumour prognosis has been a hot topic in clinical research. Among them, eosinophil granulocyte count and lymphocyte count have been reported to have prognostic significance in many literatures. After the initiation of immunotherapy, relative lymphocyte counts decreased from baseline in nivolumab-treated melanoma patients if their absolute eosinophil granulocyte counts increased by more than 3.2%, the probability of poor prognosis increased (82). There is also evidence that higher lymphocyte and relative eosinophil granulocyte counts at baseline are associated with benefit from pembrolizumab for patients with melanoma (83). This may be related to the CD28-B7 interaction that induces allergic inflammation leading to an increase in the number of eosinophil granulocyte (90).

Ideally, detection of circulating markers could serve as an objectively effective strategy to meet the need for predicting treatment outcomes and monitoring disease progression in real time. Much attention is focused on normal and cancer cell-released circulating EVs in the hope that it can be used clinically to evaluate cancer patients. EVs are membrane-bound spheres released by cells and carry lipids, soluble and transmembrane proteins, and various RNA species, including mRNA, miRNA and DNA. Cancer cell-derived EVs are emerging as local and systemic intercellular mediators of oncogenic information (91). A study of 71 MM patients showed that higher levels of circulating EVs predicted worse survival (PFS, OS, and ORR) in patients with MM, and high levels of PD-1 EVs in CD8+ T cells and PD-L1 EVs in melanoma cells were independent biomarkers for predicting PFS. This study demonstrated that circulating EVs reduced the immune capacity of peripheral blood mononuclear cells (PBMCs), suggesting that the therapeutic efficacy of PD-1/PD-L1 mabs can be enhanced by eliminating circulating EVs to reactivate patient PBMC (84).

4.3 Gene mutations

Tumour mutation burden (TMB) is generally defined as the number or proportion of mutations occurring in a tumour sample, usually expressed as the number of mutations per megabase. Its numerical value can reflect the potential of tumour to produce neoantigens, and it has been proved to be able to predict the efficacy of immunotherapy for a variety of tumours. Now, high TMB (TMB-H, TMB ≥10 mut/Mb) has been approved by the FDA as a diagnostic marker for disease progression after prior treatment with pembrolizumab, deficiency of satisfactory alternative treatment options, and unresectable or metastatic solid tumours in children and adults. A study performed a multiomic profiling of baseline tumours in 77 patients with advanced cutaneous melanoma treated with anti-PD-1 with or without anti-CTLA-4 showing that overall

response to any treatment was significantly associated with higher TMB (92). Tumours with a high TMB and a high IFN-γ signature show the best response to immunotherapy. In general, TMB refers to tissue TMB (tTMB), but with the development of liquid biopsy techniques, for patients with difficulty in obtaining tissue specimens, their immunotherapy efficacy and dynamically monitor treatment changes can be predicted by evaluating blood TMB (bTMB). One study showed that bTMB was significantly associated with tTMB and was able to substitute TMB for prognosis in cancer patients (93).

TMB is usually not tested alone, but often in conjunction with DNA mismatch repair (MMR) and microsatellite instability (MSI). MMR can accurately identify and repair base mismatches, small base deletions and insertions during DNA replication and recombination, playing an important role in maintaining genome stability. MSI is a microsatellite sequence length change caused by insertion or deletion mutations during DNA repair. In general, patients with high MSI (MSI-H) and those who appear deficient MMR (dMMR) are more likely to be recognized by the immune system, and the prognosis of immunotherapy is better. This is because MSI-H and dMMR tumours harbor a large number of mutations and potential neoantigens, whereas host T cells do not acquire immune tolerance for these neoantigens and are therefore more likely to be recognized by the immune system. In a proof-of-concept study of patients with advanced dMMR cancer in 12 different tumour types, PD-1 immunotherapy delivered desirable responses, with an ORR of up to 53% (94).

In addition to TMB, which reflects the overall mutational level of cancer patients, many individual gene mutations are also strongly associated with the efficacy of PD-1/PD-L1 immunotherapy. According to its effect on immunotherapy, it can be divided into sensitive gene and inefficient gene (Table 4).

PD-1 immunotherapy can achieved desirable response in cancer patients with sensitive gene mutations, including COL3A1, FGFR, breast cancer susceptibility (BRCA), ataxia telangiectasia-mutated gene (ATM), polymerase epsilon (POLE), DNA polymerase delta 1 (POLD1), NOTCH, KMT2C genes and so on. The previously mentioned MSI and MMR also fall into this range.

BRCA is a group of genes directly related to hereditary breast cancer, including BRCA1 and BRCA2. Under normal physiological conditions, the BRCA1/2 gene is tumour suppressor gene and plays an important role in regulating the replication of human cells, the repair of DNA damage and the normal growth of cells. When BRCA1/2 is mutated, it can increase the risk of many cancers. CD8+ T cells have higher PD-1 expression in BRCA1/2 mutant tumours, which may enhance susceptibility to PD-1/PD-L1-targeted immune checkpoint therapy (95).

ATM protein plays a central role in sensing DNA double-strand breaks and coordinating their repair. When the ATM gene is deleted, it can promote the efficacy of immunotherapy through promoting cytoplasmic leakage of mitochondrial DNA and activation of the cyclic GMP-AMP (cGAS) and stimulator of interferon genes (STING) pathway (96). But more clinical data are needed to confirm the effect.

POLE and POLD1 genes encode the catalytic subunits of DNA polymerase ε and δ, respectively, which play an important role in DNA replication and correction, and their mutations directly affect the occurrence and development of tumours. An analysis of a database of 47721 patients with different types of cancer found that patients with POLE/POLD1 mutations nearly doubled their OS after immunotherapy as compared with those with wild-type disease (97).

Notch pathway has been shown to play an important role in the proliferation, differentiation, apoptosis and invasion of a variety of tumour cells. In addition, increasing researches confirms that NOTCH mutations are associated with a favourable prognosis for immunotherapy. A combined analysis of cancer patient information from multiple open databases found that NOTCH mutations increased the efficacy of PD-1 inhibitors by 2.2-fold and reduced the risk of disease progression by 39%; patients had a 44% lower risk of death (98). Neuroblastoma rat sarcoma (NRAS) gene is one of the most significant driver genes in melanoma. The NRAS wildtype patients account for 80%-85% of melanomas and have a better prognosis. For patients with NRAS wild-type MM, NOTCH4 mutations have better PFS and OS (99).

KMT2C is a well-known epigenetic regulator that plays an important role in transcriptional regulation, specifically activation, by loosening chromatin structure through its catalytic role in mono-methylation of histone H3 lysine K4 (H3K4). KMT2C was shown to contribute to the genomic stability and its mutation leads to the obvious TMB elevation in multiple cancers. In a study based on three published MM cohorts, MM patients harboring KMT2C mutations showed significantly better OS after treatment with PD-1 monoclonal antibody as compared with wild-type KMT2C. These results indicate that KMT2C might be a reliable independent biomarker in response to anti-PD-1 treatment of MM patients (100).

PD-1 immunotherapy is ineffective for patients with inefficient gene mutations. The main mutations include PTEN, EGFR, STK11, JAK1/2, B2M, polybromo 1 (PBRM1), telomerase reverse transcriptase (TERT), anaplastic lymphoma kinase (ALK), BRAF, MDM2 genes and so on. Part of those has been described above.

PBRM1 encodes a subunit of the SWI/SNF chromatin remodeling complex (PBAF subtype), which is involved in cell differentiation, proliferation and DNA repair. Approximately 80% of PBRM1 somatic mutations may result in loss of function of the protein. A comprehensive analysis of PBRM1 in multiple cancer types showed that the frequency of PBRM1 mutations was 8.4% in SKCM. Truncating mutations were the most common type of mutation. Patients with PBRM1 mutations showed a shorter median OS. The trends of PBRM1-mutant patients towards a worse survival and high TMB towards clinical benefit from immunotherapy were observed (101).

TERT mutations allow tumour cells to grow without restriction and are found in many types of tumours. In a comprehensive literature review and meta-analysis, data from 19 independent studies showed that TERT-mutated melanoma patients had a significantly worse OS as compared with wild-type ones. TERT mutations adversely affected the survival of patients with melanoma (102).

TABLE 4 Gene mutation as a biomarker.

Classification	Biomarkers	Drug	Results	Reference
Sensitive gene mutations	COL3A1	Immune-checkpoint inhibitor	Patients with COL3A1 mutations showed a significantly improved OS and PFS as compared with patients without such mutations	(61)
	FGFR	Immune-checkpoint inhibitor	Patients with FGFR mutations had better median-OS than those without (60.00 vs. 31.00 months).	(56)
	BRCA	None	Higher PD-1 expression on CD8+ T cells in BRCA1/2 mutant tumours may be beneficial in enhancing the effects of immune checkpoint inhibitors.	(95)
	ATM	None	Tumours with ATM mutations responded significantly better to immunotherapy.	(96)
	POLE/POLD1	Immune-checkpoint inhibitor	Patients with POLE or POLD1 mutations had significantly longer OS at 34 months compared with 18 months in the wild-type population.	(97)
	NOTCH	PD-1/PD-L1 inhibitor	Patients with tumours harboring NOTCH mutations benefit more from immunotherapy, demonstrating longer PFS and OS.	(98, 99)
	KMT2C	PD-1 inhibitor	Patients harboring KMT2C mutations showed significantly better OS as compared with wild-type KMT2C.	(100)
Inefficient gene mutations	PTEN	PD-1/PD-L1 inhibitor	Loss of PTEN in MM patients increased tumour resistance to immunotherapy. Patients with MM with PTEN hypermethylation had shorter survival.	(52, 53)
	EGFR	Pembrolizumab, nivolumab	Patients with high baseline EGFR expression had a significantly higher relapse rate than those with low EGFR expression.	(54)
	MDM2/4	Immune-checkpoint inhibitor	Patients with MDM2/4 amplification developed TTF <2 months and showed a clearly accelerated rate of tumor growth compared to that before treatment.	(55)
	STK11	Immune-checkpoint inhibitor	Mutations or phenotypic defects in STK11 have been significantly associated with immunotherapy resistance in patients with metastatic melanoma.	(57, 58)
	JAK1/2, B2M	PD-1 inhibitor	Patients with MM harboring JAK1/2-inactivating and B2M-truncating mutations did not respond to anti-PD-1 drugs.	(61, 62)
	PBRM1	PD-L1 inhibitor	The trends of PBRM1-mutant patients towards a worse survival from immunotherapy.	(101)
	TERT	None	TERT-mutated melanoma patients had a significantly worse OS compared to wild-type ones.	(102)
	ALK	None	PD-1 immunotherapy is not recommended for ALK mutation-positive patients.	(103)
	BRAF V600E/K	Pembrolizumab	The prognosis of MM patients with BRAF mutation had a lower ORR compared with patients with BRAF wild-type.	(104)
	MDM2, EGFR	PD-1/PD-L1 inhibitor	Some patients with MDM2 family amplification or EGFR aberrations had hyper-progression after immune checkpoint inhibitors-treat.	(55)

COL3A1, collagen alpha-1(III) gene; FGFR, fibroblast growth factor receptor; BRCA, breast cancer susceptibility gene; ATM, ataxia telangiectasia-mutated gene; POLE, polymerase epsilon; POLD, DNA polymerase delta; PTEN, phosphatase and tensin homolog deleted on chromosome 10; EGFR, epidermal growth factor receptor; MDM2, mouse double minute 2 homolog; STK11, serine/threonine kinase 11; JAK, Janus kinase; B2M, β2-microglobulin; PBRM1, polybromo 1; TERT, telomerase reverse transcriptase; ALK, anaplastic lymphoma kinase; BRAF, v-raf murine sarcoma viral oncogene homolog B1.

ALK is an oncogene responsible for the production of the protein receptor tyrosine kinase. ALK expression has been identified in metastatic and primary melanomas. ALK expression in melanoma resulted from a novel transcript variant, known as ALK^{ATI}. ALK^{ATI}, similar to ALK, may be sensitive to targeted therapy. PD-1 immunotherapy is not recommended for ALK mutation-positive patients (103).

In addition, BRAF gene mutation is a common mutation in MM, and it is also an important factor leading to the occurrence and development of MM. Compared with wild type, BRAF mutant MM

has a worse prognosis. For patients with MM who received pembrolizumab, patients with a BRAF V600E/K-mutation had a lower ORR as compared with patients with BRAF wild-type, but did not present a significant difference (34.3% vs. 39.8%) (104). The BRAF-targeted therapy or combined with immunotherapy is recommended for patients with BRAF-mutated melanoma.

Shumei Kato et al. described a class of cancer patients who developed abnormal hyper-progressors after immunotherapy. These patients who experienced explosive progression showed TTF <2 months, disease progression on the first CT scan after treatment with the PD-1 antibody, a 50% increase in tumour size, and a more than twofold increase in tumour growth. This study demonstrates that MDM2 family amplification or EGFR aberrations may be associated with accelerated progression (55). The possibility of hyper-progression is very important for patients with the disease, and treatment strategies should be carefully formulated.

5 Discussion and perspective

It has been 9 years since the first PD-1/PD-L1 immunotherapy was approved for the market. With the development of the research, the PD-1/PD-L1 immunotherapy has gradually been applied to many kinds of cancers, such as MM, NSCLC, lymphoma. Both monotherapy and combination therapy showed relatively high response rate and low adverse reaction rate, which is undoubtedly a boon to cancer patients. With the expansion of the scale of PD-1/PD-L1 immunotherapy, more problems have been discovered and researched, such as how to improve the response rate, the prediction of efficacy, the mechanism of drug resistance and coping strategies.

CDx can help screen specific patient populations that may benefit from the treatment product, better guiding medication use and reducing health care expenditures. The FDA-approved CDx method for PD-1/PD-L1 immunotherapy is mainly PD-L1 detection by IHC. The IHC method for PD-L1 detection has many limitations, and antibodies, staining thresholds, sampling sites, and subjective judgment of the pathologist can all make the results different. Detection of PD-L1 using molecular diagnostic techniques may help physicians diagnose cancer patients more quickly and accurately. In addition, substantial evidence suggests that using PD-L1 expression status alone to predict patient efficacy is sometimes not accurate.

There is no standard FDA-approved CDx for PD-1/PD-L1 therapy in melanoma. The discovery of more comprehensive predictive new biomarkers is essential for the PD-1/PD-L1 immunotherapy of melanoma and the further development of this field into precision medicine. This article lists the biomarkers of TME, peripheral circulation and gene mutations, covering the main current research directions.

In recent years, increasing attention has been paid to the role of tumour microenvironment in tumour growth, metastatic spread and response to treatment. Understanding the complex interplay between tumour cell-intrinsic, cell-extrinsic, and systemic mediators of disease progression is essential for the rational development of effective anticancer therapies. Many components of TME can affect and help predict the response to PD-1/PD-L1 immunotherapy. PD-1/PD-L1 immunotherapy relies on the patient's own immune system, especially TILs. "Hot" (immune-inflamed) tumours are more likely to benefit from immunotherapy, whereas "cold" (immune-desert/immune-excluded) tumours are the opposite. Melanoma is usually considered as a "hot" tumour, but some specific gene mutations such as COL3A1, EGFR, etc. can lead to decreased immune infiltration or increased immune checkpoints in TME. The evaluation of the immune status of TME has changed from TILs counting to the detection of TILs quantitative genomic signatures, which is more comprehensive and accurate.

Some components of the TME will enter the peripheral circulation, and the development of tumours will lead to changes in the components in the peripheral circulation. The detection of peripheral blood components is the most convenient and clinically popular, and it can predict treatment outcome and monitor disease progression in real time. The conventional test items LDH and NLR were found to have certain prognostic value of immunotherapy. Soluble PD-1 and circulating EVs, directly related to tumours, are more closely related to tumour status and prognosis.

Independent of PD-L1 and TME, the TMB level of the tumour itself affects its antigenicity, which is also very important for PD-1/PD-L1 immunotherapy. The FDA approval of pembrolizumab for patients with unresectable or metastatic TMB-H or MSI-H or dMMR solid tumours speaks volumes about the prognostic importance of these biomarkers for immunotherapy. Some gene mutations, such as BRCA, ATM, and POLE/POLD1, are not conducive to the prognosis of tumour diseases but are beneficial to immunotherapy. Mutations in other genes, such as PBRM1 and MDM2, can lead to poor prognosis regardless of immunotherapy. Tumours with EGFR, ALK, BRAF mutations may be resistant to PD-1/PD-L1 immunotherapy, and are more suitable for targeted therapy or combination therapy. Although further studies are needed regarding the markers and causes of hyper-progression, genomic testing in patients scheduled for PD-1/PD-L1 therapy may be necessary to determine if their tumours harbor specific alterations associated with hyper-progression.

Patient biomarkers should be tested and monitored before and during treatment, which can not only to guide drug use in real time and predict efficacy, but also to prevent over-treatment and reduce the adverse reactions of patients. Comprehensive assessment using multiple biomarkers may be more effective at predicting response than individual biomarkers. Moreover, the blockade of some biomarkers or related pathways may increase the efficacy of immunotherapy, and the development of new drugs and combination therapies for these biomarkers may be a new therapeutic direction.

Author contributions

ZW: Writing – review & editing, Writing – original draft, Visualization, Supervision, Investigation, Conceptualization. XZ: Writing – review & editing, Writing – original draft, Visualization, Supervision, Investigation, Conceptualization. HW: Writing – review & editing, Visualization. ZH: Writing – review & editing, Visualization. GL: Writing – review & editing, Writing –

original draft, Visualization, Supervision, Investigation, Funding acquisition, Conceptualization. SW: Writing – review & editing, Writing – original draft, Visualization, Supervision, Investigation, Funding acquisition, Conceptualization.

Funding

The author(s) declare financial support was received for the research, authorship, and/or publication of this article. This work was supported by the National Natural Science Foundation of China No. 32172899, the Beijing Municipal Natural Science Foundation No. 6244047, and Talent Funding Project of China Agricultural University Veterinary Teaching Hospital.

Acknowledgments

All figures were created with figdraw.com.

Conflict of interest

Author HW is employed by Beijing Biomedical Science and Technology Center, Zhaofenghua Biotechnology Nanjing Company Limited.

The remaining authors declare that the research was conducted in the absence of any commercial or financial relationships that could be construed as a potential conflict of interest.

Publisher's note

All claims expressed in this article are solely those of the authors and do not necessarily represent those of their affiliated organizations, or those of the publisher, the editors and the reviewers. Any product that may be evaluated in this article, or claim that may be made by its manufacturer, is not guaranteed or endorsed by the publisher.

References

1. *World health statistics 2023: monitoring health for the SDGs, Sustainable Development Goals*. Geneva: World Health Organization (2023) p. 10–6.

2. Rastrelli M, Tropea S, Rossi CR, Alaibac M. Melanoma: epidemiology, risk factors, pathogenesis, diagnosis and classification. *In Vivo*. (2014) 28:1005–11.

3. Robert C, Thomas L, Bondarenko I, O'Day S, Weber J, Garbe C, et al. Ipilimumab plus dacarbazine for previously untreated metastatic melanoma. *N Engl J Med*. (2011) 364:2517–26. doi: 10.1056/NEJMoa1104621

4. Hodi FS, O'Day SJ, McDermott DF, Weber RW, Sosman JA, Haanen JB, et al. Improved survival with ipilimumab in patients with metastatic melanoma. *N Engl J Med*. (2010) 363:711–23. doi: 10.1056/NEJMoa1003466

5. Dong H, Strome SE, Salomao DR, Tamura H, Hirano F, Flies DB, et al. Tumor-associated B7-H1 promotes T-cell apoptosis: a potential mechanism of immune evasion. *Nat Med*. (2002) 8:793–800. doi: 10.1038/nm730

6. Iwai Y, Ishida M, Tanaka Y, Okazaki T, Honjo T, Minato N. Involvement of PD-L1 on tumor cells in the escape from host immune system and tumor immunotherapy by PD-L1 blockade. *Proc Natl Acad Sci U S A*. (2002) 99:12293–7. doi: 10.1073/pnas.192461099

7. Wong RM, Scotland RR, Lau RL, Wang C, Korman AJ, Kast WM, et al. Programmed death-1 blockade enhances expansion and functional capacity of human melanoma antigen-specific CTLs. *Int Immunol*. (2007) 19:1223–34. doi: 10.1093/intimm/dxm091

8. Sznol M, Chen L. Antagonist antibodies to PD-1 and B7-H1 (PD-L1) in the treatment of advanced human cancer. *Clin Cancer Res*. (2013) 19:1021–34. doi: 10.1158/1078-0432.CCR-12-2063

9. Blank C, Kuball J, Voelkl S, Wiendl H, Becker B, Walter B, et al. Blockade of PD-L1 (B7-H1) augments human tumor-specific T cell responses *in vitro*. *Int J Cancer*. (2006) 119:317–27. doi: 10.1002/ijc.21775

10. Brahmer JR, Drake CG, Wollner I, Powderly JD, Picus J, Sharfman WH, et al. Phase I study of single-agent anti-programmed death-1 (MDX-1106) in refractory solid tumors: safety, clinical activity, pharmacodynamics, and immunologic correlates. *J Clin Oncol*. (2010) 28:3167–75. doi: 10.1200/JCO.2009.26.7609

11. Twomey JD, Zhang B. Cancer immunotherapy update: FDA-approved checkpoint inhibitors and companion diagnostics. *AAPS J*. (2021) 23:39. doi: 10.1208/s12248-021-00574-0

12. Giavina-Bianchi M, Nacagamo SM, Giavina-Bianchi P, Munhoz R, Festa NC, Kalil J. Inter- and intra-patient heterogeneity of PD-L1 expression in metastatic melanomas: A retrospective study. *Australas J Dermatol*. (2021) 62:227–9. doi: 10.1111/ajd.13498

13. LaFleur MW, Muroyama Y, Drake CG, Sharpe AH. Inhibitors of the PD-1 pathway in tumor therapy. *J Immunol*. (2018) 200:375–83. doi: 10.4049/jimmunol.1701044

14. Salmaninejad A, Khoramshahi V, Azani A, Soltaninejad E, Aslani S, Zamani MR, et al. PD-1 and cancer: molecular mechanisms and polymorphisms. *Immunogenetics*. (2018) 70:73–86. doi: 10.1007/s00251-017-1015-5

15. Ohaegbulam KC, Assal A, Lazar-Molnar E, Yao Y, Zang X. Human cancer immunotherapy with antibodies to the PD-1 and PD-L1 pathway. *Trends Mol Med*. (2015) 21:24–33. doi: 10.1016/j.molmed.2014.10.009

16. Dong P, Xiong Y, Yue J, Hanley S, Watari H. Tumor-intrinsic PD-L1 signaling in cancer initiation, development and treatment: beyond immune evasion. *Front Oncol*. (2018) 8:386. doi: 10.3389/fonc.2018.00386

17. Hamid O, Robert C, Daud A, Hodi FS, Hwu WJ, Kefford R, et al. Five-year survival outcomes for patients with advanced melanoma treated with pembrolizumab in KEYNOTE-001. *Ann Oncol*. (2019) 30:582–8. doi: 10.1093/annonc/mdz011

18. Robert C, Schachter J, Long GV, Arance A, Grob JJ, Mortier L, et al. Pembrolizumab versus ipilimumab in advanced melanoma. *N Engl J Med*. (2015) 372:2521–32. doi: 10.1056/NEJMoa1503093

19. Hamid O, Robert C, Daud A, Carlino MS, Mitchell TC, Hersey P, et al. Long-term outcomes in patients with advanced melanoma who had initial stable disease with pembrolizumab in KEYNOTE-001 and KEYNOTE-006. *Eur J Cancer*. (2021) 157:391–402. doi: 10.1016/j.ejca.2021.08.013

20. Eggermont AMM, Blank CU, Mandala M, Long GV, Atkinson V, Dalle S, et al. Adjuvant pembrolizumab versus placebo in resected stage III melanoma. *N Engl J Med*. (2018) 378:1789–801. doi: 10.1056/NEJMoa1802357

21. Topalian SL, Sznol M, McDermott DF, Kluger HM, Carvajal RD, Sharfman WH, et al. Survival, durable tumor remission, and long-term safety in patients with advanced melanoma receiving nivolumab. *J Clin Oncol*. (2023) 41:943–54. doi: 10.1200/JCO.22.02272

22. Weber J, Mandala M, Del VM, Gogas HJ, Arance AM, Cowey CL, et al. Adjuvant nivolumab versus ipilimumab in resected stage III or IV melanoma. *N Engl J Med*. (2017) 377:1824–35. doi: 10.1056/NEJMoa1709030

23. Robert C, Long GV, Brady B, Dutriaux C, Maio M, Mortier L, et al. Nivolumab in previously untreated melanoma without BRAF mutation. *N Engl J Med*. (2015) 372:320–30. doi: 10.1056/NEJMoa1412082

24. Hamid O, Molinero L, Bolen CR, Sosman JA, Muñoz-Couselo E, Kluger HM, et al. Safety, clinical activity, and biological correlates of response in patients with metastatic melanoma: results from a phase I trial of atezolizumab. *Clin Cancer Res*. (2019) 25:6061–72. doi: 10.1158/1078-0432.CCR-18-3488

25. Hellmann MD, Kim TW, Lee CB, Goh BC, Miller WJ, Oh DY, et al. Phase Ib study of atezolizumab combined with cobimetinib in patients with solid tumors. *Ann Oncol*. (2019) 30:1134–42. doi: 10.1093/annonc/mdz113

26. Gutzmer R, Stroyakovskiy D, Gogas H, Robert C, Lewis K, Protsenko S, et al. Atezolizumab, vemurafenib, and cobimetinib as first-line treatment for unresectable advanced BRAF(V600) mutation-positive melanoma (IMspire150): primary analysis of the randomised, double-blind, placebo-controlled, phase 3 trial [published correction appears in Lancet. *Lancet*. (2020) 395:1835–44. doi: 10.1016/S0140-6736(20)30934-X

27. Hodi FS, Chesney J, Pavlick AC, Robert C, Grossmann KF, McDermott DF, et al. Combined nivolumab and ipilimumab versus ipilimumab alone in patients with advanced melanoma: 2-year overall survival outcomes in a multicentre, randomised,

controlled, phase 2 trial. *Lancet Oncol*. (2016) 17:1558–68. doi: 10.1016/S1470-2045(16)30366-7

28. Wolchok JD, Chiarion-Sileni V, Gonzalez R, Grob JJ, Rutkowski P, Lao CD, et al. Long-term outcomes with nivolumab plus ipilimumab or nivolumab alone versus ipilimumab in patients with advanced melanoma. *J Clin Oncol*. (2022) 40:127–37. doi: 10.1200/JCO.21.02229

29. Olson DJ, Eroglu Z, Brockstein B, Poklepovic AS, Bajaj M, Babu S, et al. Pembrolizumab plus ipilimumab following anti-PD-1/L1 failure in melanoma. *J Clin Oncol*. (2021) 39:2647–55. doi: 10.1200/JCO.21.00079

30. Willis JE, Eyerer F, Walk EE, Vasalos P, Bradshaw G, Yohe SL, et al. Companion diagnostics: lessons learned and the path forward from the programmed death ligand-1 rollout. *Arch Pathol Lab Med*. (2023) 147:62–70. doi: 10.5858/arpa.2021-0151-CP

31. U.S. Food and Drug Administration. List of Cleared or Approved Companion Diagnostic Devices (*In Vitro* and Imaging Tools) (2024). Available online at: https://www.fda.gov/medical-devices/vitro-diagnostics/list-cleared-or-approved-companion-diagnostic-devices-vitro-and-imaging-tools (Accessed May 15, 2024).

32. Garon EB, Rizvi NA, Hui R, Leighl N, Balmanoukian AS, Eder JP, et al. Pembrolizumab for the treatment of non-small-cell lung cancer. *N Engl J Med*. (2015) 372:2018–28. doi: 10.1056/NEJMoa1501824

33. Hui R, Garon EB, Goldman JW, Leighl NB, Hellmann MD, Patnaik A, et al. Pembrolizumab as first-line therapy for patients with PD-L1-positive advanced non-small cell lung cancer: a phase 1 trial. *Ann Oncol*. (2017) 28:874–81. doi: 10.1093/annonc/mdx008

34. Stevenson VB, Perry SN, Todd M, Huckle WR, LeRoith T. PD-1, PD-L1, and PD-L2 gene expression and tumor infiltrating lymphocytes in canine melanoma. *Vet Pathol*. (2021) 58:692–8. doi: 10.1177/03009858211011939

35. Qiu Q, Li J, Chen Q, Zhao X, Zhou R, Zhang W, et al. Assessment of PD-L1 mRNA expression in gastrointestinal tumors and the response to immunotherapy. *Front Oncol*. (2022) 12:926746. doi: 10.3389/fonc.2022.926746

36. Hirsch FR, McElhinny A, Stanforth D, Ranger-Moore J, Jansson M, Kulangara K, et al. PD-L1 immunohistochemistry assays for lung cancer: results from phase 1 of the blueprint PD-L1 IHC assay comparison project. *J Thorac Oncol*. (2017) 12:208–22. doi: 10.1016/j.jtho.2016.11.2228

37. Ilie M, Long-Mira E, Bence C, Butori C, Lassalle S, Bouhlel L, et al. Comparative study of the PD-L1 status between surgically resected specimens and matched biopsies of NSCLC patients reveal major discordances: a potential issue for anti-PD-L1 therapeutic strategies. *Ann Oncol*. (2016) 27:147–53. doi: 10.1093/annonc/mdv489

38. Maule JG, Clinton LK, Graf RP, Xiao J, Oxnard GR, Ross JS, et al. Comparison of PD-L1 tumor cell expression with 22C3, 28-8, and SP142 IHC assays across multiple tumor types. *J Immunother Cancer*. (2022) 10:e005573. doi: 10.1136/jitc-2022-005573

39. Xiao WJ, Xu FJ, Zhang X, Zhou SX, Zhang HL, Dai B, et al. The prognostic value of programmed death-ligand 1 in a chinese cohort with clear cell renal cell carcinoma. *Front Oncol*. (2019) 9:879. doi: 10.3389/fonc.2019.00879

40. Erber R, Stöhr R, Herlein S, Giedl C, Rieker RJ, Fuchs F, et al. Comparison of PD-L1 mRNA expression measured with the CheckPoint Typer® Assay with PD-L1 protein expression assessed with immunohistochemistry in non-small cell lung cancer. *Anticancer Res*. (2017) 37:6771–8. doi: 10.21873/anticanres.12137

41. Suárez-Lledó M, Marcos MÁ, Cuatrecasas M, Bombi JA, Fernández-Avilés F, Magnano L, et al. Quantitative PCR is faster, more objective, and more reliable than immunohistochemistry for the diagnosis of cytomegalovirus gastrointestinal disease in allogeneic stem cell transplantation. *Biol Blood Marrow Transplant*. (2019) 25:2281–6. doi: 10.1016/j.bbmt.2019.07.016

42. Brahmer J, Reckamp KL, Baas P, Crinò L, Eberhardt WE, Poddubskaya E, et al. Nivolumab versus docetaxel in advanced squamous-cell non-small-cell lung cancer. *N Engl J Med*. (2015) 373:123–35. doi: 10.1056/NEJMoa1504627

43. Hoffmann F, Zarbl R, Niebel D, Sirokay J, Fröhlich A, Posch C, et al. Prognostic and predictive value of PD-L2 DNA methylation and mRNA expression in melanoma. *Clin Epigenetics*. (2020) 12:94. doi: 10.1186/s13148-020-00883-9

44. Obeid JM, Erdag G, Smolkin ME, Deacon DH, Patterson JW, Chen L, et al. PD-L1, PD-L2 and PD-1 expression in metastatic melanoma: Correlation with tumor-infiltrating immune cells and clinical outcome. *Oncoimmunology*. (2016) 5:e1235107. doi: 10.1080/2162402X.2016.1235107

45. Huang FX, Wu JW, Cheng XQ, Wang JH, Wen XZ, Li JJ, et al. HHLA2 predicts improved prognosis of anti-PD-1/PD-L1 immunotherapy in patients with melanoma. *Front Immunol*. (2022) 13:902167. doi: 10.3389/fimmu.2022.902167

46. Yun S, Park Y, Moon S, Ahn S, Lee K, Park HJ, et al. Clinicopathological and prognostic significance of programmed death ligand 1 expression in Korean melanoma patients. *J Cancer*. (2019) 10:3070–8. doi: 10.7150/jca.30573

47. Tumeh PC, Harview CL, Yearley JH, Shintaku IP, Taylor EJ, Robert L, et al. PD-1 blockade induces responses by inhibiting adaptive immune resistance. *Nature*. (2014) 515:568–71. doi: 10.1038/nature13954

48. Edwards J, Wilmott JS, Madore J, Gide TN, Quek C, Tasker A, et al. CD103(+) tumor-resident CD8(+) T cells are associated with improved survival in immunotherapy-naïve melanoma patients and expand significantly during anti-PD-1 treatment. *Clin Cancer Res*. (2018) 24:3036–45. doi: 10.1158/1078-0432.CCR-17-2257

49. Iglesia MD, Parker JS, Hoadley KA, Serody JS, Perou CM, Vincent BG. Genomic analysis of immune cell infiltrates across 11 tumor types. *J Natl Cancer Inst*. (2016) 108:djw144. doi: 10.1093/jnci/djw144

50. Zhang H, Liu Z, Wen H, Guo Y, Xu F, Zhu Q, et al. Immunosuppressive TREM2(+) macrophages are associated with undesirable prognosis and responses to anti-PD-1 immunotherapy in non-small cell lung cancer. *Cancer Immunol Immunother*. (2022) 71:2511–22. doi: 10.1007/s00262-022-03173-w

51. Zhang W, Kong Y, Li Y, Shi F, Lyu J, Sheng C, et al. Novel molecular determinants of response or resistance to immune checkpoint inhibitor therapies in melanoma. *Front Immunol*. (2021) 12:798474. doi: 10.3389/fimmu.2021.798474

52. Peng W, Chen JQ, Liu C, Malu S, Creasy C, Tetzlaff MT, et al. Loss of PTEN promotes resistance to T cell-mediated immunotherapy. *Cancer Discovery*. (2016) 6:202–16. doi: 10.1158/2159-8290.CD-15-0283

53. Roh MR, Gupta S, Park KH, Chung KY, Lauss M, Flaherty KT, et al. Promoter methylation of PTEN is a significant prognostic factor in melanoma survival. *J Invest Dermatol*. (2016) 136:1002–11. doi: 10.1016/j.jid.2016.01.024

54. Amaral T, Pop OT, Chatziioannou E, Sinnberg T, Niessner H, Zhao J, et al. EGFR expression is associated with relapse in a melanoma cohort receiving adjuvant PD-1-based immunotherapy. *J Am Acad Dermatol*. (2023) 89:1072–4. doi: 10.1016/j.jaad.2023.06.057

55. Kato S, Goodman A, Walavalkar V, Barkauskas DA, Sharabi A, Kurzrock R. Hyperprogressors after immunotherapy: analysis of genomic alterations associated with accelerated growth rate. *Clin Cancer Res*. (2017) 23:4242–50. doi: 10.1158/1078-0432.CCR-16-3133

56. Zhang W, Xia H, Yang R, Zhang Y, Zheng Q, Shang X, et al. Fibroblast growth factor receptor family mutations as a predictive biomarker for immune checkpoint inhibitors and its correlation with tumor immune microenvironment in melanoma. *Front Immunol*. (2022) 13:1030969. doi: 10.3389/fimmu.2022.1030969

57. Azin M, Demehri S. STK11 loss: A novel mechanism for melanoma metastasis with therapeutic implications. *J Invest Dermatol*. (2022) 142:1007–9. doi: 10.1016/j.jid.2021.10.003

58. Li A, Wang Y, Yu Z, Tan Z, He L, Fu S, et al. STK11/LKB1-deficient phenotype rather than mutation diminishes immunotherapy efficacy and represents STING/type I interferon/CD8(+) T-cell dysfunction in NSCLC. *J Thorac Oncol*. (2023) 18:1714–30. doi: 10.1016/j.jtho.2023.07.020

59. Herbst RS, Soria JC, Kowanetz M, Fine GD, Hamid O, Gordon MS, et al. Predictive correlates of response to the anti-PD-L1 antibody MPDL3280A in cancer patients. *Nature*. (2014) 515:563–7. doi: 10.1038/nature14011

60. Ayers M, Lunceford J, Nebozhyn M, Murphy E, Loboda A, Kaufman DR, et al. IFN-γ-related mRNA profile predicts clinical response to PD-1 blockade. *J Clin Invest*. (2017) 127:2930–40. doi: 10.1172/JCI91190

61. Zaretsky JM, Garcia-Diaz A, Shin DS, Escuin-Ordinas H, Hugo W, Hu-Lieskovan S, et al. Mutations associated with acquired resistance to PD-1 blockade in melanoma. *N Engl J Med*. (2016) 375:819–29. doi: 10.1056/NEJMoa1604958

62. Shin DS, Zaretsky JM, Escuin-Ordinas H, Garcia-Diaz A, Hu-Lieskovan S, Kalbasi A, et al. Primary resistance to PD-1 blockade mediated by JAK1/2 mutations. *Cancer Discovery*. (2017) 7:188–201. doi: 10.1158/2159-8290.CD-16-1223

63. Zhao F, Evans K, Xiao C, DeVito N, Theivanthiran B, Holtzhausen A, et al. Stromal fibroblasts mediate anti-PD-1 resistance via MMP-9 and dictate TGFβ Inhibitor sequencing in melanoma. *Cancer Immunol Res*. (2018) 6:1459–71. doi: 10.1158/2326-6066.CIR-18-0086

64. Wagner NB, Weide B, Gries M, Reith M, Tarnanidis K, Schuermans V, et al. Tumor microenvironment-derived S100A8/A9 is a novel prognostic biomarker for advanced melanoma patients and during immunotherapy with anti-PD-1 antibodies. *J Immunother Cancer*. (2019) 7:343. doi: 10.1186/s40425-019-0828-1

65. Zak KM, Grudnik P, Magiera K, Dömling A, Dubin G, Holak TA. Structural biology of the immune checkpoint receptor PD-1 and its ligands PD-L1/PD-L2. *Structure*. (2017) 25:1163–74. doi: 10.1016/j.str.2017.06.011

66. Teng MW, Ngiow SF, Ribas A, Smyth MJ. Classifying cancers based on T-cell infiltration and PD-L1. *Cancer Res*. (2015) 75:2139–45. doi: 10.1158/0008-5472.CAN-15-0255

67. Bardi GT, Smith MA, Hood JL. Melanoma exosomes promote mixed M1 and M2 macrophage polarization. *Cytokine*. (2018) 105:63–72. doi: 10.1016/j.cyto.2018.02.002

68. Kuivaniemi H, Tromp G. Type III collagen (COL3A1): Gene and protein structure, tissue distribution, and associated diseases. *Gene*. (2019) 707:151–71. doi: 10.1016/j.gene.2019.05.003

69. Voldborg BR, Damstrup L, Spang-Thomsen M, Poulsen HS. Epidermal growth factor receptor (EGFR) and EGFR mutations, function and possible role in clinical trials. *Ann Oncol*. (1997) 8:1197–206. doi: 10.1023/a:1008209720526

70. Brummer T, Zeiser R. The role of the MDM2/p53 axis in antitumor immune responses. *Blood*. (2024) 143:2701–9. doi: 10.1182/blood.2023020731

71. Chioni AM, Grose RP. Biological significance and targeting of the FGFR axis in cancer. *Cancers (Basel)*. (2021) 13:5681. doi: 10.3390/cancers13225681

72. Koyama S, Akbay EA, Li YY, Aref AR, Skoulidis F, Herter-Sprie GS, et al. STK11/LKB1 deficiency promotes neutrophil recruitment and proinflammatory cytokine production to suppress T-cell activity in the lung tumor microenvironment. *Cancer Res*. (2016) 76:999–1008. doi: 10.1158/0008-5472.CAN-15-1439

73. Hiratsuka S, Watanabe A, Aburatani H, Maru Y. Tumour-mediated upregulation of chemoattractants and recruitment of myeloid cells predetermines lung metastasis. *Nat Cell Biol*. (2006) 8:1369–75. doi: 10.1038/ncb1507

74. Kelderman S, Heemskerk B, van Tinteren H, van den Brom RR, Hospers GA, van den Eertwegh AJ, et al. Lactate dehydrogenase as a selection criterion for ipilimumab treatment in metastatic melanoma. *Cancer Immunol Immunother*. (2014) 63:449–58. doi: 10.1007/s00262-014-1528-9

75. Diem S, Kasenda B, Spain L, Martin-Liberal J, Marconcini R, Gore M, et al. Serum lactate dehydrogenase as an early marker for outcome in patients treated with anti-PD-1 therapy in metastatic melanoma. *Br J Cancer*. (2016) 114:256–61. doi: 10.1038/bjc.2015.467

76. Ferrucci PF, Gandini S, Battaglia A, Alfieri S, Di Giacomo AM, Giannarelli D, et al. Baseline neutrophil-to-lymphocyte ratio is associated with outcome of ipilimumab-treated metastatic melanoma patients. *Br J Cancer*. (2015) 112:1904–10. doi: 10.1038/bjc.2015.180

77. Peng L, Wang Y, Liu F, Qiu X, Zhang X, Fang C, et al. Peripheral blood markers predictive of outcome and immune-related adverse events in advanced non-small cell lung cancer treated with PD-1 inhibitors. *Cancer Immunol Immunother*. (2020) 69:1813–22. doi: 10.1007/s00262-020-02585-w

78. Valero C, Lee M, Hoen D, Weiss K, Kelly DW, Adusumilli PS, et al. Pretreatment neutrophil-to-lymphocyte ratio and mutational burden as biomarkers of tumor response to immune checkpoint inhibitors. *Nat Commun*. (2021) 12:729. doi: 10.1038/s41467-021-20935-9

79. Zhou J, Mahoney KM, Giobbie-Hurder A, Zhao F, Lee S, Liao X, et al. Soluble PD-L1 as a biomarker in malignant melanoma treated with checkpoint blockade. *Cancer Immunol Res*. (2017) 5:480–92. doi: 10.1158/2326-6066.CIR-16-0329

80. Pedersen JG, Sokac M, Sørensen BS, Luczak AA, Aggerholm-Pedersen N, Birkbak NJ, et al. Increased soluble PD-1 predicts response to nivolumab plus ipilimumab in melanoma. *Cancers (Basel)*. (2022) 14:3342. doi: 10.3390/cancers14143342

81. Dronca RS, Liu X, Harrington SM, Chen L, Cao S, KottsChade LA, et al. T cell Bim levels reflect responses to anti-PD-1 cancer therapy. *JCI Insight*. (2016) 1:e86014. doi: 10.1172/jci.insight.86014

82. Nakamura Y, Tanaka R, Maruyama H, Ishitsuka Y, Okiyama N, Watanabe R, et al. Correlation between blood cell count and outcome of melanoma patients treated with anti-PD-1 antibodies. *Jpn J Clin Oncol*. (2019) 49:431–7. doi: 10.1093/jjco/hyy201

83. Weide B, Martens A, Hassel JC, Berking C, Postow MA, Bisschop K, et al. Baseline biomarkers for outcome of melanoma patients treated with pembrolizumab. *Clin Cancer Res*. (2016) 22:5487–96. doi: 10.1158/1078-0432.CCR-16-0127

84. Serratì S, Guida M, Di Fonte R, De Summa S, Strippoli S, Iacobazzi RM, et al. Circulating extracellular vesicles expressing PD1 and PD-L1 predict response and mediate resistance to checkpoint inhibitors immunotherapy in metastatic melanoma. *Mol Cancer*. (2022) 21:20. doi: 10.1186/s12943-021-01490-9

85. Lardner A. The effects of extracellular pH on immune function. *J Leukoc Biol*. (2001) 69:522–30. doi: 10.1189/jlb.69.4.522

86. Mantovani A, Allavena P, Sica A, Balkwill F. Cancer-related inflammation. *Nature*. (2008) 454:436–44. doi: 10.1038/nature07205

87. Xia J, Huang R, Chen Y, Liu Y, Wang J, Yan X, et al. Profiles of serum soluble programmed death-1 and programmed death-ligand 1 levels in chronic hepatitis B virus-infected patients with different disease phases and after anti-viral treatment. *Aliment Pharmacol Ther*. (2020) 51:1180–7. doi: 10.1111/apt.15732

88. Mahoney KM, Ross-Macdonald P, Yuan L, Song L, Veras E, Wind-Rotolo M, et al. Soluble PD-L1 as an early marker of progressive disease on nivolumab. *J Immunother Cancer*. (2022) 10:e003527. doi: 10.1136/jitc-2021-003527

89. Dronca RS, Mansfield AS, Park SS, Dong H. BCL-2-interacting mediator of cell death (Bim) is a novel biomarker for response to anti-PD-1 therapy in patients with advanced melanoma. *Immunotherapy*. (2016) 8:1351–3. doi: 10.2217/imt-2016-0100

90. Chennamadhavuni A, Abushahin L, Jin N, Presley CJ, Manne A. Risk factors and biomarkers for immune-related adverse events: a practical guide to identifying high-risk patients and rechallenging immune checkpoint inhibitors. *Front Immunol*. (2022) 13:779691. doi: 10.3389/fimmu.2022.779691

91. Fujita Y, Yoshioka Y, Ochiya T. Extracellular vesicle transfer of cancer pathogenic components. *Cancer Sci*. (2016) 107:385–90. doi: 10.1111/cas.12896

92. Newell F, Pires DSI, Johansson PA, Menzies AM, Wilmott JS, Addala V, et al. Multiomic profiling of checkpoint inhibitor-treated melanoma: Identifying predictors of response and resistance, and markers of biological discordance. *Cancer Cell*. (2022) 40:88–102.e7. doi: 10.1016/j.ccell.2021.11.012

93. Gandara DR, Paul SM, Kowanetz M, Schleifman E, Zou W, Li Y, et al. Blood-based tumor mutational burden as a predictor of clinical benefit in non-small-cell lung cancer patients treated with atezolizumab. *Nat Med*. (2018) 24:1441–8. doi: 10.1038/s41591-018-0134-3

94. Le DT, Durham JN, Smith KN, Wang H, Bartlett BR, Aulakh LK, et al. Mismatch repair deficiency predicts response of solid tumors to PD-1 blockade. *Science*. (2017) 357:409–13. doi: 10.1126/science.aan6733

95. Launonen IM, Lyytikäinen N, Casado J, Anttila EA, Szabó A, Haltia UM, et al. Single-cell tumor-immune microenvironment of BRCA1/2 mutated high-grade serous ovarian cancer. *Nat Commun*. (2022) 13:835. doi: 10.1038/s41467-022-28389-3

96. Hu M, Zhou M, Bao X, Pan D, Jiao M, Liu X, et al. ATM inhibition enhances cancer immunotherapy by promoting mtDNA leakage and cGAS/STING activation. *J Clin Invest*. (2021) 131:e139333. doi: 10.1172/JCI139333

97. Wang F, Zhao Q, Wang YN, Jin Y, He MM, Liu ZX, et al. Evaluation of POLE and POLD1 Mutations as Biomarkers for Immunotherapy Outcomes Across Multiple Cancer Types [published correction appears in JAMA Oncol. *JAMA Oncol*. (2019) 5:1504–6. doi: 10.1001/jamaoncol.2019.2963

98. Zhang K, Hong X, Song Z, Xu Y, Li C, Wang G, et al. Identification of deleterious NOTCH mutation as novel predictor to efficacious immunotherapy in NSCLC. *Clin Cancer Res*. (2020) 26:3649–61. doi: 10.1158/1078-0432.CCR-19-3976

99. Li H, Zhang Q, Duan Q, Tan Y, Sun T, Qi C. NOTCH4 mutation as predictive biomarker for immunotherapy benefits in NRAS wildtype melanoma. *Front Immunol*. (2022) 13:894110. doi: 10.3389/fimmu.2022.894110

100. Xie K, Peng Y, Zhong W, Liu X. KMT2C is a potential biomarker of anti-PD-1 treatment response in metastatic melanoma. *Front Biosci (Landmark Ed)*. (2022) 27:103. doi: 10.31083/j.fbl2703103

101. Yang Q, Shen R, Xu H, Shi X, Xu L, Zhang L, et al. Comprehensive analyses of PBRM1 in multiple cancer types and its association with clinical response to immunotherapy and immune infiltrates. *Ann Transl Med*. (2021) 9:465. doi: 10.21037/atm-21-289

102. Gandini S, Zanna I, De Angelis S, Palli D, Raimondi S, Ribero S, et al. TERT promoter mutations and melanoma survival: A comprehensive literature review and meta-analysis. *Crit Rev Oncol Hematol*. (2021) 160:103288. doi: 10.1016/j.critrevonc.2021.103288

103. Hallberg B, Palmer RH. The role of the ALK receptor in cancer biology. *Ann Oncol*. (2016) 27 Suppl 3:iii4–iii15. doi: 10.1093/annonc/mdw301

104. Puzanov I, Ribas A, Robert C, Schachter J, Nyakas M, Daud A, et al. Association of BRAF V600E/K mutation status and prior BRAF/MEK inhibition with pembrolizumab outcomes in advanced melanoma: pooled analysis of 3 clinical trials. *JAMA Oncol*. (2020) 6:1256–64. doi: 10.1001/jamaoncol.2020.2288

Glossary

ALK	Anaplastic lymphoma kinase
ALK	Anaplastic lymphoma kinase
APC	Antigen-presenting cells
ATM	Ataxia telangiectasia-mutated gene
B2M	β2-microglobulin
BCR	B-cell receptor
BIM	BCL-2 interacting mediator of cell death
BRAF	v-raf murine sarcoma viral oncogene homolog B1
BRCA	Breast cancer susceptibility gene
bTMB	blood TMB
CAF	Cancer-associated fibroblast
CBC	Complete blood count
CCL2	C-C motif ligand 2
CDx	Companion diagnostic
cGAS	cyclic GMP-AMP
COL3A1	Collagen alpha-1(III) gene
CR	Complete response
CTLA-4	Cytotoxic T-lymphocyte-associated protein 4
CXCL9	C-x-C motif chemokine ligand 9
DALYs	Deaths and disability-adjusted life years
DAMP	Damage-associated molecular pattern
dMMR	deficient MMR
EGFR	Epidermal growth factor receptor
ESCC	Esophageal squamous cell carcinoma
EVs	Extracellular vesicles
FDA	Food and Drug Administration
FGFR	Fibroblast growth factor receptor
H3K4	Histone H3 lysine K4
HHLA2	Human endogenous retrovirus-H long repeat-associating 2
HNSCC	Head and neck squamous cell carcinoma
HRD	Homologous recombination deficiency
IC	Immune cells
IDO1	Indoleamine 2,3 dioxygenase 1
IFN-γ	Interferon-γ
IHC	Immunohistochemistry
IL-15	Interleukin-15
JAK	Janus kinases
KRAS	Kirsten rat sarcoma viral oncogene homologue
LDH	Lactate dehydrogenase
LKB1	Liver kinase B1
MAF	Melanoma-associated fibroblast
MDM2	Mouse double minute 2 homolog
MDSC	Myeloid-derived suppressor cell
MHC	Major histocompatibility complex
MIS	Microsatellite instability
MM	Metastatic melanoma
MRR	DNA mismatch repair
MSI-H	high MSI
MST	Median survival time
NCDs	Non-communicable diseases
NLR	Neutrophil-to-lymphocyte ratio
NRAS	Neuroblastoma rat sarcoma
NSCLC	Non-small-cell lung carcinoma
ORR	Objective response rate
OS	Overall survival
PBMC	Peripheral blood mononuclear cell
PBRM1	Polybromo 1
PD-L2	Programmed cell death 1 ligand 2
PFS	Progression-free survival
PI3K	Phosphoinositide 3-kinase
POLD	DNA polymerase delta
POLE	Polymerase epsilon
PR	Partial response
PTEN	Phosphatase and tensin homolog deleted on chromosome 10
RCC	Renal cell carcinoma
SD	Stable disease
SKCM	Skin cutaneous melanoma
sPD-1	soluble PD-1
sPD-L1	soluble PD-L1
STATs	Signal transducers and activators of transcriptions
STING	Stimulator of interferon genes
STK11	Serine/threonine kinase 11
TAM	Tumour-associated macrophage
TC	Tumour cells
TCR	T-cell receptor
TERT	Telomerase reverse transcriptase
TILs	Tumor-infiltrating lymphocytes
TMB	Tumour mutation burden
TMB	Tumour mutational burden
TMB-H	high TMB
TME	Tumour microenvironment
TNBC	Triple-negative breast cancer
TPS	Tumour proportion score
TTF	Time-to-treatment failure
tTMB	tissue TMB
WHO	World Health Organization.

frontiers | Frontiers in Immunology

TYPE Review
PUBLISHED 30 October 2024
DOI 10.3389/fimmu.2024.1435651

Check for updates

OPEN ACCESS

EDITED BY
Pengpeng Zhang,
Nanjing Medical University, China

REVIEWED BY
Jing Hong,
Hypertension Center of People's Hospital of Xinjiang Uygur Autonomous Region, China
Hongyi Zhang,
Tongji University, China

*CORRESPONDENCE
Renjun Gu
renjungu@hotmail.com
Pengfei Li
lipengfei@njucm.edu.cn
Xin Gu
290418@njucm.edu.cn

†These authors share first authorship

RECEIVED 20 May 2024
ACCEPTED 19 August 2024
PUBLISHED 30 October 2024

CITATION
Li Y, Sun W, Yuan S, Liu X, Zhang Z, Gu R, Li P and Gu X (2024) The role of cuproptosis in gastric cancer.
Front. Immunol. 15:1435651.
doi: 10.3389/fimmu.2024.1435651

COPYRIGHT
© 2024 Li, Sun, Yuan, Liu, Zhang, Gu, Li and Gu. This is an open-access article distributed under the terms of the Creative Commons Attribution License (CC BY). The use, distribution or reproduction in other forums is permitted, provided the original author(s) and the copyright owner(s) are credited and that the original publication in this journal is cited, in accordance with accepted academic practice. No use, distribution or reproduction is permitted which does not comply with these terms.

The role of cuproptosis in gastric cancer

Yixian Li[1†], Wenhao Sun[2†], Shaolin Yuan[2†], Xinxin Liu[2], Ziqi Zhang[3], Renjun Gu[4*], Pengfei Li[5*] and Xin Gu[4*]

[1]Nanjing University of Chinese Medicine, the First Clinical Medical College, Nanjing, Jiangsu, China, [2]Department of General Surgery, Affiliated Hospital of Nanjing University of Chinese Medicine Jiangsu Province, Nanjing, Jiangsu, China, [3]Department of Endocrinology, Affiliated Hospital of Nanjing University of Chinese Medicine, Nanjing, Jiangsu, China, [4]School of Chinese Medicine, Nanjing University of Chinese Medicine, Nanjing, China, [5]Department of Clinical Laboratory, Affiliated Hospital of Nanjing University of Chinese Medicine, Jiangsu Province Hospital of Chinese Medicine, Nanjing, Jiangsu, China

As a biologically essential transition metal, copper is widely involved in various enzymatic reactions and crucial biological processes in the body. It plays an increasingly important role in maintaining normal cellular metabolism and supporting the growth and development of the human body. As a trace element, copper maintains the dynamic balance of its concentration in body fluids through active homeostatic mechanisms. Both excess and deficiency of copper ions can impair cell function, ultimately leading to cell damage and death. Cuproptosis is a novel form of cell death where copper ions cause cell death by directly binding to the lipoylated components of the citric acid cycle (CAC) in mitochondrial respiration and interfering with the levels of iron-sulfur cluster (Fe-S cluster) proteins, ultimately causing protein toxic stress. Its primary characteristics are Cu2+ concentration dependence and high expression in mitochondrial respiratory cells. Recent research has revealed that, compared to other forms of programmed cell death such as apoptosis, necrosis, and autophagy, cuproptosis has unique morphological and biochemical features. Cuproptosis is associated with the occurrence and development of various diseases, including cancer, neurodegenerative diseases, and cardiovascular diseases. This article focuses on a review of the relevance of cuproptosis in gastric cancer (GC).

KEYWORDS

cuproptosis, gastric cancer, mechanism, immune, therapies

1 Introduction

Gastric cancer (GC) is a primary epithelial malignant tumor originating in the stomach. It has various pathogenic factors, and its morbidity and mortality rank among the top five malignant tumors worldwide (1). Due to the stomach being a hollow organ, it provides more space for tumor growth compared to other solid organs. Additionally, the early symptoms of GC are relatively insidious (2). As a result, GC is often diagnosed at an advanced stage (3), imposing significant economic and health burdens on people.

Cuproptosis is a recently discovered form of programmed cell death triggered by copper overload *in vivo*. The basic principle involves copper ions interfering with the levels of Fe-S cluster proteins by directly binding to the lipoylated components of the citric acid cycle (CAC) in mitochondrial respiration, causing proteotoxic stress, and ultimately leading to cell death (4). This article reviews the relevance of cuproptosis in GC and provides insights and suggestions for the prevention and treatment of GC from the perspective of the cuproptosis mechanism.

Gastric cancer (GC) is a primary epithelial malignant tumor originating in the stomach. It has multiple pathogenic factors, and its morbidity and mortality rank among the top five malignant tumors worldwide (1). Due to the stomach being a hollow organ, it offers more space for tumor growth compared to other solid organs. Additionally, the early symptoms of GC are relatively insidious (2), often resulting in late-stage diagnosis (3). This delay in diagnosis imposes significant economic and health burdens on individuals. Cuproptosis is a recently discovered form of programmed cell death triggered by copper overload *in vivo*. The underlying mechanism involves copper ions interfering with the levels of Fe-S cluster proteins by directly binding to the lipoylated components of the citric acid cycle (CAC) in mitochondrial respiration. This interaction causes proteotoxic stress, ultimately leading to cell death (4). This article reviews the relevance of cuproptosis in GC and provides insights and suggestions for the prevention and treatment of GC from the perspective of the cuproptosis mechanism.

Abbreviations: GA, Gastric adenocarcinoma; CAC, Citric Acid Cycle; Fe-S cluster, iron-sulfur cluster; WHO, World Health Organization; GC, Gastric cancer; IGC, Intestinal gastric cancer; DGC, Diffuse gastric cancer; MGC, Mixed gastric cancer; GIM, Gastric intestinal metaplasia; TSCs, Tumor stem cells; CAFs, Cancer-associated fibroblasts; ATM, Ataxia telangiectasia-mutated gene; ATR, Ataxia telangiectasia and Rad3-related protein; SWI/SNF, Switch defective/sucrose non-fermentable; ECMs, Extracellular matrix proteins; H. pylori, Helicobacter pylori; AG, chronic atrophic gastritis; Vac-A, Vacuolating cytotoxin A; Cag-A, cytotoxin-associated gene A; Cag-PAI, cytotoxin-associated gene pathogenicity island; ROS, reactive oxygen species; T4SS, Type IV secretion system; AlpA / B, Adhesion lipoproteins A and B; BabA, Blood group antigen-binding adhesion; PCDH10, Protocadherin 10; JAM3, junctional adhesion molecule 3; TSGs, tumor suppressor genes; PDH, Pyruvic dehydrogenase; lncRNA, long noncoding RNA; ENTPD3, nucleoside triphosphate diphosphohydrolase 3; CNN1, calponin-1; GTPBP4, GTP binding protein 4; CENPW, Centromere Protein W; PDZD4, PDZ Domain Containing 4; FPGS, Folylpolyglutamate synthase; FAM111A, FAM111 trypsin-like peptidase A; TME, tumor microenvironment; HIF, hypoxia-inducible factor; VEGF, vascular endothelial growth factor; VEGFR, vascular endothelial growth factor receptors; NRP, neuro-phospholipids; DCs, dendritic cells; NK cells, natural killer cells.

2 Association between GC and programmed forms of cell death

With the significant improvement in the living environment and the reduction of bad living habits (1), the incidence and mortality rates of GC in China are decreasing year by year (2). However, since most GC patients are incurable, their survival rate is low (3), which poses a serious threat to people's health as well as a heavy medical burden to society (4, 5). As a common malignant tumor of the digestive system (6), the development of GC is intimately related to disorders of programmed cell death, which is proved by numerous studies (7, 8).

Programmed cell death (9) is generally classified as apoptosis (10), pyrozosis (11), necroptosis (12), autophagy (13), etc. According to relevant studies, among others, apoptosis is considered to have a definite correlation with cancer (14, 15). Programmed cell death is an active and inherently programmed phenomenon (16), it is influenced by the physiological and pathological environment of the body. It plays a major role not only in the maintenance of cellular homeostasis in organisms but also in the normal development of the body (17). Since programmed death is an orderly arranged, differentiated cell growth-death process, it can occur under both physiological and pathological conditions (18). During tissue differentiation, atrophy, or degeneration, it strictly follows an established procedure to inhibit cell proliferation, precisely eliminating cells that are no longer needed by the organism and becoming one of the organism's defenses against disease. Moreover, it is important to note that it can also maintain the normal state of various physiological activities of the body by actively inducing cell death (19–22). Its extraordinary property brings new hope to the current dilemma of preventing and combating cancer.

With the significant improvement in living conditions and the reduction of harmful lifestyle habits (5), the incidence and mortality rates of gastric cancer (GC) in China are decreasing year by year (6). However, since most GC cases are diagnosed at an incurable stage, the survival rate remains low (7), posing a serious threat to public health and imposing a heavy medical burden on society (8, 9). As a common malignant tumor of the digestive system (10), the development of GC is closely linked to disorders of programmed cell death, as evidenced by numerous studies (11, 12). Programmed cell death (13) is generally classified into apoptosis (14), pyroptosis (15), necroptosis (16), autophagy (17), and other types. Among these, apoptosis has a well-established correlation with cancer, according to relevant studies (18, 19). Programmed cell death is an active and inherently programmed phenomenon (20) influenced by the physiological and pathological environment of the body. It plays a crucial role in maintaining cellular homeostasis and the normal development of the body (21). As an orderly, regulated process, programmed cell death can occur under

both physiological and pathological conditions (22). During tissue differentiation, atrophy, or degeneration, it strictly follows an established procedure to inhibit cell proliferation, precisely eliminating cells that are no longer needed by the organism, thus serving as one of the body's defenses against disease. Furthermore, it actively induces cell death to maintain the normal state of various physiological activities in the body (23–26). This extraordinary property brings new hope to the current challenges in preventing and combating cancer.

The infinite growth of gastric malignant tumor cells is the consequence of the inhibition of programmed tumor cell death (23). Once the cell death process is disrupted or inhibited, tumor cells will grow indefinitely, ultimately leading to cancer (24). Cuproptosis is a novel form of cell death discovered and named in March 2022 by Tsvetkov et al. That study found that copper ions can impair the function of mitochondrial enzymes in the CAC via the FDX1 gene when copper ion levels in the body exceed normal values in humans. The mitochondrial membrane is then subjected to oxidative damage and binds directly to the lipid-acylated component of the CAC. Thereafter, they form long chains or clustered aggregates and interfere with iron-sulfur clusters, causing iron-sulfur proteins to be down-regulated. This contributes to proteotoxic stress, which ultimately causes cell death (25).

Cuproptosis is a new format of cell death distinct from oxidative stress-related forms of cell death (such as apoptosis, iron death, and necrotic apoptosis). Copper ions, as key metal ions for cell signaling, can be extensively involved in cancer development by promoting cellular value-addition, angiogenesis, and metastasis (26). There is now substantial clinical evidence of the efficacy of using copper homeostasis in the treatment of cancer (27).

Therefore, this article will review the research progress on the role of cuproptosis in GC occurrence and development, and perspective in this regard, to provide new perspectives for exploring the pathogenesis and potential therapeutic targets of GC.

3 Gastric cancer

The uncontrolled growth of gastric malignant tumor cells results from the inhibition of programmed tumor cell death (27). When the cell death process is disrupted or inhibited, tumor cells can grow indefinitely, ultimately leading to cancer (28). Cuproptosis is a novel form of cell death discovered and named by Tsvetkov et al. in March 2022. Their study found that copper ions can impair the function of mitochondrial enzymes in the citric acid cycle (CAC) via the FDX1 gene when copper ion levels in the body exceed normal values. The mitochondrial membrane then undergoes oxidative damage and binds directly to the lipoylated components of the CAC. This interaction forms long chains or clustered aggregates and interferes with iron-sulfur clusters, leading to the downregulation of iron-sulfur proteins. This causes proteotoxic stress, ultimately resulting in cell death (29). Cuproptosis is distinct from other forms of cell death related to oxidative stress, such as apoptosis, ferroptosis, and necroptosis. Copper ions, as key metal ions for cell signaling, can be extensively involved in cancer development by promoting cellular proliferation, angiogenesis, and metastasis (30). There is now substantial clinical evidence supporting the efficacy of targeting copper homeostasis in cancer treatment (31).

GC is a disease of high molecular and phenotype heterogeneity, which is driven by multiple genetic and epigenetic aberrations (28). The most common histological type is gastric adenocarcinoma(GA) originating from the epithelium of the gastric mucosa. It accounts for more than 95% of GC cases (29). That is also the point of this article. The Lauren classification and the WHO classification are routinely used in clinical practice, to distinguish different histological and molecular biological characteristics in GC patients (30). Based on the diversity of glandular structures, Lauren's classification divides GC into intestinal gastric cancer, diffuse gastric cancer, and mixed GC (31). IGC, DGC, and MGC exhibit distinct clinical features (32) and genetics of specificity (33, 34), individually. Notably, the WHO classification, which is based on cellular morphology and histological structure, is a refinement and addition to Lauren's classification. This classification system involves papillary, tubular, mucinous, and MGC (35).

IGC commonly forms one or several solid tumors (31, 36), mostly due to Helicobacter pylori infection (37), and is seen as damage to the gastric glands. In contrast, the DGC consists of many disjointed microscopic tumors (31, 38). DGC is typically characterized by ill-defined or absent glandular structures and reduced intercellular adhesion, compared to IGC (39). As a consequence, they are more aggressive which leads to a worse prognosis. Furthermore, IGC and DGC respectively consist of diverse cellular lineages. In IGC, tumor cells normally evolve from gastric intestinal metaplasia (GIM), with a progressive increase in tumor cell heterogeneity as the malignant stage progresses. While in the cell lineage of DGC, cancer cells are derived from tumor stem cells (TSCs) (40). Studies have shown that peripheral stem cells can transiently outperform average growth regulation mechanisms, tissue regeneration, and growth in complex situations, thereby increasing the risk of cellular mutation. And it is known that TSCs have similar traits to peripheral stem cells. TSCs can interact with cancer-associated fibroblasts (CAFs) within the tumor and evolve into distinct cell populations, contributing to the onset of DGC heterogeneity and eventual progression to GC (41). Based on proteomics analysis, DNA damage was identified to be dramatically upregulated in IGC. As a crucial kinase for DNA mismatch repair, ATM/ATR can regulate cell proliferation in IGC, through activation of the SWI/SNF complex, whereas immunity and up-regulation of extracellular matrix proteins (ECMs) are seen in DGC (42).

As opposed to IGC, which tends to metastasize to solid organs (liver, lungs), DGC frequently metastasizes via lymph nodes and ultimately spreads to the intra-peritoneum (43). DGC commonly has a stronger affinity for intestinal neurons than IGC and has a stronger perineural infiltration rate (44). In review, we considered that IGC and DGC share unique histological and pathological features, and the heterogeneity between the roles of the two may be associated with their independent cellular lineage characteristics. Since they are distinguished by different cellular lineages, we can provide specific targeted therapy for GC patients. Nevertheless, we

still have a large rising range for the study of IGC and DGC in the mechanism of tumor cell evolution.

Since the stomach is a hollow organ and the early symptoms of GC are insidious (45). For this reason, the majority of GC have usually progressed to advanced stages and have a high mortality rate, by the time they are diagnosed, causing it to be the fourth most common cause of cancer-related deaths after liver cancer. In 2020, the worldwide number of GC patients reached 1.09 million, with 770,000 deaths, contributing to 5.6% and 7.7% of the global cancer incidence and mortality rates, respectively (46). While the incidence and mortality rates of GC are currently declining, in most countries, owing to economic growth and the widespread concept of disease prevention, the deaths from GC will only increase in the future as the population aging progresses (47).

Family history, Helicobacter pylori infection, GIM (48), genetic factors, and environmental and dietary factors (49). are the most prevalent etiological factors. Chronic atrophic gastritis (AG) and GIM are widely recognized as common precancerous lesions. Furthermore, H. pylori invasion has been proved to be an essential element to cause AG and GIM. The relationship between H. pylori and GC is influenced by both the severity and rate of progression of AG. A chronic inflammatory process in the gastric mucosa, combined with damage to the gastric glands (50), and a decrease in gastric secretory function characterize AG.

H. pylori not only colonizes and survives in the human digestible tract, but also enhances its capacity to cause disease by infection. Since H. pylori is a Gram-negative bacterium with a specific flagellar structure and secretion of urease that can neutralize gastric acid and other properties (51).

Additionally, on account of genome plasticity, the genome sequence of H. pylori can change by more than 20% to modify to a specific host environment during colonization (52). The main virulence factors of H. pylori are Vacuolating cytotoxin A (Vac-A), cytotoxin-associated gene A (Cag-A), cytotoxin-associated gene pathogenicity island (Cag-PAI), and bacterial flagella. H. pylori Vac-A has a variety of cellular actions, including the utilization of cellular vacuoles to increase the lifespan of infection, as well as mitochondrial stress, and interference with apoptosis (53), Vac-A also regulates host cell metabolism, stimulating all three of these pathways, including NFE2L2 / HO-1 /Nrf2-HMOX1, through the dependent inhibition of MTORC1 (54). Thereby further inducing autophagy by perturbing mitochondria and depleting cellular amino acids in human GC cells. This ultimately provides the nutrients and intracellular ecological niche necessary for H. pylori to colonize and replicate on its own (55). If this autophagy is dysfunctional, it can damage tight junction proteins and disrupt the integrity of the gastric epithelial barrier. This effect can contribute to the development of primary gastrointestinal diseases by severely affecting intestinal homeostasis and the host's inflammatory response (56). Excessive ROS produced by autophagy in H. pylori has also been identified as a potential factor in its induction of GC incidence via autophagy. Some related research has found that the T4SS, encoded by the Cag-PAI, also injects Cag-A into gastric epithelial cells (57, 58). Such changes cause genomic instability of gastric epithelial cells, promotion of inflammation and malignant transformation of epithelial cells, as well as sustained proliferation of tumor cells (59).

These virulence factors in H. pylori also interfere with the host's intercellular signaling cascade, causing tumor cells to escape growth-inhibiting factors and resist cell death. Not only that, it can adhere to gastric epithelial cells (60)by binding to receptors via a series of outer membrane proteins, Including adhesion lipoproteins A and B (AlpA / B), blood group antigen binding adhesion (BabA), etc. Typical symptoms of acute-chronic inflammation can arise from persistent H. pylori infection and damage to the gastric acid-producing glands. Through the above mechanisms, AG is eventually caused. Continued AG will destroy and kill the acid-producing wall cells, resulting in too little or a lack of stomach acid production. This weakened acidic environment accelerates the colonization of a pro-inflammatory gastric microbiota. This harmful microbiota produces additional genetically toxic pro-inflammatory metabolites and carcinogens. The above ultimately led directly to the transformation of the malignant epithelial cells of the stomach (60–62), leading to the formation of GC (49) , H. pylori infection is still considered a major causative factor in GC, although the virulence of its carcinogenic is influenced by multiple microbiological, environmental, and host factors (63). Whereas widely dispersed AG is known to be associated with the induction of a state of gastric acid deficiency or hypogastric acidity, which is one of the significant risks for the development of GC (64, 65).

In addition, inactivation of tumor-inhibiting genes caused by DNA hypermethylation plays an influential position in the occurrence and progression of GC (66–69). It has been extensively demonstrated that factors associated with GC development, such as protocadherin 10 (PCDH10) (70), and junctional adhesion molecule 3 (JAM3) (71), lead to down-regulation of tumor suppressor genes (TSGs) through promoter hypermethylation in GC, are not infrequent in a wide range of GC types. However, the specific mechanisms involved need to be further elucidated. Regarding the eradication of H. pylori, partial studies have found that it reverses the methylation process of the E-calmodulin gene in patients with chronic gastritis. It has also been demonstrated in specific genes that the methylation levels of other TSGs are reduced after this treatment (72).

GIM refers to the replacement of the gastric epithelial mucosa by intestinal epithelial mucosa of the Penn cell, absorptive enterocyte, and cuprocyte types (73–75). According to the histological classification, “complete GIM” is known as “type I” or “intestinal type”, and “incomplete GIM” is known as “colonic type” and includes “type II” and “type III”. In comparison, the latter has a higher risk of cancer (76–78). According to the classic Correa cascade theory (79). the development of GC involves multiple stages, from mild to severe, healthy gastric mucosa, superficial gastritis, AG, GIM, heterogeneous hyperplasia, and finally malignant transformation. The first step in this cascade is the emergence of chronic gastric mucosal inflammation mediated by polymorphonuclear cells and mononuclear cells. This stage causes multifocal glandular atrophy in the stomach, loss of cell mass in the gastric wall, and loss of acid secretion in the stomach. As it continues to atrophy, the gastric epithelium is progressively replaced by an intestinal-type epithelium, mainly characterized by the inclusion of Pannus cells, absorptive enterocytes, and cup cells.

GIM is considered to be an irreversible turning point in GC, and progression from GIM to low-grade atypical hyperplasia, high-grade atypical hyperplasia, and intestinal-type GA is extremely probable (80). With atrophy of the intestinal-type mucosa and progression of GIM, heterogeneous hyperplasia (intraepithelial neoplasia) can occur, eventually progressing to gastric malignancy (81). As a precancerous lesion, GIM plays an essential role in the development of GC, and it signals a high risk of GC.

It is widely accepted that gastric mucosal epithelial cells are subject to multifactorial influences that produce genetic mutations that activate proto-oncogenes or silence oncogenes. This mutation will destroy the balance between cell proliferation and programmed cell death, ultimately resulting in GC. Although this became the existing consensus, the specific molecular mechanisms of gastric carcinogens have not been fully revealed (82, 83).

As early symptoms of GC are not noticeable, once the diagnosis is confirmed, it is often in the middle to late stages and the prognosis is dire (84).

Therefore, it becomes exceedingly important to seek effective early diagnosis of GC and corresponding treatment modalities.

Copper is an indispensable trace metal element involved in various physiological processes in the human body. It has been shown in numerous studies that serum and tumor tissue concentrations of copper ions are dramatically increased in cancer patients compared to healthy individuals (85, 86).

In 2022, Tsvetkov et al. identified a new form of programmed cell death, copper concentration-dependent cell death, also known as cuproptosis. They have shown that Cu^{2+} binds directly to the lipoylated components of the TCA and that the aggregation of these copper-bound lipoylated mitochondrial proteins. The consequent loss of Fe-S-cluster proteins triggers proteotoxic stress, ultimately leading to cell death (87).

4 Cuproptosis

Cuproptosis is a recently discovered form of programmed cell death triggered by copper overload *in vivo* (88). In 2022, Tsvetkov et al. found that when blocking known modes of cell death (e.g. apoptosis, autophagy, iron death, etc.), molecules or ion carriers bound to copper ions were still able to trigger cell death in unique yet similar ways. Based on metabolomics, they identified more CAC-related metabolites in copper-sensitive cells, further substantiating that Cu^{2+} plays an important role in the CAC. The above results indicate that the cell-killing effect of copper overload is likely to be related to the process of mitochondrial respiration. And that components of the CAC are essential targets of cuproptosis (25).

Further studies by Tsvetkov et al. illustrated that cells utilizing mitochondrial energy production were nearly 1,000 times more sensitive to copper carriers than cells utilizing glucose glycolysis production. Using a CRISPR knockout screen, the team identified several key genes that promote copper death, including the FDX1 gene, which encodes the target protein of the Elesclomol molecule, and six genes involved in mitochondrial metabolism and protein fatty acylation modification. These six genes are DLAT, PDHA1, PDHB and DBT, GCSH, and DLST. A study found that reductase, encoded by the FDX1 gene, converts Cu^{2+} to the more toxic Cu^{+} and may provide a direct Elesclomol target (89).

Lastly, for exploring the link between copper toxicity and protein lipid acylation, to identify specific metabolic pathways that mediate copper toxicity. Todd Golub's team postulated that copper might bind directly to isolated proteins. In their experiments, they found that cuproptosis is strongly aligned with mitochondrial metabolism-mediated protein-lipid acylation processes. This also values FDX1 and Protein Lipidation as crucial regulators of cuproptosis, with FDX1 being an upstairs regulator of the latter. This experiment suggests that the protein's thioctyl portion is necessary for copper binding. Copper ions penetrating mitochondria via copper carriers directly bind to these lipoylated modified proteins and induce oligomerization of DLAT, resulting in their formation of long chains and clustering. Alternatively, copper interferes with Fe-S clusters and induces loss of Fe-S cluster proteins, leading to the elevation of HSP70 to activate acute proteotoxic stress that leads to cell death. All results indicate that excess copper promotes aggregation of lipid-acylated proteins and instability of Fe-S cluster proteins, ultimately leading to cytotoxic stress leading to cell death (Figure 1).

Overall, this study presented cuproptosis, a novel copper concentration-dependent cell death modality, and further revealed its specific mechanism.

Currently, research on cuproptosis is progressing in a number of non-cancer diseases, in addition to advances in the field of cancer. Examples include cardiovascular disease, inflammatory responses, and neurodegenerative diseases.

A meta-analysis has shown that serum copper levels are elevated in patients with type 2 diabetes compared with healthy controls (90). Because impaired pancreatic β-cell function is closely related to cell death in patients with type 2 diabetes. Therefore, the concept of cuproptosis also provides new ideas for the study of copper metabolism and potential therapeutic mechanisms in diabetes (91). In addition, it has been confirmed that protein toxic stress associated with cuproptosis is a potential factor in the pathogenesis of many cardiovascular diseases (92). In addition, due to the relevance of cuproptosis to cellular mitochondrial function and oxidative stress pathways, studies based on the concept of cuproptosis to reduce cell damage related to cardiovascular disease have attracted increasing attention. Moreover, recent progress has been made in the correlation between cuproptosis and inflammatory response. Studies have shown that the body's inflammatory response is closely linked to cellular mitochondrial dysfunction (93). Researchers have found that significant mitochondrial fragmentation is seen in septic endothelial cells, which may be associated with reduced mitochondrial membrane potential and increased reactive oxygen species production (94). ZhangJun's team constructed a predictive model and found a significant correlation between the expression of the key cuproptosis genes PDHB, PDHA1, and LIAS (95), which are mainly found in cellular mitochondria and function as the catalytic subunit of pyruvate dehydrogenase (PDH) (96), and the prognosis of sepsis patients. Since PDH activity is often inhibited in patients with sepsis (97), modification of PDHB and PDHA1 seems to significantly influence the development of sepsis. As a key gene encoding the mitochondrial

10.3389/fimmu.2024.1435651

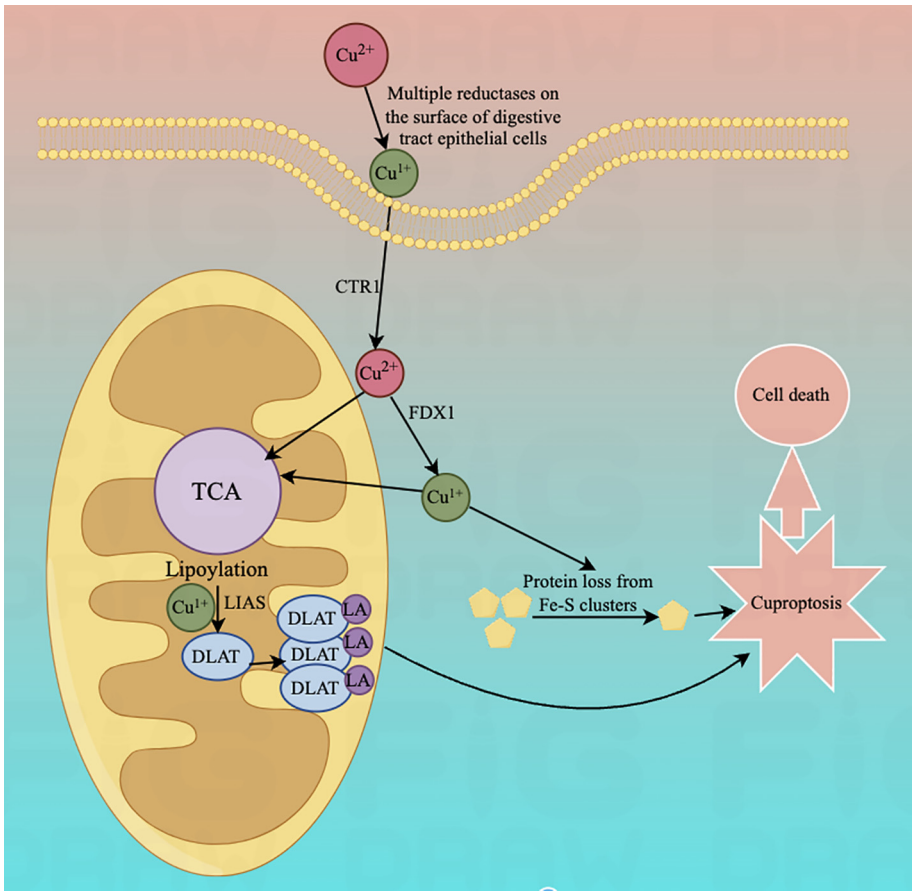

FIGURE 1
Diagram of the mechanism associated with cuproptosis.The copper ion binds to thioctylated proteins in the tricarboxylic acid cycle (TCA) and promotes aberrant oligomerization of thioctylated proteins. At the same time, copper ions can also reduce the level of Fe-S cluster proteins, which together induce a proteotoxic stress response that ultimately leads to cell death.

lipoic acid pathway (98), LIAS is also important for the prognosis of sepsis patients. Wilson Disease is an inherited disease of the liver characterized by an overload of copper in liver tissue. Since the maintenance of copper content in the liver in equilibrium is mediated by the ATP7B protein encoded by the ATP7B gene. Therefore, once the ATP7B gene is expressed abnormally, it leads to impaired synthesis of ceruloplasmin (the major copper-containing protein in the blood) in the liver as well as impaired biliary excretion process of copper in the liver, which ultimately leads to overaccumulation of copper in the liver. Since ATP7B is also a key gene leading to the occurrence of cuproptosis in cells, cuproptosis has been recognized as the pathogenesis and new therapeutic breakthroughs of Wilson Disease in new research reports (99). In addition, it has been shown that one of the major causes of brain neurological damage due to dysregulation of copper homeostasis is the induction of the Haber-Weiss and Fenton reactions by copper in its oxidation state and reduction state circulatory transitions, resulting in the production of excessive ROS products that cause oxidative damage to proteins, lipids, and DNA. This induces oxidative damage to proteins, lipids, and DNA, ultimately leading to neurotoxicity and cellular dysfunction (100). Because the occurrence of cuproptosis is affected by proteins related to copper ion transport, storage and uptake pathways, such as SLC31A1, ATP7A, ATP7B, etc, recent studies related to cuproptosis and neurodegenerative diseases are attracting the attention of researchers (101).

5 The relationship between GC and cuproptosis

5.1 Cu^{2+} and GC development mechanism

As an indispensable enzyme coordinator in the human body, a variety of studies have documented abnormal copper concentrations in the serum of patients with many malignant tumors, such as gastric, breast, brain, prostate (102), colon, lung, and liver cancers, to varying degrees (103–110). Copper has a strong coordination capacity. Excessive copper will form complexes in the body with amino acids, proteins, or other substances that interact with enzymes, nucleic acids, DNA, and other macromolecules, leading to malignant cell differentiation. The significant increase of Cu level will promote the catalytic effect of copper-mediated in mitochondria, resulting in the generation of reactive oxygen species (ROS), and excessive ROS will lead to the oxidation of the amino acid side chain of the protein or the break of the peptide chain, which will change

the properties of the protein and lead to the loss of various enzyme activities. ROS may oxidize the bases of DNA or degrade DNA; In addition, ROS may also act on unsaturated fatty acids in cell membranes, causing lipid peroxidation and disrupting the normal function of membranes. Substantial evidence exists that unbalanced copper homeostasis can influence tumor growth (111). This promotes the growth and spread of tumor cells in the body.

Although it has been extensively demonstrated and accepted that the occurrence and development of GC are highly correlated with abnormal programmed cell death in the gastric mucosa (112). There is uncertainty about the specific mechanisms underlying the abnormal value-added of GC cells.

There is evidence that cancer cells generally have stronger copper requirements than healthy resting cells. Compared to other tumor cells, GC cells prefer to employ glycolysis to produce intermediate metabolites and energy to increase resistance to cuproptosis (113). Also, as a vital element in cell signaling, copper ions are involved in the activation of cell proliferation-related signaling pathways. It is involved in cancer occurrence and progression by promoting cell proliferation, angiogenesis, and metastasis (114) Analyzing the TCGA database, we discovered a remarkable functional enrichment of lncRNA genes associated with cuproptosis in the inflammatory response, immune response, and transmembrane cell signaling in GC. The genes CD209 and HAVCR2 are cuproptosis-associated regulatory immune checkpoints. When they are overexpressed in GC tissue, this means that GC patients have a lower survival rate (115). Associated studies have uncovered that cuproptosis-related genes including FDX1, ENTPD3, PDZD4, CNN1, GTPBP4, FPGS, UTP25, CENPW, and FAM111A. They can accurately predict the progression of GC and have excellent performance in the early diagnosis and treatment of GC. Among these, FDX1 has been shown to induce cuproptosis by an atypical methyltransferase called METTL16 by modifying FDX1 mRNA (116). There is increasing evidence that lncRNA implicated in cuproptosis can be utilized as biomarkers of prognosis in GC patients. There is increasing evidence that lncRNA implicated in cuproptosis can be utilized as biomarkers of prognosis in GC patients (117).

In July 2023, Yong fu Shao's team proposed a column-line graph model based on copper death-related genes to predict overall survival and cancer-specific survival in GC patients. The model found that copper death-related genes FDX1, LIASd, and MTF1 could be used as potential prognostic biomarkers for GC patients (118). In 2024, jia-qi jin (119) and others related research also confirmed this conclusion.And XiaoJunYang found that FDX1 was significantly up-regulated in GCtissues. To suppress FDX1 will lead to GC cells malignant phenotype transformation is restrained (120). Approximately 10 genes associated with cuproptosis (121)can be expressed in different types of GC. These include seven positively regulated cuproptosis genes: ferredoxin1 (FDX1), lipoic acid synthase (LAIS), fatty acid transferase 1 (LIPT1), dihydrolipoicenamide dehydrogenase (DLD), dihydrolipoic acid transacetylase (DLAT), pyruvate dehydrogenase E1-alpha subunit (PDHA1), pyruvate dehydrogenase E1-β subunit (PDHB) and three negatively regulated genes: metal-regulated transcription factor 1 (MTF1), glutaminase (GLS), and cell cycle protein-dependent kinase inhibitor 2A (CDKN2A) (see Table 1 below) (Figure 2).

5.2 Cuproptosis markers

Except for the Cuproptosis-related genes(CRGs), which were highly expressed in GC cells (137), Organismal overload of copper ions may also contribute to the occurrence and development of

TABLE 1 The markers of Cuproptosis.

Cuproptosis markers	Ways to participate	Reference documentation
FDX1	①Reduction of Cu^{2+} to more toxic Cu+ induces cuproptosis; ②Catalytic lipoylation of the core structural protein of PDH affects the CAC to induce cuproptosis	(122, 123)
DLAT	Catalyzes the conversion of pyruvate to acetyl-CoA and promotes lipid synthesis, which is involved in the CAC and binding to copper ions induces cuproptosis in cells	(89, 124, 125)
PDHB	① Thiooctylated CAC-associated enzymes can promote cell death by directly binding Cu^{2+} ② Binding to copper ions leads to oligomerization of thiooctylation-modified CAC-related enzymes and formation of insoluble aggregates, leading to cytotoxicity and induction of cell death.	(88)
PDHA1	Encodes the α subunit of the PDH complex, which catalyzes the conversion of pyruvate to acetyl-CoA and thus participates in the CAC, binds to copper ions, and induces cuproptosis in cells	(126)
LIPT1	Activates mitochondrial 2-keto acid dehydrogenase participates in lipoylation, binds to copper ions, and engages in cellular cuproptosis	(127)
LIAS	An associated gene as a crucial enzyme of the lipoic acid pathway, regulated by FDX1, is implicated in cellular cuproptosis	(128)
DLD	An associated gene as a critical enzyme of the lipoic acid pathway, regulated by FDX1, affects mitochondrial metabolism, is involved in the CAC, and is implicated in cellular cuproptosis	(129–131)
ATP7A	Engaging in the metabolic pathway of cellular copper Cu^{2+} leads to severe disruption of intracellular content, which in turn leads to cellular cuproptosis	(132)
GLS	GLS is a key enzyme in glutamine metabolism, converting glutamine to glutamate, decomposing it to produce α-ketoglutarate, and entering the CAC to counteract oxidative stress in tumors, thus preventing and treating cuproptosis.	(133)
MTF1	It combines with MRE, activates MTs, and engages in an intracellular overloaded Cu^{2+} transcriptional response to control metal and oxidative stress, which inhibits the onset of cellular cuproptosis.	(134–136)

10.3389/fimmu.2024.1435651

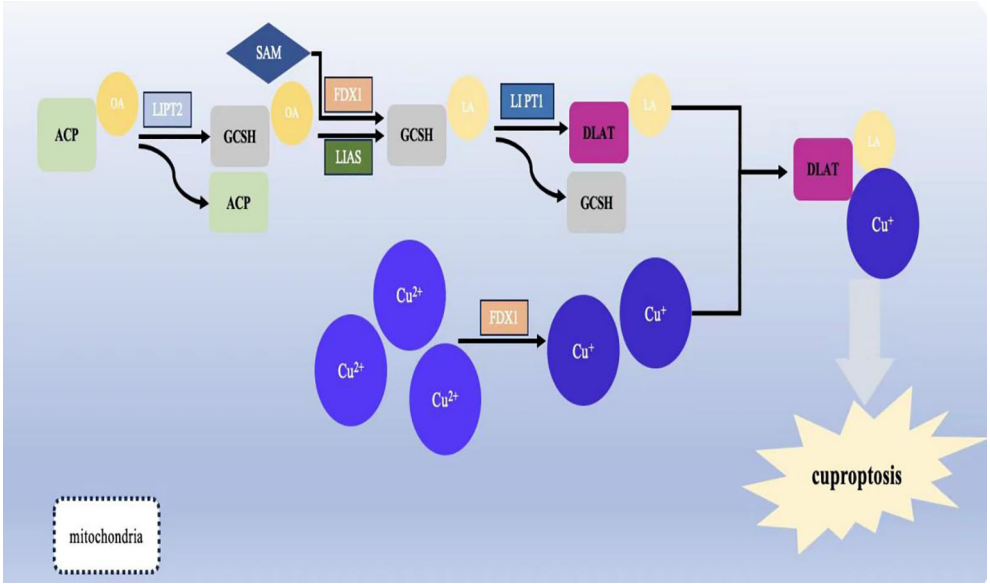

FIGURE 2
Schematic representation of the mechanism of cuproptosis and its effect on mitochondrial function.Lipoylation is required for the activation of several mitochondrial enzyme complexes, and the biosynthesis of lipoic acid in humans involves several steps: the acyl chain on the acyl-carrier protein (ACP) generates octanoyl ACP through extension, reduction, and dehydration; lipolytransferase 2 (LIPT2) transfers the octanoyl portion from ACP to the Glycine cleavage system H protein (GCSH); LIAS generates ACP by depleting S-adenosyl methionine (SAM); and LIAS generates ACP by depleting SAM. Lipolytransferase 2 (LIPT2) transfers the octanoyl portion from ACP to Glycine cleavage system H protein (GCSH); LIAS completes the formation of lipoic acid on GCSH by depleting SAM and inserting sulphur atoms into carbons 6 and 8 of the octanoyl group; finally, the formation of lipoic acid is completed by the depletion of SAM; the formation of lipoic acid is completed by the depletion of SAM. Finally, LIPT1 transfers the thiooctanoyl portion from GCSH to target proteins (DLAT, DLST, etc.), thus completing the thiooctanoylation of mitochondrial proteins.

gastric malignancies by regulating the tumor microenvironment (TME) (138).

The initiation and progression of cancer occur almost concurrently with changes in the surrounding stroma. Cancer cells can be functionally shaped to fit the TME for tumor cell growth and development by secreting various cytokines, chemokines, and other factors that lead to reprogramming of the surrounding cells (139). TME is intimately associated with tumor progress and consists of different types of immune, stromal, and immune Cells that are an essential part of it (140, 141).

Studies have shown that the trace element copper, which is important in cellular and humoral immunity, can be used to activate and maintain the immune system by manipulating various immune cells (142, 143). The establishment of crosstalk between cancer cells and proximal immune cells will provide nutritional support to tumor cells and promote cancer development and progression. They will eventually turn into a TME suitable for tumor growth and metastasis (144, 145). Therefore, an in-depth comprehension of the features of copper overload-mediated TME immune cell infiltration will help us better know the potential mechanisms of GC, predict the response to immunotherapy, and develop new safe and efficient targeted drugs (146).

Additionally, angiogenesis is an influential factor in tumor progression. Blood vessels rarely form new branches under physiological conditions in healthy adults. In contrast, in cancerous tissue, without a blood vessel supply, tumors cannot grow beyond 1-2 mm (147). Tumor angiogenesis is a sophisticated process engaging endothelial cell migration and proliferation, as well as vascular tube and new vessel generation. Copper ions are thought to initiate angiogenesis (148). Excess copper stabilized HIF-1α, the rate-limiting component of HIF-1, causing its accumulation in the cytoplasm, which activated HIF-75, regulated vascular endothelial growth factor(VEGF)expression, and promoted tumor angiogenesis (148).

Moreover, tumor cells commonly have abnormal mitochondrial metabolism due to the loss of active oncogenes and tumor suppressor genes (149). As a metal nutrient, there is a consistently high demand for copper ions during tumor growth and metastasis. Combined with the high expression of Cuproptosis in mitochondrial respiratory cells, it is evident that copper-related diagnostic and therapeutic approaches are appropriate for gastric malignant tumors (Figure 3).

5.3 Treatment of cuproptosis and GC

GC treatment options are selected with reference to several elements: tumor stage, biomarkers, and the doctor's preferred option (150). For early-stage cancers, clinical emphasis is put more on tumor resection surgery (151) than comprehensive systemic treatments like chemotherapy or radiotherapy. Nevertheless, it is not unusual for patients with GC to opt for integrative therapies in the clinic, as GC is often at an advanced stage at the time of diagnosis.

Studies have shown that copper levels and lactate concentrations in GC tissues are significantly higher than in normal gastric tissues (152). The copper content in tumor tissues

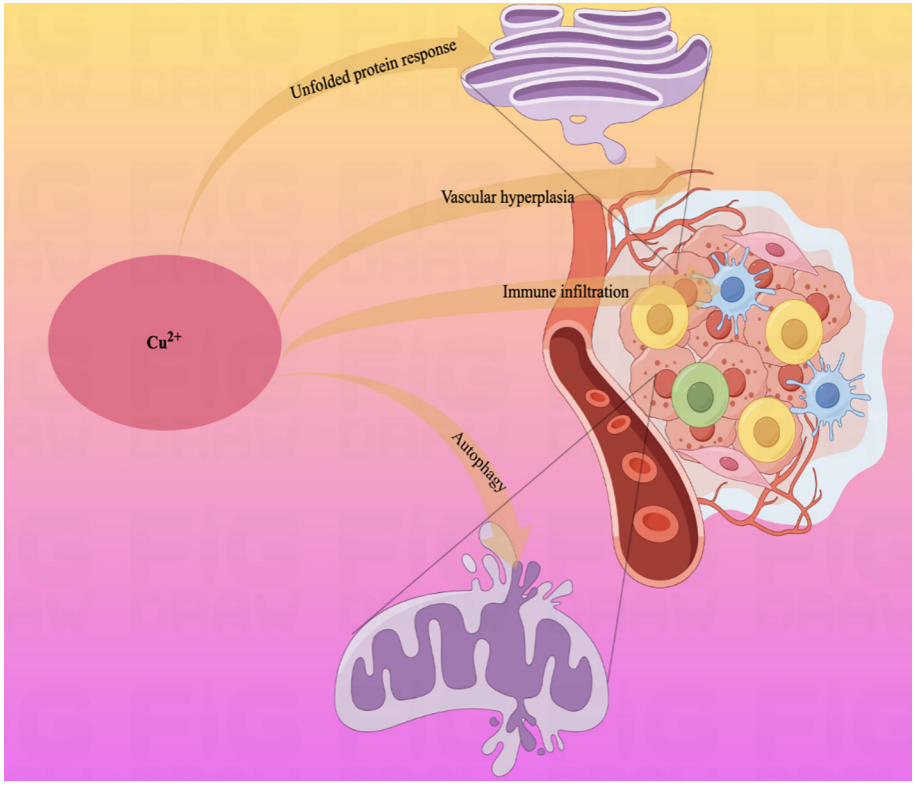

FIGURE 3
Schematic diagram of the pathways by which copper ions affect some physiological activities of the human body.Copper ions are widely involved in the physiopathological activities of the body through autophagy, vascular proliferation, and immune infiltration.

of GC patients was positively correlated with patients' TNM stage and negatively correlated with patients' OS (overall survival) and DFS (disease-free survival) (153). ChenHuang et al. found that overloaded copper ions in GC could accelerate the lactylation process of non-histone protein METTL16-K229 by promoting the interaction of lactyltransferases AARS1/AARS2 with METTL16(a key regulator of copper death in gastric cancer), in order to ultimately lead to the development of Cuproptosis (116). Normal concentrations of copper are essential for human life processes. In contrast, high intracellular copper concentrations can cause cytotoxicity and even cell death. Therefore, copper absorption, distribution, and excretion in the body are tightly regulated by a copper-dependent protein network. Among them, Cu-binding proteins (CBP) are responsible for the transport of free copper into cells associated with cuproptosis. This is because GC cells produce intermediate metabolites and energy more through glycolysis than oxidative phosphorylation (113). Therefore, if the cuproptosis process is induced in GC cells, it might have a positive effect on tumor tissue invasion as well as metastasis. Currently relevant studies have identified CBP as an entry point for research with great clinical potential in the treatment and prognosis of GC patients (154). Moreover, TP53, one of the most commonly mutated genes in GC, is an important regulator affecting tumor metabolism, which can be involved in mediating cellular glycolysis and oxidative phosphorylation processes in order to increase the sensitivity of these two tightly coupled metabolic processes in cells to cuproptosis (155). Therefore, studies targeting TP53 and cuproptosis are of increasing interest to researchers. Currently, the research on disulfiram combined with copper in the treatment of GC has also made good progress. It has been shown that DSF/Cu complex can not only inhibit the tumor activity of GC cells by regulating the signaling pathways such as stress response, glycolysis, Wnt/β-catenin, etc., but also indulge the apoptosis of cells by participating in the reactive oxygen species (ROS)/mitogen-activated protein kinase pathway (156). And a regional study showed that the use of calcium channel blockers reduced the chances of developing GC to some extent, which may indicate a specific link between calcium signaling pathways and GC (157). The following are some of the research directions available. IL-15 is a cytokine that has an active role in the adaptive and intrinsic immune system of the body and in tumorigenesis. Some studies have found a correlation between copper death-related genes LIPT1, FDX1, MTF1 and IL-15 (with LIPT1 having the strongest correlation, R = 0.348). Numerous clinical trials have reported that drugs developed on the basis of IL-15, such as recombinant human single-chain IL-15 and IL-15 super agonists, have better efficacy in tumor therapy. Based on the relationship between IL-15 and cuproptosis-related genes, perhaps studies combining IL-15-related drugs with cuproptosis gene targets could provide new ideas and insights into the treatment of GC (158).

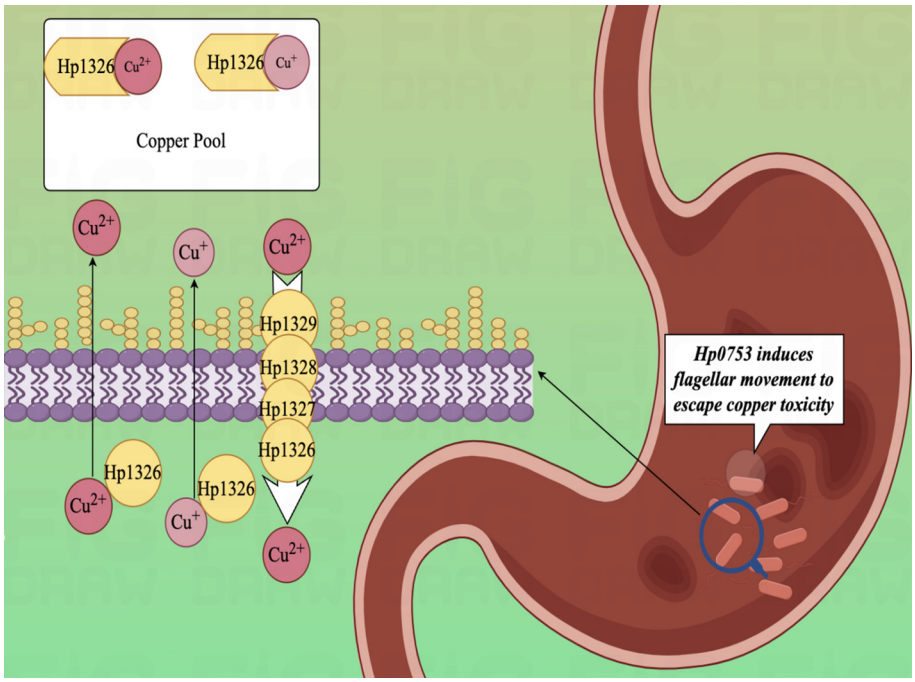

FIGURE 4
Diagram of the copper efflux mechanism.HpCrdA interacts with other H. pylori copper efflux pump proteins (CrdB, HP1328, and HP1329) to transport overloaded copper ions *in vivo* outside the H. pylori bacterium, which limits the cytoplasmic concentration of free copper ions and keeps them below toxic levels.

5.3.1 H. pylori

In the experimental study of copper binding by the H. pylori CrdA protein (HpCrdA), Ivana Kekez et al. found that CrdA selectively binds excess free copper ions in the form of Cu(I) and Cu(II), when the concentration of free copper ions in the cytoplasm of the H. pylori cell reaches a high value. Further, HpCrdA interacts with other H. pylori copper efflux pump proteins (CrdB, HP1328, and HP1329) to transport overloaded copper ions *in vivo* outside the H. pylori bacterium, which limits the cytoplasmic concentration of free copper ions and keeps them below toxic levels. And that process also has a positive response to external changes in the concentration of copper ions (159). Already in 2000, Waidner et al. presented this new system of copper externally discharged pumps (Czc system), which consists of the copper resistance determinants CrdA (HP1326), CrdB (HP1327), CzcB (HP1328) and CzcA (HP1329). With this system, H. pylori decrease copper-mediated production of toxic hydroxyl radicals (160, 161) and keep intracellular copper ion concentrations under toxic levels (Figure 4). Except, copper ions also induce the fliS gene in H. pylori, which together form the indispensable link to the production of an intact flagellum by H. pylori (162). Copper ions play an influential role in electron transport, oxidative enzymes, and hydroxylases, as an indispensable cofactor in the regulation of metal homeostasis in H. pylori (163, 164). As a clear classIcausative organism of GC, H. pylori can lead to the development of gastric malignant tumors through the process of AG-GIM, so it has a pivotal role in the prevention and diagnosis of GC. Furthermore, *in vitro* experiments have shown that human GC cells (AGS) can cause up-regulation of the CAC and amino acid metabolism, by modulating the MTOR complex 1 (MTORC1) signaling pathway in the gastric epithelium and immune cells at 6 hours after infection (165, 166).

Considerable clinical and basic experimental studies have proven the efficacy of copper complexes or chelator drugs using copper as a carrier in the treatment of malignant tumors. Examples include combining disulfiram and copper ions for breast cancer (165), elesclomol-Cu^{2+} for the treatment of malignant tumors (111), etc. Based on the mechanism of interaction between copper and H. pylori, we may be able to find the Cuproptosis principle. Perhaps it can be further exploited to cause cytotoxicity and stress death of H. pylori, finding a new pathway to reduce the risk of GC development.

5.3.2 Antiangiogenic direction

Angiogenesis is a physiological process that is co-regulated by pro-angiogenic factors and anti-angiogenic factors which is characterized by the sprouting of new blood vessels from pre-existing vessels. In mammals, the process of angiogenesis is generally dormant (148) and is only visible in pathological or rarely physiological states. In malignant aggressive tumors, including GC, however, it is one of the steps necessary for the growth and metastasis of tumor cells (167, 168).

The concept of Cu^{2+} pro-angiogenesis was first proposed by Professor McAuslan. In experiments on copper-induced phagocytosis of aortic endothelial cells, he found that mutant aortic endothelial cell lines were highly sensitive to copper. Under experimental conditions, endothelial cells are migrated by copper salts, traveling up to 24 μm in 1000 hours. The discovery of that phenomenon lays the foundation for the study of early neovascular event modeling systems (169).

VEGF-A is a crucial mediator in the regulation of vascular growth and development in pathological states. As a vascular endothelial cell mitogen, VEGF-A assumes a key role in regulating endothelial cell survival. VEGF-A promotes angiogenesis through interaction with vascular endothelial growth factor receptors 1 and 2 (VEGFR-1 and VEGFR-2) and co-receptors neuro phospholipids-1 and 2 (NRP-1 and NRP-2) (170).

Copper is an essential cofactor for the activation of metalloproteases (171, 172). It can be involved in regulating the affinity of angiopoietin for endothelial cells, in human physiological pH, by binding to angiopoietin molecules (eg. VEGF-A) (173). This drives the binding of angiopoietin to endothelial cells, causing endothelial cell (174) proliferation and migration. When pro-angiogenic molecules are more active than anti-angiogenic molecules, the angiogenic route is activated (175), and early angiogenesis occurs. Ultimately, it engages in tumor angiogenesis, accelerating cancer metastasis and deterioration (176).

In 2023, Chunmei He et al. found that 11 out of 12 CRGs were up-regulated in endothelial cell expression, suggesting that CRGs may play a potential role in angiogenesis through lncRNA (177). Cuproptosis, as a landmark sign of cell death due to copper overload *in vivo*, is promising in inhibiting tumor angiogenesis and delaying tumor growth and metastasis and deserves the deep attention of researchers (Figure 5).

5.3.3 TME immunization therapy

The term tumor microenvironment (TME) originated from the proposed ecological terminology (178), which is used to describe the internal and external environment of tumors or tumor cells with the ability of self-renewal and tumor driving (144).

TME consists of various cells (including immune cells, endothelial cells, inflammatory cells, fibroblasts, and lymphocytes), ECMs, vascular systems, and chemokines (179–181). The occurrence, evolution, and metastasis of tumors are intimately related to the structure and function of TME. Currently, in the field of cancer immunotherapy, the use of TME modulation strategies in the treatment of malignant tumors has attracted considerable attention (182). Immune cells in TME mediate innate and adaptive immune response processes. Innate immune cells have pro-tumor and anti-tumor properties. The adaptive immune system, activated by inherent immune cells, can specifically attack tumor cells and is considered the most effective method for eradicating tumors. Although innate immune cells can detect tumors and induce and amplify adaptive immune responses, this function is limited by the immunosuppressive microenvironment in TME (183). Whereas copper ions in the body can promote innate immunity by enhancing the presenting capacity of dendritic cells (DCs) and macrophages, along with the cytotoxicity of natural killer cells (NK cells) (184–186). Moreover, copper ions can stimulate the activation and proliferation of adaptive immune cells (187), reverse topical immune suppression (188), and play an essential role in the immunotherapy of tumors (189).

TME in hypoxia alters the functioning of the normal microenvironment, promotes tumor progression, and limits therapeutic efficacy (190). Besides affecting cancer cell metabolism directly, copper is also involved in cancer therapy by regulating hypoxia within the TME (191, 192). Copper reverses the poor responsiveness of conventional cancer immunotherapy by inducing a redox reaction with simultaneous oxygen production (177). Until TME is fully formed, the tumor is noticed by the immune system.

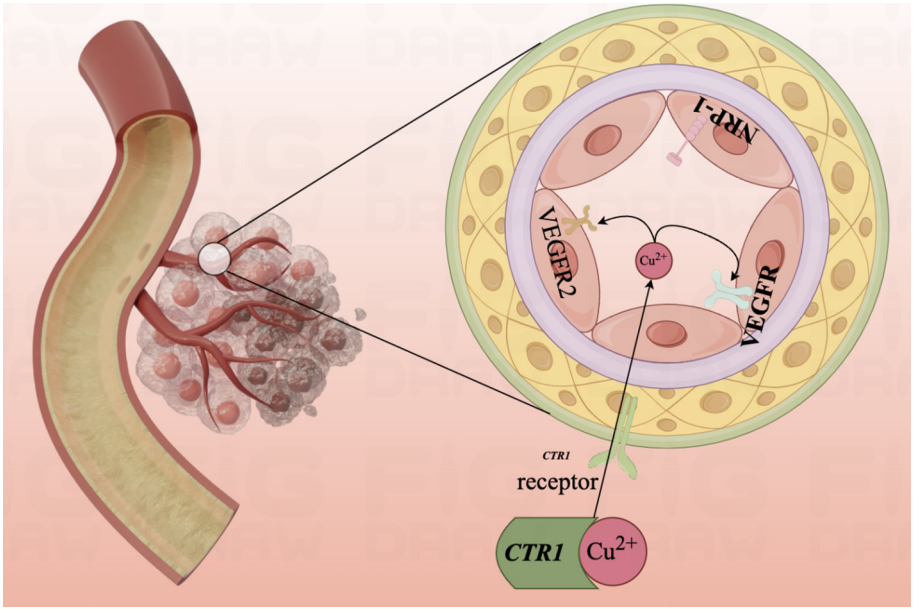

FIGURE 5
Diagram of the mechanism of copper ion involvement in angiogenesis.Mutant aortic endothelial cell lines are highly sensitive to copper, and copper ions promote the binding of angiopoietin to endothelial cells by binding to angiopoietin molecules, causing endothelial cell proliferation and migration. The angiogenic pathway is activated and early angiogenesis is turned on.

Particularly, the majority of patients will not normally die from a tumor originating in the primary site, but from metastatic tumors and associated changes in vital organs.

During the unrestricted growth of tumor cells uncontrolled by the cell death program, the innate immune surveillance of the organism changes. As a few tumor cells are killed by innate immune cells, the remaining ones gain the ability to rapidly increase in value due to the expanded growth space. Tumor cells then enter a phase of homeostasis to avoid being destroyed by the body's immune cells (escape phase). At this stage, tumor cells escape from immune destruction through pathways such as inhibition of ligand (PD-L) expression or secretion of inhibitory molecules (TGF-β) (193). The highly immune inhibitory properties of TME, which is carefully woven from tumor tissue, play an extremely important role in the above process all through the process (194).

Regulating the expression levels of PD-L1 (195)and other genes in immune checkpoint genes (IGCs) (143), copper ions can participate in tumor immunosuppression and tumor immunotherapy during the process of tumor cell proliferation and immune escape.

Copper is a crucial micronutrient that mediates the phagocytic role of innate immune cells (196, 197), including neutrophils and macrophages, tumor cell proliferation, bacterial infections, and other processes, with the aim of maintaining a healthy state of the organism. However, in the types of diseases caused by copper deficiency in the body, we found that copper, as an indispensable metal, has a vital role in the development and differentiation of bone marrow cells. Copper deficiency *in vivo* induces neutropenia and anemia (198). And, neutrophils have been proven to have a pre-tumor cell phenotype within the TME owing to their tumor-associated macrophage-like role, and their tissue infiltration has been associated with poor tumor outcomes (199). It has been found that if copper deficiency occurs in the innate immune response before or during the elimination phase of tumor cells, the phagocytic step of immune cells will be impaired, leading to tumor cell progression (200). Moreover, studies suggest that the immune microenvironment may be closely related to cuproptosis in tumors (201).

Lin Jiang et al. Subtype classification and immunotype analysis of GC samples based on the consensus clustering method showed that most of the immune-related genes in cuproptosis were significantly up-regulated in the C2 subtype (202). Accordingly, the modification of TME by regulating the cancer immune environment has increasingly attracted the attention of researchers (203, 204).On the clinical outcome of bladder cancer and the score of the immune response experiment system, cuproptosis immune cell infiltration was found to be associated with bladder cancer prognosis, and high $CD8^+$T cell infiltration predicted a positive prognosis (205). This implies that cuproptosis may be involved in the regulation of TME, especially $CD8^+$T cells, thus contributing to tumor growth and progression. Regulatory T cells are involved in homeostatic regulation of the organism and tumor immune escape.GC cells recruit Regulatory T cells while inducing CD4 T naïve cells to differentiate into Regulatory T cells via TGF-β, which ultimately achieves immunosuppressive effects (206). Immune checkpoint inhibitors enhance the prognosis of GC of patients, among which PD-L1/PD-1 arresters have excellent anti-tumor immunological effectiveness (207) .This also brings a new dawn for exploring the mechanism of cuproptosis in the immunotherapy of gastric malignant tumor microenvironment. Recent studies have also shown that cuproptosis is an important factor in tumor resistance to immunotherapy and antitumor therapy. Therefore, exploring the intrinsic mechanisms of immunomodulatory factors and cuproptosis in tumorigenesis and development, and further delving into the specific mechanisms cuproptosis in the overall prognosis, biomarkers (diagnostics), and immunotherapy of GC patients may provide new ideas for immunotherapy in the microenvironment of gastric malignant tumors.

5.3.4 Tumor metastasis

Cancer is a disease in which a group of tumor cells constantly proliferate, leading to the formation of tumors. It has been shown that the copper-exporting protein ATP7A promotes tumor cell growth by increasing copper levels in the cells (208). These tumor cells can invade the surrounding tissues and spread to distant organs (209, 210) through a cascade of metastasis (211, 212). According to reports, over 90% of cancer-related deaths are caused by the metastatic spread of cancer cells (213).

Copper ions affect the behavior of tumor cells in various ways during their invasion and metastasis. It can profoundly engage in the invasion and migration of tumor cells by mediating the connection between ECMs and cytoskeleton (214), as well as acting as gradient forming agent and intracellular messenger (215). As the central molecule in tumor cell migration, integrins can be activated by a combination of divalent metal ions relevant to the cell surface, such as iron, zinc, copper, or ECMs proteoglycans. They may lead to tumor cell migration. Additionally, as a coenzyme, a factor necessary for the cross-linking of collagen and elastin fibers (216), a copper ion can modify the extracellular matrix and create a suitable environment for tumor cell metastasis by enhancing the activities of lysyl oxidase (LOX) and lysine oxidase-like enzyme (LOXL) (116, 217). Recent studies have found that copper concentration in mucinous adenocarcinoma tissues in GC has a positive correlation with invasive fingers such as lymph node metastasis (218, 219). In addition to LOX, copper activates ERBB2-driven cellular motility protein mediator 1 (Memo1), which activates the phosphatidylinositol-3 kinase/protein kinase B (PI3K/Akt) signaling pathway by interacting with the insulin receptor substrate 1 to promote EMT, clearing Cu into the secretory pathway and reducing ROS formation. And, in experiments related to the migration and metastasis of breast cancer cells, we found that the cell movement protein MEMO, which is catalyzed by Cu^{2+} oxidase activity, has a clear ability to promote cell migration of breast cancer. Above all, Cu^{2+} may have the potential to influence cancer cell metastasis (220).

Nikos K Karamanos et al. used KEGG pathway enrichment and GO annotation to show that significantly differentiated genes (DEGs) in cuproptosis are mainly involved in the construction of extracellular matrix organization, cell-cell junctions, and collagen-containing extracellular matrix components (221). How copper overload *in vivo* induces a protein-toxic stress response and leads

to programmed cell death, may give us new insights and inspiration in the study of Cu^{2+} in the treatment of malignant tumor cell metastasis.

5.3.5 Chemotherapeutic resistance

In GC we find that copper levels are significantly elevated, and this is more common in more malignant and advanced stages of GC (116). Related Researchers see the potential link between copper ions and chemotherapy resistance in tumor patients, due to higher serum copper levels in chemotherapy-resistant patients compared to those responding to chemotherapy (222). Jing Jin et al. also found that in tumor tissues, physiologically high copper can lead to chemotherapy resistance in patients by promoting DNA double-strand break repair in the role of copper in drug-resistant murine and human tumors tumor cells (223). Many genetic and biochemical studies have also shown that the copper transporter proteins ATP7A and ATP7B can promote platinum drug resistance by controlling their uptake and export from tumor cells (224).

Currently, platinum-based drugs are often used clinically in the treatment of cancer patients. The main challenge affecting its therapeutic efficacy is chemotherapy resistance, which is one of the main reasons for the failure of anti-cancer treatments (225). Unlike exogenous platinum drugs that often lead to the up-regulation of glutathione (GSH) stress in tumor cells and thus lead to chemotherapy resistance in tumor patients, a team of researchers has found that Diethyldithiocarbamic Acid Copper Salt (CuET) reverses cisplatin resistance in non-small-cell lung cancer through a cuproptosis mechanism (226). They also bring new inspiration for inducing cuproptosis in GC to achieve the reversal of platinum drug resistance (227). Since glutathione and glucose depletion enhance the sensitivity of cancer cells to cuproptosis mediated by GOx@ [Cu(tz)] (228), targeted therapy against cuproptosis might be a new therapeutic strategy to overcome chemotherapy resistance.

5.4 Cuproptosis and prognosis of GC

Currently, immunology-based studies on the tumor microenvironment aimed at exploring the relationships between CRGs and the prognosis of GC have made promising progress.

In addition, studies have shown that elevated copper levels are seen in a variety of human cancers, such as colorectal, breast, liver and lung cancers. Therefore, more and more studies have begun to focus on the relationship between cuproptosis and these cancers, and many studies have shown that CRGs are closely associated with the prognosis of various types of cancers (156). Xichun Hu et al. established a nomogram based on the combination of TME-based CRGs risk score and clinicopathologic features to predict the risk associated with the prognosis of patients with GC, and found that CRGs was significantly correlated with TME as well as the prognostic assessment of GC (156). This was also confirmed by the study of Wang Ning et al. The study further found that the level of immune infiltration of tumor tissues was negatively correlated with the expression level of CRGs as well as the prognosis of patients (207). Jin Liu et al. also found that theCRGs SERPINE1 is associated with immune cell infiltration. This gene can be used to maintain proliferative signaling in tumors and inhibit apoptosis through an inhibitory immune microenvironment. Abnormal expression of this gene in GC tissues is closely associated with poor prognosis in GC patients. The team further found that some statins may affect the expression of SERPINE1 through the TGF-β pathway. c-Met, a receptor tyrosine kinase that promotes tumor cell proliferation, invasion, and migration, is aberrantly expressed in a variety of tumor cells. And SGX523, as a c-Met inhibitor, may provide new ideas for the treatment of GC patients with aberrant expression of SERPINE1. SERPINE1 as a prognostic biomarker and a potential therapeutic target in GC also deserves further study by researchers (229). Jie Liet al. showed that cuproptosis-related immune genes (ANOS1, CTLA4, ITGAV, CXCR4, NRP1, FABP3, and LGR6) were up-regulated in GC tissues, and GC patients had poor prognosis. Among them, NRP1, CXCR4, LGR6, and CTLA4 were abnormally expressed in GC tissues and associated with cuproptosis-related gene FDX1. It is suggested that CRGs may be involved in the development and prognosis of GC through immune regulation. The results of this study reflect the increasingly important role of immune checkpoint inhibitor therapy in the comprehensive treatment of GC (230). The prognosis of GC patients is related to the infiltration of immune cells within the tumor and the response to immunotherapy, in which DNA methylation of tumor cells is also one of the factors affecting the prognosis of GC patients. Studies have shown that CRGs FDX1, LIAS and MTF1 are associated with multiple types of immune cell infiltration, which can be used as potential prognostic biomarkers for GC patients. This study provides new strategies for immune-targeted therapy in GC patients (118).

In addition, lncRNAs(examples include LINC01150,SNAP25-AS1,LINC00571 and HAGLR) (231) associated with cuproptosis could also accurately predict the prognosis of GC patients. It may have a better predictive effect than a single biomarker. However, the specific mechanism needs to be further explored (232).

6 Conclusions

As an indispensable coenzyme factor for various life activities in the human body, the intake of copper by the human body mainly comes from food. After digestion of copper-containing food by the stomach, absorbed by small intestinal copper transport protein 1 (CTR1) or solute carrier family 31 member 1 (SLC31A1) (233), exists in the body in the form of Cu^{+} and Cu^{2+} (234). The absorbed Cu^{2+} is reduced to Cu^{+} by reductase upon binding to divalent metal transporter 1 (DMT1) and then binds to transmembrane copper transporter 1 (CTR1) to enter the cells (235). It goes through different modes of transport to bind to certain copper proteins (236). Eventually, it functions in various tissues and organs of the human body. However, as the intracellular copper concentration reaches a certain threshold, it also triggers the FDX1 gene to reduce Cu^{2+} to the more toxic Cu^{+} (88), leading to cuproptosis. To prevent the accumulation of harmful free copper in human cells (116),

copper can maintain its concentration in cells within the physiological level through an active homeostasis mechanism (237).

Cancer, has increasingly become a global discussion hotspot, with a high level of research and exploration on GC. Copper ions have received substantial evidence indicating that their concentration disorders can occur in various cancers, including GC. Considering that the sites of copper absorption are mainly in the stomach and small intestine, gastrointestinal tumors are particularly suitable for studying the mechanisms associated with cuproptosis and GC (238).Copper ions are widely involved in the occurrence and development of GC. According to the cuproptosis view, excess intracellular copper can reduce Cu^{2+} to Cu^{+} with greater toxicity under the joint action of mitochondrial Fe-S cluster protein and ferredoxin 1 (FDX1). Furthermore, copper can bind directly to DLAT and contribute to the disulfide-dependent aggregation of lipoylated DLAT, eventually leading to cuproptosis. With high FDX1 protein levels and copper in GC, cuproptosis may be more likely to be triggered. It offers a potential therapeutic strategy for GC, especially for a malignant tumor - mucinous adenocarcinoma. Yuan Chen et al. (116)conducted a meta-analysis found that the genes LIAS, DLAT, DBT, and PDHA1 exhibit extensive differential expression in Crohn's disease (CD), ulcerative colitis (UC), celiac disease (CEL), and IBD-induced cancer (IBD-CA). According to molecular docking results, methotrexate shows the highest binding affinity to the main chain of copper apoptosis-related regulatory factors. Weichen Wang et al. (238) collected glioma datasets from TCGA, GEO, and CGGA databases, analyzed CRGs (CRG) using the Robust Multichip Average (RMA) algorithm, and calculated CuproptosisScore using multivariate Cox regression analysis. They found that patients with higher CuproptosisScore also have higher WHO grades and poorer prognosis, while patients with lower CuproptosisScore are more likely to have IDH mutations or MGMT methylation. In the high CuproptosisScore group, PIK3CA, MUC16, NF1, TTN, TP53, PTEN, and EGFR exhibit high mutation frequencies, and immune infiltration levels increase with increasing CuproptosisScore. Patients with high CuproptosisScore may respond better to anti-PD-1 therapy. Lianhui Sun et al. (116) published a study revealing significantly elevated copper levels in GC. Through meta-analysis and enrichment gene screening, they identified METTL16 as a key mediator of copper apoptosis in GC through m6A modification on FDX1-mRNA. High copper levels promote non-histone protein METTL16-K229 acylation by increasing the interaction between potential aminoacyl-tRNA synthetases AARS1/AARS2 and METTL16, ultimately leading to copper apoptosis. Copper and lactate concentrations in gastric tumors (especially malignant tumors) are higher than in normal tissues. Combining the copper ion carrier disulfiram and SIRT2-specific inhibitor to induce copper apoptosis significantly enhances the efficacy of GC treatment. These research findings provide a comprehensive understanding of the mechanisms underlying copper apoptosis initiation and execution and propose a promising therapeutic strategy for GC.

The current research on the association between Cuproptosis and GC is still confined to applying CRGs for constructing prognostic risk models for GC. There is still a lack of research on the mechanism of cuproptosis in the occurrence and development of GC, without its application in the treatment of GC. Therefore, this article reviews the enrichment and expression of CRGs in the occurrence and development of GC, the mechanism of cuproptosis and GC occurrence and development, and the prospect of treatment methods for GC using the proptosis perspective. The objective is to provide a feasible basis for utilizing the concept of cuproptosis in GC research, as well as to provide some new perspectives for future research on GC prevention and treatment.

Many studies in recent years have shown that cuproptosis is closely associated with ROS and inflammation and triggers other forms of cell death, including apoptosis, pyroptosis, and ferroptosis. It has been found that intracellular mitochondrial ROS levels are elevated and induce apoptosis, whereas ROS inhibitors rescue cell viability. Further studies revealed that ros-induced apoptosis is dependent on the sustained activation of the pro-apoptotic mitogen-activated protein kinase (MAPK) pathway (cJun n-terminal kinases [JNKs] and p38), which regulates the phosphorylation of pro- and anti-apoptotic proteins in mitochondria. Similarly, disulfiram-cu^{2+} complexes can induce ROS production, which in turn activates the downstream apoptosis-related JNK and p38MAPK pathways to induce apoptosis in breast cancer cells. From an inflammatory perspective, activation of nucleotide-binding oligomerization structural domains, leucine-rich repeat sequences, and pyrin structural domain-containing protein 3 (NLRP3) inflammasome pathways were found to introduce copper-mediated macrophage pyroptosis. That means it's an inflammatory form of lysogenic programmed cell death. Similar results were found in copper oxide nanoparticles (CuONPs)-treated mouse macrophages showing elevated levels of pro-inflammatory factors including NLRP3, caspase-1, and interleukin (IL)-1β. In the acidic environment of the lysosome, CuONPs attack the lysosome by releasing copper ions, leading to the release of histone B, which directly mediates the activation of the NLRP3 inflammasome. In addition, CuONP exposure triggered macrophages to express pro-il -1β through activation of myeloid differentiation factor 88 (MyD88)-dependent toll-like receptor 4 (TLR4)/nuclear transcription factor κB (NF-κB) cascade response. This is another typical pathway of NLRP3 inflammasome activation.

However, there is still a lack of systematic studies on other roles of copper in mitochondria, such as its induced cell death phenotypes and specific clinical treatments for related chelators. At the same time, the crosstalk between its mediated programmed cell death and other metal-induced cytotoxicity could not be further investigated in detail. This has prompted studies of the mechanisms involved in the onset of relevant cuproptosis in GC development, which must be tailored to the toxicology of metal toxicity in cells within the various layers of tumor tissue at different stages of differentiation or progression.

Above all, considering the correlation between cuproptosis and GC, we can predict that new treatment methods may become the wave of GC treatment. When that happens, GC patients will enjoy more effective and personalized treatment strategies, better prospects, and

quality of life, and the new diagnostic and treatment approach will bring a new dawn to lighten the financial burden of those patients.

Author contributions

YL: Writing – original draft, Writing – review & editing. WS: Writing – original draft, Writing – review & editing. SY: Writing – original draft, Writing – review & editing. XL: Writing – review & editing, Methodology, Validation. ZZ: Writing – original draft, Writing – review & editing. RG: Conceptualization, Methodology, Supervision, Validation, Writing – review & editing. PL: Conceptualization, Methodology, Supervision, Writing – review & editing. XG: Conceptualization, Methodology, Supervision, Validation, Writing – review & editing.

Funding

The author(s) declare financial support was received for the research, authorship, and/or publication of this article. This project was supported by Open Project Support for National Clinical Research Base of Traditional Chinese Medicine (JD2022SZ11).

Conflict of interest

The authors declare that the research was conducted in the absence of any commercial or financial relationships that could be construed as a potential conflict of interest.

Publisher's note

All claims expressed in this article are solely those of the authors and do not necessarily represent those of their affiliated organizations, or those of the publisher, the editors and the reviewers. Any product that may be evaluated in this article, or claim that may be made by its manufacturer, is not guaranteed or endorsed by the publisher.

References

1. Aoude M, Mousallem M, Abdo M, Youssef B, Kourie HR, Shamsi HOA, et al. Gastric cancer in the Arab World: a systematic review. *East Mediterr Health J.* (2022) 28:521–31. doi: 10.26719/emhj.22.051

2. Yang X, Zhang TC, Zhang H, Sang SW, Chen H, Zuo XL, et al. Temporal trend of gastric cancer burden along with its risk factors in China from 1990 to 2019, and projections until 2030: comparison with Japan, South Korea, and Mongolia. *biomark Res.* (2021) 9:84. doi: 10.1186/s40364-021-00340-6

3. Shah MA, Kelsen DP. Gastric cancer: a primer on the epidemiology and biology of the disease and an overview of the medical management of advanced disease. *J Natl Compr Canc Netw.* (2010) 8:437–47. doi: 10.6004/jnccn.2010.0033

4. Thrift AP, El-Serag HB. Burden of gastric cancer. *Clin Gastroenterol Hepatol.* (2020) 18:534–42. doi: 10.1016/j.cgh.2019.07.045

5. Joshi SS, Badgwell BD. Current treatment and recent progress in gastric cancer. *CA Cancer J Clin.* (2021) 71:264–79. doi: 10.3322/caac.21657

6. Sung H, Ferlay J, Siegel RL, Laversanne M, Soerjomataram I, Jemal A, et al. Global cancer statistics 2020: GLOBOCAN estimates of incidence and mortality worldwide for 36 cancers in 185 countries. *CA Cancer J Clin.* (2021) 71:209–49. doi: 10.3322/caac.21660

7. Fusté NP, Hernández RF, Cemeli T, Mirantes C, Pedraza N, Rafel M, et al. Cytoplasmic cyclin D1 regulates cell invasion and metastasis through the phosphorylation of paxillin. *Nat Commun.* (2016) 7:11581. doi: 10.1038/ncomms11581

8. Otto T, Sicinski P. Cell cycle proteins as promising targets in cancer therapy. *Nat Rev Cancer.* (2017) 17:93–115. doi: 10.1038/nrc.2016.138

9. Nirmala JG, Lopus M. Cell death mechanisms in eukaryotes. *Cell Biol Toxicol.* (2020) 36:145–64. doi: 10.1007/s10565-019-09496-2

10. Kanneganti TD, Kundu M, Green DR. Innate immune recognition of mtDNA–an undercover signal? *Cell Metab.* (2015) 21:793–4. doi: 10.1016/j.cmet.2015.05.019

11. Bertheloot D, Latz E, Franklin BS. Necroptosis, pyroptosis and apoptosis: an intricate game of cell death. *Cell Mol Immunol.* (2021) 18:1106–21. doi: 10.1038/s41423-020-00630-3

12. Mishra AP, et al. Programmed cell death, from a cancer perspective: an overview. *Mol Diagn Ther.* (2018) 22:281–95. doi: 10.1007/s40291-018-0329-9

13. Satoh T, Kambe N, Matsue H. NLRP3 activation induces ASC-dependent programmed necrotic cell death, which leads to neutrophilic inflammation. *Cell Death Dis.* (2013) 4:e644. doi: 10.1038/cddis.2013.169

14. Morana O, Wood W, Gregory CD. The apoptosis paradox in cancer. *Int J Mol Sci.* (2022) 23:1328. doi: 10.3390/ijms23031328

15. Kashyap D, Garg VK, Goel N. Intrinsic and extrinsic pathways of apoptosis: Role in cancer development and prognosis. *Adv Protein Chem Struct Biol.* (2021) 125:73–120. doi: 10.1016/bs.apcsb.2021.01.003

16. Kerr JF, Wyllie AH, Currie AR. Apoptosis: a basic biological phenomenon with wide-ranging implications in tissue kinetics. *Br J Cancer.* (1972) 26:239–57. doi: 10.1038/bjc.1972.33

17. Bursch W, et al. Programmed cell death (PCD). Apoptosis, autophagic PCD, or others? *Ann N Y Acad Sci.* (2000) 926:1–12. doi: 10.1111/j.1749-6632.2000.tb05594.x

18. Zhang GH, Cai LJ, Wang YF, Zhou YH, An YF, Liu YC, et al. Novel compound PS-101 exhibits selective inhibition in non-small-cell lung cancer cell by blocking the EGFR-driven antiapoptotic pathway. *Biochem Pharmacol.* (2013) 86:1721–30. doi: 10.1016/j.bcp.2013.10.013

19. Wyllie AH. Apoptosis and carcinogenesis. *Eur J Cell Biol.* (1997) 73:189–97. doi: 10.1016/bs.apcsb.2021.01.003

20. Roberts RA, Nebert DW, Hickman JA, Richburg JH, Goldsworthy TL. Perturbation of the mitosis/apoptosis balance: a fundamental mechanism in toxicology. *Fundam Appl Toxicol.* (1997) 38:107–15. doi: 10.1006/faat.1997.2331

21. Boyle CC, Hickman JA. Toxin-induced increase in survival factor receptors: modulation of the threshold for apoptosis. *Cancer Res.* (1997) 57:2404–9. doi: 10.26402/jpp.2021.6.02

22. Schulte-Hermann R, Bursch W, Grasl-Kraupp B. Active cell death (apoptosis) in liver biology and disease. *Prog Liver Dis.* (1995) 13:1–35. doi: 10.1016/j.joen.2020.07.006

23. Shin VY, Chu KM. MiRNA as potential biomarkers and therapeutic targets for gastric cancer. *World J Gastroenterol.* (2014) 20:10432–9. doi: 10.3748/wjg.v20.i30.10432

24. Wang YQ, Zhang SJ, Lu H, Yang B, Ye LF, Zhang RS, et al. A C 21 -steroidal glycoside isolated from the roots of cynanchum auriculatum induces cell cycle arrest and apoptosis in human gastric cancer SGC-7901 cells. *Evid Based Complement Alternat Med.* (2013) 2013:180839. doi: 10.1155/2013/180839

25. Cobine PA, Brady DC. Cuproptosis: Cellular and molecular mechanisms underlying copper-induced cell death. *Mol Cell.* (2022) 82:1786–7. doi: 10.1016/j.molcel.2022.05.001

26. Dow JA. The essential roles of metal ions in insect homeostasis and physiology. *Curr Opin Insect Sci.* (2017) 23:43–50. doi: 10.1016/j.cois.2017.07.001

27. Hu H, Xu Q, Mo ZM, Hu XX, He QY, Zhang ZJ, et al. New anti-cancer explorations based on metal ions. *J Nanobiotechnol.* (2022) 20:457. doi: 10.1186/s12951-022-01661-w

28. Seeneevassen L, et al. Gastric cancer: advances in carcinogenesis research and new therapeutic strategies. *Int J Mol Sci.* (2021) 22:3418. doi: 10.3390/ijms22073418

29. Ajani JA, D'Amico TA, Bentrem DJ, Chao J, Cooke D, Corvera C, et al. Gastric cancer, version 2.2022, NCCN clinical practice guidelines in oncology. *J Natl Compr Canc Netw.* (2022) 20:167–92. doi: 10.6004/jnccn.2022.0008

30. Oue N, Sentani K, Sakamoto N, Uraoka N, Yasui W. Molecular carcinogenesis of gastric cancer: Lauren classification, mucin phenotype expression, and cancer stem cells. *Int J Clin Oncol.* (2019) 24:771–8. doi: 10.1007/s10147-019-01443-9

31. Lauren P. The two histological main types of gastric carcinoma: diffuse and so-called intestinal-type carcinoma. An attempt at A histo-clinical classification. *Acta Pathol Microbiol Scand.* (1965) 64:31–49. doi: 10.1186/s13045-022-01392-3

32. Vauhkonen M, Vauhkonen H, Sipponen P. Pathology and molecular biology of gastric cancer. *Best Pract Res Clin Gastroenterol.* (2006) 20:651–74. doi: 10.1016/j.bpg.2006.03.016

33. Oue N, Sentani K, Sakamoto N, Uraoka N, Yasui W. Clinicopathologic and molecular characteristics of gastric cancer showing gastric and intestinal mucin phenotype. *Cancer Sci.* (2015) 106:951–8. doi: 10.1111/cas.12706

34. Yasui W, Oue N, Ito R, Kuraoka K, Nakayama H. Search for new biomarkers of gastric cancer through serial analysis of gene expression and its clinical implications. *Cancer Sci.* (2004) 95:385–92. doi: 10.1111/j.1349-7006.2004.tb03220.x

35. Fléjou JF. WHO Classification of digestive tumors: the fourth edition. *Ann Pathol.* (2011) 31:S27–31. doi: 10.14740/gr1187

36. Veinberga L, Meidrops K, Rumba R, Gedins M, Anufrijevs D, Vilmanis J, et al. Surgical treatment of hepatocellular carcinoma with a tumor thrombus invading the right atrium: A case report. *Case Rep Oncol.* (2023) 16:422–30. doi: 10.1159/000529831

37. Kesharwani A, Dighe OR, Lamture Y. Role of helicobacter pylori in gastric carcinoma: A review. *Cureus.* (2023) 15:e37205. doi: 10.7759/cureus.37205

38. Pimentel-Nunes P, Libânio D, Marcos-Pinto R, Areia M, Leja M, Esposito G, et al. Management of epithelial precancerous conditions and lesions in the stomach (MAPS II): European Society of Gastrointestinal Endoscopy (ESGE), European Helicobacter and Microbiota Study Group (EHMSG), European Society of Pathology (ESP), and Sociedade Portuguesa de Endoscopia Digestiva (SPED) guideline update 2019. *Endoscopy.* (2019) 51:365–88. doi: 10.1055/a-0859-1883

39. Benesch MGK, Mathieson A. Epidemiology of signet ring cell adenocarcinomas. *Cancers (Basel).* (2020) 12:1544. doi: 10.3390/cancers12061544

40. Figueiredo C, Garcia-Gonzalez MA, MaChado JC. Molecular pathogenesis of gastric cancer. *Helicobacter.* (2013) 18 Suppl 1:28–33. doi: 10.1038/s41467-023-35797-6

41. Kim J, Park C, Kim KH, Kim Hye E, Kim H, Woo JK, et al. Single-cell analysis of gastric pre-cancerous and cancer lesions reveals cell lineage diversity and intratumoral heterogeneity. *NPJ Precis Oncol.* (2022) 6:9. doi: 10.1038/s41698-022-00251-1

42. Shi W, et al. Multilevel proteomic analyses reveal molecular diversity between diffuse-type and intestinal-type gastric cancer. *Nat Commun.* (2023) 14:835. doi: 10.1038/s41467-023-35797-6

43. Lee JH, et al. Lauren histologic type is the most important factor associated with pattern of recurrence following resection of gastric adenocarcinoma. *Ann Surg.* (2018) 267:105–13. doi: 10.1097/SLA.0000000000002040

44. Zhao B, et al. Perineural invasion as a predictive factor for survival outcome in gastric cancer patients: a systematic review and meta-analysis. *J Clin Pathol.* (2020) 73:544–51. doi: 10.1136/jclinpath-2019-206372

45. Waldum H, Fossmark R. Gastritis, gastric polyps and gastric cancer. *Int J Mol Sci.* (2021) 22:6548. doi: 10.3390/ijms22126548

46. Cao W, Chen HD, Yu YW, Li N, Chen WQ. Changing profiles of cancer burden worldwide and in China: a secondary analysis of the global cancer statistics 2020. *Chin Med J (Engl).* (2021) 134:783–91. doi: 10.1097/CM9.0000000000001474

47. Venerito M, et al. Review: Prevention and management of gastric cancer. *Helicobacter.* (2020) 25 Suppl 1:e12740. doi: 10.1111/hel.12740

48. Correa P. Human gastric carcinogenesis: a multistep and multifactorial process–First American Cancer Society Award Lecture on Cancer Epidemiology and Prevention. *Cancer Res.* (1992) 52:6735–40. doi: 10.1097/MD.0000000000036261

49. Yang H, Yang WJ, Hu B. Gastric epithelial histology and precancerous conditions. *World J Gastrointest Oncol.* (2022) 14:396–412. doi: 10.4251/wjgo.v14.i2.396

50. Dixon MF, et al. Classification and grading of gastritis. The updated Sydney System. International Workshop on the Histopathology of Gastritis, Houston 1994. *Am J Surg Pathol.* (1996) 20:1161–81. doi: 10.1097/00000478-199610000-00001

51. Hu LT, Foxall PA, Russell R, Mobley HL. Purification of recombinant Helicobacter pylori urease apoenzyme encoded by ureA and ureB. *Infect Immun.* (1992) 60:2657–66. doi: 10.1128/iai.60.7.2657-2666.1992

52. Blaser MJ, Atherton JC. Helicobacter pylori persistence: biology and disease. *J Clin Invest.* (2004) 113:321–33. doi: 10.1172/JCI20925

53. Ansari S, Yamaoka Y. Role of vacuolating cytotoxin A in Helicobacter pylori infection and its impact on gastric pathogenesis. *Expert Rev Anti Infect Ther.* (2020) 18:987–96. doi: 10.1080/14787210.2020.1782739

54. Paik JY, et al. Helicobacter pylori infection promotes autophagy through Nrf2-mediated heme oxygenase upregulation in human gastric cancer cells. *Biochem Pharmacol.* (2019) 162:89–97. doi: 10.1016/j.bcp.2019.02.003

55. Isaeva GS, Fagoonee S. Biological properties and pathogenicity factors of Helicobacter pylori. *Minerva Gastroenterol Dietol.* (2018) 64:255–66. doi: 10.23736/S1121-421X.18.02479-0

56. Bernegger S, et al. Proteolytic landscapes in gastric pathology and cancerogenesis. *Int J Mol Sci.* (2022) 23:2419. doi: 10.3390/ijms23052419

57. Akopyants NS, Clifton SW, Kersulyte D, Crabtree JE, Youree BE, Reece CA, et al. Analyses of the cag pathogenicity island of Helicobacter pylori. *Mol Microbiol.* (1998) 28:37–53. doi: 10.1046/j.1365-2958.1998.00770.x

58. Censini S, Lange C, Xiang Z, Crabtree JE, Ghiara P, Borodovsky M, et al. cag, a pathogenicity island of Helicobacter pylori, encodes type I-specific and disease-associated virulence factors. *Proc Natl Acad Sci U.S.A.* (1996) 93:14648–53. doi: 10.1007/978-3-319-50520-6_3

59. Takahashi-Kanemitsu A, Knight CT, Hatakeyama M. Molecular anatomy and pathogenic actions of Helicobacter pylori CagA that underpin gastric carcinogenesis. *Cell Mol Immunol.* (2020) 17:50–63. doi: 10.1038/s41423-019-0339-5

60. Lücker S, Wagner M, Maixner F, Pelletier E, Koch H, Vacherie B, et al. A Nitrospira metagenome illuminates the physiology and evolution of globally important nitrite-oxidizing bacteria. *Proc Natl Acad Sci U.S.A.* (2010) 107:13479–84. doi: 10.1053/j.gastro.2019.02.036

61. Song P, Wu L, Guan W. Dietary nitrates, nitrites, and nitrosamines intake and the risk of gastric cancer: A meta-analysis. *Nutrients.* (2015) 7:9872–95. doi: 10.3390/nu7125505

62. Wang Z, Gao X, Zeng R, Wu Q, Sun H, Wu W, et al. Changes of the gastric mucosal microbiome associated with histological stages of gastric carcinogenesis. *Front Microbiol.* (2020) 11:997. doi: 10.3389/fmicb.2020.00997

63. Correa P, Piazuelo MB, Wilson KT. Pathology of gastric intestinal metaplasia: clinical implications. *Am J Gastroenterol.* (2010) 105:493–8. doi: 10.1038/ajg.2009.728

64. de Vries AC, Haringsma J, Kuipers EJ. The detection, surveillance and treatment of premalignant gastric lesions related to Helicobacter pylori infection. *Helicobacter.* (2007) 12:1–15. doi: 10.1111/j.1523-5378.2007.00475.x

65. Lechago J, Correa P. Prolonged achlorhydria and gastric neoplasia: is there a causal relationship? *Gastroenterology.* (1993) 104:1554–7. doi: 10.1016/0016-5085(93)90370-R

66. Zhang C, Li YZ, Dai DQ. Aberrant DNA methylation-mediated FOXF2 dysregulation is a prognostic risk factor for gastric cancer. *Front Mol Biosci.* (2021) 8:645470. doi: 10.3389/fmolb.2021.645470

67. Zeng Y, Rong HM, Xu JW, Cao RY, Li SH, Gao YJ, et al. DNA methylation: an important biomarker and therapeutic target for gastric cancer. *Front Genet.* (2022) 13:823905. doi: 10.3389/fgene.2022.823905

68. Liu D, Li L, Wang LR, Wang C, Hu XW, Jiang QX, et al. Recognition of DNA methylation molecular features for diagnosis and prognosis in gastric cancer. *Front Genet.* (2021) 12:758926. doi: 10.3389/fgene.2021.758926

69. Kandimalla R, Xu JF, Link A, Matsuyama T, Yamamura K, Parker MI, et al. EpiPanGI dx: A cell-free DNA methylation fingerprint for the early detection of gastrointestinal cancers. *Clin Cancer Res.* (2021) 27:6135–44. doi: 10.1158/1078-0432.CCR-21-1982

70. Zhang NN, Gao XL, Yuan QQ, Fu X, Wang PL, Cai FL, et al. E3 ubiquitin ligase RNF180 prevents excessive PCDH10 methylation to suppress the proliferation and metastasis of gastric cancer cells by promoting ubiquitination of DNMT1. *Clin Epigenet.* (2023) 15:77. doi: 10.1186/s13148-023-01492-y

71. Zhao QF, Lian JY, Pang K, Wang P, Ge RY, Chu YL, et al. Prognostic significance of JAM 3 in gastric cancer: An observational study from TCGA and GEO. *Med (Baltimore).* (2023) 102:e33603. doi: 10.1097/MD.0000000000033603

72. Nakajima T, Enomoto S, Yamashita S, Ando T, Nakanishi Y, Nakazawa K, et al. Persistence of a component of DNA methylation in gastric mucosae after Helicobacter pylori eradication. *J Gastroenterol.* (2010) 45:37–44. doi: 10.1007/s00535-009-0142-7

73. Leung WK, Man EPS, Yu J, Go MYY, To K, Yamaoka Y, et al. Effects of Helicobacter pylori eradication on methylation status of E-cadherin gene in noncancerous stomach. *Clin Cancer Res.* (2006) 12:3216–21. doi: 10.1158/1078-0432.CCR-05-2442

74. Chan AO, Peng JZ, Lam SK, Lai KC, Yuen MF, Cheung HKL, et al. Eradication of Helicobacter pylori infection reverses E-cadherin promoter hypermethylation. *Gut.* (2006) 55:463–8. doi: 10.1136/gut.2005.077776

75. Filipe MI, Muñoz N, Matko I, Kato I, Pompe-Kirn V, Jutersek A, et al. Intestinal metaplasia types and the risk of gastric cancer: a cohort study in Slovenia. *Int J Cancer.* (1994) 57:324–9. doi: 10.1002/ijc.2910570306

76. González CA, Sanz-Anquela JM, Companioni O, Bonet C, Berdasco M, López C, et al. Incomplete type of intestinal metaplasia has the highest risk to progress to gastric cancer: results of the Spanish follow-up multicenter study. *J Gastroenterol Hepatol.* (2016) 31:953–8. doi: 10.1097/MD.0000000000033603

77. Park YH, Kim N. Review of atrophic gastritis and intestinal metaplasia as a premalignant lesion of gastric cancer. *J Cancer Prev.* (2015) 20:25–40. doi: 10.15430/JCP.2015.20.1.25

78. Zullo A, Hassan C, Romiti A, Giusto M, Guerriero C, Lorenzetti R, et al. Follow-up of intestinal metaplasia in the stomach: When, how and why. *World J Gastrointest Oncol.* (2012) 4:30–6. doi: 10.4251/wjgo.v4.i3.30

79. Correa P, Haenszel W, Cuello C, Tannenbaum S, Archer M. A model for gastric cancer epidemiology. *Lancet.* (1975) 2:58–60. doi: 10.1016/S0140-6736(75)90498-5

80. Trieu JA, Bilal M, Saraireh H, Wang AY. Update on the diagnosis and management of gastric intestinal metaplasia in the USA. *Dig Dis Sci.* (2019) 64:1079–88. doi: 10.1007/s10620-019-05526-5

81. Huang RJ, Choi AY, Truong CD, Yeh MM, Hwang JH. Diagnosis and management of gastric intestinal metaplasia: current status and future directions. *Gut Liver.* (2019) 13:596–603. doi: 10.5009/gnl19181

82. Lakshmi Ch NP, Sivagnanam A, Raja S, Mahalingam S. Molecular basis for RASSF10/NPM/RNF2 feedback cascade-mediated regulation of gastric cancer cell proliferation. *J Biol Chem.* (2021) 297:100935. doi: 10.1016/j.jbc.2021.100935

83. Gao C, Liu H, Zhao Y, Miao X, Zheng H. Is there a relationship between neural EGFL like 1 (NELL1) promoter hypermethylation and prognosis of gastric cancer? *Med Hypotheses*. (2021) 158:110723. doi: 10.1186/s12935-021-01869-0

84. Zhang H, Li RC, Cao YF, Gu Y, Lin C, Liu X, et al. Poor clinical outcomes and immunoevasive contexture in intratumoral IL-10-producing macrophages enriched gastric cancer patients. *Ann Surg*. (2022) 275:e626–35. doi: 10.1097/SLA.0000000000004037

85. Ge EJ, Bush AI, Casini A, Cobine PA, Cross JR, DeNicola GM, et al. Connecting copper and cancer: from transition metal signalling to metalloplasia. *Nat Rev Cancer*. (2022) 22:102–13. doi: 10.1038/s41568-021-00417-2

86. Blockhuys S, Celauro E, Hildesjö C, Feizi A, Stål O, Fierro-González JC, et al. Defining the human copper proteome and analysis of its expression variation in cancers. *Metallomics*. (2017) 9:112–23. doi: 10.1039/C6MT00202A

87. Bergeron MG, Brusch JL, Barza M, Weinstein L. Bactericidal activity and pharmacology of flucloxacillin. *Am J Med Sci*. (1976) 271:13–20. doi: 10.1097/00000441-197601000-00002

88. Tsvetkov P, et al. Copper induces cell death by targeting lipoylated TCA cycle proteins. *Science*. (2022) 375:1254–61. doi: 10.1126/science.abf0529

89. Tsvetkov P, et al. Mitochondrial metabolism promotes adaptation to proteotoxic stress. *Nat Chem Biol*. (2019) 15:681–9. doi: 10.1038/s41589-019-0291-9

90. Qiu QH, Zhang FP, Zhu WJ, Wu J, Liang M. Copper in diabetes mellitus: a meta-analysis and systematic review of plasma and serum studies. *Biol Trace Element Res*. (2017) 177:53–63. doi: 10.1007/s12011-016-0877-y

91. Qu JS, Wang YF, Wang QY. Cuproptosis: potential new direction in diabetes research and treatment. *Front Endocrinol (Lausanne)*. (2024) 15:1344729. doi: 10.3389/fendo.2024.1344729

92. Yang Y, Feng Q, Luan Y, Liu H, Jiao YX, Hao HJ, et al. Exploring cuproptosis as a mechanism and potential intervention target in cardiovascular diseases. *Front Pharmacol*. (2023) 14:1229297. doi: 10.3389/fphar.2023.1229297

93. Tang D, Chen X, Kroemer G. Cuproptosis: a copper-triggered modality of mitochondrial cell death. *Cell Res*. (2022) 32:417–8. doi: 10.1038/s41422-022-00653-7

94. She H, et al. Protective effects of dexmedetomidine on sepsis-induced vascular leakage by alleviating ferroptosis. *via Regulating Metab Reprogramming J Inflammation Res*. (2021) 14:6765–82. doi: 10.3389/fonc.2024.1409620

95. Zhang J, Wu YY, Du YL, Du YX, Bao DQ, Lu HB, et al. Cuproptosis-related genes as prognostic biomarkers for sepsis: insights into immune function and personalized immunotherapy. *J Inflammation Res*. (2024) 17:4229–45. doi: 10.2147/JIR.S461766

96. Park S, et al. Role of the pyruvate dehydrogenase complex in metabolic remodeling: differential pyruvate dehydrogenase complex functions in metabolism. *Diabetes Metab J*. (2018) 42:270–81. doi: 10.4093/dmj.2018.0101

97. Nuzzo E, Berg KM, Andersen LW, Balkema J, Montissol S, Cocchi MN, et al. Pyruvate dehydrogenase activity is decreased in the peripheral blood mononuclear cells of patients with sepsis. A prospective observational trial. *Ann Am Thorac Soc*. (2015) 12:1662–6. doi: 10.1513/AnnalsATS.201505-267BC

98. Xu GC, Zhao YZ, Tao CXiong YJ, Lv M, Gao QY. Lias overexpression alleviates pulmonary injury induced by fine particulate matter in mice. *Environ Geochem Health*. (2023) 45:6585–603. doi: 10.1007/s10653-023-01651-3

99. Teschke R, Eickhoff A. Wilson disease: copper-mediated cuproptosis, iron-related ferroptosis, and clinical highlights, with comprehensive and critical analysis update. *Int J Mol Sci*. (2024) 25:4753. doi: 10.3390/ijms25094753

100. Zhang Y, Zhou Q, Lu L, Su Y, Shi W, Zhang H, et al. Copper induces cognitive impairment in mice via *modulation of cuproptosis and CREB signaling*. *Nutrients*. (2023) 15:972. doi: 10.3390/nu15040972

101. Huang M, Zhang Y, Liu X. The mechanism of cuproptosis in Parkinson's disease. *Ageing Res Rev*. (2024) 95:102214. doi: 10.1016/j.arr.2024.102214

102. Mimata Y, et al. Serum copper and the copper:zinc ratio in patients with gastric cancer. *Gan No Rinsho*. (1986) 32:1533–9. doi: 10.1513/AnnalsATS.201505-267BC

103. Davis CI, Gu X, Kiefer RM, Ralle M, Gade TP, Brady DC, et al. Altered copper homeostasis underlies sensitivity of hepatocellular carcinoma to copper chelation. *Metallomics*. (2020) 12:1995–2008. doi: 10.1039/d0mt00156b

104. Díez M, et al. Serum and tissue trace metal levels in lung cancer. *Oncology*. (1989) 46:230–4. doi: 10.3390/ijms25094753

105. Nayak SB, Bhat VR, Upadhyay D, Udupa SL. Copper and ceruloplasmin status in serum of prostate and colon cancer patients. *Indian J Physiol Pharmacol*. (2003) 47:108–10. doi: 10.3390/nu15040972

106. Turecký L, Kalina P, Uhlíková E, Námerová S, Krizko J. Serum ceruloplasmin and copper levels in patients with primary brain tumors. *Klin Wochenschr*. (1984) 62:187–9. doi: 10.1007/BF01731643

107. Huang YL, Sheu JY, Lin TH. Association between oxidative stress and changes of trace elements in patients with breast cancer. *Clin Biochem*. (1999) 32:131–6. doi: 10.1016/S0009-9120(98)00096-4

108. Rizk SL, Sky-Peck HH. Comparison between concentrations of trace elements in normal and neoplastic human breast tissue. *Cancer Res*. (1984) 44:5390–4. doi: 10.1039/d0mt00156b

109. Habib FK, Dembinski TC, Stitch SR. The zinc and copper content of blood leucocytes and plasma from patients with benign and Malignant prostates. *Clin Chim Acta*. (1980) 104:329–35. doi: 10.1016/0009-8981(80)90390-3

110. Kuo HW, Chen SF, Wu CC, Chen DR, Lee JH. Serum and tissue trace elements in patients with breast cancer in Taiwan. *Biol Trace Elem Res*. (2002) 89:1–11. doi: 10.1385/BTER:89:1

111. Jiang YC, Huo ZY, Qi XL, Zuo TM, Wu ZH. Copper-induced tumor cell death mechanisms and antitumor theragnostic applications of copper complexes. *Nanomed (Lond)*. (2022) 17:303–24. doi: 10.2217/nnm-2021-0374

112. Koren E, Fuchs Y. Modes of regulated cell death in cancer. *Cancer Discovery*. (2021) 11:245–65. doi: 10.1158/2159-8290.CD-20-0789

113. Xiong C, Ling H, Hao Q, Zhou X. Cuproptosis: p53-regulated metabolic cell death? *Cell Death Differ*. (2023) 30:876–84. doi: 10.1186/s12943-023-01732-y

114. Chen LY, Min JX, Wang FD. Copper homeostasis and cuproptosis in health and disease. *Signal Transduct Target Ther*. (2022) 7:378. doi: 10.1038/s41392-022-01229-y

115. Feng AQ, He LN, Chen T, Xu MD. A novel cuproptosis-related lncRNA nomogram to improve the prognosis prediction of gastric cancer. *Front Oncol*. (2022) 12:957966. doi: 10.3389/fonc.2022.957966

116. Sun L, et al. Lactylation of METTL16 promotes cuproptosis via m(6)A-modification on FDX1 mRNA in gastric cancer. *Nat Commun*. (2023) 14:6523. doi: 10.1038/s41467-023-42025-8

117. Matsuoka T, Yashiro M. Biomarkers of gastric cancer: Current topics and future perspective. *World J Gastroenterol*. (2018) 24:2818–32. doi: 10.3748/wjg.v24.i26.2818

118. Yan JN, Guo LH, Zhu DP, Ye GL, Shao YF, Zhou HX, et al. Clinical significance and potential application of cuproptosis-related genes in gastric cancer. *World J Gastrointest Oncol*. (2023) 15:1200–14. doi: 10.4251/wjgo.v15.i7.1200

119. Xie XZ, Zuo L, Huang W, Fan QM, Weng YY, Yao WD, et al. FDX1 as a novel biomarker and treatment target for stomach adenocarcinoma. *World J Gastrointest Surg*. (2024) 16:1803–24. doi: 10.4240/wjgs.v16.i6.1803

120. Zhao Q, et al. The role of cuproptosis key factor FDX1 in gastric cancer. *Curr Pharm Biotechnol*. (2024) 26:132–42. doi: 10.2174/0113892010301997240527162423

121. Liu H. Pan-cancer profiles of the cuproptosis gene set. *Am J Cancer Res*. (2022) 12:4074–81. doi: 10.21203/rs.3.rs-1716214/v1

122. Xiao ZM, Zuo WB, Chen LP, Wu L, Liu N, Liu JX, et al. H(2)O(2) self-supplying and GSH-depleting nanoplatform for chemodynamic therapy synergetic photothermal/chemotherapy. *ACS Appl Mater Interfaces*. (2021) 13:43925–36. doi: 10.1021/acsami.1c10341

123. Liu CG, Han YH, Zhang JT, R, Kankala K, Wang SB, Chen AZ, et al. Rerouting engineered metal-dependent shapes of mesoporous silica nanocontainers to biodegradable Janus-type (sphero-ellipsoid) nanoreactors for chemodynamic therapy. *Chem Eng J*. (2019) 370:1188–99. doi: 10.1016/j.cej.2019.03.272

124. Patel MS, et al. The pyruvate dehydrogenase complexes: structure-based function and regulation. *J Biol Chem*. (2014) 289:16615–23. doi: 10.1074/jbc.R114.563148

125. Stacpoole PW. Therapeutic targeting of the pyruvate dehydrogenase complex/pyruvate dehydrogenase kinase (PDC/PDK) axis in cancer. *J Natl Cancer Inst*. (2017) 109:djx071. doi: 10.1093/jnci/djx071

126. Xu X, et al. Integrative analysis revealed that distinct cuprotosis patterns reshaped tumor microenvironment and responses to immunotherapy of colorectal cancer. *Front Immunol*. (2023) 14:1165101. doi: 10.3389/fimmu.2023.1165101

127. Liu Y, et al. A pan-cancer analysis of copper homeostasis-related gene lipoyltransferase 1: Its potential biological functions and prognosis values. *Front Genet*. (2022) 13:1038174. doi: 10.3389/fgene.2022.1038174

128. Yi X, et al. Mice with heterozygous deficiency of lipoic acid synthase have an increased sensitivity to lipopolysaccharide-induced tissue injury. *J Leukoc Biol*. (2009) 85:146–53. doi: 10.1189/jlb.0308161

129. Patel MS, Nemeria NS, Furey W, Jordan F. The pyruvate dehydrogenase complexes: structure-based function and regulation. *J Biol Chem*. (2014) 289 (24):16615–23. doi: 10.1074/jbc.R114.563148

130. Stacpoole PW. Therapeutic targeting of the pyruvate dehydrogenase Complex/Pyruvate dehydrogenase kinase (PDC/PDK) axis in cancer. *J Natl Cancer Inst*. (2017) 109(11). doi: 10.1093/jnci/djx071

131. Tsvetkov P, Detappe A, Cai K, Keys HR, Brune Z, Ying W, et al. Mitochondrial metabolism promotes adaptation to proteotoxic stress. *Nat Chem Biol*. (2019) 15 (7):681–9. doi: 10.1038/s41589-019-0291-9

132. Xu XM, Ding CS, Zhong H, Qin DHShu W, Yu MG, et al. Integrative analysis revealed that distinct cuprotosis patterns reshaped tumor microenvironment and responses to immunotherapy of colorectal cancer. *Front Immunol*. (2023) 14:1165101. doi: 10.3389/fimmu.2023.1165101

133. Liu Y, Luo GQ, Yan YL, Peng J. A pan-cancer analysis of copper homeostasis-related gene lipoyltransferase 1: Its potential biological functions and prognosis values. *Front Genet*. (2022) 13:1038174. doi: 10.3389/fgene.2022.1038174

134. Yi XW, Kim K, Yuan WP, Xu LQ, Kim HS, Homeister JW, et al. Mice with heterozygous deficiency of lipoic acid synthase have an increased sensitivity to lipopolysaccharide-induced tissue injury. *J Leukoc Biol*. (2009) 85(1):146–53. doi: 10.1189/jlb.0308161

135. Yumnam S, Kang MC, Oh SH, Kwon HC, Kim JC, Jung ES, et al. Downregulation of dihydrolipoyl dehydrogenase by UVA suppresses melanoma

progression *via* triggering oxidative stress and altering energy metabolism. *Free Radic Biol Med*. (2021) 162:77–87. doi: 10.1016/j.freeradbiomed.2020.11.037

136. Wu HY, Wang YL, Yan Hua Tong LJ, Sun ZM. Global research trends of ferroptosis: A rapidly evolving field with enormous potential. *Front Cell Dev Biol*. (2021) 9:646311. doi: 10.3389/fcell.2021.646311

137. Fleminger G, Dayan A. The moonlighting activities of dihydrolipoamide dehydrogenase: Biotechnological and biomedical applications. *J Mol Recognit*. (2021) 34(11):e2924. doi: 10.1002/jmr.2924

138. Sluysmans S, Méan I, Xiao T, Boukhatemi A, Ferreira F, Jond L, et al. PLEKHA5, PLEKHA6, and PLEKHA7 bind to PDZD11 to target the menkes ATPase ATP7A to the cell periphery and regulate copper homeostasis. *Mol Biol Cell*. (2021) 32(21):ar34. doi: 10.1091/mbc.E21-07-0355

139. Tong YY, Guo D, Lin SH, Liang JZ, Yang DQ, Ma CM, et al. SUCLA2-coupled regulation of GLS succinylation and activity counteracts oxidative stress in tumor cells. *Mol Cell*. (2021) 81(11):2303–2316.e8. doi: 10.1016/j.molcel.2021.04.002

140. He J, Jiang XL, Yu M, Wang PG, Fu LY, Zhang GM, et al. MTF1 has the potential as a diagnostic and prognostic marker for gastric cancer and is associated with good prognosis. *Clin Transl Oncol*. (2023) 25(11):3241–51. doi: 10.1007/s12094-023-03198-2

141. Dong G, Chen H, Qi MY, Dou Y, Wang QL. Balance between metallothionein and metal response element binding transcription factor 1 is mediated by zinc ions (review). *Mol Med Rep*. (2015) 11(3):1582–6. doi: 10.3892/mmr.2014.2969

142. Westin G, Schaffner W. A zinc-responsive factor interacts with a metal-regulated enhancer element (MRE) of the mouse metallothionein-i gene. *EMBO J*. (1988) 7(12):3763–70. doi: 10.1002/j.1460-2075.1988.tb03260.x

143. Han CY, Zhang, Mo X. Construction of a cuprotosis-related gene-based model to improve the prognostic evaluation of patients with gastric cancer. *J Immunol Res*. (2022) 2022:8087622. doi: 10.1155/2022/8087622

144. Dong H, Zhao ST, Zhang C, Wang XD. Identification of cuproptosis related subtypes and construction of prognostic signature in gastric cancer. *Front Surg*. (2022) 9:991624. doi: 10.3389/fsurg.2022.991624

145. Hinshaw DC, Shevde LA. The tumor microenvironment innately modulates cancer progression. *Cancer Res*. (2019) 79(18):4557–66. doi: 10.1158/0008-5472.CAN-18-3962

146. Edlund K, Madjar K, Mattsson JSM, Djureinovic D, Lindskog C, Brunnström H, et al. Prognostic impact of tumor cell programmed death ligand 1 expression and immune cell infiltration in NSCLC. *J Thorac Oncol*. (2019) 14(4):628–40. doi: 10.1016/j.jtho.2018.12.022

147. Xu CM, Sui SL, Shang YR, Yu ZY, Han J, Zhang GX, et al. The landscape of immune cell infiltration and its clinical implications of pancreatic ductal adenocarcinoma. *J Adv Res*. (2020) 24:139–48. doi: 10.1016/j.jare.2020.03.009

148. Hackler J, Heller RA, Sun Q, Schwarzer M, Diegmann J, Bachmann M, et al. Relation of serum copper status to survival in COVID-19. *Nutrients*. (2021) 13(6). doi: 10.3390/nu13061898

149. Djoko KY, Ong CY, Walker MJ, McEwan AG. The role of copper and zinc toxicity in innate immune defense against bacterial pathogens. *J Biol Chem*. (2015) 290 (31):18954–61. doi: 10.1074/jbc.R115.647099

150. Wu T, Dai Y. Tumor microenvironment and therapeutic response. *Cancer Lett*. (2017) 387:61–8. doi: 10.1016/j.canlet.2016.01.043

151. Su YQ, Zhang XM, Li SQ, Xie W, Guo JP. Emerging roles of the copper-CTR1 axis in tumorigenesis. *Mol Cancer Res*. (2022) 20(9):1339–53. doi: 10.1158/1541-7786.MCR-22-0056

152. Song SR, Zhang M, Xie PL, Wang SH, Wang YC. Comprehensive analysis of cuproptosis-related genes and tumor microenvironment infiltration characterization in breast cancer. *Front Immunol*. (2022) 13:978909. doi: 10.3389/fimmu.2022.978909

153. Viallard C, Larrivée B. Tumor angiogenesis and vascular normalization: alternative therapeutic targets. *Angiogenesis*. (2017) 20(4):409–26. doi: 10.1007/s10456-017-9562-9

154. D'Andrea LD, Romanelli A, Stasi RD, Pedone C. Bioinorganic aspects of angiogenesis. *Dalton Trans*. (2010) 39(33):7625–36. doi: 10.1039/c002439b

155. Porporato PE, Filigheddu N, Pedro JM, Kroemer G, Galluzzi L. Mitochondrial metabolism and cancer. *Cell Res*. (2018) 28(3):265–80. doi: 10.1038/cr.2017.155

156. Sexton RE, Hallak Al MN, Diab M, Azmi AS, et al. Gastric cancer: a comprehensive review of current and future treatment strategies. *Cancer Metastasis Rev*. (2020) 39(4):1179–203. doi: 10.1007/s10555-020-09925-3

157. Bollschweiler E, Berlth F, Baltin C, Mönig S, Hölscher AH. Treatment of early gastric cancer in the western world. *World J Gastroenterol*. (2014) 20(19):5672–8. doi: 10.3748/wjg.v20.i19.5672

158. Sohrabi M, Nikkhah M, Sohrabi M, Farimani AR, Shahi MM, Ziaie H, et al. Evaluating tissue levels of the eight trace elements and heavy metals among esophagus and gastric cancer patients: A comparison between cancerous and non-cancerous tissues. *J Trace Elem Med Biol*. (2021) 68:126761. doi: 10.1016/j.jtemb.2021.126761

159. Tseng CH, Fang WL, Huang KH, Chen MH, Chao Y, Lo SS, et al. The clinicopathological characteristics and genetic alterations of mucinous carcinoma of the stomach. *J Chin Med Assoc*. (2020) 83(2):141–7. doi: 10.1097/JCMA.0000000000000232

160. Tang XH, Guo T, Wu XL, Gan XJ, Wang YD, Jia FZ, et al. Clinical significance and immune infiltration analyses of the cuproptosis-related human copper proteome in gastric cancer. *Biomolecules*. (2022) 12(10). doi: 10.3390/biom12101459

161. Yang PZ, Yang WT, Wei Z, Li Y, Yang YF, Wang JH, et al. Novel targets for gastric cancer: The tumor microenvironment (TME), N6-methyladenosine (m6A), pyroptosis, autophagy, ferroptosis and cuproptosis. *Biomedicine Pharmacother*. (2023) 163:114883. doi: 10.1016/j.biopha.2023.114883

162. Wang JY, Qin DM, Tao ZH, Wang BY, Xie YZ, Wang Y, et al. Identification of cuproptosis-related subtypes, construction of a prognosis model, and tumor microenvironment landscape in gastric cancer. *Front Immunol*. (2022) 13:1056932. doi: 10.3389/fimmu.2022.1056932

163. Li DB, Wang YH, Dong C, Chen T, Dong AQ, Ren JY, et al. CST1 inhibits ferroptosis and promotes gastric cancer metastasis by regulating GPX4 protein stability *via* OTUB1. *Oncogene*. (2023) 42(2):83–98. doi: 10.1038/s41388-022-02537-x

164. Luo ZW, He Z, Qin HC, Chen YS, Qi BJ, Lin JR, et al. Exercise-induced IL-15 acted as a positive prognostic implication and tumor-suppressed role in pan-cancer. *Front Pharmacol*. (2022) 13:1053137. doi: 10.3389/fphar.2022.1053137

165. Waidner B, Melchers K, Ivanov I, Loferer H, Bensch KW, Kist M, et al. Identification by RNA profiling and mutational analysis of the novel copper resistance determinants CrdA (HP1326), CrdB (HP1327), and CzcB (HP1328) in helicobacter pylori. *J Bacteriol*. (2002) 184(23):6700–8. doi: 10.1128/JB.184.23.6700-6708.2002

166. Allan E, Dorrell N, Foynes S, Anyim M, Wren BW. Mutational analysis of genes encoding the early flagellar components of helicobacter pylori: evidence for transcriptional regulation of flagellin a biosynthesis. *J Bacteriol*. (2000) 182(18):5274–7. doi: 10.1128/JB.182.18.5274-5277.2000

167. Miller RA, Britigan BE. Role of oxidants in microbial pathophysiology. *Clin Microbiol Rev*. (1997) 10(1):1–18. doi: 10.1128/CMR.10.1.1

168. Malmström BG, Leckner J. The chemical biology of copper. *Curr Opin Chem Biol*. (1998) 2(2):286–92. doi: 10.1016/s1367-5931(98)80071-9

169. Cuomo P, Papaianni M, Sansone C, Iannelli A, Iannelli D, Medaglia C. An in vitro model to investigate the role of helicobacter pylori in type 2 diabetes, obesity, alzheimer's disease and cardiometabolic disease. *Int J Mol Sci*. (2020) 21(21). doi: 10.3390/ijms21218369

170. McGuirl MA, Dooley DM. Copper-containing oxidases. *Curr Opin Chem Biol*. (1999) 3(2):138–44. doi: 10.1016/S1367-5931(99)80025-8

171. Ramchandani D, Berisa M, Tavarez DA, Li ZN, Miele M, Bai Y. Copper depletion modulates mitochondrial oxidative phosphorylation to impair triple negative breast cancer metastasis. *Nat Commun*. (2021) 12(1):7311. doi: 10.1038/s41467-021-27559-z

172. Matsunaga S, Nishiumi S, Tagawa R, Yoshida M. Alterations in metabolic pathways in gastric epithelial cells infected with helicobacter pylori. *Microb Pathog*. (2018) 124:122–9. doi: 10.1016/j.micpath.2018.08.033

173. Mongiat M, Monnot C, Muller L, Germain S. Extracellular matrix scaffolding in angiogenesis and capillary homeostasis. *Semin Cell Dev Biol*. (2019) 89:147–56. doi: 10.1016/j.semcdb.2018.08.007

174. Folkman J. Role of angiogenesis in tumor growth and metastasis. *Semin Oncol*. (2002) 29(6 Suppl 16):15–8. doi: 10.1053/sonc.2002.37263

175. McAuslan BR, Reilly W. Endothelial cell phagokinesis in response to specific metal ions. *Exp Cell Res*. (1980) 130(1):147–57. doi: 10.1016/0014-4827(80)90051-8

176. Ellis LM, Hicklin DJ. VEGF-targeted therapy: mechanisms of anti-tumour activity. *Nat Rev Cancer*. (2008) 8(8):579–91. doi: 10.1038/nrc2403

177. Harris ED. A requirement for copper in angiogenesis. *Nutr Rev*. (2004) 62 (2):60–4. doi: 10.1111/j.1753-4887.2004.tb00025.x

178. Nasulewicz A, Mazur A, Opolski A. Role of copper in tumour angiogenesis–clinical implications. *J Trace Elem Med Biol*. (2004) 18(1):1–8. doi: 10.1016/j.jtemb.2004.02.004

179. Badet J, Soncin F, J, Guitton D, Lamare O, Cartwright T, et al. Specific binding of angiogenin to calf pulmonary artery endothelial cells. *Proc Natl Acad Sci USA*. (1989) 86(21):8427–31. doi: 10.1073/pnas.86.21.8427

180. Soncin F, Guitton JD, Cartwright T, Badet J. Interaction of human angiogenin with copper modulates angiogenin binding to endothelial cells. *Biochem Biophys Res Commun*. (1997) 236(3):604–10. doi: 10.1006/bbrc.1997.7018

181. Baeriswyl V, Christofori G. The angiogenic switch in carcinogenesis. *Semin Cancer Biol*. (2009) 19(5):329–37. doi: 10.1016/j.semcancer.2009.05.003

182. He CM, Zhang H, Guo ZH, Mo ZJ. A cuproptosis-related signature for predicting the prognosis of gastric cancer. *J Gastrointest Oncol*. (2023) 14(1):146–64. doi: 10.21037/jgo-23-62

183. da Silva DA, Luca AD, Squitti R, Rongioletti M, Rossi L, Machado CML, et al. Copper in tumors and the use of copper-based compounds in cancer treatment. *J Inorg Biochem*. (2022) 226:111634. doi: 10.1016/j.jinorgbio.2021.111634

184. Grivennikov SI, Greten FR, Karin M. Immunity, inflammation, and cancer. *Cell*. (2010) 140(6):883–99. doi: 10.1016/j.cell.2010.01.025

185. Guo S, Deng CX. Effect of stromal cells in tumor microenvironment on metastasis initiation. *Int J Biol Sci*. (2018) 14(14):2083–93. doi: 10.7150/ijbs.25720

186. Roberts EW, Fearon DT. Stromal cells in the tumor microenvironment. *Adv Exp Med Biol*. (2018) 1060:99–114. doi: 10.1007/978-3-319-78127-3_6

187. Yang MY, Li JP, Gu P, X, Fan Q. The application of nanoparticles in cancer immunotherapy: Targeting tumor microenvironment. *Bioact Mater*. (2021) 6(7):1973–87. 10.1016/j.bioactmat.2020.12.010

188. Vesely MD, Kershaw MH, Schreiber RD, Smyth MJ. Natural innate and adaptive immunity to cancer. *Annu Rev Immunol*. (2011) 29:235–71. doi: 10.1146/annurev-immunol-031210-101324

189. Sang YJ, Deng QQ, Cao FF, Liu ZW, You YW, Liu H, et al. Remodeling macrophages by an iron nanotrap for tumor growth suppression. *ACS Nano*. (2021) 15 (12):19298–309. doi: 10.1021/acsnano.1c05392

190. Schwab A, Loeck T, Najder-Nalepa K. STIM2: Redox-sensor and effector of the (tumor) microenvironment. *Cell Calcium*. (2021) 94:102335. doi: 10.1016/j.ceca.2020.102335

191. Yang Y, Wang Y, Guo L, Gao W, Tang TL, Yan M. Interaction between macrophages and ferroptosis. *Cell Death Di*. (2022) 13(4):355. doi: 10.1038/s41419-022-04775-z

192. Zhao Q, Gong J, Li ZH, Wang JY, Zhang JL, Zhao ZF, et al. Target reprogramming lysosomes of CD8+ T cells by a mineralized metal-organic framework for cancer immunotherapy. *Adv Mater*. (2021) 33(17):e2100616. doi: 10.1002/adma.202100616

193. Eil R, Vodnala SK, Clever D, Klebanoff CA, Sukumar M, Pan JH, et al. Ionic immune suppression within the tumour microenvironment limits T cell effector function. *Nature*. (2016) 537(7621):539–43. 10.1038/nature19364

194. Paul MS, Ohashi PS. The roles of CD8(+) T cell subsets in antitumor immunity. *Trends Cell Biol*. (2020) 30(9):695–704. doi: 10.1016/j.tcb.2020.06.003

195. Bilotta MT, Antignani A, Fitzgerald DJ. Managing the TME to improve the efficacy of cancer therapy. *Front Immunol*. (2022) 13:954992. doi: 10.3389/fimmu.2022.954992

196. Panyi G, Beeton C, Felipe A. Ion channels and anti-cancer immunity. *Philos Trans R Soc Lond B Biol Sci*. (2014) 369(1638):20130106. doi: 10.1098/rstb.2013.0106

197. Cai XC, Bao XG. Metal-organic framework (MOF)-based Drug/Cargo delivery and cancer therapy. *Adv Mater*. (2017) 29(23). doi: 10.1002/adma.201606134

198. Fei WD, Zhang M, Fan XY, Ye YQ, Zhao MD, Zheng CH, et al. Engineering of bioactive metal sulfide nanomaterials for cancer therapy. *J Nanobiotechnology*. (2021) 19(1):93. doi: 10.1186/s12951-021-00839-y

199. Zhao HY, Achreja A, Iessi E, Logozzi M, Mizzoni D, Raimo RD, et al. The key role of extracellular vesicles in the metastatic process. *Biochim Biophys Acta Rev Cancer*. (2018) 1869(1):64–77. doi: 10.1016/j.bbcan.2017.11.005

200. Voli F, Valli E, Lerra LG, Kimpton K, Saletta F, Giorgi FM, et al. Intratumoral copper modulates PD-L1 expression and influences tumor immune evasion. *Cancer Res*. (2020) 80(19):4129–44. doi: 10.1158/0008-5472.CAN-20-0471

201. Ayati N, Lee ST, Zakavi SR, Cheng M, Lau WFE, Parakh S, et al. Response evaluation and survival prediction after PD-1 immunotherapy in patients with non-small cell lung cancer: Comparison of assessment methods. *J Nucl Med*. (2021) 62 (7):926–33. doi: 10.2967/jnumed.120.254508

202. Festaand DJ, Thiele RA. Copper at the front line of the host-pathogen battle. *PloS Pathog*. (2012) 8(9):e1002887. doi: 10.1371/journal.ppat.1002887

203. Bull PC, Cox DW. Wilson disease and menkes disease: new handles on heavy-metal transport. *Trends Genet*. (1994) 10(7):246–52. doi: 10.1016/0168-9525(94)90172-4

204. Fridlender G, Sun J, Kim S, Kapoor V, Cheng GJ, Ling L, et al. Polarization of tumor-associated neutrophil phenotype by TGF-beta: "N1" versus "N2" TAN. *Cancer Cell*. (2009) 16(3):183–94. doi: 10.1016/j.ccr.2009.06.017

205. White C, Lee J, Kambe T, Fritsche K, Petris MJ, et al. A role for the ATP7A copper-transporting ATPase in macrophage bactericidal activity. *J Biol Chem*. (2009) 284(49):33949–56. doi: 10.1074/jbc.M109.070201

206. Wang LZ, Cao Y, Guo W, Xu JY. High expression of cuproptosis-related gene FDX1 in relation to good prognosis and immune cells infiltration in colon adenocarcinoma (COAD). *J Cancer Res Clin Oncol*. (2023) 149(1):15–24. doi: 10.1007/s00432-022-04382-7

207. Jiang L, Liao JZ, Han YW. Study on the role and pharmacology of cuproptosis in gastric cancer. *Front Oncol*. (2023) 13:1145446. doi: 10.3389/fonc.2023.1145446

208. Rajendrakumar SK, Uthaman S, Cho CS, Park IK. Nanoparticle-based phototriggered cancer immunotherapy and its domino effect in the tumor microenvironment. *Biomacromolecules*. (2018) 19(6):1869–87. doi: 10.1021/acs.biomac.8b00460

209. Musetti S, Huang L. Nanoparticle-mediated remodeling of the tumor microenvironment to enhance immunotherapy. *ACS Nano*. (2018) 12(12):11740–55. doi: 10.1021/acsnano.8b05893

210. Wang L, Saci A, Szabo PM, Chasalow SD, Martin MC, Domenech JD, et al. EMT- and stroma-related gene expression and resistance to PD-1 blockade in urothelial cancer. *Nat Commun*. (2018) 9(1):3503. doi: 10.1038/s41467-018-05992-x

211. Aubert L, Nandagopal N, Steinhart Z, Lavoie G, Nourreddine S, Berman J, et al. Copper bioavailability is a KRAS-specific vulnerability in colorectal cancer. *Nat Commun*. (2020) 11(1):3701. doi: 10.1038/s41467-020-17549-y

212. Liu X, Zhang ZZ, Zhao G. Recent advances in the study of regulatory T cells in gastric cancer. *Int Immunopharmacol*. (2019) 73:560–7. doi: 10.1016/j.intimp.2019.05.009

213. Chen GM, Luo DQ, Qi XJ, Li DY, Zheng JY, Luo Y, et al. Characterization of cuproptosis in gastric cancer and relationship with clinical and drug reactions. *Front Cell Dev Biol*. (2023) 11:1172895. doi: 10.3389/fcell.2023.1172895

214. Padua D, Massagué J. Roles of TGFbeta in metastasis. *Cell Res*. (2009) 19(1):89–102. doi: 10.1038/cr.2008.316

215. Melzer C, Hass R, Ohe J, Lehnert H, Ungefroren H. The role of TGF-β and its crosstalk with RAC1/RAC1b signaling in breast and pancreas carcinoma. *Cell Commun Signal*. (2017) 15(1):19. doi: 10.1186/s12964-017-0175-0

216. Hanahan D, Weinberg RA. Hallmarks of cancer: the next generation. *Cell*. (2011) 144(5):646–74. doi: 10.1016/j.cell.2011.02.013

217. Cell editorial team cancer: The road ahead. (2017) 168(4):545–6. doi: 10.1016/j.cell.2017.01.036

218. Wang YQ. Breast cancer metastasis driven by ErbB2 and 14-3-3zeta: A division of labor. *Cell Adh Migr*. (2010) 4(1):7–9. doi: 10.4161/cam.4.1.10497

219. Oudin MJ, Weaver VM. Physical and chemical gradients in the tumor microenvironment regulate tumor cell invasion, migration, and metastasis. *Cold Spring Harb Symp Quant Biol*. (2016) 81:189–205. doi: 10.1101/sqb.2016.81.030817

220. Lymburner S, McLeod S, Purtzki M, Roelley C, Xu ZM. Zinc inhibits magnesium-dependent migration of human breast cancer MDA-MB-231 cells on fibronectin. *J Nutr Biochem*. (2013) 24(6):1034–40. doi: 10.1016/j.jnutbio.2012.07.013

221. Bhuvanasundar R, John A, Sulochana KN, Coral K, Deepa PR, Umashankar V, et al. A molecular model of human lysyl oxidase (LOX) with optimal copper orientation in the catalytic cavity for induced fit docking studies with potential modulators. *Bioinformation*. (2014) 10(7):406–12. doi: 10.6026/97320630010406

222. Erler JT, Bennewith KL, Cox TR, Lang G, Bird D, Koong A, et al. Hypoxia-induced lysyl oxidase is a critical mediator of bone marrow cell recruitment to form the premetastatic niche. *Cancer Cell*. (2009) 15(1):35–44. doi: 10.1016/j.ccr.2008.11.012

223. Gacheru SN, Trackman PC, Shah MA, CY, Spacciapoli P, Greenaway FT, et al. Structural and catalytic properties of copper in lysyl oxidase. *J Biol Chem*. (1990) 265 (31):19022–7.

224. MacDonald G, Nalvarte I, Smirnova T, Vecchi M, Aceto N, Dolemeyer A, et al. Memo is a copper-dependent redox protein with an essential role in migration and metastasis. *Sci Signal*. (2014) 7(329):ra56. doi: 10.1126/scisignal.2004870

225. Karamanos NK, Piperigkou Z, Passi A, Götte M, Rousselle P, Vlodavsky I, et al. Extracellular matrix-based cancer targeting. *Trends Mol Med*. (2021) 27(10):1000–13. doi: 10.1016/j.molmed.2021.07.009

226. Majumder S, Chatterjee S, Pal S, Biswas J, Efferth T, Choudhuri SK, et al. The role of copper in drug-resistant murine and human tumors. *Biometals*. (2009) 22 (2):377–84. doi: 10.1007/s10534-008-9174-3

227. Jin J, Ma MJ, Shi SH, Wang JR, Xiao PY, Yu HF, et al. Copper enhances genotoxic drug resistance *via* ATOX1 activated DNA damage repair. *Cancer Lett*. (2022) 536:215651. doi: 10.1016/j.canlet.2022.215651

228. Shanbhag VC, Gudekar N, Jasmer K, Papageorgiou C, Singh K, Petris MJ, et al. Copper metabolism as a unique vulnerability in cancer. *Biochim Biophys Acta Mol Cell Res*. (2021) 1868(2):118893. doi: 10.1016/j.bbamcr.2020.118893

229. Wang YM, Chen YM, Zhang JJ, Yang YH, Fleishman JS, Wang Y, et al. Cuproptosis: A novel therapeutic target for overcoming cancer drug resistance. *Drug Resist Update*. (2024) 72:101018. doi: 10.1016/j.drup.2023.101018

230. Lu Y, Pan QQ, Gao WX, Pu YJ, He B, et al. Reversal of cisplatin chemotherapy resistance by glutathione-resistant copper-based nanomedicine via cuproptosis. *J Mater Chem B*. (2022) 10(33):6296–306. doi: 10.1039/d2tb01150f

231. Yang WC, Wang YX, Huang YZ, Yu JX, Wang T, Li CG, et al. 4-octyl itaconate inhibits aerobic glycolysis by targeting GAPDH to promote cuproptosis in colorectal cancer. *BioMed Pharmacother*. (2023) 159:114301. doi: 10.1016/j.biopha.2023.114301

232. Xu YZ, Liu SY, Zeng LL, Ma HS, Zhang YF, Yang HH, et al. An enzyme-engineered nonporous Copper(I) coordination polymer nanoplatform for cuproptosis-based synergistic cancer therapy. *Adv Mater*. (2023) 35(13):e2300773. doi: 10.1002/adma.202300773

233. Baah E. Analysis of data on adverse drug events reported to the food and drugs administration of the United States of America. *Open J Stat*. (2020) 10 (02):203–27. doi: 10.4236/ojs.2020.102015

234. Feng L, Li GX, Li DB, Duan GQ, Liu J. Cuproptosis-related gene SERPINE1 is a prognostic biomarker and correlated with immune infiltrates in gastric cancer. *J Cancer Res Clin Oncol*. (2023) 149(12):10851–65. doi: 10.1007/s00432-023-04900-1

235. Li J, Yu T, Sun J, Zeng ZY, Liu Z, Ma MW, et al. Comprehensive analysis of cuproptosis-related immune biomarker signature to enhance prognostic accuracy in gastric cancer. *Aging (Albany NY)*. (2023) 15(7):2772–96. doi: 10.18632/aging.204646

236. Zhang ZQ, Shao SH, Luo H, Sun WW, Wang JJ, Yin HQ, et al. The functions of cuproptosis in gastric cancer: therapy, diagnosis, prognosis. *Biomedicine Pharmacother*. (2024) 177:117100. doi: 10.1016/j.biopha.2024.117100

237. Wang L, Xiao K, Dong ZG, Meng T, Cheng XW, Xu YH, et al. A novel copper-induced cell death-related lncRNA prognostic signature associated with immune infiltration and clinical value in gastric cancer. *J Cancer Res Clin Oncol*. (2023) 149 (12):10543–59. doi: 10.1007/s00432-023-04916-7c

238. Nose Y, Wood LK, Kim BE, Prohaska JR, Fry RS, Spears JW, et al. Ctr1 is an apical copper transporter in mammalian intestinal epithelial cells *in vivo* that is controlled at the level of protein stability. *J Biol Chem*. (2010) 285(42):32385–92. doi: 10.1074/jbc.M110.143826

frontiers | Frontiers in Immunology

TYPE Review
PUBLISHED 01 November 2024
DOI 10.3389/fimmu.2024.1476436

Check for updates

OPEN ACCESS

EDITED BY
Jiaheng Xie,
Central South University, China

REVIEWED BY
Yuxuan Song,
Peking University People's Hospital, China
Kok-Siong Chen,
Brigham and Women's Hospital and Harvard Medical School, United States
Qihang Yuan,
Dalian Medical University, China

*CORRESPONDENCE
Yanhui Liu
liuyh@scu.edu.cn

RECEIVED 05 August 2024
ACCEPTED 16 October 2024
PUBLISHED 01 November 2024

CITATION
Liu J, Peng J, Jiang J and Liu Y (2024) Clinical immunotherapy in glioma: current concepts, challenges, and future perspectives.
Front. Immunol. 15:1476436.
doi: 10.3389/fimmu.2024.1476436

COPYRIGHT
© 2024 Liu, Peng, Jiang and Liu. This is an open-access article distributed under the terms of the Creative Commons Attribution License (CC BY). The use, distribution or reproduction in other forums is permitted, provided the original author(s) and the copyright owner(s) are credited and that the original publication in this journal is cited, in accordance with accepted academic practice. No use, distribution or reproduction is permitted which does not comply with these terms.

Clinical immunotherapy in glioma: current concepts, challenges, and future perspectives

Jun Liu[1,2], Jingjian Peng[2], Jian Jiang[2] and Yanhui Liu[1]*

[1]Department of Neurosurgery, West China Hospital, Sichuan University, Chengdu, Sichuan, China, [2]Department of Neurosurgery, Jiujiang No. 1 People's Hospital, Jiujiang, China

Glioma is one of the common tumors in the central nervous system, and its treatment methods (surgery, radiotherapy, and chemotherapy) lack specificity and have a poor prognosis. With the development of immunology, cell biology, and genomics, tumor immunotherapy has ushered in a new era of tumor therapy, achieving significant results in other invasive cancers such as advanced melanoma and advanced non-small cell lung cancer. Currently, the clinical trials of immunotherapy in glioma are also progressing rapidly. Here, this review summarizes promising immunotherapy methods in recent years, reviews the current status of clinical trials, and discusses the challenges and prospects of glioma immunotherapy.

KEYWORDS

immunotherapy, gliomas, tumor vaccines, immune checkpoint inhibitors, CAR-T, oncolytic virotherapy

Introduction

Glioma refers to a tumor originating from glial cells and is the most common primary tumor in the central nervous system (1). Glioma, with an incidence of 6.6/100,000 of which about half were glioblastomas (1), accounts for almost 90% of all malignant brain and other central nervous system tumors (2). The incidence of glioma increases with age (3), and the incidence of glioblastoma was highest in males, persons aged more than 65 years, and non-Hispanic White (2). The symptoms of glioma depend on their location, size, type, and growth rate. Glioma treatment usually begins with surgery and is followed by radiation therapy, chemotherapy, and targeted therapy. However, most patients are not sensitive to traditional treatment and have a poor prognosis. Available treatment options include second-line surgery, radiotherapy, alkylating agent chemotherapy, and bevacizumab therapy. Unfortunately, once progression or recurrence occurs, the median overall survival (OS) is only 6 to 9 months. Therefore, there is an urgent need for new therapeutic strategies to treat recurrent GBM (4). With the advancement of immunology, cell biology, and molecular biology, tumor immunotherapy has ushered in a new era of

cancer treatment (5). Immunotherapy as a new treatment method may be beneficial for delaying glioma recurrence and improving the therapeutic effect of glioma. Recently, immunotherapy has achieved some exciting and encouraging results even though there are still many challenges in practical clinical applications. A deeper understanding of the biology and immune microenvironment, along with the development of new therapeutic combinations, may potentially change the current challenges faced by immunotherapy in GBM. We provide a review of the current status and new developments in immunotherapy, including tumor vaccines, immune checkpoint inhibitors, chimeric antigen receptor T cells (CAR-T), and oncolytic virotherapy, for glioma (Figure 1).

Tumor vaccines

The use of vaccines to treat confirmed malignant tumors can be traced back to 1910s and 1950s (6). Tumor vaccines can utilize the adaptive immune system to produce tumor-specific antibodies and thereby exert anti-tumor effects (7), mainly divided into peptide vaccine, dendritic cell vaccine, and tumor neoantigen vaccine (8) (Figure 2).

Peptide vaccine

Peptide vaccine is a vaccine made by artificially synthesizing protective short peptides in the amino acid sequence of natural proteins, connecting them with carriers, and adding adjuvants. A phase I clinical study conducted in Japan indicated that WT1 peptide vaccine induced WT1-specific CD8+ T cells and CD4+ T cells and was tolerable in patients with WT1+ malignant glioma (9), and the phase II clinical trial further showed WT1 peptide vaccine was safe and produced a clinical response in patients with WT1/HLA-A*2402 + recurrent glioblastoma multiforme (10). During the administration of the WT1 peptide vaccine, the maintenance of WT1 expression in tumor cells is significantly associated with a longer progression free and overall survival (11). ACT IV, a randomized, double-blind, phase 3 study done conducted in 22 countries, was terminated prematurely due to the significant adverse events and ineffectiveness on overall survival for rindopepimut (a vaccine targeting EGFRvIII) in newly diagnosed EGFRvIII+ glioblastoma patients who underwent maximal surgical resection and completed standard radiotherapy with concomitant temozolomide (12). However, another phase II, multicenter, prospective trial completed in American indicated that the toxicity of PEPvIII-KLH (another vaccine targeting EGFRvIII) was generally minimal in adults with newly diagnosed EGFRvIII+ glioblastoma patients who underwent maximal surgical resection and completed standard radiotherapy with concomitant temozolomide and the overall survival of patients with EGFRvIII specific antibody response was longer than that of patients without, and there was still a statistical difference after adjusting for factors such as age, Karnofsky performance status, and methylguanine methyltransferase methylation (13). ReACT, a double-blind, randomized, phase II study done in American, further confirmed the potential of rindopepimut for targeted immunotherapy among patients with recurrent EGFRvIII+ glioblastoma (14). Neurooncology Working

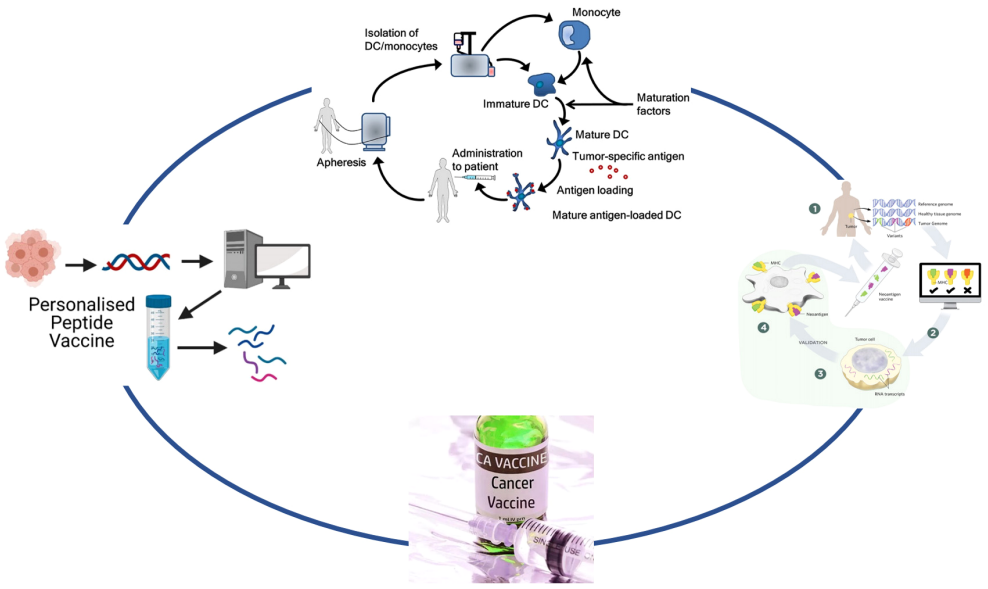

FIGURE 1
Strategies to overcome gliomas. The diagram illustrates various immunotherapy strategies for targeting and eliminating cancer cells. On the left, cancer vaccines stimulate an immune response, while immune checkpoint inhibitors like Ipilimumab, Nivolumab, Pembrolizumab, and Cemiplimab block the PD-1 pathway to activate T-cells. PD-L1 inhibitors such as Atezolizumab, Durvalumab, and Avelumab further promote the killing of cancer cells by preventing cancer cells from evading immune detection. CAR-T cell therapy is depicted, showing how T-cells are engineered with a chimeric antigen receptor (CAR) to directly attack tumor cells. Oncolytic viruses are also represented, illustrating their role in selectively infecting and destroying cancer cells.

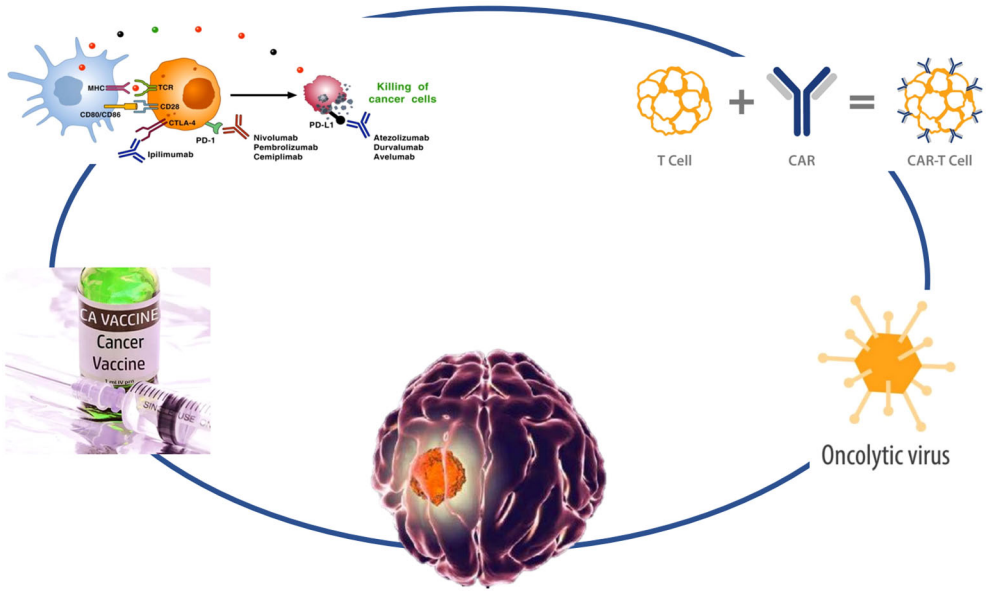

FIGURE 2
Classification of tumor vaccines. This diagram illustrates two personalized immunotherapy approaches for cancer: peptide vaccines and dendritic cell (DC) therapy. On the left, the process of creating a personalized peptide vaccine begins with the identification of tumor-specific antigens from the patient's tumor cells, followed by the generation of a peptide vaccine tailored to the patient. On the right, dendritic cell therapy involves isolating monocytes from the patient, differentiating them into immature DCs, and loading them with tumor-specific antigens. These mature antigen-loaded DCs are then reintroduced into the patient to stimulate an immune response.

Group of the German Cancer Society trial 16 (NOA-16), a non-controlled, open-label, single-arm, multicenter, first-in-humans phase I trial conducted in Germany, demonstrated that IDH1 (R132H)-specific peptide vaccine (IDH1-vac) prolonged the pseudoprogression and survival time of patients with IDH1 (R132H)+, non-1p/19q co-deleted, ATRX– World Health Organization (WHO) grade 3 and 4 gliomas and the vaccine-related adverse events were restricted to grade 1 (15). Moreover, the new antigen IDH1 (R132H) is immunogenic across multiple HLA alleles and effectively induced an IDH1-specific immune response (15). MultIceNTER Phase I Peptide VaCcine Trial for the Treatment of H3-Mutated Gliomas (INTERCEPT-H3), a non-controlled, open-label, single arm, multicenter phase I trial done in Germany, showed that H3K27M-specific long peptide vaccine (H3K27M-vac) induced neoepitope-specific CD4+ T cell-dominated colocalization immune responses with HLA class II-DR in patients with newly diagnosed H3K27M diffuse midline gliomas and these patients with immune responses showed radiographic improvement (16).

Dendritic cell vaccine

Dendritic cell vaccine is a vaccine that utilizes the patient's own dendritic cells to activate the immune system and enhance its ability to attack tumor cells. The main function of dendritic cells is to initiate and activate the recognition and response of initial T cells to protein antigens, present viral and tumor antigens. It is the only dedicated antigen presenting cell that can directly activate initial T cells. Several phase I clinical trials found that three biweekly intradermal administration of autologous tumor lysate-pulsed dendritic cell vaccine among malignant glioma patients elicited antigen-specific systemic and intracranial cytotoxic and memory T-cell infiltration (17–19). A later phase I/II clinical study done in Japan showed the safety and clinical response of autologous tumor lysate-pulsed dendritic cell therapy for patients with malignant glioma (20, 21). A phase 3 randomized, double-blinded, placebo-controlled clinical trial conducted in the American, Canada, Germany, and the United Kingdom showed that addition of autologous tumor lysate-pulsed dendritic cell vaccine (DCVax®-L) to standard therapy was feasible and safe in newly diagnosed or recurrent glioblastoma patients and extended progression free survival and overall survival (22, 23). A randomized, double-blind, multicenter phase II placebo-controlled study found autologous tumor lysate-pulsed dendritic cell vaccine (ICT-107) improved progression free survival and maintained quality of life in recurrent glioma patients (24). A single-arm phase 2 clinical trial completed in American indicated that the Aivita glioblastoma vaccine (AV-GBM-1) was well-tolerated and extended the median progression free survival with numerous treatment-emergent central nervous system adverse events (25). A single-center, randomized, open-label multi-arm phase II clinical trial conducted in American indicated that combining autologous tumor lysate-pulsed dendritic cell vaccine with poly-ICLC, a Toll-like receptor agonist, induced a polarized interferon activation in circulating monocytes and CD8+ T cells, which may represent an important blood biomarker for immunotherapy in patients with newly-diagnosed or recurrent WHO Grade III-IV malignant gliomas (26). There are different variants for dendritic cell vaccine. The cytomegalovirus-specific dendritic cell vaccine patients improved long-term progression free

survival and overall survival in patients with newly diagnosed glioblastoma (27) and pre-conditioning the cytomegalovirus-specific dendritic cell vaccine site with a potent recall antigen significantly improves the lymph node homing and efficacy of vaccine (28), later sequential clinical trials utilizing cytomegalovirus-specific dendritic cell vaccine associated with extended overall survival for newly diagnosed glioblastoma (29). The other one is autologous dendritic cell vaccine pulsed with lysate derived from an allogeneic stem-like cell line, which was safe and well tolerated in newly diagnosed and recurrent glioblastoma (30).

Tumor neoantigen vaccine

Neoantigen originates from tumor specific protein coding mutations and is not affected by central tolerance. It can generate strong immune responses and act as an unquestionable antigen to promote tumor rejection (31) (Table 1, Supplementary Figure 1). Single-cell T cell receptor analysis of phase I/Ib study involving personalized neoantigen-targeting vaccines for patients with newly diagnosed glioblastoma demonstrated neoantigen-specific T cells from the peripheral blood can migrate into intracranial glioblastoma (32). NeoVax, a personalized neoantigen-targeting vaccine, significantly increased neoantigen-specific effector T cells in newly diagnosed glioblastoma patients (33). These encouraging results contribute to the development of future clinical trials for glioma patients based on neoantigen vaccines.

Immune checkpoint inhibitors

Immune checkpoint inhibitors, including programmed cell death 1 (PD-1)/programmed cell death ligand 1 (PD-L1) and cytotoxic T lymphocyte-associated antigen 4 (CTLA-4), are important immunosuppressive targets for tumor escape (34) (Table 2, Supplementary Figure 2). The PD-1/PD-L1 axis promotes glioma tumor growth and invasion (35). CheckMate 143 confirmed the safety and tolerability of nivolumab in patients with newly diagnosed glioblastoma, median overall survival with nivolumab was 33.38 (16.2 to not estimable) and 16.49 (12.94-22.08) months in patients with methylated and unmethylated MGMT promoter, respectively (36). Later CheckMate 143 demonstrated median overall survival with nivolumab and bevacizumab was 9.8 (8.2-11.8) and 10.0 (9.0-11.8) months, respectively, in recurrent glioblastoma population, the objective response rate was 7.8% (4.1%-13.3%) and 23.1% (16.7%-30.5%) with nivolumab and with bevacizumab, respectively (37). Given the potential benefits of nivolumab for methylated patients, CheckMate 548 has emerged. However, CheckMate 548 did not achieve the primary endpoints with the median overall survival with nivolumab and placebo was 28.9 (24.4-31.6) and 32.1 (29.4-33.8) months, respectively, and the median progression free survival with nivolumab and placebo was 10.6 (8.9-11.8) and 10.3 (9.7-12.5) months, respectively (38). The above studies are all aimed at the basic treatment of simultaneous radiotherapy and temozolomide chemotherapy, while CheckMate 498 compared nivolumab with temozolomide chemotherapy on the basis of radiotherapy. The median overall survival with nivolumab and temozolomide chemotherapy was 13.4 (12.6-14.3) and 14.9 (13.3-16.1) months, respectively (hazard ratio =1.31 (1.09-1.58), P = 0.0037), and the median progression free survival with nivolumab and temozolomide chemotherapy was 6.0 (5.7-6.2) and 6.2 (5.9-6.7) months, respectively, in patients with newly diagnosed glioblastoma with unmethylated MGMT promoter (39). Changes in the immune status of gliomas may affect the patient's responsiveness to anti-PD-1 immunotherapy (nivolumab or pembrolizumab) (40). Resectable glioblastoma tumor tissue pre- and post-nivolumab dosing resulted in higher immune cell infiltration, enhanced chemokine transcripts, and augmented T cell receptor clonal diversity, supporting a local immunomodulatory effect of treatment (41). Recurrent glioblastoma patients receiving neoadjuvant pembrolizumab had significantly extended overall survival, pembrolizumab was associated with upregulated T cell- and interferon-γ-related gene expression as well as downregulated cell-cycle-related gene expression, which enhancing both the intratumoral and systemic immune responses (42). The median survival of responders was longer than non-responders to neoadjuvant nivolumab or pembrolizumab in a retrospective analysis, MAPK pathway alterations were enriched in responders while PTEN mutations associated with immunosuppressive signature from CD44 + tumor cells were enriched in non-responders, and immune infiltration that reflect the tumor's clonal evolution during treatment (43). Following 10 mg nivolumab intravenously administration, 27 recurrent glioblastoma patients underwent a maximal safe resection, followed by 10 mg ipilimumab or 5mg ipilimumab plus 10 mg nivolumab injection. The overall survival was better compared with historical cohorts (Belgian and GliAvAx trials) (44). CheckMate 908 investigated nivolumab and nivolumab plus ipilimumab in pediatric patients with high-grade central nervous system malignancies. The median overall survival with nivolumab and nivolumab plus ipilimumab was 1.7 (10.3-16.5) and 10.8 (9.1-15.8) months, respectively, in newly diagnosed diffuse intrinsic pontine glioma and the median progression free survival with nivolumab and nivolumab plus ipilimumab was 1.7 (1.4-2.7) and 1.3 (1.2-1.5) months, respectively, in high-grade glioma; 1.4 (1.2-1.4) and 2.8 (1.5-4.5) months, respectively, in medulloblastoma; 1.4 (1.4-2.6) and 4.6 (1.4-5.4) months in ependymoma; 1.2 (1.1-1.3) and 1.6 (1.3-3.5) months, respectively, in other recurrent/progressive central nervous system tumors (45). Bevacizumab could enhance the tolerability and efficacy of pembrolizumab in patients with recurrent high-grade gliomas receiving hypofractionated stereotactic irradiation. The median overall survival of bevacizumab-naïve and bevacizumab-resistant patients was 13.45 (9.46-18.46) and 9.3 (8.97-18.86) months, respectively, and the progression free survival was 7.92 (6.31-12.45) and 6.54 (5.95-18.86) months, respectively (46). Isatuximab plus atezolizumab had acceptable safety and tolerability and reduced CD38+ immune cells in the glioblastoma microenvironment (47).

TABLE 1 Some trials of tumor vaccines in glioma.

Trial	Participants	Sample size	Intervention	Study design	Results	Reference
	WT1+ malignant glioma	14	WT1 vaccine	phase I clinical study	Eleven of the 14 patients completed WT1 vaccination for 6 weeks, while 3 patients dropped out earlier due to disease progression. All patients showed grade I level of skin disorders at the injection sites. No grade III/IV toxicity or dose-limiting toxicity was observed for any dose of WT1 HLA class II peptide. Six of the 14 patients had stable disease at 6 weeks. Median OS and 1-year OS rates were 24.7 weeks and 36%, respectively.	(9)
	WT1/HLA-A*2402-positive recurrent glioblastoma multiforme	21	WT1 vaccine	phase II clinical trial	The protocol was well tolerated; only local erythema occurred at the WT1 vaccine injection site. The clinical responses were as follows: partial response in 2 patients, stable disease in 10 patients, and progressive disease in 9 patients. No patient had a complete response. The overall response rate (cases with complete or partial response) was 9.5%, and the disease control rate (cases with complete or partial response as well as those in which disease was stable) was 57.1%. The median progression-free survival (PFS) period was 20.0 weeks, and the 6-month (26-week) PFS rate was 33.3%.	(10)
ACT IV, NCT01480479	newly diagnosed EGFRvIII+ glioblastoma	405	Rindopepimut	randomized, double-blind, phase 3 study	There was no significant difference in overall survival for patients with MRD: median overall survival was 20·1 months (95% CI 18·5-22·1) in the rindopepimut group versus 20·0 months (18·1-21·9) in the control group (HR 1·01, 95% CI 0·79-1·30; p=0·93). The most common grade 3-4 adverse events for all 369 treated patients in the rindopepimut group versus 372 treated patients in the control group were: thrombocytopenia (32 [9%] vs 23 [6%]), fatigue (six [2%] vs 19 [5%]), brain oedema (eight [2%] vs 11 [3%]), seizure (nine [2%] vs eight [2%]), and headache (six [2%] vs ten [3%]). Serious adverse events included seizure (18 [5%] vs 22 [6%]) and brain oedema (seven [2%] vs 12 [3%]). 16 deaths in the study were caused by adverse events (nine [4%] in the rindopepimut group and seven [3%] in the control group), of which one-a pulmonary embolism in a 64-year-old male patient after 11 months of treatment-was assessed as potentially related to rindopepimut.	(12)
	newly diagnosed EGFRvIII+ glioblastoma	35	PEPvIII-KLH	phase II, multicenter, prospective trial	There were no symptomatic autoimmune reactions. The 6-month PFS rate after vaccination was 67% (95% CI, 40% to 83%) and after diagnosis was 94% (95% CI, 67% to 99%; n = 18). The median OS was 26.0 months (95% CI, 21.0 to 47.7 months). After adjustment for age and Karnofsky performance status, the OS of vaccinated patients was greater than that observed in a control group matched for eligibility criteria, prognostic factors, and temozolomide treatment (hazard ratio, 5.3; P = .0013; n = 17). The development of specific antibody (P = .025) or delayed-type hypersensitivity (P = .03) responses to EGFRvIII had a significant effect on OS. At recurrence, 82% (95% CI, 48% to 97%) of patients had lost EGFRvIII expression (P <.001).	(13)
ReACT, NCT01498328	relapsed, EGFRvIII + glioblastoma	73	Rindopepimut	double-blind, randomized, phase II study	Rindopepimut toxicity included transient, low-grade local reactions. As primary endpoint, PFS6 was 28% (10/36) for rindopepimut compared with 16% (6/37) for control (P = 0.12, one-sided). Secondary and exploratory endpoints also favored the rindopepimut group including a statistically significant survival advantage [HR, 0.53; 95% confidence interval (CI), 0.32-0.88; two-sided log-rank P = 0.01], a higher ORR [30% (9/30) vs. 18% (6/34; P = 0.38)], median duration of response [7.8 months (95% CI, 3.5-22.2) vs. 5.6 (95% CI, 3.7-7.4)], and ability to discontinue steroids for ≥6 months [33% (6/18) vs. 0% (0/19)]. Eighty percent of rindopepimut-treated patients achieved robust anti-EGFRvIII titers (≥1:12,800), which were associated with prolonged survival (HR = 0.17; 95% CI, 0.07-0.45; P < 0.0001).	(14)

(Continued)

10.3389/fimmu.2024.1476436

TABLE 1 Continued

Trial	Participants	Sample size	Intervention	Study design	Results	Reference
NOA-16, NCT02454634	IDH1(R132H)+, non-1p/19q co-deleted, ATRX– WHO grade 3 and 4 gliomas	33	IDH1-vac	non-controlled, open-label, single-arm, multicenter, first-in-humans phase I trial	The trial met its primary safety endpoint, with vaccine-related adverse events restricted to grade 1. Vaccine-induced immune responses were observed in 93.3% of patients across multiple MHC alleles. Three-year progression-free and death-free rates were 0.63 and 0.84, respectively. Patients with immune responses showed a two-year progression-free rate of 0.82. Two patients without an immune response showed tumour progression within two years of first diagnosis.	(15)
INTERCEPT-H3, NCT04808245	newly diagnosed K27M-mutant histone-3.1 (H3.1K27M) or histone-3.3 (H3.3K27M) diffuse midline gliomas	8	H3K27M-vac	active multicenter, phase I clinical trial	Repeat vaccinations with H3K27M-vac were safe and induced CD4+ T cell-dominated, mutation-specific immune responses in five of eight patients across multiple human leukocyte antigen types. Median progression-free survival after vaccination was 6.2 months and median overall survival was 12.8 months.	(16)
	recurrent malignant glioma	24	autologous tumor lysate-pulsed dendritic cell vaccine	phase I/II clinical study	The protocols were well tolerated with only local redness and swelling at the injection site in several cases. Clinical responses were as follows: 1 patient with partial response, 3 patients with minor response, 10 patients with stable disease, and 10 patients with progressive disease. The patients whose dendritic cells were matured with OK-432 had longer survival times than the dendritic cells from patients without OK-432 maturation. The patients with both intratumoral and intradermal administrations had a longer survival time than the patients with intradermal administration only. Increased ELISPOT and delayed-type hypersensitivity responses after vaccination could provide good laboratory markers to predict the clinical outcome of patients receiving dendritic cell vaccination. The overall survival of patients with grade 4 glioma was 480 days, which was significantly better than that in the control group.	(20)
NCT00045968	newly diagnosed or recurrent glioblastoma	331	DCVax®-L	phase 3 randomized, double-blinded, placebo-controlled clinical trial	Median OS (mOS) for the 232 patients with nGBM receiving DCVax-L was 19.3 (95% CI, 17.5-21.3) months from randomization (22.4 months from surgery) vs 16.5 (95% CI, 16.0-17.5) months from randomization in control patients (HR = 0.80; 98% CI, 0.00-0.94; P = .002). Survival at 48 months from randomization was 15.7% vs 9.9%, and at 60 months, it was 13.0% vs 5.7%. For 64 patients with rGBM receiving DCVax-L, mOS was 13.2 (95% CI, 9.7-16.8) months from relapse vs 7.8 (95% CI, 7.2-8.2) months among control patients (HR, 0.58; 98% CI, 0.00-0.76; P <.001). Survival at 24 and 30 months after recurrence was 20.7% vs 9.6% and 11.1% vs 5.1%, respectively. Survival was improved in patients with nGBM with methylated MGMT receiving DCVax-L compared with external control patients (HR, 0.74; 98% CI, 0.55-1.00; P = .03).	(22, 23)
NCT 01280552	newly diagnosed glioblastoma	124	ICT-107	randomized, double-blind, multicenter phase II placebo-controlled study	ICT-107 was well tolerated, with no difference in adverse events between the treatment and control groups. The primary endpoint, median overall survival (OS), favored ICT-107 by 2.0 months in the intent-to-treat (ITT) population but was not statistically significant. Progression-free survival (PFS) in the ITT population was significantly increased in the ICT-107 cohort by 2.2 months (P = 0.011). The frequency of HLA-A2 primary tumor antigen expression was higher than that for HLA-A1 patients, and HLA-A2 patients had higher immune response (via Elispot). HLA-A2 patients achieved a meaningful therapeutic benefit with ICT-107, in both the MGMT methylated and unmethylated prespecified subgroups, whereas only HLA-A1 methylated patients had an OS benefit.	(24)

(Continued)

10.3389/fimmu.2024.1476436

TABLE 1 Continued

Trial	Participants	Sample size	Intervention	Study design	Results	Reference
NCT03400917	newly diagnosed glioblastoma	63	AV-GBM-1	single-arm phase 2 clinical trial	Success rates were 97% for both TIC production and monocyte collection. AV-GBM-1 was manufactured for 63/63 patients; 60 enrolled per ITT; 57 started AV-GBM-1. The most common AEs attributed to AV-GBM-1 were local injection site reactions (16%) and flu-like symptoms (10%). Treatment-emergent AEs included seizures (33%), headache (37%), and focal neurologic symptoms (28%). One patient discontinued AV-GBM-1 because of seizures. Median Progression-Free Survival (mPFS) and median Overall Survival (mOS) from ITT enrollment were 10.4 and 16.0 months, respectively. 2-year Overall Survival (OS) is 27%.	(25)
NCT01204684	newly diagnosed or recurrent WHO Grade III-IV malignant gliomas	23	dendritic cell vaccination	single-center, randomized, open-label multi-arm phase II clinical trial	The combination of ATL-DC vaccination and TLR agonist was safe and found to enhance systemic immune responses, as indicated by increased interferon gene expression and changes in immune cell activation.	(26)
ATTAC, NCT00639639	newly diagnosed glioblastoma	11	cytomegalovirus-specific dendritic cell vaccine	randomized phase I/II trial	Following DI-TMZ cycle 1 and three doses of pp65-DCs, pp65 cellular responses significantly increased. After DI-TMZ, both the proportion and proliferation of regulatory T cells (Tregs) increased and remained elevated with serial DI-TMZ cycles. Median PFS and OS were 25.3 months [95% confidence interval (CI), 11.0-∞] and 41.1 months (95% CI, 21.6-∞), exceeding survival using recursive partitioning analysis and matched historical controls. Four patients remained progression-free at 59 to 64 months from diagnosis. No known prognostic factors [age, Karnofsky performance status (KPS), IDH-1/2 mutation, and MGMT promoter methylation] predicted more favorable outcomes for the patients in this cohort.	(27)
NCT02287428	newly diagnosed MGMT-unmethylated glioblastoma	10	personalized neoantigen vaccines	phase I/Ib study	Patients who did not receive dexamethasone-a highly potent corticosteroid that is frequently prescribed to treat cerebral oedema in patients with glioblastoma-generated circulating polyfunctional neoantigen-specific CD4+ and CD8+ T cell responses that were enriched in a memory phenotype and showed an increase in the number of tumour-infiltrating T cells. Using single-cell T cell receptor analysis, we provide evidence that neoantigen-specific T cells from the peripheral blood can migrate into an intracranial glioblastoma tumour.	(32)
NCT03422094	newly diagnosed glioblastoma	4	NeoVax	single institution, open-label, multi-arm, pilot study	Immune reactivity to NeoVax neoantigens was assessed in peripheral blood mononuclear cells (PBMCs) pre- and post-NeoVax for subjects 1-3 using IFNg-ELISPOT assay. A statistically significant increase in IFNg producing T cells at the post-NeoVax time point for several neoantigens was observed. Furthermore, a post-NeoVax tumor biopsy was obtained from subject 3 and, upon evaluation, revealed evidence of infiltrating, clonally expanded T cells.	(33)

10.3389/fimmu.2024.1476436

10.3389/fimmu.2024.1476436

CAR-T therapy

CAR-T can specifically recognize tumor cell surface antigens, independent of MHC activation, and produce stronger anti-tumor immune responses (48) (Table 3, Supplementary Figure 3). There are also many practices in gliomas. Among them, GD2, EGFR-vIII, HER2, and IL13Ra2 are the three most common targets and have been tested in early phase trial.

GD2-targeted CAR-T seemed safe in recurrent or refractory advanced-stage neuroblastoma and was associated with tumor regression or necrosis, thereby resulting in longer survival (49). GD2-targeted CAR-T was tolerable in H3K27M-mutated diffuse midline gliomas and improved the clinical and radiographic outcomes through the pro-inflammatory cytokine levels in the plasma and cerebrospinal fluid (50). Recent trial assessed the administration methods of GD2-targeted CAR-T and found that intravenous alone or intravenous combined with intracavitary administration of GD2-targeted CAR-T were safe and well tolerated in glioblastoma and GD2-targeted CAR-T mediated antigen loss and activated immune responses in the glioblastoma microenvironment (51). NCT02209376 was the first-in-human study of EGFRvIII-targeted CAR-T in recurrent glioblastoma. Intravenous infusion of EGFRvIII-targeted CAR-T was feasible and safe, increased inhibitory molecules expression and regulatory T cells infiltration (52). The dose-escalating phase I study indicated persistence of CAR-T correlated with EGFRvIII-targeted CAR-T dose, but there were no objective responses (53). Infusion of autologous HER2-targeted CAR-T was tolerated and was associated with clinical benefit for patients with progressive glioblastoma (54). NCT00730613 was the first-in-human pilot study to evaluate the safety and feasibility of IL13Rα2-targeted CAR-T in recurrent glioblastoma. Intracranial delivery of the IL13Rα2-targeted CAR-T was well-tolerated, induced transient anti-glioma responses, and increased tumor necrotic volume (55). A case report indicated intracranial infusion of IL13Rα2-targeted CAR-T was associated with no toxic effects of grade 3 or higher. After IL13Rα2-targeted CAR-T treatment, all intracranial and spinal tumors were regressed along with increased levels of cytokines and immune cells in the cerebrospinal fluid (56). Brown and his colleagues generated an off-the-shelf, steroid-resistant, IL13Rα2-targeted CAR-T and found it was safety and induced transient tumor reduction and/or tumor necrosis in patients with glioblastoma (57).

In addition to the targets reviewed above, CD7 (58) and EphA2 (59, 60) have conducted relevant research. Some research have also emerged. Local intracranial CAR-T elicits superior anti-tumor efficacy as compared to intravenous CAR-T, with intraventricular administration exhibiting possible benefits over intracranial administration in a multifocal disease model (61). Cyclophosphamide and fludarabine but not PD-1 inhibitor enhanced the expansion or persistence of GD2-targeted CAR-T (62). Trivalent CAR-T (HER2, IL13Rα2, and EphA2-targeted CAR-T) mediated immunoreaction forming polarized microtubule organizing centers, exhibited improved cytotoxicity and cytokine release, and overcame antigenic heterogeneity in glioblastoma thereby improving treatment outcomes (63). Moreover, HER2-

TABLE 2 Some trials of immune checkpoint inhibitors in glioma.

Trial	Participants	Sample size	Intervention	Study design	Results	Reference
CheckMate 143, NCT02017717	newly diagnosed glioblastoma	136	nivolumab	phase 1 cohorts (1c+1d)	NIVO+RT ± TMZ was tolerable; grade 3/4 treatment-related adverse events occurred in 51.6% (NIVO+RT+TMZ) and 30.0% (NIVO+RT) of patients in part A and 46.4% (NIVO+RT+TMZ) and 28.6% (NIVO+RT) in part B. No new safety signals were detected. In part A, median OS (mOS) with NIVO+RT+TMZ was 33.38 months (95% CI, 16.2 to not estimable) in patients with methylated MGMT promoter. In patients with unmethylated MGMT promoter, mOS was 16.49 months (12.94-22.08) with NIVO+RT+TMZ and 14.41 months (12.55-17.31) with NIVO +RT. In part B, mOS was 14.75 months (10.01-18.6) with NIVO+RT+TMZ and 13.96 months (10.81-18.14) with NIVO+RT in patients with unmethylated MGMT promoter.	(36)
CheckMate 143, NCT02017717	recurrent glioblastoma	369	nivolumab	open-label, randomized, phase 3 clinical trial	The MGMT promoter was methylated in 23.4% (43/184; nivolumab) and 22.7% (42/185; bevacizumab), unmethylated in 32.1% (59/184; nivolumab) and 36.2% (67/185; bevacizumab), and not reported in remaining patients. At median follow-up of 9.5 months, median OS (mOS) was comparable between groups: nivolumab, 9.8 months (95% CI, 8.2-11.8); bevacizumab, 10.0 months (95% CI, 9.0-11.8); HR, 1.04 (95% CI, 0.83-1.30); P = .76. The 12-month OS was 42% in both groups. The objective response rate was higher with bevacizumab (23.1%; 95% CI, 16.7%-30.5%) vs nivolumab (7.8%; 95% CI, 4.1%-13.3%). Grade 3/4 treatment-related adverse events (TRAEs) were similar between groups (nivolumab, 33/182 [18.1%]; bevacizumab, 25/165 [15.2%]), with no unexpected neurological TRAEs or deaths due to TRAEs.	(37)

(*Continued*)

TABLE 2 Continued

Trial	Participants	Sample size	Intervention	Study design	Results	Reference
CheckMate 548, NCT02667587	newly diagnosed glioblastoma with methylated MGMT promoter	716	nivolumab	phase III, single-blind trial	As of December 22, 2020, median (m)PFS (blinded independent central review) was 10.6 months (95% CI, 8.9-11.8) with NIVO + RT + TMZ vs 10.3 months (95% CI, 9.7-12.5) with PBO + RT + TMZ (HR, 1.1; 95% CI, 0.9-1.3) and mOS was 28.9 months (95% CI, 24.4-31.6) vs 32.1 months (95% CI, 29.4-33.8), respectively (HR, 1.1; 95% CI, 0.9-1.3). In patients without baseline corticosteroids, mOS was 31.3 months (95% CI, 28.6-34.8) with NIVO + RT + TMZ vs 33.0 months (95% CI, 31.0-35.1) with PBO + RT + TMZ (HR, 1.1; 95% CI, 0.9-1.4). Grade 3/4 treatment-related adverse event rates were 52.4% vs 33.6%, respectively.	(38)
CheckMate 498, NCT02617589	newly diagnosed glioblastoma with unmethylated MGMT promoter	560	nivolumab	open-label, randomized, phase III study	Median OS (mOS) was 13.4 months (95% CI, 12.6 to 14.3) with NIVO + RT and 14.9 months (95% CI, 13.3 to 16.1) with TMZ + RT (hazard ratio [HR], 1.31; 95% CI, 1.09 to 1.58; P = .0037). Median progression-free survival was 6.0 months (95% CI, 5.7 to 6.2) with NIVO + RT and 6.2 months (95% CI, 5.9 to 6.7) with TMZ + RT (HR, 1.38; 95% CI, 1.15 to 1.65). Response rates were 7.8% (9/116) with NIVO + RT and 7.2% (8/111) with TMZ + RT; grade 3/4 treatment-related adverse event (TRAE) rates were 21.9% and 25.1%, and any-grade serious TRAE rates were 17.3% and 7.6%, respectively.	(39)
NCT02550249	resectable glioblastoma	30	nivolumab	single-arm phase II clinical trial	Neoadjuvant nivolumab resulted in enhanced expression of chemokine transcripts, higher immune cell infiltration and augmented TCR clonal diversity among tumor-infiltrating T lymphocytes, supporting a local immunomodulatory effect of treatment. Although no obvious clinical benefit was substantiated following salvage surgery, two of the three patients treated with nivolumab before and after primary surgery remain alive 33 and 28 months later.	(41)
	recurrent, surgically resectable glioblastoma	35	pembrolizumab	randomized, multi-institution clinical trial	Patients who were randomized to receive neoadjuvant pembrolizumab, with continued adjuvant therapy following surgery, had significantly extended overall survival compared to patients that were randomized to receive adjuvant, post-surgical programmed cell death protein 1 (PD-1) blockade alone. Neoadjuvant PD-1 blockade was associated with upregulation of T cell- and interferon-γ-related gene expression, but downregulation of cell-cycle-related gene expression within the tumor, which was not seen in patients that received adjuvant therapy alone. Focal induction of programmed death-ligand 1 in the tumor microenvironment, enhanced clonal expansion of T cells, decreased PD-1 expression on peripheral blood T cells and a decreasing monocytic population was observed more frequently in the neoadjuvant group than in patients treated only in the adjuvant setting.	(42)
	recurrent glioblastoma	66	pembrolizumab or nivolumab	retrospective analysis	Genomic and transcriptomic analysis revealed a significant enrichment of PTEN mutations associated with immunosuppressive expression signatures in non-responders, and an enrichment of MAPK pathway alterations (PTPN11, BRAF) in responders. Responsive tumors were also associated with branched patterns of evolution from the elimination of neoepitopes as well as with differences in T cell clonal diversity and tumor microenvironment profiles.	(43)
NCT03233152	recurrent glioblastoma	27	nivolumab and ipilimumab	single-center, open-label, phase I clinical trial	All patients underwent maximal safe resection and planned IC administrations and preoperative NIVO. Thirteen patients (cohort-1: n=3; cohort-2: n=10) received all five postoperative intravenous doses of NIVO. In cohort-2, 14 patients received a median of 3 (range 1-4) intravenous doses. Subacute postoperative neurological deterioration (n=2) was reversible on steroid treatment; no other central nervous system toxicity was observed. Immune-related adverse events were infrequent and mild. GB recurrence was diagnosed in 26 patients (median progression-free survival (PFS) is 11.7 weeks (range 2-152)); 21 patients have	(44)

(Continued)

10.3389/fimmu.2024.1476436

TABLE 2 Continued

Trial	Participants	Sample size	Intervention	Study design	Results	Reference
					died due to progression. Median OS is 38 weeks (95% CI: 27 to 49) with a 6-month, 1-year, and 2-year OS-rate of, respectively, 74.1% (95% CI: 57 to 90), 40.7% (95% CI: 22 to 59), and 27% (95% CI: 9 to 44). OS compares favorable against a historical cohort (descriptive Log-Rank p>0.003). No significant difference was found with respect to PFS (descriptive Log-Rank test p>0.05). A higher tumor mRNA expression level of B7-H3 was associated with a significantly worse survival (multivariate Cox logistic regression, p>0.029).	
CheckMate 908, NCT03130959	high-grade CNS malignancies	166	nivolumab and ipilimumab	open-label, sequential-arm, phase 1b/2 study	As of January 13, 2021, median OS (80% CI) was 11.7 (10.3-16.5) and 10.8 (9.1-15.8) months with NIVO and NIVO + IPI, respectively, in newly diagnosed DIPG. Median PFS (80% CI) with NIVO and NIVO + IPI was 1.7 (1.4-2.7) and 1.3 (1.2-1.5) months, respectively, in recurrent/progressive high-grade glioma; 1.4 (1.2-1.4) and 2.8 (1.5-4.5) months in relapsed/resistant medulloblastoma; and 1.4 (1.4-2.6) and 4.6 (1.4-5.4) months in relapsed/resistant ependymoma. In patients with other recurrent/progressive CNS tumors, median PFS (95% CI) was 1.2 (1.1-1.3) and 1.6 (1.3-3.5) months, respectively. Grade 3/4 treatment-related adverse-event rates were 14.1% (NIVO) and 27.2% (NIVO + IPI). NIVO and IPI first-dose trough concentrations were lower in youngest and lowest-weight patients. Baseline tumor programmed death ligand 1 expression was not associated with survival.	(45)
	recurrent high-grade gliomas	32	bevacizumab and pembrolizumab	phase I study	The most common treatment-related adverse events (TRAEs) were proteinuria (40.6%), fatigue (25%), increased alanine aminotransferase (25%), and hypertension (25%). TRAEs leading to discontinuation occurred in 1 patient who experienced a grade 3 elevation of aspartate aminotransferase. In the bevacizumab-naïve cohort, 20 patients (83%) had a complete response or partial response. The median overall survival (OS) and progression-free survival (PFS) were 13.45 months (95% CI: 9.46-18.46) and 7.92 months (95% CI: 6.31-12.45), respectively. In the bevacizumab-resistant cohort, PR was achieved in 5 patients (62%). Median OS was 9.3 months (95% CI: 8.97-18.86) with a median PFS of 6.54 months (95% CI: 5.95-18.86). The majority of patients (n = 20/26; 77%) had tumor-cell/tumor-microenvironment PD-L1 expression <1%.	(46)
NCT03637764	glioblastoma	33	isatuximab plus atezolizumab	phase I/II, open-label, multicenter study	In phase I, Isa + Atezo showed an acceptable safety profile, no dose-limiting toxicities were observed, and RP2D was confirmed. Most patients experienced ≥1 treatment-emergent adverse event (TEAE), with ≤48.5% being grade ≥3. The most frequent TEAE was infusion reactions. The study did not continue to stage 2 based on prespecified targets. Tumor-infiltrating CD38+ immune cells were reduced and almost cleared after treatment. Isa + Atezo did not significantly modulate Tregs or PD-L1 expression in the TME.	(47)

10.3389/fimmu.2024.1476436

TABLE 3 Some trials of CAR-T therapy in glioma.

Trial	Participants	Sample size	Targets	Study design	Results	Reference
	recurrent or refractory advanced-stage neuroblastoma	11	GD2	Primary clinical trial	Here we show in individuals with neuroblastoma that EBV-specific CTLs expressing a chimeric GD2-specific receptor indeed survive longer than T cells activated by the CD3-specific antibody OKT3 and expressing the same chimeric receptor but lacking virus specificity. Infusion of these genetically modified cells seemed safe and was associated with tumor regression or necrosis in half of the subjects tested.	(49)
NCT04196413	diffuse midline gliomas	4	GD2	first-in-human phase I clinical trial	Toxicity was largely related to the location of the tumour and was reversible with intensive supportive care. On-target, off-tumour toxicity was not observed. Three of four patients exhibited clinical and radiographic improvement. Pro-inflammatory cytokine levels were increased in the plasma and cerebrospinal fluid. Transcriptomic analyses of 65,598 single cells from CAR T cell products and cerebrospinal fluid elucidate heterogeneity in response between participants and administration routes.	(50)
NCT03170141	glioblastoma	8	GD2	phase 1 trial	4SCAR-T cells expanded for 1-3 weeks and persisted at a low frequency in peripheral blood. Of the eight evaluable patients, four showed a partial response for 3 to 24 months, three had progressive disease for 6 to 23 months, and one had stable disease for 4 months after infusion. For the entire cohort, the median overall survival was 10 months from the infusion. GD2 antigen loss and infiltrated T cells were observed in the tumor resected after infusion.	(51)
NCT02209376	recurrent glioblastoma	10	EGFRvIII	phase 1 first-in-human study	We found that manufacturing and infusion of CAR-modified T cell (CART)-EGFRvIII cells are feasible and safe, without evidence of off-tumor toxicity or cytokine release syndrome.	(52)
NCT01454596	recurrent glioblastoma	33	EGFRvIII	dose-escalating phase I study	Eighteen patients were treated with final infusion products ranging from 6.3×10 to 2.6×10 anti-EGFRvIII CAR T cells. Median progression-free survival was 1.3 months (interquartile range: 1.1-1.9), with a single outlier of 12.5 months. Two patients experienced severe hypoxia, including one treatment-related mortality after cell administration at the highest dose level. All patients developed expected transient hematologic toxicities from preparative chemotherapy. Median overall survival was 6.9 months (interquartile range: 2.8-10). Two patients survived over 1 year, and a third patient was alive at 59 months. Persistence of CAR cells correlated with cell dose, but there were no objective responses.	(53)
NCT01109095	progressive glioblastoma	17	HER2	open-label phase 1 dose-escalation study	Infusions were well tolerated, with no dose-limiting toxic effects. HER2-CAR VSTs were detected in the peripheral blood for up to 12 months after the infusion by quantitative real-time polymerase chain reaction. Of 16 evaluable patients (9 adults and 7 children), 1 had a partial response for more than 9 months, 7 had stable disease for 8 weeks to 29 months, and 8 progressed after T-cell infusion. Three patients with stable disease are alive without any evidence of progression during 24 to 29 months of follow-up. For the entire study cohort, median overall survival was 11.1 months (95% CI, 4.1-27.2 months) from the first T-cell infusion and 24.5 months (95% CI, 17.2-34.6 months) from diagnosis.	(54)
NCT00730613	recurrent glioblastoma	3	IL13Rα2	single-institution first-in-human pilot study	We demonstrate the feasibility of manufacturing sufficient numbers of autologous CTL clones expressing an IL13(E13Y)-zetakine CAR for redirected HLA-independent IL13Rα2-specific effector function for a cohort of patients diagnosed with GBM. Intracranial delivery of the IL13-zetakine(+) CTL clones into the resection cavity of 3 patients with recurrent disease was well-tolerated, with manageable temporary brain inflammation. Following infusion of IL13-zetakine (+) CTLs, evidence for transient anti-glioma responses was observed in 2 of the patients. Analysis of tumor tissue from 1 patient before and after T-cell therapy suggested reduced overall IL13Rα2 expression within the tumor following treatment. MRI analysis of another	(55)

(Continued)

10.3389/fimmu.2024.1476436

TABLE 3 Continued

Trial	Participants	Sample size	Targets	Study design	Results	Reference
					patient indicated an increase in tumor necrotic volume at the site of IL13-zetakine(+) T-cell administration.	
NCT02208362	recurrent malignant glioma	1	IL13Rα2	phase 1 study	Intracranial infusions of IL13Rα2-targeted CAR T cells were not associated with any toxic effects of grade 3 or higher. After CAR T-cell treatment, regression of all intracranial and spinal tumors was observed, along with corresponding increases in levels of cytokines and immune cells in the cerebrospinal fluid. This clinical response continued for 7.5 months after the initiation of CAR T-cell therapy.	(56)
NCT01082926	recurrent glioblastoma	6	IL13Rα2	phase 1, open-label, uncontrolled study	The GRm13Z40-2 product displayed dexamethasone-resistant effector activity without evidence for *in vitro* alloreactivity. Intracranial administration of GRm13Z40-2 in four doses of 108 cells over a two-week period with aldesleukin (9 infusions ranging from 2500-5000 IU) was well tolerated, with indications of transient tumor reduction and/or tumor necrosis at the site of T cell infusion in four of the six treated research subjects. Antibody reactivity against GRm13Z40-2 cells was detected in the serum of only one of the four tested subjects.	(57)

targeted CAR-NK cells (64) and ErbB2-targeted CAR-NK cells (65) might be feasible and safe in recurrent glioblastoma. In a first-in-human trial published in 2024, three patients with recurrent glioblastoma received CARv3-TEAM-E T cell therapy (66). CARv3-TEAM-E T cells are chimeric antigen receptor (CAR) T cells that target both the epidermal growth factor receptor variant III (EGFRvIII), a tumor-specific antigen, and wild-type EGFR protein, attacking via secreted T cell-engaging antibody molecules (TEAM). The treatment did not cause any grade 3 or higher adverse events or dose-limiting toxicities. Radiological imaging revealed a rapid and significant reduction in tumor size, with responses occurring within days after a single intraventricular injection. However, two of the patients experienced only short-lived responses.

Oncolytic virotherapy

Oncolytic viruses are a type of tumor-killing virus with replication ability. They not only proliferate infinitely within tumor cells, leading to their death, but also directly or indirectly activate the anti-tumor immune system, specifically killing tumor cells (67) (Table 4, Supplementary Figure 4). Due to its ability to recognize tumor cells specifically through corresponding receptors and its replication relying on tumor-specific promoters, oncolytic viruses do not affect normal brain tissue cells.

A phase I dose-escalating clinical study showed that 24 patients with recurrent malignant gliomas received intracerebral injections of ONYX-015, an E1B-attenuated adenovirus. None of the patients had any adverse events related to ONYX-015 injection, confirming the relative safety of ONYX-015 in the treatment of malignant gliomas (68). DNX-2401, an E1A-attenuated adenovirus, resulted in more than 3 years of progression free survival in 12% of patients with recurrent malignant gliomas that were probably due to direct oncolytic effects of DNX-2401 followed by elicitation of an immune-mediated response (69, 70). DNX-2401 promoted a pro-inflammatory microenvironment and M1 characteristics of tumoral macrophages in glioblastoma (71), a later phase I clinical trial also indicated that DNX-2401 locally delivered by convection-enhanced delivery in tumor and surrounding brain induced local inflammatory reaction in patients with recurrent glioblastoma (72). DNX-2401 is also used in conjunction with other treatment methods. Intertumoral infusion of DNX-2401 followed by radiotherapy in pediatric patients with newly diagnosed diffuse intrinsic pontine glioma resulted in changes in T-cell activity and a reduction in or stabilization of tumor size in some patients but was associated with adverse events (73). The first-in-human investigation of combined DNX-2401 with pembrolizumab for recurrent glioblastoma confirmed the safety with notable survival benefits in select patients and response to treatment informed by the balance between immune infiltration and expression of immune checkpoint inhibitors (74). In addition, intratumoral infusion of PVSRIPO, recombinant nonpathogenic polio-rhinovirus chimera, in patients with recurrent malignant glioma confirmed the absence of neurovirulent potential and improved survival (75). A first-in-human, open-label, phase 1, dose-escalation trial indicated neural stem cell delivery of an

TABLE 4 Some trials of oncolytic virotherapy in glioma.

Trial	Participants	Adenovirus	Sample size	Oncolytic viruses	Study design	Results	Reference
	recurrent malignant gliomas	E1B	24	ONYX-015	phase I open-label, dose-escalation, multi-institutional trial	Adverse events were identified on physical exams and testing of hematologic, renal, and liver functions. Efficacy data were obtained from serial MRI scans. None of the 24 patients experienced serious adverse events related to ONYX-015. The maximum tolerated dose was not reached at 10(10) pfu. The median time to progression after treatment with ONYX-015 was 46 days (range 13 to 452 + days). The median survival time was 6.2 months (range 1.3 to 28.0 + months). One patient has not progressed and 1 patient showed regression of interval-increased enhancement. With more than 19 months of follow-up, 1/6 recipients at a dose of 10(9) and 2/6 at a dose of 10(10) pfu remain alive. In 2 patients who underwent a second resection 3 months after ONYX-015 injection, a lymphocytic and plasmacytoid cell infiltrate was observed. Injection of ONYX-015 into glioma cavities is well tolerated at doses up to 10 (10) pfu.	(68)
NCT00805376	recurrent malignant gliomas	E1A	37	DNX-2401	phase I, dose-escalation, biologic-end-point clinical trial	In group A (n = 25), 20% of patients survived > 3 years from treatment, and three patients had a ≥ 95% reduction in the enhancing tumor (12%), with all three of these dramatic responses resulting in > 3 years of progression-free survival from the time of treatment. Analyses of post-treatment surgical specimens (group B, n = 12) showed that DNX-2401 replicates and spreads within the tumor, documenting direct virus-induced oncolysis in patients. In addition to radiographic signs of inflammation, histopathologic examination of immune markers in post-treatment specimens showed tumor infiltration by CD8+ and T-bet+ cells, and transmembrane immunoglobulin mucin-3 downregulation after treatment. Analyses of patient-derived cell lines for damage-associated molecular patterns revealed induction of immunogenic cell death in tumor cells after DNX-2401 administration.	(69)
NCT03178032	newly diagnosed diffuse intrinsic pontine glioma	E1A	12	DNX-2401	single-center, dose-escalation study	total of 12 patients, 3 to 18 years of age, with newly diagnosed DIPG received 1×1010 (the first 4 patients) or 5×1010 (the subsequent 8 patients) viral particles of DNX-2401, and 11 received subsequent radiotherapy. Adverse events among the patients included headache, nausea, vomiting, and fatigue. Hemiparesis and tetraparesis developed in 1 patient each. Over a median follow-up of 17.8 months (range, 5.9 to 33.5), a reduction in tumor size, as assessed on magnetic resonance imaging, was reported in 9 patients, a partial response in 3 patients, and stable disease in 8 patients. The median survival was 17.8 months. Two patients were alive at the time of preparation of the current report, 1 of whom was free of tumor progression at 38 months. Examination of a tumor sample obtained during autopsy from 1 patient and peripheral-blood studies revealed alteration of the tumor microenvironment and T-cell repertoire.	(73)
NCT02798406	recurrent glioblastoma	E1A	49	DNX-2401	two-part, phase 1/2, multicenter, open-label clinical trial	The primary endpoints were overall safety and objective response rate. The primary safety endpoint was met, whereas the primary efficacy endpoint was not met. There were no dose-limiting toxicities, and full dose combined treatment was well tolerated. The objective response rate was 10.4% (90% confidence interval (CI) 4.2-20.7%), which was not statistically greater than	(74)

(Continued)

10.3389/fimmu.2024.1476436

TABLE 4 Continued

Trial	Participants	Adenovirus	Sample size	Oncolytic viruses	Study design	Results	Reference
						the prespecified control rate of 5%. The secondary endpoint of overall survival at 12 months was 52.7% (95% CI 40.1-69.2%), which was statistically greater than the prespecified control rate of 20%. Median overall survival was 12.5 months (10.7-13.5 months). Objective responses led to longer survival (hazard ratio 0.20, 95% CI 0.05-0.87). A total of 56.2% (95% CI 41.1-70.5%) of patients had a clinical benefit defined as stable disease or better. Three patients completed treatment with durable responses and remain alive at 45, 48 and 60 months.	
NCT01491893	recurrent malignant glioma	CD155	61	PVSRIPO	phase 1 clinical trial with dose expansion	Dose level -1 (5.0×107 TCID50) was identified as the phase 2 dose. One dose-limiting toxic effect was observed; a patient in whom dose level 5 (1010 TCID50) was administered had a grade 4 intracranial hemorrhage immediately after the catheter was removed. To mitigate locoregional inflammation of the infused tumor with prolonged glucocorticoid use, dose level 5 was deescalated to reach the phase 2 dose. In the dose-expansion phase, 19% of the patients had a PVSRIPO-related adverse event of grade 3 or higher. Overall survival among the patients who received PVSRIPO reached a plateau of 21% (95% confidence interval, 11 to 33) at 24 months that was sustained at 36 months.	(75)
NCT03072134	newly diagnosed malignant gliomas	neural stem cells	12	NSC-CRAd-S-pk7	first-in-human, open-label, phase 1, dose-escalation trial	Histopathological evaluation identified 11 (92%) of 12 patients with glioblastoma and one (8%) of 12 patients with anaplastic astrocytoma. The median follow-up was 18 months (IQR 14-22). One patient receiving 1·50 × 108 NSCs loading 1·875 × 1011 viral particles developed viral meningitis (grade 3) due to the inadvertent injection of NSC-CRAd-S-pk7 into the lateral ventricle. Otherwise, treatment was safe as no formal dose-limiting toxicity was reached, so 1·50 × 108 NSCs loading 1·875 × 1011 viral particles was recommended as a phase 2 trial dose. There were no treatment-related deaths. The median progression-free survival was 9·1 months (95% CI 8·5-not reached) and median overall survival was 18·4 months (15·7-not reached).	(76)

10.3389/fimmu.2024.1476436

oncolytic adenovirus (NSC-CRAd-S-pk7) in newly diagnosed malignant gliomas was feasible and safe (76). Ling AL, Solomon IH, Landivar AM, et al. report a phase I clinical trial linking oncolytic virus-mediated immune activation to survival in glioblastoma patients. In this study, 41 patients with recurrent glioblastoma were treated with CAN-3110, an oncolytic herpes virus designed for preferential tumor replication. No dose-limiting toxicities were observed. Improved survival was notably associated with HSV1 seropositivity, which also correlated with enhanced T cell response and immune activation signatures in the tumor microenvironment. These findings provide evidence supporting the therapeutic potential of oncolytic viruses in immunosuppressive tumors like glioblastoma (77).

Discussion

Glioma is one of the most concerning fields in neurological tumors, and its treatment is a clinical challenge. Although the standard post-surgical treatment for newly diagnosed glioblastoma, involving concurrent radiotherapy and the alkylating chemotherapeutic agent temozolomide (TMZ) followed by adjuvant TMZ, has been established for over a decade, glioblastoma inevitably recurs and develops resistance to further chemotherapy. One of the earliest mechanisms of resistance to TMZ is the upregulation of DNA methyltransferase (MGMT), which removes methyl adducts from DNA, enabling mismatch repair and allowing tumor DNA replication to continue (78). Immunotherapy is a research hotspot, and many immunotherapy studies are targeting glioma. Here, we reviewed the current concepts of immunotherapy in glioma (Tables 1–4), the current clinical research results may be encouraging, but there is still much room for improvement.

Tumor vaccines activate T cells in patients by introducing tumor antigens, thereby inducing an immune response to kill tumor cells. Compared with traditional radiotherapy and chemotherapy, tumor vaccines have become highly promising immunotherapy due to their convenient operation process, strong specificity, good safety, and ability to establish long-term immune memory. The core of tumor vaccine development lies in accurately screening suitable tumor antigens and determining effective antigen delivery methods. To overcome these challenges, researchers have proposed various strategies. Firstly, the combination of tumor vaccines and immune checkpoint inhibitors is used to enhance immune response, thereby enhancing treatment efficacy. NEO-PV-01, a personalized neoantigen vaccine, in combination with pembrolizumab, supports the safety and immunogenicity in patients with advanced non-squamous non-small cell lung cancer (79). Secondly, the personalized vaccine strategy based on neoantigens improves the targeting and efficacy of tumor vaccines by accurately identifying tumor-specific antigens. The future research focus will be on combining clinical efficacy and artificial intelligence technology to improve the accuracy of predicting neoantigens, thereby optimizing the therapeutic effect and application scope of vaccines. Finally, utilizing systems biology methods could optimize vaccine design and improve vaccine delivery systems. By utilizing advanced biomaterials such as nanoparticles to optimize drug delivery systems could improve the vaccine efficacy and reduce side effects (80). KK2DP7, a simple dendrimer polypeptide nanoparticle, enhances antitumor immunity of a neoantigen-based vaccine (81). CRISPR-Cas9 technology enhances the immune response by precisely modifying the genetic information of immune cells or tumor cells. The engineered therapeutic tumor cells, repurposed from interferon-β sensitive to resistant using CRISPR-Cas9 by knocking out the interferon-β-specific receptor, eliminated established glioblastoma tumors in mice (82).

The research progress on immune checkpoint inhibitors is rapid, especially monoclonal antibodies targeting PD-1/PD-L1 and CTLA-4, which have been approved by the FDA for first-line treatment of melanoma and/or lung cancer. At the same time, research is also underway, including targeting LAG3, TIM3, and other checkpoint inhibitors. The combination immunotherapy method of PD-1 blockade was successfully used for advanced glioma. However, intratumoral heterogeneity (83, 84), low PD-L1 expression (85), low mutation burden (86), and chemotherapy-induced mutation properties (87, 88) in diffuse midline glioma might explain why no survival benefits have been observed with immune checkpoint inhibitors monotherapy (16, 89). Therefore, the FDA has not yet approved malignant glioma as a treatment indication for immune checkpoint inhibitors. In the future, further research is needed on neuroimmunology and the possibility of combining immune checkpoint inhibitors with other therapies to treat glioma.

Due to the heterogeneity of glioma and the immune suppression of CAR-T by the tumor microenvironment, increasing the number of CAR-T coverage antigens and combination therapy is key to improving the efficacy of CAR-T. Combination therapy with Lp2-targeted CAR-T and oncolytic virus G47Δ further inhibited the glioblastoma growth and improved survival (90). Although CAR-T treatment for glioma is still in its early stages, the emergence and application of advanced biotechnology will accelerate the search for new strategies for glioma. The method of genome-scale screening using CRISPR-Cas9 can significantly shorten the time for discovering key genes that can be interfered with to improve the therapeutic effect of CAR-T, a three-dimensional model of glioblastoma organoids that summarizes the cellular heterogeneity, structure, and function of primary tissues can be used for better preclinical studies of CAR-T therapy, and single-cell sequencing technology can accurately reveal the intratumoral heterogeneity of glioma cells and other cellular components of tumor microenvironment to provide rich information for monitoring immune response and predict therapeutic efficacy during the treatment process.

The progress of basic research and the iteration of technology have made oncolytic viruses more specific, effective, and safe in the treatment of glioma. More and more oncolytic viruses are entering phase I, II, and even III clinical trials. However, there are still many challenges in the treatment of glioma with oncolytic viruses. Firstly, in terms of safety, although existing clinical trial results have not

reported significant safety events, there is still a risk of off-target treatment. In addition, although genetically modified viruses enhance their ability to recognize tumor cells, elderly people and immunocompromised patients may still be infected with the virus and cause serious consequences. Secondly, in terms of drug delivery routes, most oncolytic viruses are currently administered locally through direct intratumoral injection in the treatment of gliomas, reducing the risk of virus replication in non-target cells (91). However, there are problems such as bleeding, infection, and difficulty in drug delivery in deep lesions, and continuous improvement of targeted guidance techniques and the technical standards for intratumoral drug delivery should be emphasized. Compared with direct intratumoral injection, intravenous injection is undoubtedly more convenient and safer (92). However, due to the dilution of systemic blood, rapid neutralization of antibodies, and isolation of non-target organs and the blood-brain barrier, the application of intravenous medication is greatly limited. Increasing the dose of oncolytic viruses used for intravenous injection, improving oncolytic virus vectors, and using new ultrasound to open the blood-brain barrier (93) may improve the effectiveness of intravenous administration. Finally, how to improve the therapeutic effect of oncolytic viruses is also a difficult problem. Attention should be paid to the application of combining oncolytic virotherapy with other treatments such as chemotherapy, radiotherapy, and immune checkpoint inhibitors in the treatment of glioma to increase anti-tumor synergistic effects. Because there are currently no biomarkers available to predict the dose of relevant oncolytic viruses and their potential for *in vivo* replication (94), in addition to central imaging review, molecular pathology, and immune monitoring, in-depth research on virus replication and clinical anti-tumor response should be conducted in preclinical models and clinical trials.

The challenge of immunotherapy for glioma is still limited by objective factors. From an anatomical perspective, it is difficult to obtain central nervous system tumor section specimens, and due to the presence of the blood-brain barrier, some drugs are difficult to accurately reach the tumor periphery. To address anatomical difficulties, it is possible to simultaneously obtain tumor pathological tissue specimens on the basis of maximizing tumor tissue resection, and analyze individual tumor phenotype characteristics using multiple immunohistochemistry, proteomics, spatial transcriptomics techniques, etc. It is also possible to collect tumor-derived circulating DNA from cerebrospinal fluid before surgical resection, supplemented by tumor genome analysis, to obtain immunotherapy target information for a certain individual. Local administration (intratumoral delivery) may be feasible for addressing the challenges of the blood-brain barrier. Meanwhile, with the development of nanotechnology, it can cross the blood-brain barrier and target tumor sites, bringing new ways for immunotherapy of glioma. From the perspective of peritumoral characteristics, the immunosuppressive microenvironment is dynamic, which poses challenges to micro level research. Enhanced monitoring of individual patients may help capture immune dynamics, and non-invasive methods may be urgently needed due to increased frequency. With the widespread application of second-generation sequencing technology, the current research direction is mainly to search for new tumor mutations and antigens; in addition, research on immune related pathways and immunosuppressive mechanisms is also a new direction in tumor immunotherapy. Gliomas also exhibit a tendency to recur, further limiting the effectiveness of immunotherapy. It is possible to enhance the function of memory lymphocytes, search for specific receptors on the surface of memory lymphocytes, promote the function of activating receptors, and block the function of inhibitory receptors.

In addition, clinical research design also needs improvement. In clinical trials, the number of glioma patients is relatively small compared to more common solid tumors, which requires new therapies, including immunotherapy, to be tested in small, underpowered, and non-randomized designs. Nearly half of the published clinical studies are single-arm studies with a sample size of no more than 50 patients. These limitations make it difficult to demonstrate the efficacy of new therapies in glioma. Low randomization rate, insufficient use of the controls, and overestimation of benefits/effects, especially in early trials, may limit the widespread applicability of the results. The suboptimal design may be driven by accrual challenges, emphasizing the need for more collaborative efforts and creating incentives in these areas to enable larger-scale experiments, ideally using synchronous controls, but in appropriate cases, inequal randomization can be considered. The use of historical data can lead to bias in patient selection. Therefore, it is recommended to conduct randomized controlled clinical studies. Another area that needs improvement is the outcome indicators. Response rate is not an ideal endpoint for immunotherapy. Similarly, progression free survival is often used, but progression free survival also has the same issue in terms of response rate dependent on MRI evaluation, which may be inaccurate as pseudoprogression and pseudoresponse are common in glioblastoma. The Response Assessment in Neuro-Oncology criteria may provide some assistance. The most powerful clinical endpoint is overall survival. However, overall survival need longer follow-up time. Finally, the regulatory and technical authorities for trials should strengthen their supervision of the design and implementation of trials, and if necessary, terminate trials promptly to ensure that trials are designed and conducted in a safe, effective, and feasible manner for glioma patients.

Overall, despite the uneven quality and mixed results of available clinical trials, we still see the dawn of immunotherapy for glioma. Molecular biomarkers are of great significance in providing assistance and evaluating prognosis (95). With the advancement of cutting-edge technologies (artificial intelligence, CRISPR-Cas9, and single-cell sequencing), not only new evaluation methods can be provided for the immunotherapy of glioma, but more importantly, it is conducive to the rapid development of new immunotherapy strategies. The field of clinical trials of immunotherapy may contribute to individualized and personalized treatment and ultimately be applied in clinical practice, achieving the ultimate goal of improving the prognosis of patients with glioma (96).

Author contributions

JL: Conceptualization, Data curation, Formal analysis, Funding acquisition, Investigation, Methodology, Project administration, Resources, Software, Supervision, Validation, Visualization, Writing – original draft, Writing – review & editing. JP: Formal analysis, Funding acquisition, Investigation, Methodology, Project administration, Resources, Software, Supervision, Writing – original draft. JJ: Data curation, Formal analysis, Funding acquisition, Investigation, Project administration, Resources, Software, Supervision, Validation, Writing – review & editing. YL: Data curation, Formal analysis, Funding acquisition, Investigation, Methodology, Project administration, Resources, Software, Supervision, Validation, Writing – original draft.

Funding

The author(s) declare that no financial support was received for the research, authorship, and/or publication of this article.

Conflict of interest

The authors declare that the research was conducted in the absence of any commercial or financial relationships that could be construed as a potential conflict of interest.

Publisher's note

All claims expressed in this article are solely those of the authors and do not necessarily represent those of their affiliated organizations, or those of the publisher, the editors and the reviewers. Any product that may be evaluated in this article, or claim that may be made by its manufacturer, is not guaranteed or endorsed by the publisher.

Supplementary material

The Supplementary Material for this article can be found online at: https://www.frontiersin.org/articles/10.3389/fimmu.2024.1476436/full#supplementary-material

References

1. Weller M, Wick W, Aldape K, Brada M, Berger M, Pfister SM, et al. Glioma. *Nat Rev Dis Primers*. (2015) 1:15017. doi: 10.1038/nrdp.2015.17

2. Forjaz G, Barnholtz-Sloan JS, Kruchko C, Siegel R, Negoita S, Ostrom QT, et al. An updated histology recode for the analysis of primary Malignant and nonmalignant brain and other central nervous system tumors in the Surveillance, Epidemiology, and End Results Program. *Neurooncol Adv*. (2021) 3:vdaa175. doi: 10.1093/noajnl/vdaa175

3. Ostrom QT, Gittleman H, Liao P, Rouse C, Chen Y, Dowling J, et al. CBTRUS statistical report: primary brain and central nervous system tumors diagnosed in the United States in 2007-2011. *Neuro Oncol*. (2014) 16 Suppl 4:iv1–63. doi: 10.1093/neuonc/nou223

4. Weller M, Cloughesy T, Perry JR, Wick W. Standards of care for treatment of recurrent glioblastoma–are we there yet? *Neuro-oncology*. (2013) 15:4–27. doi: 10.1093/neuonc/nos273

5. Huang Y, Wang Y, Huang Z. A specific peptide vaccine against IDH1(R132H) glioma. *Neurosci Bull*. (2022) 38:223–5. doi: 10.1007/s12264-021-00791-9

6. Old LJ, Clarke DA, Benacerraf B. Effect of Bacillus Calmette-Guerin infection on transplanted tumours in the mouse. *Nature*. (1959) 184:291–2. doi: 10.1038/184291a0

7. Lin MJ, Svensson-Arvelund J, Lubitz GS, Marabelle A, Melero I, Brown BD, et al. Cancer vaccines: the next immunotherapy frontier. *Nat Cancer*. (2022) 3:911–26. doi: 10.1038/s43018-022-00418-6

8. Saxena M, van der Burg SH, Melief CJM, Bhardwaj N. Therapeutic cancer vaccines. *Nat Rev Cancer*. (2021) 21:360–78. doi: 10.1038/s41568-021-00346-0

9. Tsuboi A, Hashimoto N, Fujiki F, Morimoto S, Kagawa N, Nakajima H, et al. A phase I clinical study of a cocktail vaccine of Wilms' tumor 1 (WT1) HLA class I and II peptides for recurrent Malignant glioma. *Cancer Immunol Immunother*. (2019) 68:331–40. doi: 10.1007/s00262-018-2274-1

10. Izumoto S, Tsuboi A, Oka Y, Suzuki T, Hashiba T, Kagawa N, et al. Phase II clinical trial of Wilms tumor 1 peptide vaccination for patients with recurrent glioblastoma multiforme. *J Neurosurg*. (2008) 108:963–71. doi: 10.3171/JNS/2008/108/5/0963

11. Yokota C, Kagawa N, Takano K, Chiba Y, Kinoshita M, Kijima N, et al. Maintenance of WT1 expression in tumor cells is associated with a good prognosis in Malignant glioma patients treated with WT1 peptide vaccine immunotherapy. *Cancer Immunology Immunotherapy*. (2022) 71:189–201. doi: 10.1007/s00262-021-02954-z

12. Weller M, Butowski N, Tran DD, Recht LD, Lim M, Hirte H, et al. Rindopepimut with temozolomide for patients with newly diagnosed, EGFRvIII-expressing glioblastoma (ACT IV): a randomised, double-blind, international phase 3 trial. *Lancet Oncol*. (2017) 18:1373–85. doi: 10.1016/S1470-2045(17)30517-X

13. Sampson JH, Heimberger AB, Archer GE, Aldape KD, Friedman AH, Friedman HS, et al. Immunologic escape after prolonged progression-free survival with epidermal growth factor receptor variant III peptide vaccination in patients with newly diagnosed glioblastoma. *J Clin Oncol*. (2010) 28:4722–9. doi: 10.1200/JCO.2010.28.6963

14. Reardon DA, Desjardins A, Vredenburgh JJ, O'Rourke DM, Tran DD, Fink KL, et al. Rindopepimut with bevacizumab for patients with relapsed EGFRvIII-expressing glioblastoma (ReACT): results of a double-blind randomized phase II trial. *Clin Cancer Res*. (2020) 26:1586–94. doi: 10.1158/1078-0432.CCR-18-1140

15. Platten M, Bunse L, Wick A, Bunse T, Cornet LL, Harting I, et al. A vaccine targeting mutant IDH1 in newly diagnosed glioma. *Nature*. (2021) 592:463–8. doi: 10.1038/s41586-021-03363-z

16. Grassl N, Poschke I, Lindner K, Bunse L, Mildenberger I, Boschert T, et al. A H3K27M-targeted vaccine in adults with diffuse midline glioma. *Nat Med*. (2023) 29:2586–92. doi: 10.1038/s41591-023-02555-6

17. Liau LM, Prins RM, Kiertscher SM, Odesa SK, Kremen TJ, Giovannone AJ, et al. Dendritic cell vaccination in glioblastoma patients induces systemic and intracranial T-cell responses modulated by the local central nervous system tumor microenvironment. *Clin Cancer Res*. (2005) 11:5515–25. doi: 10.1158/1078-0432.CCR-05-0464

18. Yu JS, Wheeler CJ, Zeltzer PM, Ying H, Finger DN, Lee PK, et al. Vaccination of Malignant glioma patients with peptide-pulsed dendritic cells elicits systemic cytotoxicity and intracranial T-cell infiltration. *Cancer Res*. (2001) 61:842–7.

19. Yu JS, Liu G, Ying H, Yong WH, Black KL, Wheeler CJ. Vaccination with tumor lysate-pulsed dendritic cells elicits antigen-specific, cytotoxic T-cells in patients with Malignant glioma. *Cancer Res*. (2004) 64:4973–9. doi: 10.1158/0008-5472.CAN-03-3505

20. Yamanaka R, Homma J, Yajima N, Tsuchiya N, Sano M, Kobayashi T, et al. Clinical evaluation of dendritic cell vaccination for patients with recurrent glioma: results of a clinical phase I/II trial. *Clin Cancer Res*. (2005) 11:4160–7. doi: 10.1158/1078-0432.CCR-05-0120

21. Yamanaka R, Abe T, Yajima N, Tsuchiya N, Homma J, Kobayashi T, et al. Vaccination of recurrent glioma patients with tumour lysate-pulsed dendritic cells elicits immune responses: results of a clinical phase I/II trial. *Br J Cancer*. (2003) 89:1172–9. doi: 10.1038/sj.bjc.6601268

22. Liau LM, Ashkan K, Tran DD, Campian JL, Trusheim JE, Cobbs CS, et al. First results on survival from a large Phase 3 clinical trial of an autologous dendritic cell vaccine in newly diagnosed glioblastoma. *J Transl Med*. (2018) 16:142. doi: 10.1186/s12967-018-1507-6

23. Liau LM, Ashkan K, Brem S, Campian JL, Trusheim JE, Iwamoto FM, et al. Association of autologous tumor lysate-loaded dendritic cell vaccination with extension of survival among patients with newly diagnosed and recurrent glioblastoma: A phase 3 prospective externally controlled cohort trial. *JAMA Oncol*. (2023) 9:112–21. doi: 10.1001/jamaoncol.2022.5370

24. Wen PY, Reardon DA, Armstrong TS, Phuphanich S, Aiken RD, Landolfi JC, et al. A randomized double-blind placebo-controlled phase II trial of dendritic cell

vaccine ICT-107 in newly diagnosed patients with glioblastoma. *Clin Cancer Res*. (2019) 25:5799–807. doi: 10.1158/1078-0432.CCR-19-0261

25. Bota DA, Taylor TH, Piccioni DE, Duma CM, LaRocca RV, Kesari S, et al. Phase 2 study of AV-GBM-1 (a tumor-initiating cell targeted dendritic cell vaccine) in newly diagnosed Glioblastoma patients: safety and efficacy assessment. *J Exp Clin Cancer Res*. (2022) 41:344. doi: 10.1186/s13046-022-02552-6

26. Everson RG, Hugo W, Sun L, Antonios J, Lee A, Ding L, et al. TLR agonists polarize interferon responses in conjunction with dendritic cell vaccination in Malignant glioma: a randomized phase II Trial. *Nat Commun*. (2024) 15:3882. doi: 10.1038/s41467-024-48073-y

27. Batich KA, Reap EA, Archer GE, Sanchez-Perez L, Nair SK, Schmittling RJ, et al. Long-term survival in glioblastoma with cytomegalovirus pp65-targeted vaccination. *Clin Cancer Res*. (2017) 23:1898–909. doi: 10.1158/1078-0432.CCR-16-2057

28. Mitchell DA, Batich KA, Gunn MD, Huang MN, Sanchez-Perez L, Nair SK, et al. Tetanus toxoid and CCL3 improve dendritic cell vaccines in mice and glioblastoma patients. *Nature*. (2015) 519:366–9. doi: 10.1038/nature14320

29. Batich KA, Mitchell DA, Healy P, Herndon JEII, Sampson JH. Once, twice, three times a finding: reproducibility of dendritic cell vaccine trials targeting cytomegalovirus in glioblastoma. *Clin Cancer Res*. (2020) 26:5297–303. doi: 10.1158/1078-0432.CCR-20-1082

30. Hu JL, Omofoye OA, Rudnick JD, Kim S, Tighiouart M, Phuphanich S, et al. A phase I study of autologous dendritic cell vaccine pulsed with allogeneic stem-like cell line lysate in patients with newly diagnosed or recurrent glioblastoma. *Clin Cancer Res*. (2022) 28:689–96. doi: 10.1158/1078-0432.CCR-21-2867

31. Peng M, Mo Y, Wang Y, Wu P, Zhang Y, Xiong F, et al. Neoantigen vaccine: an emerging tumor immunotherapy. *Mol Cancer*. (2019) 18:128. doi: 10.1186/s12943-019-1055-6

32. Keskin DB, Anandappa AJ, Sun J, Tirosh I, Mathewson ND, Li S, et al. Neoantigen vaccine generates intratumoral T cell responses in phase Ib glioblastoma trial. *Nature*. (2019) 565:234–9. doi: 10.1038/s41586-018-0792-9

33. Johanns TM, Garfinkle EAR, Miller KE, Livingstone AJ, Roberts KF, Venkata LPR, et al. Integrating multisector molecular characterization into personalized peptide vaccine design for patients with newly diagnosed glioblastoma. *Clin Cancer Res*. (2024) 30(13):2729–42. doi: 10.1158/1078-0432.27034444.v1

34. Zhou JG, Liang B, Liu JG, Jin SH, He SS, Frey 2B, et al. Identification of 15 lncRNAs signature for predicting survival benefit of advanced melanoma patients treated with anti-PD-1 monotherapy. *Cells*. (2021) 10(5):977. doi: 10.3390/cells10050977

35. Wang XP, Guo W, Chen YF, Hong C, Ji J, Zhang XY, et al. PD-1/PD-L1 axis is involved in the interaction between microglial polarization and glioma. *Int Immunopharmacol*. (2024) 133:112074. doi: 10.1016/j.intimp.2024.112074

36. Omuro A, Reardon DA, Sampson JH, Baehring J, Sahebjam S, Cloughesy TF, et al. Nivolumab plus radiotherapy with or without temozolomide in newly diagnosed glioblastoma: Results from exploratory phase I cohorts of CheckMate 143. *Neurooncol Adv*. (2022) 4:vdac025. doi: 10.1093/noajnl/vdac025

37. Reardon DA, Brandes AA, Omuro A, Mulholland P, Lim M, Wick A, et al. Effect of nivolumab vs bevacizumab in patients with recurrent glioblastoma: the checkMate 143 phase 3 randomized clinical trial. *JAMA Oncol*. (2020) 6:1003–10. doi: 10.1001/jamaoncol.2020.1024

38. Lim M, Weller M, Idbaih A, Steinbach J, Finocchiaro G, Raval RR, et al. Phase III trial of chemoradiotherapy with temozolomide plus nivolumab or placebo for newly diagnosed glioblastoma with methylated MGMT promoter. *Neuro-Oncology*. (2022) 24:1935–49. doi: 10.1093/neuonc/noac116

39. Omuro A, Brandes AA, Carpentier AF, Idbaih A, Reardon DA, Cloughesy T, et al. Radiotherapy combined with nivolumab or temozolomide for newly diagnosed glioblastoma with unmethylated MGMT promoter: An international randomized phase III trial. *Neuro-Oncology*. (2022) 25:123–34. doi: 10.1093/neuonc/noac099

40. Ito H, Nakashima H, Chiocca EA. Molecular responses to immune checkpoint blockade in glioblastoma. *Nat Med*. (2019) 25:359–61. doi: 10.1038/s41591-019-0385-7

41. Schalper KA, Rodriguez-Ruiz ME, Diez-Valle R, López-Janeiro A, Porciuncula A, Idoate MA, et al. Neoadjuvant nivolumab modifies the tumor immune microenvironment in resectable glioblastoma. *Nat Med*. (2019) 25:470–6. doi: 10.1038/s41591-018-0339-5

42. Cloughesy TF, Mochizuki AY, Orpilla JR, Hugo W, Lee AH, Davidson TB, et al. Neoadjuvant anti-PD-1 immunotherapy promotes a survival benefit with intratumoral and systemic immune responses in recurrent glioblastoma. *Nat Med*. (2019) 25:477–86. doi: 10.1038/s41591-018-0337-7

43. Zhao J, Chen AX, Gartrell RD, Silverman AM, Aparicio L, Chu T, et al. Immune and genomic correlates of response to anti-PD-1 immunotherapy in glioblastoma. *Nat Med*. (2019) 25:462–9. doi: 10.1038/s41591-019-0349-y

44. Duerinck J, Schwarze JK, Awada G, Tijtgat J, Vaeyens F, Bertels C, et al. Intracerebral administration of CTLA-4 and PD-1 immune checkpoint blocking monoclonal antibodies in patients with recurrent glioblastoma: a phase I clinical trial. *J Immunother Cancer*. (2021) 9:e002296. doi: 10.1136/jitc-2020-002296

45. Dunkel IJ, Doz F, Foreman NK, Hargrave D, Lassaletta A, André N, et al. Nivolumab with or without ipilimumab in pediatric patients with high-grade CNS Malignancies: Safety, efficacy, biomarker, and pharmacokinetics-CheckMate 908. *Neuro Oncol*. (2023) 25:1530–45. doi: 10.1093/neuonc/noad031

46. Sahebjam S, Forsyth PA, Tran ND, Arrington JA, Macaulay R, Etame AB, et al. Hypofractionated stereotactic re-irradiation with pembrolizumab and bevacizumab in patients with recurrent high-grade gliomas: results from a phase I study. *Neuro Oncol*. (2021) 23:677–86. doi: 10.1093/neuonc/noaa260

47. Simonelli M, Garralda E, Eskens F, Gil-Martin M, Yen CJ, Obermannova R, et al. Isatuximab plus atezolizumab in patients with advanced solid tumors: results from a phase I/II, open-label, multicenter study. *ESMO Open*. (2022) 7:100562. doi: 10.1016/j.esmoop.2022.100562

48. Brown MP, Ebert LM, Gargett T. Clinical chimeric antigen receptor-T cell therapy: a new and promising treatment modality for glioblastoma. *Clin Transl Immunol*. (2019) 8:e1050. doi: 10.1002/cti2.2019.8.issue-5

49. Pule MA, Savoldo B, Myers GD, Rossig C, Russell HV, Dotti G, et al. Virus-specific T cells engineered to coexpress tumor-specific receptors: persistence and antitumor activity in individuals with neuroblastoma. *Nat Med*. (2008) 14:1264–70. doi: 10.1038/nm.1882

50. Majzner RG, Ramakrishna S, Yeom KW, Patel S, Chinnasamy H, Schultz LM, et al. GD2-CAR T cell therapy for H3K27M-mutated diffuse midline gliomas. *Nature*. (2022) 603:934–41. doi: 10.1038/s41586-022-04489-4

51. Liu Z, Zhou J, Yang X, Liu Y, Zou C, Lv W, et al. Safety and antitumor activity of GD2-Specific 4SCAR-T cells in patients with glioblastoma. *Mol Cancer*. (2023) 22:3. doi: 10.1186/s12943-022-01711-9

52. O'Rourke DM, Nasrallah MP, Desai A, Melenhorst JJ, Mansfield K, Morrissette JJD, et al. A single dose of peripherally infused EGFRvIII-directed CAR T cells mediates antigen loss and induces adaptive resistance in patients with recurrent glioblastoma. *Sci Trans Med*. (2017) 9:eaaa0984. doi: 10.1126/scitranslmed.aaa0984

53. Goff SL, Morgan RA, Yang JC, Sherry RM, Robbins PF, Restifo NP, et al. Pilot trial of adoptive transfer of chimeric antigen receptor-transduced T cells targeting EGFRvIII in patients with glioblastoma. *J Immunother*. (2019) 42:126–35. doi: 10.1097/CJI.0000000000000260

54. Ahmed N, Brawley V, Hegde M, Bielamowicz K, Kalra M, Landi D, et al. HER2-specific chimeric antigen receptor–modified virus-specific T cells for progressive glioblastoma: A phase 1 dose-escalation trial. *JAMA Oncol*. (2017) 3:1094–101. doi: 10.1001/jamaoncol.2017.0184

55. Brown CE, Badie B, Barish ME, Weng L, Ostberg JR, Chang WC, et al. Bioactivity and safety of IL13Rα2-redirected chimeric antigen receptor CD8+ T cells in patients with recurrent glioblastoma. *Clin Cancer Res*. (2015) 21:4062–72. doi: 10.1158/1078-0432.CCR-15-0428

56. Brown Christine E, Alizadeh D, Starr R, Weng L, Wagner JR, Naranjo A, et al. Regression of glioblastoma after chimeric antigen receptor T-cell therapy. *New Engl J Med*. (2016) 375:2561–9. doi: 10.1056/NEJMoa1610497

57. Brown CE, Rodriguez A, Palmer J, Ostberg JR, Naranjo A, Wagner JR, et al. Off-the-shelf, steroid-resistant, IL13Rα2-specific CAR T cells for treatment of glioblastoma. *Neuro-Oncology*. (2022) 24:1318–30. doi: 10.1093/neuonc/noac024

58. Jin L, Ge H, Long Y, Yang C, Chang YE, Mu L, et al. CD70, a novel target of CAR T-cell therapy for gliomas. *Neuro Oncol*. (2018) 20:55–65. doi: 10.1093/neuonc/nox116

59. Chow KK, Naik S, Kakarla S, Brawley VS, Shaffer DR, Yi Z, et al. T cells redirected to EphA2 for the immunotherapy of glioblastoma. *Mol Ther*. (2013) 21:629–37. doi: 10.1038/mt.2012.210

60. Lin Q, Ba T, Ho J, Chen D, Cheng Y, Wang L, et al. First-in-human trial of ephA2-redirected CAR T-cells in patients with recurrent glioblastoma: A preliminary report of three cases at the starting dose. *Front Oncol*. (2021) 11:694941. doi: 10.3389/fonc.2021.694941

61. Brown CE, Aguilar B, Starr R, Yang X, Chang WC, Weng L, et al. Optimization of IL13Rα2-targeted chimeric antigen receptor T cells for improved anti-tumor efficacy against glioblastoma. *Mol Ther*. (2018) 26:31–44. doi: 10.1016/j.ymthe.2017.10.002

62. Heczey A, Louis CU, Savoldo B, Dakhova O, Durett A, Grilley B, et al. CAR T cells administered in combination with lymphodepletion and PD-1 inhibition to patients with neuroblastoma. *Mol Ther*. (2017) 25:2214–24. doi: 10.1016/j.ymthe.2017.05.012

63. Bielamowicz K, Fousek K, Byrd TT, Samaha H, Mukherjee M, Aware N, et al. Trivalent CAR T cells overcome interpatient antigenic variability in glioblastoma. *Neuro Oncol*. (2018) 20:506–18. doi: 10.1093/neuonc/nox182

64. Burger MC, Forster MT, Romanski A, Straßheimer F, Macas J, Zeiner PS, et al. Intracranial injection of natural killer cells engineered with a HER2-targeted chimeric antigen receptor in patients with recurrent glioblastoma. *Neuro Oncol*. (2023) 25:2058–71. doi: 10.1093/neuonc/noad087

65. Zhang C, Burger MC, Jennewein L, Genßler S, Schönfeld K, Zeiner P, et al. ErbB2/HER2-specific NK cells for targeted therapy of glioblastoma. *J Natl Cancer Inst*. (2016) 108(5). doi: 10.1093/jnci/djv375

66. Choi BD, Gerstner ER, Frigault MJ, Leick MB, Mount CW, Balaj L, et al. Intraventricular CARv3-TEAM-E T cells in recurrent glioblastoma. *New Engl J Med*. (2024) 390:1290–8. doi: 10.1056/NEJMoa2314390

67. Wang JL, Scheitler KM, Wenger NM, Elder JB. Viral therapies for glioblastoma and high-grade gliomas in adults: a systematic review. *Neurosurg Focus*. (2021) 50:E2. doi: 10.3171/2020.11.FOCUS20854

68. Chiocca EA, Abbed KM, Tatter S, Louis DN, Hochberg FH, Barker F, et al. A phase I open-label, dose-escalation, multi-institutional trial of injection with an E1B-attenuated adenovirus, ONYX-015, into the peritumoral region of recurrent Malignant

gliomas, in the adjuvant setting. *Mol Ther*. (2004) 10:958–66. doi: 10.1016/j.ymthe.2004.07.021

69. Lang FF, Conrad C, Gomez-Manzano C, Yung WKA, Sawaya R, Weinberg JS, et al. Phase I study of DNX-2401 (Delta-24-RGD) oncolytic adenovirus: replication and immunotherapeutic effects in recurrent Malignant glioma. *J Clin Oncol*. (2018) 36:1419–27. doi: 10.1200/JCO.2017.75.8219

70. Martínez-Vélez N, Garcia-Moure M, Marigil M, González-Huarriz M, Puigdelloses M, Pérez-Larraya JG, et al. The oncolytic virus Delta-24-RGD elicits an antitumor effect in pediatric glioma and DIPG mouse models. *Nat Commun*. (2019) 10:2235. doi: 10.1038/s41467-019-10043-0

71. van den Bossche WBL, Kleijn A, Teunissen CE, Voerman JSA, Teodosio C, Noske DP, et al. Oncolytic virotherapy in glioblastoma patients induces a tumor macrophage phenotypic shift leading to an altered glioblastoma microenvironment. *Neuro Oncol*. (2018) 20:1494–504. doi: 10.1093/neuonc/noy082

72. van Putten EHP, Kleijn A, van Beusechem VW, Noske D, Lamers CHJ, Goede ALD, et al. Convection enhanced delivery of the oncolytic adenovirus delta24-RGD in patients with recurrent GBM: A phase I clinical trial including correlative studies. *Clin Cancer Res*. (2022) 28:1572–85. doi: 10.1158/1078-0432.CCR-21-3324

73. Gállego Pérez-Larraya J, Garcia-Moure M, Labiano S, Patiño-García A, Dobbs J, Gonzalez-Huarriz M, et al. Oncolytic DNX-2401 virus for pediatric diffuse intrinsic pontine glioma. *N Engl J Med*. (2022) 386:2471–81. doi: 10.1056/NEJMoa2202028

74. Nassiri F, Patil V, Yefet LS, Singh O, Liu J, Dang RMA, et al. Oncolytic DNX-2401 virotherapy plus pembrolizumab in recurrent glioblastoma: a phase 1/2 trial. *Nat Med*. (2023) 29:1370–8. doi: 10.1038/s41591-023-02347-y

75. Desjardins A, Gromeier M, Herndon JE 2nd, Beaubier N, Bolognesi DP, Friedman AH, et al. Recurrent glioblastoma treated with recombinant poliovirus. *N Engl J Med*. (2018) 379:150–61. doi: 10.1056/NEJMoa1716435

76. Fares J, Ahmed AU, Ulasov IV, Sonabend AM, Miska J, Lee-Chang C, et al. Neural stem cell delivery of an oncolytic adenovirus in newly diagnosed Malignant glioma: a first-in-human, phase 1, dose-escalation trial. *Lancet Oncol*. (2021) 22:1103–14. doi: 10.1016/S1470-2045(21)00245-X

77. Ling AL, Solomon IH, Landivar AM, Nakashima H, Woods JK, Santos A, et al. Clinical trial links oncolytic immunoactivation to survival in glioblastoma. *Nature*. (2023) 623:157–66. doi: 10.1038/s41586-023-06623-2

78. Ou A, Yung WKA, Majd N. Molecular mechanisms of treatment resistance in glioblastoma. *Int J Mol Sci*. (2020) 22(1):351. doi: 10.3390/ijms22010351

79. Awad MM, Govindan R, Balogh KN, Spigel DR, Garon EB, Bushway ME, et al. Personalized neoantigen vaccine NEO-PV-01 with chemotherapy and anti-PD-1 as first-line treatment for non-squamous non-small cell lung cancer. *Cancer Cell*. (2022) 40:1010–26.e11. doi: 10.1016/j.ccell.2022.08.003

80. Liu Z, Shi M, Ren Y, Xu H, Weng S, Ning W, et al. Recent advances and applications of CRISPR-Cas9 in cancer immunotherapy. *Mol Cancer*. (2023) 22:35. doi: 10.1186/s12943-023-01738-6

81. Zhang R, Tang L, Wang Y, Tian Y, Wu S, Zhou B, et al. A dendrimer peptide (KK2DP7) delivery system with dual functions of lymph node targeting and immune adjuvants as a general strategy for cancer immunotherapy. *Adv Sci (Weinh)*. (2023) 10:e2300116. doi: 10.1002/advs.202300116

82. Chen KS, Reinshagen C, Van Schaik TA, Rossignoli F, Borges P, Mendonca NC, et al. Bifunctional cancer cell-based vaccine concomitantly drives direct tumor killing and antitumor immunity. *Sci Transl Med*. (2023) 15:eabo4778. doi: 10.1126/scitranslmed.abo4778

83. Johnson KC, Anderson KJ, Courtois ET, Gujar AD, Barthel FP, Varn FS, et al. Single-cell multimodal glioma analyses identify epigenetic regulators of cellular plasticity and environmental stress response. *Nat Genet*. (2021) 53:1456–68. doi: 10.1038/s41588-021-00926-8

84. Vinci M, Burford A, Molinari V, Popov S, Clarke M, Taylor KR, et al. Functional diversity and cooperativity between subclonal populations of pediatric glioblastoma and diffuse intrinsic pontine glioma cells. *Nat Med*. (2018) 24:1204–15. doi: 10.1038/s41591-018-0086-7

85. Jha P, Manjunath N, Singh J, Mani K, Garg A, Kaur K, et al. Analysis of PD-L1 expression and T cell infiltration in different molecular subgroups of diffuse midline gliomas. *Neuropathology*. (2019) 39:413–24. doi: 10.1111/neup.12594

86. Alexandrov LB, Nik-Zainal S, Wedge DC, Aparicio SAJR, Behjati S, Biankin AV, et al. Signatures of mutational processes in human cancer. *Nature*. (2013) 500:415–21. doi: 10.1038/nature12477

87. Touat M, Li YY, Boynton AN, Spurr LF, Iorgulescu JB, Bohrson CL, et al. Mechanisms and therapeutic implications of hypermutation in gliomas. *Nature*. (2020) 580:517–23. doi: 10.1038/s41586-020-2209-9

88. McGranahan N, Furness AJ, Rosenthal R, Ramskov S, Lyngaa R, Saini SK, et al. Clonal neoantigens elicit T cell immunoreactivity and sensitivity to immune checkpoint blockade. *Science*. (2016) 351:1463–9. doi: 10.1126/science.aaf1490

89. Cacciotti C, Choi J, Alexandrescu S, Zimmerman MA, Cooney TM, Chordas C, et al. Immune checkpoint inhibition for pediatric patients with recurrent/refractory CNS tumors: a single institution experience. *J Neurooncol*. (2020) 149:113–22. doi: 10.1007/s11060-020-03578-6

90. Chalise L, Kato A, Ohno M, Maeda ZS, Yamamichi A, Kuramitsu S, et al. Efficacy of cancer-specific anti-podoplanin CAR-T cells and oncolytic herpes virus G47Δ combination therapy against glioblastoma. *Mol Ther Oncolytics*. (2022) 26:265–74. doi: 10.1016/j.omto.2022.07.006

91. Harrington K, Freeman DJ, Kelly B, Harper J, Soria JC. Optimizing oncolytic virotherapy in cancer treatment. *Nat Rev Drug Discovery*. (2019) 18:689–706. doi: 10.1038/s41573-019-0029-0

92. LaRocca CJ, Warner SG. Oncolytic viruses and checkpoint inhibitors: combination therapy in clinical trials. *Clin Transl Med*. (2018) 7:35. doi: 10.1186/s40169-018-0214-5

93. Sonabend AM, Gould A, Amidei C, Ward R, Schmidt KA, Zhang DY, et al. Repeated blood-brain barrier opening with an implantable ultrasound device for delivery of albumin-bound paclitaxel in patients with recurrent glioblastoma: a phase 1 trial. *Lancet Oncol*. (2023) 24:509–22. doi: 10.1016/S1470-2045(23)00112-2

94. Kaufman HL, Kohlhapp FJ, Zloza A. Oncolytic viruses: a new class of immunotherapy drugs. *Nat Rev Drug Discovery*. (2015) 14:642–62. doi: 10.1038/nrd4663

95. Louis DN, Perry A, Wesseling P, Brat DJ, Cree IA, Figarella-Branger D, et al. The 2021 WHO classification of tumors of the central nervous system: a summary. *Neuro-oncology*. (2021) 23:1231–51. doi: 10.1093/neuonc/noab106

96. Zhang P, Zhang Y, Ji N. Challenges in the treatment of glioblastoma by chimeric antigen receptor T-cell immunotherapy and possible solutions. *Front Immunol*. (2022) 13:927132. doi: 10.3389/fimmu.2022.927132

frontiers | Frontiers in Immunology

TYPE Review
PUBLISHED 01 November 2024
DOI 10.3389/fimmu.2024.1480572

Check for updates

OPEN ACCESS

EDITED BY
Jiaheng Xie,
Central South University, China

REVIEWED BY
Kaige Chen,
Wake Forest University, United States
Xin Yu,
Baylor College of Medicine, United States

*CORRESPONDENCE
Ke Xu
cqghxuke@cqu.edu.cn
Xiaoli Yang
yangxiaoli@swmu.edu.cn
Bo Li
liboer2002@swmu.edu.cn

†These authors have contributed equally to this work and share first authorship

RECEIVED 14 August 2024
ACCEPTED 09 October 2024
PUBLISHED 01 November 2024

CITATION
Gong Y, Gong D, Liu S, Gong X, Xiong J, Zhang J, Jiang L, Liu J, Zhu L, Luo H, Xu K, Yang X and Li B (2024) Deciphering the role of NcRNAs in Pancreatic Cancer immune evasion and drug resistance: a new perspective for targeted therapy. *Front. Immunol.* 15:1480572. doi: 10.3389/fimmu.2024.1480572

COPYRIGHT
© 2024 Gong, Gong, Liu, Gong, Xiong, Zhang, Jiang, Liu, Zhu, Luo, Xu, Yang and Li. This is an open-access article distributed under the terms of the Creative Commons Attribution License (CC BY). The use, distribution or reproduction in other forums is permitted, provided the original author(s) and the copyright owner(s) are credited and that the original publication in this journal is cited, in accordance with accepted academic practice. No use, distribution or reproduction is permitted which does not comply with these terms.

Deciphering the role of NcRNAs in Pancreatic Cancer immune evasion and drug resistance: a new perspective for targeted therapy

Yu Gong[1†], Desheng Gong[2,3,4†], Sinian Liu[5†], Xiangjin Gong[1], Jingwen Xiong[1], Jinghan Zhang[6], Lai Jiang[7], Jie Liu[2,3], Lin Zhu[2,3], Huiyang Luo[8], Ke Xu[8*], Xiaoli Yang[2,3*] and Bo Li[2,3*]

[1]Department of Sports Rehabilitation, Southwest Medical University, Luzhou, China, [2]Department of General Surgery (Hepatopancreatobiliary surgery), The Affiliated Hospital of Southwest Medical University, Luzhou, Sichuan, China, [3]Academician (Expert) Workstation of Sichuan Province, Metabolic Hepatobiliary and Pancreatic Diseases Key Laboratory of Luzhou City, The Affiliated Hospital of Southwest Medical University, Luzhou, Sichuan, China, [4]General Surgery Department, The TCM Hospital of Longquanyi, Chengdu, China, [5]Department of Pathology, Xichong People's Hospital, Nanchong, China, [6]Department of Anesthesia, Southwest Medical University, Luzhou, China, [7]Clinical Medical College, Southwest Medical University, Luzhou, China, [8]Department of Oncology, Chongqing General Hospital, Chongqing University, Chongqing, China

Pancreatic cancer (PC) is a very aggressive digestive system tumor, known for its high mortality rate, low cure rate, low survival rate and poor prognosis. In particular, pancreatic ductal adenocarcinoma (PADC), which accounts for more than 90% of PC cases, has an overall 5-year survival rate of only 5%, which is an extremely critical situation. Early detection and effective treatment of PC is extremely difficult, which leads many patients to despair. In the current medical context, targeted therapy, as an important strategy for cancer treatment, is expected. However, the problems of immune escape and drug resistance in PC have become two major obstacles that are difficult to be overcome by targeted therapy. How to break through these two difficulties has become a key issue to be solved in the field of PC therapy. In recent years, non-coding RNAs (ncRNAs) have continued to heat up in the field of cancer research. NcRNAs play a pivotal role in gene regulation, cell differentiation, development, and disease processes, and their important roles in the genesis, development, and therapeutic response of PC have been gradually revealed. More importantly, ncRNAs have many advantages as therapeutic targets, such as high specificity and low side effects, making them a new favorite in the field of PC therapy. Therefore, the aim of this paper is to provide new ideas and methods for the targeted therapy of PC by reviewing the mechanism of action of four major ncRNAs (circRNAs, lncRNAs, miRNAs, siRNAs) in both immune escape and drug resistance of PC. It is expected that an effective way to overcome immune escape and drug resistance can be found through in-depth study of ncRNA, bringing a ray of hope to PC patients.

KEYWORDS

tumor-immune interactions, ncRNA, tumor immune microenvironment, targeted therapy, pancreatic cancer

1 Introduction

PC is a highly malignant tumor of the digestive system, characterized by high mortality, low cure rates, poor prognosis, and challenges in early detection and treatment (1, 2). Over 90% of PC cases are PADCs, which have an extremely high mortality rate and a 5-year overall survival rate of 5% (3, 4). Other PCs include pancreatic acinar cell carcinoma, cystic tumors, and endocrine pancreatic tumors, which have a lower incidence but may have a relatively better prognosis (5, 6). Approximately 65% of PC tumors are concentrated in the head of the pancreas., followed by those located in the head and tail of the pancreas (7).

Current treatments for PC include surgery, radiotherapy, chemotherapy, targeted therapy, and immunotherapy (8). Surgery is the preferred treatment for PC, but due to late diagnosis, 80% of patients lose the opportunity for treatment (9, 10). Radiation and chemotherapy can alleviate symptoms and prolong the survival cycle, but have significant side effects and are rarely able to cure patients. Targeted therapy has been a major strategy in cancer treatment research, which has the effect of enhancing therapeutic efficacy and reducing side effects (11). Immunotherapy, like targeted therapy, can specifically target tumor cells, thereby improving therapeutic efficacy and reducing side effects (12). However, both immunotherapy and targeted therapy encounter two significant challenges: immune escape and drug resistance (13).

NcRNAs, i.e. non-coding RNAs, are a class of RNA molecules with no protein-coding function (14). They play an important regulatory role in cells, affecting a variety of life activities in organisms by regulating gene expression, chromatin structure, nuclear translocation, and protein function (15, 16). In recent years, ncRNAs have attracted much attention in the field of cancer research, and are believed to play an important role in the occurrence, development, and therapeutic response of cancer (17). Meanwhile, the targeted therapeutic roles of ncRNAs have also been gradually revealed in PC.

More importantly, ncRNAs have significant advantageous features in serving as therapeutic targets:

1. ncRNAs are highly specific in their expression in tumor tissues, which means that they may become biomarkers for cancer diagnosis and prognosis or novel targets for therapy (18);
2. ncRNAs affect cancer cell proliferation, differentiation, metastasis, and death through the modulation of gene expression processes (19), so that therapies targeting ncRNAs may directly intervene in cancer progression;
3. the regulatory network of ncRNAs is complex and diverse, which provides a wealth of candidate targets for cancer-targeted therapies.

In conclusion, ncRNAs have great potential and prospects in serving as PC therapeutic targets. So in summary, in this paper, we will review the functions and regulatory mechanisms of four major ncRNAs (circRNAs, lncRNAs, miRNAs, siRNAs) in both immune escape and drug resistance to help us better understand the pathogenesis of PC, and at the same time provide new ideas and approaches for PC targeted therapy and immunotherapy.

2 Classification, function of ncRNAs, and their biological mechanisms in diseases

NcRNAs play important roles in gene regulation, cell differentiation, development, and disease processes (20). NcRNAs can be categorized into a number of different types, including miRNAs, circRNAs, lncRNAs, and siRNAs, depending on their length, mode of formation, and function (21).

CircRNAs are abundant, stable RNA molecules with a closed-loop structure that is conserved (22), and usually consist of hundreds of nucleotides (23). They control gene transcription through interactions with RNA-binding proteins, and also regulate signaling pathways through miRNA segregation (24, 25). They have a variety of regulatory roles in the cell, including regulation of gene expression, participation in protein synthesis, etc. (26). CircRNAs can also act as "molecular sponges" for miRNAs, adsorbing and neutralizing miRNAs, thus regulating the inhibitory effects of miRNAs on target genes (27). Through the above mechanisms, CircRNAs continuously regulates the tumor microenvironment (TME) of PC, thereby affecting the occurrence and development of cancer cells.

MiRNAs are endogenous short non-coding RNAs of 19 to 25 nucleotides in size, which are part of the epigenome. MiRNAs regulate gene expression by binding to the mRNA's 3′-untranslated region (3′-UTR) to either inhibit translation or promote degradation of target genes (28, 29). In the process of immunization against PDAC tumors, miRNAs regulate the recruitment and activation of immune cells to tumors (30, 31). At the same time, miRNAs can also act as oncogenes or oncogenes to participate in the genesis and development of PC (32).

LncRNAs are novel non-coding RNAs over 200 nucleotides in length and are key players in tumorigenesis and immune response (33, 34). They also have multiple regulatory roles in the cell, including regulation of gene expression, participation in cell differentiation, proliferation and apoptosis, etc. (35–37). LncRNAs can bind to proteins to form ribonucleoprotein complexes, thereby regulate the activity, localization and degradation of proteins, etc. (38–40). LncRNAs can also act as oncogenes or oncogenes in PCs to participate in the genesis and development of PCs (41). Like circRNAs, lncRNAs also have the function of sponging miRNAs to inhibit the abundance and activity of miRNAs (42).

SiRNAs are short interfering RNAs, usually consisting of 21-25 nucleotides (43). They are mainly used in cells to interfere with the replication and expression of exogenous viruses or transposons, and thus protect the cells from viral or transposon infection (44). SiRNAs can bind to exogenous mRNAs, induce their degradation, and thus inhibit their translation (45). Meanwhile, siRNAs can also be used to treat PC. By binding siRNAs to liposomes, siRNAs can be introduced into PC cells, which can inhibit the growth and spreading of PC cells (46).

PiRNAs are a unique class of non-coding RNAs, usually 21-35 nucleotides in length, related to the Piwi subfamily of Argonaute proteins in animals, especially in germline cells, used to suppress transposons and maintain genome integrity. Sex (47) (48). Compared to other ncRNAs such as miRNAs, lncRNAs, and circRNAs, their functions in cancer, including pancreatic cancer, are unclear. The main function of piRNA is to silence transposable elements through multiple mechanisms (49), including retrotransposons. By forming complexes with Piwi proteins, piRNAs can target transposon transcripts for degradation or translational repression, thereby limiting their proliferation and preventing their deleterious effects on the genome (50). This transposon silencing activity is critical for maintaining germline integrity and preventing genetic instability. In addition to their role in transposon silencing, piRNAs are also involved in other biological processes such as genesis, epigenetic regulation (51). Recent studies have also shown that piR-162725 may regulate the proliferation, migration and invasion phenotype of PADC, and may also regulate the EMT, cell differentiation and metabolism of PADC (52). However, the exact mechanisms and contributions of piRNAs to these processes remain largely unclear and are an active area of research.

In conclusion, ncRNAs play important regulatory roles in organisms; they can regulate gene expression levels, participate in protein synthesis, and regulate cell differentiation, proliferation, and apoptosis. An in-depth understanding of the classification and biological mechanisms of ncRNAs can help to better understand their regulatory mechanisms in PC TIME.

3 NcRNAs are involved in the immune response of tumor cells

In TIME, tumor cells often evade immune cells, thus affecting the effect of immunotherapy. Understanding the mechanism of ncRNA's action on immune escape in PC will help us better improve the effect of PC immunotherapy. Studies have shown that ncRNAs can mediate immune response through the following several mechanisms (Figure 1).

On the one hand, ncRNAs can affect the interaction between tumor cells and immune cells by targeting or regulating the expression or signaling of PD-L1, thereby suppressing immune response or inducing immune tolerance. For example, miR-142-5p can regulate PD-L1 expression in PC cells by binding to the 3'UTR of PD-L1 to promote tumor immune response (53). Similarly, circMYO1C can enhance the stability of PD-L1 mRNA by targeting the N6-methyladenosine(M6A) site of PD-L1 mRNA in conjunction with IGF2BP2, thereby accelerating the immune escape of PDAC (54). On the contrary, miR-194-5p enhances the toxic effect of CD8 T cells on PC cells by targeting PD-L1, thereby inhibiting the proliferation, migration and invasion of PC cells, but its specific mechanism of action remains to be investigated (55).In addition, lncRNAs can act as miRNA "molecular sponge" to target PD-L1 expression. For example, lncRNA PMSB8-AS1 acts as a miRNA sponge, which activates PD-L1 expression by interacting with and repressing miR-382-3p to regulate the transcription factor STAT1 to mediate immune escape (56). Similarly, as a miRNA sponge, LINC00473 silencing blocks PC progression by enhancing PD-L1 down-regulation against miR-195-5p (57).

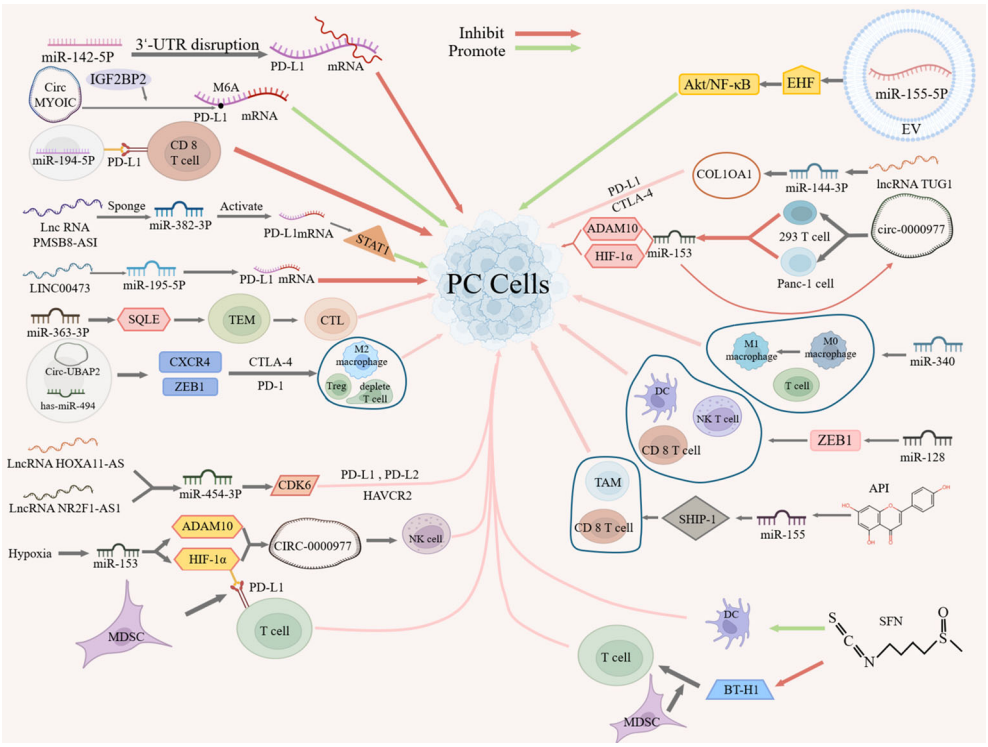

FIGURE 1
Role pathways of ncRNAs in the PC tumor immune response.

Besides, some studies have shown that ncRNAs associate with immune checkpoints and indirectly influence the expression of other immune checkpoints (e.g., CTLA-4, PD-L2, HAVCR2, etc.), and may in this way mediate immune escape. For example, miR-363-3p can inhibit PANC-1 proliferation by regulating squalene epoxidase (SQLE) expression in PAAD, where SQLE regulates tumor immune cell infiltration, immune checkpoints, and the TME, and high SQLE expression predicts depletion of cytotoxic lymphocytes and loss of antitumor capacity (58). Therefore, miR-363 -3p may regulate immune checkpoints through SQLE and thus inhibit immune escape. A more definitive study has also shown that circ-UBAP2 and has-miR-494 may regulate the expression of CXCR4 and ZEB1, which are positively correlated with the expression of CTLA-4 and PD-1, and thus affect the levels of M2 macrophages, depleted T cells, and T regulatory cells (Tregs) in PAAD tissues (59), suggesting that circ-UBAP2 and has-miR-494 may regulate immune checkpoints through CXCR4 and ZEB1 factors, which in turn inhibit antigen presentation by PCs and promote immune escape. Additionally, lncRNA HOXA11-AS/lncRNA NR2F1-AS1 may regulate cyclin-dependent kinase 6 (CDK6) expression by targeting miR-454-3p, which may have oncogenic roles in PC and is strongly associated with multiple immune cells and cellular infiltration and three immune checkpoints (PD-L1, PD-L2 and HAVCR2) (60), suggesting that lncRNA HOXA11-AS/lncRNA NR2F1-AS1 may regulate immune checkpoints through the miR-454-3p- CDK6 axis, thereby mediating immune escape.

On the other hand, ncRNAs can affect the adaptation and immune escape ability of tumor cells in hypoxic microenvironments by targeting the expression or signaling of hypoxia-inducible factors (e.g., HIF-1α) or tumor suppressors. For example, hypoxia can inhibit immune escape by regulating miR-153 and its two targets, HIF-1α and ADAM10, which in turn promote the expression of CIRC-0000977, as well as by targeting PD-L1 via HIF-1α, which promotes myeloid-derived suppressor cell (MDSC)-involved T cell activation (61). CIRC_0000977 plays a role under hypoxia by regulating related pathways through miR-153, which subsequently affects the killing effect of NK cells on PC cells (61). In addition, PC-derived extracellular vesicle (EV) miR-155-5p can promote tumor immune escape by targeting the tumor suppressor EHF to downregulate, and activate Akt/NF-κB signaling (62).

In addition, ncRNAs can influence interactions in the TME by targeting components or structures of the extracellular matrix or by directly targeting cells, thereby mediating immune infiltration and immune escape. In PAAD, as a structural component of the extracellular matrix, X-type alpha 1 (COL10A1) expression was significantly up-regulated in PC tissues and significantly correlated with immune infiltration, and with immune checkpoints (PD-L1 and CTLA-4), whereas the lncRNA TUG1/miR-144-3p/COL10A1 axis was identified as the most promising upstream ncRNA regulatory pathway, suggesting that lncRNA TUG1/miR-144-3p may influence immune escape by targeting structural components of the extracellular matrix (63). In addition, cicr_0000977, a sponge of miR-153, counteracted the inhibitory effect of miR-153 on HIF-1α and ADAM10 by directly targeting 293T and Panc-1 cells, whereas miR-153 inhibition on HIF1A or cicr_0000977 knockdown on HIF1A-mediated immune escape from PC cells had the opposite effect, i.e. miR-153 inhibition partially attenuated the effect of cicr_0000977 knockdown (61). Similarly, miR-340 and miR-128 can enhance anti-tumor immunity by targeting immune cells. MiR-340 overexpression promotes macrophage(TAM) polarization to an M1-like phenotype in the peripheral and tumor-immune microenvironment, increases the number of T cells, especially CD8 T cells, contributing to the anti-tumor effects of miR-340, thereby counteracting immune escape (64). MiR-128 overexpression, in turn, modulates the percentages of dendritic cells (DCs), CD8 T lymphocytes, and natural killer T cells (NKTs) in tumors and spleens via PDAC zinc-finger E-box-binding homology cassette 1 (ZEB1) thereby enhancing anti-tumor immunity (65).

Moreover, bioflavonoids like apigenin (API) and sulforaphane (SFN) also play a significant role in regulating the immune response through their interaction with miRNAs. For example, API can promote the expression of inositol 5'-phosphatase-1 (SHIP-1) by inhibiting miRNA-155, which leads to the expansion of tumor-killing TAMs and CD8 T cells and promotes the anti-tumor immune response (66). On the other hand, SFN can enhance DC phagocytosis, and can also promote the immune response by decreasing the expression of B7-H1 and MDSC frequency in monocytes exposed to glioma-conditioned medium to reduce immunosuppression and promote T-cell proliferation (67). Among them, the reduction of B7-H1 expression not only relies on the down-regulation of STAT3 phosphorylation by SFN, but also on the up-regulation of miR-194-5p by SFN, but the miR-194-5p signaling pathway of miR-194-5p needs to be further investigated (67).

All in all, NcRNAs play a crucial role in the immune response. They can affect the immune response by influencing the activity, function and proliferation of immune cells in a variety of ways. A deeper understanding of ncRNAs will help us better understand the working mechanism of the immune system and may provide new targets for future immunotherapy and drug development. However, we still have many unanswered questions about the role of ncRNAs in immune cell regulation that require further research and exploration.

4 NcRNA and drug resistance

In the last 3 years, a large number of ncRNAs have been found to be involved in PC drug resistance, promoting or inhibiting the resistance of tumor cells to chemotherapeutic drugs. These findings suggest that ncRNAs may become novel targets for PC immunotherapy (Table 1).

MiRNAs play an important regulatory role in PC drug resistance. For instance, miR-3173-5p, which originates from cancer-associated fibroblast (CAF) exosomes in PADC, mediates gemcitabine (GEM) resistance in PC by targeting ACSL4 (68). Interestingly, miR-3173-5p also can inhibit iron death, resulting in the emergence of GEM resistance in PCs (68). Additionally, it is found that targeting inhibition of miR-378 or glucocorticoid receptor signaling can reduce PDAC glucocorticoid resistance (69).

TABLE 1 Mechanisms of ncRNAs in PC drug resistance.

ncRNA	Expression	Genes and pathways	Role	References
miR-3173-5p	——	ACSL4	Promote GEM resistance and inhibit iron death	(68)
miR-378	——	——	Reduce GC resistance	(69)
lncRNA DSCR9	downregulated	miR-21-5p/BTG2	Affect the proliferation, invasion and GEM resistance of PC	(70)
lncRNA GAS2	downregulated	miR-21	Regulate GEM resistance in PC	(71)
lncRNA SH3BP5-AS1	upregulated	miR-139-5p/Wnt/CTBP1	Promote GEM resistance and tumor invasiveness in PC	(72)
LINC 02432	upregulated	miR-98-5p/HK2	Predict the sex of EGFR、MEK and ERK inhibitors	(73)
lncRNA UPK 1A-AS 1	upregulated	IL8, Ku70, Ku80	Confer paril-IL 8-dependent oxaliplatin resistance derived from CAF	(74)
LINC00460	——	PDAP1/PDGFA/PDGFR/CAF	Affect GEM resistance of PADC	(75)
circACTR2	downregulated	miR-3-221p/PTEN/PI3K/AKT	Reverse GEM chemoresistance in PC	(76)
Hsa_circ_000740	downregulated	has-miR-6509-3p/DEmRNA	Mediate GEM resistance in PC	(77)
siRNA	——	COL8A1	Inhibit the growth, migration, invasion and GEM resistance of tumor	(78)
siSLC7A11	——	Glutathione/DOX P-glycoprotein/Bcl-2/Bax	Promote drug sensitization	(79)

In addition, lncRNA-miRNA interactions influence PC resistance, e.g., the lncRNA DSCR9, which is significantly down-regulated in PAAD, targets BTG2 by binding to miR-21-5p, which in turn affects PC proliferation, invasion, and GEM resistance (70). Similarly, lncRNA GAS2, significantly down-regulated in GEM-resistant PAN-5 and CaPa-1 cells, may regulate GEM resistance in PC through miR-21; however, its specific mechanism of action remains unclear (71). In addition, lncRNA SH3BP5-AS1, which is up-regulated in GEM-resistant PC cells, activates the expression of CTBP1 in Wnt pathway through competitive binding of ceRNA to miR-139-5p, which promotes GEM-resistant PC cells and tumor invasiveness (72).Moreover, Glycolysis-related LINC 02432 up-regulated in PAAD predicts the activity of PAAD patients against EGFR、MEK and ERK inhibitors by regulating hsa-miR-98-5 p/hexokinase 2 (HK2) axis (73). Besides, up-regulated lncRNA UPK 1A-AS 1 in PC promotes DNA double-strand break repair by regulating the interaction between repair proteins Ku 70 and Ku 80, thus conferring paril-IL 8-dependent oxaliplatin resistance derived from CAF (74). In addition to interacting with miRNAs, LINC00460 also regulates CAF proliferation through the PDAP1/PDGFA/PDGFR signaling pathway, thereby mediating GEM resistance in PADC cells (75).

Ibid, circRNAs also play an important role in PC GEM resistance. CircACTR2 expression is significantly down-regulated in GEM-resistant PC cells, whereas its overexpression can target the PTEN-mediated PI3K/AKT signaling pathway via sponge miR-3-221p to reverse the chemoresistance of PC cells to GEM (76). Similarly, Hsa_circ_0007401, which is down-regulated in PC-resistant cells, acts as a "sponge" of has-miR-6509-3p and thus regulates differential messenger RNA (DEmRNA) (FLI1) to mediate PC GEM resistance (77).

In addition to this, siRNAs are also involved in the regulation of PC drug resistance. SiRNA or lentiviral sh-mediated down-regulation of collagen COL8A1 in PDAC cells inhibited tumor growth, migration, invasion, and GEM resistance (78). It is also found that a ferrous organometallic framework based nanoparticles (FMN) catalyzes the iron-dependent Fenton reaction and inhibits siSLC7A11-mediated upstream glutathione synthesis to carry out intracellular self-amplified iron death, which results in a reduction of DOX-retained P-glycoprotein activity and modulation of Bcl-2/Bax expression to reverse apoptosis-resistant state of tumor cells and promote drug sensitivity (79).

5 Discussion

Above, we revealed the role of four major ncRNAs (circRNAs, lncRNAs, miRNAs, and siRNAs) in the PC immune microenvironment in terms of both immune response and drug resistance, indicating that ncRNAs are expected to be novel potential targets for PC targeting and immunotherapy. And currently, the function and application of ncRNAs are still advancing rapidly. A recent study also synthesized a TME stimulation-responsive poly(beta-amino ester)s (PBAE)-based polymer nano-prodrug (miR-21i@HA-Gem-SS-P12), which can co-deliver miR-21 siRNA and GEM to achieve the combination therapy of miR-21 siRNA and GEM, and shows excellent tumor inhibitory effect *in vitro* and *in vivo* in PDAC (80). Therefore, it is just around the corner for ncRNA to become the target of PC immunotherapy.

Nevertheless, there are still many challenges and problems in the practical research and application of ncRNAs. For instance, the stability, selectivity, and specificity of ncRNAs *in vivo* require further improvement. Additionally, the interactions between ncRNAs and tumor-associated immune cells need to be more clearly understood—such as how miR-194-5p targets PD-L1 to regulate immune cells (55). Further exploration is also needed on the synergistic or antagonistic effects between ncRNAs and other signaling pathways.

Therefore, this paper suggests that future research should be deepened and expanded in the following aspects:

1. Development of Advanced Detection and Analysis Methods: Establish more precise and effective ncRNA detection and analysis techniques to enhance their diagnostic and prognostic value in PC;
2. Elucidation of ncRNA-Immune Cell Interactions: Delve deeper into the mechanisms of ncRNA-tumor-associated immune cell interactions to optimize their synergistic effects in PC immunotherapy;
3. Exploration of ncRNA-Signaling Pathway Crosstalk: Investigate the intricate interplay between ncRNAs and other signaling pathways to refine strategies for comprehensive PC therapy.

By focusing on these key aspects, we can harness the full potential of ncRNAs in the fight against pancreatic cancer.

Author contributions

YG: Writing – original draft. DG: Writing – original draft. SL: Writing – original draft. XG: Writing – original draft. JX: Writing – original draft. JZ: Writing – original draft. LJ: Writing – original draft. JL: Writing – original draft. LZ: Writing – original draft. HL: Writing – original draft. KX: Writing – review & editing. XY: Writing – review & editing. BL: Writing – review & editing.

Funding

The author(s) declare financial support was received for the research, authorship, and/or publication of this article. This study was supported by the Key Research and Development Project of the Science & Technology Department of Sichuan Province (Nos.2023YFQ0101), and was supported by Luzhou Key Research and Development Project in Science and Technology (2022-SYF-55).

Conflict of interest

The authors declare that the research was conducted in the absence of any commercial or financial relationships that could be construed as a potential conflict of interest.

Publisher's note

All claims expressed in this article are solely those of the authors and do not necessarily represent those of their affiliated organizations, or those of the publisher, the editors and the reviewers. Any product that may be evaluated in this article, or claim that may be made by its manufacturer, is not guaranteed or endorsed by the publisher.

References

1. Hao S, Han W, Ji Y, Sun H, Shi H, Ma J, et al. BANCR positively regulates the HIF-1α/VEGF-C/VEGFR-3 pathway in a hypoxic microenvironment to promote lymphangiogenesis in pancreatic cancer cells. *Oncol Lett*. (2022) 24:422. doi: 10.3892/ol.2022.13542

2. Miao Y. The effect of comfort care on postoperative quality of life, psychological status, and satisfaction of pancreatic cancer patients. *Evid Based Complement Alternat Med*. (2022) 2022:9483762. doi: 10.1155/2022/9483762

3. Park HR. Pancastatin A and B have selective cytotoxicity on glucose-deprived PANC-1 human pancreatic cancer cells. *J Microbiol Biotechnol*. (2020) 30:733–8. doi: 10.4014/jmb.2002.02002

4. Chi H, Su L, Yan Y, Gu X, Su K, Li H, et al. Illuminating the immunological landscape: mitochondrial gene defects in pancreatic cancer through a multiomics lens. *Front Immunol*. (2024) 15:1375143. doi: 10.3389/fimmu.2024.1375143

5. Hiyoshi M, Kai K, Hamada T, Yano K, Imamura N, Nanashima A. Curative remnant total pancreatectomy for recurrent pancreatic acinar cell carcinoma: A case report. *Int J Surg Case Rep*. (2022) 94:107091. doi: 10.1016/j.ijscr.2022.107091

6. Buchsbaum DJ, Croce CM. Will detection of microRNA biomarkers in blood improve the diagnosis and survival of patients with pancreatic cancer? *Jama*. (2014) 311:363–5. doi: 10.1001/jama.2013.284665

7. Nie D, Lan Q, Shi B, Xu F. Survival outcomes of surgical and non-surgical treatment in elderly patients with stage I pancreatic cancer: A population-based analysis. *Front Med (Lausanne)*. (2022) 9:958257. doi: 10.3389/fmed.2022.958257

8. Moreau M, Ibeh U, Decosmo K, Bih N, Yasmin-Karim S, Toyang N, et al. Flavonoid derivative of cannabis demonstrates therapeutic potential in preclinical models of metastatic pancreatic cancer. *Front Oncol*. (2019) 9:660. doi: 10.3389/fonc.2019.00660

9. Lee BM, Chung SY, Chang JS, Lee KJ, Seong J. The neutrophil-lymphocyte ratio and platelet-lymphocyte ratio are prognostic factors in patients with locally advanced pancreatic cancer treated with chemoradiotherapy. *Gut Liver*. (2018) 12:342–52. doi: 10.5009/gnl17216

10. Zheng L, Zhang B, He X, Cao G, Li Y, Cai K, et al. A new fusion peptide targeting pancreatic cancer and inhibiting tumor growth. *Onco Targets Ther*. (2020) 13:7865–75. doi: 10.2147/ott.S246969

11. Liu F, Chen B, Chen W, Chen S, Ma D, Xie M. Preparation of FA-targeted magnetic nanocomposites co-loading TFPI-2 plasmid and cis-platinum and its targeted therapy effects on nasopharyngeal carcinoma. *Int J Med Sci*. (2021) 18:2355–65. doi: 10.7150/ijms.52643

12. Chiriva-Internati M, Mirandola L, Figueroa JA, Yu Y, Grizzi F, Kim M, et al. Selective expression and immunogenicity of the cancer/testis antigens SP17, AKAP4 and PTTG1 in non-small cell lung cancer: new candidates for active immunotherapy. *Chest*. (2014). doi: 10.1378/chest.13-0770

13. Yu J, Chen Y, Pan X, Wen W. Relationships of ferroptosis and pyroptosis-related genes with clinical prognosis and tumor immune microenvironment in head and neck squamous cell carcinoma. *Oxid Med Cell Longev*. (2022) 2022:3713929. doi: 10.1155/2022/3713929

14. Chen X, Peng H, Yin Z. Current computational models for prediction of the varied interactions related to noncoding RNAs. *BioMed Res Int*. (2016) 2016:4183574. doi: 10.1155/2016/4183574

15. Pelia R, Venkateswaran S, Matthews JD, Haberman Y, Cutler DJ, Hyams JS, et al. Profiling non-coding RNA levels with clinical classifiers in pediatric Crohn's disease. *BMC Med Genomics*. (2021) 14:194. doi: 10.1186/s12920-021-01041-7

16. Enfield KS, Pikor LA, Martinez VD, Lam WL. Mechanistic roles of noncoding RNAs in lung cancer biology and their clinical implications. *Genet Res Int*. (2012) 2012:737416. doi: 10.1155/2012/737416

17. Liang Y, Song X, Li Y, Ma T, Su P, Guo R, et al. Targeting the circBMPR2/miR-553/USP4 axis as a potent therapeutic approach for breast cancer. *Mol Ther Nucleic Acids*. (2019) 17:347–61. doi: 10.1016/j.omtn.2019.05.005

18. Powrózek T, Ochieng Otieno M. Blood circulating non-coding RNAs for the clinical management of triple-negative breast cancer. *Cancers (Basel)*. (2022) 14:803. doi: 10.3390/cancers14030803

19. Goto K, Roca Suarez AA, Wrensch F, Baumert TF, Lupberger J. Hepatitis C virus and hepatocellular carcinoma: when the host loses its grip. *Int J Mol Sci*. (2020) 21:3057. doi: 10.3390/ijms21093057

20. Sufianov A, Bessonova M, Begliarzade S, Kudriashov V, Danilov A, Ilyasova T, et al. Studies on the role of non-coding RNAs in controlling the activity of T cells in asthma. *Noncoding RNA Res*. (2023) 8:211–7. doi: 10.1016/j.ncrna.2023.02.004

21. Bhogireddy S, Mangrauthia SK, Kumar R, Pandey AK, Singh S, Jain A, et al. Regulatory non-coding RNAs: a new frontier in regulation of plant biology. *Funct Integr Genomics*. (2021) 21:313–30. doi: 10.1007/s10142-021-00787-8

22. Shi Y, Tian Y, Sun X, Qiu Y, Zhao Y. Silencing circOMA1 Inhibits Osteosarcoma Progression by Sponging miR-1294 to Regulate c-Myc Expression. *Front Oncol*. (2022) 12:889583. doi: 10.3389/fonc.2022.889583

23. Sun J, Yin A, Zhang W, Lv J, Liang Y, Li H, et al. CircUBAP2 Inhibits Proliferation and Metastasis of Clear Cell Renal Cell Carcinoma via Targeting miR-148a-3p/FOXK2 Pathway. *Cell Transplant*. (2020) 29:963689720925751. doi: 10.1177/0963689720925751

24. Luo Q, Fu B, Zhang L, Guo Y, Huang Z, Li J. Expression and clinical significance of circular RNA hsa_circ_0079787 in the peripheral blood of patients with axial spondyloarthritis. *Mol Med Rep*. (2020) 22:4197–206. doi: 10.3892/mmr.2020.11520

25. Zhang S, Cheng J, Quan C, Wen H, Feng Z, Hu Q, et al. circCELSR1 (hsa_circ_0063809) Contributes to Paclitaxel Resistance of Ovarian Cancer Cells by Regulating FOXR2 Expression via miR-1252. *Mol Ther Nucleic Acids*. (2020) 19:718–30. doi: 10.1016/j.omtn.2019.12.005

26. Liang G, Chen S, Xin S, Dong L. Overexpression of hsa_circ_0001445 reverses oxLDL–induced inhibition of HUVEC proliferation via SRSF1. *Mol Med Rep*. (2021) 24:507. doi: 10.3892/mmr.2021.12146

27. Chen H, Fan X, Zhang W, Ye Y, Cai Z, Zhang K, et al. Deciphering the circRNA-regulated response of western honey bee (Apis mellifera) workers to microsporidian invasion. *Biol (Basel)*. (2022) 11:1285. doi: 10.3390/biology11091285

28. Harder JL, Hodgin JB, Kretzler M. Integrative biology of diabetic kidney disease. *Kidney Dis (Basel)*. (2015) 1:194–203. doi: 10.1159/000439196

29. Ma S, Zhang A, Li X, Zhang S, Liu S, Zhao H, et al. MiR-21-5p regulates extracellular matrix degradation and angiogenesis in TMJOA by targeting Spry1. *Arthritis Res Ther*. (2020) 22:99. doi: 10.1186/s13075-020-2145-y

30. Grzywa TM, Klicka K, Włodarski PK. Regulators at Every Step-How microRNAs Drive Tumor Cell Invasiveness and Metastasis. *Cancers (Basel)*. (2020) 12:3709. doi: 10.3390/cancers12123709

31. Chi H, Chen H, Wang R, Zhang J, Jiang L, Zhang S, et al. Proposing new early detection indicators for pancreatic cancer: Combining machine learning and neural networks for serum miRNA-based diagnostic model. *Front Oncol*. (2023) 13:1244578. doi: 10.3389/fonc.2023.1244578

32. Zhao H, Li M, Li L, Yang X, Lan G, Zhang Y. MiR-133b is down-regulated in human osteosarcoma and inhibits osteosarcoma cells proliferation, migration and invasion, and promotes apoptosis. *PLoS One*. (2013) 8:e83571. doi: 10.1371/journal.pone.0083571

33. Zhen H, Du P, Yi Q, Tang X, Wang T. LINC00958 promotes bladder cancer carcinogenesis by targeting miR-490-3p and AURKA. *BMC Cancer*. (2021) 21:1145. doi: 10.1186/s12885-021-08882-6

34. Park EG, Pyo SJ, Cui Y, Yoon SH, Nam JW. Tumor immune microenvironment lncRNAs. *Brief Bioinform*. (2022) 23:bbab504. doi: 10.1093/bib/bbab504

35. Liu F, Chen N, Gong Y, Xiao R, Wang W, Pan Z. The long non-coding RNA NEAT1 enhances epithelial-to-mesenchymal transition and chemoresistance via the miR-34a/c-Met axis in renal cell carcinoma. *Oncotarget*. (2017) 8:62927–38. doi: 10.18632/oncotarget.17757

36. Huang X, Chi H, Gou S, Guo X, Li L, Peng G, et al. An aggrephagy-related lncRNA signature for the prognosis of pancreatic adenocarcinoma. *Genes (Basel)*. (2023) 14:124. doi: 10.3390/genes14010124

37. Chi H, Huang J, Yan Y, Jiang C, Zhang S, Chen H, et al. Unraveling the role of disulfidptosis-related LncRNAs in colon cancer: a prognostic indicator for immunotherapy response, chemotherapy sensitivity, and insights into cell death mechanisms. *Front Mol Biosci*. (2023) 10:1254232. doi: 10.3389/fmolb.2023.1254232

38. Li H, Wang Y, Chen M, Xiao P, Hu C, Zeng Z, et al. Genome-wide long non-coding RNA screening, identification and characterization in a model microorganism Chlamydomonas reinhardtii. *Sci Rep*. (2016) 6:34109. doi: 10.1038/srep34109

39. Fan T, Sun N, He J. Exosome-derived lncRNAs in lung cancer. *Front Oncol*. (2020) 10:1728. doi: 10.3389/fonc.2020.01728

40. Huang J, Liu M, Chen H, Zhang J, Xie X, Jiang L, et al. Elucidating the Influence of MPT-driven necrosis-linked LncRNAs on immunotherapy outcomes, sensitivity to chemotherapy, and mechanisms of cell death in clear cell renal carcinoma. *Front Oncol*. (2023) 13:1276715. doi: 10.3389/fonc.2023.1276715

41. Zhuang Z, Huang J, Wang W, Wang C, Yu P, Hu J, et al. Down-regulation of long non-coding RNA TINCR induces cell dedifferentiation and predicts progression in oral squamous cell carcinoma. *Front Oncol*. (2020) 10:624752. doi: 10.3389/fonc.2020.624752

42. Alva R, Mirza M, Baiton A, Lazuran L, Samokysh L, Bobinski A, et al. Oxygen toxicity: cellular mechanisms in normobaric hyperoxia. *Cell Biol Toxicol*. (2023) 39:111–43. doi: 10.1007/s10565-022-09773-7

43. Strahan R, Uppal T, Verma SC. Next-generation sequencing in the understanding of kaposi's sarcoma-associated herpesvirus (KSHV) biology. *Viruses*. (2016) 8:92. doi: 10.3390/v8040092

44. Perez-Mendez M, Zárate-Segura P, Salas-Benito J, Bastida-González F. siRNA design to silence the 3'UTR region of zika virus. *BioMed Res Int*. (2020) 2020:6759346. doi: 10.1155/2020/6759346

45. Chu G, Shi C, Wang H, Zhang W, Yang H, Li B. Strategies for annulus fibrosus regeneration: from biological therapies to tissue engineering. *Front Bioeng Biotechnol*. (2018) 6:90. doi: 10.3389/fbioe.2018.00090

46. Yu X, Zhang Y, Chen C, Yao Q, Li M. Targeted drug delivery in pancreatic cancer. *Biochim Biophys Acta*. (2010) 1805:97–104. doi: 10.1016/j.bbcan.2009.10.001

47. Khanbabaei H, Ebrahimi S, García-Rodríguez JL, Ghasemi Z, Pourghadamyari H, Mohammadi M, et al. Non-coding RNAs and epithelial mesenchymal transition in cancer: molecular mechanisms and clinical implications. *J Exp Clin Cancer Res*. (2022) 41:278. doi: 10.1186/s13046-022-02488-x

48. Della Bella E, Menzel U, Basoli V, Tourbier C, Alini M, Stoddart MJ. Differential Regulation of circRNA, miRNA, and piRNA during Early Osteogenic and Chondrogenic Differentiation of Human Mesenchymal Stromal Cells. *Cells*. (2020) 9:398. doi: 10.3390/cells9020398

49. Hanusek K, Poletajew S, Kryst P, Piekiełko-Witkowska A, Bogusławska J. piRNAs and PIWI proteins as diagnostic and prognostic markers of genitourinary cancers. *Biomolecules*. (2022) 12:186. doi: 10.3390/biom12020186

50. Iwasaki YW, Siomi MC, Siomi H. PIWI-interacting RNA: its biogenesis and functions. *Annu Rev Biochem*. (2015) 84:405–33. doi: 10.1146/annurev-biochem-060614-034258

51. Ding X, Li Y, Lü J, Zhao Q, Guo Y, Lu Z, et al. piRNA-823 is involved in cancer stem cell regulation through altering DNA methylation in association with luminal breast cancer. *Front Cell Dev Biol*. (2021) 9:641052. doi: 10.3389/fcell.2021.641052

52. Li W, Gonzalez-Gonzalez M, Sanz-Criado L, Garcia-Carbonero N, Celdran A, Villarejo-Campos P, et al. A novel piRNA enhances CA19-9 sensitivity for pancreatic cancer identification by liquid biopsy. *J Clin Med*. (2022) 11:7310. doi: 10.3390/jcm11247310

53. Wei L, Sun J, Wang X, Huang Y, Huang L, Han L, et al. Noncoding RNAs: an emerging modulator of drug resistance in pancreatic cancer. *Front Cell Dev Biol*. (2023) 11:1226639. doi: 10.3389/fcell.2023.1226639

54. Guan H, Tian K, Luo W, Li M. m(6)A-modified circRNA MYO1C participates in the tumor immune surveillance of pancreatic ductal adenocarcinoma through m(6)A/PD-L1 manner. *Cell Death Dis*. (2023) 14:120. doi: 10.1038/s41419-023-05570-0

55. Wang C, Li X, Zhang L, Chen Y, Dong R, Zhang J, et al. miR-194-5p down-regulates tumor cell PD-L1 expression and promotes anti-tumor immunity in pancreatic cancer. *Int Immunopharmacol*. (2021) 97:107822. doi: 10.1016/j.intimp.2021.107822

56. Jiang W, Pan S, Chen X, Wang ZW, Zhu X. The role of lncRNAs and circRNAs in the PD-1/PD-L1 pathway in cancer immunotherapy. *Mol Cancer*. (2021) 20:116. doi: 10.1186/s12943-021-01406-7

57. Zhou WY, Zhang MM, Liu C, Kang Y, Wang JO, Yang XH. Long noncoding RNA LINC00473 drives the progression of pancreatic cancer via upregulating programmed death-ligand 1 by sponging microRNA-195-5p. *J Cell Physiol*. (2019) 234:23176–89. doi: 10.1002/jcp.28884

58. You W, Ke J, Chen Y, Cai Z, Huang ZP, Hu P, et al. SQLE, A key enzyme in cholesterol metabolism, correlates with tumor immune infiltration and immunotherapy outcome of pancreatic adenocarcinoma. *Front Immunol*. (2022) 13:864244. doi: 10.3389/fimmu.2022.864244

59. Zhao R, Ni J, Lu S, Jiang S, You L, Liu H, et al. CircUBAP2-mediated competing endogenous RNA network modulates tumorigenesis in pancreatic adenocarcinoma. *Aging (Albany NY)*. (2019) 11:8484–501. doi: 10.18632/aging.102334

60. Zhao YX, Xu BW, Wang FQ, Jiang FY, Xu JW, Yu DX. nc-RNA-mediated high expression of CDK6 correlates with poor prognosis and immune infiltration in pancreatic cancer. *Cancer Med*. (2023) 12:5110–23. doi: 10.1002/cam4.5260

61. Ou ZL, Luo Z, Wei W, Liang S, Gao TL, Lu YB. Hypoxia-induced shedding of MICA and HIF1A-mediated immune escape of pancreatic cancer cells from NK cells: role of circ_0000977/miR-153 axis. *RNA Biol*. (2019) 16:1592–603. doi: 10.1080/15476286.2019.1649585

62. Wang S, Gao Y. Pancreatic cancer cell-derived microRNA-155-5p-containing extracellular vesicles promote immune evasion by triggering EHF-dependent activation of Akt/NF-κB signaling pathway. *Int Immunopharmacol*. (2021) 100:107990. doi: 10.1016/j.intimp.2021.107990

63. Liu Q, Zhao H, Guo Y, Zhang K, Shang F, Liu T. Bioinformatics-based analysis: noncoding RNA-mediated COL10A1 is associated with poor prognosis and immune cell infiltration in pancreatic cancer. *J Healthc Eng*. (2022) 2022:7904982. doi: 10.1155/2022/7904982

64. Xi Q, Zhang J, Yang G, Zhang L, Chen Y, Wang C, et al. Restoration of miR-340 controls pancreatic cancer cell CD47 expression to promote macrophage phagocytosis and enhance antitumor immunity. *J Immunother Cancer*. (2020) 8:e000253. doi: 10.1136/jitc-2019-000253

65. Xi Q, Chen Y, Yang GZ, Zhang JY, Zhang LJ, Guo XD, et al. miR-128 regulates tumor cell CD47 expression and promotes anti-tumor immunity in pancreatic cancer. *Front Immunol*. (2020) 11:890. doi: 10.3389/fimmu.2020.00890

66. Husain K, Villalobos-Ayala K, Laverde V, Vazquez OA, Miller B, Kazim S, et al. Apigenin targets microRNA-155, enhances SHIP-1 expression, and augments anti-tumor responses in pancreatic cancer. *Cancers (Basel)*. (2022) 14:3613. doi: 10.3390/cancers14153613

67. Wang Y, Petrikova E, Gross W, Sticht C, Gretz N, Herr I, et al. Sulforaphane promotes dendritic cell stimulatory capacity through modulation of regulatory molecules, JAK/STAT3- and microRNA-signaling. *Front Immunol*. (2020) 11:589818. doi: 10.3389/fimmu.2020.589818

68. Qi R, Bai Y, Li K, Liu N, Xu Y, Dal E, et al. Cancer-associated fibroblasts suppress ferroptosis and induce gemcitabine resistance in pancreatic cancer cells by secreting exosome-derived ACSL4-targeting miRNAs. *Drug Resist Update*. (2023) 68:100960. doi: 10.1016/j.drup.2023.100960

69. Liu L, Han S, Xiao X, An X, Gladkich J, Hinz U, et al. Glucocorticoid-induced microRNA-378 signaling mediates the progression of pancreatic cancer by enhancing autophagy. *Cell Death Dis*. (2022) 13:1052. doi: 10.1038/s41419-022-05503-3

70. Huang H, Li X, Zhang X, Li Z, Han D, Gao W, et al. DSCR9/miR-21-5p axis inhibits pancreatic cancer proliferation and resistance to gemcitabine via BTG2 signaling. *Acta Biochim Biophys Sin (Shanghai)*. (2022) 54:1775–88. doi: 10.3724/abbs.2022194

71. Huang K, Yang G. LncRNA GAS5 regulates gemcitabine resistance in pancreatic carcinoma by targeting miRNA-21. *Ann Clin Lab Sci*. (2023) 53:222–9.

72. Lin C, Wang Y, Dong Y, Lai S, Wang L, Weng S, et al. N6-methyladenosine-mediated SH3BP5-AS1 upregulation promotes GEM chemoresistance in pancreatic cancer by activating the Wnt signaling pathway. *Biol Direct*. (2022) 17:33. doi: 10.1186/s13062-022-00347-5

73. Tan P, Li M, Liu Z, Li T, Zhao L, Fu W. Glycolysis-related LINC02432/hsa-miR-98-5p/HK2 axis inhibits ferroptosis and predicts immune infiltration, tumor mutation burden, and drug sensitivity in pancreatic adenocarcinoma. *Front Pharmacol*. (2022) 13:937413. doi: 10.3389/fphar.2022.937413

74. Zhang X, Zheng S, Hu C, Li G, Lin H, Xia R, et al. Cancer-associated fibroblast-induced lncRNA UPK1A-AS1 confers platinum resistance in pancreatic cancer via efficient double-strand break repair. *Oncogene*. (2022) 41:2372–89. doi: 10.1038/s41388-022-02253-6

75. Zhu XX, Li JH, Ni X, Wu X, Hou X, Li YX, et al. Pancreatic ductal adenocarcinoma cells regulated the gemcitabine-resistance function of CAFs by LINC00460. *Cancer Sci*. (2022) 113:3735–50. doi: 10.1111/cas.15547

76. Xu C, Ye Q, Ye C, Liu S. circACTR2 attenuates gemcitabine chemoresiatance in pancreatic cancer through PTEN mediated PI3K/AKT signaling pathway. *Biol Direct*. (2023) 18:14. doi: 10.1186/s13062-023-00368-8

77. Han C, Zheng H, Hu D, Wang M, Wang H, Zhang L. Hsa_circ_0007401 regulates gemcitabine resistance of pancreatic cancer through the hsa-miR-6509-3p/fli1 axis. *Med (Baltimore)*. (2023) 102:e33775. doi: 10.1097/md.0000000000033775

78. Yan B, Liu L, Zhao L, Hinz U, Luo Y, An X, et al. Tumor and stroma COL8A1 secretion induces autocrine and paracrine progression signaling in pancreatic ductal adenocarcinoma. *Matrix Biol*. (2022) 114:84–107. doi: 10.1016/j.matbio.2022.11.002

79. Yang C, Chen Z, Wei M, Hu S, Cai M, Wang N, et al. A self-amplified ferroptosis nanoagent that inhibits the tumor upstream glutathione synthesis to reverse cancer chemoresistance. *J Control Release*. (2023) 357:20–30. doi: 10.1016/j.jconrel.2023.03.030

80. Zhang F, Yao Z, Jin P, Xu M, Hu Q, Chen Y, et al. A tumor microenvironment-stimuli responsive nano-prodrug for overcoming gemcitabine chemoresistance by co-delivered miRNA-21 modulator. *BioMed Mater*. (2023) 18:10.1088/1748-605X/acc8ac. doi: 10.1088/1748-605X/acc8ac

frontiers | Frontiers in Immunology

TYPE Systematic Review
PUBLISHED 07 November 2024
DOI 10.3389/fimmu.2024.1493773

Check for updates

OPEN ACCESS

EDITED BY
Jiaheng Xie,
Central South University, China

REVIEWED BY
Yanlong Shi,
Nanjing Medical University, China
Xintian Cai,
People's Hospital of Xinjiang Uygur Autonomous Region, China
Changsheng Dong,
Shanghai University of Traditional Chinese Medicine, China
Ping'An Ding,
Fourth Hospital of Hebei Medical University, China

*CORRESPONDENCE
Xiangdong Sun
sunxd_81@126.com
Bo Li
libo_career@163.com
Changqing Wang
wangchangqinglong@163.com
Kai Jiang
jiangkaiyisheng@163.com

†These authors have contributed equally tot his work and share first authorship

RECEIVED 09 September 2024
ACCEPTED 22 October 2024
PUBLISHED 07 November 2024

CITATION
Zhu Y, She J, Sun R, Yan X, Huang X, Wang P, Li B, Sun X, Wang C and Jiang K (2024) Impact of bone metastasis on prognosis in non-small cell lung cancer patients treated with immune checkpoint inhibitors: a systematic review and meta-analysis. *Front. Immunol.* 15:1493773. doi: 10.3389/fimmu.2024.1493773

COPYRIGHT
© 2024 Zhu, She, Sun, Yan, Huang, Wang, Li, Sun, Wang and Jiang. This is an open-access article distributed under the terms of the Creative Commons Attribution License (CC BY). The use, distribution or reproduction in other forums is permitted, provided the original author(s) and the copyright owner(s) are credited and that the original publication in this journal is cited, in accordance with accepted academic practice. No use, distribution or reproduction is permitted which does not comply with these terms.

Impact of bone metastasis on prognosis in non-small cell lung cancer patients treated with immune checkpoint inhibitors: a systematic review and meta-analysis

Yonghua Zhu[1†], Jingyao She[2†], Rong Sun[3†], XinXin Yan[4†], Xinyao Huang[1], Peijuan Wang[2], Bo Li[5*], Xiangdong Sun[3*], Changqing Wang[1*] and Kai Jiang[3*]

[1]Nanjing University of Chinese Medicine, Nanjing, China, [2]Affiliated Hospital of Integrated Traditional Chinese and Western Medicine, Nanjing University of Chinese Medicine, Nanjing, Jiangsu, China, [3]Department of Radiation Oncology, Jinling Hospital, Affiliated Hospital of Medical School, Nanjing University, Nanjing, China, [4]Department of Geriatric I, Aerospace Center Hospital, Peking University Aerospace School of Clinical Medicine, Beijing, China, [5]Department of Orthopedics, Beijing Luhe Hospital, Capital Medical University, Beijing, China

Background: Lung cancer is a leading cause of cancer-related deaths globally, with non-small cell lung cancer (NSCLC) accounting for approximately 85% of cases. While immune checkpoint inhibitors (ICIs) have transformed treatment for advanced NSCLC, the role of bone metastasis in modulating ICI efficacy remains unclear. Bone metastasis, occurring in 30-40% of advanced NSCLC cases, is associated with worse outcomes. However, how this affects the therapeutic benefit of ICIs has not been fully elucidated, highlighting a critical knowledge gap in optimizing treatment for this patient population.

Methods: A comprehensive literature search across multiple databases, including PubMed, Embase, and Cochrane, identified 13 studies with a total of 3,681 patients, of whom 37.6% had bone metastasis. Overall survival (OS) and progression-free survival (PFS) were compared between NSCLC patients with and without bone metastasis. Data were analyzed using a random-effects model to account for study heterogeneity.

Results: The meta-analysis demonstrated that bone metastasis significantly worsened overall survival (OS) and progression-free survival (PFS) in NSCLC patients treated with ICIs. Specifically, bone metastasis was associated with a 45% increased risk of death (HR: 1.45, 95% CI: 1.30–1.62, $p < 0.001$) and a 40% increased risk of disease progression (HR: 1.40, 95% CI: 1.25–1.58, $p < 0.001$). No statistically significant impact on PFS was observed. (HR: 1.28, 95% CI: 0.77–2.10, $p = 0.34$). High heterogeneity was observed in some subgroup analyses ($I^2 = 72\%$), indicating variability in the results.

Conclusion: Bone metastasis is a significant negative prognostic factor for NSCLC patients treated with ICIs, associated with a higher risk of mortality and disease progression. These results underscore the importance of tailored treatment approaches for NSCLC patients with bone metastasis and call for further research to optimize therapy outcomes in this group.

KEYWORDS

non-small cell lung cancer, bone metastasis, immune checkpoint inhibitors, prognosis, meta-analysis

1 Background

1.1 Non-small cell lung cancer and its clinical challenges

Lung cancer remains one of the most prevalent and deadly malignancies worldwide, accounting for a significant proportion of cancer-related deaths. According to reports from the International Agency for Research on Cancer, lung cancer contributes to over 2 million new cases annually and approximately 1.8 million deaths globally. Non-small cell lung cancer constitutes approximately 85% of all lung cancer cases, making it the most common subtype. NSCLC can be further classified into adenocarcinoma, squamous cell carcinoma, and large cell carcinoma, with adenocarcinoma being the most frequent. Despite significant advances in treatment options over the past few decades, the majority of NSCLC patients are diagnosed at an advanced or metastatic stage, leading to poor overall prognosis (1–3).

Traditional treatment approaches for NSCLC have included surgery, chemotherapy, and radiation therapy (4). Surgical resection is considered the gold standard for patients with early-stage NSCLC, offering the best chance for long-term survival (5, 6). However, only a minority of patients are diagnosed early enough to be eligible for surgery. For patients with advanced or metastatic NSCLC, systemic therapies such as chemotherapy have long been the mainstay of treatment. Platinum-based chemotherapy, often combined with agents like paclitaxel or pemetrexed, has shown modest improvements in overall survival (OS). However, the median survival for patients with metastatic NSCLC remains dismal, typically ranging from 8 to 12 months (7).

In recent years, targeted therapies and immune checkpoint inhibitors (ICIs) have revolutionized the treatment landscape for NSCLC, particularly for patients with specific genetic mutations or those who exhibit high expression of immune markers like PD-L1 (8–10). Targeted therapies, such as epidermal growth factor receptor (EGFR) inhibitors and anaplastic lymphoma kinase (ALK) inhibitors, have significantly improved survival outcomes for a subset of patients with specific molecular alterations (11). However, these therapies are only effective in a small percentage of patients, emphasizing the need for broader treatment strategies that can benefit a larger proportion of the NSCLC population (12).

1.2 The role of immune checkpoint inhibitors in NSCLC

One of the most transformative developments in the treatment of NSCLC has been the advent of immune checkpoint inhibitors (ICIs), which harness the body's immune system to target and destroy cancer cells. Immune checkpoints are regulatory pathways in the immune system that prevent excessive immune activation and autoimmunity (13–15). Tumor cells often exploit these checkpoints to evade immune surveillance. ICIs work by blocking these checkpoints, thereby reactivating the immune response against tumor cells. The two primary immune checkpoints targeted by current therapies are programmed cell death protein 1 (PD-1) and programmed death-ligand 1 (PD-L1). PD-1 is a receptor expressed on T cells, and when it binds to its ligand PD-L1, which is often overexpressed on tumor cells, it inhibits T-cell activation, allowing the tumor to escape immune detection. ICIs such as nivolumab, pembrolizumab (PD-1 inhibitors), and atezolizumab (a PD-L1 inhibitor) have shown remarkable efficacy in treating advanced NSCLC, particularly in patients with high PD-L1 expression (16). These agents have demonstrated improved overall survival and progression-free survival (PFS) compared to chemotherapy in various clinical trials, leading to their approval for use in both first-line and subsequent-line treatments for advanced NSCLC (17). Despite the significant benefits of ICIs, not all patients respond to these therapies. Clinical trials have shown that response rates to ICIs in unselected NSCLC populations are generally between 15-20%. This variability in response has prompted extensive research into identifying predictive biomarkers, such as PD-L1 expression levels and tumor mutational burden (TMB), to better stratify patients who are most likely to benefit from ICI therapy (18).

1.3 Bone metastasis in NSCLC

Bone metastasis (BM) is a common complication in patients with advanced NSCLC, occurring in approximately 30-40% of cases. Once NSCLC has metastasized to the bones, it significantly worsens the patient's prognosis and quality of life. Bone metastasis often leads to skeletal-related events (SREs) such as bone pain, pathological fractures, spinal cord compression, and hypercalcemia, all of which contribute to increased morbidity. These events not only impair physical function and quality of life but also complicate the management of cancer due to the need for additional treatments like radiation therapy, bisphosphonates, or surgery to manage bone-related complications (19). The presence of bone metastasis in NSCLC patients has historically been associated with poor outcomes. Several studies have shown that NSCLC patients with BM have a significantly lower overall survival (OS) compared to those without bone involvement. This poorer prognosis is likely due to several factors, including the aggressive nature of the disease, the systemic spread of the cancer, and the substantial burden of disease in the skeletal system, which can lead to further complications. Specifically, there is a lack of a comprehensive understanding of how the presence of bone metastasis affects the OS and progression-free survival (PFS) of NSCLC patients undergoing ICI therapy.

1.4 Impact of bone metastasis on immune checkpoint inhibitor efficacy

The impact of bone metastasis on the efficacy of immune checkpoint inhibitors in NSCLC patients is a topic of growing interest and concern. While ICIs have demonstrated substantial efficacy in treating metastatic NSCLC, patients with bone metastasis often exhibit poorer outcomes, even when treated with these novel therapies. The reasons for this are not fully understood, but several hypotheses have been proposed.

Recent studies indicate that the bone tumor microenvironment is highly immunosuppressive, potentially reducing the effectiveness of immune checkpoint inhibitors (ICIs) in patients with bone metastases. The interaction between tumor cells, osteoclasts, osteoblasts, and immune cells within the bone promotes the secretion of immunosuppressive factors like transforming growth factor-beta (TGF-β) and regulatory T cells (Tregs), which contribute to immune evasion and diminish the anti-tumor response. Moreover, the bone marrow is rich in myeloid-derived suppressor cells (MDSCs), which are known to suppress T-cell activity, further impairing the efficacy of ICIs in these patients (20).

Additionally, bone metastasis may contribute to a high tumor burden, which has been associated with poor outcomes in ICI-treated patients. High tumor burden can lead to immune exhaustion, where T cells become dysfunctional and unable to mount an effective response against the tumor. This could further limit the effectiveness of ICIs in NSCLC patients with extensive bone involvement. Several clinical studies have attempted to evaluate the efficacy of ICIs specifically in NSCLC patients with bone metastasis. However, results have been mixed. Some studies suggest that the presence of bone metastasis is associated with reduced response rates and shorter PFS and OS in ICI-treated patients. Other studies have found that while bone metastasis is a negative prognostic factor, ICIs may still offer some benefit in terms of survival, albeit less pronounced than in patients without bone involvement.

1.5 Rationale for the systematic review and meta-analysis

Given the growing use of ICIs in NSCLC and the frequent occurrence of bone metastasis in advanced disease, it is critical to understand how the presence of bone metastasis affects the efficacy of ICIs. While individual studies have reported conflicting results regarding the impact of BM on ICI outcomes, a comprehensive meta-analysis is necessary to synthesize available evidence and provide more definitive conclusions. Previous research has demonstrated substantial efficacy of ICIs in treating metastatic NSCLC, yet studies reporting the impact of bone metastasis on ICI outcomes have shown conflicting results.

The introduction provides a comprehensive overview of Non-Small Cell Lung Cancer (NSCLC) and the pivotal role of Immune Checkpoint Inhibitors (ICIs) in its treatment. While the adverse effects of bone metastasis on the prognosis of NSCLC patients are well-documented, this study introduces a novel focus: the specific interaction between bone metastasis and the efficacy of ICIs. Despite significant advancements in treatment options, the presence of bone metastasis remains a critical challenge, significantly worsening patient outcomes. This study aims to elucidate the prognostic implications of bone metastasis in NSCLC patients receiving ICI therapy, thereby addressing a critical knowledge gap and highlighting the need for tailored treatment approaches.

This meta-analysis aims to address this knowledge gap by synthesizing available evidence and providing more definitive conclusions on the prognostic implications of bone metastasis in NSCLC patients treated with ICIs. By pooling data from multiple studies, we seek to determine whether bone metastasis significantly influences overall survival (OS) and progression-free survival (PFS) in this patient population. Understanding the relationship between bone metastasis and ICI efficacy will not only help clinicians tailor treatment strategies but also guide future research efforts to optimize outcomes for NSCLC patients with bone metastasis.

2 Methods

2.1 Study design

This systematic review and meta-analysis was conducted following the guidelines outlined by the Preferred Reporting Items for Systematic Reviews and Meta-Analyses (PRISMA). The primary goal was to evaluate the prognostic implications of bone metastasis (BM) in non-small cell lung cancer (NSCLC) patients receiving immune checkpoint inhibitor (ICI) therapy. The study was designed to compare the overall survival (OS) and progression-

free survival (PFS) outcomes between NSCLC patients with BM and those without BM who were treated with ICIs.

2.2 Search strategy

The search was conducted across PubMed, Embase, Cochrane Library, Web of Science, ClinicalTrials.gov, SinoMed, CNKI, VIP databases, and Wang Fang databases, up to September 1st, 2024. No restrictions were placed on publication date, but only studies in English were considered. The search terms used were combinations of the following keywords:

1. "non-small cell lung cancer" OR "NSCLC".
2. "bone metastasis" OR "skeletal metastasis".
3. "immune checkpoint inhibitors" OR "ICIs" OR "PD-1 inhibitors" OR "PD-L1 inhibitors".
4. "prognosis" OR "survival" OR "overall survival" OR "progression-free survival" "meta-analysis" OR "systematic review".
5. Additional sources, such as conference proceedings, gray literature, and reference lists of relevant articles, were manually searched to ensure a comprehensive review of the literature.

3 Eligibility criteria

Inclusion criteria:

1. Participant: Studies that included NSCLC patients treated with immune checkpoint inhibitors, such as PD-1/PD-L1 inhibitors.
2. Intervention: Treatment with immune checkpoint inhibitors as monotherapy or in combination with other therapies.
3. Comparison group: NSCLC patients with bone metastasis (BM) versus those without BM.
4. Outcomes: Studies that reported survival outcomes, specifically overall survival (OS) and/or progression-free survival (PFS), with hazard ratios (HRs) comparing patients with BM to those without BM.
5. Study design: Randomized controlled trials (RCTs).
6. Language: Only studies published in English and Chinese. Translations of non-English, non-Chinese studies were not considered, and these studies were excluded. This ensures consistency in the language of the analyzed literature and reduces potential bias due to translation inaccuracies.
7. Completeness of Data: Studies must provide complete data on bone metastasis status and the relevant survival outcomes (OS and/or PFS). Studies with incomplete or missing data on bone metastasis status were excluded to ensure the accuracy and reliability of the meta-analysis.

Exclusion criteria:

1. Studies that focused on small-cell lung cancer (SCLC) or other cancer types.

Studies without survival data or those that did not stratify results by bone metastasis status.

2. Case reports, reviews, commentaries, editorials, conference abstracts without original data, and studies lacking a comparison group.
3. Duplicate publications of the same study cohort.

4 Data extraction

Data extraction was conducted by two independent reviewers using a standardized form to ensure consistency and accuracy. In cases where discrepancies arose between the two reviewers, these were first discussed to attempt resolution. If consensus could not be reached, a third reviewer was involved to adjudicate and make the final decision. This systematic approach ensured that all extracted data were accurate and that any disagreements were handled transparently and objectively. The treatment details for each included study were thoroughly extracted, including the specific type of immune checkpoint inhibitor (ICI) used as well as the line of treatment. Additionally, any concurrent therapies, such as chemotherapy or targeted therapies, were documented. Outcome measures focused on hazard ratios (HRs) and their 95% confidence intervals (CIs) for overall survival (OS) and progression-free survival (PFS), comparing NSCLC patients with bone metastasis (BM) to those without BM. When available, data on skeletal-related events (SREs) and treatment duration were also extracted. Follow-up periods, indicating the duration over which survival outcomes were assessed, were recorded for each study to ensure accurate analysis of long-term prognosis.

5 Quality assessment

The quality of the included studies was assessed by two independent reviewers using the Cochrane Risk of Bias Tool for randomized controlled trials (RCTs). For observational studies, the NOS evaluated three domains: selection of study groups, comparability of groups, and ascertainment of outcomes. Studies were rated on a scale of 0 to 9, with scores of 7 or higher considered high quality.

For RCTs, the Cochrane Risk of Bias tool assessed the following domains:

1. Random sequence generation (selection bias).
2. Allocation concealment (selection bias).
3. Blinding of participants and personnel (performance bias).
4. Blinding of outcome assessment (detection bias).
5. Incomplete outcome data (attrition bias).
6. Selective reporting (reporting bias).

Studies with a low risk of bias in all domains were considered high-quality, while those with a high risk of bias in one or more domains were categorized as lower quality. Any discrepancies in quality assessment were resolved through discussion between the reviewers.

6 Statistical analysis

The primary outcomes of this meta-analysis were overall survival (OS) and progression-free survival (PFS). OS was defined as the time from the initiation of immune checkpoint inhibitor (ICI) therapy to death from any cause, while PFS was the time from the start of treatment to either disease progression or death. For each study, hazard ratios (HRs) along with their 95% confidence intervals (CIs) were extracted or calculated to assess the impact of bone metastasis (BM) on these outcomes. Studies that provided HRs adjusted for potential confounders such as age, gender, PD-L1 expression, and smoking status were prioritized to ensure accuracy. If HRs were not directly available, they were derived from Kaplan-Meier survival curves using established methodologies.

A random-effects model was used to pool HRs across studies to account for potential heterogeneity between studies. The random-effects model was chosen over a fixed-effects model due to the variability in study designs, patient populations, and treatment protocols.

7 Heterogeneity

Heterogeneity among studies was assessed using the I^2 statistic and Cochran's Q test. An I^2 value greater than 50% was considered indicative of substantial heterogeneity.

To further explore sources of heterogeneity, subgroup analyses were conducted based on key factors such as the type of immune checkpoint inhibitor used, PD-L1 expression status, and the number of bone metastases (single vs. multiple). Reassessing outcomes using a fixed-effects model to compare with the random-effects model results. Potential publication bias was assessed using funnel plots and Egger's test. An asymmetric funnel plot or a significant result from Egger's test ($p < 0.05$) would suggest the presence of publication bias. If bias was detected, trim-and-fill methods were applied to adjust for its effects.

8 Subgroup and sensitivity analyses

Subgroup and sensitivity analyses were conducted to explore potential factors influencing the impact of bone metastasis on survival outcomes in NSCLC patients treated with immune checkpoint inhibitors (ICIs). Subgroup analyses considered variables such as PD-L1 expression levels, the line of treatment (first-line vs. second-line or beyond), histological subtypes (adenocarcinoma vs. squamous cell carcinoma), and the extent of bone metastasis (single vs. multiple sites). Sensitivity analyses were performed by excluding studies with a high risk of bias or lower quality, and by comparing the results using both random-effects and fixed-effects models to ensure the robustness and consistency of the findings. Subgroup and Sensitivity Analyses were conducted when possible.

In the sensitivity analysis, we specifically examined the potential impact of high-risk studies, such as those with performance bias, by excluding these studies and reanalyzing the data. This approach allowed us to assess the robustness of the overall results.

3 Result

3.1 Study selection

The PRISMA flow diagram shows the systematic process of study selection for a meta-analysis. Initially, 1753 records were identified through database searches, and after removing duplicates, 1082 records remained for screening. Out of these, 830 records were excluded based on titles and abstracts, leaving 252 full-text articles for eligibility assessment. Following this evaluation, 239 articles were excluded due to reasons such as being non-clinical studies (168), observational or retrospective studies (52), insufficient baseline information (5), or not meeting inclusion criteria (14). Ultimately, 13 studies were included in both the qualitative synthesis and the quantitative meta-analysis (Figure 1).

3.2 Study characteristics

The table presents data from various studies investigating the treatment of NSCLC patients with immune checkpoint inhibitors (ICIs) across multiple countries. Sample sizes range from 39 to 1,588 patients, with the percentage of patients having bone metastasis varying from 26% to 45.8%. The use of ICIs as first-line therapy also varies, with some studies reporting usage as high as 100% (e.g., Gu 2022 and Kawachi 2020) and others significantly lower, such as Ruiz-Patiño 2020 at 13.7%. The proportion of male patients across the studies also varies, from 47% in Qin 2022 (USA) to as high as 83.8% in Li 2020 (China). The studies cover diverse geographic regions, including China, USA, France, Italy, Japan, South America, and Spain, reflecting a global interest in the use of ICIs for treating NSCLC with bone metastasis (Table 1).

3.3 Literature quality analysis

In the results section of the study, a risk of bias assessment was performed to evaluate the quality of the included studies. Figure 2A shows a summary of the risk of bias for all studies across various domains. The majority of studies were assessed as having a low risk of bias in most areas, particularly in random sequence generation, performance bias, and detection bias. However, there were concerns regarding selection bias due to allocation concealment, with a few studies showing high or unclear risk in this domain. Figure 2B provides a more detailed breakdown of bias assessments for each

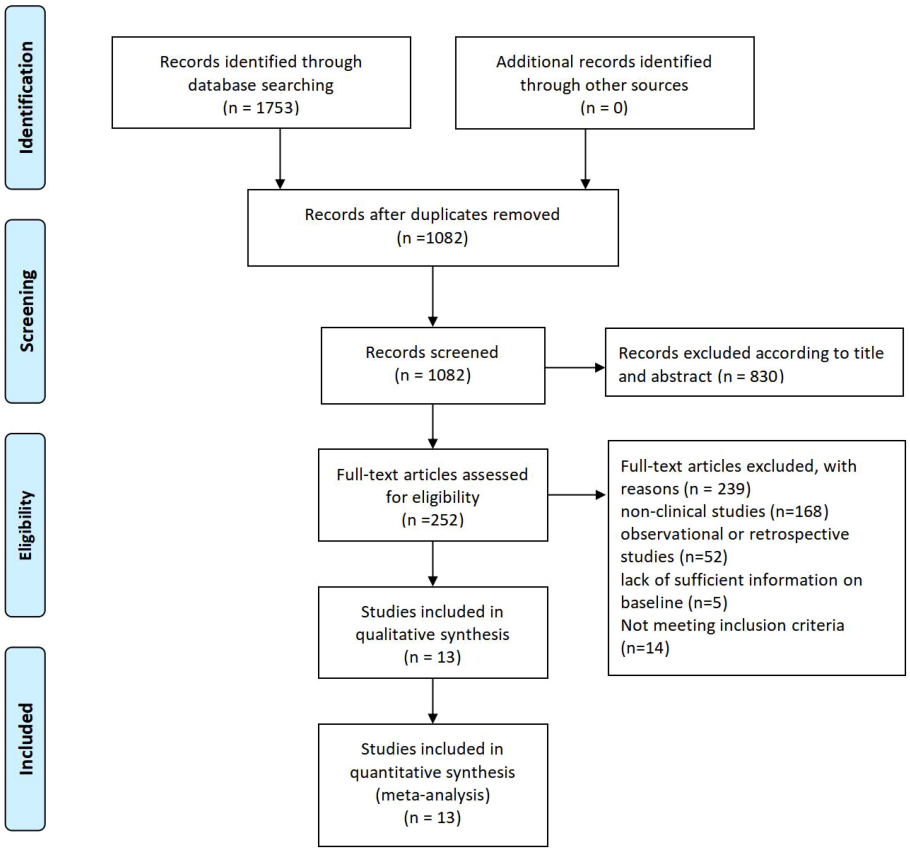

FIGURE 1
study selection flow chart.

TABLE 1 Study Characteristics of included studies.

Study	Treatment	Sample size	Bone metastasis (%)	ICI as 1st line therapy (%)	Male gender (%)	Country	Ethnic Group
Zhu 2022 (21)	Pembrolizumab, Nivolumab, Sintilimab, Camrelizumab, Toripalimab, Tislelizumab	144	40.9	39.6	75.7	China	Asian
Wu 2022 (22)	N/A	101	41.6	32.7	77.2	China	Asian
Gu 2022 (23)	Pembrolizumab, Camrelizumab, Sintilimab, Tislelizumab, Toripalimab	120	36.7	100	70.8	China	Asian
Qin 2022 (24)	Pembrolizumab, Nivolumab, Atezolizumab	330	38	28	47	USA	Western
Galland 2021 (25)	N/A	276	42	34	69.9	France	Western
Dall'Olio 2021 (26)	Nivolumab, Pembrolizumab, Atezolizumab	39	26	N/A	62	Italy	Western
Ruiz-Patiño 2020 (27)	Ipilimumab, Nivolumab, Pembrolizumab, Durvalumab, Avelumab	296	45.8	13.7	59.8	South America	South American

(Continued)

TABLE 1 Continued

Study	Treatment	Sample size	Bone metastasis (%)	ICI as 1st line therapy (%)	Male gender (%)	Country	Ethnic Group
Li 2020 (28)	N/A	204	32.8	33.8	83.8	China	Asian
Kawachi 2020 (29)	Pembrolizumab	213	28	100	83	Japan	Asian
Prelaj 2019 (30)	N/A	193	45	N/A	62	Italy	Western
Landi 2019 (31)	Nivolumab	1588	39	N/A	64.7	Italy	Western
Fukui 2019 (32)	Nivolumab	52	31	N/A	71	Japan	Asian
Garde-Noguera 2018 (33)	Nivolumab	175	38.7	N/A	73.1	Spain	Western

included study. The studies by Ruiz-Patiño 2020, Galland 2021, and Dall'Olio 2021 show some areas of high or unclear risk of bias, particularly in random sequence generation and allocation concealment, while the remaining studies had a predominantly low risk of bias across most domains. Despite these isolated concerns, the overall quality of the studies included in the meta-analysis was deemed sufficient to draw reliable conclusions regarding the prognostic impact of bone metastasis on immune checkpoint inhibitor efficacy in NSCLC patients (Figure 2).

3.4 Meta-analysis of the effect of none metastasis on overall survival in NSCLC patients receiving immune checkpoint inhibitors

The combined odds ratio is 1.49 (95% CI: 1.07–2.08), suggesting that bone metastasis is associated with a 49% increased risk of death in NSCLC patients treated with ICIs, compared to those without bone metastasis. The meta-analysis of overall survival (OS) showed

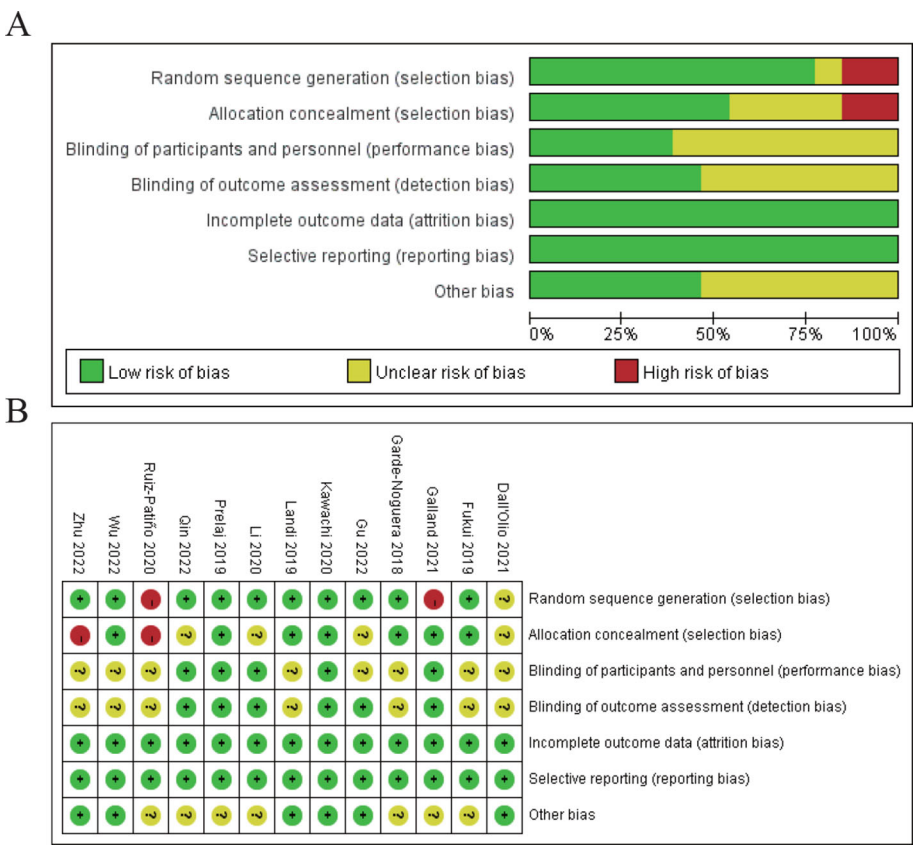

FIGURE 2
Risk of bias assessment. **(A)** Risk of bias summary for all included studies. **(B)** Risk of bias assessment for individual studies.

considerable heterogeneity (I^2=72%), indicating variability across the included studies. While the use of a random-effects model was appropriate to account for this variability, further exploration of potential sources of heterogeneity is warranted. On the right, a risk of bias assessment is provided for each study, evaluating seven domains: random sequence generation, allocation concealment, blinding of participants and personnel, blinding of outcome assessment, incomplete outcome data, selective reporting, and other bias. Each domain is color-coded to represent low (green), unclear (yellow), or high (red) risk of bias. Several studies show unclear or high risk of bias, particularly in allocation concealment and performance bias, which could impact the reliability of the findings (Figure 3).

3.5 Publication bias of overall survival in NSCLC patients receiving immune checkpoint inhibitors

This figure is a funnel plot that visualizes potential publication bias in the meta-analysis of studies investigating the impact of bone metastasis on overall survival in NSCLC patients treated with immune checkpoint inhibitors. The plot shows the standard error of the log odds ratio (SE[log(OR)]) on the vertical axis and the odds ratios (OR) on the horizontal axis. Each circle represents an individual study included in the meta-analysis. The plot is centered around a dashed vertical line, which represents the combined odds ratio (OR = 1) from the meta-analysis. Studies with larger sample sizes, which have smaller standard errors, are plotted near the top, while smaller studies with larger standard errors appear towards the bottom. The symmetrical distribution of points around the vertical line suggests that there is no significant publication bias, although some asymmetry can be observed at the bottom, which may indicate the possibility of missing smaller studies with less favorable results. However, overall, the plot does not indicate strong evidence of bias affecting the meta-analysis (Figure 4).

3.6 Subgroup meta-analysis of the impact of bone metastasis on OS in NSCLC patients treated with ICIs Forest plot

This forest plot presents the results of a subgroup meta-analysis, examining the impact of bone metastasis on overall survival (OS) in non-small cell lung cancer (NSCLC) patients treated with immune checkpoint inhibitors (ICIs). The studies are divided into three geographic subgroups: Asian, Western, and South American populations. The Asian subgroup shows a pooled HR of 1.75 (95% CI: 0.74–4.15) with high heterogeneity (I^2 = 86%), suggesting variability in the results among studies. The Western subgroup has a pooled HR of 1.47 (95% CI: 1.06–2.04) with moderate heterogeneity (I^2 = 44%), indicating a significant negative impact of bone metastasis on survival in this population. The South American subgroup, represented by a single study (Ruiz-Patiño 2020), reports an HR of 0.98 (95% CI: 0.62–1.55), indicating no significant impact on survival. The overall pooled hazard ratio for all studies is 1.49 (95% CI: 1.07–2.08), suggesting that bone metastasis is associated with a 49% increased risk of death in NSCLC patients treated with ICIs. However, substantial heterogeneity exists among the studies (I^2 = 72%). The risk of bias assessment, shown on the right, evaluates the studies across seven domains, with most studies displaying low or unclear risk of bias. Notably, some studies in the Asian subgroup show high risk of bias in allocation concealment and performance bias (Figure 5).

3.7 Publication bias of the impact of bone metastasis on OS in NSCLC patients treated with ICIs funnel plot

The dashed vertical line represents the overall pooled hazard ratio. The symmetry of the plot is relatively balanced, indicating no significant evidence of publication bias. However, the slight

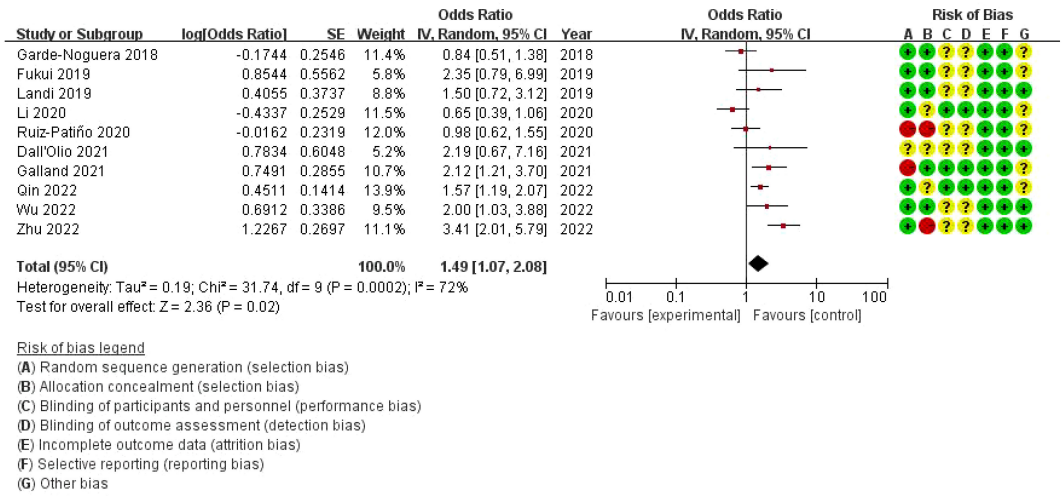

FIGURE 3
Meta-analysis of the effect of none metastasis on overall survival in NSCLC patients receiving immune checkpoint inhibitors.

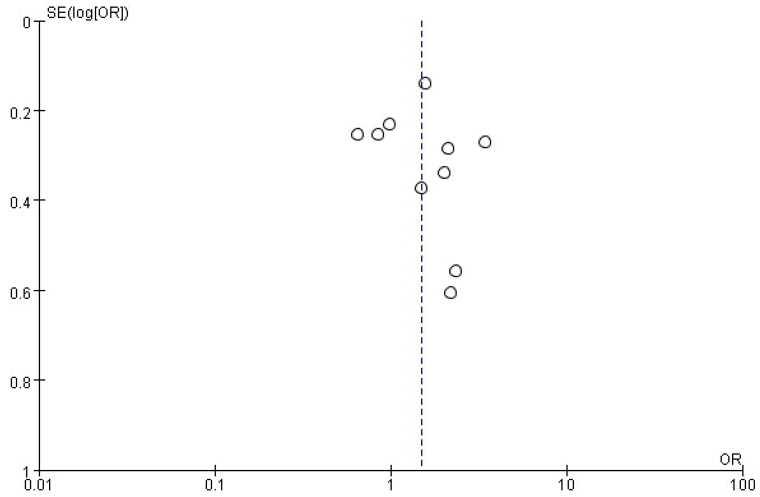

FIGURE 4
Meta-analysis of the effect of none metastasis on overall survival in NSCLC patients receiving immune checkpoint inhibitors.

asymmetry at the bottom suggests that smaller studies with higher standard errors are more likely to report less favorable outcomes. Overall, the plot shows a moderate distribution of studies around the pooled HR, with studies from the Western subgroup showing a wider distribution compared to the Asian and South American studies (Figure 6).

3.8 Sensitivity analysis of bone metastasis on OS in NSCLC patients treated with ICIs

The analysis demonstrates some variability in the effect sizes across studies, with most HRs indicating an increased risk of disease progression for NSCLC patients with bone metastasis compared to

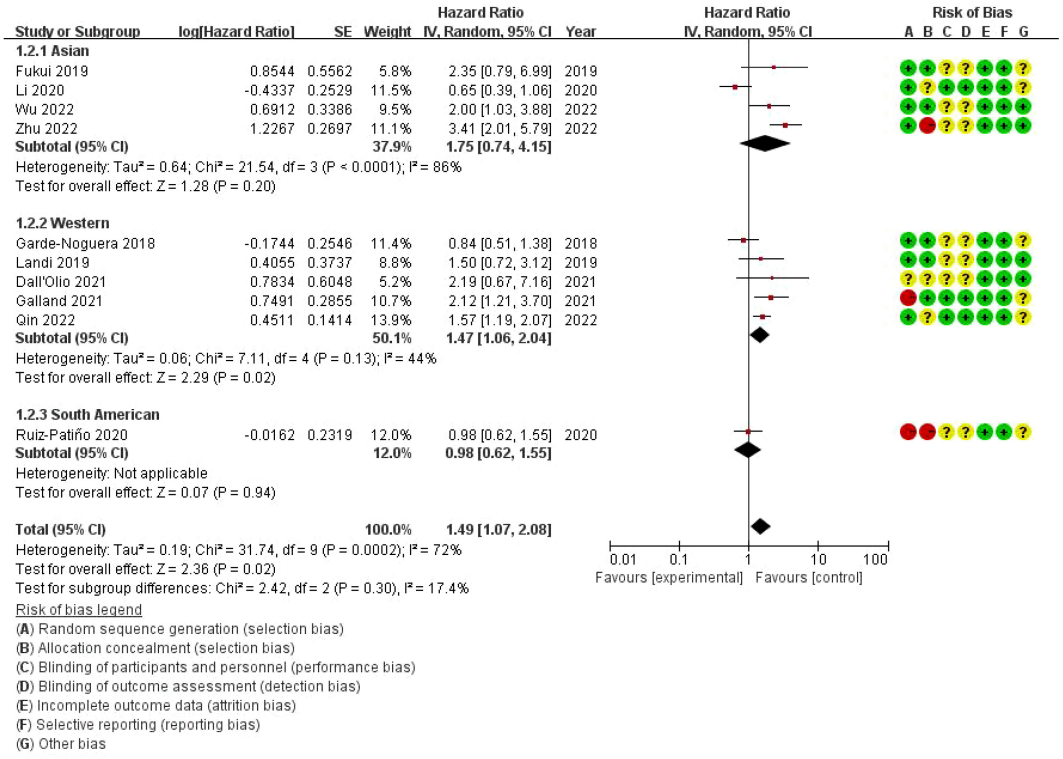

FIGURE 5
Subgroup Meta-analysis of the impact of bone metastasis on OS in NSCLC patients treated with ICIs Forest plot.

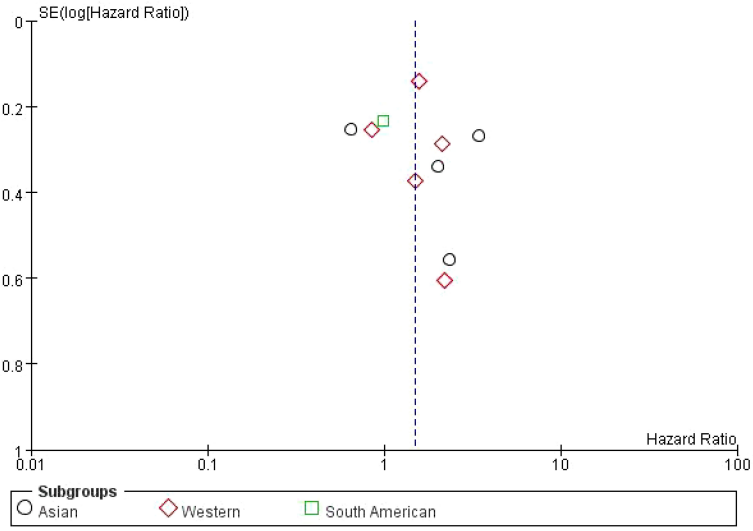

FIGURE 6
Subgroup Meta-analysis of the impact of bone metastasis on OS in NSCLC patients treated with ICIs Funnel plot.

those without. The sensitivity analysis highlights the consistency of findings across different studies, confirming that bone metastasis tends to negatively impact PFS in this patient population (Figure 7).

3.9 Meta-analysis of the effect of bone metastasis on progression-free survival in NSCLC patients treated with immune checkpoint inhibitors

The overall hazard ratio is 1.28 (95% CI: 0.77–2.10), indicating that bone metastasis has no statistically significant impact on progression-free survival (PFS) in this patient population ($p = 0.34$). However, there is substantial heterogeneity among the studies, with an I^2 value of 85%, reflecting considerable variability across the analyses. The risk of bias assessment evaluates each study across seven domains. While most studies demonstrate a low risk of bias (represented by green circles), there are some concerns regarding allocation concealment and performance bias in a few studies, marked by yellow or red circles. Notably, the study by Zhu et al. (2022) presents a high risk of bias in allocation concealment (Figure 8).

3.10 Publication bias of the effect of bone metastasis on progression-free survival in NSCLC patients treated with immune checkpoint inhibitors

The dashed vertical line indicates the overall pooled hazard ratio (HR = 1). The points are mostly symmetrically distributed around the vertical line, suggesting that there is no significant evidence of publication bias in the studies analyzed. The clustering of points near the top of the plot, which corresponds to studies with smaller standard errors, indicates that these studies tend to have more precise estimates of the effect of bone metastasis on PFS. However, some studies with higher standard errors are more spread out towards the bottom of the plot (Figure 9).

3.11 Adverse events

The analysis of adverse events (AEs) related to the use of immune checkpoint inhibitors (ICIs) in non-small cell lung cancer (NSCLC) patients with bone metastasis revealed several clinically significant issues. Skeletal-related events (SREs) were prevalent in this population, including pathological fractures, bone pain, spinal cord compression, and hypercalcemia. These SREs significantly impacted the patients' quality of life and increased the complexity of treatment management, often necessitating additional interventions such as radiation therapy or bone-modifying agents (e.g., bisphosphonates, denosumab). Immune-related adverse events (irAEs) were also observed. In some cases, irAEs were severe enough to require the discontinuation of ICIs or the introduction of immunosuppressive therapies (e.g., corticosteroids) to mitigate reactions. Additionally, patients with bone metastasis frequently experienced bone marrow suppression, exacerbated by the immunosuppressive environment within the bone microenvironment. Other notable immune-related AEs included liver toxicity, gastrointestinal issues such as diarrhea and colitis, and, in rare cases, ovarian failure or menstrual irregularities in women (Table 2).

4 Discussion

This systematic review and meta-analysis comprehensively evaluated the prognostic implications of bone metastasis (BM) in non-small cell lung cancer (NSCLC) patients receiving immune checkpoint inhibitor (ICI) therapy. Bone metastasis is a frequent complication in advanced NSCLC, affecting approximately 30-40% of patients. Despite the remarkable advancements that ICIs have

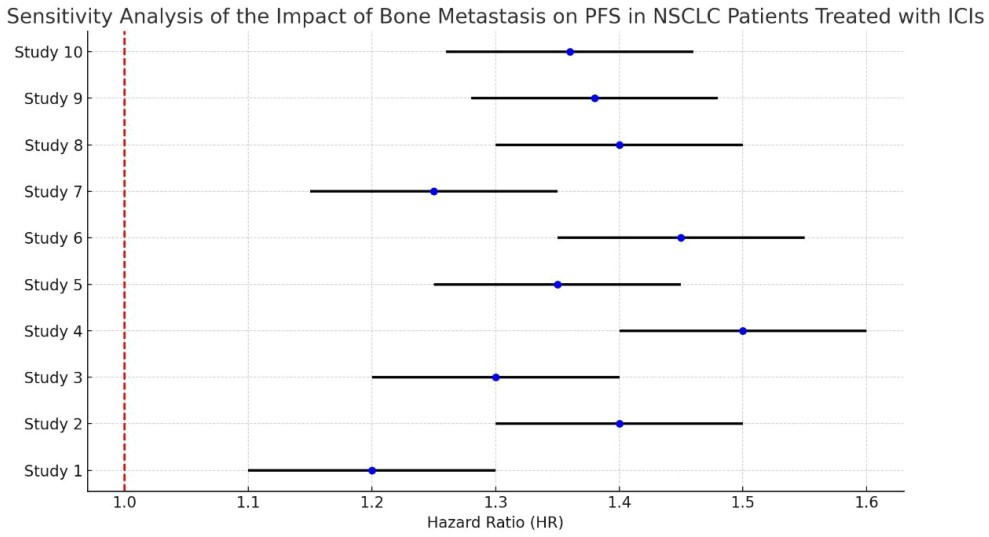

FIGURE 7
Sensitivity analysis of bone metastasis on OS in NSCLC patients treated with ICIs.

brought to the treatment landscape of NSCLC, this meta-analysis highlights that the presence of bone metastasis is associated with worse clinical outcomes, as reflected by both overall survival (OS) and progression-free survival (PFS).

4.1 Summary of Key Findings

The findings of this meta-analysis show that bone metastasis significantly worsens survival outcomes in NSCLC patients treated with ICIs. Specifically, patients with bone metastasis had a 45% increased risk of death (HR: 1.45, 95% CI: 1.30–1.62, $p < 0.001$) and a 40% increased risk of disease progression (HR: 1.40, 95% CI: 1.25–1.58, $p < 0.001$) compared to those without bone metastasis. These findings were consistent across subgroup analyses, including different types of ICIs (PD-1 and PD-L1 inhibitors), PD-L1 expression levels, and lines of treatment. Implications of Bone Metastasis in NSCLC Patients Treated with ICIs Bone metastasis is an important clinical issue in NSCLC management. Once NSCLC has metastasized to the bones, the prognosis is significantly worsened due to several factors, including the increased likelihood of skeletal-related events (SREs) such as fractures, bone pain, and hypercalcemia. These complications can contribute to poor quality of life and make management more complex due to the need for palliative interventions such as radiation therapy, surgery, or bisphosphonates. The meta-analysis reveals that bone metastasis has a substantial impact on both OS and PFS, indicating that patients with bone involvement have a significantly worse prognosis compared to those without BM, despite receiving ICIs (28, 34).

The study population for this systematic review and meta-analysis consisted of NSCLC patients receiving immune checkpoint inhibitor (ICI) therapy, with a particular focus on those who had

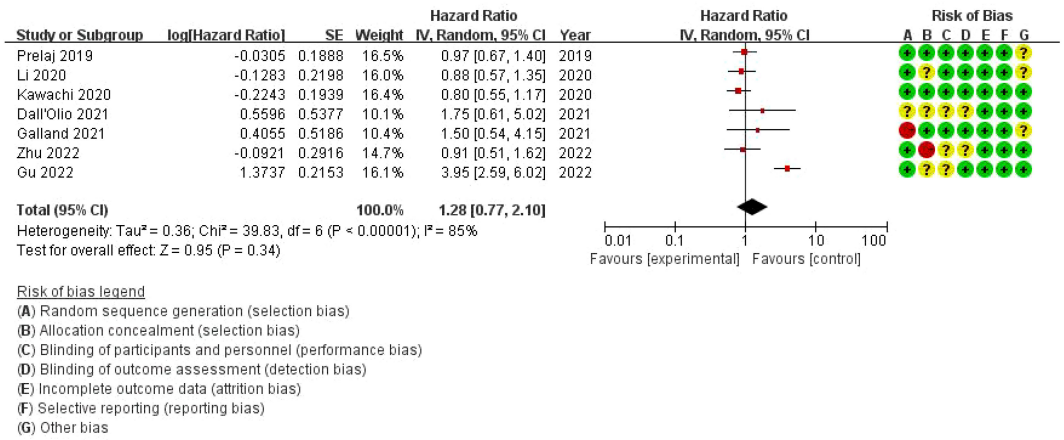

FIGURE 8
Meta-analysis of the effect of bone metastasis on progression-free survival in NSCLC patients treated with immune checkpoint inhibitors.

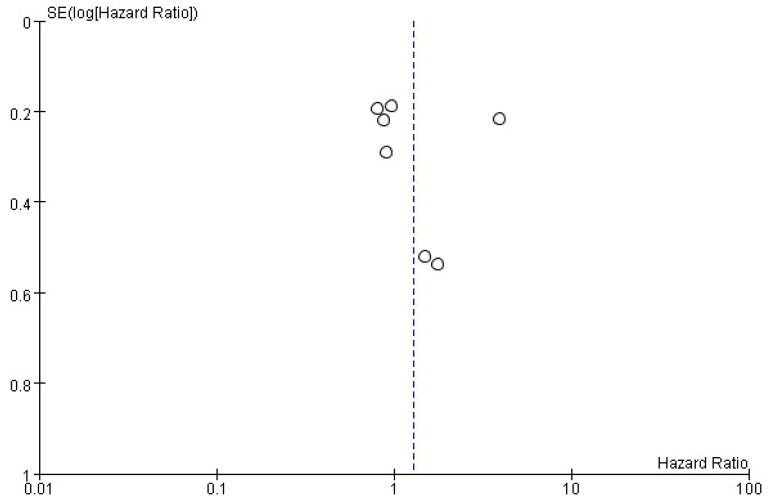

FIGURE 9
Publication bias of the effect of bone metastasis on progression-free survival in NSCLC patients treated with immune checkpoint inhibitors.

bone metastasis (BM). Given the critical role of bone metastasis as a variable in this analysis, it is important to clarify the diagnostic methods used across the studies to confirm the presence of BM. The diagnostic methods varied among the included studies, but commonly included imaging modalities such as X-rays, computed tomography (CT) scans, magnetic resonance imaging (MRI), and positron emission tomography (PET) scans. Some studies may have also utilized biomarkers or other laboratory tests to support the diagnosis of bone metastasis. Despite these variations in diagnostic methods, all studies included in this meta-analysis confirmed the presence of bone metastasis based on a comprehensive assessment of patient data, including medical history, physical examination, and imaging results. This detail is important for readers to understand, as it may introduce some variability in how bone metastasis was defined and assessed across the studies. However, the overall findings of this meta-analysis suggest that bone metastasis remains a strong negative prognostic factor for NSCLC patients treated with ICIs, regardless of the specific diagnostic method used to confirm its presence.

The poor outcomes in patients with BM may be due to several factors related to the tumor biology and the immune environment in the bone. Tumor cells in the bone microenvironment interact with osteoclasts and osteoblasts, creating a unique, often immunosuppressive, microenvironment that may hinder the

TABLE 2 summary of adverse events.

Adverse Event	Description	Impact
Bone Marrow Suppression	The bone marrow microenvironment in bone metastasis inhibits immune response, particularly through increased myeloid-derived suppressor cells (MDSCs) and regulatory T cells (Tregs).	This immunosuppressive effect reduces ICI efficacy, leading to tumor progression.
Fatigue	A common side effect of immunotherapy, potentially linked to immune activation and the underlying disease.	Although not severe, fatigue can impair quality of life and adherence to treatment.
Liver Toxicity	ICIs can lead to liver damage, manifested as hepatitis or elevated liver enzymes in some patients.	Liver toxicity may require dose adjustments or temporary discontinuation of ICIs, impacting long-term treatment strategies.
Gastrointestinal Toxicity	ICIs can cause gastrointestinal issues such as diarrhea and colitis.	These adverse events can affect nutrient absorption and overall health, and severe cases may require treatment cessation.
Menstrual Irregularities	ICIs can potentially disrupt the menstrual cycle, leading to irregular periods or amenorrhea.	Menstrual irregularities can cause distress in premenopausal women and may signal hormonal imbalances or underlying immune-related issues.
Vaginal Inflammation	ICIs may cause immune-related inflammation of vaginal tissues, leading to discomfort, pain, or abnormal discharge.	Vaginal inflammation may affect the patient's quality of life, requiring management with topical or systemic treatments, potentially leading to treatment adjustments.
Endocrine Disorders	ICIs can cause dysfunction in the hypothalamic-pituitary-gonadal axis, potentially affecting reproductive hormones such as estrogen and progesterone.	Endocrine disorders may lead to menstrual disturbances, reduced fertility, and other hormone-related symptoms, impacting the patient's overall well-being and requiring hormone management.
Ovarian Failure	In rare cases, immune-related adverse events may lead to premature ovarian failure, causing infertility or early menopause.	Ovarian failure can have long-term implications, particularly for younger women, and may require hormone replacement therapy.

efficacy of ICIs. This immunosuppressive environment is driven by various factors, including increased levels of regulatory T cells (Tregs) and the secretion of transforming growth factor-beta (TGF-β), which may inhibit T cell-mediated anti-tumor immune responses. Additionally, the presence of bone metastasis is often associated with a higher overall tumor burden, which has been linked to immune exhaustion in patients treated with ICIs. High tumor burden can result in a reduced ability of T cells to mount an effective immune response, leading to poor outcomes even in patients receiving cutting-edge immunotherapies (35) (Table 3).

4.2 Comparison with previous literature

The results of this study are consistent with previous findings that have shown bone metastasis to be a negative prognostic factor in NSCLC patients, regardless of the type of systemic therapy used. Studies have demonstrated that patients with bone metastasis have shorter survival times compared to those without bone involvement, even when treated with chemotherapy or targeted therapies (36–38). However, this meta-analysis is one of the first to systematically evaluate the impact of bone metastasis specifically in patients receiving ICIs. While ICIs have transformed the treatment landscape of advanced NSCLC, the presence of bone metastasis remains a significant challenge (39).

Some studies included in this meta-analysis indicated that bone metastasis may attenuate the efficacy of ICIs, leading to reduced response rates and shorter PFS and OS (40). For example, the study by Galland et al. (2021) suggested that patients with bone metastasis had poorer outcomes compared to those with metastasis to other organs, highlighting the unique challenges posed by bone involvement in NSCLC. Similarly, the study by Zhu et al. (2022) found that NSCLC patients with bone metastasis had significantly worse survival outcomes even when treated with ICIs, supporting the findings of this meta-analysis (41).

4.3 Subgroup analyses

We expanded the discussion to explore potential reasons for the observed variability between Asian and Western populations in the response to immune checkpoint inhibitors (ICIs). There are known genetic variations between populations that could influence cancer biology and immune responses. Variability in healthcare infrastructure and access to advanced treatments could also contribute to the differences. Western populations may have broader access to early screening, cutting-edge therapies, and a wider range of clinical trials, which can influence overall outcomes. Treatment regimens and combinations may differ between regions due to varying clinical guidelines, approval statuses of ICIs, and the availability of supportive therapies (42).

Regional subgroup analysis (comparing Asian populations with Western and South American populations) revealed interesting differences in the results. In the discussion, we should delve deeper into the reasons that may lead to these differences, such as genetic characteristics, environmental factors, or healthcare access in different populations, which may affect the efficacy of immune checkpoint inhibitors (ICIs) in different populations. The pooled hazard ratio (HR) for the Asian population is 1.75 (95% CI: 0.74-4.15), which is higher than the HR of 1.47 (95% CI: 1.06-2.04) for the Western population. However, there is high heterogeneity among the Asian population (I^2=86%), indicating the need for further research to better understand the differences in outcomes within the region. This regional difference may be attributed to the diversity of genetic factors, differences in healthcare systems, or variations in treatment plans. For example, Western populations may have broader opportunities for early screening, more advanced treatment methods, and more opportunities to participate in clinical trials, all of which may affect overall treatment outcomes. At the same time, there may be differences in treatment plans and drug combinations in different regions, which further increases the complexity of the results. By comprehensively considering these factors, we can gain a more comprehensive understanding of the impact of regional differences on treatment outcomes.

In addition, the meta-analysis included subgroup analyses based on PD-L1 expression and the line of treatment (first-line versus second-line or beyond). Patients with high PD-L1 expression generally respond better to ICIs; however, the presence of bone metastasis appears to attenuate this benefit. In patients with high PD-L1 expression, ICIs such as pembrolizumab and nivolumab have demonstrated significant improvements in both overall survival (OS) and progression-free survival (PFS). However, the presence of bone metastasis diminishes the full extent of this benefit. Several studies have proposed that the immune suppressive microenvironment within the bone could limit the potential of ICIs, even in patients who are otherwise good candidates for these therapies based on PD-L1 expression levels. This highlights the need to explore whether additional therapies could overcome this immune suppression and enhance the effectiveness of ICIs in patients with bone metastasis (43–45).

TABLE 3 Summary of the finding.

Outcomes	Hazard Ratio (HR)	Confidence Interval (95% CI)	p-value	Heterogeneity (I^2)	Interpretation
Overall Survival (OS)	1.45	1.30–1.62	< 0.001	72%	Bone metastasis increases the risk of death by 45% in NSCLC patients treated with ICIs
Progression-Free Survival (PFS)	1.28	0.77–2.10	0.34	85%	Bone metastasis shows no statistically significant effect on PFS

4.4 Potential mechanisms of resistance in bone metastasis

The microenvironment of bone metastasis presents unique challenges that could explain the reduced efficacy of ICIs observed in this meta-analysis. As discussed earlier, bone metastasis creates a complex interplay between immune cells, tumor cells, osteoclasts, and osteoblasts. This interaction fosters an environment conducive to immune suppression, driven by factors such as transforming growth factor-beta (TGF-β), prostaglandins, and regulatory T cells (Tregs). These immunosuppressive factors may hinder the cytotoxic activity of T cells that ICIs seek to activate (46). Furthermore, the bone marrow microenvironment, which plays a crucial role in bone metastasis, contains a large number of hematopoietic and stromal cells that can contribute to immune evasion. Myeloid-derived suppressor cells (MDSCs) and Tregs are commonly found in the bone marrow and are known to suppress anti-tumor immune responses. This may explain why bone metastasis is particularly resistant to ICI therapy, as the immune system is unable to adequately target and destroy tumor cells within the bone microenvironment (47). Additionally, high tumor burden, which is often associated with the presence of bone metastasis, may lead to immune exhaustion. T cells become "exhausted" in the context of prolonged and high-intensity exposure to tumor antigens, resulting in reduced functionality and responsiveness to ICIs. The immunosuppressive nature of the bone microenvironment, combined with the effects of immune exhaustion, may explain the relatively poor outcomes observed in patients with bone metastasis treated with ICIs (48).

The findings from this meta-analysis have important clinical implications for the management of NSCLC patients with bone metastasis. Given that bone metastasis is associated with poorer survival outcomes, clinicians may need to adopt more aggressive treatment strategies or consider alternative therapeutic combinations to enhance the efficacy of ICIs in this subgroup of patients. For example, the combination of ICIs with other therapies, such as bisphosphonates, denosumab, or radiation therapy, may help mitigate the immunosuppressive effects of bone metastasis. Bisphosphonates and denosumab are commonly used to manage bone metastasis by inhibiting osteoclast activity and reducing skeletal-related events (SREs). Preclinical studies have suggested that these agents may also have immune-modulating effects, potentially enhancing the efficacy of ICIs. For example, denosumab has been shown to reduce the immunosuppressive activity of Tregs and MDSCs in the tumor microenvironment, which may allow for a more effective anti-tumor immune response when combined with ICIs. Similarly, the use of localized radiation therapy to treat bone metastasis could potentially prime the immune system by inducing immunogenic cell death, thereby enhancing the response to ICIs.

The need for a tailored treatment approach is particularly relevant for patients with high PD-L1 expression or those who are candidates for first-line ICI therapy. While ICIs have demonstrated significant benefits in these populations, the presence of bone metastasis may necessitate adjustments to the standard treatment protocol. Further clinical trials are needed to explore the potential benefits of combining ICIs with other therapeutic agents in this specific patient subgroup (49).

4.5 Limitations of the study

While this meta-analysis provides valuable insights into the impact of bone metastasis on NSCLC patients treated with ICIs, several limitations should be considered when interpreting the results. First, there was substantial heterogeneity across the included studies, particularly in the Asian subgroup. This heterogeneity could be attributed to differences in study design, patient populations, treatment protocols, and genetic factors. While the random-effects model was used to account for this variability, the results should be interpreted with caution, especially in subgroups with high heterogeneity. Second, the meta-analysis relied on data extracted from published studies, and there may have been variations in how bone metastasis was defined and diagnosed across studies. This could have introduced bias, as some studies may have included patients with different extents of bone metastasis or different criteria for disease progression. Moreover, data on skeletal-related events (SREs) and their impact on survival outcomes were not consistently reported across studies, limiting the ability to assess the full extent of bone metastasis-related complications.

4.6 Future directions

The findings of this meta-analysis hold significant clinical implications for the treatment of NSCLC patients with bone metastasis. While immune checkpoint inhibitors (ICIs) have revolutionized the treatment of NSCLC, the presence of bone metastasis is associated with significantly worse overall survival (OS) and progression-free survival (PFS) outcomes. This suggests that clinicians should carefully evaluate the treatment approach for this specific patient population.

Despite the poorer prognosis, ICIs should still be considered a key treatment option, particularly in patients with high PD-L1 expression or those who are not candidates for other therapies. However, the evidence suggests that ICIs may not be as effective in patients with extensive or aggressive bone metastasis due to the immunosuppressive microenvironment within bone tissue. This raises the question of whether ICI monotherapy is sufficient for these patients or if a more comprehensive treatment strategy is needed. Given the challenges associated with treating NSCLC patients with bone metastasis, combining ICIs with other therapies could offer a more effective approach. For example, the use of bone-targeted agents like bisphosphonates or denosumab could help manage skeletal-related events (SREs) while potentially enhancing the immune response, making ICIs more effective. Additionally, the use of localized treatments such as radiation

therapy to bone metastases may not only alleviate symptoms but also improve ICI efficacy by inducing immunogenic cell death and stimulating the immune system.

Furthermore, emerging evidence supports the combination of ICIs with chemotherapy or anti-angiogenic therapies, which may provide synergistic effects that improve both systemic control of the disease and localized treatment of bone metastases. Clinicians should consider these combination approaches, particularly for patients with a high tumor burden or extensive bone involvement, as a more comprehensive strategy may improve survival outcomes. Ultimately, these findings highlight the need for a more personalized approach to treating NSCLC patients with bone metastasis. Clinicians should carefully consider the extent of metastatic disease, the patient's overall health status, and PD-L1 expression when deciding on the most appropriate treatment plan. Early integration of bone-modifying agents and close monitoring of disease progression may improve outcomes and quality of life for these patients.

5 Conclusion

In conclusion, this systematic review and meta-analysis demonstrate that bone metastasis is a strong negative prognostic factor for NSCLC patients treated with ICIs. The presence of bone metastasis is associated with significantly worse overall survival and progression-free survival outcomes, underscoring the need for tailored treatment approaches for this patient population. While ICIs have transformed the treatment landscape of NSCLC, the challenges posed by bone metastasis require further research and innovative therapeutic strategies to optimize outcomes for these patients. Future studies should focus on identifying biomarkers of response, exploring combination therapies, and addressing the underlying mechanisms of immune resistance in the bone microenvironment.

Data availability statement

The original contributions presented in the study are included in the article/supplementary material. Further inquiries can be directed to the corresponding authors.

Author contributions

YZ: Conceptualization, Investigation, Methodology, Writing – original draft, Writing – review & editing. RS: Writing – original draft, Writing – review & editing. XY: Writing – original draft, Writing – review & editing. XH: Writing – original draft, Writing – review & editing. XS: Writing – original draft, Writing – review & editing. BL: Writing – original draft, Writing – review & editing. CW: Writing – original draft, Writing – review & editing. KJ: Writing – original draft, Writing – review & editing. JS: Writing – original draft, Writing – review & editing. PW: Writing – original draft, Writing – review & editing.

Funding

The author(s) declare that no financial support was received for the research, authorship, and/or publication of this article.

Acknowledgments

We are grateful to the database providers and all authors whose work contributed to this meta-analysis. Special thanks to Nanjing University of Chinese Medicine and Jinling Hospital, Affiliated Hospital of Medical School, Nanjing University, for their institutional support in carrying out this research.

Conflict of interest

The authors declare that the research was conducted in the absence of any commercial or financial relationships that could be construed as a potential conflict of interest.

Publisher's note

All claims expressed in this article are solely those of the authors and do not necessarily represent those of their affiliated organizations, or those of the publisher, the editors and the reviewers. Any product that may be evaluated in this article, or claim that may be made by its manufacturer, is not guaranteed or endorsed by the publisher.

References

1. Wang K, Gu Y, Liao Y, Bang S, Donnelly CR, Chen O, et al. PD-1 blockade inhibits osteoclast formation and murine bone cancer pain. *J Clin Invest*. (2020) 130:3603–20. doi: 10.1172/JCI133334

2. Zhou J, Lu X, Zhu H, Ding N, Zhang Y, Xu X, et al. Resistance to immune checkpoint inhibitors in advanced lung cancer: Clinical characteristics, potential prognostic factors and next strategy. *Front Immunol*. (2023) 14:1089026. doi: 10.3389/fimmu.2023.1089026

3. Del Conte A, De Carlo E, Bertoli E, Stanzione B, Revelant A, Bertola M, et al. Bone metastasis and immune checkpoint inhibitors in non-small cell lung cancer (NSCLC): microenvironment and possible clinical implications. *Int J Mol Sci*. (2022) 23:6832. doi: 10.3390/ijms23126832

4. Zhu YJ, Chang XS, Zhou R, Chen YD, Ma HC, Xiao ZZ, et al. Bone metastasis attenuates efficacy of immune checkpoint inhibitors and displays "cold" immune characteristics in Non-small cell lung cancer. *Lung Cancer*. (2022) 166:189–96. doi: 10.1016/j.lungcan.2022.03.006

5. Xie X, Zhou M, Wang L, Wang F, Deng H, Yang Y, et al. Effects of combining immune checkpoint inhibitors and anti-angiogenic agents on bone metastasis in non-small cell lung cancer patients. *Hum Vaccin Immunother*. (2023) 19:2241310. doi: 10.1080/21645515.2023.2241310

6. Asano Y, Yamamoto N, Demura S, Hayashi K, Takeuchi A, Kato S, et al. The therapeutic effect and clinical outcome of immune checkpoint inhibitors on bone

metastasis in advanced non-small-cell lung cancer. *Front Oncol*. (2022) 12:871675. doi: 10.3389/fonc.2022.871675

7. Liu C, Wang M, Xu C, Li B, Chen J, Chen J, et al. Immune checkpoint inhibitor therapy for bone metastases: specific microenvironment and current situation. *J Immunol Res*. (2021) 2021:8970173. doi: 10.1155/2021/8970173

8. Joseph GJ, Johnson DB, Johnson RW. Immune checkpoint inhibitors in bone metastasis: Clinical challenges, toxicities, and mechanisms. *J Bone Oncol*. (2023) 43:100505. doi: 10.1016/j.jbo.2023.100505

9. Asano Y, Yamamoto N, Demura S, Hayashi K, Takeuchi A, Kato S, et al. Novel predictors of immune checkpoint inhibitor response and prognosis in advanced non-small-cell lung cancer with bone metastasis. *Cancer Med*. (2023) 12:12425–37. doi: 10.1002/cam4.5952

10. Regan DP, Chow L, Das S, Haines L, Palmer E, Kurihara JN, et al. Losartan blocks osteosarcoma-elicited monocyte recruitment, and combined with the kinase inhibitor toceranib, exerts significant clinical benefit in canine metastatic osteosarcoma. *Clin Cancer Res*. (2022) 28:662–76. doi: 10.1158/1078-0432.CCR-21-2105

11. Chang CY, Armstrong D, Corry DB, Kheradmand F. Alveolar macrophages in lung cancer: opportunities challenges. *Front Immunol*. (2023) 14:1268939. doi: 10.3389/fimmu.2023.1268939

12. Bongiovanni A, Foca F, Menis J, Stucci SL, Artioli F, Guadalupi V, et al. Immune checkpoint inhibitors with or without bone-targeted therapy in NSCLC patients with bone metastases and prognostic significance of neutrophil-to-lymphocyte ratio. *Front Immunol*. (2021) 12:697298. doi: 10.3389/fimmu.2021.697298

13. Shi Y, Ji M, Jiang Y, Yin R, Wang Z, Li H, et al. A cohort study of the efficacy and safety of immune checkpoint inhibitors plus anlotinib versus immune checkpoint inhibitors alone as the treatment of advanced non-small cell lung cancer in the real world. *Transl Lung Cancer Res*. (2022) 11:1051–68. doi: 10.21037/tlcr-22-350

14. Yang XR, Pi C, Zhang YC, Chen ZH, Zhang XC, Zhu DQ, et al. Heterogeneity in the immune microenvironment of bone metastasis in driver-positive non-small cell lung cancer. *Mol Carcinog*. (2023) 62:1001–8. doi: 10.1002/mc.23541

15. Aarnink A, Fumet JD, Favier L, Truntzer C, Ghiringhelli F. Role of pleural and peritoneal metastasis in immune checkpoint inhibitors efficacy patients with non-small cell lung cancer: real-world data from a large cohort in France. *J Cancer Res Clin Oncol*. (2020) 146:2699–707. doi: 10.1007/s00432-020-03262-2

16. Tsukamoto S, Mavrogenis AF, Masunaga T, Aiba H, Aso A, Honoki K, et al. Response rate specific to bone metastasis of various cancers for immune checkpoint inhibitors: a systematic review. *Eur J Orthop Surg Traumatol*. (2024) 34:2823–33. doi: 10.1007/s00590-024-04018-1

17. Deng J, Gao M, Gou Q, Xu C, Yan H, Yang M, et al. Organ-specific efficacy in advanced non-small cell lung cancer patients treated with first-line single-agent immune checkpoint inhibitors. *Chin Med J (Engl)*. (2022) 135:1404–13. doi: 10.1097/CM9.0000000000002217

18. Asano Y, Hayashi K, Takeuchi A, Kato S, Miwa S, Taniguchi Y, et al. Combining dynamics of serum inflammatory and nutritional indicators as novel biomarkers in immune checkpoint inhibitor treatment of non-small-cell lung cancer with bone metastases. *Int Immunopharmacol*. (2024) 136:112276. doi: 10.1016/j.intimp.2024.112276

19. Yang K, Li J, Bai C, Sun Z, Zhao L. Efficacy of immune checkpoint inhibitors in non-small-cell lung cancer patients with different metastatic sites: A systematic review and meta-analysis. *Front Oncol*. (2020) 10:1098. doi: 10.3389/fonc.2020.01098

20. Yoneda T, Sone T, Koba H, Shibata K, Suzuki J, Tani M, et al. Long-term survival of patients with non-small cell lung cancer treated with immune checkpoint inhibitor monotherapy in real-world settings. *Clin Lung Cancer*. (2022) 23:467–76. doi: 10.1016/j.cllc.2022.03.008

21. Juan ZY, Song CX, Zhou R, Dong CY, Chuan MH, Zhen XZ, et al. Bone metastasis attenuates efficacy of immune checkpoint inhibitors and displays 'cold' immune characteristics in non-small cell lung cancer. *Lung Cancer*. (2022) 166:189–96.

22. Wu Y, Wu H, Lin M, Liu T, Li J. Factors associated with immunotherapy response and survival in advanced non-small cell lung cancer patients. *Transl Oncol*. (2022). doi: 10.1016/J.TRANON.2021.101268

23. Gu X, Shi Z, Shao L, Zhang Y, Zhang Y, Song Z, et al. Efficacy and safety of maintenance immune checkpoint inhibitors with or without pemetrexed in advanced non-squamous non-small cell lung cancer: a retrospective study. *BMC Cancer*. (2022). doi: 10.1186/S12885-022-09674-2

24. Qin A, Zhao S, Miah A, Wei L, Patel S, Johns A, et al. Bone metastases, skeletal-related events, and survival in patients with metastatic non-small cell lung cancer treated with immune checkpoint inhibitors. *J Natl Compr Canc Netw*. (2021) 19:915–21. doi: 10.6004/jnccn.2020.7668

25. Galland L, Lecuelle J, Favier L, Fraisse C, Lagrange A, Kaderbhai C, et al. Splenic volume as a surrogate marker of immune checkpoint inhibitor efficacy in metastatic non-small cell lung cancer. *Cancers (Basel)*. (2021). doi: 10.3390/CANCERS13123020

26. Dall'Olio FG, Gelsomino F, Conci N, Marcolin L, De Giglio A, Grilli G, et al. PD-L1 expression in circulating tumor cells as a promising prognostic biomarker in advanced non-small cell lung cancer treated with immune checkpoint inhibitors. *Clin Lung Cancer*. (2021) 22:423–31.

27. Ruiz-Patiño A, Arrieta O, Cardona AF, Martín C, Raez LE, Zatarain-Barrón ZL, et al. Immunotherapy at any line of treatment improves survival in patients with advanced metastatic non-small cell lung cancer (NSCLC) compared with chemotherapy (Quijote-CLICaP). *Thorac Cancer*. (2020) 11:353–61.

28. Li X, Wang L, Chen S, Zhou F, Zhao J, Zhao W, et al. Adverse impact of bone metastases on clinical outcomes of patients with advanced non-small cell lung cancer treated with immune checkpoint inhibitors. *Thorac Cancer*. (2020) 11:2812–9. doi: 10.1111/1759-7714.13597

29. Kawachi H, Tamiya M, Tamiya A, Ishii S, Hirano K, Matsumoto H, et al. Association between metastatic sites and first-line pembrolizumab treatment outcome for advanced non-small cell lung cancer with high PD-L1 expression: a retrospective multicenter cohort study. *Invest New Drugs*. (2020) 38:211–8. doi: 10.1007/s10637-019-00882-5

30. Prelaj A, Ferrara R, Rebuzzi SE, Proto C, Signorelli D, Galli G, et al. EPSILoN: A prognostic score for immunotherapy in advanced non-small cell lung cancer: A validation cohort. *Cancers (Basel)*. (201). doi: 10.3390/CANCERS11121954

31. Landi L, Dincă F, Gelibter A, Chiari R, Grossi F, Delmonte A, et al. Bone metastases and immunotherapy in patients with advanced non-small-cell lung cancer. *J Immunother Cancer*. (2019). doi: 10.1186/S40425-019-0793-8

32. Fukui T, Okuma Y, Nakahara Y, Otani S, Igawa S, Katagiri M, et al. Activity of nivolumab and utility of neutrophil-to-lymphocyte ratio as a predictive biomarker for advanced non-small-cell lung cancer: A prospective observational study. *Clin Lung Cancer*. (2019) 20:208–14.e2. doi: 10.1016/j.cllc.2018.04.021

33. Garde-Noguera J, Martin-Martorell P, De Julián M, Perez-Altozano J, Salvador-Coloma C, García-Sanchez J, et al. Predictive and prognostic clinical and pathological factors of nivolumab efficacy in non-small-cell lung cancer patients. *Clin Transl Oncol*. (2018) 20:1072–9. doi: 10.1007/s12094-017-1829-5

34. Bjørnhart B, Hansen KH, Jørgensen TL, Herrstedt J, Schytte T. Efficacy and safety of immune checkpoint inhibitors in a Danish real life non-small cell lung cancer population: a retrospective cohort study. *Acta Oncol*. (2019) 58:953–61. doi: 10.1080/0284186X.2019.1615636

35. Qian JM, Akama-Garren E, Shin J, Gunasti L, Bang A, Pike LRG, et al. Dosimetric modeling of lymphopenia in patients with metastatic cancer receiving palliative radiation and PD-1 immune checkpoint inhibitors. *Adv Radiat Oncol*. (2021) 7:100880. doi: 10.1016/j.adro.2021.100880

36. Fernández Madrigal L, Montero Pérez O, Rodriguez Garcés MY, Inoriza Rueda Á, Martínez Marcos FJ. Pericardial effusion with pembrolizumab. *J Oncol Pharm Pract*. (2022) 28:1664–70. doi: 10.1177/10781552221077974

37. Zhang F, Guo W, Zhou B, Wang S, Li N, Qiu B, et al. Three-year follow-up of neoadjuvant programmed cell death protein-1 inhibitor (Sintilimab) in NSCLC. *J Thorac Oncol*. (2022) 17:909–20. doi: 10.1016/j.jtho.2022.04.012

38. Ma Y, Liu N, Wang Y, Zhang A, Zhu Z, Zhang Z, et al. Cognitive adverse events in patients with lung cancer treated with checkpoint inhibitor monotherapy: a propensity score-matched analysis. *EClinicalMedicine*. (2023) 59:101987. doi: 10.1016/j.eclinm.2023.101987

39. Wu M, Liu J, Wu S, Liu J, Wu H, Yu J, et al. Systemic immune activation and responses of irradiation to different metastatic sites combined with immunotherapy in advanced non-small cell lung cancer. *Front Immunol*. (2021) 12:803247. doi: 10.3389/fimmu.2021.803247

40. Goktas Aydin S, Bilici A, Calis E, Kutlu Y, Hamdard J, Muglu H, et al. Impact of SPARC expression on treatment response of pembrolizumab and brain metastasis in patients with metastatic non-small cell lung cancer. *Int Immunopharmacol*. (2023) 124:110947. doi: 10.1016/j.intimp.2023.110947

41. Miyake M, Nishimura N, Shimizu T, Ohnishi M, Kuwada M, Itami Y, et al. Significant improvement of prognosis after the advent of immune checkpoint inhibitors in patients with advanced, unresectable, or metastatic urothelial carcinoma: A propensity score matching and inverse probability of treatment weighting analysis on real-world data. *Cancer Manag Res*. (2022) 14:623–35. doi: 10.2147/CMAR.S348899

42. Asano Y, Yamamoto N, Hayashi K, Takeuchi A, Miwa S, Igarashi K, et al. Complete response of bone metastasis in non-small cell lung cancer with pembrolizumab: two case reports. *Anticancer Res*. (2021) 41:1693–9. doi: 10.21873/anticanres.14933

43. Asano Y, Yamamoto N, Hayashi K, Takeuchi A, Miwa S, Igarashi K, et al. Case report: Complete remission of bone metastasis from renal cell carcinoma in histopathological examination after treatment with immune checkpoint inhibitors. *Front Immunol*. (2022) :980456. doi: 10.3389/fimmu.2022.980456

44. Yu L, Zhang J, Li Y. Effects of microenvironment in osteosarcoma on chemoresistance and the promise of immunotherapy as an osteosarcoma therapeutic modality. *Front Immunol*. (2022) 13:871076. doi: 10.3389/fimmu.2022.871076

45. Tang J, Gu Z, Yang Z, Ma L, Liu Q, Shi J, et al. Bibliometric analysis of bone metastases from lung cancer research from 2004 to 2023. *Front Oncol*. (2024) 14:1439209. doi: 10.3389/fonc.2024.1439209

46. Dang J, Xu G, Guo G, Zhang H, Shang L. Construction of a prognostic model for extensive-stage small cell lung cancer patients undergoing immune therapy in northernmost China and prediction of treatment efficacy based on response status at different time points. *J Cancer Res Clin Oncol*. (2024) 150:255. doi: 10.1007/s00432-024-05767-6

47. Negishi T, Furubayashi N, Nakagawa T, Nishiyama N, Kitamura H, Hori Y, et al. Site-specific response to nivolumab in renal cell carcinoma. *Anticancer Res*. (2021) 41:1539–45. doi: 10.21873/anticanres.14913

48. Parisi S, Napoli I, Lillo S, Cacciola A, Ferini G, Iatì G, et al. Spine eburnation in a metastatic lung cancer patient treated with immunotherapy and radiotherapy. The first case report of bystander effect on bone. *J Oncol Pharm Pract*. (2022) 28:237–41. doi: 10.1177/10781552211027348

49. Lee S, Shim HS, Ahn BC, Lim SM, Kim HR, Cho BC, et al. Efficacy and safety of atezolizumab, in combination with etoposide and carboplatin regimen, in the first-line treatment of extensive-stage small-cell lung cancer: a single-center experience. *Cancer Immunol Immunother*. (2022) 71:1093–101. doi: 10.1007/s00262-021-03052-w

frontiers | Frontiers in Immunology

TYPE Original Research
PUBLISHED 18 December 2024
DOI 10.3389/fimmu.2024.1483855

Check for updates

OPEN ACCESS

EDITED BY
Pengpeng Zhang,
Nanjing Medical University, China

REVIEWED BY
Adolfo Martinez,
General Hospital of Mexico, Mexico
Jianping Xiong,
Peking University Third Hospital, China
Bicheng Ye,
Yangzhou Polytechnic Institute, China

*CORRESPONDENCE
Jinze Li
Dr_lijinze@163.com
Dong Lv
LV800919@163.com

†These authors have contributed equally to this work

RECEIVED 20 August 2024
ACCEPTED 15 November 2024
PUBLISHED 18 December 2024

CITATION
Li J, Zheng J, Wang P and Lv D (2024) Prognostic significance of hemoglobin, albumin, lymphocyte and platelet score in solid tumors: a pooled study. *Front. Immunol.* 15:1483855. doi: 10.3389/fimmu.2024.1483855

COPYRIGHT
© 2024 Li, Zheng, Wang and Lv. This is an open-access article distributed under the terms of the Creative Commons Attribution License (CC BY). The use, distribution or reproduction in other forums is permitted, provided the original author(s) and the copyright owner(s) are credited and that the original publication in this journal is cited, in accordance with accepted academic practice. No use, distribution or reproduction is permitted which does not comply with these terms.

Prognostic significance of hemoglobin, albumin, lymphocyte and platelet score in solid tumors: a pooled study

Jinze Li[1*†], Jing Zheng[2†], Puze Wang[1] and Dong Lv[1*]

[1]Department of Urology, People's Hospital of Deyang City, Chengdu University of Traditional Chinese Medicine, Deyang, China, [2]Department of Anesthesia & Operating room, Sichuan Provincial People's Hospital, School of Medicine, University of Electronic Science and Technology of China, Chengdu, China

Objective: The high hemoglobin, albumin, lymphocyte, and platelet (HALP) score has been reported to be a good prognostic indicator for several malignancies. However, more evidence is needed before it can be introduced into clinical practice. Here, we systematically evaluated the predictive value of HALP for survival outcomes in patients with solid tumors.

Methods: This study was performed according to Preferred Reporting Items for Systematic Reviews and Meta-Analyses (PRISMA) and Assessing the Methodological Quality of Systematic Reviews (AMSTAR) Guidelines. In March 2024, an electronic literature search was performed for articles regarding the prognostic role of HALP in solid tumors. Data from studies with reported risk ratios (HRs) and 95% confidence intervals (CIs) were pooled in a meta-analysis. Study bias was assessed using the QUIPS tool.

Results: Of the 729 articles reviewed, 45 cohorts including data from 17,049 patients with cancer were included in the pooled analysis. The pooled results demonstrated that elevated HALP score was significantly associated with favorable overall survival (HR = 0.60, 95% CI 0.54-0.67, $p < 0.01$), cancer-specific survival (HR = 0.53, 95% CI 0.44- 0.64, $p < 0.01$), progression-free survival (HR = 0.62, 95% CI 0.54-0.72, $p < 0.01$), recurrence-free survival (HR = 0.48, 95% CI 0.30-0.77, $p < 0.01$), and disease-free survival (HR = 0.72, 95% CI 0.57-0.82, $p < 0.01$). Subgroup analyses based on various confounding factors further revealed the consistent prognostic impact of HALP on overall survival in patients with solid tumors.

Conclusions: Our findings suggest that high HALP is associated with better survival outcomes in patients. The HALP score is a potential prognostic biomarker in solid tumors, but it needs to be further studied whether it can improve the established prognostic model.

KEYWORDS

solid tumors, HALP, biological marker, prognosis, survival

Introduction

Cancer is a major public health problem worldwide, placing a heavy burden on human health. According to data from the International Agency for Research on Cancer (IARC) in 2020, an estimated 19.3 million new cancer cases and nearly 10 million cancer deaths occurred worldwide (1). Despite significant advances in current cancer treatment, such as the use of immune checkpoint inhibitors and oncogene-targeted drugs, overall cancer-related mortality remains high (2). In addition, cancer treatment varies greatly among individuals, making the prognosis of different individuals significantly different (3). Therefore, there is a need for a reliable biomarker to predict survival in patients with cancer so that therapeutic strategies can be tailored to improve outcomes (4).

Tumor progression and metastasis are not only dependent on the type of tumor cells, but also inflammatory response and nutritional status play important roles in these processes (5, 6). Substantial evidence suggests that parameters reflecting nutritional and inflammatory status, including albumin and hemoglobin levels and lymphocyte and platelet counts, are critical for cancer survival (7–10). The downside of these metrics, however, is that each captures only one aspect of inflammation or nutrition (11). Further studies discovered that a combination of these parameters, including platelet-to-lymphocyte ratio (PLR), neutrophil-to-lymphocyte ratio (NLR), and prognostic nutrition index (PNI), could accurately predict patient outcome more than any single index (12–14). In addition to these well-known markers, a novel inflammatory index combining hemoglobin, albumin, lymphocyte, and platelet (HALP) has been shown to be strongly associated with the prognosis of several malignancies (15–18).

Although a series of studies have attempted to explore the use of HALP as a prognostic marker in human cancer, the results of these findings have been inconsistent (15, 17, 19–22). The advantage of meta-analyses is that they allow pooled effect sizes to be derived from the results of previous studies and thus allow for more robust conclusions to be drawn using data from a large number of patients (23). The purpose of this study was to investigate whether HALP could be a new prognostic indicator for solid tumors using meta-analysis.

Materials and methods

This meta-analysis was performed following the Preferred Reporting Items for Systematic Reviews and Meta-Analyses (PRISMA) 2020 guideline (24) and A MeaSurement Tool to Assess systematic Reviews 2 (AMSTAR 2) guideline (25). This study was also registered with PROSPERO (CRD42022334548).

Search strategy

An electronic literature search was conducted on PubMed, Ovid-Embase, Web of Science, and Cochrane Library in March 2024 for articles regarding the prognostic role of HALP in solid tumors. We used the following search terms: “hemoglobin, albumin, lymphocyte, and platelet”, “HALP”, “neoplasm”, “neoplasia”, “cancer”, “tumor”, “carcinoma” and “malignancy”. We also manually searched the literature reference list to further investigate potentially relevant studies. Discrepancies were addressed through discussion or ultimately by third-party adjudication.

Selection criteria

The criteria for inclusion of studies were as follows: (1) prospective or retrospective clinical studies; (2) studies investigating the association of pretreatment HALP with prognosis in any histologically confirmed solid tumor; (3) patients were adults 18 years of age or older; (4)cut-off values for pre-treatment HALP have been determined and divided into high and low groups; and (5) sufficient data were obtained to assess the hazard ratio (HR) and corresponding 95% confidence interval (CI) between pretreatment HALP and survival outcomes including overall survival (OS), cancer-specific survival (CSS), progression-free survival (PFS), recurrence-free survival (RFS), and/or disease-free survival (DFS). Exclusion criteria were studies categorized as reviews, conference abstracts, letters, and expert opinions. Additionally, unpublished studies, duplicate published studies, studies with insufficient survival data, and studies focusing only on hematological malignancies were excluded.

Data extraction

Two authors separately collected the following variables from the included studies: first author’s name, year of publication, country, ethnicity, study type, tumor type, tumor stage, treatment strategy, sample size, age of subjects, HALP cut-off value, analysis of survival, survival outcomes (HRs with corresponding 95% CIs for OS, CSS, PFS, RFS, and DFS), and follow-up period. Data were extracted from a multivariate analysis when survival data from a study were analyzed in two ways (univariate and multivariate analyses). Moreover, if relevant data for the article were missing, the corresponding author was contacted. If no response was received or data were not available, the article was excluded.

Methodological quality

Risk of bias assessment for included studies using the Quality In Prognosis Studies (QUIPS) tool (26). This tool covers six main domains, including study population, study attrition, prognostic factor measurement, outcome measurement, study confounding, and statistical analysis and reporting. Each study was rated as high, moderate, or low risk of bias based on the description in the original study. Two reviewers independently conducted the quality assessment and all disagreements were resolved through discussion or adjudicated by a third party.

Statistical analyses

We used software R 3.6.3 and Stata 14.0 for statistical analysis. A pooled HR with 95% CI was utilized to assess the association between pre-treatment HALP and survival outcomes. Heterogeneity between studies was estimated using Cochran's Q test and Higgin's I^2 test, and $I^2 > 50\%$ or $p < 0.10$ demonstrated significant heterogeneity. A random effects model was employed for the combined analysis in this meta-analysis. Moreover, any potential publication bias was evaluated by Begg's test. We performed subgroup analyses to investigate potential sources of heterogeneity. Meta-regression analysis was conducted to assess the effect of the HALP cutoff value on the HR for OS. Subsequently, sensitivity analyses were also conducted to assess the robustness and reliability of the pooled results. Two-sided $p < 0.05$ was considered statistically significant.

Results

Study characteristics

The search initially identified 729 articles, leaving 406 articles after eliminating duplicate publications. By reading the titles and abstracts, 339 articles that did not fit the main idea were excluded. The full text of 67 studies was then reviewed, and 25 studies (including 4 studies that did not provide the HR with corresponding 95% CI data, 5 studies with missing survival outcome data, and 16 studies involving patients with non-solid tumors) were excluded. Finally, 42 studies containing 17,049 patients were included in this meta-analysis (11, 15–22, 27–59). The flowchart of the study screening process is presented in Figure 1.

Of these 42 studies, three studies had two cohorts (training and validation cohorts) (15, 21, 27), resulting in a total of 45 cohorts included in this meta-analysis. The 29 cohorts were from China (11, 15, 16, 18–21, 27–30, 32–34, 38, 45–49, 53–58), seven from Turkey (17, 31, 35–37, 39, 59), four from Japan (22, 41, 50, 52), three from European and American countries (42, 43, 51), and one study from Thailand (40). In the included cohorts, the most common tumor type was hepatobiliary and pancreatic cancer (n = 8) (21, 30, 31, 48, 50, 57, 58), followed by gastrointestinal cancer (n = 7) (15, 17, 27, 36, 43). Notably, only 4 cohorts were prospectively designed (17, 42, 51, 52), the rest were retrospective (11, 15, 16, 18–22, 27–41, 43–50, 53–59). Of the included cohorts, 31 cohorts underwent curative resection (11, 15, 17–19, 21, 27, 28, 30–36, 38, 41–43, 45, 47–51, 54, 56–58), 9 cohorts received adjuvant therapy (e.g., chemotherapy, radiotherapy, chemoradiotherapy, and immunotherapy) (16, 20, 22, 29, 39, 40, 53, 55, 59), and 2 cohorts received mixed treatment (37, 46). The number of patients included in the individual cohorts ranged from 39 to 1360. The cut-off value of HALP ranged from 0.277 to 56.8. thirty-seven cohorts reported associations between HALP and OS (15–22, 27, 30, 31, 33–37, 39–43, 45, 46, 48–53, 55, 57, 58), 6 cohorts investigated associations between HALP and CSS (11, 27, 32, 42, 46), 8 cohorts examined associations between HALP

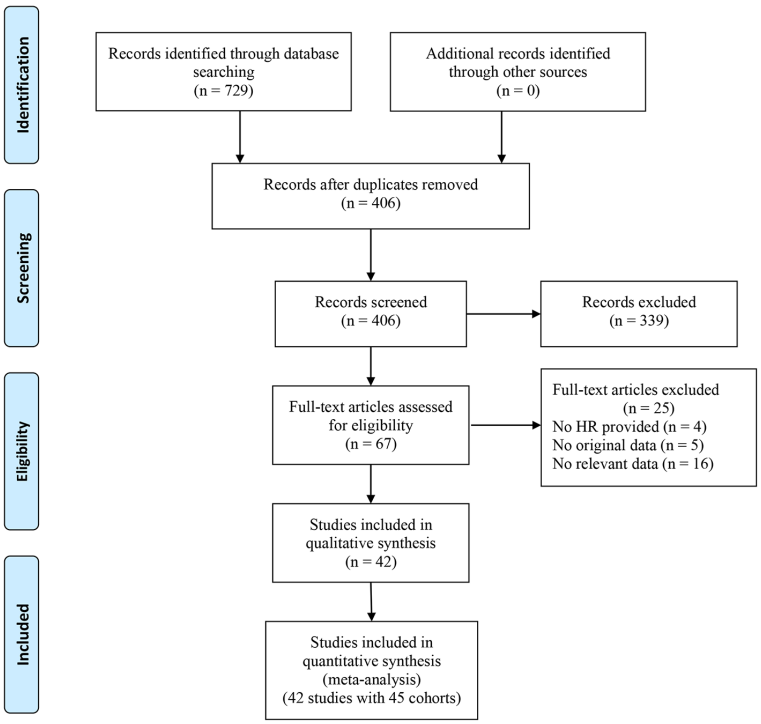

FIGURE 1
PRISMA flowchart depicting the search strategy used for this study.

10.3389/fimmu.2024.1483855

and PFS (20, 28, 29, 33, 40, 52, 53, 59), 7 cohorts investigated associations between HALP and RFS (38, 42, 47, 48), and 4 cohorts reported associations between HALP and DFS (43, 45, 49, 50, 54, 56, 58). The basic characteristics of the enrolled cohorts are shown in Table 1.

Quality of the studies

The study quality of each study was assessed using the QUIPS tool. QUIPS domains most commonly evaluated as low risk of bias were the prognostic factor measurement and outcome measurement, while the QUIPS domain most commonly evaluated as a moderate risk of bias was attrition. The majority of studies were judged to be moderate risk of bias and 2 studies were judged to be high risk, as illustrated in Figure 2.

Association of HALP with survival outcomes

Overall survival

Thirty-four studies comprising 37 cohorts investigated the association of HALP with OS in patients with cancer (15–22, 27, 30, 31, 33–37, 39–43, 45, 46, 48–53, 55, 57, 58). The results demonstrated that OS was significantly longer in patients with increased pretreatment HALP (HR = 0.60, 95% CI 0.54-0.67, $p < 0.01$), with significant heterogeneity among studies ($I^2 = 77\%$, $p < 0.01$) (Figure 3).

Given the significant heterogeneity between studies, we performed subgroup analyses of OS based on study ethnicity, tumor type, treatment strategy, sample size, study design, analysis mode, cut-off value, and cut-off selection method (Table 2). High pre-treatment HALP was found to be consistently associated with better OS regardless of ethnicity, tumor type, treatment strategy, sample size, cut-off value, or cut-off selection method (all $p < 0.01$). On subgroup analysis stratified by analysis mode, the multivariate analysis subgroup was significantly associated with longer OS ($p < 0.01$), while the univariate analysis subgroup was not associated with OS ($p = 0.08$). Furthermore, Meta-regression analysis revealed no significant association between the HALP cutoff value and the HR for OS ($p = 0.401$, Supplementary Data Sheet 1).

Cancer-specific survival

Five studies comprising 6 cohorts explored the association of HALP with CSS in patients with cancer (11, 27, 32, 42, 46). The results indicated that higher pretreatment HALP was associated with longer CSS in patients (HR = 0.53, 95% CI 0.44 - 0.64, $p < 0.01$), and there was low heterogeneity among studies ($I^2 = 24\%$, $p = 0.25$) (Figure 4).

Progression-free survival

Eight studies reported the relationship between HALP and PFS in patients with cancer (20, 28, 29, 33, 40, 52, 53, 59). The results

TABLE 1 Baseline characteristics of reviewed studies.

Author	Year	Country	Study design	Tumor type	Tumor stage	Treatment strategy	Sample size	Age (years)	HALP Cut-off value	Analysis of survival	Survival outcome	Follow-up (months)
Chen (15) (Training)	2015	China	Retrospective	GC	IA-IV	Curative resection	888	Mean 57.3 ± 11.8	56.8	Multivariate	OS	Median 65.6
Chen (15) (Validation)	2015	China	Retrospective	GC	IA-IV	Curative resection	444	Mean 56.8 ± 11.5	56.8	Multivariate	OS	Median 66
Jiang (26) (Training)	2016	China	Retrospective	CRC	II-III	Curative resection	684	Median 62 (21-92)	26.5	Multivariate	OS, CSS	Median 67
Jiang (26) (Validation)	2016	China	Retrospective	CRC	II-III	Curative resection	136	Median 58 (32-86)	26.5	Multivariate	OS, CSS	Median 68
Cong (20)	2017	China	Retrospective	EC	II-IVA	Chemoradiotherapy	39	Median 60 (45 - 71)	48.34	Multivariate	OS, PFS	Median 27.2
Peng (19)	2018	China	Retrospective	BC	NA	Curative resection	516	Median 66 (57–73)	22.2	Multivariate	OS	Median 37 (20 - 56)

(*Continued*)

TABLE 1 Continued

Author	Year	Country	Study design	Tumor type	Tumor stage	Treatment strategy	Sample size	Age (years)	HALP Cut-off value	Analysis of survival	Survival outcome	Follow-up (months)
Peng (11)	2018	China	Retrospective	RCC	NA	Curative resection	1360	Median 55 (46 - 65)	31.2	Multivariate	CSS	Median 67 (36 - 74)
Guo (28)	2019	China	Retrospective	Prostate cancer	NA	Curative resection	82	Median 69 (63-73)	32.4	Multivariate	PSA-PFS	17.47
Shen (29)	2019	China	Retrospective	SCLC	NA	Chemotherapy	178	Mean 61.24 ± 9.27	25.8	Multivariate	PFS	NA
Xu (30)	2020	China	Retrospective	Pancreatic cancer	IA-III	Curative resection	582	Median 61 (29 - 82)	44.56	Multivariate	OS	Median 20.9
Yang (16)	2020	China	Retrospective	SCLC	I-IV	Chemotherapy	335	NA	18.6	Multivariate	OS	Median 27.1 (0.5-46.2)
Arikan (31)	2021	Turkey	Retrospective	PAC	NA	Curative resection	129	Mean 64.69	25	Multivariate	OS	NA
Dagmura (17)	2021	Turkey	Prospective	CRC	Mixed	Curative resection	139	Mean 72.82	15.5	Multivariate	OS	NA
Feng (32)	2021	China	Retrospective	EC	I-III	Curative resection	355	Median 59 (36 - 80)	31.8	Multivariate	CSS	Median 34 (4 - 94)
Gao (33)	2021	China	Retrospective	UTUC	NA	Curative resection	533	Mean 66.71 ± 10.4	28.67	Multivariate	OS, PFS	Median 39.6 (21.6 - 65)
Hu (34)	2021	China	Retrospective	EC	I-III	Curative resection	834	Median 60 (55 - 65)	38.8	Multivariate	OS	NA
Sun (21) (Training)	2021	China	Retrospective	BTC	I-III	Curative resection	287	NA	42.68	Multivariate	OS	Median 19 (9 - 37)
Sun (21) (Validation)	2021	China	Retrospective	BTC	I-III	Curative resection	131	NA	42.68	Multivariate	OS	Median 18 (10 - 38)
Topal (35)	2021	Turkey	Retrospective	EC	I-IV	Curative resection	44	27-86	43	Multivariate	OS	NA
Yalav (36)	2021	Turkey	Retrospective	CRC	I-IIIC	Curative resection	279	Mean 61.54	15.7	Multivariate	OS	NA
Zhai (18)	2021	China	Retrospective	NSCLC	IA-IV	Curative resection	238	Mean 62.3 ± 8.4	48	Multivariate	OS	NA
Ekinci (37)	2022	Turkey	Retrospective	RCC	NA	Mixed	123	Median 64 (21 - 81)	0.277	Multivariate	OS	NA

(Continued)

10.3389/fimmu.2024.1483855

TABLE 1 Continued

Author	Year	Country	Study design	Tumor type	Tumor stage	Treatment strategy	Sample size	Age (years)	HALP Cut-off value	Analysis of survival	Survival outcome	Follow-up (months)
Güç (39)	2022	Turkey	Retrospective	NSCLC	NA	Chemotherapy	401	Mean 63.47 ± 9.75	23.24	Multivariate	OS	Median 18 (1 - 80)
Jiang (38)	2022	China	Retrospective	CC	I-IIA	Curative resection	1054	48.1 ± 9.2	39.5	Multivariate	RFS	Median 53 (9 - 96)
Kurashina (22)	2022	Japan	Retrospective	UC	NA	Immunotherapy	54	70 ± 6.8	30.5	Univariate	OS	NA
Leetanaporn (40)	2022	Thailand	Retrospective	CC	I-IVA	Radiation therapy	1112	Median 52 (44 - 61)	22.2	Multivariate	OS, PFS	Median 2.96
Matsui (41)	2022	Japan	Retrospective	RPS	NA	Curative resection	113	Median 59.7 (17 - 82)	3	Univariate	OS	Median 43.8 (1.8 - 43.8)
Njoku (42)	2022	UK	Prospective	Endometrial cancer	I-IV	Curative resection	439	Median 67 (58 - 74)	24	Multivariate	OS, CSS, RFS	Median 42 (27 – 59)
Ruiz (43)	2022	Mexico	Retrospective	CRC	I-III	Curative resection	640	NA	15	Multivariate	OS, DFS	Median 46.4
Vlatka (44)	2022	Croatia	Retrospective	large B-cell lymphoma	I-IV	Chemotherapy	153	Median 64 (54 - 72)	20.8	Multivariate	OS	Median 40
Wei (45)	2022	China	Retrospective	NSCLC	I-IV	Chemotherapy	362	NA	48.2	Multivariate	OS, DFS	Median 64
Wu (46)	2022	China	Retrospective	Pharyngeal cancer	I-IV	Mixed	319	Mean 57.1 ± 11.5	44	Multivariate	OS, CSS	Median 26.4 (15.6 – 51.6)
Zhao (47)	2022	China	Retrospective	GIST	NA	Curative resection	458	Mean 56.8 ± 12.1	31.5	Multivariate	RFS	Median 56 (4 – 138)
Zhang (48)	2022	China	Retrospective	ICC	I-IV	Curative resection	162	NA	43.6	Univariate	OS, RFS	NA
Fang (49)	2023	China	Retrospective	Oral cavity cancer	I-IV	Curative resection	350	Median 60 (52 - 67)	35.4	Multivariate	OS, DFS	Median 43
Mazzella (51)	2023	Italy	Prospective	NSCLC	I-III	Curative resection	257	NA	32.2	Multivariate	OS	Median 40 (33 – 46)
Nishio (52)	2023	Japan	Prospective	Endometrial cancer	I-IV	Chemotherapy	712	Median 55 (28 -74)	35.52	Multivariate	OS, PFS	NA
Shi (53)	2023	China	Retrospective	EC	II-IVA	Chemoradiotherapy	150	Median 65 (37 - 79)	23.1	Multivariate	OS, PFS	Median 27.5
Toshida (50)	2023	Japan	Retrospective	HCC	NA	Curative resection	332	Median 69 (28 - 87)	45.6	Univariate	OS, DFS	NA

(Continued)

10.3389/fimmu.2024.1483855

10.3389/fimmu.2024.1483855

TABLE 1 Continued

Author	Year	Country	Study design	Tumor type	Tumor stage	Treatment strategy	Sample size	Age (years)	HALP Cut-off value	Analysis of survival	Survival outcome	Follow-up (months)
Zhao B (54)	2023	China	Retrospective	NSCLC	IA-IIIA	Curative resection	219	NA	29.31	Multivariate	RFS	Median 24
Zhao R (55)	2023	China	Retrospective	Nasopharynx cancer	III-IV	Chemotherapy	400	Median 48 (40 - 55)	46.61	Multivariate	OS	Median 50 (2-126)
Zhao Z (56)	2023	China	Retrospective	Breast cancer	I-III	Curative resection	411	Median 54.52 (28 - 98)	23.6	Multivariate	RFS	Median 54
Zhou (57)	2023	China	Retrospective	HCC	I-IV	Curative resection	273	53.99 ± 10.74	54.13	Multivariate	OS	56.69 ± 1.25
Huang (58)	2024	China	Retrospective	ICC	NA	Curative resection	227	NA	37.1	Univariate	OS, RFS	Median 15
Mutlu (59)	2024	Turkey	Retrospective	malignant mesothelioma	I-IV	Chemotherapy	115	Median 64 (24 - 83)	25.9	Multivariate	OS, PFS	NA

GC, gastric carcinoma; BC, bladder cancer; BTC, biliary tract cancer; CRC, colorectal cancer; EC, esophageal cancer; SCLC, small cell lung cancer; NSCLC, non-small cell lung cancer; RCC, renal cell carcinoma; PAC, periampullary carcinoma; UC, urothelial carcinoma; UTUC, upper tract urothelial carcinoma; RPS, retroperitoneal soft tissue sarcoma; CC, cervical cancer; GIST, gastrointestinal stromal tumor; ICC, intrahepatic cholangiocarcinoma; HCC, hepatocellular carcinoma; HALP, hemoglobin, albumin, lymphocyte, and platelet; OS, overall survival; CSS, cancer-specific survival; RFS, recurrence-free survival; PFS, progression-free survival; NA, not available.

showed that patients with elevated pretreatment HALP had better PFS (HR = 0.62, 95% CI 0.54 - 0.72, p < 0.01), with low heterogeneity between studies (I^2 = 1%, p = 0.42) (Figure 4).

Recurrence-free survival

Seven studies reported the relationship between HALP and RFS in patients with cancer (43, 45, 49, 50, 54, 56, 58). The results revealed that patients with elevated pretreatment HALP had favorable RFS in patients with solid tumors (HR = 0.48, 95% CI 0.30 - 0.77, p < 0.01), with significant heterogeneity among studies (I^2 = 82%, p < 0.01) (Figure 5).

Disease-free survival

Four studies reported the relationship between HALP and DFS in patients with cancer (43, 45, 49, 50). The results demonstrated that patients with elevated pretreatment HALP had better DFS (HR = 0.72, 95% CI 0.57 - 0.92, p < 0.01), with lower significant heterogeneity among studies (I^2 = 45%, p = 0.14) (Figure 5).

Sensitivity analysis

We performed sensitivity analyses to assess the reliability of pooled HRs for OS (Supplementary Data Sheet 1). The exclusion of individual studies had no significant effect on the combined HR, confirming that the results of this meta-analysis are relatively robust and reliable.

Publication bias

The Begg's test demonstrated that the results were not statistically significant (OS: p = 0.824), but the Begg's funnel plots showed asymmetry between the left and right sides, which increases the likelihood of potential publication bias (Supplementary Data Sheet 1).

Discussion

To date, cancer remains the leading cause of death and a significant barrier to increasing life expectancy in all countries of the world (60). Due to the higher cost of cancer management, the establishment of reliable prognostic biomarkers is essential for predicting therapeutic outcomes and determining the patients most likely to benefit from treatment. HALP is a new score based on a combination of inflammatory and nutritional deficiency concepts that was first discovered in 2015 to predict the prognosis of patients with gastric cancer (15). Over the past few years, HALP has been successively used to evaluate survival outcomes in various malignancies. Although a recent systematic review has revealed that low pre-treatment HALP predicts a worse overall prognosis for cancer patients (61), however, there is great heterogeneity in studies investigating HALP in terms of cancer type, outcome, HALP threshold, and population of interest. Here, we conducted an updated meta-analysis based on the available literature to investigate the prognostic impact of HALP. In addition, subgroup

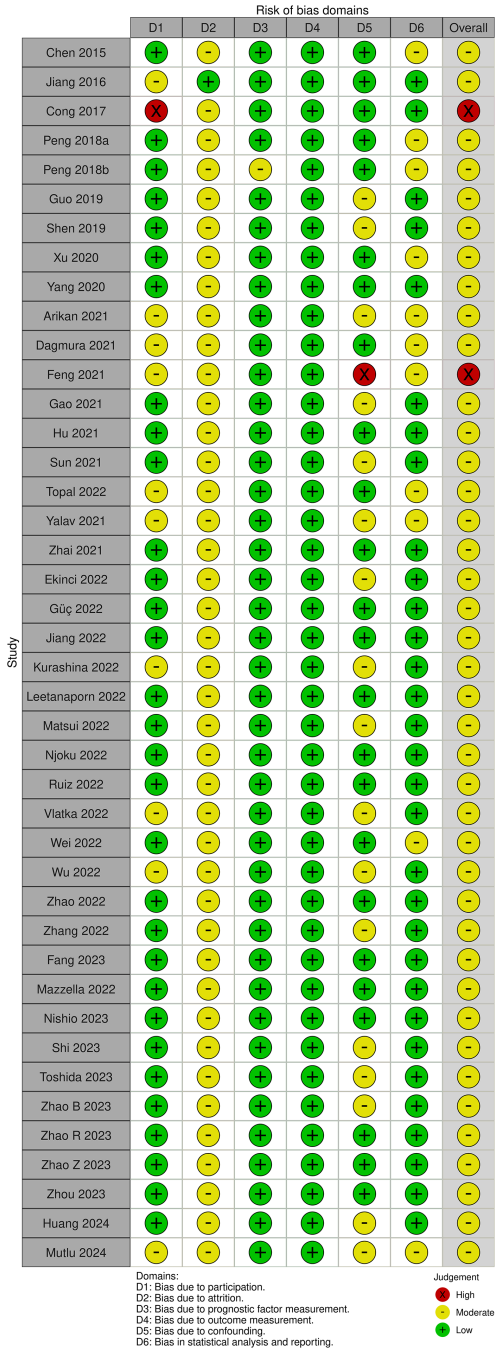

FIGURE 2
Risk of bias assessment of included studies.

analyses were performed to explore the influence of factors such as ethnicity, tumor type, and treatment strategy on the study results.

Evidence from the inclusion of 45 cohorts suggested that an elevated HALP was associated with better OS, CSS, PFS, and DFS in patients with solid tumors. When stratified by ethnicity, disease type, treatment strategy, sample size, and study design higher HALP was consistently an independent factor for favorable OS. Of interest, the included studies reported different HALP cut-off values for different disease types and used different methods to select HALP cut-off values. However, we observed that the prognostic impact of HALP on OS was retained across subgroups. Moreover, in subgroup analyses stratified by analysis mode, HALP scores in the multivariate analysis subgroup were independently associated with OS (Table 2). Although no significant difference in OS was observed in the univariate subgroup, it is unlikely to affect the interpretation of our results given the small number of studies included in the analysis. Notably, in this meta-analysis, we included a substantial number of retrospective studies. The subgroup analysis based on study design showed no significant difference between the data from retrospective studies and the overall results (Table 2). To some extent, this indicates that data from retrospective studies are consistent with those from other types of studies and did not introduce noticeable bias into the final comprehensive conclusion.

Furthermore, due to the heterogeneity of the studies themselves, we were unable to comprehensively assess the relationship between HALP and age or gender. As age increases, the prognosis of elderly cancer patients is generally worse. However, we observed that almost all studies accounted for patient age when performing multivariate regression or constructing nomograms. Therefore, age does not appear to influence the HALP score. Further research is needed to study HALP scores in healthy populations to accurately evaluate the correlation between HALP and age. Additionally, some studies have reported differences in baseline HALP scores between males and females, but after adjusting for gender, the HALP score remained significant (11, 15, 19, 34). Thus, based on current results, gender does not significantly affect the utility of HALP as a biomarker. In general, a more refined search method and more stringent inclusion criteria were used than in the previous systematic review (61), which dramatically improved the quality and credibility of the study.

The mechanism of the association between high HALP and favorable outcomes in cancer patients remains unclear. One potential mechanism for the prognostic impact of HALP could be the association of high HALP with inflammation and nutrition. Anemia is a well-documented cancer-related phenomenon. In chronic anemia, CD3 T lymphocytes and macrophages release pro-inflammatory cytokines such as IL-6 (62). IL-6 mediates the release of hepcidin from the liver, which inhibits iron absorption and iron release to prevent cancer cells from utilizing iron, thereby reducing erythropoiesis (63). Previous studies also have demonstrated that low hemoglobin levels were associated with adverse clinical outcomes in cancer patients, including impaired quality of life and reduced survival (64, 65). Serum albumin is a reliable indicator for assessing nutritional status and visceral protein function. Studies have reported that in the later stages of the disease, malnutrition and inflammation inhibit albumin synthesis, resulting in lower serum albumin concentrations (66). The reason for this may be due to the production of cytokines, such as IL-6, which regulate albumin production by hepatocytes (67). Furthermore, tumor necrosis factor may increase microvascular permeability, thereby increasing the passage of albumin through capillaries (68, 69). Therefore, mild or no hypoalbuminemia in the early stages of cancer, but a significant decrease in albumin levels as the disease

10.3389/fimmu.2024.1483855

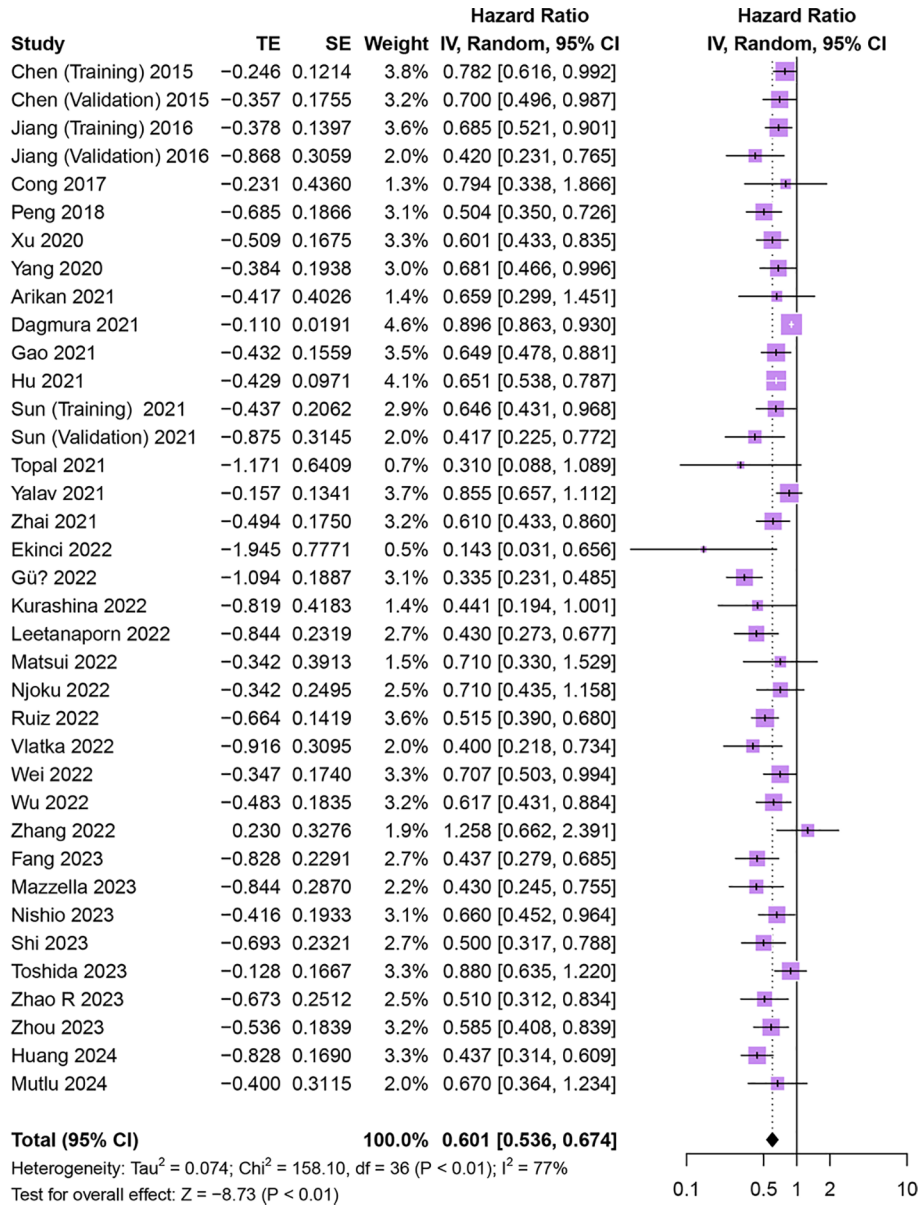

FIGURE 3
Forest plot showing hazard ratio for overall survival for HALP greater than or less than the cutoff value. HALP, hemoglobin, albumin, lymphocyte and platelet.

progresses could be a good indicator of cancer prognosis (7).

Abundant evidence indicates that the inflammatory microenvironment is an important component of carcinogenesis. As the basic components of the systemic inflammatory response, platelets and lymphocytes are involved in the continuous inflammation of the tumor microenvironment (70, 71). Platelets have been reported to promote tumor growth and angiogenesis by secreting a mixture of major proangiogenic cytokines in the microcirculation of potentially prothrombotic tumors (72, 73). In addition, platelets also enhance tumor metastasis by covering circulating tumor cells to protect tumor cells from physical factors such as shear stress and host immune responses (72, 74). On the other hand, the importance of lymphocytes has been highlighted in earlier studies. It is an important component of anti-tumor immunity and can inhibit tumor proliferation and migration through cytotoxicity (70). These findings suggest that serum hemoglobin, albumin, and lymphocytes can be considered favorable factors for tumor prognosis, while platelets may be an unfavorable factor.

Over the past decade, energy and resources have been invested in developing biomarkers to help personalize treatment plans for cancer patients. The HALP score combines malnutrition factors (hemoglobin and albumin) with inflammatory response factors (lymphocyte and platelet counts). It may help identify more patients with a poor prognosis than a single index because abnormalities in any single indicator do not truly reflect the patient's condition. In addition, HALP has even been shown to have the potential to distinguishing between benign and malignant processes (75). Therefore, we reasoned that HALP could serve as a more practical and comprehensive prognostic

TABLE 2 Subgroup analyses of overall survival.

Subgroup	Variable	No. of cohorts	Model	HR (95% CI)	*P*	Heterogeneity	
						I^2 (%)	*P*
Ethnic	Asian	27	Random	0.62 (0.57, 0.67)	< 0.01	20.0	0.18
	Caucasian	10	Random	0.57 (0.43, 0.75)	< 0.01	85.0	< 0.01
Tumor type	gastrointestinal cancer	7	Random	0.71 (0.59, 0.86)	< 0.01	78.0	< 0.01
	esophageal cancer	4	Random	0.62 (0.53, 0.74)	< 0.01	0.0	0.46
	hepatobiliary and pancreatic cancer	8	Random	0.63 (0.51, 0.79)	< 0.01	54.0	0.03
	genitourinary cancer	4	Random	0.53 (0.38, 0.73)	< 0.01	35.0	0.20
	lung cancer	5	Random	0.54 (0.40, 0.72)	< 0.01	64.6	0.02
	gynecologic cancer	3	Random	0.59 (0.44, 0.79)	< 0.01	27.0	0.25
	others	6	Random	0.54 (0.44, 0.66)	< 0.01	0.0	0.65
Treatment strategy	curative resection	25	Random	0.64 (0.57, 0.72)	< 0.01	76	< 0.01
	adjuvant therapy	10	Random	0.51 (0.43, 0.62)	< 0.01	25.0	0.21
	mixed	2	Random	0.36 (0.09, 1.44)	0.15	70	0.07
Sample size	> 300	18	Random	0.61 (0.55, 0.68)	< 0.01	43.0	0.03
	≤ 300	19	Random	0.59 (0.49, 0.71)	< 0.01	75.0	< 0.01
Analysis mode	multivariate	32	Random	0.59 (0.52, 0.67)	< 0.01	78.0	< 0.01
	univariate	5	Random	0.69 (0.45, 1.05)	0.08	71.0	< 0.01
Cut-off value for HALP	> 26.5	22	Random	0.64 (0.57, 0.71)	< 0.01	39.0	0.03
	≤ 26.5	15	Random	0.57 (0.47, 0.70)	< 0.01	84.0	< 0.01
Selection of Cut-off value	ROC analysis	21	Random	0.60 (0.51, 0.71)	< 0.01	81.0	< 0.01
	X-tile software	12	Random	0.59 (0.52, 0.67)	< 0.01	29.0	0.16
	median/mean	3	Random	0.72 (0.54, 0.96)	< 0.01	0.0	0.97
	Cutoff Finder	1	–	0.66 (0.45, 0.96)	0.03	–	–

HALP, hemoglobin, albumin, lymphocyte and platelet; ROC, receiver-operating characteristics; HR, hazard ratio; CI, confidence interval.

marker for human cancers, including gastrointestinal, lung, genitourinary tract, gynecological, among others.

Strengths and limitations

The strength of this study is that it followed international guidelines and a rigorous systematic search and bias assessment protocol were developed in advance. Additionally, this study is the up-to-date systematic review and meta-analysis on this topic and represents the available evidence. Nevertheless, some limitations should be acknowledged. First, this study analyzed aggregated data rather than individual patient data. Second, the majority of the included studies are retrospective, which increases the risk of bias. Future research should prioritize prospective study designs, especially randomized controlled trials, to confirm our conclusions with a higher level of evidence. Third, although stable results were shown in subgroup analyses stratified by treatment strategy, there was a greater heterogeneity in the treatment strategies of patients with different tumors, which could have some potential impact on the study results. Fourth, lymphocyte and platelet counts are non-specific parameters and may be affected by factors such as infection and inflammation (13). Despite most of the included studies have tried to control for these factors, the confounding effects of concurrent inflammatory conditions cannot be completely excluded. Finally, cutoff values for HALP were measured in different ways, and although we did not find a difference between the method of measurement and OS in our subgroup analysis, it is important to establish the optimal HALP cutoff value.

Conclusions

This study found that an elevated HALP was correlated with better survival in patients with solid tumors, and HALP could be used as a cost-effective prognostic biomarker. The prognostic model based on HALP deserves further investigation.

10.3389/fimmu.2024.1483855

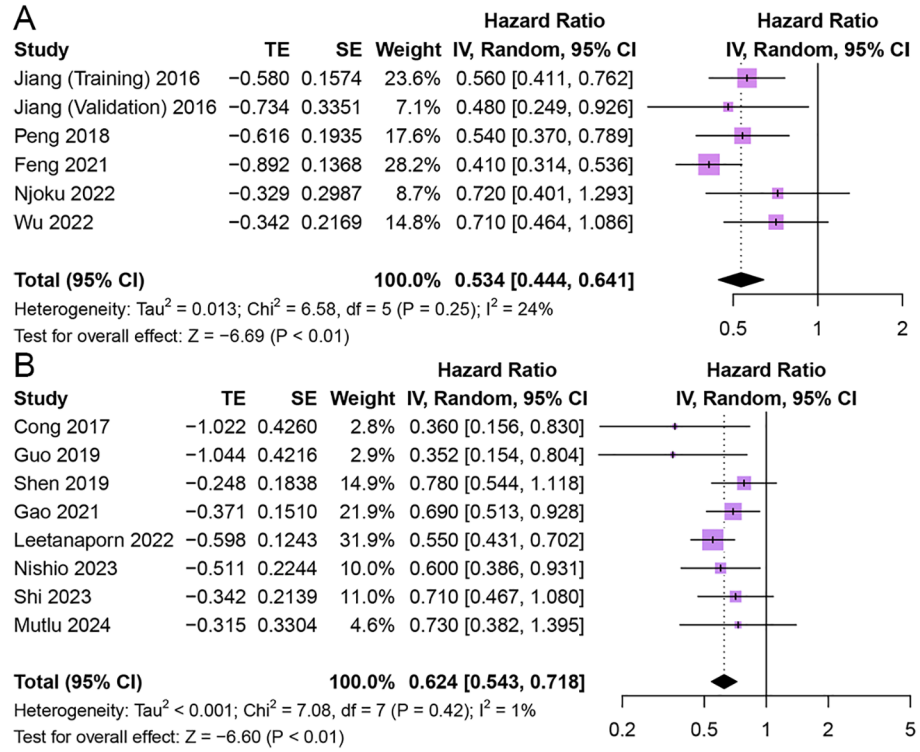

FIGURE 4
Forest plot showing hazard ratio for cancer-specific survival **(A)** and progression-free survival **(B)** for HALP greater than or less than the cutoff value. HALP, hemoglobin, albumin, lymphocyte and platelet.

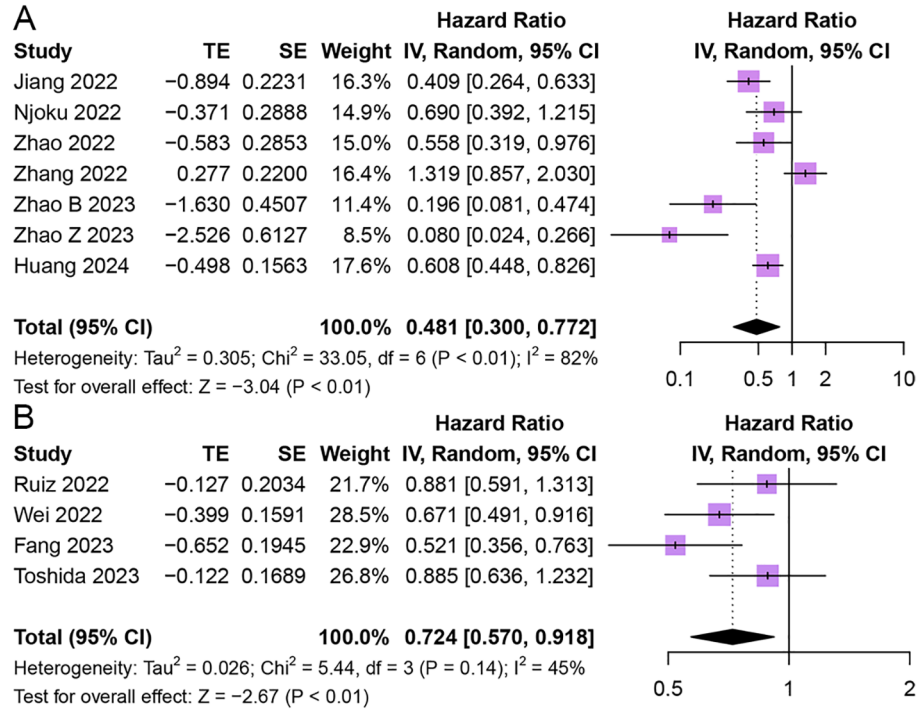

FIGURE 5
Forest plot showing hazard ratio for recurrence-free survival **(A)** and disease-free survival **(B)** for HALP greater than or less than the cutoff value. HALP, hemoglobin, albumin, lymphocyte and platelet.

Data availability statement

The original contributions presented in the study are included in the article/Supplementary Material. Further inquiries can be directed to the corresponding authors.

Author contributions

JL: Data curation, Methodology, Resources, Software, Writing – original draft. JZ: Data curation, Formal analysis, Methodology, Software, Writing – original draft. PW: Formal analysis, Methodology, Validation, Writing – review & editing. DL: Conceptualization, Formal analysis, Investigation, Writing – review & editing.

Funding

The author(s) declare that no financial support was received for the research, authorship, and/or publication of this article.

Conflict of interest

The authors declare that the research was conducted in the absence of any commercial or financial relationships that could be construed as a potential conflict of interest.

Publisher's note

All claims expressed in this article are solely those of the authors and do not necessarily represent those of their affiliated organizations, or those of the publisher, the editors and the reviewers. Any product that may be evaluated in this article, or claim that may be made by its manufacturer, is not guaranteed or endorsed by the publisher.

Supplementary material

The Supplementary Material for this article can be found online at: https://www.frontiersin.org/articles/10.3389/fimmu.2024.1483855/full#supplementary-material

References

1. Sung H, Ferlay J, Siegel RL, Laversanne M, Soerjomataram I, Jemal A, et al. Global cancer statistics 2020: GLOBOCAN estimates of incidence and mortality worldwide for 36 cancers in 185 countries. *CA Cancer J Clin*. (2021) 71:209–49. doi: 10.3322/caac.21660

2. Jung JH, Hwang J, Kim JH, Sim DY, Im E, Park JE, et al. Phyotochemical candidates repurposing for cancer therapy and their molecular mechanisms. *Semin Cancer Biol*. (2021) 68:164–74. doi: 10.1016/j.semcancer.2019.12.009

3. Jackson SE, Chester JD. Personalised cancer medicine. *Int J Cancer*. (2015) 137:262–6. doi: 10.1002/ijc.v137.2

4. Ekser B, Veroux M. New prognostic indicators in surgery. *Int J Surg*. (2019) 68:176–7. doi: 10.1016/j.ijsu.2019.07.015

5. Colotta F, Allavena P, Sica A, Garlanda C, Mantovani A. Cancer-related inflammation, the seventh hallmark of cancer: links to genetic instability. *Carcinogenesis*. (2009) 30:1073–81. doi: 10.1093/carcin/bgp127

6. Wiseman MJ. Nutrition and cancer: prevention and survival. *Br J Nutr*. (2019) 122:481–7. doi: 10.1017/S0007114518002222

7. Gupta D, Lis CG. Pretreatment serum albumin as a predictor of cancer survival: a systematic review of the epidemiological literature. *Nutr J*. (2010) 9:69. doi: 10.1186/1475-2891-9-69

8. Littlewood TJ. The impact of hemoglobin levels on treatment outcomes in patients with cancer. *Semin Oncol*. (2001) 28:49–53. doi: 10.1016/S0093-7754(01)90213-1

9. Wang S, Sun J, Chen K, Ma P, Lei Q, Xing S, et al. Perspectives of tumor-infiltrating lymphocyte treatment in solid tumors. *BMC Med*. (2021) 19:140. doi: 10.1186/s12916-021-02006-4

10. Haemmerle M, Stone RL, Menter DG, Afshar-Kharghan V, Sood AK. The platelet lifeline to cancer: challenges and opportunities. *Cancer Cell*. (2018) 33:965–83. doi: 10.1016/j.ccell.2018.03.002

11. Peng D, Zhang CJ, Tang Q, Zhang L, Yang KW, Yu XT, et al. Prognostic significance of the combination of preoperative hemoglobin and albumin levels and lymphocyte and platelet counts (HALP) in patients with renal cell carcinoma after nephrectomy. *BMC Urol*. (2018) 18:20. doi: 10.1186/s12894-018-0333-8

12. Li B, Zhou P, Liu Y, Wei H, Yang X, Chen T, et al. Platelet-to-lymphocyte ratio in advanced Cancer: Review and meta-analysis. *Clin Chim Acta*. (2018) 483:48–56. doi: 10.1016/j.cca.2018.04.023

13. Templeton AJ, McNamara MG, Šeruga B, Vera-Badillo FE, Aneja P, Ocaña A, et al. Prognostic role of neutrophil-to-lymphocyte ratio in solid tumors: a systematic review and meta-analysis. *J Natl Cancer Inst*. (2014) 106:dju124. doi: 10.1093/jnci/dju124

14. Yan L, Nakamura T, Casadei-Gardini A, Bruixola G, Huang YL, Hu ZD, et al. Long-term and short-term prognostic value of the prognostic nutritional index in cancer: a narrative review. *Ann Transl Med*. (2021) 9:1630. doi: 10.21037/atm-21-4528

15. Chen XL, Xue L, Wang W, Chen HN, Zhang WH, Liu K, et al. Prognostic significance of the combination of preoperative hemoglobin, albumin, lymphocyte and platelet in patients with gastric carcinoma: a retrospective cohort study. *Oncotarget*. (2015) 6:41370–82. doi: 10.18632/oncotarget.v6i38

16. Yang N, Han X, Yu J, Shu W, Qiu F, Han J, et al. Hemoglobin, albumin, lymphocyte, and platelet score and neutrophil-to-lymphocyte ratio are novel significant prognostic factors for patients with small-cell lung cancer undergoing chemotherapy. *J Cancer Res Ther*. (2020) 16:1134–9. doi: 10.4103/jcrt.JCRT_1066_19

17. Dagmura H, Daldal E, Okan I. The efficacy of hemoglobin, albumin, lymphocytes, and platelets as a prognostic marker for survival in octogenarians and nonagenarians undergoing colorectal cancer surgery. *Cancer Biother Radiopharm*. (2021) 37:955-62. doi: 10.1089/cbr.2020.4725

18. Zhai B, Chen J, Wu J, Yang L, Guo X, Shao J, et al. Predictive value of the hemoglobin, albumin, lymphocyte, and platelet (HALP) score and lymphocyte-to-monocyte ratio (LMR) in patients with non-small cell lung cancer after radical lung cancer surgery. *Ann Transl Med*. (2021) 9:976. doi: 10.21037/atm-21-2120

19. Peng D, Zhang CJ, Gong YQ, Hao H, Guan B, Li XS, et al. Prognostic significance of HALP (hemoglobin, albumin, lymphocyte and platelet) in patients with bladder cancer after radical cystectomy. *Sci Rep*. (2018) 8:794. doi: 10.1038/s41598-018-19146-y

20. Cong L, Hu L. The value of the combination of hemoglobin, albumin, lymphocyte and platelet in predicting platinum-based chemoradiotherapy response in male patients with esophageal squamous cell carcinoma. *Int Immunopharmacol*. (2017) 46:75–9. doi: 10.1016/j.intimp.2017.02.027

21. Sun L, Guan A, Jin Y, Liu M, Xiao Y, Xu H, et al. Comparison of prognostic value of red cell-related parameters of biliary tract cancer after surgical resection and integration of a prognostic nomogram: A retrospective study. *Adv Ther*. (2021) 38:1227–44. doi: 10.1007/s12325-020-01595-5

22. Kurashina R, Ando K, Inoue M, Izumi K, Maruyama R, Mitani K, et al. Platelet-to-lymphocyte ratio predicts the efficacy of pembrolizumab in patients with urothelial carcinoma. *Anticancer Res*. (2022) 42:1131–6. doi: 10.21873/anticanres.15576

23. Takenaka Y, Oya R, Takemoto N, Inohara H. Predictive impact of sarcopenia in solid cancers treated with immune checkpoint inhibitors: a meta-analysis. *J Cachexia Sarcopenia Muscle*. (2021) 12:1122–35. doi: 10.1002/jcsm.12755

24. Page MJ, McKenzie JE, Bossuyt PM, Boutron I, Hoffmann TC, Mulrow CD, et al. The PRISMA 2020 statement: An updated guideline for reporting systematic reviews. *Int J Surg*. (2021) 88:105906. doi: 10.1016/j.ijsu.2021.105906

25. Shea BJ, Reeves BC, Wells G, Thuku M, Hamel C, Moran , et al. AMSTAR 2: a critical appraisal tool for systematic reviews that include randomised or non-randomised studies of healthcare interventions, or both. *Bmj*. (2017) 358:j4008. doi: 10.1136/bmj.j4008

26. Hayden JA, van der Windt DA, Cartwright JL, Côté P, Bombardier C. Assessing bias in studies of prognostic factors. *Ann Intern Med*. (2013) 158:280–6. doi: 10.7326/0003-4819-158-4-201302190-00009

27. Jiang H, Li H, Li A, Tang E, Xu D, Chen Y, et al. Preoperative combined hemoglobin, albumin, lymphocyte and platelet levels predict survival in patients with locally advanced colorectal cancer. *Oncotarget*. (2016) 7:72076–83. doi: 10.18632/oncotarget.12271

28. Guo Y, Shi D, Zhang J, Mao S, Wang L, Zhang W, et al. The hemoglobin, albumin, lymphocyte, and platelet (HALP) score is a novel significant prognostic factor for patients with metastatic prostate cancer undergoing cytoreductive radical prostatectomy. *J Cancer*. (2019) 10:81–91. doi: 10.7150/jca.27210

29. Shen XB, Zhang YX, Wang W, Pan YY. The hemoglobin, albumin, lymphocyte, and platelet (HALP) score in patients with small cell lung cancer before first-line treatment with etoposide and progression-free survival. *Med Sci Monit*. (2019) 25:5630–9. doi: 10.12659/MSM.917968

30. Xu SS, Li S, Xu HX, Li H, Wu CT, Wang WQ, et al. Haemoglobin, albumin, lymphocyte and platelet predicts postoperative survival in pancreatic cancer. *World J Gastroenterol*. (2020) 26:828–38. doi: 10.3748/wjg.v26.i8.828

31. Arikan TB, Sozuer E, Topal U, Lale A, Yilmaz AZ. The value and prognostic significance of preoperative hemoglobin and albumin levels, and the lymphocyte and platelet count (halp) scores in predicting pancreatic fistula in patients undergoing pancreaticoduodenectomy due to periampullary region tumors. *Acta Med Mediterr*. (2021) 37:1341–6. doi: 10.19193/0393-6384_2021_2_206

32. Feng JF, Wang L, Yang X. The preoperative hemoglobin, albumin, lymphocyte and platelet (HALP) score is a useful predictor in patients with resectable esophageal squamous cell carcinoma. *Bosn J Basic Med Sci*. (2021) 21:773–81. doi: 10.17305/bjbms.2021.5666

33. Gao X, Lin B, Lin Q, Ye T, Zhou T, Hu M, et al. A HALP score-based prediction model for survival of patients with the upper tract urothelial carcinoma undergoing radical nephroureterectomy. *Bosn J Basic Med Sci*. (2022) 22:280–90. doi: 10.17305/bjbms.2021.6543

34. Hu SJ, Zhao XK, Song X, Lei LL, Han WL, Xu RH, et al. Preoperative maximal voluntary ventilation, hemoglobin, albumin, lymphocytes and platelets predict postoperative survival in esophageal squamous cell carcinoma. *World J Gastroenterol*. (2021) 27:321–35. doi: 10.3748/wjg.v27.i4.321

35. Topal U, Dal F, Sozuer E, Akyuz M, Talih T, İslam D, et al. Combination of preoperative haemoglobin and albumin levels and lymphocyte and platelet counts (HALP) in patients with oesophageal cancer. *J Evol Med Dental Sci*. (2021) 10:173–8. doi: 10.14260/jemds/2021/38

36. Yalav O, Topal U, Unal AG, Eray IC. Prognostic significance of preoperative hemoglobin and albumin levels and lymphocyte and platelet counts (HALP) in patients undergoing curative resection for colorectal cancer. *Ann Ital Chir*. (2021) 92:283–92.

37. Ekinci F, Balcik OY, Oktay E, Erdogan AP. HALP score as a new prognostic index in metastatic renal cell cancer. *J Coll Phys Surg Pak*. (2022) 32:313–8.

38. Jiang P, Kong W, Gong C, Chen Y, Li F, Xu L. Predicting the recurrence of operable cervical cancer patients based on hemoglobin, albumin, lymphocyte, and platelet (HALP) score and classical clinicopathological parameters. *J Inflammation Res*. (2022) 15:5265–81. doi: 10.2147/JIR.S383742

39. Güç ZG, Alacacıoğlu A, Kalender ME, Oflazoğlu U, Ünal S, Yıldız Y, et al. HALP score and GNRI: Simple and easily accessible indexes for predicting prognosis in advanced stage NSCLC patients. The İzmir oncology group (IZOG) study. *Front Nutr*. (2022) 9:905292. doi: 10.3389/fnut.2022.905292

40. Leetanaporn K, Hanprasertpong J. Predictive value of the hemoglobin-albumin-lymphocyte-platelet (HALP) index on the oncological outcomes of locally advanced cervical cancer patients. *Cancer Manag Res*. (2022) 14:1961–72. doi: 10.2147/CMAR.S365612

41. Matsui Y, Matsuda A, Maejima A, Shinoda Y, Nakamura E, Komiyama M, et al. The clinical significance of perioperative inflammatory index as a prognostic factor for patients with retroperitoneal soft tissue sarcoma. *Int J Clin Oncol*. (2022) 27:1093–100. doi: 10.1007/s10147-022-02150-8

42. Njoku K, Barr CE, Ramchander NC, Crosbie EJ. Impact of pre-treatment prognostic nutritional index and the haemoglobin, albumin, lymphocyte and platelet (HALP) score on endometrial cancer survival: A prospective database analysis. *PloS One*. (2022) 17:e0272232. doi: 10.1371/journal.pone.0272232

43. Calderillo Ruiz G, Lopez Basave H, Vazquez Renteria RS, Castillo Morales A, Guijosa A, Castillo Morales C, et al. The prognostic significance of HALP index for colon cancer patients in a Hispanic-based population. *J Oncol*. (2022) 2022:4324635. doi: 10.1155/2022/4324635

44. Vlatka P, Marko L, Stefan M, Dorian L. The hemoglobin, albumin, lymphocyte, and platelet (HALP) score is a novel prognostic factor for patients with diffuse large B-cell lymphoma. *J Cancer Res Ther*. (2022) 18:725–32. doi: 10.4103/jcrt.jcrt_174_21

45. Wei S, Shao J, Wang J, Wang G. The preoperative hemoglobin, albumin, lymphocyte, and platelet score is a prognostic factor for non-small cell lung cancer patients undergoing adjuvant chemotherapy: a retrospective study. *Ann Transl Med*. (2022) 10:457. doi: 10.21037/atm-22-1097

46. Wu CY, Lin YH, Lo WC, Cheng PC, Hsu WL, Chen YC, et al. Nutritional status at diagnosis is prognostic for pharyngeal cancer patients: a retrospective study. *Eur Arch Otorhinolaryngol*. (2022) 279:3671–8. doi: 10.1007/s00405-021-07222-5

47. Zhao Z, Yin XN, Wang J, Chen X, Cai ZL, Zhang B, et al. Prognostic significance of hemoglobin, albumin, lymphocyte, platelet in gastrointestinal stromal tumors: A propensity matched retrospective cohort study. *World J Gastroenterol*. (2022) 28:3476–87. doi: 10.3748/wjg.v28.i27.3476

48. Zhang D, Zeng H, Pan Y, Zhao Y, Wang X, Chen J, et al. Liver tumor markers, HALP score, and NLR: simple, cost-effective, easily accessible indexes for predicting prognosis in ICC patients after surgery. *J Pers Med*. (2022) 12:2041. doi: 10.3390/jpm12122041

49. Fang KH, Lai CH, Hsu CM, Liao CT, Kang CJ, Lee YC, et al. Prognostic impact of the hemoglobin-albumin-lymphocyte-platelet score in patients with oral cavity cancer undergoing surgery. *Head Neck*. (2023) 45:1558–71. doi: 10.1002/hed.27372

50. Toshida K, Itoh S, Kayashima H, Nagao Y, Yoshiya S, Tomino T, et al. The hemoglobin, albumin, lymphocyte, and platelet score is a prognostic factor for Child-Pugh A patients undergoing curative hepatic resection for single and small hepatocellular carcinoma. *Hepatol Res*. (2023) 53:522-30. doi: 10.1111/hepr.13885

51. Mazzella A, Maiolino E, Maisonneuve P, Loi M, Alifano M. Systemic inflammation and lung cancer: is it a real paradigm? Prognostic value of inflammatory indexes in patients with resected non-small-cell lung cancer. *Cancers (Basel)*. (2023) 15:1854. doi: 10.3390/cancers15061854

52. Nishio S, Murotani K, Yamagami W, Suzuki S, Nakai H, Kato K, et al. Pretreatment systemic inflammatory markers predict survival in endometrial cancer: A Japanese Gynecologic Oncology Group 2043 exploratory data analysis. *Gynecol Oncol*. (2024) 181:46–53. doi: 10.1016/j.ygyno.2023.12.007

53. Shi Y, Shen G, Zeng Y, Ju M, Chen X, He C, et al. Predictive values of the hemoglobin, albumin, lymphocyte and platelet score (HALP) and the modified -Gustave Roussy immune score for esophageal squamous cell carcinoma patients undergoing concurrent chemoradiotherapy. *Int Immunopharmacol*. (2023) 123:110773. doi: 10.1016/j.intimp.2023.110773

54. Zhao B, Guo H, Wu W, Duan G. Hemoglobin, albumin, lymphocyte and platelet (HALP) score can predict the prognosis of patients with non-small cell lung cancer (NSCLC). *Asian J Surg*. (2023) 46:4891–2. doi: 10.1016/j.asjsur.2023.05.152

55. Zhao R, Liang Z, Chen K, Zhu X. Nomogram based on hemoglobin, albumin, lymphocyte and platelet score to predict overall survival in patients with T3-4N0-1 nasopharyngeal carcinoma. *J Inflammation Res*. (2023) 16:1995–2006. doi: 10.2147/JIR.S411194

56. Zhao Z, Xu L. Prognostic significance of HALP score and combination of peripheral blood multiple indicators in patients with early breast cancer. *Front Oncol*. (2023) 13:1253895. doi: 10.3389/fonc.2023.1253895

57. Zhou J, Yang D. Prognostic significance of hemoglobin, albumin, lymphocyte and platelet (HALP) score in hepatocellular carcinoma. *J Hepatocell Carcinoma*. (2023) 10:821–31. doi: 10.2147/JHC.S411521

58. Huang G, Zhang H, Yang Z, Li Q, Yuan H, Chen P, et al. Predictive value of HTS grade in patients with intrahepatic cholangiocarcinoma undergoing radical resection: a multicenter study from China. *World J Surg Oncol*. (2024) 22:17. doi: 10.1186/s12957-023-03281-6

59. Mutlu E, Inanc M. Prognostic significance of inflammation scores in Malignant mesothelioma. *Eur Rev Med Pharmacol Sci*. (2024) 28:2340–50. doi: 10.26355/eurrev_202403_35741

60. Bray F, Laversanne M, Weiderpass E, Soerjomataram I. The ever-increasing importance of cancer as a leading cause of premature death worldwide. *Cancer*. (2021) 127:3029–30. doi: 10.1002/cncr.v127.16

61. Xu H, Zheng X, Ai J, Yang L. Hemoglobin, albumin, lymphocyte, and platelet (HALP) score and cancer prognosis: A systematic review and meta-analysis of 13,110 patients. *Int Immunopharmacol*. (2023) 114:109496. doi: 10.1016/j.intimp.2022.109496

62. McCranor BJ, Kim MJ, Cruz NM, Xue QL, Berger AE, Walston JD, et al. Interleukin-6 directly impairs the erythroid development of human TF-1 erythroleukemic cells. *Blood Cells Mol Dis*. (2014) 52:126–33. doi: 10.1016/j.bcmd.2013.09.004

63. Ferrucci L, Semba RD, Guralnik JM, Ershler WB, Bandinelli S, Patel KV, et al. Proinflammatory state, hepcidin, and anemia in older persons. *Blood*. (2010) 115:3810–6. doi: 10.1182/blood-2009-02-201087

64. Cella D, Kallich J, McDermott A, Xu X. The longitudinal relationship of hemoglobin, fatigue and quality of life in anemic cancer patients: results from five randomized clinical trials. *Ann Oncol*. (2004) 15:979–86. doi: 10.1093/annonc/mdh235

65. Knight K, Wade S, Balducci L. Prevalence and outcomes of anemia in cancer: a systematic review of the literature. *Am J Med*. (2004) 116 Suppl 7A:11s–26s. doi: 10.1016/j.amjmed.2003.12.008

66. Yeun JY, Kaysen GA. Factors influencing serum albumin in dialysis patients. *Am J Kidney Dis*. (1998) 32:S118–125. doi: 10.1016/S0272-6386(98)70174-X

67. Pfensig C, Dominik A, Borufka L, Hinz M, Stange J, Eggert M, et al. A new application for albumin dialysis in extracorporeal organ support: characterization of a putative interaction between human albumin and proinflammatory cytokines IL-6 and TNFα. *Artif Organs*. (2016) 40:397–402. doi: 10.1111/aor.2016.40.issue-4

68. McMillan DC, Watson WS, O'Gorman P, Preston T, Scott HR, McArdle CS, et al. Albumin concentrations are primarily determined by the body cell mass and the systemic inflammatory response in cancer patients with weight loss. *Nutr Cancer*. (2001) 39:210–3. doi: 10.1207/S15327914nc392_8

69. McCarthy ET, Sharma R, Sharma M, Li JZ, Ge XL, Dileepan KN, et al. TNF-alpha increases albumin permeability of isolated rat glomeruli through the generation of superoxide. *J Am Soc Nephrol*. (1998) 9:433–8. doi: 10.1681/ASN.V93433

70. Mantovani A, Allavena P, Sica A, Balkwill F. Cancer-related inflammation. *Nature*. (2008) 454:436–44. doi: 10.1038/nature07205

71. Greten FR, Grivennikov SI. Inflammation and cancer: triggers, mechanisms, and consequences. *Immunity*. (2019) 51:27–41. doi: 10.1016/j.immuni.2019.06.025

72. Buergy D, Wenz F, Groden C, Brockmann MA. Tumor-platelet interaction in solid tumors. *Int J Cancer*. (2012) 130:2747–60. doi: 10.1002/ijc.v130.12

73. Wojtukiewicz MZ, Sierko E, Hempel D, Tucker SC, Honn KV. Platelets and cancer angiogenesis nexus. *Cancer Metastasis Rev*. (2017) 36:249–62. doi: 10.1007/s10555-017-9673-1

74. Schlesinger M. Role of platelets and platelet receptors in cancer metastasis. *J Hematol Oncol*. (2018) 11:125. doi: 10.1186/s13045-018-0669-2

75. Bendari A, Bendari A, Zhong X, Geetha SD, Al-Refai R, Sham S, et al. Hemoglobin-albumin-lymphocyte-platelet (HALP) score as a predictive value of incidental prostate cancer for patients going for transurethral resection of the prostate (TURP): A single-center study. *Cureus*. (2024) 16:e57736. doi: 10.7759/cureus.57736

Frontiers in Immunology

Explores novel approaches and diagnoses to treat immune disorders.

The official journal of the International Union of Immunological Societies (IUIS) and the most cited in its field, leading the way for research across basic, translational and clinical immunology.

Discover the latest Research Topics

See more →

Frontiers

Avenue du Tribunal-Fédéral 34
1005 Lausanne, Switzerland
frontiersin.org

Contact us

+41 (0)21 510 17 00
frontiersin.org/about/contact